ESS Technical Design Report

Åberg, M.; Ahlfors, N. ; Ainsworth, R. ; Alba-Simionesco, C. ; Alimov, S. ; Aliouane, N. ; Alling, B. ; Andersson, Kasper Grann; Andersen, Niels Hessel; Hansen, Britt Rosendahl

Total number of authors:
24

Publication date:
2013

Document Version
Publisher's PDF, also known as Version of record

ESS Technical Design Report

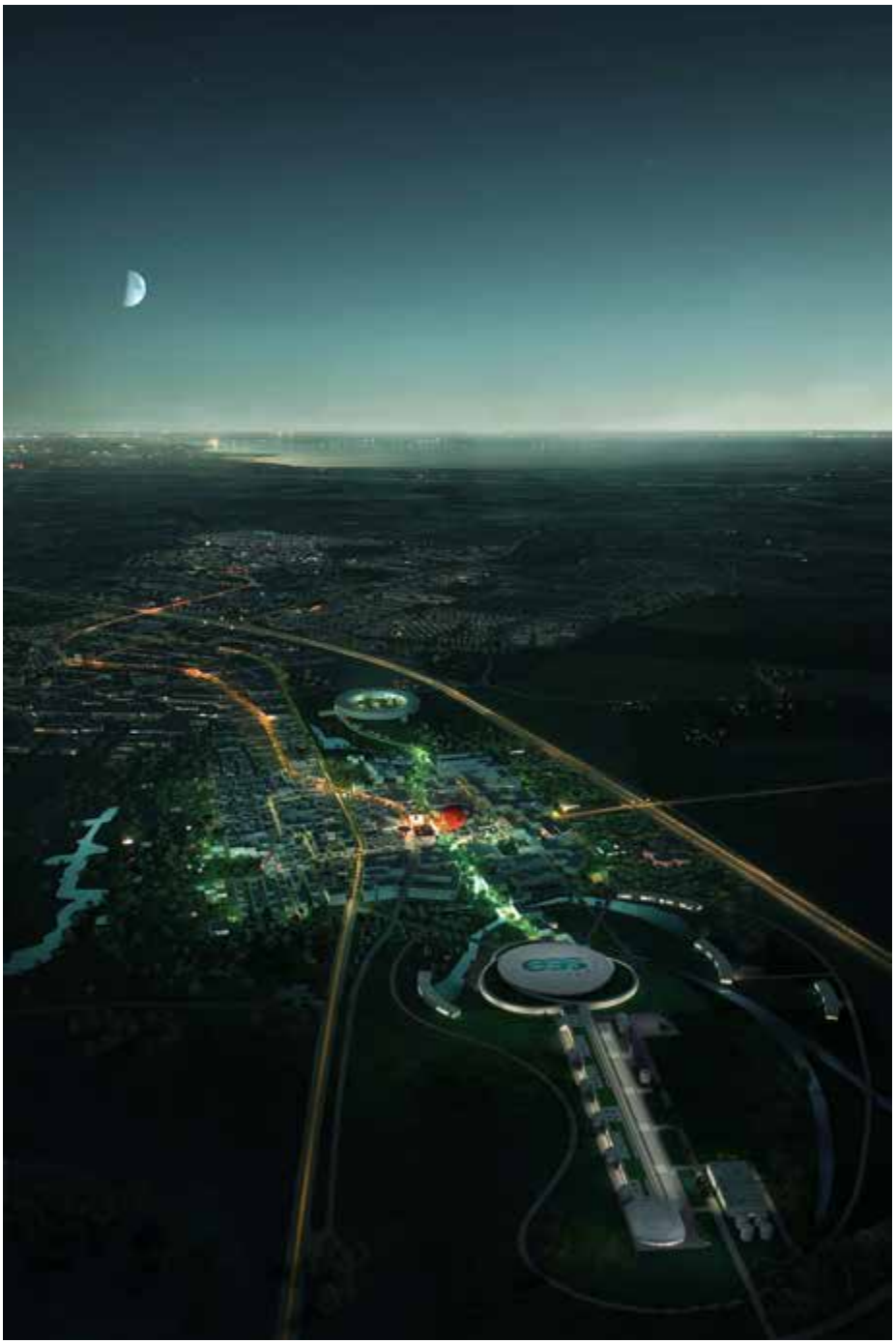

April 23, 2013

ESS Technical Design Report
April 23, 2013
ESS-doc-274
http://europeanspallationsource.se/documentation/tdr.pdf

ISBN 978-91-980173-2-8

Executive editor: S. Peggs[1].

Structural editor: R. Kreier[1].

Contributing editors: C. Carlile[1], R. Miyamoto[1], A. Påhlsson[2], M. Trojer[2], J. G. Weisend II[1].

Chapter editors: M.-L. Ainalem[1], K. H. Andersen[1], K. Batkov[1], P. Carlsson[1], D. Ene[1], B. Hedén[1], K. Hedin[1], A. J. Jackson[1], P. Jacobsson[1], O. Kirstein[1], G. Lanfranco[1], Y. Lee[1], M. Lindroos[1], J. Malovrh Rebec[3], G. Trahern[1], J. Yeck[1].

Contributors: M. Åberg[1], N. Ahlfors[1], R. Ainsworth[4], C. Alba-Simionesco[5], S. Alimov[6] N. Aliouane[7] B. Alling[8], K. Andersson[9], M. Andersson[1], N. H. Andersen[9], D. Anevski[10], S. Ansell[11], V. Antonelli[12], D. Argyriou[1], L. Arleth[13], E. Babcock[14], S. Barbanotti[15], F. Beckmann[16], P. M. Bentley[1], P. Beran[17], L. Bérden[1], F. Bergstedt[1], J. Bermejo[18], M. Berrada[14], M. Bertelsen[13], Y. Beßler[14], T. Bigault[19], J. Birch[8], J. O. Birk[13], J. Bobnar[3], C. Böhme[1], A. Bollhalder[7], P. Böni[12], H. N. Bordallo[13], P. Bosland[5], S. Bousson[20], W. G. Bouwman[21], G. Brandl[12], S. Brault[20], J. Brinch[21], R. Brinkmann[15], H. Brueck[15], T. Brückel[14], J. C. Buffet[19], M. Bulat[6], R. Bürge[7], I. Bustinduy[18], M. Butzek[14], X. X. Cai[22], R. Caniello[23], M. Cardenas[13], G. Castro[24], H. Carlsen[13], L. Celona[21], Y. Chen[25], N. Cherkashyna[1], S. Choroba[15], B. Cheymol[1], M. Christensen[26], N. B. Christensen[27], E. P. Cippo[28], A. Class[25], K. Clausen[19], U. Clemens[14], J. F. Clergeau[19], M. Comunian[21], C. Cooper-Jensen[1], J. Correa[19], G. Croci[23], G. Čuk[3], L. Cussen[6], Y. Dai[7], H. Danared[1], D. Dancila[29], C. Darve[1], T. Davenne[11], P. de Vicente[18], P. P. Deen[1], M. Dell'Anno Boulton[1], S. Deledda[22], C. Densham[11], R. De Prisco[1], M. Desmons[5], G. Devanz[5], F. M. Dominguez[18], P. Duchesne[20], R. Duperrier[1], P. Duthil[20], H. Eckerlebe[16], S. Eckert[30], H.-J. Eckholt[15], T. Ekelöf[29], J. Embs[7], M. Eneroth[1], R. Engels[14], C. Engling[15], M. Eshraqi[1], R. Fabbri[14], C. Fazio[25], J. Fenske[16], J. Fetzer[25], U. Filges[7], U. Fischer[25], K. G. Fissum[10], M. Forster[7], A. France[5], A. Franciosi[31], P. Freeman[6,32], H. Frielinghaus[14], C. Fröjdh[33], C. Frost[11], T. Gahl[1], S. Gallimore[1], S. Gammino[21], N. Gandalfo[20], R. Georgii[12], G. Gerbeth[30], G. Gervasini[23], B.-E. Ghidersa[25], A. Ghiglino[18], L. Giacomelli[28], O. Gonzalez[18], G. Gorini[28], V. Goryashiko[29], M. Göhran[1], K. Gajewski[29], A. Goukassov[26], D. Graf[7], F. Grespan[24], A. Gromov[7], G. Grosso[23], U. Greuter[7], C. Grünzweig[7], B. Guérard[19], S. Gysin[1], K. Habicht[6], H. Hahn[1], E. A. L. Håkansson[34], S. Hall[1,10], R. Hall-Wilton[1], B. R. Hansen[9], U. B. Hansen[35], T. Hansson[1], T. Haraldsen[22], V. Haramus[16], C.-H. Hårdh[1], H. Hassan[1], H. Hassanzadegan[1], B. C. Hauback[22], W. Häussler[12], W. Hees[1], G. Helgesen[22], P. Henry[1], L. Hermansson[29], A. Hiess[1], A. Hilger[6], T. Hofmann[6], C. Höglund[1,8], L. Hoitzner[7], A. I. S. Holm[27], S. Holm[36], L. Høpfner[35], C. Horstmann[16], A. Houben[37], L. Hultman[8], M. Imam[1,8], A. Ioffe[14], J. Iversen[15], S. Iyengar[34], P. Jacobs[37], C. L. Jacobsen[35], H. Jacobsen[35], J. Jacobsen[13], A. Jansson[1], K. Jensch[15], J. Jensen[8], M. Jensen[9], X. J. Jin[25], A. J. Johansson[34], R. Jongeling[1], F. Juranyi[7], C. Kagi[7], R. Kampmann[16], K. Kanaki[1], N. Kardjilov[6], S. Kecskes[25], P. Keller[7], G. Kemmerling[14], M. Kenzelmann[7], A. Khaplanov[1], C. Kharoua[1], I. Khokhriakov[16], K. Kiefer[6], B. Kildetoft[1], T. Kittelmann[1], H. Kleines[14], K. Klenø[35], E. B. Klinkby[9], B. Klösgen[38], E. B. Knudsen[9], K. Knudsen[22], J. Kohlbrecher[7], M. Könnecke[7], A. Konobeev[25], P. Korelis[7], T. Köttig[1], L. Krämer[12], J. Krašna[3], J. Krebs[7], Ž. Kroflič[3], V. Krsjak[39], S. Kynde[13], B. Laatsch[14], P. Ladd[1], E. Laface[1], B. Lauritzen[9], R. E. Lechner[1], K. Lefmann[35], E. Lehmann[7], M. Lehmann[7], F. Leseigneur[20], K. Lieutenant[6], L. Lilje[15], R. Linander[1], H. Lindblad[1], B. Lindenau[14], I. Llamas-Jansa[22], T. Lofnes[29], W. Lohstroh[12], D. Lott[16], P. Lukáš[17], J. Lundgren[1], M. Lundin[40], H. Möller[1], M. Maǵan[18], I. Manke[6], M. Marko[7], N. Martin[12], D. Mascali[24], A. Matheisen[15], S. Mattauch[14], D. McGinnis[1], M. Meissner[1], P. Mereu[24], M. Meshkian[34], F. Mezei[1], W.-D. Moeller[15], J. Molander[1], S. Molloy[1], K. Mortensen[13], J.-F. Moulin[16], A. Milocco[28], M. Monkenbusch[14], M. Morgano[7], T. Mühlebach[7], M. Müller[16], J. L. Muñoz[18], G. Nagy[7], D. Nekrassov[6], L. Neri[24], K. Neuhaus[15], J. Neuhausen[7], C. Niedermayer[7], J. B. Nielsen[9], S. Nielsen[9], B. Nilsson[40], P. Nilsson[1], E. Noah[1], E. Nonboel[9], P. Norby[9], A. Nordt[1], G. Nowak[16], E. Oksanen[1], G. Olivier[20], G. Olry[20], T. Panzner[7], S. Pape-Møller[27], C. Pappas[21], T. Parker[1], S. Pasini[14], H. Pedersen[8], S. Peetermans[7], J. Persson[1], B. Petersen[15], S. Petersson[33], S. Petersson Årsköld[1], J. Pieper[41], A. Pietropaolo[23], J. Pilch[17], A. Piquet[5], F. Piscitelli[19], A. Pisent[24], E. Platacis[25], F. Plewinski[1], J. Plomp[21], J. Plouin[5], A. Ponton[1], S. Pospisil[42], B. Pottin[5], H. F. Poulsen[9], S. O. Poulsen[9], P. Rådahl[1], P. K. Pranzas[16], M. Proell[15], O. Prokhnenko[6], K. Prokeš[6], E. Rampnoux[20], E. Rantsiou[7], N. Rasmussen[35], O. Rasmussen[9], K. Rathsman[1], M. Rebai[28], T. Reiss[7], M. Reščič[3], D. Reschke[15], C. Rethfeldt[6], M. Reungoat[44], D. Reynet[20], D. Richter[14], M. Rieth[25], T. H. Rod[35], D. M. Rodriguez[1], I. Rodriguez[1,14] K. Rolfs[6], M. Rouijaa[16], R. Ruber[29], U. Rücker[14], C. Rüegg[7], H. Rønnow[32], M. Russina[6], A. Ryberg[29], P. Sabbagh[1], A. Sadeghzadeh[1],

M. Sales[6,36], Z. Salhi[14], R. Santiago-Kern[29], J. Šaroun[17], T. Satogata[45], F. Saxild[9], J. Schaffran[15], J. Schefer[7], J. Scherzinger[10], M. Schild[7], B. Schillinger[12], H. Schlarb[15], P. Schmakat[12], A. Schreyer[16], W. Schroeder[14], P. Schurtenberger[10], C. Schulz[6], M. Schulz[12], W. Schweika[1,14], M. Seifert[12], G. Severin[9], R. Seviour[1], M. Sharp[1], T. Shea[1], P. Sievers[1], L. Silvi[12], G. G. Simeoni[12], W. Singer[15], P. Šittner[46], R. Sjöholm[1], N. Skar-Gislinge[13], S. Skelboe[35], F. Sordo[18], J. Stahn[7], P. Staron[16], I. Stefanescu[12], F. Stefani[30], W.-D. Stein[6], R. Steitz[6], H. Stelzer[14], A. Steuwer[1], M. Störmer[16], M. Strobl[1,6], P. Stronciwilk[14], P. Strunz[17], A. Sukhanova[14], I. Sutton[1], K. Svedin[1], H. Svensson[40], A. Takibayev[1], V. Talanov[7], M. Tardocchi[23], L. Tchelidze[1], M. Telling[11], S. Terron[18], K. Theodor[35], J-P. Thermeau[20], H. D. Thomsen[27], K. Thomsen[7], A. Tibbelin[1], C. Tiemann[14], M. Trapp[6], N. Tsapatsaris[1], L. Udby[13], A. Ushakov[6], P. Van Esch[19], L. Van Eijck[21], S. van Waasen[14], A. A. Van Well[21], C. Vasi[48], E. Vassallo[23], C. Vettier[1], A. Vickery[35], N. Violini[14], M. Vitorovič[3], R. Vivanco[18], E. Vogel[15], J. Voigt[14], L. Von Moos[13], H. P. Wacklin[1], X. Wang[15], X. L. Wang[1], T. Weber[12], R. Wedberg[29], S. Weichselbaumer[12], B. Weinhorst[25], H. Weise[15], A. Weisenburger[25], P. K. Willendrup[9], R. Willumeit[16], T. Wilpert[6], A. Wischnewski[14], M. Wohlmuther[7], J. Wolters[14], R. A. Yogi[29], L. Zanini[1], K. Žagar[3], K. Zeitelhack[12], C. Zendler[6], R. Zeng[1], V. Ziemann[29], M. Zoppi[49], A. Zugazaga[18].

[1]European Spallation Source
[2]ÅF Consult
[3]Control System Laboratory
[4]Royal Holloway, University of London
[5]Commissariat à l'Énergie Atomique et aux énergies alternatives
[6]Helmholtz-Zentrum Berlin für Materialien und Energie
[7]Paul Scherrer Institut
[8]Linköping University
[9]Technical University of Denmark
[10]Lund University
[11]Science and Technology Facilities Council
[12]Technische Universität Mnchen
[13]Københavns Universitet
[14]Forschungszentrum Jülich
[15]Deutsches Elektronen-Synkrotron
[16]Helmholtz-Zentrum Geesthacht
[17]Nuclear Physics Institute ASCR, Řež
[18]European Spallation Source – Bilbao
[19]Institut Laue-Langevin
[20]Institut de Physique Nucléaire
[21]Delft University of Technology
[22]Institute for Energy Technology
[23]Consiglio Nazionale delle Ricerche – Milano
[24]Istituto Nazionale di Fisica Nucleare
[25]Karlsruhe Institute of Technology
[26]Laboratoire Léon Brillouin
[27]Aarhus University
[28]Milano-Bicocca University
[29]Uppsala University
[30]Helmholtz-Zentrum Dresden-Rossendorf
[31]Sincrotrone Trieste S.C.p.A. di interesse nazionale
[32]École Polytechnique Fédérale de Lausanne
[33]Mid Sweden University
[34]Lunds Tekniska Högskola
[35]Niels Bohr Institute
[36]Copenhagen University
[37]Rheinisch-Westfälische Technische Hochschule Aachen
[38]University of Southern Denmark
[39]Slovak University of Technology, Bratislava
[40]The MAX IV Laboratory
[41]University of Tartu
[42]Czech Technical University in Prague
[43]Institute of Nuclear Techniques – Budapest
[44]Centrum výzkumu Řež s.r.o.
[45]Thomas Jefferson National Accelerator Facility
[46]Institute of Physics of the ASCR, Prague
[47]IHEP – Protvino
[48]Consiglio Nazionale delle Ricerche – Messina
[49]Consiglio Nazionale delle Ricerche – Firenze

Brief Contents

Contents

List of Figures

List of Tables

Executive Overview

Introduction: The evolving story

ESS, the European Spallation Source, will be a major user facility at which researchers from academia and industry will investigate scientific questions using neutron beams. Neutron methods provide insights about the molecular building blocks of matter not available by other means. They are used for both basic and applied research.

ESS will be a slow neutron source of unparallelled power and scientific performance. It will deliver its first protons to a solid, rotating tungsten target in 2019, which will in turn generate neutrons for delivery to an initial suite of seven neutron scattering research instruments. ESS will reach its full design specifications in 2025, with a suite of 22 research instruments. The publication of the *Technical Design Report* in 2013 represents an important milestone for the ESS project, marking its readiness to move forward with construction activities. This executive overview provides a brief summary of the key insights and findings of the *Technical Design Report.*

The road to achieve such a European high-power spallation source has been long and winding. The neutron itself was discovered in 1932 in Cambridge by James Chadwick. During the 1950s, research installations in the north American subcontinent developed the early instrumental techniques that used neutrons to unravel the atomic structures and dynamics of relatively simple materials. Cliff Shull and Bert Brockhouse received the Nobel prize in physics in 1994 for this work. A rapid rise in technical capabilities culminated, in the late 1960s, in the construction in Grenoble of a purpose-built high flux reactor source of slow neutrons. The *Institut Laue-Langevin* (ILL), as it was named, became the flagship of neutron research. In parallel, and with a somewhat different purpose, accelerator-driven sources of neutrons were also being developed. These facilities were excellent generators of fast neutrons that were used to compile a nuclear cross section database of all the elements and their isotopes in order to support the nuclear power industry. The early exemplars of such sources were based on electron linear accelerators, which, unfortunately, have significant background problems caused by the intense gamma radiation bursts that they generate.

In the late 1970s and early 1980s, scientists began to explore the use of proton-driven neutron sources, employing cyclotrons, synchrotrons or linear accelerators. Proton sources avoid the problems with gamma background from which electron sources suffer. Proton sources also hold a significant technological advantage over the most intense research reactors because the spallation reaction employed in proton machines generates significantly less heat per useful neutron than does a fission reactor. In addition, the generation of neutrons in pulses provides peak brightnesses that far exceed those available from reactors. ISIS, a proton spallation source that was powerful enough to challenge the supremacy of ILL, was built near Oxford in the late 1970s.

In 1998, the OECD research ministers endorsed a Megascience Forum report recommending that a megawatt-class spallation neutron source be built in each of the three developed regions of the world. Over the next five years, alternative configurations were studied. In 2003, following a plenary meeting of some 700 scientists and science policy-makers in Bonn, a new concept was put forward for ESS comprising a 5 MW proton linear accelerator delivering a 2 to 3 millisecond-long pulse to a single target station surrounded by a suite of 20 to 25 neutron instruments. This initiative held out the promise of neutron intensities that were a factor of six more intense, per megawatt of proton beam power, than contemporary existing or planned facilities. The user community in Europe endorsed this concept, and it has provided the framework for the ESS design process that is now nearing completion.

The decision to locate ESS near Lund was taken in Brussels on 28 May, 2009, after a competitive process

Parameter	Unit	Value
Average beam power	MW	5
Number of target stations		1
Number of instruments in construction budget		22
Number of beam ports		48
Number of moderators		2
Separation of ports	degrees	5
Proton kinetic energy	GeV	2.5
Average macro-pulse current	mA	50
Macro-pulse length	ms	2.86
Pulse repetition rate	Hz	14
Maximum accelerating cavity surface field	MV/m	40
Maximum linac length (without 100 m upgrade space)	m	482.5
Annual operating period	h	5000
Reliability	%	95

Table 1: High level parameters, approved by the ESS Steering Committee on 18 April, 2011.

facilitated by the European Strategy Forum for Research Infrastructures (ESFRI) and the Czech Republic's Ministry of Research during its period of Presidency of the European Union. At the time of writing – April 2013 – ESS AB is a shareholding company under Swedish law in which Sweden holds approximately 75% of the shares and Denmark holds the remaining 25%. Its Steering Committee currently includes 17 partner countries: Sweden, Denmark, Norway, Latvia, Lithuania, Estonia, Iceland, Poland, Germany, France, the United Kingdom, the Netherlands, Hungary, the Czech Republic, Switzerland, Spain, and Italy. The 17 partner countries support ESS both through financial contributions and through in-kind contributions of materials, equipment and expert scientific and technical services.

Table 1 records the high level parameters of ESS, and its guiding scientific goals. The ESS Steering Committee approved these parameters on 18 April, 2011 at its inaugural meeting in Copenhagen. The three year-long ESS pre-construction phase is now coming to an end. Currently, ESS has close to 200 employees, and the organisation is in a period of rapid growth. The construction phase begins in 2013, followed by the start of the operations phase of the ESS life-cycle in 2017. The machine will reach full specifications in 2025 and continue to serve the European neutron research community, which currently includes approximately 6000 researchers, until 2065.

Neutron science and instruments

Neutron scattering techniques offer a unique combination of high sensitivity and high penetration as they monitor structure and motion at a molecular level. They address today's cutting edge research questions, and will be even more important to meet tomorrow's technological challenges. Their impact spans many scientific disciplines including physics, chemistry, biology, materials science, engineering and archaeology. Neutrons can probe magnetism and superconductivity, guide the development of new materials, "look inside" an operating car engine, or illuminate an old master's painting technique without damaging his priceless masterpiece. These techniques further industrial and technological progress, contributing to advances in fields ranging from pharmaceutical development to fuel cell technology. The neutron also holds promise of helping to unravel fundamental puzzles of the universe, such as why there is more matter than antimatter. Figure 1 illustrates the ability of neutrons to examine the internal structures of precious, irreplaceable materials (in this case, an Indonesian dagger sheath) without causing damage. The two images in Figure 2 exemplify the major contributions neutron techniques have made to understanding the magnetic properties of matter.

No single probe can cover the whole span of time and length scales that the various fields of science encompass. Techniques are often complementary rather than competitive even when their temporal and spatial scales overlap, because different probes access different kinds of information, realising powerful synergies. The particular strengths of neutrons include sensitivity to light elements such as hydrogen; the ability to distinguish between different elements; the non-destructiveness of the beam in terms of sample

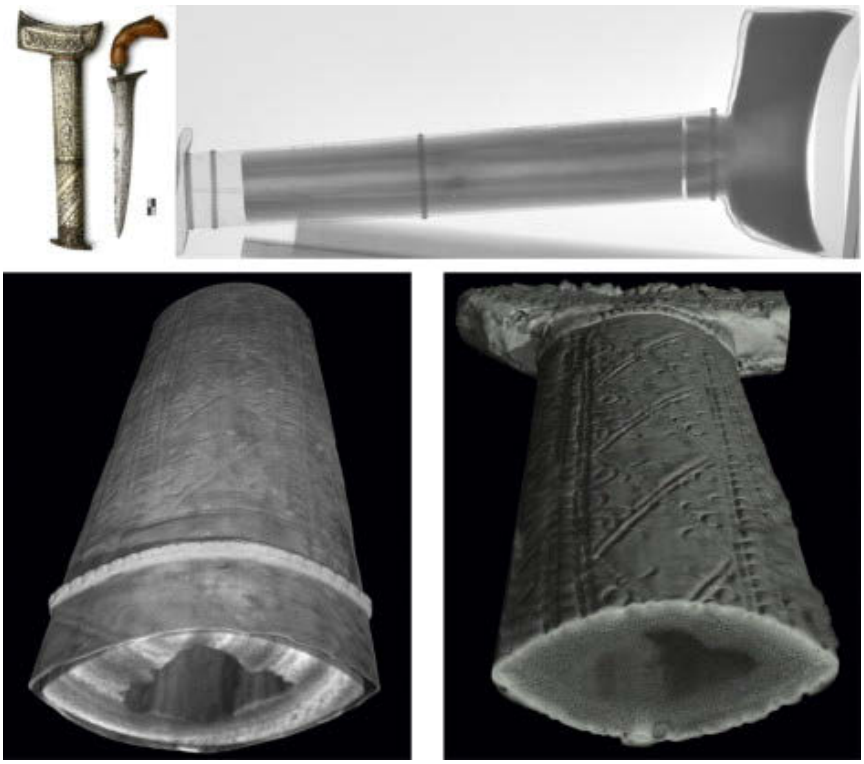

Figure 1: Non-destructive imaging of an Indonesian dagger sheath, illustrating how neutrons mitigate the obscuring effects of the outer metal cover on images of the inner wooden parts. Top left: A photograph of the dagger and the sheath, which has an outer metal cover (containing silver) and an inner wooden structure. Top right: A neutron transmission (radiography) image. Bottom left and right: 3D renderings of neutron and X-ray tomography data, respectively. Courtesy of E.H. Lehmann [1].

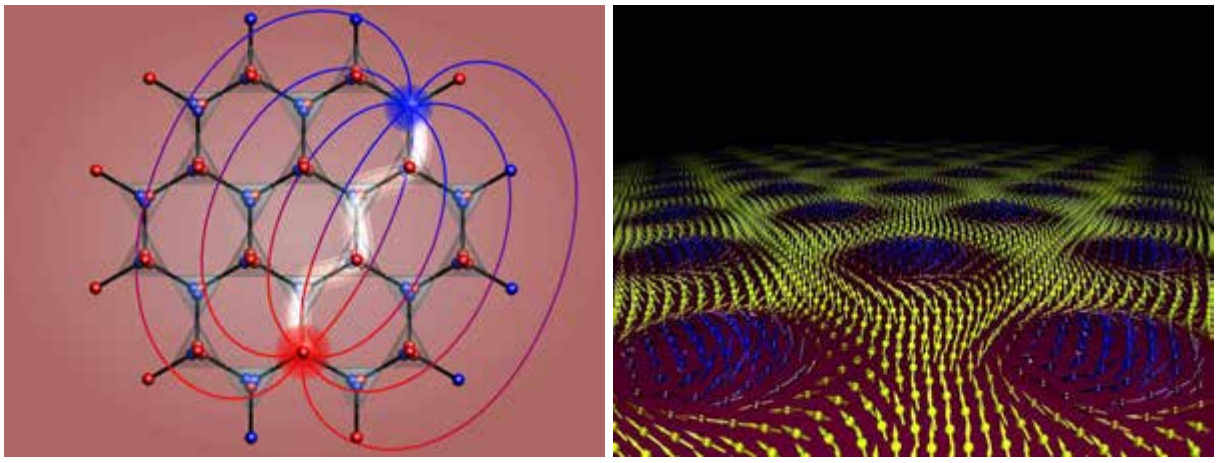

Figure 2: Dirac strings and a Skyrmion lattice. Left: A pair of separated monopoles, in red and blue, with a chain of inverted dipoles between them. Dirac strings are highlighted in white with the associated magnetic field lines [2]. Right: Magnetic vortex spin ordering in a Skyrmion lattice as first revealed by neutron scattering [3].

integrity; the power to probe magnetic structure; and the capability to penetrate many materials, making possible the investigation of samples in environments that would stop other forms of radiation.

The value of a scattering probe also depends on the performance of available sources of radiation. In that respect, investigations using X-rays have experienced dramatic progress through the ongoing development of synchrotron light sources and X-ray free electron lasers. Electron microscopy and nuclear magnetic resonance (NMR) methods also have benefited from significant ongoing advances. Similarly, ESS will offer gain factors of more than an order of magnitude over current neutron sources.

ESS will have a unique ability to study a broad range of structures and time scales due to its long, high-intensity neutron pulses. ESS will offer neutron beams of unparallelled brightness, delivering a peak flux 30 times higher than the world's most powerful reactor-based neutron source, and five times more power than any accelerator-based spallation source. Its high brightness will provide an unprecedented ability to probe weak signals and systems that change over time, or to measure within a small volume. This last ability is particularly useful for real-world heterogeneous samples or for materials for which only small sample quantities are available. The bright neutron beams will be delivered in a unique time structure, with long neutron pulses (2.86 ms) at low frequency (14 Hz). This structure is very well matched to the requirements of long-wavelength neutrons. To fully exploit the long-pulse structure, ESS will rely on components such as guides and choppers to adapt resolution and dynamic range to each individual experiment, rather than hard-wiring these parameters into the design of the source and instruments as has been done at current spallation and reactor sources. The result will be unmatched instrument flexibility, which will allow the user to zoom in or out of the features of interest while varying the resolution to exactly match the time or spatial correlations under study. The high flux and unique time structure will make possible many investigations that are out of range today, significantly expanding the scientific possibilities.

The spallation source will deliver neutron beams to a suite of research instruments, each devised to extract different kinds of information from the samples studied. The instruments will be adapted to meet the requirements of a wide range of scientific disciplines. The science drivers identified for ESS are soft condensed matter, life science, magnetic and electronic phenomena, chemistry of materials, energy research, engineering materials and geosciences, archaeology and heritage conservation, and fundamental and particle physics. Many of these areas have long traditions using neutron techniques, while in others, the use of neutron techniques is on the rise. It is important that ESS accommodate the science of today while allowing flexibility to meet the developments of tomorrow. The specialised instruments will collectively provide researchers with vital information complementary to information from other methods, such as the X-rays provided by the MAX IV synchrotron that will be ESS's immediate neighbour. To fully exploit the source performance, ESS's instruments will employ new technology and novel approaches in their design.

Figure 3 shows the neutron beamline and instrument layout for a reference suite of 22 instruments, selected for illustrative purposes from the 40-odd instrument concepts presently under development. The instruments that actually will be built are likely to be quite different from those in the reference suite, since instrument selection will take place in a staged process, starting in 2013. The design phase for the instruments will continue past 2020, when the final two instrument concepts are slated for selection. This staged approach will permit ESS to remain engaged with the European user community and to choose instrument designs that are state-of-the-art and scientifically relevant when they enter user operation.

In order to make use of the enormous flexibility that the long neutron pulse provides, ESS will use neutron choppers to variably select the sections of the pulse that are needed for a specific instrument. To realise the optimum use of the high flux available, neutron optical components such as focusing guides and polarising mirrors also will be used. In each neutron research instrument, neutrons are detected by a nuclear interaction in a "converter material." Most flagship instruments at current sources use an isotope of helium, ^{3}He, as this converter material. New kinds of neutron detectors are urgently needed, due to the very limited availability of ^{3}He. For this reason, the Detector Group was the first neutron technology group established in Lund in July 2010. ESS has established collaborations to develop ^{10}B-based detector technology. The collaborations aim both to build up a core of competence in detector development in the Lund region to support ESS's needs during the construction phase, and to develop capacity in Europe as a whole.

Specialised instruments will not be sufficient by themselves to fully exploit the potential of ESS. Extensive infrastructure also will be required to enable users to make the most productive use of research instruments. This area will be a key strength of ESS. Crucial user infrastructure will include sample preparation, characterisation, and specialised synthesis laboratories; detector and sample environment systems; and information technology and computational support. ESS users will benefit from the Data Management

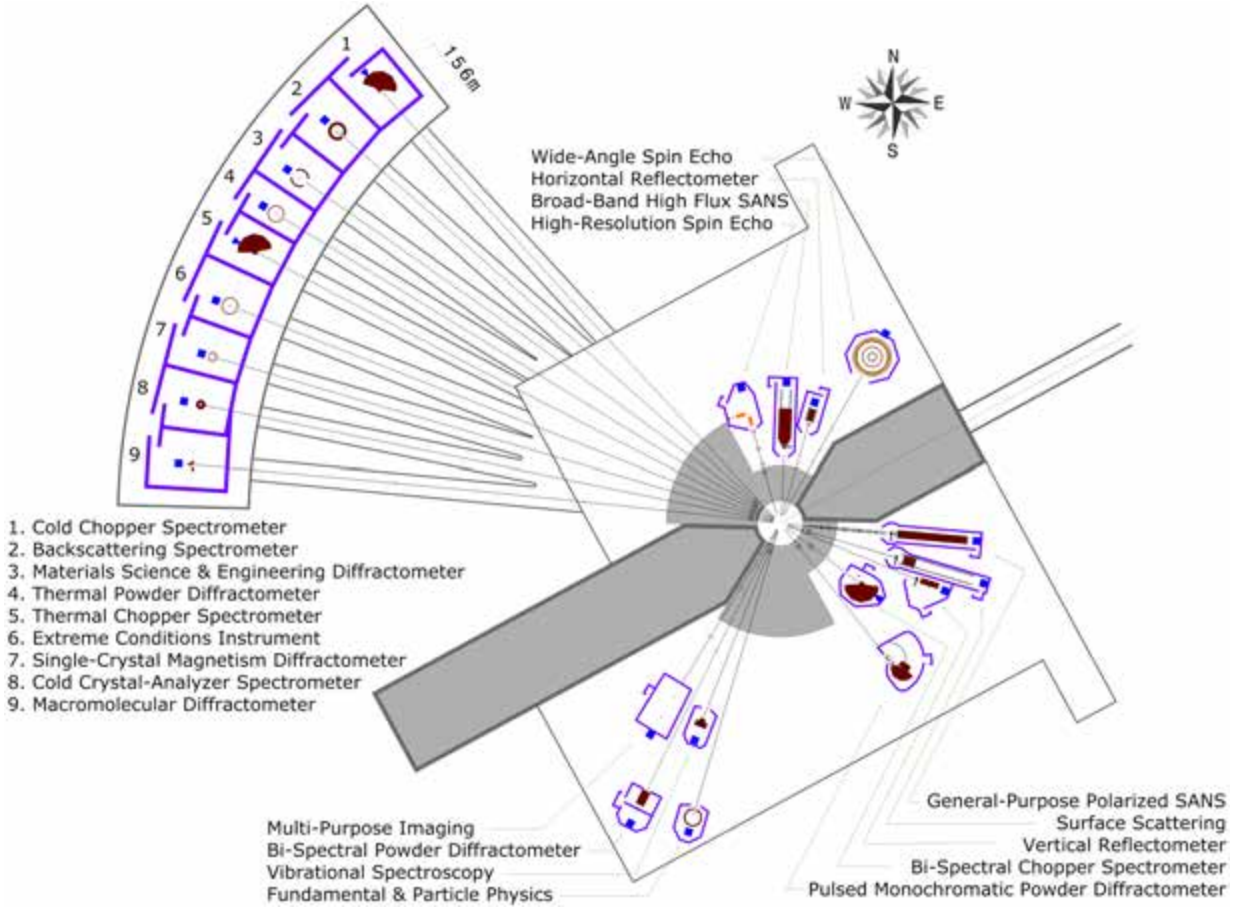

Figure 3: Neutron beamline and instrument layout for the reference instrument suite, which is presented for illustrative purposes. The instruments that actually will be built will be chosen in an ongoing process in which several instrument concepts are selected every year, starting in 2013 and ending in 2020. Labels for the nine numbered instruments in the upper left of the figure are listed below the image.

and Software Centre (DMSC) that will be located at the Nørre Campus of the University of Copenhagen across the Öresund from the experimental stations in Lund. The computational and software solutions being developed at DMSC will provide users with a coherent experience, providing user-centred software for instrument control, efficient data reduction, real-time data visualisation, intuitive data analysis and computational support for modelling and simulations. This comprehensive set of computational solutions will add value to the neutron data collected, and will establish a new standard for neutron facilities. It also will make neutron techniques more accessible to researchers from fields that do not have long histories using these tools, but for which neutrons hold significant promise of yielding new insights.

An ongoing series of ESS science symposia and workshops promotes communication between ESS and the scientific community, ensuring that the instrument suite, supporting infrastructure and computational options will be able to respond to the diverse needs of researchers from a broad range of disciplines as they evolve over time.

The target station

The main function of the target station is to convert the high-energy proton beam from the accelerator into low-energy neutron beams with the greatest possible efficiency. Three groups of target station subsystems deliver this key functionality. The first group consists of the target monolith and the components it houses, including the target wheel. The second group is made up of fluid systems, including the closed cooling circuits and the radioactive gaseous effluents and confinement (RGEC) system. The third group

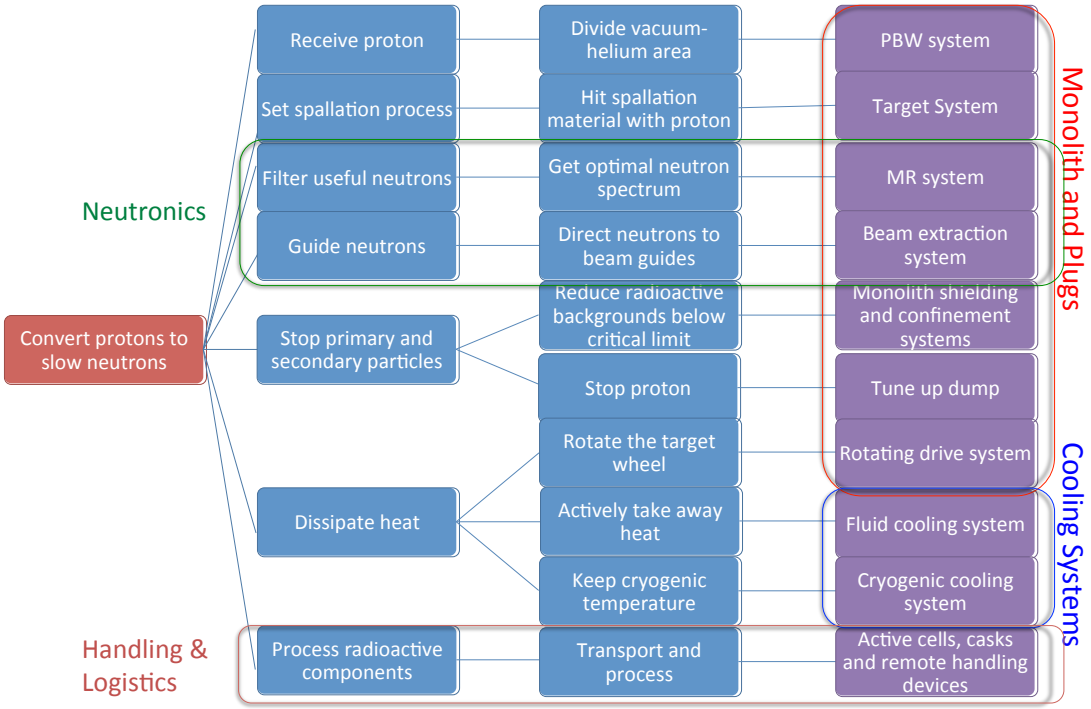

Figure 4: Target station functionalities.

includes the handling and logistics subsystems for the radioactive components from the target station operation. This group includes active cells, casks and remote handling systems. These subsystems transport, exchange, maintain, process, package, store and release the used radioactive components from the target station operation. Figure 4 provides an overview of the target station functionalities.

Target station interfaces with the rest of the ESS project are complex. Target station design has been coordinated with accelerator design and with the requirements of the neutron scattering instruments. The target station safety system also has a number of protected interfaces with the facility-wide integrated control system, and the target station design has a large impact on target building and conventional facilities design, and vice versa. For robust and cost-effective design of the target station components, ESS has used advanced multi-physics simulation techniques in an iterative fashion, both for optimising neutron beam performance and for addressing issues of technical realisation and operation. This approach begins with calculation of the beam profile using beam dynamics calculation tools. A particle transport code is then applied to calculate volumetric heat depositions in irradiated target station components. Finally, the calculated local volumetric heat deposition configurations are used in advanced coupled flow, thermal and mechanical simulations to estimate the thermal and mechanical loads on the system. A database of the characteristics of the irradiated and un-irradiated materials used in the target system has been constructed using information from experiments, design codes and the scholarly literature. This database provides a crucial underpinning for the engineering design of target system components.

The monolith, target and associated subsystems will interact directly with protons and/or neutrons. This group of target subsystems includes the proton beam window, the rotating target wheel system, the moderator-reflector assembly and the beam extraction system. The self-contained target safety system, which overarches the whole target station and provides for facility safety at the highest level, is also a crucial part of this group. The target material (tungsten) will transform high-energy protons to fast neutrons. The moderator-reflector system surrounding the target will transform the fast neutrons into slow neutrons. These neutronically-activated subsystems will be housed in the target monolith, which will be composed of 7000 tons of steel shielding. The target monolith has been designed to contain the highly-penetrating gamma and fast neutron radiation that will be created by the spallation and radioactive decay processes. The baseline technology chosen for the ESS target design is a rotating tungsten target cooled by inert helium gas. The target surface area will be large enough so that in the event of a loss of power, passive

conduction, convection and radiative cooling would prevent the afterheat of radioactive decay from leading to unsafe temperatures with a significant safety margin.

In order to provide a complete and robust technical underpinning for the ESS design, two other target concepts have been explored in addition to the baseline design. A water-cooled rotating tungsten target has been designated as the back-up option. A lead-bismuth-eutectic (LBE) target, using liquid metal both as target material and coolant, was studied as a comparative option particularly with respect to environmental considerations. The results of this comparative study proved favourable to the baseline option.

The accelerator

ESS is an accelerator-driven neutron spallation source. The linear accelerator, or linac, is thus a critical component. The role of the accelerator is straightforward. It creates protons at the ion source, accelerates them to an appropriate energy, and steers them onto the target to create neutrons via the spallation process for use by a suite of research instruments. The general lay-out of the ESS linac is shown in Figure 5.

The proton ion source is a compact electron cyclotron resonance source (ECR) similar to those currently in operation in Catania, Sicily and at CEA-Saclay outside Paris. The beam from the ion source is transported through a low energy beam transport (LEBT) section to the radio-frequency quadrupole (RFQ) for bunching and acceleration. A similar RFQ presently under commissioning at CEA-Saclay, will be tested with realistic ESS performance parameters. The beam is transported from the RFQ and matched to the normal conducting drift tube linac (DTL) through a medium energy beam transport (MEBT) section. Leaving the DTL, the beam enters the superconducting portion of the linac, where acceleration is accomplished via superconducting radio frequency (SRF) cavities constructed from niobium. The low temperatures required for superconduction are achieved by immersing the cavities in liquid helium at a nominal temperature of 2 K. An individual helium tank surrounds each cavity. From the superconducting portion of the linac, the beam is transported via the high energy beam transport (HEBT) section to the target.

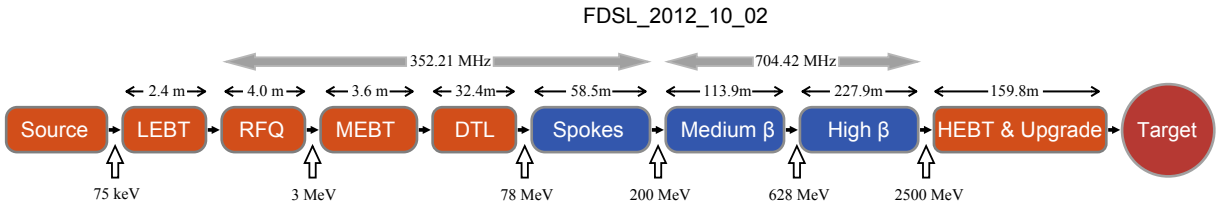

Figure 5: Block diagram of the ESS accelerator. Orange items (such as the radio frequency quadrupole and the drift tube linac) are normal conducting, while blue items (the spoke resonators and the medium- and high-β elliptical cavities) are superconducting.

The energy that accelerates the proton beam is provided by the radio frequency (RF) system that converts the AC power from the electrical grid to the appropriate RF frequencies required to drive the various accelerator components. This system includes the RF sources and conditioners (klystrons and modulators), the RF distribution system and the RF controls. The high level requirement of 95% reliability (availability) strongly influences the baseline design choices. High reliability requires that the accelerator must run, after re-tuning, even if multiple RF source-cavity stations are inoperable. It also requires a segmented cryomodule design, in which each cryomodule may be cooled down or warmed up independently of the others. Figure 6 shows a view of the tunnel including cryomodules.

The beam physics design of the linac has reached a high level of maturity. Inputs to the design include ESS's high-level parameters; mechanical properties such as the length of all linac components; constraints such as the maximum cavity gradients and the rating of the power couplers; optimisation criteria such as a desire for a minimum linac length and for small numbers of cavities and cryomodules; the need for high beam quality and small losses; and external factors such as the development of production capabilities and collaborations. The resulting configuration is a robust lattice with very small emittance growth, in which design margins and tolerances to faults and parameter variations are balanced with effectiveness in terms of cost and schedule. The linac configuration must be tolerant against static and dynamic variations

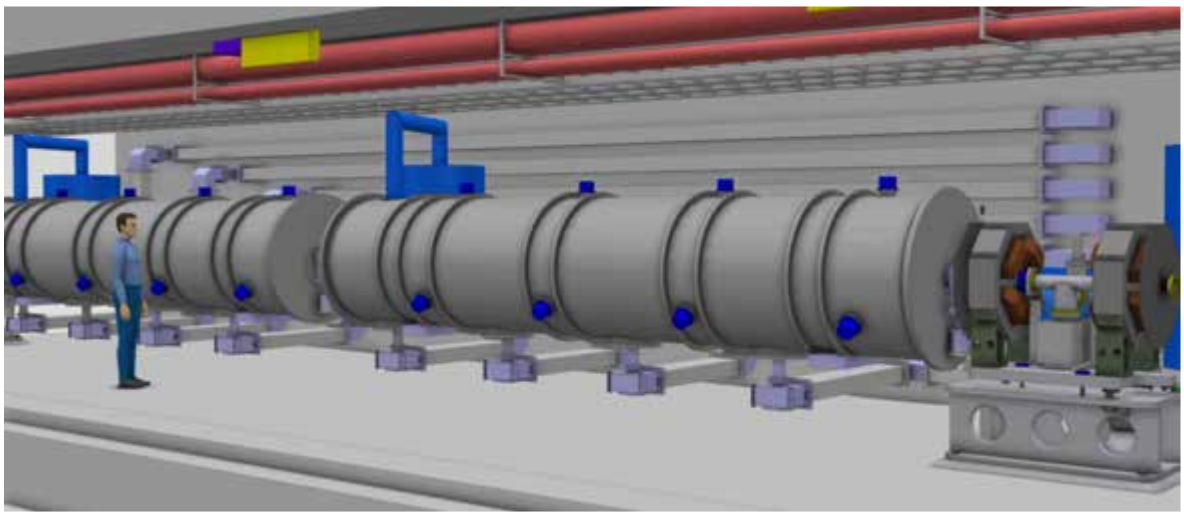

Figure 6: Tunnel perspective, showing elliptical cavity cryomodules, jumper connections, valve boxes and cryogenic transfer lines.

in parameter values, and beam losses must stay small within the range of expected variations. Also, the machine should, as far as possible, be able to run even if some components fail. To address these issues, a comprehensive study of alignment and field errors has been initiated, and investigations of the effects of faults and failures have begun. Figure 7 shows simulations of the maximum radius of the proton beam at different points along the linac for an ideal machine and for machines with various amplitudes of errors.

Successful operation of the accelerator requires detailed knowledge of the condition and location of the proton beam. The accelerator will be equipped with an array of beam instrumentation for this purpose. Beam loss monitoring (BLM) is arguably the most important diagnostic system of the linac. It will serve the dual purpose of keeping the machine safe from beam-induced damage and avoiding excessive machine activation by providing critical input to the machine protection system. Thus, the system will be designed so as not to have any blind spots. As the BLM system will be a major tool for beam tune-up, it also will be designed in a way that enables it to pinpoint the loss location as precisely as possible.

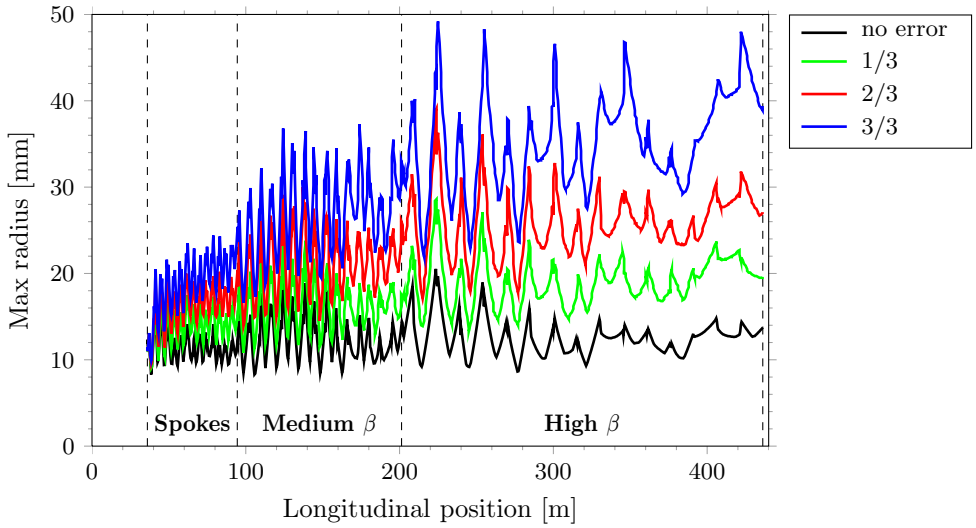

Figure 7: Robust design requires that the linac function even in the presence of alignment and field errors. The plot shows results from the simulation of maximum beam radius for an ideal machine (black curve) and for machines with various amplitudes of deviation from that ideal (coloured curves).

The integrated control system

The integrated control system (ICS) is responsible for the whole ESS machine and facility: Accelerator, target, neutron scattering instruments and conventional facilities. This unified approach keeps the costs of development, maintenance and support relatively low. ESS has selected a standardised, field-proven controls framework, the Experimental Physics and Industrial Control System (EPICS), which was originally developed jointly by Argonne and Los Alamos National Laboratories in the United States of America. Complementing this selection are best practices and experience from similar facilities regarding platform standardisation, control system development and device integration and commissioning. The components of ICS include the control system core, the control boxes, the database management system, and the human machine interface.

The control system core is a set of systems and tools that make it possible for the control system to provide required data, information and services to engineers, operators, physicists and the facility itself. The core components are the timing system that makes possible clock synchronisation across the facility, the machine protection system (MPS) that helps avoid damage to the machine's equipment due to beam losses, the personnel protection system (PPS) that prevents harm due to radiological risks, and a set of control system services that help with maintenance and operations.

Control boxes are servers that control a collection of equipment (for example a radio frequency cavity). ICS will include many control boxes, each of which can be assigned to one supplier, such as an internal team, a collaborating institute or a commercial vendor. This approach facilitates a clear division of responsibilities and makes integration much easier. A control box is composed of a standardised hardware platform, components, development tools and services. On the top level, it interfaces with the core control system components (timing, MPS, PPS) and with the human-machine interface. At the bottom, it interfaces with the equipment and parts of the facility through a set of analogue and digital signals, real-time control loops and other communication buses.

The central data management system is named BLED (beam line element databases). BLED is a set of databases, tools and services that is used to store, manage and access data. It holds vital control system configuration and physics-related (lattice) information about the accelerator, target and instruments. It facilitates control system configuration by bringing together direct input-output controller configuration and real-time data from proton and neutron beam line models. BLED also simplifies development and speeds up the code-test-debug cycle. The set of tools that access BLED will be tailored to the needs of different categories of users, such as staff physicists, engineers, and operators; external partner laboratories; and visiting experimental instrument users.

The human-machine interface will be vital to providing a high-quality user experience. It encompasses a wide array of devices and software tools, from control room screens to engineering terminal windows; from beam physics data tools to post-mortem data analysis tools. It will serve users with a wide range of computer skills from widely varied backgrounds. ESS is developing a set of user profiles to accommodate this diverse range of use-cases and users.

Specialised technical services

ESS requires three specialised technical systems: The cryogenic system, the vacuum system and the test stands. These systems support all three areas of the ESS: Accelerator, target and experiments. The system designs are conservative and based on experience at other facilities such as CERN in Geneva, Switzerland; SNS in Oak Ridge, Tennessee; and CEA-Saclay.

The cryogenic system consists of the linac cryoplant that provides cooling for cryomodules; the test and instruments cryoplant that provides cooling for test stands and liquid helium for instruments; the target cryoplant that provides 16 K helium cooling for the target station's hydrogen moderators; and the distribution system that connects the linac cryoplant to cryomodules. The linac cryoplant and test/instrument cryoplant share common gas management and storage systems. The target cryoplant system is completely separate due to the potential for tritium contamination. The cryogenic systems have been designed to meet sustainability goals through measures such as helium conservation and heat recovery. The cryogenic system also has been designed with an adequate margin of error to assure that its capacity will be large enough to meet ESS's needs.

The vacuum system provides vacuum for the linac beam line, target system and instrument lines. It

Figure 8: Maps of the ESS location. Left: Copenhagen/Malmö area. Right: Northeastern outskirts of Lund. The ESS site is shaded in blue. The MAX IV site is shaded in pink to the southwest of the ESS site.

uses well-established technology and procedures based on experience at similar facilities, including SNS in the United States, and J-PARC in Japan. It poses low technical risk.

Test stands provide testing and validation of both RF equipment (klystrons and modulators) and cryomodules. Cryogenic connection to cryomodules in the test stands will prototype similar connections in the linac tunnel. The test stand programme is robust against uncertainty in the ESS construction schedule by allowing for RF equipment testing in a temporary location if necessary. All cryomodules will be tested at nominal temperatures and RF power levels before tunnel installation. Cryomodule testing will take place at test stands in Lund and Uppsala.

Conventional facilities

The term "conventional facilities" refers to the spaces required to house ESS research equipment, machines and instruments and to accommodate the human beings who will either make use of the facility directly, or who will support its operation and maintenance. The overarching goal of the Conventional Facilities (CF) project is to deliver the physical space for a sustainable research facility in an environmentally friendly way. This includes meeting energy-related objectives and requirements; creating a good, safe and accessible working environment; creating an outdoor environment that promotes biodiversity and sustainable transportation; and using environmentally sound materials. During construction, CF will adopt a life-cycle perspective on the ESS facility, fulfilling requirements imposed as part of the Swedish environmental and construction permitting process and delivering the project within schedule and within budget. CF is also responsible for the mechanical and electrical services necessary for the proper functioning of the facility. Figure 8 locates the ESS site on maps of the region, while Figure 9 provides a preliminary sketch of the layout of the main components of the facility.

ESS will locate its facility on a 74.2 hectare site situated northeast of the town of Lund in the region of Skåne in southern Sweden. The site is located between Odarslövsvägen and the E22 highway, shaded in blue in the right hand panel of Figure 8. CF has studied the location and conditions at the site in terms of geography, current infrastructure, archaeology, and scientific and industrial environment. CF has also carried out extensive studies of ground conditions at the site, and evaluated alternative approaches to providing the facility's foundations in light of those ground conditions. The site, on the outskirts of the Brunnshög district of the city of Lund, is located in a highly developed scientific and industrial environment, providing access to an educated and technically skilled workforce, and proximity to Lund University and several major research centres. In addition, Lund and the surrounding region are home to

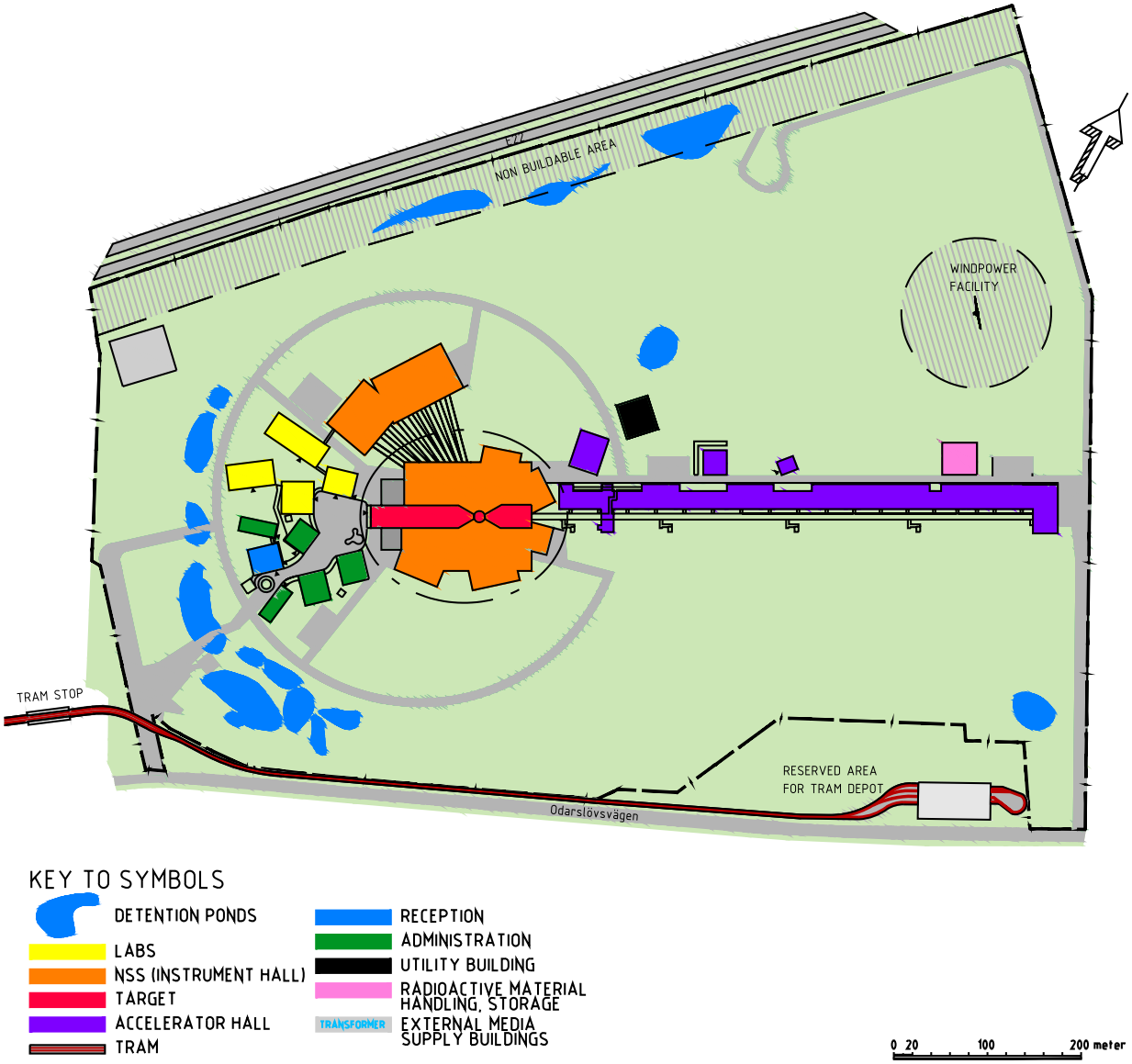

Figure 9: Preliminary layout of the main components on the ESS site.

a thriving knowledge-based industrial sector, including such major international companies as Ericsson, Tetra Pak and Alfa Laval. ESS's immediate neighbours will include the MAX IV synchrotron and Lund Science Village. Brunnshög is undergoing extensive growth and development. Regional land use plans call for a mixed-use neighbourhood with about 3000 dwellings, and with businesses providing employment for 20,000 to 25,000 individuals by 2025. Regional authorities will construct a tramway from Lund Central Station to the area. In addition, local buses and bicycle routes will be available.

The facility stretches over a considerable area. It is the responsibility of CF to create an efficient and functional logistics network and to provide a transportation system that will facilitate communication, social interaction, and the gradual addition of further buildings and instrument halls. Notable logistical challenges include the design of facilities and procedures to handle the complex and delicate sample materials that will be investigated by the ESS instruments, and the provision of remote handling and other systems required to deal with activated materials. CF is also responsible for planning and constructing the earthworks needed to create roads, parking spaces and landscaping, including the detention ponds required to treat storm water. The specific requirements of the storm water system that will protect external recipients from pollution from the facility receive particular attention. Buildings must reflect ESS's core values of excellence, openness and sustainability. The main buildings include the accelerator buildings,

Figure 10: The central campus, in an artist's impression by the Henning Larsen Architects in collaboration with COBE and NNE Pharmaplan. The target station is in the background, instantly recognisable by its overhanging, oval roof.

target station buildings, experimental halls, central laboratory building, and office building.

The scientific and symbolic value of the facility calls for a work of architectural and functional excellence. The summer of 2012 saw the launch of the ESS architectural design competition, undertaken under European Union rules and regulations. Experts in architecture, landscaping, economy and user aspects were invited to advise the jury. On 19 February, 2013, a team headed by Henning Larsen Architects was selected. The winning proposal provides a clear concept for the overall design of the site. The centrepiece target building is instantly recognisable by its overhanging, oval roof. The roof provides an ordering principle for the various buildings around the target area. In front of the target building, a dense campus area is planned, as shown in Figure 10.

Integration

The ESS integration strategy facilitates the success of the programme by progressively combining system elements in accordance with design requirements. It sets out procedures to ensure that interim assembly configurations are tested repeatedly, in order to assure the necessary flow of information and data across interfaces, to reduce interference risk and to minimise errors. ESS is implementing a quality management system based on the principles of ISO-9001. Systems engineering will ensure the efficient management of non-conformities and change requests. ESS's building information modelling system defines a uniform way of operating in civil engineering work and facility construction. The internal manual, *Standards, Norms and Guidelines Recommended for the Design and Construction of ESS,* constitutes a platform of standards recognised to be valid and applicable. The Standards Working Group is responsible for keeping the platform current with evolving norms and standards adopted by relevant national and international agencies and

professional groups. Design integration focuses on the interconnections between system components. The plant breakdown structure allows easy interface identification and provides a framework for the coherent organisation of documents and CAD assembly structures. Configuration management is achieved through configuration identification, interface and document management and change control. The plant layout is the three-dimensional model virtualisation of the facility. It is robustly linked to the proton and neutron beam lattices by BLED, the centralised system of databases and tools and services that is used to store, manage and access data.

Survey and alignment helps to accomplish the required positioning accuracy of the ESS components. A surface monument network will be connected to the accelerator axis, the target ports and the neutron lines in order to establish a relation between the global position coordinates and the components. ESS will maintain a centralised, freely accessible database of standardised components that will guide personnel in Lund and at partner laboratories during the selection of devices for their applications. Benefits from component standardisation include economies of scale, reduced burden on procurement offices, ease of maintenance and supply, and more efficient management of inventory. Product life-cycle management (PLM) encompasses the tools and procedures developed to ensure component traceability from design through installation, operation and decommissioning. Integration activities include a variety of quality-related tasks, such as acceptance testing and component alignment. The first major challenge for integration activities is to successfully bring the facility through the installation process. The final goal is to achieve system assembly and interconnection.

Commissioning

For a complex facility such as ESS, the transition from construction to operation has to be planned early in the construction phase so that it can be made in an organised and effective manner. The transition from construction to operations will stretch from 2017, when the first building is completed and taken into operation, to 2025 when the last of the 22 instruments is completed and 5 MW of power is reached. Building on experience from other research facilities, ESS has developed a commissioning strategy and methodology. A main element of this strategy is an initial proton beam commissioning with a staged approach and early start. This will be followed by an aggressive early increase in beam power, in order to identify any machine limitations as soon as possible, before a large number of users are expecting reliable beam. Naturally, the commissioning and power ramp-up will comply with the limits set by the licenses and permits ESS has been granted by the relevant legal authorities. Systems will be commissioned first without beam, and later with beam.

The conventional facilities commissioning includes bringing all the conventional parts and systems of the facility into an operational state such that they perform all intended functions and meet design and operational criteria. Buildings and systems will be completed and commissioned in a timely fashion in order to allow efficient and early installation and commissioning of machine and instruments systems. The accelerator will be commissioned in stages: The front-end and ion source will be commissioned first, followed by the drift tube linac, the superconducting linac with spoke resonators, all medium-β and high-β elliptical cavities, and finally the high energy beam transport and the transfer to the target. For commissioning of the first stages, a movable beam dump and a provisional control system will be used to allow parallel installation of the later stages. The target station will be the last major machine component to be commissioned. It includes the neutron production systems (target, moderators and pre-moderators, reflectors, proton beam window), the ancillary systems and the safety systems (shielding, confinement barriers). Activation levels will be kept low during the initial stages of commissioning in order to allow hands-on work. The neutron instruments will be commissioned individually as the construction of each instrument is completed. The instruments will first be commissioned without beam, followed by a commissioning with beam, and later, a period of scientific commissioning during which the instrument will be brought into scientific operation suitable for external users.

Emission control

ESS has prioritised developing a waste management strategy for irradiated materials that addresses regulatory requirements, radiological characterisation, waste treatment and conditioning, waste disposal, de-

commissioning, and environmental concerns. ESS is very serious about planning for the safe operation of the facility, and for its safe decommissioning at the end of its operating life.

The handling and conditioning of radioactive waste requires complex engineering solutions that are strictly regulated under Swedish law. As the pre-construction and design phase of ESS's life-cycle nears its end, ESS has already made substantial progress in estimating levels of radioactive waste and emissions, and in developing protocols for managing waste. A series of technical reports detailing quantitative results and concrete plans demonstrates the commitment and organisational and intellectual capacity of ESS to meet the demands of Swedish law and regulation and to comply with Swedish waste management policy. Collectively, these analyses make it clear that ESS will be a good neighbour, and will not damage the health of the community or the environment. Within the Swedish system, the generator of radioactive waste must provide information about the radionuclide inventory before the removal of the waste into final repositories is permitted. ESS will rely on three complementary methods for waste characterisation. These methods are Monte Carlo calculations, the matrix method, and on-site radiation detection and measurement.

ESS has developed a waste management logistical plan that divides ESS waste streams into categories according to a risk-based assessment, and proposes a treatment protocol optimised for each specific material's characteristics. Treatment, shipping and disposal of ESS waste are feasible within the Swedish system. ESS has also made preliminary estimates of the radioactive waste and emissions generated in fluid systems. The outcomes of these studies provide data for the environmental impact analysis of normal ESS operation. In addition, ESS has conducted a parametric study of the performance of the purification system within the helium cooling circuit. This work confirmed that safe management of radionuclides is readily achievable. As required for environmental impact analyses under Swedish law, the annual dose to a reference person from exposure due to routine release of radionuclides was estimated. Calculations indicated that dominant contributions come from linac emissions through the stack, while the contribution from dismantling the target every five years is almost negligible. Under the study's assumptions, doses are less than the ESS limit of 10 μSv/year for a single pathway. Rough modelling of activity transport within groundwater under very conservative assumptions indicated a negligible contribution to the total annual dose to the public. The radiological consequences of potential accidental releases were also estimated. Contaminants that could be released during the most severe hypothetical design basis accident (DBA) were ranked by their importance with respect to dose. For the very conservative value of 0.5% volatile release fraction, the total estimated dose to individuals in the immediate vicinity of the facility was around 6 mSv.

When the facility enters the final phase of its life-cycle, decommissioning will take place over a period of five years. ESS has chosen immediate dismantling as its decommissioning reference strategy. Several factors favour this approach over phased decommissioning, perhaps the most important of which is being able to draw on the accumulated experience of ESS's operating staff during decommissioning. ESS will return the site to green field status, permitting unrestricted future use.

Safety and security

ESS prioritises prevention of harm to employees, the public, and the environment from both radiation and conventional safety threats. In 2011, ESS formally adopted the following project-wide set of General Safety Objectives:

- *"To protect individuals, society and the environment from harm arising from the construction, operation and decommissioning of the ESS facility.*
- *To ensure that in normal operation, exposure of personnel to hazards within the facility is controlled, kept within prescribed limits, and minimised.*
- *To prevent accidents with high confidence.*
- *To ensure that any abnormal operational event has minimal consequences for ESS personnel and for the public.*
- *To minimise the hazardous waste arising from the operation and decommissioning of ESS, both in its quantity and level of hazard potential."*

These overarching goals will guide ESS through all phases of its multi-decade life-cycle. They apply to all aspects of safety at the facility, including radiation, fire, cryogenics, chemicals, heavy loads and other hazardous items or situations. The security systems of the facility will be designed to meet basic in-house security needs such as deterrence of theft and vandalism and to comply with regulatory requirements, while also taking into account the need for users and personnel to work in an open and friendly atmosphere.

While ESS is classified as a non-nuclear facility from the standpoint of Swedish law, it will produce activated materials. In developing its safety programmes, ESS has profited from decades of collaboration and exchange among regulators and facility operators within the nuclear community about how to handle such materials. This accumulated collective knowledge base informs ESS's own safety objectives and programme. The ESS licensing process is governed by three Swedish laws: the Radiation Protection Act, the Environmental Code and the Planning and Building Act. On 15 March 2012, ESS submitted a formal application for a permit to begin construction to the Swedish Radiation Safety Authority (SSM). On the same day, ESS also sent in its application to the Swedish Environmental Court.

In accordance with well-established international best practices, a few basic principles constitute the framework for the ESS safety programme: Exposure to hazards will be as low as reasonably achievable (ALARA); multiple and redundant levels of safety barriers and protective systems will provide defence-in-depth; ESS design will incorporate both passive and active safety measures; and an ongoing process of review and assessment of safety systems will shape the entire engineering design process. These principles will enforce the safety culture within the ESS organisation. Maintaining that safety culture will be a top priority for ESS management. In accordance with the ALARA principle, ESS guidelines call for more restrictive dose limits than does Swedish law. ESS will apply the defence-in-depth concept in order to minimise deviations from normal operation, to prevent accidents, and to mitigate the consequences of abnormal events. ESS will use a set of physical confinement barriers that operate independently of one another to prevent and mitigate potential releases of radioactive isotopes. Three confinement barriers will contain the nuclide inventory in the target, caused by proton bombardment. All possible other nuclide inventories at ESS will have at least two safety barriers.

Passive safety systems rely on facility features whose very nature acts to prevent accidents or to limit the adverse consequences of accidents independently of human intervention. The ESS design incorporates two important passive safety systems. First, the linac will depend on the continuous input of power from the electrical grid to produce beam. This is a powerful safety feature, because if the external power supply is interrupted for any reason, the accelerator will automatically shut itself down. Unlike nuclear reactors, there is no danger of ESS "going critical" once it has been accidentally or deliberately cut off from the power grid. The second important feature of the ESS design from the safety perspective involves the ESS target station cooling system. The most likely reason for a loss of cooling system function is an electric power interruption. Although this guarantees an instantaneous shut-down of the accelerator, heat production in the target will continue for some time. ESS's rotating, helium-gas-cooled tungsten target, with its 2.5 m diameter, offers a large enough surface area for passive cooling to avoid dangerous temperatures with a significant safety margin, eliminating the risk of target overheating, even in the absence of an active cooling system.

ESS's active safety systems will include mechanical, electrical, and instrumentation and control components. They will ensure that the facility operates safely, and that safety is maintained in the event of an incident. Active safety systems also encompass ESS protocols governing installations and training programs to ensure that all employees act in accordance with prevailing instructions and in compliance with Swedish regulation. ESS protocols will lay out a fixed schedule for maintenance, testing and adjustment of many mechanical and electrical safety devices, and for radiation monitoring of the experimental instruments.

Conclusion

After more than 20 years of work we find ourselves at the point where the construction of ESS will begin. This comes about thanks to the dedication of countless hundreds, and perhaps thousands, of people who have contributed to bringing the project to where it is today. The publication in 2013 of the *Technical Design Report* demonstrates the fruits of that work – the scientific drive, the technological inventiveness, the administrative determination. We could not have reached this point without the support of our funding bodies and, ultimately, of the taxpayers who support the funding bodies. We are well aware of

the responsibility we carry. We will deliver.

The TDR comes one year after the *Conceptual Design Report* (CDR) was published. It is not simply one year advanced from the CDR, but rather contains the work, the studies and the designs contributed by perhaps four times as many people as contributed to the CDR. There has been a multiplicative process in play. Equally well, whilst the CDR was more or less a stand-alone document, the TDR is but one of the whole sheaf of documents of more than one thousand pages that together represent the current state of knowledge. They in turn stand on the foundation studies and technical reports that have been produced over the last few years in Lund, in the laboratories of our partner countries and indeed around the world.

This body of knowledge has reached a certain state of maturity. It is, thanks to the nature of a scientific facility, incomplete. It will always be incomplete. However it represents what is both necessary and sufficient to allow a clear decision from funding bodies around Europe to officially start the construction phase of ESS.

As Ivan Turgenev said:

> *If we wait for the moment when everything, absolutely everything is ready, we shall never begin.*

It is time to begin!

Chapter 1

Introduction

1.1 The evolving story

ESS, the European Spallation Source, will be a major user facility at which researchers from academia and industry will investigate scientific questions using neutron beams. Neutron methods provide insights about the molecular building blocks of matter not available by other means. They are used for both basic and applied research. European nations are working together in order to build, in southern Scandinavia, this slow neutron source of unparallelled power and scientific performance. ESS will deliver its first protons to a solid, rotating tungsten target in 2019, which will in turn generate neutrons for delivery to an initial suite of seven neutron scattering research instruments. ESS will reach its full design specifications in 2025, with a suite of 22 research instruments.

The road to achieve such a European high-power spallation source has been long and winding, with many twists and turns, but always with a determination to succeed. The production of this *Technical Design Report* is a concrete demonstration that this project, long in gestation, is now reaching a state of maturity signalling its readiness to move forward with construction activities.

Let us look briefly at the history of the project. Neutron scattering, as a tool for the investigation of materials in all their diversity and complexity, was pioneered in the north American sub-continent in the 1950s. The neutron itself had been discovered in 1932 in Cambridge by James Chadwick. The first moderately intense sources of neutron beams, as shown in Table 1.1, were extracted from the early research reactors that were first constructed in a number of national laboratories in the USA as well as in Canada. It was on these research installations that the early instrumental techniques using neutrons were developed in order to begin to unravel the atomic structures of relatively simple materials and, uniquely, the atomic dynamics of these same materials. For this work Cliff Shull and Bert Brockhouse were awarded the Nobel prize in physics in 1994, too many years after their pioneering work had been done, but at a time when the power of neutron beams to investigate the very wide spectrum of materials upon which much of our daily lives depend had been well and truly demonstrated.

As with all new technologies, there was a rapid rise in capabilities over the following two decades that culminated, in the late 1960s, in the construction in Grenoble in south-eastern France of a purpose-built high flux reactor source of slow neutrons that was rapidly to become the focus of world attention and scientific endeavour in this discipline. Building upon the global effort in instrumentation, the *Institut Laue-Langevin*, as it was named, became the flagship of neutron research and an exemplary demonstration of how two European countries could work together for the good of mankind. ILL secured a scientific lead that, even 40 years later, it has retained and in many ways, consolidated.

In parallel, and with a somewhat different purpose, accelerator-driven sources of neutrons were also being developed. These facilities were excellent generators of fast neutrons that were used to great effect to compile a nuclear cross section database of all the elements and their isotopes in order to support the nuclear power industry. These sources were pulsed in nature with a very high peak brightness. It was realised rather early on that such accelerator-driven sources held out significant opportunities for neutron beam experimentation on materials, provided that some of the disadvantages could be overcome. The early sources of this genre were based on electron linear accelerators that had significant background problems caused by the very intense gamma radiation bursts which were generated. Nevertheless, opportunities for neutron scattering investigations were demonstrated with these early machines, which were built around

Facility	Location	Status	First operation	Power [MW]	Instruments	Flux Average	Flux Peak
						[10^{15}cm^{-2}s^{-1}]	
ESS	Lund	Pre-construction	2019	5.0	22	1.60	40
J-PARC	Tokai	Operating	2009	.3	20	.10	20
ISIS-TS2	Oxford	Operating	2009	.03	7	.01	6
SNS	Oak Ridge	Operating	2006	1.0	14	.10	8
LANSCE	Los Alamos	Operating	1988	.1	13	.01	3
ISIS-TS1	Oxford	Operating	1984	.13	20	.01	2
SINQ	Villigen	Operating	1996	1.0	15	.15	–
IBR-II	Dubna	Upgrading	1977	2.0	12	.01	5
PIK	St. Petersburg	Construction	2014-15	100	10	1.20	–
CRR-II	Beijing	Operating	2010	60	6	.80	–
ARR-III	Sydney	Operating	2006	20	12	.20	–
FRM-II	Munich	Operating	2004	20	24+6	.80	–
JRR-III	Tokai	Operating	1990	20	34	.27	–
RSG	Serpong	Operating	1987	30	10	.25	–
Dhruva	Mumbai	Operating	1985	100	15	.18	–
BER-II	Berlin	Operating	1984	10	16+3	.12	–
LLB	Saclay	Operating	1980	14	22+3	.30	–
ILL	Grenoble	Operating	1971	58	27+10	1.30	–
NIST	Washington	Operating	1967	20	30	.40	–
HFIR	Oak Ridge	Operating	1965	85	11	1.50	–
LVR	Řež	Operating	1957	10	10	.15	–

Table 1.1: The European Spallation Source facility in comparison to other high-level neutron sources that are operating, or are close to operation.

the world. These machines produced their beams of neutrons as sharp pulses, unlike the research reactors that produced continuous beams. Each type of source has its own unique characteristics that can be harnessed for the study of materials. The complementarity evident then still exists today.

At about this time – the late 1970s and early 1980s – the use of proton-driven neutron sources, generated by cyclotrons, synchrotrons, or linear accelerators, was beginning to be explored. Proton sources do not suffer from the gamma background problems that affect electron sources, overcoming the fundamental disadvantages of the earlier machines. Pioneering work at Argonne National Laboratory and Los Alamos National Laboratory in the USA and in Tsukuba in Japan indicated that pulsed proton sources held out a significant technological advantage over the most intense research reactors. This was because the spallation reaction employed in proton machines generates significantly less heat per useful neutron than does a fission reactor. In addition, the generation of neutrons in pulses provides peak brightnesses that far exceed those available from reactors.

The enthusiasm for such proton machines led to ambitious conceptual designs for neutron sources that went well beyond the technological capabilities of the time. Far-sighted projects such as the Intense Neutron Generator (ING) in Canada, the *Spallations Neutronen Quelle* (SNQ) project in Germany and the pulsed reactor SORA (*Sorgente Rapida*) of the European Community were planned. None of these were ever built, but they provided the seeds from which the European Spallation Source has grown. In the late 1970s, construction began on the world's first proton spallation source that was powerful enough to challenge the supremacy of ILL. It was a pioneering endeavour that had many doubters but which succeeded, over a difficult decade, in achieving its design specification and overturning the accepted wisdom. This source, built close to Oxford in the UK, was called ISIS. Despite having a design power of only 180 kW, it demonstrated that world-class science could be carried out very effectively on such sources. ISIS was the birthplace of many new instrument concepts, some of which had been prototyped on other neutron sources. ISIS also provided a degree of support to the user community that surpassed the contemporary accepted

relationship between the central facility and its user community.

The next chapter in this story sees the OECD Megascience Forum producing a study of the future evolution and needs for neutron beams in a global context. This study took place in the early 1990s. It resulted in a report to the research ministers of the OECD countries in 1998 that recommended that a megawatt-class spallation neutron source be built in each of the three developed regions of the world, a recommendation that the OECD Ministers endorsed [4–6].

Europe in the late 1990s was therefore in an enviable position in this scientific field. It not only had the world's leading reactor and accelerator-based neutron sources, but it also was blessed with a network of medium and low intensity neutron sources that were breeding grounds for innovative instrumentation built by excellent young scientists, which proved to be the origin of new scientific ideas. Accordingly, the community of researchers in Europe who used neutrons for a significant part of their scientific research programme, grew rather spectacularly in number and in scientific diversity. The figure today, according to a survey made by the European Neutron Scattering Association, sits at around 6000 individuals [7, 8]. It was therefore a completely logical step that many of these scientists started to lay down plans for the European facility that had been foreshadowed in the OECD recommendation. An international task force was assembled, originating from around 20 countries, which began the task of defining the scientific case for such a facility and designing a neutron source that would be capable of delivering this scientific goal. This resulted in a 2002 design study for ESS that comprised a 10 MW spallation source with two targets and that was furnished with more than 40 neutron instruments [9–11]. It was to be powered, not by a proton accelerator, but rather by an H-minus accelerator, the beams from which could be injected into a compressor ring and compressed in time to less than 1 μs in duration. By this time, the United States and Japan had both begun the construction of megawatt capacity spallation neutron sources, SNS and J-PARC, both of which are operational today.

Europe however, furnished with its rich network of neutron sources, collectively allowed itself a more relaxed procedure which has, in the long-run, been beneficial, even though at that time this slowness in decision-making was not universally appreciated. This ongoing deliberation resulted in a comprehensive set of documents being produced that laid down the scientific case for ESS together with extensive technical documentation and costings [9–13]. These studies were presented to a plenary meeting of ESS stakeholders in May 2002 in Bonn attended by more than 700 scientists and science policy-makers. Although this meeting was a very positive endorsement of the use of neutrons for materials science and was excellently organised, in retrospect it proved to be the beginning of a reshaping of the whole project that created an opportunity for sites other than those in Germany and Britain to consider bidding for the location of ESS. In 2003, a new concept was put forward for ESS that involved descoping the whole facility and a fundamental change of technical orientation. The new design comprised a 5 MW proton linear accelerator delivering a 2 to 3 millisecond-long pulse to a single target station surrounded by a suite of 20 to 25 neutron instruments. The H-minus beam, the compressor ring, the second target station and the constrained moderator configuration were all abandoned. This initiative held out the promise of neutron intensities that were a factor of six more intense, per megawatt of proton beam power, than contemporary existing or planned facilities.

It is this concept from 2003, which was endorsed by the user community in Europe and which is now nearing the end of its pre-construction period, that will deliver first neutrons in 2019. During this pre-construction period, ESS has completed an update of its design, and a totally revised cost estimate and time-schedule. It is poised to begin with construction, with ground breaking scheduled to commence in 2014. In the intervening years from 2003 to 2009, a number of significant steps were taken. Following the Bonn meeting, the British and German sites were withdrawn as site candidates. At the same time, three new sites emerged as contenders for the location of ESS. These were Debrecen in eastern Hungary, Bilbao in northern Spain, and Lund in southern Sweden. The three site contenders worked both competitively and collaboratively in an intense and determined process which led, via the European Strategy Forum for Research Infrastructures (ESFRI) and ultimately overseen by the Czech Republic's Ministry of Research during its period of Presidency of the European Union, to the selection of Lund in Scandinavia as the preferred site. This choice followed a site review process during the summer of 2008 that resulted in a report presented to the major ESS stakeholders in September of that year. In Brussels on the evening of May 28, 2009 a decision on the site was made. It was a milestone.

Thereafter, following further negotiations, Spain and then Hungary endorsed the choice of Lund. The team in Lund had, since the year 2000, been administered within Lund University as a special entity and funded by Scandinavian organisations. With the site decision, a new governance of the growing

organisation, with its important tasks to fulfil, was put in place. ESS Aktiebolag (ESS AB) was established. Two lines of governance were created: A Steering Committee with representatives from the scientific institutes and Research Ministries of the various partner countries, and a legal Board representing the formal owners of the project which were, for administrative and legal purposes, Sweden and Denmark who were co-hosts and therefore co-owners of the emerging facility. At the time of writing – April 2013 – ESS AB is a shareholding company under Swedish law with Sweden holding approximately 75% of the shares and Denmark holding the remaining 25%. The Steering Committee includes representatives from 17 partner countries: Sweden, Denmark, Norway, Latvia, Lithuania, Estonia, Iceland, Poland, Germany, France, the United Kingdom, the Netherlands, Hungary, the Czech Republic, Switzerland, Spain, and Italy. Various advisory committees actively provide counsel to the ESS organisation and the governing bodies. The 17-partner international collaboration was secured by the signing of a memorandum of understanding (MOU) in Paris at the Swedish Embassy on 3 February, 2011. This MOU was a non-binding agreement that contained three guiding principles. These were an acceptance of Lund as the site for ESS, an agreement to engage in and to proceed with the update of the design, and an agreement to make best efforts to continue on to the construction phase in a timely manner.

This present *Technical Design Report* represents the technical and scientific work carried out during

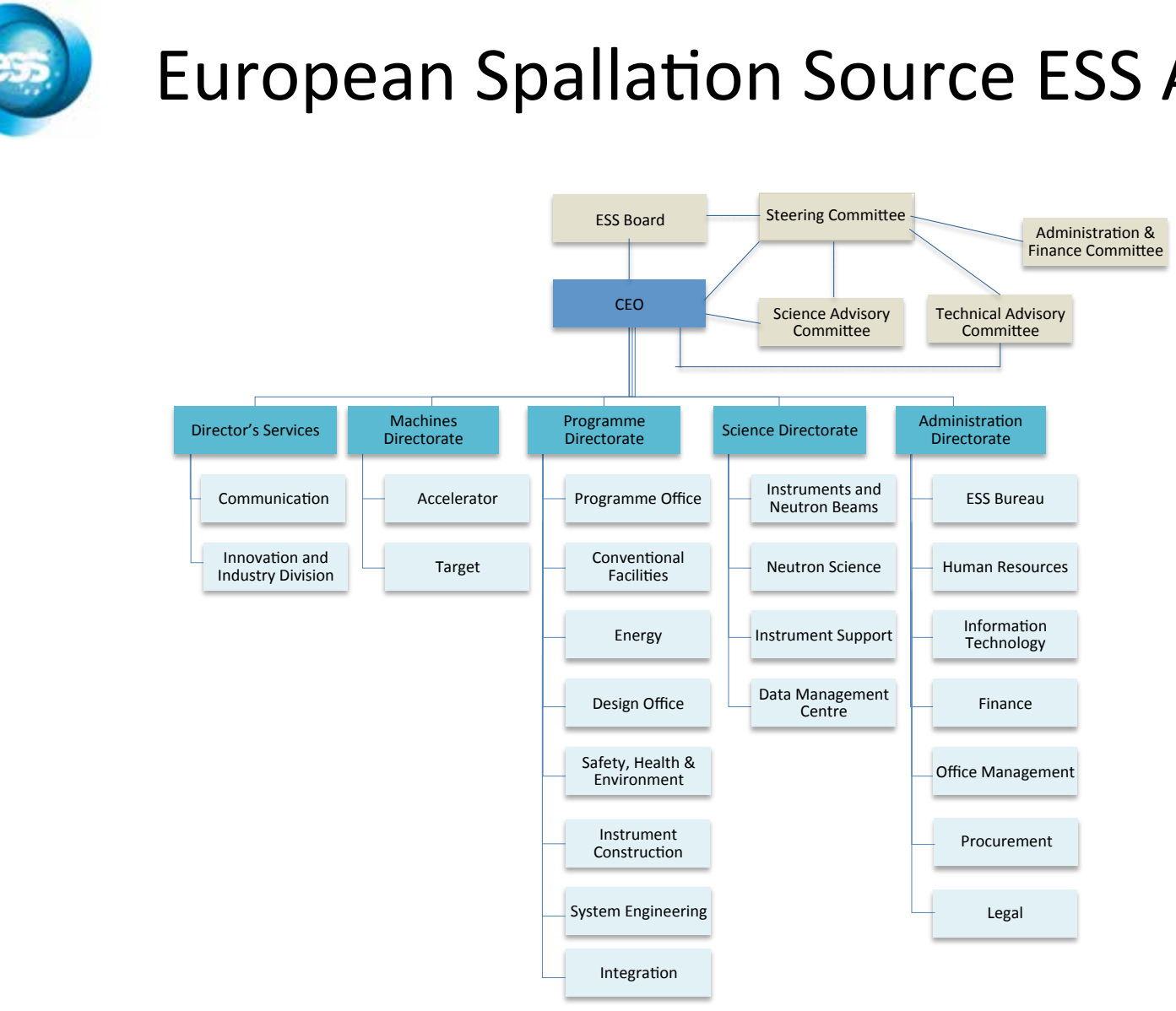

Figure 1.1: ESS high level organigramme.

Top

1.2 The ESS programme

With 17 European partners committed to construct ESS, it is inevitable that a significant source of revenue will be components manufactured and supplied as in-kind contributions. For planning purposes, the ESS organisation has worked under the expectation that 75% of the capital cost will be covered by cash contributions and that 25% will be in-kind. Currently, representatives appointed by the Swedish and Danish governments are engaged in bilateral discussions with the other partners in order to determine the potential of each country to engage in the construction process starting in 2013. The significant fraction of in-kind contributions brings with it particular challenges. Management of in-kind contributions is the key issue in delivering the ESS on time, to budget and fully operational. The technical risks of managing interfaces need special attention. Additional resources will be required to do this effectively, and 100 M€ is not an unrealistic sum for this purpose.

The governance of ESS is illustrated diagrammatically in Figure 1.1. Legally and administratively, ESS reports to a governing Board populated by Swedish and Danish members reflecting the 3:1 shareholding of the two countries and their status as co-hosts. A Steering Committee (STC), which gathers together delegates from the 17 partner countries, functions in parallel to the ESS AB Board. The STC is a more traditional governing body, being populated by scientists with experience of large scientific infrastructures together with ministerial or research council personnel who are close to the funding authorities from their individual countries. The STC is aided in its job by an Administrative and Finance Committee, which is formally a sub-committee of the STC, populated by national delegates. Two further advisory committees exist that are directly related to the ESS organisation itself and are the source of independent advice. These are the Scientific and Technical Advisory Committees. They are populated by international scientific and technical experts and are nominated by the ESS organisation itself. They do not map onto the 17 ESS partner countries.

The ESS organisation itself is undergoing rapid growth. This requires careful guidance and management. Currently ESS is composed of 200 people organised into five directorates. The five directorates are: Director General's Services, Machine, Science, Administration and Programme Office. The organisation operates on a customer-supplier basis managed by the ESS Management Team (EMT), which the Director General chairs. The architecture of authority and responsibility is not organised in a vertical hierarchical structure but rather is built on a strong team with distributed authority and responsibility. The organisation is significantly flatter than equivalent organisations set up in the second half of the twentieth century, with which ESS is often compared.

Table 1.2 records ESS's high level parameters, and its guiding scientific goals. The starting point for the generation of these parameters was the 2008 ESFRI Roadmap specification. The parameters shown were updated and approved on April 18, 2011 by the ESS Steering Committee. ESS will offer unparallelled cold neutron beam brightness, delivering a peak flux 30 times higher than the world's brightest neutron source, and 5 times more power than any spallation source. ESS's pre-construction period, which was

Parameter	**Unit**	**Value**
Average beam power	MW	5
Number of target stations		1
Number of instruments in construction budget		22
Number of beam ports		48
Number of moderators		2
Separation of ports	degrees	5
Proton kinetic energy	GeV	2.5
Average macro-pulse current	mA	50
Macro-pulse length	ms	2.86
Pulse repetition rate	Hz	14
Maximum accelerating cavity surface field	MV/m	40
Annual operating period	h	5000
Reliability	%	95

Table 1.2: High level parameters, approved by the ESS Steering Committee on April 18, 2011.

launched in 2009, is now over, following the timeline shown in Figure 1.2. The programme contains within it three additional life-cycle phases:

1. Construction.
2. Operations.
3. Decommissioning.

As shown in Figure 1.2, construction activities will take place over a period of 12 years. They will partly overlap with operations activities, which will last for 45 years, beginning in 2017.

This *Technical Design Report* is the fruit of design activities that took place during the pre-construction period. The task of the design phase is to complete an exercise in conception, design, computation and, critically, project organisation. The goal is to deliver a design for the whole facility, rather than a ready-for-procurement design. Detailed design will be an ongoing activity using resources as and when necessary to ensure on-time procurement, manufacture and delivery. A central part of this process will be an updated time plan and an updated costing report indexed to 2013 values. In the meantime, ESS works with its current time plan, which calls for first protons to the target and first neutrons to the day-one suite of seven instruments in 2019, with full specification achieved in 2025. At that point, the accelerator will be operating at 5 MW proton power, 22 neutron scattering instruments will be taking data, and a healthy but still growing neutron user community will be generating top-class science. Opportunities for future

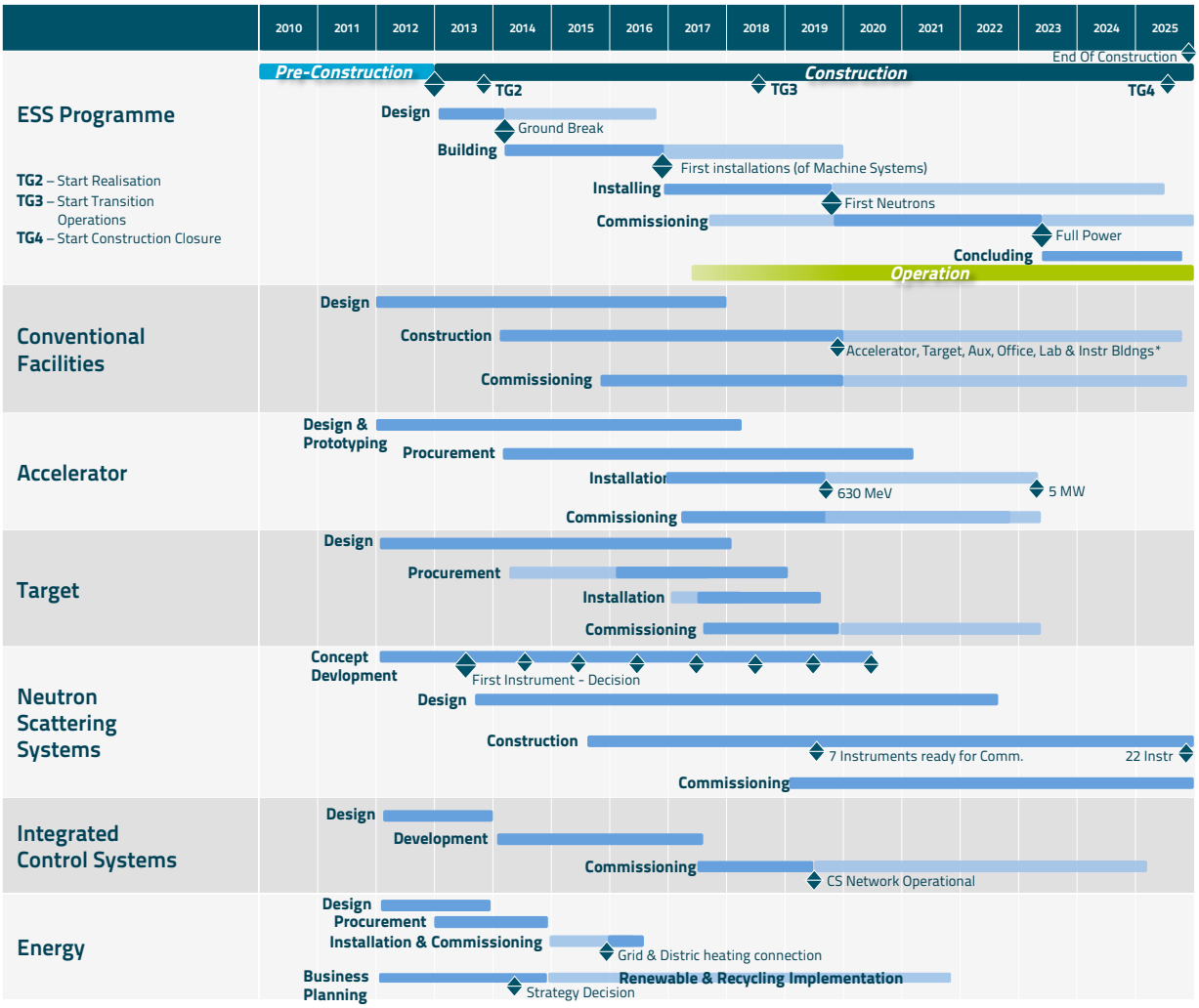

Figure 1.2: An overview of the schedule for key activities during the Construction Phase.

While the major thrust of the *Technical Design Report* is to describe the design of the major components of the operating facility, the report also encompasses planning for the factory and site acceptance testing of key components, such as RF cavities and cryomodules, and for the installation and commissioning of accelerator, target and instruments that will occur as the programme makes the transition to operations (see Chapter 9). In addition, the report describes the general approach that ESS will take towards decommissioning, in particular, the decision to return the site to greenfield status and to do so through a strategy of immediate dismantlement that will make it possible to take advantage of the accumulated experience of the facility's operating staff (see Chapter 10). This approach is outlined in the preliminary decommissioning plan that ESS has prepared as part of the Swedish licensing process for the facility.

Chapter 2

Neutron Science and Instruments

Chapter abstract

Summary: This chapter describes the uses of neutron scattering techniques, their place in the wider science landscape, and the ways in which they complement other experimental techniques. It discusses ESS's strengths in studying and understanding complex materials and presents a reference suite of 22 instruments selected to illustrate capabilities and scientific impact. The chapter also describes the multi-faceted research infrastructure that will surround the facility and enhance its productivity. While the publication of this report marks the end of the design phase for the accelerator and target station, the design phase for the neutron instrument suite will continue past 2020, when the final two instrument concepts are slated for selection. The instruments that will be built are therefore likely to be quite different from the reference suite described here. The phased instrument selection and design process will make it possible to respond flexibly and creatively to changing research needs and to take advantage of evolving technology.

Neutron science makes it possible to explore the complexity of condensed matter, furthering both technological progress, and humanity's understanding of nature. While no single probe can cover the whole span of time and length scales required for scientific enquiry, neutrons are a crucially important research tool. Neutron scattering techniques can, among other things, probe the molecular basis of superconductivity, guide the development of new materials or "look inside" an operating car engine.

ESS will push the frontiers of neutron science due to its capabilities in two key areas: Its unique characteristics as a neutron source, and an integrated scientific and computing infrastructure. It will be able to study a broad range of structures and time scales, offering neutron beams of unparallelled brightness, delivering more neutrons than the world's most powerful reactor-based neutron source with higher peak intensities than other spallation sources. Its user infrastructure will include sample preparation, characterisation, and specialised synthesis laboratories; detector and sample environment systems; and information technology and computational support designed for a broad range of disciplines.

State-of-the-art neutron scattering instruments depend on sophisticated hardware components, such as choppers, detectors, neutron guides, advanced neutron optics and sophisticated shielding. Progress in defining and developing these technologies is described here, and is illustrated by a science-driven, 22-instrument reference suite that matches the capabilities of individual instruments to specific areas of societal, scientific and technological interest.

Software and data management infrastructure will harness the scientific potential of the instruments and their sophisticated technology, integrating the control of each neutron instrument and its sample environment with the processing, real-time visualisation, analysis and preparation for publication of the data. This infrastructure also will provide for permanent storage and public access to the data, and will make neutron techniques more accessible to researchers from fields that do not have long histories using these tools, but for which neutrons hold significant promise of yielding new insights.

2.1 Neutrons in the scientific landscape

The scientific case for building a next-generation spallation source in Europe was presented in 2002 [9, 10]. This resulted in the inclusion of ESS in the European roadmap for research infrastructures [14] in 2006. Several years of planning and technical development later, we are now on the verge of realising this vision for neutron science in Europe. At the time of writing, ESS is actively engaging with the neutron user community to gather valuable input from different user groups via the ongoing series of ESS Science Symposia [15], from published perspectives [16, 17] and from participation in workshops and conferences. By pursuing these interactions, ESS is continuously developing and updating a scientific strategy in parallel to the development of instrumentation. In this chapter we build on both the established science case and the input provided by the community to present specific science drivers for ESS and relate these to a reference suite of instruments. It is important to stress that the design phase for the neutron instrument suite will continue past 2020, when the final two instrument concepts are slated for selection. The instruments that will be built are therefore likely to be quite different from the reference suite described here. The phased instrument selection and design process will make it possible to respond flexibly and creatively to changing research needs and to take advantage of evolving technology.

2.1.1 The complexity of nature

Every day, humanity reaps the fruits of the remarkable scientific and technological advances of the previous century. In the microscopic world, we enjoy insight into the basic nature of atoms and molecules, and of the forces that govern their interaction with one another. In the macroscopic world, we have achieved extensive knowledge about the properties of the materials surrounding us – man-made and naturally occurring – and we are adept at wielding them to serve our needs. We have also begun to explore assemblies at mesoscopic scales, larger than atoms, but small enough to exhibit quantum effects. These systems raise questions about our fundamental understanding of nature while opening the door to technological progress that will help us tackle society's grand challenges. This is the realm of neutron science, as neutron methods reveal the structure and dynamics of atoms and molecules, relating molecular-scale properties to the macroscopic characteristics of matter. With unparallelled neutron brightness and a unique time structure, ESS will facilitate new levels of understanding of the complexity of matter, challenging our minds and contributing to our progress.

The complex assemblies ripe for exploration take on many different forms. In the geosciences, topical challenges span deep-Earth mineral crystal structures and phase transitions, mineral alterations and metamorphism, and material responses to changes in pressure and temperature. Biological systems such as enzymes, cells, or whole organs rely on the intricate interplay of large molecules, such as proteins, with smaller molecules, such as hormones and metabolites. Functional materials such as catalysts and polymers are similarly complex, with molecular diversity leading to a range of competing interactions and intricate structures, with a wide range of tangible qualities and functionalities. Quantum interactions in advanced electronic and magnetic materials lead to new states of matter such as spin-ices, magnetic monopoles and Skyrmions [3]. These new states were first revealed by neutrons, and have far-reaching consequences for our understanding of nature itself. They also hold promise of new technologies. In addition to being a probe of matter, the neutron may hold the key to fundamental puzzles of our universe such as the question of why there is more matter than antimatter. The answer hinges precariously on the confirmation of a non-zero electric dipole moment of the neutron itself [18, 19].

The undertaking of modern research entails more than deciphering the workings of complex systems at several different length and time scales. The greater task is to bring these effects together into coherent theoretical frameworks that provide holistic insight and promote development. How do structural changes of minerals at very high pressure and temperature relate to large-scale phenomena such as deep-focus earthquakes and volcanic activity? How can we store data using the magnetic state of individual ions rather than today's macroscopic blocks, thereby going beyond the predicted limitations of data storage capacity? How does repeated oxidative damage by free radicals to tissue lead to cancer, and how can it be inhibited? ESS will be instrumental in identifying the answers to questions like these, providing insights relevant for technological progress and the future prosperity of society.

2.1.2 The grand challenges of society

As a result of a growing global population of increasing average age and high demands on living standards, humanity is facing daunting challenges related to supply and sustainability. The tools of science are being deployed to find smart solutions, aiming to maintain living standards within the finite resources with which we are endowed, and to pass a healthy planet on to future generations. ESS will play a role in addressing and solving the grand challenges of society, as many of the emerging smart solutions are based on insights at the molecular or atomic level of matter, an area in which neutron science offers unique investigative powers. The following examples are described further in Section 2.2.

Energy. In the face of diminishing fossil fuel reserves, we are in urgent need of more renewable energy sources, more effective engines, materials for lower heat loss and less energy spill and greener processes for industry. Neutrons are an important analytical tool that aids the understanding and development of promising novel materials for solar cells [20–22], batteries [23], fuel cells [24, 25], thermoelectric materials for waste-heat recovery and refrigeration [26], and reversible hydrogen storage materials for safe usage of hydrogen as an energy carrier [27, 28]. ESS will deliver the information required to engineer novel, smart materials.

Climate. The developments towards carbon-neutral energy options also address the climate challenge brought on by large-scale consumption of carbon-based fuels. Furthermore, ESS will provide important advances in the development of carbon sequestration solutions [29–31].

Health. Our ageing population brings with it a changing disease landscape, calling for better treatments of illnesses such as cancer, diabetes, and Alzheimer's disease. Furthermore, multi-resistant bacterial strains are a growing threat to our collective health and safety. Neutrons further our understanding of the mechanisms of disease [32, 33], help us develop drug delivery systems [34–36] and contribute to the formulation of drugs into effective pharmaceuticals. Neutron techniques are also used to develop potential new materials for implants and health-care devices.

Agriculture. The neutron methods that serve the health sciences also address the agricultural challenges: the large environmental footprint, the demand on crop production for biofuels as well as food and feed, and global food security. By elucidating the molecular intricacies of plant metabolism and of pest, disease and drought resistance, these issues can be addressed. Neutron methodologies can decipher vital molecular mechanisms through structural and dynamic analysis of complex assemblies [37,38], and neutron imaging shows promise for whole-plant water-uptake analysis [39].

Digital society. Societal infrastructure relies on accomplished and increasingly distributed IT systems, and the IT landscape is evolving more rapidly than any other area. This brings with it challenges of energy supply for the server parks and information security, and entails a significant vulnerability. Neutron scattering has a strong track record in clarifying the inner workings of data storage materials, and is a key tool for developing better ones [40, 41]. The neutron-aided development of new energy materials also plays a large role in this context. A side benefit of building large-scale research infrastructures is the concomitant advancement of innovative IT solutions born from such endeavours, a prominent example being the development of the world wide web at CERN.

These grand challenges present us with a complexity as profound as the whole of science, and many parallel avenues of enquiry must be pursued in order to meet them. The science community is taking on these challenges, hand in hand with industrial research and development – recognising that dedicated development is needed to bring today's knowledge to applications, and that free fundamental science is a prerequisite for the unveiling of tomorrow's insights and solutions. Both the commercial and the academic perspectives are needed, and for both, success requires the development and maintenance of state-of-the-art research infrastructure. ESS will provide powerful tools for solving the urgent issues of society, facilitating both academic and industrial research and development [42].

2.1.3 Neutrons in the landscape of experimental techniques

In order to address these issues, researchers need access to a range of different experimental methods. No single probe can cover the whole span of time and length scales that the various fields of science encompass. Moreover, no single experimental probe can inspect all properties or characteristics of materials. Figure 2.1 gives an overview of how different methods cover different parts of the experimental space, displayed as a graph of time scales versus length scales. It is clear that the various neutron-based methods cover a wide and important part of parameter space, both in spectroscopy, where neutrons probe structure and

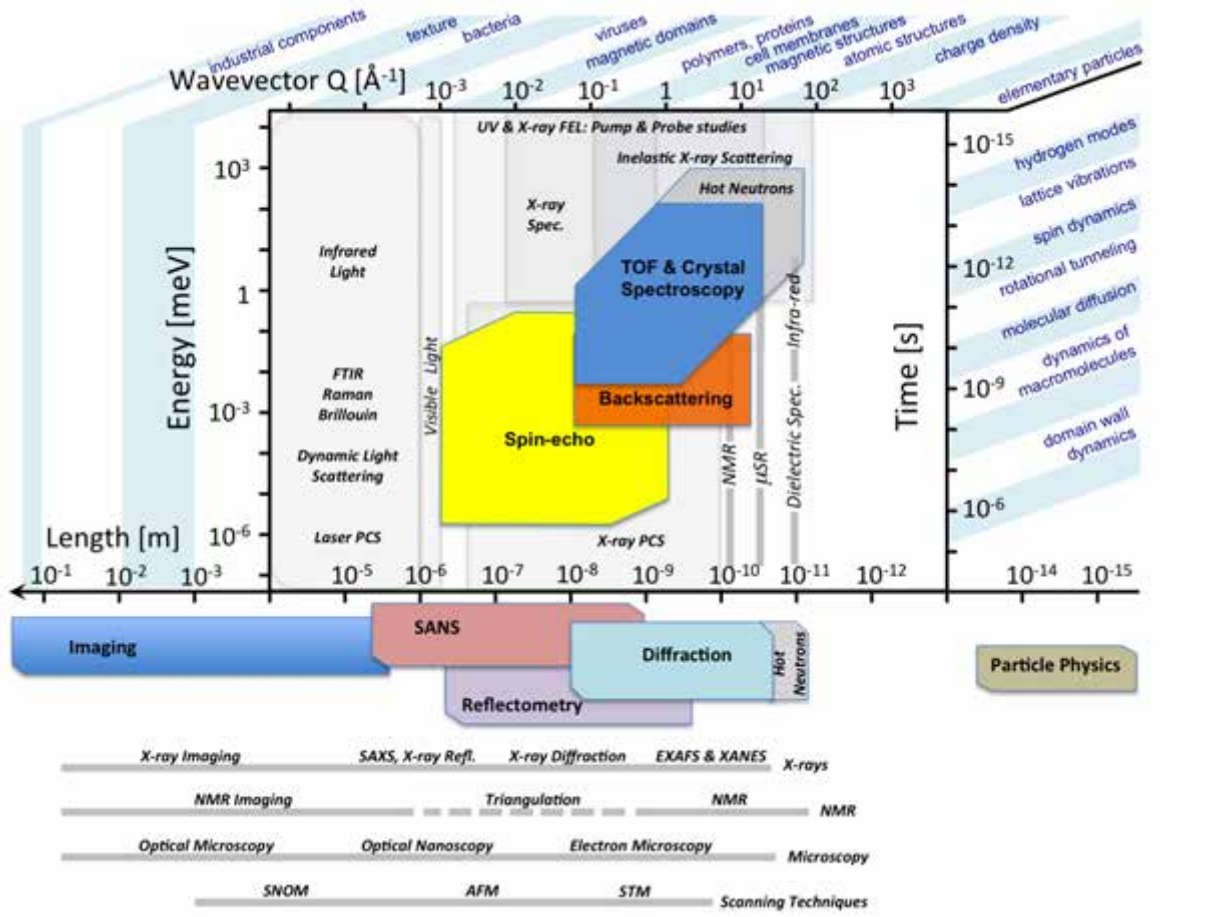

Figure 2.1: Using neutrons and complementary techniques to explore different length and time scales. The horizontal axes indicate real and reciprocal length scales, while the vertical axes refer to time and energy scales. Scientific areas falling within different length and time scales are indicated along the edges.The experimentally accessible areas of the various neutron-based techniques available at ESS are shown as polygons in strong colours. Those techniques that are sensitive to both time and length scales are represented above the main horizontal axis; those that measure only length-scales below. In addition to the neutron-based techniques covered by ESS, the analogous areas for a selection of complementary experimental techniques are shown in grey. Areas labelled "Hot Neutrons" refer to neutron-based techniques which will not be available at ESS.

dynamics in parallel, and in the purely structural methods found below the horizontal axis.

Techniques are often complementary rather than competitive when their temporal and spatial scales overlap, because spatial and temporal needs are not the sole determinants of usefulness. Different probes access different kinds of information, so the methods of Figure 2.1 are often used in combination, unleashing powerful synergies. The particular strengths of neutrons include sensitivity to light elements such as hydrogen, the ability to distinguish between different elements, the non-destructiveness of the beam in terms of sample integrity, the power to probe magnetic structure, and the capability to penetrate many materials, making possible the investigation of samples in a wide range of relevant sample environment set-ups that would stop other forms of radiation. These strengths are discussed further in Section 2.2. A combination of different approaches and techniques is necessary to answer many scientific questions. Moreover, the continuously evolving landscape of available tools drives the continuing need to try and test new combinations of experimental techniques. Multi-probe experiments that combine different probe techniques on the same site are becoming increasingly possible – for example, using both Raman and neutron scattering. There are many examples of combined studies.

Studies of polymer relaxation processes that exploit neutron spin-echo methods, light scattering,

nuclear magnetic resonance (NMR) and X-ray or visible light photon correlation spectroscopy to span more than 10 decades of time scales.

Magnetic structure determinations are uniquely and easily performed using powder or single crystal neutron diffraction, while subtle details can be obtained from X-ray magnetic diffraction.

Experiments at extremely low temperatures are impossible with X-rays due to the deposition of heat by the incident beam, while the heating created by neutrons is negligible. Special environmental conditions must be compatible with the characteristics of the probe. In this case the penetrating capabilities of neutrons play an important role.

Energy scales that drive magnetic properties of solids are determined by using neutrons to probe local and exchange parts, complemented by the use of X-rays to identify the electronic component.

Atomic motion and dynamics in condensed matter are probed both by X-rays and by neutron inelastic scattering. While X-rays are especially useful in the case of disordered systems, neutrons offer the proper energy resolution for looking at incipient modes that lead to phase transformations.

Macromolecular structure determination (for example for proteins) relies on X-rays to provide the detailed overall structure, while neutrons provide accurate data on the location of the functionally pivotal protons and water molecules in the structure.

The value of a scattering probe also depends on the performance of available sources of radiation. In that respect, X-rays have experienced dramatic progress through the ongoing development of synchrotron light sources and X-ray free electron lasers. Electron microscopy and NMR methods also have benefited from significant ongoing advances. Similarly, ESS will offer gain factors of more than one order of magnitude over previous neutron sources. ESS is an essential element in the diverse toolkit that scientists will use in their quest for comprehensive understanding of complex systems. In order to harness the full potential of complementarity, a number of other laboratory-scale techniques will be available in conjunction with the neutron instruments. Located adjacent to the next-generation synchrotron light source MAX IV, ESS will play its role in allowing the newest achievements of both synchrotron X-rays and neutron methods to be synergistically combined.

2.1.4 ESS in the landscape of neutron sources

Neutrons are wonderful, but there are too few of them! Although neutrons represent half the mass of the visible matter in the universe, it is not straightforward to extract them from nuclei and to produce bright neutron beams. Neutron sources on Earth are low-brilliance particle sources compared to their electron or photon counterparts. The reactor technology that developed rapidly in the late 1940s reached a plateau in neutron performance in the 1970s with the construction of ILL in France, and HFIR in the United States of America. The spallation process, which was discovered in the 1970s, opened the opportunity to produce brighter neutron beams than reactor-based installations. Currently operating high-flux spallation sources include ISIS in the United Kingdom, SNS in the United States of America, and the MLF at J-PARC in Japan. Thanks to its modern technology, ESS will surpass current neutron sources.

The long pulse and low repetition rate time structure of the proton pulses will make ESS the ideal source for long-wavelength neutrons, with energies in the range of about 0.1 meV to 50 meV. Existing pulsed neutron sources deliver short pulses, because the emphasis at the time of their construction was on higher energy neutrons, typically in the range of 100 meV to 1,000 meV. Science priorities have evolved and broadened. Current trends in condensed matter sciences (soft matter and life science, magnetism and engineering materials) stress the importance of slow dynamics and large-scale fluctuations of multi-component systems. ESS addresses these scientific trends by focusing on cold and thermal neutrons, in part by adopting a long-pulse time structure. Cold and thermal neutrons at ESS will be complementary to the hot neutron beams delivered by reactor-based sources and by short-pulse accelerator-based spallation sources.

2.1.5 The unique capabilities of ESS

Figure 2.2 illustrates how the unique capabilities of ESS will help to push forward the frontiers of neutron science. The quadrants in the top of the figure explore the implications of *high brightness* and *long pulses*, while the bottom quadrants explore *advanced computations and software*, and *real world capabilities*. Its unique capabilities make ESS a key tool for peering deeper, wider and more clearly into the structure of materials and their dynamics. ESS will be a source for discovery when these capabilities are combined

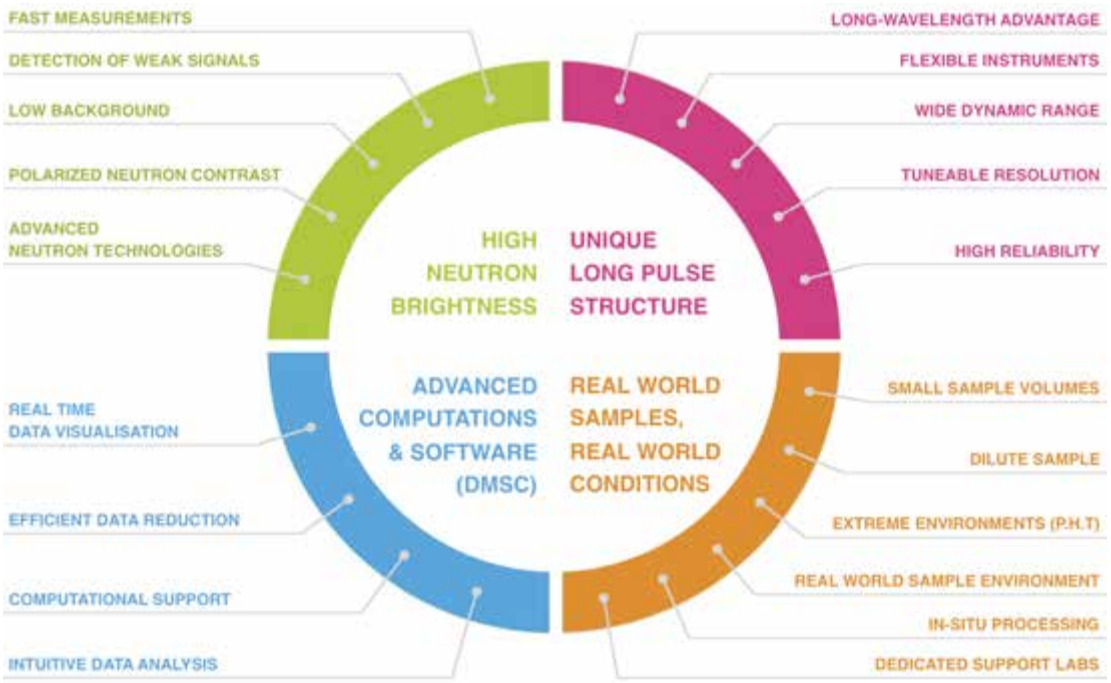

Figure 2.2: The unique capabilities of ESS.

with the ability to carry out experiments under realistic conditions, to visualise data using sophisticated software, and to make theoretical simulations of the experiment live in real time.

High neutron brightness. ESS will be at least 5 times more powerful than the world's leading neutron sources, offering unparallelled cold neutron beam brightness. High fluxes will make possible many investigations that are impossible today by allowing faster measurements, measurements of smaller samples, increased use of polarised neutrons, and the detection of weaker signals.

Unique long-pulse structure. The bright neutron beams will be delivered in a unique time structure, with long neutron pulses (2.86 ms) at low frequency (14 Hz). This structure will make possible the use of long-wavelength neutrons, which will be exploited by novel neutron technologies to allow instruments to achieve a wider dynamic range, bispectral beams, and tunable resolution as needed. All of this contributes to significantly expanded scientific capabilities.

Real-world samples, real-world conditions. While experiments under controlled conditions are the cornerstone of experimental methodology, the ultimate goal is to understand the behaviour of real-world samples in real-world conditions. This may entail monitoring specific parameters in biological samples under physiological conditions; searching for new quantum states under high magnetic fields and low temperatures; or coming to terms with the behaviour of commercial catalysts under the high temperatures and unusual gas atmospheres that reflect the reality of industrial processes. These investigations often require extreme or demanding conditions, achieved through unwieldy sample environment set-ups that limit the volume available for the sample itself. The smaller the sample volume required, the larger the range of thermodynamic conditions that can be explored. In other areas of science, such as macromolecular crystallography, the availability or concentration of the sample material is limited. In either case, ESS will provide the opportunity to go beyond what is currently possible due to its higher source brightness. This will be fully exploited by providing a range of state-of-the-art sample environments, including extreme condition and *in operandi* processing for engineering studies. Furthermore, scientific support laboratories including deuteration and crystallisation platforms will enhance the scientific output of the facility.

Advanced computations and software. Realistic computer simulations that model physical system interactions over length scales from the microscopic to the macroscopic must be combined with physical observations, in order to extend the dynamic range of analytical techniques and to gain insights into the complexity of real-world systems. The computational and software solutions being developed at the Data Management and Software Centre (DMSC) in Copenhagen aim to provide the user with a coherent

experience, providing user-centred software for instrument control, efficient data reduction, real-time data visualisation, intuitive data analysis and computational support for modelling and simulations. This comprehensive set of computational solutions will add value to the neutron data collected, and will establish a new standard for neutron facilities. It will also make neutron techniques more accessible to researchers from fields that do not have long histories using these tools, but for which neutrons hold significant promise of yielding new insights.

2.2 Science drivers for the instrument suite

Neutron scattering encompasses a diverse range of analytical techniques that exploit the unique properties of the neutron summarised in the box below. These neutron-based techniques make it possible to extract subtle information about the characteristics and behaviour of different materials and systems. This is achieved by monitoring structure and dynamics over wide time- and length-scales as illustrated in Figure 2.1.

The unique properties of neutrons

Probing structure and motion: Neutron scattering enables us to study the structure and dynamics of atoms and molecules over an enormous range of distances and times.

A gentle probe: Neutrons pass easily through most materials, enabling the study of large or bulk samples and buried interfaces. This also allows for samples to be studied under extreme conditions, such as very high temperature or pressure, as makes possible the investigation of low-temperature states without any deteriorating beam heating. Neutrons are non-destructive, so delicate materials or precious objects can be studied without fear of damage.

A precise tool: Neutrons provide an extremely precise tool. Their interactions with matter are not too strong, which makes quantitative analysis and interpretation of the data straightforward.

High sensitivity: Since neutrons are scattered by atomic nuclei, they report which element and which isotope is present. Neutrons are particularly sensitive to protons and can distinguish between protons and deuterium. This facilitates highlighting particular groups of atoms in mixtures, complex biological and other hydrogen-containing materials.

A unique probe for magnetism: The neutron has an internal magnetic moment but no charge, so it can be used to study the microscopic magnetic structure and spin dynamics of matter.

A probe of fundamental properties: Studies of the properties of the neutron itself elucidate events ranging from the creation of fundamental particles and forces shortly after the Big Bang, to the explosions of massive stars, such as supernovae, in which most of the heavier elements were created.

Having no charge, neutrons penetrate the electron density in a sample, and scatter off the atomic nuclei of the molecules under scrutiny. This has a number of advantageous consequences. Their relatively weak interaction with matter makes it possible for neutrons to probe deeply into condensed matter, without damaging the sample during the investigation. The direct interaction with nuclei also gives neutron methods the power to discern between elements that are adjacent in the periodic table, and between different isotopes of the same element. Since neutron scattering intensity does not scale with the size of the electron cloud, it is not partial to heavier elements – rather, light elements such as hydrogen show up clearly. Furthermore, the inherent magnetic moment of the neutron makes it possible to monitor magnetic structure, a key property in many electronic and data storage materials. These characteristics inspired

the Nobel laureate Bertram Brockhouse to say in the 1950s, "if the neutron hadn't been discovered ... it would have been invented" – and neutrons are still indispensable to science today.

This section describes how ESS will address important science topics. Each of the following subsections presents a scientific area, including challenges specific to each field, and outlines the prospects for its future. Relevant examples of past and current neutron applications are described, as are potential contributions linked to specific instruments in the reference suite.

The common theme uniting the use of neutron-based techniques across areas of scientific enquiry is the drive towards understanding increasingly complex phenomena. Complexity manifests itself in investigations of multiple interrelated physical properties within materials, and in studies of realistic heterogeneous samples within extreme and/or natural environments, and requires experimental instruments capable of probing a range of length and energy scales. Increased complexity calls for sharpening and diversifying experimental tools, and also for more advanced data analysis and modelling.

The high brightness and long pulse structure will allow the study of real-world samples, similar to those used for complementary investigations with non-neutron techniques. This will have a bearing on many different scientific disciplines. It opens up the possibility of addressing currently intractable problems, as interesting samples often are available only in limited quantities and may be unstable over time. Smaller samples also tend to be more homogeneous, increasing the precision of the results obtained and making possible more advanced investigations. Reduced gauge volumes will allow better-controlled studies under extreme or biological conditions. Scanning techniques with optimised gauge volumes are especially useful for heterogeneous samples. Instruments will be flexible and will permit trade-offs between brightness and better resolution, optimisation of signal-to-noise ratio, and the use of polarised neutrons when necessary.

2.2.1 Soft condensed matter research

Soft condensed matter is a rapidly expanding and highly interdisciplinary area of research concerned with systems that respond to weak external stress or thermal fluctuations. Polymers, surfactants, foams, gels, and many biological materials fall into this category. The fundamental science determining their behaviour is at the core of industrial applications such as organic photovoltaics, polymer batteries, sensors, personal care products, pharmaceutical drug delivery systems and food products. Designing, manipulating and processing these materials requires in-depth understanding of their components and interactions. Neutrons are well-suited for this task and ESS will enhance soft condensed matter research significantly: Time-resolved investigations of self-assembly will be performed in combination with high-throughput manipulation of samples using in situ *equipment; Collective dynamics in polymeric materials in pursuit of future battery technologies will be probed; Time-dependent surface dynamics and reactions at interfaces will be investigated to create novel sensors and nanoscale switches.*

Soft materials such as polymers and emulsions are already used widely in products as diverse as packaging, medicines and Kevlar body armour. In the future, the goal is to construct soft, nano-sized building blocks of various shapes and to assemble them into structures that provide technologically useful properties. Ideally, this goal should be met through directed self-assembly processes that are environmentally benign and sustainable, mimicking in many respects processes seen in the natural world. Devices that can be expected to benefit from such "designer materials" include photonic materials for optical signal transmission, rapid and inexpensive genome sequencing kits and organic photovoltaic devices. Designing, manipulating and processing these complex materials at the same microscopic level as that reached for inorganic materials during the twentieth century is thus one of the major challenges for the future. It will require a comprehensive understanding of the structures and dynamics of the constituent components over length and time scales for which neutron scattering techniques are well-suited.

Neutron scattering has played a pivotal role in this area, making important contributions to the fundamental understanding of soft matter during the latter part of the twentieth century. These important developments in soft matter are largely based on the fact that neutrons scatter differently from hydrogen than they do from deuterium, a feature realised by the Nobel laureate de Gennes, who published influential papers on polymer dynamics in which he developed theoretical descriptions of quasi-elastic scattering from single polymer chains in solution. This isotopic contrast between hydrogen and deuterium, which is unique to neutrons, allows various parts of soft matter systems to be labelled so that their structure and dynamics can be distinguished. It is this contrast variation technology, plus the fact that cold neutrons

provide simultaneous access to the relevant length and time scales, that make neutrons so useful as probes of soft matter.

As indicated by the name, soft condensed matter can easily be deformed through applications of weak external stresses or thermal fluctuations. A non-invasive characterisation is therefore imperative, and handling these materials often imposes demanding requirements for sample environment and on-site preparation. Moreover, many interesting features of soft matter are linked to non-equilibrium states and closely related to the application of external fields and variable conditions. These require suitable tools for a time-resolved and *in situ* characterisation, parallel investigations with complementary methods, and experiments that involve complex sample environments that make it possible to duplicate industrial processing conditions at the neutron instrument.

It is important to understand the equilibrium and non-equilibrium properties of soft condensed matter not only in well defined model systems, but also in everyday life and industrial and technological applications. To make significant advances on this front, it is necessary to probe considerably smaller (gauge) volumes within larger and often complex samples, over a wide range of length scales and with high temporal resolution. This will be an area of strength for ESS. The key techniques for addressing soft matter will be small angle neutron scattering (SANS), reflectometry, neutron spin-echo spectroscopy and quasi-elastic neutron spectroscopy.

Self-assembled colloids

The development of new colloids and hybrid nanostructures offers the possibility of exciting new applications and permits researchers to explore unusual phenomena that result from the unique microscopic structure of these novel materials. Predicting the behaviour of these materials [43] requires the development of theoretical models and detailed structural investigations over a wide range of conditions. Likewise, the fundamental interactions of surfactants form the basis of their behaviour in commercial formulations. Deuterium labelling gives superior contrast, allowing investigation of the roles of different components. Time-resolved studies are crucial to detect how surfactant molecules self-assemble into micelles and how such structures transform into different shapes [44,45]. These studies rely on a high neutron flux to detect transformations on the millisecond to second timescale, and on high-throughput manipulation of the samples using *in situ* equipment integrated into the neutron instrument. Such studies will benefit from the high flux in the **general purpose polarised SANS instrument** and the **broadband small sample SANS instrument**, and from the ability of the latter instrument to probe small gauge volumes and cover a broad simultaneous range of scattering vectors to address different length scales.

In order to understand how self-assembling colloidal suspensions behave under manufacturing conditions, many state-of-the-art applications rely on investigations of non-equilibrium structures and material responses to external stimuli. For example, personal care formulations and food are exposed to shear stresses in confined geometries during processing, making it of significant interest to study colloidal structures under flow. Figure 2.3 shows a map of SANS patterns collected across a flow cell mimicking processing conditions. The map reveals two coexisting micellar structures at different locations in the flow profile, which is indicative of partial de-mixing of the surfactant components. Such studies require small, high intensity beams of neutrons to make possible spatially resolved measurements [46], which currently severely limits the ability to use this approach. ESS will expand possibilities to map flow fields in a wide range of commercially interesting systems [47,48].

Polymers

Polymers are in widespread commercial use and represent an active area of scientific research in which neutron scattering already has a high impact. Polymer-polymer interactions and phase behaviour have important applications. For example, polymer hydrogels are attractive candidates for soft tissue replacement, since they can contain a very high fraction of water, which allows them to support living cells. However, such hydrogels are typically very fragile, and significant effort is being directed at improving their mechanical strength by using interpenetrated polymer networks [50]. These networks have hierarchical structures on several length scales from 5 Å up to several microns, so their investigation calls for SANS measurements across a wide simultaneous Q-range, a capability offered by the **broadband small sample SANS instrument** in the reference suite.

In polymers, atomic motions define the overall structural configuration and determine macroscopic

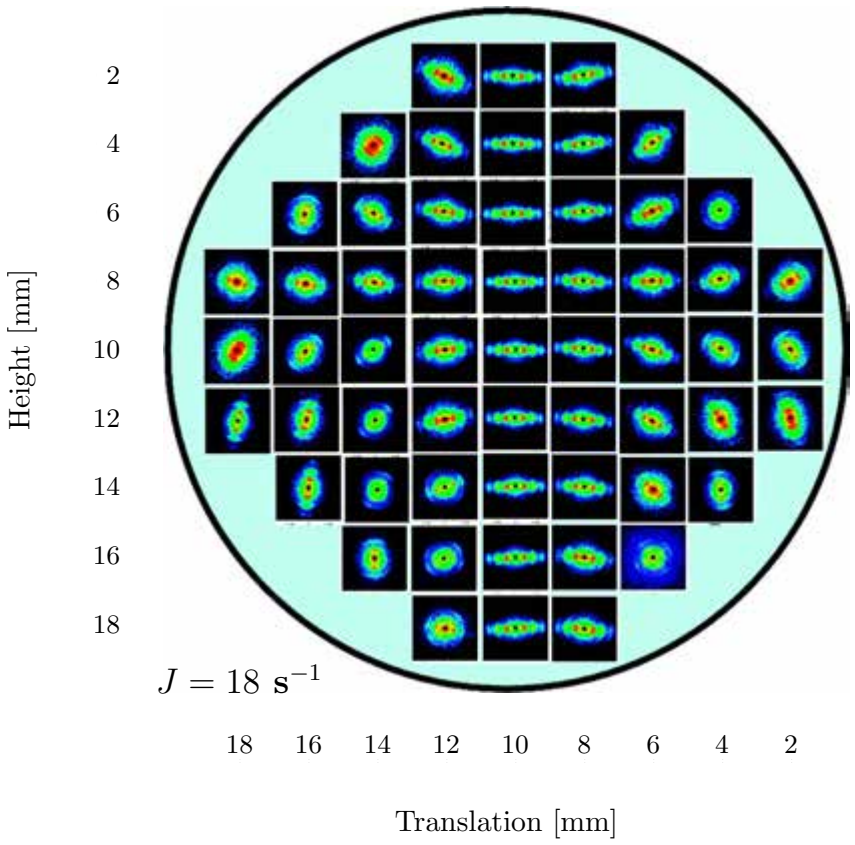

Figure 2.3: SANS imaging of a mixed surfactant suspension under an elongational flow profile. Images taken at different positions across the flow profile (measured at 2 mm intervals) indicate partial de-mixing of the components [49].

Figure 2: 2.6

properties. Therefore, many technological applications involve tailoring the dynamic properties of polymer materials. For example, ion transport in lithium batteries depends on polymer chain dynamics [51]. Information on the collective dynamics, correlated over distances of several atomic spacings, is of particular importance for determining material functions. However, in soft disordered materials it is difficult to investigate dynamics at all relevant length scales as this implies assessing signals that are two to three orders of magnitude smaller than those in crystalline materials. The high flux in the instruments will open up possibilities to study new materials and new phenomena across various length scales.

Low frequencies are difficult to access with optical techniques, so neutrons remain the only experimental probe able to deliver information in the correct space and time ranges to explore and understand these intermediate scale dynamics. Such an approach has been used to monitor the surface association state of polyethylene oxide intercalated between graphite oxide layers during graphene templating [52], as shown in Figure 2.4, and to follow the dynamics of water in polyamide engineering plastics [53]. The gain in sensitivity for inelastic scattering spectroscopy provided by the spectrometer suite will make more such experiments possible. Moreover, a strong link between neutron scattering, and rapidly advancing molecular dynamics model calculations will allow researchers to investigate increasingly complex phenomena.

The reference suite includes a number of instruments well adapted to investigate polymer dynamics, namely, the **vibrational spectrometer**, **backscattering spectrometer**, **cold and bispectral chopper spectrometers**, **wide-angle neutron spin-echo spectrometer** and the **high-resolution spin-echo spectrometer**, covering the time window from local dynamics up to slower correlated motions – from picoseconds to nanoseconds. High flux instruments with tunable resolution will allow access to a broader dynamic range and higher energy resolution than is possible with existing instruments. This will open up new possibilities to study and observe areas such as changes in rotational dynamics, and slower motions and more dilute systems such as thin films and nanostructured materials.

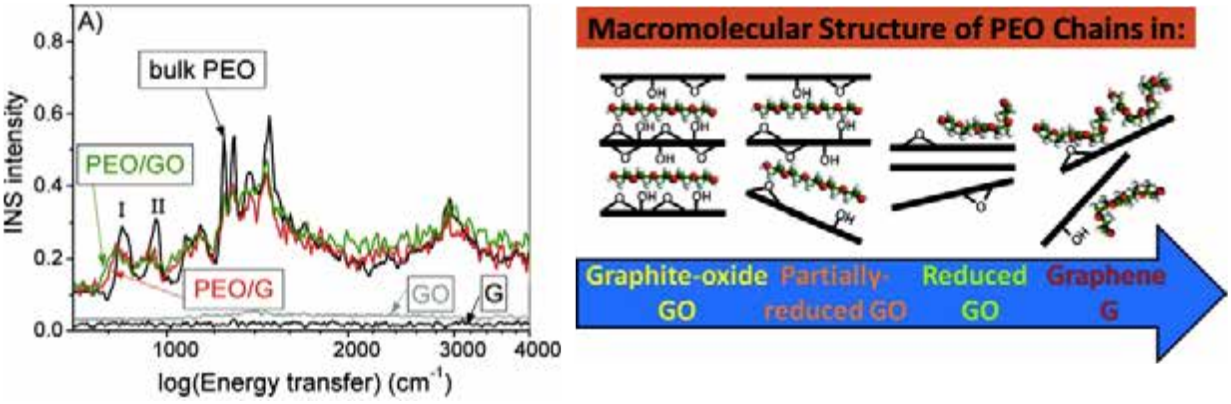

Figure 2.4: Vibrational spectra from polyethylene oxide polymer chain conformation under confinement during graphene templating from graphite oxide [52].

Thin film devices

Polymer thin films are widely used in advanced device technologies, and understanding their structure is a prerequisite to optimising performance. Neutron reflectometry and grazing incidence SANS (GISANS) are well-suited to probing these materials, in which the active layers are often buried deep within the device structure. Neutrons penetrate more easily and non-invasively than do X-ray or electron beams. In state-of-the art organic photovoltaic solar cells, high performance requires the acceptor to be uniformly distributed within the donor polymer matrix [20], whereas in organic light emitting diodes (OLEDs), the adjacent polymer layers need to be stable under operating conditions without significant interdiffusion [54]. In chemical sensors for organic explosives such as TNT, the film structure needs to be optimised for fast and reversible response with maximum sensitivity for the analyte [55]. Studying these issues non-invasively *in situ* is possible using neutron reflection, which allows the structural changes to be correlated directly to the signal output (such as photoluminescence). However, many advanced structures, especially those including inorganic nanostructures, are typically available only in small volumes, and therefore reducing the beam size will allow more widespread investigation using neutrons. In the reference suite, the **vertical sample reflectometer** would permit studies of very small samples with dimensions of a millimetre or less.

Reactive surfaces and interfaces

Time-dependent surface processes and reactions on the millisecond to second timescale are important in a range of soft materials. Neutron reflectivity provides unique information about changing surface structures, because deuterium labelling allows the *in situ* detection of different components in the reacting or forming films. This is particularly important for understanding the realistic conditions in which commercial detergent formulations are used, where dynamic adsorption of surfactant and polymer mixtures occurs at flowing water surfaces on sub-second to second timescales [56]. Fast occurring phase transitions, such as the swelling of polymer hydrogel films, can be tuned for use as nano-scale switches in miniaturised sensors [57]. Liquid-liquid interfaces (for example oil-water [58]), are of significant interest for emulsion technologies, but experiments are limited by the strong attenuation of neutrons by liquids. The ESS flux will enable a significant reduction in the experimental path length, allowing time-resolved experiments. Fast, low-resolution studies of this type would be one of the main strengths of the **horizontal sample reflectometer**, which covers a broad Q-range simultaneously at this time scale.

For the development of environmentally friendly formulations, mixtures of biosurfactants have been characterised to identify the functionality of the most active compounds in complex mixtures [59]. The high flux and ability to work with small samples will facilitate high-throughput and rapid scanning of a large number of samples to solve the functionality of complex mixtures more efficiently than is possible at the moment.

Nanostructured and patterned surfaces

One of the biggest current challenges in soft condensed matter is to understand and manipulate thin 2D or 3D nanostructures formed at interfaces, for example by block copolymers on nano-patterned surfaces [60] or surface-induced colloidal crystals [61]. To do so, it is necessary to use SANS, grazing incidence SANS (GISANS) and off-specular reflectometry to obtain a view of the thin film structures in all 3 dimensions. ESS will be well placed to further advance these emerging applications through use of the **surface scattering instrument**. Spin-echo encoding of polarised neutrons will additionally give access to the longer length scales, up to microns, that are found in many hierarchical materials such as food and composite materials.

Composite materials

Nanoparticles are often included in composite polymers or fibrous materials to provide enhanced strength [62] or flexibility (e.g. in plastics), where the state of dispersion and aggregation of the nano-fillers has significant impact on the final properties obtained [63]. A practical example is flexible Kevlar body armour fabric [64], which is reinforced by a colloidal suspension of silica nanoparticles that stiffens reversibly under impact due to the phenomenon of shear-thickening [65], without impairing mobility. In such materials, neutron scattering can detect the multiple components, allowing the relationship of their properties to the performance to be elucidated. Quasielastic neutron spectroscopy has also been used to detect how polymer segmental dynamics in grafted silica-polymer composites are coupled to the aggregation of the nanoparticles, which gives rise to the solidification of the material [66]. Composite materials often exhibit structure on the nanometre to micron length scale. The high flux and wide Q range of the **broadband small sample SANS** would be ideal for studies of nano-composite materials both in their final state and under processing conditions, whereas the **multipurpose imaging instrument** could be used to detect structural or texture variation over larger areas, which can influence material performance in applications.

Drug delivery systems and theranostics

Soft matter forms the foundation of many novel theranostic (both therapeutic and diagnostic) materials. These materials exploit the self-assembly and phase behaviour of biocompatible amphiphiles, such as polymers, lipids, and polysaccarides, in advanced drug delivery systems for improved drug circulation, and controlled or targeted release. Both structure and dynamics influence the material's response to external stimuli (such as a change in pH), its interaction with biological tissues [67], and the drug release profile [68]. This behaviour can be probed using neutron reflectometry and SANS combined with neutron inelastic, quasi-elastic and spin-echo spectroscopy. A significant amount of effort is directed at the synthesis and characterisation of new drug delivery materials, particularly for "stealth" carriers [34], which also reduce the toxicity and side-effects of drugs. Using deuterium labelling, neutron scattering can probe the structures and dynamics of the carrier material, encapsulated drug, and water in these systems. A prominent example is polymersomes used to encapsulate magnetic nanoparticles for combined MRI imaging and magneto-chemotherapy, as shown in Figure 2.5. The mechanism of targeted doxorubicin release, induced by a magnetic field deforming the polymer membrane, was first demonstrated using SANS [36]. Neutrons are also sensitive to the magnetic structure of materials. Studies of magnetic nanoparticles could benefit from polarised neutron experiments on the **general purpose polarised SANS instrument** in the reference suite.

Water dynamics also play an important role in drug release characteristics, for example from novel injectable drug delivery media made from thermo-responsive polymer micro-capsules [35]. Such dynamics can be probed by quasi-elastic neutron spectroscopy (QENS) on the picosecond to nanosecond timescale. The **cold and bispectral chopper spectrometers** and **backscattering spectrometers** have a broad dynamic range to investigate phenomena at different timescales, typical of those needed to investigate drug delivery systems with structure and confinement effects on multiple length scales.

Food science

Many natural and processed foods contain colloidal structural elements that give them their characteristic properties and determine how they feel in the mouth, how they are formed or how they are digested. In the near future, functional foods using nanotechnologies are expected to have a huge impact in controlling

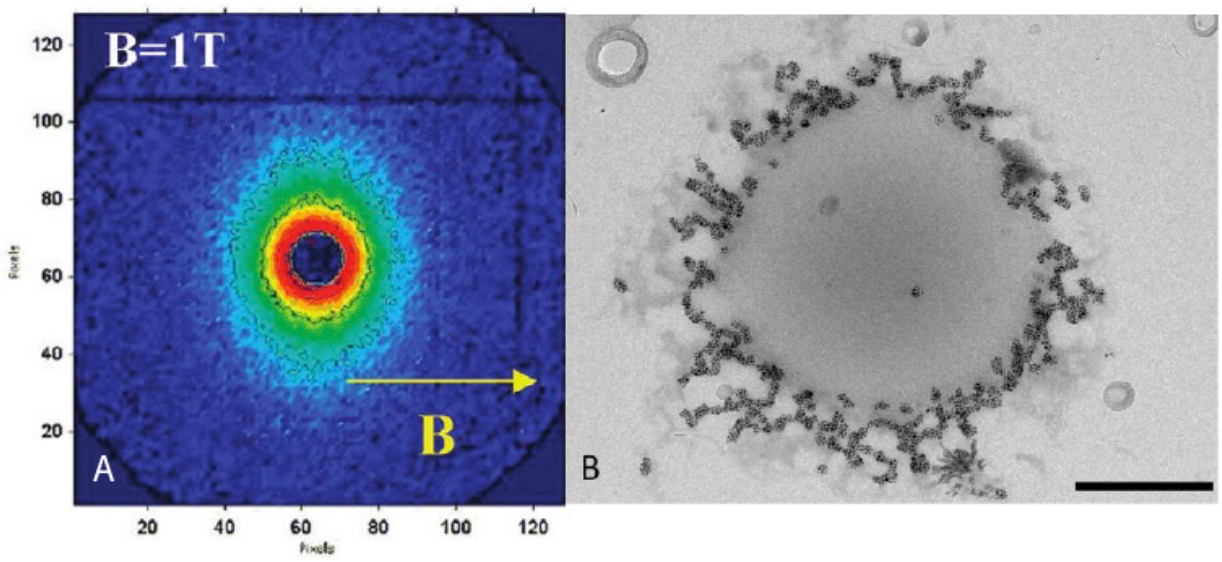

Figure 2.5: Small angle neutron scattering was used to elucidate the mechanism of doxorubicin release by deformation of polymersomes loaded with magnetic nano particles for combined MRI imaging and magneto-chemotherapy. Left: Anisotropy of the SANS pattern due to polymersome deformation in a magnetic field. Right: Cryo-TEM image of the polymersomes loaded with nanoparticles [36].

or enhancing nutrient release. Soft materials are also the key components in advanced packaging using antimicrobial surfaces, and microporous and biodegradable materials. Neutron scattering has already provided important insights, for example by employing deuterium labeling to distinguish different components in milk, in tannin precipitates in wine, and in protein-lipid nanoparticles for controlled release [69]. There is the potential to do significantly more, particularly by investigating food and packaging materials under realistic processing conditions over several length scales. This would be facilitated by the combination of the **multi-purpose imaging instrument**, the **broadband small sample SANS instrument**, the **horizontal reflectometer** and the **instrument for surface scattering** for measuring structure, while the **high resolution spin echo** and **wide angle spin echo spectrometers** would cover fluctuation measurements.

In summary, ESS will provide a wide range of high performance instrumentation to address twenty-first century challenges in soft condensed matter research with higher throughput, faster time resolution, detection of more dilute components, and imaging of structure and dynamics across a broad range, which will further systematic studies of these complex multi-component materials. While the actual instruments built will differ to a greater or lesser extent from those included in the reference suite, nonetheless the instruments in the reference suite serve to illustrate these capabilities.

2.2.2 Life science

Modern life science faces the challenge of deciphering intricate cellular and molecular mechanisms in the dynamic chemical environments of living systems. To address issues such as healthy ageing and food security, information ranging from atomic details to the workings of entire organisms is required. Neutrons excel in discerning structure and dynamics on many different time and length scales, particularly in hydrogen-rich materials. With unprecedented neutron flux, ESS will open up new paths of research. ESS will be used to explore how individual proteins aggregate and cause degenerative disease; to visualise biological material in three-dimensions; to identify key protonation states when drugs interact with drug targets; to elucidate molecular interactions at membrane surfaces; and to understand in detail structure and dynamics of complex multi-component systems in solution.

Deciphering the mechanisms behind health and disease and understanding the intricacies of plant biochemistry and other complex biological processes are crucial for tackling many of the challenges facing

humanity. Ageing, illness and the environmental impact of agriculture all involve complex biological systems, the mechanistic understanding of which calls for information ranging from atomic and molecular detail to the structure and functioning of an entire organism.

Neutrons have many advantages as a probe for structure and dynamics in biological systems, as biological samples with their high hydrogen content are easily damaged by X-ray or electron-scattering techniques. Despite this, the use of neutrons in biology has not yet reached its full potential. The field has to date been limited by a number of factors. Relatively low source brightness has demanded large samples; the isotope labelling techniques required to make full use of neutron methods are not yet fully developed for biology; and the number of neutron instruments appropriate for biological samples is limited today. A bright source will allow the investigation of small samples not amenable to neutron work today. Furthermore, long neutron pulses are particularly well suited for a number of neutron techniques relevant for biological systems. In combination with modern isotope labelling techniques, ESS will open up opportunities for experiments on biologically interesting samples that were previously impervious to neutron methods.

Macromolecular structures at an atomic level of detail

X-ray protein crystallography has provided monumental insights into the complex structure and inner workings of proteins. While X-ray techniques provide valuable structural information, they cannot in general determine the positions of hydrogen atoms, which are crucial in many biochemical processes. Determination of these hydrogen positions by neutron crystallography offers a key advantage in understanding phenomena such as enzyme mechanisms, protein-ligand interactions or proton transport across membranes. Understanding enzyme mechanisms in detail is not only of fundamental chemical interest, but is also essential for designing better inhibitors for use as pharmaceuticals and for engineering industrial enzymes. For example, Figure 2.6 illustrates how a combined neutron and X-ray crystallographic study of the drug acetazolamide bound to its target protein, carbonic anhydrase II [70], definitively shows the protonation state of the drug. This allows the rational design of better inhibitors for this important class of enzymes, relevant in, for example, convulsion, obesity and cancer.

While the complementarity between neutron and X-ray macromolecular crystallography is increasingly deployed on complex biological problems, this methodology remains underused – partly due to limited access to suitable neutron instruments worldwide and partly due to the relatively low brightness of currently available neutron sources. With the enhanced ESS flux, it will become possible to apply the methodology described above to more challenging systems, such as proton-pumping membrane proteins that are crucial for bioenergetics and photosynthesis [71], nerve and muscle function [72], or plant drought re-

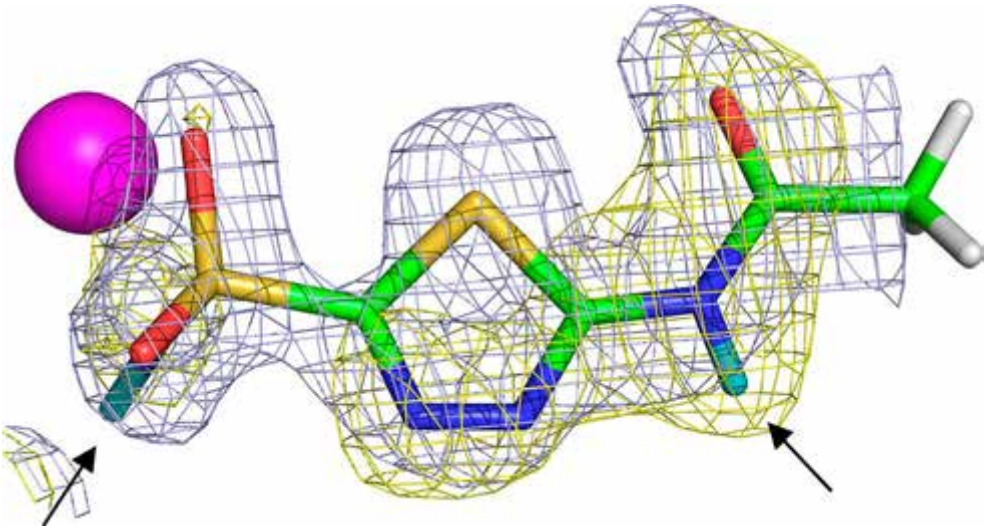

Figure 2.6: A nuclear scattering length density map of the drug acetazolamide in the active site of human carbonic anhydrase II, showing the unambiguous identification of hydrogen atom locations using neutron crystallography [70].

sistance [73]. Expanding the scope of neutron macromolecular crystallography will make possible more systematic combined neutron and X-ray studies of protein-ligand complexes in the search for new drugs. A **macromolecular diffractometer** in the reference suite, dedicated to biological crystallography, addresses these challenges.

Solution structures of macromolecular complexes

The large, multi-component complexes involved in the biological function of most macromolecules are often transient and inherently flexible, and hence difficult to crystallise. However, such structures can be elucidated in solution to intermediate resolution using small angle neutron scattering in combination with selective deuteration. By changing the isotopic composition of the individual components of the complex and the solvent, the structures of different parts of the complex can be determined, and the information combined to yield a full quaternary structure of the multi-component complex. Because of its ability to discern separate components and subunits and their motions, this method is able to make important contributions to understanding the intricate interactions between biological macromolecules in solution.

SANS on selectively deuterated samples is complementary to similar X-ray methods (SAXS). Together with other techniques such as electron microscopy (EM), these methodologies are delivering important insights in the biosciences. For example, the complex formed between myosin-binding protein C and filamentous actin was studied with SANS and contrast variation, showing how these molecular interactions regulate heart muscle contractions [32]. A combination of SANS, SAXS and mass spectrometry was used to elucidate the role of a conformational change of the Munc18-Syntaxin protein complexes [33] involved in vesicle fusion – a process crucial, for example, in the function of nerve synapses and carbohydrate storage. Understanding such processes in molecular detail is instrumental to developing new treatments for heart diseases, neurological disorders and obesity, among other conditions.

High brightness will increase the range of problems that can be addressed using SANS, as the protein material of the biologically most interesting systems is often available in quantities too small for present-day neutron experiments. More importantly, high flux will open opportunities to perform time-resolved studies with macromolecular complexes. The **broadband small sample SANS** instrument is well adapted for such experiments.

Dynamics of biomolecules

Biological macromolecules are not static structures and their dynamics are pivotal to their function. The dynamic processes in such systems are difficult to monitor and successful research draws on a variety of methods, including the use of neutrons, X-rays, nuclear magnetic resonance (NMR) and optical spectroscopy. These methods are highly complementary, illuminating different aspects of the dynamic activities of biological systems.

Inelastic neutron scattering techniques are used to elucidate internal protein dynamics over many length- and time-scales, from very fast dynamics on the atomic scale to the slow domain of motions taking place over much longer distances. For example, the changes in the vibrational dynamics of dihydrofolate reductase – an important target of antimicrobial and cancer drugs – upon binding of the drug methotrexate were shown to have a significant effect on the binding free energy [74]. Other examples include water and lipid dynamics at biological interfaces [37], and large amplitude domain motions in proteins [75]. The functionally pivotal dynamics of biological membranes can also be monitored, as described in the following section. Importantly, it is possible to follow the dynamic changes of biological macromolecules in response to external stimuli. For instance, Figure 2.7 illustrates how the light-driven proton pump bacteriorhodopsin was monitored using quasi-elastic neutron scattering (QENS) whilst being driven through a series of specific functional states using laser excitation [38]. A set of instruments is needed, including a **cold chopper spectrometer** and a **backscattering spectrometer**, in addition to **high-resolution spin echo** and **wide-angle spin echo**, to probe the range of time and length scales involved. High neutron brightness together with the advantages of modern dynamics simulation tools will allow the study of time-resolved changes of dynamics in even more complex systems, and will facilitate the exploration of how changes in protein dynamics correlate to biological function.

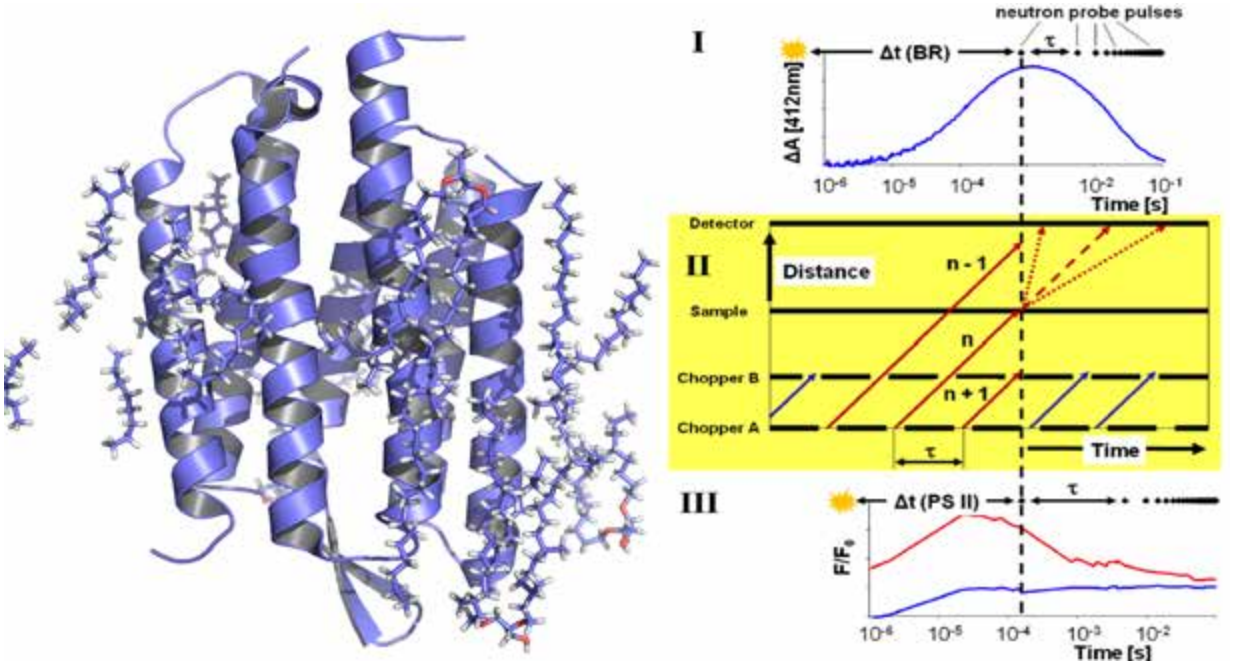

Figure 2.7: The membrane protein bacteriorhodopsin is a light-driven proton pump whose function is associated with a large conformational change. Using QENS, it has been shown that the conformational change is preceded by a significant change in the dynamic modes of the protein, establishing a direct link between internal protein dynamics and protein function [38].

Biological membrane assemblies

Biological membranes are complex functional assemblies that form the interface between organelles and the cytosol, and between the cells and their environment. They also play a key role in larger structures such as blood vessels and skin. Biological membranes constitute soft interfaces that mediate or regulate many cellular functions [76]. The lipid matrix contains or anchors a wide range of membrane proteins, carrying out specific tasks such as transport across the membrane and signalling between cells. The integrated functionality of lipids and proteins was clarified in recent decades, in the so-called lipid-raft model [77]. Subsequently, lipid membrane structures, lipid domain coexistence, and the role of cholesterol in the structural properties of membranes have been subjected to intense investigations.

A range of methods are used for exploring biological membrane structure, including neutron scattering, NMR, fluorescence microscopy and MD simulations. With neutron reflectometry and SANS, deuterium labelling allows unique information to be obtained about the structure across the membrane. Observing the nuclear scattering length density profile perpendicular to the membrane surface gives information about the internal structure, such as the location [78], dimensions [79] and orientation [80] of membrane proteins under physiologically relevant, non-crystalline conditions. Time-of-flight neutron reflectometry and SANS can be used to study the mechanisms of molecular interactions and transfer processes at biological interfaces, such as how natural antibiotics penetrate the outer membrane of a bacterium [81] or how cholesterol is transferred across a membrane [82]. Neutron reflectometry gave insight into the aggregation state and process by which the anticancer and anti-HIV plant peptides Kalata B1/B2 insert into membranes [83]. Time-resolved reflectometry can also be used to follow chemical reactions at biological interfaces, such as the toxic interaction of ozone with lipids lining the lung alveoli [84]. At ESS, it will be possible to study smaller samples with better time-resolution, elucidate biochemical mechanisms, and help design new therapeutic agents. It will also be possible to study the lateral structure in biological membranes [85], using grazing incidence SANS, which extends the one-dimensional information obtained from reflectometry to two-dimensional structures. In addition to the **broadband small sample SANS instrument**, the **horizontal reflectometer** and the **surface scattering instrument** would be useful for these investigations.

The dynamics of membranes have received much less attention than membrane structure, despite

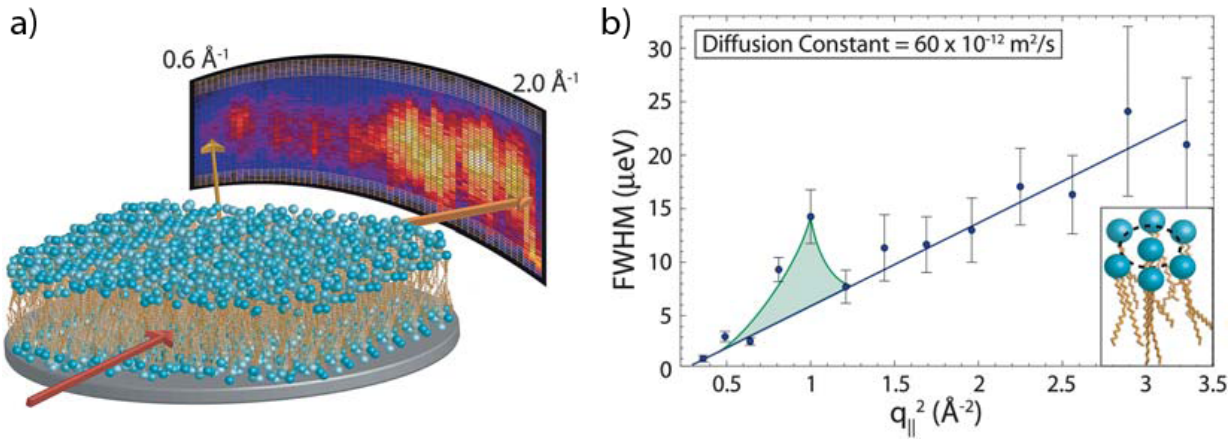

Figure 2.8: A state-of-the art quasi-elastic neutron scattering study using 30 single-supported lipid bilayers showed that molecular diffusion is continuous and the rates are comparable to the bulk lamellar phase [89]. Left: The plane scattering experimental detection geometry. Right: The full-width half-maximum of the quasi-elastic peak as a function of Q^2, revealing enhanced diffusion around $q_{\|} \simeq 1$ Å^{-1} corresponding to the in-layer lipid molecule distance.

their importance [86]. Today mainly X-ray or visible light photon correlation spectroscopy is used but neutron inelastic scattering has the potential to offer many new insights into this still relatively unexplored area [87–90]. Figure 2.8 illustrates how lipid molecular vibrations could be probed at the picosecond timescale using the **cold chopper spectrometer**, while collective motions, rotations and diffusion could be probed using the **backscattering spectrometer**. This instrument in the reference suite provides an unprecedented versatility, stemming from its ability to trade neutron flux for spectral resolution, while bridging the gap to the **high resolution spin echo** and **wide angle spin echo spectrometers**, which can also probe the membrane fluctuations.

The crowded interior of cells

The cytoplasm of a living cell is a mixture of thousands of proteins, together with nucleic acids, metabolites and signalling substances, adding up to a very high total concentration. Despite the fact that the cellular proteins often contain opposite charges and differ widely in size, shape and interactions, the intracellular fluid is normally stable. However, there are cases in which the proteins do become unstable, and this is typically at the onset of protein condensation diseases such as cataract, sickle cell disease and many others. In recent years, it has also become clear that the common denominator of many neurodegenerative diseases is uncontrolled protein aggregation. Science has not yet arrived at a detailed understanding of the molecular origins of these diseases.

Neutron scattering possibilities, combined with other techniques, will further understanding of what makes proteins aggregate at the onset of a condensation disease, and help decipher the role that individual proteins play. SANS combined with selective isotope labelling is well suited to investigate macromolecules and complexes in highly concentrated solutions often inaccessible with other techniques. By manipulating the contrast of the crowding agent, contributions from a highly concentrated solution can be minimised while studying the complex in crowded conditions. In combination with detailed molecular dynamics simulations, this approach has already shed light on interactions among proteins in the eye lens, creating the basis for a scientific understanding of cataract formation [91].

Any attempt to understand nature's cellular machinery will also need to address the dynamic properties of proteins. The diffusion of proteins in the dense and crowded environment of the cell is an essential topic, as it strongly influences processes such as signal transmission or reactions between proteins. Combined with modern colloid theories for hydrodynamic interactions in dense solutions and computer simulations, neutron backscattering and spin echo spectroscopy have already made it possible to disentangle internal protein dynamics and overall diffusion in a crowded environment [92, 93], thus raising hopes of one day perfecting a quantitative understanding of protein diffusion and its role in a variety of biological processes.

Current limits on sample volume and neutron flux, and the current state-of-the-art of preparing par-

tially deuterated proteins at concentrations comparable to that of the cell cytosol, make many important experiments unfeasible today. The proposed **broadband small sample SANS instrument**, with its superior flux and broad simultaneous range of scattering vectors, could bring closer a breakthrough in the understanding of living cells and protein condensation diseases. Dynamics studies using backscattering and neutron spin echo techniques will considerably benefit from high flux and relaxed wavelength resolution. The **backscattering**, **wide-angle spin echo** and **high-resolution spin echo instruments** combined with the possibilities offered by the planned deuteration laboratory and computer modelling activities will have the potential to make important contributions to systems biology through investigation of macromolecular crowding and protein dynamics under conditions that mimic the cell cytoplasm.

Imaging organism-level complexity

Biological imaging is an area of wide interest that has made considerable progress in recent years, using a number of different probes. While imaging using neutrons is currently underexploited for biological applications, there are some key advantages of neutron imaging that make this an avenue worth exploring. These are the high penetrating power of neutrons through material that scatters light, the contrast between different light elements often present in biological samples, and the absence of radiation damage to the sample. Because of these characteristics, neutrons can be used to image processes at the organism level under realistic conditions. For example, neutron imaging has been used to study the time course of water uptake in plant roots [39], an agriculturally important process that is difficult to image with light microscopy through the surrounding soil. High brightness will make such studies more rapid, improve the time resolution and allow a more widespread use of tomographic imaging to study the three-dimensional organisation of biological tissues and organisms in conditions not easily amenable to light microscopy. The **multi-purpose imaging** instrument is well suited for such applications.

2.2.3 Magnetic and electronic phenomena

> *Understanding magnetic and electronic phenomena is key to improving materials used in advanced technologies, and also to enhancing fundamental knowledge about quantum matter. Their investigation represents a core activity for both basic and applied research. With their unique sensitivity to magnetism, neutrons have been extremely successful in identifying the static and dynamic properties in a broad range of materials, from magnetic hetero-structures, molecular magnets and magnetic nano-particles promising novel electronic devices to unconventional superconductors and novel quantum states of matter. The versatile ESS instrumentation will provide unprecedented simultaneous coverage of length and time scales to identify how and why these quantum states are realised. The long-pulse flexibility will make it possible to use the high neutron flux to carry out higher precision measurements, and to study quantum materials* in situ *and* in operandi *under extreme environments, as required for the study of quantum phase transitions. Providing high precision maps of the magnetic polarisation and spin dynamics using polarisation analysis provides a yard stick for theoretical modelling, and yields quantitative information unavailable with any other measurement technique.*

Huge technological advances are being made by better understanding and manipulating the electronic properties of materials. Examples are giant magnetoresistance (GMR) compounds, high temperature superconductors and, most recently, topological phases and graphene. For many of these important materials, neutron methods have played a pivotal role in bringing insights that could not have been realised by other means, including accurate crystal and magnetic structure determination; investigation of magnetic resonance in superconductors; and greater clarity about exchange bias in GMR films.

The strength of neutron- and non-neutron-based scattering techniques lies in their ability to measure spatial and temporal correlations simultaneously, thus providing information about the different length and energy scales responsible for electronic phenomena. The direct microscopic information yielded by using neutron spin as a quantitative probe makes neutron scattering very useful for benchmarking theoretical models against experimental results. While there have been very recent exciting developments in measuring high-energy magnetic excitations with broad resolution using resonant inelastic X-ray scattering, the impact of neutron scattering in the field of magnetism is extremely important. The energy scales of many of these emerging magnetic and electronic phenomena lie in the sub-meV to tens of meV energy regime

where high resolution and precision is required to untangle the competing interactions that underpin much of the physics of these materials. ESS, with its strength in low energy cold neutrons and novel long pulse time structure, will be a valuable tool in the investigation of low energy magnetic and electronic phenomena. The enhanced brightness will allow the study of novel materials that are synthesised in quantities too small for present-day neutron investigations. In addition, it will be possible to make more use of polarised neutron scattering than was possible at earlier neutron facilities. Polarised neutron scattering is very important for the study of magnetism, but places huge demands on neutron flux that were beyond the capacity of earlier facilities in many circumstances.

Currently, about one quarter of available neutron beam time is used to study magnetic and electronic phenomena, driven by both fundamental and applied research interests. Though the majority of publications result from powder diffraction investigations, all neutron techniques are used for magnetic investigations. In the next section, a few select examples are given to illustrate the wealth and breadth of uses of neutron scattering within this field and how ESS will transcend many of the current limitations on the power and range of neutron scattering techniques, furthering investigation of some of the most exciting materials of the 21st century.

Symmetries in emergent complex phenomena such as high temperature superconductivity

The behaviours of individual electrons and lattices are fairly well understood, yet the electronic properties of high temperature superconductivity and the electronic charge and spin ordering observed in multiferroics cannot be predicted. As such, collective behaviour cannot be determined from individual constituents. Emergent complex phenomena are currently viewed as fundamental research. Nevertheless, an understanding of these phenomena will be the starting point for future innovative technologies. One example is the studies of flux-line lattices of practical superconductors, in which the effects of applied magnetic fields are of crucial importance to increasing the efficiencies of materials that are necessary to create the high-field magnets that are ubiquitous in medical imaging.

The nature of high temperature superconductivity and its relation to magnetism remains one of the great scientific enigmas, as outlined during the Nobel lecture of V.L. Ginzburg [94]. By studying changes in the symmetry of spin dynamics upon entry into the superconducting state, neutron scattering has revealed the features of superconducting phases relative to the symmetries and energy scales involved [95–97]. The observations challenge the well-established BCS theory of phonon-driven superconductivity and help to benchmark theoretical models evoking magnetism not only for long-studied copper oxide-based high temperature superconductors, but also for the rare earth- and iron-based unconventional superconductors. Probing the excitation spectrum has been simplified recently with the possibility to measure four dimensional spatial and energy neutron scattering maps using chopper spectrometers with position sensitive detectors that were not available when the first wave of high temperature superconductors was discovered [95]. However, present-day neutron spectroscopic instrumentation is limited to specific energy regions – cold or thermal neutron scattering – while emergent complex phenomena affect dynamic behaviour over broad energy scales. Novel bispectral instrumentation such as the **bispectral chopper spectrometer** will provide extended energy ranges in this field.

Orbital current excitations are believed to be pivotal to high temperature superconductivity. An extensive study of the neutron spin-polarisation dependence of their signal is necessary to obtain a conclusive explanation of this phenomenon [98]. These signals are very weak and overlay with other strong features such as phononic scattering. The future for crystal analyser spectrometers and chopper spectrometers lies in providing full polarisation analysis to separate these weak signals. In addition, the relevant signatures are often revealed at specific positions in momentum space and need to be studied as a function of external parameters such as temperature, pressure and magnetic field. The **crystal analyser spectrometer** in the reference suite is optimised for such parametric studies under extreme conditions.

Novel states of matter

Novel states of matter are states that clearly deviate from the current canonical description. These phases have many exotic properties, and their study is driven by scientific curiosity about fundamental issues. Interestingly, certain solid state phenomena have cosmological analogues, such as magnetic monopoles that interact in a class of magnets knows as spin ice [2, 3, 99, 100], as illustrated on the left of Figure 2.9. The cosmological Higgs mechanism can be evoked to explain how the magnetic monopoles in spin ice undergo an

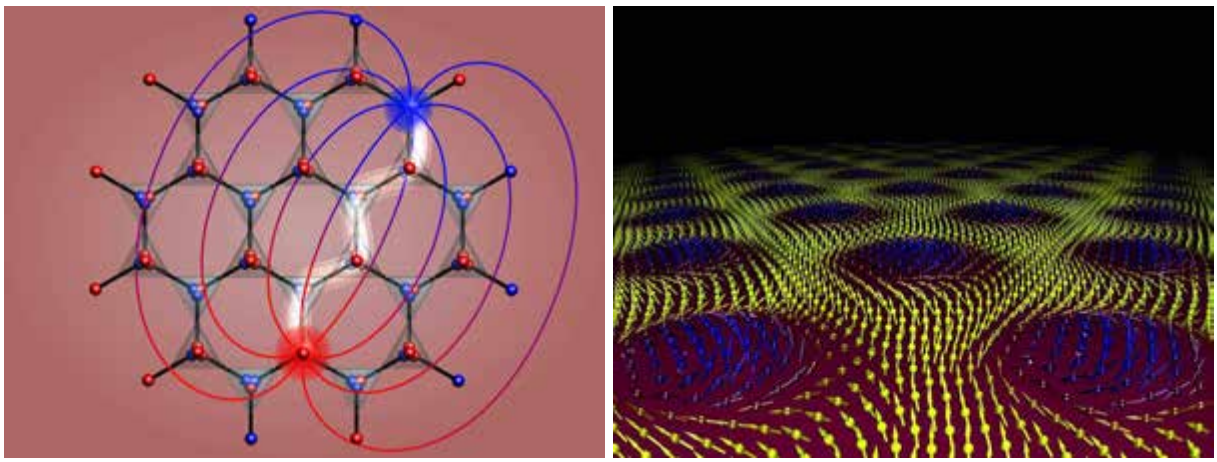

Figure 2.9: Left: A pair of separated monopoles, red and blue, with a chain of inverted dipoles between them. "Dirac strings" are highlighted in white with the associated magnetic field lines [2]. Right: Magnetic vortex spin ordering in a Skyrmion lattice as first revealed by neutron scattering [3].

unusual first order phase transition. The Higgs mechanism observed in spin ice confines the magnetic field in a manner analogous to the mechanism that causes the weak nuclear force to confine the nucleus [101]. The experimental signatures of these phases could only have been determined via the unique properties of neutron scattering and, in particular, by using information gleaned from polarisation analysis. The **single-crystal magnetism diffractometer** in the reference suite would contribute to further research in this field of enquiry.

These novel states can all be understood to arise from a phenomenon known as magnetic frustration, which displays low frequency spin dynamics due to its degenerate ground state. Due to the low energy scales, the excitations are inaccessible by non-neutron scattering methods. Typically, they are probed by cold neutrons on chopper spectrometers, backscattering instruments and via the Fourier time of a spin echo instrument such as the **cold chopper spectrometer**, the **backscattering instrument** or the **wide angle spin echo instrument** in the reference suite. The dynamics in these compounds are complex and cover a wide energy range. Longer Fourier times, coupled with greater flux and higher energy and spatial resolutions will be available to dissociate relaxational dynamics from more exotic experimental signatures.

The interplay of topology and magnetism has revealed a number of exciting new magnetic states. One of these is the Skyrmion lattice, as shown on the right of Figure 2.9, which originates from a charged topological spin texture due to strong electronic correlations. Neutron scattering was able to reveal this highly complex order to be a chiral lattice of topological particles [3]. Although chirality and topology are old concepts in theoretical terms, recent research is discovering them in an ever-growing number of compounds. The study of their behaviour requires all the experimental attributes that have been mentioned thus far. Of particular importance for future instrumentation will be low-Q capabilities on all wide-mapping diffraction instruments, such as the **single crystal magnetism diffractometer** and **bispectral powder diffractometer**, and on spectroscopic instruments, including **chopper spectrometers** and the **cold crystal-analyser spectrometer**, with polarisation analysis capabilities to separate the chiral terms, and high Q and E resolution to probe the finely detailed structures.

Quantum critical behaviour shows phase transitions that cannot be mimicked in the classical world. Quantum fluctuations give rise to an abrupt change in the ground state when their energy scales (1 meV, 11.56 K, and 10 T for 1 μ_B) exceed those of thermal fluctuations. They can be accessed by tuning a phase transition to $T = 0$ K via external or chemical pressure or magnetic field. The scattering profiles obtained tend to be broad, and as the quantum critical point is approached, the signal is intrinsically weak [102]. A key requirement is to map out the dynamic response over a wide range of momentum and energy space as a function of temperature concomitant with magnetic field or external pressure. The high penetration power of neutrons permits extreme sample environment equipment to be used during a neutron experiment, and neutron scattering avoids beam-heating the sample when performing measurements at sub-Kelvin temperatures. On the other hand, these restrictive sample environments result in small sample volumes. In addition, it is necessary to synthesise samples with homogeneous doping, which again leads

to small sizes. The dedicated **cold crystal-analyser spectrometer** and the **extreme conditions instrument** are well suited to providing extreme environments with focusing optics for small samples and restrictive sample environments.

Fractional excitations observed in low dimensional magnetism are another manifestation of novel states of matter. This phenomenon provides a distinct opportunity to study the ground and excited states of quantum model systems. In particular, the 1D Heisenberg antiferromagnetic chain has proved fertile ground for the interplay between theory and neutron scattering by recently revealing a four-spinon continuum at high energies that emerges when long range magnetic order is destroyed via quantum fluctuations [103]. The low energy scales involved are well matched to neutron methods and inaccessible with other scattering methods such as resonant inelastic X-ray scattering. However, current neutron scattering experimental limits arise from the intrinsically small magnetic moments and the subtle experimental manifestations that distinguish the disparate theories. Wide mapping instruments such as chopper spectrometers will continue to play an important role in these strongly correlated behaviours in which weak scattering signals are distributed over broad regions of momentum and energy space. The greater brilliance, together with polarisation on large mapping instruments such as the **chopper spectrometers** in the reference suite, holds great promise for the generation of data that can be benchmarked against theoretical models.

Non-equilibrium quantum phenomena

Using magnetic materials in technological applications includes manipulating and perturbing a magnetic system to create non-equilibrium states that will pave the way for novel scientific phenomena. This perturbation is possible via magnetic switching by ultrafast, 2 picosecond magnetic field pulses [104]; manipulation of the energy landscape by strong single cycle electric field pulses [105]; and ferromagnetic to antiferromagnetic phase transitions induced by femtosecond laser pulses. The physical mechanisms behind these transitions are not fully understood, although a dedicated research effort is under way, in particular, at pulsed X-ray laser facilities [106]. ESS will enter this pump-pulse field in the microsecond time range to complement pulsed X-ray work. *In situ* measurements such as these do not require a drastic change in instrumentation, but the experimental requirements for applying *in situ* external stimuli such as electric fields, lasers or microwave radiation must be considered carefully in the instrument design. The optimisation of the **crystal analyser spectrometer** for investigations within a horizontal scattering plane plays to its strength when the sample environment imposes restrictions on the scattering geometry.

Thin film heterostructures

Thin film and multi-layer structures comprising oxide heterostructures give rise to novel concepts for electronic devices. These heterostructures are based on metal oxide materials that display a broad range of physical phenomena. These phenomena include large spin polarisation; colossal magnetoresistance; electronic phase ordering; and charge, orbital and spin ordering [107–109]. Such phenomena are altered in thin film structures due to surface and interface effects that are probed using polarised neutron reflectometry complementary to X-ray investigations. ESS will offer the possibility to measure the static and dynamic behaviour of thin film heterostructures that have been reduced in size with the concomitant size effects realised in novel electronic devices. Novel instrumentation that profits from a gain in the source brightness will enable reflectometers, such as the **vertical reflectometer**, to routinely measure the very weak scattering signals that hamper current day investigations.

Molecular magnets, nanoparticles and excitons in confined systems

Molecular magnets, nanoparticles and excitons in confined systems realise the trend towards the miniaturisation of electronic and biological devices to an extreme degree. Molecular magnets are new classes of magnetic materials at the nano-scale. Research is underway to create multifunctional molecules whose properties can be fine tuned at the molecular level, offering superior performance for spintronics as well as for biological and medical applications. Indeed, molecular magnets will be used to facilitate the separation, purification and concentration of different biomolecules encased within magnetic molecules from the bulk solution through the application of a magnetic field. Their function depends on microscopic correlations revealed via single crystal neutron studies. Recent inelastic neutron scattering work determined the unusual spin dynamics [110] of a molecular magnet. These experiments are challenging to conduct, since these materials are often only available in small single crystals resulting in a limited scattering signal. Instruments

optimised for small samples will form an essential part of the instrument suite, and may include the **bispectral chopper spectrometer**, **vibrational spectrometer**, **cold crystal-analyser spectrometer**, **single-crystal magnetism diffractometer** and the **extreme conditions instrument**.

Significant potential applications in ultrahigh-density magnetic recording, information processing, and magnetic sensing result from the confined nature of magnetic antidot arrays [40,41]. Specific attention has been devoted to recording processes, with studies of the magnetic domain configuration to obtain regions where basic units of information will be stored. Spatial information obtained by neutron scattering is essential to determine the properties of these magnetic antidot arrays. The reduced sizes of these structures have revealed novel spin states and corresponding excitations not observed in bulk materials. These nano-sized structures can be observed using the **vertical reflectometer** or the **general purpose polarised SANS instrument**. Dynamics can be probed using the **cold chopper spectrometer**. Polarised neutron scattering with micro-focused neutron beams from ordered nanometer-sized magnetic regions on such antidot arrays also hold great potential for detecting local versus global structures, scanning lateral inhomogeneities and correlating nuclear and magnetic structures. Currently, polarisation analysis is hampered by the great loss of incident flux during the polarisation and analysis of the neutrons. As such, experiments that employ polarisation, essential for a full quantitative description of such anti-dot arrays, will benefit from the flux increase that ESS will realise.

2.2.4 Chemistry of materials

> *The search for new materials with novel and attractive properties is as alluring as it is scientifically challenging. Neutrons are an indispensable tool to reveal and understand the role of light elements in ever more complex and versatile materials. Advances built into ESS will meet the increasing demands of modern materials chemistry in respect to real time studies using smaller gauge volumes or samples in more dilute forms than is possible with neutrons today.* In situ *and* in operandi *views of processes with simultaneous determination of structure and dynamics will make movies of the chemistry of materials possible in realistic conditions with unmatched clarity.*

Human demands on materials drive their increasing complexity. Society needs better catalysts, improved construction materials and safer pharmaceuticals. Discovering where atoms are, and what they do is key to understanding their properties, which in turn makes it possible to design and tailor materials for a variety of applications that benefit society. ESS, with its unparallelled brightness and innovative instrument suite, will be an important tool for understanding the physics and chemistry of materials. This field is extremely multidisciplinary, intersecting with energy, chemical, environmental and life sciences and with electronics and geoscience. The goal that unites these disparate fields is the desire to understand and impart functionality to materials.

Although there have been significant advances in diffraction and spectroscopic techniques with a new generation of synchrotron light sources, the unique capabilities of neutron-based instruments still make them the tool of choice to gain critical insights into new materials. Neutrons provide absolute structure factors and total magnetic moments that can be directly tested against theoretical predictions. The isotopic variation of the neutron's scattering length between hydrogen and deuterium is an irreplaceable tool in many applications involving hydrogen-containing materials such as pharmaceutical and cements. The touchstone for modern advanced materials research is the determination of the structure and dynamics of realistic materials under realistic conditions. The deeply penetrating power of the neutron allows researchers to peer into the material itself while it is in action, yielding insights that can not be obtained by other means. High brilliance will allow researchers to view decreasing gauge volumes inside devices, gaining insight into physical and chemical processes in real time with second to millisecond resolution. This will make it possible to study the ever-increasing complexity and nano-structure of functional materials, which will be studied with greater precision and in more dilute realistic forms. For an advanced understanding of physical and chemical properties, scientists will be able to harness the combined power of advances in experimental, theoretical and computational methods. The key experimental techniques are diffraction, small angle neutron scattering and imaging for structure, and inelastic neutron scattering, quasi-elastic neutron scattering and spin-echo for dynamics.

Novel materials

A recent review stated that superconducting materials are, "still alluring but hard to predict ..." [111]. This encapsulates the great challenge in materials chemistry: Even after centuries of research and development in experimental and theoretical methods, it remains difficult to predict novel properties of materials. While our society greatly benefits from novel materials exhibiting negative thermal expansion, new light-emitting compounds or novel high temperature superconductors, our ability to discover them largely relies on scientific experience and intuition. In recent years, the chemical processes for forming new, technologically important compounds have become ever more extreme conditions in terms of pressure and temperature [112–114]. This leads to smaller and more complex samples whose structure and chemistry must be understood [115].

Neutrons and X-rays are the basic tools for characterising these new materials. While X-rays often provide highly accurate information on complex symmetry, neutrons are best suited for accurately determining the positions of atoms. These tools are indispensable for advancing understanding of novel materials and their properties. Often these advances in chemistry have proved resistant to the important information that neutrons can deliver. ESS will make possible a suite of diffractometers that will be able to measure ever smaller and more complex novel materials under realistic processing conditions, which promises critical acceleration of materials discovery. The dedicated **cold crystal-analyser spectrometer** and the **extreme conditions instrument** are well suited to provide extreme environments with focusing optics for small samples and restrictive sample environments.

Structure and *in situ* processing

Crystallography is the cornerstone of materials characterisation, determining where atoms are in space. Without this knowledge, it would be impossible to relate structure to properties [116–118]. Neutron scattering is highly complementary to X-ray scattering and, ideally, requires flexible instrument set-up (resolution, Q-range and flux), which is inherent to the long pulse source. *In-situ* processing [119–121] is an extension of crystallography – investigation of a system in real-time as a function of changing variables, such as time [122], temperature, pressure, magnetic field and/or chemical potential [123, 124]. It can also be applied to investigate the evolution of dynamics and changes in microstructure over time. Neutron scattering has barely scratched the surface of possibilities offered by high flux, high time- and spatial-resolution instruments [125–128]. At ESS, scientists will perform multi-technique measurements and combine them with computational modelling, connecting theory and experiment to understand processes in great detail. The reference instrument suite reflects the various needs for structural investigation by providing the **general-purpose polarised SANS** and **broadband small sample SANS instruments**, the **thermal powder diffractometer**, **bispectral powder diffractometer**, **pulsed monochromatic powder diffractometer**, **materials science and engineering diffractometer**, **extreme conditions instrument** and the **single crystal magnetism diffractometer**.

Catalysis

Catalysis, the ability of some substances to alter the rate of chemical reactions without being consumed, was recognised more than 150 years ago and has been applied on an industrial scale since the beginning of the last century. To understand catalytic activity, or to tailor a catalyst to do a specific job, it is necessary to understand the individual steps in the catalytic process in detail. Many experimental techniques, from NMR to synchrotron radiation and microscopy, are employed to understand and tailor these materials for their realistic applications. The unique advantage of neutrons resides in their ability to locate hydrogen atoms and determine their chemical state [129–131], providing critical insight into catalytic activity. While quenching a catalytic system *in operandi* is often used to perform quasi-static neutron measurements of the frozen state [132], this method is of limited practical use, as the system is not investigated in its active states. ESS will facilitate routine, time-resolved measurements breaking new ground in fast catalytic processes at the gas-solid interface. The combination of these measurements with computer simulations of model and real systems (facilitated via the ESS-DMSC) delivers the potential to provide new insight into the structure and function of catalysts. Key instruments that address these needs in the reference suite are the **thermal powder diffractometer**, **pulsed monochromatic powder diffractometer**, **bispectral powder diffractometer**, **cold chopper spectrometer**, **vibrational spectroscopy instrument** and **backscattering spectrometer**.

Health and pharmaceutical drugs

The development of pharmaceutical drugs must proceed through several stages in order to ensure their safety and efficacy before their introduction into the market. Many problems that delay new drug approvals are related to insufficient understanding of the drug's physical properties and manufacturing processes [133]. Although the intrinsic activity of an active pharmaceutical ingredient is determined by its chemical structure in solution and how it interacts with its targets (i.e. receptors and enzymes), the effectiveness of a drug's delivery depends largely on its physicochemical and materials properties in the solid state. It is critical to identify the degree of polymorphism and stability of the active ingredient in the presence of other polymorphs before development. Choosing the lowest free energy polymorph usually leads to dissolution problems and low bioavailability, whereas the highest energy polymorph may yield high solubility that is accompanied by high toxicity and a very short half life. Selecting the appropriate level of free Gibbs energy of the active ingredient is crucially important as the consequences of incomplete evaluation can be disastrous. For example, the lowest energy polymorph of the HIV protease inhibitor Ritonavir rendered the bioactive higher energy polymorph inactive [134].

Despite all the experimental tools available, the energy landscape of drug polymorphs is not exhaustively investigated during the discovery phase. Such a task is not straightforward and in most cases Raman scattering and powder X-ray diffraction are insufficient. Access to both spatial and time correlations, and the absence of selection rules are unique to neutron spectroscopy. Wider use of neutron scattering techniques has the potential to make a big impact in this evaluation process [128, 135–137]. Combining neutron techniques with the existing arsenal of other methodologies will make it possible to locate the hydrogen atoms in a more precise way and to understand their dynamics in molecular drugs, thus mapping the energy landscape more precisely and understanding polymorphism more accurately. For structural studies, higher fluxes and the flexibility to tailor long pulse will be valuable for studying processes *in situ* using instruments like the **thermal powder diffractometer** and the **pulsed monochromatic powder diffractometer**. Dynamics could be determined by neutron spectroscopy using the **vibrational spectroscopy instrument**, the **backscattering spectrometer**, the **cold chopper spectrometer** or the **bispectral chopper spectrometer**.

Environmental and green chemistry

Modelling of cloud formation by atmospheric aerosol droplets [138, 139] as well as safe and economical processes for water purification in developing countries [140] are examples in environmental chemistry for which neutron investigations have already played an important role. Investigating the environmental fate and the structure-activity relationship of engineered nanomaterials is essential to understanding their environmental impact and to providing a framework for improved nanomaterials that are more environmentally benign. Only a few structure-activity relationships have been completely elucidated [141]. In addition to SANS, the **multi-purpose imaging station** will allow materials to be studied non-destructively and under operational conditions. Following processes *in situ* will also play a fundamental role in developing alternatives that have a lower environmental footprint. The high neutron flux of the **horizontal reflectometer** could make possible studies of interfacial reactions at the millisecond to second timescale, allowing the kinetics and mechanism of processes to be understood.

Waste management

Natural and engineered clay barriers appear in the multi-barrier concept used for the disposal of high and long-life radioactive wastes at great depth, while concrete, the world's most versatile and most widely used material, is commonly used for repository barriers for intermediate-level waste. The quality of these barriers and their resistance to water is critical in safeguarding the environment. The quality of hardened concrete is strongly influenced by the water confined in the cementitious materials and by water transmission through cracks and pores. In the case of clays, the dynamic properties of water molecules in the interlayer spacing is responsible for a wide range of water activity. In both cases, environmental conditions can interfere with these barriers and influence their service life. Neutron scattering offers unique advantages for understanding how water transmission is affected by confinement in such waste management materials [142–145].

Figure 2.10 illustrates how quasi-elastic neutron techniques have provided information about the dynamics of water molecules and their mobility. SANS, with its sensitivity to nanometer structural features, has made it possible to look into pores and water adsorption [146, 147], and neutron imaging has revealed

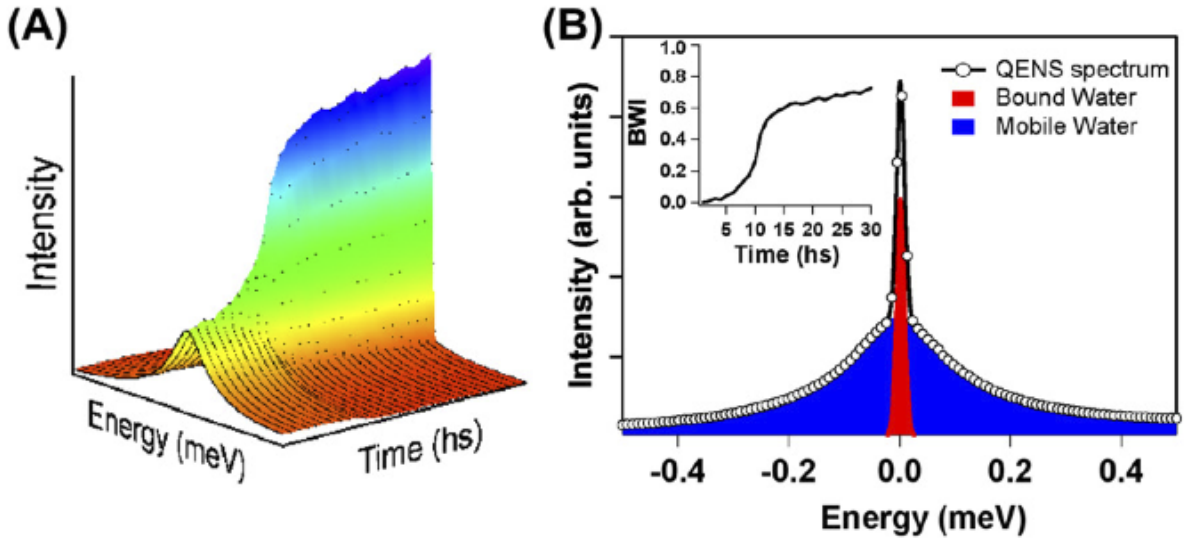

Figure 2.10: A 3D representation of the time evolution for a quasi-elastic neutron spectroscopy spectrum. Left: A hydrating cement paste [142]. Right: Elastic and quasi-elastic components contributing to a QENS spectrum at a given time after cement mixing. The inset records the bound water index as a function of time.

the pore size distribution and the extent of cracking [122]. The **multi-purpose imaging**, **general-purpose polarised SANS** and **broadband small sample SANS instruments** promise a better grasp of the nuances of the hydration process of various waste management materials, allowing for a better understanding of their structure. In the reference suite, the dynamics of the various water populations found in concrete and clays are covered by the **cold chopper**, **bispectral chopper** and **backscattering spectrometers**, as well as by the **instrument for vibrational spectroscopy**. The combination of experiments on these instruments with computer modelling insights into the dynamics of water facilitated by DMSC could further the development of better and more durable barriers for waste management.

2.2.5 Energy research

The properties of the neutron are well suited to investigating the structural and dynamic processes responsible for relevant macroscopic properties in energy materials such as polymer solar cells, batteries, fuel cells, thermoelectric materials and materials used in hydrogen technologies. The high penetration depth of the neutron can be used to probe complex systems and assemblies under working conditions. The presence of light atoms such as oxygen, lithium and hydrogen require neutron-based techniques to elucidate structure and to determine mechanistic pathways since these are difficult to detect with X-ray scattering techniques. The high ESS brilliance will be valuable in the study of physical properties and processes in advanced materials, which are typically synthesised in small quantities. Investigating the electrochemistry of batteries and fuel cells may lay important foundations for a possible hydrogen-based energy economy in the future.

In a recent book about energy research in the European Union [148], the crucial importance of a reliable and sustainable energy supply is highlighted:

> Reliable and sustainable energy supply is fundamental to the economic and social fabric of nations, and to the well-being and quality of life for their citizens. In an age when the demand for traditionally exploited natural resources is outpacing supply, conventional industrial practices are contributing to undesirable climatic change and developing regions are competing for a greater share of finite fuel stocks, the search for innovative ways to meet this need becomes more urgent than ever.

Materials research provides the foundation for developing novel technologies for a clean, reliable and efficient energy supply. In particular, the advent of nano-materials has placed materials research at the forefront of developing sustainable technologies for energy conversion and storage. Principal areas of interest include polymer-based solar cells, batteries, fuel cells, thermoelectric materials and hydrogen technologies. The properties of the neutron are well suited to investigating the structural and dynamic processes responsible for relevant macroscopic properties. The high penetration depth of the neutron can be used to probe complex systems and assemblies under working conditions. The advantage of isotopic contrast provided by neutron-based technologies, and their sensitivity to light atoms such as oxygen, lithium and hydrogen, are valuable for elucidating structure and determining mechanistic pathways which are difficult to detect with X-ray scattering techniques. High neutron brilliance will provide new opportunities in the study of physical properties and processes in advanced energy materials.

Fuel cells

Fuel cells have great potential to aid in overcoming global energy challenges, by combining efficient conversion technology and hydrogen as a clean energy carrier. They will play a significant role in a number of energy end-use sectors, from electric vehicles to power plants. Neutron scattering is integral [149] in designing and evaluating novel candidate materials [24,150], as well as in elucidating mechanisms [151,152] that will lead to improvements in energy efficiency, performance and sustainability. In addition, because of the non-damaging nature of the neutron and the large penetration depth, neutron scattering is particularly powerful for understanding the underlying causes of failures and inefficiencies in components [25] and in operating fuel cells [153] as shown in Figure 2.11, as well as for monitoring the in-operation performance and lifetime of membrane-electrode assemblies and operating fuel-cell stacks. The key challenge in this field is to optimise the energy efficiency of fuel cells. This requires a greater understanding of the relationship between proton diffusion and chemical structure, which will require tunable resolution in space and time. While there is a plethora of advanced tools deployed to track the location and motion of light atoms in fuel cells, real- and reciprocal-space neutron images of fuel cells are unparallelled. The long pulse advantage will make versatile instruments possible that will cover the extended spatial domains needed to optimise the efficiency of fuel cells. Relevant instruments in the reference suite include the **thermal powder diffractometer**, **pulsed monochromatic powder diffractometer**, **bispectral powder diffractometer**, **vertical reflectometer** and **multi-purpose imaging instrument**.

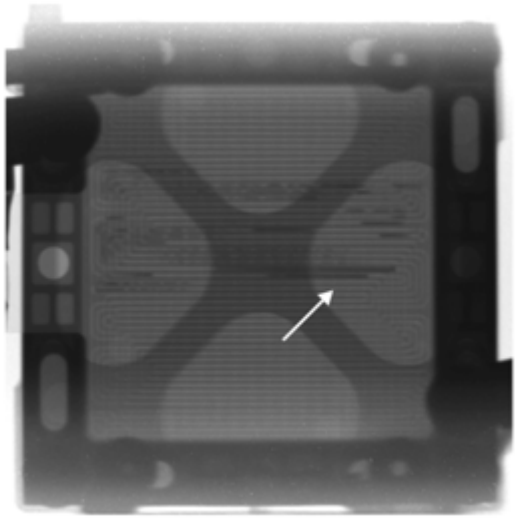

Figure 2.11: A radiographic image of an operating PEM fuel cell (140 mm × 140 mm). The dark horizontal lines indicated by the arrow are large water accumulations in the gas flow channels.

Gas storage materials

The broad class of gas storage materials includes hydrides, hydrates, clathrates, frameworks, metal-organic frameworks and nanotubes, with an emphasis on reversible hydrogen storage; encapsulation of other small molecules, such as alkanes; and trapping of harmful gases, such as carbon dioxide. Storing hydrogen safely, efficiently and reversibly is one of the main technological challenges which must be met before hydrogen can be adopted as a widespread energy carrier. *In situ* neutron diffraction has been widely used to monitor hydrogenation and dehydrogenation reactions and site preferences [27,154–156]. Such work could be further advanced by the capabilities of the **thermal powder diffractometer** and the **pulsed monochromatic powder diffractometer** instruments, while the **general-purpose polarized SANS** and **broadband small sample SANS** instruments are powerful tools for studying the effects of small molecules confined in gas reservoirs, such as shale gases in coal, with implications for carbon dioxide sequestration [29, 30].

By measuring the characteristic rotational spectrum of hydrogen models, inelastic neutron scattering [28,158,159], quasi-elastic neutron scattering [160] and neutron vibrational spectroscopy [161, 162] are uniquely able to identify the amount of un-bound hydrogen in a sample and to reveal if it is present as dihydrogen [163]. The **backscattering** and **wide-angle neutron spin-echo spectrometer** instruments in the reference suite could be used to investigate the hydrogen diffusion mechanism in hydrogen-storage materials. Understanding how clathrates form, coexist, transform and decompose [164, 165] under particular conditions of temperature and pressure is crucial to their use as fuel sources and to investigating the origins of pipeline blockages due to the formation of clathrate plugs. Also of interest is carbon dioxide

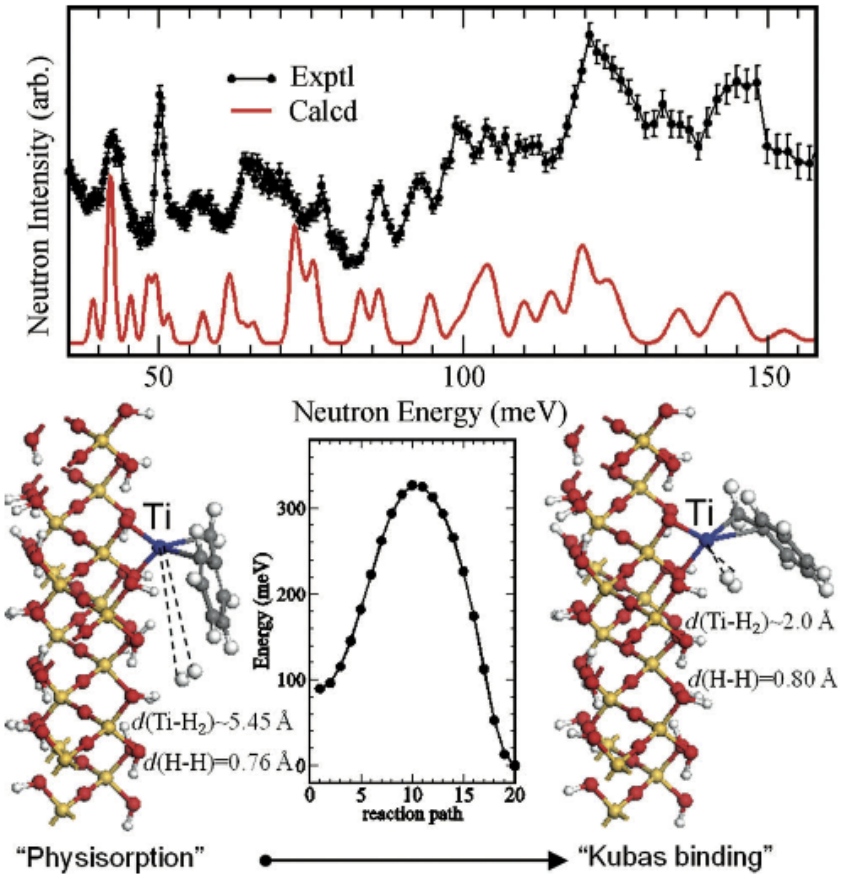

Figure 2.12: Top: A comparison of the inelastic neutron scattering spectra of activated dihydrogen-Ti binding on a silica-supported Ti^{III} organometallic complex and a simple density functional theory model in which Ti-benzyl is attached to two layers of hydrogen-passivated silicon dioxide. Bottom: The calculated reaction path from physisorption to Kubas-like dihydrogen binding with an activation barrier that is consistent with the neutron measurements shown above [157].

sequestration and understanding the implications for climate change of uncontrolled release of methane and carbon dioxide from undersea clathrate beds. The **cold chopper spectrometer** and **vibrational spectrometer** are well suited for this work. As illustrated in Figure 2.12, it is useful to combine advanced computational methods such as molecular dynamics and density functional theory [157] with experimental measurements. Provided with adequate tools, scientists will be able to gain new insights into how gases actually anchor in these complex frameworks and how new materials can be tailored to meet society's future needs.

Battery materials

Batteries represent the most widely available solution to energy storage in a huge range of applications, from personal batteries in smoke detectors to backup energy supply in case of mains failure. Many batteries rely on ion exchange and/or the ionic conductivity properties of lithium and hydrogen, making them prime candidates for investigations using neutron scattering methods in operation [23, 166–168]. Time-dependent studies could be performed using the **thermal powder diffractometer**, **pulsed monochromatic powder diffractometer**, **bispectral powder diffractometer**, **vertical reflectometer** and **multi-purpose imaging** instruments. Higher brilliance instruments will allow faster time dependent studies, but just as important, imaging techniques offer the opportunity to visualise working batteries under charge and discharge conditions [167, 168]. The **multi-purpose imaging instrument** provides novel capabilities for spatially resolved neutron scattering studies with the full range of high resolution attenuation contrast options to image subtle effects. Quasi-elastic neutron scattering could be used for diffusion measurements on the weakly scattering lithium ions, thus making it possible to study the diffusion mechanism directly. QENS on operating battery materials would be possible using the **backscattering** and **chopper spectrometers**, while the **wide-angle neutron spin-echo spectrometer** could be used for probing dynamic properties, especially in lithium-ion battery materials.

Thermoelectric materials

Thermoelectric materials hold great potential to further sustainability by applications in thermoelectric devices for waste-heat recovery and in the refrigeration industry. With more efficient, cheaper and environmentally friendly materials, markets for these devices will grow enormously. The research roadmap is clear. Better performance will be found by combining low thermal conductivity with high electrical conductivity – the so-called "phonon glass-electron crystal" concept [26]. Many thermoelectric materials exhibit cage-like host structures with heavy rattling ions, which act as wave breakers to the dispersive and heat-transporting acoustic phonons. The interaction of local phonon modes with the acoustic phonon

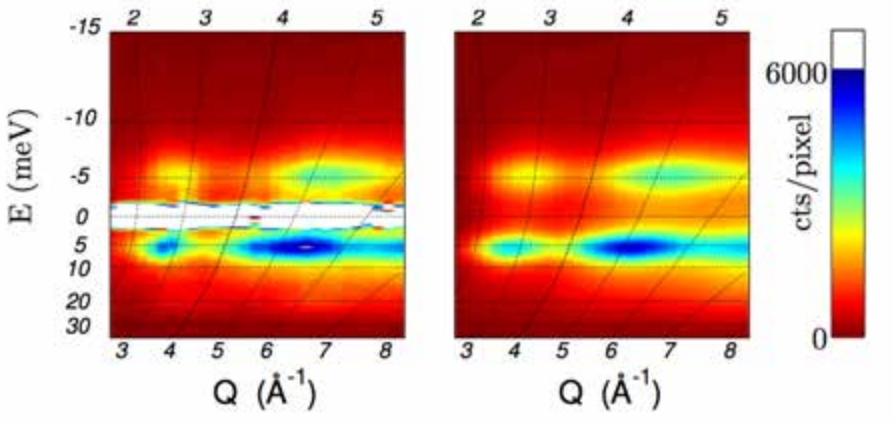

Figure 2.13: The phonon response of the thermoelectric material Zn_4Sb_3 is hallmarked by anisotropic rattling of Sb_2 dumbbells. Left: Neutron time-of-flight data at 300 K. Right: A model calculation of the same data [169].

branches affects phonon lifetimes and reduces thermal conductivity [169, 170], as illustrated in Figure 2.13.

While Inelastic X-ray scattering offers the possibility to measure phonons from tiny crystalline samples, it provides neither the S(Q, ω) mapping capabilities nor the energy resolution to map out phonon anomalies. For this purpose, inelastic neutron scattering is a key technique for determining lattice vibrations and revealing the microscopic origin of the low thermal conductivity with the degree of precision required to verify theoretical models. Current research trends move towards nano-structured materials and increasingly larger unit cells. High resolution experiments, ideally on single crystalline material, are required to benchmark the modelling results. In the reference suite, the **thermal chopper spectrometer** and **bispectral chopper spectrometer** are well suited for this work, providing high resolution data on the full 4D phonon dispersion.

Solar cells and photovoltaics

Photovoltaic solar cells were originally developed for space applications in the 1950s and are now widely used in consumer products, mounted on roofs of houses, and assembled into power stations. Photovoltaics may well become a major source of clean electricity in the future. Given their low manufacturing cost, organic polymer-based photovoltaics have begun to rival silicon-based cells. Current research aims to improve the efficiency of converting sunlight into electricity for these polymer-based solar cells. Neutron scattering is widely used in this field to characterise bulk structural properties of novel materials that have enhanced efficiencies [21]. Neutrons are also successfully used to understand the morphology involved and to study interfaces in thin-film blends or monitor time dependent composition [22]. Optimised performances in organic photovoltaic devices depends on the structure of the active layer, in particular on a uniform distribution of the active component [20]. Relevant instruments in the reference suite include the **vertical reflectometer** for thin film investigations, as well as the **thermal powder diffractometer**, **pulsed monochromatic powder diffractometer** and **bispectral powder diffractometer** for studies of bulk crystallographic properties. With the high flux of the **backscattering** and **chopper spectrometers** it would become feasible to tackle basic questions of molecular dynamics in organic photovoltaic devices and relate those to their performance.

2.2.6 Engineering materials and geosciences

> *The deep material penetration of neutrons allows non-destructive investigations of inner structure, properties and processes locally within bulk materials and complex assemblies (e.g., multi-component devices) with high precision and sensitivity. This penetration capability also makes possible studies within complex sample environments that replicate realistic or extreme operating and processing environments of the study materials, components and devices. These capabilities are of great importance in engineering science and geoscience research. The brightness of the ESS neutron beam, combined with cutting edge instrumentation, and in conjunction with complementary non-neutron-based methods, will facilitate previously unfeasible investigations of materials and processes: ESS promises new understanding of the fundamental mechanisms that drive earth processes and it also will facilitate the development of new materials and material-processing techniques to enhance material durability and reduce environmental impact.*

The use of neutron scattering is widespread in engineering materials and geoscience research, ranging from investigations with direct application in industrial research and development to analyses of geomaterials that further understanding of the fundamental processes of the planet. In such applications, the deep penetration capability of neutrons is of primary importance, allowing scientists to carry out non-destructive investigations of inner structure, properties and processes locally within bulk materials and complex assemblies (e.g., multi-component devices) with high precision and sensitivity. Furthermore, this penetration capability makes possible studies with complex sample environments that replicate realistic or extreme operating and processing environments of the study materials, components and devices. A key feature common to many engineering and geoscience samples is that they are multi-component systems with sensitivities to different, perhaps multiple, physical, chemical and thermal interactions, which is in contrast to isolated and well defined samples used for fundamental studies; with this comes an associated set of specific challenges.

The range of applications of neutron scattering in the fields of materials engineering and geosciences studies is vast. The discussion here is restricted to a few key areas and challenges that the facility will be well

equipped to address. The brightness of the neutron beam, combined with its cutting-edge instrumentation, will allow researchers to investigate phenomena that at present can not be studied. Compared to neutron

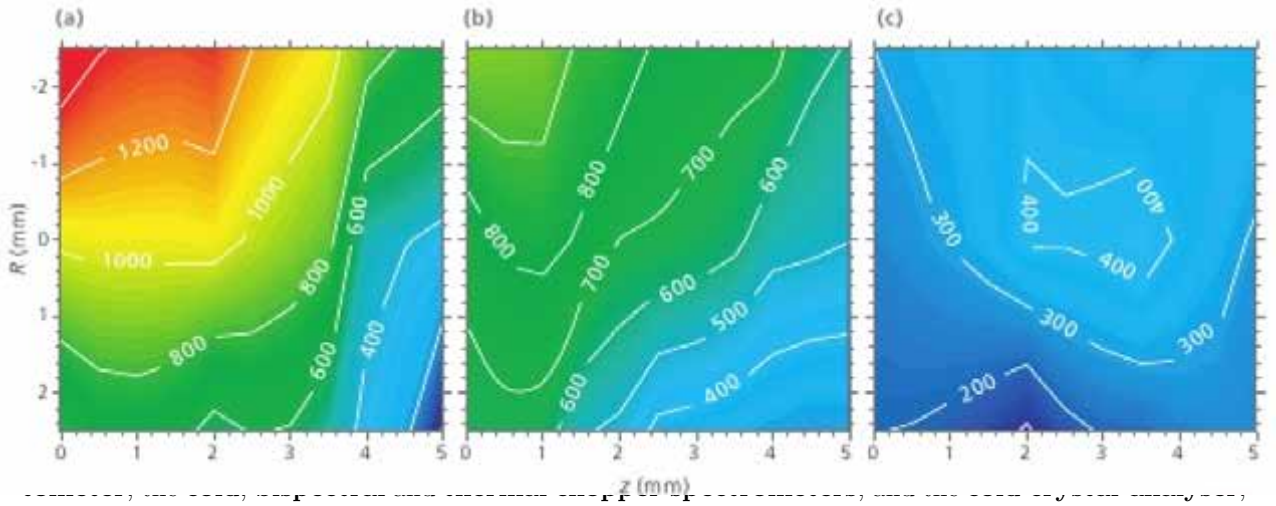

vibrational and **backscattering spectrometers**.

Figure 3: 2.14

Engineering materials

Neutron scattering can provide information about the composition, phases, microstructure and stresses in materials in ambient conditions and as functions of different external parameters. Examples of applications in engineering materials science include alloy development, materials processing and joining technology. Unique insight can be gained into the characteristics and behaviour of realistic engineering components used in a host of contexts, from aircraft to power generation. Specific materials science diffraction methodologies (like SPEED, the structure pulsed concept; or CEED the extreme environment concept), imaging capabilities and small angle scattering instrumentation, will make possible *in situ* studies of joining, processing and deformation, as well as investigations of thermo-mechanical treatments, near-surface measurements of the effects of surface treatments and combined macro- and micro-structural studies of components and new materials.

Higher spatial resolution (down to the important sub-millimetre region) will enable further progress in monitoring residual stress, including at high pressure and high temperatures, and for detecting interfacial diffusion and reactions at interfaces in metals. High intensity will allow *in situ* real time experiments, routine determination of 3D maps of stress and texture within real engineering components; tomographic

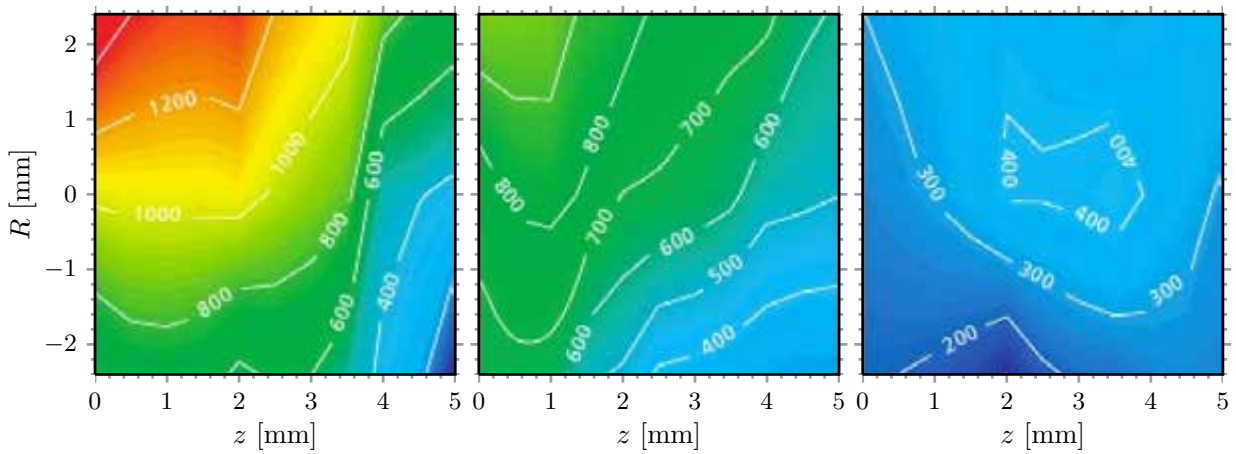

Figure 4: 2.14

Figure 2.14: Neutron diffraction results of the residual stresses (in MPa) in inertia welded turbine disks. Left: After initial welding. Middle, Right: After two different post-weld heat treatments leading to significant reduction in the residual stress.

images of machine parts under working conditions in real time and with structural sensitivity; and investigation of fast, time-dependent phenomena with isotope sensitivity. Many such investigations will be driven by technological demands for advanced materials, such as novel transformation-induced plasticity steels or precipitation-hardening alloys used in aerospace applications, such as aluminium and nickel super alloys. Instruments in the reference suite that offer the possibility to study magnetic phenomena of engineering relevance such as domain-structure design in transformer steels, include the **multi-purpose imaging** and **general-purpose polarized SANS** instruments. In many areas, engineering and energy materials applications overlap, including, for example, the study of materials used in turbines and cars, an area in which material optimisation could lead to higher efficiency and lower energy consumption. Figure 2.14 shows an example of an engineering science application in which neutron residual stress measurements have been performed in inertia-welded turbine discs. These measurements improve researchers' understanding of the stresses induced in manufacture, which could lead to improved fabrication processes.

Earth and environmental sciences

Neutron diffraction techniques are an important tool in geoscience research. They are used to make measurements of structural changes in minerals at very high pressures and temperatures; to assess the locations of light elements (in particular hydrogen) in complex structures; and to measure strain in polycrystalline aggregates under non-ambient (and extreme) conditions. ESS will provide advanced facilities for the study of structure-property relationships in mineral phases, as well as for the study of the structure, reactivity and physical properties of multi-component melts and fluids. The relevant instruments in the reference suite are the **thermal**, **bispectral** and **pulsed monochromatic powder diffractometers**. The **extreme conditions instrument** would make it possible to perform such studies under geological conditions with *in situ* measurements, while the **materials science and engineering diffractometer** would make possible highly detailed measurements of texture, anisotropy and stress in polymineralic rocks such as the gneiss shown in Figure 2.15, contributing to understanding the evolution of the Earth. Neutron spectroscopy can be employed to measure dynamic properties such as the small-scale mobility of water in a system, as would be possible using the **cold chopper**, **vibrational spectroscopy** and **backscattering spectrometers**, while neutron imaging permits characterisation of bulk samples or systems, including

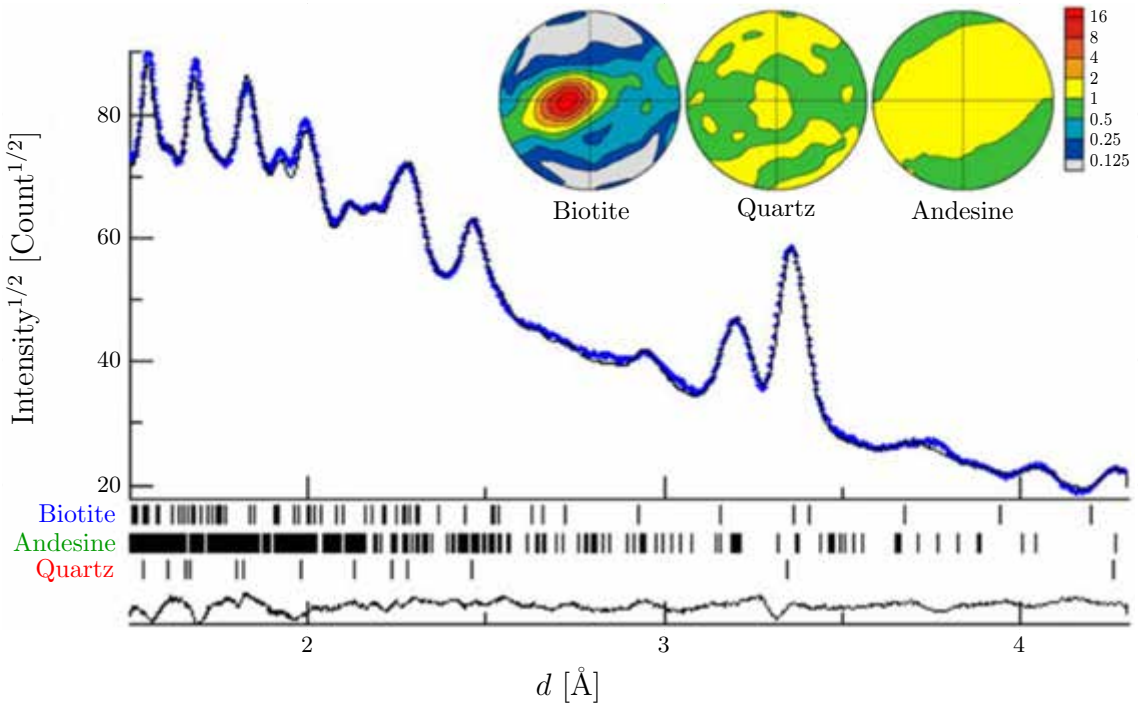

Figure 2.15: Neutron diffraction results and texture measurements of gneiss composed of quartz, feldspar (andesine), and mica (biotite) with the Rietveld method. Courtesy H.-R. Wenk [171].

Figure 6: 2.15

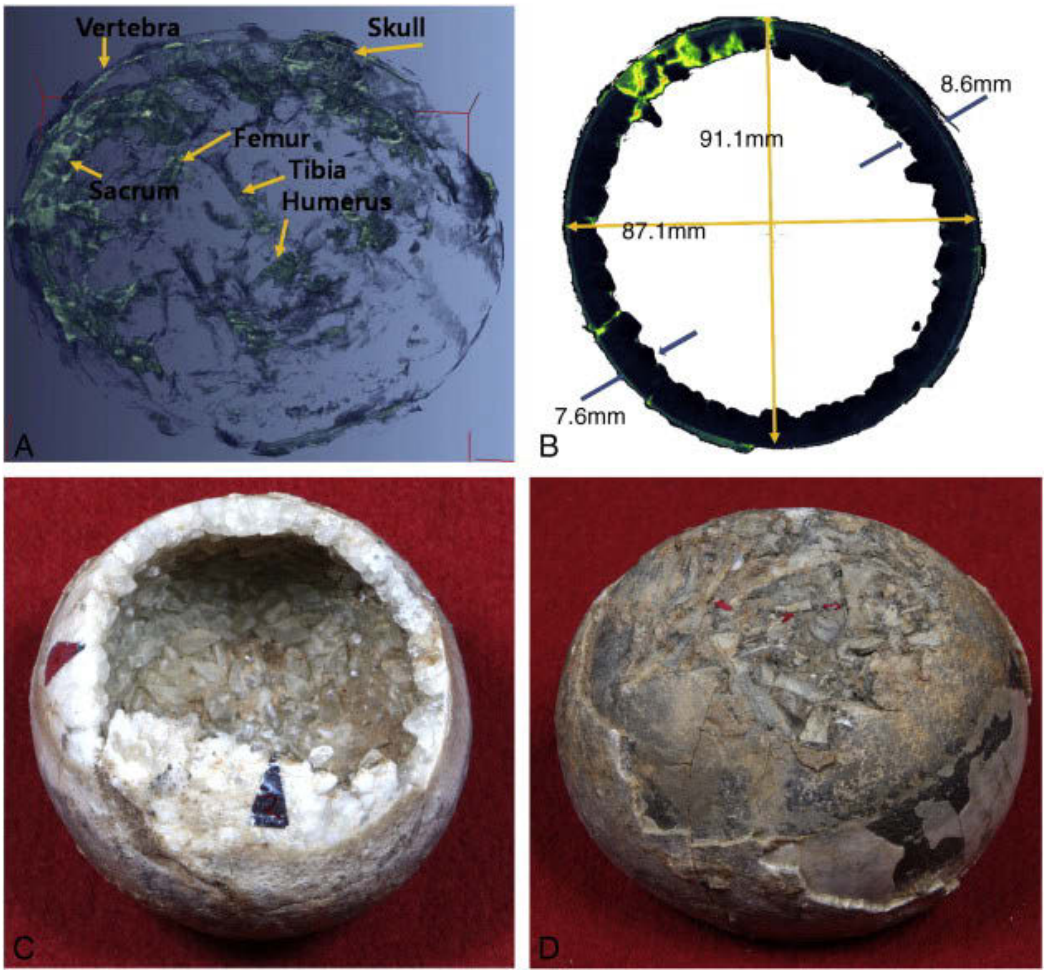

Figure 2.16: Top left: Neutron tomography scan of a titanosaur, showing a fairly articulated and complete embryo. Top right: The relatively small spherical egg ranges from 87.1 mm to 91.1 mm in diameter, with a maximum wall thickness, including the calcite crystal, of 8.6 mm. The embryo, visible here in a different colour in the top left quadrant, is preserved within the thin calcite layer. Bottom left: View of the inside of the egg with calcite crystals that grew inward from the egg outer rim. Bottom right: Part of the embryo skeleton surface where the eggshell was naturally eroded. Six arrows point to the skull, vertebrae, sacrum, humerus, femur, and tibia. Courtesy of Grellet and Tinner [172].

the movements of fluids and chemicals through them. The **multi-purpose imaging instrument** would make possible 4D studies with unprecedentedly high resolution of, for example, water transport in rocks and soils.

Imaging can also lead to new understanding of the evolution of life through 3D investigations of paleontological samples that are impenetrable by other non-destructive methods. In some cases, the contrast between fossilised material and the surrounding minerals, and thus the inner structure of fossils, can only be resolved by using the phase change of neutron waves. Figure 2.16 shows a complete and articulated specimen of a titanosaur embryo *in ovo*, which is the first of its kind yet discovered and is hence too valuable for destructive testing. Neutron tomography permitted full 3D imaging of the embryo that provided indisputable proof that lithostrotian titanosaurs were reproducing at the Aptian-Albian Algui Ulaan Tsav in Mongolia.

Information made available through neutron measurements can further fundamental understanding of the properties and processes in the Earth, and can further understanding of the origins of life. This information may be integrated into numerical simulations to clarify large-scale geologic phenomena such as deep-focus earthquakes and volcanic activity, or to may help to develop responses to important societal challenges, such as the transport and disposal of pollutants (for example, geologic carbon dioxide seques-

tration) or fluid movement with relevance in agriculture (for example, root growth and water uptake).

Paleoclimatology and climate change

Paleoclimatology is the study of climate over long periods of time. Core samples from ice sheets contain a wealth of information about past climate changes that could help to understand contemporary short- and long-term climate fluctuations, including global warming. Of particular interest in connection with neutron scattering is the analysis of proton ordering in ice. Proton disorder can provide evidence about an abundance of defects, and different defects give rise to different creep behaviour, with consequences for the modelling of ice sheet dynamics that play a key role in the analysis of global climate change. Whether ice can become partially proton ordered is subject to much debate. Neutron diffraction studies have played an important role in this debate (see, for example, the discussion in Fortes [173]). However, incoherent scattering from the hydrogen in ice limits standard neutron scattering investigations. The **pulsed monochromatic powder diffractometer** in the reference suite would overcome such issues by making possible time-of-flight measurements that would eliminate the dominant inelastic part of the incoherent scattering in ice cores and other hydrogenous materials.

2.2.7 Archaeology and heritage conservation

Archaeological and cultural artefacts are generally one-of-a-kind objects from which information about human origins and cultural heritage may be gained. It is essential to be able to study such irreplaceable objects non-destructively. A key strength of neutron techniques is the ability to probe internal composition and structure through coatings and layers of corrosion, reducing the need for potentially damaging cleaning and sample preparation. ESS will make important contributions in these fields though the development of instruments capable of assessing interconnections between macroscopic and microscopic structures, without damaging the sensitive samples. By exploiting the long pulse structure, simultaneous measurements that combine the strengths of diffraction, SANS and imaging will allow investigations of artefacts such as weapons and tools in three dimensions. These measurements will combine chemical and structural sensitivities related to phase and texture revealing historic manufacturing techniques and technological standards.

The ability of neutrons to non-destructively probe deeply into the interior of complex specimens is valuable for determining the composition and structure of precious archaeological and cultural artefacts. Neutrons penetrate coatings and layers of corrosion, reducing the need for potentially damaging cleaning or sample preparation [174–177]. Wide fields-of-view and deep penetration make neutrons useful for studying large artefacts. In addition, neutrons also have a special advantage in the investigation of wooden artefacts (for which the material contrasts produced using other techniques are often small), and in the investigation of artefacts containing both wood and other materials such as metal (in which the more absorbing material often impedes imaging of the wood). For example, Figure 2.17 illustrates the use of neutron imaging for a metal and wooden dagger sheath from Indonesia [1]. Neutron methods also contribute to understanding artistic, cultural and ancient manufacturing techniques and methods used to create historical artefacts. For example, an energy dispersive imaging approach allowed researchers to identify specific characteristics related to forging methods that were used by different schools and traditions in Japan, in the construction of Japanese swords from the Koto (987–1596) and Shinto (1596–1781) periods [178].

As it will do for the study of complex devices and processes for industry, ESS will develop instruments capable of assessing interconnections between macroscopic and microscopic structures and features without damaging sensitive samples that are of historical and cultural value. In such studies it will, for example, be possible to perform simultaneous measurements that combine the strengths of diffraction, SANS and imaging. The relevant instruments in the reference suite are the **thermal powder diffractometer**, **materials science and engineering diffractometer**, and the **general-purpose SANS** and **multi-purpose imaging instruments**. In addition, ESS will facilitate efficient time-of-flight tomographic investigations of metallic artefacts such as weapons and tools, with a chemical and structural sensitivity related to phase and texture.

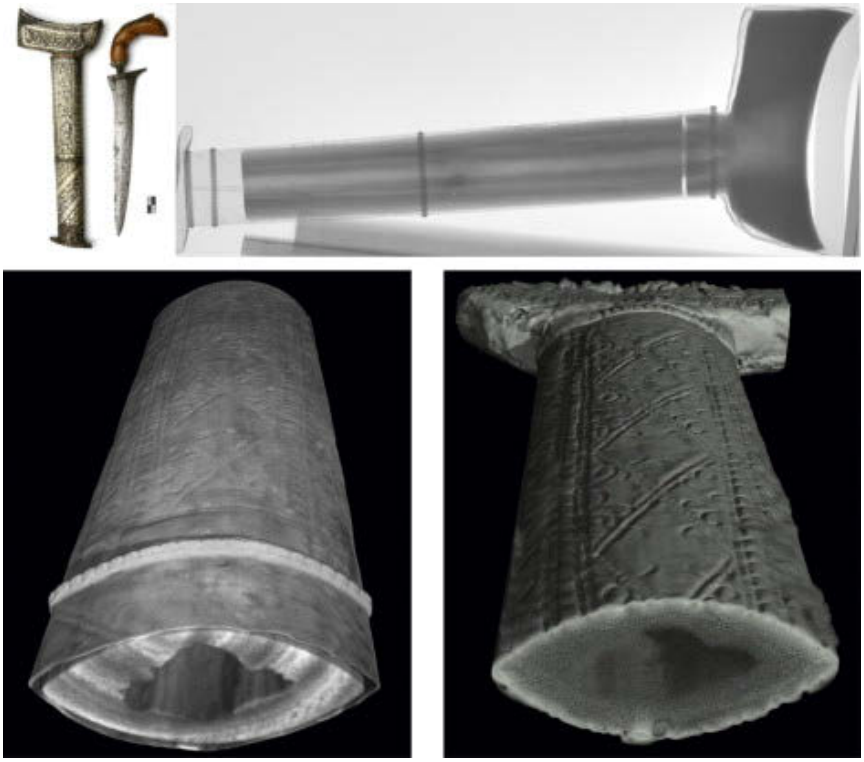

Figure 2.17: Non-destructive imaging of an Indonesian dagger sheath, illustrating how neutrons mitigate the obscuring effects of the out metal cover on images of the inner wood parts. Top left: A photograph of the dagger and the sheath, which has an outer metal cover (containing silver) and an inner wooden structure. Top right: A neutron transmission (radiography) image. Bottom left and right: 3D renderings of neutron and X-ray tomography data, respectively. Courtesy of E.H. Lehmann [1].

2.2.8 Fundamental and particle physics

Fundamental physics seeks to understand the "what" and the "how" of the universe. Even slight deviations from the predictions of the Standard Model, which embodies our current state of understanding of particle physics, would have important implications for both cosmology and particle physics. Fundamental neutron physics offers high precision tests of this model. High brightness and long pulses will allow a wide range of fundamental phenomena to be probed with sensitivity superior to that which is possible at present.

Fundamental physics currently stands at the interface of particle physics with nuclear physics, astrophysics, and cosmology, as illustrated in Figure 2.18. For three decades, the Standard Model of particle physics has successfully provided the framework for explaining phenomena involving three of the four known forces of nature. However, there exist many reasons to believe that the Standard Model is not the complete theory. Besides the high-energy frontier, there exists another frontier in the search for what is called the New Standard Model – the high precision frontier. The pattern of deviations (or their absence) that emerges from precision experiments is a "footprint" of new forces. The higher brightness and the pulse structure of ESS provide new possibilities for fundamental neutron physics experiments. It will be possible to investigate a wide range of fundamental phenomena with a sensitivity superior to that of previous experiments. A review of possible topics in which the gain factor over current facilities is expected to be large can be found in articles by Rathsman and Sand [180,181]. The fundamental physics science topics mentioned above are addressed by the **fundamental and particle physics beamline** in the reference suite.

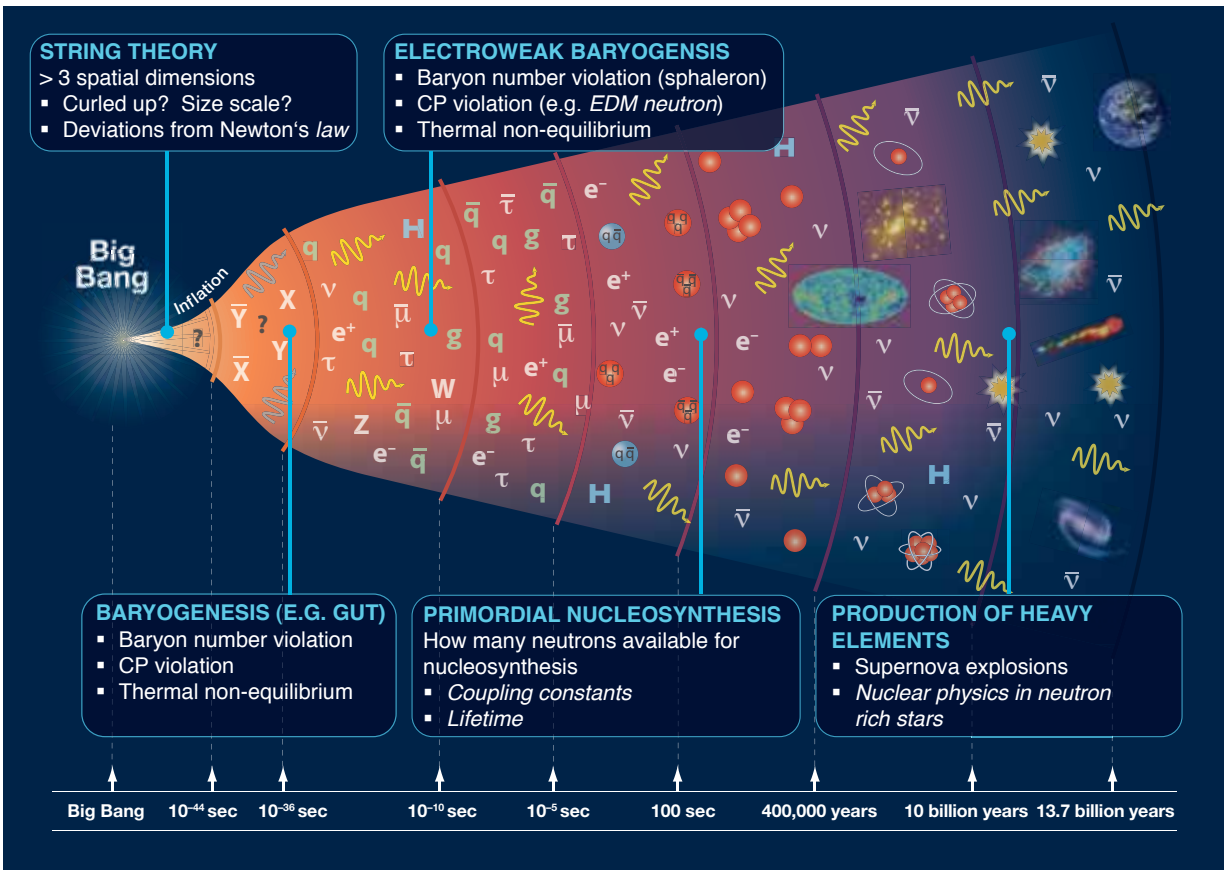

Figure 2.18: Illustration of the structure and development of the universe in space (vertical direction) and time (horizontal axis). The time axis is quasi-logarithmic. The diagram depicts the different phases of the universe corresponding to the Standard Model of cosmology. Many features are strongly model-based and lack experimental support. Also indicated is the role of measurements performed with neutrons and their impact on supporting the present conception. Courtesy of S. Paul [179].

Neutron electric dipole moment and the origin of matter

The search for the neutron electric dipole moment is motivated by one of the outstanding puzzles at the interface of particle physics with cosmology: Why is there more visible matter than antimatter in the universe? The observation of a non-zero electric dipole moment of the neutron could signal the presence of the CP-violating interactions needed to produce the early universe charge asymmetries [18,182]. CP violation is a violation of the postulated CP-symmetry – the combination of C-symmetry (charge conjugation symmetry between particles and anti-particles) and P-symmetry (parity symmetry between left and right). To date, only upper limits have been determined for the magnitude of the neutron electric dipole moment, and for the electric dipole moments of other systems, such as neutral atoms, from which it is possible to deduce an upper limit for the electron electric dipole moment. Since the origin of the CP-violation needed to explain the abundance of matter is not known, it is important to search for the electric dipole moments of a variety of systems. Consequently, the neutron electric dipole moment program should be viewed in the broader context of electric dipole moment searches as a whole. The current neutron electric dipole moment limit is, nevertheless, compatible with predictions of supersymmetry, in particular, "supersymmetric electroweak baryogenesis," under the right conditions for the superpartner spectrum. It would likely take future electric dipole moment searches with two orders of magnitude better sensitivity to conclusively test this possibility [182]. Experiments underway at ILL, PSI, and SNS are working toward this horizon. It may be that a future experiment at ESS, with its significantly higher neutron flux, could

push the neutron electric dipole moment program across the finish line in the search for cosmologically relevant CP-violation [183,184].

Neutron decay

The neutron decay physics programme is rich and includes precision tests of the Standard Model and the search for physics beyond the Standard Model. In contrast to the electric dipole moment experiments, precise studies of neutron decay parameters, such as the neutron lifetime and decay correlation coefficients, start off by measuring quantities that often are not suppressed in the Standard Model. In these cases, the goal is to look for extremely small deviations from the non-zero Standard Model predictions that could signal the presence of virtual new particles that were more active in the early universe. There is an interplay between the level of experimental uncertainty and the ability to make precise predictions from the Standard Model. To illustrate, consider tests of the unitarity of the Cabibbo-Kobayashi-Maskawa (CKM) matrix or "quark mixing matrix", for which super-allowed nuclear β-decay provides the most input in the guise of V_{ud}. V_{ud} is one of the elements of the CKM matrix, which is related to the probability that a down quark decays into an up quark via the weak interaction. Combining the results of an extensive programme of experimental lifetime, branching ratio, and Q-value measurements with recent progress in computing hadronic contributions to Standard Model electroweak radiative corrections, one obtains a value for V_{ud} with a precision of a few times 10^{-4} [18, 19]. Looking to the future, if progress is made in reducing the uncertainties associated with V_{ud}, the limit in CKM unitarity tests may again be set by V_{ud}. In this respect, a programme of neutron decay studies that include a more precise determination of the lifetime and one or more of the decay correlation coefficients, may provide a path forward [185]. The nuclear decay determinations of V_{ud} are likely to reach an irreducible uncertainty associated with nuclear structure corrections to the fit values. In addition, certain neutron decay correlations may provide information about new interactions that do not have pure left- or right-handed character or exotic particles such as leptoquarks.

Neutron-antineutron oscillations

An observation of neutron-antineutron oscillations would constitute a discovery of fundamental importance for particle physics and cosmology. The required change in baryon number by 2 units with no change in lepton number would signal physics beyond the Standard Model and could be relevant for understanding the matter-antimatter asymmetry of the universe. Recent developments in cold neutron technology may make possible improvements in sensitivity to the free neutron oscillation probability by factors of 100 to 1000. One might reduce the transverse size of the beam (and therefore the cost of an ESS experiment) using a phased supermirror reflector array. One issue that a search for neutron-antineutron oscillations addresses is the ultimate stability of matter. In the Standard Model, there seem to be two globally-conserved quantum numbers: baryon number B and lepton number L. Extensions to the Standard Model are not expected to conserve either B or L, however, and baryon number violation leads to matter instability – there is no longer an obvious physical principle that forbids nucleons from decaying into lighter particles. Proton decay has never been seen: typical upper limits for the proton decay time range from 10^{32} to 10^{33} years. If a neutron oscillates into an antineutron inside a nucleus, the antineutron annihilates and the nucleus explodes. Again, this phenomenon has never been observed [186]. Standard Model extensions can lead to B violation by 2 units and not 1 unit [187]. The improvements in sensitivity that could be reached by an ESS experiment would extend the proton decay time upper limit towards the 10^{36} year range. A null result would therefore place the most stringent existing limit on a possible decay mode for the "normal" matter whose mass dominates our everyday world.

The neutron as a quantum wave

As massive particles, neutrons exhibit all quantum effects and can be harnessed to yield new insight into the quantum world. Many neutron interference experiments have been performed with perfect crystal interferometers and various Larmor interferometer methods [188–190]. Since several interpretations of quantum physics are presently being considered [191,192], new experiments may determine whether a more complete theory exists or can be formulated in the future. Questions about reality, locality and causality can be tackled by neutron quantum optics methods. Experiments on entanglement, contextuality and

quantum states of neutrons in the gravitational field are interesting topics for related experiments at ESS. Many such experiments require ultra-cold neutrons, which can be efficiently produced at ESS.

Neutron bound beta decay

Neutron decay has been the subject of intense studies for many years, as it reveals detailed information about the structure of the weak interaction [193]. Using the two-body neutron β-decay into a hydrogen atom and an electron antineutrino, the hyperfine population of the emerging hydrogen atom can be investigated [194]. By investigating the spin states, beyond-Standard Model quantities can be accessed and tested [195–198].

2.3 Design drivers for the instrument suite

Based on the analysis of the science drivers in the preceding section, a number of key instrument themes have been identified, mapping the science drivers onto the inherent instrumentation advantages presented by the long-pulse concept:

1. **Flexibility.** Many of the problems that ESS will address require the measurement of structures or dynamics over several length or time scales. Being able to tailor the resolution and bandwidth of the measurement to the sample behaviour is key. The long-pulse concept is inherently advantageous for designing such flexibility into instrument performance. At long-pulse sources, the resolution is often set by controlling the opening time of a pulse-shaping chopper, instead of hard-wiring the resolution into the moderator line-shape as is done for instruments at a short-pulse source. The systematic use of repetition-rate multiplication and wavelength-frame multiplication allows the full time-frame to be used, while tailoring the bandwidth of the measurement to the requirements of each experiment.

2. **Small sample volumes.** ESS's high flux is well suited for accessing small sample volumes, particularly when combined with the latest advances in focusing optics. By designing instruments to probe smaller volumes than can be reached now, it will be possible to measure materials that are only available in small quantities, which is often the case for newly-developed materials and for biological and soft-matter systems for which the use of larger sample volumes can be prohibitively costly or time-consuming. The ability to investigate smaller volumes will also make it possible to scan for local variations across larger samples, for example when measuring systems under flow, and to reach more extreme conditions using complex sample environments, such as high pressure or high magnetic fields.

3. **Cold and bispectral neutron beams.** Cold neutrons are required to elucidate the structures and dynamics of biological and soft-matter systems, and of many types and aspects of hard condensed matter, as well. ESS's source brightness and time structure are particularly well suited to cold neutrons, providing high flux and a wide dynamic range. The dynamic range is especially important for hierarchical systems and other systems that need to be covered over multiple length or time scales. Instruments using a bispectral extraction system will be able to access an unprecedented dynamic range. The spectral brightness of thermal neutrons will also be world-leading.

4. **Polarised neutrons.** The inherent strengths of neutrons in being able to see hydrogen atoms and magnetism can be significantly enhanced by manipulating the neutron spin. This has applications throughout biology, soft matter, chemistry and physics. The use of polarised beams and polarisation analysis allows the unambiguous separation of structural, magnetic and incoherent scattering contributions. ESS's high brightness will greatly enhance the feasibility of this inherently flux-demanding technique.

Instruments optimised for a long-pulse neutron source are in many ways intermediate between those on a short-pulse source and those on a continuous source. Short-pulse instruments benefit from the high peak brightness of the short pulse, but are constrained by the need to match their requirements to the time-widths imposed by the choice of moderator. Time-of-flight instruments at continuous sources offer complete freedom to choose their time structures using chopper systems, but make it necessary to live with the inherently lower peak brightness imposed by their sources. A comparison of the peak brightnesses of

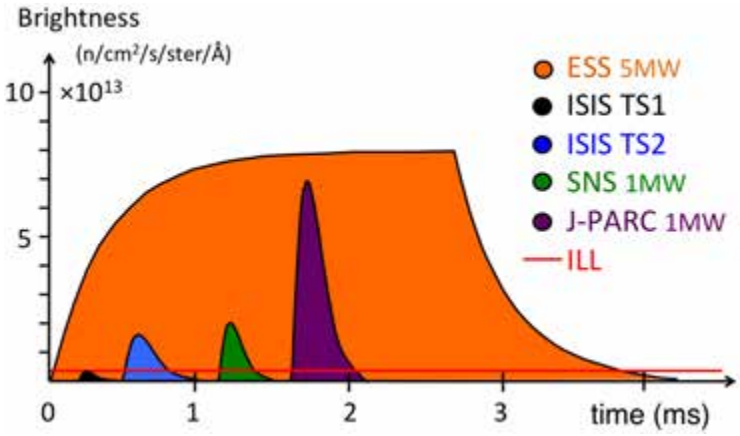

Figure 2.19: Single-pulse source brightness as a function of time at a wavelength of 5 Å at ESS, ILL, SNS, J-PARC and ISIS target stations 1 and 2. In each case, the cold moderator with the highest peak brightness is shown.

the world's leading neutron facilities is made in Figure 2.19. The peak brightness at ESS will be higher than that of any of the short pulse sources, and will be more than an order of magnitude higher than that of the world's leading continuous source. The time-integrated brightness at ESS will also be one to two orders of magnitude larger than is the case at today's leading pulsed sources.

The designs of instruments at ESS will be less limited by the time-structure of their long-pulse source than are instruments at short-pulse sources. They will benefit from a substantially higher peak brightness, combined with a time-average brightness which is much higher than that at any short-pulse source, while retaining much of the flexibility of continuous-source instruments.

Many of the instruments will be substantially longer than their counterparts at short-pulse sources. The underlying reason is the requirement for good wavelength resolution; the pulse length at the source represents the uncertainty in the emission time of the neutrons, which can be reduced compared to their time-of-flight by making the instrument longer. However, the instrument length also directly affects the bandwidth; that is, the longest wavelength that can be measured from a particular source pulse before it overlaps in time with the shortest wavelength emitted from the following pulse. Pulse-shaping choppers are an alternative method of improving wavelength resolution. Placed close to the source, they effectively reduce the pulse length, and hence the resolution, without making it necessary to increase instrument length. A large part of the optimisation of the instrument suite consists of balancing resolution and bandwidth considerations through appropriate combinations of instrument lengths and chopper systems.

2.3.1 White-beam instruments

The majority of the instruments at ESS will use a substantial part of the full white beam. Their bandwidth will be limited by their length and choice of pulse suppression, and it will be possible to tailor their resolution using a pulse-shaping chopper. They fall into two categories – large pulse width and small pulse width – depending on the required pulse width compared to the intrinsic length, $\tau = 2.86$ ms, of the neutron pulse.

Full pulse width $\simeq \tau$

SANS, spin-echo, macromolecular crystallography, and particle physics: There are seven instruments in this category in the ESS reference suite, all of which are well suited to the long-pulse time structure. They can use the full ESS pulse width and thus benefit from the high peak and time-average brightness. The ESS instruments will significantly outperform equivalent present-day instruments, due to the often unnecessarily good wavelength resolution of those instruments at contemporary short-pulse sources, and to the inherently lower peak brightness available to instruments at continuous sources.

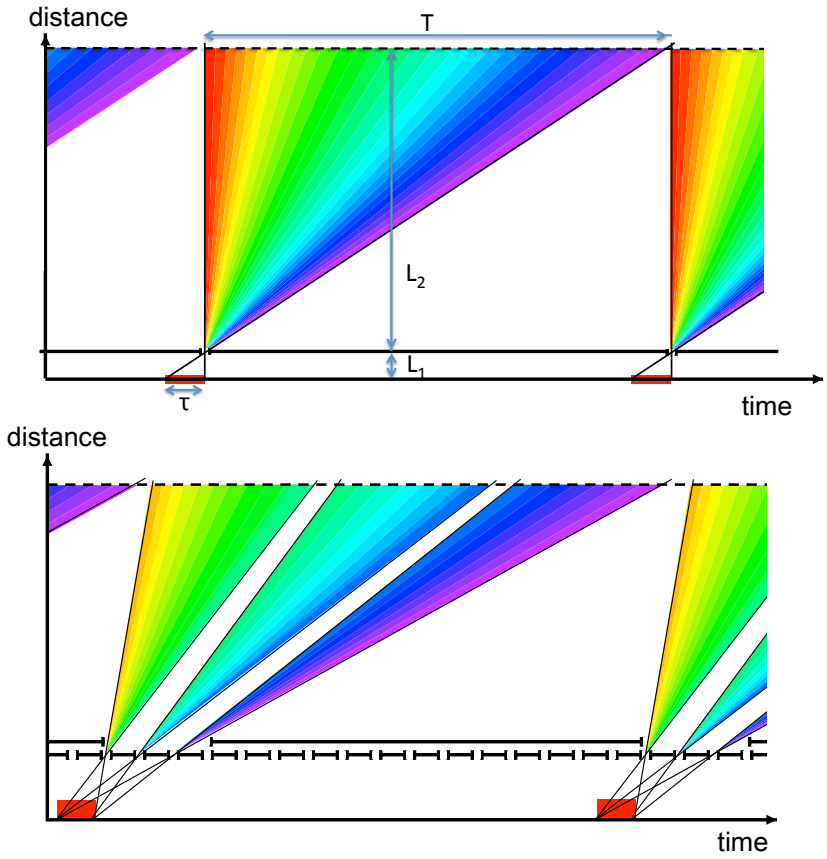

Figure 2.20: Time-distance diagrams for white-beam instruments. Top: An instrument with a pulse-shaping chopper, where τ and T are the source pulse width and repetition period, and L_1 and L_2 are the source-to-chopper and chopper-to-detector distances. The figure shows the "natural" length that fully fills the time frame without wavelength-frame multiplication for an instrument with a pulse-shaping chopper. Bottom: An instrument with a pulse-shaping chopper and triple wavelength-frame multiplication.

Flexible pulse width $< \tau$

Single-crystal and powder diffraction, crystal-analyser spectroscopy, reflectometers, backscattering, imaging: This will be the largest group of instruments at ESS, and so 11 of the 22 instruments selected for the reference suite fall into this category. These instruments employ a pulse-shaping chopper to reduce the length of the source pulse in order to achieve the required wavelength resolution. This makes them intrinsically very flexible, as it is possible to make them gain flux by relaxing resolution when appropriate. The pulse-shaping chopper is placed as close to the source as possible, which at ESS will be at the edge of the target monolith, at 6 m from the moderator. It can be seen from Figure 2.20 (top) that the pulse-shaping chopper, in addition to improving the resolution, also has the effect of reducing the bandwidth. When the instrument length after the chopper reaches 150 m, this bandwidth is sufficient to fill the full time frame (T) between adjacent pulses. The instrument length of 156 m is therefore considered the "natural" length for an instrument with a pulse-shaping chopper, which is achieved when $L_1/\tau = L_2/T$, where L_1 and L_2 are the source-to-chopper and chopper-to-detector distances, respectively. Instruments shorter than the natural length require wavelength-frame multiplication (WFM) in order to fill the time-frame, as shown in the bottom panel of Figure 2.20 for an instrument that is one third of the natural length. Detailed WFM calculations have demonstrated the feasibility of the method in simulations. Test experiments and prototyping are well under way at the time of writing.

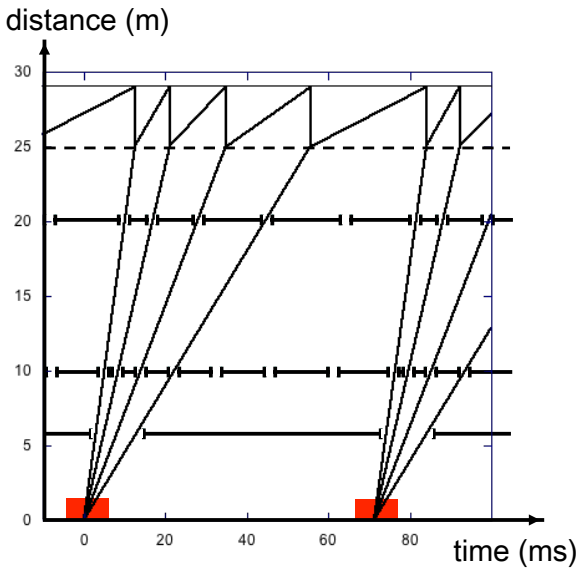

Figure 2.21: Time-distance diagram of a 25 m chopper spectrometer, using 4-fold repetition-rate multiplication (RRM) to cover incident energies from 1 to 20 meV in a single measurement.

2.3.2 Monochromatic instruments

There are three **chopper spectrometers** in the reference suite, ranging in length from 25 m to 156 m. These instruments will employ repetition-rate multiplication (RRM) in order to make full use of the long repetition period of ESS, as illustrated in Figure 2.21. The figure illustrates the need for using different frame lengths for each of the individual neutron energies selected in the incident beam. Several different chopper schemes for RRM have been identified that can achieve this effect, and whose study and optimisation are in process. In general, it is clear that both short and long instruments will be able to perform survey measurements using RRM, covering several orders of magnitude in energy scales in a single measurement, while the longer instruments will also be able to select smaller ranges of incident energy to provide very high counting rates over a smaller Q-energy area.

Only one instrument in the reference suite uses a **crystal monochromator**: The pulsed monochromatic powder diffractometer. This type of instrument is envisaged to function in a similar manner to analogous instruments at continuous sources. However, the ESS time structure allows several new modes of operation: Using the higher orders from the monochromator to provide separate data sets, similarly to what is done with RRM; separating elastic from incoherent-inelastic scattering from hydrogenous samples by time-of-flight; or performing ms-resolution stroboscopic or kinetic measurements which would make use of the very high flux on the sample for the duration of the pulse.

2.3.3 Neutron optics and transport

Considerable effort is going into the development of novel concepts for optimising the long-pulse performance, while ensuring the appropriate balance between novelty and low risk. Particular emphasis is being placed on studying chopper systems for RRM and WFM, as described in the previous two sub-sections, and also on optimising the performance of the many long guides which will be required. The work is still on-going, but it is already clear that the feasibility of transporting neutrons over very long distances is limited essentially by the cost of the guides and shielding, rather than by any fundamental or technical problem. Cold and thermal neutron guides on the order of 100 m already exist at today's reactor and spallation sources, and recent simulation work has shown that guides as long as 300 m can deliver almost perfect brightness transfer up to the sample for realistic beam divergences of both thermal and cold neutrons [199].

Many of the instruments employ an "eye-of-the-needle" concept for beam extraction, in which the relatively large area (12 cm $\times$ 12 cm) of the moderator is viewed through a small aperture at the edge of the target monolith 6 m away. When more divergence is required than such a setup can allow, a focusing

in-pile guide section is used, commonly referred to as a "feeder" section. There are several advantages to such a setup:

1. **Lower fast-neutron background.** The solid-angle acceptance for high-energy neutrons which might otherwise contribute to the background on the instrument is greatly reduced.

2. **Improved resolution and flux.** Instruments that use a pulse-shaping chopper should place it at the position of minimum beam size in order to reduce the sweep time across the beam, thus allowing shorter opening times, which in turn make it possible to reach higher resolution and allow for a more rectangular opening function, which provides a considerably higher flux than the typical triangular opening functions obtained when the sweep time is similar to the opening time.

3. **Improved Q-resolution and slow-neutron background.** By an appropriate choice of guide geometry, such as a single or two sequential ellipses, it is possible to image the beam profile and divergence at the target monolith exit on the sample. This results in a very uniform beam distribution at the sample, both in space and divergence, with clear benefits for Q-resolution. It also minimises the halo around the beam, which can be an additional source of background.

Further enhancement of the signal over noise will be achieved by designing-in suppression of fast neutrons and other sources of background, using a combination of shielding, heavy choppers and various types of kinked and curved guides. The count rates, spatial resolution, area coverage, efficiency and availability of neutron detectors are also the subject of intense study and R&D. Technical aspects associated with all the neutron technology components required for the various instruments are addressed in Section 2.7.

2.4 The reference instrument suite

A total of 22 public instruments will be built at ESS to serve the neutron user community, with the initial seven instruments coming online in 2019, and the full suite operational by 2025. To deliver the required instrument designs, around 40 instrument concepts are currently in various stages of design by ESS scientists and scientific partners around Europe. From among these concepts, a reference suite of 22 instruments has been assembled here to showcase ESS capabilities and to serve as a basis for the costing and planning of the facility. The selection of instruments in the reference suite focuses on the natural strengths of the long-pulse concept in order to maximise scientific output, while addressing a broad science base and employing state-of-the-art instrument techniques. The reference suite is not identical with the instruments that ultimately will be built.

Selection of instruments

The choice of instruments to build will take place as an ongoing process in which a number of concepts are selected every year, starting in 2013. This staged approach will allow ESS to remain engaged with the European neutron community and to choose instrument designs that are state-of-the-art and scientifically relevant when they enter user operation. As mentioned above, about 40 instrument concepts are currently under study. Other conceptual studies will be added as ideas and resources progress. As each conceptual study reaches a sufficient level of maturity, a proposal will be submitted for its construction. The proposals will be evaluated each year by review panels which will make recommendations for construction to ESS management. The evaluation criteria are scientific impact, user base and demand, instrument performance, strategy and uniqueness, technical maturity and costing. It is important to stress that the instruments that will be built have not yet been chosen. The reference suite described here does not, and cannot, represent the precise instrument suite that actually will be built, as the process for selection of instruments will run over several years and has only just begun.

Presentation of the reference suite

The instruments of the reference suite are presented in this and the following section. They can be categorised by instrument class, with the coverage of length- and time-scales accessed by each instrument class shown in Figure 2.1. A selection of the scientific areas addressed by the various instrument types is indicated in the plot, illustrating the mapping between scientific needs and instrumental capabilities. Also

shown are the analogous areas for selected complementary techniques, such as microscopy and synchrotron x-ray scattering.

Neutron imaging

Neutron imaging is a real-space technique examining the inner structure of potentially highly complex components by looking at the transmitted beam. The **multi-purpose imaging beamline** pushes spatial resolutions down to the micron range thanks to the high brightness of ESS, coupled with ongoing advances in detector technology. The pulsed nature of the source will give access to wavelength-resolved information, yielding a qualitative informational advance over the state-of-the-art today. The instrument offers its users a variety of imaging techniques for the characterisation of objects, covering cultural heritage, energy materials, magnetic phenomena and fuel cells as well as inspection of engineering components. Different imaging techniques, from traditional attenuation-based imaging to advanced dark field or Bragg edge imaging, are available with unprecedented efficiency and detail. The instrument concept takes full advantage of the flexibility made possible by the ESS time structure, allowing wavelength resolution, bandwidth and collimation to be tuned for each application.

Small angle neutron scattering

Small angle neutron scattering (SANS) provides access to the largest length scales possible with neutron scattering. SANS instruments are white-beam instruments requiring a large pulse-width, as described in Section 2.3.1, and so are perfectly adapted to the long-pulse ESS time structure. As an illustration, Figure 2.22 shows a comparison between a SANS instrument adapted to the ESS source and a present-day world-leading SANS instrument. Not only is the counting rate for the ESS instrument higher by an order of magnitude, but the Q-range covered in a single measurement is also an order of magnitude greater. There are three SANS instruments in the reference suite. The **general-purpose polarized SANS instrument** simultaneously covers the Q-range of current conventional SANS instruments, 10^{-3} Å^{-1} to 0.1 Å^{-1}, using multiple detector banks. It is particularly powerful when high resolution is needed, and for industrial processes requiring bulky sample environment. The instrument will have flexible resolution and bandwidth and will make available the option of reaching very low Q, possibly using specialised optics for accessing the very-small-angle regime. The **broadband small sample SANS instrument** is a shorter instrument and covers a very large Q-range in a single measurement. It is a lower-resolution instrument optimised for very high counting rates and smaller samples. The key science areas are in soft matter and

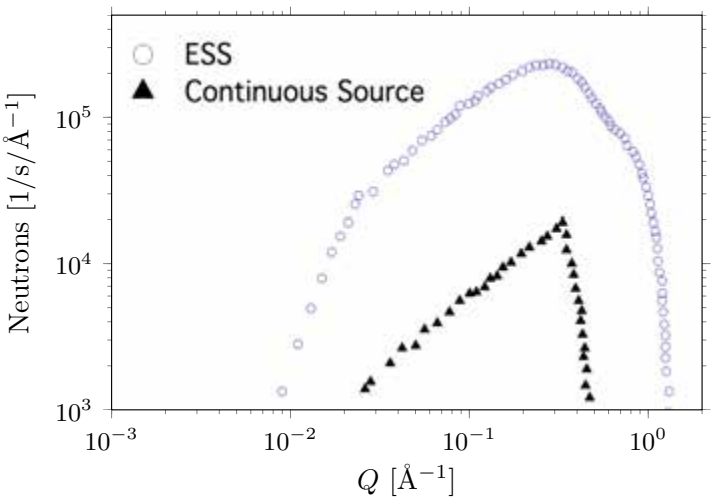

Figure 2.22: A comparison of the count rate obtained as a function of Q on a SANS instrument at ESS and on a world-leading SANS instrument at a continuous source. The curves were generated using simulations of isotropic scattering from 1 mm of water. Using the entire long pulse and cold spectrum, SANS at the ESS gains as neutrons of all wavelengths contribute to scattering at all Q values, whereas at a continuous source a narrow wavelength band must be selected using a velocity selector.

biology. The high counting rate will also make it a very powerful instrument for parametric studies, e.g. temperature, electric and magnetic fields, and pH. While the SANS community today is primarily focused on bulk samples, it is expected that the high source brightness of ESS will allow many of these studies to be extended to surface structures. The **surface scattering instrument** will probe the lateral topology of surfaces with a controlled penetration depth. By adjusting the incident angle of the beam, it will be possible to measure the structure of horizontal sample surfaces, opening grazing-incidence SANS to the study of free liquid interfaces, an area which is only just beginning to be explored at existing facilities.

Neutron reflectometry

Neutron reflectometry is used to probe the structure of surfaces and interfaces in the Å to micron range. The **horizontal reflectometer** uses an inclined beam to measure horizontal surfaces, particularly liquid-air interfaces, covering the full Q-range of interest without moving the sample. The instrument is optimised for very fast measurements with moderate resolution, with particular applications for kinetics of structural changes in biological systems and soft matter. The **vertical reflectometer** is a versatile instrument for measuring solid interfaces with high resolution and on small samples. It employs a novel double-elliptical mirror setup which allows flexible tailoring of the beam divergence to the resolution and background requirements of the samples. The beam size can be adapted to the measurement of mm-sized samples which are inaccessible on current instruments.

Powder diffraction

Powder diffraction is covered by five instruments in the reference suite. ESS's unique pulse structure makes possible a very wide dynamic range, while the inherent long-pulse flexibility allows the resolution to be tuned to the requirements of each experiment by adjusting the opening time of the pulse-shaping chopper. This capability is illustrated in Figure 2.23, which shows the resolution and intensity of a range

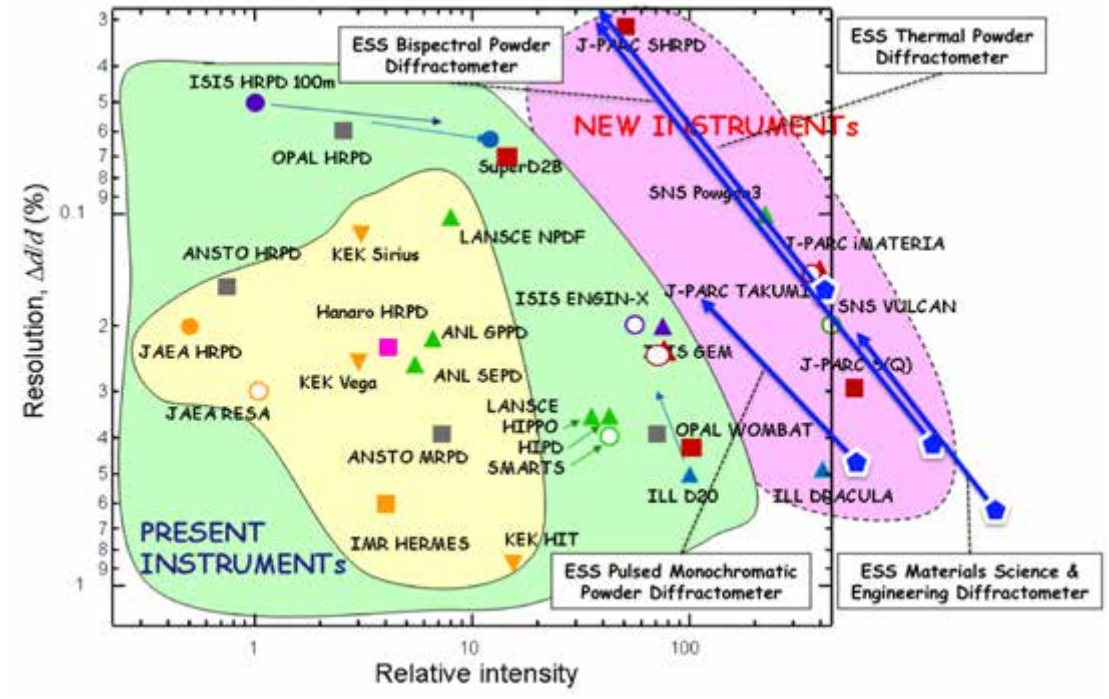

Figure 2.23: Performance of powder diffractometers at leading large-scale facilities (adapted from Kamiyama [200]) with the expected performance of reference suite diffractometers marked as blue pentagons with extended arrows to illustrate the count rate/resolution flexibility afforded by tuning the pulse width for the time-of-flight diffractometers, or the monochromator takeoff angle for the pulsed monochromatic diffractometer. The instruments in the area labelled "New Instruments" are currently in various stages of commissioning and have not yet reached the performance shown here.

of neutron powder diffractometers at leading large-scale facilities around the world. The performance of current instruments and their specialisation for high flux or high resolution are shown by various symbols, while continuous lines show how instrument performance can be selected depending on the needs of the experiment, for four of the five powder diffractometers in the reference suite. (The extreme conditions instrument is not shown.) The reference suite instruments match the projected best performance of today's new instruments, though there are limitations in comparison to short-pulse sources at large Q, which do not appear in such a figure.

The **thermal powder diffractometer** covers the core crystallography and *in situ* processing science case for thermal neutrons up to a Q_{max} of around 25 Å^{-1}. The pulse-shaping chopper allows the wavelength resolution to be matched to experimental requirements over a very wide range, in the best case achieving a resolution of $< 0.01\%$. The **bispectral powder diffractometer** can access longer wavelengths and hence, larger d-spacings in backscattering. It is well suited for powder magnetic structure determination, larger unit cell powder crystallography and *in situ* experiments in the intermediate Q range ($Q_{max} <$ 13 Å^{-1}). The **pulsed monochromatic powder diffractometer** is a high-throughput instrument for *in situ* chemical processing, crystallography, pole figures, high time-resolution kinetics and hydrogen-containing materials, with the option for variable resolution inelastic scattering mapping. It uses a set of crystal monochromators with access to a wide range of takeoff angles to tune the accessible Q range, flux and instrument resolution. The **materials science & engineering diffractometer** allows users to study mechanical and micro-structural properties, texture, phase transformations and kinetics in engineering and functional/smart materials. Dedicated sample environments allow a wide range of conditions to be probed. Structural studies include the determination of residual stresses in engineering materials and components, an important area in welding and joining R&D. The **extreme conditions instrument** is built around bulky, complex sample environments (high pressure, high magnetic field) and the limitations that imposes on detector coverage and geometry. It is a multi-role instrument to perform diffraction, spectroscopy, SANS and imaging experiments. For all the diffraction instruments, the resolution and bandwidth can be tailored to each application.

Single-crystal diffraction

Single-crystal diffraction is required for solving complex or large unit cell structures and profits largely from the the ESS long pulse structure. The **single-crystal magnetism diffractometer** has a polarised incoming beam with optional full polarisation analysis. It is optimised for the determination of complex magnetic structures, spin density distributions, local susceptibility measurements and diffuse scattering. The **macromolecular diffractometer** is dedicated to biological crystallography and is optimised for sub-millimetre single-crystal samples with large unit cells. The flux increase made possible by the use of the full pulse allows the study of systems such as membrane proteins which currently cannot be addressed with neutrons. The objective is to bring neutrons into the mainstream of protein crystallography, currently addressed almost exclusively by synchrotron light sources.

Time-of-flight and crystal spectroscopy

Time-of-flight and crystal spectroscopy is carried out by two types of instruments: Chopper spectrometers and crystal-analyser instruments. There are three chopper spectrometers in the reference suite which are designed for optimised RRM for all experiments, as described in Section 2.3.2, using sophisticated multiplexing chopper systems. The range of incident energies for these types of instruments will be adapted to the range of time scales that need to be covered, while the spacing between adjacent incident energies will be adjusted to cover the width of the inelastic scattering. Due to the very high ESS peak brightness, the flux of each individual wavelength frame incident on the sample will be significantly higher than on today's world-leading chopper spectrometers. The additional pulses arising from the RRM system will bring the total flux on the sample up to more than an order of magnitude greater than what is possible today while simultaneously probing a far larger dynamic range in both Q and energy. The **cold chopper spectrometer** is specialised for cold neutrons and the measurement of single-crystal samples. It is optimised for low background and high resolution and is thus ideally suited for probing weak signals and collective excitations. The **bispectral chopper spectrometer** provides a one-shot measuring technique for covering dynamics over a very wide simultaneous energy range of $0.1 - 100$ meV. It is a wide-mapping instrument optimised for quasi-elastic scattering on small samples, allowing more than three orders of magnitude in fluctuation

times to be covered in a single measurement. The **thermal chopper spectrometer** is a high-resolution, narrow-bandwidth instrument for fast dynamics. It allows incident energies up to 150 meV with flexible resolution both in energy and Q. The beam optics are tunable, allowing efficient focusing for small samples as well high Q-resolution single-crystal measurements. The **cold crystal-analyser spectrometer** uses graphite crystals to cover a quasi-continuous range of scattering angles in the horizontal plane. This a high-flux instrument, particularly well suited for measuring samples in constrained horizontal geometries that are imposed by high-field or high-pressure sample environment. The **instrument for vibrational spectroscopy** will have variable resolution to allow measurements up to 300 meV, with a variable energy resolution down to 2% with very little energy-dependence. The instrument characteristics are well suited to the mapping of molecular vibrational modes and collective excitations of hydrogenated materials in heterogeneous catalysis, energy storage systems and hydrogen-bonded scaffolds in pharmaceuticals.

Backscattering

The **backscattering spectrometer** provides access to a unique combination of high energy resolution, intermediate Q, and large dynamic range. It uses Si 111 and Si 311 analyser crystals arranged in near-backscattering geometry, and the flexible chopper cascade is matched to the source time structure to allow a continuous variation of the energy resolution between 2 μeV and 300 μeV together with a variable dynamic range down to about 1 meV. ESS's low repetition rate provides the instrument with an unparallelled dynamic range that is perfectly suited for studies of localised relaxational atomic motions with overlapping collective long-range motions, as well as quantum-mechanical tunnelling. It addresses all disciplines of condensed matter from physics to chemistry and biology via soft matter and energy materials.

Spin-echo spectroscopy

Spin-echo spectroscopy reaches the longest time scales accessible with neutrons, allowing the measurement of polymer and protein dynamics, membrane fluctuations, confined liquids, micro-emulsions and magnetism. This type of instrument will accept the full pulse width of ESS, giving rise to a very large improvement in performance compared to the best instruments available today. The **high-resolution spin echo spectrometer** provides the highest energy resolution available in the reference suite. It measures dynamics, predominantly of large-scale structures, with fluctuation times of up to 1 μs, covering a dynamic range of six decades. The **wide-angle spin echo spectrometer** provides the bridge in fluctuation times between the backscattering and cold chopper spectrometers at one end, and high-resolution spin-echo spectrometers at the other. By covering a large range of Q, it is able to probe nanosecond fluctuations over many length-scales simultaneously, while the large solid-angle coverage of the analysers and detectors provides a counting rate two orders of magnitude higher than any comparable instrument today.

Particle physics

Particle physics is covered by the **fundamental and particle physics beamline**, which addresses precision tests of the Standard Model, and searches for new interactions and symmetries. The range of Standard Model tests and searches that such a beamline could competitively address is wide. Therefore, the instrument is designed to be highly configurable, analogous to similar beamlines at current sources.

2.4.1 A balanced reference suite

Table 2.1 provides an overview of the reference suite instruments, including instrument lengths and the main science drivers relevant to each instrument. The reference suite has been chosen to cover a broad range of science, as well as a broad range of instrument types and degrees of specialisation and complexity. Some instruments have a narrowly focused science case, while others address a diverse user community. Some are workhorse instruments, which will have very high throughput and a limited degree of configurability, while others will need to be configured specifically for each experiment, requiring strong scientific collaborations between users and ESS scientific staff. In all cases, the instruments will be accessible by both non-expert and expert users, placing strong requirements on beam access, staff quality and software.

Instrument length is a key performance driver, determining constraints on bandwidth and resolution. It also drives the instrument layout on the ESS site, which is shown in Figure 2.24 at the beginning of Section 2.5. Due to the design of the moderator-reflector assembly and the beam extraction within the

Instrument name	**Moderator to sample distance** [m]	**Sample to detectors distance** [m]	**Science drivers**
Multi-purpose imaging	50	10	LIF, SOF, MAG, ENG
General-purpose polarized SANS	30	20	MAG, SOF, CHE, NRG
Broadband small sample SANS	20	10	SOF, LIF
Surface scattering	30	15	SOF, LIF, CHE, MAG
Horizontal reflectometer	27	3	SOF, LIF, CHE
Vertical reflectometer	52	6	MAG, CHE, NRG, SOF
Thermal powder diffractometer	156	2	CHE, NRG, ENG, MAG
Bispectral powder diffractometer	75	1.5	MAG, CHE, NRG, ENG
Pulsed monochromatic powder diffractometer	46+4	2.5	CHE, NRG, MAG
Materials science & engineering diffractometer	156	2	ENG, CHE
Extreme conditions instrument	156	4	ENG, MAG, CHE
Single-crystal magnetism diffractometer	156	1	MAG, CHE
Macromolecular diffractometer	156	1	LIF
Cold chopper spectrometer	156	4	LIF, CHE, MAG
Bispectral chopper spectrometer	25	4	LIF, SOF, CHE, MAG
Thermal chopper spectrometer	156	6	CHE, NRG, MAG
Cold crystal-analyser spectrometer	156	3	CHE, NRG, MAG, ENG
Vibrational spectroscopy	60	1	CHE, NRG, MAG
Backscattering spectrometer	156	5	LIF, SOF, CHE
High-resolution spin echo	30	5	LIF, SOF, CHE, NRG
Wide-angle spin echo	50	3.5	NRG, MAG, LIF, SOF
Fundamental & particle physics	70	30	FUN

Table 2.1: Instrument names and lengths, as shown in Figure 2.24. For the *pulsed monochromatic powder diffractometer*, the first distance is shown as a two-term sum, indicating the distance from the moderator to the monochromator and then to the sample. The science drivers for each instrument are listed in order of decreasing importance. The acronyms are as follows. LIF: Life science, SOF: Soft condensed matter, CHE: Chemistry of materials, NRG: Energy research, MAG: Magnetism and superconductivity, ENG: Engineering materials and geosciences, ARC: Archaeology and heritage conservation, FUN: Fundamental and particle physics.

target monolith, all beamlines have the freedom to view either a cold or a thermal source, or a combination of the two. All beamlines also will view roughly the same time structure, as the long-pulse time structure of the proton beam means that there is no need for decoupled or poisoned moderators, such as are used at short-pulse sources. The choice of beam port for each instrument is therefore primarily driven by operational convenience and the desire to save cost, with little or no compromise on performance.

The nine instruments in the reference suite which are 156 m long are housed together in the west experimental hall, where they can comfortably be accommodated next to each other with 5° of beamline separation. Instruments between 50 m and 80 m long are in the south experimental hall, while the short ($<$ 50m) instruments are arranged in two sectors – one each in the north and east experimental halls – that are adjacent to the incoming proton beam, where the fast-neutron background is expected to be the lowest. The distribution of instruments in the north and east halls has been determined first by the need to allow them sufficient lateral space for shielding and convenient operation (as has been done for all the instruments), and then by the need to separate the spin-echo spectrometers from instruments that are likely to need large superconducting magnets for their sample environment. The floor of the hall in the north sector, where the spin-echo and non-magnetic instruments are housed, has also been made 1 m lower than that of the other halls, in order to provide a magnetically cleaner environment for the spin-echo instruments. The grey area around the target monolith in Figure 2.24 shows the common bunker in which the first sections of the guides outside the target monolith are housed. This allows for an effective shielding assembly enclosing the guides, choppers and optical elements near the monolith.

2.5 Catalogue: The reference suite

This catalogue presents the 22-instrument reference suite. Its layout is shown in Figure 2.24, while the instrument names and lengths are summarised in Table 2.1. The reference suite has been assembled to showcase the scientific and technical capabilities that ESS is expected to have, and also to provide a basis for costing and planning the facility. It does not represent the precise instrument suite that will actually be built, since the process of choosing those instruments has only just started at the time of writing and will continue until 2020. The reference instrument suite is discussed at length in Section 2.4.

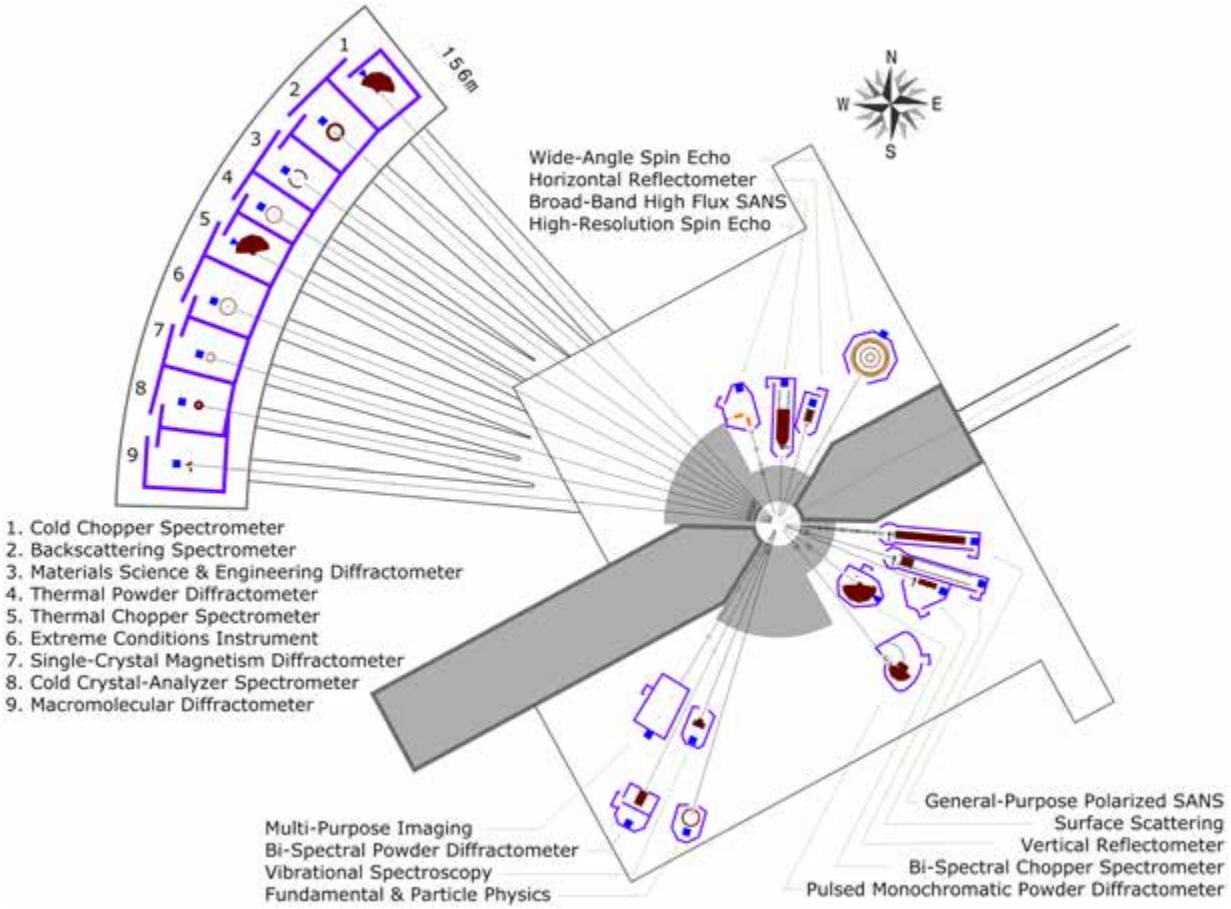

Figure 2.24: Neutron beamline and instrument layout of the reference instrument suite.

Multi-Purpose Imaging

Multi-Purpose Imaging

Fuel cells
Battery materials
Nano-composite materials
Engineering materials
Macroscopic magnetism
Biological organisms
Food science
Geosciences
Archeology
Heritage conservation

A unique instrument that combines imaging with reciprocal space techniques in a novel way. It represents a versatile instrument concept using high-resolution attenuation-based imaging as well as time-of-flight neutron imaging techniques with novel capabilities based on spatially resolved scattering effects. The variable choice of wavelength resolutions between 0.3% and 10% over tunable wavelength bands combined with polarization analysis opens up the possibility of highly efficient polarized-neutron and Bragg-diffraction imaging as well as dark-field imaging options. The instrument is also capable of spatially resolved SANS investigations.

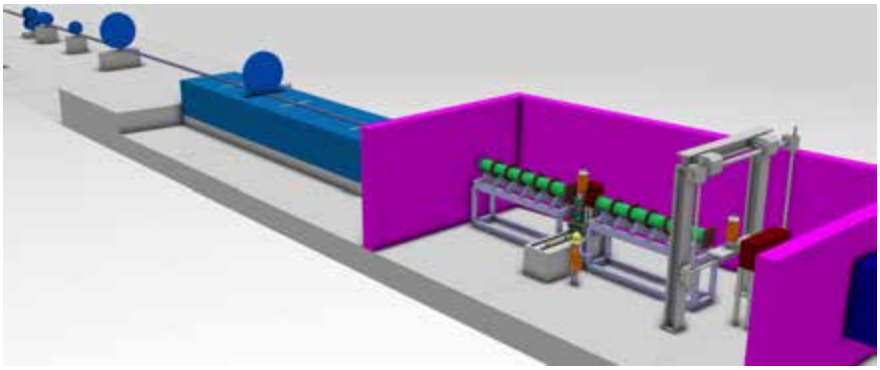

Instrument Description

The unique source characteristics of ESS allow the instrument to be optimized for a large variety of neutron imaging techniques with high efficiency. The high source brightness, a bi-spectral extraction and an optimized neutron guide system enable not only high resolution and high-speed attenuation contrast imaging, but also permit the user to take advantage of corresponding energy-selective measurements increasing e.g. sensitivity. The length of the instrument, chosen to 60 m to the detector, provides sufficient wavelength resolution for efficient time-of-flight dark-field contrast imaging. This corresponds to measuring small-angle scattering where the spatial resolution is determined by beam modulation techniques. Other imaging modes profit from the potential to tune the time-of-flight resolution from 1% down to 0.3% with a wavelength frame multiplication chopper system. It features an optically blind, pulse shaping, double chopper system. In this system the variable distance of the disks, operated such that the closing of the first disk coincides with the opening of the second disk, defines the wavelength resolution at the detector. Both the separation of the wavelength frames (bands) as well as the choice of the wavelength band with or without pulse suppression require additional choppers. The corresponding wavelength resolution provides efficient polarized neutron imaging or Bragg edge studies. The prompt pulse background is avoided by a T_0 chopper at 9m from the moderator.

Polarized neutron imaging is based on keeping track of the neutron polarization as it passes through a magnetic field, and can be used for quantitative investigations of magnetic fields and structures with spatial resolution. Bragg edges are steps in the transmitted total cross section deriving from coherent elastic (Bragg) scattering. Measuring the Bragg edge pattern in the transmitted spectrum with 1% and 0.3% wavelength resolution can be utilised to map crystalline phases or texture and lattice strains, somewhat akin to conventional diffraction.

The integrated flux and beam homogeneity, e.g. for white beam imaging, is comparable to the source brightness at the highest flux continuous sources. Consequently this can provide orders of magnitude gains for all wavelength-resolved techniques when compared to the most productive and world-leading imaging facilities today. Just as in conventional imaging instruments, a variable pinhole D at a variable distance L (up to 13m) upstream, combined with a variable detector systems allows the tailoring of the collimation ratio L/D to the spatial resolution and flux requirements of specific measurements. At a typical L/D ratio of 500, the flux using the full pulse will be approximately 10^8n/cm^2/s, and when shaping the pulse to achieve a wavelength resolution of 1%, the instrument will deliver a flux of the order of 10^7n/cm^2/s at the sample position, outperforming currently world-leading instruments by orders of magnitude.

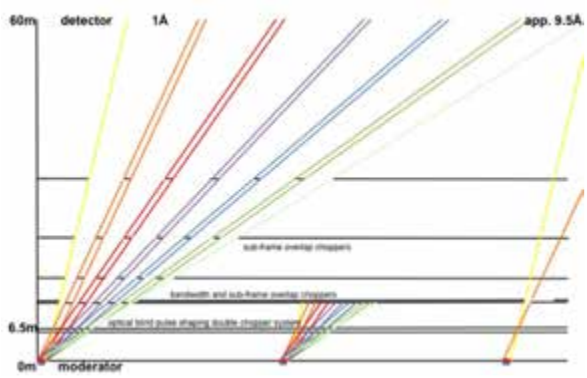

A comprehensive wavelength frame multiplication chopper system allows to tune the wavelength resolution and to suppress every other pulse if required to enable a large variety of measurements with maximum efficiency.

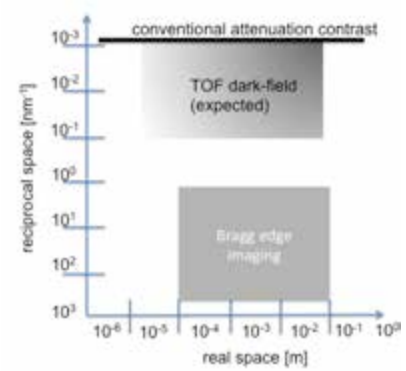

Novel TOF imaging methods like Bragg edge and dark-field imaging allow for extending the range of applications significantly and into Q-space, i.e. beyond direct spatial resolution.

Instrument Parameters	
Moderator	cold/thermal bispectral extraction
Moderator to sample distance	variable: 50-60m
Methods and Add-Ons	White beam attenuation, Bragg edge transmission Dark-Field Imaging (add-on), Polarization Analysis
Mode 1: Bandwidth	4.8Å/10Å(at 14Hz/7Hz depending on pulse suppression)
Mode 1: Wavelength range	1-20Å
Mode 1: Wavelength Res.	<10%
Mode 2: Bandwidth	4.6Å/9.6Å (at 14Hz/7Hz)
Mode 2: Wavelength range	1-9.6Å
Mode 2: Wavelength Res.	0.3% -1%
Collimation ratios L/D	40-4000
Max Field of view	25×25cm^2

General-Purpose Polarized SANS

General-Purpose Polarized SANS

Polymers
Magnetic Nanoparticles
Superconductivity
Nano-composite materials
In-situ processing
Drug delivery systems
Gas storage materials
Engineering materials

This SANS instrument incorporates a very flexible sample space, flexible optics, a polarized neutron beam and polarization analysis.

The length of the instrument means that it will have good Q resolution across the whole Q range enabling the study of materials with correlated structures such as concentrated colloids. Combining the good resolution with polarized neutrons and space for magnets will make this instrument particularly well suited to hard condensed matter studies such as flux line lattice measurements.

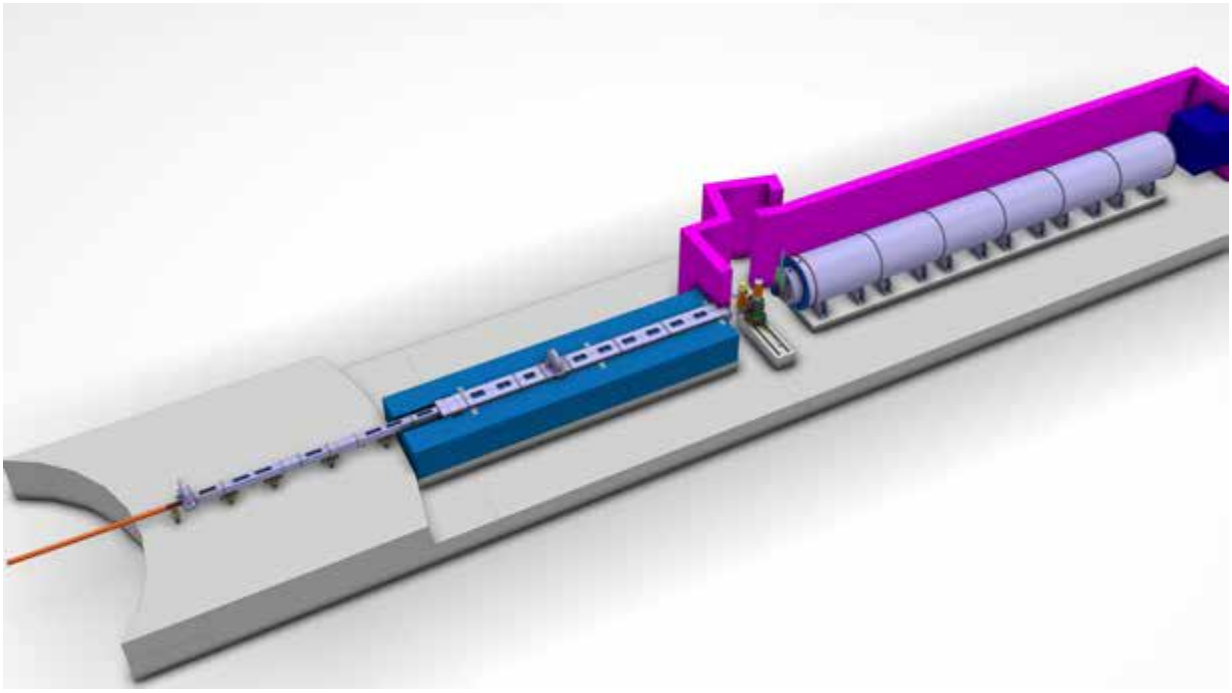

Instrument Description

The instrument begins 2m from the moderator with a 5 m long curved guide with a radius of curvature of 200 m. This is followed by a 1m polarizing cavity and space for a spin flipper. The first collimation section of 8 m contains removable guide sections and is narrow to fit into the space available and allow for the necessary shielding. The second collimation section of 12 m is wider, allowing space for installation of optical components in addition to guides such as focussing optics for accessing even lower Q, or spin-echo modulation coils.

Bandwidth selection and frame-overlap suppression is achieved by a series choppers which will also allow for operation of the instrument at 7 Hz, thus doubling the available bandwidth from 6 Å to 12 Å

The sample position can accommodate equipment with a footprint of up to 2.5 m $\times$ 2.5 m allowing the use of large cryo-magnets, industrial processing equipment and ^{3}He polarisation analysis cells.

The detectors are arranged with a front "picture frame" detector of 2 m $\times$ 2 m and a rear high resolution area detector, both on moveable carriages. The use of multiple detector banks provides good simultaneous Q range and their movability allows optimised use of the good Q resolution of this instrument.

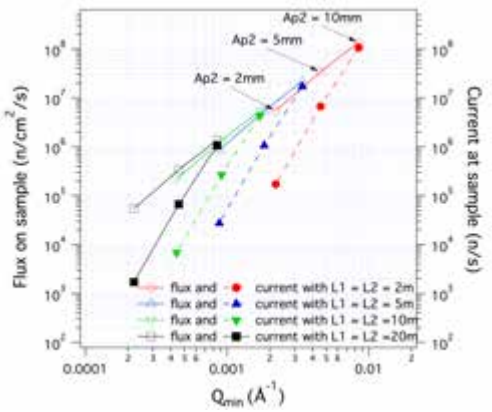

Estimated neutron flux and current at the sample position as a function of collimation length, beam size at sample (Ap2) and minimum accessible Q.

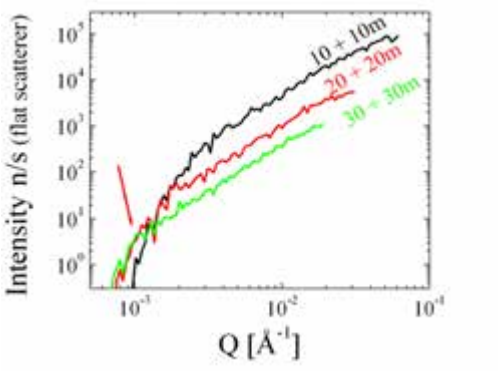

Optimisation of instrument length using a flat scatterer. A 20 m collimation length provides the best balance of flux and minimum Q.

Through the use of a polarised neutron beam and a ^{3}He analyser after the sample, it is possible to separate the magnetic scattering from the nuclear scattering and furthermore to analyse the magnetic scattering parallel and perpendicular to the applied field. This allows studies such as shown here examining the magnetic structure of magnetite nanoparticles [201]. A core-shell magnetic structure was determined (green fit in figure), with canted spins at the surface, despite the nanoparticles being chemically uniform. The *General-Purpose Polarized SANS* instrument, having high flux and good Q resolution, will be especially well suited to this type of study, which is often flux limited.

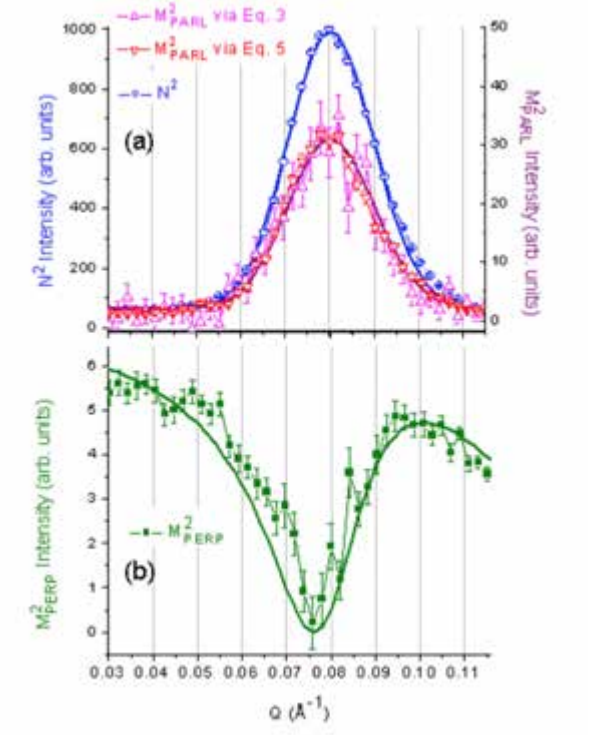

Instrument Parameters	
Moderator	Cold
Moderator - Sample distance	30 m
Wavelength Range	4 to 10 Å at 14 Hz 4 to 16 Å at 7 Hz
Wavelength Resolution	4% at 6Å and L2 = 20 m
Max Simultaneous Q-range	$1.5 \times 10^{-4} < Q < 1$Å^{-1} @ 7Hz with 2mm sample $9 \times 10^{-4} < Q < 1$Å^{-1} @ 14Hz with 10mm sample
Sample to Detector distance	Variable 2m to 20m
Detectors	Front: 3.5 m^2 of 8 mm pitch detectors Rear: 1 m^2 of 2 mm pitch detectors

Broad-Band Small Sample SANS

Broad-Band Small Sample SANS

Self-assembled colloids
Solutions of macromolecules
Biological membrane assemblies
Materials under flow
Nano-composite materials
Food science
Environmental chemistry
Engineering materials

This instrument provides a broad simultaneous Q range, up to 4 orders of magnitude, which is particularly useful for kinetics measurements and small sample volumes.

This is a short SANS instrument with the sample only 20 m from the source. It will therefore have a broad wavelength band allowing access to a wide simultaneous Q range. The instrument will enable single pulse scattering measurements on strongly scattering samples of around 5 mm x 5 mm. It will also be suitable for the use of sample beam sizes, around 1 mm in diameter, enabling measurements on small volume samples and on small areas of larger samples. The instrument will be equipped with a variety of soft matter sample environment including flow-through cells for biological solution scattering.

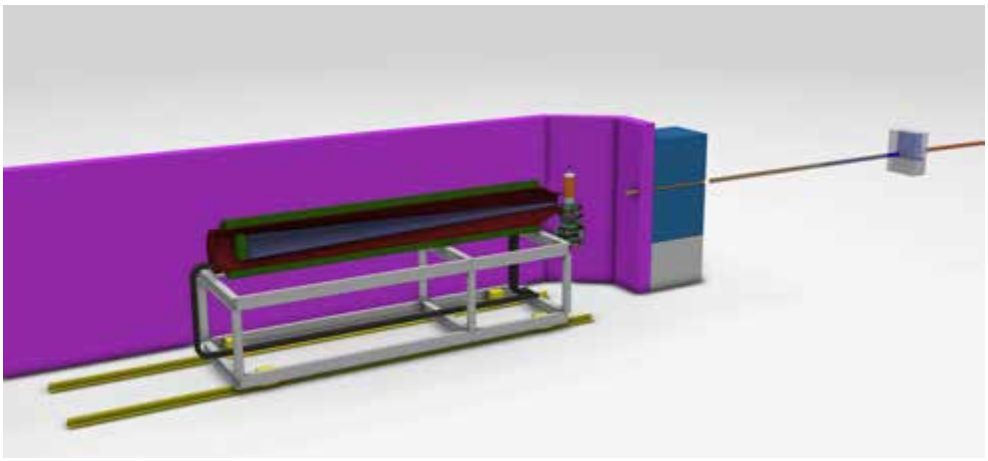

Instrument Description

The primary flight path of the instrument begins at 2m from the moderator with a multi-channel bender. The bender is optimised for transfer of neutrons above 3 Å and rejection of short wavelengths whilst ensuring that line-of-sight from the source is closed before the start of the collimation section of the instrument. Wavelength band selection is performed by a frame-overlap mirror and a chopper. The instrument can operate in its highest flux mode by stopping the chopper but this limits the maximum wavelength that can be obtained to that which fits into the source frame. There is then 3 m of straight guide to re-distribute the neutron divergence before the collimation begins at 10 m.

The collimation is variable from 2m to 10m with interchangeable apertures to give a choice of beam size from 1 mm $\times$ 1 mm up to 10 mm $\times$ 10 mm. The last section of interchangeable collimation has space for focussing optics to be employed in order to access low Q values with larger samples, or to focus the beam on the sample in cases where the resolution requirements can be relaxed, but a very small, high-flux beam is needed.

The sample position has space for the use of sample environment with a footprint of up to 1.5 m $\times$ 2.5 m allowing for the use of sample changers, flow-through cells, shear and rheology equipment and electromagnets.

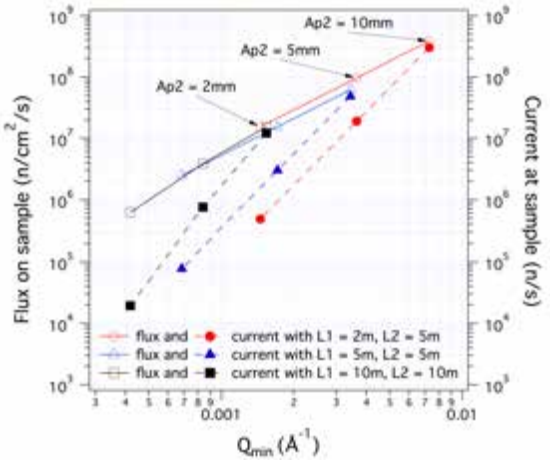

Estimated neutron flux and current at the sample position as a function of collimation length, beam size at sample (Ap2) and minimum accessible Q. Values are given for operation with no chopper.

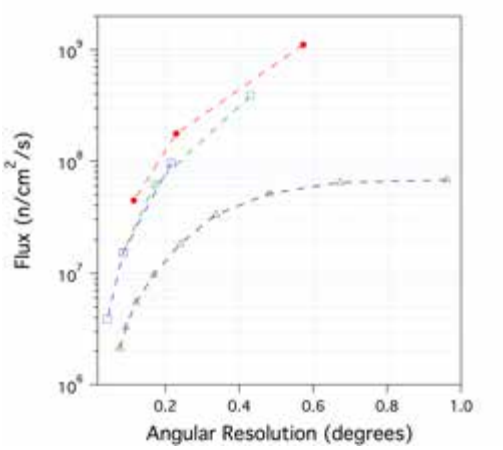

Estimated neutron flux at the sample as a function of angular resolution (red, green and blue curves) compared to the currently world-leading SANS instrument (black curve). Values are given for operation with no chopper.

The detector makes use of ^{10}B thin film detectors in grazing incidence geometry. The detector elements are arranged parallel to the beam direction around the outside of an evacuated flight tube. At the end of the tube is a high resolution area detector and instrumented beamstops capable of measuring a time-of-flight spectrum. In order to increase the space available at the sample position in order to accommodate larger sample environment, the detector array is moveable.

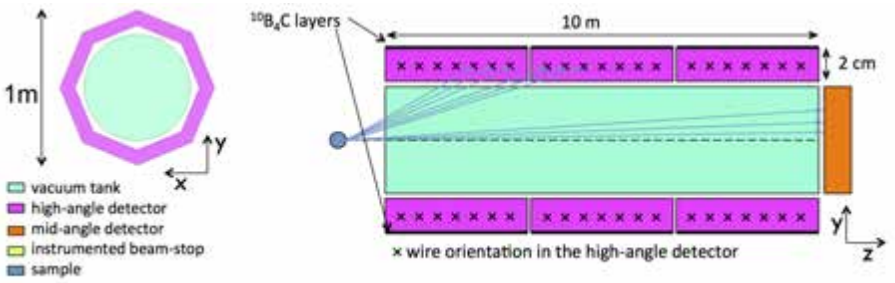

Detector layout using ^{10}B thin film detectors around a tube.

Instrument Parameters	
Moderator	Cold
Moderator - Sample distance	20 m
Wavelength Range	2 to 13 Å at 14 Hz
Wavelength Resolution	9% at 4Å and L2 = 10 m
Simultaneous Q Range	2×10^{-4} <Q< 2Å^{-1} @ 7 Hz with 2 mm diameter sample 1.6×10^{-3} <Q< 2Å^{-1} @ 14 Hz with 10 mm diameter sample
Sample to Detector distance	Detector bank from 1 m to 10 m High resolution low-angle detector moves from 5 m to 10 m
Detectors	35 m^2 of 5 cm pitch ^{10}B detectors 0.4 m^2 of 2 mm pitch detectors Beamstop detectors

Surface Scattering

Surface Scattering

Nanostructured and patterned surfaces
Polymer thin films
Self-assembled colloids
Biological membrane assemblies
Energy materials
Drug delivery systems
Food science

This instrument will be optimised for high flux grazing incidence SANS (GISANS) on horizontal surfaces, but will also be well-suited for complementary surface scattering measurements (reflectometry, surface diffraction and transmission SANS). Approaching the sample surface from either above or below the horizon will allow the study free liquid surfaces and wide range of nanostructured thin film applications using **in-situ techniques** and sample environments.

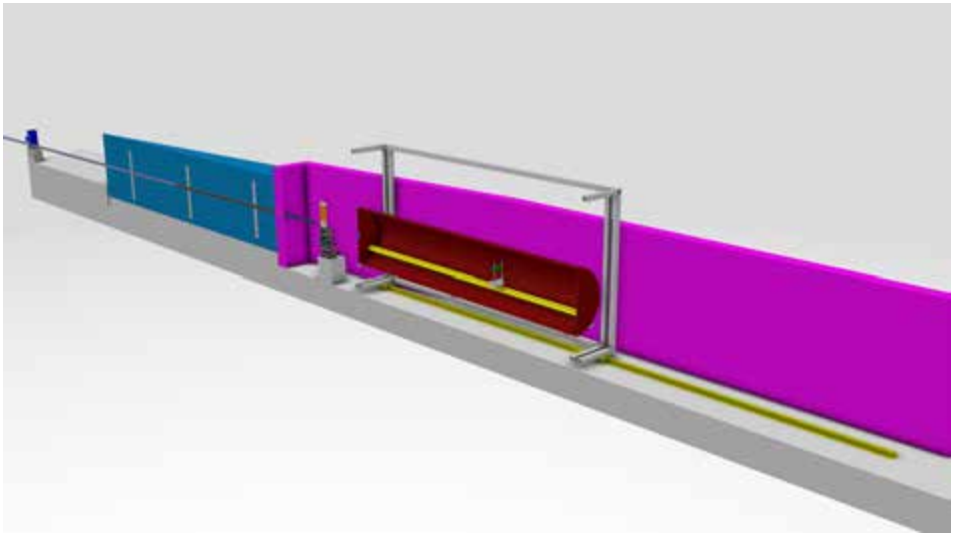

Instrument Description

The instrument begins 2 m from the moderator with a multi-channel bender to take the instrument out of line of sight of the source. The guide is inclined up at 0.5° to enable access from below the sample horizon when using in-situ environments such as cone-plate rheometers. The sample position is located 30m from the moderator. 20 m from the source the collimation section begins, with slit and pinhole collimation up to 10 m for SANS and GISANS measurements, as well as vertical slit collimation for reflectometry. In order to access free liquid surfaces, the last two guide sections will be coated on the top and bottom with m=6 supermirrors to allow the beam to be deflected up to 4.8 ° up or down, giving access to an angular range up to 5.3 ° from below and 4.3 ° the sample surface. At a typical collimation and a 3m detector distance for specular reflectivity measurements the usable bandwidth of 2-9Å allows a competitive Q_z-range of 0.0050-0.47 (0.58) $Å^{-1}$ to be covered for both liquid and solid interfaces. For GISANS and SANS measurements, the instrument will have a variable detector position from 1-15m from the sample, giving a Q_{xy} range of 1 x 10^{-3} - 2 $Å^{-1}$.

The instrument will have a 0.5 m × 0.5 m high-resolution detector (< 1mm pixel size) inside a short evacuated tank. The detector will be able to move within the tank to vary the accessible Q range and to match the incident collimation. For higher specular angles the detector can be brought forward to 1m from the sample.

Understanding self-assembly of 2-3D nanostructures at surfaces and interfaces is a challenge in both soft and hard condensed matter. The structures of interest range from a few nanometers up to micrometers in dimensions, and are often difficult to characterise using optical techniques due to their small size, or because many interesting phenomena take place at buried interfaces. Small angle scattering in a grazing incidence geometry allows such structures to be characterised revealing lateral morphology, particle size and inter-particle distances. GISANS is a technique that the ESS is well placed to develop further, as the demand for it is high but the scattering from thin films is flux limited. Time of flight GISANS has the additional advantage of being able to monitor structures at different distances from the interface using the wavelength dependent penetration depth of evanescent neutrons. Such experiments have successfully been demonstrated, as illustrated in the figure below, but widespread use is limited by a lack of dedicated high flux instruments.

The collimation, bandwidth and resolution requirements for GISANS differ significantly from those that are optimal for specular reflectometry, and thus GISANS measurements are difficult to accommodate on reflectometers designed for specular applications. A dedicated instrument is thus required to optimise Tof-GISANS for advanced applications and weakly scattering thin films. Particular applications that will benefit from the geometry of this instrument will be free-liquid interfaces and in-situ experiments employing special sample environments (such as cone-plate rheometers) or complementary optical techniques (such as ellipsometry or fluorescence microscopy). The instrument will additionally be capable of the specular measurements required for a full 3D analysis laterally structured thin films.

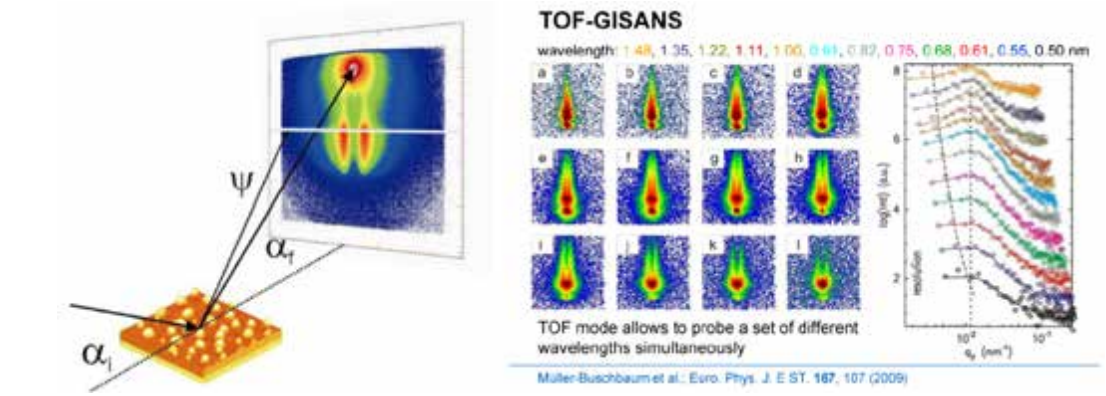

Tof-GISANS recorded from a submonolayer of polymer islands, using the variation of penetration depth of different wavelengths to probe the structure at different distances from the surface [202].

Instrument Parameters	
Moderator	Cold
Wavelength Range	variable depending on detector position
Moderator - sample distance	30 m
Sample to Detector distance	1-15m
Q_z-range	0.005 - 0.47 (0.58) Å^{-1}
Q_{xy}-range	1×10^{-3} - 2 Å^{-1}
Flux at Sample	Depends on collimation and geometry
Sample environnements	Air-liquid, solid-liquid, *in-situ* techniques (rheometry, microscopy
Detectors	0.5m x 0.5m with 0.5mm resolution for GISANS, low resolution/ wide angle banks for SANS

Horizontal Reflectometer

Horizontal Reflectometer

Soft condensed matter
Reactive surfaces
Biological membranes
Drug delivery systems
Environmental chemistry
Thin film devices

This high-flux instrument is optimised for the study of free liquid interfaces with 4-20% wavelength resolution and an extended simultaneous Q-range for kinetic experiments on the millisecond to second timescale, realised using a fast shutter system to select angles of incidence with the pulse sequence.

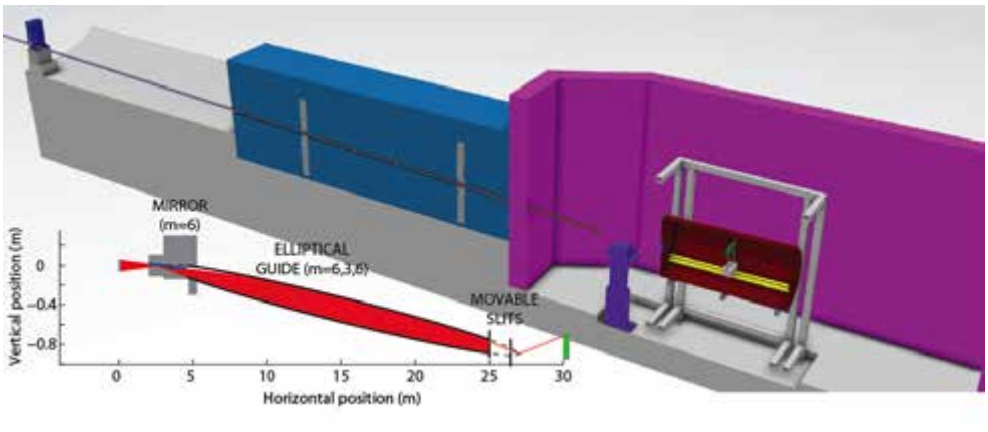

Instrument Description

The primary motivation for this instrument is to allow faster time-dependent processes to be studied with better structural resolution by extending the simultaneously measured Q-range. The instrument has an elliptical guide inclined at -2.1 degrees transporting a broad angular divergence of neutrons towards a horizontal sample surface. Reflectivity can be measured by sequentially choosing angles of incidence from the divergence profile with 2 slit collimation, as shown in the inset to the instrument layout. This allows the full Q-range to be covered without moving the liquid samples. In addition to the slit collimation to limit divergence, a fast shutter system will open and close the slits with fast time-resolution in order to record the full Q-range quasi-simultaneously from changing surface structures. The broad wavelength range allows flexible choice of the incident angles used according to the sample reflectivity profile. The illumination of the sample is homogeneous within a 4cm × 4cm area and samples as small as 5mm × 5mm should be possible to measure due to the high brightness at ESS.

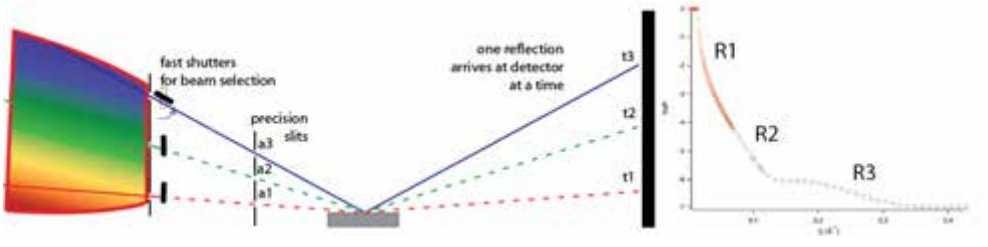

Beam selection principle: from the wide divergence neutron beam (0.2-4.1°), incident angles a1-a3 can be collimated using the two sets of precision slits for sequential measurement of reflectivities R1-R3 shown on in the reflectivity graph on the right. A system of fast rotating shutters will allow rapid selection of these angle for kinetic experiments to record the full reflectivity range within milliseconds-seconds.

The instrument has the potential for very high flux and high throughput measurements of 1-10 nanometre thick films at relaxed resolution. The figure below shows a comparison of the simulated time-averaged flux as a function of Q to the currently world-leading liquids reflectometer, at a comparable wavelength and angular resolution, as well as the simulated reflectivity profile and estimated counting time required for an air-D_2O interface. The main origin of the higher flux is the higher source brightness, and the use of the natural wavelength resolution of the instrument rather than inserting resolution-modifying disc choppers as on reactor instruments, but also from the use of more advanced optics. A wavelength frame multiplication chopper system will be used for higher resolution studies of thicker films.
To limit the incoherent background from the sample, which is typically a problem for simultaneous multi-angle measurements, a beam-selecting fast shutter will be placed in front of each precision slit set to collimate the beam to a specific angle and resolution. This allows the reflection at each angle to be measured on the detector at a unique time, allowing background subtraction from all angles which would otherwise overlap in time and space.

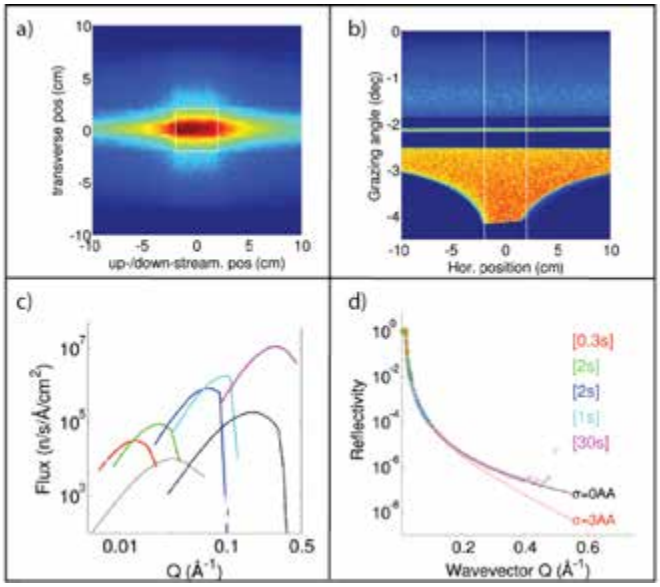

Instrument simulations: a) Footprint of the uncollimated beam b) full range of incident angles on the horizontal sample, c) simulated flux at $\Delta\theta/\theta = 2.94\%$ and an average $\Delta\lambda/\lambda = 8\%$ at 0.2-4.11°, compared to the currently world-leading liquids reflectometer (grey and black curves at 0.62° and 3.8°), d) Simulated reflectivity on a 4×4 cm^2 D_2O surface including an incoherent background of 10^{-6}.

Instrument Parameters	
Moderator	Cold
Moderator to sample distance	27m
Wavelength range	2-9.5Å
Q-range on liquids	0.006-0.45$Å^{-1}$
Q-range on solids	0.001-2$Å^{-1}$
Wavelength Resolution	4-19%
Beam Size at sample	4×4 cm^2
Divergence at guide exit	4.2° (Vertically)
Sample to Detector distance	1-3m
Detector Technology	1×1 mm^2 spatial resolution.
Sample environment	air-liquid, liquid-liquid and solid-liquid

Vertical Reflectometer

Vertical Reflectometer

Thin film magnetism
Thin film devices
Solar cells & photovoltaics
Chemical sensors
Battery materials
Fuel cells

A versatile high-flux vertical-sample instrument optimised for specular reflectivity studies of small and ultra-small samples with 2-10% wavelength resolution and broad accessible Q-range. A polarized incident beam with optional polarization analysis will allow magnetic studies, with additional energy-angle encoding available using a multilayer monochromator.

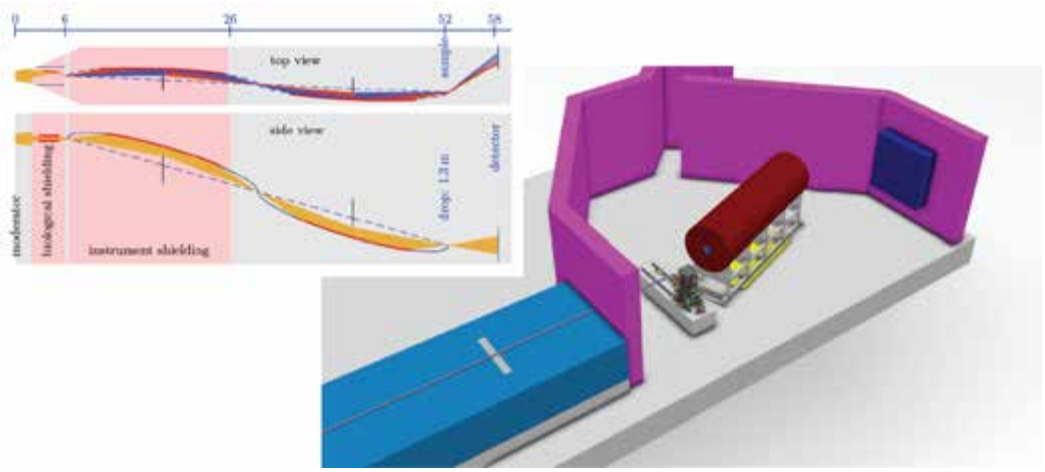

Instrument Description

The vertical reflectometer utilizes the Selene concept [203] of two identical elliptical reflectors to focus the neutron beam and deliver a broad angular divergence onto the sample surface. The design allows a gain in flux relative to conventional two-slit collimation, and it has the additional advantage that by using elliptical focusing optics, only the desired neutrons are transported to the sample, reducing background levels. The double elliptical optics has several modes of operation as illustrated in the figure below. The design offers the possibility to use the full divergence to increase the simultaneously measured Q-range, which at an angular resolution of 5% gives rise to a flux gain of 10 on the sample compared to the almost conventional set up.

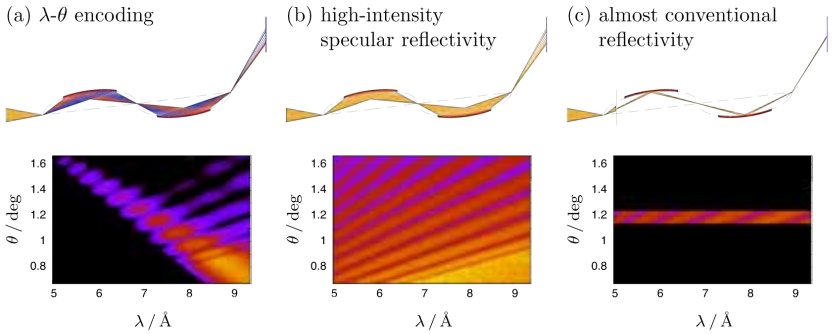

Three operational modes of the instrument simulated on a 5 x 5 mm^2 sample. a) Angle-wavelength encoding using a multilayer monochromator mirror, b) the wide divergence mode for rapid scanning of ultra-small samples and c) the limited divergence mode giving rise to an almost conventional set up.

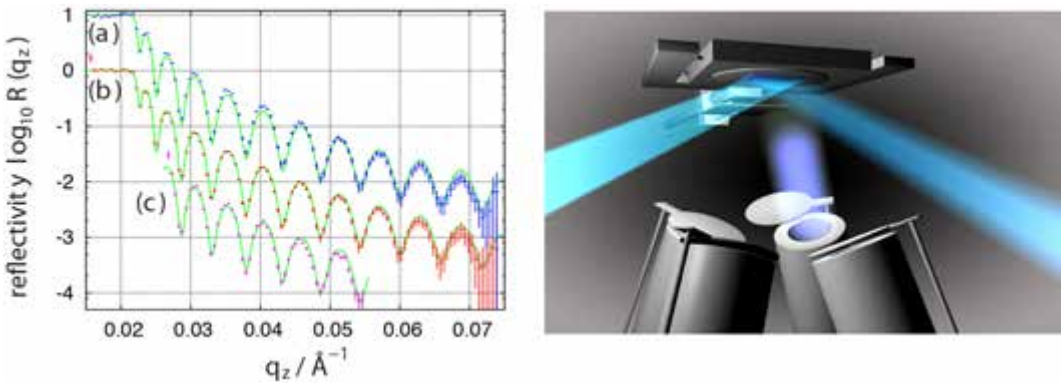

Left: Specular reflectivity of a 1000 Ni film on glass simulated using (a) the wavelength-angle encoding mode (60s), (b) the wide-divergence mode (1s) and (c) the almost conventional set up (10s). Right: Potential applications include very small samples in complex environments e.g. in-situ MBE deposition.

In the wide-divergence mode the angle of incidence is resolved on the position sensitive time-of-flight detector. The angular divergence of the instrument will be 1° in the scattering plane, which gives a simultaneous Q-range of 0.005 - 0.5 $Å^{-1}$, using 0.2-1.2°. In cases where the full divergence cannot be used due to incoherent background from the samples, the beam divergence can be limited by a slit rendering the measurement equivalent to a conventional double-slit collimation system, but still using a beam focusing on the sample plane instead of a divergent beam. For particularly small samples, or for scanning local structures, the guide system can be tuned to select only the most focused part of the beam, leading to beam spots of 200-300 micrometres in dimensions. For samples that exhibit both specular and off-specular scattering, these can be separated using a multilayer monochromator to encode wavelength with reflection angle and measuring the time-of-flight. The divergence within the sample plane can be used for focusing in grazing incidence small angle scattering (GISANS) experiments, if the detector is brought forward to the sample position. The guide geometry leaves several meters of space around the sample, so that using large sample environment and *in-situ* characterisation and deposition techniques is possible.

Instrument Parameters	
Moderator	Cold
Moderator to sample distance	52m
Wavelength range	5-9.4Å
Wavelength Resolution	2-10%
Q_z-range	0.005 - 2$Å^{-1}$
Beam Size at sample	0.1x0.1 to 1x1cm^2
Divergence at sample	$\Delta\theta_{xz} = 1°$, $\Delta\theta xy = 2°$
Sample to Detector distance	1-6m
Detector Technology	0.5 x 0.5 mm^2 spatial resolution.
Detector Range	$-5 < 2\,\theta < +40^o$
Sample environment	in-situ MBE, contacted devices

Vertical Reflectometer

Thermal Powder Diffractometer

Thermal Powder Diffractometer

Structure & in-situ processing
Catalytically-active materials
Novel materials
Health & pharmaceuticals
Fuel cells
Battery materials
Gas storage materials
Solar cells & photovoltaics
Engineering & geosciences
Archeology & heritage conservation

This is a thermal neutron, time-of-flight diffractometer with variable wavelength resolution ($\Delta\lambda/\lambda$ from $\approx 0.02\%$ to 5%), provided by a pulse shaping chopper, and a useful Q_{max} of ≈ 25 Å^{-1} for medium and high-resolution powder crystallography. The usable wavelength band in the time-frame is 1.9 Å (normal operational mode λ = 0.5 - 2.4 Å) and is optimised for shorter wavelengths for structural characterisation and *in situ* processing when extended Q-data are required. The flexibility of the instrument allows a wide-range of materials to be investigated. While the instrument is optimised for thermal neutron powder diffraction, it can also perform single crystal diffraction measurements in a quasi-Laue mode.

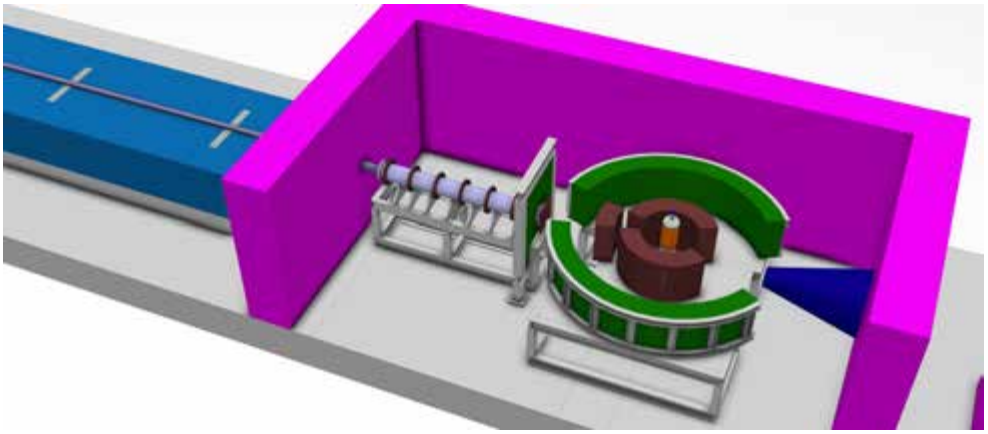

Instrument Description

The beam transport system is based on a kinked double ellipse geometry, in order to avoid line-of-sight from the thermal moderator. A pulse shaping chopper allows the wavelength resolution to be tuned from 0.02% to 5% for the central wavelength of 1.45 Å. The guide is optimised for the transport of short wavelength neutrons, giving the standard operational mode wavelength band of 0.5 - 2.4 Å, ideal for small to intermediate unit cell crystallography. Using short wavelengths also avoids problems with the prompt pulse for almost the entire wavelength band. The wavelength band can be tuned across the range available from the thermal moderator (0.5 - 6 Å) but, for longer wavelength bands, the *bispectral powder diffractometer* is preferred. Vertical focussing of the guide means that cylindrical sample geometry is preferred. A large cylindrical 2-D detector ($10° < 2\theta < 160°$) with a height of at least 1 m and high spatial resolution (2 mm in the scattering plane, 5 mm in the vertical plane) matches the sample geometry, allowing both angle dispersive and time-of-flight information to be collected across a wide angular range. A backscattering detector array is also envisaged for high resolution studies. The ability to tune the instrument resolution to the experimental system is a key advantage of the ESS suite. The combination of the very flexible instrument set-up, event mode data acquisition and optimised sample environments are key to the impact of this instrument across a broad range of science. Additionally, the cylindrical detector geometry will allow single crystal data collection using the quasi-Laue technique but the instrument is not optimised for this purpose. Polarisation of the incoming beam is also foreseen as an upgrade path.

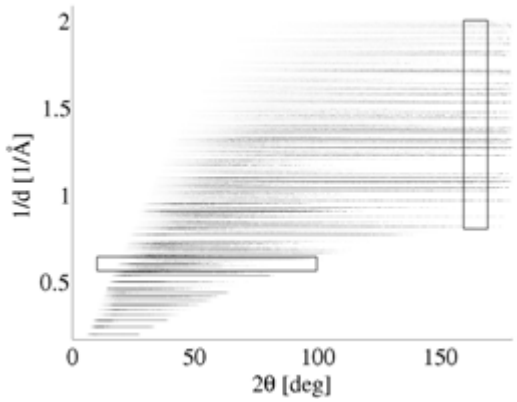

Simulation of powder diffraction data for a NaCaAlF standard for a two-dimensional detector over the full detector scattering angle.

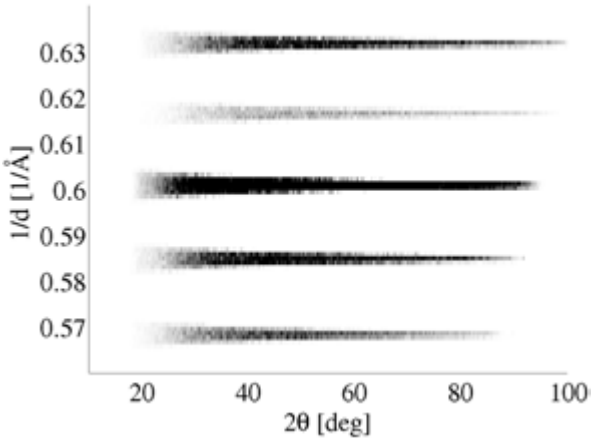

Bragg diffraction peak width as a function of detector scattering angle showing the variation in the instrument resolution function.

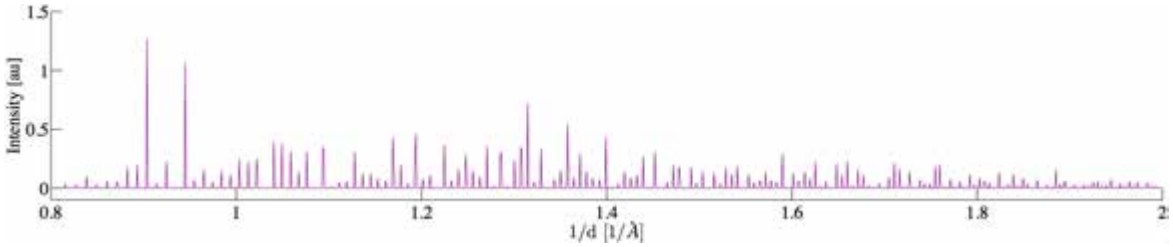

Standard one-dimensional powder diffraction pattern obtained by summation of the data within the box at high scattering angle (160-170°) in the above left figure.

Diffraction data is simulated above assuming a cylindrical detector geometry and plotted in 1/d in order to illustrate the instrument characteristics (Figure top left). Detector summing over a restricted scattering angle range to give one-dimensional data is the usual method to produce data for Rietveld refinement (Figure bottom) but summing the data into one-dimension across a larger detector angle leads to broader Bragg reflections (Figure top right) and the loss of information due to increased peak overlap. The goal is to develop multi-dimensional Rietveld analysis software to refine the full detector image, where the variation in the instrument resolution as a function of detector scattering angle can be modelled.

Instrument Parameters	
Moderator	thermal
Moderator - Sample distance	156 m
Wavelength Range	0.5 - 2.4 Å in standard mode; full range 0.5 - 6 Å
Wavelength Resolution	≈0.02% (10 μs) - 5% (full pulse) at $\lambda = 1.45$ Å
d-range	0.25 - 14 Å in standard mode; full range 0.25 - 35 Å
Q-range	0.5 - 25 Å^{-1} in standard mode
Beam Size at sample	full beamsize 2 × 1 cm^2 with optional additional focussing (0.5 × 0.5 cm^2)
Sample to Detector distance	wide angle bank - 2 m, backscattering bank - up to 2.5 m
Detector Technology	Boron-10 or wavelength shifting fibre, spatial resolution ≈ 2 mm in scattering plane and 5 mm in vertical plane, efficiency > 50% (for $\lambda > 1$ Å)
Detector Coverage	$10° < 2\theta < 160°$ on both sides with separate backscattering detector array from 160-180°

Bispectral Powder Diffractometer

Bispectral Powder Diffractometer

Novel &materials
Structure & in-situ processing
Catalytically-active materials
Fuel cells
Battery materials
Solar cells & photovoltaics
Novel states of matter
Engineering & geosciences
Archeology & heritage conservation
Earth & environmental sciences

This time-of-flight diffractometer combines the flux of a thermal and coupled cold moderator for an efficient use of a broad wavelength band with flexible time resolution, which makes it ideal to determine larger units cells of complex materials, or magnetic superstructures simultaneously with the atomic structure including light elements. The instrument is 75 m long and uses two wavelength frames with a total bandwidth of 3.8 Å. The choppers will typically be phased to select 0.8 to 4.6 Å, yielding a Q_{max} of 15 $Å^{-1}$ and can be tuned to provide wavelengths up to 10 Å. The pulse shaping chopper system provides a flexible time resolution and efficient wavelength frame multiplication, in addition to the ability to shift the wavelength band and to suppress the background of the prompt pulse. The beam divergence and detector resolution are also well adapted to single crystal diffraction studies. With an optional monochromating chopper, the instrument can be converted to a special multispectral spectrometer optimized for small samples and low divergence.

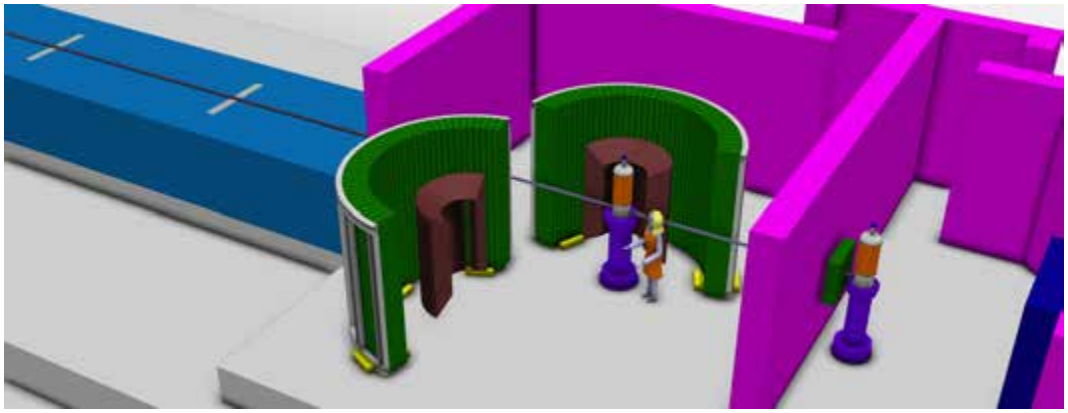

Instrument Description

The bispectral extraction system, consisting of a super-mirror stack inserted in the monolith, allows the instrument to view simultaneously both the thermal and cold moderators. The pulse shaping chopper (PSC) uses the eye-of-the-needle concept in both space and time and is placed at the first focal point of the double elliptic guide system, mirroring the phase space density at the PSC to the sample position.
The final section of the guide will contain exchangeable parts to vary the beam size and divergence at the sample position. The detector system covers a large solid angle with 2D position sensitivity at 3 mm spatial resolution and will likely be composed of units based on wavelength shifting fiber scintillation detectors. A cylindrical detector geometry with the cylinder axis along beam and a dedicated backscattering detector are foreseen. The measurements provide angle and wavelength dispersive data for powder diffraction, as illustrated for the *Thermal powder diffractometer*, and multi-dimensional Rietveld analysis software, currently under development, will be used for data analysis. The beam is further guided out of the experimental section to a second station, which can use the transmitted beam for neutron Laue characterization and test experiments.

Time resolution options

$\delta t(\lambda_1)$	$\delta t(\lambda_1 + 1.9\text{Å})$	(Hz) : (Hz)
27.5 μs	82.5 μs	84 : 70
60.6 μs	181.8 μs	45 : 28
151.5 μs	353.5 μs	28 : 14
227.4 μs	606.3 μs	14 : 14
378.8 μs	681.8 μs	0 : 14

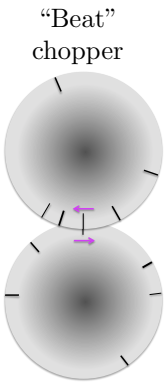

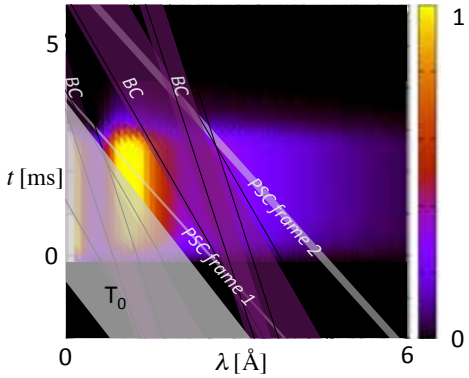

The pulse shaping chopper consists of two counter-rotating discs of 75 cm diameter rotating with different multiples of the source frequency to produce short pulses as a 14 Hz "beat" of the ESS source frequency. The choice of slit pair provides a large flexibility in time/wavelength resolution: for high resolution backscattering diffraction $\delta t/t$ can be tuned to the range of 10^{-3} to 10^{-4} and can be relaxed to increase flux in fine incremental steps up to 1% resolution. The acceptance diagram (right-hand figure) shows the selection of the chopper system from the bispectral moderator distribution. The stripes indicate the opening time of the PSC and the closing time for the Bandwidth Control (BC) choppers and the T_0 chopper. The BC choppers remove the background from the long time decay of the source pulse, while a massive T_0 chopper suppresses the prompt pulse. For a typical medium resolution setting of $\delta d/d \sim 0.005$ at $2\theta = 90°$, a pulse width of 100 to 600 μs, depending on wavelength, matches the divergence given by the instrument geometry and detector specification. The wavelength band can easily be shifted by phase-shifting the choppers to match the required Q-range.

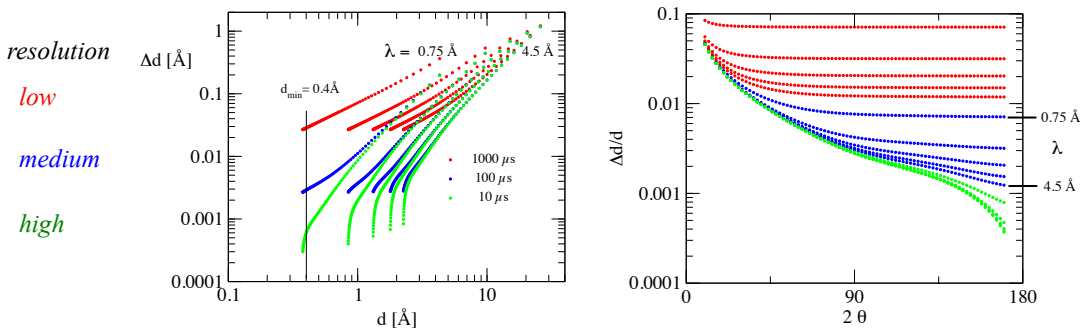

Instrument Parameters	
Moderator	bispectral cold/thermal
Moderator - Sample distance	75 m
Wavelength Range	0.8 - 10 Å
d-range	0.4 - 30 Å
Q-range	0.2 -15 Å^{-1}
Beam size at sample	full beamsize 1 × 1 cm^2 with optional focussing (0.5 × 0.5 cm^2)
Background suppression	T_0 chopper
Sample to Detector distance	about 1.5 m
Detector Technology	Wavelength shifting fibre, Boron-10 blade, or $^{10}BF_3$ volume spatial resolution 3 mm, efficiency > 50% (for $\lambda > 1$ Å)
Detector Coverage	$10° < 2\theta < 170°$

Pulsed Monochromatic Powder Diffractometer

Pulsed Monochromatic Powder Diffractometer

Structure & in-situ processing
Fuel cells
Battery materials
Gas storage materials
Solar cells & photovoltaics
Catalytically-active materials
Novel materials
Health & pharmaceuticals
Novel states of matter
Engineering & geosciences
Paleoclimatology & climate change
Earth & environmental sciences

The instrument is a thermal neutron, crystal monochromator diffractometer with variable $\Delta d/d$ resolution from $> 1\%$ to $< 0.1\%$ covering a Q-range up to ≈ 12.5 Å^{-1}. The complete diffraction pattern over a scattering angle of 160° can be obtained in a few seconds, ideal for parametric investigations, and the out-of-plane scattering angle coverage is matched to the requirements of complex sample environments. The variable take-off angle to the monochromators (continuous from 40° to $\approx$ 130°) increases the flexibility of the instrument, allowing trade of flux for resolution. Several additional modes of operation are foreseen to take advatnage of the pulsed source: simultaneous multiple wavelength data collection, the possibility to separate the inelastic incoherent scattering contribution from hydrogenous materials and fixed incident energy inelastic scattering mapping.

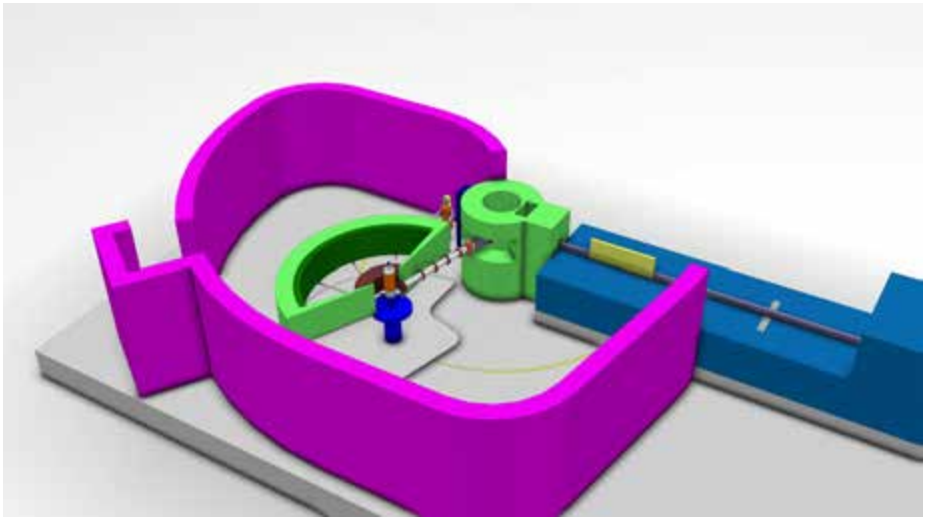

Instrument Description

The beam transport system will be optimised for thermal neutrons and starts with an in-pile feeder focussing through a 4 cm × 4 cm aperture at 6 m. A half-elliptical guide section (horizontal and vertical directions) will transport the neutrons to a point where the guide will be split, allowing an upgrade path to several instruments on the same beamport as, for this instrument, only 1/3 of the guide is required (horizontally). In the near future, we shall evaluate an angled straight guide section after the splitting point to avoid direct line-of-sight of the monochromator to the moderator, so as to reduce background. The total flight-path length from the moderator surface to the monochromator face is 46 m, allowing full illumination of at least a 30 cm high vertically-focussing (variable curvature) monochromator through the aperture at 6 m (natural divergence of ± 0.2°). A fixed-collimation carousel will determine the divergence acceptance onto the monochromator and a carousel with several monochromators offers flexibility. The operational take-off angle to the monochromators can be varied between 40° and 130°. The secondary evacuated flight path length (monochromator to sample) is 4 m with variable apertures to vary the beam divergence at the sample position, followed by a final set of beam-defining jaws. The sample - detector distance is 2.5 m, including a radial oscillating collimator (to suppress parasitic sample environment scattering) at the detector entrance and an evacuated detector housing (to reduce air scattering).

Crystal Mono.	d-spacing (Å)	Wavelength (Å) ($2\theta = 90°$)	Wavelength (Å) ($2\theta = 40°$)
HOPG(002)	3.355	4.743	2.295
HOPG(004)	1.677	2.372	1.147
Ge(220)	2.000	2.828	1.368
Ge(440)	1.000	1.414	0.684
Ge(400)	1.414	2.000	0.967

Table showing some possible composite monochromators based on HOPG and Ge.

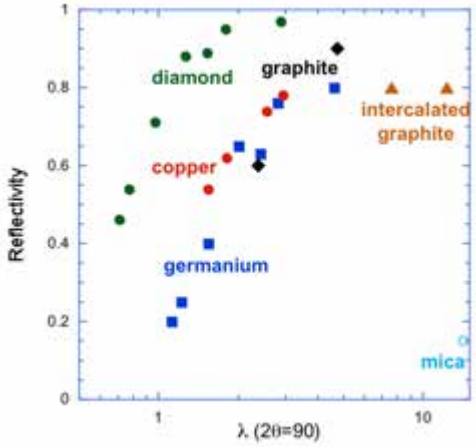

Comparison of diamond reflectivity (green) to other materials for crystal monochromators - Ge (blue), Cu (red) and graphite (black).

The instrument is similar to a conventional reactor-based diffractometer, such as D20 at the ILL, in the single wavelength mode of operation, as the time-averaged flux of the ESS is comparable to that of the ILL. However, the background is reduced *cf.* existing reactor instruments by discarding events outside the elastic line boundary time-of-flight conditions, increasing the effective signal-to-background ratio. Furthermore, multiple monochromatic wavelengths can be generated from monochromators (through co-aligned reflecting planes and/or higher order reflections) or by developing composite sandwich monochromators (see Table above left). The individual pulsed wavelengths are separated at the detector using the total path-length time-of-flight difference, not possible at a continuous source. Other monochromator materials will be investigated, such as diamond for its superior reflectivity in the wavelength range of interest (see Figure right) and layered materials (more higher order reflections). The monochromatic pulse structure is also well matched to fast kinetic measurements (sampling rate 4-5 ms at 14 Hz) and has potential with triggered cyclic measurements under extreme conditions, such as pulsed high-magnetic fields. The sample - detector flight-path can be used to separate inelastic incoherent scattering contributions, in time-of-flight, from elastic scattering in hydrogenous materials. Fixed incident energy inelastic scattering mapping can be performed with the full pulse (low energy resolution) or with a shaped pulse (variable energy resolution) using the optional chopper placed before the monochromator, offering a variable pulse-width from tens of μs to the full pulse-width. RRM-like measurements can also be replicated using the composite monochromator and/or higher order reflection set-up. Thus, while optimised for diffraction and *in situ* processing, several additional modes of operation are envisaged.

Instrument Parameters	
Moderator	Thermal
Moderator – monochromator distance	46 m
Monochromator – sample distance	4 m
Sample – detector distance	2.5 m
Q-range	0.1 -12.5 Å^{-1}
Beam size at sample position	maximum 40 mm height × 15 mm width
Normal Monochromators	diamond(111), diamond(220), Ge(113), HOPG(002)
Composite Monochromators	Example - Ge(220) / Ge(440) / Ge(400)
Detector technology	$^{1}0B$ or wavelength shifting fibre, resolution 2.5 mm
Detector coverage	160° 2-D cylindrical detector of 30 cm height (± 6.8° acceptance)

Materials Science & Engineering Diffractometer

Materials science
Engineering materials
Structure & in-situ processing
Residual stress & texture
Novel materials
Geosciences
Earth & environment sciences
Archeology & heritage conservation

A unique instrument for a broad range of scientific and industrial applications with a special emphasis on in-situ investigations of mainly engineering materials. The user will have the choice of multiplexing for fast time-resolved measurements or to trade resolution, divergence, beam size etc. versus flux in a single-frame pulse shaping mode. Flexible resolution is achieved by utilizing a double chopper system for pulse shaping, where different distances between the two chopper discs can be chosen. It will have the option of standard pulse shaping on a natural length instrument (Complex Environment Engineering Diffractometer "CEED" concept) or applying the structured pulse modulating (SPEED) concept. The latter allows modulation of the broad ESS pulse and thus to multiplication of the signal and efficiency especially for high-symmetry materials and strain measurements. Other concepts such as pulse-overlap are also being considered.

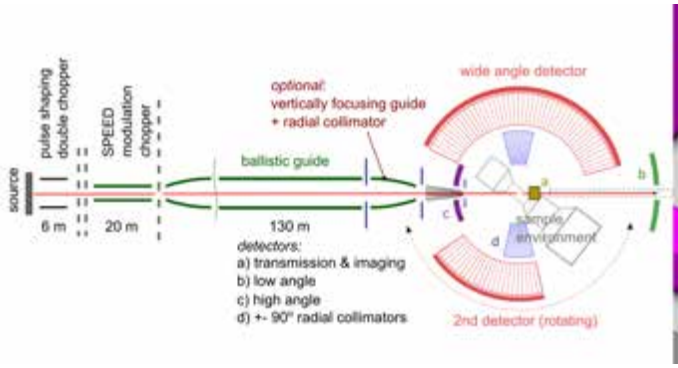

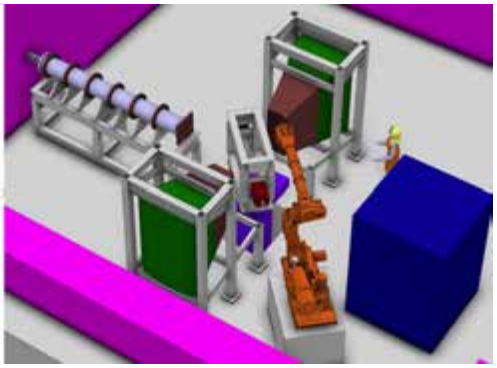

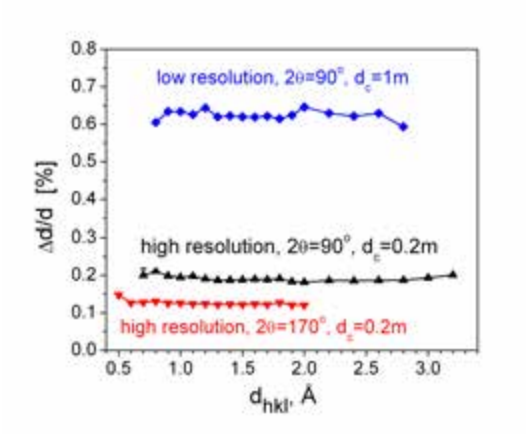

Nearly constant $\Delta\lambda/\lambda$ resolution as produced by the double chopper for different distances, d_c, between the chopper discs (simulation for pulse suppression mode with double band width).

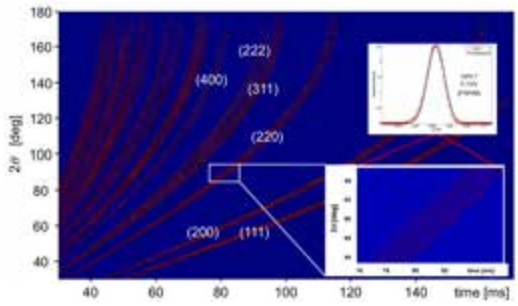

A diffraction pattern simulated in the SPEED mode displays the modulation of the broad source pulse for each Bragg peak. The top inset shows the high intensity and resolution obtained by integrating over the range shown in the lower inset.

Instrument Description

In addition to the pulse shaping and frame overlap choppers the instrument will possess the option to run a modulation chopper positioned in the first third of the instrument's total length of about 160 m. This device allows for chopping the beam into short subframes i.e. pulses, which then overlap at the detector position. Nevertheless the signal can be separated in many cases, especially when highly symmetric crystal lattices are under investigation, due to the corresponding angular offset of the Bragg peaks registered by the detector. In this way the signal is multiplied independently of the resolution, which may boost the efficiency for many engineering applications.

The instrument will be equipped with a wide range of sample environments dedicated for in-situ testing and characterization of engineering materials exposed to complex thermal, mechanical and electric or magnetic field loading. Under particular consideration are (i) physical simulations of fabrication and processing of engineering materials, (ii) long-lasting creep and fatigue experiments, (iii) investigation of magnetic materials in pulsed magnetic field and (iv) combination of in-situ diffraction and micro-imaging. Physical simulation of materials fabrication, processing and/or end use involves the exact laboratory reproduction of the thermal and mechanical processes that the engineering material is subjected to in the large scale production or end use. In-situ neutron diffraction during the physical simulation provides supplemental information about the evolution of texture, preferred orientation of martensitic variants, elastic and plastic anisotropy, dislocations and many other aspects. This additional information is expected to significantly improve the chance of achieving the optimisation of material performance through physical simulation. The instrument will also be used for texture and residual stress measurements in engineering components which are of major interest for industry. The basic instrument concept involves conventional detector banks located at right angles to the incident beam, coupled with flexible radial collimators (thus providing two distinct Q-vectors or independent directions of strain). Together with the incident slits, these define a gauge volume that allows spatially resolved measurements (of strain, texture etc) by moving the sample. Extension of the 90° banks to include back-scattering or forward scattering are to be considered. This would give better coverage for texture measurements and more directions of strain, but has to be balanced with the spatial and logistical requirements demanded from the advanced and potentially bulky sample environment. For residual stress measurements, the resolution and vertical divergence can be relaxed considerably (up to 1%) in order to gain flux.

Instrument Parameters	
Moderator	Thermal &Cold Bi-spectral
Moderator - Sample distance	156 m
Wavelength Range	0.5-5Å(0.5%)
Resolution	0.1% to 1% at 90°
Beam Size at sample	$0.5 \times 0.5\text{mm}^2$ to $10 \times 20\text{mm}^2$
Detector Technology	Boron-10, with mm spatial resolution
Detector Coverage	Initially 2θ=90° ± 20°, two banks but with extensions, possibly transmission detector
Sample environment	In-situ materials testing equipment, stress rigs, furnaces, cryo-cooling, robotics

Extreme Conditions Instrument

Extreme Conditions Instrument

Novel materials
Structure & in-situ processing
Geosciences
High-Tc superconductivity
Molecular magnets
Novel states of matter
Earth & environmental sciences

This instrument is optimised for effective use of state-of-the-art sample environments, in particular high-field ($\geq$ 25 T) magnets or high-pressure cells, including multi-anvil presses high temperature presses (up to 30 GPa at 2000 K). It can perform diffraction and spectroscopy measurements, and has additional SANS capabilities with bispectral extraction from the moderators to cover the widest possible Q/energy range. For wide angle diffraction the useful Q_{max} is 12 Å^{-1} and the usable wavelength band is 1.9 Å. For the spectroscopy option, the instrument covers an energy range of 1 - 80 meV with a variable energy resolution of up to 5%. The detector set-up is modular and will be matched to the sample environment. The instrument has a broad range of applications ranging from the physics and chemistry of materials to applied science.

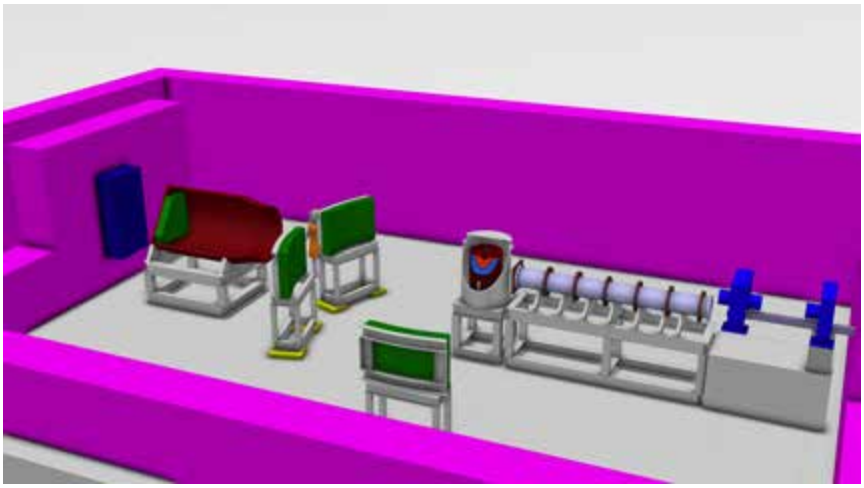

Instrument Description

The primary instrument is very flexible, due to the quite different requirements for diffraction, spectroscopy and SANS, while the secondary instrument matches the sample environment. Bispectral extraction from both moderators significantly expands the range of wavelengths accessible at the instrument and allows conventional diffraction, cold spectroscopy or SANS under the same experimental conditions. The wavelength resolution can be tuned by choppers from <0.1% to several % depending on the incident wavelength band, the former resolution is preferred for diffraction and the latter for SANS. For the spectroscopy option, either full or shaped pulse operation is foreseen depending on the required energy resolution. The direct spectrometer mode gives flexibility in choosing the incident energy from an extended energy range of 1 to 80 meV with a resolution that can be varied between 1 and 5%, enhanced by RRM. The beam delivery system has a kinked double ellipse geometry, similar to that proposed for the *thermal powder diffractometer* in order to bend out of the line-of-sight of the moderator to reduce background. The final section of the guide will contain slit systems to optimise the spatial and divergence acceptances at the sample position, offering great flexibility to tune the instrument set-up to those required by the experiment. Extreme conditions mean small sample sizes and/or severely restricted sample geometry and the maximum beam size is 1×1 cm^2, with optional focusing to reduce the beam to mm dimensions.

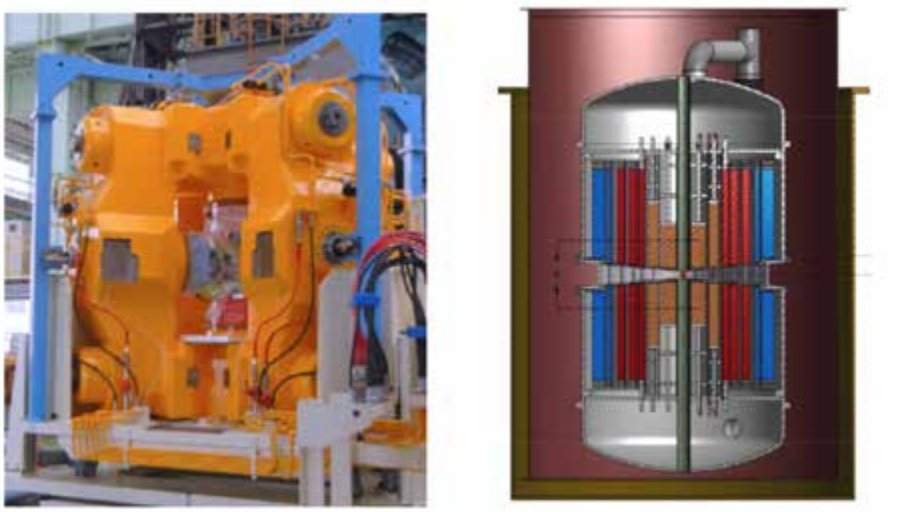

Possible sample environment types: (left) Multi-anvil pressure apparatus installed at PLANET (J-Parc) and (right) 25 T high-field split-pair magnet. Other alternatives include split magnets with wedge openings or superconducting horizontal magnets (not shown).

The secondary instrument is adapted to the dedicated sample environment (see Figure). Depending on the type of magnet, the scattering angle can be either limited to 30° in- and out-of-plane in forward and backscattering directions or be as wide as 300° in-plane but only a few degrees out-of-plane. For a high-pressure apparatus, the most useful scattering angle is around 90°, whereas forward and backward scattering positions are similar to those for the high-field magnet. For the system robustness, a modular detector panel configuration is planned for all the diffraction and spectroscopy modes, with an additional SANS detector bank in forward scattering that can be installed at a distance of 6 - 8 m from the sample position. To define the gauge volume and avoid parasitic scattering from the sample environment, a high degree of collimation is required in the secondary instrument. The non-magnetic and evacuated detector chambers will therefore incorporate radial collimation (not shown in the instrument overview). Combined with the long distance from the source and the kinked guide, this will provide a very low background and maximize the signal-to-noise ratio, crucial for small sample volumes.

Instrument Parameters	
Moderator	bispectral cold/thermal
Moderator - sample distance	156 m
Wavelength range	1 - 15 Å
d-range (Q-range)	0.5 - 600 Å (0.01 - 12 $Å^{-1}$) including SANS mode
Energy range (resolution)	1 - 80 meV (1 - 5%)
Beam size at sample	1×1 cm^2 (optional focusing)
Sample - detector distance	up to 4 m
Detector technology	Diffraction/spectroscopy: Boron-10 or wavelength shifting fibres, spatial resolution 2.5 mm, efficiency > 50% (for $\lambda > 1$ Å); SANS: (see Broad-band small sample SANS)
Detector Coverage	modular detector panels 1.5×1 m^2, SANS detector 1×1 m^2
Dedicated sample environment	superconducting high field magnet (>25T), multi-anvil press (6-axis press with max. load 500 ton/axis), diamond anvil pressure cells

Single-Crystal Magnetism Diffractometer

Single-Crystal Magnetism Diffractometer

Highly frustrated magnetism and emergent phenomena
Structure & in-situ processing
Molecular magnets & nanoparticles
Novel states of matter
Spin densities
Site susceptibilities

A time-of-flight (TOF) Laue instrument with the option to use polarized neutrons and full polarization analysis. Applications include magnetic structure determination for small single crystals including polarimetry, site susceptibilities, spin density distributions, hydrogen bonding, diffuse magnetic scattering, parametric real-time exploration of reciprocal space and monitoring the order parameters of weak signals.

The instrument takes full advantage of the ESS long pulse structure, its high flexibility and low background allowing to measure very small samples. Measurements using the TOF Laue method can very efficiently cover the reciprocal space of interest by a single or just a few sample settings.

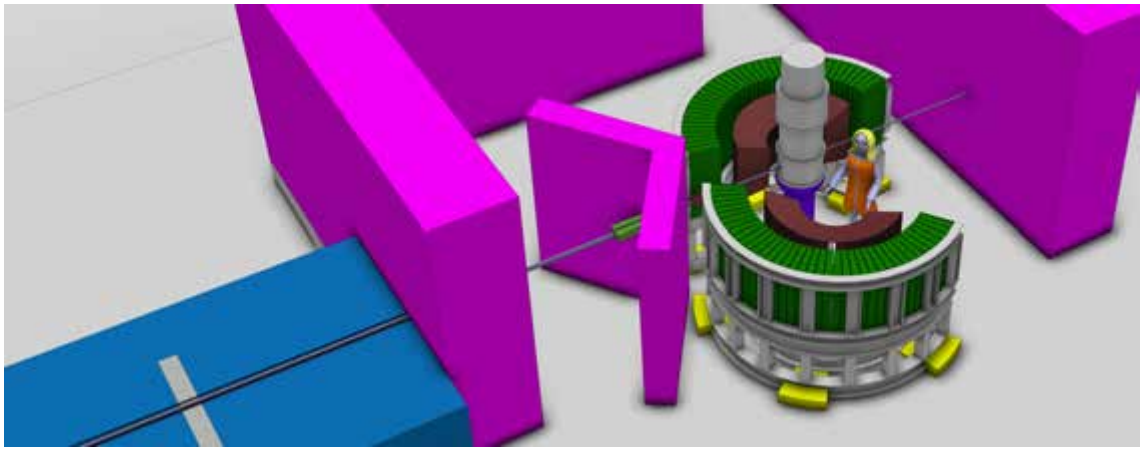

Instrument Description

Details on site susceptibilities and spin density distributions are obtained by polarized *thermal* neutron diffraction under magnetic field reversal, whereas *cold* polarized neutrons with polarization analysis can favourably be used for complex magnetic ordering and diffuse magnetic scattering. In order to enable both of these two standard modes of operation, the wavelength band can be shifted within the spectrum of a bi-spectral moderator, a flexibility which also allows efficient survey measurements, as well as parametric studies focused on small regions of reciprocal space.

With a simple spin-echo technique, it is possible to set a common coordinate system for the polarization analysis in *white* beam TOF Laue polarimetry, a method that rigorously disentangles the various nuclear and magnetic scattering terms on the full measured range of Bragg peaks in a single shot.

The spectrum of a bi-spectral moderator feeds a neutron guide system avoiding direct line of sight. The background is minimized by elliptic guide elements for focusing on small samples. Beam polarization is achieved by super mirrors. Half-polarized experiments with thermal neutrons can be performed with a 10 T asymmetric split-coil magnet giving large access to solid angle and reciprocal space. Polarization analysis and polarimetry are applied for separating magnetic, nuclear coherent, spin-incoherent scattering and interference terms.

The detector at 1 m distance from the sample, 1 m high, will be based on a thin film $^{10}B_4C$ converter, with 50% efficiency at 1 Å, which can achieve a spatial resolution of 2.5 mm fitting to a crystal mosaicity of 0.15°.

The user may benefit from the versatility of the instrument by adjusting wavelength band, pulse duration and focusing to the required reciprocal space, resolution and sample size. A large section of reciprocal space can be covered in a single sample setting, or alternatively, a continuous sample rotation can be chosen for data acquisition. The choice of a 156 m long instrument using a single wavelength frame gives a simple, adaptable time structure. For most needs the instrument exploits the full long source pulse. In order to resolve Bragg peaks at large Q with constant high resolution, the thermal spectrum of the pulse can be adapted to the unit cell dimensions, using a pulse-shaping chopper to provide a wavelength-dependent pulse length, as shown in the figure below.

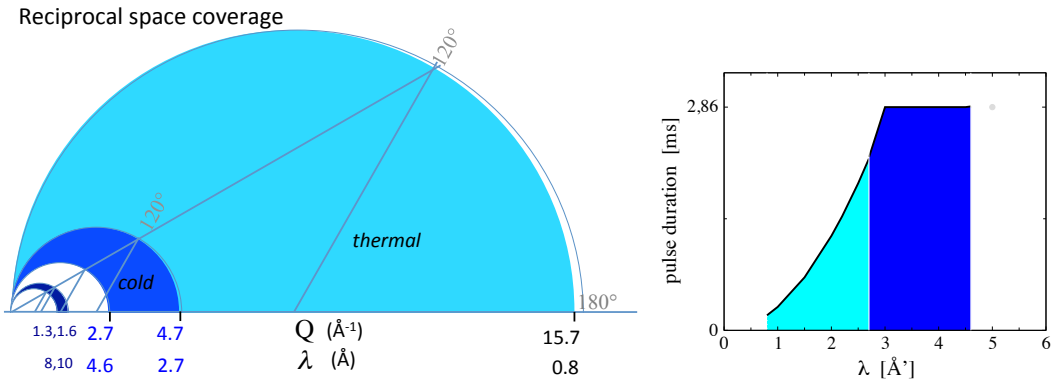

The left figure, a cut through the Ewald sphere, displays the reciprocal space coverage for different selected wavelength bands, with thermal (cyan) and cold (blue) choices and scattering angles up to 180°. The 2D detector also gives access to vertical Q-components (< 2.7 Å^{-1}) and completes the picture to both sides of the incoming beam.
The right figure shows the pulse-shaping required for a constant absolute resolution of $\Delta k_i \leq 0.05$Å^{-1}; for cold neutrons the resolution improves considerably even using the full pulse. At a wavelength resolution of 1%, the flux at the sample position will be 5×10^8n/cm^{2}s.

Instrument Parameters	
Moderator	bispectral cold/thermal
Moderator - sample distance	156 m
Wavelength range	0.8 - 10 Å
d-range (resolution)	0.4 - 60 Å ($\sim$ 1%)
Q-range (resolution)	0.1 -15 Å^{-1}
	($\sim$ 1%, flexible ΔQ ≤ 0.05Å^{-1})
divergence	$0.3° - 0.6°$ (thermal−cold, FWHM)
Background	no direct line of sight
Beam size at sample	typical $< 0.5 \times 0.5$ cm^2
Sample size	0.1 - 10 mm^3
Sample to detector distance	1 m
Detector technology	^{10}B-foil, efficiency $> 50\%$ for $\lambda > 1$Å
	spatial resolution 2.5 mm
Detector coverage	horizontal $10° < 2\theta < 170°$
	vertical $-20° < \chi < 20°$
Special sample environment	asymmetric vertical 10 T magnet for half-polarized setup
wide angle polarization analysis	^{3}He spin-filter cell applying for full the 2D detector or,
and neutron polarimetry	super mirror analyzer for applied fields, high polarization
	and 25° vertical acceptance, ($\lambda = 2 - 10$Å)

Macromolecular Diffractometer

Macromolecular Diffractometer

Macromolecular structures
Enzyme mechanisms
Protein-ligand interactions
Proton transport

Dedicated to biological neutron crystallography, this instrument is a single crystal quasi-Laue TOF diffractometer optimised for sub-millimeter crystals with large unit cells. The instrument should be able to routinely study 30-40 kDa proteins in unit cells with 100-150 Å edges. The determination of the hydrogen positions requires a d_{min} of the order of 2 Å, even for large unit cells. The flexible detector geometry allows larger unit cells to be studied at the expense of longer data collection times.

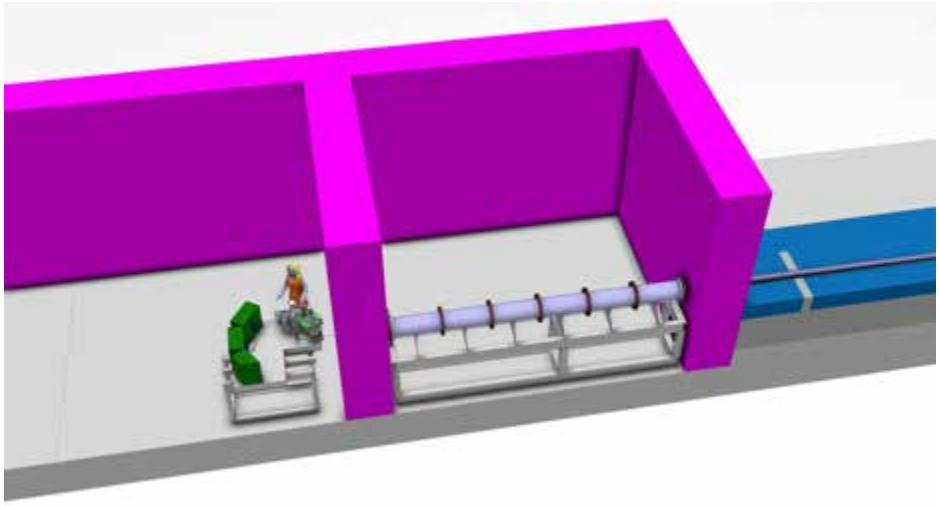

Instrument Description

The 156 m instrument length allows a wavelength frame of ca. 1.8 Å to be used, while the wavelength resolution using the full 2.86 ms pulse is ca. 2-5 %. Since the main advantage of TOF in macromolecular Laue crystallography is to spread the scattering background from the crystal to many time bins, this time resolution is sufficient to separate the spots in the Laue pattern while making full use of the integrated intensity of the long pulse. The width of the wavelength frame fits well with the wavelength range typically accepted in the quasi-Laue technique. Separating the crowded Laue pattern in TOF not only distributes the background into multiple time bins, but also allows spatially overlapping reflections to be separated by three-dimensional profile fitting.

In order to maximise the signal-to-background ratio, the beam delivery system is optimised to match the beam size to typical crystal sizes of 0.2-1 mm and the beam divergence to typical crystal mosaicities of ca. $\pm 0.1°$. A curved guide with a low m-value coating is sufficient to deliver the required divergence at the sample and avoid a direct line-of-sight to the moderator.

The detector setup allows both the sample-detector distance and the 2θ angle at the center of the detector to be changed. Increasing the detector distance allows the reflections from larger unit cells to be better separated on the detector plane. As the fraction of reciprocal space covered at one crystal orientation is then smaller, more crystal orientations have to be used to obtain a complete data set, leading to a longer data collection time. Several options for the detector technology required to achieve 0.2 mm spatial resolution with acceptable efficiency and time resolution are under development. Existing scintillator detectors with 0.5 mm resolution can be used as a fall-back option at the expense of either larger detector area or increased data collection time.

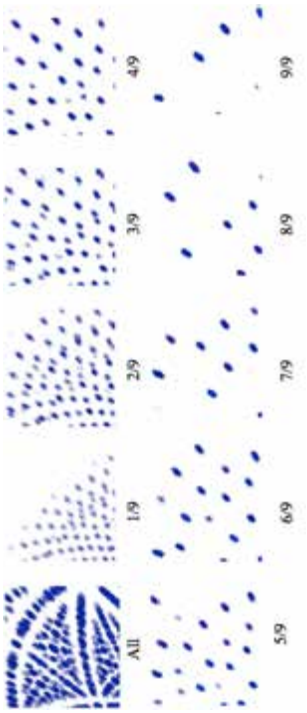

A crowded part of a simulated Laue pattern split into ten time bins.

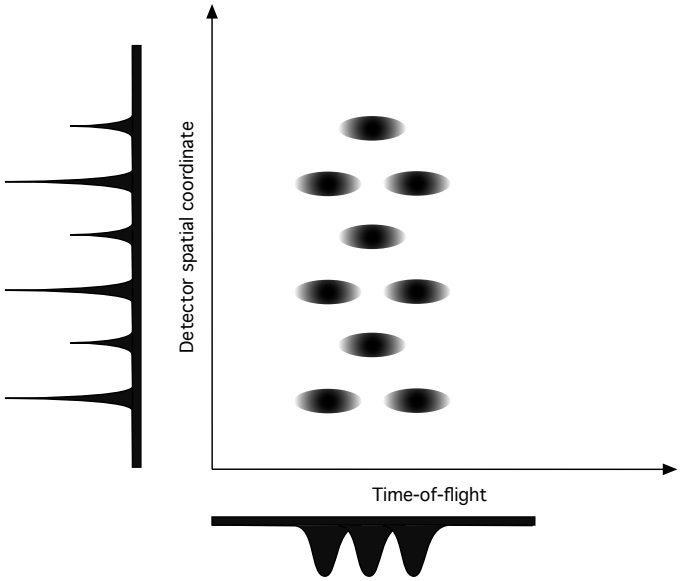

Separation of diffraction spots of a given width in the spatial and time-of-flight dimensions.

The high time-averaged flux of the ESS combined with the effective background reduction by using TOF will reduce the required crystal volume currently required for a given size of unit cell by more than an order of magnitude. This will allow much more challenging, but scientifically highly interesting targets such as integral membrane proteins to be investigated using neutron crystallography.

Producing sufficient amounts of perdeuterated protein material and growing large and well-ordered crystals remains the most time-consuming part of the structure determination effort. In order to make the most efficient use of the instrument time, the ESS will provide supporting facilities to help the users with these steps and ensure that the samples have been thoroughly optimised before the neutron experiment.

Instrument Parameters	
Moderator	Bispectral/cold
Moderator - Sample distance	156 m
Wavelength Range	1.5-3.3 Å
Energy Resolution	5-2%
dmin (Crystallographic resolution)	1.2 Å
Beam Size at sample	$3 \times 3 - 0.2 \times 0.2 mm^2$
Divergence at sample	$\pm 0.1^\circ$
Sample to Detector distance	0.2-1.0 m
Detector Technology	Three 60 × 60 cm^2 solid state Gd or ^{10}B detectors with 0.2 mm spatial resolution.
Detector Coverage	$2\theta = \pm 165^\circ$ (0.2 m)-$\pm 50^\circ$ (1.0 m)
Sample environment	Cryostream, humidity control, X-ray diffraction

Cold Chopper Spectrometer

Cold Chopper Spectrometer

Novel states of matter
High-Tc superconductivity
Molecular magnets & confined systems
Solar cells & photovoltaics
Drug delivery systems
Catalytically active materials
Gas storage materials
Battery materials
Polymers
Biological membrane assemblies
Biomolecules
Geosciences

A versatile instrument with a scientific focus on single crystal magnetism, providing an intense cold neutron beam with high energy and angular resolution in addition to a beam profile optimised for scattering from single crystal samples. This instrument is well optimized for magnetism and will also appeal to the soft matter and biological communities. The majority of experiments are expected to utilise an energy resolution of 50 - 200 μeV, but much higher energy resolution is also possible, reaching 8 μeV at a wavelength of 9 Å. The incident beam will provide a very clean resolution function and divergence profile to produce high resolution in both wavevector and energy transfer. Polarisation analysis will be a day one option to enable the separation of nuclear and magnetic signals. These features will yield a cold chopper spectrometer which is perfectly suited to probe novel dynamic behaviour in single crystal samples.

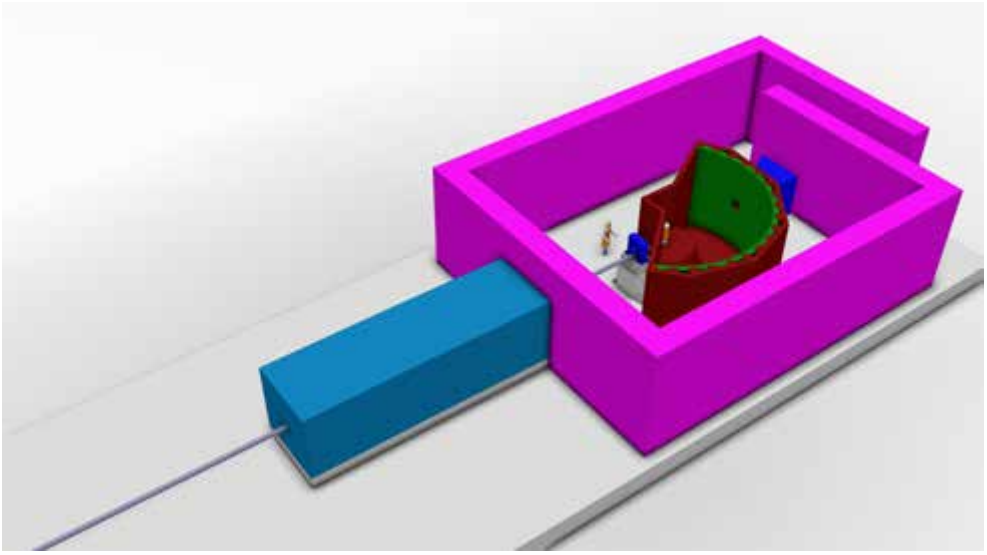

Instrument Description

The conceptual design foresees an instrument length of 156 m from moderator to sample, viewing the cold moderator. The background from the prompt pulse neutrons will be minimised by avoiding direct line of sight to the moderator through the use of an S-shaped ballistic guide which yields a spatially homogenous beam distribution at the sample position and provides a very clean short-wavelength cut-off. The choppers will be integrated into the guide design with a counter-rotating pulse-shaping chopper pair placed at 7 m, a frame overlap chopper at 13 m, another frame-overlap chopper at 1.4 m from the sample, and a counter-rotating monochromating chopper pair immediately after. Interchangeable guide sections just before the sample will make it possible to vary the beam size and divergence at the sample position and optimize the flux and Q-resolution conditions for each experiment.

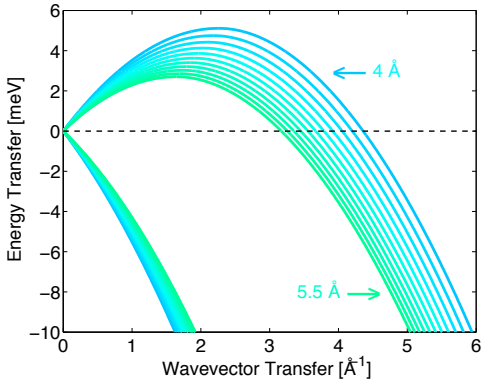

The energy and wavevector transfer reached for an incident bandwidth of 4 Å $< \lambda_i <$ 5.5 Å via the use of RRM. 10 incident energy frames can be measured simultaneously in this mode. The dashed lines shows elastic scattering. The figure shows how close the scattering profiles are in energy and wavevector transfer thereby making it possible to combine these data with a greatly enhanced resultant flux.

In a single time frame a range of incident energies covering a wavelength range of 1.88 Å is probed via repetition rate multiplication (RRM). The long length of the instrument results in only a small wavelength spacing between adjacent pulses on the sample. The focus on cold neutrons ensures that the resultant range of incident energies is small, and it is therefore envisaged that these individual datasets will be combined to provide a single dataset with substantially improved statistics. Combining these datasets will require sophisticated software tools as provided by the Data Management and Software Centre.

Special attention is paid to obtaining a clean energy resolution function and divergence profile to ensure an instrument which is well-suited for single crystal measurements. Selecting an incident pulse length of 1000 μs results in an energy resolution of ΔE = 86 μeV at an incident wavelength of 5 Å with a Q resolution of 0.01 Å^{-1}. Higher energy resolution measurements up to 8 μeV at 9 Å with good flux are possible by further pulse shaping, due to the high peak brightness of the source and the flexible chopper system.

The frame overlap chopper at 6 m from the pulse-shaping chopper prevents overlap between subsequent source pulses. The position and the opening times are chosen so as not to restrict the wavelength band, while allowing a flexible choice of RRM configurations: a large number of incident energies for quasielastic measurements or fewer energy windows when inelastic signals need to be probed. The neutron flux in each individual energy window will be significantly higher than the world-leading instruments of this type today, resulting in more than an order-of-magnitude performance enhancement when taking the multiple frames into account. The incident beam will be polarised with an exchangeable polarising guide section before the monochromating choppers. Analysis of the scattered neutrons will be performed by a ^{3}He cell, allowing XYZ polarization analysis.

Instrument Parameters	
Moderator	Cold
Moderator - Sample distance	156 m
Wavelength Range	2 - 20 Å
Energy Resolution (elastic line)	ΔE/E = 1% - 2.7%
Beam Size at sample	from 1 × 1 cm^2 to 2 × 4 cm^2
Sample to Detector distance	4 m
Detector Technology	Boron 10
Detector Coverage	-30 $< 2\,\theta <$ 150^o
Sample environment	High magnetic fields
	Polarization analysis
	Time-dependent phenomena
	Levitation experiments
	Secondary in-situ measurements (e.g. IR, Raman)

Cold Chopper Spectrometer

Bispectral chopper Spectrometer

Bispectral Chopper Spectrometer

Novel states of matter
High-Tc superconductivity
Molecular magnets & confined systems
Solar cells & photovoltaics
Drug delivery systems
Catalytically active materials
Gas storage materials
Battery materials
Polymers
Biological membrane assemblies
Biomolecules
Geosciences

A high resolution direct geometry spectrometer that gives the possibility to measure dynamics simultaneously over a very extended energy range. This instrument will be used as (a) a wide energy and wavevector transfer mapping instrument and (b) to determine energy scales, in a single snap shot, that cover many energy (or time) decades. It will be possible to relax the energy resolution from the high resolution set-up $\Delta E/E \sim 1\%$ to 10 %. This will enable the user to trade flux for resolution and thus optimise for the scattering signal and energy resolutions required. The guide design will be optimised for samples as small as a few mm^3 in size. Scattering from liquids or biological samples and small single crystals in complex sample environments will become routine.

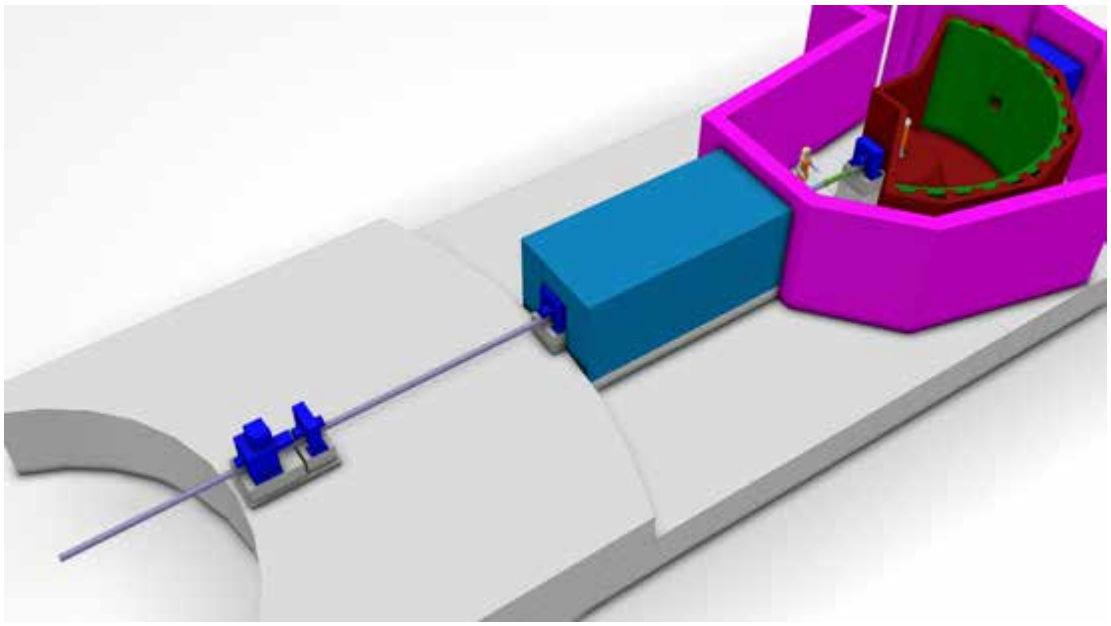

Instrument Description

The bi-spectral chopper spectrometer will be a short instrument; 25.3 m from moderator surface to sample, with a 4 m sample to detector distance. Bi-spectral extraction is possible either via the use of a supermirror switch to reflect cold neutrons into the guide, or by pointing the guide to the edge of the cold moderator to access a warmer spectrum. This will allow a large dynamic range to be probed in a single shot via the use of repetition rate multiplication (RRM). A large dynamic range has been highlighted as important for a variety of scientific cases as diverse as magnetism, soft matter dynamics and hydrogen storage materials. Polarisation analysis is important to all these fields and will be used to separate coherent from incoherent scattering in soft matter dynamics and to determine the direction of magnetic correlations. Polarisation analysis will be implemented via removable polarising guides in the incident beam and a wide-angle ^{3}He cell for spin analysis.

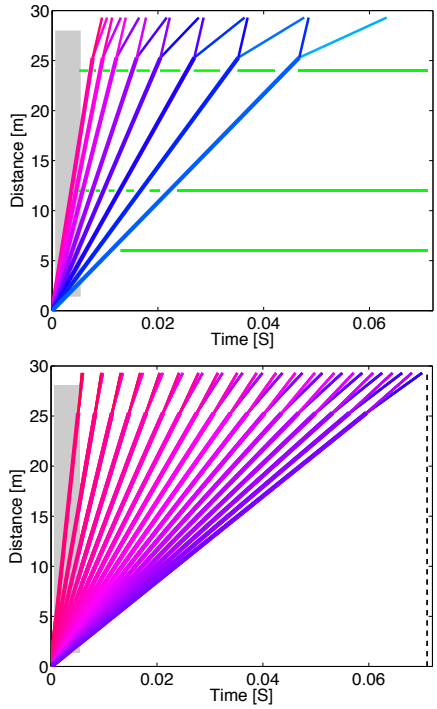

Time-distance diagram for the bi-spectral chopper spectrometer for (top) an inelastic measurement and (bottom) quasielastic scattering. The grey region illustrates the trajectory of fast neutrons from the prompt pulse. The dotted line indicates the full frame of the ESS time structure. The coloured lines follow the paths for neutrons with $1.2 < \lambda < 7.3$ Å for an inelastic measurement (up to 80% energy loss and ambient temperature energy gain) and $1.0 < \lambda < 9.5$ Å for the quasielastic measurement (20 % energy loss and gain).

The figure to the left shows the time-distance diagram of the bi-spectral spectrometer for (top) inelastic scattering and (bottom) quasielastic scattering. All measurements will be performed in the first time frame, avoiding possible problems arising from the prompt pulse; fast neutrons emitted while the proton pulse is incident on the target. The bi-spectral chopper instrument will therefore have a very well defined low background with a world-leading signal to noise ratio. This is particularly important for quasielastic scattering as found in biological samples and the weak diffuse signals found in frustrated magnetism. Chopper positions will be optimised for RRM to provide a range of incoming energies. When measuring inelastic signals far from the elastic peak, it is important that the energy window at the detector, covers up to 80% or more in energy loss and up to ambient temperature on the energy gain side. However there are many cases where only quasielastic scattering is required in which case a ±20% energy range is acceptable and many more incident energy frames can be measured in a single ESS time frame, as shown in the lower figure. A rather sophisticated and flexible chopper system is required to satisfy both requirements.

- One-shot technique for measuring dynamics over a wide energy range.
- Excellent signal to noise ensured by always measuring after the prompt pulse.
- Trade flux for resolution over a large resolution window (1-10 % at 10 Å).
- Three dimensional polarisation analysis as a day-one option.
- Flexible frame length for switching between inelastic and quasielastic modes.
- Good overlap in energy resolution with backscattering instrumentation.

Instrument Parameters	
Moderator	Bispectral extraction
Moderator - Sample distance	25.3 m
Wavelength Range	1 – 20 Å
Sample to Detector distance	4 m
Detector Technology	Boron 10
Detector Coverage	$-30 < 2\theta < 150^o$
Sample environment	Polarisation Analysis as day 1 option High magnetic field (16 Tesla) Lateral access for levitation experiments Non-equilibrium experiments.

Bispectral chopper Spectrometer

Thermal Chopper Spectrometer

Thermal Chopper Spectrometer

Novel states of matter
High-Tc superconductivity
Thermoelectric materials
Battery materials
Geosciences

An instrument designed for broad mapping of thermal excitations with high energy and spatial resolution in hard condensed matter. The $\sim$ 2 Å wavelength band of this 156 m instrument will provide a large bandwidth of thermal neutron energies so that it is possible to measure between with incident wavelengths between 0.7 Å and 2.5 Å in a single measurement thus probing $11 < E_i < 167$ meV simultaneously via repetition rate multiplication (RRM). The long-pulse nature of the ESS source allows a versatile energy resolution that can be varied between 1 % and 6 %. The instrument will be optimised for 1 % energy resolution. Position-sensitive detectors with a 1 cm spatial resolution in addition to homogenous flux and divergence profiles across the sample will provide a very high **Q** resolution as required for studies of single crystals. Polarisation analysis will be a day-one option to enable the measurement of complex magnetic components and to separate coherent from incoherent scattering contributions.

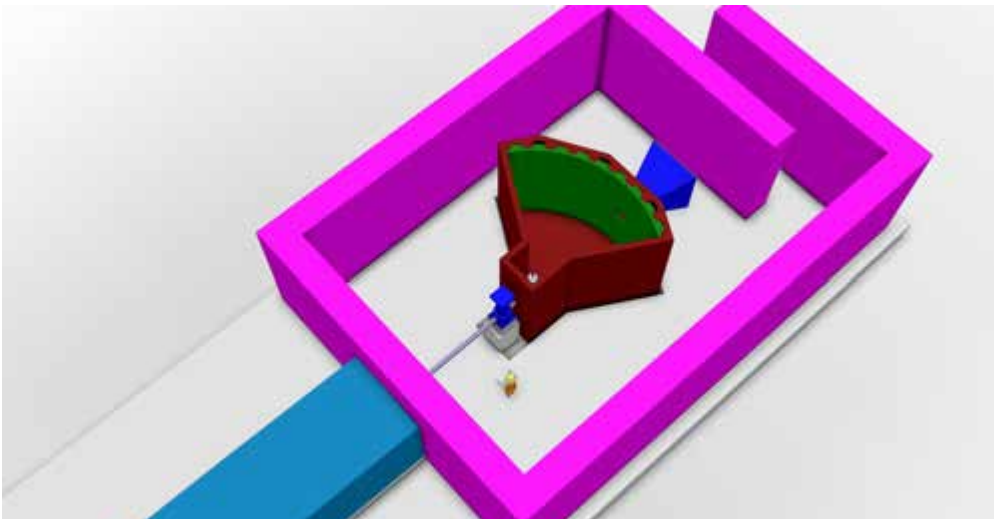

Instrument Description

The high resolution thermal chopper spectrometer is $\sim$ 156 m from moderator to sample. A pulse-shaping chopper is placed at 6 m while a Fermi chopper is situated 1.3 m from the sample to monochromate the beam and provide RRM. To ensure a high signal to noise ratio the sample space will be placed at least 1.5 times out of line of sight of the moderator via the use of a curved guide. The fast neutron spectra that arise from the prompt pulse will be further reduced via the use of a T0 chopper placed close to the monolith. The sample - detector distance is 6 m which, along with the detector depth, will determine the highest resolution possible of ΔE/ E = 1%. The instrument will have an angular detector coverage of 90° in the horizontal plane and $\pm$ 30° in the vertical plane. Polarisation analysis will be a day one option. The incident beam will be polarised with an exchangeable polarising guide section before the Fermi chopper. Analysis of the scattered neutrons will be performed by a ^{3}He spin-filter cell.

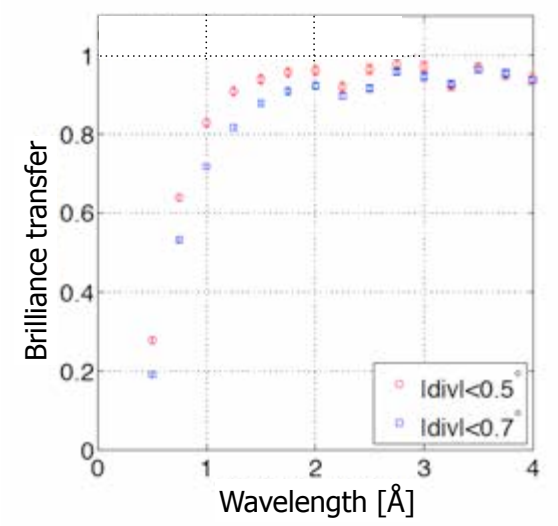

This instrument is well-suited for single crystal experiments. The brilliance transfer of the guide is almost perfect for $\lambda > 1$ Å and 40% at 0.6 Å. Variable divergence profiles are available by exchanging the final guide portions with absorbing pieces that make it also possible to alter the beam profile at the sample position.

A large dynamic range is probed in a single shot via the use of RRM. The figures below show a series of simulated data sets with a range of incident energies that can be obtained in a single time frame, from a sample with a gapped excited state - a magnon or phonon for example. These data, obtained via McStas simulations, reveal the broad range of resultant energy and wavevector transfer resolutions. Multiple energy scans such as these permit a full understanding of the scattering from the sample. RRM data sets also allow the extraction of multiple-scattering and other systematic error effects due to their Q, energy and resolution dependence, ensuring quantitative data analysis, free of spurious background effects. The performance of this instrument is world-leading, with a counting rate for just a single RRM data set comparable to the best instruments today.

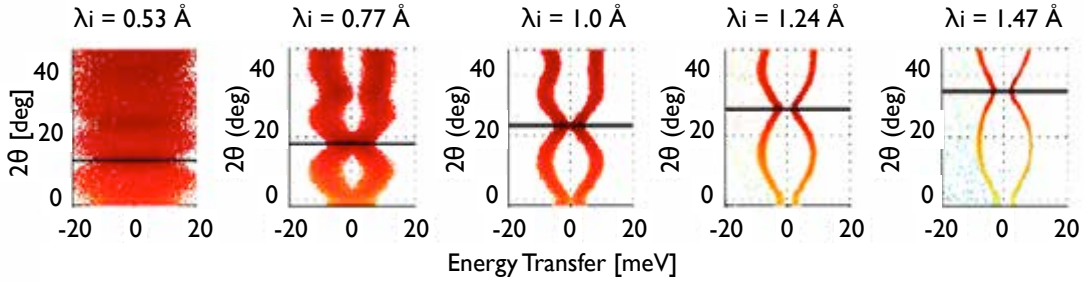

Scattering profiles of a simulated sample with a gapped excited state using RRM on the thermal chopper spectrometer. The range of incident wavelengths in a single ESS time frame gives rise to a large range of wavevector and energy transfer resolutions.

Instrument Parameters	
Moderator	Thermal
Moderator to sample distance	156m
Wavelength Range	0.5-4 Å
Energy Resolution (elastic line)	1 - 6 %
Beam Size at sample	2×2 cm^2
Sample to Detector distance	6 m
Detector Technology	Boron 10
Detector Coverage	$-30 < 2\,\theta < 60^o$
Specially considered sample environment	High Fields, Polarization Analysis

Cold Crystal-Analyser Spectrometer

Cold Crystal-Analyser Spectrometer

Novel states of matter
Molecular magnets & confined systems
High-Tc superconductivity
Novel materials
Thermoelectric materials
Non-equilibrium quantum phenomena
Geosciences

A very high intensity, medium to high resolution, indirect geometry spectrometer covering a wide Q-range. It is especially suited for studies of excitation spectra as a function of wavevector transfer in the areas of functional materials, quantum materials, and geoscience. These investigations use real-world samples and sample environments with the restricted angular access imposed by high-field magnets or high-pressure equipment. The instrument is designed to accept the full ESS long pulse and combines wide angular coverage in the horizontal plane with simultaneous detection of multiple energies using the CAMEA (Continuous Angle Multiple Energy Analyser) concept. Although primarily envisaged as a single crystal spectrometer, it can be employed for the study of powders and liquids and can also function as a diffractometer.

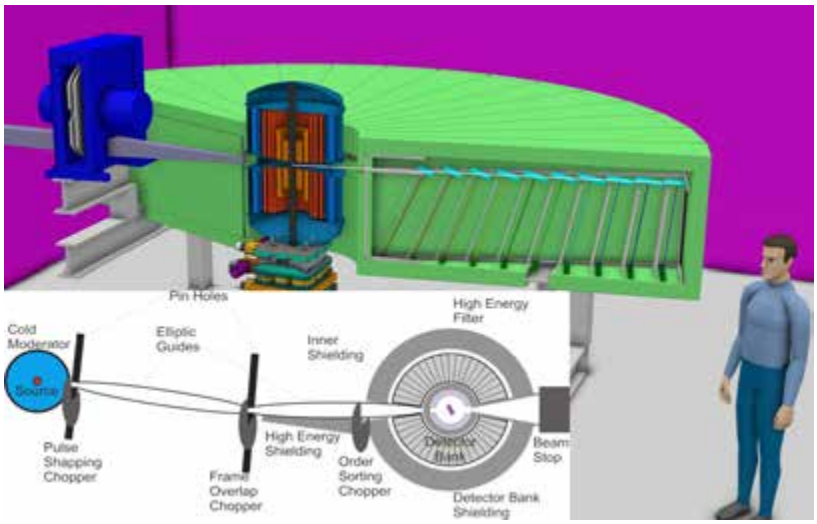

Instrument Description

The instrument uses an inverse time-of-flight geometry, in which the final energy is determined by analyser crystals, while the initial energy is determined through time-of-flight. The spectrometer uses a pseudo-white beam at the sample with a wavelength band of 1.8 Å. The band can be chosen within the interval from 1 Å to 8 Å.

The instrument will use the full pulse width of the ESS when running in high-flux mode, resulting in a flux at the sample of more than 10^{10}n/cm^2/s at an energy resolution $dE/E = 4\%$ and an incident divergence of $\pm 2^\circ/\pm 1.5^\circ$ (vertical/horizontal). For the high resolution mode, a pulse shaping chopper is used, placed as close as possible to the moderator. The distance from moderator to sample is 156 m, which is covered by two consecutive elliptic guides of equal length, with a kink to avoid direct line-of-sight. A frame overlap chopper is positioned between the two elliptic sections.

The secondary spectrometer will consist of 32 analyser detector modules covering all scattering angles between 5° and 165° in the horizontal plane. Each analyser detector module uses 10 graphite crystal analysers placed behind each other to simultaneously record different energies. The analysers cover 4° in the vertical scattering direction and focus to detectors placed below the scattering plane, as shown in the figure above.

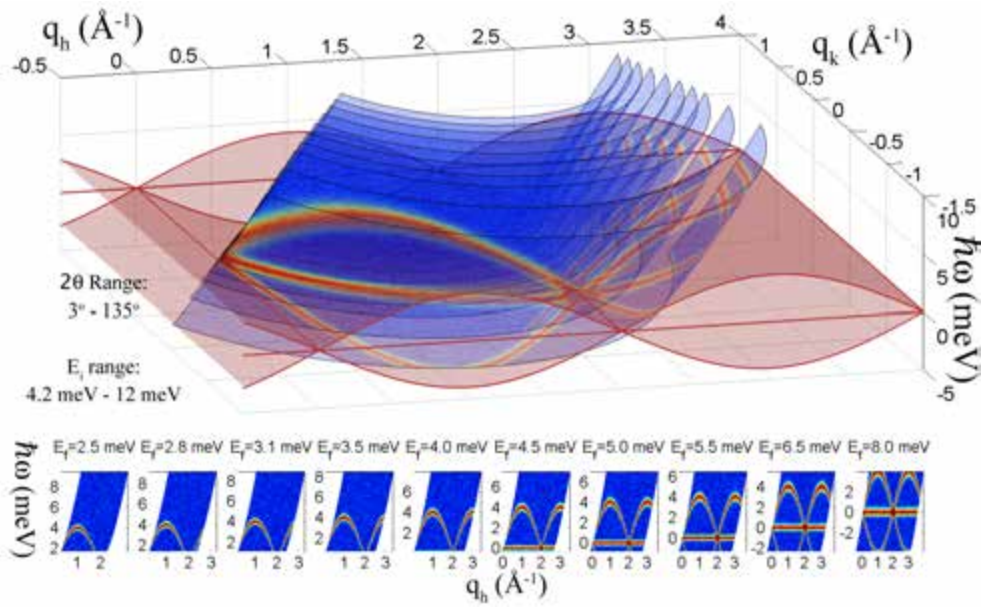

Spin wave dispersion and elastic line simulated using PG002 scattering from the different analysers in maximum flux mode with an energy resolution of 4 %.

Using the PG002 reflection the analysers will cover an energy range from 2.5 meV and 8 meV. The arrangement of the crystals allows for energy resolutions down to $dE/E = 1.2\%$. Placing an order-sorting chopper 2 m before the sample permits recording simultaneously the scattering from the PG002 and PG004 reflections of the analyzer crystals extending the energy range to 32 meV.
In this spectrometer, each analyser will span a parabolic surface in momentum and energy space. In a single acquisition, the consecutive energy-momentum surfaces already provide good coverage (see figure), which can be complemented by sample rotation. The key advantage of this instrument is that coverage is concentrated in the horizontal scattering plane, resulting in good counting statistics within a short time, enabling fast parametric studies as a function of temperature, magnetic field, pressure, etc. The instrument will have polarization analysis and a Be filter will be used for background suppression when covering an energy range below 5 meV.

Instrument Parameters	
Moderator	Cold / Bispectral
Moderator - Sample distance	156 m
Incident Wavelength Range	1 - 8 Å
Energy Resolution	adjustable between ΔE/E = 1.2-6% at 5meV
Q-range	0.04 - 7.8 $Å^{-1}$
Divergence at Sample	adjustable up to ±2°/±1.5° Vertical/Horizontal
Final Energy Coverage of Analysers	for PG002: 2.5, 2.8, 3.1, 3.5, 4, 4.5, 5, 5.5, 6.5, 8 meV for PG004: 10, 11.2, 12.4, 14, 16, 18, 20, 22, 26, 32 meV
Scattering Angle Coverage	$5° < 2\theta < 165°$ for each final energy
Sample to Detector Distance	1.8 - 3.25 m
Detector Technology	^{3}He or solid state detectors, (3.5 m^2)
Sample Environment	High Pressure, High magnetic fields, Extreme temperatures, Pump probe experiments

Vibrational Spectroscopy

Catalytically active materials
Gas storage materials
Waste management
Polymers
Earth & environmental sciences
Molecular magnets & confined systems
Health & pharmaceuticals
In-situ processing
Geosciences
Earth & environmental sciences

A workhorse instrument that is indispensable to energy and catalysis science, and complements neutron diffraction techniques in complex structure determination. It is particularly powerful in optically dense materials compared to non-neutron optical spectroscopies. It complements Raman and IR spectroscopies especially when dipole selection rules complicate the analysis. It is a wide energy range, medium-resolution instrument which allows the measurement of molecular modes, as well as collective excitations under in situ conditions. With an emphasis on the lower energy phenomena such as molecular rotations, lattice vibrations and collective motions, this instrument will also measure hydrogen stretch modes up to about 500 meV with an almost constant resolution $\Delta E/E$ of 2%.

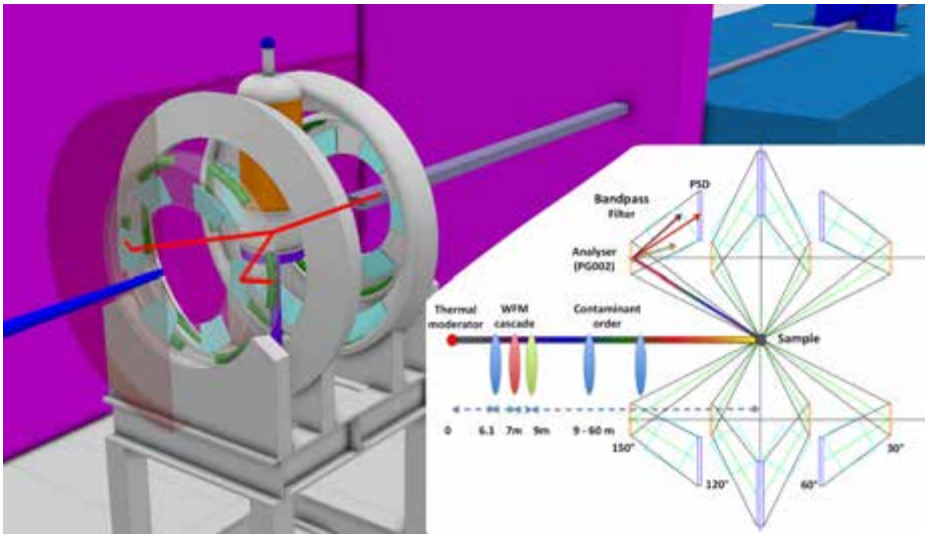

Instrument Description

The concept of the vibrational spectroscopy instrument will take advantage of the flexibility of the long-pulse structure of ESS by trading flux for resolution when applicable, using a flexible chopper cascade. It features a three-interval wavelength frame multiplication scheme, using three independent pulse-shaping choppers to provide 503.6 - 29.7 meV, 37.8 - 7.4 meV, and 8.3 - 3.6 meV with almost constant relative energy resolution. Calculation of the energy transfer is performed using the total time of flight in the primary and secondary spectrometer. The secondary spectrometer is static and energy discrimination of the final energy is accomplished by selecting the final energy using graphite 002 crystal analysers. The four banks of crystal analyser arrays time-focus the forward- and back-scattered neutrons onto the detector banks. Thanks to recent progress in the electronics speed, it will be possible to use position sensitive detection to increase angular selectivity and, therefore, resolution. This provides an increase in neutron count rate, while maintaining a constant energy resolution. Higher order contaminants and incoherent background will be suppressed by cryogenically cooled Be filters. The instrument can access an extended dynamic range starting below the elastic line by rephasing the pulse-shaping choppers.

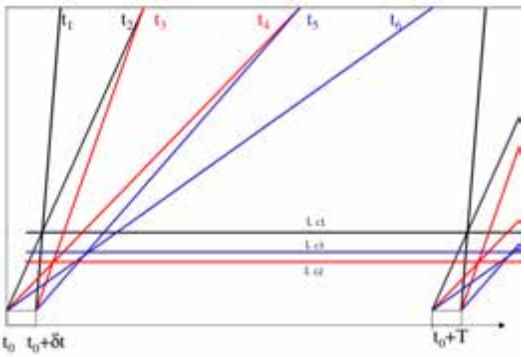

Time distance diagram illustrating the 3 frames which will allow cover a total energy range of 4 - 503 meV. Primary path length of 60 m with 3 independent pulse-shaping choppers at 9.0m, 6.1m and 7.0m

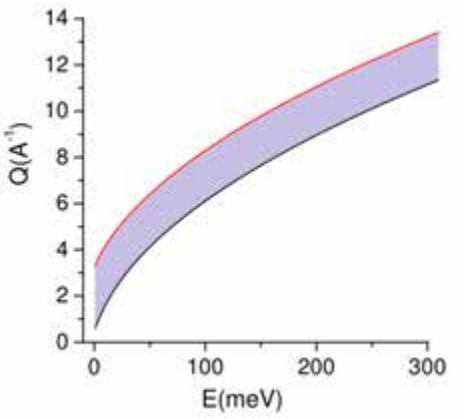

Accessible momentum transfer range over energy for 4 analyser banks centered at 30° 60° 120° 150°.

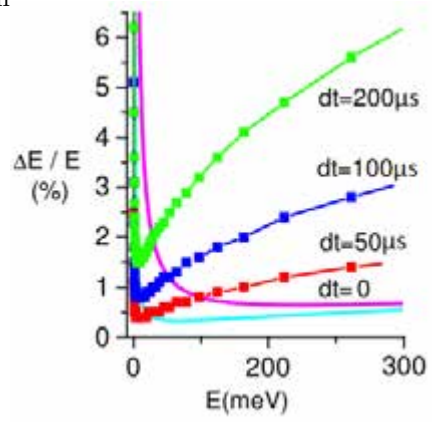

Contribution from the pulse width of the pulse-shaping chopper and the scattering angle (light blue: 30° and 150°; magenta: 60° and 120°) to the instrumental resolution.

A guide focusing option is envisaged to increase the flux on the sample and to facilitate measurements under environmental conditions as well as using a Fourier deconvolution method, by time-modulating the ESS long pulse structure. The estimated measurement times of typical hydrogenated samples at lower energy transfers are expected to be between 1 - 30 minutes per spectrum.

Instrument Parameters	
Moderator	Thermal/Bispectral
Moderator - Sample distance	60 m
Wavelength Range	0.4 - 5 Å
Energy Resolution	ΔE/E better than 2% using PG002 Graphite Analysers
Q-range	1 - 15 $Å^{-1}$
Beam Size at Sample	2×2 cm^2 (Focusing option: 0.5×0.5 cm^2)
Divergence at Sample	±2.5°/±2.5° (Vertical)/(Horizontal)
Sample to Detector Distance	1 m
Detector Technology	^{3}He
Analyser-Detector Banks	4 banks centered at 30° 60° 120° 150°
Sample Environment	High and Low Pressure and Temperature, Controlled Gas Adsorption

Backscattering Spectrometer

Backscattering Spectrometer

Dynamics of biomolecules
Biological membrane assemblies
Cell function
Drug delivery systems
Health & pharmaceuticals
Confined systems
Polymers
Battery materials
Catalytically active materials
Waste management
Gas storage materials
Geosciences

The Backscattering Spectrometer offers access to a unique combination of high energy resolution, intermediate Q coverage, and large dynamic range. The slow repetition rate of the long-pulse source provides the instrument with an unparalleled dynamic range that is well suited for studies of localized relaxational atomic motions overlapping with collective long-range motions, as well as quantum-mechanical tunneling and low-frequency vibrational densities of states. The instrument covers the range of time and length scales between those of chopper spectrometers and neutron spin-echo instruments. The long-pulse time structure of the ESS permits continuous variation of the energy resolution from 2 to 300 μeV, and a broad dynamic range allowing high-resolution spectroscopic in all areas of condensed matter science including chemistry, physics and biology.

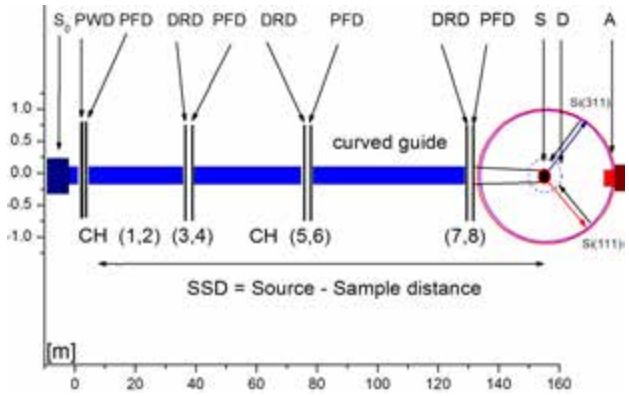

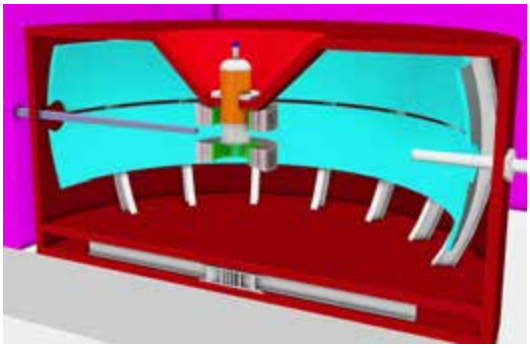

Instrument Description

The instrument uses a chopper cascade in the primary spectrometer, and Si(111) and Si(311) analyzer crystals in the secondary part of the spectrometer. The analyzer crystals are positioned at 2.5m from the sample position and arranged on a spherical surface in near-backscattering geometry. The long-pulse time structure of the ESS permits a continuous trade-off between flux and resolution by varying the opening time of the pulse-shaping chopper. The elastic energy resolution can be chosen between 2 and 50 μeV for the Si(111) configuration and up to 300 μeV for Si(311). The dynamic range can be selected by the choice of analyzer crystals: -500 to +500 μeV with Si(111) and -3.5 to +3.5 meV with Si(311), or by skipping pulses if an even larger dynamic range is required.

The instrument will have a very low background by moving out of the direct line of sight of the source using a curved guide, while an exchangeable radial collimator will minimize the observed scattering from sample-environment equipment. The combination of low energy neutrons and analyzers covering a large vertical solid angle, allows the use of highly divergent beams. State-of-the-art neutron optics will efficiently select and deliver large portions of neutron phase space to the sample position. The high source brightness of the ESS will allow a very large flux at the sample, while the time structure will provide an unprecedented dynamic range. This combination results in an order-of-magnitude performance increase compared to currently world-leading backscattering instruments.

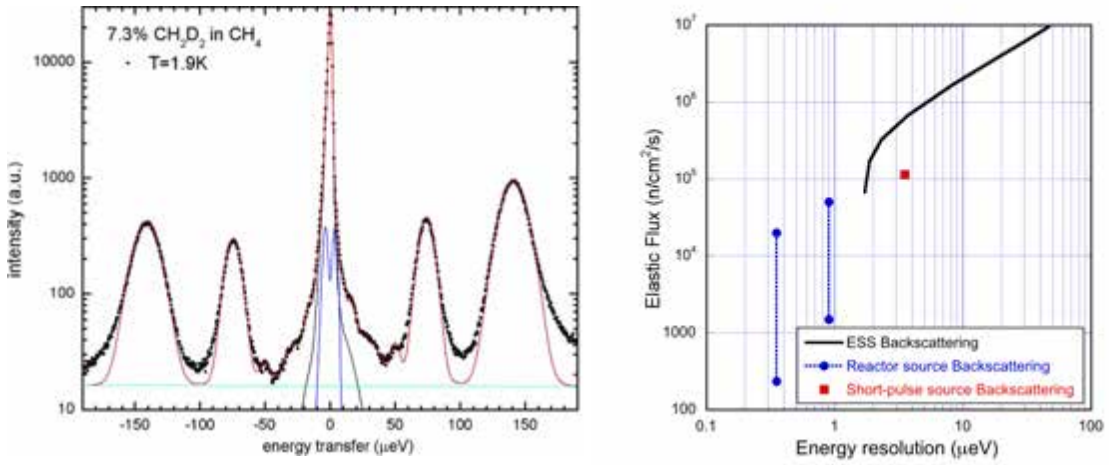

The left-hand figure shows a tunneling spectrum of CH_2D_2 in CH_4, measured on BASIS at the SNS, exemplifying the importance of combining high resolution with a wide dynamic range in fundamental research. The figure on the right shows the calculated elastic flux, defined as the spectral flux on the sample, integrated over the energy acceptance of the analyser crystals, compared to today's world-leading backscattering spectrometers at pulsed and continuous neutron sources. The flux of the ESS instrument is shown as a solid black line, illustrating how the resolution and hence the flux, can be tuned by modifying the opening time of the pulse-shaping choppers. At comparable resolution, the ESS instrument is seen to outperform the currently world-leading instrument by a factor of five. In reality that gain factor will be considerably larger, as it can reasonably be expected that another factor of two can be achieved by transporting a larger divergence to the sample.

At comparable resolution, with 5-10 times higher flux than the currently world-leading instrument, the ESS instrument simultaneously achieves a dynamic range which is three times larger. The continuous-source instrument has two flux conditions shown for the two resolution configurations, each corresponding to measurements with the monochromator Doppler drive on and off. The lower flux number corresponds to normal measurement conditions with the Doppler drive on, for which this instrument has a dynamic range of 30μeV, for comparison with the 1 meV dynamic range of the ESS instrument. With the Doppler drive off, the dynamic range of the continuous-source instrument is not used, but the elastic flux is integrated over the resolution width.

Instrument Parameters	
Moderator	Cold
Moderator - Sample Distance	156 m
Wavelength Range	2 Å - 8 Å
Energy Resolution	2 - 50 μeV for Si(111), 8 - 300 μeV for Si(311)
Dynamic Range	1 meV for Si(111), 7 meV for Si(311)
Q-range	0.1 Å^{-1} - 3.8 Å^{-1}
Beam Size at Sample	variable between 0.5 × 0.5 cm^2 and 3 × 3 cm^2
Divergence at Sample	Up to ±3°/ ±3° (Vertical)/(Horizontal)
Sample to Analyzer Distance	2.5 m
Detector Technology	^{3}He tubes
Detector Coverage	2 banks of $10° < 2\theta < 170°$
Sample Environment	Low and High Temperature, High Pressure, Humidity and Gas control, Pump Probe

High-Resolution Spin Echo

Dynamics of biomolecules
Biological membrane assemblies
Polymers
Cell function
Self-assembled colloids
Food science
Drug delivery systems
Confined systems

Used to measure slow dynamics, this instrument covers a broad energy (10 ps - 1 μs) and Q-range (0.01 - 2 Å^{-1}), but will be optimised for the study of large structures, i.e. for measurements at low Q. This makes the instrument particularly well suited for the investigation of complex soft matter systems, proteins and other biomolecules, dynamics under confinement and colloid physics.

The instrument is a high-resolution neutron spin-echo spectrometer, using the neutron spin to encode very small changes in the velocity of the neutron, thus decoupling the energy resolution and intensity. This instrument reaches the highest energy resolution at the ESS. It is optimised to provide maximum flux on the sample, at the expense of reaching higher Q-values. Due to the large wavelength bandwidth a very large time and spatial range can be covered within one experiment.

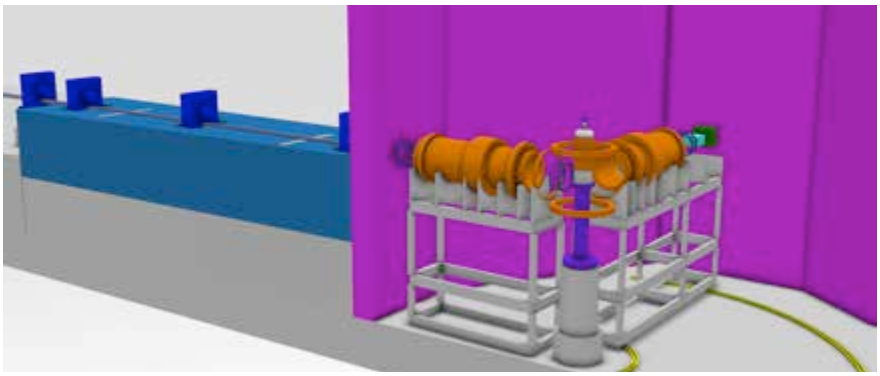

Instrument Description

A total instrument length of 35 m allows for a usable wavelength band of around 8 Å, allowing for a broad simultaneous $Q-t$-range to be accessed, with an excellent intensity and sufficient wavelength resolution. The instrument will use superconducting solenoids for the main coils, allowing field integrals of more than 1 Tm to be obtained. The choice to use superconducting technology comes from the dual requirement of high field integrals and excellent field homogeneity for reaching the very highest resolution. This technology for the main coils was first implemented at the SNS-NSE spectrometer and has been shown to work well [204]. The optimised coil configuration is inspired by the IN15 renovation project at the ILL, and is expected to lead to significant gains, since it will be possible to reach an equivalent Fourier time resolution using a shorter wavelength than previously (alternatively, one can reach longer Fourier times using the same wavelength).

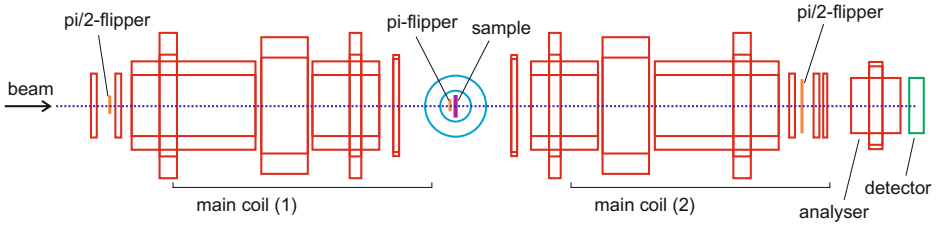

Sketch of the possible coil configuration for the high-resolution spin-echo instrument.

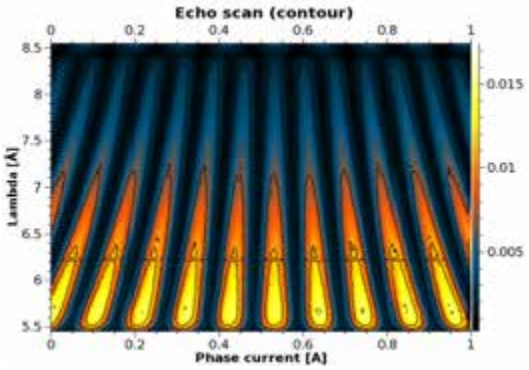

Contour plot of the obtained echo as a function of wavelength at the high-resolution SNS-NSE spectrometer.

For the correction elements it is planned to use two correction coils in each spectrometer arm. It is assumed that performance of these coils will at a minimum match those currently used in high-resolution NSE spectrometers. These combine two quadratic corrections x^2 and y^2 to a radial corrective action r^2 (Pythagoras coils). If new developments allow for the manufacture of sufficiently accurate radial correctors, further enhancement of performance can be achieved.

Incident beam polarisation will be possible via an FeSi supermirror bender, although the option of using a kink with a single reflection from a straight wall is also being considered. Both options perform well at the longer wavelengths, which are critical for the resolution, but the bender is able to extend the performance to shorter wavelengths. The polariser also plays the important role of bringing the instrument out of the direct line of sight of the source.

The instrument will outperform current world-leading NSE instruments by at least an order of magnitude, due to the source brightness, including an excellent flux at long wavelengths, the nature of the long-pulse source, as well as the large field integral which will be achieved.

It is essential for the performance of the instrument that magnetic disturbances are minimised. The instrument will therefore be placed in the North sector of the main experimental hall, together with other instruments which do not use cryo-magnets. In the north sector of the hall the beam height is 3.1 m, which will provide extra distance from any magnetic impurities in the floor.

Instrument Parameters	
Moderator	Cold
Moderator - Sample distance	30 m
Wavelength Range	4-25 Å
Wavelength band	8 Å
Q-range (Resolution)	0.01 - 2 $Å^{-1}$ (< 10%)
Fourier time range	10 ps - 1 μs
Field integral	>1 Tm
Beam Size at sample	3×3cm^2, optional smaller pinhole
Divergence at sample	±0.5°
Sample to Detector distance	5 m
Detector	30 × 30 cm^2 He 3 area detector
Angular range	$0 < 2\,\theta < 90°$
Sample environment	Standard temperature equipment, dedicated pressure cell

Wide-Angle Spin Echo

Wide-Angle Spin Echo

Novel materials
Battery materials
Gas storage materials
Polymers
Novel states of matter
Dynamics of biomolecules
Biological membrane assemblies
Cell function
Food science
Drug delivery systems

Measuring slow dynamics over a wide simultaneous Q-range this instrument is able to reach up to $Q = 4$ Å^{-1}, while still achieving a good energy resolution (1ps - 100ns). The instrument is therefore particularly well-suited for studies at high-Q in systems such as glass-forming polymers and magnetically frustrated materials, as well as for studying slow diffusional processes in for example functional materials such as fuel cell membranes. With an excellent Q-resolution it will also be well-suited for the study of crystalline samples.

It uses the neutron spin to encode very small changes in the velocity of the neutron, thus decoupling the energy resolution and intensity. Compared to the high-resolution spin-echo instrument, this is a medium energy resolution instrument optimised for large scattering angles and with a large detector solid angle, allowing for a very broad simultaneous Q-range to be measured with a very high count rate.

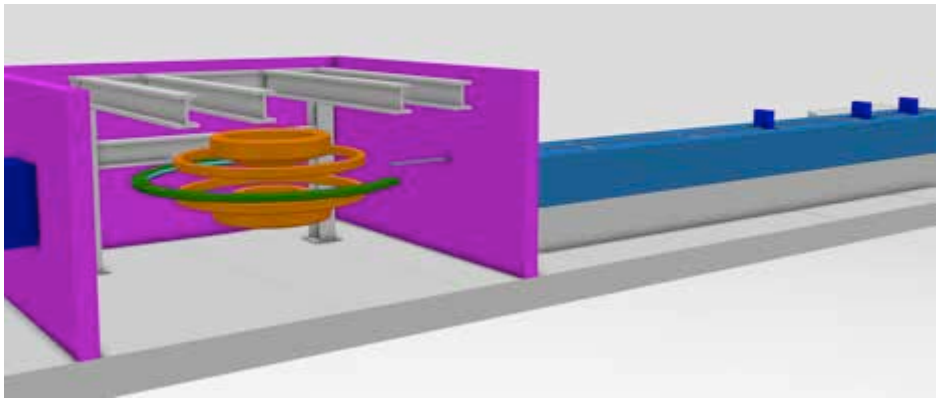

Instrument Description

The wide-angle spin-echo spectrometer is based on the SPAN@HZB / WASP@ILL designs [205]. For this instrument the main coils are arranged in a 'quasi-anti-Helmholtz' configuration, i.e. there are two circular coils placed symmetrically above and below the horizontal scattering plane using opposite currents. The field in the horizontal plane is then rotationally symmetric, allowing the use of a large detector bank.

The spectrometer will have a longer moderator-to-sample distance compared to the high-resolution spin-echo instrument. While this means that the instrument will have a smaller useable wavelength band, it provides a better wavelength, and hence Q-resolution, improving performance for studies of crystalline samples. An optional pulse-shaping chopper will be used to further improve the Q-resolution at the expense of flux.

The instrument length allows for a wavelength band of 5 Å, which, compared to currently world-leading instruments using a 10 % velocity selector, will lead to improvement in performance of up to an order of magnitude - in particular at the shorter wavelengths, which is where the majority of the measurements on this instrument will be done. Furthermore, compared to currently existing spin-echo instruments, there will be a enhancement in performance from the use of the wide detector bank.

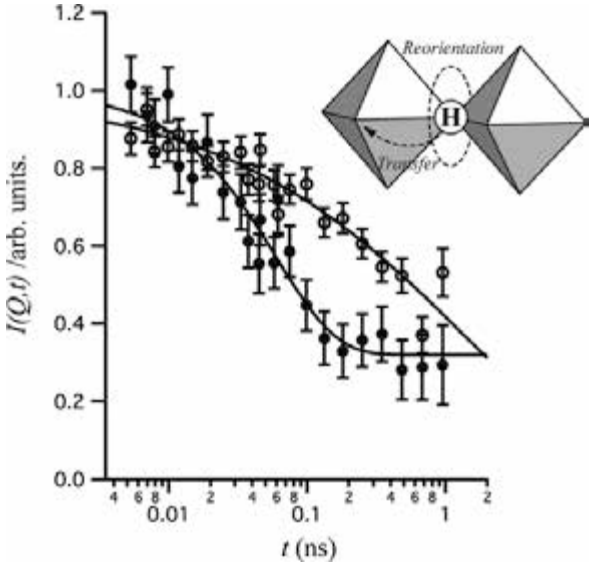

Intermediate scattering function obtained for proton-conducting perovskites at Q= 1.05 Å^{-1} using NSE [206]. The wide-angle spin-echo instrument at ESS will be well suited for this type of study of energy materials at high Q-values.

The wide-angle spin-echo instrument will use normal-conducting wire for the main coils, with a diameter of around 3 m, giving a total diameter of the instrument of 7 m. The expected field integral provided by these coils is of the order of 0.3 Tm. Supermirrors will be employed for both the polariser and analysers. It is expected that the polariser will be a bender, since the performance at shorter wavelengths, which are key for reaching the highest Q-values, is better for this option. The polariser will also play the important role of bringing the instrument out of the direct line of sight of the source.

The instrument will be placed in the North sector of the main experimental hall, where the floor height is lowered to avoid magnetic interferences from impurities in the ground, together with the other instruments which do not use cryo-magnets, since it is critical to the instrument performance that magnetic disturbances are minimised. It will therefore also be placed away from the high-resolution spin echo spectrometer to avoid magnetic interference between the two spin-echo instruments.

Instrument Parameters	
Moderator	Cold
Moderator - Sample distance	50 m
Wavelength Range	3-15 Å
Wavelength band	5 Å
Q-range (Resolution)	0.01 - 4 Å^{-1} (< 5%)
Fourier-time range	1 ps - 100 ns
Beam Size at sample	3x3cm ^{2}, optional smaller pinhole
Divergence at sample	±0.5° / ±1.0°
Sample to Detector distance	4 m
Analysers	Supermirror
Detector Technology	He-3 or B-10
Angular Coverage	-130 < 2 θ < 130°
Sample environment	Standard temperature equipment, dedicated pressure cell, cryopad [207]

Fundamental & Particle Physics

Neutron electric dipole moment
Origin of matter
Neutron decay
Neutron-antineutron oscillations
The neutron as a quantum wave
Neutron bound beta decay

A beamline for precision tests of the standard model, quantitative understanding of the nucleon and its interactions, and searches for new interactions and symmetries. Topics that may be addressed with such a beam line include searches for nucleon-nucleon weak interactions and possible exotic neutron interactions, and neutron beta decay correlation measurements. These investigations require a pulsed beam and would therefore benefit from a factor 10 gain over existing beamlines.

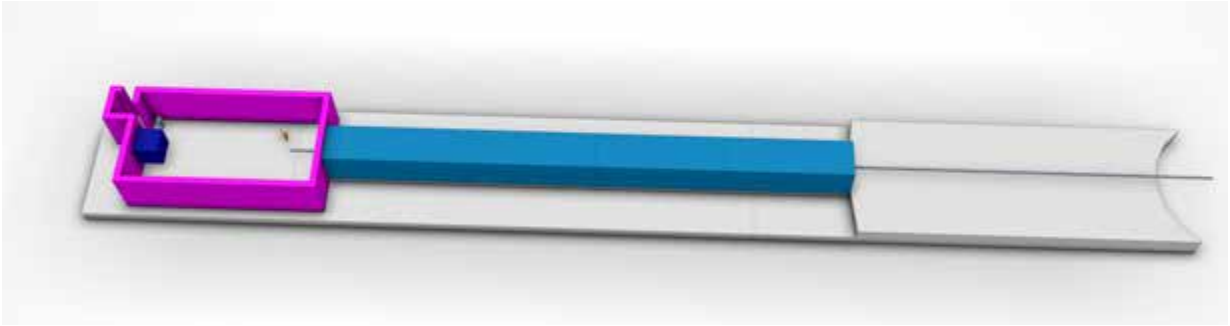

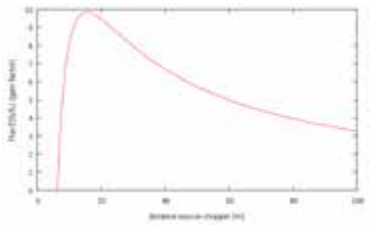

A versatile well-defined cold neutron beamline with a versatile arrangement allowing a broad range of fundamental physics to be investigated. A large experimental area allows detectors to be exchanged, and additionals, such as polarisation and polarisation analysis to be added.

Instrument Parameters	
Moderator	Cold
Moderator - Sample distance	70m
Wavelength Range	5- 30 Å
Energy Resolution (elastic line)	N/A
Q-range (Resolution)	N/A
Guide geometry	No line of sight to moderator
Beam Size at sample	100×120 mm^2
Divergence at sample	2°
Sample to Detector distance	Up to 30m in length, 6m height and width
Detector Technology	Various: ^{3}He, Microchannel Plates, Semiconductor, Scintillator
Detector Coverage	typically <10cm^2
Sample environment	High accuracy polarisation and polarisation analysis available

2.6 Neutron science support facilities

ESS will be part of the future suite of European research infrastructures that will provide experimental possibilities for research from both academia and industry. For its scientific success, ESS has to be governed by the scientific needs of its users. This goal determines the outline of this section on science support facilities. The outlined facilities are required independently of the different user access modes. However, it is evident that these plans will evolve during the transition from construction to operation depending on the policies adopted concerning user access modes (both proprietary and public), in-house research, intellectual property and data ownership, scientific collaboration, education and outreach [42]. In the current situation, emphasis is put on scientific motivation as well as on defining interfaces and requirements for building ESS facilities.

2.6.1 User programme, academic activities and sample handling

Extrapolating from data from similar user facilities, Table 2.2 summarises key estimated parameters for the ESS user programme, which depend on the number of operational instruments, the number of beam days available for research using neutrons and the average experiment duration. The number of operational instruments will steadily increase from seven in 2019 to 22 in 2025. The duration of experiments varies significantly over the instrument suite, defining both the level of ESS staff and support and the on-site user presence required. Experience from other facilities indicates that experiment duration does not decrease as quickly as instrument performance improves. Instead, improvements in instrument performance lead researchers to undertake more challenging experiments, for instance, using a larger number of samples, or undertaking more sophisticated measurements. In the period from 2019 to 2025, the average experiment duration is therefore likely to decrease from five days initially to three days as full power is reached. The available beam days for research using neutrons is expected to ramp up to about 225 days per year. Given these assumptions, the number of experiments, users on-site and activated samples (sample lots) requiring storage can be estimated. It is also assumed that three scientists visit for every experiment and stay for the duration of the experiment plus one day. About 1.5 scientists per instrument will stay for some additional time, for example, for sample preparation and special instrument set-up. Therefore, facilities will be available to meet the needs of 121 users on-site at any given time including workspace (office, computer network access and library); networking (lecture hall, meeting rooms, and areas for social mingling); accommodation (guesthouse); catering (canteen and coffee shop); and recreational possibilities (gym). Rapid and convenient transportation will be possible among scientific sites (ESS, MAX IV, Lund University) and to Lund Central Railway Station at all times. Additional details are available in Sections 7.2.1 and 7.3.3.

The user office will be equipped with the IT tools necessary to run the user programme, which will support researchers from the inception of a scientific idea through to publication. The user office will be

Parameter	2020	2025
Experiments		
Number of operational instruments	7	22
Beam days available for neutron experiments	100	225
Average experiment duration in days	5	3
Number of experiments per year	140	1650
Users		
Average number of users per experiment	3	3
Total number of user visits per year	420	4950
Typical number of users performing experiments	25	88
Typical number of users preparing samples or experiments	10	33
Typical total number of users on site at any one time	35	121
Lab space		
Work spaces per instrument	2	2
Total number of work spaces	14	44
Storage for activated samples (stored for 2 years)	280	3300

Table 2.2: Estimates of user key programme parameters in 2020 and 2025.

responsible for registering users and maintaining the web portal. It will administer the proposal system, including evaluation, and the assignment and scheduling of instrument, equipment, and other resources. It will handle user visits, including arrangements for travel, accommodation, safety training, and expense reimbursement. And it will support virtual experiments, sample handling, user-specific data access, and publication tracking. Details are presented in Section 2.8.2.

As outlined in the previous section, ESS will make possible experiments on challenging "real-world" samples, which will be prepared, handled or investigated in diverse optimised sample environments, some of them with extreme conditions, that could not be handled at earlier facilities. Users will be provided with facilities for on-site sample preparation and conditioning. Since beam time is a precious resource, it is crucial to assist users, ensuring the measured sample has the expected characteristics and has not, for example, been damaged during travel. The facilities will complement those available at the home institute or at more specialised local infrastructure, taking the special requirements of neutron samples, such as isotope substitution or special containment, into account. The flow of samples at ESS is illustrated in Figure 2.25.

Appropriate and safe handling are prerequisites for a successful research project. Samples have to be handled safely before, during and after experiments at ESS, taking potential risks into account including radiological, biological and chemical hazards. Disposal routes for radiological, conventional and chemical/biological laboratory waste will be established, and controlled access zones will be planned to ease sample transport between the various laboratories. Logistic support and infrastructure (pathways) will be provided to ensure safe and efficient transport of samples, equipment and users under controlled environments, taking into account the size of the facility and the distances involved. (See also the general discussion of facilities for handling samples in Section 7.3.)

The technical support required prior to and during a user visit is determined by the nature of the specific experiment. Workshops with mechanical technical capabilities will often be required in close to the instruments to prepare items in a timely manner. Following the recent trend at other neutron facilities and in accordance with safety requirements, user laboratories in the controlled areas will all provide the capability to condition the samples promptly before the experiment with adequate capacity to accommodate users in accordance with the estimates presented in Table 2.2. These facilities will include equipment for sample handling, preparation, and storage appropriate for different types of materials, such as biological, active, or chemical materials. User laboratories will be cost-effectively grouped in instrument halls each serving the scientific needs of several instruments. Most samples will arrive prior to the experiment from the user's home institute or other facilities and will be tracked and stored. After the experiment, the samples will either be disposed of on-site or shipped back to the user's home institute.

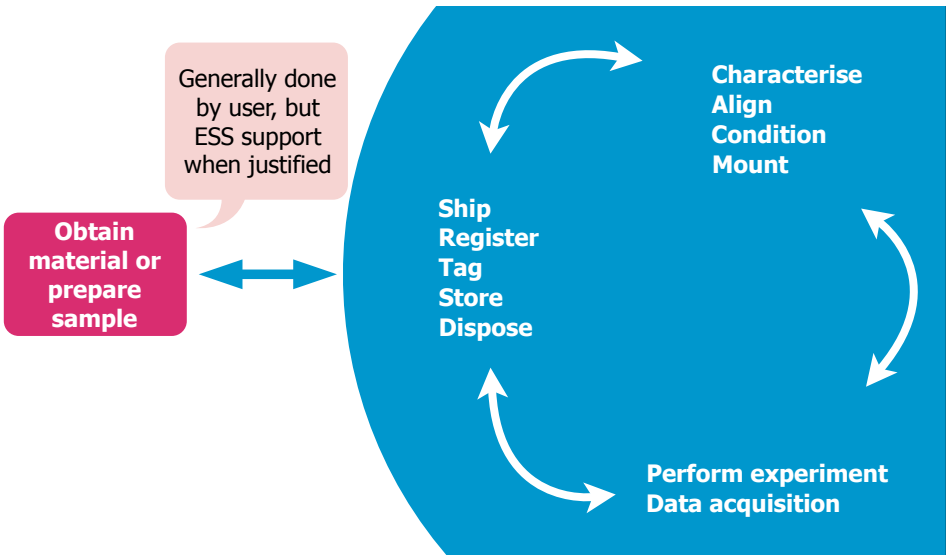

Figure 2.25: Flow of neutron experiment samples, indicating core activities performed on-site (cyan), and supplementary activities concerning sample preparation (purple) that require dedicated access modes and intermediate involvement of the user group.

In both cases, radiological activation will require special precautions and temporary storage in adequate conditions for time periods ranging from a few days to up to two years, following guidelines described in Chapters 10 and 11.

2.6.2 Laboratories for life science and soft condensed matter research

It is a great challenge for many experiments in biology and soft condensed matter (SCM) to obtain the optimal sample, and to condition and characterise it properly before and during the experiment. Successfully meeting this challenge calls for well equipped sample handling and characterisation laboratories in the immediate vicinity of the instruments, and central support facilities for sample production techniques specific to neutron experiments, particularly deuteration.

Most experiments in biology and SCM require the timely preparation and thorough characterisation of the sample, either *in situ* or just prior to the experiment. Samples often have to be handled in a controlled environment with respect to temperature, humidity and other conditions. For this reason, sample handling and characterisation laboratories will be located very close to the instruments within the controlled zone. These facilities will be open automatically to all users who have been scheduled for beam time.

Exhaustive, partial or selective deuteration of the sample material is often necessary in biological and SCM research, either to reduce the incoherent scattering background or to provide contrast variation to highlight molecules in multi-component systems. Since many potential users will not be experts in producing and characterising deuterium-labelled sample materials, ESS will provide support and expertise in these techniques in addition to the sample-handling laboratories. The effort and resources required for this support are small in comparison to the cost of beam time and are more than justified by the higher-impact experiments they will allow to be performed. The main categories of sample material that benefit from these techniques are recombinant proteins, deuterated surfactants and polymers, and other macromolecules for crystallography, SANS, reflectometry and spectroscopy experiments, and deuterated lipids or other amphiphiles for SANS and reflectometry. Small quantities of other small molecules, such as ligands and cofactors or pharmaceutical agents, are also required, and can usually be obtained by custom synthesis. Biological and chemical perdeuteration are well established for nuclear magnetic resonance (NMR) experiments, for example. Since not all users will have expertise in these techniques, ESS will provide laboratories for both chemical and biological deuteration, and staff them with personnel competent to help users with both techniques.

In neutron macromolecular crystallography, the main bottleneck is growing large, high-diffraction quality crystals. While the methods for growing protein crystals for X-ray crystallography are fairly mature, they are optimised for producing crystals smaller than 50 μm, while neutron crystallography requires much larger samples. A large majority of users will not be experts in the specialised techniques for optimisation of large crystal growth, and will not possess the necessary equipment. Thus, ESS will provide a specialised environment for protein crystallisation to support neutron macromolecular diffraction.

Sample handling and characterisation laboratories

Bulk sample characterisation equipment such as dynamic and static light scattering instruments, optical and infrared spectrometers and densitometers will be available in the sample handling and characterisation laboratories. Equipment for surface characterisation, such as an ellipsometers, quartz crystal microbalances, Langmuir troughs and contact angle goniometers will be provided. There will also be research-grade optical microscopes available. Complementary measurements for small angle scattering and reflectometry using X-rays will be provided either with laboratory X-ray equipment, or through easy and rapid access to MAX IV beamlines. At full user operations, 30 to 40 people will use the laboratories at any one time. The laboratories will be accessible from all the instruments applicable to SCM and biology.

The instrument layout envisaged for ESS will mean that the halls with instruments used for biological and SCM experiments will need laboratory space within the controlled zone for sample handling and characterisation, which can be grouped within the instrumental halls housing the relevant instruments, but may also need to be duplicated or shared in some cases. When the sample can be safely transported off-site to MAX IV or other facilities in Lund, these will provide additional access to a large suite of specialist characterisation tools in a collaborative framework.

Deuteration facilities

The ESS deuteration laboratory will provide all the necessary equipment for the production and purification of deuterated sample materials, as well as access to characterisation techniques such as mass spectrometry or NMR on a collaborative basis within the local academic environment. Recombinant proteins are typically produced in a microbial host such as the bacterium *Escherichia coli* or yeast cells grown in D_2O with a deuterated carbon source. Either shaker flasks or specialised fermentors are used for the culture, depending on the quantities required.

The production of deuterated lipids and many synthetic compounds, such as polymers and surfactants, is generally achieved either by exchanging the hydrogens in a chemical reactor or by extracting natural compounds from cells grown in deuterated media. The former option involves process chemistry and custom synthesis techniques in which few users have expertise and for which commercial suppliers do not exist, so a dedicated ESS laboratory is well justified. The extraction method is in many ways similar to the production of deuterated proteins in microbial cultures and will be realised using large-scale fermentors as part of the biological deuteration facility. Having facilities for both chemical and biological deuteration on-site will allow ESS to create synergies by using one approach to produce raw materials for the other (e.g. sugars for chemical modification, or specially synthesised amino acids or other small molecules for labelling proteins or as precursors to synthetic compounds).

For routine projects, the facility will operate in service mode, but for more challenging projects, users will be expected to send personnel for an extended stay. Such extended stays will have the added advantage of building user expertise in these techniques to support future research. Because the techniques and equipment for protein expression and purification are not specific to perdeuteration, the ESS deuteration facility will be able to be part of a larger platform such as the LP3 protein production platform at Lund University. This will offer economies of scale, and will also allow efficient sharing of expertise between ESS and the university and provide a stimulating scientific environment. The deuteration laboratory will also actively develop labelling methodology. The expected mass for deuterated protein when ESS is in full operation with 22 instruments is more than 10 g of pure protein per year from more than 100 constructs with more than 20 users at any one time.

Biocrystallisation facility

A biocrystallisation facility will provide users with access to equipment and expert support in obtaining the largest crystals possible, thus reducing data collection time. Equipment for controlled crystal growth using both temperature and concentration as variables will be provided. While the number of users at any one time will be about five, storage and automated visualisation of the crystals will be provided for more than 50 projects per year. Based on those requirements, the deuteration and biocrystallisation facility will consist of about 750 m^2 of laboratory space situated outside the controlled zone. These laboratories may be located within the joint infrastructure for ESS and MAX IV. While the laboratories for sample handling and characterisation will be available to all users coming for an experiment, both deuteration and biocrystallisation facilities will require specific access modes.

2.6.3 Laboratories for chemistry, physics and materials science

Chemistry, physics and materials science researchers will require sample conditioning and preparation facilities (including adequate storage space) located as close as possible to an instrument, preferably with separate facilities for non-radioactive and radioactive samples. These laboratories will be equipped with four or five-decimal place balances so that sample absorption corrections can be calculated, and with gases (air, nitrogen and argon/helium) so that samples can be loaded under inert atmospheres in glove bags and cells.

Chemistry laboratories

Well equipped chemistry laboratories, occupying about 100 m^2 per instrument hall, will be used not only for *ex situ* sample conditioning but also to support *in situ* equipment on the instruments. Several hundred users per year will use the chemistry laboratories. The instruments requiring support in the form of chemistry laboratories are spread out in all instrumental halls, implying replication of chemistry facilities. Two to three groups of three scientists are expected to require access to the chemistry laboratory space

dedicated to a given instrument at any one time. Equipment will include dedicated fume cupboards for each user group for work with organic solvents, plus an additional cupboard for acids; wet and dry glove boxes; bench space; vacuum and drying ovens for samples and glassware; a densitometer; ultrasound-bath; die press to make pellets; refrigerators and freezers providing both conventional cooling and -80°C for delicate samples; a cold room; general laboratory equipment; and access to acids, bases, solvents and general chemicals. One of the chemistry laboratories within the instrumental halls will house a chemical storage facility; furnaces for annealing samples under gas flow and under air (up to 1500°C); dielectric spectroscopy; thermogravimetric analysis and differential scanning calorimetry.

Physics laboratories

Due to its sensitivity to both magnetic and structural properties, condensed matter physics is a core business for neutron scattering. Because of the different energy scales governing the properties of the sample, requirements for extreme conditions in terms of temperature, magnetic field, and pressure are significant. Neutron experiments often require *in situ* measurements of magnetic and other electronic properties to link results together. To prepare for these *in situ* measurements, but also for supplementary *ex situ* measurements on the same samples prior to and/or after the neutron experiments, a dedicated hard condensed matter laboratory is required. The equipment will be compatible with the sample environment used on the instrument, including some of the sample environments for extreme conditions. The laboratory will contain basic measurement equipment for magnetic susceptibility, electrical resistivity and specific heat.

For many experiments, cutting, orienting, co-aligning and mounting the sample is a prerequisite. Mounting samples will require on-the-spot tailored mounts manufactured in on-site workshops. Co-alignment may be (semi)-automated using robotics. Both gluing and bonding may be used to mount samples. Equipment for sample cutting and polishing will be available. A single crystal neutron alignment facility will be provided for sample quality control and orientation, which will be complemented by X-ray equipment.

Laboratories for highly radioactive samples

Actinide-based samples, special isotopes and other highly activated samples will be handled in dedicated laboratories, enforcing approved handling procedures. Equipment will include glove boxes; equipment for container leak testing, sealing and/or encapsulation; and dedicated storage space. The facilities discussed in this paragraph will be co-located with the spaces required for sample environment (as discussed in Section 2.7) due to their close link with extreme sample environment. Laboratories for highly radioactive samples will be located within the controlled zone in order to deal with sample activation.

2.6.4 Facilities for engineering and other research areas

Engineering facilities to handle bulky real world samples will be provided for material scientists, geoscientists and cultural heritage scientists from both public and private institutions. The engineering and geoscience facility will consist of several laboratories with at least 150 m^2 surface area placed in close proximity to the materials science & engineering diffractometer and also accessible by users of the multi-purpose imaging instrument. The facility will be accessible to lorries and its floors will have a load carrying capacity of 5 tonnes per square metre. Rooms will be provided for user support, sample environment, materials characterisation and storage. Computers for data analysis and integrated workstations for laser scanning, robotics, and instrument setup will be available to the users.

The sample environment laboratory will be equipped with an overhead crane with a 5 tons load-bearing capacity and the ability to store large pieces of equipment. It will also be equipped with typical *in situ* equipment, including a variety of servo-hydraulic testing rigs and power supplies, furnaces, electrical supplies (piezoelectric), laser scanner, robots and sample changing equipment. The materials characterisation laboratory will be built with vibration-proof flooring and exhaust pipes. Automated hardness tester, laboratory X-ray machine(s), microscope, metallurgy suite, SEM, 3D measurement systems, welding and deformation equipment will be available. A safe room will be provided for the storage of irradiated and precious samples, such as irreplaceable works of art, archaeological artefacts, and palaeontological specimens.

Laboratory work space	Location	Number of user group work spaces	Area [m^2]
Life sciences & soft condensed matter			
Extended preparation	Controlled zone	6+extra	250
Basic preparation	Controlled zone	12	300
Deuteration and biocrystallisation	On site or in science village		750
Chemistry & physics			
Extended chemistry	Controlled zone	6+extra	250
X-ray and physical characterisation	Controlled zone	4+extra	200
Radioactive samples	Controlled zone	extra	25
Basic chemistry	Controlled zone	12	300
Engineering & cultural heritage			
Engineering	Controlled zone	2+extra	200
Cultural Heritage	Controlled zone	2+extra	100

Table 2.3: Estimated requirements of laboratories indicating location, the number of workplaces for teams of 3 persons each and the approximate area. User groups are assumed to consist of 3 persons, on average, each requiring 25 m^2 of work space. The basic preparation laboratories will be distributed among the different instrument halls.

2.6.5 Laboratory work space requirements

Table 2.3 summarises the requirements for the laboratories that will be constructed (but not equipped) as part of the conventional facilities activities discussed in Chapter 6. The work space per experimental team is estimated to be 25 m^2, but extra space will be required for one of the topical laboratories grouping the more advanced equipment.

2.7 Instrument support and neutron technologies

State-of-the-art neutron scattering instruments require sophisticated hardware components and systems to fully exploit the unique source characteristics of ESS. Following established best practice at other leading facilities, technical groups will maintain, test, diagnose and improve existing hardware solutions. Critical instrument components will be matched by groups specialising in detector systems; chopper systems; neutron optics and polarisation; sample environment; and electronics, hardware units, motion control and personal protection systems. These groups will be able to provide technical expertise and experimental support once ESS starts operating neutron scattering instruments. They will manage standardisation of systems, parts and components; have access to spares; and be prepared to provide rapid response in case of either mechanical or electronic failure of critical components to minimise the loss of valuable beam time. In addition to service, the neutron scattering instruments will require specific research and development activities over their lifetime, and the lifetime of the facility as a whole. The groups will carry out R&D in conjunction with European partners. This implies not only sufficient staffing levels but also dedicated workspaces, labs and assembly areas, indicated in Table 2.4. Delivery, installation and development of instrument components will continue well into the operations phase.

2.7.1 Detector systems

Neutrons are indirectly detected by a nuclear interaction in a converter material, which leads to the destruction of the neutron in the process. The daughter products of this nuclear interaction are then characterised electronically by the detector. Most flagship instruments at current sources use ^{3}He gas as this converter material. New kinds of neutron detectors that are not based on ^{3}He are urgently needed, due to the very limited availability of ^{3}He. For this reason, the ESS detector group was established in 2010. Good progress on R&D has been made since then, but detector development will continue into the

Support group	Workspace functions	Controlled access	Total area [m^2]
Detector	Gas storage		410
	Mechanical and electronics lab		
	Assembly area		
Chopper	Mechanical and electrical workshop	Yes	180
	Operational area	Yes	
Neutron optics	^{3}He polarisation area	Yes	360
	Mechanical and glass workshop		
	Assembly area		
Sample environment	Mechanical and electrical workshop	Yes	380
	Gas storage	Yes	
	Preparation and test area	Yes	
Electrical engineering	Mechanical and electrical workshop		300
	Storage		
	Assembly area		

Table 2.4: Laboratory requirements for individual technical groups performing instrument support. Some group laboratories will be inside controlled access areas. The sample environment lab space might be subdivided and located to accommodate needs in different instrument halls. Assembly, operational, and preparation and test areas will all have a crane capacity of at least 2.5 tonnes.

construction phase. A strong core detector group is foreseen in Lund, and extensive collaborative links have been established. The aim of these collaborative links is twofold: to build up a core of competence in detector development in the Lund region to support needs during the ESS construction phase, and to develop capacity in Europe to provide detectors for ESS. The goal is to develop detectors that cost-effectively meet the needs of ESS's instruments and enable them to contribute to cutting-edge research from 2019 onwards.

^{3}Helium supply

In the last few years, demands for ^{3}He have increased, mainly due to U.S. Homeland Security programmes, which in the past five years have used 85% of the U.S. supply; in turn, much of this supply has been met by the depletion of reserves. Since the end of the Cold War, production of this rare gas has been very limited because its main source is the radioactive decay of tritium [209]. This has led to shortages and unaffordable prices (>50 times pre-crisis norms), especially for users outside the U.S. [210], and an urgent need for alternatives to ^{3}He-based neutron detectors for large scale neutron research facilities [209–211]. The need is especially critical for new large-area neutron detectors. Over the past few years, several observers have predicted that existing facilities would require in excess of the complete U.S. supply of ^{3}He by 2012 [209, 210]. The severity of the supply shortage is illustrated in Figure 2.26. Requirements for ESS instruments were not included in these estimates and would increase this demand further.

Recently, the situation has eased slightly for U.S.-based users [212], with a limited supply being made available for scientific usage, although this is not expected to significantly change the situation for European users. These factors put ^{3}He out of range for any future request for large- and medium-area neutron detectors. This dilemma was recognised by the neutron research community in 2009, and led to the formation of the International Collaboration for the Development of Neutron Detectors, ICND [213], to investigate and develop alternatives for large-area detectors. In particular, three joint research activity (JRA) working groups were formed focusing on scintillator detectors, ^{10}B thin film gaseous detectors and BF_3 gaseous detectors. In the discussion below, extant technologies such as image plates and scintillator/CCD imagers are not mentioned. Although they are well proven technologies, and readily available, they have poor time resolution, which makes them inappropriate primary detectors for ESS's flagship instruments.

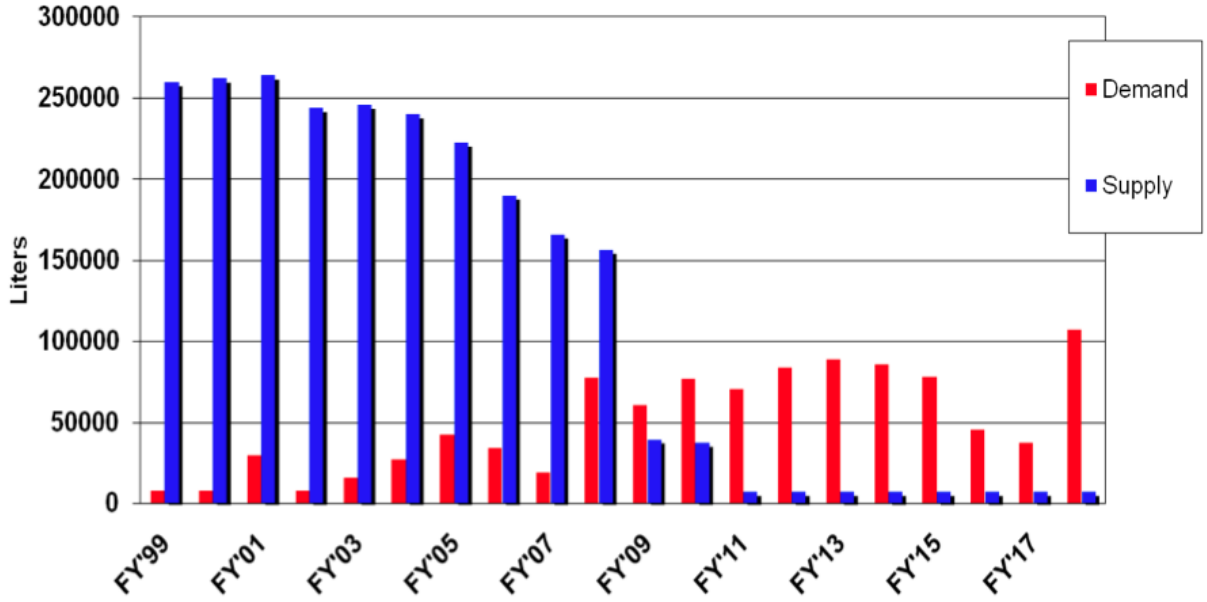

Figure 2.26: Global supply and demand situation for ^{3}He gas in bar-litres as reported in late 2011 [208]. The demand here excludes the requirements of ESS and other future spallation sources.

Detector requirements for the instruments

The estimated detector requirements for the 22 reference neutron scattering instruments outlined in this document are summarised in Table 2.5.

^{10}Boron thin film gaseous detectors

One possible replacement for ^{3}He for neutron detection is the boron isotope ^{10}B. ^{10}B has a relatively high neutron absorption cross section, resulting in an absorption efficiency of 70% compared to ^{3}He, at a neutron wavelength of 1.8 Å. Naturally occurring boron contains 20% of ^{10}B. Due to the almost 10% difference in mass from the other boron isotope, ^{11}B, it is relatively easy to separate the two isotopes. A detector based on ^{10}B absorption of the incident neutrons typically contains aluminium sheets that are coated with $^{10}B_4C$ (boron carbide) layers. The nuclear reaction results in lithium and helium ions. Both the ^{7}Li and ^{4}He ions can be detected, with both temporal and spatial resolutions, in a detecting gas. Due to a reduced escape probability for the reaction particles with increasing depth of the events (typically a few microns), a detector, on which the neutrons impinge at normal incidence, will be based on consecutive multiple (∼30) thin (1 μm) conversion layers, consisting of ^{10}B-containing films, which will be traversed by the neutrons. To overcome the reduction in escape probability with depth, it is also possible to incline the layers at high angles to increase the effective interaction length, without adversely affecting the escape efficiency. This has the additional benefit of potentially improving the position resolution for a given readout segmentation. It does, however, complicate the design of such a detector; such a configuration is termed an "inclined geometry" detector.

The potential of boron thin film gaseous detectors is evidenced by the resources devoted to research in this area. There are presently more than 10 ongoing R&D efforts, featuring both "normal" and "inclined" geometry configurations. The discussion below will concentrate on three illustrative well-advanced developments – one aimed at normal geometry detectors, one towards inclined geometry and one that seeks to match the two approaches. A more complete overview of the promising results can be found in the papers and talks from a recent workshop [214]. These detectors offer the potential for ^{3}He replacements at a price that is competitive with the historical costs of ^{3}He detectors. High quality coatings containing ^{10}B are the primary ingredient for these boron thin-film gaseous detectors. Since pure boron is a poor conductor and oxidises readily in air, boron carbide, which is stable and an electrical conductor, is typically chosen. However, strain in boron carbide layers can be very high, with the result that layers thicker that a few

Instrument	**Detector area** [m^2]	**Wavelength range** [Å]	**Time resolution** [μs]	**Spatial resolution** [mm]
Multi-purpose imaging	0.5	1 - 20	1	0.001 - 0.5
General purpose polarised SANS	5	4 - 20	100	10
Broad-band small sample SANS	14	2 - 20	100	1
Surface scattering	5	4 - 20	100	10
Horizontal reflectometer	0.5	5 - 30	100	1
Vertical reflectometer	0.5	5 - 30	100	1
Thermal powder diffractometer	20	0.6 - 6	< 10	2×2
Bi-spectral powder diffractometer	20	0.8 - 10	< 10	2.5×2.5
Pulsed monochromatic powder diffractom.	4	0.6 - 5	< 100	2×5
Material science & engineering diffractom.	10	0.5 - 5	10	2
Extreme conditions instrument	10	1 - 10	< 10	3×5
Single crystal magnetism diffractometer	6	0.8 - 10	100	2.5×2.5
Macromolecular diffractometer	1	1.5 - 3.3	1000	0.2
Cold chopper spectrometer	80	1 - 20	10	10
Bi-spectral chopper spectrometer	50	0.8 - 20	10	10
Thermal chopper spectrometer	50	0.6 - 4	10	10
Cold crystal-analyser spectrometer	1	2 - 8	< 10	5 - 10
Vibrational spectroscopy	1	0.4 - 5	< 10	10
Backscattering spectrometer	0.3	2 - 8	< 10	10
High-resolution spin echo	0.3	4 - 25	100	10
Wide-angle spin echo	3	2 - 15	100	10
Fundamental & particle physics	0.5	5 - 30	1	0.1
Total	**282.6**			

Table 2.5: Estimated detector requirements for the 22 reference instruments in terms of detector area, typical wavelength range of measurements and desired spatial and time resolution.

tens of nanometres spall off [215–220]. Development efforts have concentrated on overcoming these effects and on developing techniques to deposit layers of the required thickness (several μm) at reasonable cost over several square metres.

The Thin Film Physics Division at Linköping University, in collaboration with ESS, has used an industrial physical vapour deposition DC magnetron sputtering system to develop an appropriate recipe for depositing boron carbide [221, 222]. A system has already been designed to scale up this deposition approach to larger areas. The deposition system is shown in Figure 2.27, alongside scanning electron microscopy (SEM) cross sections of deposited layers on a silicon substrate, which show an amorphous film with a dense columnar structure and a smooth surface. Elastic recoil detection analysis (ERDA) measurements of the elemental composition of the layers show a very low level of impurities and approximately 80% composition of ^{10}B, demonstrating that high quality layers can be produced with few impurities. During 2011, 7 m^2 of coating was produced during a 10 day period, showing that high rates of production can be obtained from such a deposition system.

An alternative approach for the fabrication of thin-film boron carbide by the Helmholz-Zentrum Geesthacht (HZG) group is also very promising; here a large deposition system, developed specifically for depositing very flat X-ray mirrors over long lengths for the European X-ray Free Electron Laser (XFEL), has been used. This approach concentrates on depositing the highest quality layers over a larger area at one go. It is possible to deposit adhesive, stable, continuous, natural, ^{10}B-enriched and μm-thick conver-

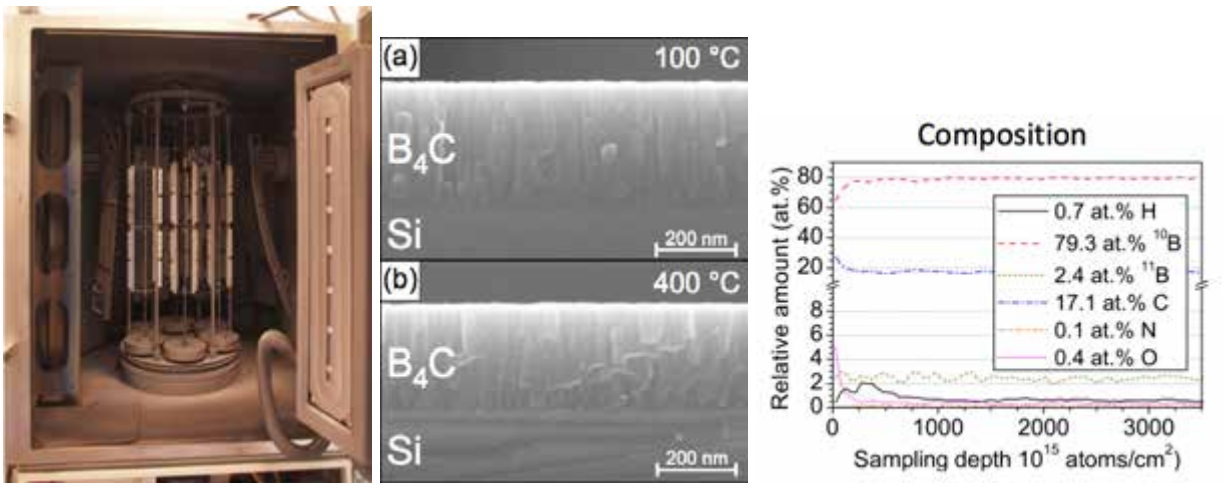

Figure 2.27: Thin film vapour deposition by magnetron. Left: Physical vapour magnetron deposition system at Linköping University. Middle: Typical cross-sectional SEM images, showing boron carbide thin films deposited onto silicon at substrate temperatures of 100°C and 400°C. Right: ERDA measurement of elemental composition of the ^{10}boron carbide thin films.

sion layers on thin aluminium plates over large scales up to 0.1 m × 1.5 m. The interior of the deposition chamber is shown in Figure 2.28. The thickness deviation is below 4% over the whole deposition area due to the high precision and good stability of the sputtering facility. The ratio of boron to carbon is 3.6, which is similar to that of the sputtering target content. Furthermore, the elemental and isotopic composition is uniform in depth. The contents of oxygen and nitrogen are quite low, less than 5%.

In addition, chemical vapour deposition (CVD) techniques for boron carbide coatings have been looked at, though mostly unsuccessfully, with one notable exception. The advantage of chemical vapour deposition is that irregular surfaces can be coated with uniform thickness. However, when ordinary thermally activated CVD is used at substrate temperatures below 500°C, the impurity level is high, which results in inferior neutron detection efficiencies [223]. Low temperature CVD techniques are being looked at to improve the coating's properties. Coating with gadolinium, another potential neutron converter material, with the highest neutron cross section of all elements, is also under investigation [224].

To demonstrate the feasibility of these new technologies for the large-area detectors needed for some instruments, a programme of prototypes is foreseen. In summer 2011, the ^{10}B thin films collaboration

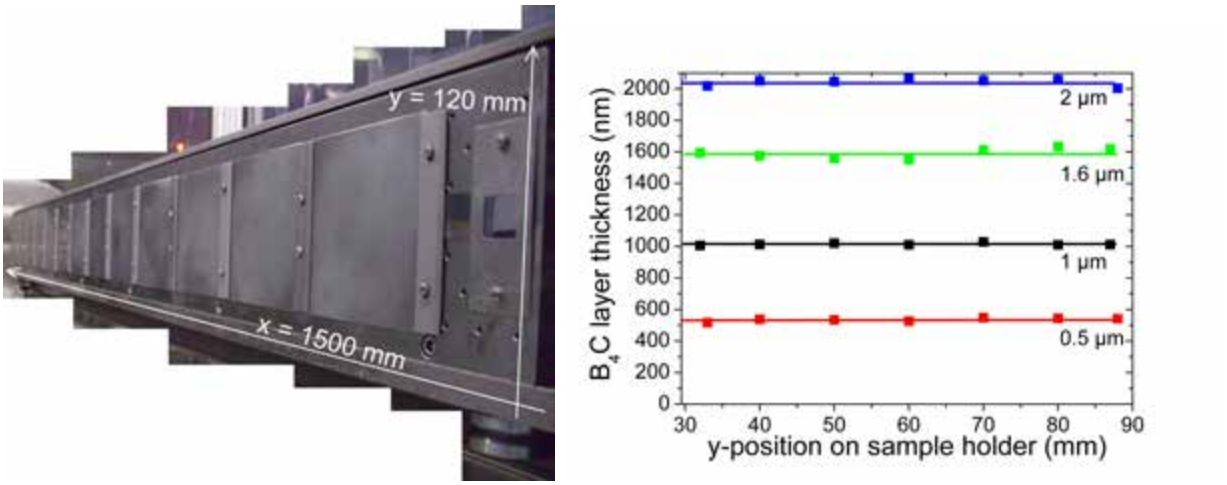

Figure 2.28: Large-area thin film deposition of boron carbide. Left: Deposition chamber at HZG. Right: Boron carbide layer thickness across the substrates.

between ILL, ESS and Linköping University successfully completed a ^{3}He-free prototype detector with a 2 cm $\times$ 10 cm active area with 30 ^{10}B conversion layers, each 1 μm thick) [225, 226]. The prototype was tested on the CT2 test beamline at ILL, as can be seen from Figure 2.29. This proved the feasibility of constructing and assembling such large-area detectors. The results from the initial tests show that the performance of the detector agrees well with results obtained from simulations. The efficiency of the detector has been determined experimentally to be about 50% for neutrons with a wavelength of 2.5 Å. Insensitivity to gamma background at the 10^{-5} to 10^{-7} level has also been shown.

The strategy for this stage of research is to produce modules for existing instruments that replace ^{3}He modules, so that their performance can be evaluated directly against that of existing ^{3}He detectors. The first such demonstration took place on the IN6 instrument at ILL in late 2012. Design and construction of a full scale module (2.4m^2) for the flagship IN5 instrument [227] at ILL will follow during 2013 to 2014. Due to the larger number of layers typically needed, the ^{10}B thin film detectors will need approximately 15 times as many channels as are needed for ^{3}He detectors. This leads to a roughly commensurate increase in the maximum rate of operation for the detector for a fixed design, increasing the requirements for electronics, which are addressed later in this section. To illustrate the potential of ^{10}B thin film detectors incorporating an inclined geometry, an extreme inclined geometry can be considered, in which the angle of incidence is such that the neutron is absorbed in a single layer. Such a prototype is shown under test in Figure 2.30. Impressive efficiencies were achieved in this proof of concept. Full-scale prototypes are now planned, and work towards a full demonstration module of this detector technology is moving forward.

There has been an effort at FRM-II to develop a cathode design that provides an efficiency superior to that of a planar cathode of the same active area. The increased efficiency of the single layer will allow a reduction in the number of cathodes needed in order to reach the desired efficiency. This will lead to a decrease in the number of electronic channels, size and cost of the detector. The investigated design consists of grooves of a certain height with an opening angle of 45 degrees separated by small flat portions in the double-sided format shown in Figure 2.31. This approach makes it possible to use the inclination of the boron layer to increase sensitivity without altering the physical volume of the detector. The design of the cathode has been optimised using the GEANT4 simulation package. Such calculations indicate that cathodes with grooves higher than 2 mm are up to 40% more efficient than a planar cathode of the same active area, as can be seen in the plot in the right hand panel of Figure 2.31. The performance of various cathodes with grooves of various heights and coated with 3 μm of enriched $^{10}B_4C$ was investigated with a moderated Cf-source and a well-defined neutron beam of 4.7 Å at the TREFF beamline at FRM-II. The transmission and efficiency of the various cathodes were measured by making use of a multi-wire proportional counter, which also allowed evaluation of the charge collection efficiency for each design. Good agreement with theoretical predictions has been observed.

The next step is to incorporate the optimal cathode design into a detector prototype. Such a detector prototype would simultaneously demonstrate the performance of the macro-structure cathode concept and that of the flat-cathode, multi-layer ^{10}B thin film's multi-wire proportional counter.

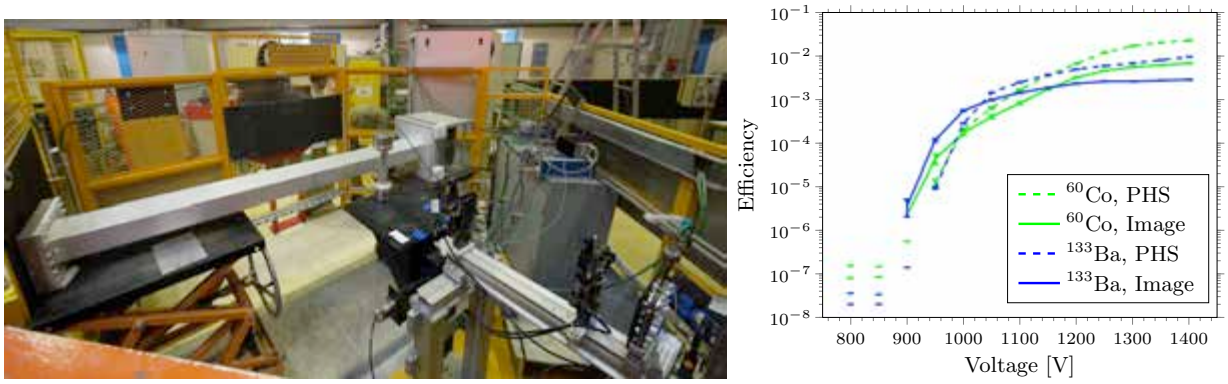

Figure 2.29: Prototype tests of thin film technologies. Left: Prototype under test on the CT2 beamline at ILL. Right: Measurement of γ efficiency as a function of anode wire voltage.

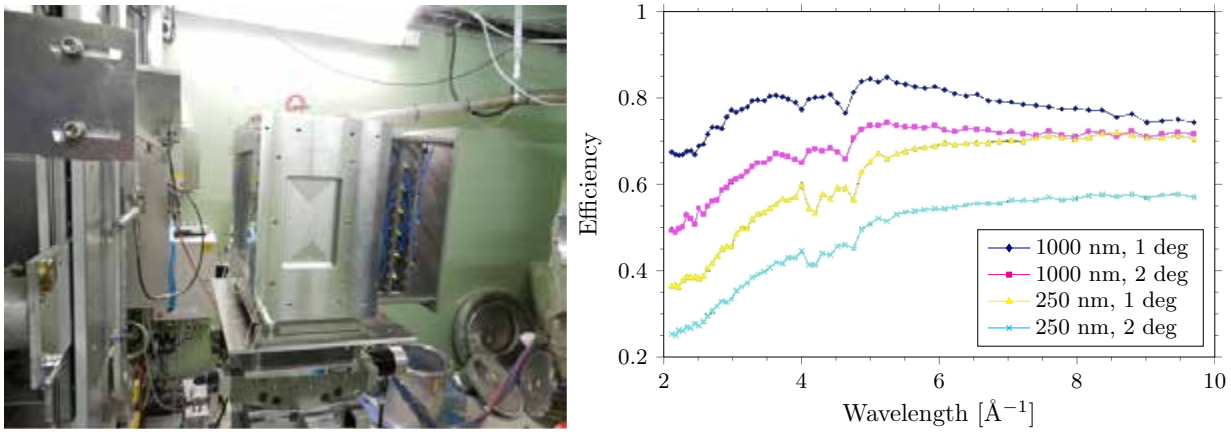

Figure 2.30: Prototype tests incorporating ^{10}B thin films. Left: HZG prototype with thin films at very small angles (one or two degrees) to the incident neutron under test at the REFSANS time-of-flight reflectometer at FRM-II. Right: The efficiency of detection measured as a function of incident neutron wavelength for two angles of incidence (1 degree and 2 degrees) and for two thicknesses (250 nm and 1000 nm).

Small area ^{3}helium detectors

There may be a class of instruments for which ^{3}He gaseous detectors remain the appropriate technology choice, despite the scarcity and cost of the ^{3}He gas. These are instruments for which small areas need to be covered with high efficiency; hence the requirements in terms of bar-litres of ^{3}He are small. ESS does not plan to build any ^{3}He detectors in-house. Any requirements for ^{3}He detectors will be met from parties who already possess the appropriate expertise, and who already supply the community with these detectors, such as ILL or commercial companies.

BF_3 gas detectors

Historically, BF_3 detectors were superseded by ^{3}He detectors, due to safety considerations and the superior detection properties of ^{3}He detectors. As part of the ICND activity, HZB and ILL are exploring potential ways to overcome the shortcomings of BF_3 detectors. BF_3 is extremely toxic, corrosive and reactive, so the safety issue is the biggest problem, in particular for testing, handling and transport. Even during stable, steady-state detector operation, BF_3 represents a constant risk. Therefore, BF_3 is viewed as a backup

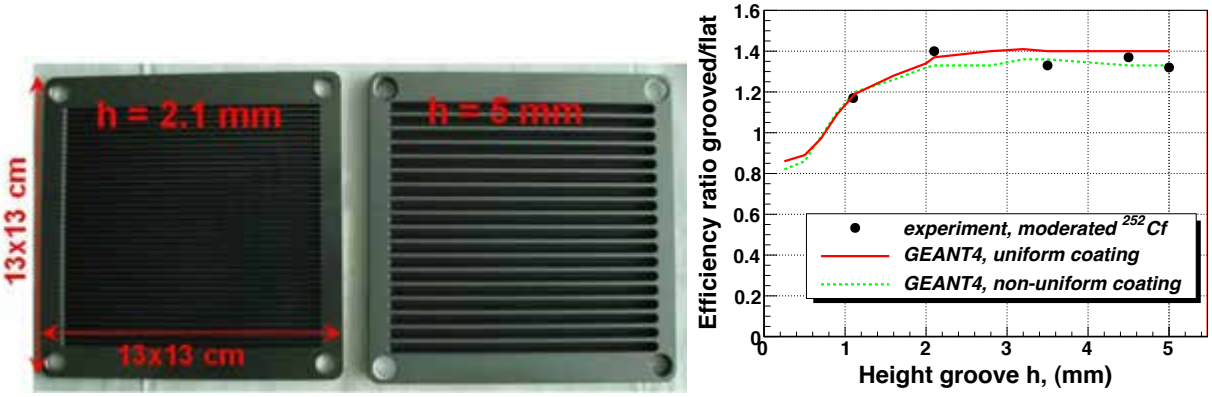

Figure 2.31: Coated grooved cathodes for improved detection efficiency. Left: Photograph of two coated grooved cathodes indicating h, the height of the grooves. Right: Ratio of the efficiency of grooved cathodes compared to flat cathodes of the same active area, as a function of the groove height. Lines show the calculated ratios while points show measured values.

detector technology of last resort for ESS instruments.

Scintillator-based detectors

Neutron detectors based on solid state scintillators have been in use for a long time and offer some attractive properties with respect to installations at pulsed-source instruments. The relatively high density of the scintillation material allows for thin (∼mm) neutron converters with high detection efficiency and a well defined interaction point of the neutron. As a result of the low thickness, scintillation detectors also have almost no parallax effects and usually offer a high time resolution for neutron capture. Today, Li-glass or LiF/ZnS scintillators are most often used for neutron detection. The properties of neutron scintillation detectors depend heavily on the scintillation material and the light detection method. "GS20" glass scintillators with 6.6 percent by weight of enriched ^{6}Li are desirable for high rate detectors. Scintillators of this type have a fast light emission decay time of about 60 ns. With scintillation material about 1 mm thick, they offer a detection efficiency of about 75% for thermal neutrons. The gamma sensitivity of Li-glass is strongly dependent on the gamma energy. The detection of gammas can be suppressed by discrimination methods for gamma energies of less than 1 MeV, but gamma detection is an issue for higher energies, as gammas at these energies produce a light yield equivalent to that of neutrons.

Ceramic scintillators based on a mixture of LiF and ZnS are also often used for neutron detection. These scintillators have a very high light yield, but, unfortunately, both components are opaque. Thus, due to the self-absorption of the emitted light, the thickness of the scintillation material is limited to 450μm to 500μm, which impacts detection efficiency. Another drawback of such scintillators is the rather high decay time of the light emission, which is a few μs and which limits the count rate capability. The gamma sensitivity can be reduced to 10^{-5} by pulse shape discrimination methods. The light detection within scintillation detectors is usually performed by photomultiplier tubes (PMT), which present a well proven technology that is easy to operate. However, operation in magnetic fields is an issue due to the deflection of the internal electron current, which can partly be cured by Mu-metal shielding.

The high light yield of LiF/ZnS scintillators offers the possibility of a fibre-based readout of the scintillation light, which is an appropriate method for large area neutron scintillation detectors of several square metres. One example is the detector for the general materials (GEM) neutron diffractometer, in operation since 2009 at the ISIS pulsed neutron source [228]. It has 77 modules with 1152 PMTs and a total of 7270 elements for readout. The detector modules are equipped with a LiF/ZnS scintillator from which the light of the converted neutron is captured by a clear fibre and transported to a photomultiplier tube. The position reconstruction is done by a fibre combination over a selection of photomultiplier tubes.

Wavelength-shifting fibres

Another option for fibre-based readout of the LiF/ZnS scintillation light is the use of wavelength-shifting fibres (WSF), an approach first applied at the powder diffractometer POWGEN at the Spallation Neutron Source (SNS) at Oak Ridge National Laboratory [229]. This instrument (though presently only fractionally instrumented due to budgetary constraints) requires a detector array with large, 6 mm × 40 mm, pixels and an area of several square meters. The detector uses a two-dimensional grid of wavelength-shifting fibres to collect the scintillation, with the fibre axes parallel to the scintillator screen. The fibre ends for each pixel go to a specific set of four photomultiplier tubes, so that the position of each event can be determined by a 4-tube coincidence system developed for GEM. A corrugated and grooved ^{6}LiF/ZnS scintillator is used that shows a detection efficiency comparable to a 6.6 bar ^{3}He tube. The observed maximum light yield with the ^{6}LiF/ZnS neutron scintillation screen, summed over four tubes, is greater than 200 photons/neutron, which is about 0.13% of the 180,000 photons/neutron produced in the scintillator. This light yield is sufficient to allow pulse discrimination between neutron signals and gamma-ray background. These modules are commercially available [230].

At the Japan Proton Accelerator Research Complex (J-PARC), a compact, high position-resolution neutron imaging detector prototype was developed with 0.5 mm thick wavelength-shifting fibres sandwiched between two LiF/ZnS scintillator screens [231]. The prototype detector exhibited a position resolution of 0.5 mm, which would be very useful for neutron scattering experiments, for which high resolution and the lowest possible amount of dead area (non-sensitive regions) are mandatory. The detector of the SENJU instrument at J-PARC – a time-of-flight Laue single crystal diffractometer – will be established with 1 mm thick WSF sandwiched between two B_2O_3/ZnS scintillators of optimised thickness [232]. Thirty-one

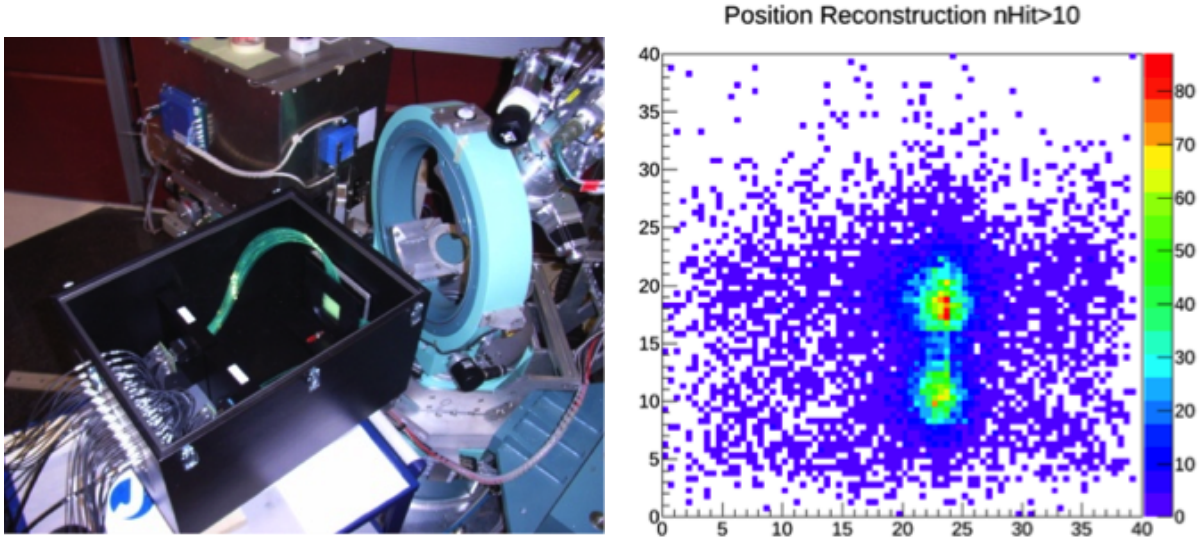

Figure 2.32: Prototype of a small wavelength-shifting fibre detector under test. Left: At the instrument HEIDI at FRM-2. Right: Reconstructed image of a diaphragm measurement with two holes, each with a 2 mm diameter.

modules, 30 cm × 30 cm each, will form the total detector area of 2.8 m^2. The pixel size will be 4 mm^2. An efficiency of 40% has been measured with a prototype at 1.6 Å.

As WSF-based detectors are viewed as advantageous for future large-area scintillation detectors, they are currently objects of research at several neutron scattering labs, as well as in other disciplines. At Forschungszentrum Jülich (FZJ), studies of light emission and detection are being carried out with a small, 4 cm × 4 cm detector prototype and precise time stamping readout electronics, as shown in Figure 2.32. These studies aim to develop suitable event recognition algorithms, which may improve detection efficiency and gamma discrimination. Additional gains in WSF detector performance may be achieved by further optimisation of the fibre-bending radii and of the fibre and scintillator arrangement. Also, the light detection at the end of a single fibre and the readout electronics may be improved. The use of multi-anode photomultipliers with chip-based readout electronics would allow for a compact detector design. There are currently several WSF detector prototypes under preparation at different groups that should yield further improvements of this detector technology.

The Anger method

One possibility to realise position-sensitive neutron detectors is through the Anger method [233], as shown in Figure 2.33. In this approach, the light produced by a neutron event is spread by a disperser glass on an array of light detection devices. By analysing the signals of the light detection devices, the position of the neutron capture can be derived. The position resolution largely depends on the light yield of the scintillator and is to some degree adjustable by the dimensions of the light detection devices. The two SANS instruments, KWS-1 and KWS-2, which are in operation at the Munich reactor FRM-II, are both equipped with position sensitive Anger-based scintillation detectors, as illustrated in Figure 2.33. The detectors have an active area of 60 cm × 60 cm and consist of a GS20 ^{6}Li glass scintillator of 1 mm thickness and an 8 × 8 array of photomultipliers of 7.5 cm diameter each [234, 235]. Measurements at KWS-1 and KWS-2 showed that the detectors provide a statistical count rate capability of 150 kHz at 10% dead time with a maximum count rate of 60 kHz and position resolution of less than 6.3 mm.

For a higher position resolution, the size of the light detection devices can be reduced. For example, the single-crystal diffractometer TOPAZ at SNS is equipped with Anger camera modules of 15 cm × 15 cm active area, with GS20 ^{6}Li-glass scintillator as neutron absorber and a 3 × 3 array of multi-anode H8500 flat panel-photomultiplier tubes from Hamamatsu for light detection. A position resolution of 1.0 mm has been achieved. These modules are becoming commercially available [230]. If the modularity to cover larger areas is not needed, a more straightforward technique to obtain such a position resolution is the use

Figure 2.33: The Anger method of neutron detection. Left: Schematic of the setup of an Anger camera. Middle: Mechanics of the KWS-1 Anger detector with 64 photomultiplier tubes during construction at FZJ. Right: Demonstration of the image quality at KWS-1 during a measurement with a triblock.

of position sensitive photomultipliers; the subsequent position reconstruction is carried out by the pulse division method [236]. A statistical count rate capability of 60 kHz at 10% dead time can be achieved with such detectors. There are ongoing efforts to improve the performance of Li-glass-based Anger detectors. Tapered based solutions, in which the number of light detection devices is lower, may lead to a reduction in the cost of Anger detectors. At FZJ, the silicon photomultiplier (SiPM) technology for light detection with on-board chip-based readout electronics also is being evaluated. With the considerably higher pixellation of these devices, a drastic increase of count rate capability may be achieved simultaneously with an inherently higher position resolution. This technology would also allow for operation in a higher magnetic field.

It is reasonable to expect that a significant fraction of ESS instruments might employ scintillator detectors. In analogous ways to designs for ^{10}B thin film detectors, inclined geometry configurations might be incorporated in the design to increase performance, in particular with respect to resolution and efficiency.

Micropattern devices

Micropattern device detector technology is a fast-paced and active multidisciplinary field. The development of micropattern detectors originated in neutron scattering, with the invention in 1988 of micro-strip gas counters (MSGCs) at ILL, which were first used on the D20 instrument there. Since then, many species of micropattern devices have emerged, and they have become widely used in other fields. Several options exist or are being investigated for neutron detection, and such devices will certainly be part of the mix for ESS instruments [237]. In general, the advantage of these devices is that they excel in performance in terms of count rate capability and/or resolution. Count rate capability is likely to be a limiting issue for several ESS instruments, and superior resolution will open up potential new applications. The Gd-MSGC detectors developed at Helmholtz-Zentrum Berlin (HZB), which are shown in Figure 2.34, consist of a 0.5-1.5 μm-thick gadolinium conversion layer, in which the electrons are emitted as part of the nuclear conversion (with an 80% probability) and are further amplified by a CsI layer immediately on top of the Gd layer. The electrons then enter a gas mixture (such as Isobutane or Ar/CO_2), and the subsequent ionisation of the gas is detected on a micro-strip plate, which has x-y patterns laid down on glass, allowing a 2D measurement to be made. These detectors have the potential to achieve resolutions of up to 100 μm with suitable algorithms, and a very good rate capability. The gamma rejection capability has not yet been evaluated, and further work will also be needed to investigate methods to reduce manufacturing costs.

Gas electron multipliers (GEMs) concentrate the electric field in small holes in an insulating Kapton polyimide foil to amplify the signal. The mechanical simplicity of such devices means that they have the potential to be deployed on a larger scale. One such neutron-sensitive device, CASCADE, is already commercially available in a 20 cm $\times$ 20 cm format, and is in use on two instruments at FRM-II. Developments are ongoing to increase the efficiency of such devices and their range of applications. Developments have also started on 'Micromega' detectors, using a boron conversion layer. There is another category of detectors, typically used at present for neutron imaging applications, which aim at the highest possible spatial resolution. Micro-channel plates are one type of detector belonging to this category. In micro-channel

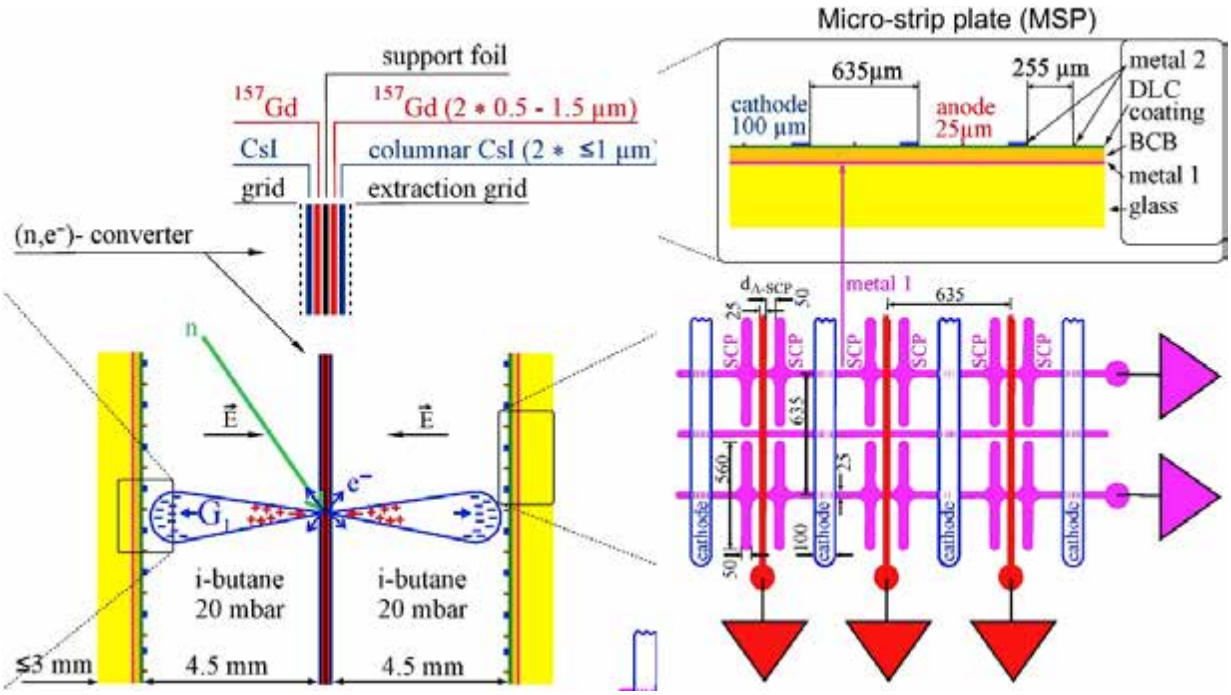

Figure 2.34: A micropattern detector using Gd-MSGC. Left: Concept. Right: Microstrip plate pattern.

plates, the neutron is converted in boron-loaded glass or plastic, and the signal is amplified in the micro-channel walls by a cascade of secondary electrons. Studies of the potential of such devices have been made, and developments are already underway to demonstrate their operational potential for the future IMAT instrument at ISIS. Semiconductor detectors have made a huge impact in other disciplines, as they are able to combine very high spatial and time resolution with good rate capability. More recently, larger areas have been shown to be feasible. A suitable semiconductor device that is sensitive for neutron detection is not currently available; however, there have been several studies showing proof of principle. Given the tendency for instruments to acquire better resolution over time, it is likely that neutron semiconductor detectors will become available for a growing niche of applications.

Table 2.6 summarises the matrix of possible options for detector technology to fulfil the requirements of the reference instrument suite. Minimising the cost of these detectors for the instruments is a key factor in the options presented here, as is ensuring that ESS instruments deploy state-of the-art detectors at the time that they become operational. The above discussion makes clear that while the detectors for the majority of ESS instruments rely on upcoming developments, for most instruments robust secondary technological options exist, as shown in Table 2.6.

Detector electronics

Electronics are a key consideration for detectors for ESS instruments. Three factors in particular drive the importance of electronics:

1. The larger detector active area needed by ESS instruments.
2. The push to superior spatial resolution for detectors, which increases the channel count quadratically.
3. Technologies such as the ^{10}B thin film detectors, micropattern detectors, and scintillator detectors, which are designed to operate in high rate environments, and which therefore drive the channel count per unit area much higher than has been the case for previous generations of instruments.

High channel count rates have several implications. It is estimated that electronics will represent half the cost of the detectors for instruments, so attention needs to be paid to this issue. While generic solutions should be applied where possible, some optimisation is likely to be needed for each instrument class, and for detector species. As an illustration of the growth in channel count requirements, the IN5 instrument at

Instrument	Detector technology						
	^{10}B thin films		Scintillators		^{3}He	Micropattern	
	⊥	∥	WSF	Anger		Rate	Resolution
Multi-purpose imaging	-	-	-	-	-	o	+
General purpose polarised SANS	o	+	-	+	o	+	-
Broad-band small-sample SANS	o	+	-	+	-	+	-
Surface scattering	o	+	-	+	o	+	-
Horizontal reflectometer	-	o	-	+	+	o	-
Vertical reflectometer	-	o	-	+	+	o	-
Thermal powder diffractometer	o	+	+	-	-	o	-
Bi-spectral powder diffractometer	o	+	+	-	-	o	-
P-M powder diffractometer	o	+	+	-	-	o	-
MS engineering diffractometer	o	+	+	-	-	o	-
Extreme conditions diffractometer	o	+	+	-	-	o	-
Single crystal diffractometer	o	+	+	-	-	o	-
Macromolecular diffractometer	-	o	o	o	-	+	+
Cold chopper spectrometer	+	o	o	-	-	-	-
Bi-spectral chopper spectrometer	+	+	o	-	-	-	-
Thermal chopper spectrometer	+	+	+	-	-	-	-
Cold crystal analyser spectrometer	-	o	-	+	+	-	-
Vibrational spectrometer	-	o	-	o	+	-	-
Backscattering spectrometer	-	o	-	+	+	-	-
High-resolution spin echo	-	o	-	o	+	+	-
Wide-angle spin echo	-	o	-	o	+	+	-
Fundamental & particle physics	-	-	-	-	+	+	+

Table 2.6: Appropriate detector technology options for the 22 reference instruments. The detector technologies are grouped into perpendicular (⊥) and inclined (∥) neutron incidence geometries for ^{10}B thin film detectors; wavelength shifting fibres (WSF) and Anger cameras for scintillator detectors; and ^{3}He detectors and high count rate and high resolution detectors for microstructure and imaging detectors. In the matrix of options, '+' indicates that this technology is presently seen as a strong possibility, '-' indicates that it is a disadvantageous technology for this instrument, and 'o' means that it is considered an option, though not the primary one.

ILL [227] has 375 tubes with double-ended readout, resulting in a total of about 750 electronics channels. An equivalent instrument at ESS using ^{10}B thin film detectors may have a channel count of several tens of thousands. This means that while channel-economising techniques such as charge division, and channel sharing might be employed, the electronics also need a step change. It can be expected that the single channel electronics presently used will be replaced by integrated ASIC chips, which digitise the analogue signals at a very early stage. It can also be expected that the subsequent digital processing will take place before the readout data acquisition stage – to some extent on the ASIC, but also possibly in FPGAs in the front-end electronics or in the data acquisition cards in the readout crates. In terms of data format, it is also the case that nearly all instruments will use "event mode", in which each neutron interaction detected "event" is read out, rather than a "histogramming mode" summarising the data. It is possible, given the processing power that will be available in the readout electronics, to produce the histogramming data parasitically. Such ASICs and readout electronics are complicated solutions; however there are already several quite suitable possibilities as prototypes for ESS electronics that have been identified. These approaches have been used extensively in other disciplines.

One contemporary example, developed for the Gd-MSGC prototypes mentioned above, relies on such an ASIC/FPGA combination for the high channel count and degree of processing required to determine the resolution to sufficient accuracy. The CASCADE detector electronics are already commercially available. They are shipped in units of up to 256 channels. These were developed within the high energy physics community ten years ago, but have been specifically adapted to neutron scattering. Another possibility identified and being investigated is the 2000-channel crate demonstrator developed within the EUDET project. This already offers the correct channel density in a single unit. For certain high resolution applications, pixelated chips, such as the MEDIPIX series (MEDIPIX and TIMEPIX) or the PSI series (such as PILATUS or EIGER) may be appropriate. Such chips typically come with highly specialised and adaptable readouts.

While significant effort will have to go into characterising and evaluating these options, it is encouraging that a number of suitable options already exist at an affordable price. This means that the high channel count should not be seen as posing undue risk; in fact, to fully take advantage of the ESS long pulse source without saturating instruments — as happens presently at many instruments — it is only logical to progress to more sophisticated detector electronics. The timing system, and time distribution between parts of the detector, must be fully integrated into the readout electronics. This is important both for operation, and for calibration purposes. As such, the site-wide timing system should be used. The timing system will be a part of the integrated control system (ICS). It is described in more detail in Section 5.2.6. Parts of the ICS extended and implemented by the DMSC will be already be integrated into the readout during the prototype stage.

Standards

To optimise the performance of instruments and to minimise operational and lifetime costs, strict standards will be defined for all detectors and associated electronics and software. In terms of detector technologies, all options will need to be qualified as appropriate for ESS applications. Dedicated prototyping for all instruments is planned, as well as demonstration on extant instruments, to determine performance and to enable objective comparisons between options for detector technology. In terms of front-end and readout electronics, crates, timing and control software, there are numerous interfaces between groups at ESS. Care will be taken to ensure that this is managed smoothly. The imposition of standards on such items serves multiple goals. It helps to ensure that detector systems are easy and cheap to maintain, and have a known level of reliability. The level of expert help and number of hot spares needed is also reduced. Settling on a limited number of solutions for electronics, for example, has the potential to significantly reduce the per-channel cost of the electronics, which are expected to be a large part of the cost of detector systems. At the same time as ESS imposes standardisation, care will also be taken to ensure that there are several vendor options, and that single-source supplier problems are avoided.

Laboratories, workshops and testing facilities

In order to accommodate different activities within the Detector Group, specific laboratories and workshops are necessary. The requirements are indicated in Table 2.4. Dedicated testing facilities for detectors at the Institute for Energy Technology (IFE) in Kjeller, Norway have been secured. IFE will provide the Detector Group with full access to two dedicated beam lines (R2D2 and beam line 10), as well as assistance during the operations carried out on these instruments.

2.7.2 Chopper systems

Chopper systems are one of the principal building blocks of all neutron spectrometers, and will be present in one form or another on nearly all of the instruments. The pulse structuring and waveband selection functions performed by neutron choppers are central to instrument performance at all facilities, and will be critical to unlocking the full potential of the long pulse source. However, systems performance will not be judged in isolation but also in terms of equally important operational criteria such as serviceability, maintainability and accessibility of the individual systems and units in order to ensure the highest instrument availability achievable.

Period	Phase	Prompt pulse suppression T_0	Bandwidth	Fermi E_0
2013 – 2016	Technology development	4	6	2
2017 – 2019	Day-1 suite of 7 instruments	6	27	32
2020 – 2025	Full complement of 22 instruments	10	77	10
2030 – 2035	Upgrade potential	8	30	5

Table 2.7: Time frames and counts for different styles of neutron choppers systems.

Instrument requirements

At ESS, choppers will be required to perform all the functions typically encountered on instruments at other facilities, but they will also face a number of new challenges specifically due to the source's pulse characteristics. Functions such as pulse shaping, pulse suppression, coarse and narrow bandwidth selection and background noise reduction will be required. A number of system architectures and mechanical configurations or types are envisaged, and strategies are under study as part of instrument concepts. The implementation of techniques such as frame rate multiplication [238] and advanced guide systems are envisaged and are poised to push beyond the performance envelope of current chopper systems, requiring ESS to engage with new developments. Current estimates for the number of axes required are represented in Table 2.7. The equipment supply schedule is based on the instrument installation program with chopper system deliveries advanced by approximately one year to permit systems testing and integration prior to installation on site, as shown in Figure 2.35.

Operational requirements

Serviceability, maintainability, and accessibility (SMA) of chopper systems is of crucial importance. The reliability and availability of chopper systems is often wrongly viewed as secondary to neutronic performance. ESS will not make this mistake. SMA criteria will figure highly in the design, development and implementation of chopper systems in order to reduce the "lost time due to component failure" (LTCF), and keep instrument availability high. In order to ensure that all issues relating to systems' SMA are

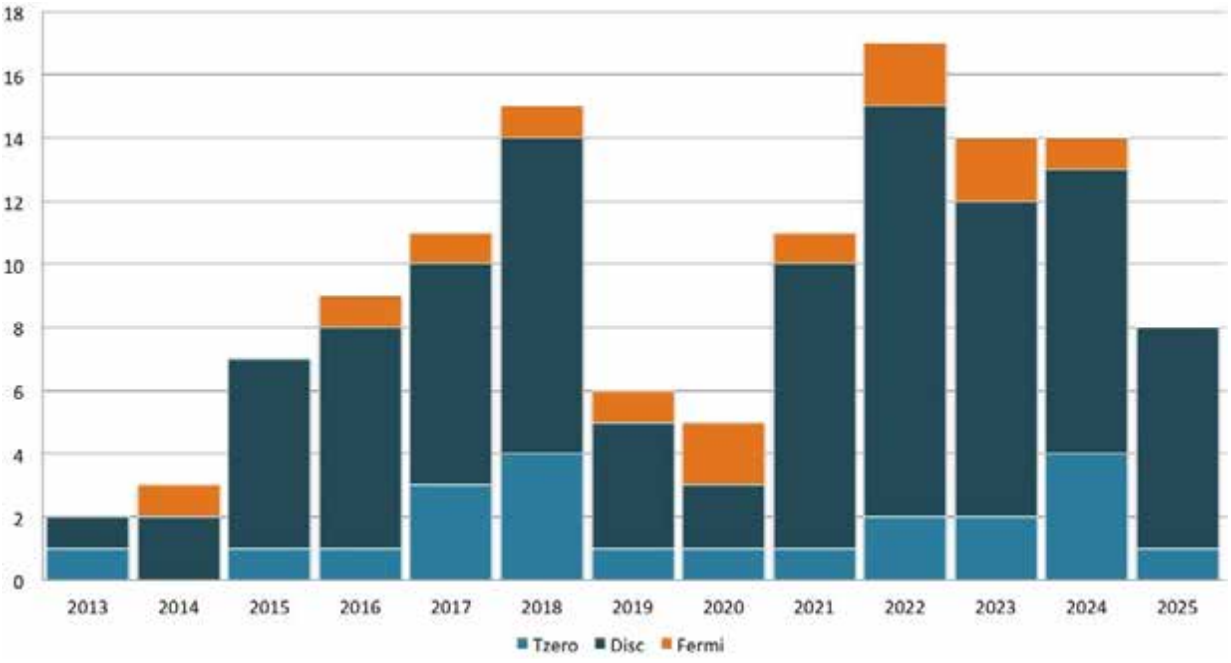

Figure 2.35: Delivery schedule for neutron chopper systems.

considered holistically, all steps of the design, procurement and integration process will either be carried out or overseen by the group's personnel. Since many of the choppers will be located close to the monolith, assuring ease of access for maintenance or repair will be an important issue in the design of instruments. Best practices at existing facilities will be used as guidelines.

Diagnostics

In order to maintain the highest degree of equipment reliability, and to provide advance warning before failure, all chopper units will be equipped with sensors to monitor critical functions. These systems will also permit the optimisation of maintenance schedules, and in case of breakdown, will provide valuable information to the crew, assisting with the diagnosis of the causes of failure and with preparation before repair work starts, thus reducing the number of lost neutron beam days.

Radiation damage and activation

Many devices will operate in high-radiation environments within heavy beamline shielding, often close to the target monolith. In particular, the T_0 choppers will be directly exposed to high integrated doses of radiation. These extreme conditions are expected to result in the premature degradation of directly exposed and adjacent components and significant component activation. The negative consequences will be mitigated in the design and the selection of materials, however, and parallel irradiation tests on critical components will be carried out. Component activation accumulated during service may reach levels such that it becomes a hazard to personnel during removal and maintenance operations and, as a result, personnel shielding and remote handling equipment will be used.

Standardisation

At existing facilities many additional costs during installation and running of chopper systems can be attributed to the complexity of maintaining a heterogeneous park of equipment. ESS will mitigate these issues by standardising chopper systems and subsystems across the facility wherever possible. Through the standardisation of components, such as spindles, control systems and housings, development costs are spread, parts inventories are decreased and larger order volumes offer potential for cost reductions through lower per unit prices. At the same stroke, maintenance procedures are simplified, reducing errors, and tooling and equipment obsolescence issues can be considered in a holistic manner. One of the principal tasks of the Chopper Group during the pre-construction phase has been to establish the range of chopper parameters for the future instrument suite and to study the feasibility of developing a suite of modular chopper platforms to fulfil all requirements with combinations of standardised parts. The "platform" approach will permit the majority of systems to be built up from common components yielding improvements in SMA during maintenance, and LTCF during operation. The platform will also form a basis for the development of special "one off" machines for particular requirements. This approach will require dedicating resources to the design and development of chopper platforms. However, the in-house knowledge and capacity will ensure that the group is well equipped to provide effective support to instruments and a degree of independence from suppliers.

Procurement

The procurement strategy for this equipment is heavily dependent on that of the facility as a whole. Due to the complexity and limited market for these systems, only a handful of suppliers exist worldwide and a limited range of products is available. Where commercial systems conforming to established ESS standards are available at an acceptable cost, external procurement is the preferred option. However, the equipment presently on offer cannot meet the complete range of requirements. A number of well developed systems are commercially available for pulse-shaping and bandwidth-limiting applications typically performed by either (light) disc or (light) Fermi choppers. In order to preserve serviceability and reduce maintenance costs through standardisation, ESS will develop and enforce strict specifications concerning the type and supply of critical components such as spindles and controllers. Currently, no commercial systems are available for prompt pulse suppression at a long pulse facility. T_0 systems have unique engineering requirements and all devices installed today result from in-house efforts at the various facilities. In these circumstances, systems

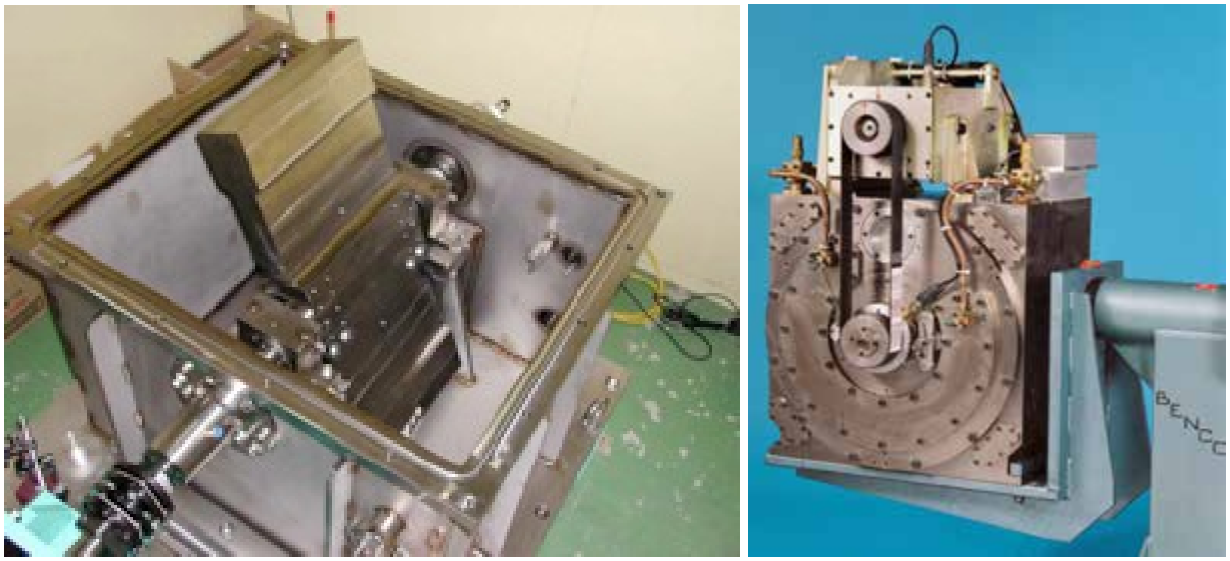

Figure 2.36: Parallel axis prompt pulse T_0 choppers. Left: Developed at J-PARC. Right: Developed at ISIS.

have been designed and developed in-house by group personnel before being manufactured externally, and ESS will follow this approach.

Prompt pulse T_0 choppers

T_0 choppers are designed to block fast neutrons and gamma rays generated during the prompt pulse. As the proton beam is incident on the target, highly energetic particles are produced, which are not of use in experiments and which, if permitted to propagate, would generate background radiation and noise on instrument detectors. The T_0 chopper's role is to block this pulse by closing the beam with a thick absorber of high cross section material, and to open rapidly permitting the slower, useful neutrons to pass though. Choppers for this application, such as those shown in Figure 2.36, will be equipped with thick metallic rotors and rotate at a multiple of the source frequency with precise phasing to match the proton pulse. Due to the high mass in rotation, ensuring adequate support is paramount to performance and reliability. Devices typically employ contact bearings on each side of the rotor, which places upper limits on rotational frequency. A number of magnetically suspended, perpendicular axis machines (Fermi type) have been developed at Forschungszentrum Jülich (FZJ). These devices are well suited for applications for which higher rotational speeds are essential, while the bandwidth limitations and limited absorption characteristics of this type of rotor are acceptable.

Engineering challenges

The necessity of employing massive rotors, and operation at high rotational speeds, generate high loads on machine components and bearings in particular. High standards of engineering design and execution are required in order to ensure safe operation and high neutronic performance. Experience from existing facilities has shown that the frequency and elevated costs of maintenance are critical issues on these devices. Current designs often demonstrate operational lives much shorter than those of other instrument components, requiring regular outages for overhaul or replacement. In this respect, replacing the conventional bearings with zero maintenance magnetic bearings would be a major step forward. A considerable development effort driven by ESS offers strong promise of producing a successful design for the very heavy rotor using this technology. Preliminary research is being pursued with the FZJ Magnetic Bearings Group.

Choppers for bandwidth limitation and pulse shaping

Bandwidth limiting and pulse shaping functions on thermal and cold neutron beamlines are typically performed by parallel-axis, disc rotor-type choppers. Neutrons of cold and thermal energies are readily

absorbed by, for example, boron supported by a light aluminium or reinforced plastic disc rotor. Openings in the rotor permit the passage of neutrons and phasing the openings of multiple rotors permits pulse shaping and/or neutron energy selection. For this purpose, these choppers typically require an opening angle that is tuned to meet the wavelength requirements of a particular experiment. Bandwidth-limiting choppers rotate at some multiple or sub-multiple of the source frequency and in phase with the source. For applications requiring lower rotational speed, aluminium rotors and conventional bearings are often employed successfully and cost effectively. Two examples are pictured in Figure 2.37.

At slow and intermediate rotational speeds, stress levels are sufficiently low to allow the construction of rotors in high strength aluminium alloy. This material is easily machined, and gives design flexibility to optimise rotors to different guide dimensions and to varying window openings for experimental purposes. For applications requiring higher rotational speeds, carbon fibre-reinforced (CFR) rotors are preferred due to their superior mechanical properties, and magnetic bearings are favoured because the service life of contact bearings becomes unacceptably short at very high speeds and in vacuum. A recent design study achieved a maximum rotation speed of 27,500 rpm (until failure of the disc) with a CFR disc and TOF-TOF geometry [239]. The limitations of the current design have been identified and further development will in all likelihood result in discs with a diameter of about 600 mm that can be operated at approximately 28,000 rpm [240].

Fermi or E_0 choppers

E_0 choppers are designed to transmit only a very narrow bandwidth of neutrons and/or to define very narrow pulses of neutrons. They are typically used on instruments employing time-of-flight (TOF) techniques, rotating at a multiple of the source frequency with very precise phase control. When employed in combination with large neutron beam cross sections, or high energy neutrons, rotor weight can be high, on the order of 40 kg. Due to the high rotation speed, often above 600 Hz, Fermi choppers are supported on magnetic bearings and operate under vacuum. Despite the high performance of these systems, experience shows that reliability can be excellent, with systems running for periods of years with minimal or no maintenance. Certain experiments on some instruments require the ability to modify the energy resolution of the chopper. This is achieved by equipping the cavity in the rotor with a slit package or other optical devices that can be exchanged. The facility requirements of E_0 choppers, rotors and rotor payloads have been estimated based on data from other facilities. A limited range of Fermi choppers and light rotors is commercially available, however, they do not cover the full range of requirements for ESS instruments. Meeting some of these requirements will demand a considerable development effort driven by ESS to produce a successful design in partnership with industrial partners. Efforts to address this issue have already begun with FZJ.

As a result of their high rotational speed, the rotors of Fermi choppers possess significant kinetic energy which present a hazard to unprotected personnel during operation. At ESS, where large rotors

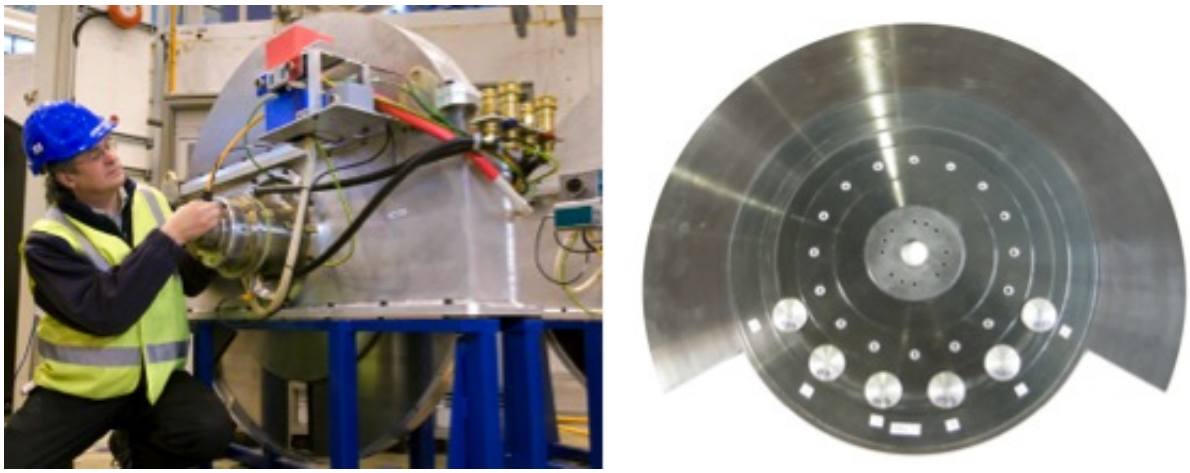

Figure 2.37: Choppers with aluminium discs and conventional bearings Left: 1.2 m chopper developed at ISIS. Right: A carbon fibre-reinforced rotor developed at Technical University Munich.

may be required to suit large guide cross sections, kinetic energy could become a major issue. Efforts are currently underway to replace heavy Fermi choppers with an array of small and very fast rotating pencil-like choppers [241], as shown in Figure 2.38.

Facility standards and Infrastructure

The neutron chopper systems will be designed taking into consideration facility-wide software and hardware standardisation and maintainability. The chopper systems will be fully integrated into ICS including the ICS-supported safety systems.

Laboratories and workshops

Currently, two areas within the facility have been set aside for the establishment and operations of the neutron chopper group. A chopper development laboratory of 80 m^2 has allocated lab space close to the experimental hall. In this area, chopper prototype assembly and testing will be carried out. Three test cells, two mechanical and one electrical, are planned for this area, along with equipment for high precision and balancing work. Within the experimental hall, a further 100 m^2 have been allocated for the chopper operations facility in which the group's integration, inspection, commissioning and maintenance functions will take place, as is indicated in Table 2.4. Within the area, a small workshop with dedicated machine tools will permit final adjustment of parts during construction, and repair of damaged components.

2.7.3 Neutron optics

The performance of the neutron scattering instruments will rely on bespoke neutron optical systems finely tailored to the requirements of the individual instruments. These systems will transport and condition

Figure 2.38: Fermi (E_0) choppers. Left: An operational FZ Jülich "heavy" Fermi chopper installed on HET at ISIS. Middle: A recent "heavy" Fermi prototype developed at FZJ. Right: Pencil Fermi concept developed at FZ Jülich.

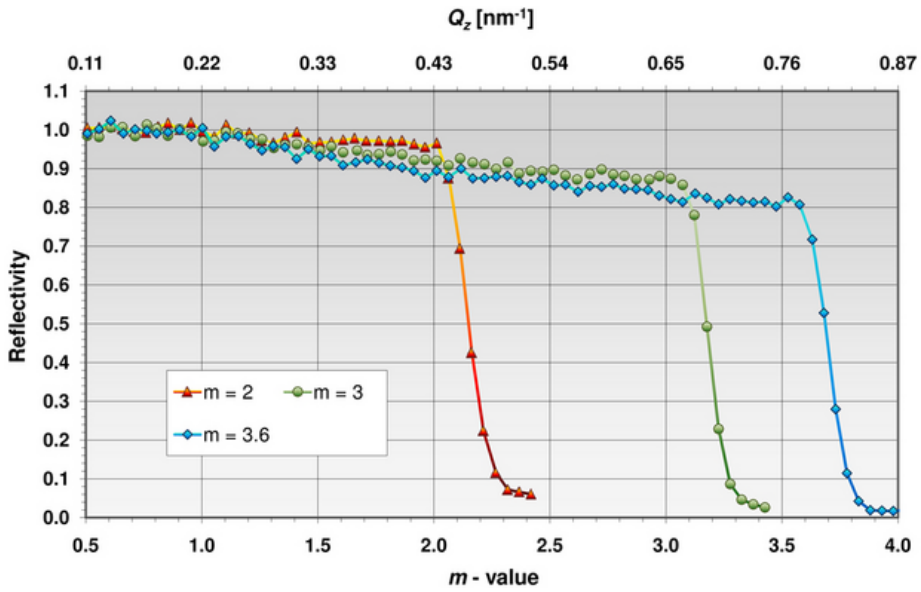

Figure 2.39: Measured reflectivity curves of supermirrors from one of three specialised vendors. Courtesy of Swiss Neutronics.

the neutron beams to provide the best performance reasonably achievable. At the same time, the design goals include minimising experimental background, elimination of magnetic materials from sensitive experimental areas, maintaining a safe working area, and protecting the environment from the final waste footprint.

Optical requirements for the instruments

Broadly speaking, the optical requirements are similar for each instrument:

1. **Performance.** Maximum transport efficiency of the neutron beam, while offering good rejection of neutrons that lie outside the required phase space for the desired instrument resolution.

2. **Clean signal and safety.** Strong suppression of background contributions, both continuous and time structured, including the attenuation of cross-talk between the beamlines.

3. **Long component lifetime.** Once installed, the systems should operate for a minimum of 10 years without replacement.

4. **Spin polarised beams.** Many instruments require a carefully prepared spin polarised beam with a well controlled magnetic environment.

Performance

The highest quality neutron guides will be used with the most modern, advanced supermirrors. Reflectivity is measured on an m-scale relative to natural nickel ($m = 1$), which has the largest critical angle of total external reflection for neutrons. Mirrors with larger m values are made by depositing supermirrors, which are comprised of a large number of layers of nickel and titanium. Supermirror fabrication is a specialised and complex process, and modern supermirrors offer high reflectivity across a wide angular range, as illustrated in Figure 2.39. Beam delivery systems based on ballistic neutron guide geometries [242], and the special case of ballistic guides forming an elliptic shape [243], meet the needs of the chosen instruments and have been adapted on a case-by-case basis to the specific geometrical requirements of the neutron beam. Both ballistic guides and elliptic guides reduce the number of reflections in the guides. This increases the performance of the instruments considerably for beam transport over large distances, and provides maximum scientific return on capital investment.

It is generally advantageous to avoid a direct line-of-sight to the target monolith. For shorter instruments, this requires a deflection of the neutron beam through large angles of more than one or two degrees. Neutron guides with multiple channels known as "benders" are used to steer the neutron beam, in a manner similar to the way fibre optic connectors work. For a number of instruments, a bender design offers the best balance of simple, efficient beam delivery, and good rejection of unwanted short wavelength neutrons and high energy particles from the target monolith.

Focusing elements

For experiments in which small samples require an increase in the neutron flux at the expense of angular resolution in one or more axes, there are a number of technologies available, including both mature approaches and recent innovations. The method of shaping the final sections of the supermirror to match a conical section shape is well established [244, 245]. For more demanding, optically precise measurements based on reflective elements, Walter optics can be deployed [246, 247]. Refractive elements are also available, either in the form of compound refractive lenses (CRL) [248], or Fresnel lenses [249]. Each of these technologies has relative merits and drawbacks, which are evaluated in light of the requirements of the particular experiment and sample size. Decisions about deploying these technologies across ESS will be made on a case-by-case basis, taking into account considerations of cost, operational reliability and performance.

Supermirrors for adaptive optics and background reduction

One of the challenges in focusing on extremely small samples is aligning the focusing element with the sample. To facilitate the study of very small samples, several adaptive focusing devices are currently being

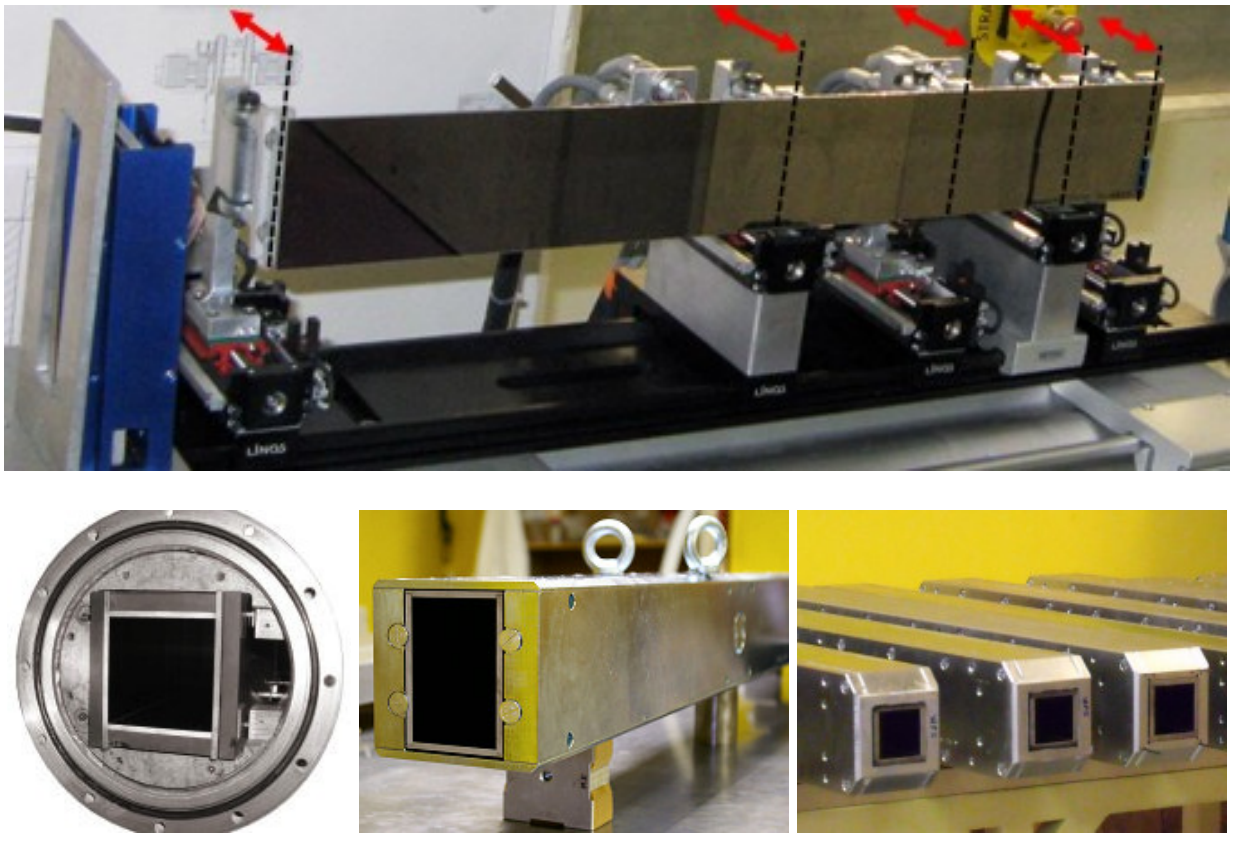

Figure 2.40: Adaptive optics and shielded neutron guides. Top: Adaptive optics elements developed with collaborators at PSI, Switzerland. The red arrows show actuators that bend the shape of the mirror, so that the neutron beam focusing can be adjusted for each experiment. Bottom left: In-pile guides shrouded in steel. Bottom middle: Shutter guides shrouded in steel. Bottom right: Steel sandwich guides. Courtesy of Mirrotron.

tested at PSI [250]. One way to adjust the focusing characteristics of a neutron guide is to change the curvature of the focusing device. The photograph at the top of Figure 2.40 shows how the bending of a uniform substrate by five actuators, in one of three different concepts that have already been investigated and measured at the BOA beamline at PSI's SINQ. Minimising the background from neutrons and gamma rays is essential for productive experimental facilities, for providing a healthy working area, and for protecting the environment by minimising activation and waste. ESS will use proven methods to block unwanted neutrons and gamma rays around the neutron beams based on knowledge gleaned from decades of operations at facilities around the world. These include neutron guides clad in neutron-absorbing boron, and gamma-absorbing steel and concrete, in combination with other hydrogenated materials, so that, to as large a degree as is reasonably achievable, only the clean neutron beam is transmitted into the experimental halls. An example of shielded guides for use in the shielding walls near the neutron source is shown at the bottom of Figure 2.40. Many of the instruments will be obscured from the neutron source by avoiding a direct line-of-sight back to the moderator. Those that are not so situated will be heavily shielded from neighbouring instruments. In all cases, the beam delivery system will employ multiple absorbing materials to reduce the quantity of high energy particles that contribute to the background as far as is reasonably achievable, taking into consideration cross sections and interactions over the full energy range to the ceiling of 2.5 GeV that the proton beam provides.

Radiation and heat-tolerant supermirrors

It is essential that the capital investment in ESS results in a reliable facility with minimum disruption to operations caused by component failure. The neutron beams are designed so that the optical components will have an expected life time in excess of 10 years with only monitoring and minor preventative maintenance required. Achieving this becomes more challenging near the source of the neutrons, due to heating and radiation damage. Where necessary, ESS will deploy radiation-tolerant and heat-tolerant materials in these areas to ensure a long life without degradation in performance over time. Two examples are shown in Figure 2.41.

Spin polarising supermirrors

Spin polarising supermirrors based on various multilayer systems, such as Fe/Si and FeCoV/TiNx, are used in neutron instrumentation to provide a polarised neutron beam and to analyse the polarisation of the scattered beam. The multiple magnetic and nonmagnetic layers have different scattering contrasts for neutrons with either up or down polarisation. Moreover, the internal stresses of the multilayer systems

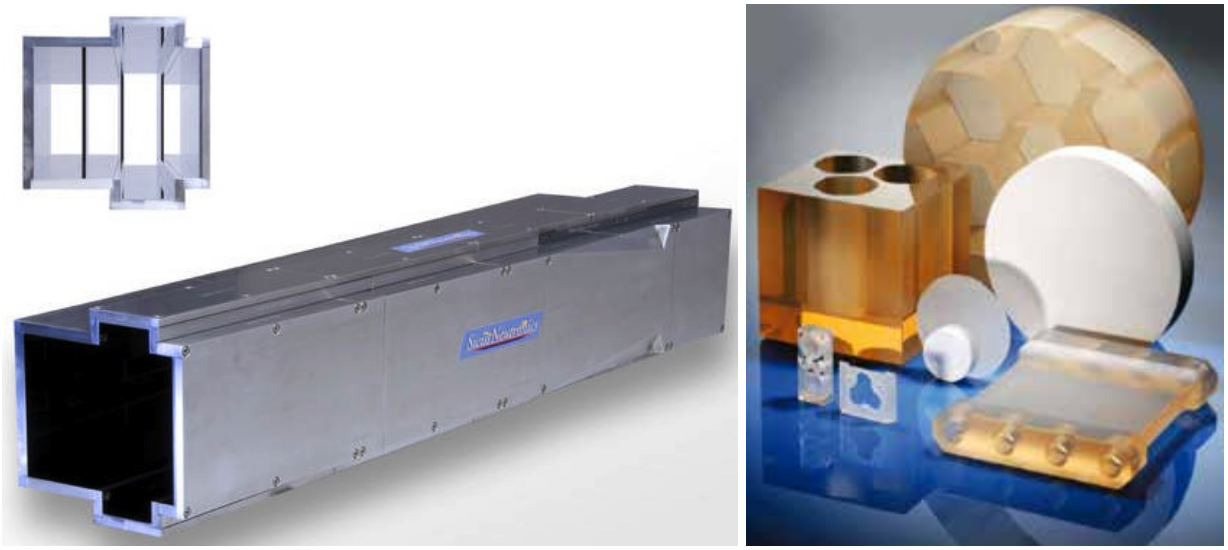

Figure 2.41: Radiation and heat tolerant neutron guides. Left: Metal substrates are radiation and heat resistant, and can be reliably made in complex geometrical shapes. Right: Radiation and heat resistant guides made from Zerodur Glass-Ceramic, which can be finely machined.

are manipulated in such a way that the polariser can be used in its remanent state. In particular, FeCoV polarisers have the property that the magnetisation can be induced with an external magnetic field of only 2−4 mT. This feature makes the FeCoV polariser very important if polarisation is needed together with a cryomagnetic sample environment. PSI is developing polarisers based on FeCoV/TiNx technology in partnership with ESS. The 60 degree supermirror analyser based on FeCoV/TiNx multi-layers shown in Figure 2.42 was built and tested at SINQ at PSI in 2011. It reached a polarisation of more than 95% with a transmission of 45% for the spin-up component at 5 Å. The main feature of the device is that the assembled 960 polarisers are positioned without any gaps. The present limitation of the FeCoV polariser is the maximal m value of around 3. The goal of the project is to increase the quality of the polariser – a higher m value without a significant decrease in reflectivity – and to reduce the potential for ^{60}Co activation.

^{3}He devices

The long neutron pulse requires that polarising devices at ESS be effective over a broad wavelength band, and be able to cope with an increased angular acceptance. Conceptual designs of an in-beam spin exchange optical pumping (SEOP) analyser, which can be used for a small angle neutron scattering instrument, are currently being developed with partners at FZJ and TUM [251]. For inelastic spectrometers, the key technical problem is to cover both a wide range in scattering angle and a broad wavelength range with the neutron spin analyser. Another area of ongoing research addresses this need [251] by developing improved ^{3}He wide angle cells.

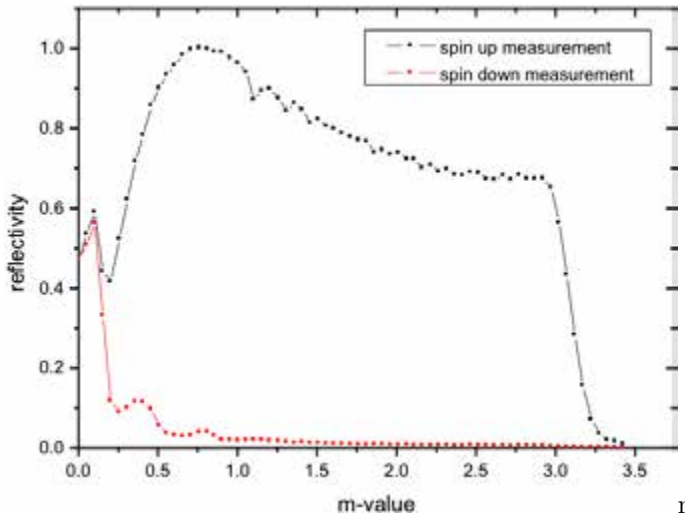

multi-layers

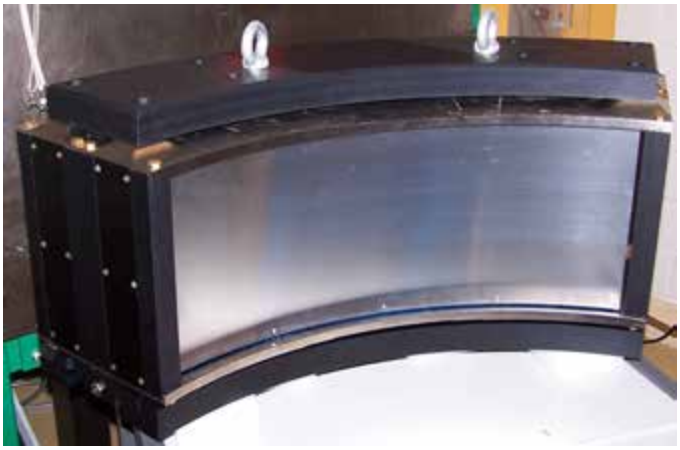

Figure 2.42: Spin polarising supermirror analyser. Top: Reflectivity curves (spin up and down) for a FeCoV polariser. Bottom: Wide angle analyser (60 degrees) without gaps based on FeCoV/TiNx polarisers.

Neutron optics simulation software

In partnership with ESS, PSI in Switzerland and DTU in Denmark are developing the capability to merge advanced simulation software used in the nuclear industry (MCNPX) with neutron modelling software (McStas), enabling ESS to design its neutron beams with a better idea of backgrounds and beam transport simultaneously in the same piece of software. Furthermore, DTU and Copenhagen University in Denmark are using these tools to study the background and shielding requirements of the very long guides that ESS necessarily needs to maximise instrument performance. In order to validate the recently developed software, a real experiment was performed at the BOA beamline at PSI, in which a beam was split and one half of the neutrons passed through a polyethylene block. Figure 2.43 shows the agreement between the simulation and the measured data. Other aspects of this work are discussed in Section 3.2.8.

Technology deployment

The technologies described in this section may be matched on a case-by-case basis to the instruments, in order to establish the total requirements of the facility, as shown in Table 2.8. While the addition of polarisation analysis may be an attractive option for many, if not all, of the instruments later in the lifetime of the facility, there are a number of instruments for which polarisation is extremely important from day one of operations. These instruments are labelled "Y" in Table 2.8.

2.7.4 Sample environment

Sample environment plays a key role in the success of a neutron user facility – the control and variation of parameters such as temperature, magnetic or electric field, pressure, humidity or material deposition (including liquid, vapour and gas flow) is in almost all cases an essential part of a neutron experiment. These sample parameters have to be provided in a very reliable way and over a broad range. Temperatures from mK to thousands of degrees K, magnetic fields from "zero" to 17 T, and pressures up to several GPa are standard at contemporary leading neutron sources. Examples of sample environment infrastructure are shown in Figure 2.44. ESS's high flux imposes special requirements on sample environment devices, beyond simple provision of broad access to parameter space. Waiting times – for example, for temperature equilibration or for sample changes – will be minimised for optimal beam time usage. Automatic sample handling and positioning by means of robotic machines will be adapted to the various instrument needs and to the specific sample environment system (e.g. low temperature cryostats and magnets). Some sample environment systems can be very bulky, circumstances in which neutrons compare advantageously to X-rays, for which the photons are rapidly absorbed. A modular approach is planned, with interchangeable sample environments for standard experiments, combined with highly specialised sample environments for

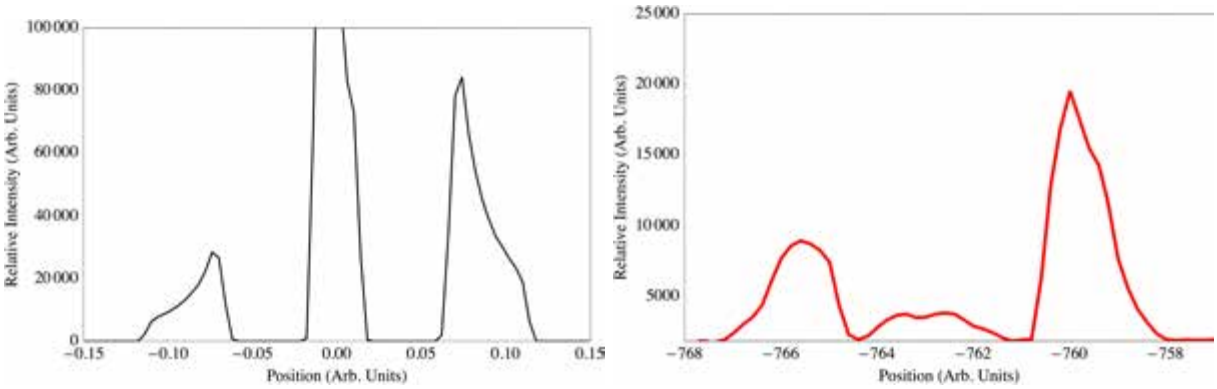

Figure 2.43: Comparison of simulated and measured neutron beam profiles. Left: Simulation of a neutron beam profile using MCNPX and McStas together. Right: Measurements on the BOA beamline. The large central peak in the simulated data is suppressed on the actual instrument by curving the neutron guide, so it does not appear so prominently in the measured data. The beam is split into two parts before the adaptive optics shown in Figure 2.40 refocuses the two beams while leading the left beam through a block of polyethylene, causing its peak height to be reduced.

Instrument	Wavelength range [Å]	Neutron optics technology					
		^{3}He	SM	FO	AO	BG	Bdr	LOS
Multi-purpose imaging	1 - 20	Y	Y	Y		Y		Y
General purpose polarised SANS	4 - 16	Y	Y				Y	
Broad-band small sample SANS	2 - 13							
Surface scattering	4 - 10			Y			Y	
Horizontal reflectometer	2 - 9.5		Y			Y		
Vertical reflectometer	5 - 9	Y	Y	Y	Y			
Thermal powder diffractometer	0.5 - 6			Y		Y		
Bi-spectral powder diffractometer	0.8 - 10			Y		Y		Y
Pulsed monochromatic powder diffractom.	0.6 - 10							
Material science & engineering diffractom.	0.5 - 5			Y		Y		
Extreme conditions instrument	1 - 10			Y	Y			
Single crystal magnetism diffractometer	0.8 - 10	Y	Y	Y		Y		
Macromolecular diffractometer	1.5 - 3.3							
Cold chopper spectrometer	1 - 20	Y	Y			Y		
Bi-spectral chopper spectrometer	0.8 - 20	Y	Y	Y				Y
Thermal chopper spectrometer	0.6 - 4	Y	Y	Y		Y		
Cold crystal analyser spectrometer	2 - 10			Y		Y		
Vibrational spectroscopy	0.4 - 5			Y	Y	Y		Y
Backscattering spectrometer	2 - 8			Y		Y		
High-resolution spin echo	4 - 25		Y				Y	
Wide-angle spin echo	2 - 15		Y					
Fundamental & particle physics	5 - 30			Y				

Table 2.8: Instrument-by-instrument deployment of neutron optics technologies. Key: SM: Polarised supermirrors; FO: (Removable) focusing optics, either supermirror-based or refractive; AO: Adaptive optics; BG: Ballistic guides; Bdr: Bender guides; LOS: Line-of-sight optics straight to the moderator would benefit these instruments at short wavelengths.

highly specialised neutron experiments. Standardisation of mechanical dimensions and software interfaces will ease the fast exchange of sample environment devices. Sophisticated equipment, controls and cabling can be highly complex. Standardisation of procedures and systems, following best practice in leading institutions worldwide, will be the guiding principle to efficiently use valuable beam time [251]. ESS will continue to seek input from the user community through science symposia and workshops during the construction phase of the facility, in order to identify requirements, facilities, and desirable features related to sample environment that will make the most productive scientific use of the beamlines.

Low temperature and magnetic fields

Desirable features for low temperature and magnetic field sample environments include superconducting (symmetric and asymmetric) vertical and horizontal cryomagnets (using liquid helium and/or dry cryo-cooler technology) to provide the highest available magnetic fields; modular low temperature inserts (dilution and ^{3}He); pulsed high field magnets ($\geq$ 40 T) with fast repetition rates; cryogenic polarisers that allow access to magnetisation distributions in molecular magnets, nanoscale samples, et cetera, on powder diffractometers; and magnets with arbitrary orientation relative to the scattering vector, which are useful for investigating complex magnetic structures including multiferroics.

Figure 2.44: Typical sample environments addressing, for example, low temperature, soft matter or material science applications. Left: Cryogen-free dilution refrigerator. Middle: Shear cell. Right: Custom made load frame for material testing. Required modifications to allow existing hardware to be used on the instruments will be done by the Sample Environment group in close collaboration with the manufacturers.

High or low temperature in combination with pressure

Desirable features for sample environments that combine high or low temperatures with pressure include vacuum furnaces with high heating and cooling rates and *in situ* reaction chambers up to 1800°C. Levitation furnaces that are part of the European NMI3 project will greatly improve the ability to assess materials at higher temperatures (up to 3000°C) and will have an important impact on research about high temperature innovative materials. Also desirable are dedicated and optimised pressure cells that, for example, reproduce conditions found deep within the earth's crust that are of interest to the geophysical community, but which could also address other scientific problems and needs (e.g. hydrogen storage). Combinations of temperature T (varying from mK to 3000 K and offering high heating and cooling rates), pressure p (varying up to e.g. 1 GPa), magnetic field B (varying up to 20 T or even higher for pulsed magnet options) will be possible. Combinations of parameters suited for approaches such as quantum magnetism studies or the application of electric fields to study multiferroics will be made available.

Soft condensed matter

Desirable features for soft condensed matter sample environments include shear cells in which the shear direction is perpendicular and/or parallel to the neutron beam direction; sample cells for fast and accurately controlled variation of temperature and pressure; *in situ* liquid handling on ml and μl volume scales [250] to be used, for example, on SANS instruments or reflectometers; stopped flow devices for SANS and surface studies; kinetic experiments with variable external parameters such as temperature, humidity controlled environments, controlled gas environments; and hybrid pump-probe laser techniques.

Material science

Desirable features for material science sample environments include furnaces for the application of high temperatures such as vacuum furnaces up to 1800°C or levitation devices to reach even higher temperatures; load frames for the application of external forces, combined with temperature and/or torsion. Such devices must allow for rotation of the sample in the neutron beam to accommodate, for example, texture measurements, which are of interest to the geophysics community, among others; and equipment that allows for dynamic thermo-mechanical testing of materials (e.g., dilatometer deformation system and DSC thermocaloric unit) and physical simulation of processes *in situ* in the neutron beam.

Identifying requirements

Continuous, on-going consultation with the different user communities and with leading researchers is of paramount importance in determining priorities and research trends. ESS will continue to actively pursue such consultation during the construction phase of the facility. Present necessities for instruments need

to be addressed, and future trends need to be anticipated, allowing critical scientific experiments to be performed in a timely manner. Specific sample environments that will likely operate synchronously with the ESS pulse structure will be identified and developed in more detail, once a firm decision on the seven day-one instruments has been reached. Consequently, the above mentioned sample environment systems are not exhaustive, but rather are indicative of what the user community anticipates will be required.

Standards and infrastructure

Where sensible, ESS will standardise the hardware and procedures surrounding the sample position of the relevant instrument. The use of standardised communication and control interfaces, as well as of sophisticated handling devices such as robotic systems, will help to achieve a high sample throughput to make effective use of neutron beam time. The Sample Environment Group will establish proper standards and procedures, and will develop sample environment hardware in close collaboration with the user community and the instrument scientists at ESS, working in parallel while the instruments are being constructed. This activity will closely interact with the activities of the Controls Group and DMSC, who will develop the control systems for the sample environment. The Electrical Engineering Group will be tasked with developing the instrument motion control system in coordination with ICS, as is discussed in more detail in the next section.

2.7.5 Electrical engineering

The Electrical Engineering Group (EEG) will develop motion control systems for general automation with an emphasis on standardisation, maintainability, and compatibility between instruments and instrument control systems [252]. The group will interface closely with the Detector Group, for example via the data acquisition system, with the Data Management and Software Centre (Section 2.8) and with the Integrated Control System Project (Chapter 5).

Motion control

Motion control in neutron instrumentation is very complex as it involves nearly every part of a modern neutron scattering instrument. A non-exhaustive list of areas requiring motion control includes positioning of samples or detectors, as well as controlling the movements of components such as collimators, moving slits, filters, and even whole neutron guides. Motion control must be able to position a small sample of a few milligrammes with sub-micron precision and also to manipulate tons of shielding with millimetre resolution. Motion control in neutron instrumentation also demands the ability to exercise control within extreme environments, with extremes of vacuum, radiation, temperature and/or magnetic fields [253]. The movement itself may be either a rotation, a linear motion or a combination of the two. Motion is controlled mostly in a closed control loop consisting of motor and power driver (actor), encoder (position or speed sensor) and control electronics. Appropriately placed switches limit movement in case of control failure or serve as reference points. Motion control loops interface naturally to both the remote control electronics and software on one side and the related instruments mechanics on the other side with a borderline marked by the so-called mechatronics components – motor and encoder switches – as shown in Figure 2.45.

Cable topologies

The classical centralised cable topology for a motion control system is shown on the left of Figure 2.46. All the electronics are located in a 19-inch rack outside the instrument area, and cabling must stretch from that rack to all the different corners of the instrument to provide connections to all components. In contrast, modern integrated motors with built-in driver and control electronics allow for a decentralised cabling structure like that shown in Figure 2.46 on the right side. Encoders and switches are cabled directly into the motor and the different positioning modules need only be connected by a field bus and a power supply cable.

Special instrumentation requirements

The unique features of the ESS neutron source together with the latest developments in neutron scattering instruments have a huge impact on motion control for the instruments. In particular, the high brightness

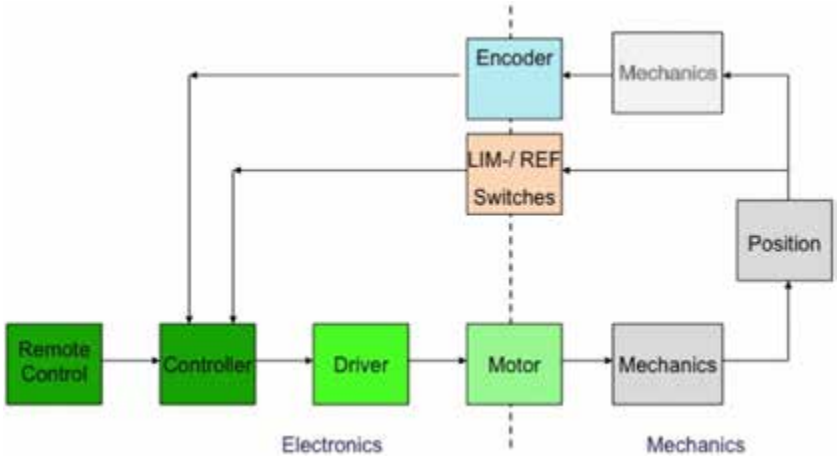

Figure 2.45: Motion control components forming a closed control loop linking the mechanics with the electronics.

and the size and layout of the facility will impose challenging requirements. Some of the challenges include small sample sizes requiring high positioning precision; positioning inside cryogenic environments; short experiments, requiring faster positioning in order to make the most productive use of beam time; high radiation fields, requiring identification of radiation-proof components; large distances between instrument components, requiring distributed and synchronised motion control units, capable of self- and distance-diagnostics; high magnetic stray fields, requiring identification of magnetic field-proof components; and high security levels requiring components with redundancy or status check.

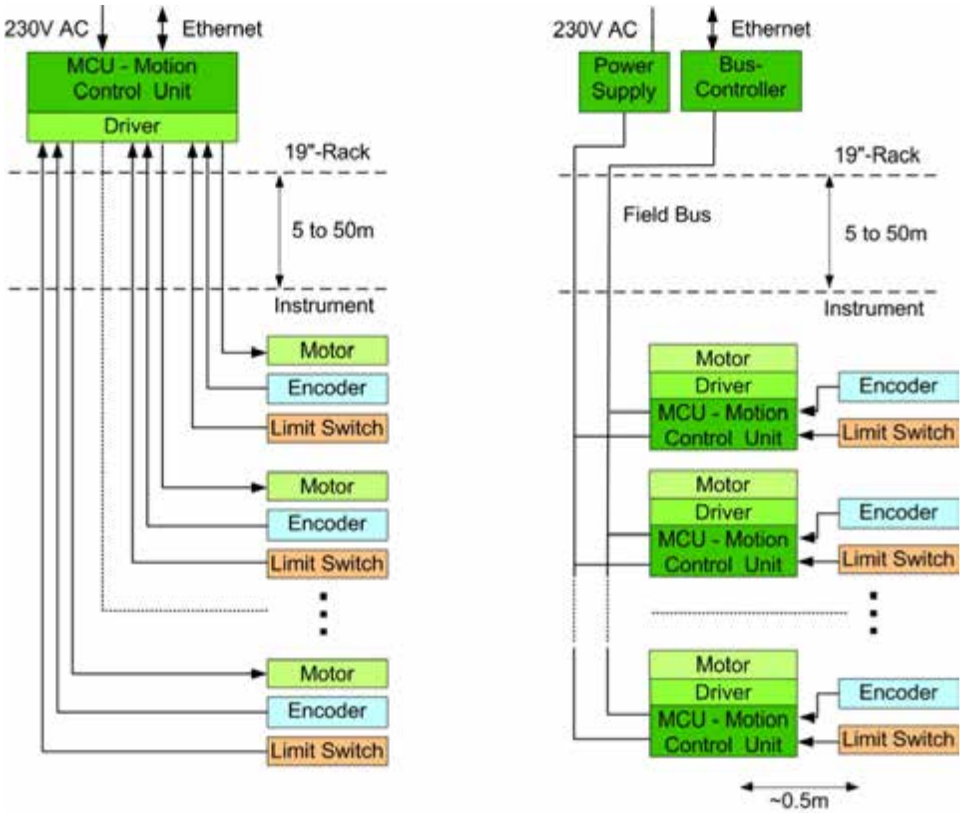

Figure 2.46: Cable topologies for instrument motion control technologies. Left: Centralised. Right: Decentralised.

Latest industrial developments

The motion control technology chosen for neutron instrumentation will be the facility standard for a relatively long period compared to regular production cycles known in industry. It is therefore essential to include the latest improvements and developments for the first instruments. These will include coordinated movements of a large number of axes; decentralised cable topology with integrated motors and controllers; synchronised motion control units with real-time field bus (EtherCat); two encoders for one axis (e.g. absolute and incremental) to optimise performance; piezo technology for precise positioning; and linear motors for faster movements.

Instruments personal protection system

The instruments branch of the personnel protection system, or PPS, which is discussed in more detail in Section 5.2.3, will be designed to allow users to easily access and operate the neutron scattering instruments while ensuring that the system complies with local Swedish laws, rules and regulations. This branch of PPS will be designed in concert with the ICS Project as it will be fully integrated in the site-wide PPS, which is the responsibility of ICS. It will also interface, communicate with and provide feedback to the machine protection system, or MPS, which is described in Section 5.2.2.

Standards and non-standards

The design of the electronics in combination with the software will integrate the neutron scattering instrument. The choice of hardware and low-level control will be defined taking into consideration standardisation, expandability, upgradeability and maintainability. Choices will be made in close communication with the neutron scattering community, and will fulfil the requirements of the instruments as defined by the instrument scientists. A standard list of motors, encoders, limit switches,and cables and connectors will be compiled following best practices at other leading neutron facilities [254–256]. This will serve as a compulsory guideline for instrument teams as well as for internal and external designers of instrument hardware. Definition of a carefully selected, limited number of parts, components and interfaces based on experience with existing systems will facilitate a proper integration of hardware, and will also be more cost effective over the lifetime of the instrument and the facility as a whole. Nevertheless, many hardware solutions will be cutting-edge projects from the scientific and technical points of view. EEG will support the development of solutions for special applications with ambitious requirements where standard parts cannot not be used. In recognition of the need for customised solutions, flexibility will be provided for further specifications to be assessed and approved as the selection of the motion control concept proceeds. However, solutions will only be accepted if they either fulfil the standard specifications already in place or have been explicitly approved by EEG.

Collaborations

Existing solutions for motion control at other facilities will be evaluated and collaborations pursued depending on requirements. Potential models include the modular control system SINQ-MCU developed at the Paul-Scherrer-Institute [257], or the motion system IcePAP [258] developed at the European Synchrotron Radiation Facility. The Experimental Physics and Industrial Control System (EPICS) will be used as a control framework, in combination with the control box approach discussed in Section 5.3. This mitigates risk associated with development, allows instruments to benefit from developments done in the Integrated Control System project, and maintains standardisation across the facility. EPICS is a software framework used to develop and implement distributed control systems to operate devices such as accelerators, telescopes and other large experiments [259]. It is a quasi-industry standard that is well maintained and documented, and has the support of a large number of large scale scientific facilities, including the SNS and Diamond Light Source. In fact, the SNS is gradually upgrading their EPICS systems to unify the existing accelerator and target control system with the neutron scattering instruments. The development of specific EPICS drivers in conjunction with the ICS project could potentially be performed in close collaboration with the SNS and ISIS, thus benefiting the neutron user community as a whole. The designers of the motion control system will interact closely with the Sample Environment Group, as robotic systems for sample environments become increasingly important and require systems that integrate motion and

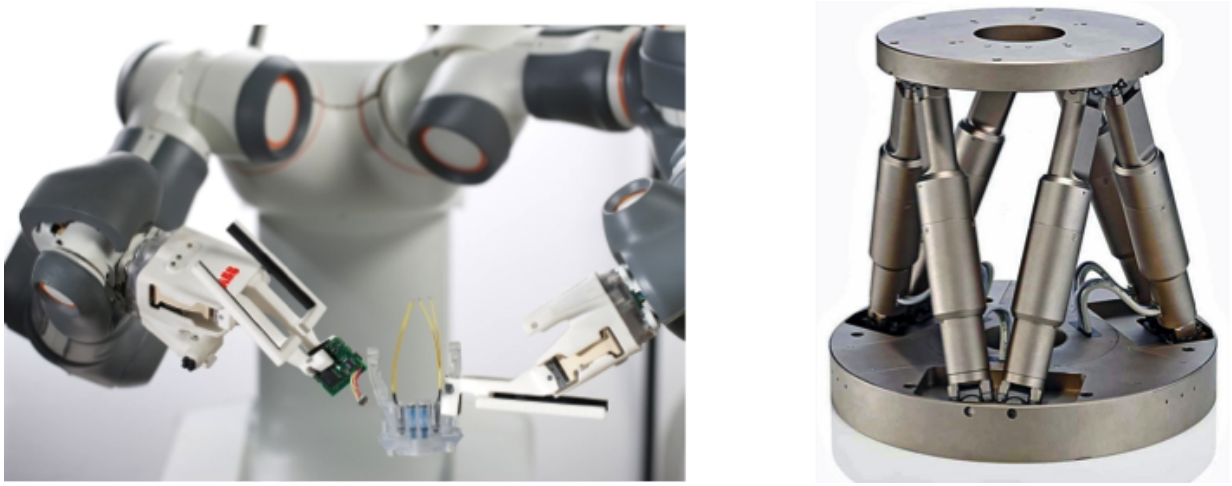

Figure 2.47: Multi-axis robotic and hexapod sample tables. Left: Conceptual robot FRIDA [260]. Courtesy of ABB. Right: A Hexapod robotics system for sample positioning [261]. Courtesy of Physikalische Instrumente.

control of complex hardware at optimised cost-to-performance ratios with a high degree of scalability. Examples of multi-axis robotic and hexapod sample tables are shown in Figure 2.47.

2.8 Data management and software for instruments and users

To fully exploit the information power of ESS, a new approach for software and data management is needed that intuitively integrates control of the neutron instrument and its sample environment; data processing, visualisation, analysis and publication; and permanent storage and public access. Realising this vision of a fully integrated e-science solution from idea to publication will be one of ESS's major contributions. The ESS-Data Management and Software Centre (DMSC) will tackle this e-science challenge, delivering a 24/7 e-science service programme to cover the complete research cycle from idea to publication as illustrated in Figure 2.48. The programme will provide an Internet-based system for interactions of the user community with ESS. It will include a user proposal system and peer review management; high-end tools for virtual experiments in order to plan, optimise and model measurements; a homogeneous instrument control platform across the instrument suite, which will be fully integrated with sample environments and ancillary measurements that generate meta data. It will also provide tools to enable researchers to interact remotely with experiments and ESS staff in real time; a platform that seamlessly integrates neutron and meta data and facilitates data reduction, visualisation and analysis in an intuitive manner; and state-of-the-art computational tools and computing platforms integrated with theoretical support in order to exploit the full scientific potential of ESS measurements. Finally, the programme will provide state-of-the-art data archiving and e-science tools to make data available to the scientific community in an appropriate form.

ESS-DMSC will be an integral part of ESS, located on the campus of University of Copenhagen in Denmark where it will host the ESS staff and IT equipment required to achieve its mission. Figure 2.49 provides an overview ESS-DMSC linkages. Reliability, usability, maintainability, and high quality will be ensured by using best practices in the development of the IT infrastructure. The complex IT infrastructure that is required to support scientific activities will be composed of dedicated networks, work stations, supercomputers, file systems, and long term storage. Figure 2.49 shows how the different components of the IT infrastructure will be distributed between the different physical locations in Lund and in Copenhagen. DMSC will provide and maintain updated infrastructure for high-performance computing during the construction phase for instrument simulations, simulations of the target, and for the online model of the accelerator. The use of this infrastructure will naturally extend into the operation phase, where it will form the starting point for the computational infrastructure required by the instruments and user programme. Moreover, DMSC will ensure that the McStas [262] software that is used for instrument simulations is properly maintained and further developed. Software development environments will also

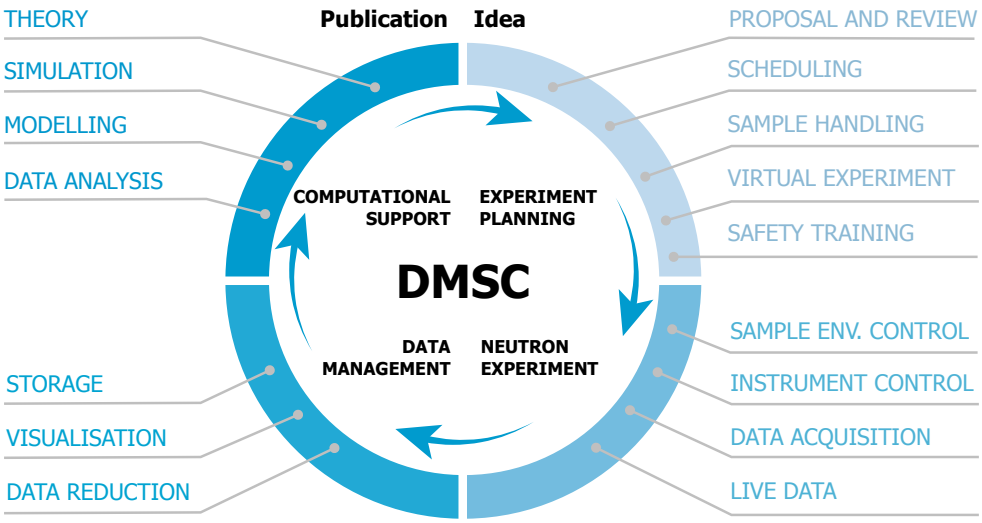

Figure 2.48: IT services and infrastructure provided by the Data Management and Software Centre, in each step of the research cycle from idea to publication, beginning with experiment planning, followed by the actual neutron experiment, data management, and finally computational support. This in turn may result in publications as well as new ideas and experiments.

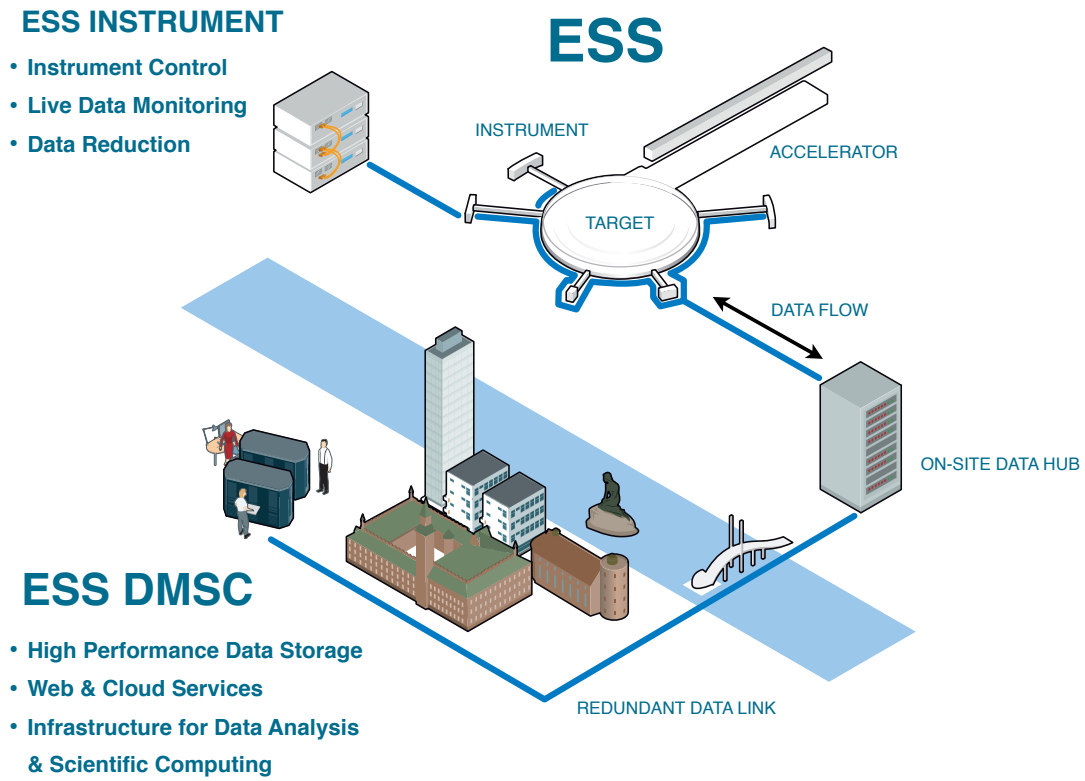

Figure 2.49: The relationship between the ESS-DMSC in Copenhagen, and ESS in Lund.

be required for research and development in the Detector Group and in the Integrated Control System group.

2.8.1 Requirements

In order to reach its full potential, ESS will need software and IT infrastructure for its instruments and user programme that are reliable, maintainable, usable, and supportable. Given the multi-decade duration of the ESS project and the rapid pace of technological change, ongoing software projects may easily span successive generations of technological developments. ESS will need the flexibility to cater for changing user requirements over its life time, and to interface to new or user-supplied equipment. In particular, the software provided through the user programme must be easy to learn and use for users with vastly different backgrounds and experiences in order to reduce the burden of support and avoid waste of beam time.

Instrument user interfaces

ESS will offer different instrument user interfaces in order to support researchers who will have very different backgrounds. For example, visiting scientists are likely to include both archaeologists who may visit the facility once a year for a few days, and physicists who visit on a regular basis. Interfaces will support users who need to perform complicated tasks as well as those requiring routine services, including software developers, instrument scientists, and support staff. To cater for these different types of users, an application programming interface (API) will be developed, as well as a domain specific command line interface (CLI) and a graphical user interface (GUI), as is common in modern scientific software. The interface will also support users who are not comfortable with command line interfaces in setting up sequences of operations. It will be possible to use a sequencer table interface, which resembles a spreadsheet in look-and-feel and functionality, to set up a sequence of operations for execution. The sequencer table will be an integral part of the graphical user interface. A uniform look-and-feel will be maintained across the software suite, and different programs will work seamlessly together. This will save user time, and increase the research productivity of the facility.

Software architecture

The same architecture will be used for all components of the software suite used across the entire research cycle from idea to publication, as is illustrated in Figure 2.48. This uniformity is important for building an efficient software development organisation, and will make it easier and cheaper to ensure that different components of the software suite indeed work together seamlessly. A software architecture that spans the needs is outlined in Figure 2.50. The central component is an API that will be used to interface to various libraries, including graphical components, databases, and third-party applications. The API will in turn be used to develop domain-specific command line interfaces, graphical user interfaces, and browser-based services. The preferred option for the implementation is based on Python for the API, C++ for performance intensive libraries, and Qt as a graphical library, as shown in Figure 2.50. This approach is becoming a standard software framework for scientific applications, in part due to the extensive selection of scientific libraries. Many facilities already use, or have plans to use Python as a scripting language, including the Diamond Light Source, ISIS, and SNS. This architecture also is used by the data reduction and analysis program, Mantid [263]. For this reason, Mantid has been selected as a cornerstone of the software suite. Many other programs of relevance for ESS-DMSC are also based on this architectural choice, such as the Python-based Hierarchical ENvironment for Integrated Xtallography (PHENIX) for macromolecular structure solution [264]. Some level of web development (which could be based on HTML5, for example) will take place because some components of the software solution, such as the user office software, must be browse- based. Indeed, ideally, the software suite as a whole will work as a web application.

Command line interface

A command line interface will be made available for instrument control, data reduction and data analysis. It will be possible to use the command line interface interactively as well as to execute scripts consisting of several lines of codes, a capability already available in Python. Users will be able to generate their own scripts, test that they work as intended through a dry-run, and save them for later use or for distribution

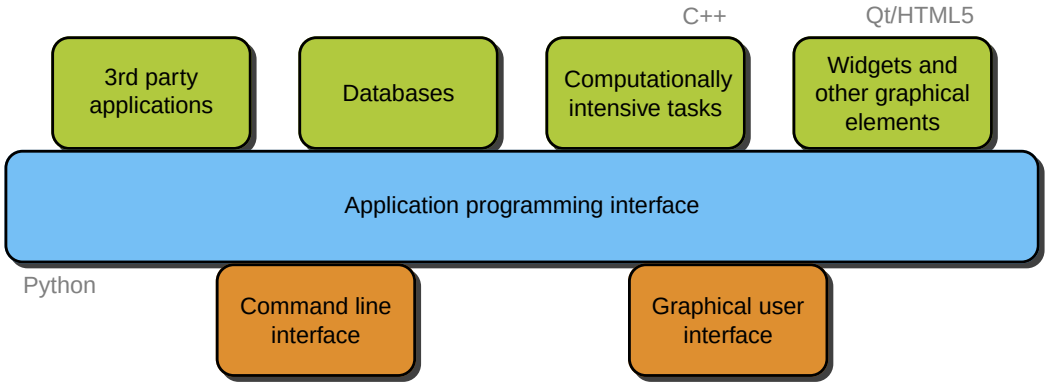

Figure 2.50: The architecture that will be used for the software suite that will support users from idea to publication. Python, C++, Qt, and HTML5 are the current preferred options. Language use locations are indicated.

to other users. The latter makes it possible for instrument scientists to optimise the path from idea to publication for specific types of experiments by scripting predefined procedures for the user community. Whether run interactively on the command line, through a script, or via the graphical user interface, all steps will be time stamped and logged as a new script. This will make it easy for users to repeat the various steps of an experiment (instrument control, reduction, or analysis), or to make variations over the same experiment by modifying the logged script. The time stamping will also make possible the alignments of logged commands with data acquired from the experiment, facilitating the creation of a detailed log book from the experiment.

Graphical user interface

The graphical user interface will be self-explanatory for the users of the instruments. It will be customised for each instrument. It will be possible for the instrument scientist, users, and technical support staff to selectively enable features for a given experiment. The graphical user interface will support advanced tasks through a shell for executing commands of the command line interface, a library of predefined scripts, and a sequencer table interface, which will allow the execution of commands via a spreadsheet-like interface. The sequencer table interface is expected to appeal to many users because it resembles the spreadsheet interfaces that they are already familiar with, and because it will enable them to do fairly complicated tasks without scripting through the command line interface.

Remote access and web applications

Users will be given secure remote access to software services. In fact, much of the software required by ESS will be developed as web applications, including types of software that traditionally have been thought of as standalone applications. Web applications offer many advantages. Web-based solutions will enable DMSC to avoid providing support for a multitude of current and future hardware platforms and operating systems. Web applications will also spare users the hassle of software installation. In addition, web applications will make in-house resources available to users remotely. It will be possible to analyse experimental data by means of computers and software running with a minimum of data transfer.

Security and access control

Many of the risks related to remote access, if not all, can be mitigated by implementing proper authorisation policies and security measures. DMSC has a strategy to monitor developments in IT security, hacking, and network penetration techniques and will ensure that the systems in place remain at the forefront of recommended practice. The final line of defence for a successful penetration will be the provision of an operation mode under which ESS is completely disconnected from the Internet. To avoid unwanted intrusions into the ESS network, user credentials (such as user name and password) will be required to

access DMSC software services. A single set of credentials will give access to all services that the user has permission to use. Moreover, single sign on (SSO) [265] will be used for all web applications, such as user office services, data access, and remote monitoring of experiments. Where feasible, SSO will also be used for software programs that are not web applications. It is currently the plan to mesh SSO with existing methods, developed as part of PaNData [266], CRISP [267], and eduroam [268]. Authentication (the ability for users to prove who they are) and authorisation (the different rights a user has in the system) are discussed in more detail in relation to user office software in Section 2.8.2.

2.8.2 Experiment planning and the user office

A number of administrative and planning tasks need to be completed before an experiment can take place. First, the experiment must be approved for beam time. Subsequently, scheduling, sample handling, and safety training (among other procedures) must be taken care of. The user office, which will be under the responsibility of the Neutron Science Division, will play a pivotal role in accomplishing these practical tasks. It will be the user's primary point of entry to ESS. The functionality of the user office software that DMSC will provide will have a significant impact on the efficiency of the user office and on the user's experience at ESS. Besides administrative matters, both visiting users and ESS staff involved in an experiment, may plan the execution of the experiment in detail, and practice operation of the instrument and its associated software through virtual instruments, for instance through computer simulations. The user office will have both an online and a physical presence which will come into play during experiment planning, and at other stages of the user's involvement with the facility. The user office will offer both end-users (visitors) and staff a simple and comprehensive gateway to the information required to make the visiting scientist's stay successful. The gateway will be a mostly paperless, integrated solution that does not duplicate information across various systems or require constant manual re-entry of information already in the system. The user office software will play a central role at the facility since the information gathered by the user office will feed into many systems across the facility. Such information exchange is required, for example, to facilitate scheduling and planning. In developing the user office software, special care will therefore be taken to identify and manage information exchange. European data protection laws, in addition to Swedish and Danish regulations, provide very specific requirements for the collection and retention of data, and DMSC will adhere to these standards. The scope of the user office software is quite broad, as also are the different areas of responsibility within the user office, including a user database, proposal system, scheduling, invitation procedure, sample handling, and post-experiment activities.

Instrument user database

Users will have to be registered in the instrument user database in order to access various services at the facility. There will be different kinds of users at the facility, including external users who visit the facility to conduct experiments and permanent staff, who also will need to access various functions of the user office systems. Provision may also be made for other classes of users, such as those proposal reviewers who may be neither staff nor visitor. The instrument user database will provide both authentication (the ability for users to prove who they are) and authorisation (the different rights a user has in the system). The information required to authenticate and authorise a user will vary depending on the level of access they are granted to the facility. An external user will be able to create an online account for the purpose of submitting proposals without providing proof of identity. However, such proof, for example through the provision of identity papers, will be required before a user is granted further access to the facility. The status of trust in a user's identity will be kept updated in the system. Identity information may also come from other sources, such as other trusted facilities or through a federated identity management service.

Proposal system

During calls for proposals, registered users will be able to create, view, edit, submit, and withdraw proposals. A given user may have one or more active proposals. For each proposal, users will be able to enter various types of information, for example, title, type, instrument, the purpose of the data collected (e.g., whether it is used for thesis work), subject and research areas, abstract, related proposals, information about the team, samples and sample environment. Users also will be able to attach files with supporting material. Once a proposal has been submitted, a proposal ID will be allocated, which the user will be

able to use to view and track the proposal as it makes its way through the review process. During the submission process, users may be required to agree to various conditions before being allowed to submit proposals, including conditions governing access to data generated at the facility, intent to publish, and compliance with safety procedures. Once a user has submitted a proposal, it will be possible for administrators to view it and to assign reviewers to it. The reviewers will be able to view the contents of the proposal and submit evaluations, which initially will not be visible to the proposer. Before the results are released, the successful proposals will be ranked and scheduled. Once the review deadline has passed, users will be informed of the result of the review of their proposal. If review results are favourable, the proposing team will receive an invitation to visit the facility to conduct its experiment. At that point, proposers also will be able to view the details of the evaluation.

Scheduling

Scheduling is an integral part of the proposal process. The schedule of each instrument will be stored and will be query-able, and alterable. In addition to the instruments, other components will also be scheduled, including sample environment and the instrument team. Care will be taken to make sure that crucially important scheduling information is disseminated correctly throughout the facility.

Invitation procedure

Once a successful proposal has been scheduled, the proposing user will be formally invited to the facility. Invitation procedures involve informing the user of the invitation, of course, but also ensuring that the proposer and other members of the scientific team are ready to visit the facility. Along with the invitation there are a number of practical matters that the proposal system will be equipped to deal with, including booking, confirming, and providing opportunity to review accommodations at the facility; travel arrangements, when required; ensuring that site access is granted for the duration of the experiment and that conditions for granting that access have been met, such as the completion of safety and instrument training, submission of health certificates, and dosimetry handling. These procedural matters will be addressed during the period of time between the issuing of the invitation and the beginning of the experiment. In some cases, such as travel arrangements, activity will be initiated by the user, but will usually require action from user office staff. Other matters can be entirely automated, such as safety training. It is important to ensure that these practical matters do not become burdensome for staff and visitors.

Sample handling

Some users will send in their samples, rather than showing up physically at the facility. The system will be able to handle the registration of samples, shipping, storage, safety evaluation, and location tracking at the facility, using identifying markers such as barcodes, QR codes, or electronic tags. Both users and ESS personnel will be able to add, view, and update information about samples, and this information will be automatically included in the metadata of an experiment. If the user is off-site, the system will also grant remote access to the instrument during scheduled beam time. Once the sample has been exposed to the beam, it may need to be quarantined for some time before being returned or disposed of. The software will keep track of the location of the sample, as well as the custodian who should be contacted once the sample has been released from storage.

Post-experiment activities

Although many responsibilities of the user office are related to experiment planning, there are also a number of post-experiment activities that the system will enable the user to complete. The user office system will be able to handle the creation, editing, and approval or rejection of reimbursement forms, and to facilitate communication about these forms where clarification is required. The user office software will make it possible to attach necessary documentation to the reimbursement forms. A simple and well documented workflow will be established for completing these forms. The software will also make provisions to elicit feedback from users at the conclusion of their stays. After the user has published or otherwise made use of the experimental data collected at ESS, data about outcomes will be recorded in the system. While some users may take the initiative themselves to collect and track this information, user office staff will often play this role. Outcomes of interest might be reports, publications, or intellectual property

such as patents attributable to the research carried out at the facility. Along with the specific services above, the user office will provide some generic services in order to support day-to-day functions, such as content management for training materials, instructions, and help related to user office procedures; and a method to administer tests and provide feedback forms. The user office will play a central role in user authentication and authorisation. This will apply to both electronic and physical access to the facility. Electronic access will encompass the various user office facilities and remote access to instruments, which will be limited to the period during which the user is scheduled to use the instrument ,and to data once the experiment has concluded. Physical access to the facility will also be limited to the period during which the user is scheduled to use the instrument.

Training

Besides safety training, training in performing an experiment at ESS will be provided to novices before the experiment takes place. This will avoid unnecessary waste of beam time. Training may take the form of face-to-face workshops at DMSC or of electronic courses, including online courses. In either case, users in the training sessions will engage with software identical to that which they will need to use during the experiment to operate the instrument and analyse resulting data. They will be given the opportunity to perform dry runs using the software with artificial data.

Virtual experiments

Monte Carlo ray-tracing simulations using programs like McStas [262] or Vitess [269] have already been deployed in the design update phase for evaluation and design of instruments, neutron optics and time structure of the ESS source. For each instrument constructed, ESS will develop a detailed instrument model that mimics the real instruments. A limited number of sample models for McStas exists today. This library of sample models will be expanded significantly in the future, based partly on a systematic development chain from quantum chemistry calculations (for example, density functional theory) to McStas model. With a model of instrument, sample environment and sample in hand, it will be possible to simulate a complete experiment, which in turn will become a tool for training users and staff in how to operate the instrument and perform data analysis. Users may also employ the virtual instruments to evaluate experiment ideas and to optimise experimental procedures prior to scheduled beam time. In the long term, it may become common practice to include complete simulations of experiments in applications for beam time.

2.8.3 Instrument control and data acquisition software

Software is required for controlling the instrument and sample environments, and also for acquiring neutron and metadata from ancillary measurements. Live data processing will enable experimentalists to better control the experiment to increase research productivity. The term “instrument control” is used here exclusively to refer to the process of controlling the instrument through commands (slow control), while the term “data acquisition” is used to refer to the process of acquiring data from sensors or detectors, whether it is neutron data (fast control) or metadata (typically slow control).

Instrument control software

The devices that need to be controlled in order to perform an experiment are associated with the neutron scattering instruments, sample environments, or detectors. Technical details for these systems are discussed in Section 2.7, and layouts for specific instruments in the reference instrument suite are discussed in Section 2.4. Neutron scattering instruments typically are associated with a number of controllable devices, including choppers (as discussed in Section 2.7.2); motors for positioning and aligning the sample and for operating the shutter; and associated sensors for monitoring frequency and phase of the choppers, position of the motors, intensity of the neutron beam, and pressure (to verify the existence of vacuum in the beamline). Vendor-supplied goniometer systems and robots for picking up samples and aligning them in the beam may also be part of a neutron scattering instrument. Depending on the specific instrument, there may be other components along the beam line that need to be controlled via motors, such as collimators and removable polarisers. In some cases, highly integrated motion control systems with complex trajectories and/or a high number of coupled axes maybe needed, as discussed in Section 2.7.5. A complete list of

devices will be available only after the instruments have been selected for construction and completely designed.

Sample environments are discussed in Section 2.7.4. They will have vastly different configurations depending on their purpose. They may be equipped with temperature, pressure or applied force regulation; magnetic and electric fields; and/or access for chemicals, for instance by means of syringes in stopped flow experiments or valves for gases. At a lower level, this implies the existence of heaters, coolers, cryostats, magnets, pumps, motors, and various sensors, including thermometers, pressure sensors, pH-meters, and flow-meters. In addition to instrument-specific sample environments, there will also exist a set of standardised sample environments that will be compatible with several instruments. Furthermore, some users are expected to provide their own sample environment equipment, and ESS will provide standard interfaces to facilitate these experiments. The sample environment will be controllable by the same means and through the same user interface as the beamline instrument, and thus the sample environment will be plug and play. All detectors will need to be controlled and will require monitoring of magnitudes such as voltage and gas-related settings. Furthermore, whilst the majority of instruments will have a fixed geometry, some instruments may have movable detector banks requiring motors, as is the case for the materials science and engineering diffractometer in the reference suite. Detection of neutron events will take place in hardware systems, and is discussed in detail in Section 2.7.1. The various devices will be controlled by a user through a control console. Control consoles ready for use will be available in the main control room, and also in satellite control areas associated with each neutron scattering instrument, and via a mobile device. This is discussed further in Section 5.1.2.

Integrated control system

The instrument control will be part of the integrated control system (ICS), which in addition to the instruments also will control the accelerator, target, and conventional facilities. The integrated control system will facilitate standardisation and collaboration, for example, on driver development, across ESS. Moreover, required information from the accelerator and target will be provided by ICS, such as moderator temperature and flux of the proton pulse. Time signals from the master oscillator, machine protection system (MPS) and personnel protection system (PPS) also will be provided by ICS. ICS will be based on EPICS [259] for the device layer (drivers) and EPICS channel access middleware for communication between devices and between devices and control units. Control boxes will be employed to ensure modularisation and standardisation across ESS, as described in detail in Section 5.3.

Requirements for instrument control

The general requirements outlined in Section 2.8.1 are also valid for the instrument control software. Both a command line interface and a graphical user interface will be available. The same software will be implemented on all beamlines in order to reduce development and maintenance costs and to facilitate the transfer of knowledge and experience among instruments. Other software will only be implemented for instrument control where there are substantial benefits that balance the additional cost of supporting multiple solutions. Examples of such exceptions might be the existence of a standard solution within a given technique or a desire to support cross-facility experiments, for instance between ESS and MAX-lab, in which case it will be desirable for users to encounter the same software at the two facilities. There is no *de facto* standard for instrument control user interfaces at neutron scattering facilities, and no interface currently fulfils all the required specifications described above. ESS will monitor developments in existing projects and will decide to what extent it will be advantageous to use existing solutions in the near future.

Data acquisition

In order to fully preserve all the information from an experiment and allow for more powerful and flexible data analysis, instrument data acquisition will be based on event mode as far as possible and appropriate. In event mode, a detected event is time stamped with a value from the central timing system provided by ICS, as described in Section 5.2.6. ICS will employ current practices of accurate timekeeping, in partnership with the chopper and instrument groups, to ensure that recorded data are accurate and reliable and properly aligned in time with other events across the facility. Three categories of data events will be generated for experiments: Neutron data, metadata events, and absolute time records. Neutron data will be sent from the detector electronics in a binary data format containing the relative timing information

and the index of the detectors being hit by a neutron, as described in Section 2.7.1. Metadata events will be provided by the control boxes associated with the relevant devices in a binary format containing the required information about parameter, time, and value. The exceptions from this are user, sample, and proposal tags which will be obtained from the software suite provided by DMSC, as will be the case for the user office. Absolute time records will contain absolute time and will be provided by the central timing system.

Data transfer will take place by means of two types of data streams. One will contain neutron data events and the other will contain metadata events. In both cases, the streams also will contain absolute time records in order to ensure that all events can be properly aligned on an absolute time scale. Details about the data format can be found in [270]. A non-exhaustive list of relevant metadata includes experiment data on users, team members, local contact, and system under study; proton pulse data; moderator temperature; neutron flux; chopper settings; measured speed and phase; position of detector banks; instrument settings and sample positions including motor axle positions; pressure, humidity, temperature, and alignment on optical systems; beam monitor counts. For sample environment, metadata will include temperature, pressure, magnetic field, mechanical strain; and user-supplied commands, as discussed in Section 2.8.1. All data will be streamed to the live-processing system, which is discussed below, and to the data storage system discussed in Section 2.8.4, where they will be saved in the form of NeXus files, with a NeXus file for each experiment or measurement performed.

Live-acquisition processing, visualisation and automation

Live-acquisition processing and visualisation will enable researchers to get feedback in real time during their experiments. Data processing and visualisation are discussed in more detail in the next section. An efficient infrastructure will be developed to give fast access to stored data and sufficient CPU power

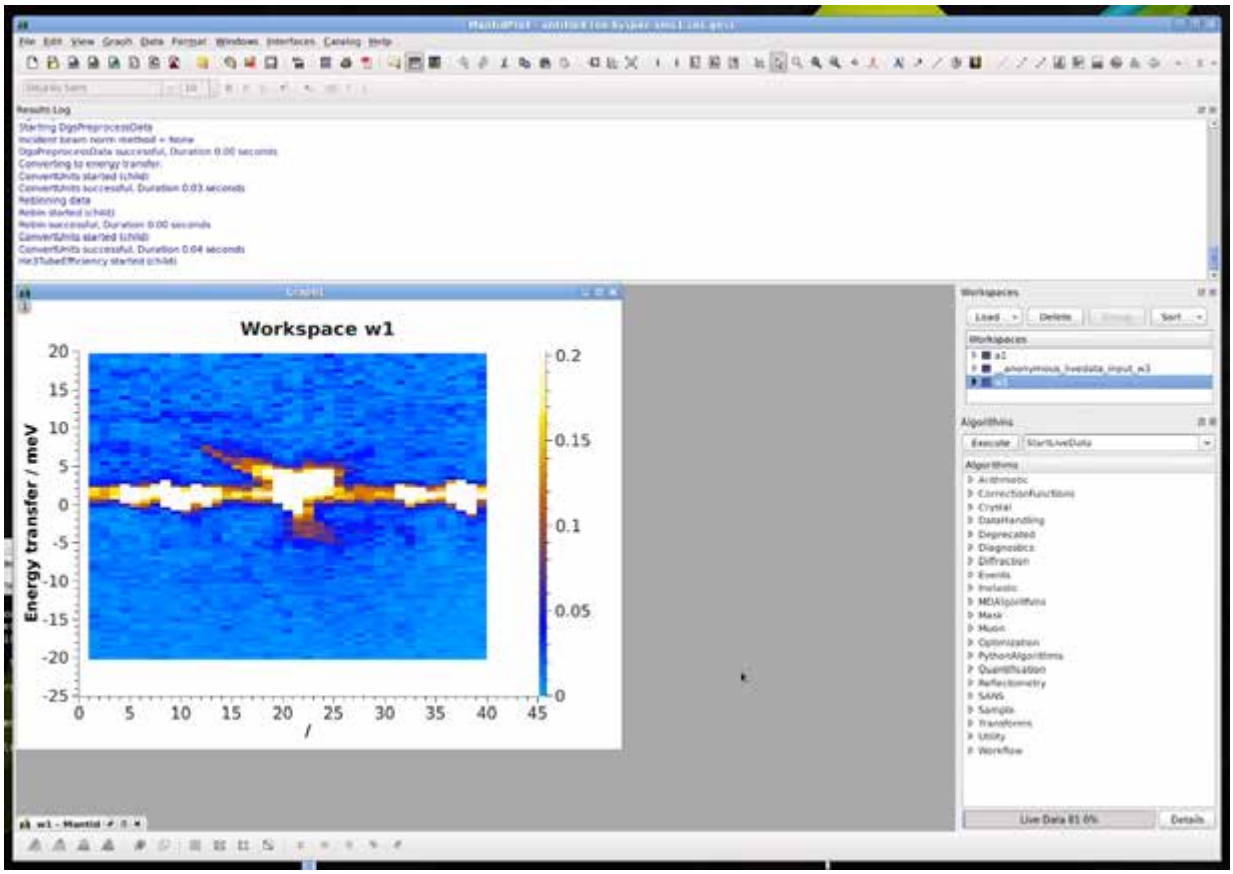

Figure 2.51: Snapshot of live streaming data reduction with Mantid and the ADARA system developed at Oak Ridge National Laboratory [271, 272].

for live-acquisition processing as well as for post-acquisition processing. Given the high neutron fluxes, significant computer resources will be required on site in Lund for processing of acquired data in real time. The ADARA system shown in Figure 2.51, which was developed at ORNL, will be used for live processing, and further developed so that it will be able to cope with ESS's high data flow rates. It may be possible to use libraries from the ROOT data handling system at CERN [273], which can handle data streams on the same order as may be required at ESS. Various levels of automation will be employed. Scripting and the sequencer table interface will provide the means to do so and the software will make it possible to use data from the live-acquisition processing to automatically advance to the next step in a sequence of measurements once sufficient statistics have been obtained. This will enable scientists to concentrate on the scientific aspects of the experiment rather than the technical details of running routine tasks on the instrument.

2.8.4 Data management

An experiment or sequence of experiments generally results in a large number of documents, simulation results, measurement data, analysis results and scientific papers. All this information will be stored at DMSC and DMSC will provide tools and services to ensure that researchers are able to access the data and the required computational resources to manipulate this data at all stages of the scientific process in accordance with the security policies described in Section 2.8.1. Much of the information will be made browsable and searchable, including metadata. Besides metadata and raw neutron data originating from measurements, logs of applied data analysis and information about the employed software and resulting publications also will be stored in the data management system.

Data reduction

Data reduction describes the process of correcting and transforming acquired raw data into physically interpretable data. It is an essential part of an experiment. The algorithms for data reduction are instrument-specific, and software for reducing data acquired at a given instrument will thus be considered an integral part of that instrument. Preliminary data reduction and real time analysis and visualisation will assist users in performing an experiment as described in the previous section. However, at any given time after the experiment, a user also will be able to access the data and process them or visualise them without transferring the data out of the facility. Thus data reduction is intimately linked to data management. That being said, the user will also be able to copy data to the home institution, where a user will be able to use his or her own software or software provided by DMSC, which will be open source to the extent feasible.

Data reduction consists of filtering, correction, mathematical operations, binning and presentation. Filtering ensures that only data that fulfils specification will be used in the subsequent processing. Data may fail to meet specifications for a variety of reasons. For example, data generated before choppers have settled to the specified speed and phase will be rejected, as will be data generated when sample environment conditions have not yet met specifications, or when neutron pulses are of inferior quality. All raw data will be stored, so no data will actually be discarded in the filtering process. Data will be corrected to compensate for spurious effects. This may include, but will not be limited to, normalising a data set by the incident flux; determining variations in detector sensitivity using a vanadium sample and normalising data accordingly; or correcting for background obtained by measurement. Data sets may also be corrected for scattering from the instrument itself or from the sample environment or corrected for multiple scattering effects by measurement or instrument simulations using, for example, Monte Carlo ray-tracing codes.

Mathematical operations will be used to slice, project, interpolate or otherwise manipulate data into a scientifically appropriate form. The extensive use of wavelength frame multiplication and repetition rate multiplication at ESS will augment the complexity of this task, which underscores the importance of providing adequately reduced data in order to realise the full potential of the long-pulsed source. Binning is a procedure that converts the set of remaining events to histograms that may be multidimensional. In the general case, events will be converted to a histogram depicting neutron intensities (event counts) as a function of parameters of interest. The accumulated data from each detector pixel will be presented to the user graphically, and it will be possible to replay the accumulation of data over time. It will be possible

to plot graphs and histograms in one and two dimensions, and also to visualise data in 3, 4 or even more dimensions, based on the slicing and projection of data for final presentation on a graphics terminal.

Virtual instruments for data reduction

Virtual instruments based on Monte Carlo ray-tracing software will play an important role in the development of data reduction and analysis software for the instruments while the real instruments are being constructed. This will be particularly important for researching and developing algorithms for data reduction and analysis for wavelength frame and repetition rate multiplication where no standard methods exist at the present time. The use of virtual instruments will make it possible to develop and test software for data reduction even though the instruments have not yet been constructed and put into operation. This, in turn, reduces the risk that adequate software will not be ready once the target instruments enter the commissioning phase. Virtual instruments are also expected to play an important role during the operational phase. Advanced data reduction can be performed with a realistic sample model, making it possible to simulate the complete experiment to obtain good agreement between simulation and experiment. Once that has been obtained, the individual contributions to the observed scattering pattern can be separated, as illustrated in Figure 2.52. With the single coherent, incoherent and multiple scattering patterns available, more reliable data analysis can be performed. Furthermore, simulations can be used to estimate contributions from the surrounding sample container and cryostat.

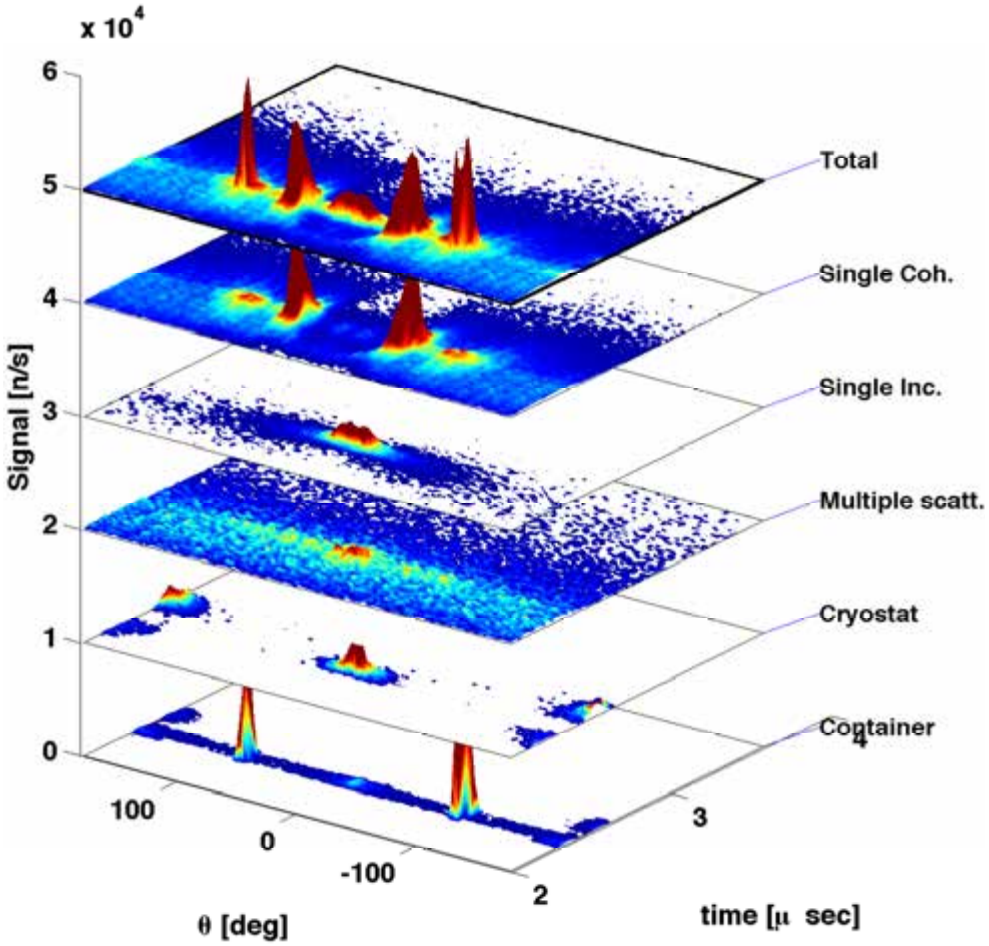

Figure 2.52: Simulated total signal from l-Rb at 350 K separated into coherent, incoherent, multiple scattering, cryostat, and container contributions. The cryostat and multiple scattering signals are multiplied by a factor of ten.

Options and system architecture for data management

The preferred option for a data format for storage is the NeXUS file format [274], which is a customisation of the HDF format to data from neutron scattering experiments. ICAT [275] is an example of a data management system that could be used, in which all metadata are stored in a relational database and made browsable and searchable. Links to the raw data files are stored, and in this way a single point of entry to information from the experiment from idea to publication is obtained. Solutions for data reduction and visualisation will likely be developed in the Mantid framework, which fulfils most requirements with respect to architecture, user interfaces, and development as discussed in Section 2.8.1. Mantid, which has both a graphical user interface and a command line interface, is being developed for reduction, analysis, and visualisation of data acquired at ISIS and at SNS [263], and may be adopted by J-PARC [276] and ILL. Thus, by joining the Mantid project, ESS will be able to deploy data reduction software with which users are already very familiar. Mantid can already be used for processing live data streams [277], has excellent visualisation capabilities, and can handle data of high dimensionality [263]. A project has been launched to connect McStas and Mantid so that algorithms in Mantid can be applied to data generated in silico by McStas. This would make possible the use of virtual instruments in the software development process.

The data management system will reside on a high performance file system at DMSC. A data volume of the order of multiple petabytes per year is expected. The file system will be based on both disk and tape to assure fast access to frequently used data and reliable storage for all data. A total backup of the storage system will be located in Lund to assure physical separation of the master data and the backup data. Data will be transferred between Copenhagen and Lund over a dedicated fibre connection that will be doubled for reliability reasons; one fibre will pass over the Öresund bridge and one fibre will pass under the Öresund between Denmark and Sweden. If all connections between Lund and Copenhagen fail, data will remain in the back-up facility in Lund until the connection is reestablished. A high performance computing cluster for post-acquisition processing will interface directly with the data storage system to ensure the highest data-transfer bandwidth during reduction and analysis and will make it possible for users to process their data with a minimum level of data transfer out of the IT infrastructure.

2.8.5 Computational support for analysis

Data analysis will require new sophisticated software, powerful computing hardware, and expert knowledge in scientific computing if ESS is to reach its full potential. Two examples of how scientific computing can be used in the data analysis process are given in Figure 2.53. DMSC will prioritise making it easy to integrate new data analysis methods and algorithms into the software to increase research productivity and the potential for new breakthroughs in experimental techniques. Indeed, scientific computation and theory will be critical in providing added value to the data measured at ESS. Recent development of supercomputing infrastructures (e.g. the Cray XT5 computer at Oak Ridge National Laboratory) has allowed the timescale and system size attainable by molecular dynamics simulations to reach timescales on the order of 1 μs and sizes in the order of 10 million atoms. Extrapolation of this performance indicates that it probably will become possible to perform molecular dynamics simulations of systems of 10 billion explicit interacting atoms (i.e., approximately the size of a living cell) within the time frame of ESS's operational life [281]. Simulations at this level will complement the length and timescales of systems that can be characterised by the instruments at ESS, as discussed in Section 2.2. This rapid development in computing power will thus bring unprecedented capabilities to scientific computing and make it possible to employ new algorithms for analysis, for instance based on quantum chemical calculations or molecular dynamics simulations.

In most cases, data analysis consists of resolving a spectrum into individual peaks or other curve forms by means of curve fitting followed by modelling. Data analysis allowing for multi-dimensional fitting will be particularly important for ESS because data will be acquired in event mode. Figure 2.54 illustrates this in the (simulated) case of a powder diffraction pattern, where existing analysis tools only use a tiny fraction of the available information. By developing methods that use all data, the beam time required to obtain sufficient statistics can be drastically reduced. In some cases, the subsequent modelling step is more or less standardised, and users will be able to go from data acquisition to resolved structures in a single step through reduction, fitting, and modelling. However, this only works for perfect crystal structures, whereas structures with defects or amorphous and porous materials (for example, polymers and concrete) are more

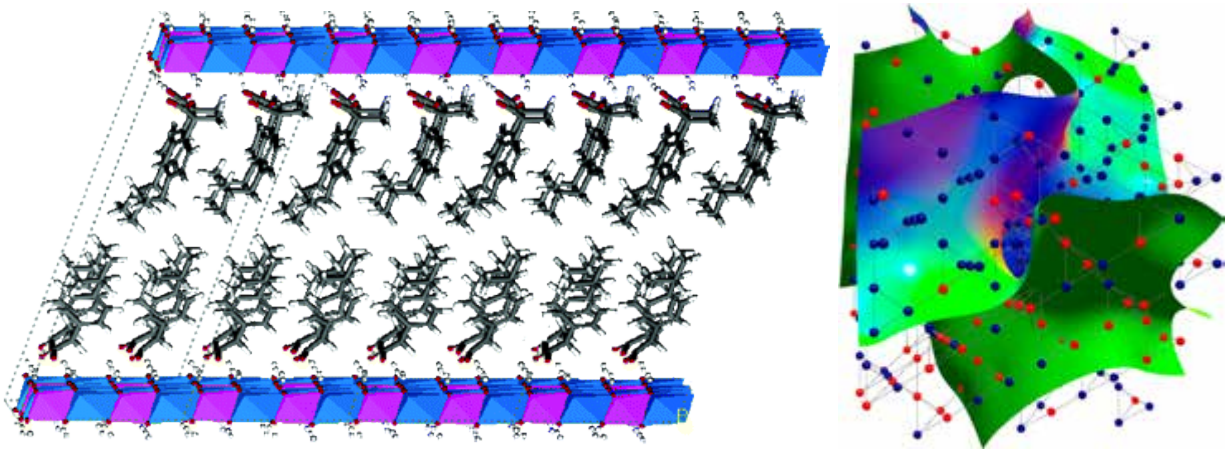

Figure 2.53: Two examples of how intensive computing can be used in data interpretation. Left: Snapshots of the simulation of Mg-Al intercalated drug hybrids, in this case ibuprofen (indicated by sticks). Dashed lines indicate the initial simulation unit cell. Colour code: Blue N, green Cl, red O, gray C, white H, pink Al, and blue-green Mg [278]. Neutron scattering data is indispensable to confirm or constrain these simulations. Right: Computer reconstruction of the surface morphology of a percolation cluster surface in $Y(Mn_{1-x}Fe_x)_2$. Colour code: Red Fe and blue Mn. Magnetic small angle neutron scattering experiments show that the morphology is similar to that of microemulsions [279].

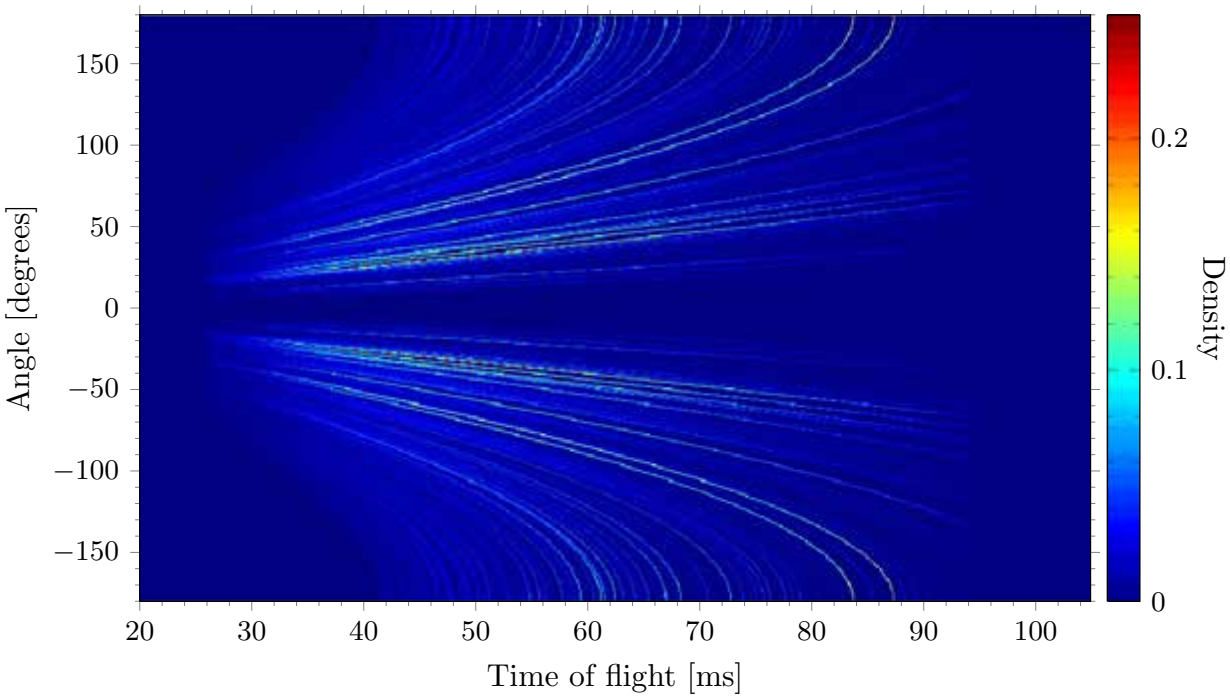

Figure 2.54: Simulated density plot based on ray tracing simulations showing intensity of detected neutrons as function of scattering angle and time-of-flight for a thermal powder diffractometer. Bragg's law ($\lambda = 2d\sin\theta$) manifests itself in the shape of the curves. Each curve corresponds to one value of the lattice plane distance d [280]. Existing analysis tools only use a tiny fraction of the available information.

challenging. In the case of Portland cement concrete – the world's most widely used manufactured material – the internal structure and water content, and their effect on concrete behaviour is only beginning to be understood. Figure 2.55 shows results from grand canonical Monte Carlo simulations of water adsorption in concrete based on molecular models [282]. It is now recognised that water molecules can be adsorbed not only in the interlayer space, but also in small cavities present in the defective structure. This knowledge was crucial for understanding the high mass density measured in complementary small-angle neutron scattering measurements [283].

Inelastic neutron scattering is an example of a technique that can easily be interfaced to computer simulations and applied in a complementary fashion to other spectroscopic probes. This complementarity spans from identifying specific interactions of a hemoprotein involved in carcinogenesis and drug metabolism [284] to the most fundamental understanding of the dynamics of functional groups in pharmaceutical analysis [137], as illustrated in Figure 2.56. In more general terms, the combination of neutron scattering techniques with other techniques, whether computationally or experimentally (e.g. Raman, NMR, or X-ray) is fundamental for interpreting neutron scattering experiments and key to understanding fundamental processes (e.g. in biology) and for developing new advanced functional materials and devices. Providing interfaces for external sources of information to the software suite at ESS will make it easier for users to exploit this information, and will encourage the development of new advanced analysis tools that make possible the use of such external information. An example of such an interdisciplinary analysis tool is the ComQum-X program that makes possible structure refinement of metal-containing enzymes without

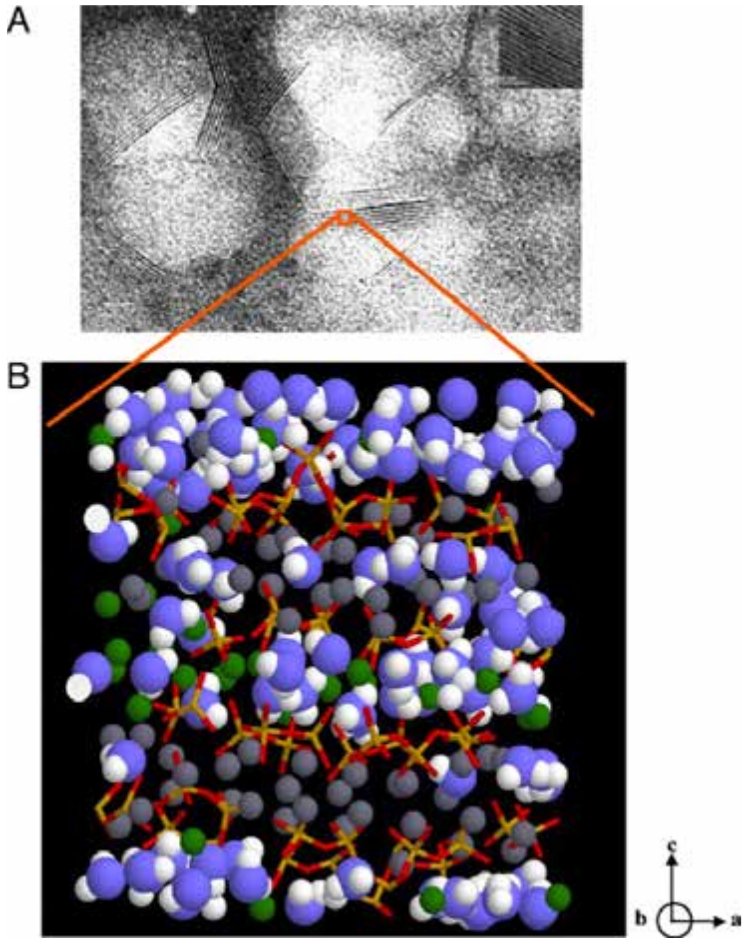

Figure 2.55: Results from grand canonical Monte Carlo simulations of water adsorption in concrete. Top: Transmission electron microscopy image of clusters of C-S-H, tobermorite-14, that occurs in cement paste. Courtesy of A. Baronnet. Bottom: The molecular model of C-S-H [282]. Blue and white spheres are oxygen and hydrogen atoms of water molecules, respectively; the green and grey spheres are inter and intra-layer calcium ions, respectively; yellow and red sticks are silicon and oxygen atoms in silica tetrahedra.

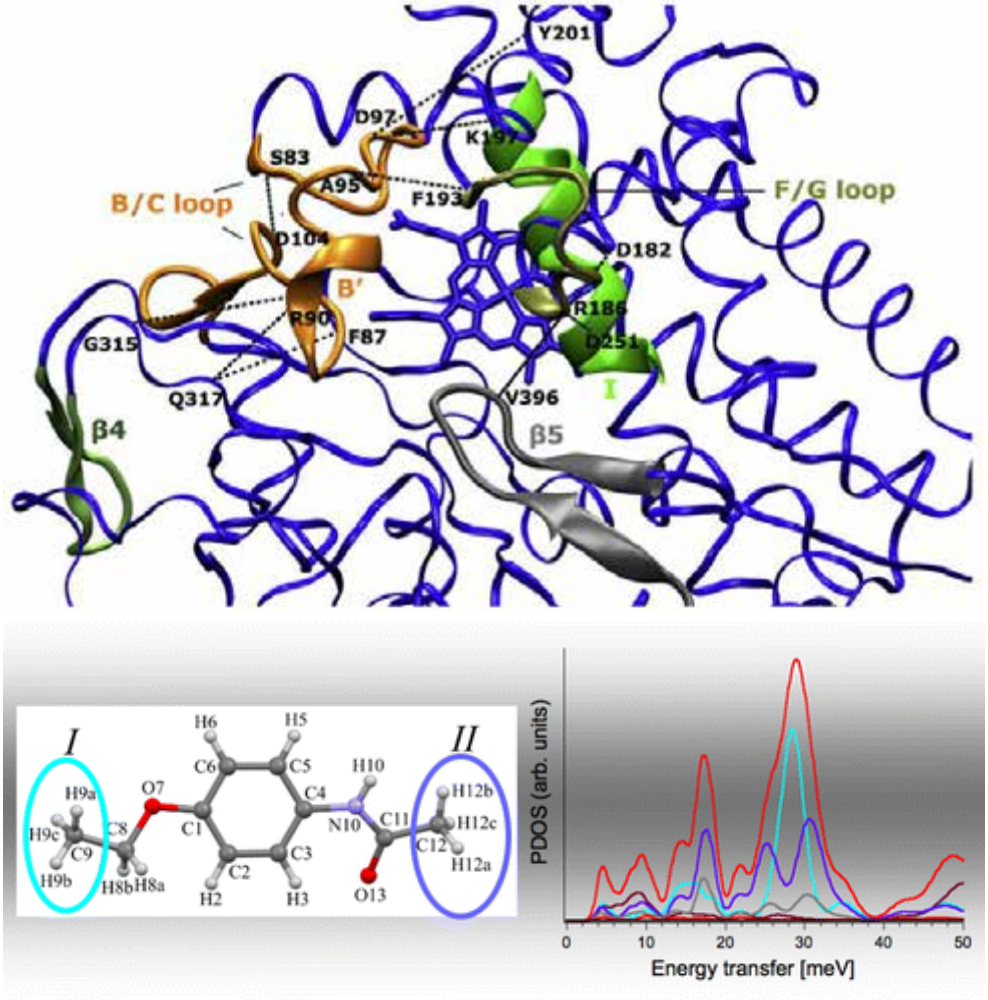

Figure 2.56: Two examples of complementary neutron scattering and scientific computing techniques. Top: Molecular dynamics simulations combined with quasi-elastic neutron scattering and nuclear magnetic resonance imaging, used to study the dynamics of the enzyme cytochrome P450cam at different timescales [284]. Bottom: Inelastic neutron scattering in combination with methods based on density functional theory, used to study the dynamics of the pharmaceutical compound phenacetin [137].

prior knowledge of the metal-bonds by using methods based on density functional theory in combination with X-ray data [285].

Data analysis software options

Virtual instruments may be used to make the data reduction stage an integral part of the data analysis process. When a sample model with a number of free parameters is available, it may be possible to perform the data analysis as an inverse problem in which the free parameters are determined to obtain agreement between the measured and simulated scattering patterns. Solutions for data analysis and visualisation can with advantage be developed in the Mantid framework and as part of the Mantid project or interfaced to Mantid. ESS is expected to host instruments for which there are currently no satisfactory data analysis programs. The strategies chosen by DMSC will provide maximum flexibility for such instruments in the future. Many programs besides Mantid could provide significant leverage when integrated into the software suite, such as GSAS-II for diffraction, PHENIX for macromolecular diffraction [264], StockFit [286, 287] and GenX [288, 289] for reflectometry. Moreover, several existing programs have been, are being, or will be integrated in Mantid [290], such as HORACE [291], TobyFit [292], McPhase [293], and SANSView [294]. The Atomistic Simulation Environment (ASE) [295] can be used with advantage to interface molecular

and materials modelling and simulation programs to the software suite at ESS provided the architecture in Figure 2.50 is used. ASE supports a large selection of "calculators", such as VASP [296, 297] for DFT calculations and LAMPPS for MD simulations [298]. DMSC will work with various existing projects in order to make tools available to the user community and, if necessary, to develop them further. Moreover, a well defined API will make it possible for external software developers to ensure that the software developed by them can work in combination with the software suite at ESS.

Chapter 3

Target Station

Chapter abstract

Summary: The main function of the target station is to convert the high-energy proton beam from the accelerator into low-energy neutron beams with the greatest possible efficiency, safety and reliability. This chapter describes three groups of target station subsystems, and the design characteristics that enable them to deliver this key functionality. The first group consists of the target monolith and the components it houses, including among others the target wheel, the moderator-reflector and the beam extraction systems. The second group is made up of fluid systems. The third group includes the handling and logistics subsystems for radioactive components of the target station operation.

Target monolith and associated subsystems. The first group of subsystems will interact directly with protons and/or neutrons. It includes the proton beam window, the rotating target wheel system, the moderator-reflector assembly and the beam extraction system. The target station safety system is also a crucially important part of this group. The target material (tungsten) will transform high-energy protons to fast neutrons. The moderator-reflector system surrounding the target will transform the fast neutrons into slow neutrons, which will be guided to neutron scattering experimentalists via the beam extraction system. These neutronically active subsystems will be housed in the target monolith, which is composed of 7000 tons of steel shielding. The target monolith is designed to contain the highly-penetrating gamma and fast neutron radiation that will be created by the spallation and radioactive decay processes. The baseline technology chosen for the target is a rotating tungsten wheel cooled by inert helium gas. The surface area of the wheel is large enough that, in the event of a loss of power and/or coolant, passive cooling would prevent unsafe target temperatures with a significant safety margin.

Fluid systems. The second group of subsystems consists of fluid systems, including the closed cooling circuits and the radioactive gaseous effluents and confinement system.

Handing and logistics subsystems. The third group of subsystems includes active cells, casks and remote handling systems. These subsystems transport, exchange, maintain, process, package, store and release the used radioactive components from the target station operation.

Fallback and comparative target technologies. Two other target concepts are explored, in order to provide a complete and robust technical underpinning for the ESS design. A water-cooled rotating tungsten target is the designated back up option, while a lead-bismuth-eutectic (LBE) target is used as a comparative option, primarily to assess environmental impact.

Target station interfaces with the rest of the facility are complex. Chapters 5, 8 and 9 detail ESS integration strategies.

Target design support. Advanced multi-physics simulations of target subsystem components are used in an iterative fashion, to optimise neutron beam performance, to address issues of technical realisation and operation, and to ensure a robust and cost-effective design. A database of the characteristics of the irradiated and un-irradiated materials used in the target system provides a crucial underpinning for the engineering design of target system components.

3.1 General description

3.1.1 Summary of basic requirements and design choices

The function of the target station is to convert the intense proton beam from the accelerator into a number of intense neutron beams. This conversion is achieved by the interplay of a number of basic functions. The heavy metal target absorbs the impinging proton beam radiation from the accelerator and transforms it via the spallation process into fast neutrons as the useful product, while generating a large amount of heat, radioactive isotopes and prompt radiation as unavoidable by-products. The moderator-reflector assembly surrounding the target transforms the fast neutrons emitted by the target into slow neutrons, which are the final form of useful radiation provided by the neutron source, while further radioactive waste is produced by the absorption of neutrons by various target structures. (Here, "fast" means neutrons with velocities in the range of 10% of the velocity of light and "slow" means velocities comparable to the speed of sound.) These two neutronically active systems are surrounded by a radiation shielding system of approximately 7000 tons of steel, in order to contain the extreme level of highly penetrating gamma and fast neutron radiation created in the target and its vicinity. The beam extraction system provides intense slow neutron beams through beam guides which traverse the target shielding. These neutron beam guides are accessible at the surface of the shielding, for delivery to and use at the neutron-scattering instruments facing the beam ports at variable distances. The proton beam window separates the high vacuum in the accelerator from the atmospheric-pressure inert helium gas inside a large container vessel, in which all of these systems are housed. They form, together with the tight container, the target monolith, which takes the shape of a 12 m diameter and 10 m high cylinder.

At ESS, the proton beam will deliver 5 MW power in the form of kinetic energy. About 10% of this energy is converted to mass through the nuclear reactions in the spallation process that produces neutrons, other nuclear fragments, isotopes and gamma radiation. The kinetic energy of these particles makes up the remaining 90% of the proton beam energy, and it is almost all deposited within a distance of 1 m from the site of proton beam impact in the target. Different cooling circuits in the target monolith remove this large amount of heat from the target itself (3 MW), from the moderator-reflector assembly (1.2 MW) and from the monolith shielding (0.3 MW). The proton beam window is directly heated by the traversing beam and requires cooling of about 6 kW, though this value is strongly dependent on window design details.

Radiation damage and fatigue limit the lifetime of the three most strongly affected systems: the target, the reflector-moderator assembly and the proton beam window. All of these systems will need to be changed multiple times during the lifetime of the facility, with frequencies ranging between 6 months and 5 years, as conservatively estimated on the basis of available experience at spallation sources. The removed used components represent a considerable amount of radioactive waste. The other part of the radioactive waste consists of gases, volatiles and airborne particles, which will be continuously captured by a variety of efficient filters and traps. (See Chapter 10 for further discussion of emission and waste control, management and disposal.)

These functional properties determine the basic requirements that the target station must fulfil:

1. Maximising the neutron yield from the moderators for a given proton beam energy requires keeping the volume of the target on which the proton beam impinges as small as possible, using a target material of high atomic number and high density. At ESS, the effective proton beam cross section on the target will be 100 cm^2, and tungsten has been selected as the affordable, high-density target material. Tungsten is one of the most commonly used and well-established choices at existing spallation sources, albeit of much lower power level than ESS.

2. The optimal design of the moderator-reflector system is the other requirement for providing maximal neutron beam performance. For this purpose, the ESS target station will be built with two state-of-the-art, liquid-hydrogen cold neutron moderators, partially surrounded by a water premoderator and beryllium reflector. For each beamline, provision will be made for extracting both cold and thermal beams within the same neutron guide when appropriate, with the help of the bispectral beam extraction concept successfully developed and implemented at HZB. The moderator-reflector design concept allows for the regular implementation of future technical improvements during the lifespan of the facility, whenever the used reflector-moderator system is exchanged for a new one.

3. The viewed, neutron-beam emitting surfaces of the moderators need to be well coupled to the supermirror-based neutron optical beam extraction systems, both for conventional and bispectral

neutron beam guides. Carefully balancing the need to make room for beam extraction openings against the need to maximise the reflector volume is necessary to achieve the best moderator brightness possible.

4. Providing adequate cooling for the target at the 5 MW power level of ESS requires distributing the heat over a much larger volume than the few litres instantaneously irradiated by the proton beam. This can be achieved by a rotating target, with a total active volume much larger than the one momentarily irradiated by each proton beam pulse. The same goal has been attained by other existing modern high-power spallation sources by using circulating liquid mercury as the target material.

5. Cost efficient operation requires a reasonable target lifetime. The principle of a rotating target also dilutes the radiation damage to the materials constituting the target and provides for an adequately long target lifetime of as much as 5 years, estimated on the basis of existing experience with spallation targets built and operated to date.

6. The radioactivity created in the spallation process must be safely contained both in normal operation and in case of accidents, in order to avoid harm to inhabitants living around the facility, personnel and the environment. The radioactivity of the irradiated target material leads to the phenomenon of afterheat, that is, to the development of heat over an extended period of time in the used target even when the proton beam is switched off. Overheating could lead to the escape of radioactivity, so a key safety requirement is to secure a fully fail-safe mechanism for removing the afterheat in the case of loss of cooling, for example in the case of a loss of electric power.

7. The exchange of used, highly radioactive system components requires careful design, planning and extensive auxiliary equipment for protecting workers and the environment in all phases along the path from removal from the monolith through handling, storage, preparation for transport to the disposal site, transport and disposal.

8. The presence of a considerable radioactive inventory inside the monolith and also in the temporary storage on-site requires extensive safety systems for controlling and mitigating the consequences of both operational accidents and the impact of external natural or man-made disasters (earthquake, airplane crash, etc.).

Fulfilling all of these requirements is crucial for the safety of ESS operation, and it has significant implications for the construction and operating costs of the target station and for its performance in delivery of high intensity neutron beams. Optimisation of the cost-to-benefit ratio is an important design goal, which very strongly impacts the total value delivered by the whole facility. In particular, the target station accounts for only about 9% of the total ESS investment, which implies a high leverage in the impact of investments in target performance on the performance of ESS as a whole. For example, a 10% variation in neutron production efficiency of the target would be equivalent for facility output to a variation in similar proportion of the accelerator power, a parameter with very substantial consequences for the total project costs.

Target baseline and options

A helium-gas cooled rotating tungsten target of 2.5 m diameter has been selected as the baseline and a water-cooled rotating tungsten target of the same dimensions as the back-up option. A lead-bismuth eutectic liquid metal target has also been studied as a comparative option for environmental safety assessment. The baseline option offers the highest neutronic performance and the lowest inherent environmental safety risks and mitigation costs for ESS, which will be a spallation source operating at an unprecedented power level. The choice of the target wheel diameter assures distribution of the total heat deposition, activation and afterheat over 33 target sectors forming the circumference of the target wheel, with each sector receiving 1 in every 33 proton beam pulses. The surface area of the target wheel will be large enough that passive cooling by radiation and heat conductivity of stagnant helium gas will preclude dangerous overheating of the target in the case of accidental loss of active cooling, for example, due to loss of electric power. Helium gas cooling has been developed and extensively tested as an option for nuclear power plants

and it is being developed in fusion research for cooling tungsten diverters at much higher power levels than ESS.

The water-cooled rotating target back-up option is intended to occupy the same space as the baseline target. It would require the use of heavy water coolant to match the neutronic performance of the helium-cooled version. This reliance on heavy water, coupled with the inevitable protective enclosure of the tungsten target material against the corrosive water environment if tantalum (the most common choice) is used for the protective enclosure, result in higher radioactive inventory and significantly higher afterheat. The presence of water vapour makes the target more vulnerable to overheating due to the onset of target vapourisation at about 700°C by exothermic water reduction reaction. Similar behaviour of zircaloy is a well-known issue in nuclear safety

A liquid metal target is the alternative solution to a rotating wheel for the dilution of the heat deposition and afterheat. In studying liquid metal designs, mercury has not been considered for ESS due to the absence of an established and approved disposal technology for this material after irradiation. The development of such a technology would require too much time to be feasible and its costs could very well prove to be comparable to a large fraction of the construction cost of the entire target station. In contrast, lead-bismuth eutectic is solid at room temperature and is acceptable for irradiated waste disposal. From an environmental point of view, however, its operation creates higher radioactive inventory and involves higher risk of the escape of volatile radioactivity in case of accidental overheating than the rotating tungsten target. It also has different spatial requirements compared to the rotating tungsten target baseline. For these reasons, it was not selected as the preferred back-up option.

Neutron beamlines

The traditional layout scheme of beamlines at pulsed spallation sources is a relatively uniform, predetermined distribution around the target station covering between 110 degrees and 120 degrees of beam extraction sector on each side of the target monolith, with respect to the proton beam direction. However, the intensity of the neutron beams can be enhanced by reducing the accumulated angle of the beam extraction sectors, that is by minimising the associated removal of reflector material around the moderators. For a given number of beamlines, this implies grouping them in bundles as close to each other as possible. For this reason, about 1.5 degrees of separation is the general practice for beamlines using neutron guides at continuous neutron sources. Target engineering studies have shown that 5 degrees minimum angular separation is feasible for ESS, although it might be too small for a number of short instruments.

Creating a 5 degree grid of possible beam port positions in the target monolith design offers the possibility to flexibly group the beamlines in beam extraction sectors with minimal angular width during the full life-cycle of the facility, as the detailed requirements of early and later instrument suites take shape. For instruments that need more lateral space (primarily short instruments), 10 degrees or 15 degrees of separation with respect to neighbouring beam lines can be selected. For example, of the 22 instruments in the ESS reference suite presented in Chapter 2, 60% are longer instruments with 5 degree beam separations and the rest are shorter instruments requiring 10 degree separations. In this arrangement, the neutron beam intensity will be 15% to 18% higher than it would be using the common approach of predetermined beam positions spread more widely around the monolith.

An additional important feature of beam extraction at ESS is that every beamline will have the option either to use both cold and thermal neutrons by bispectral beam extraction, or to extract only one of these spectra. Experience with the prototype bispectral beam system built at the BER-II reactor in Berlin shows that the unmodified beryllium reflector around the cryogenic liquid hydrogen moderator is by itself a good source of thermal neutrons. Neutronics studies by ESS and collaboration partners demonstrated better thermal neutron performance by using extended viewable surfaces of the water premoderator next to the hydrogen moderators.

The target design choices presented here represent an advanced, but not yet final stage of optimisation. Meeting the April 2019 project milestone to start commissioning the target station with neutron beam production requires that the design be finalised and frozen by the third quarter in 2014. The time until this date will be used to fine-tune, further optimise and demonstrate the engineering design of the target station.

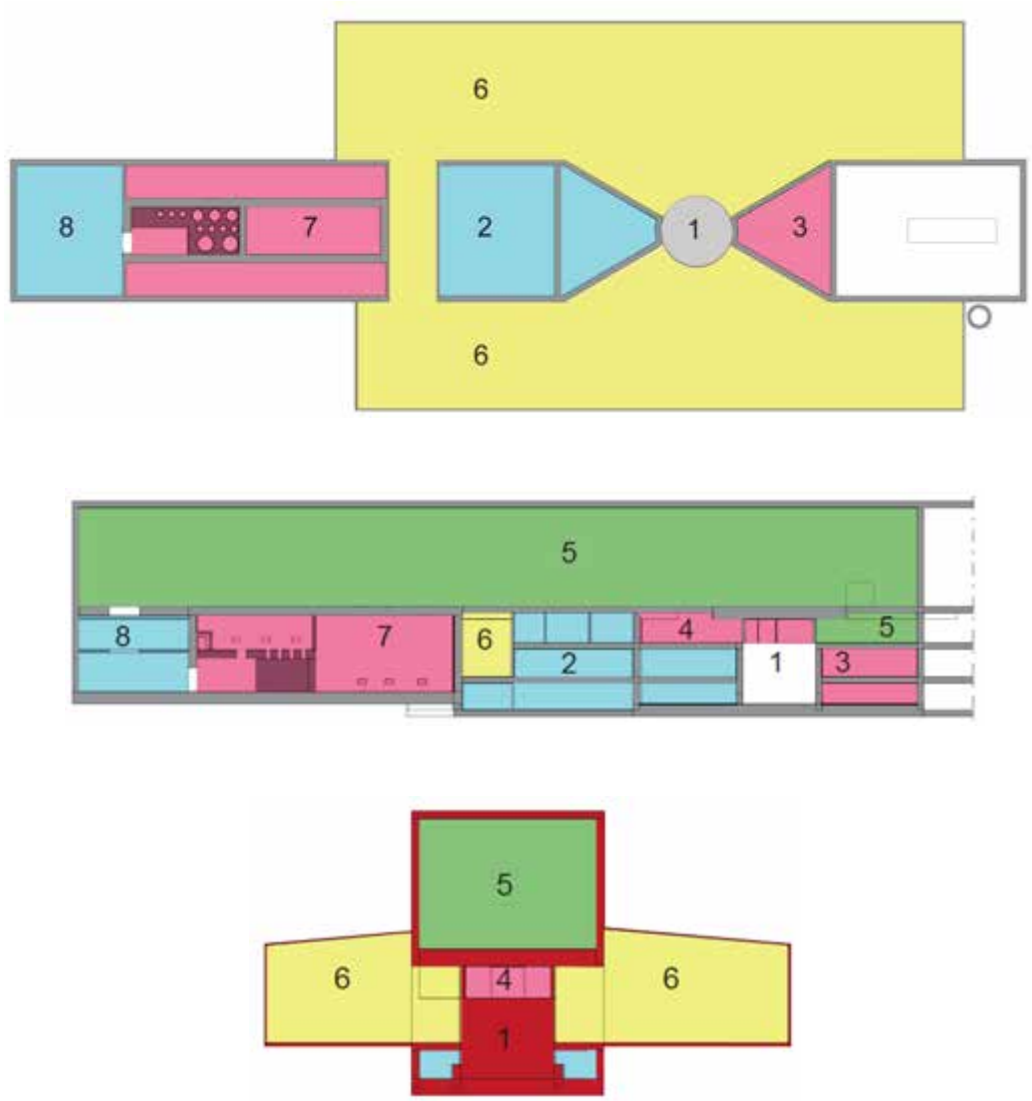

Figure 3.1: Target station building. Top: Plan view at the proton beam elevation. Middle: Side view along the proton beam. Bottom: Side view facing upstream.

3.1.2 Target station layout

The target station (TS) building is divided into several building parts, with different operational functions and different requirements for confinement and shielding in terms of user access during operation and maintenance. Figure 3.1 illustrates the building part-numbering convention. The **monolith** (part 1) contains mainly the target, the moderators and the shielding. The **utility rooms** (part 2) house different target systems connected to the monolith, including the helium cells, the utility cells and the target basement. The **accelerator-to-target (A2T)** section (part 3) is the interface between the accelerator and the target station. The **connection cells** (part 4) are located on top of the monolith, where circuits penetrate into it. These target station building parts 1 to 4 mainly house the target station systems related to the proton beam and the neutron beams. Two additional parts, the **active cells** (part 7), which are used to process radioactive components, and the **transport hall** (part 8) for the external shipment and reception of large components, are connected to the beams-related systems by the **high bay** (part 5), which permits all transfers and movements of components. Figure 3.2 gives an overview of the target station building. The two **experimental halls** (part 6) around the monolith house the short instruments and the neutron guides serving long instruments (located in other buildings), and are connected by a

Figure 3.2: Perspective view of the target station building through a vertical section.

passage for personnel and components.

The experimental hall constitutes the reference level for the instruments (ground floor), around which the other main levels are positioned. Tables 3.1 and 3.2 summarise the dimensions, relative heights and absolute altitudes of the main TS parts and levels. The proton beam level is 1.8 m above the ground floor. The two reference levels for the neutron beam guides are located approximately 0.18 m above and below this proton beam level, facing respectively the top and bottom moderators.

The **A2T** section (TS building part 3) hosts the tune-up dump in the lower room, which is used to tune the linac when the proton beam is not being sent to the target wheel. The lower room is located on the same level as the accelerator tunnel. In the upper room, the A2T hosts the last collimator before the high-β protons pass the opening of the confinement valve of the target monolith. This A2T confinement valve forms a part of the second barrier for the primary radioactive inventory, which is an extension of the monolith liner. Table 3.3 gives barrier definitions. The proton beam tube connects the A2T confinement valve to the proton beam window. During shutdown periods, if activated components (the collimator, the tune up dump, the proton beam tube, the A2T confinement valve, etc.) need to be replaced, their handling will be carried out towards the high bay, for a final transfer to the active cells. A cask will be used for handling if the level of remaining activation makes this necessary. For this reason, the above-mentioned A2T components are designed for remote handling. These systems are shielded below and laterally by steel blocks, and by the concrete structural walls and floors of the A2T itself. The upper shielding is composed of removable parts, and is accessible from the high bay. Specific shielded plugs are foreseen for the A2T confinement valve and proton beam diagnostic systems, which are located downstream of the collimator. These components are designed to allow their exchange during normal maintenance periods.

Parameter	**Dimension** [m]
Total building length	133
Internal building width	22
Monolith external diameter	12
Length from monolith centre to upstream building end	18
Length from monolith centre to downstream building end	115
Total length of the connection cells	24
Total length of the helium cells	30
Total length of the active cells	45
Total length of the transport hall	18
Floor slab and wall thickness (current zones)	1.0
Free space above the experimental hall floor (near monolith)	9.5

Table 3.1: Main target station building dimensions.

Target station rooms and floors	Relative height [m]	Altitude [m]
Utility rooms (basement)	−5.50	73.1
Tune-up dump room	−3.80	74.8
Active cells and transport hall	−3.50	75.1
Experimental halls, collimator room, utility rooms	0.00	78.6
Connection cells	5.50	84.1
High bay	11.50	90.1
Crane hook maximum height	24.00	102.6

Table 3.2: Target station room and floor heights and altitudes.

The **monolith** (TS building part 1) is a cylinder made of steel and reinforced concrete, housing the irradiated components during ESS operation, as described in Section 3.3. The steel monolith is encapsulated in a steel liner that isolates the steel shielding from the concrete to assure high quality helium throughout the lifetime of the target station and contains radioactive isotopes inside the monolith in normal and accidental situations. This steel shielding and the reinforced concrete volume inside the monolith are structurally connected. This structural block is anchored both in the supporting slab and in the V-shaped walls of the A2T (upstream of the monolith) and of the utility rooms (downstream of the monolith). The V-shaped walls for the A2T and the utility rooms are symmetrically laid out around the proton beam axis, to allow a flexible distribution of 22 neutron beam guides of the construction phase, among the 48 potential neutron beam ports. From a structural viewpoint, the monolith's structures are not connected to the connection cells that are located above it. This assures the stability of the monolith during normal and accidental situations, including aeroplane crash and earthquake.

The **connection cells** (TS building part 4) are located just above the monolith, as shown in Figures 3.1 and 3.3. This is the location in which the permanent circuits are connected to the vertical plugs in the monolith. The functions of the connection cells include confinement, since the cells serve as part of the second confinement barrier, and separation of hazards related to the target station circuits, such as tritium, cryogenics, hydrogen explosion, et cetera. The connection cell walls include a network of horizontal structural beams between the connection cell floor level and the high bay slab level. This entire structure, composed of structural beams, connection cell floors and the high bay slab, is connected to the two V-shaped structural walls.

The **utility rooms** (TS building part 2) are located downstream of the monolith and connection cells, as shown in Figures 3.1 and 3.3. They contain, from the top to the bottom levels, the helium cells, the utility cells and the target basement. The helium cells contain the helium circuits and associated systems, such as the pressure control system (PCS), and the purification and filtering systems, as discussed in Section 3.4.1. The utility cells host permanent circuits connected to the monolith, the intermediate cooling circuits and their interfaces with conventional facilities (mainly external cooling systems). The target basement houses

Inventory type	Barrier number	During powered operation	During maintenance
Primary	1	Target cooling helium circuit	Connection cells, monolith & target cask
	2	Monolith liner & connection cells	High bay
	3	High bay	
Secondary	1	Monolith liner & circuits in utilities block	Connection cells, monolith, utility rooms & casks
	2	Utility rooms	High bay
	3	High bay	
Tertiary	1	Containing circuits, casks	Containing circuits, casks
	2	High bay, utility rooms	High bay, utility rooms

Table 3.3: Confinement barrier definitions for primary, secondary and tertiary inventories.

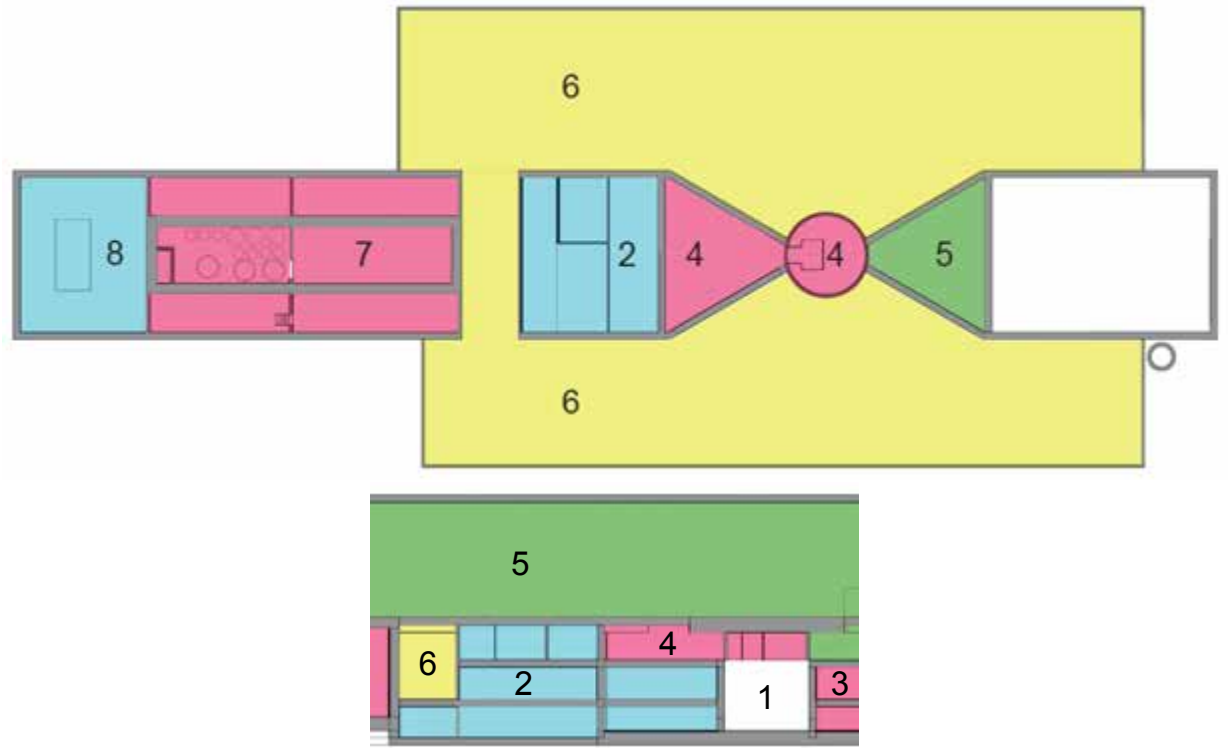

Figure 3.3: Target station utility rooms. Top: Plan view of the target station building at the utility room level. Bottom: Side view of the utility rooms, showing the helium cells in green.

additional contaminated systems such as fluid storage systems and is a prolongation of the utility cells. It extends around the monolith and houses the monolith atmosphere system, the contaminated liquid effluent storage and over tanks, and some penetrations in the target station building for the ancillaries provided by the conventional facilities.

The **high bay** (TS building part 5) spans the A2T, the connection cells and utility rooms, the passage between the two experimental halls, the active cells and the transport hall. The transfer of components from the ground floor is possible. Irradiated components such as internal neutron beam guides and internal supports are mainly transported through the hatches in the high bay slab from the passage joining the two experimental halls, and the non-irradiated components are mainly transported through those from the transport hall. The high bay contains safety-classified ancillary systems and facilities (radioactive gaseous effluents and confinement (RGEC) systems, temporary storage area for irradiated components, etc.), non safety-classified ancillary systems and facilities (external cooling water; heat, ventilation and air conditioning (HVAC) system for the TS building; temporary storage zone for non irradiated components), handling systems (casks, mock-up area for plugs, casks and tooling) and some penetrations in the target station building for the ancillaries provided by the conventional facilities. The high bay floor is flat, so all transfers of heavy components can be made either by the high bay crane at a minimised height above the high bay floor or by rolling devices and casks, in order to avoid major structural damages in case of load fall. Several penetrations are available in the high bay for transferring components to and from the active cells (process cell, maintenance cell and storage pits), by connecting internal shielding casks to lids and sliding doors. A large opening is available above the transport hall to deliver large spare components in the high bay for temporary storage, until they are installed during maintenance periods, as shown in Figure 3.3. A pit in the high bay, located upstream of the monolith and at the level of the connection cells, houses the hydrogen systems for the cold moderators.

The functions and characteristics of the **active cells** (TS building part 7) are described in Section 3.5. Access to the neutron beam windows (part of the monolith liner, the second confinement barrier), internal inserts and neutron guides is only possible from the **experimental halls** (TS building part 6). The exchange and maintenance of these internal structures in the monolith are performed during proton beam

Location	During powered operation		During maintenance	
	Gas	Pressure [kPa]	Gas	Pressure [kPa]
Target system	Helium	200	Air or helium	−0.20
Monolith	Helium	−0.30	Air	−0.06
Connection cells	Air	−0.30	Air	−0.06
Helium cells	Air	−0.30	Air	−0.06
Utility rooms	Air	−0.12	Air	−0.06
High bay	Air	−0.06	Air	−0.06
Accelerator-to-target	Air	−0.12	Air	−0.06
Experimental halls	Air	−0.12	Air	0

Table 3.4: Pressure cascade values in different zones of the target station building during powered operation and during maintenance, relative to atmospheric pressure.

shutdown periods. When the neutron beam windows are open during the maintenance period, access to the area within a 6 m radial distance from the monolith surface will be subject to the same protective measures as access in the immediate monolith area in the absence of the confinement barrier, as shown in Figure 3.63 and as discussed in Sections 3.3.9 and 3.5.2. The junctions between the additional shielding blocks surrounding the external neutron guides and other components on the experimental lines are specifically designed to avoid any aggression of the shielding blocks on the second confinement barrier (steel liner and neutron beam windows) during an accidental scenario, such as an earthquake, aeroplane crash or shielding block handling accident.

Confinement barrier concept

The confinement barrier concept addresses the risk of dissemination of radioactive contaminants. It considers the different radioactive inventories present in the target station building and their capacity to disseminate in the environment (with different transfer factors for noble gases, volatiles and other elements). For each inventory, this chapter discusses a life-cycle approach for the operation and maintenance phases. The decommissioning phase is treated in Chapter 10. The radioactive inventories are classified into three types. The freshly irradiated spallation target wheel and spallation products are classified as the primary inventory. The other radioactive isotopes in the monolith (and those transported from it by the fluid circuits that traverse it) are classified as the secondary inventory, and the additional minor radioactive inventories that are not connected to the monolith (radioactive liquid effluents, empty transfer casks, etc.) are classified as the tertiary inventory. As these inventories are naturally decreasing with time, they are progressively declassified from one inventory to another during the decay process. As a result, the spallation target material is declassified from the primary to the secondary inventory after a few weeks of decay time. The target station confinement barriers are defined in Table 3.3 [299]. Confinement is assured preferentially by a static confinement or by a pressure cascade maintained dynamically with the radioactive gaseous effluents and confinement (RGEC) systems. Table 3.4 presents the pressure cascade during

Location	Air pressure [kPa]
Process cell	−0.23
Maintenance cell	−0.20
Storage pits	−0.20
Transfer zone	−0.10
Technical galleries	−0.10
Transport hall	−0.06

Table 3.5: Air pressure cascade values in the active cell rooms and in the transfer hall during normal operation, relative to atmospheric pressure.

power operation of the neutron source and during its maintenance. For the active cells during normal cells operation, the first confinement barrier is the active cells' external wall and penetrations, and the second confinement barrier is the high bay. The pressure cascade in active cell rooms and in the transfer hall are presented in Table 3.5.

Shielding concept

The shielding concept addresses the risk of direct radiation exposure to prompt radiation from the interaction of the proton beam with matter, and to decay radiation from radioactive inventories. The shielding concept also addresses contamination transfer issues. It considers the different radioactive inventories present in the target station building and their capacity to irradiate personnel in the vicinity. For each inventory, a life-cycle approach is developed for operation and maintenance phases. During beam operation, the necessary shielding is provided by the monolith structures, the connection cell walls, the high bay floor, the A2T shielding and the utility rooms. The monolith, the connection cells and some cells in the utility rooms (those housing filters or water with ^{16}N, for example) are off limits for personnel during beam operation and the decay time immediately following it. The slab above the connection cells (22 m $\times$ 22 m) is up to 2 m thick, as shown in Figure 3.3. Additional movable shielding blocks are necessary around the monolith, up to an height of 6 m above the ground floor. During maintenance phases, some shielding only required during beam operation can be removed to maintain or exchange irradiated components. Both adapted shielding structures and remote handling procedures are implemented to minimise the radiological impact on workers during these phases. The shielding concept during beam operation is described in more details in Section 3.3 [300], and the one related to the transfer casks and the active cells is presented in Section 3.5.

Zoning concept

ESS has developed an internal system to zone different areas of the facility in terms of required safety measures. The zoning concept mainly addresses those risks associated with non-radioactive inventory (conventional risks) that have a potential impact on radioactive safety functions. A specific radioactive risk addressed by the zoning concept in the target station building is the risk due to tritium. Although all kinds of conventional risks are potentially concerned, the non-conventional hazards present for the target station are hydrogen explosion, fire and usage of beryllium.

3.1.3 Quality assurance and risk analysis

Quality assurance

Quality assurance for the target station (TS) from the standpoint of nuclear safety is considered in this section. Broader issues of ESS quality management and quality assurance are addressed in Section 8.2. Nuclear safety quality assurance (QA) will be applied to activities related to systems and subsystems that are safety-classified and which can have an impact on nuclear safety, and to activities related to these systems and subsystems. The list of systems and subsystems of concern for nuclear safety QA is defined in the preliminary safety analysis report and safety analysis report. (See Chapter 11 for further discussion of these safety reports.) These are the systems participating in the radioactive confinement functions (first, second and third confinement barriers), including the normal release of radioactive gaseous effluents; the systems participating in evacuation of radioactive effluents (liquid and gaseous) and wastes (solid) outside the target station building; the systems participating in radioactive shielding functions; the systems participating in the shutdown of the proton beam, when this shutdown is required to avoid confinement system damages; and the systems participating in monitoring of the previous systems.

Quality assurance activities are defined in the ESS quality management plan [301]. For the target station, these activities include design, production, testing and storage of QA-related systems and their components; operation and maintenance of QA-related systems (including periodic tests); characterisation and analysis of radioactive inventories and releases; monitoring of QA-related systems; training and qualification for personnel, acceptance and processing of non-conforming situations; and review and feedback for TS processes and its QA-related systems documentation (listing all activities above). The activities performed by TS personnel or by TS subcontractors without their own QA manual will be subject to the

TS quality management plan. When a TS subcontractor has his own quality management plan, the scope of the QA plan must be dealt with on a case-by-case basis.

Risk analysis

For the construction phase of the ESS target station, the risks from the perspectives of the availability of human and financial resources, technical challenges, regulatory frame such as licensing, political environment and organisational issues have been identified and their potential impact on costs, schedule and performances has been analysed [302]. Having identified these risks, an action plan was developed and risk mitigation strategies have been implemented and reviewed since 2011 [302].

3.1.4 Target station operations and maintenance

This section presents the main characteristics of operating cycles, such as the annual number of days of operation, number of annual restarts and shutdowns, or the number of annual maintenance days, for target station design. Only the nominal situation is defined, based on ESS high-level requirements described in Chapter 1. Operation and maintenance conditions such as load cases drive the thermo-mechanical design of the target station components.

Abnormal situations (incidents and accidents), including beyond-design-basis accident scenarios, are addressed in the conceptual design of the target station, which will be further refined as ESS works with Swedish regulatory authorities on its safety analysis report. Details can be found in Chapter 11. To define the different load cases for the detailed design of the target station, an iterative method is used, starting with different operating modes for the ESS facility and progressively honing in on different target station systems in more and more well-defined modes, as the design options are selected. For the machine as a whole, ESS operating cycles will permute among four modes corresponding to specific needs such as machine development and qualification, power ramp-up, neutron production, cooling time and maintenance, as indicated in Figure 3.4. The four modes are:

1. Production mode, which prevails when the facility is delivering stable beam to its scientific users;
2. Maintenance mode, during which broad access to most systems is permitted for preventive and curative maintenance;
3. Studies mode, during which tests, studies, and activities to develop or qualify the accelerator are performed; and
4. Restart mode, which prevails during the transition from very low power to nominal power.

Target station modes for different classes of target station systems

Target station systems fall into two classes. The *beam class* includes those systems that are directly involved in the production of neutrons, and which become activated as a consequence of that involvement. These encompass all the systems in the monolith, all fluid systems transiting through the monolith, the movable shielding, and all the systems in the A2T area. The *enabling class* includes the TS systems that do not have direct involvement in neutron production, that is, the active cell systems, the radioactive handling systems, the radioactive liquid storage system, the confinement systems and the storage areas. For each of the four ESS modes described above, the beam-class TS systems operate in one of several TS-specific sub-modes:

1. Production mode is associated with several TS stable nominal power modes, each corresponding to a different level of maximal allowable power.
2. Maintenance mode is associated with TS decay mode (for radioactive and thermal decay of components); TS maintenance mode (for component handling and access); and TS conditioning mode (for circuit reconditioning and system preparation to restart).
3. Studies mode is associated either with TS decay, maintenance and condition modes (when the tuning beam dump is being used by the accelerator) or with TS calibration mode (for system requalification) or with TS ramping-up and nominal power modes.

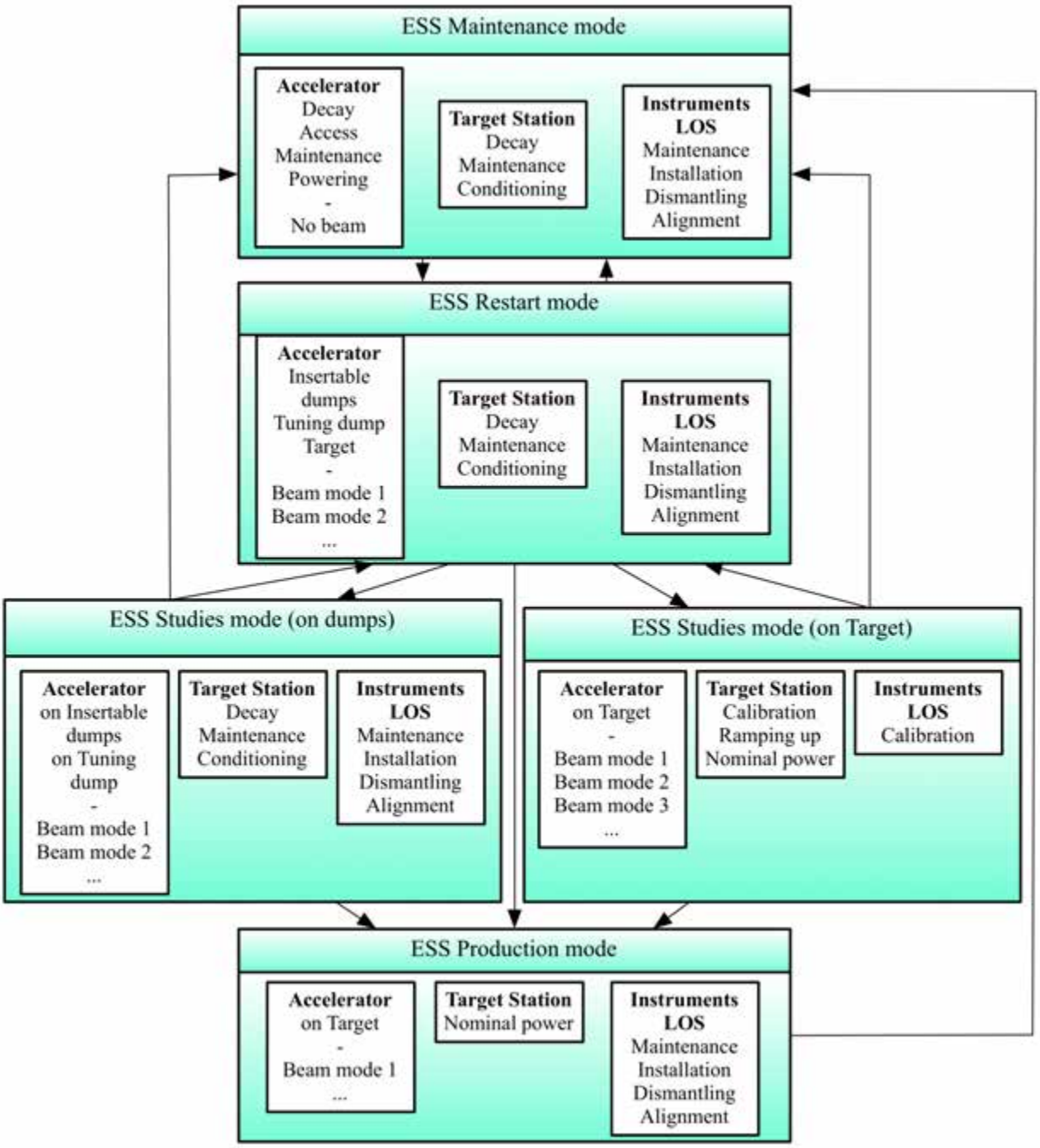

Figure 3.4: State diagram for transitions between ESS modes during normal operations.

4. Restart mode is associated with TS ramping-up mode and TS nominal power mode.

However, enabling-class TS systems have their own specific modes for maintenance, qualification and operation. The three enabling-class modes are requalification, operation and preventive maintenance. The modes for the beam class TS systems are illustrated in Table 3.6. The operational modes of the two classes of TS systems will be different from, but not independent of each other, as systems in the two classes interact with and are constrained by each other. The ways in which the operational modes of the two classes constrain each other can be depicted by a compatibility matrix.

ESS mode	Accelerator mode	Target mode	Instrument mode
Maintenance	Decay Access Maintenance Powering	Decay Maintenance Conditioning	Several
Studies	Insertable dump Tune-up dump	Decay Maintenance Conditioning	Several
	Beam on-target	Calibration Ramping-up Nominal power	Several
Restart	Insertable dump Tune-up dump Beam on-target	Ramping-up Nominal power	Several
Production	Beam on-target	Nominal power	Several

Table 3.6: ESS operational modes and associated accelerator, target station and instrument modes.

Target station systems design assumptions

The target station systems are designed on the basis of a set of assumptions about operation and maintenance conditions, which is presented in Table 3.7, and assumes the reference beam trip rate that is shown in Figure 3.5. The design loads in normal situations for each beam-class TS system can be derived from the appropriate columns of Table 3.7, integrating across operational modes. Pressure loads, static and dynamic loads, thermal loads and fatigue loads are derived from proton beam power. The fatigue cycles are derived from the number of occurrences a year and from proton beam trips, creep analysis duration and irradiation damages duration of occurrence, as shown in Figure 3.6. The enabling-class TS systems are designed taking into account the irradiation characteristics of the beam-class systems, for example, the irradiation time for radioactive inventories, or replacement frequencies from irradiation damages and loads. Enabling-class designs also are informed by the mode compatibility matrix, which imposes constraints on the number and duration of periods available annually to perform necessary TS system maintenance.

ESS mode	Beam power [MW]	Occurrence rate [per year]	Duration [days]	Beam trip rate [× reference]	Down time [days/year]
Maintenance	0	1	64	–	64
		1	10	–	10
		2	3	–	6
(sub-total)		4			80
Studies	0.05	33	1	10	33
		5	3	10	15
(sub-total)		38			48
Restart	< 5.0	21	1/3	2	7
		5	1	2	5
(sub-total)		26			12
Production	5.0	17	12	1	204
		3	7	1	21
(sub-total)		20			225

Table 3.7: Operation and maintenance conditions assumed for the design of target station systems. The reference beam trip rate is shown in Figure 3.5.

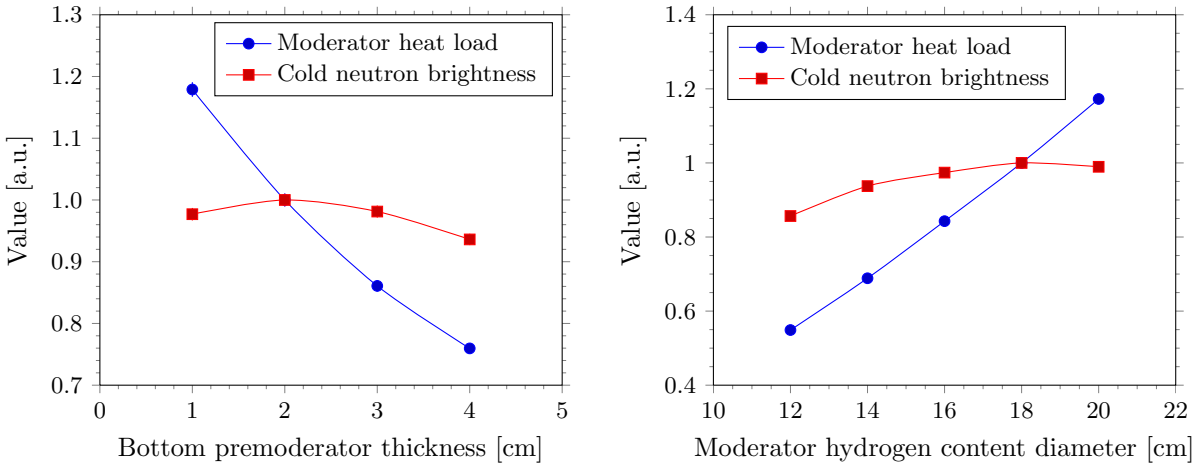

Figure 3.5: Proton beam trip assumptions for beam-class target station systems. The reference rate is for nominal power operation in the production mode.

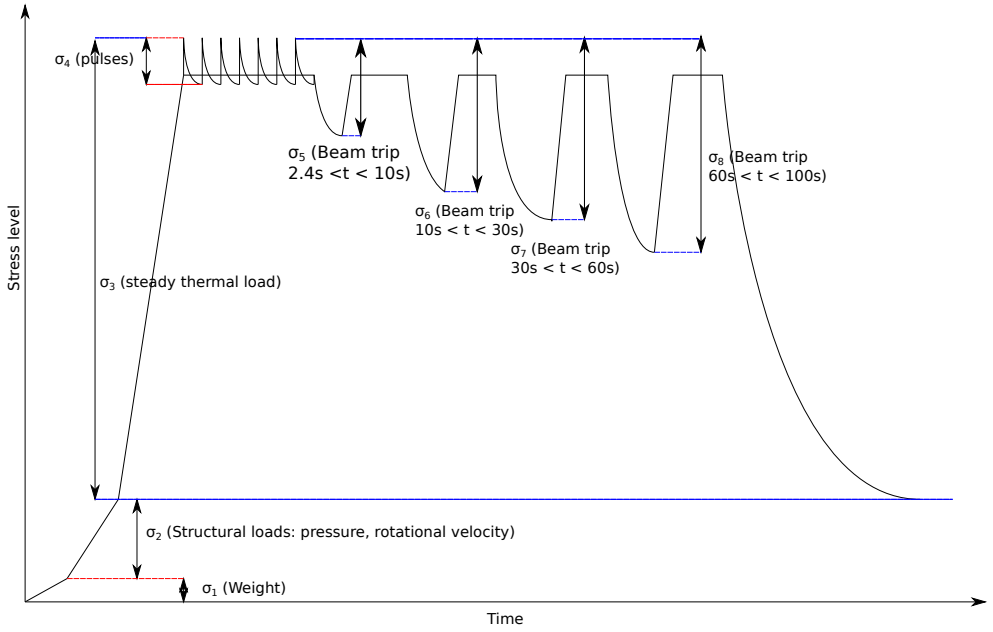

Figure 3.6: Description of the beam trip cycles for the target.

3.1.5 Target station control system

Monitoring and control of the target station systems is performed through the integrated control system (ICS) and a consistent set of three safety systems. The target control system is a part of the ICS, which is a non-safety class system that provides normal controls, regulation functions, settings archiving and data logging functions for the target station.

The first safety system, the **machine protection system (MPS)**, protects equipment against damage due to beam losses and malfunctioning equipment components. The MPS is classified as non-safety; however the MPS contributes to overall safety by triggering alarms and actions (e.g. performing an emergency shutdown of the machine and beams) when safety classified functions operated by target station systems are detected operating outside permitted ranges. The MPS will then act as a preventative system before the target safety system operates. MPS will be a very fast, reliable and fail-safe system, based on hardware and software described in Sections 5.2.2 and 5.2.3.

The second safety system is the **target safety system (TSS)**, which is subject to the highest relia-

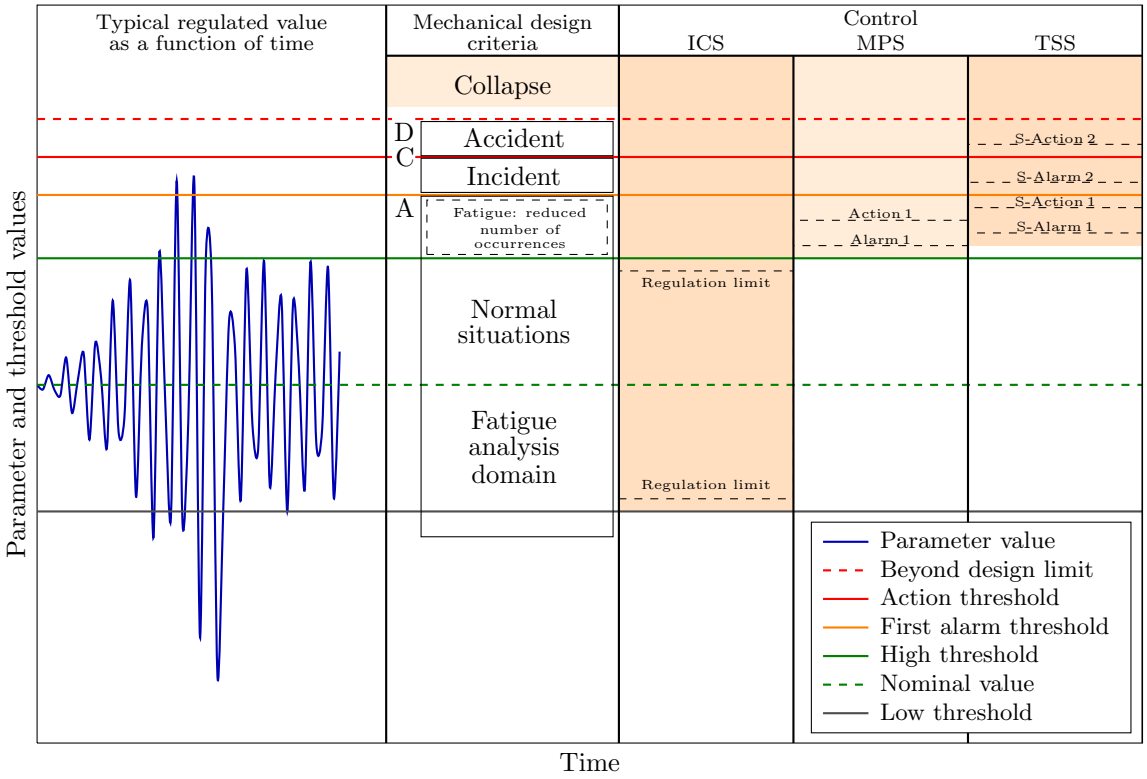

Figure 3.7: Relationship between ICS thresholds, mechanical design values and operating domains.

bility demands in ESS safety operation, as illustrated in Figure 5.4. The TSS guarantees that the target station operates within the design domain. If an abnormal situation occurs, the TSS triggers and controls mitigation functions in both internal and external associated target station systems. The main external trigger signal is to shutdown the proton beam. From an operational point of view, TSS is also a back up for MPS for the target station. However, in that case, there is no guarantee the systems will be kept in the normal operation domain, so the restart of the facility is not optimised. The TSS is essentially dedicated to the nuclear safety functions of protecting workers and the public from exposure to unsafe levels of radiation, and preventing the release of radioactive material beyond permissible limits. The TSS will be installed based on hardware or a highly reliable software system. Figure 3.7 illustrates control hierarchy for these first three control systems.

The third safety system is the **personnel protection system (PPS)**, which is largely dedicated to the nuclear safety function of protecting personnel against irradiation when the transfer of contamination is not an issue. The PPS also protects operators from non-radiological hazards, but these functions are not addressed in this chapter. The PPS stops the proton beam when openings are made in the shielding barrier, by monitoring the doors and locks, and by assuring they are closed during operational states. PPS manages the entrance and egress from radiation-controlled areas according to a pre-defined classification. The target station PPS branch is a part of the global PPS system for ESS, as discussed in Section 5.2.4.

Target station system operating domains, associated actions and mechanical design criteria

The evolution of parameter measurements during operation will be continuously monitored by the control system, which will assure that target station systems operate within their design values. In normal situations, the values of operating parameters will be kept within their normal operating range by the non safety classified control system, ICS. A value evolving outside this normal operating range will trigger the MPS to take precautionary measures to prevent an incidental situation. As long as it is possible to rely on MPS to take protective actions, the target station will avoid a situation in which safety concerns might delay restart of the facility. Should MPS fail to act, TSS will take independent action, for example, by shutting down the accelerator, when its operating parameters cross specified thresholds. Crossing a

first threshold will trigger S_Alarm1 and S_Action1, and crossing a second threshold will trigger S_Alarm2 and S_Action2. The TSS serves as a failsafe mechanism to keep the systems within the design domain in both incidental and accidental situations. For that reason, triggering TSS actions could lead to delays in restarting the plant. The principles illustrating the relative threshold values for an ICS, MPS and TSS operating parameter are depicted in Figure 3.7.

Target safety system principles

The role of the target safety system is to bring the target station into a safe state in case of an abnormal event from a nuclear safety point of view, in order to reduce the risk of harm to people, equipment and environment. This will be accomplished through the emergency shutdown of the proton beam and actions on the target internal isolation barriers. Potential abnormal events are listed in the risk analysis report for the target station [302]. ESS risk analysis documents define a *top event* as an undesired event that poses a risk to people or to the environment. An *initiating event* is defined as any event or circumstance that heralds the occurrence of a top event. A top event may have one or many initiating events, and an initiating event may have the potential to trigger a top event on its own or in combination with other initiating events. The *consequence* is defined as the impact of a top event on people or the environment. Although TSS risk analysis focuses on abnormal events, ESS will also conduct risk analysis for the other operating modes of the target station, such as maintenance. In addition to the risk analysis, functional analysis is underway to detail activity flow in different operational modes for each target system, defining instrumentation; regulation process under normal conditions; and alarms, interlock and activities to be undertaken following an initiating event in order to move the target station to a safe state in a controlled way. An important issue in design and implementation of the TSS is licensing. ESS is a non-nuclear facility. However, many parts of TSS have to be licensed by the Swedish radiation safety authority (SSM), as discussed in Chapters 10 and 11. Standard guidelines will be used for both software and hardware implementation. International Electrotechnical Commission (IEC) standards potentially applicable to TSS development are listed in Table 3.8.

Safety standard	NPP related	Description
IEC 61226	Yes	Instrumentation and control systems important to safety: This standard is used to assign the instrument and control functions of a nuclear power plant to one of three categories.
IEC 61513	Yes	Instrumentation and control important to safety: This standard provides requirements and recommendations for the instrumentation and control of systems important to the safety of nuclear power plants.
IEC 61511	No	Functional safety: Safety instrumented systems for the process industry sector.
IEC 61508	No	Functional safety of electrical/electronic/programmable electronic (E/E/PE) safety-related systems.
IEC 60880	Yes	Instrumentation and control systems important to safety: This standard serves as a reference for IEC 61513, which deals with the system aspects of high integrity computer-based I&C used in safety systems of nuclear power plants.
IEC 60709	Yes	Instrumentation and control systems important to safety: Separation. This standard defines the technical requirements to be met for I&C systems and their cables, in order to achieve adequate physical separation between redundant sections of a system and between one system and another system.
IEC 60987	Yes	Instrumentation and control systems important to safety: Hardware design requirements for computer-based systems.
IEC 61500	Yes	Instrumentation and control systems important to safety: Data communication in systems performing category A functions.

Table 3.8: International Electrotechnical Commission (IEC) standards potentially applicable for target safety system development. NPP stands for nuclear power plant.

Target safety system functions

For each operating mode, TSS will have different functions and actions that may be either external to the target, such as emergency shutdown of the proton beam and machine, or internal, such as static and dynamic confinements of affected TS systems. As fatigue for mechanical systems components can be a parameter relevant for nuclear safety analysis, another TSS function will be to monitor and trace the cyclic load history when required.

Target safety system architecture

The TSS design uses highly reliable programmable logic controller (PLC) systems designed and qualified to be used as plant safety systems. In order to achieve the high reliability required, the TSS will have two, separated, redundant, safety-qualified PLCs as shown in Figure 3.8 to meet the ESS risk probability goal of 10^{-6}. Each safety-qualified PLC will have fault-tolerant processors and will include diagnostics designed to detect failures and ensure failsafe operation of the I/O and communication networks. The TSS design will include capabilities to facilitate periodic testing in order to certify that its components are functional and continue to maintain the design value of the probability of failure on demand. Several networking methods are under study to achieve the required millisecond shutdown response time required for some design basis accidents. The TSS PLCs will be located outside areas classified as explosive. The safety-related devices that are in areas classified as explosive will be designed and installed to meet industry standards that ensure they will not initiate a hydrogen gas explosion.

The TSS triggers proton beam shutdown to ensure design basis accidents do not harm workers or the public. The safety integrity level of the TSS will be determined using the guidance in the standard IEC 61508 and the hazard analysis risk determinations. In accordance with this standard, the TSS will have instruments, networks, cabling, and final actuator elements separated from non-safety equipment and between redundant channels, to prevent propagation of failures in non-safety systems from affecting the TSS safety functions. The two redundant final actuator elements will de-energise contactors that will shut down the proton beam by de-energising either the ion source or the low energy beam transport (LEBT) chopper.

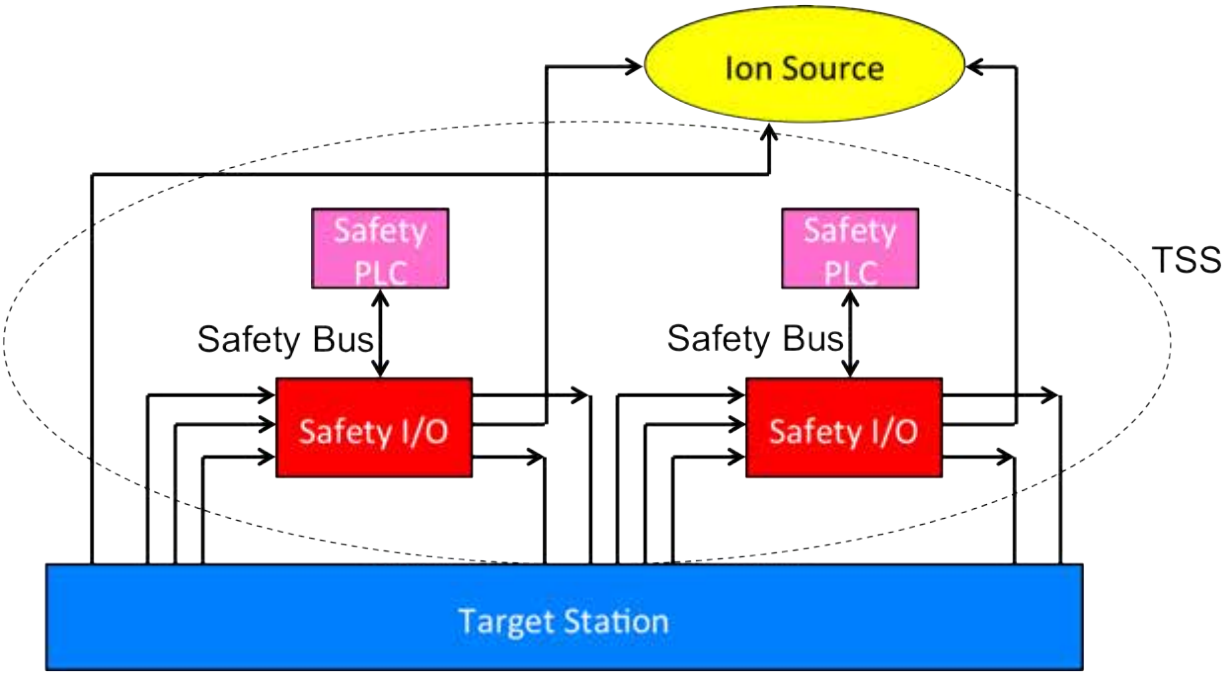

Figure 3.8: Illustration of TSS interfaces to external systems, e.g. ICS and PPS.

3.1.6 Global simulation of target station system

Global simulations will be performed for the target station, consisting of mechanical and fluid analyses. Both types of analysis will be performed at the end of the design process, after the mechanical and fluid systems have been fully defined.

The target station has a number of different fluid systems under different operating conditions defined, for example, by temperature and pressure. The physical parameters of these systems are subject to strong transient effects due to dynamic operations such as the shutting down and starting up of the pumps or the beam trips. These transient effects have an impact on operating conditions which must be understood to ensure safe operation. Furthermore, in case of accidents, it is important to understand the behaviour of these systems in order to react appropriately. Since target station fluid systems are all embedded within ESS's global fluid systems, and since fluid systems interact with beam control systems, it is of importance to simulate this behaviour in a global setting. The purpose of this global simulation is to link control, different operating modes (normal, tuning and abnormal) and different loop parameters together, including cryogenic systems, ensuring the compliance of target systems with safety, operational and control requirements, even during transient situations. The global mechanical analysis will cover the impact of an earthquake on the monolith and an aeroplane crash on the target station building. As this kind of analysis is quite standard, the mechanical analysis will not be discussed further in this section.

Methodology

The global simulation of TS fluid systems, will be undertaken in the following steps. After having benchmarked the chosen software to ensure its suitability, the different operational modes and scenarios will be defined in the first step of the analysis. These modes will exhibit different behaviours, placing different loads on the systems. The next step is then to build independent models for each system and subsystem, following which, the independent models are implemented and connected to the global target station model. Before starting the simulation, all necessary transient situations have to be defined and qualified. After

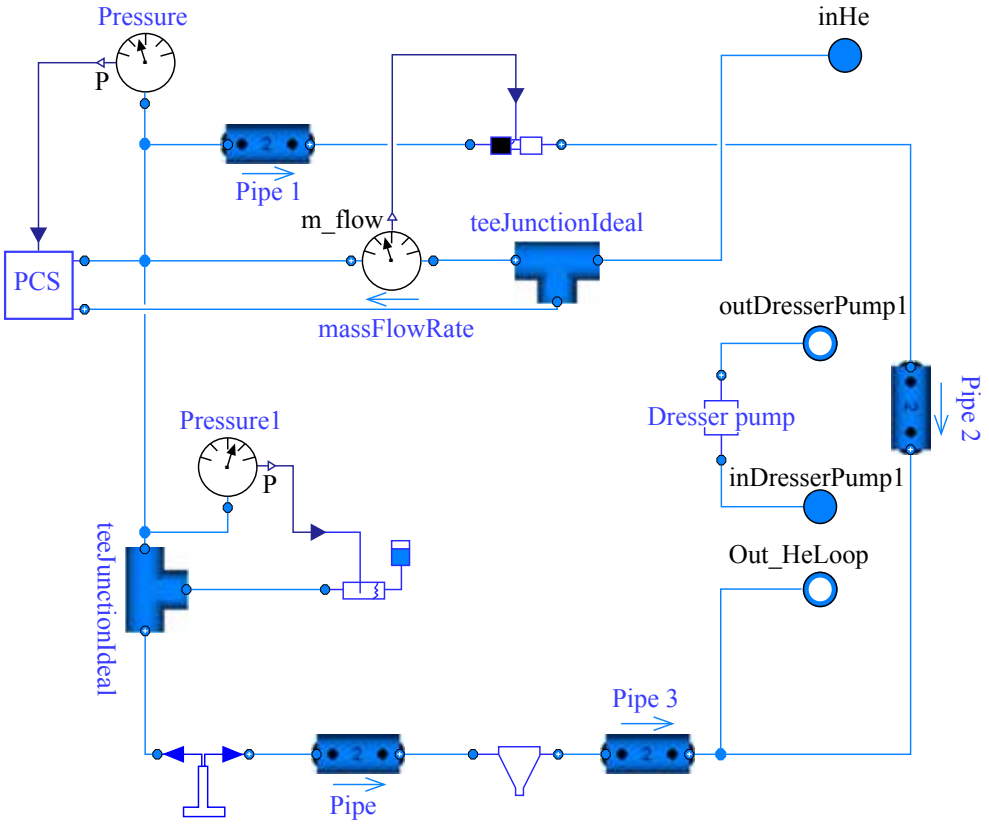

Figure 3.9: The model of the target helium loop.

calculations, they can be analysed and updated in the way that satisfies control and safety requirements.

While each system can be modelled independently of the others, potential connections have to be prepared, so that the connections among system models can be made later. Hence, it is important to prepare all piping and instrumentation diagrams (P&ID) in a detailed way and to clearly define the interfaces to other systems such as the control systems. This means that all P&IDs must contain all components (heat exchangers, filters, valves, etc.), and that the control of these components and the loops must be defined during this phase as well. A checklist will provide the most flexible and efficient way to build the global model of the ESS target station. As an example, the gaseous cooling system for the target cooling is composed of a primary helium circuit and intermediate nitrogen circuit, as discussed in Section 3.4. At the subsystem level, either the He-loop or the N_2-loop can be analysed separately. Figure 3.9 shows the helium loop model prepared for simulation and analysis. This model has free connections to other systems, so that it can be implemented in a more global model. When all the subsystems have been prepared, which includes cryogenic, moderator, target and control systems, they can be connected to the global system. For example, the full target loop is shown in Figure 3.10.

The global model will encompass the component system models, the ways that they are controlled and the different interfaces between the systems. Several operating modes have been defined in Section 3.1.4. The various modes are subject to different beam powers, changing the general behaviour of the facility. In order to design all the system correctly and ensure the reliability of the systems in all those cases, the different operating modes have to be clearly defined.

Prior to analysis, transient effects must be sorted into two different categories, one corresponding to normal operation and the other corresponding to incidental and accidental scenarios. The accidental scenarios are defined in close collaboration with the ESS safety division and can be found in the risk analysis report [302]. Transient effects that have to be analysed as part of normal operation are those associated with the start up or shut down of the facility or its components, and the beam trips. Transient effects that have to be analysed as part of incidental and accidental events are those associated with undesirable occurrences such as the leakage of a loop, obstruction of a loop, heat exchanger leakage, retarded rotation of the target wheel, or failure of sensors in the control system.

Dymola [303] has been chosen for the simulation tool. This is a modelling and 1-D simulation tool for dynamic multi-field systems. Models created with this software can combine fluid, mechanical, thermodynamic and control systems. All these fields can interact with each other, allowing a better simulation of the facility. Other software tools are available for this type of simulation analysis, including Cathare (CEA) and Relap5 (Idaho National Laboratory). However, Dymola suits ESS needs better. First, it is based on the Modelica language [304], which is an open source language. This makes it extremely flexible and means that there exist a large number of model libraries that can be shared or bought. EDF, Air Liquide and Linde, for example, use Modelica libraries to simulate the behaviour of products and equipment. This also makes it easier to develop specific model libraries that will fit ESS needs. Second, Dymola is a Dassault product that can be embedded in the ESS Enovia system. This facilitates the exchange of data and model archiving. Finally, Dymola is a multi-engineering tool, so that the TS global model will be able to combine

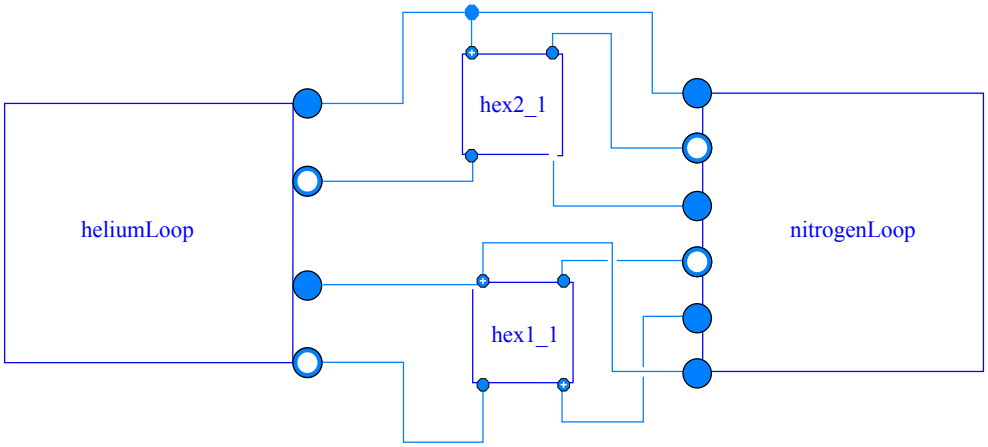

Figure 3.10: Model of the full target loop.

control, thermodynamic and fluidic effects, which will make the dynamic behaviour more realistic.

ESS will undertake a benchmark study to validate Dymola results. For this purpose, it has been proposed to operate the low pressure helium loop of HELOKA at the Karlsruher Institut für Technologie (KIT) under conditions similar to those at ESS, and to compare Dymola simulation results with experimental results for HELOKA [305–307]. Discussion with Swedish licensing authorities will be more informative after ESS has the results of this benchmark study.

3.1.7 Material properties

As is the case for existing spallation targets such as SNS, SINQ, and ISIS, the lifetime of the ESS target will be limited by materials performance in normal operating conditions. The behaviour of materials during normal and abnormal conditions sets requirements on other target station systems such as safety and filtering systems. Due to its special design based on a helium gas-cooled rotating solid tungsten target, the materials issues encountered in the ESS target will differ from those of the liquid metal targets at SNS, J-PARC and MEGAPIE and the water-cooled solid targets at SINQ and ISIS. This section discusses materials issues related to the helium gas-cooled rotating solid tungsten target design, based on target operating conditions and previous experience at other spallation targets and published materials data obtained in the spallation, fusion and fission materials communities. The main focus is on those materials exposed to high fluxes of protons and spallation neutrons, which are used for the target wheel, the proton beam window, and the moderator-reflector system. Some materials data are provided here for guidance, with the knowledge that the detailed design of components will draw materials data from the body of knowledge currently available and the recognition that, as with all spallation sources built and operated to date, component lifetimes will increase with operating experience.

Pure tungsten has been selected as the target material, beryllium as the reflector material, austenitic stainless steel (SS) 316L(N) as the structural material for the target shroud and reflector container, and aluminium-alloy Al-6061-T6 as the material for the proton beam window and moderator canister. According to the latest calculations, the operation temperature range is 25°C to 600°C for the tungsten, 25°C to 150°C for beryllium, 25°C to 300°C for SS 316L(N), and 20 K to 293 K for Al-6061. Detailed information about the distribution of irradiation dose, temperature and thermal mechanical stress, etc. can be found in other sections of this report. This section describes relevant information for these materials in the ESS temperature range. The nominal chemical compositions of the materials are given in Table 3.9. As a general rule, the concentration of an alloying element may vary by up to 10% around its nominal value. Some of the data in Table 3.9 have been applied to neutronic calculations [308].

In thermo-mechanical and flow dynamics calculations, physical properties, such as thermal conductivity, thermal expansion and specific heat, and mechanical parameters such as Young's modulus and the Poisson ratio are often used. These properties are usually temperature dependent. In the relevant temperature ranges mentioned above, the numerical value of each of these properties can be expressed by the polynomial $A+B\,T+C\,T^2+D\,T^3$ where T is the absolute temperature and A, B, C and D are coefficients that depend

Material	**Al** [%]	**C** [%]	**Cr** [%]	**Cu** [%]	**Fe** [%]	**Mg** [%]	**Mn** [%]	**Mo** [%]	**Ni** [%]	**Si** [%]	**Ta** [%]	**Ti** [%]	**Zn** [%]
Beryllium	.02	.04			.06	.01				.03			
Al-6061	97.3		.195	.275	.35	1.0	0.075			.6		.075	.125
$AlMg_3$	95.9		.030	.080	.30	3.0	0.300			.3		.020	.050
SS316L		.03	17.0		65.7		1.80	2.5	12.5	.4			
SS316LN		.03	17.0		65.6		1.80	2.5	12.5	.4			
Tungsten*	5	10	5	5	10	10		20		5	10		

Table 3.9: The nominal chemical compositions of the target materials, measured in percentage weight (except for tungsten*, where the unit is parts per million). In addition to the listed components, SS316L and SS316LN contain 0.03% cobalt, 0.02% phosphorous, and 0.01% sulphur, while SS316LN also contains 0.07% nitrogen, beryllium includes 0.64% beryllium oxide, and tungsten includes 5 parts per million of oxygen. The values given for tungsten correspond to PLANSEE's pure tungsten product, and the values given for beryllium correspond to Brush Wellman's Be S-65 product.

Material		Thermal conductivity [W/(m.K)]	Thermal expansion [10^{-6}/K]	Specific heat [J/(kg.K)]	Young's modulus [GPa]	Poisson ratio
Al-6061	A	116.4	19.96	156.6	78.01	0.33
300 K – 400 K	B	0.2865	6.133×10^{-3}	5.761	-2.801×10^{-2}	
	C	-4.938×10^{-4}	1.230×10^{-5}	-0.01488	1.758×10^{-5}	
	D	3.282×10^{-7}	-1.246×10^{-8}	1.310×10^{-5}	-8.030×10^{-8}	
SS316L	A	10.145	14.287	185.7	217.6	0.263
300 K – 600 K	B	1.253×10^{-2}	-1.120×10^{-3}	1.332	-6.899×10^{-2}	1.022×10^{-4}
	C	2.1927×10^{-6}	2.021×10^{-5}	-1.642×10^{-3}	-9.414×10^{-6}	-2.132×10^{-8}
	D		-1.636×10^{-8}	7.28×10^{-7}		
Tungsten	A	247.3	4.049	120.8	417.2	2.826×10^{-1}
300 K – 900 K	B	-3.164×10^{-1}	1.9×10^{-3}	0.048	-3.767×10^{-2}	7.479×10^{-6}
	C	2.720×10^{-4}	-1.664×10^{-6}	-3.577×10^{-5}	2.133×10^{-6}	2.830×10^{-9}
	D	-8.494×10^{-8}	7.319×10^{-10}	1.697×10^{-8}	-2.604×10^{-9}	3.647×10^{-13}

Table 3.10: Physical and mechanical properties of Al-6061, SS316L(N), and tungsten [309]. The four coefficients A, B, C and D describe a cubic fit: $A+B\,T+C\,T^2+D\,T^3$, where T is the absolute temperature. The thermal expansion is the mean coefficient rather than the instantaneous value.

on the material and the property under consideration. Table 3.10 presents the values of A, B, C and D for these properties for tungsten, SS 316L and Al-6061.

Properties of structural materials

SS 316L(N) is one of the most widely used structural materials in existing spallation neutron sources and in nuclear installations. It is normally used in the solution-annealed condition, denoted by the letter "N" in parentheses, and its properties are extensively studied. Table 3.11 presents the typical tensile data for non-irradiated SA316L(N) [310]. Based on its tensile properties, design stress can be considered to be 150 MPa to 125 MPa in the temperature range of 300 K to 500 K [311].

Austenitic steels are one of the main classes of materials irradiated in the SINQ target irradiation program (STIP). Several kinds of austenitic steels from Europe, Japan and the USA have been irradiated to a maximum dose of about 20 dpa and a sample of the specimens have been tested [312]. After irradiation at temperatures below 350°C, the yield stress (YS) and the ultimate tensile strength (UTS) increase, while the uniform elongation or strain to necking (STN) and total elongation (TE) decrease with irradiation dose. After irradiation, the difference between YS and UTS is much smaller than that before irradiation at zero dpa. This implies that the steels lose their work hardening capability after irradiation due to irradiation-induced hardening. Although the STN drops significantly to very low level, TE remains generally at about 8%, indicating that the steels still have relatively good ductility at 10 dpa to 20 dpa. The tensile data of the STIP specimens and the experience of SINQ targets indicate that SA 316L(N)

Temperature [K]	Yield stress [MPa]	Ultimate tensile stress [MPa]	Ultimate elongation [%]	Total elongation [%]
300	305	610	48	62
350	250	550	41	53
500	203	500	31	41
600	190	490	31	40
700	162	490	34	42

Table 3.11: The tensile properties of non-irradiated SA316L [310].

can certainly withstand 10 dpa in the above-mentioned conditions, which corresponds to approximately 8 years of lifetime for the target vessel as can be deduced from Table 3.15.

If the thermal stress in the shroud is found to be too high to use SA 316L(N), annealed inconel 718 can be considered as an alternative. Annealed inconel 718 has been used at the proton beam window of SNS and LANSCE. Some results obtained from specimens irradiated in STIP show excellent ductility after irradiation up to about 18 dpa [313]. Martensitic steels are less desirable because of the relatively low operation temperature of the shroud. The ductile-to-brittle transition temperature (DBTT) may increase rapidly to the operation temperature at above 10 dpa. Aluminium alloys are widely used in existing spallation neutron sources. All cold moderator tanks are made of Al-alloys. For instance, Al-6061 is used for the moderator tanks at SNS, LANSCE and J-PARC, while $AlMg_3$ is used for those at SINQ. $AlMg_3$ is also used as the proton beam window material at J-PARC and the target container material at SINQ.

The properties of Al-6061-T6 are reviewed in detail in an article published by LANL [309]. Irradiation in the fission neutron spectrum at 423 K and below can introduce significant hardening and embrittlement effects [314]. However, the reduction of ductility saturates at high irradiation doses and TE maintains at above 8% at a dose of 3×10^{27} neutrons/m^2 (approximately equivalent to 400 dpa). Al-6061-T6 is currently used as the material for the moderator canister at SNS. Exchange of the moderator tank is planned for 2015. By then, the material will have received a dose of about 21 dpa in the peak position [315]. [1] Extrapolating from SNS and J-PARC experience to ESS conditions indicates a moderator lifetime of slightly more than a year.

$AlMg_3$ has been used in SINQ since 1997 as the material for the target container and the moderator tank. In the proton beam window position of the target container, the material receives both high-energy proton and spallation neutron irradiation. The maximum irradiation temperature is about 330 K. The proton beam window of the SINQ Target-3 was investigated. The tensile test results indicate strong irradiation hardening and embrittlement effects [316]. At the maximum dose of 3.6 dpa, the TE decreased from 22% in non-irradiated condition to about 8%. It is expected that the ductility of $AlMg_3$ will further decrease with increasing irradiation dose. Nevertheless, in SINQ, no problems have been encountered with the target containers since the first one operated in 1997. In the last target, the proton beam window of the $AlMg_3$ container received a dose of about 8 dpa and 2000 appm He. The post-irradiation examination will be conducted on the proton beam window to demonstrate whether it can be exposed to higher irradiation dose in such a severe irradiation environment. The present moderators in SINQ have been used since 2000. This also indicates that $AlMg_3$ has a good resistance to neutron irradiation.

It can be seen that both Al-alloys have good track records in applications in spallation sources. There is much more neutron irradiation information available for Al-6061-T6 than there is proton irradiation. Nevertheless, the excellent experiences obtained from SINQ, operating at 1 MW continuous proton beam, demonstrate that $AlMg_3$ performs well in both proton beam window and moderator tank applications. As the ESS moderator will be subject to higher energy deposition, it is worth considering applying zircaloy for some parts of the moderator tanks, for example, for the exterior envelope, since its use may reduce the moderator heat load at equivalent mechanical resistance.

Properties of non-structural materials

In the ESS baseline design, the target wheel is composed of bare pure tungsten slabs in various sizes. There are two requirements from the material point of view, which the tungsten slabs must satisfy. First, although tungsten will not play a structural role due to its brittleness, it must retain structural integrity over the lifetime of the target to avoid blocking the cooling channels. Second, the radioactive inventory should be retained in the slabs as much as possible to minimise contamination of the helium cooling loop.

The mechanical properties of tungsten depend strongly on production procedures. Normally, the sintered tungsten has a few per cent of porosity with isotropic grain structure and grain size between 50 and 200 μm. Pores of sizes up to a few μm are closed and located mostly at grain boundaries. Sintered tungsten is very brittle and has low ductility and high DBTT. Hot deformation is therefore required at about 1000°C. However, hot deformation is usually applicable only to thin ($\simeq$20 mm) plates or rods. Hot-deformed tungsten exhibits a texture grain structure with grain sizes of a few μm in diameter and a few tens of μm length, and grain sizes increase with distance to the outer surface of a plate or rod. As

[1] Although for direct comparisons, dpa remains the most often quoted unit, another unit to express radiation damage in Al-alloys such as neutron fluence or silicon production might be desirable in the future.

usual, a hot-deformed tungsten plate or rod has higher fracture resistance in transverse direction. Irradiation data of tungsten are very limited, particularly in the spallation irradiation case. Compression tests conducted on small tungsten rods irradiated at LANSCE to a maximum dose of 23 dpa at 270°C show that irradiation induced hardening and embrittlement effects increase with irradiation dose [317]. Testing at 475°C exhibits further increased brittleness than that observed from testing at room temperature.

Concerning water-cooled targets, online operation and post-irradiation examinations of the irradiated LANSCE tungsten target showed high water corrosion rates which increase with irradiation dose [318]. Early experience at the first generation (MK-0) tungsten target of LANSCE also revealed severe cracking caused by a steep temperature gradient under beam [319]. All these observations led to the adoption of various cladding or canning techniques with materials such as tantalum and stainless steel 304L in the LANSCE and ISIS targets.

Unlike the situation with a water-cooled tungsten target, coolant flow-induced corrosion damage is not expected with the helium-cooled tungsten target at ESS. However, since the pulsed proton beam will induce cycling stress as high as 300 MPa in tungsten slabs, care must be taken to maintain the mechanical integrity of the tungsten slabs. To avoid cracking, the tungsten slabs must be designed to have the lowest possible thermal stress during full beam power operation. It is also important to pay careful attention to the surface treatment of the slabs, in order to reduce the risk of having micro-cracks on the surface. Transmutation of tungsten to osmium and rhenium in large enough quantities could also contribute to increased embrittlement, but this is not expected to be a significant problem at ESS.

Neutron irradiation experiments demonstrate that pure tungsten may undergo swelling at a rate of 0.2% per dpa at temperatures above 600°C [320]. Although there is no experimental data, the swelling effect is expected to be less pronounced in the ESS target, because the temperature is lower, and furthermore, the helium produced by spallation reactions can form stable clusters around vacancies, which significantly suppresses void formation.

Another important issue posed by using bare tungsten as the target material is tungsten dust production. In high purity helium atmosphere, the tungsten dust will come from the tungsten grains detached from the surface of tungsten slabs. The pure tungsten grain sizes are large enough that the cyclonic filters can remove them with high efficiency, as discussed in Section 3.4.1. If oxygen incidentally infiltrates the helium loop, the tungsten will be oxidised at high temperatures and tungsten oxide dust will be produced. W-Ni-Cu and W-Ni-Fe alloys exposed briefly in He+5%O_2 gas showed significant oxidation above 600°C [321]. A more significant level of oxidation was observed from pure tungsten exposed to air in the same temperature range [322], with oxidation beginning take place at 550°C. The size of oxide particles varies from 0.1 to about 400 μm in the testing temperature range of 550°C to 800°C [322]. Handling this issue is difficult, because the size of the volatile oxide particle is unknown. To collect tungsten oxide dust, various filters will be installed in the helium loop. However, the cyclonic filters that work well for filtering pure tungsten dust would be significantly less efficient if the oxides should turn out to be in the sub-micron range. Therefore, impurity level of the helium cooling gas must be kept as low as possible during operation.

It is difficult to make an accurate assessment of dust production in a helium-cooled tungsten spallation target, due to the lack of direct measurements under representative environments. For safety and licensing and for maintainability of the helium loop components, a good understanding of this issue is needed. In order to get necessary information to support the target design, a number of experiments on bare tungsten in both non-irradiated and irradiated conditions will be planned and the issues discussed here will be investigated. Tungsten samples clad, canned or coated with various techniques and materials will be studied as well. Irradiation of various kinds of samples will be performed in the next STIP irradiation campaign in the temperature range relevant to ESS.

Reflector materials also will not have structural functions. At present, beryllium is commonly used for nuclear applications as a neutron multiplier and reflector material. Though it is very suitable for these purposes, some aspects, such as tritium inventory and the structural integrity of beryllium blocks should be investigated with account taken of the differences between spallation and fission reactor environments.

Neutron irradiation leads to complex changes in the micro-structure of beryllium, which may lead to swelling resulting from the formation of He bubbles. There are two important pathways for gas production. One is the (n, 2n) reaction in which the ^{9}Be is reduced to ^{8}Be, which then splits into two ^{4}He atoms. The second is the (n, α) reaction in which the ^{9}Be absorbs a neutron and then splits to form a ^{4}He and a ^{6}He. The ^{6}He rapidly decays to become ^{6}Li. The ^{6}Li then reacts with a thermal neutron to produce ^{4}He and ^{3}H. Therefore, a large amount of helium and tritium may be produced in the beryllium reflector, as indicated

by the neutronic calculation results presented in Table 3.14. Nevertheless, since the operation temperature of the reflector is low, the swelling rate also is expected to be low. Fusion materials studies concluded that for an irradiation temperature below about 400°C, swelling of beryllium containing 1,500 appm of helium is less than about 1% [323]. Neutron irradiation at low temperatures will induce embrittlement as well. However, as the stress level in the reflector should not be high, the embrittlement may not cause serious failure in the integrity of the reflector during the design lifetime of more than one year.

3.2 Neutronic design

3.2.1 Target and moderator concepts

The main goal of the neutronic study of the ESS target station is to define the parameters of the target moderator-reflector configuration for a neutron source with excellent neutronic performance. Another objective is to provide data essential to the engineering design, such as heat deposition, gas production and radiation damage. This work is done using advanced Monte Carlo simulation codes. The determination of the absolute neutronic performance is important, in order to compare the expected performance with existing facilities and validate the choice to enter into construction. In order to achieve this goal, validated codes must be used, and uncertainties must be estimated from the different sources, coming for instance from the libraries and models used. The most important figure of merit is the source brightness, defined as the neutron flux per unit of solid angle, per neutron wavelength, in units of $[\mathrm{cm}^{-2}\,\mathrm{s}^{-1}\,\mathrm{sr}^{-1}\,\text{Å}^{-1}]$. This quantity is independent of the distance from the surface of the moderator, and is therefore an indication of the performance of the facility.

The chosen spallation material for neutron production is tungsten, which is known to be among those materials yielding the highest numbers of neutrons per incoming proton [324]. In terms of neutrons leaking from the surface of a target per incoming proton, tungsten gives an excellent performance. Its choice for the target material is not, however, driven primarily by neutronic issues, but rather by arguments related to cooling and safety, which are discussed in other parts of this chapter. Similarly, the rotating target concept described in Section 3.3 was chosen because it makes it possible to cool at full beam power. The neutronic design helped in this case in determining the thickness of the target, which was chosen after a neutronic optimisation that also took into account the proton beam profile and the presence of moderators and reflectors.

For the moderators, the design philosophy is determined by the constraint of the start date of 2019 for neutron production at ESS. New design concepts typically require a decade or more to go from the first tests to production. Therefore, it is wise to rely for the start-up on the best existing state-of-the art technologies, to provide the best possible neutron source from the beginning. At the same time, development of innovative concepts, such as directional moderators, will be pursued. This strategy is justified by the expected lifetime of the moderators (on the order of one year) due to radiation damage. Thus, there will be opportunity in the future to install moderators exploiting new concepts that are currently under study, or, perhaps, that have not yet even been conceived of.

The choice of the type of moderator is also related to the proton pulse structure of the ESS accelerator, 2.857 ms pulse length at 14 Hz. Since the pulse is remarkably long, compared to a short pulse facility, a coupled moderator is proposed. Neutron pulses are shaped by choppers, eliminating the need for the decoupled or poisoned moderators used at short pulse facilities such as SNS, J-PARC, and ISIS. The best choice for a long-pulse source is a coupled moderator of relatively large volume. Volume moderators, of cylindrical shape, filled with supercritical para-hydrogen have been shown to provide the highest peak flux [325, 326]. Also, the high energy of the protons forces the use of a wing-type moderator, in order to reduce the flux of fast neutrons and the associated radiation background in the experimental lines. The choice of moderator is also related to the power of the facility. At ESS power levels, the only sensible choice for a cold moderator is supercritical H_2.

The cross sections for ortho- and para-hydrogen differ significantly in the low-energy region: the neutron scattering cross section in pure para-H_2 drops significantly below about 15 meV of neutron energy, while the cross section for ortho-H_2 increases [324]. This implies that the moderator of pure para-H_2 becomes almost transparent for low-energy neutrons, thus favouring neutron extraction from the moderator, while at the same time the number of collisions and thus the probability of neutron capture, is reduced. Another concept that has been shown to work at the research reactor HZB in Berlin, and that is of great interest for

the ESS user community, is bispectral neutron extraction [327]. This option provides the opportunity to offer both full thermal and cold neutron spectra in the same beam line and enhances the dynamic range of the instruments. The challenge is to design a moderator with high performance for both cold and thermal neutrons. Calculations have been performed using MCNPX [328] and PHITS [329] codes. Details about the codes and options (models and libraries) used are given below.

3.2.2 Description of the model

Figure 3.11 shows the global MCNPX model of the target station monolith. Two horizontal cuts are shown corresponding to the centre of the top moderator and to the centre of the target. Figure 3.12 shows details of the proton interaction zone in the target and of the moderators. Two supercritical, cylindrical H_2 moderators are placed above and below the tungsten target. On the side of the cold moderators, extensions filled with ambient light water are placed for moderation of neutrons to thermal temperatures. A beryllium reflector that maximises the neutron flux surrounds both moderator and premoderator. Materials definitions according to the chemical compositions listed in Section 3.1.7 were used. Details of the neutronic calculations leading to this design choice are reported below. The presence of ortho-hydrogen considerably reduces neutron brightness, so catalytic converters will be considered for use in the cryogenics systems, in order to guarantee the highest possible concentration of para-hydrogen.

3.2.3 Neutronic codes and nuclear data

Neutronic design studies were performed using MCNPX and PHITS, with MCNPX used as the primary simulation option due to its long history of validation and benchmarking as well as due to a number of features not available in PHITS (e.g. next event estimators and ability to mix models and libraries freely). Auxiliary codes used for visualisation and data processing include MORITZ, MCAM and MCCAD [330–333]. The quality of the neutronic design strongly depends on the quality of the nuclear interaction models and nuclear data libraries used. In order to assess the influence of models and libraries on the neutronics of the target-moderator-reflector system, two integral parameters were analysed: 1) cold brightness (brightness of the moderator surface integrated over the 0-5 meV energy range), and 2) moderator heat load or total heat deposited in the cryogenic part of the moderator suite due to prompt nuclear interactions. The first parameter reflects neutronic performance, while the second reflects engineering constraints and limits.

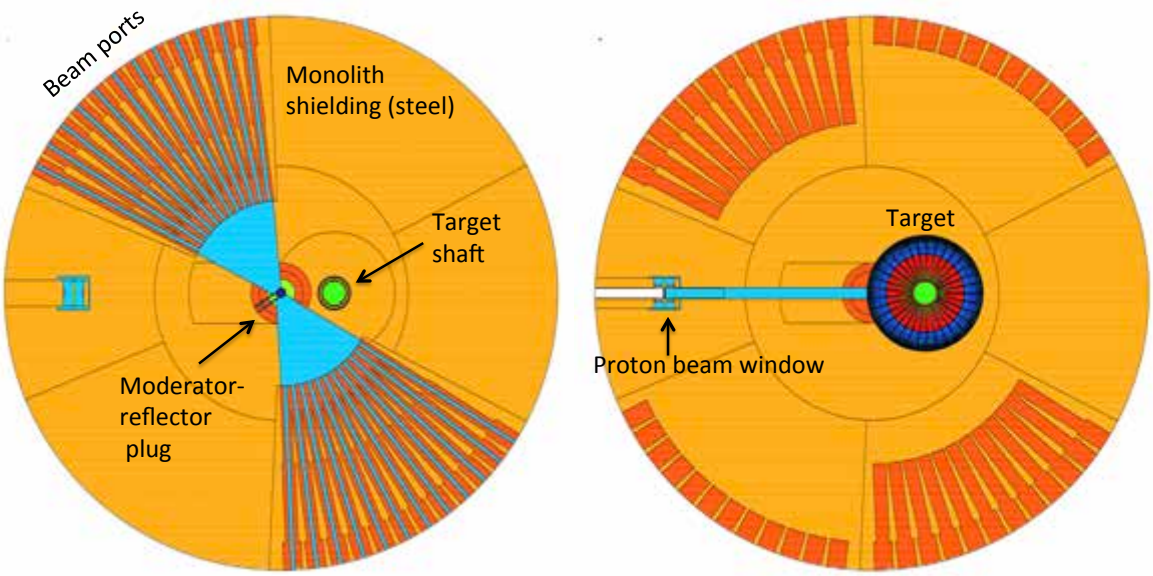

Figure 3.11: MCNPX model of the target station monolith. Left: Horizontal cut through the top moderator. Right: Horizontal cut through the proton beam line and target.

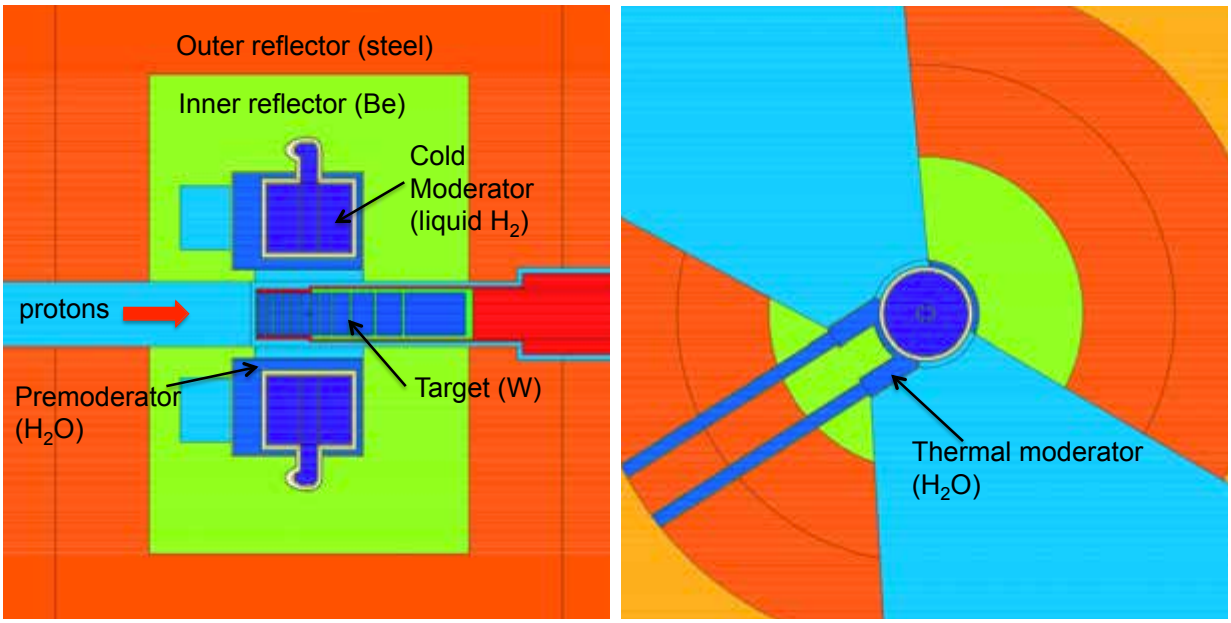

Figure 3.12: MCNPX model of the moderators and target zone. Left: Vertical cut showing top and bottom cold moderators. Right: Horizontal cut showing top cold moderator and water extensions for bispectral neutron beam extraction.

Several intra-nuclear cascade (INC) models (Bertini, Isabel, INCL4) and evaporation/fission models (Dresner, ABLA), as well as the self-contained package CEM03, were employed for simulation of high-energy physics in MCNPX. The results are shown in Figure 3.13 (top left). Apart from the INCL4 INC model, the models returned values within ± 5% of each other for neutronic performance and heat deposition. The intermediate energy region (above a few eV) is especially important for the neutronics of moderators and reflectors. Three neutron libraries, ENDF/B-VII.0 (US), JENDL-4.0 (Japan), and JEFF3.1 (Europe), were tested on system components, with the results shown in Figure 3.13 (top right). The differences in neutronic performance was again found to be within ± 5%. Neutron scattering kernels are used for detailed simulation of neutron transport at thermal energies and below. Figure 3.13 (bottom left) shows that the use of scattering kernels at ambient temperatures is not crucial: the difference between free gas treatment and $S(\alpha, \beta)$ formalism is within 5% for non-cryogenic parts. Scattering kernels are, however, absolutely necessary for cryogenic parts, for example, liquid hydrogen. The difference in neutronic performance and heat deposition due to the difference in para-hydrogen scattering kernels is illustrated in Figure 3.13 (bottom right).

The analysis shows that uncertainties associated with nuclear interaction models and nuclear data libraries are expected to be about 15%. While almost any combination of models and libraries studied would suffice (with the notable exception of the outdated MCNPX INCL4 INC model), the default MCNPX Bertini-Dresner model coupled with ENDF/B-VII.0-based neutron libraries and scattering kernels (whenever available) are recommended to simplify inter-comparison of neutronic results. The default MCNPX nuclear interaction model is generally accepted by the spallation source community for calculating most quantities of interest, such as neutronic performance and nuclear heating [334]. In addition, it requires less computing time than other models and is therefore preferred for optimisation studies.

3.2.4 Optimisation of the beam-target interface

Optimisations of the neutronic design were performed by choosing integral values of the cold or thermal neutron brightness as the figure of merit:

$$FoM = \int_0^{\infty} dt \int_0^{E_c} \Phi(t, E) dE \tag{3.1}$$

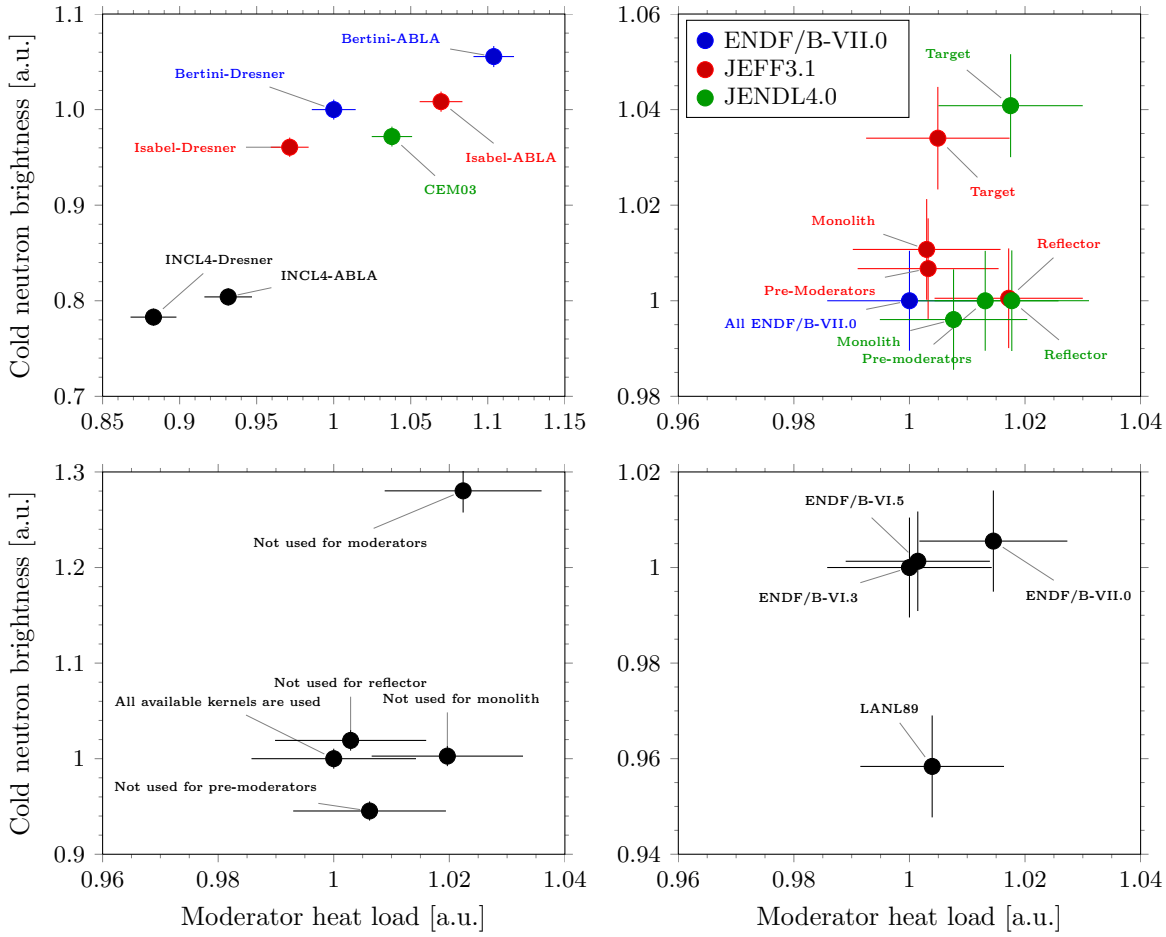

Figure 3.13: Cold brightness and moderator heat load obtained under different simulation conditions. Top left: With different nuclear interaction models. Top right: With different neutron libraries. Bottom left: With and without scattering kernels. Bottom right: With different para-hydrogen scattering kernels.

where $\Phi(t, E)$ is the neutron brightness as a function of time and energy, $E_c = 5$ meV for the cold neutrons and $E_c = 0.5$ eV for thermal neutrons. The results of these optimisations are summarised below. For more details, the reader is referred to the paper by Batkov et al. [335].

A sensitivity analysis of this figure of merit as a function of the height of spallation material was performed for different beam profile configurations. The optimal value for the target thickness was found at 8 cm. The shape and footprint of the proton beam affect important target station parameters such as material damage and cooling, which in turn contribute to defining the engineering constraints that limit possible beam profile configurations. Monte Carlo simulations were performed using PHITS 2.30 [329]

Parameter	**Unit**	**Baseline**	**Neutronic maximum:**	
			Parabolic	**Uniform**
Proton beam width	cm	16	3.5	1.5
Proton beam height	cm	6	0.01	1.0
Moderator heat load	kW	10.5 ± 0.2	10.8 ± 0.2	10.7 ± 0.2
Maximum heat load density in tungsten	kW/cm^3	3.2 ± 0.2	23.9 ± 0.5	27.7 ± 0.5
Cold neutron brightness efficiency	%	96	100	100

Table 3.12: Beam profile optimisation results. The baseline beam profile gives 96% of the maximum theoretical performance achieved in the limit of a zero emittance beam.

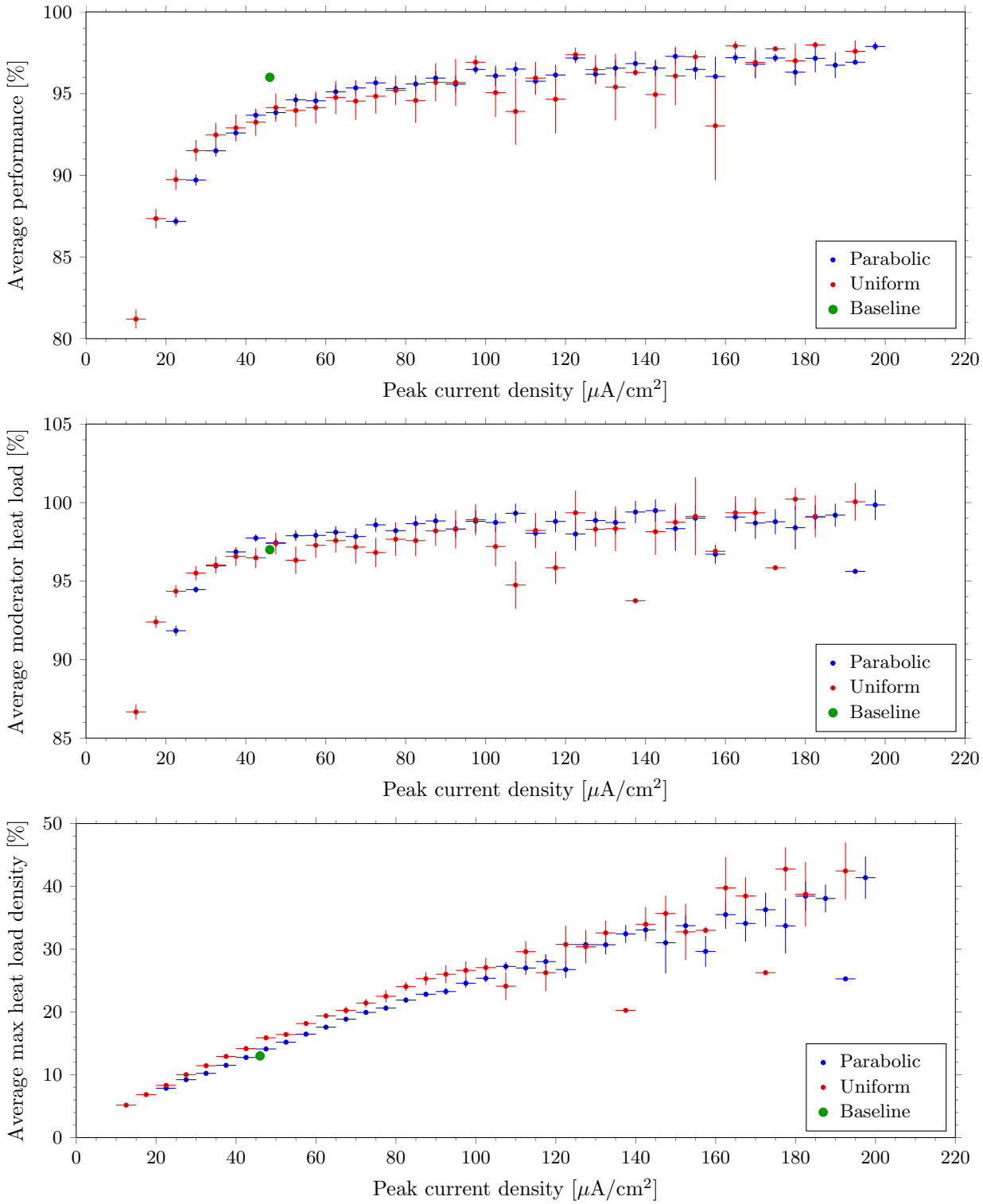

Figure 3.14: Neutronic performance and moderator heat load as a function of proton peak current density, for parabolic, uniform and baseline beam distributions. Top: Average neutronic performance. Middle: Average moderator heat load. Bottom: Average maximal heat load density in the target wheel.

and MCNPX 2.7 [328] codes with the JAM [336] and Bertini [337] models, respectively, and coupled with ENDF/B-VII data libraries [338]. The beam divergence between the proton beam window and target was not taken into account in this work. Two proton beam profile distributions were studied, a parabolic and a uniform distribution. In each distribution, the overall width and height of the beam footprint varied between 0.01 cm and 25 cm, and between 0.01 cm and 10 cm, respectively, thus spanning the phase-space of realistic beam profiles.

For MCNPX, the figure of merit was calculated by a standard sample biasing technique of scoring neutron flux at a point detector behind an ideal collimator, followed by a solid angle correction. A surface-crossing tally was used for the figure of merit in PHITS. The results of the optimisation are summarised in Table 3.12. From a theoretical point of view, a zero emittance proton beam would provide the best neutronic performance, at the cost of a huge peak current density. However, the baseline double parabolic profile configuration [339] gives only 4% lower performance than the neutronically optimal beam. This result holds true despite the use of a double parabolic beam profile with a peak current density of 47 μA/cm^2 in the simulations, slightly different from the peak current density of 52 μA/cm^2 that has been derived from the beam dynamics calculations described in Section 4.7.

Figure 3.14 shows how average values of neutronic performance and heat load depend on the peak current density of the proton beam. All of these figures support the conclusion that, for a given peak current density, there is no significant difference between the parabolic and uniform beam profiles. The main results of this optimisation study are: 1) the baseline beam parameters give 96% of the maximum neutronic performance achieved with a pencil-like beam; and 2) there is no significant difference in the neutronic performance and engineering parameters studied between parabolic and uniform beam profiles, as long as the peak current density is the same [335].

3.2.5 Neutronic design of the target-moderator-reflector system

The geometrical configuration of the bispectral moderator is shown in Figure 3.15. This model was used as a reference in a parametric optimisation process, during which each of the system parameters was varied in a sequential way, until the optimal configuration shown in Figure 3.12 was reached. Figure 3.16 (right) indicates that the optimal diameter is around 18 cm for a conventional pure para-hydrogen moderator, although the loss in neutronic performance is not dramatic when a smaller moderator is used. ESS has chosen a diameter of 16 cm in order to reduce the heat load on the moderator, and thus, the cryogenic system requirements of the facility. Another parameter related to neutronic performance and the design of moderators is the dimension of the premoderator. In particular, a thicker water layer between the target

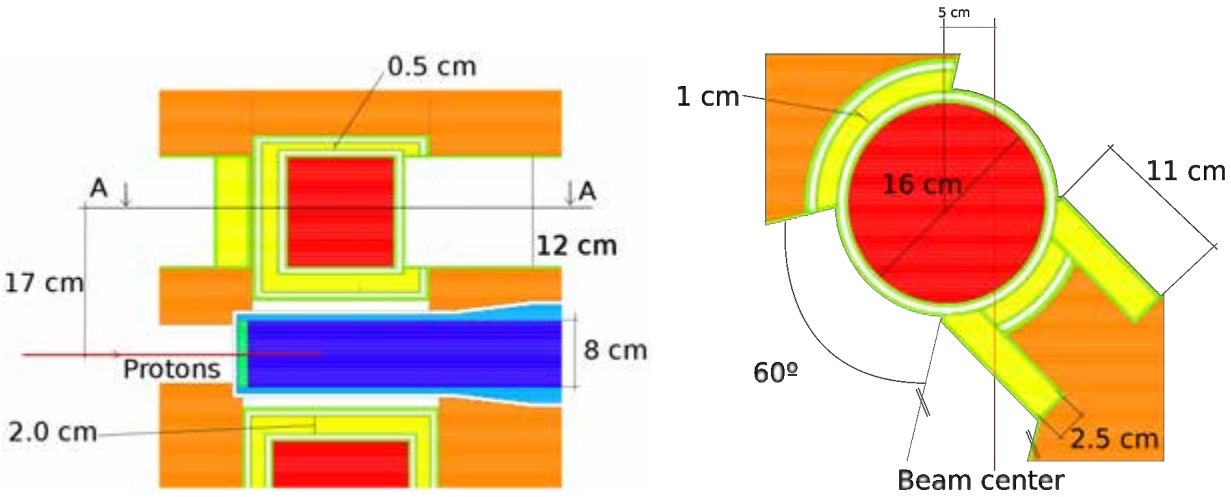

Figure 3.15: MCNPX model of the target and surrounding moderator and reflector. The cold moderator is shown in red, the thermal moderator for bispectral beam extraction and the premoderator are in yellow, and the beryllium reflector is in orange. Left: Longitudinal view. Right: Top moderator showing the thermal extensions for bispectral extraction.

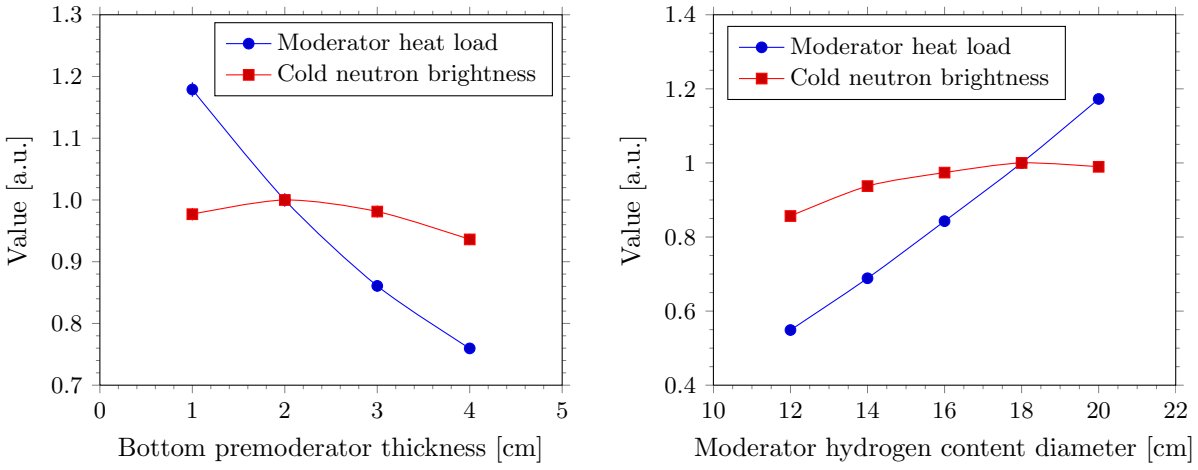

Figure 3.16: Sensitivity studies of the bottom premoderator and moderator dimensions. Left: Premoderator thickness. Right: Moderator diameter. Variation of these parameters strongly influences the heat load on the cryogenic moderator, dictating the choice of the optimal dimensions.

and the moderator can reduce heat deposition in the moderator, while at the same time improving its neutronic performance. Figure 3.16 (left) shows that thick ambient water premoderators placed between moderator and target can substantially decrease the heat load on moderators without compromising their neutronic performance.

The thermal moderator extensions provide thermal neutrons for bispectral extraction. The bispectral moderators are positioned so as to optimise the flow of neutrons from the target to the cold moderators, which implies that the thermal moderators will not receive optimal neutron flow from the target. Nevertheless, as shown below, their neutronic performance is excellent. The thermal moderator extensions affect the brightness of the cold moderator, because their presence makes it necessary to reduce the amount of

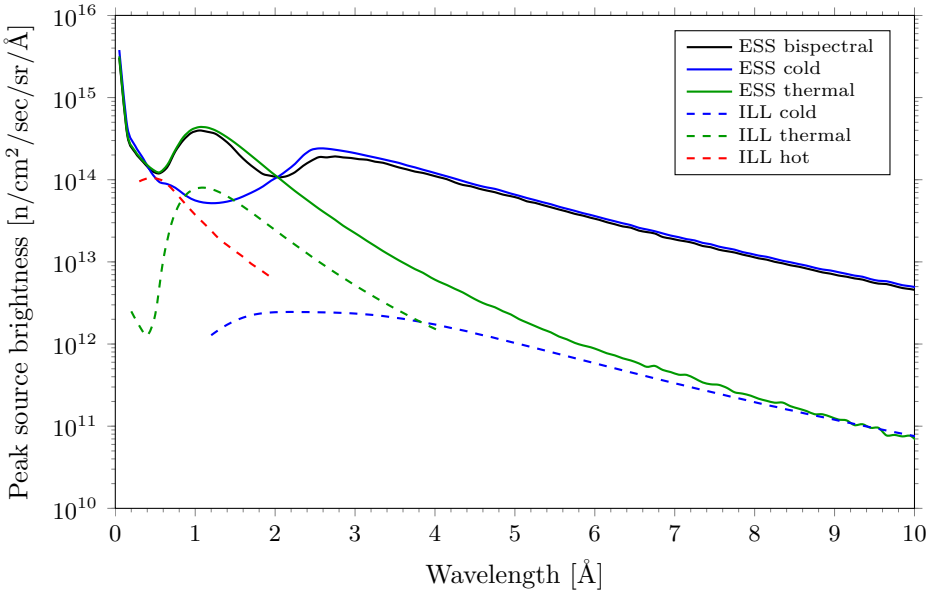

Figure 3.17: ESS absolute peak brightness [339] compared to ILL yellow book data [340]. "ESS bispectral" is the weighted sum of "ESS cold" and "ESS thermal" using calculated weight factors corresponding to a typical bispectral beam extraction neutron guide configuration [341]. The ILL spectra are accurate to within about a factor of 2: slightly too high for thermal neutrons and too low for cold neutrons.

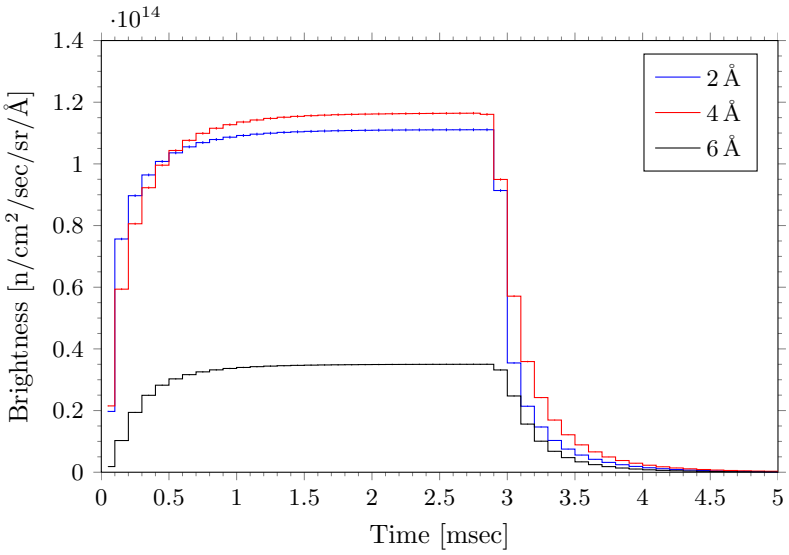

Figure 3.18: Neutron pulse shapes at 2 Å, 4 Å and 6 Å out of the moderator, with the same parameters as in Figure 3.17.

reflector surrounding the cold moderator. This effect was studied, comparing the calculated flux from an isolated cold moderator with the flux from a cold moderator with thermal extensions on the side. The addition of thermal extensions was found to result in a 15% reduction in cold neutron brightness. Earlier studies carried out by J-PARC and SNS show that beryllium is the optimum reflector material to maximise cold brightness in a coupled moderator. Based on previous experience, ESS has selected a composite reflector, with an inner reflector made of beryllium and an outer reflector made of steel. The main nuclear properties of beryllium when it is used as a reflector material are that it introduces a significant moderation, has a very low threshold for the (n, xn) reactions and does not have an important capture cross section. The diameter of the inner reflector in the baseline design is 60 cm.

Cold and thermal brightness

Figure 3.17 shows the spectral brightness of the ESS moderators. The absolute brightness was calculated at a distance of 10 m from the moderators, using collimators to view only the moderator surfaces. The peak cold brightness is a factor of 75 larger that at ILL at 4 Å, a factor of 61 larger at 6 Å, and a factor of 65 larger at 10 Å [340]. The thermal neutron brightness is at the same level as that called for in the 2003 design [334]. In summary, the proposed configuration for the cold moderator with thermal extensions allows the production of thermal neutrons in conditions that are similar to those for the long pulse moderator of 2003, while the production of cold neutrons is significantly increased. Further optimisation of the design of the thermal moderator is expected to increase thermal neutron brightness. The peak of the thermal spectrum is about 2.5 times higher than the cold peak. It is interesting to compare this relationship with the situation at the HZB reactor, which has bispectral extraction. At HZB, the cold moderator is a liquid H_2 bottle, while the thermal neutrons are extracted from the beryllium reflector surrounding the core. The ratio of thermal to cold is about five; one can expect that with an optimised cold moderator like the one for ESS, this ratio would drop by about a factor of 2, consistent with the present results.

In summary, Figure 3.18 shows the time distribution of the neutron pulse for wavelengths of 2, 4 and 6 Å. The calculations take into account the presence of a beryllium reflector, for which neutron flux almost reaches a saturation value after about 1 ms, although the value does increase slightly over time thereafter.

3.2.6 Support to beam extraction

Neutron beam extraction and beam delivery are inseparable. Their task is to make possible an efficient transfer of neutrons by matching the phase space distribution at the sample to the phase space distribution at a position close to the moderator surface, while rejecting as many neutrons as possible from outside

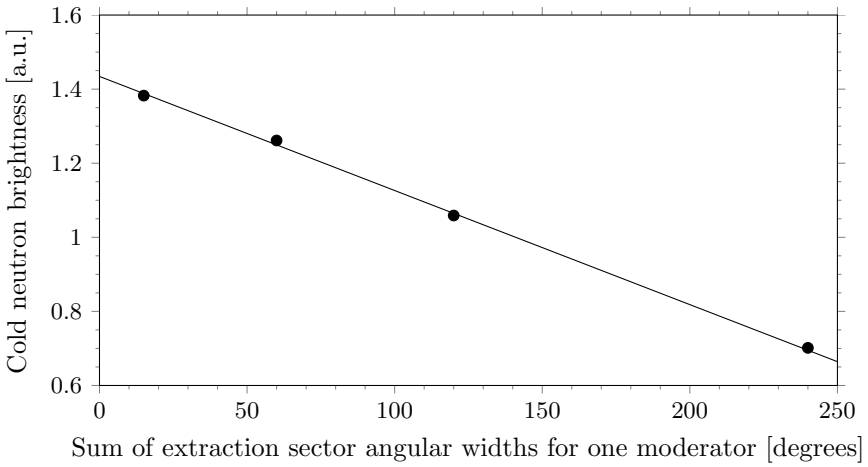

Figure 3.19: Calculated dependence of cold neutron brightness on total opening angle around a cold moderator.

the desired phase space volume. This requires high quality reflective optics, and careful design of the geometry of the optical system and the shielding. The beam extraction layout and its engineering design concepts are described in Section 3.3.9. This section discusses aspects of the layout related to openings in the reflector for optimal beam extraction, and to the use of shutters.

Viewing angles from the moderators

The amount of reflector around the moderator affects its neutronic performance; any reduction in the amount of beryllium will negatively affect neutronic performance. In the ESS baseline configuration, the reflector material around each moderator has two 60 degree openings which allow for the extraction of neutrons to the guides and instruments. The brightness of the moderator is a function of the total angular size of its openings. Figure 3.19 shows the brightness calculated from the moderator surface for different angular values of the openings. The brightness decreases with increasing angular values, and the effect is only slightly dependent of the number of openings; that is, the brightness calculated with one opening of 120 degrees is nearly the same as that calculated with two openings of 60 degrees each. The brightness can be increased by reducing the beam extraction angular range, in a way similar to common practice in reactors (i.e., with openings of 10 degrees to 15 degrees per moderator). This opens the opportunity for an innovative ESS beam extraction layout. Instead of fixed beamline positions uniformly covering about 240 degrees, as is the current practice at pulsed spallation sources, a flexible grid will be used of possible beamline positions every 5 degrees, which would be able to accommodate changing instrumentation over the lifetime of the facility. This will make it possible to group beamlines depending on instrumental needs, with minimal angular spread. By using this approach, it will be possible, for instance, to reach a brightness of 15% to 20% above baseline with 22 operational beamlines. This approach would create the option to close one opening in the beryllium reflector in the moderator plug, when the corresponding beam ports were not being used for a period of time.

Experience from PSI on shutter design

The layout of the shutters is discussed in Section 3.3.9. In general, two different solutions are available for closing the primary neutron beam ports at neutron sources. The first approach uses a so-called high energy shutter system, in which a strong shutter (more than 1.5 m thick) is incorporated into the biological shielding. Such a system allows access at any time to all components of the beam line. The second concept is based on a “light” shutter solution. In this approach, the light shutter is positioned at the end of the biological shielding where it provides shielding from secondary radiation (mainly activation) when the neutron source is switched off. Such a light shutter system is installed on various beamlines at the spallation source SINQ. Three days after the SINQ shutdown in 2012, gamma and neutron measurements were performed to check the radiation levels with closed and opened light shutter. The measured dose

Figure 3.20: Neutron and gamma dose rate measurement configuration at SINQ. Measurements were performed three days after the shutdown.

rates were 0.5 μSv hr^{-1} with a closed shutter and 450 μSv hr^{-1} with an open shutter. The light shutter itself is a 30 cm thick steel block positioned about 6 m away from the SINQ target. Figure 3.20 shows the measurement setup employed at one of the SINQ beamlines.

In addition, ESS has also performed simulations to analyse the shielding behaviour of a light shutter during normal neutron production. As a first step, simulations assumed the use of a simple, 0.5 m thick steel block as a shutter. Using the ESS spectrum as input, this shutter was able to reduce the neutron dose rate by a factor of 500. Optimisation of the system with further simulations increased this by a factor of two, without any loss of gamma shielding ability. The optimised solution was found to be a layered block of borated epoxy and tungsten.

3.2.7 Neutronic support to engineering design

Within the framework of neutronics to engineering activities, detailed assessment of heat deposition, gas production, and radiation damage throughout the target station monolith was performed. Selected findings are presented here. The results are normalised to the baseline time average beam current of 2 mA and peak current density of 47 μA cm^{-2}. Divergence of the beam was not taken into account since the proton beam profile at the accelerator-to-target interface has not been fixed yet.

The prompt heat deposited in various parts of the target station monolith is summarised in Table 3.13. The peak heat deposition in the PBW is an average over the central part of the structure. Total production

Component	**Materials**	**Total** [kW]	**Peak value** [W cm^{-3}]
Target	Tungsten, stainless steel, helium	2800	3100
Target vessel	Stainless steel	62	940
Target shaft	Stainless steel	53	11
Cold moderators	Para-hydrogen, aluminium	19	19
Water moderators	Water, aluminium	51	29
Inner reflector	Beryllium, aluminium	300	21
Outer reflector	Stainless steel	840	18
Proton beam window plug	Aluminium, stainless steel, helium	2.9	34
Neutron beam extraction	Stainless steel	7.5	0.014
Shielding & monolith structure	Iron, helium	290	0.82

Table 3.13: Prompt heat deposition in various parts of the target station monolith.

Component	Gas production [litres/GW-day]					
	^{1}H	^{2}H	^{3}H	^{3}He	^{4}He	H+He total
Target	82	18	8.6	1.7	17	130
Target vessel	3.4	0.39	0.069	0.061	0.70	4.6
Target shaft	2.6	0.33	0.054	0.053	0.53	3.5
Cold moderators	0.57	28	0.0058	0.00048	0.094	29
Water moderators	1.9	23	0.044	0.0068	1.0	26
Inner reflector	5.6	1.6	2.8	0.31	120	130
Outer reflector	29	3.4	0.48	0.42	6.1	39
Proton beam window plug	0.079	0.012	0.0047	0.0049	0.021	0.12
Neutron beam extraction	0.048	0.0052	0.00069	0.00052	0.010	0.065
Shielding & monolith structure	7.7	1.1	0.16	0.15	1.7	11

Table 3.14: Total gas production in various parts of the target station monolith.

Component	Stainless steel, iron	Aluminium	Tungsten
Target	0.58		0.90
Target vessel	1.2		
Target shaft	0.081		
Cold moderators		8.9	
Water moderators		19	
Inner reflector		17	
Outer reflector	3.6		
Proton beam window plug	0.0072	2.7	
Neutron beam extraction	0.0020		
Shielding & monolith structure	0.15		

Table 3.15: Peak values of the number of displacements per atom (dpa) per GW-day in various parts of the target station monolith.

of light gases (hydrogen and helium) within the target station monolith is shown in Table 3.14. The values are normalised to 1 GW-day of proton beam energy, which is equivalent to 200 days of operation at 5 MW power, and then converted to litres (1 mol = 22.4 litres) for convenience. Note that part of the hydrogen produced will be bound within various compounds. Only production data are given; depletion due to intra-hydrogen and intra-helium transitions is not taken into account. Radiation-induced damage of the main structural materials (stainless steel and aluminium), as well as of tungsten, is given in Table 3.15, again normalised to 1 GW-day of proton beam energy. These data, as well as gas production in steel and tungsten, were evaluated on the basis of cross sections provided by KIT [342].

3.2.8 Development of optimisation tools

Besides the main task of the neutronic design of the target-moderator-reflector system, as described above, some effort is being devoted to development of tools based on the available transport codes, which will be important for future work in the construction phase, in particular for cross-functional activities with instrument design experts. On the one hand, considerable effort has been dedicated to the coupling of the Monte Carlo transport code MCNPX with the ray-tracing code McStas, mainly for use in applications to beam extraction, but also with an eye to future work on advanced moderators. On the other hand, a more elaborated figure of merit could be beneficial, for instance, a more detailed specification of the range of wavelengths that instruments may need, and of the ratio of thermal to cold neutrons required by the experiments. Recent progress in these areas is reported below.

Interfacing MCNPX and McStas for simulations of neutron transport

Simulations of the target-moderator-reflector system at spallation sources are conventionally carried out using MCNPX [328], whereas simulations of neutron transport from the moderator and the instrument response are performed by neutron ray tracing codes such as McStas [343, 344]. The coupling between the two simulation suites typically consists of providing analytical fits of MCNPX neutron spectra to McStas. This method is generally successful but has limitations, for example, it does not allow for re-entry of neutrons into the MCNPX regime. These shortcomings can be resolved by interfacing MCNPX and McStas by direct or indirect coupling [345]. Some of the coupling options ESS has implemented are briefly described below.

At present, the tally option is the default approach. It is based on fitting MCNPX neutron distributions such as those at the moderator surface, making it possible to model neutron states on a statistical basis. In short, a detailed MCNPX simulation of a target, reflector and moderator system at a given neutron facility is performed and the resulting neutron fluxes and spectra at the moderator surface are approximated by simple distributions. McStas then "draws" random neutron states from these distributions. One challenge posed by using this approach is correctly describing the correlations between the parameters constituting a neutron state. For example, non-trivial phase space correlations could exist, such as those between the neutron location and momentum at the moderator surface. Quantifying correlations is thus an important part of employing this method. The tally method has the advantage that the time consuming MCNPX simulation step is decoupled from McStas and therefore only needs to be carried out once. This makes subsequent McStas simulations faster and therefore this method is very useful for applications such as instrument design.

A second option is to use the MCNPX source surface write/read (SSW/SSR) feature that permits a user to stop a simulation at a given surface, and restart it later. A new interpreter has been developed, allowing McStas to run based on SSW/SSR file input, and to produce a SSW/SSR output once the McStas simulation is complete [345]. The main advantage of this approach is that MCNPX runs can be based on the SSW/SSR input files. In this way, one can first do a MCNPX simulation, for example, of thermal neutron moderation. Once the neutrons enter the beam extraction region, the neutron states are handed to the SSW/SSR interface, and based on this input, a McStas simulation is carried out, for example, a simulation involving mirrors and coherent scattering (which is not possible in MCNPX). The scattered and/or the non-scattered neutrons can then be handed back to MCNPX using the same interface. One example application of the SSW/SSR interface is shown in Figure 3.21, where the cold neutrons emitted from the moderator side surface are shown.

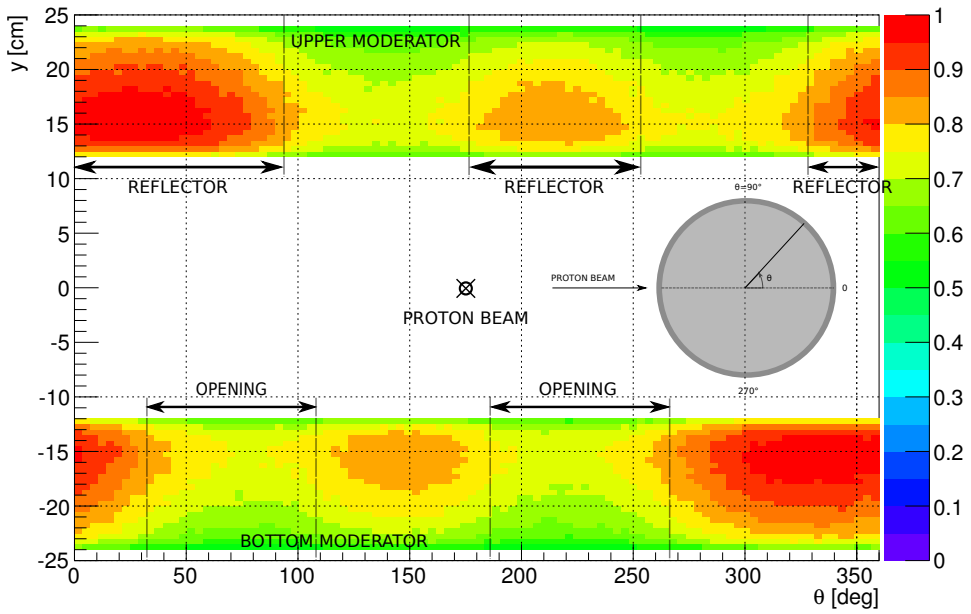

Figure 3.21: Map of cold neutrons emitted from the surface of the moderator at different angles and longitudinal positions.

The supermirror option is the third possibility. This option is based on modifying the MCNPX source code [346,347]. In this case, however, the idea is not to launch a McStas simulation from within MCNPX, but rather to extend MCNPX with functionality inspired by McStas. The most important shortcoming of using MCNPX for cold neutron applications is the lack of coherent scattering. Coherent scattering can be described as a neutron wave interacting with a lattice, while MCNPX only addresses scattering on single particles. The process gives rise to wavelength-dependent reflection and can for present purposes be well approximated by the following expression:

$$R = \begin{cases} R_0 \times \left(1 - \tanh \frac{(Q-m)Q_c}{W}\right) \times (1 - \alpha(Q - Q_c))/2 & \text{for } Q > Q_c, \\ R_0 & \text{otherwise} \end{cases} \tag{3.2}$$

where Q is the scattering vector, Q_c is the critical scattering vector, R_0 is the low angle reflectivity constant, W is the width of supermirror cut-off, α is the reflectivity slope, and m is the m-value of the material.

In order to validate the recently developed software, an experiment was performed at the BOA beamline at PSI to demonstrate how the MCNPX-McStas interface can be used to analyse an experimental setup. Other activities planned for the future include 'cradle-to-grave' simulations of BOA, starting with an energetic proton bunch reaching the target and concluding with cold neutrons giving signals on simulated detectors in the instrumental hall. It is foreseen that this cradle-to-grave setup will be useful for such purposes as redesigning or re-optimising the moderator shape, since it will provide the means to see the effects of alternative geometries directly on neutron distributions at the sample position, without relying on questionable assumptions such as fits taking into account only parts of the neutron phase space.

Extension of the figure of merit

The figure of merit has been extended, based on a survey of the broad user community that was conducted among neutron instrument scientists and beam users at the Paul Scherrer Institut. A number of figures of merit that emphasise different interests can be optimised simultaneously [348].

The moderator performance is expressed numerically by a set of quantities, representing the shape of the neutron flux spectrum extracted from the surface of the moderator. Such a numerical representation is critical when a programming automation of the optimisation process is used, in order to derive at each optimisation step the value for the figure of merit. Figure 3.22 shows a theoretical bispectral spectrum that is composed of two separate Maxwellian distributions. The first Maxwellian distribution, Φ_{th}, simulates the thermal neutron spectrum, and the second, Φ_c, simulates the cold one. Each of these distributions is characterised by the position of its peak, λ^p_{th} and λ^p_c, by the value of the neutron flux at the peak, $\Phi(\lambda^p_{th})$ and $\Phi(\lambda^p_c)$, by the position of the crossing point between thermal and cold peaks, λ_x, and by the value of the neutron flux at the crossing point, $\Phi(\lambda_x)$.

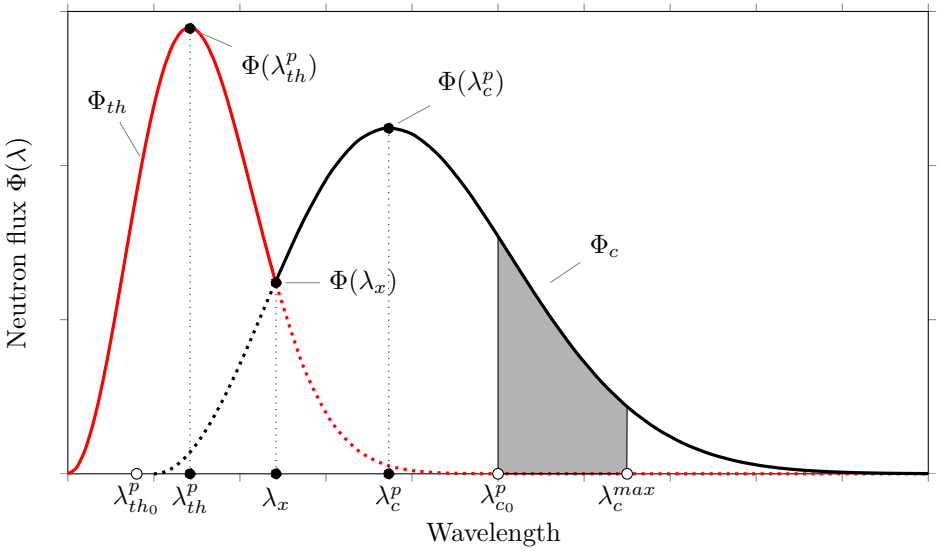

Figure 3.22: Graphical description of the bispectral spectrum.

In the optimisation process, the positions and peak values of thermal ($\Phi(\lambda^p_{th})$) and cold ($\Phi(\lambda^p_c)$) fluxes are extracted from the neutron spectrum estimated by a point detector tally with a solid viewing angle limited to the side surface of the moderator of 12 cm × 24 cm. The integral neutron fluxes Φ_{th_I} and Φ_{c_I} of the thermal $[\lambda^p_{th_0}, \lambda^{\max}_{th}]$ and cold $[\lambda^p_{c_0}, \lambda^{\max}_{c}]$ parts of the spectrum are compared to optimisation requirements. The optimisation framework follows the procedure described in a 2010 article discussing the design of a solid rotating target [349], although new expressions for the figure of merit are implemented, which allow both thermal and cold neutron fluxes to be simultaneously maximised. In particular:

1. Thermal performance of the moderator can be evaluated by maximising neutron flux in the thermal part of the spectrum by setting the figure of merit to be:
$$FoM_1 \;=\; \Phi(\lambda^p_{th}).$$
2. Similarly, cold performance of the moderator can be studied by maximising the cold neutron flux:
$$FoM_2 \;=\; \Phi(\lambda^p_{c}).$$
3. Bispectral performance of the moderator can be optimised by establishing some ratio between the peak values of thermal and cold neutron flux, for example by requiring these values to be equal and maximal simultaneously:
$$FoM_3 \;=\; \min(\Phi(\lambda^p_{th}), \Phi(\lambda^p_{c})).$$
4. Assuming effective ranges of the measurements as required by the instruments, integral values of thermal and cold neutron flux can also be maximised while keeping them equal with the following figure of merit:
$$FoM_4 \;=\; \min(\Phi_{th_I}, \Phi_{c_I}).$$

In this last expression the thermal neutron flux is given by

$$\begin{aligned} \Phi_{th_I} \quad &= \quad \int_{1.4\ \mathring{\mathrm{A}}}^{\lambda_{\mathrm{x}}} \Phi(\lambda)\, d\lambda \\ \text{where} \qquad \Phi(\lambda_{\mathrm{x}}) \quad &= \quad \min_{\lambda \in [\lambda^p_{th},\, \lambda^p_c]} \Phi(\lambda) \end{aligned} \tag{3.3}$$

while the cold neutron flux is

$$\Phi_{c_I} = \int_{4.1\ \mathring{\mathrm{A}}}^{6\ \mathring{\mathrm{A}}} \Phi(\lambda)\, d\lambda \tag{3.4}$$

This approach has been used successfully for the optimisation of bispectral extraction on the basis of a box-shaped moderator model, similar to that of the 2003 design [348]. In such a model, the bispectral moderator contains two separated moderating materials, liquid cold 100% para-H_2 at 20 K and room temperature H_2O, side-by-side in the common 12 cm × 12 cm × 24 cm moderator volume. Target geometry, bottom moderator, and reflector are assumed to be the same as in the previous sections. The model can be used with up to 30 parameters. The important ones are the relative offset of the moderator centre on (y, z) and the position of the hydrogen/water separator with respect to the middle of the moderator box [348].

3.3 Monolith and plugs

3.3.1 Monolith

The design of the monolith is based on the general design, dimensions and handling philosophies of the target station baseline design [339]. The main purpose of the monolith is to provide sufficient shielding to reduce neutron background in the experimental hall and to allow personnel access close to the monolith wall. Besides the shielding function, the monolith needs to be designed to allow neutron extraction to the instruments and handling of components located inside the monolith. Shielding of high-energy neutrons requires high-density material. Early studies showed that steel is the most cost effective shielding material for the target shielding monolith [350]. Calculations indicate that more than 7 m of steel shielding will

be necessary in the proton beam forward direction [300]. Nevertheless, for simplicity and the requirement for the instruments to allow a first chopper position as close to 6 m from the moderator as possible, it was decided to design the monolith fixed structure with a constant radius of 6 m. The neutron beam line shielding outside of the monolith boundary will provide the additional necessary shielding. Figure 3.23 shows the general layout of the monolith.

The monolith can be subdivided into different areas with respect to design, choice of material, power deposition and manufacturing tolerances. The handling of components internal to the monolith, during exchange or maintenance, is described in Section 3.5. Minimising the costs of material and manufacturing is important in light of the very large volumes in question, especially of the bulk steel shielding. Access to components should be facilitated in accordance with their expected lifetime and reliability. Alignment of critical components must be achievable in a robust manner.

These design objectives are met through the following key features. Access to all components and shielding blocks that potentially can fail will be assured by design. The design facilitates exchange for components with limited lifetimes. On the other hand, for parts of the monolith that are unlikely to fail, the design may require longer maintenance periods for exchange or repair, in return for a simpler and more cost effective design. Water cooled shielding blocks that do not need to be moved for regular handling procedures will have redundant cooling channels where justified. A potential leaking channel can then be shut off and repair can be postponed to a suitable long maintenance period. A drain pipe connected to the lowest point of the monolith is installed for drainage of eventual spills and potential condensate. A base plate, manufactured with high accuracy, will allow installation of neutron beam guide inserts with a minimum of alignment features. It also offers the possibility to optimise the monolith with respect to choice of shielding type within different sections in order to reduce costs.

While the primary function of the monolith is to provide adequate shielding, it contains eight key components of the target station, which are described below, and shown in Figure 3.23. The rotating target system with long shaft is located near the central part of the monolith, while the drive, seal and bearing units are positioned on top of the monolith, reaching into the connection cells while still being part of the monolith helium system. The moderator-reflector (MR) plug, consisting of cold and thermal moderators as well as the inner and outer reflector, constitutes the central part of the monolith. It is attached to a backpack-shielding block, which allows the plug to be handled. The proton beam window (PBW), located upstream of the proton beam relative to the target, separates the high vacuum of the accelerator from the helium at atmospheric pressure inside the monolith. A separate helium valve plug will make the removal and exchange of the proton beam window possible, while preserving most of the helium atmosphere of the monolith. A proton beam diagnostic plug will house several diagnostic devices

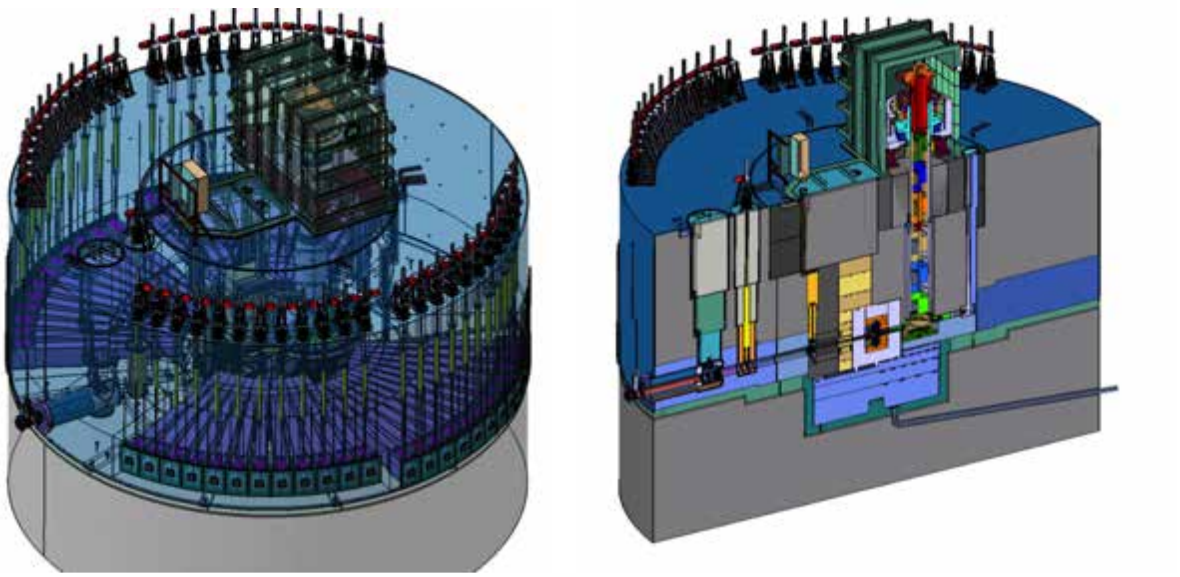

Figure 3.23: Monolith general layout. Left: 3D perspective view. Right: Side view along the vertical plane of the incident proton beam.

to monitor the proton beam footprints on the PBW and on the target as well as at the location of the diagnostic plug. Potentially, a target diagnostic plug will be introduced for online monitoring of the rotating target downstream of the proton beam, as well.

The monolith shielding design provides for 48 possible beam port positions arranged in four beam extraction sectors of 60 degrees each, with 5 degree angular separation between neighbouring beamline positions. Any of these positions may either be closed by a shielding block or opened as a beamline by replacing the shielding block by a neutron beam guide insert (NBGI). The large flexibility offered by the 5-degree grid of possible beam line positions will allow for optimally positioning the open beamlines during the whole lifetime of the facility. For the suite of 22 instruments funded within the ESS construction phase, this implies using 5 degrees of separation for as many instruments as feasible in order to maximise neutron flux for all instruments by minimising the volume of reflector removed for beam extraction purposes and placing instruments that need more lateral space at 10 or 15 degrees from the neighbouring open beamlines. Light shutters and associated drive units will be integrated into the monolith [339]. The shutters will open and close the neutron beam ports to block gamma radiation from the target and the moderator-reflector plug, allowing human access to beamline components outside the monolith when beam is off.

Liner

The liner system confines the helium atmosphere, at a slight under-pressure, inside the monolith. Figure 3.24 shows its general layout. It represents one of the safety-relevant barriers of the ESS target station confinement barrier system, as discussed in Section 3.1.2, requiring the best possible helium tightness. On the other hand, some components inside the monolith need regular and frequent handling. The liner system consists of a base plate, including a cup-like structure supporting the inner lower cooled shielding; the cylindrical wall of the monolith; and the top plate, including covers for frequent and scheduled access as well as a cover to access water-cooled shielding blocks that are designed for the lifetime of the facility but still need to be accessible in case of unexpected damage. The base plate consists of several segments to facilitate manufacturing and transportation to the site. These segments will be placed on the lower shielding, levelled and grouted in place. Finally, the gaps between the segments will be welded together to create a tight seal. This seal weld is not intended to transfer loads.

While the lower part of the liner system is a fully welded structure, the covers on the top plate are either welded for higher helium tightness for the less frequently accessed components, or equipped with

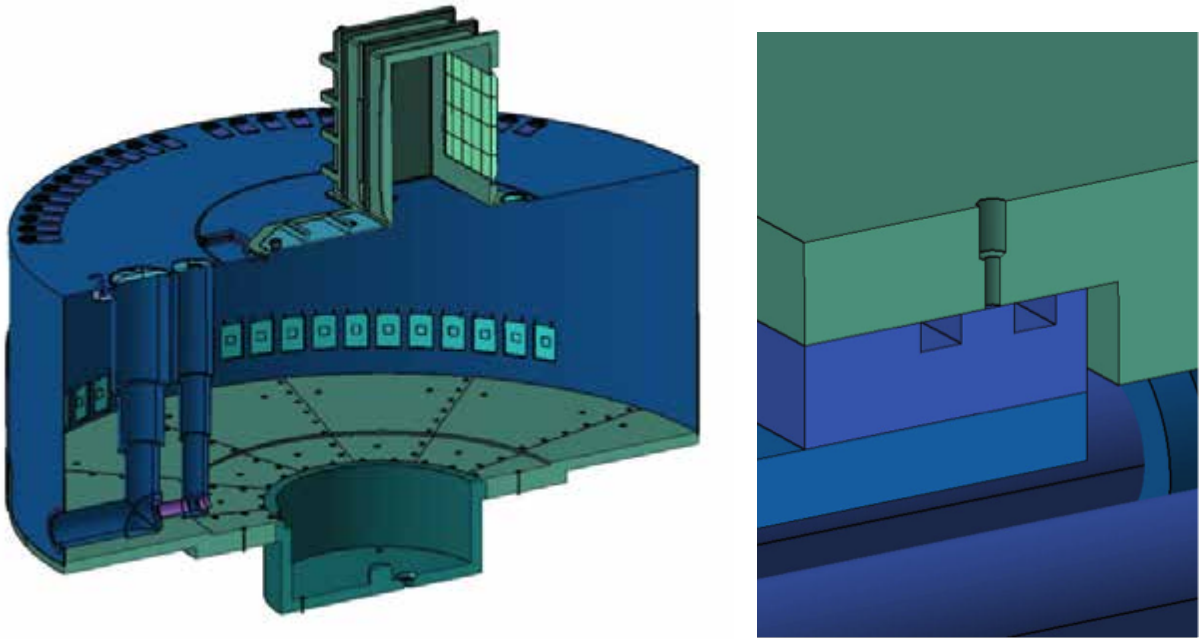

Figure 3.24: The general layout of the liner system (left) and generic double seal design with monitored interstitial gap for removable covers (right).

a double seal with monitored interstitial space to access the more frequently exchangeable components, as shown in Figure 3.24. In addition to the liner system, the confinement barrier will be completed by a fast-acting valve in the proton beamline outside the monolith, as well as by neutron beam windows allowing the neutrons to leave the confinement barrier towards the instruments. All liner components will be manufactured from stainless steel and will be welded together on site. Special care will be taken to monitor the weld quality. The total volume of the liner system will be 543 m^3 most of which is filled with shielding and components. The gaps between components making up the free volume will amount to about 34 m^3. This void volume may be increased if found necessary to cope with a target or moderator shell rupture and the consequent pressure build-up in the atmosphere within the monolith.

The target drive, seal and bearing system extends over the top plate, and is covered by a housing which is a part of the liner confinement barrier. In order to allow gas evacuation of the monolith before opening any lid or cover for handling components, the liner system will be designed for vacuum. This is accomplished by ribs on the covers as well as resting points on the top of the shielding to allow the top plate to touch inner shielding blocks during evacuated conditions.

Monolith shielding blocks and internal structure

The monolith shielding will be composed of the lower permanent shielding, the base plate, neutron beamline shielding block segments, lower semi-permanent shielding, water-cooled inner shielding blocks, removable shielding blocks and passive (helium-cooled) shielding blocks. The lower permanent shielding will consist of low tolerance and low quality steel embedded in high-density grout, ensuring low cost. Cast blocks made from pre-irradiated material can potentially be used for this shielding [351].

The base plate will consist of 13 parts: 12 segments and one cup-like centre piece. Each segment will be machined to tolerances up to ±0.25 mm in the workshop. All segments will be assembled on site, levelled and adjusted using a laser tracker. Bolts will be used to adjust the height of each segment individually. After all segments are in place and adjusted, the space underneath will be filled with low shrink grout. The segments will be bolted together. The gap between adjacent segments will be welded to achieve a helium tight layer. The hole in the centre of the base plate (diameter 4 m) will be closed with a cup-like, thick-walled vessel to carry the centre shielding blocks that need active water-cooled shielding. The lower permanent shielding will be far enough from the spallation centre not to require active cooling.

The neutron beamline shielding blocks will be placed directly on top of the levelled smooth surface of the base plate. The neutron beam line shielding blocks themselves will be manufactured to high tolerances and thus form the geometric basis for the guide-insert alignment. Despite tight tolerances required to avoid radiation streaming, the surfaces will be stepped as much as is geometrically possible. Due to seismic requirements, these blocks will most likely be bolted to the base plate. Due to the high number of neutron beam lines in combination with the spatial requirements of the large rotating target, limited space is available for supporting the structural loads of the shielding. The major load is supported through the outer shielding ring with radius larger than 2.7 m. In the area of the neutron beamlines, the small wedges between the openings for the inserts will be used to support the loads. Figure 3.25 illustrates the sequence of the shielding assembly.

Two approaches are used for the inner water-cooled shielding. The blocks that will not be removed during regular handling will be equipped with redundant water cooling channels. For the remaining blocks, only a single channel is foreseen. Cooling channels inside the shielding blocks consist of grooves inside the single layers of each block. Depending on the specific heat load, the layers are thinner in areas with high heat load and larger in areas in which the specific heat load is lower. Figure 3.25 shows as an example the water-cooled block underneath the MR plug. The inlet water supply will be at a pressure of about 1.0 MPa with a temperature of 20°C to 30°C. The maximum global block temperature is about 50°C, with some allowance for very local regions of slightly higher temperature.

3.3.2 Target design requirements and configuration

The target wheel will consist of 33 sectors, to ensure mechanical integrity of the target vessel while resulting in minimal loss of neutronic performance. Proton beam pulses will be synchronised with the target rotation speed. The number of sectors has been chosen in order to have an arc length for each sector large enough to accommodate the beam footprint, given the 2.5 m diameter of the wheel. The odd number of sectors also will eliminate direct line-of-sight via the helium cooling channels in the event that a desynchronised

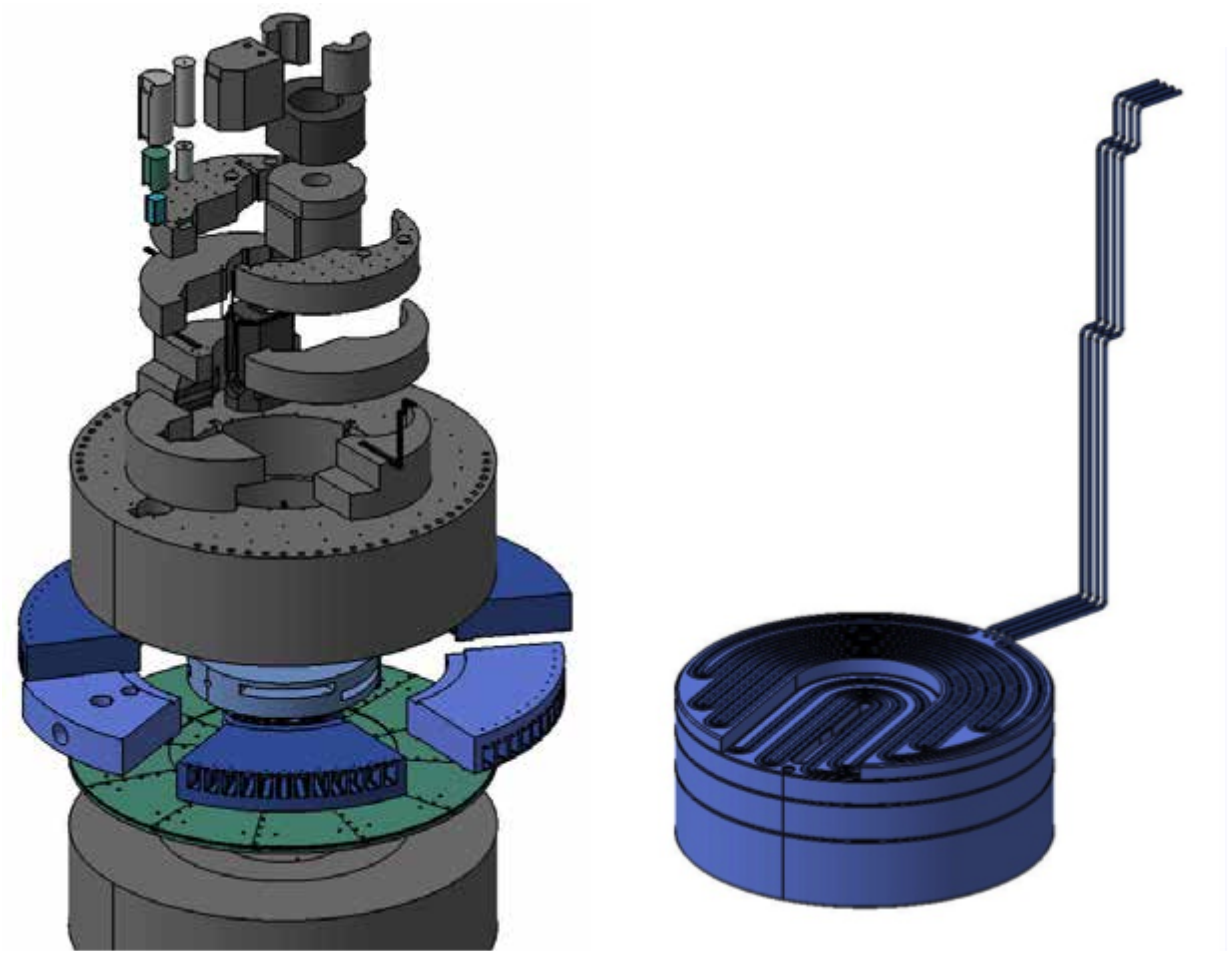

Figure 3.25: Left: Exploded view of the bulk shielding assembly. Right: The water-cooled shielding block.

proton pulse hits the target in between two sectors. Channels on the side, and gaps above and below the tungsten blocks have been designed to provide adequate cooling through helium flow. The gaps above and below the tungsten blocks also will prevent direct contact between the tungsten slabs and the steel vessel, which would lead to excessive heating of the steel at the points of contact.

Several factors have been taken into account in the arrangement of the spallation material. The proton beam will deposit most of its heat in the region near the outer rim of the target, mainly in the first 10 cm, while the coolant (helium) will be brought through the shaft from the back of the target. As previously discussed, the beam and the target will be synchronised, so straight channels will be used to move the coolant towards the outer rim of the target where the spallation material is located. The structural material will be kept at temperatures below 500°C, in order to avoid significant creep behaviour. The maximum temperature of the spallation material will be kept as low as possible, and the surfaces of the tungsten slabs will not exceed 500°C to avoid oxidation of the tungsten in the event that air infiltrates the target vessel. The beam entrance window (BEW) will be as thin as possible to minimise proton loss at the point of beam entry into the target material. Therefore, the BEW also will require substantial cooling so that its local maximum temperature can be kept low enough during beam operation.

The tungsten slabs will be arranged in three groups. The first group of tungsten slabs will be located at the outermost radial part of the target wheel, where the highest heat load is expected. It will consist of six slightly curved slabs, which will cover the area facing the two moderators. The tungsten slabs in this group will be between 12 and 14 mm thick, and will be separated from one another by 2.5 mm wide cooling channels. The second group of tungsten slabs will be located just interior to those of the first group. It will consist of four slabs, which will form the transition area between the outer rim portion of the target wheel with highest heat load, and the inner rim portion with negligible heat load. The tungsten slabs in

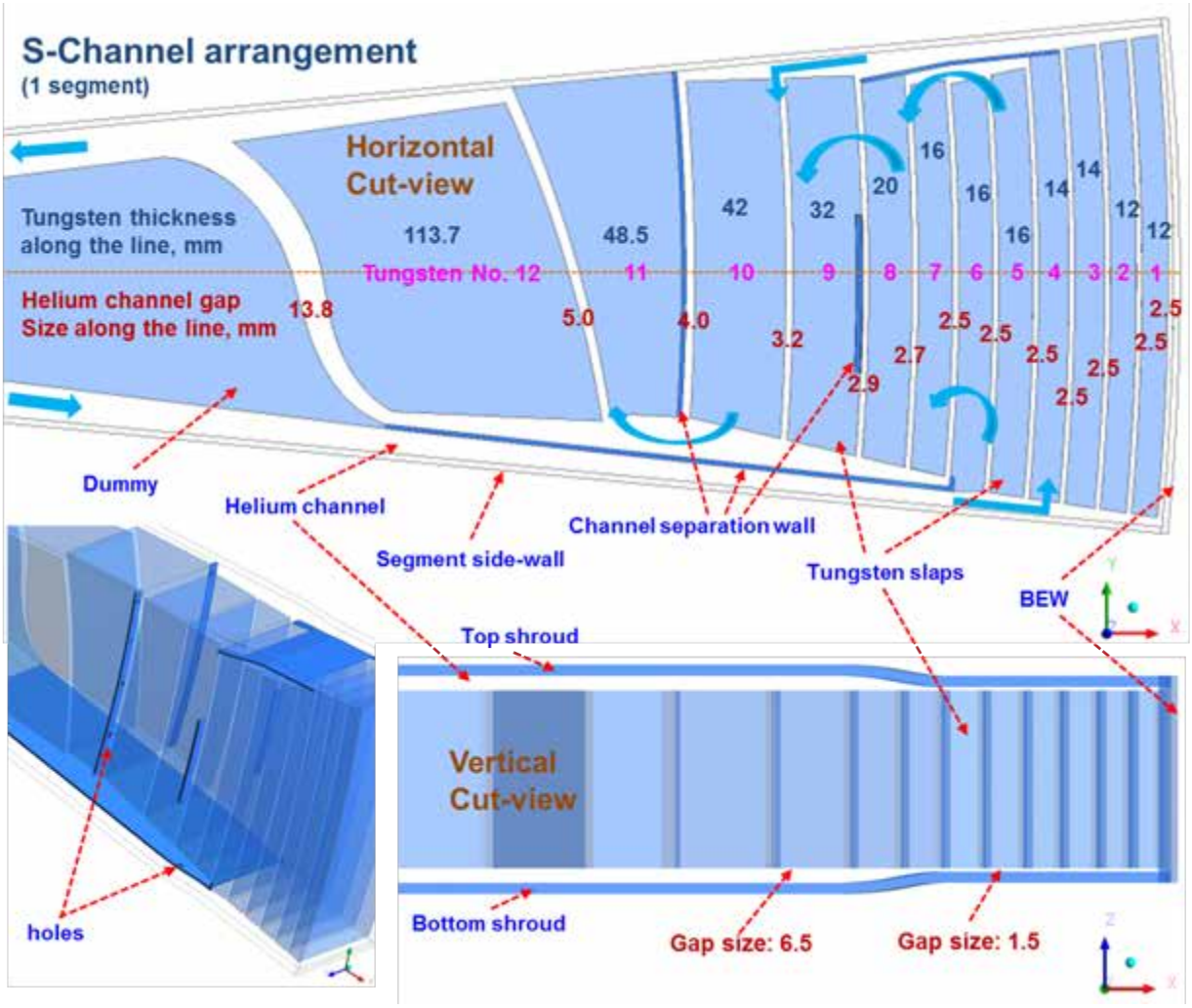

Figure 3.26: Spallation material arrangement. The helium flow follows a serpentine pattern through the tungsten slabs, guided by the channel separation walls. Blue arrows indicate direction of helium flow.

this second group will have rectangular cross sections with thicknesses between 14 and 32 mm. The third group of tungsten slabs will be located at the innermost radial part of the target wheel. It will consist of three thick slabs with rectangular cross sections. These three groups inside each of the 33 sectors will be cooled in series, using helium flow entering the target wheel, with mass flux of 3 kg s^{-1} total (or 91 g s^{-1} per sector) and inlet temperature of 25°C. The global arrangement of the tungsten slabs in one of the 33 target wheel sectors is shown in Figure 3.26. In the so-called "S-channel" arrangement, the coolant will flow in a serpentine pattern through the tungsten slabs, as shown in more detail in the figure.

As described in the following sections, the target material and flow configuration presented here ensures that the front part of the target, which will be exposed to the highest load, will be properly cooled by the cold helium flow, which will enter the target wheel area from the shaft. As a consequence, the peak temperature of the tungsten slabs will be kept below 500°C. Temperatures in the BEW will be held below 200°C during normal operation. The thermo-mechanical analyses presented in this section are based on the parabolic proton beam profile with peak current density of 64 μA cm^{-2} unless otherwise specified [339]. This peak current density value is conservative, compared to the value of 52 μA cm^{-2} that is derived from beam dynamics calculations in Section 4.7, for the beam footprint shown in Figure 4.86.

3.3.3 Analysis of spallation material arrangement and behaviour

Thermal-hydraulic simulations were carried out with ANSYS-CFX V14.0 [352]. The estimated Reynolds number is about 2.2×10^5 using the shaft inlet hydraulic diameter as the reference length, and it is about 1.0×10^4 using the equivalent hydraulic diameters of the narrow channels between tungsten slabs. Under these conditions, the turbulent model $k - \omega$ SST was selected for these simulations, based on previous validation work done for similar applications [353].

Steady state flow analysis

For the steady state flow analysis, the simulation domain was one target wheel sector with flow inlet and outlet sections. For the steady state simulations, the target wheel was treated as stationary. The effects of rotation were not taken into account for this analysis, as the angular speed of rotation, 25 rpm, is small compared to the beam pulse length of 2 ms. The time-averaged volumetric heat deposition obtained from particle transport simulations was used for steady state thermo-mechanical simulations [354]. The periodic boundary condition was applied on both sidewalls of the sector under consideration.

Tables 3.16 and 3.17 list the simulated temperatures and amounts of heat generation resulting from the beam interaction. The total heat generation over the whole target wheel is about 2.45 MW. The highest heat density is located in the second tungsten slab. These values correspond to the beam footprint defined in the baseline target design [339]. The simulated pressures and area-averaged temperatures at the inlet and outlet of the helium flow are P_{in} = 374 kPa, P_{out} = 316 kPa, T_{in} = 25.1°C and T_{out} = 181.1°C, respectively. The fluid temperature rises 156°C with a pressure drop of 58 kPa. The maximum temperatures in the beam entrance window and vessel are 175°C and 221°C, respectively. The maximum temperature of tungsten, 462°C, is observed in tungsten slab number 9 in Figure 3.26, a temperature that is below the critical temperature of 500°C.

Figure 3.27 shows the streamlines of the coolant flow, where the flow between the tungsten slabs shows an S-shape. Also shown in Figure 3.27 is the temperature distribution of the wall surfaces. The hot regions correspond to the local flow recirculation between the tungsten slabs and vessel. The holes on the separation walls help to break up the flow circulations. Without these holes, the temperature of the hot regions would increase by about 20°C. Figure 3.28 shows the calculated temperature field along the cut-planes in tungsten and the heat flux at the interface between the tungsten and helium flow, while Figure 3.29 shows the calculated velocity and pressure fields in helium flow. A low temperature zone is observed in Figure 3.28, at the inlet-side of the first tungsten group. This region is cooled by the cold fluid coming directly from the sector inlet. The highest temperature is observed in the second tungsten

Target component	$T_{average}$ [°C]	$T_{minimum}$ [°C]	$T_{maximum}$ [°C]	$P_{nuclear}$ [kW]	$P_{density}$ [W/m^3]
Beam entrance window	91.1	54.2	174.8	0.49	7.39×10^6
Dummy	148.8	59.0	234.0	1.48	5.89×10^5
Walls	132.5	42.6	221.4	1.07	3.34×10^5

Table 3.16: Simulated temperature T, heat generated by nuclear interaction $P_{nuclear}$, and power density $P_{density}$ in target components, assuming an inlet pressure of 374 kPa and a mass flow rate of 3 kg/s.

Param.	**Unit**	**Tungsten block number**											
		1	2	3	4	5	6	7	8	9	10	11	12
T_{ave}	[C]	210	215	224	223	243	275	337	316	347	296	256	276
T_{min}	[C]	61	58	60	60	69	138	195	173	193	187	176	218
T_{max}	[C]	400	411	421	405	413	420	458	436	461	366	303	302
$P_{nuclear}$	[kW]	5.93	6.19	6.91	6.40	6.60	5.85	5.10	5.44	6.89	6.34	4.74	4.70
$P_{density}$	[W/cm^3]	28.0	29.9	29.4	27.9	26.0	23.6	21.7	19.0	15.7	11.8	7.2	3.7

Table 3.17: Simulated temperature T, heat generated by nuclear interaction $P_{nuclear}$, and power density $P_{density}$ in different tungsten blocks, assuming an inlet pressure of 374 kPa and a mass flow rate 3 kg/s.

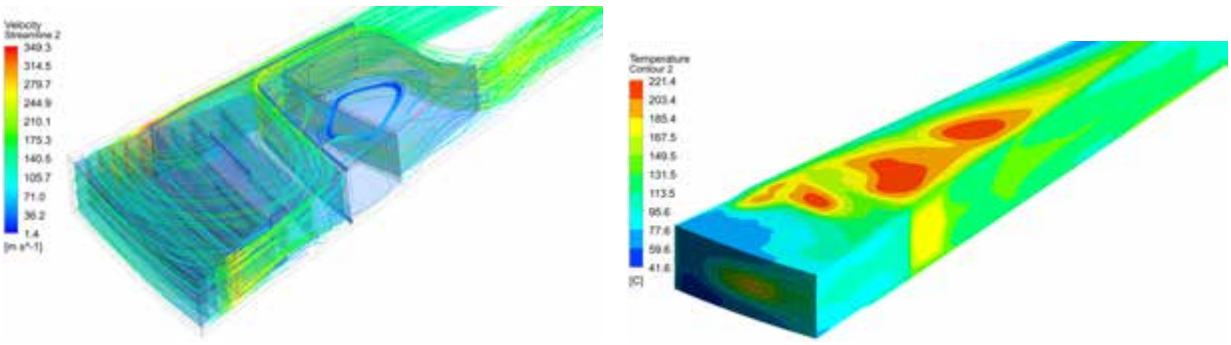

Figure 3.27: Calculated helium flow and temperature distributions in the target vessel and the beam entrance window. Left: Helium velocity streamlines. Right: Temperature.

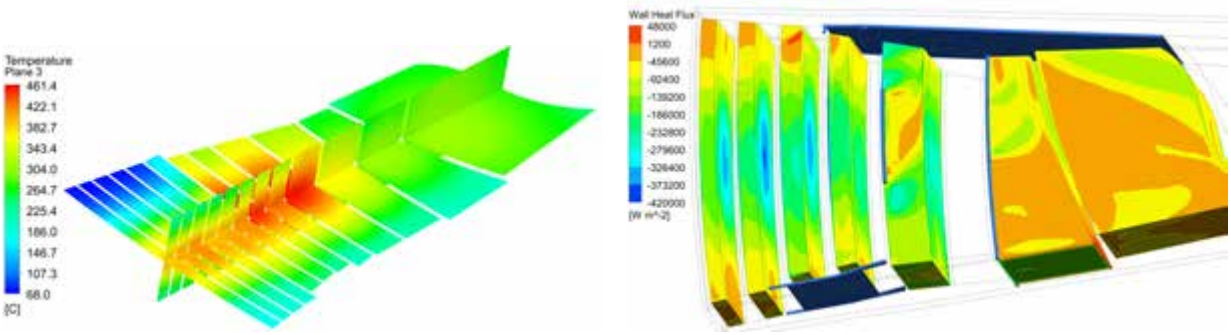

Figure 3.28: The calculated temperature field along the cut-planes in tungsten and the heat flux at the interface between the tungsten and helium flow.

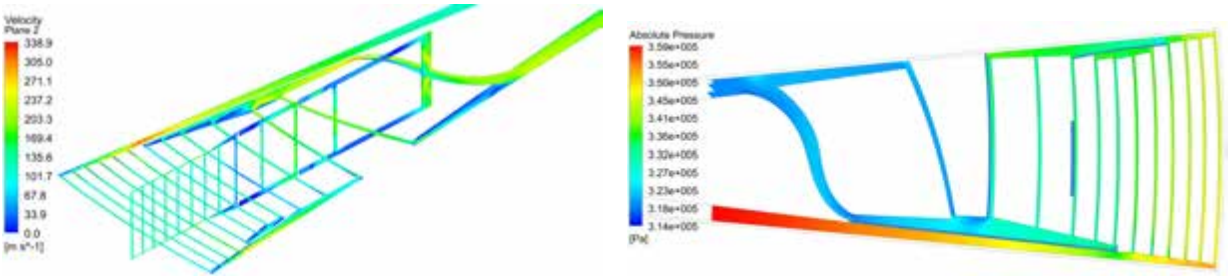

Figure 3.29: The calculated velocity and pressure fields in helium flow.

group, where the coolant flow rate between the tungsten slabs is relatively low, as shown in Figure 3.29. This behaviour arises from the fact that more fluid is drawn into the top and bottom channels as the channel gaps between the vessel and the tungsten blocks enlarge from 1.5 mm to 6.5 mm wide in the second tungsten group. The highest heat flux region is observed on the middle of the channel sidewalls between tungsten slab 2 and 3, as shown in Figure 3.28 (right). The heat flux on the top and bottom walls of the tungsten slabs is much smaller.

Transient flow analysis

For the transient flow analysis simulations, only the transient beam pulses were considered, not taking the effects of wheel rotation into account. The beam frequency used was 14 Hz with a pulse duration of 2.86 ms and a waiting period of 68.57 ms. Decay heat was assumed to be generated during the waiting period, the intensity of which was assumed to be 0.5% of the active value, based on neutronic calculations by the International Fusion Materials Irradiation Facility, IFMIF, in Japan. With an angular speed of rotation of 25.45 rpm, a given sector will be hit by the beam every 2.358 seconds.

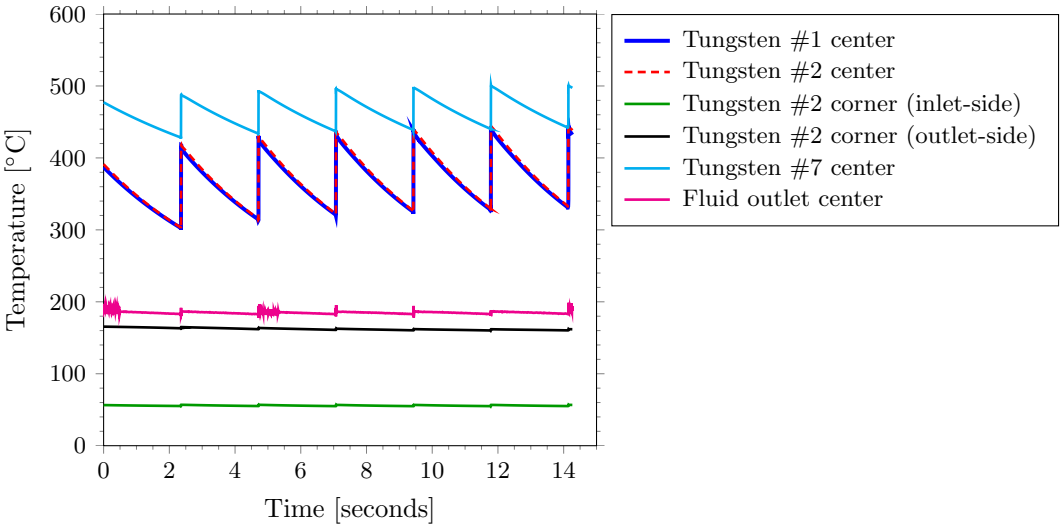

Figure 3.30: Transient temperature for a given sector at different locations.

In the simulation, the steady-state results were used as the initial state. Figure 3.30 shows the transient temperatures over time at chosen locations. After 4 or 5 cycles, the temperature stabilises. The temperatures in the centre of tungsten slabs 1 and 2 are close to each other, while the temperatures at the corners of tungsten slab 2 are much lower. The temperature decreases exponentially during the waiting period and it increases rapidly when the beam is activated. The amplitude of temperature oscillation is about 110°C at the centre of tungsten slab 2, and about 60°C at the centre of tungsten slab 7. Compared to the steady state results, the maximum temperature in tungsten slab 2 is higher by about 50°C. The flow parameters at the channel outlet oscillate after the beginning of the beam pulse. The amplitude of the oscillation is about 10°C for the fluid temperature, 20 m/s for the velocity and 1 kPa for the pressure. The oscillations in pressure are due to fast transient change in gas density, which is caused by powerful pulsed heating.

The three panels in Figure 3.31 show the temperature on the top of the vessel, in the tungsten (central cut-view) and on the BEW at the front surface reconstructed in four sectors, respectively. The beam axis is along the centre line of the first sector from the bottom. The target wheel is assumed to rotate clockwise. The temperatures are calculated at the point in time 14.145 s after an active beam pulse. Therefore, the solid temperature of the first sector from the bottom is the highest, while the temperature of the second

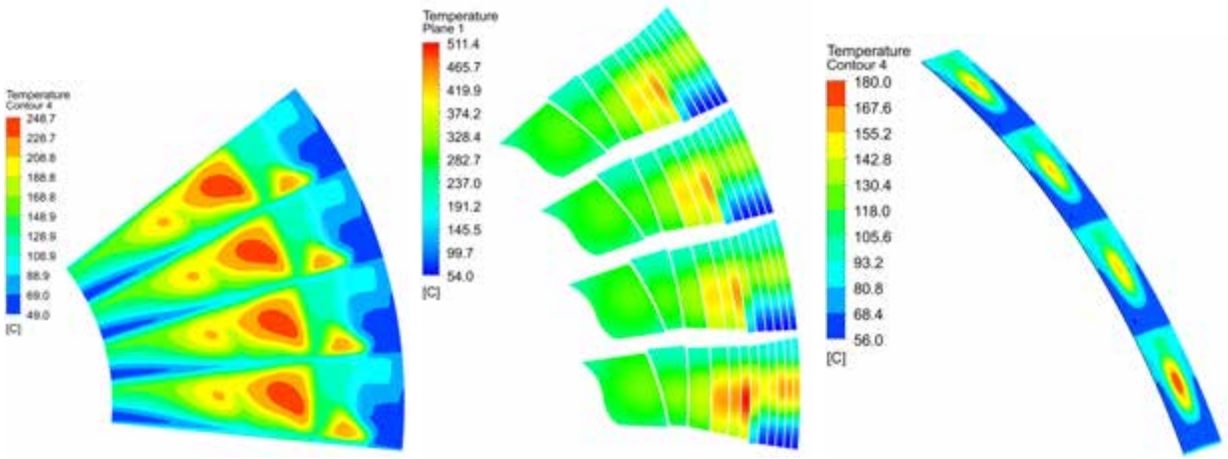

Figure 3.31: Calculated temperature fields. Left: At four sectors in the vessel. Middle: At four sectors in the tungsten. Right: At four sectors on the beam entrance window surface.

sector is the lowest. The peak temperature of the vessel shows less than 1°C variation during one cycle. The peak temperatures of the tungsten and the BEW change by about 110°C and 20°C during one cycle, as previously shown and in agreement with Figure 3.30.

Afterheat analysis

Afterheat (or decay heat) is the residual power in the irradiated tungsten due to the decay of radioactive species, about 47 kW [355]. The results presented below were calculated on the basis of this residual power estimate combined with the heat profile of the proton beam deposition shown in Figure 3.3.3. Heat is transferred between the target and the surrounding shielding, which is actively cooled by water during operation, since about 30% of the 5 MW beam power is deposited there [354]. The target and this shielding are not in direct thermal contact. Therefore, the heat transfer mechanisms that transport the power from the tungsten towards the shielding are: 1) heat conduction though the helium that fills the gap between the target and the shielding, 2) the free convection due to the helium surrounding the target, and 3) the thermal radiation from the vessel surface towards the shielding block surface. The radiation mechanism is ensured to function at all times, while the convection and conduction within the helium are not.

To be conservative, only the radiative heat transfer was taken into account in the first stage of analysis. In the second stage, the heat conduction effect of helium was added for thermal analysis. Finally, the effect

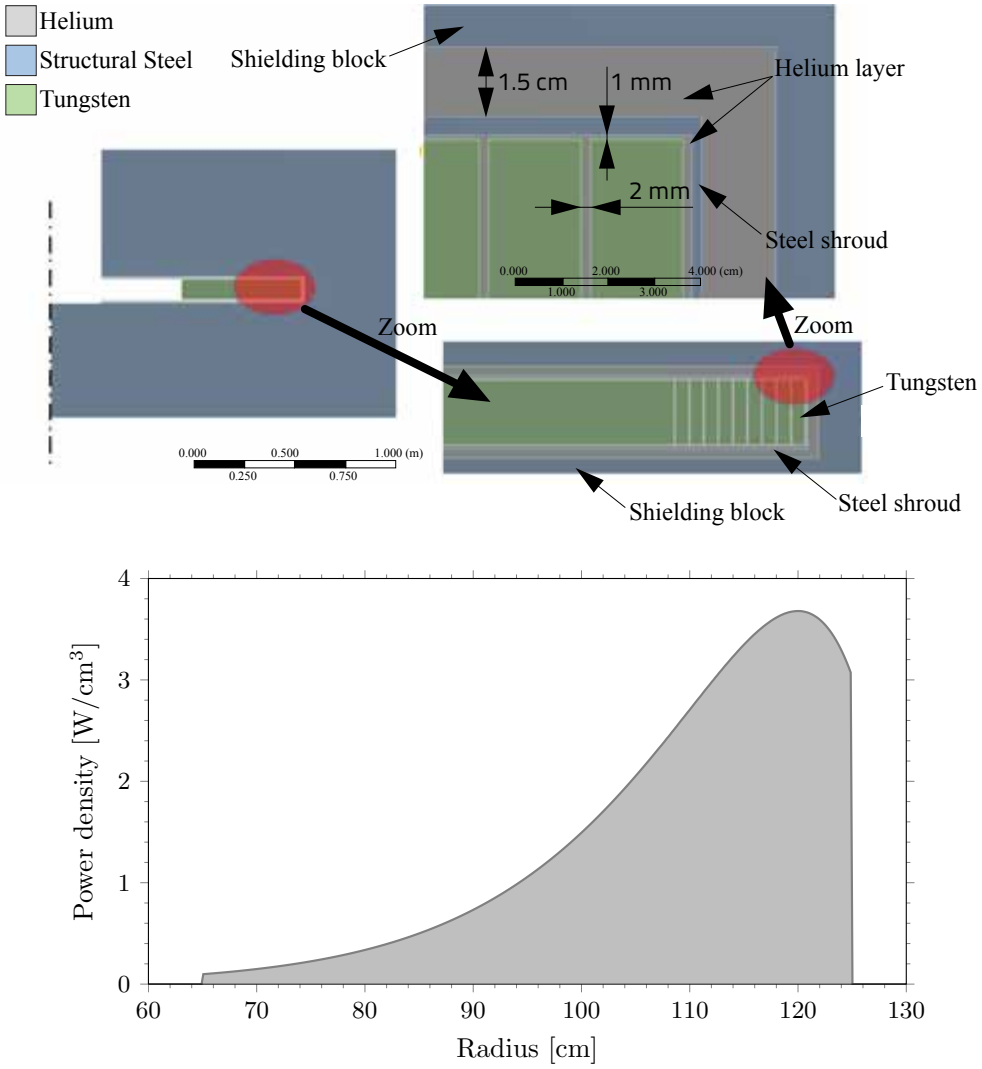

Figure 3.32: Top: The geometry of heat transfer between the target and the surrounding shielding. Bottom: The power density profile of the proton beam heat deposition.

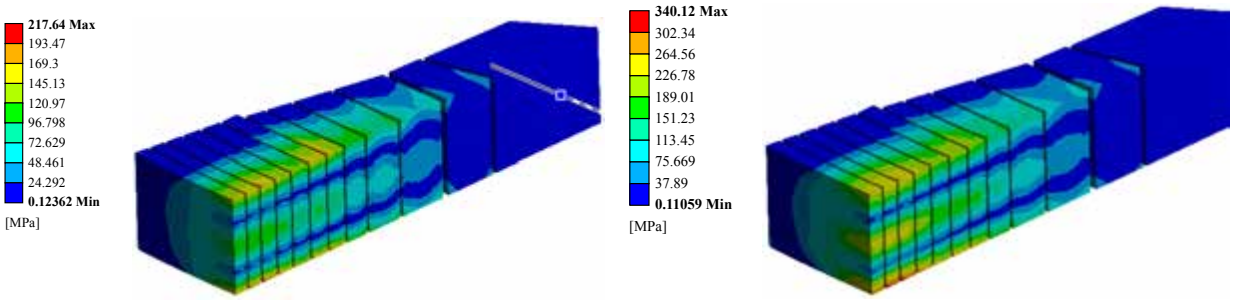

Figure 3.33: Von Mises stress distribution in tungsten, with only half of the tungsten volume shown, cut along the vertical plane. Left: Just before the proton pulse. Right: Just after the proton pulse.

of free convection was also taken into account. The overall thermal analysis showed that heat conduction through the helium between the target and the monolith played a significant role. The size of these helium gaps determined the temperature gradient between the target and the monolith. When the decay heat from the target was balanced solely by radiative heat transfer, a maximum temperature of 550°C was reached in the tungsten, assuming conservative values for the surface emissivity of the target material. A full thermal analysis, including all three types of heat transfer mechanisms, yielded a maximum temperature of 480°C [356]. If the helium were to be replaced by air, the conductive heat transfer would be lower and therefore the maximum temperature would be higher.

Afterheat will not bring the tungsten to a temperature at which oxygen ingress can start an oxidation reaction. Passive cooling due to heat transfer between the target and the monolith will evacuate the heat inside the target at a sufficient rate. The monolith will not suffer from afterheat due to its huge thermal inertia. Instead, the monolith will act as a heat sink for the target afterheat. The maximum temperature of the tungsten could be reduced by increasing the emissivity through surface treatment, such as sand blasting. The benefits of such a surface treatment have to be balanced against possible effects on the mechanical performance of the vessel, especially with respect to fatigue limits.

Mechanical behaviour of the tungsten

The mechanical behaviour of the tungsten was also analysed. In steady state, the calculated maximum value of von Mises stress is 225 MPa. Before and after pulses, the maximum stress levels reach 218 MPa and 340 MPa respectively, as shown in Figure 3.33, leading to a a stress range during operation of roughly

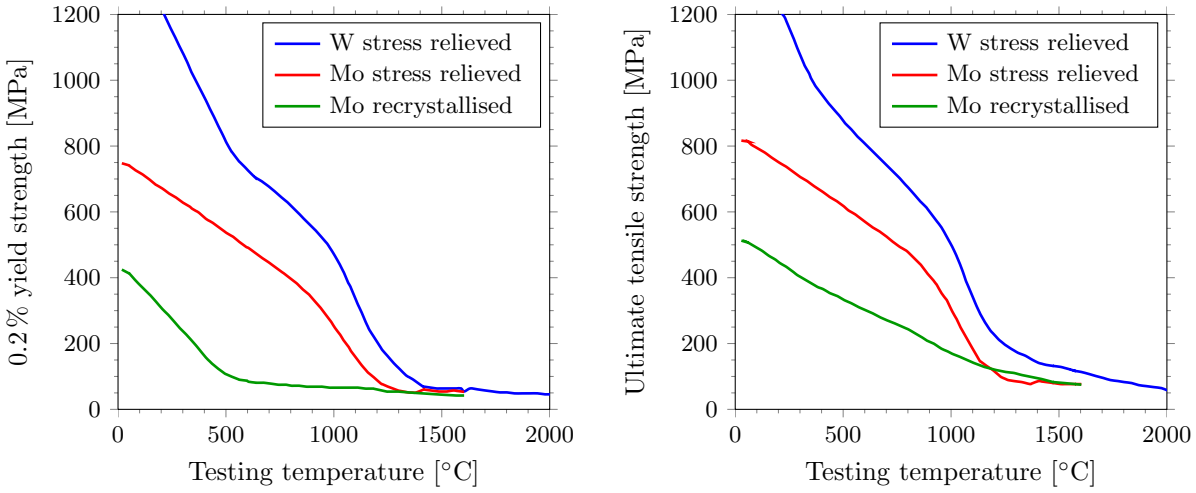

Figure 3.34: Tungsten and molybdenum sheet material in stress-relieved and recrystallised condition [357]. The tungsten and molybdenum sheets are 1 mm and 2 mm thick, respectively. Left: Typical 0.2% yield strength. Right: Ultimate tensile strength.

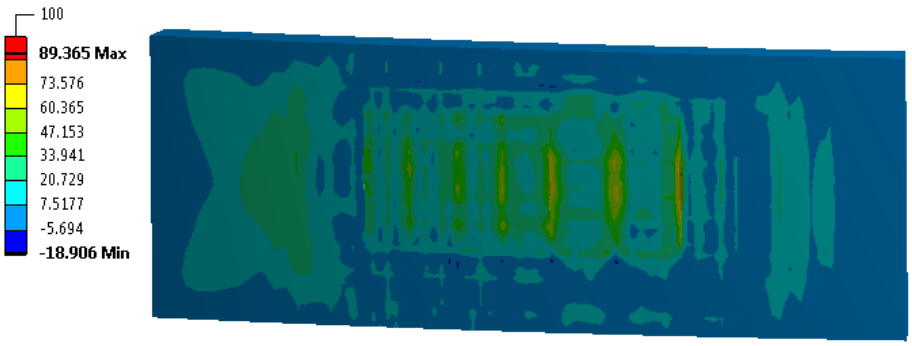

Figure 3.35: The maximum principal stress distribution in a vertically sliced tungsten plate. This shows show that effective options exist to reduce stress levels, if this is found to be to be necessary.

120 MPa (0.03% of strain). The calculated maximum stresses are below the yield stress limits shown in Figure 3.34. Furthermore, the maximum stress level in tungsten slabs could be further relaxed by taking measures such as machining a nut in the plates, resulting in a greater margin of safety. Figure 3.35 illustrates an option to relax maximum stress levels in tungsten. The stress configuration shows the effect of vertically slicing the tungsten slab. This solution would require further elaboration on the holder arrangement, but shows a dramatic reduction in the maximum stress level. The vertically sliced tungsten slab option is not intended as recommendations for a new design, but rather as an example to show that effective options exist to solve the problem if stress levels in the tungsten slabs are found to be excessive at a future date.

3.3.4 Target vessel and beam entrance window

Thickness optimisation of the target vessel

The baseline target design calls for 33 target sectors, each made up of slabs of tungsten, the spallation material, held in place between two structural holder beams. The 33 beams delimit the target sectors and are connected to a massive central hub that makes the transition to the shaft, as shown in Figure 3.36. The 33 sectors of spallation material and structural beams are contained between top and bottom ring-shaped lids welded to the periphery of the central hub, with a rim composed of the beam entrance windows and their frames. The target wheel rotates around a vertical axis. The shrouds and rim form the gas-tight target vessel, which, together with the structural beams to which it is welded, forms the target's pressure container.

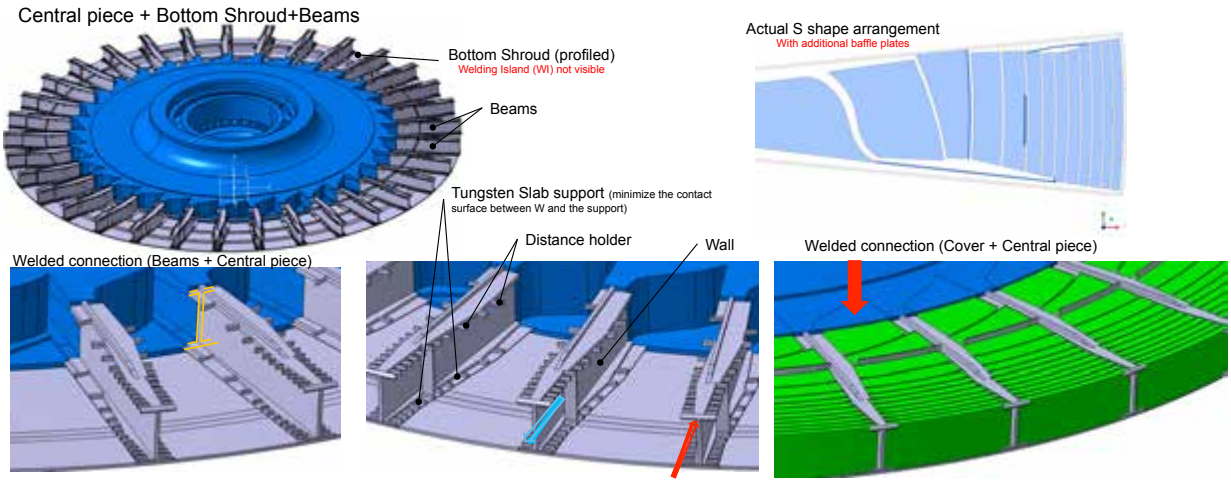

Figure 3.36: The 33 target sectors, separated by 33 structural beams.

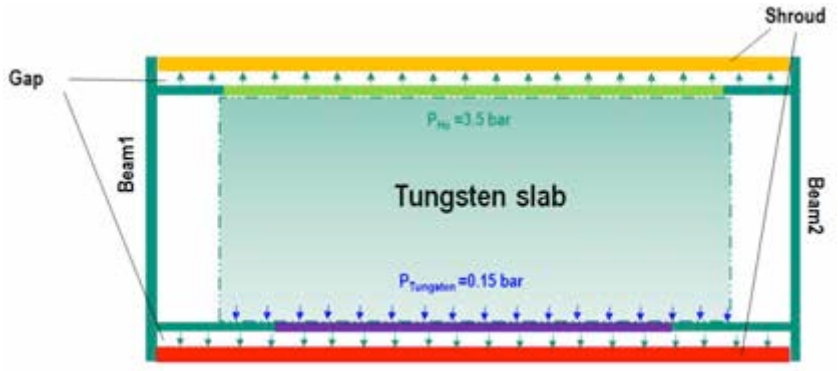

Figure 3.37: Schematic cross section of the target vessel with SHELL model applied pressure values.

In order to determine the optimal thicknesses for the walls of the structural beams and target vessel, a SHELL model in ANSYS Workbench was used to perform the thickness optimisations for one target sector. The material of the pressure container will be 316L(N) annealed austenitic stainless steel with controlled nitrogen content. As the primary loading on the container is the pressure, only this physical boundary condition was taken into account. The mechanical gravitational load from the weight of the spallation and structural materials was treated as negligible for the first pass analysis. Figure 3.37 shows the cross section of one sector, with emphasis on the pressure-loaded parts and the mechanical connections between the structural beams, vessel and tungsten slabs.

Mechanical analysis was performed for different wall thicknesses. Five mm was found to be optimal for the vessel thickness, and 6 mm was found to be optimal for the thickness of the walls of the supporting beams. Figure 3.38 shows the results of the mechanical calculations (total von Mises stress distribution and the total deformation) for the optimal thicknesses. As the next step in the design, a solid finite element (FE) model was developed for one sector including more construction details. For the meshing of the model, solid 90 and solid 186-187 element types in ANSYS were applied while performing the thermal and structural calculations, respectively. In this FE model, besides the primary loading (internal pressure), temperature loading was included as a secondary load on the vessel. Only pure thermal conductance was taken into account to obtain the temperature distribution in the solid parts. However, the full range of mechanical loads were included in the FE simulations, including the weights of the tungsten and structural material, the inertial forces of the tungsten slabs due to wheel rotation, temperature field of the vessel from CFD calculations, and inner pressure.

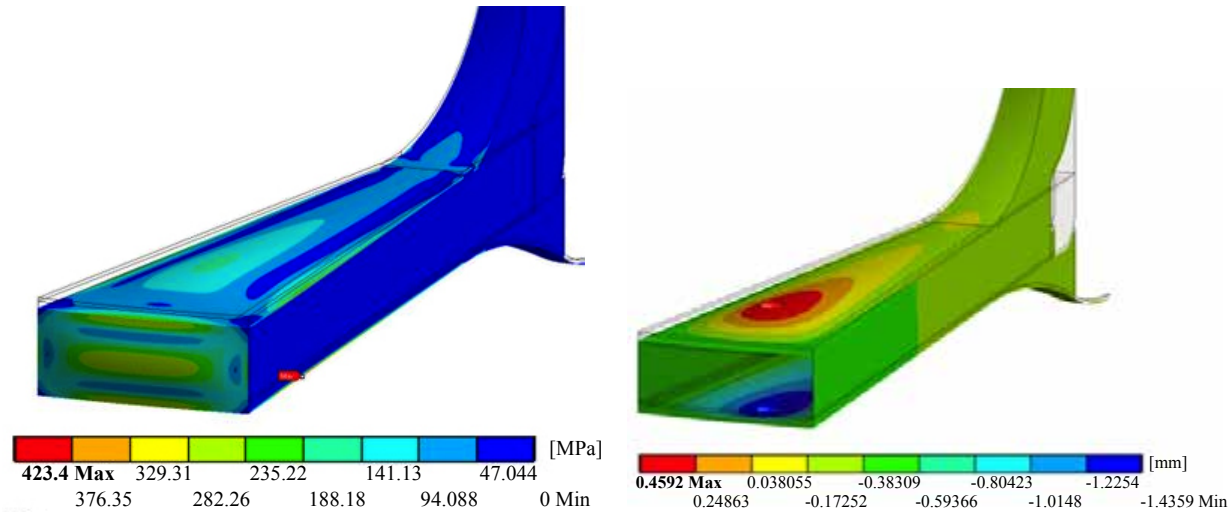

Figure 3.38: Finite element model results for the target wheel, with a vessel thickness of 5 mm and a structural beam thickness of 6 mm. Left: Von Mises stress distribution. Right: Vertical deformation.

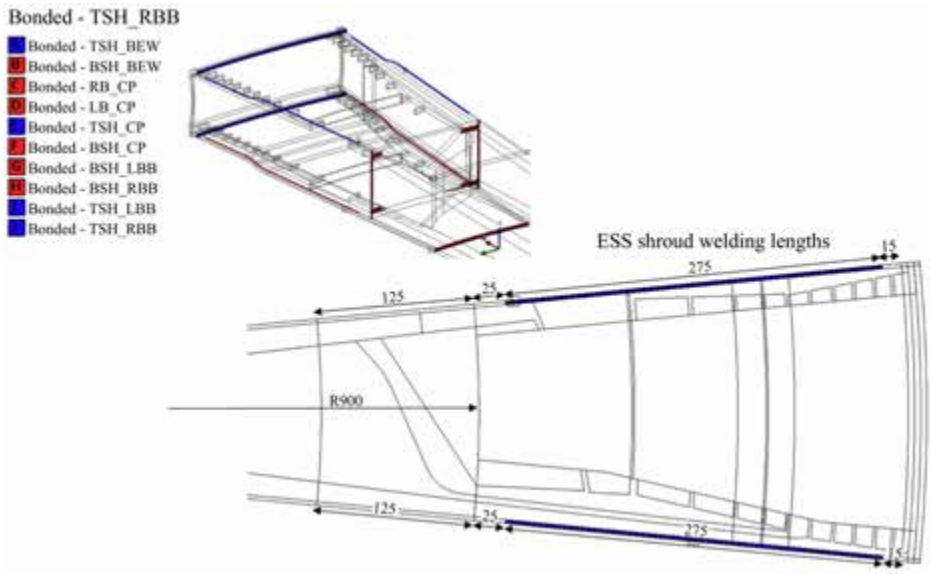

Figure 3.39: The ESS target vessel with positions and contact surfaces.

Steady state structural results

The target vessel was designed for a relative pressure of 0.26 MPa, with internal pressure of 0.36 MPa and environmental pressure in the target monolith of 0.1 MPa. The vessel will be welded onto the structural beams by a welding island, as illustrated in Figure 3.39, which shows the design with one welding island. (ESS has also studied solutions with two welding islands: a final decision on the number of welding islands has not yet been made.) Von Mises stresses and total deformation of the target vessel were simulated, taking into account both pressure and thermal loading. In all cases, the welding islands were modelled as a bonded linear contact between the edge of the vessel and the top and bottom of the holder beams. The results of the mechanical calculations presented in Figure 3.40 were assessed according to the rules

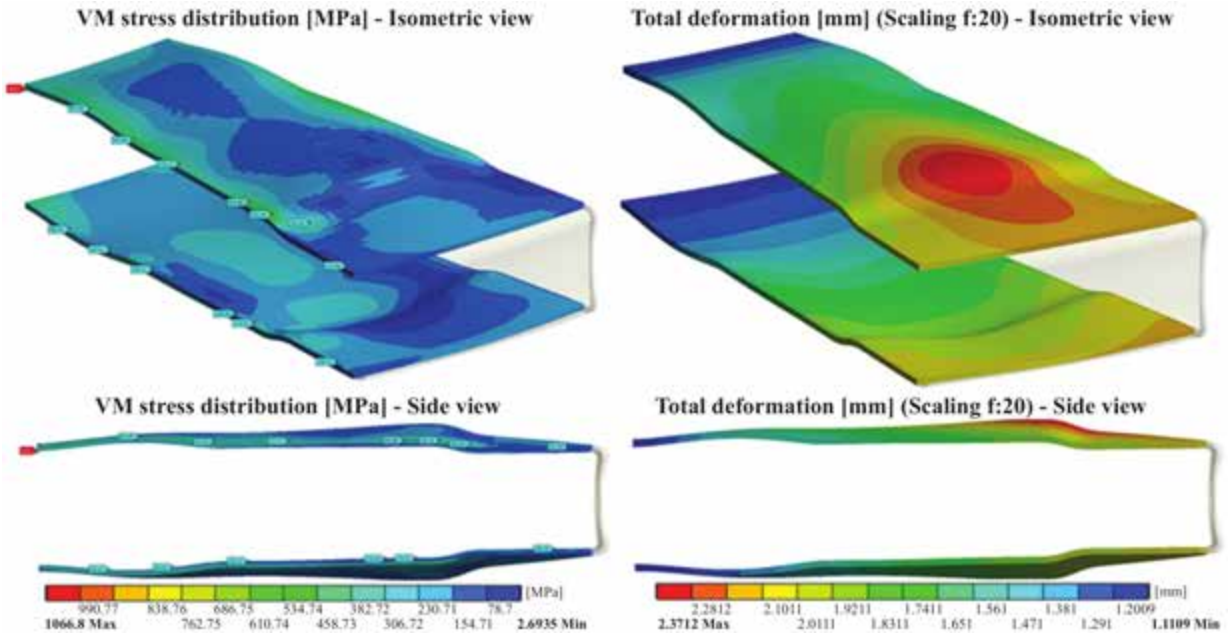

Figure 3.40: Target vessel von Mises stress field and total deformation under loading, from simulation results that combine primary and thermal loading.

Parameter	Unit	Path number										
		1	2	3	4	5	6	7	8	9	10	11
P_m	MPa	61.7	237	110	101	94.8	80.2	58.5	18.5	56.0	41.6	82.2
$P_m + Qm$	MPa	302	279	204	186	133	126	119	106	120.4	173	234
P_{mb}	MPa	65.3	271	118	118	102	85.3	62.7	20.3	74.6	78.4	82.8
PQ_{mb}	MPa	354	480	348	464	294	215	155	110	246	334	317
$P_{mb} + Q + F$	MPa	353	481	351	475	306	210	134	111	243	341	318
S_m	MPa	147	147	145	147	147	147	147	147	134	135	128
1.5 S_m	MPa	221	221	218	221	221	221	221	221	201	203	192
3 S_m	MPa	441	441	435	441	441	441	441	441	401	405	384
$P_m < S_m$	True/False	T	F	T	T	T	T	T	T	T	T	T
Margin	%	42	162	76	69	65	55	40	13	42	31	64
$P_{mb} < 1.5S_m$	True/False	T	F	T	T	T	T	T	T	T	T	T
Margin	%	30	123	54	54	46	39	28	9	37	39	43
$PQ_{mb} < 3S_m$	True/False	T	F	T	F	T	T	T	T	T	T	T
Margin	%	80.3	109	80	105	67	49	35	25	61	83	83

Table 3.18: Target vessel stresses calculated for various paths, compared with acceptance criteria contained in RCC-MR 2007. P_m is the primary membrane stress. Q_m is the secondary membrane stress. P_b is the primary bending stress, Q and F are respectively the secondary stress and the peak stress, S_m is the allowable stress, $P_{mb} = P_m + P_b$, $Q_{mb} = Q_m + Q_b$ and $PQ_{mb} = P_{mb} + Q_{mb}$.

and standards in AFCEN's RCC MR 2007 code [358], using several representative points and paths on the vessel. The outcome of this assessment is summarised in Table 3.18, while the path positions are illustrated in Figure 3.41. For most of the regions of the vessel, the acceptance criteria are met by the calculated values. However, in some areas, the calculated values do not fulfil the acceptance criteria. This is mainly due to the presence of artificial stress concentration in the simulation model associated with contacts between the vessel and the holding beams. While initial results are promising, further investigation with more advanced and detailed modelling is required.

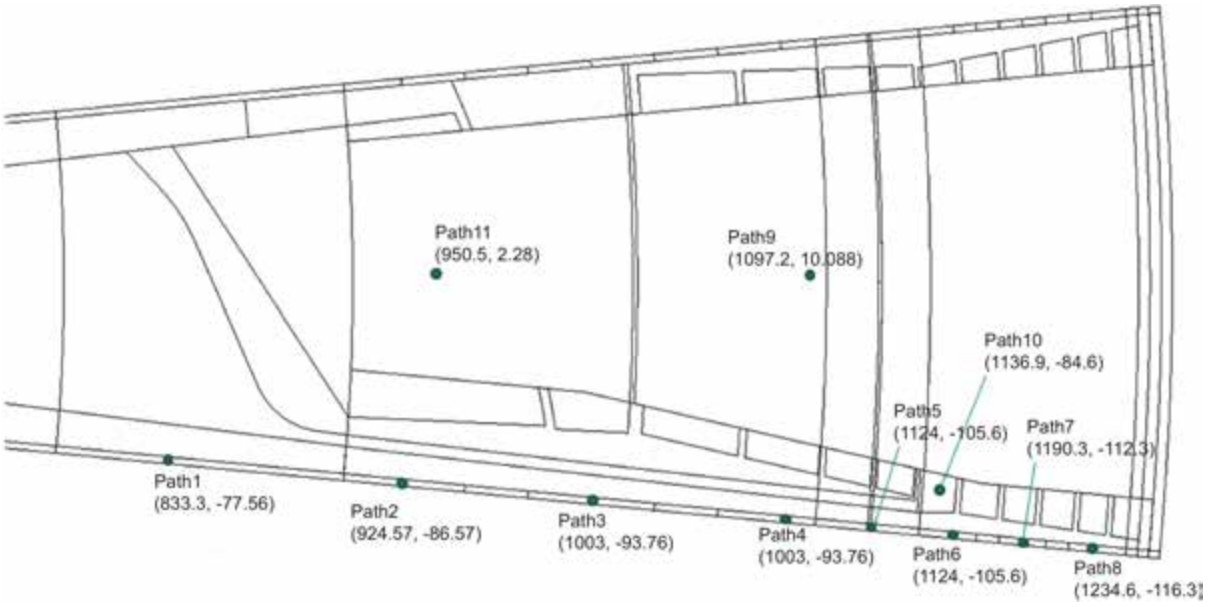

Figure 3.41: Path positions for the structural assessment of the target vessel. Numbers in parentheses indicate the (x, y) co-ordinates of each path, where x and y are, respectively, horizontal and vertical displacements measured in millimetres.

Fatigue analysis of the beam entrance window

The beam entrance window has the optimised shape of a rectangular concave wall with a minimum thickness of 2 mm in the beam path, and a maximum thickness of 5 mm at the outer corners. This maintains structural integrity under a pressure of about 0.3 MPa and under the thermal load from the proton beam, while minimising the neutronic penalty. In order to ensure the reliability of the target wheel, it is important to assess potential fatigue damages during the design phase. As the beam entrance window is exposed directly to the incoming proton beam and must contain inventories from the target material and helium coolant volume without leaking, the fatigue reliability of the BEW has a primary importance for robust target wheel design. ESS is using the methodology proposed by RCC-MRx draft (2010) [359] for its BEW fatigue analysis. This methodology is based on the accumulation of damage, similar to Miner's rule. Material data provided by the design standard are based on neutron irradiation. Hence, calculations must include sufficient margin to ensure reliable results, considering that target materials are exposed to a high power proton beam. Proton beam footprint profile parameters are defined in two technical reports [339,360].The cycling history over the lifetime of the target must be defined, in order to carry out the fatigue analysis. All cycles are divided into sub-cycles of definite strain ranges, for each of which an individual usage factor (IUF) is calculated. The IUF is defined by the number of cycles experienced during one lifetime, divided by the allowable number of cycles. The cumulative fatigue usage factor (CUF) – the sum of all the IUFs – must be less than one in order not to have a fatigue failure during the lifetime of the BEW. An internal document defines a set of 8 possible events in the target cycle [361]. Table 3.19 summarises the IUFs and the CUF for the beam entrance window, based on the frequency of each type of event. The baseline design provides sufficient margins for 5 years of target lifetime, even with proton irradiation [362].

Stress load	**Number of occurrences** [10^3]	**IUF** [10^{-3}]	**IUF per occurrence** [10^{-9}]
Mass itself	0.001	10^{-16}	10^{-10}
Pressure and rotation speed	0.175	5×10^{-6}	0.027
Average thermal load	9.0	0.015	1.600
Proton beam pulse	43,600	0.636	0.015
Beam trips from 2.4 s to 10 s	39.1	0.046	1.200
Beam trips from 10 s to 30 s	31.2	0.006	0.190
Beam trips from 30 s to 60 s	26.0	0.004	0.140
Beam trips from 60 s to 100 s	21.7	0.002	0.070
Cumulative usage factor	–	0.687	–

Table 3.19: Individual Usage Factors (IUFs) and the cumulative usage factor – the sum of all IUFs – for the beam entrance window for a set of 8 possible events [361], showing sufficient margins over the design target lifetime of 5 years. The accumulation of beam pulses is more than 10 times more damaging than the accumulation of beam trips.

3.3.5 Target shaft, seal, bearing and drive

The spallation material will be placed in a rotating target wheel, which will be connected to a long vertical shaft reaching out through the top plate of the monolith, where the driving and bearing system will be located, as shown in Figure 3.42. The target container, the outer wall of the shaft and all pipes of the cooling circuit will be part of the first barrier of the system that will prevent the escape of highly activated particles from the cooling loop. The spallation zone will be enclosed by the shielding blocks of the monolith, forming part of the necessary biological shielding and reducing the radiation to levels allowing the use of radiation-sensitive devices and materials. To avoid radiation streaming through the shaft, a helical inset will be used which, just by virtue of its geometry, will attain a shielding effect of 50% compared to the bulk monolith. Using a high-density material for this inset could increase the shielding efficiency even further, should this be found necessary to avoid or reduce activation of components in the service area above the monolith.

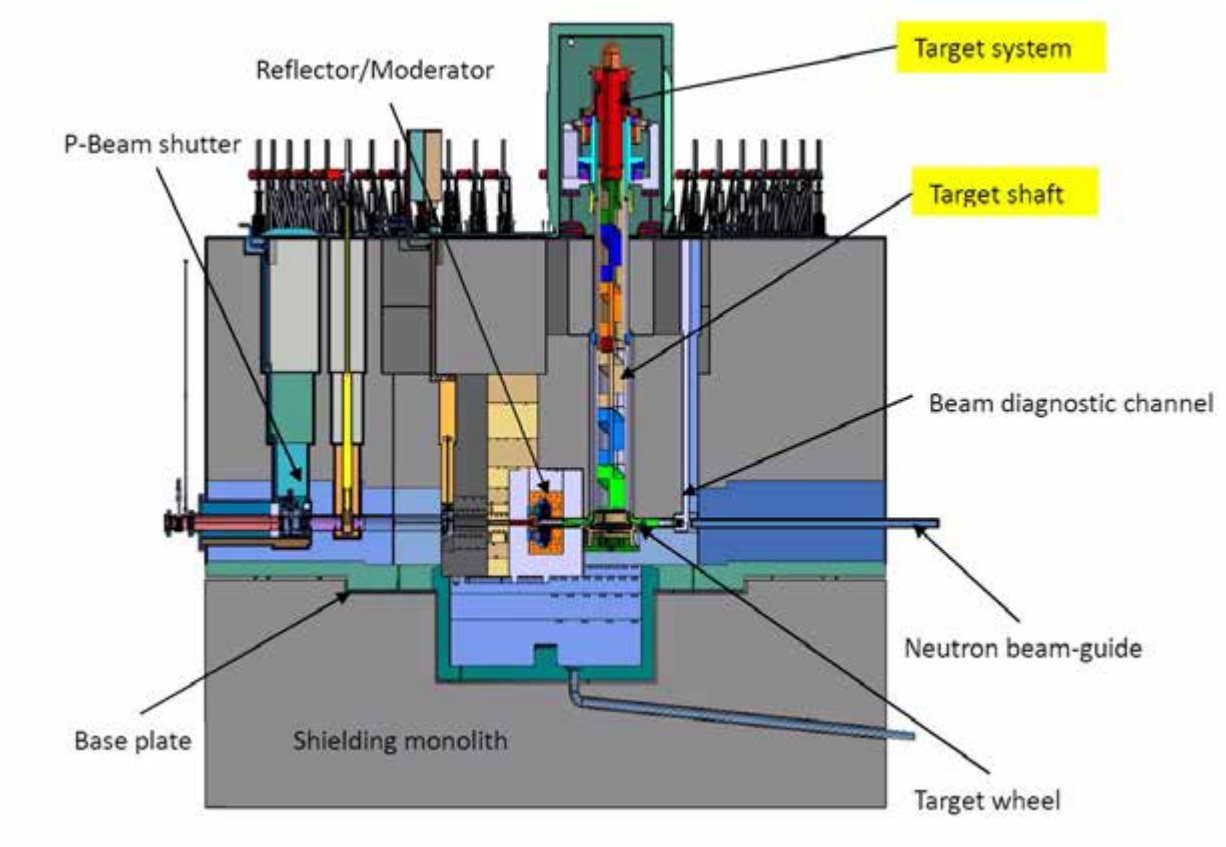

Figure 3.42: The target shaft installation environment.

The driving and bearing system on top of the monolith will be the interface between the stationary and rotating parts of the target system, including the stationary and rotating parts of the first barrier between the contaminated cooling circuit and the helium atmosphere in the monolith. Therefore, adequate sealing of the first barrier and leakage monitoring are vital for this system. The accessible box on top of the monolith will enclose the whole bearing and driving unit and will be part of the monolith helium system and thus part of the second barrier for the cooling helium.

Target shaft

The concept of driving a rotating target from a long shaft was initially considered in the design study for the low to medium power spallation source for the Basque Country [363]. This design used water as the cooling medium. The concept was worked out in more detail in the design study for the second target station for SNS [349]. The long shaft has the advantage that all system-relevant components are located at a significant distance ($\simeq$5 m) from the spallation zone and thus from the high radiation area. The target shaft forms the interface between the spallation zone and the functional system groups, as shown in Figure 3.43.

The envelope of the ESS target shaft will consist of two tubes, with dimensions (outer diameter, inner diameter, and length) of 600 mm $\times$ 540 mm $\times$ 1900 mm and 700 mm $\times$ 640 mm $\times$ 2390 mm, which will be welded together using a connecting piece at the interface. The resulting offset in the outer contour of the shaft will serve, together with the fitting contour of the monolith, as a step to reduce radiation streaming in the unavoidable gap between the shaft and the surrounding shielding blocks. The driving torque will be transferred by the outer envelope of the target shaft from the driving unit to the target wheel. The outer envelope of the shaft also will provide mechanical stiffness to the whole arrangement. Within the shaft there will be two concentrically arranged pipes for separating the inlet and outlet flow. These pipes will be centred relative to the outer envelope of the shaft by three circumferentially distributed spacers. The gap between the outer and inner pipes will serve as the helium inlet for target cooling and will have a

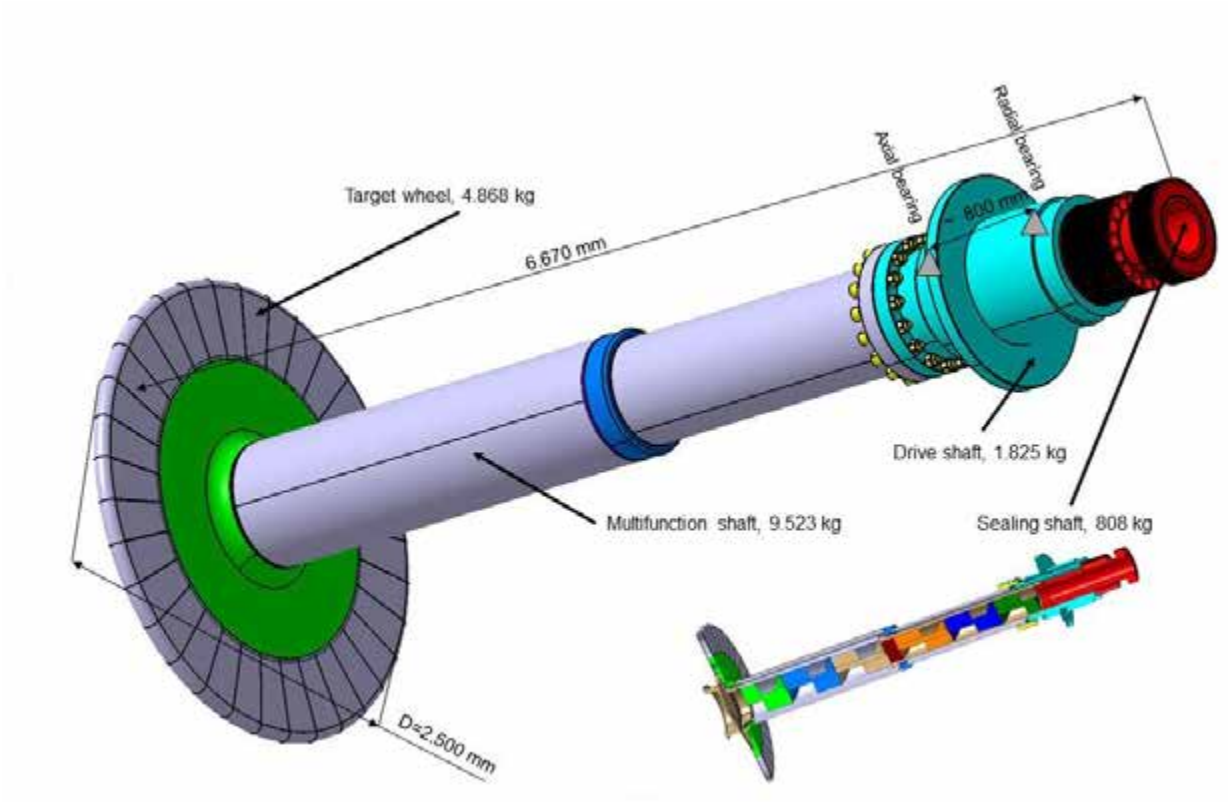

Figure 3.43: The target shaft design concept.

cross section of 77,000 mm^2 in the upper part and 75,400 mm^2 in the lower part of the shaft, respectively. The central pipe including the helical insert will be used for the helium return flow. Due to the presence of the helical insert, the return flow will also acquire an angular momentum, which may serve the purpose of separating large contaminated particles from the flow, thus preventing them from leaving the shielded area of the target station. Further calculations and experiments will be needed to validate this separation feature. The smallest cross section of the outlet is 54,000 mm^2 in the present design.

The target shaft will be welded to the container of the target vessel. Therefore the shaft and the target wheel will be handled as a single unit during installation and dismantling. The total mass of this unit will be about 17,200 kg while the total moment of inertia will be about 5,730 kg/m^2.

Seal

An interface is needed between the helium inlet and outlet to the rotating target shaft and the stationary helium loop. For this interface, a sealing is necessary which is suitable for helium, resists wear and has a lifetime of at least 5 years in an area of modest radiation. Moreover, the sealing must sustain the role of the first safety barrier for the target-cooling medium. The most promising solution for this sealing is a double labyrinth seal together with an additional pressurised seal gas which guarantees that leakage always flows from non-contaminated to contaminated volumes. Figure 3.44 shows the planned configuration. The red lines indicate rotating parts of the target wheel and the blue lines stationary parts. The red areas indicate contaminated helium within the first barrier and the green areas indicate monitored and clean helium.

The coolant will be fed into the target through the inlet with a pressure of 0.36 MPa and will leave the target shaft with a pressure of about 0.30 MPa. A small amount of the helium flow, the bypass flow, will pass a labyrinth seal directly to the outlet, as shown in Figure 3.44. To prevent contaminated helium from getting into the helium atmosphere of the monolith, a seal gas will be used at a pressure of 0.38 MPa. The non-contaminated seal gas (He_b) will pass a labyrinth seal and will enter the contaminated helium coolant loop (He_c). The pressurised seal gas will also pass another labyrinth seal and will enter the helium

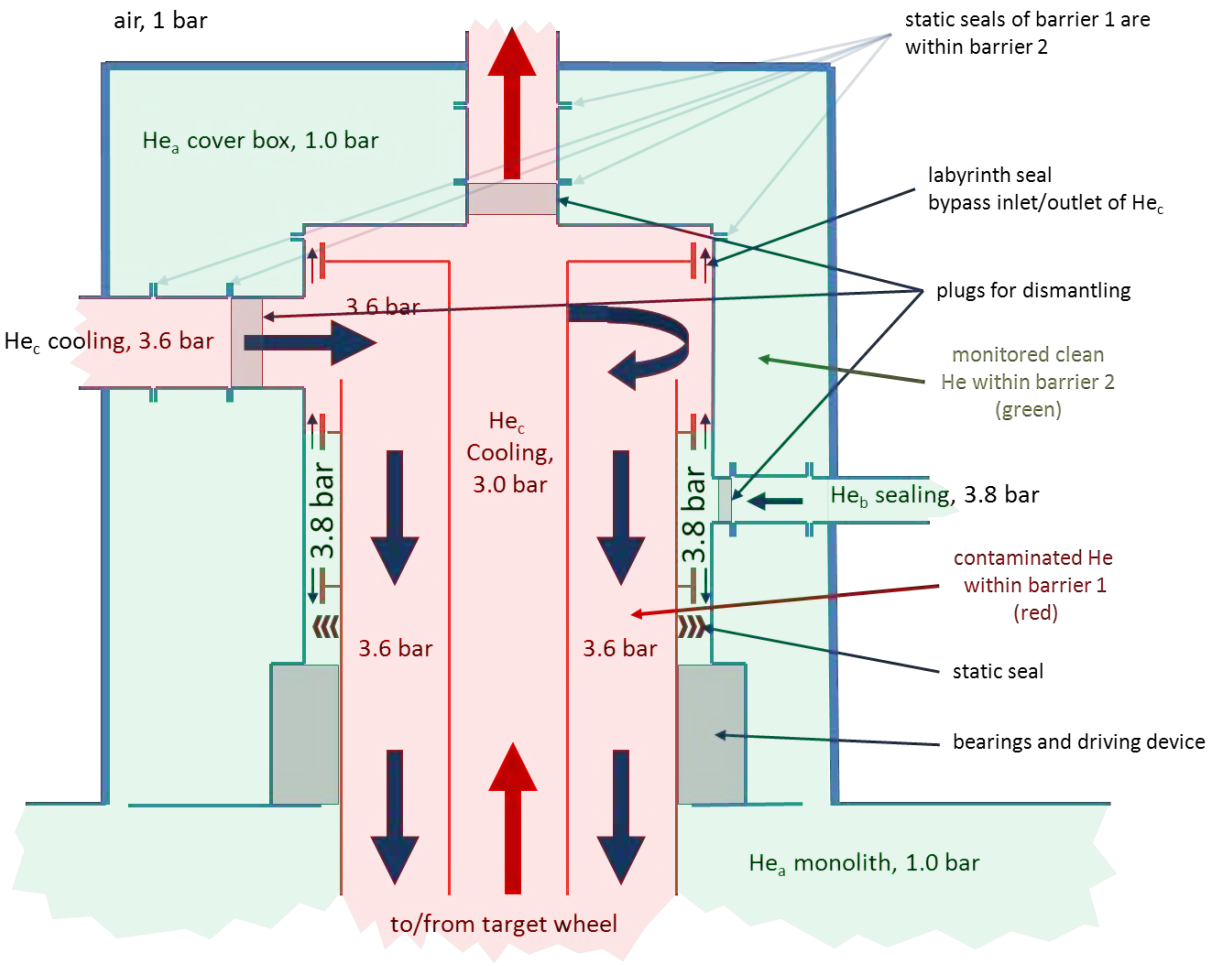

Figure 3.44: The sealing concept for the target wheel's bearing and drive unit: The red lines indicate rotating parts and the blue lines stationary parts. The red areas indicate contaminated helium within barrier 1 and the green areas indicate monitored clean helium.

atmosphere of the monolith (He_a). The total amount of seal gas needed to compensate for the leakage through these labyrinth seals was calculated to be about 10 g/s, which have to be released continuously from the helium atmosphere of the monolith and from the cooling helium storage tank. (Section 3.4.4 gives more details.) The calculated value of 10 g/s consists of a $\simeq$3 g/s flow towards the cooling loop and a $\simeq$7 g/s flow towards the monolith. The values were calculated using an analytical, semi-empirical method backed up by computational fluid dynamics (CFD) calculations [364].

For safety reasons, the barrier system will have a back-up seal, as shown in Figures 3.44 and 3.45. During normal operation this seal will be opened by applying low inward pressure. If the target wheel rotation stopped, whether during normal shutdown or in the event of a failure (e.g. due to loss of electrical power), the seal would be vented and would close itself due to spring pressure. The static seal concept is shown in Figure 3.45. The contact surfaces are polished to minimise leakage through the closed seal. The static seal is necessary avoid evacuation of the whole monolith chamber through the labyrinth seals (and vice versa) when the helium loop and the target are evacuated. It remains to be evaluated to what extend organic material can be used at this position to improve tightness of the static seal.

Bearing and drive system

The drive, the seal and the bearing units are illustrated in Figure 3.46. The design of the bearing and drive system [365] was driven by a number of requirements. Easy access to all components is necessary so that inspections can take place without opening barrier 1 or rearranging the components outside of barrier

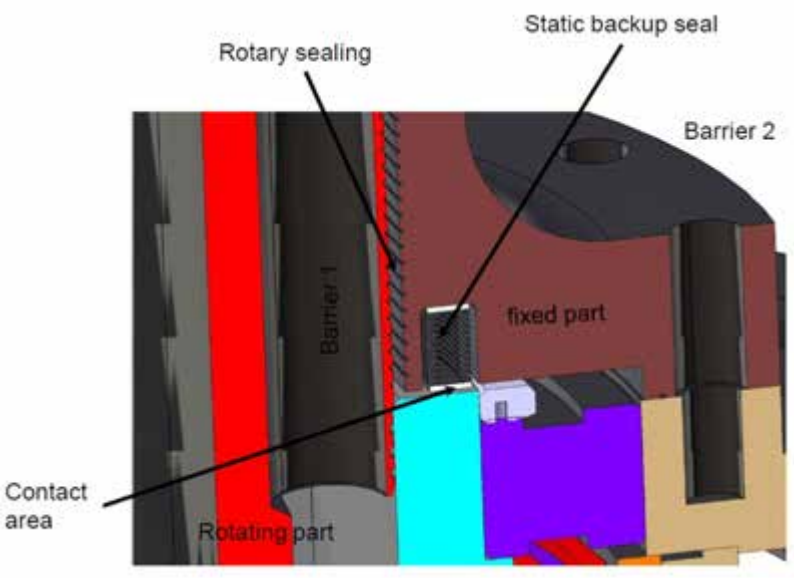

Figure 3.45: The static seal configuration.

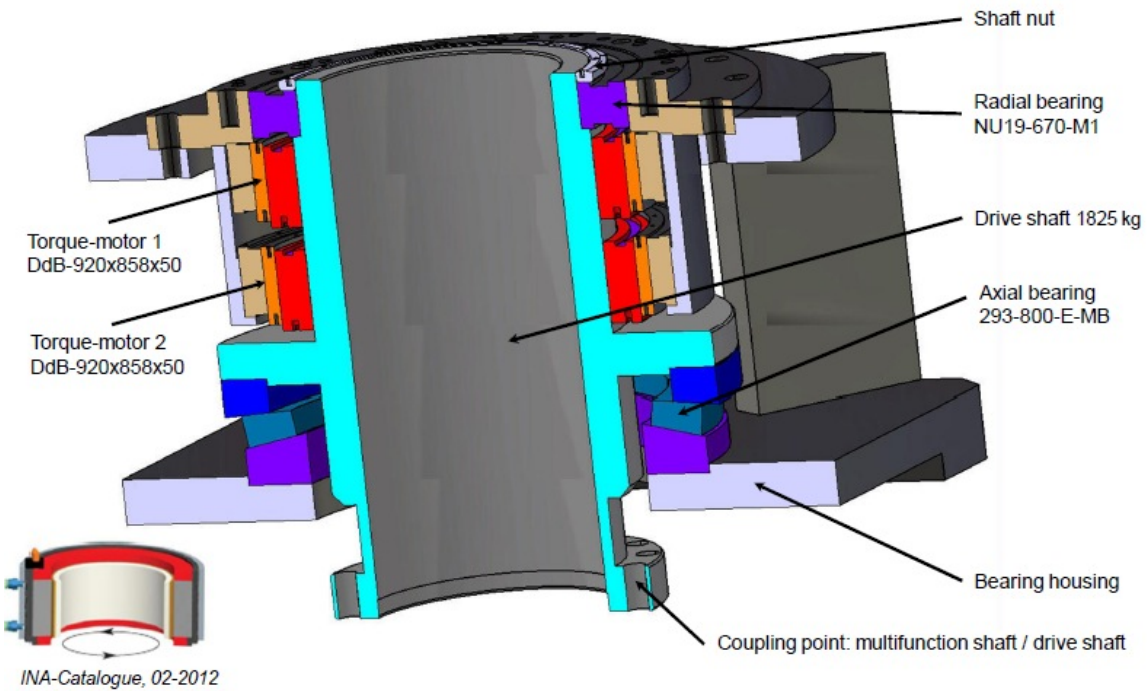

Figure 3.46: Drive, seal and bearing unit.

1 and within barrier 2. The second barrier should cover the whole bearing and drive unit and the flanges of the cooling loop in order to monitor possible leakage of barrier 1 seals in this area. It should be possible to easily exchange the bearings and drives. Redundancy in the drive system is essential to avoid long shutdown periods if a drive unit fails. Separable connection between the target shaft and the bearing and drive unit is also necessary, so that the bearing and drive unit can be reused after exchange of the target wheel and shaft. The connection to the monolith must be robust, in order to guarantee stable support of the target wheel. Sensors must be integrated into the drive system to make it possible to monitor the system's behaviour. Finally, fully developed technology with a track record of robustness should be used whenever possible.

ESS has selected a torque motor [366,367] with a maximum torque of 2,500 Nm and a power of 8 kW for the drive unit for the target wheel. The torque motor will drive the shaft directly without requiring gears or belt to transmit torque to the shaft. This choice took into account the total 17,200 kg mass of the target and shaft unit, and a ramp-up time of 20 seconds until the nominal rotational speed of 25.5 rpm is reached. Depending on the reaction time available to readjust the target velocity after detecting a desynchronisation between the target rotation and the proton beam pulses, the necessary power and moment might even be higher. In this case drive units of the design selected for ESS providing torques up to 10,250 Nm are available in 1,250 Nm increments. Sufficient cooling with water will be provided to implement this approach. Although the motor does not feature gears, lubricant or other sliding parts, investigations about operation in helium atmosphere are still necessary.

3.3.6 Target monitoring instrumentation

Successful operation of the target to produce neutron beams for the research instruments will require real-time monitoring of a number of system parameters, as well as data archiving for subsequent analysis. Table 3.20 presents a summary of the parameters and locations which will be monitored during operation of the target wheel. Details of each parameter, and monitoring approaches are discussed below.

Location	System	Monitored parameters
Helium cell	Helium circuit	Radioactive release, pressure, temperature, tungsten dust, oxygen and other gas content
Target rear plug	Target vessel	Temperature, velocity, displacement, vibration and gamma spectra
Drive unit	Target rotating seal & bearing	Vibration, rotation velocity and helium leaks

Table 3.20: Summary of the target parameters monitored during operation.

Target vessel temperature

Through the spallation processes in the tungsten target material, considerable heat will be generated, which will expose the steel target vessel to thermal stress. Unlike the tungsten, the steel target vessel and structural beams, will function as the first safety barrier between the target wheel and the outside environment, as explained in Section 3.1.2. For this reason, its temperature will be monitored to ensure that the wheel is cooled sufficiently to function properly and to prevent structural failure in the vessel. The target vessel is rather large and it will be difficult to monitor its whole surface using thermocouples. ESS will use an alternative approach, integrating an optical path into the monolith to monitor the target vessel via an infrared camera placed at a distance from the harsh irradiation area, as illustrated in Figure 3.47. This will give accurate measurements of first safety barrier temperature. Each section of the wheel will be monitored once every full rotation. The optical path for target wheel monitoring will be placed in the beam instrumentation plug shown in Figure 4.117, located between the PBW plug and the MR plug. This makes the replacement of aging monitoring components easier, without requiring a complicated remote handling process such as target exchange.

Target vessel vibration and displacement

The optical path will also be used to track structure vibration with a laser Doppler vibrometer (LDV). A three-dimensional scanning laser vibrometer is a unique tool which makes it possible to accurately determine the operational deflection shapes and eigenmodes of the target across a wide range of frequencies. Measurement data are reliable as they reflect the actual vibration characteristics of the real object in comparison to accelerometers directly placed on the structure. Nevertheless, it is mandatory to also have at least two accelerometers on the target to properly calibrate the LDV. These sensors will be placed close to the harsh irradiation area, which will severely limit their lifetimes. In comparison, the LDV and the infrared camera will be well protected.

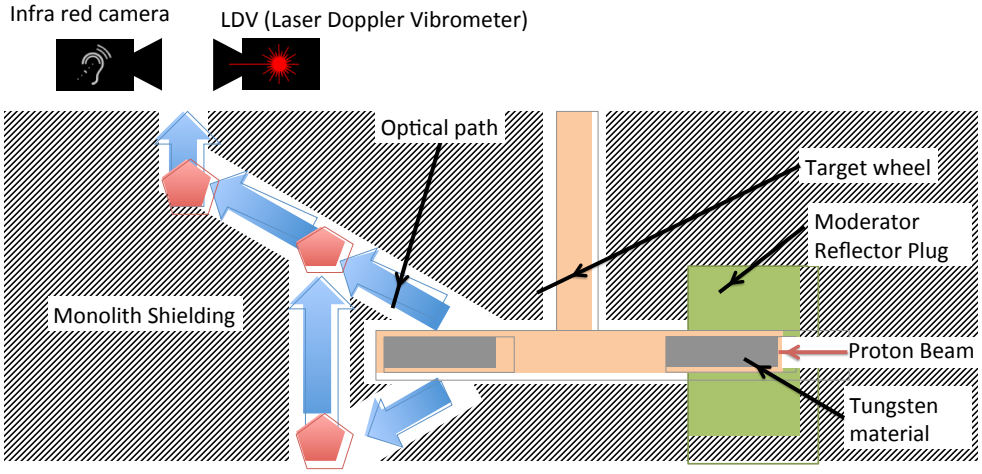

Figure 3.47: An optical path through the monolith to monitor target vessel temperatures and vibrations, using an infrared camera and a laser Doppler vibrometer placed away from the harsh irradiation area.

Tungsten material temperature

The thermal and mechanical failure of a tungsten block within the target wheel can be diagnosed by monitoring the temperature of each target block. Any mechanical change in the tungsten block causes a change in the heat exchange mechanism between the tungsten and the helium coolant, which leads to an anomalous temperature change in the target material. However, as there are a large number of target blocks inside the target vessel in constant revolution, it is technically difficult to monitor tungsten temperatures directly. Therefore, thermal sensors that are placed on strategically chosen measuring points on the target vessel will indirectly monitor the tungsten temperature. Extrapolation from the monitored temperature data on the target vessel will provide thermal information about the tungsten blocks inside the target wheel, using a methodology presented in a technical report [368].

Small leak detection

J-PARC has developed a system based on mass spectrometry of the helium in its target vessel interstices [369] to detect spallation products in the helium gap which indicate if the mercury vessel is corrupted somewhere. A similar approach will be used to monitor vessel integrity at ESS through analysis of the helium flowing around the target within the target vessel. Small tubes will be inserted at strategic points to sample the helium in order to detect spallation products from the tungsten. CFD analysis will be used to determine the appropriate placement of these tubes.

Target wheel assembly balance

The target wheel loaded with tungsten must be balanced in order to reduce vibration and ready it for operation. After achieving required balance accuracy, vibration will be monitored at different locations in the top of the shaft and wheel vessel to provide baseline information about the vibrational characteristics of the undamaged target before operation begins. During operation, the target will deform due to its own weight, rotation acceleration and proton beam load. The thermal load from the proton beam stopping in the target will extend the radius of the target and cause a displacement of the target material by 2 mm, compared to its beam-off state. This thermal deformation changes the balance and vibrational behaviour of the wheel, and these changes must be monitored during operation. The target wheel can become unbalanced during operation if the target material is displaced due to local mechanical failure of the wheel structure. For reliable operation of the target station, this anomalous dynamic mechanism must be diagnosed in real time by an appropriate monitoring system for the assessment of failure locations and the degree of material displacements. Once the target has cooled off after proton beam shutdown, the balance of the target must be checked in more detail. Slow rotation could compromise the accuracy of this measurement. Therefore, details of the mechanical balance of the target wheel must be checked by

rotating the target at a much higher angular speed than the nominal one. This testing technology has been extensively used in the turbo machinery industry, for instance, where the rotation velocity is much higher. Such tests will be conducted at ESS after every short shut down.

3.3.7 Moderators and reflector system

Requirements

One of the key challenges for the engineering design of the moderators and reflector (MR) system is the heat load produced by the 5 MW proton beam power. It will be roughly five times higher than that of the most powerful spallation sources worldwide, SNS and J-PARC. From this 5 MW beam power, approximately 1.2 MW will be deposited in the (cold) hydrogen and water moderators as well as in the reflector [339]. A large engineering effort needs to be put into the design of the moderator vessels and the H_2 circuit because of the heat load (approximately 8.3 kW) deposited in each of the H_2 moderators. Although the heat load is relatively small compared to the total deposited, it is the fact that it occurs in the cryogenic (20 K) H_2 that significantly increases the challenge. For the other components (the water moderators consisting of pre- and thermal parts and the reflector) water will be used for moderation and cooling. Figure 3.48 shows temperature distributions in the liquid hydrogen (LH_2) moderators, calculated and derived by CFD simulation. The basic dimensions of the major components were obtained by neutronic calculations [339]. The engineering design takes into account all applicable loads, stresses and temperatures and conforms to applicable design rules, standards and regulations. Cost and manufacturing issues were also considered. The engineering outcome is iterated with the neutronic performance (using the more realistic engineering geometry), for purposes of optimisation.

Cold moderator

For the cold moderator, liquid hydrogen (LH_2) at approximately 20 K and 1.5 MPa is used as the moderating medium. The structural material for the moderator vessel is required to be tolerant to radiation damage, as transparent as possible for neutrons at all energies, and suitable for cryogenic temperatures. Operational experience and assessments at other neutron sources led to the selection of Al-6061-T6, a high strength aluminium alloy also used at SNS and J-PARC [370]. Specific heat load in the aluminium is about three times higher than in the LH_2 itself and because of this, efforts have to be made to minimise the wall thickness. Local overheating in the LH_2 and high temperature gradients across the vessel's walls are to be avoided. Coupled fluid dynamics and structural mechanics calculations led to a wall thickness of 3 mm, as shown in Figure 3.49. Even with an optimised flow pattern providing efficient cooling of the wall, as shown in Figure 3.48, the 3 mm vessel wall thickness is about the maximum permissible to handle the thermal stresses induced by the temperature gradient, at least in the highest heat load region close to the target. The operating pressure of 1.5 MPa, in contrast, requires a greater wall thickness for simple box geometry to stay within the allowable stress limits. This tension led to a more complex design using a cone-like

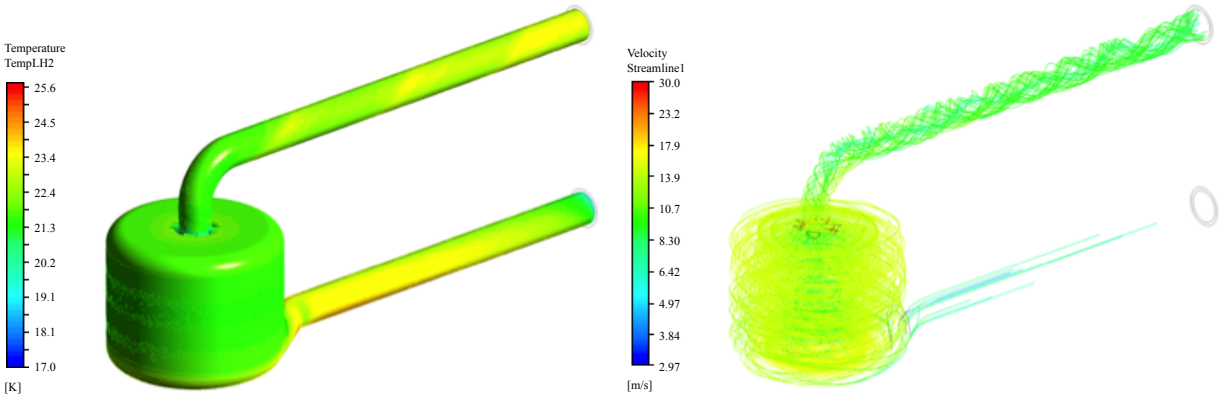

Figure 3.48: Computational fluid dynamic results for the liquid hydrogen moderator. Left: Temperature field. Right: Liquid hydrogen streamlines.

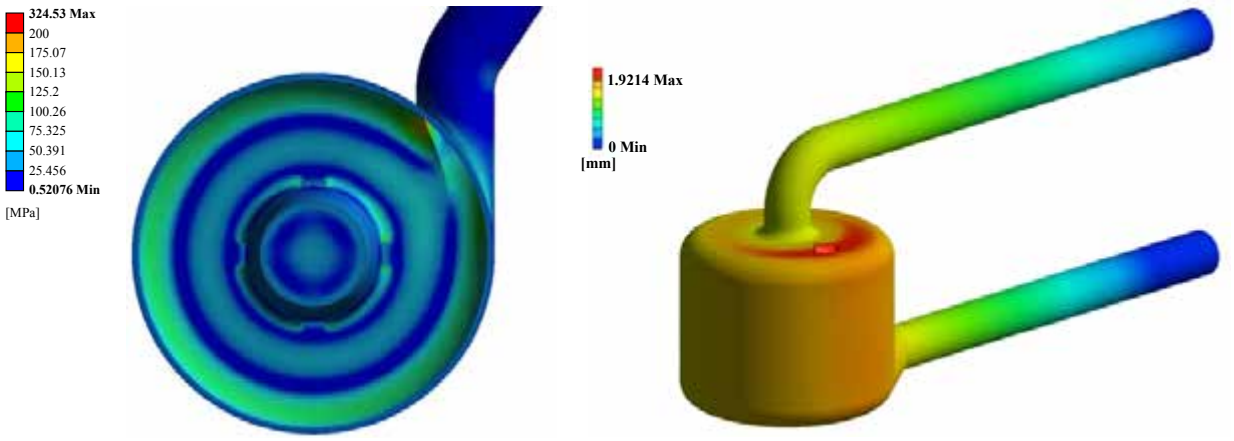

Figure 3.49: Finite element modelling results for the cold moderator. Left: Von Mises stress. Right: Deformation.

structure in the centre of the moderator to route the flow while also connecting the top and bottom flat surfaces to reduce deformation and stress. Figure 3.50 shows a cross section through the moderator that shows the centre cone-shaped inner duct.

Compared to the concentric inlet-outlet arrangement used for cold moderators at other sources, a swirl flow pattern was identified as a solution to enhance wall cooling and avoid stagnation zones. The vessel features a tangential LH_2 inlet close to the bottom (facing towards the target). This leads to a highly turbulent spiral flow pattern that routes some of the flow along the cylindrical vessel wall and up to the top where it enters the inner duct (connecting the top and bottom surfaces) through holes and leaves the vessel. The remainder of the flow enters the inner duct at the bottom and flows up through the centre. Thus, this duct acts both as a flow guide and as a stiffener.

Despite this optimisation, stresses in the vessel wall are still significant, and a thorough material investigation is necessary. Testing was performed for welded and un-welded assemblies at both room temperature (RT) and 77 K. Figure 3.51 shows some of the test results. Further testing will include the

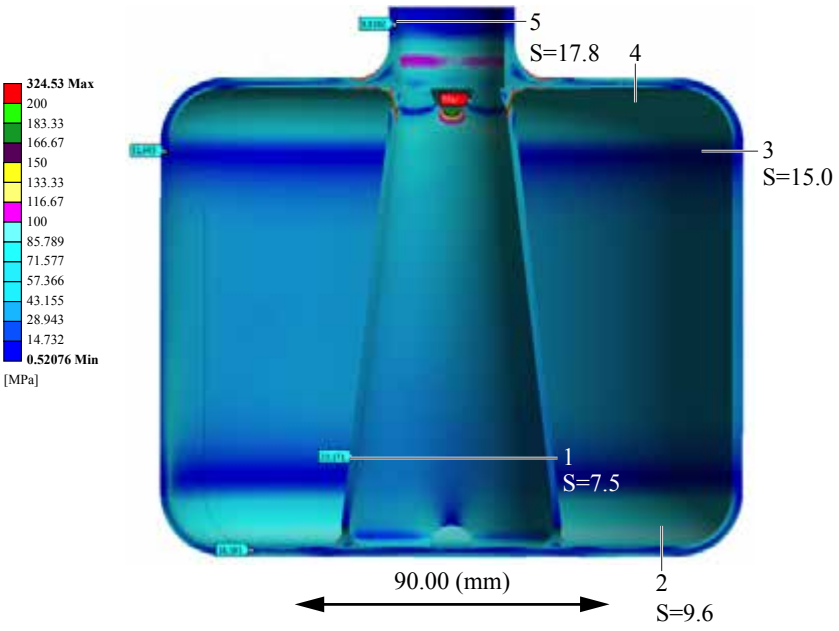

Figure 3.50: Weld positions (in red) for the cold moderator test vessel, and the associated stress safety factors at these positions. The stress safety factor S is the ratio of the yield stress to the actual stress.

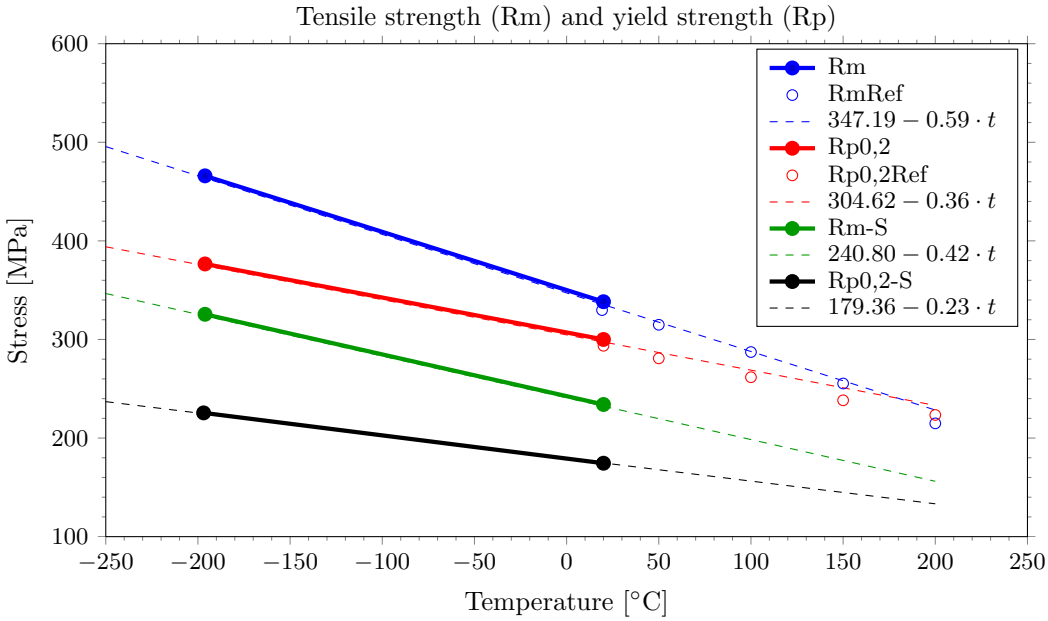

Figure 3.51: Measured tensile strengths and yield strengths for Al-6061-T6 samples at 77 K and 293 K. Two samples were tested; one was an unwelded simple solid, while the other was composed of two Al-6061-T6 halves that were welded together in the middle. Tensile and yield strengths are labelled as Rm and Rp0.2 for the unwelded sample, and Rm-S and Rp0.2-S for the welded sample.

test manufacture of sample moderator vessels. The high strength of Al-6061-T6 is due to a tempering process (denoted by the T6). Some of the strength is lost in the welding seam and in the heat-affected zone because of the temperatures reached in these regions during fabrication. This is taken into account by the careful positioning of the welds in areas of low stress. Continuing investigations are looking into how much of the strength can be recovered by post-weld heat treatment. Figure 3.50 shows the positions of the weld seams and associated stress safety factors against strength at these positions. For assessment and later optimisation of the manufacturing processes, test vessels will be produced. This will also allow pressure testing and thus benchmark the calculation results. Test vessels will be thermally cycled (from room temperature to 77 K) to simulate thermal stress ageing.

Water moderator assembly

The water moderator assembly shown in Figure 3.52 is made up of two parts. The first part is a water premoderator that surrounds the liquid hydrogen cold moderator. The second part consists of extended wings, which constitute the thermal moderator, which makes possible bispectral neutron beam extraction from the moderator assembly. The assembly also makes up part of an insulating vacuum layer for the cold moderator. The total heat load to each water moderator assembly is calculated to be 24.2 kW [339]. Compared to the cold moderator, heat removal for the water moderator assembly is of less concern because higher temperature differences can be allowed in the water. Due to the thermal wings, the design of the water moderator assembly is rather complex and includes two independent water flow paths. Figure 3.52 shows the design of the two parts forming the water moderator assembly. For the final assembly, the cold LH_2 moderator vessel will be positioned inside the premoderator (Figure 3.52, left) and then the thermal part of the moderator is added (Figure 3.52, right). The water moderator assembly will be welded together, thus forming the insulation vacuum for the cryogenic vessel.

This system does not feature a separate helium blanket as is usually seen in other cryogenic LH_2 installations. The main reason for this is that the vessel wall between the vacuum layer and the helium blanket would lack sufficient cooling and would overheat at the ESS power level. To assure detection of small water leaks into the insulating vacuum (and the associated risk that oxygen might freeze out on the cold surfaces), it is proposed to saturate the water with helium gas. In case of leakage, helium gas would enter the insulation vacuum (it would not freeze because its liquefaction temperature is lower

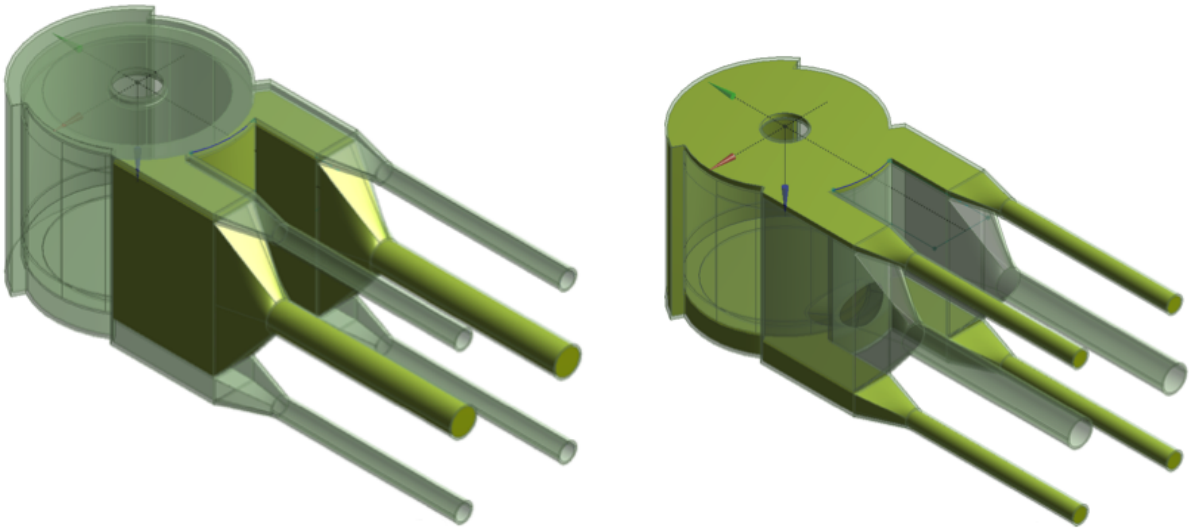

Figure 3.52: The parts of the water moderator. Left: The premoderator, highlighted in solid green. Right: The thermal moderator.

than the temperature of LH_2 operation) and be detected by monitoring instrumentation in the insulation vacuum system. Final proof of this concept will have to be shown by experiment. Figure 3.53 shows fluid dynamics simulation results for the water-aluminium boundary layer for the two parts of the water moderator assembly. Although the temperatures shown are already acceptable, further optimisation will be performed. Due to the low pressure drop and reasonable temperature rise per water moderator part (pre- and thermal moderators) both can be operated in series, reducing the necessary amount of piping from the MR plug to the top of the monolith.

Reflector

The reflector is composed of inner and outer parts. The inner reflector, which extends to a diameter of 0.6 m and a height of 0.9 m, will be made from beryllium. The outer reflector will most likely be made from steel and will feature a diameter of 1.3 m and height of 1.5 m. The frequent exchange of shielding blocks outside the outer reflector is not expected during the lifetime of the facility.

The inner reflector is housed inside an aluminium vessel. The beryllium will be introduced in slices

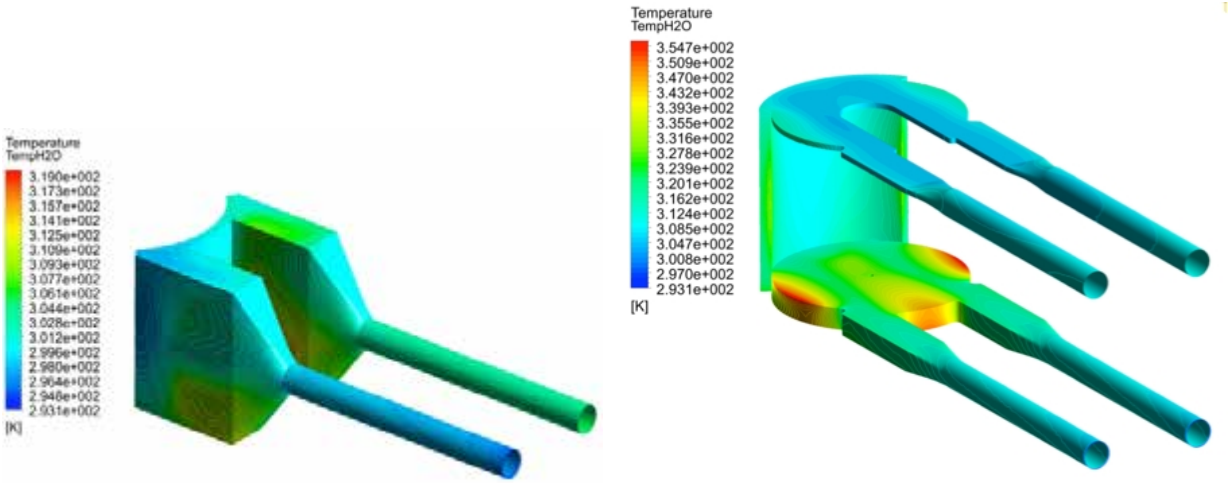

Figure 3.53: Computational fluid dynamics results for the water temperature field in the two parts of the water moderator. Left: The premoderator. Right: The thermal moderator.

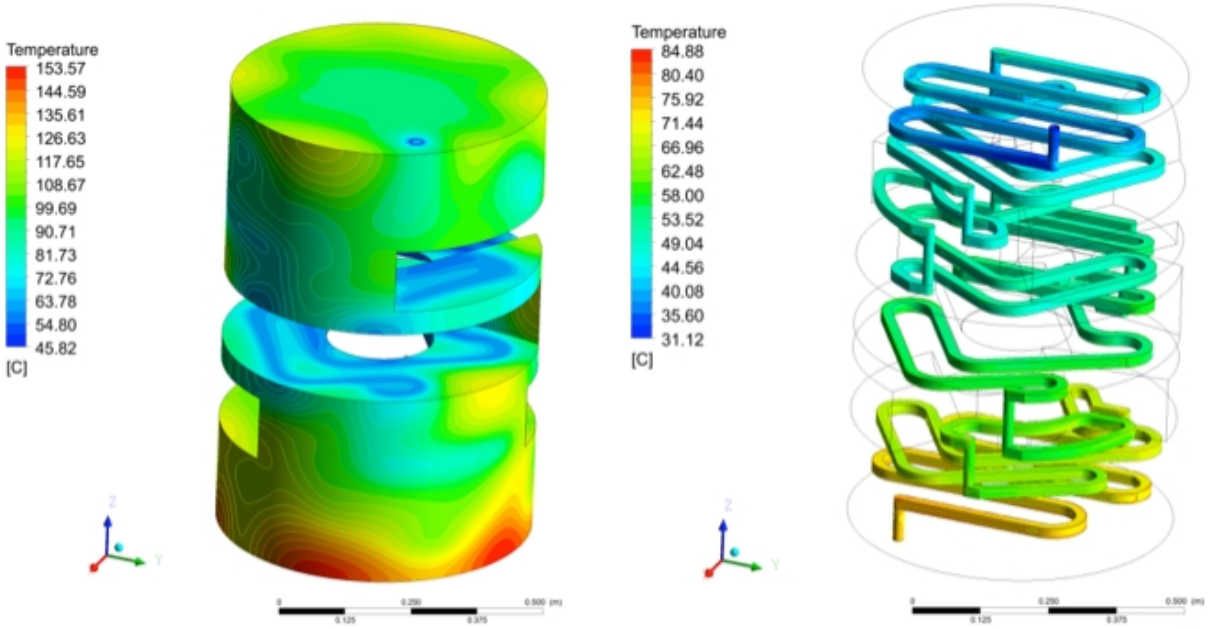

Figure 3.54: Computational fluid dynamics results for the temperature field in the inner reflector. Left: In the beryllium. Right: In the water-cooling channels.

with grooves machined in them for the cooling water flow. Since the total heat load to the inner reflector of 350 kW is not homogeneously spread, as shown in Figure 3.54, the slices are dimensioned to deal with the heat load profile. The water-routing grooves for each slice are connected by vertically drilled holes. Since the beryllium is housed in an aluminium vessel, the contact area between slices does not need to be hermetically tight. A small bypass flow can be tolerated and actually is helpful for cooling the vessel itself. Figure 3.54 shows the temperatures in the beryllium of the inner reflector and in the water-cooling channels. The rather complex routing of the flow results in a pressure drop of 0.75 MPa [371]. This leads to a water-cooling loop operating at at least 1.0 MPa. The maximum temperature in the cooling water is 85°C for a 30°C inlet temperature and the maximum beryllium temperature will be in the range of 150°C. From a neutronic point of view, this seems to be acceptable. The ratio between beryllium and water averaged over the whole inner reflector is about 96.5%, with higher peak water content close to the target.

Moderator-reflector plug and moderator plug

Figure 3.55 shows the assembled MR plug including the inner and outer reflector, the two moderator plugs and the backpack block designed for handling and routing piping with appropriate stepping to avoid radiation streaming. The assemble sequence is as follows; first the inner reflector will be attached to the water piping and lowered into the centre of the outer reflector and then a cover block will be fitted on top to complete the outer reflector, then the backpack block will be bolted to the outer reflector. After this the two moderator plugs (each containing a cold moderator, a water moderator assembly, their associated piping and back-filling material, mainly beryllium) will be horizontally inserted into their openings. Finally, some in-fill blocks (shown in dark brown in Figure 3.55) will be attached to the backpack block filling in some cutouts in the shielding necessary to assemble the piping.

The lifetime of the moderator plug will be limited by radiation damage to structures close to the target to a little over one year at full power. It is expected that this lifetime can be extended after gaining operational experience with the system. The remaining components of the MR plug will have longer lifetimes. Thus, it will be possible to reuse the longer lifetime components of the MR plug by removing the whole plug as one unit from the monolith and transporting it to the active cells. The plug will be replaced by a spare unit. During the operation time of the spare unit the horizontal moderator plugs will be removed from the remaining MR plug and replaced by new units. Figure 3.56 show cut views of the

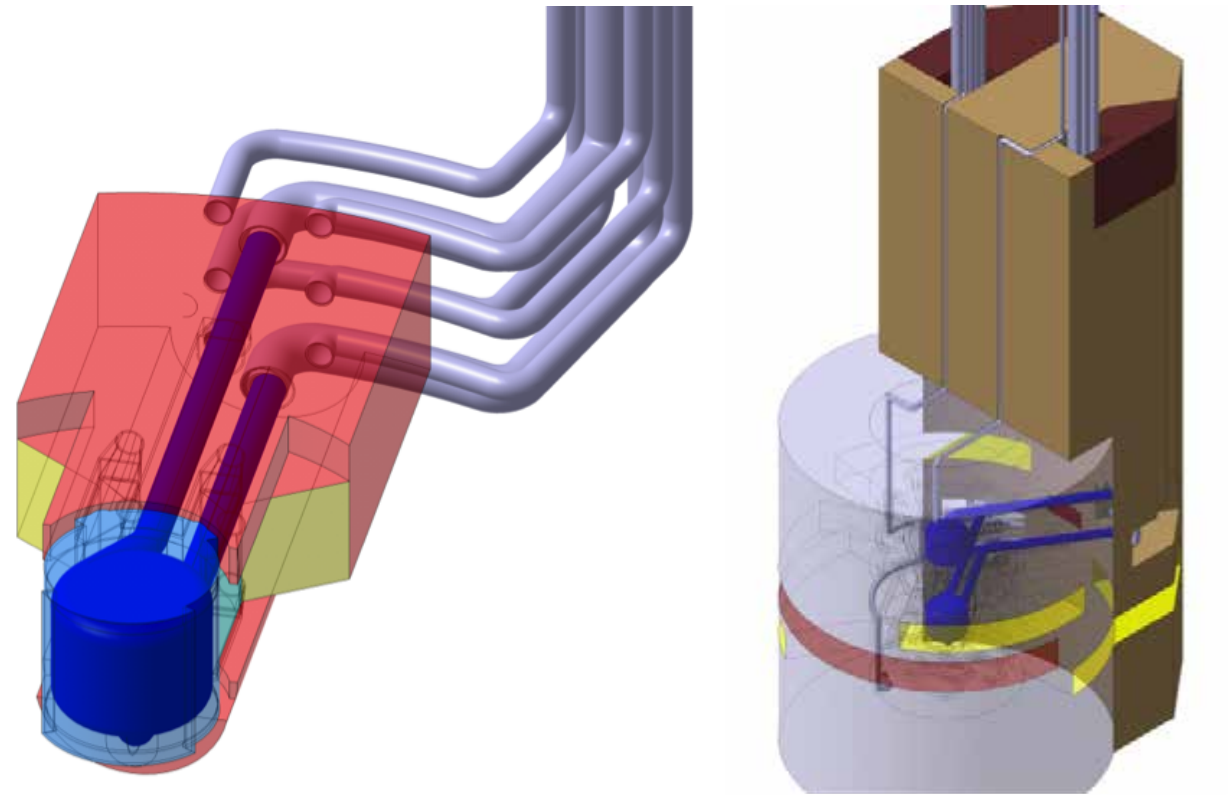

Figure 3.55: Left: The moderator plug. Right: The moderator-reflector plug, including the inner and outer reflectors. Also shown is the backpack block that handles and routes piping, with steps to avoid radiation streaming.

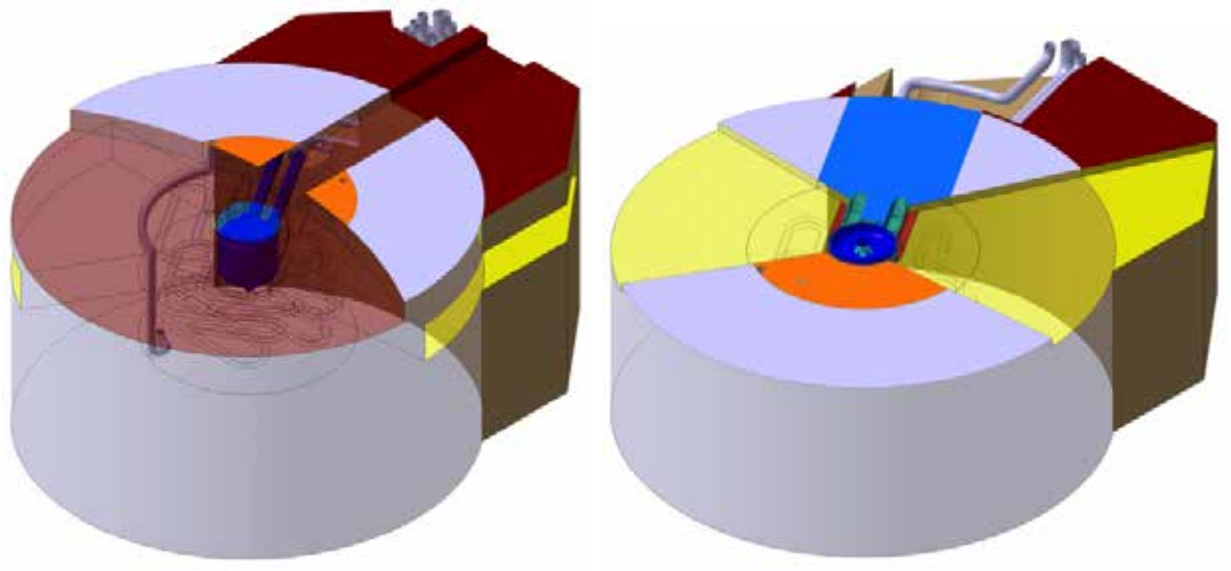

Figure 3.56: Cut views through the moderator plug. Left: Through the target plane. Right: Through the instrument plane, where the cut blue surface represents the horizontal moderator plug. The outer reflector is shown in grey, the inner reflector orange and the steel backpack block is shown in dark red.

target and instrument planes of the moderator plug. The mass of the assembled MR plug will be about 24 tons. It will be transported to and from the active cells using a dedicated handling cask. The MR plug will be handled in a two-axis movement. First, the plug will be moved horizontally from the operating position close to the target to a position further upstream, in order to get clear of the target wheel and allow vertical movement into the shielded handling cask. While the lifting process is facilitated by the tools inside the handling cask, a special machine will be used to allow horizontal movement with the required accuracy both with respect to the operating position and with respect to the position to start vertical handling.

The horizontal handling machine will be a separate tool that can be stored in the high bay area until needed. For operation, it will be lowered on the rails mounted on top of the monolith by the high bay crane. The rails are equipped with limit stops for both positions ("operation" and "ready for vertical handling"). These limit stops will be adjusted during initial installation using a dummy PR plug equipped with end switches to sense the accurate positions at target elevation. This will allow the relevant positions to be duplicated for operation and vertical handling on the target level to the limit stops on the rails. This duplication procedure can be repeated even after the facility has been activated if made necessary by significant geometric changes due to monolith settling, seismic events, or the necessity to disassemble the rails or if modifications are made that change the plug's centre of gravity. The handling machine will be equipped with a bridge for horizontal movement carrying a lifting device that can be attached to the plug. For attachment, there will be two self-aligning bolts and a threaded centre bolt available. The centre bolt will carry the load of the plug. The lifting device will only need to lift the plug by a couple of millimetres to allow horizontal movement without friction and to avoid touching the target wheel. The lifting device is not intended to lift the plug to a higher position. The drive system for horizontal movement will be designed to allow only very low speeds to avoid any dynamic response of the plug hanging underneath. Figure 3.57 illustrates the vertical handling tool for the MR plug.

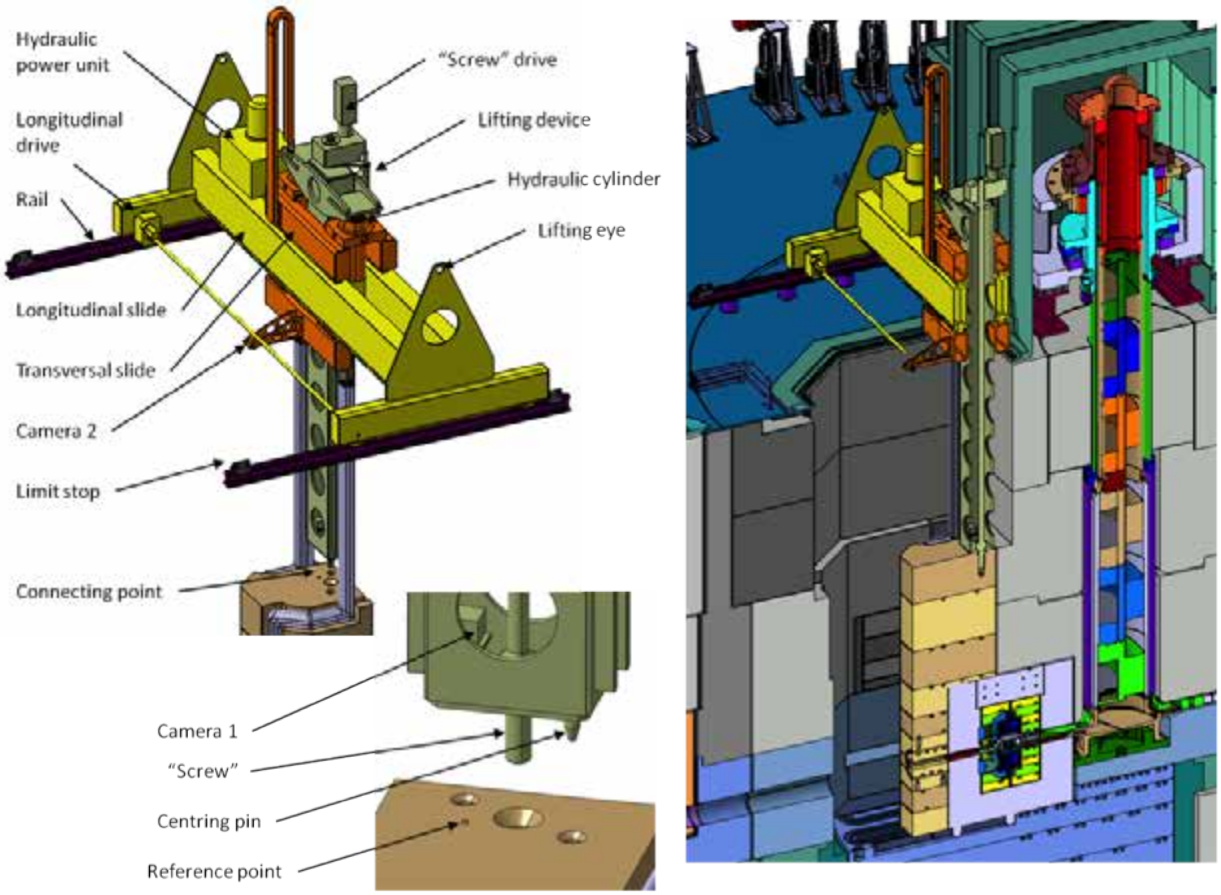

Figure 3.57: Vertical handling tool for the moderator-reflector plug.

3.3.8 Proton beam window

Requirements and configuration

The proton beam window (PBW) module will consist of the window itself – a rectangular curtain of hollow pipes machined from a solid block of aluminium – welded into an aluminium frame, which, in turn, will be mounted between two steel flanges. The PBW will separate the high vacuum of the accelerator beam tube from the helium atmosphere in the monolith. As this window will be stationary, it will be subjected to much higher radiation damage than the beam entrance windows of the rotating target wheel. In addition to the radiation damage issue, the need to provide cooling for 5 MW beam power and up to 85 μA/cm^2 beam current density at the PBW is a major design driver. Aluminium is a good material for the window because of its low density and consequent low specific heat deposition, which enable it able to withstand high accumulated proton beam intensity, and to generate relatively little heat as the proton beam penetrates the window. In addition, aluminium's high stress tolerance will make it possible to circulate the helium coolant through the window at high pressure.

Using aluminium for the PBW, as has been done in other facilities such as SINQ/PSI, leads to an expected window lifetime on the order of one half to one year at full power. Given this comparatively short lifetime, the PBW is designed so that it can be easily replaced. It is thus designed as a module that can be exchanged from the top of the monolith, in a fashion similar to the design at SNS and J-PARC. In order to maintain the helium atmosphere inside the monolith during handling, a special valve between the PBW and the target wheel has been included in the design layout. Since the PBW will be subject to very high radiation damage, the window may not serve as part of the second safety barrier system. Therefore, a fast-acting valve in the proton beam tube upstream of the window will serve as the safety-relevant boundary of the second barrier. The PBW is designed to withstand the differential pressure of 0.1 MPa between the monolith helium atmosphere and the accelerator vacuum as well as the pressure of the helium coolant circulating through the window.

Water is used for PBW cooling at other facilities, including SNS, J-PARC ISIS and SINQ. ESS's baseline design calls for the use of helium gas for this purpose, just as it relies on helium gas as the coolant for the target. Using helium gas to cool the PBW will mitigate the effects of a PBW break on the accelerator beam tube, and will also avoid the tritium production that would occur with water-cooling. The PBW is located about 4.5 m upstream of the centre of the monolith. The proton beam will be more focused at the PBW than at the target. Therefore, the profile at the target entrance window was used for the PBW design, but with an appropriately scaled higher peak current density. This scaling results in a conservative calculated value corresponding to more than 5 MW proton beam power. At a later stage, this conservatism can be reduced by using a more realistic definition of the beam profile at the PBW.

A special coating will be used on the downstream (helium) side of the window, in order for the integrated control system (ICS) to monitor the proton beam profile, Luminescence from this coating will be viewed from the proton beam diagnostic plug, which will be located half way between the PBW and the target. Since this coating will produce an additional heat load on the window, it has to be as thin as possible. The most recent calculations do not include the effect of the additional heat load from the coating, but this will be taken into account as the PBW design is refined.

Window design

The window will be composed of a series of pipes through which the helium coolant will flow continuously. These pipes will form a "curtain," rather like a panpipe. Their diameter will be small enough to enable them to withstand cooling medium circulating under high pressure with relatively low stresses. The diameter will also be small enough to make the pipes stiff enough to withstand the bending load from the 0.1 MPa differential in pressure between the monolith atmosphere and the accelerator vacuum over the window height. Internal pressure loads from the monolith atmosphere under accident conditions will be further investigated before the design is finalised. The window will be manufactured from a solid block of aluminium by high-speed milling and computer controlled drilling of the holes. The general feasibility of manufacture has been demonstrated by the machining of a sample window section. This window will be welded into a larger aluminium frame that will provide mechanical support and will be equipped with channels to guide the flow of the cooling medium into the window, as shown in Figure 3.58.

The panpipe section of the window will be 70 mm in height and 192 mm in width. This is enough to allow a beam of 60 mm $\times$ 160 mm with $\pm$6 mm variation of the real proton beam from the nominal axis.

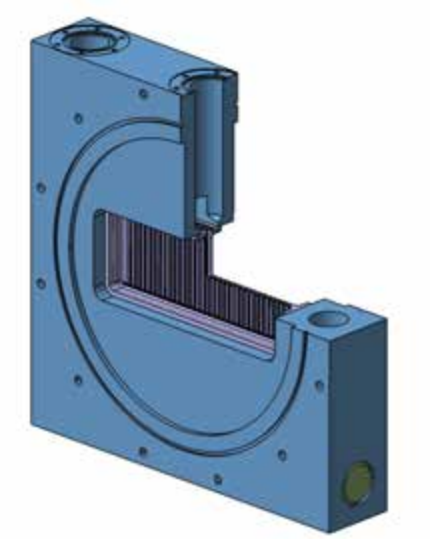

Figure 3.58: The proton beam window and frame.

The pipes feature an outer diameter of 6 mm and a wall thickness of 0.3 mm and are placed with a centre-to-centre distance of 6 mm. The intersection between the pan pipe section of the window and its much larger frame is flexible in the vertical direction to compensate for thermal expansion in the longitudinal direction. Moreover, this flexible clamping compensates for the tilting effect at the end of the pipe section that is a consequence of the window deflection caused by the pressure difference over the window.

As Al-6061-T6 has been chosen for the window material, the maximum temperature is limited to approximately 100°C, because at temperatures above 130°C the material will lose its tempered state and consequently its strength [372]. Preliminary analytical calculations using formulae for pipe flows have shown that for an inlet temperature of 20°C, a helium mass flow rate of 0.1 kg/s is needed to achieve this design criterion. In order to further reduce thermal stresses, a mass flow rate of 0.2 kg/s was selected for the reference design calculation. For this mass flow rate, detailed CFD flow simulations and FEM thermo-mechanical calculations were performed for a parabolic and time-averaged heat deposition profile with a peak value of 0.5 kW/cm^3 and footprint dimensions of 160 mm $\times$ 60 mm. The maximum temperature for the time-averaged heat deposition is approximately 65°C, which will occur in the centre of the beam footprint. Considering a temperature increment in the centre of the PBW of about 15°C during one pulse, the maximum temperature for the pulsed operation will vary between approximately 73°C at the end of one pulse and 56°C prior to the next pulse. The maximum temperature of 73°C will give leeway to increase the helium inlet temperature at a later stage of the project without exceeding the temperature limit for the chosen aluminium alloy.

Relevant stresses emerge in the flexible intersection between the panpipe section of the window and its massive frame and thus outside the beam penetration zone. The maximum local stress is about 83 MPa and emerges at the end of the cylindrical part of the central cooling channel. Relevant bending and membrane stresses of about 67 MPa are expected at the flexible intersection that has to compensate for the thermal expansion of the PBW. Dynamic amplification due to the pulsed operation can be neglected in this case, because the pulse length is much longer than the period time of relevant eigenmodes. Nevertheless, the pulsed operation has a significant impact on fatigue. One can expect stress amplitude of about 10 MPa for the flexible intersection during pulsed operation and resulting temperature oscillations. These are postulated to occur about 3×10^8 times during the lifetime of the window. In addition to these stress cycles during normal operation, cyclic stresses due to beam trips have to be considered. Beam trips of more than 0.5 s will lead to a complete cool-down of the PBW and consequently to stress cycles that might – depending on the expected number of beam trips – require additional measures to reduce fatigue damage. One remedy is to further increase the helium mass flow rate. However, fatigue evaluations show that the PBW structure can withstand more than 2.9×10^4 postulated trips in a year.

Proton beam window plug

The PBW frame is mounted between two stainless steel flanges forming a PBW module, as shown in Figure 3.59. These flanges are actively water-cooled and carry the inflatable metal seals. The module can be exchanged as one unit from the top of the monolith. For installation and alignment purposes the module is equipped with guides that engage into grooves in the proton beam window duct structure. These grooves define the exact position of the PBW module. The module can be adjusted after initial assembly of the monolith.

The general sealing technology is similar to that used at the neutron sources at SNS and J-PARC. The inflatable seals are double seals with an interstitial space that can be monitored and evacuated for leak detection and better sealing quality. The PBW duct will be operated in a rough vacuum so that requirements on the seals are reduced. The first seal (viewed from the monolith helium atmosphere) seals the helium against the rough vacuum, while the second seal seals the rough vacuum against the high quality vacuum of the proton beam tube. The counterpart for the inflatable seals is a polished metal sealing surface. In order not to damage this surface, the inflatable seals will be retracted by evacuating the seals. In any case, should the surfaces be scratched it is possible to exchange the beam tube section containing these seals, as shown in Figure 3.59. This is done horizontally, after extracting the first 2 or 3 meters of beam tube upstream of the monolith. All necessary piping, helium-cooling, water-cooling and vacuum lines, will be routed from the module to the top of the monolith. Flexible hoses can be used to cope with tolerances as well as thermal expansion of the piping. The routing of the piping has been designed so that the shielding blocks above the PBW module can be retracted without touching the piping.

The handling sequence is as follows; first the cooling helium loop will be emptied, flushed and refilled with an inert gas or dry air. Then cooling water circuits will be emptied, flushed and dried. After this, both the vacuum valve in the proton beam tube towards the accelerator and the helium valve downstream of the PBW will be closed. After venting the PBW duct with air or an inert gas, the upper cover (in the connection cell) can be removed in order to enable hands-on disconnection of the pipe elbows right underneath the cover. Now the shielding blocks above the PBW module can be removed. Depending on the accumulated activation, the lower one may be removed using a shielded flask due to activation on its lower end. After this, the PBW module itself can be removed into a shielded flask. The piping can be cut down at the module with a hydraulic remote pipe cutter. This allows independent pipe removal, thus relaxing size requirements on the flask. After a remote inspection of the sealing surfaces, the new PBW module can be lowered into position guided by the pre-aligned groove in the duct structure. The remaining work will be done in reverse order.

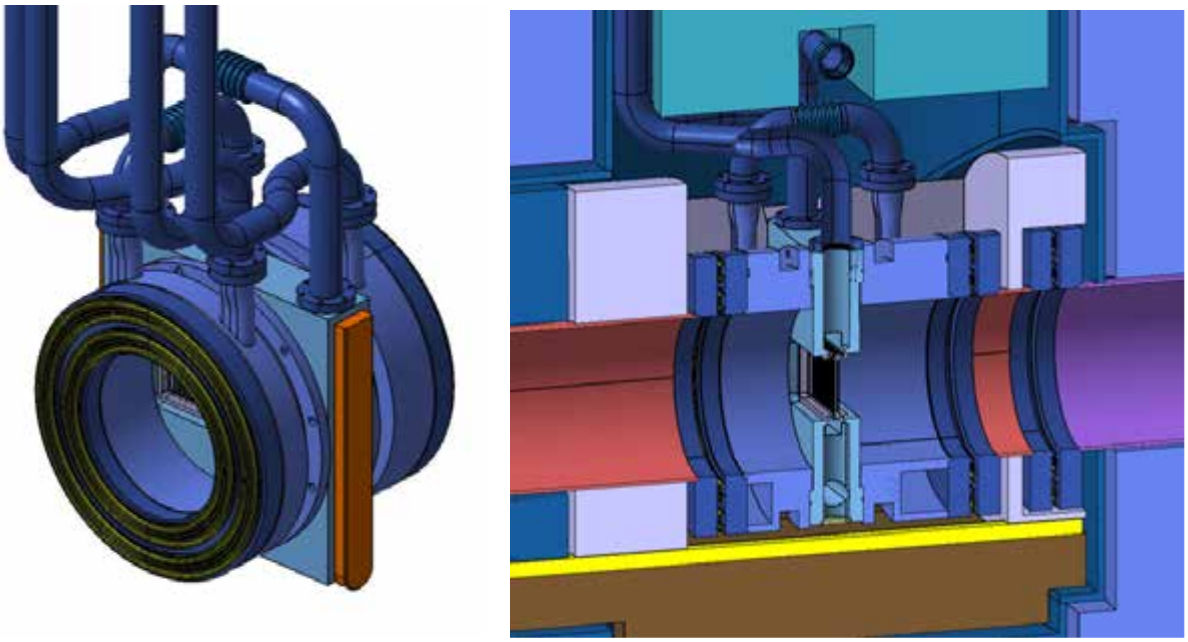

Figure 3.59: The proton beam window module and plug. Left: Inflatable seals. Right: Plug sealing system.

3.3.9 Beam ports and beam extraction system

The target monolith structure must have at least 22 openings for neutron beam guide inserts NBGI, in order to accommodate the full suite of 22 neutron instruments.

The current design of the beam extraction system includes 48 possible beamline positions in four fan-shaped beam extraction sectors, as shown in Figure 3.60. Each beam extraction sector is 60 degrees wide and has 12 possible positions with 5 degrees of angular separation, each of which can be opened for a beamline. For shorter instruments that need more than 5 degrees of angular space to the neighbouring instrumented beamlines, 10 degrees or even 15 degrees of separation can be achieved by keeping the neighbouring beamline positions closed. Current estimates suggest that about 40% of the instruments will need more than 5 degrees of beam separation from their neighbours, which implies that a maximum of about 36 open beam lines can be placed on the 5 degree grid of the 48 possible beam port positions. This design offers high flexibility to optimise beamline distributions to instrument suites that will vary over the lifetime of the facility. For example, with the 22 instruments slated to be built during the ESS construction phase divided into 40% short instruments that require 10 degrees of angular separation from neighbouring beam lines, and 60% longer instruments that require only 5 degrees of separation, the neutron flux gain for the whole facility will amount to 13% compared to a conventional uniform distribution, as discussed in Section 3.2.6. Implementing this flexibility involves marginal additional costs during the initial construction phase because, as shown in Figure 3.61, it implies the use of a larger number of smaller, removable shielding blocks compared to a smaller number of larger shielding blocks installed permanently for the lifetime of the facility. Opening additional beam ports at positions initially not prepared during the construction of the monolith would be prohibitively complex and expensive.

The beam ports will be arranged in two layers. The centre axes of the ports in the top layer will be directed towards the top moderator assembly, which will be situated 180 mm above the proton beamline.

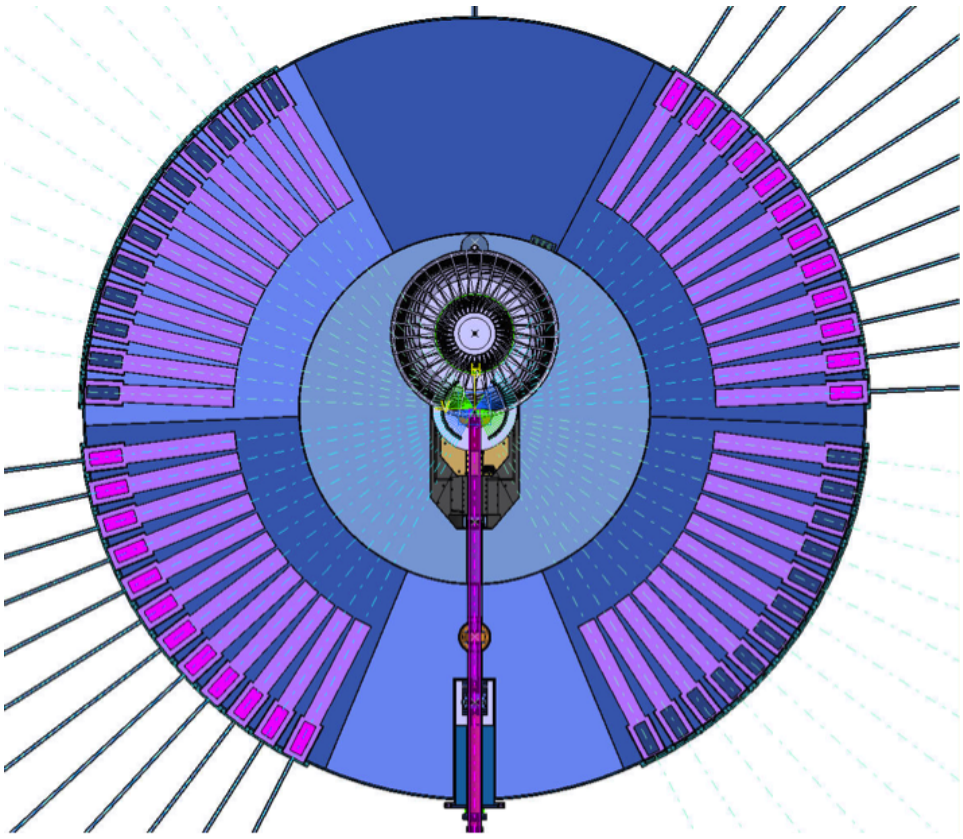

Figure 3.60: The potential neutron beam port configuration from a horizontal plane view. The 48 possible beamline positions are laid out in two vertical levels. Colours of the light shutters distinguish the different levels. The blue represents the upper level and the pink represents the lower level.

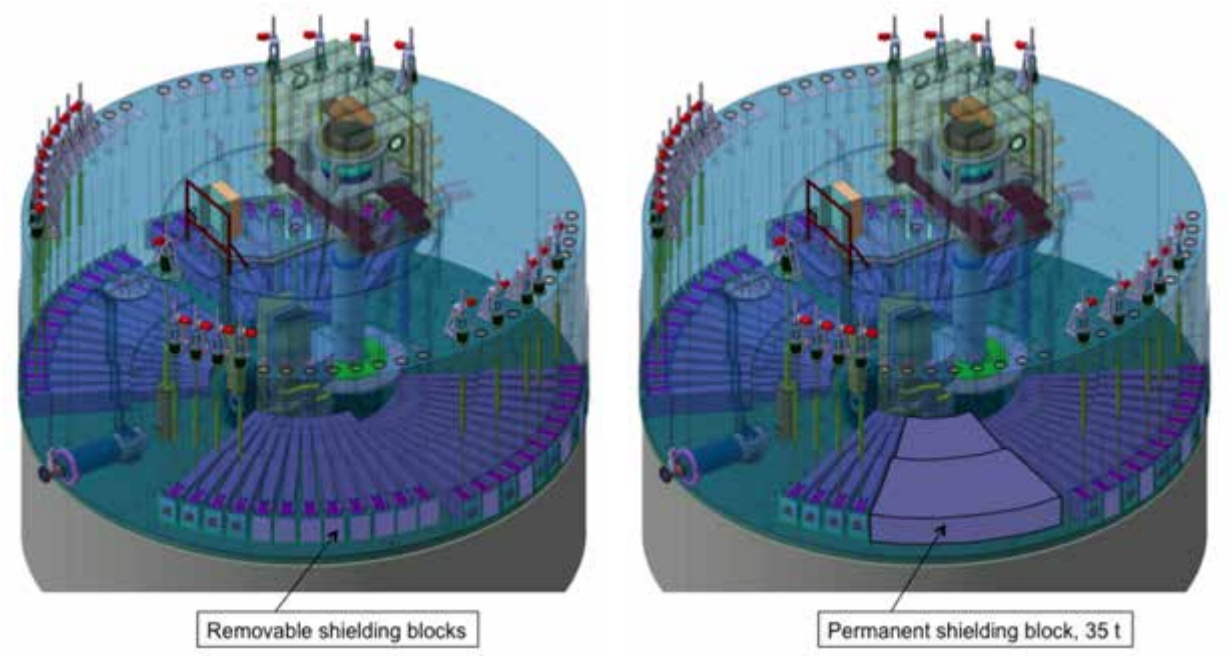

Figure 3.61: Two ways to shield closed beamline positions. Left: With removable shielding blocks. Right: With permanent shielding blocks.

The centre axes of the ports in the bottom layer will be directed towards the bottom moderator assembly, which will be situated 180 mm below the proton beamline. It will be possible for the neutron beam guides inserted into the ports to view both parts of the moderator assembly (thermal and cold), thus allowing bispectral extraction, in those cases where the dimensions of the guide permit this flexibility. The approximate separation of 170 mm at 2 m from the centre of the monolith (where the beam guide inserts originate) between neighbouring beamline axes with a 5 degree separation, allows good visibility of both types of moderator. Moving further out from the centre, adequate space becomes available to accommodate the installation of ballistic or elliptical guides.

All the beamline inserts will be identical in outer shape. The baseline design preliminarily calls for each insert to be equipped with a 500 mm thick light shutter which, when closed, will provide adequate shielding to allow access to beamline components outside the monolith after the proton beam is shut down. Unlike full heavy shutters, these light shutters are not able to block high-energy neutrons while the beam is on target. The final combination of no shutter, light shutter and heavy shutter solutions will be consolidated at the beginning of the construction phase.

Neutron beam guide inserts and shutters

A neutron beam guide insert NBGI will consist of a solid block of steel that is stepped on the outside to avoid streaming of radiation through the gap between the insert and the opening in the monolith-shielding block. Due to the narrow angular separation of adjacent beamlines, there is limited space for stepping. The design takes this tight spacing into account by setting strict manufacturing tolerances for the blocks at the beamline level as well as the inserts themselves. The resulting small gaps allow minimal stepping to be effective in reducing streaming and thus unwanted background radiation. The insert will be loaded and unloaded horizontally using a rail system, which will be built into the high precision-machined monolith shielding blocks. Figure 3.62 shows a neutron beam port with a shielded handling cask in place.

Due to the 5 degree separation between beam port sites, the width of the insert at the upstream end will be as low as 170 mm. The insert outer geometry will widen to 210 mm as soon as geometrically possible. The front section of the insert will be 270 mm high and the height will increase in steps to 400 mm. The helium inside the guide insert will be part of the monolith's helium atmosphere. Since the neutron beamline inside the monolith will feature a light shutter, alignment between the upstream guide element and the guide segment that travels with the shutter gate has to be guaranteed. The resting points

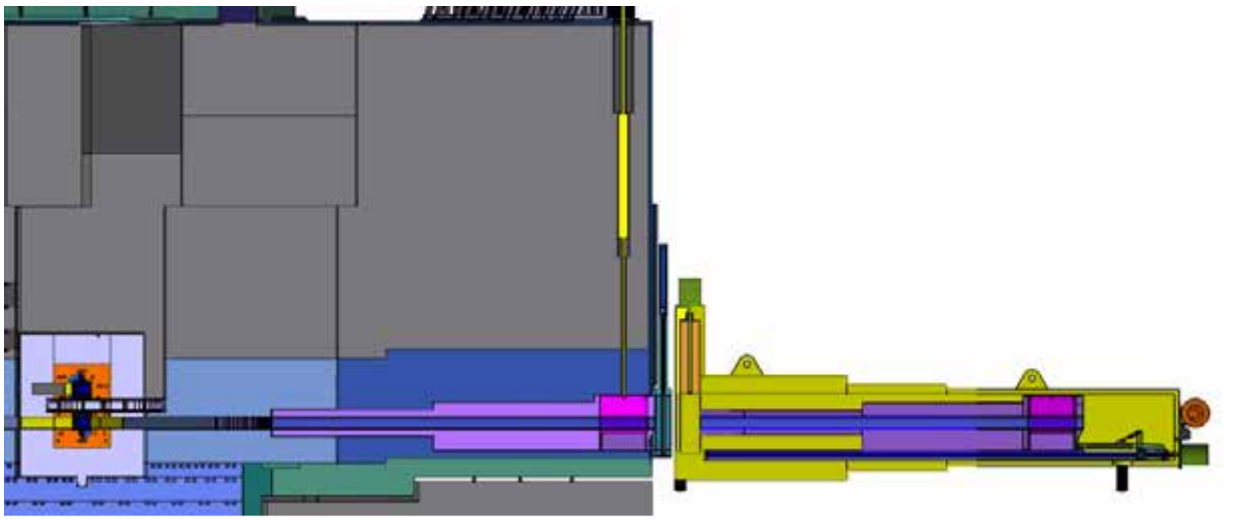

Figure 3.62: A cross section view of the neutron beam port with shielded handling cask in place.

for the shutter gate in the open position will be so-called "highly repeatable" kinematic mounts, that is, kinematic mounts that make it possible to repeatedly precisely position a moving component on the mount. The shutter will be made an integral part of the guide insert, with the shutter gate's open-position resting points attached directly to the insert. Thus, it will be possible to align the guides inside the insert, as well as the gate, to the outer surface of the insert and to each other in the open position. In order to assure failsafe operation, the shutter gate is designed to be closed in the down position.

The drive system for the shutter gate will be mounted on the top of the monolith, outside the helium atmosphere. Metal bellows will separate the drive system from the pull rod that reaches down to the shutter gate. The pull rod will be engaged in the gate and will pull it towards the kinematic joints. Springs in the drive system will allow the rod to securely press the gate to the kinematic joints while not allowing the whole insert to be lifted. Thus, access will be provided to mechanical components such as drives and motors for repair without interfering with the monolith helium or creating a need for remote handling. Water cooling connections for the guide insert will be provided from the downstream side before mounting the neutron beam window.

Handling of the insert will be performed by a shielded horizontal handling cask, as shown in Figure 3.62. In order to remove and reinstall a guide insert, the first 6 m of neutron beamline outside the monolith for the relevant instrument, and perhaps for the two neighbouring instruments as well, will have to be removed. Outside of the monolith, every beamline will be equipped with kinematic mounts to allow the flask to be positioned exactly in front of the beam port. The handling cask will feature a double door to minimise the potential for spreading contamination from the monolith into the experimental hall. Nevertheless, removal and reinstallation of the neutron beam window will open the experimental hall to the monolith atmosphere for a brief period of time.

Neutron beam windows

The neutron beam windows will separate the monolith atmosphere from the experimental hall. Thus, they will be part of the monolith liner confinement barrier. In order to minimise their effect on the neutron spectrum, the windows will be made of aluminium and have been designed to be as thin as possible. To provide a margin of safety, a double wall window design with monitored interstitial space has been adopted, as shown in Figure 3.63. The inner window (on the monolith side) is designed to withstand evacuation of the monolith and thus a 0.1 MPa pressure differential. The outer window (on the instrument side) will be only about 0.5 mm thick and so will require careful monitoring for even small pressure differentials. The frames of adjacent beamline windows will abut each other leaving very little space between window flanges.

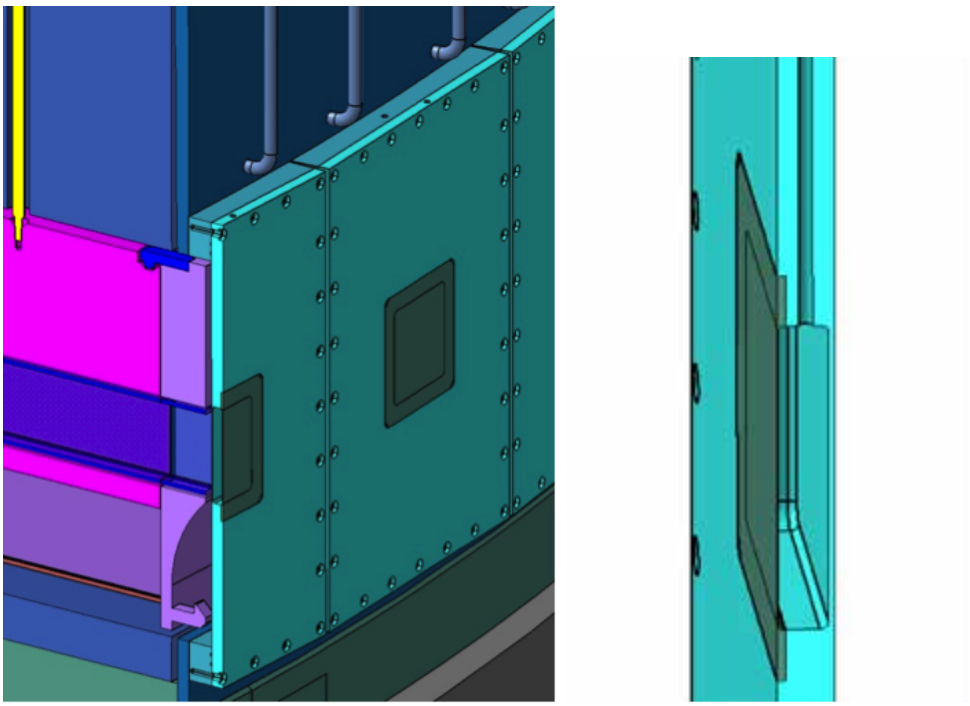

Figure 3.63: Left: The neutron beam ports. Right: A close up view of the double walled neutron beam window.

3.3.10 Irradiation ports

The main goal of ESS is to generate thermal and cold neutron spectra that will be used by the neutron-scattering research instruments. In addition, fast neutron spectra (possibly mixed with proton spectra) can be extracted from the monolith, in order to irradiate samples and components. The primary goal is to irradiate components or materials as part of ESS's own program of target station R&D. Other applications could also be investigated, however, such as irradiation of materials for fusion research or tests of microchips.

Two possible irradiation concepts are of interest, either placing samples close to the target, moderator and reflector, or placing samples in the path of fast neutrons extracted through irradiation ports. In turn, three different possibilities for irradiation ports have been considered. One is a high energy beam transport (HEBT) port located in the proton beam horizontal plane, in a backward direction at an angle of about 160 degrees with respect to the proton beam axis, in order to disturb neither the neutron guides nor target handling, as shown on the left of Figure 3.64. Another possibility is a forward fast neutron port, located in the forward zone close to the proton beam axis, starting at the target wheel opposite the proton footprint, and continuing through an opening in the monolith shielding, as shown on the right of Figure 3.64. Again, this arrangement would not disturb the neutron guides or target handling. A third possibility is a fast neutron basement port leading from the target wedge on which the protons impinge, but on the opposite side from the proton footprint. A possible path, taking into account monolith design constraints, travels downwards in the monolith, below the wheel shaft, as also shown in Figure 3.64.

Samples could be placed inside the target, or in the moderator plug close to the neutron production zone, to be irradiated for short time (in which case a system for inserting and removing the samples would be needed), or for a longer term (one or more years), in which case samples would be inserted and removed during operations on the MR plug. The design of removable irradiated components (such as a target, PMR plugs, PBW plug, and shielding) would include the ability to retrieve samples after their dismantling or during their maintenance phase in the hot cells, in order to monitor irradiation damage. This would provide important information for improving the design and lifetime of regularly replaced target subsystems, over the 45 year lifetime of the facility.

The MCNPX input file for the target station was modified to include possible fast neutron ports. Neutron fluxes and radiation damage parameters were calculated for some representative locations: in the

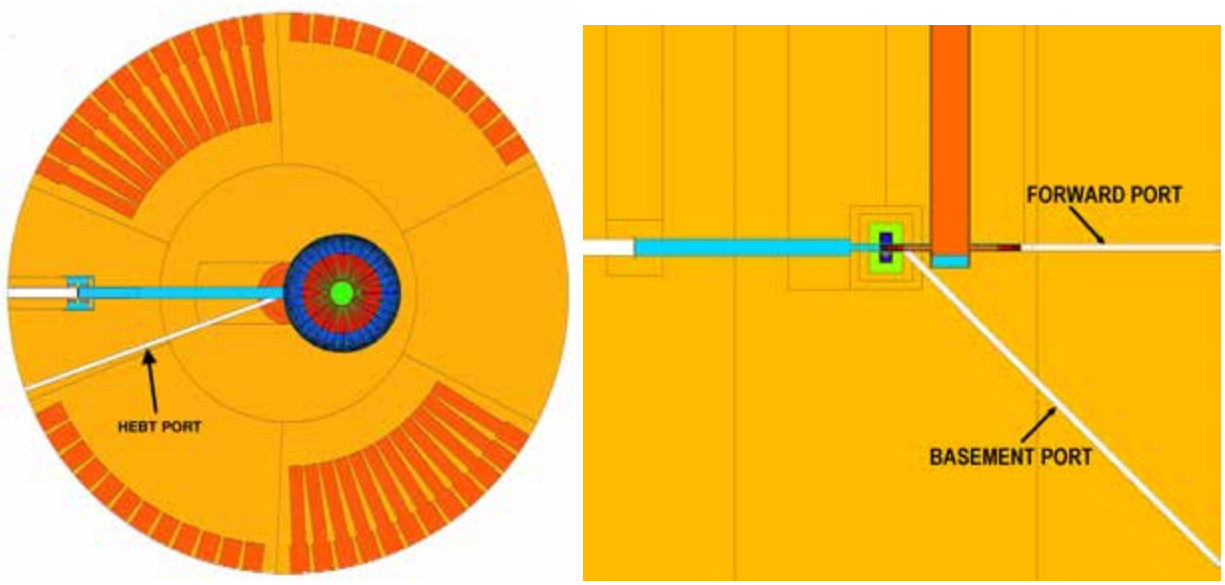

Figure 3.64: Three potential locations for fast neutron ports. Left: High energy beam transport port. Right: Forward port and basement port.

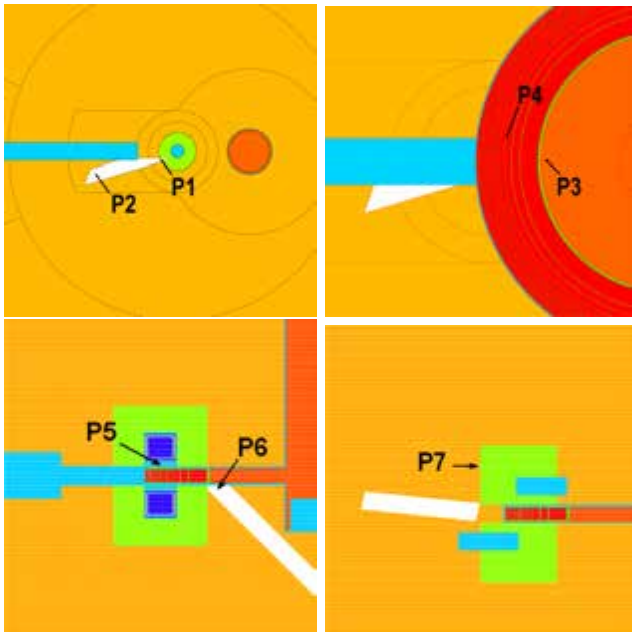

Figure 3.65: MCNPX model layout describing locations P1 to P7, from the HEBT port closest to the reflector and the proton beam, to the reflector plug.

forward irradiation port close to the wheel, and in the HEBT port close to the reflector and close to the proton beam (positions P1 and P2 in Figure 3.65), inside the target in a location representative of the sector edge and in the wheel body close to the tungsten sector (positions P3 and P4), in the space between target and moderator at the moderator radial centre (position P5), at the beginning of the HEBT port, close to the wheel (position P6), and in the position where the reflector plug is set (position P7). Calculated fast neutron spectra above 1 MeV are plotted in Figure 3.66. The maximum neutron flux is reached at the moderator centre. Interesting positions for flux magnitude in the energy region of fusion applications (10 to 20 MeV) are P1, P3 and P6. Figure 3.66 shows the mapping of the neutron flux integrated between 10

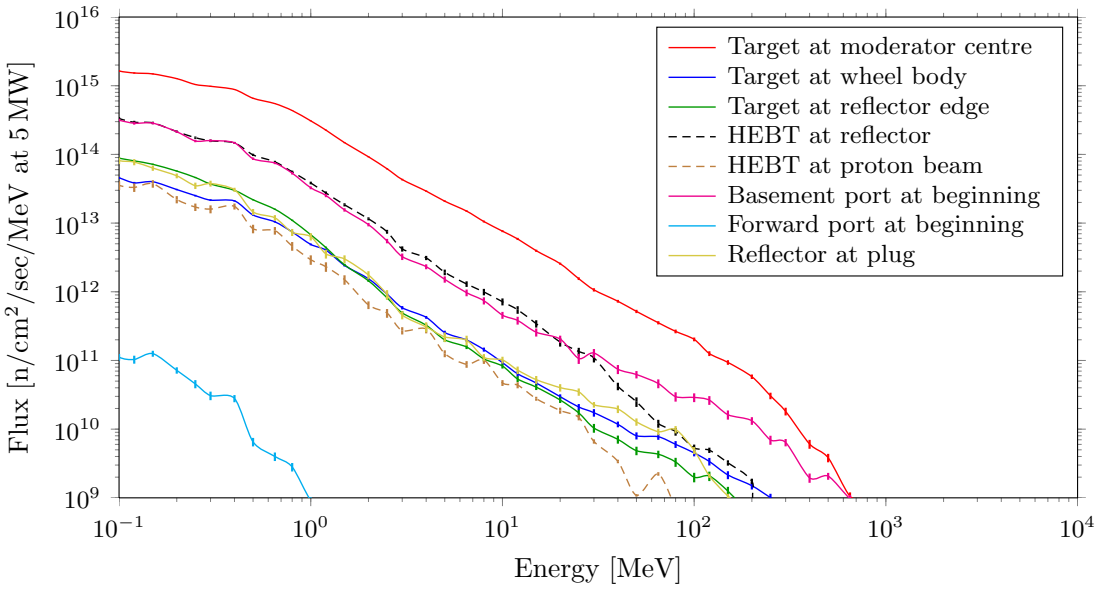

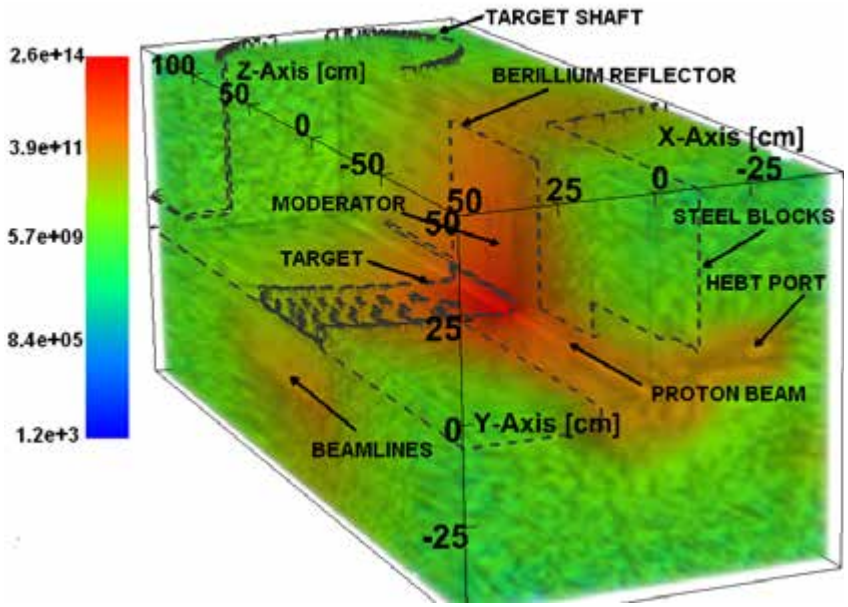

Figure 3.66: Calculated neutron behaviour in the target-moderator-reflector assembly. Top: Neutron spectra at the reference locations P1 to P7. Bottom: Integrated neutron flux between 10 MeV and 20 MeV.

and 20 MeV in the TMR region. The effects of radiation damage have been addressed by calculation of the displacement per atom (dpa) over the course of an operational year of 5000 hours, and the hydrogen and helium gas production rates measured in atomic parts per million (appm) per dpa. These calculations relied on cross sections for iron reported in recent KIT evaluations [342]. The calculations were performed in the positions listed above. The results are reported in Table 3.21. For comparison, the estimated parameters of radiation damage in the planned DEMO fusion reactor are also presented [373].

Location	**Radiation damage** [dpa]	**Hydrogen gas production rate** [appm/dpa]	**Helium gas production rate** [appm/dpa]
Forward port at wheel	8.5×10^{-5}	–	–
HEBT port at ion tube (P2)	0.1	18.7	4.7
HEBT port at reflector (P1)	1.2	23.2	5.6
Reflector at plug (P7)	0.2	44.7	11.4
Basement port at target (P6)	1.3	86.5	20.0
Target at inner body (P4)	0.2	5.4	1.2
Target at sector edge (P3)	0.2	1.9	0.5
Moderator at centre (P5)	11.7	48.5	11.6
DEMO fusion reactor first wall	20	46	11

Table 3.21: Radiation damage and gas production in the target-moderator-reflector assembly, at the positions shown in Figure 3.65, and in the DEMO fusion reactor first wall [373].

3.3.11 Tune-up dump

The tune-up dump will stop the proton beam during accelerator tuning. It will be located in the basement of the target station in the A2T area of the target building. By design, it will be a passive device, which will last for the life span of the facility, although it will operate only during periods of accelerator tuning. The baseline design calls for a graphite core embedded in aluminium cladding, cooled by water circulating through several channels. Alternative metallic materials could replace the graphite if necessary.

Figure 3.67 shows that the tune-up dump will be separated from the accelerator proton beam tube by a window. The current design of the dump's enclosure tank includes a cylindrical graphite core 2 m in length and 0.3 m in diameter, with 0.05 m thick aluminium cladding. Four cooling channels are drilled along the aluminium cladding, each 0.02 m in diameter. Together, the channels make possible a total mass flow rate for the water of 2 kg/s. The tune-up dump window consists of two thin (3 mm thick) aluminium layers cooled by a water film in between. The tune-up dump is designed to require minimal handling and maintenance during its lifespan. What regular handling is necessary will be conducted from outside the dump window. The tube between the dump and the window, shown in Figure 3.67, passes through a concrete wall. Maintenance will thus be conducted manually or semi-remotely from the other side of the wall, out of the direct line-of-sight of the activated graphite, with limited dose rates. As mentioned above, the tune-up dump will be located in the basement of the target station in the A2T area, straight ahead from the accelerator proton beam tube. The high bay overhead crane will cover this area. If the dump

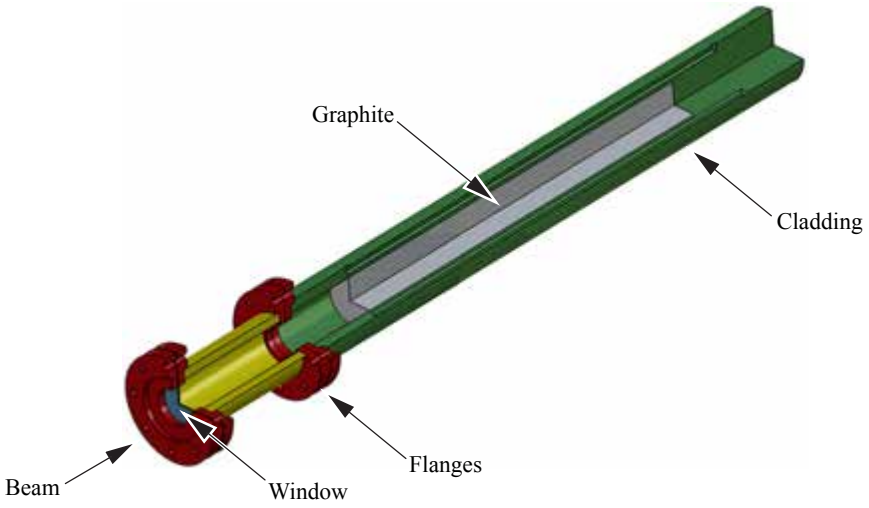

Figure 3.67: Tune-up dump overview.

Beam mode	**Min. rms beam size** [mm]	**Max. deviation** [mm]	**Pulse length** [μs]	**Max. current** [mA]	**Rep. rate** [Hz]	**Beam energy** [GeV]	**Average current** [mA]	**Temp. rise** [K]
1	9	6	10	55	14	2.5	7.7	0.4
2	9	6	10	55	14	0.2	7.7	1.8
3	9	6	105	55	1	2.5	5.8	4.2
4	9	6	105	55	1	0.2	5.8	18.4
5	0.5	31	10	55	2	2.5	1.1	96.9
6	0.5	31	10	55	2	0.2	1.1	194.4
7	9	6	3000	55	0.034	2.5	5.6	124.9
8	9	6	3000	55	0.034	2.0	5.6	121.7

Table 3.22: Beam modes and parameters for the A2T tune-up dump.

should have to be accessed for handling, the accelerator components and tube, as well as the shielding required for the accelerator above the dump will have to be removed. The dump could then be lifted to the high bay.

A shutter system will be placed between the tune-up dump and the accelerator, upstream from the dump window. The shutter will be closed when the dump is not in use in order to limit dose rates in the HEBT area, allowing for operation or maintenance of the accelerator components. The dump will be in its own vacuum environment, separated from the accelerator vacuum by the dump window. The environment around the dump will consist of low-pressure helium. The emission of activated volatile compounds and failure of the cooling channels will be monitored. Any graphite dust produced during dump operation will be removed from the dump environment.

Eight beam modes have been defined for the tune-up process, as shown in Table 3.22, which also includes thermal simulation results [374]. These beam modes present a Gaussian beam profile. The cooling scheme for the dump has been analysed for each of these modes and no feasibility issues have been detected. All cooling tubes will be joined in a manifold that will serve as the interface with the cooling system handled by the target systems. The maximum temperature of the graphite during transients will be low enough to guarantee its stability. The graphite core is the only part of the tune-up dump that will be subject to thermal stresses, but it is not a structural material for the dump. Thus, the graphite could break down without compromising the integrity of the dump. Because of the low thermal expansion coefficient of graphite, the aluminium will not be deformed by thermal stresses. Average operating temperatures are low enough to guarantee safe operation even when thermal contact between aluminium and graphite is not perfect.

3.4 Fluid systems

The target station fluid circuits are of two distinct types, the closed circuits and the open circuits. The closed systems include the water, helium, nitrogen and cryogenic liquid hydrogen circuits. The open circuits are the ventilation and the confinement air systems.

Closed circuits

The closed circuits are dedicated to power removal from the active zones of the target station or, for the helium flowing within the monolith, to avoiding accumulation of radioactive products and corrosion inside the large, irradiated containment vessel. They are staged in primary circuits that directly carry the heat away from the spallation zone, and in intermediate circuits. The intermediate circuits exchange the heat taken from the primary circuits with external circuits flowing outside the target station areas, and with conventional facilities located in non-monitored areas. A notable characteristic of these external circuits is that these are not individually controlled online, from a radiological point of view. The closed fluid circuits are organised so that all the primary circuits running through the activating fluxes of primary and secondary particles and gammas are confined within controlled areas, which are not accessible during power operation modes. These primary fluid circuits are slightly activated by protons and neutrons, or

contaminated by corrosion products, or by outgassing from their activated containment parts, in normal situations. However, these primary circuits are physically separated from the non-monitored areas by intermediate fluid circuits, and heat is transferred from the primary to the intermediate circuits via heat exchangers. Consequently, any transfer of contamination from these circuits will be contained within the target station areas where it can be detected online or during periodic tests. This general layout principle guarantees that no transfer of radioactive contaminant outside the target station area can occur either in normal operating circumstances, or in case of incidents or accidents. It would require at least a double failure for unplanned radioactive releases to occur. The water circuits are organised so that the different functions, such as removing energy, draining circuits, filling circuits, or filtering fluids, are separated as much as possible from one another, for reasons of safety and operational convenience. All the liquid circuits will drain to designated activated water storage facilities and will be collected inside the target station building during maintenance. All the potentially contaminated circuits will also be ventilated via the radioactive gaseous effluents and confinement system (RGEC), which will make it possible to route them through a decay tank and purification subsystem if necessary. Additional information about fluid system interfaces can be found in Chapter 7.

Open systems

The radioactive gaseous effluents and confinement system will be an open-air circuit. It will take air from different target station building volumes and extract it to the exhaust stack. Since the entrance of air will be managed by the target station building's heating, ventilation and air conditioning (HVAC) system, there will be no air conditioning function in the RGEC system, as discussed in Chapter 7. The RGEC system will connect to a number of circuits ventilating different portions and individual rooms in the target station. The RGEC functions are required both during the power operation and the maintenance periods of the target station. The RGEC system contributes to the functioning of the confinement barriers, assuring dynamic confinement when the intrinsic barrier tightness is not sufficient, especially during target station maintenance periods. It also enhances confinement performance to limit the radiological impact of released contamination during abnormal situations. The RGEC system is composed of sub-branches serving various parts of the target station, including the active cells (transfer zones in and out of the cells in the processing, handling and storage zones); the connection cells in direct communication with the monolith atmosphere during maintenance; and the internal neutron guide extraction zone (located within the additional shielding surrounding the neutron beam windows in the experimental hall, which are open during neutron guide insert exchange). The RGEC also serves areas with subject to much lower levels of contamination than the active cells, including the target station high bay, the utility rooms hosting the primary fluid circuits including the target station basement where the radioactive fluid storage tanks are located and the target station A2T zone.

3.4.1 Gaseous cooling circuits

There are four independent gaseous cooling systems in the target station. These are the target cooling system, the proton beam window cooling system, the monolith atmosphere system and the intermediate gas cooling systems. Each cooling system is based on system-specific purification and filter-handling concepts, and are therefore treated separately below.

Target cooling system

The target will be cooled by circulating helium gas. The coolant temperature at the inlet to the target must be as low as possible and as close as possible to the installation temperature. This will reduce the operating temperature level of the target and also will minimise target displacement due to thermal elongation of the shaft during the ramp-up period from zero-proton current to operating temperature. The design must allow online purification of the coolant, and must be able to handle the potential of dust contamination, mainly from the tungsten spallation material. Based on these considerations, an O-shaped cooling system configuration has been selected, as shown in Figure 3.68.

A helium compressor will drive the helium around the O-shaped circuit at a flow rate of 3 kg/s, which is the rate necessary to cool the target below the critical temperature, as discussed in Section 3.3.2. Given the rated compression ratio of 1.5, the helium from the compressor will be heated to about 70°C, and will

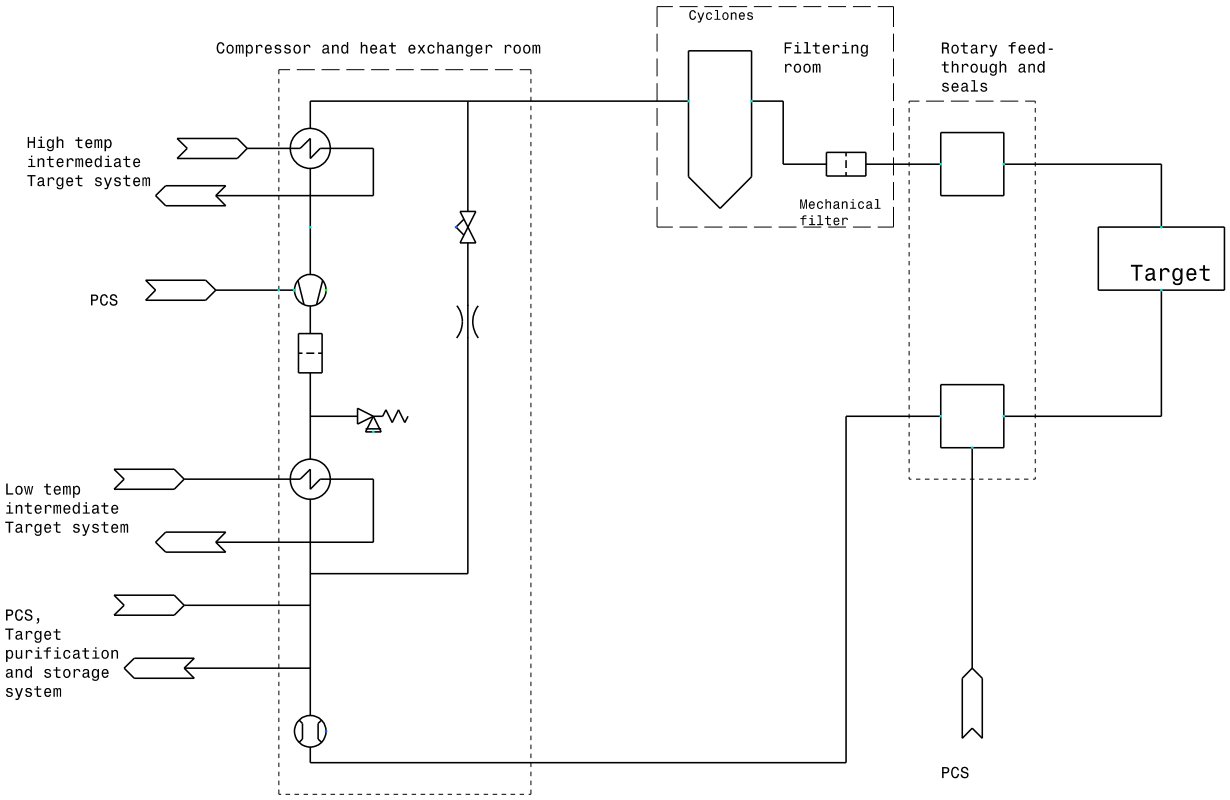

Figure 3.68: The helium circuit of the target cooling system and its principal components.

then be cooled to 20°C by a heat exchanger. The cold helium flow will go directly to the target system through the rotary feedthrough. In the target, the helium will be heated to about 220°C. The leak rate from the target cooling helium circuit is conservatively estimated to be less than 0.1% per day, based on the operating experiences of the HELOKA test loop at KIT [375].

In order to prevent dust contamination of the helium circuit by tungsten or other (active) solid particles, a mechanical filtering system will be installed downstream of the target. To ensure stable operating conditions for the compressor, a second cooler will be installed between the filter and the compressor, in order to cool the hot helium flow from the target to 20°C. A purification system connected on a bypass to the compressor will make it possible to purify the helium online. This system will cope with volatile and gaseous components that need to be removed from the coolant stream. The bypass itself will also be dimensioned to control the helium flow rate through the target.

The helium circuit will deliver a relatively high volumetric flow of approximately 6.4 m^3/s at a relatively low pressure of 0.3 to 0.4 MPa. The goal of the relatively low pressure is to relax constraints on the design of the target vessel and, especially, of the beam entrance windows (BEW) along the rim of the target shroud. The structure exposed to the proton flux will receive a volumetric power deposition from beam stopping and scattering. The associated thermal stresses, combined with mechanical stresses due to the filling pressure of the cooling flow, determine the required design thickness of the BEWs and the shroud. As a thicker target shroud results in reduced neutronic performance of the target system, it is important to make the BEWs and the shroud as thin as possible, which is facilitated by the low filling pressure. The top and bottom covers of the target wheel, which are most subject to the pressure load, are flat and therefore difficult to reinforce against internal pressure. This is also an important issue for the optimisation of the target, and especially for the neutronic performance of the system. The high flow rates at low pressure induce high velocity. It is therefore important to carefully assess the pressure drop along the circuit. Figure 3.68 illustrates the global layout of the circuit and the placement of each component. Table 3.23 summarises the circuit's essential parameters.

A multi-stage compressor will be used for circulating helium for target cooling. The commercially available helium compressors that meet the target cooling circuit requirements described above are typically

Parameter	Units	Value
Pump head, or total head loss	MPa	0.1
Inlet pressure	MPa	0.3
Design pressure (relative)	MPa	0.35
Helium mass flow rate	kg s^{-1}	3
Pumping power	kW	800
Bulk temperature at target inlet	°C	20
Bulk temperature at target outlet	°C	220
Pipe diameter	mm	250 – 300
Pipe total length	m	185
Cyclone filter volume	m^3	3.2
Total volume of the circuit	m^3	15 – 23

Table 3.23: Key parameters of the target cooling system helium circuit.

about 4 m × 8 m large, with a required electrical power rating of approximately 800 kW. This power rating implies that the helium temperature at the outlet of the compressor will rise to about 70°C. The operating pressures at the inlet and at the outlet are 0.3 MPa and 0.4 MPa respectively, for commercially available helium compressor technical specifications [376, 377].

An important aspect of compressor performance is the leak rate. The compressor will have two rotating seals. A dedicated inflow of clean and controlled helium will leak towards the atmosphere, creating a negative pressure across the sealing and preventing helium from the target cooling circuit from leaking. The leak rate – the required helium supply – is estimated to be about 2 Nm^3/hr, where "Nm^3" is a normal cubic metre of gas at a temperature and pressure of 0°C and 0.1 MPa. Figure 3.69 presents the principle of a sealing solution. The enclosure has a pressure of helium slightly higher than the pressure inside the core of the pump. That will insure that the helium can only flow from this enclosure towards the helium circuit. Some helium will leak though the last seal towards the atmosphere, but this will be the controlled helium fed by the supply directed to the enclosure. This concept will also be considered for the rotary feedthrough, which will provide the helium from the fixed part of the circuit to the rotating target shaft.

Two kinds of dust filters are under consideration for use in the helium circuit. For small particles, standard filters could be used. They would be placed on the bypass circuit, for instance in the purification

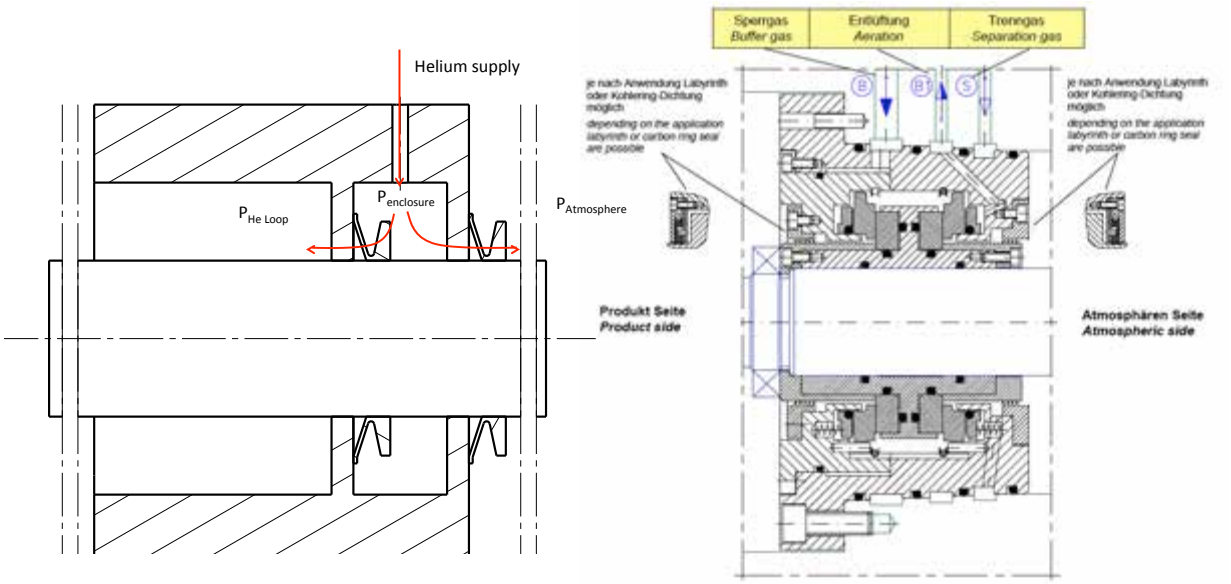

Figure 3.69: A double seal with an enclosure fed by helium. Left: Conceptual sketch. Right: Existing technology (from John Crane Ltd).

circuit, as shown in Figure 3.68. The use of cyclonic filters in the main helium stream is also under consideration. Such filtering systems are widely used in industry, even in harsh environments. The high density of tungsten makes it suitable for this type of filter.

The goal of the filtering system is to capture and remove from the helium stream any tungsten particles that may have been flushed away from the target. A hurricane, or cyclonic, system would be be the simplest, most robust and cost effective technical solution. The efficiency of the global filtering system is enhanced by adding a mechanical recirculator to the simple hurricane system. The efficiency is further enhanced by adding an electrostatic recirculator. The purpose of the recirculator is to reintroduce the fine non-captured particles into the cyclone after these have been driven to the outer walls of the recirculator by centrifugal forces. The mechanical recirculator decreases emissions 40% to 60% more than does the simple hurricane filter, and the electrostatic recirculation system reduces particle emissions even further. In the electrostatic approach, a DC high voltage is applied to the concentrator, allowing the recirculation of very fine particles, which are more resistant to centrifugal forces, to the cyclone collector. After having been separated in the recirculator and concentrated in the recirculation flow, electrically charged particles are attracted by the cyclone walls, while agglomerating with larger particles entering the system, both facilitating capture. A hurricane system equipped with an electrostatic recirculator is illustrated on the left of Figure 3.70.

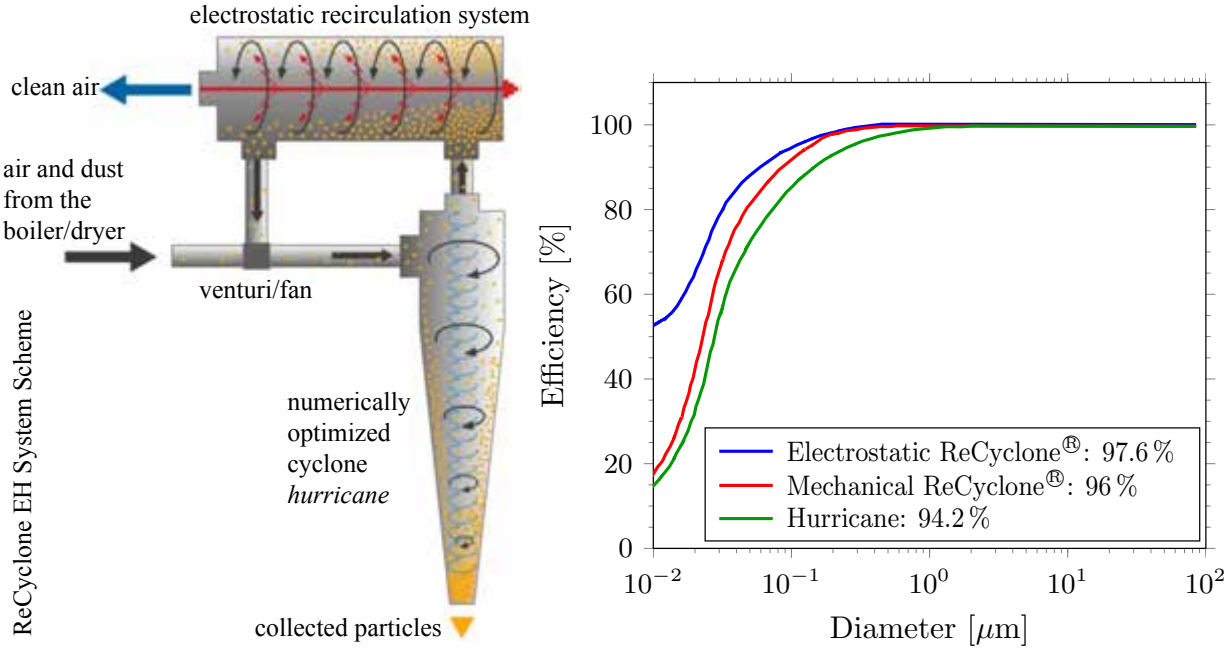

Figure 3.70: A cyclonic filtering system equipped with an electrostatic recirculator to capture dust in the helium circuit. Left: Typical filter configuration (Courtesy of ACS). Right: Predicted filtration efficiency versus particle size for three different configurations.

A preliminary analysis has been made of the filtration efficiency of commercially available cyclonic systems, assuming a conservative particle size distribution (PSD) over grain sizes between 0.01 μm and 100 μm, and for a particulate emission density of 0.27 μg/(Nm)^3 [378]. The result are summarised on the right of Figure 3.70, which shows the particle size dependent filtration efficiencies for three configurations. The simulated overall efficiencies range from 94.2% to 97.6%, agreeing well with measured efficiencies between 92.9% and 98.9% [378]. The measured pressure drop in the cyclonic system is 1.3 kPa, negligible compared to the overall pressure drop in the helium circuit. The filtration efficiency of ESS cyclonic systems will be close to 100% under normal operational conditions, considering that the grain size of the tungsten target material is expected to be approximately 10 μm [379]. Some additional issues remain to be analysed, especially regarding the handling of the container. These should not be difficult to deal with, but some key parameters must be better determined before the maintenance routine can be fully specified. Finally, the chosen configuration was assessed for its ability to deal with the formation of tungsten trioxide (WO_3) dust, which would occur in the event of air ingress if the tungsten temperature were to rise above 500°C. The analysis relied on earlier estimates of the tungsten trioxide erosion rate and particle size

Parameter	Units	Value
Tungsten trioxide (WO_3) erosion flux	kg m^{-2} s^{-1}	5×10^{-5}
Total surface area potentially eroded	m^2	17.5
Tungsten trioxide erosion rate	kg/s	8.7×10^{-4}
Average WO_3 concentration in the flowing helium	kg/m^3	8.2×10^{-5}
Expected WO_3 emission density	$\mu g/(Nm)^3$	1.76
Expected total filtration efficiency for the nominal PSD	%	95.41 – 97.47

Table 3.24: Expected filtration efficiency for tungsten trioxide dust in the event of air ingress [379].

distribution [322, 380]. The parameters used for the analysis and the expected filtration efficiency for the nominal PSD are summarised in Table 3.24.

The target cooling circuit is a closed circuit which will require pressure control. Since the coolant is gas, any change in the mean temperature of the system will have an impact on the pressure. Particularly during start-up, the helium temperature on the return line will increase by about 160°C, while the temperature in the rest of the circuit will remain unchanged. In order to maintain the pressure level, a fraction of helium will have to be removed from the system, since the volume of the circuit is constant. In addition, during operation, there will be helium inserted into the system through the rotating seals at the helium pump and the target shaft. Assuming that the pipes and filter volume is 23 m^3, the total amount of helium that will have to be removed will be about 9 m^3. This can be accomplished by putting the surplus of helium in an intermediate buffer, and then compressing it for storage.

Due to the fact that the compressor is a centrifugal machine, there is no separation of volumes in the circuit, and the connecting point of the pressure control system (PCS) can be located anywhere along the circuit. However, it is desirable to put it downstream of the machine for the stability of the compressor. Another source of pressure increase comes from the positive leakage that occurs at the labyrinth. The helium constantly put into the system has to be removed. This can be achieved with the same system, as described above. To reduce the loss of helium and simplify inventory tracking, circuit helium storage could be used as helium supply for the rotating seals. In order to do that, it is necessary to purify the gas from the buffer first, as discussed in Section 3.4.4.

In order to study the dynamic behaviour of the whole target cooling system, a thermal-hydraulic model has been built using the RELAP5-3D system code [381]. This code has been developed for the best-estimate transient simulation of light water reactor coolant systems, during postulated accidents. It includes libraries for helium properties, which allow the simulation of this gas as a working fluid. The model is built up, starting from modelling one sector, then setting up the target wheel model by connecting 33 sectors in parallel and, finally, generating the model of the whole helium circuit. For one sector, the model gives a total temperature rise of the helium of 150 K and a pressure drop of 46 kPa. These results are comparable to the CFD results presented in Section 3.3.3. The RELAP model gives lower values than the maximum temperature level from the CFD analysis, due to its coarser meshing. Using shaft design data, the flow to the wheel is modelled as an annulus flow and the return flow is modelled as a pipe flow. The pipe diameter corresponding to the equivalent hydraulic diameter of the spiral is modelled as a branch flow for each sector. The target wheel is modelled using 33 sector models installed in parallel. The model also takes the heat transfer between the inlet and outlet flow in the shaft region into account. The model is calibrated in such a way that the flow is equally distributed for the 33 sectors for the cold run at 20°C.

In a transient simulation, the pulsed operation is started at 50 s from the cold stage. For this simulation, a perfect synchronisation between the wheel and the beam is assumed. Between the pulses, in each sector, the decay heat is simulated for 47 kW of power, as discussed in Section 3.3.2. Figure 3.71 shows the simulation results. The temperature increase of the target wheel is 150°C and the total pressure drop is 51.6 kPa. The total pressure drop of the target including the shaft is estimated at 60.7 kPa. In a similar way as for one sector, the time constant of the target is calculated to be 44 s.

Proton beam window cooling system

The proton beam window (PBW) is cooled by helium at a mass flow rate of 0.2 kg/s, as described in Section 3.3.8. This cooling is provided by a closed cooling circuit, in which the helium takes heat in the PBW and gives it to the intermediate water-cooling circuit for gas described in Section 3.4.2, via a heat

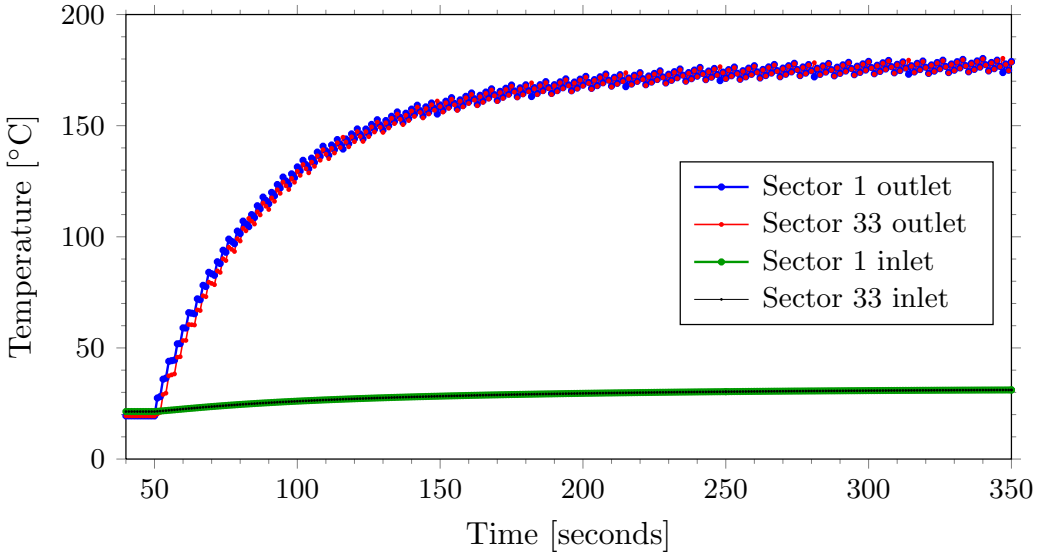

Figure 3.71: Temperature evolution of the target wheel cooling system after start-up in pulsed beam operation with decay heat.

exchanger. The system works as follows. A blower blows the helium through a filter and a heat exchanger which cools the helium to room temperature before it is led into the PBW. The filter takes care of traces of lubricants from the blower. The flow rate and pressure are controlled either by speed control or bypass. In the PBW, the helium is heated, mainly by the thin window walls and the inlet and outlet manifolds. The pulse temperature in PBW material is about 100°C, but time spent in the window is short and the area is small. Therefore, the bulk temperature increase in the helium in the cooling system is lower by an order of magnitude than the pulse temperature. After the PBW, the helium passes through another filter to remove dust from the window and protect the following components. After this, it enters the blower again.

There are also a number of side connections to the circuit. In order to stabilise the pressure in the circuit, there is a small accumulator tank connected to the circuit after the blower. Before and after the blower, there are connections to the gas purification system, as discussed in Section 3.4.4. The pressure level is maintained via a connection to the helium purification and storage system, which is also used to fill and refill the system after outages.

Monolith atmosphere system

The helium inside the monolith will have to be circulated in order to avoid pockets of stagnant hot or possibly contaminated helium. The best way to ensure movement of the helium, at least in the vicinity of the target where hot spots might occur, is under evaluation. One source of helium injection into the monolith atmosphere will be the barrier gas used for the rotating seal for the target shaft. Direct injection or extraction of helium in the vicinity of the hot components, the target and the moderator-reflector system close to the target could also be beneficial. Further calculations may show that cooling the upstream end of the guide insert can be done by moving helium only, avoiding the need for a water-cooled insert.

Intermediate gas cooling systems

In addition to the cryogenic refrigeration systems, which may be viewed as intermediate but are described in Section 3.4.3, the only intermediate cooling system working with gas is the intermediate target cooling system. This system takes heat from the primary target cooling system, and gives it to the conventional facilities cooling system via heat exchangers between the systems. The purpose is to protect and isolate the latter from contamination in the former. In order to ensure that no water can enter the primary target coolant circuit, even in the event of a heat exchanger failure, this intermediate circuit uses nitrogen. The risks and remedies for nitrogen ingress in the main target circuit have been extensively investigated [382].

Measures will be taken to protect against this eventuality, such as the placement of rupture discs in the primary helium circuit.

The flow rate in the intermediate target cooling system is about 60 kg/s. The system works as follows. A compressor presses the nitrogen through a filter at 1 MPa. The filter takes care of traces of lubricants from the compressor. The flow rate and pressure are controlled either by speed control or bypass. After the filter, the flow passes a heat exchanger where the nitrogen compressor heat is transferred to the conventional facilities cooling system. Then the nitrogen flow is divided into two parallel paths. The first path goes to the heat exchanger before the primary target-cooling compressor and takes out the heat from the target. This means that the available temperature difference on the primary helium side of this heat exchanger is about 200°C. The second path goes to the heat exchanger after the primary target-cooling compressor. This means that the available temperature difference on the primary helium side of this heat exchanger is about 50°C. After cooling the two target cooling system heat exchangers in parallel, the nitrogen flows are united again, before entering another heat exchanger in the nitrogen system. Here, the heat from the primary target cooling system is removed, and the nitrogen is cooled to room temperature before it enters the compressor again.

There are also a number of side connections to the circuit. In order to stabilise the pressure in the circuit, there is a small accumulator tank connected to the circuit after the pump. This connection is also used to evacuate the system and lower the pressure if needed. The pressure is maintained via a connection to the nitrogen supply system, which is also used to fill and refill the system after outages.

3.4.2 Water cooling systems

Water moderator cooling

All parts of each of the two water moderator assemblies above and below the target (discussed in Section 3.3.7) are connected to one closed water circuit, which is cooled via the intermediate water system that is, in turn, cooled with water from conventional facilities. Within the closed circuit, the cooling water from the water moderators first passes a delay tank to allow decay of short-lived isotopes, thus reducing radiation exposure of the components downstream. After the delay tank, the water goes into a tank for gas and liquid separation, where gaseous radiolysis products are either recombined in the gas separator or sent to the cover gas system. Water from the gas and liquid separation tank goes through a heat exchanger and a pump, before re-entering the water moderators. Downstream of the pump, a small bypass flow is directed to the water purification system, consisting of filters and ion exchangers. Purified water is returned to the system to the suction side of the pump. The system can be drained to a storage tank for maintenance. The water moderators will operate at close to room temperature, i.e. at about 20°C. The temperature rise in the water is expected to be approximately 10°C [371]. A heat load of about 25 kW has been estimated for each of the water moderators, making 50 kW in total [339, 371]. The operating pressure for structural integrity is set to 1.1 MPa [371]. This power, pressure and temperature will require an approximate flow rate of 0.9 kg s^{-1} per water moderator assembly.

Reflector cooling

The basic configuration of the inner (beryllium) reflector is analogous to that of the moderator described above, although the heat deposition and thus required mass flow rate are different. This cooling circuit will also operate at about room temperature. The heat load to the inner beryllium reflector is calculated to be 350 kW [339]. Due to the higher heat load, the temperature increase will be about 60°C [371]. This power and temperature difference results in a required flow rate of roughly 2 kg/s. The operating pressure is set to 1.1 MPa [371]. The outer reflector will be cooled by the shielding, plugs and component cooling system, which is described in the following section.

Shielding, plugs and component cooling

This system contains circuits for all parts within the monolith that require water-cooling, except the moderators and the inner (beryllium) reflectors. It also contains circuits for the tune-up beam dump and the fixed proton collimator in the A2T part of the high energy beam transport (HEBT), as discussed in Sections 3.1.2 and 4.7. The radiation exposure of the water system will be lower than the exposure of the water circuits serving the moderators and inner reflector, although it will still be significant. Hence,

requirements on the gas and liquid separator tank, delay tank and filters are a little more relaxed. This circuit's basic design will be similar to that of the other water-cooling circuits described above. The system will operate at approximately room temperature with an outlet temperature set to be lower than 35°C, and the operating pressure will be 1.1 MPa.

All components within the monolith with operational cooling requirements have active cooling systems. The shielding cooling circuits are thus designed to provide cooling to all shielding blocks in the monolith that have been identified as needing active cooling. The current basis for design is that all areas with a specific heat load higher than 1 kW/m^3 will need water-cooling. The total power deposited in the inner (cooled) shielding is calculated to be 290 kW [339], leading to a required flow rate of 14 kg/s in the region. The outer reflector cooling circuit power is calculated to be 780 kW [339], giving a required flow rate of 46 kg/s. The cooling powers required for the proton beam window plug and the proton beam diagnostics plug have not yet been estimated, but will probably be small compared to requirements for shielding and reflector cooling. The cooling power for the tune-up dump is limited to a maximum of 50 kW in total [339], giving a required flow rate of about 0.6 kg/s. Similarly, the collimator cooling requirement is estimated to be 35 kW, yielding a circulation requirement of 0.4 kg/s.

In total, the cooling requirement and water flow rates for this system are 1.2 MW and a little over 50 kg/s. The system is designed with redundancy to take at least 1.6 MW, in order to ensure removal of the full beam power, minus target, moderator and inner reflector cooling.

Intermediate water cooling systems

There are two intermediate cooling systems working with water, separating the primary systems from direct exchange with the conventional facilities. The intermediate water system for water serves as an intermediate for all the primary water systems, which include those of moderators, (inner) reflectors, and shielding systems. The intermediate water system for gas serves as an intermediate for all the primary gas systems, which include those of monolith flush and atmosphere, proton beam window and gas purification systems. Though the total power transferred in the system for the water is several times larger, because these systems receive more heat, the two intermediate systems are similar. They operate as follows. A pump generates a flow through a heat exchanger, where the intermediate water is cooled by water from the conventional facilities cooling system. Then the water flow is divided in parallel paths for each primary system to be cooled. The flow rate in each path may be controlled depending on the cooling needs in the primary systems. After the parallel paths, the flows are united again and go into a combined accumulator and gas separation tank. After this tank, the water is led back to the suction side of the pump. There are also side connections to water purification (for the unlikely event of contamination), to conventional facilities sewage and to water refill.

3.4.3 Moderator liquid hydrogen cooling circuit

The hydrogen circuit supplies supercritical liquid hydrogen (LH_2) at a flow rate of approximately 0.8 kg/s and a cooling capacity of about 20 kW at 20 K. The cryogenic system required to achieve this can be subdivided into three main sections, as illustrated in Figure 3.72. The first section represents the medium supply. Besides hydrogen, helium and liquid nitrogen are supplied from storage tanks kept separate from the main circuit components. Helium is used for the cooling of hydrogen, as discussed in Section 6.1.3, as a blanket gas and as a purge gas for safety reasons. Liquid nitrogen can be used for pre-cooling and in a gaseous form, as a blanket gas. Nitrogen will also be used to dilute the hydrogen inventory to well below the flammable limit in the case of a vent release through the stack.

The second section contains the main components of the hydrogen circuit as shown in Figure 3.72, which includes the circulators, the hydrogen-to-helium heat exchanger, the accumulator, a hydrogen heater and the ortho-to-para converter. It is necessary to avoid leakage of hydrogen to the outside and ingress of air (thus oxygen) towards the cold surfaces of the liquid hydrogen circuit, so the main components of the circuit are housed in a double-walled vacuum vessel with an interstitial helium blanket layer. Leaks and air ingress can be detected by the use of appropriate instrumentation to monitor off-gas in the exhaust of the vacuum pump and the hydrogen concentration in the blanket gas. The components in this vacuum vessel are connected via transfer lines and an appropriate coupling system to the cryogenic moderator vessels. The vessels and the in-monolith piping represent the third section of the system.

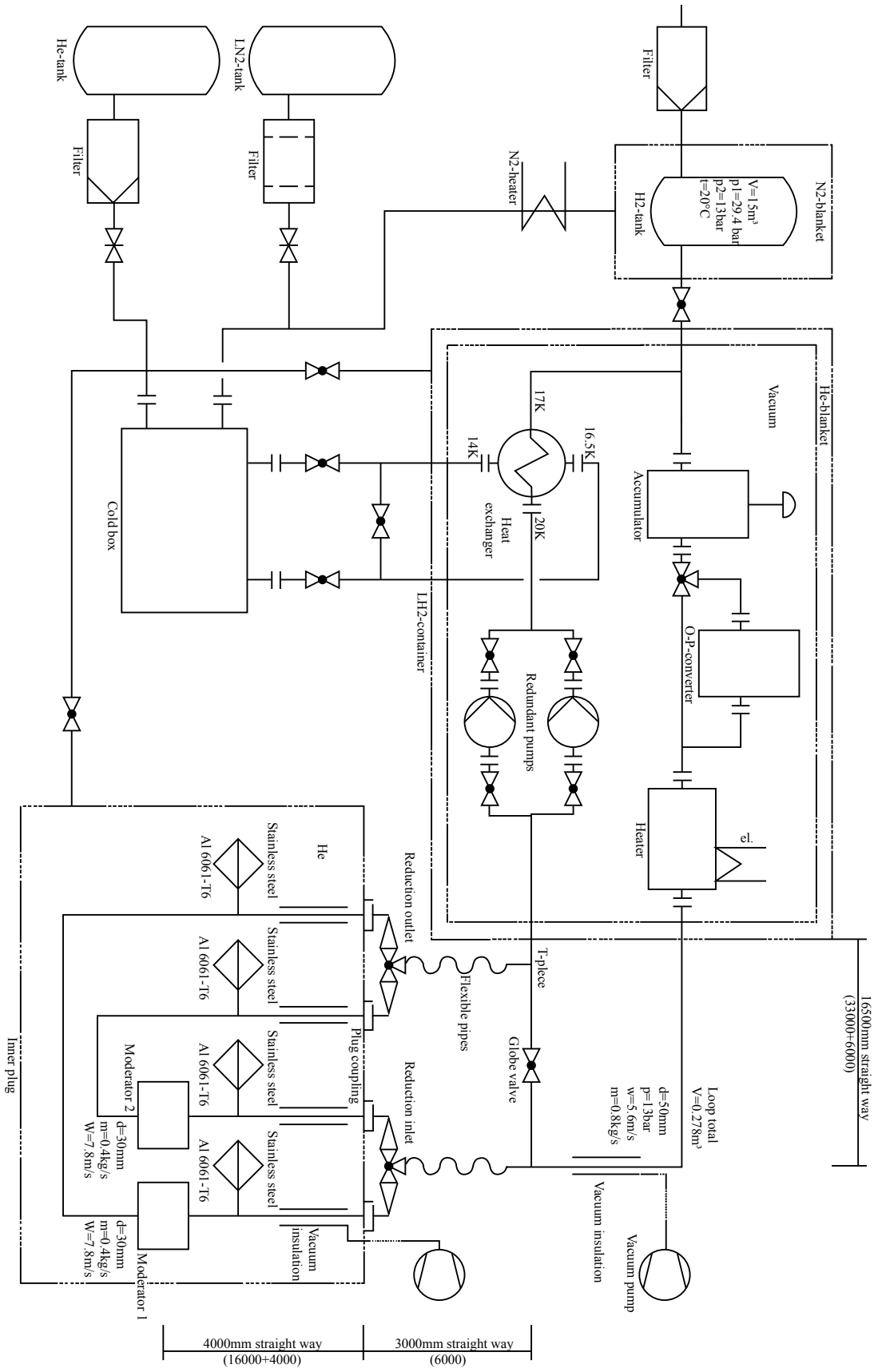

Figure 3.72: Liquid hydrogen cryogenic system flow diagram, showing three main sections: medium storage and supply, the hydrogen circuit, and vessels and in-monolith piping. Courtesy of Y. Beßler.

The main hydrogen circuit consists of pump, heat exchanger, accumulator, heater and ortho-to-para converter. With current technology and commercially available equipment, achieving the necessary mass flow rate will be a challenge for the circulation system. Discussions with potential pump manufacturers led to the conclusion that it is possible to manufacture a suitable pump, although there is currently no such pump readily available on the market. Nevertheless, it was decided to plan the circuit with two pumps both capable of the full mass flow, running at 50% of the rated power during normal operation. If one pump fails, the system will be able to operate for a limited time using the remaining pump. This technique also avoids having a "warm" redundant pump. The main source of heat into the cryogenic H_2 system will be from neutronic heating inside the moderator vessel. This heat load scales directly with the proton beam power. In order to continue operation during beam trips and short shut downs, a heater will provide heat to substitute for the neutronic heat load to the circuit. In addition, an accumulator will dampen the remaining volumetric changes.

Since the moderator dimensions are optimised for pure para-hydrogen, an ortho-to-para converter will be installed in the circuit. At 20 K, the natural equilibrium of hydrogen is very close to 100% para-hydrogen (at $T = 300$ K the natural para concentration is 25%). As the temperature of the hydrogen is reduced, a natural conversion takes place, but it is a very slow process and thus the ortho-to-para catalytic converter will be used to markedly reduce the required time of conversion. It is proposed to operate the converter in a bypass line as the heat load and irradiation could potentially reconvert para to ortho hydrogen and this will allow for flexibility in terms of the amount of fluid passed through during operation.

The hydrogen circuit in the current design has an inventory of about 280 litres of liquid hydrogen. This leads to a need for 265 m^3 of gaseous hydrogen (at 300 K and 1 MPa) for each filling.

3.4.4 Active fluids purification and storage systems

Water purification and storage systems

The target water systems will all be connected to the water purification and storage systems. These systems will serve as a base point for supply and storage of activated and non-activated water. Tanks in the storage system will be available to hold system water of all types, depending on contamination levels. The active water tank will be shielded and large enough to simultaneously contain the water of all possibly contaminated water systems. The pure water tank will contain deionised water from the conventional facilities water supply, or purified and conditioned water from the water systems. It will serve as a buffer tank for water supply and also as a control tank before release into the conventional facilities sewage system. The tanks will be kept within the controlled areas. Filters and ion exchanger columns in the water purification systems will remove contaminants, either by continuous circulation of the water or by passage between the active and pure water tanks. It will also be possible to add traces of hydrogen in the water purification and storage systems, in order to remove oxygen from the circuits and thus decrease oxidation.

Gas purification and storage systems

The target helium systems, with the exception of the hydrogen cryo-system, will all be connected to the gas purification and storage systems. These systems will serve as a base point with supply and storage of activated as well as non-activated gas. They will be shielded and located in dedicated rooms in the utilities block. It will be possible to remove filters and other contaminated components in casks via the high bay above. The connection of the target cooling helium circuit and the monolith atmosphere circuit, due to the injection in the rotating seals, imposes special demands on the purification system. The closed balance of these systems is described below in normal operation, excluding all ancillaries for purposes of clarity. More details can be found in a technical report [383].

A simplified sketch of the connections of these systems, including the purification system, is shown in Figure 3.73. Several planned connections, such as the connection to the helium supply and exhaust, have been left out of the figure, because these circuits will work together as a closed volume in normal operation. The target circuit contains cyclone filters (C), heat exchangers (HX1 and HX2) and a circulator (CT). The target circuit mass flow rate is denoted $\dot{m}_T$. Low and high pressure tanks (TP1 and TP2) for the target circuit pressure control system (PCS) and the purification compressor (CP) are shown. The purification mass flow rate ($\dot{m}_P$) must be at least as large as the sum of the target injection mass flow rates ($\dot{m}_{ST}+\dot{m}_C$), in order not to raise the target circuit pressure. Purified flow in excess of the injected flow

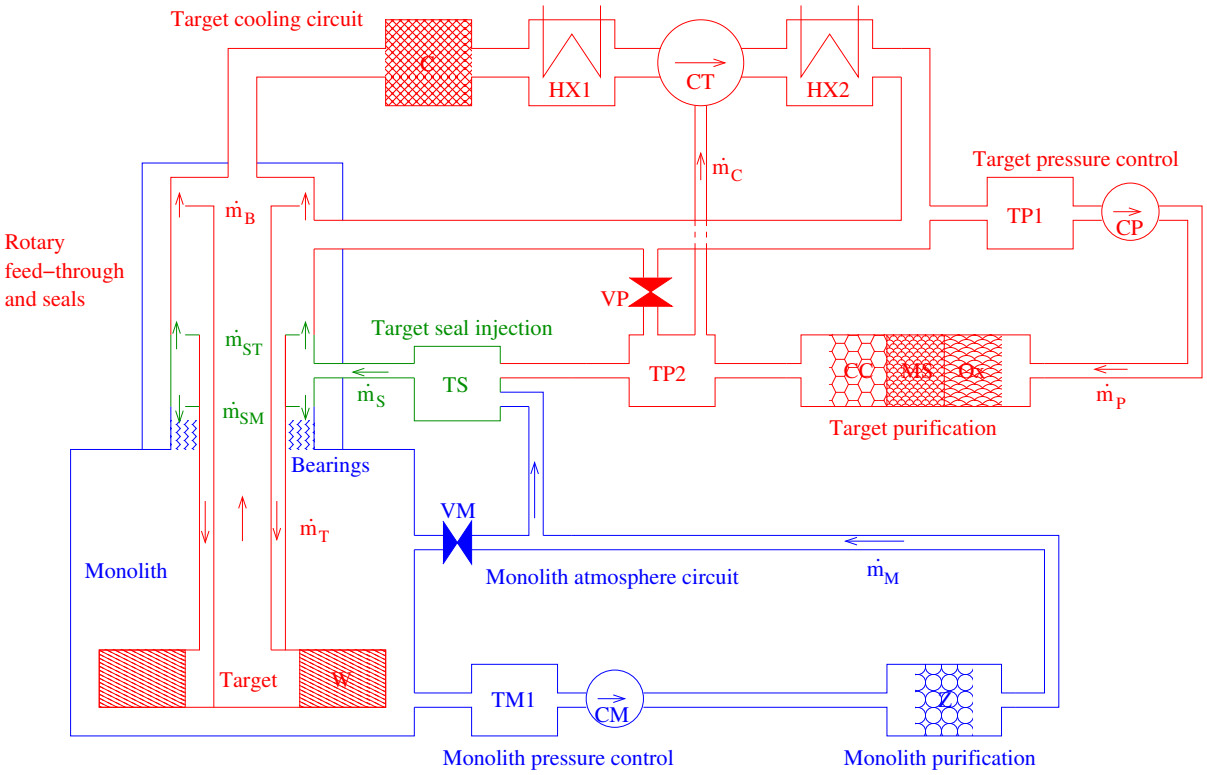

Figure 3.73: Simplified flow chart of helium in the target, monolith and purification systems, showing only the basic components and connections for helium balance in user mode operation.

is led back into the target circuit via a valve (VP). The monolith pressure control contains the monolith compressor (CM) and the low pressure monolith circuit tank (TM1). The valve VM connects back to the monolith to allow circulation, analogous to VP for target circuit purification. The monolith atmosphere mass flow rate is denoted $\dot{m}_M$.

Figure 3.73 shows the three seals in the rotary feedthrough, and indicates their leakage mass flow rates. (The three-seal concept for the bearing and drive unit is also shown in Figure 3.44, and is discussed in Section 3.3.5.) The by-pass leakage flow rate out of the top seal into the target circuit is denoted $\dot{m}_B$, while the leakage out of the bottom seal into the monolith is $\dot{m}_{SM}$, and $\dot{m}_{ST}$ is the leakage from the middle seal into the target circuit. The total seal flow rate is thus $\dot{m}_S = \dot{m}_{SM} + \dot{m}_{ST}$. The seal buffer tank, TS, is used to control the seal pressure and thus ensure the seal flow rate. There is also a lower seal flow, $\dot{m}_C$, into the smaller seals of the circulator (CT). The maximum seal flow of pure helium into the monolith is $\dot{m}_{SM} = 7$ g/s. Helium will be removed from the monolith atmosphere at the same rate in order to maintain the pressure cascade. At zero recirculation (with valve VM closed) this is also the flow rate in the monolith atmosphere circuit $\dot{m}_M$. There also will be a continuous injection of purified helium into the target circuit via the rotating seals. The maximum injection rate in the target wheel seal is $\dot{m}_{ST} = 3$ g/s.

The rotational seals in the cooling circulator will be of a multi-level type used in chemical industry, as shown in Figure 3.69 and discussed in Section 3.4.1. Purified helium is injected as a buffer gas between the first and second circulator labyrinth seals, with a maximum injection rate of 0.1 g/s. Some of this goes inward through the first seal into the target circuit. The rest goes outward through the second seal and is collected at lower pressure between the second and the third circulator seals. The purified helium collected between the second and the third seals is led back and re-injected. Due to the low pressure between the second and third seals, the leakage of purified helium outward through the third seal will be very low, comparable to diffusion in narrow gaps and within the leak rate of 0.1% per day. As already been noted in Section 3.4.1, this is a conservative estimate based on operating experiences at comparable facilities. Optionally, an additional level with a fourth seal and an additional separation gas could be added. It will be possible to temporarily operate both the target and circulator seal flows using fresh helium from storage tanks if the purification system is not available. The compressors in the purification circuit and

monolith atmosphere circuit (CP and CM) will be smaller and of a different type, which does not require a seal injection flow.

The target helium purification system will contain several subsystems. Before the first purification step, there will be a tank that ensures that the flow through the purification steps is continuous and controlled. Then there will be a mechanical filter. The first step of the purification will be oxidation at elevated temperature with copper oxide (Ox). Here, all oxidisable substances will be oxidised, with special focus on binding hydrogen, including isotopes such as tritium, in water. The oxide carrier may be re-generated by disconnecting the helium flow and injecting oxygen. In a second step, after the oxidation, the flow will be cooled and the water will be captured in molecular sieves (MS). The third step of the purification, low temperature adsorption in charcoal (CC), will remove substances with boiling points down to that of nitrogen and also will capture any remaining iodine. This will include noble gases from argon and up, and also oxygen and nitrogen, among other substances. The cooling in this last step will be accomplished by liquid nitrogen or a cryogenic refrigeration system. After the last step, there will be another tank to ensure a controlled flow. Purification systems working with these principles (Ox+MS+CC) and capacity (3 g/s), have been investigated and verified by measurements [384–386].

After purification, the gas is led to the seal injection tank (TS) and to the target system via opening VP shown in Figure 3.73. It may also be led to used gas storage or to the stack, although this option is not shown in the figure. Different purification steps may be used depending on the gas to be purified. All the different connections – used, for example, to lead all helium through the purification system during maintenance, including the PBW cooling helium – are not shown in Figure 3.73. In normal operation, the purification system will be continuously available, to keep the levels of contamination low, particularly in the primary target cooling system. It is however also possible to operate for a limited time using the storage tanks. Helium storage that is used, for example, for maintenance purposes, is also not shown in Figure 3.73. There will be a compressor after the purification chain, which may fill either of two used gas tanks. The used helium tank will be large enough to contain all helium used in the target systems, that is, the target cooling, monolith and PBW systems. There also will be a buffer for helium supply. Just as for helium, there will be tanks for the nitrogen in the intermediate target cooling system. As the intermediate system will not be contaminated in normal operation, there will be no continuous purification system – only filters. The used nitrogen tank will be able to contain all nitrogen used. It also will serves as a buffer for all nitrogen in the intermediate target cooling system.

Gases from the gas and liquid separation tanks in the water systems will be led to a system in which water vapour will be condensed in a heat exchanger connected to the intermediate water system for gas. The condensed water will return to the water purification and storage system. The gases may go via delay tanks and monitoring to the stack, or may be led to the storage systems.

3.5 Handling and logistics

3.5.1 Active cells

The active cells facility is designed to maintain, process, package and store used radioactive components from the target station operation. It is located in the target station building, downstream of the monolith relative to the proton beam direction. The active cells are bordered on the top by the high bay floor, and on the bottom by the ground concrete slab. The layout of the active cells facility is shown in a 3D view in Figure 3.74, and in a side view along the vertical cut in Figure 3.75. The important dimensions of the facility are summarised in Table 3.25.

The active cells facility will consist of five main areas, the process cell, the maintenance cell, the storage cell, the transfer area and the technical galleries. These areas have different functions related to the treatment, storage and shipment of radioactive components. On each side of the active cells, the technical galleries will be located on two levels in order to provide access to the full height of the active cells. From these areas, workers will be able to control and perform remote handling operations in the maintenance cell and the process cell. They will be able to make use of through-wall master-slave manipulators, as well as of a power manipulator and in-cell crane. The galleries will contain enough lead glass windows to facilitate operations as well as monitors and control boards for in-cell cameras and equipment. The technical galleries also will be equipped with wall penetrations through which the cells will be supplied with the electricity and compressed air needed by the active cells' equipment.

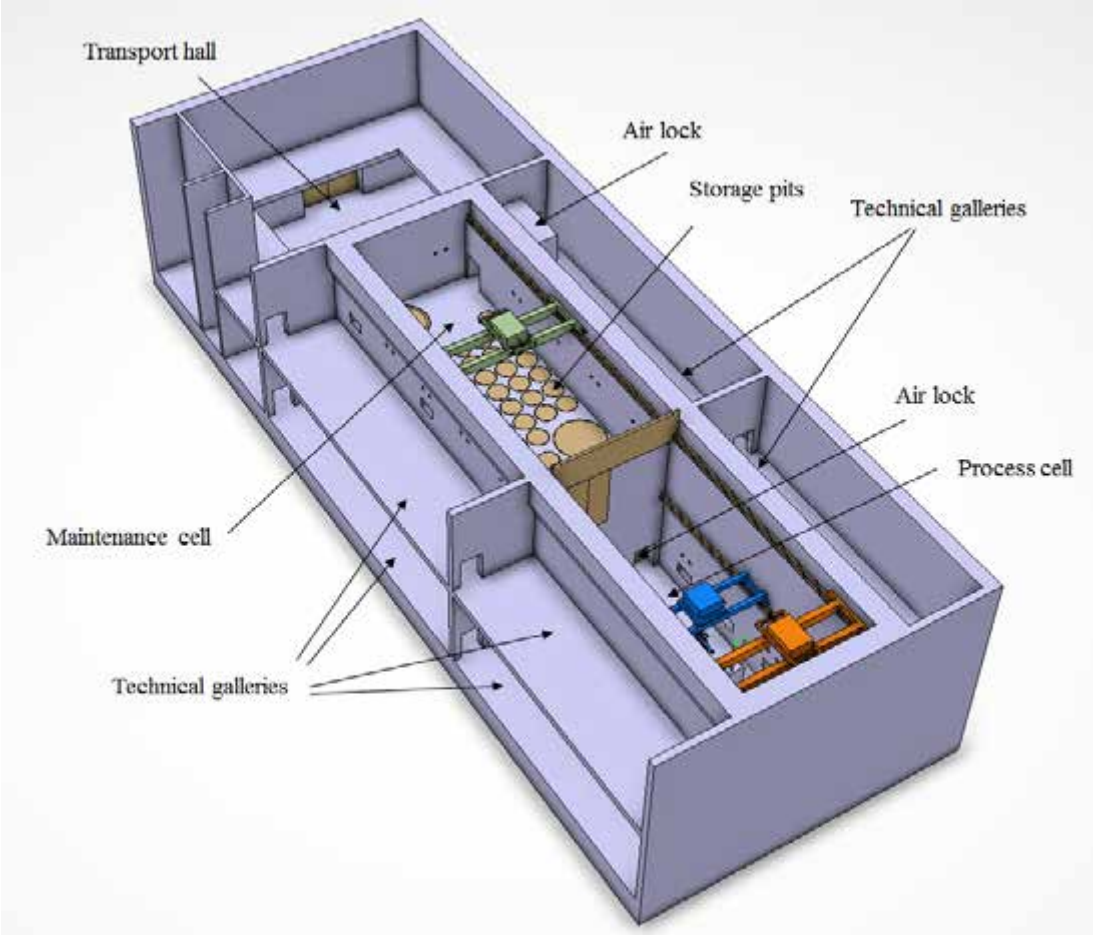

Figure 3.74: The active cells system layout.

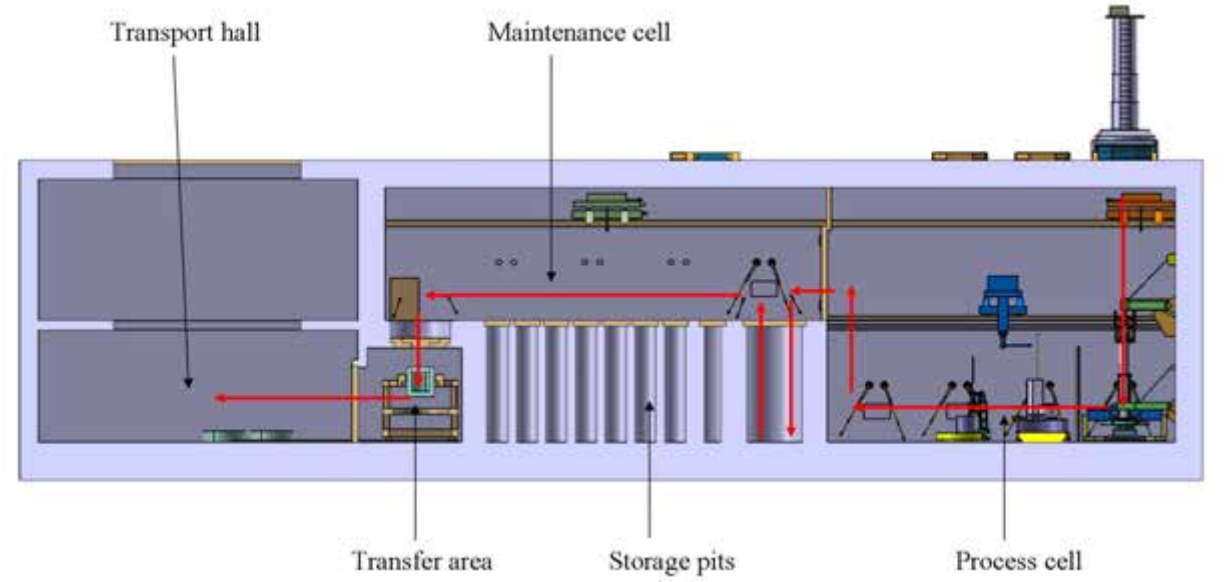

Figure 3.75: The flow of active cell logistics, and a side view of the system of active cells along a vertical cut, including (from left to right) the transport hall, transfer area, maintenance cell, storage cell and process cell.

	Length (external) [m]	**Width (internal)** [m]	**Height (external)** [m]
Active cells facility	45	22	16
Process cell	20	8	16
Maintenance cell	25	8	8
Storage pits	25	8	8
Transfer area	6	5	5

Table 3.25: Dimensions of active cells.

Confinement

The active cells facility is designed to prevent unintended escape of radioactivity through its confinement barriers. This will be achieved by good confinement design and proper management of contaminated wastes and components, and will be under constant and ongoing measurement, monitoring and control.

The confinement design concept can be divided into two categories, static confinement and dynamic confinement. Static confinement will be achieved by the structural elements delimiting the active cells, including walls, stainless steel liner, HEPA filters, and lead glass windows. In order to satisfy the general safety objectives' dose limits for ESS radiation workers laid out in Table 11.3, the walls of the active cells will be made of heavy concrete and will be 1.45 m thick [387], which will make it possible for a person to work in the technical galleries for as many as 2000 h/year without exceeding dose limits. Dynamic confinement prevents the escape of contamination through the openings of the structural elements that provide static confinement. This is achieved by the ventilation system that determines air circulation rates and pressure levels. A pressure cascade will be established so that pressure in the active cells is approximately 230 Pa below the reference pressure. The process cell and the maintenance cell will have individual ventilation systems. When the intra-bay door between these two cells is open, contamination in the maintenance cell will be avoided by forcing external air to flow from the maintenance cell toward the process cell. The dynamic confinement design complies with all relevant international standards. [388–390].

Access protocol

Permitted levels of access will vary across different areas of the active cells facility, depending on contamination and operational status. All the areas around the active cells will be classified as controlled areas because of potential contamination risk during an incident scenario.

For the technical galleries and the transfer area, no contamination is expected under normal working conditions and unlimited access will be permitted to ESS personnel. As mentioned above, shielding will be sufficient to allow any individual to work in these areas up to 2000 hours per year. Even under incident conditions, contamination in these areas will be low. In general, access to the high bay will also be unlimited for personnel. However, radiation and contamination risks in the high bay area will be higher than those in the technical galleries and transport hall during the transport and docking of casks containing irradiated material from the monolith to the active cells. Therefore, human access to the high bay will be limited during critical operations.

Human access to the maintenance cell will be permitted only if all of the following conditions have been satisfied: no waste or baskets containing irradiated components are located in the cell, all the storage pit lids are closed, the intra-bay shielded door is closed, no shipment cask containing irradiated waste is docked to the maintenance cell, and the contamination level in the cell is below an established threshold. If the contamination level is above the threshold, the maintenance cell must be decontaminated, and remote handling equipment will be required for this purpose. Since the waste and components will have been transferred to sealed baskets before entering the maintenance cell and no cutting operations will take place in this cell, the level of contamination in the maintenance cell will be low. Nevertheless, human access to the maintenance cell will be permitted only with protective equipment since it will be difficult to ensure that the maintenance cell is completely sealed off from the process cell and airborne contamination may occur in the process cell.

In general, human access will not be permitted to the process cell during normal working conditions.

However, some exceptional maintenance operations may require human access. In this case, the process cell will be emptied of contaminated components and decontaminated with slave manipulators before personnel with protective equipment are allowed access via the airlock connecting the process cell and the technical galleries. Due to the cutting operations that will take place in the process cell, and the chips that they will produce, the contamination level is expected to be high, but decontamination using robust procedures will be possible. To facilitate decontamination, liquid coolant will not be used during cutting operations. The decontamination of the process cell will be quite time consuming, so human access will be restricted to a limited set of circumstances in which operations cannot be performed by remote handling.

Component logistics

Most of the irradiated materials will consist of radioactive and/or contaminated components and waste transferred from the monolith to the active cells facility. The major features of the logistics for radioactive materials transport are described here. Shielding blocks that are removed to permit access to the target monolith will be stored in specified areas in the high bay during monolith component maintenance operations. Many components of the target station will require regular exchange and maintenance. To facilitate these activities, these components have, in most cases, been housed within plugs that can be removed or exchanged as a single module with minimal disturbance to surrounding systems. After shut down, the monolith will be conditioned to permit opening and relevant shielding will be removed, opening access to the plug requiring exchange or maintenance.

The handling cask for the plug will be stationed on the floor valve installed on top of the monolith, as shown in Figure 3.76 and discussed in Section 3.5.2. The component will be lifted from the monolith into the handling cask via a lifting unit that is built into the cask and that will be equipped with a dedicated handling grip for each irradiated component. The high bay crane will be used for heavy lifting operations. It will move the handling cask holding the component and will dock it to the active cells facility. The floor valves will be opened and the component will be delivered either to the process cell or to the maintenance cell pit for intermediate storage before process cell operations. The schematics of the flow of components, and of the waste generated during components maintenance and processing inside the active cells facility are illustrated in Figure 3.75. The component will be processed (cut or dismantled) in the process cell and the waste will be placed in baskets. The baskets will be decontaminated and transferred with the crane to a dedicated storage pit beneath the maintenance cell. When the activity of the waste has been reduced to an acceptable level, it will be inserted via the maintenance cell into a waiting shipment cask docked in the transfer area. The shipment cask will be moved to the transport hall and prepared for shipment off-site.

Process cell

The process cell is where all the processing operations of inserted components will occur. This includes activities such as cutting, refurbishing and packing. This cell will have the highest contamination levels of all the active cells during normal operations, due to dust and particles arising from processing operations. The process cell has three floor valves that connect it to the high bay. These valves will allow the entrance of radioactive waste coming from the monolith. The cell will also have a shielded door that will allow human access from the technical gallery via the airlock located below the maintenance cell. This will occur only in exceptional circumstances. One lateral intra-bay shielded door and one upper shielded door separate the process cell from the maintenance cell. The functions provided by the process cell will be determined by the particular radioactive components being processed. The main components, which have been the focus of attention in the design of the process cell, are the target, the MR plug and the PBW plug. Schematics of the main components of the process cell are given in Figure 3.77, and processing of the main radioactive components is described below.

The target will be introduced into the process cell from its handling cask through a floor valve. It will then be placed in a handling basket previously fixed on a translating worktable located on the process cell floor. A lifting system fixed on the process cell wall will clamp and hold the target steady, and a gripping system also fixed on the process cell wall will secure the shaft. A band saw will cut the shaft from the wheel, and the wheel will remain in the handling basket. The handling basket containing the wheel will be moved backward with the worktable translation and transferred with the crane into a containment basket. A lid will be mechanically fixed onto the containment basket and then welded to it in order to ensure a good sealing. After decontamination, the containment basket will be stored in a dedicated storage pit.

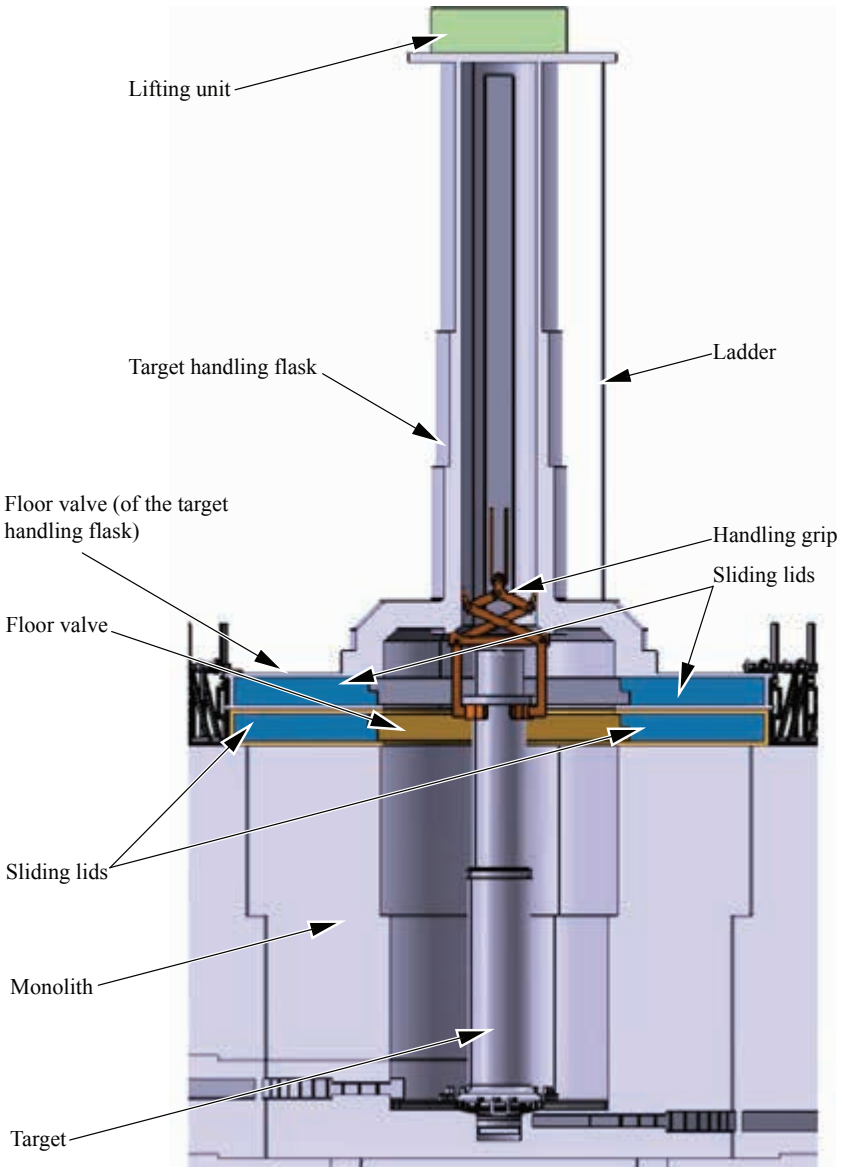

Figure 3.76: Shielded cask on top of active cell.

The same procedures are used to cut the shaft into smaller pieces.

The MR plug will be lowered through a floor valve from its handling cask to a turning table located on the process cell floor. A mechanical structure attached on the turning table will ensure that the centre of the moderator is aligned with the centre of the turning table. A moderator assembly exchange device that can turn around the turning table will be used to extract the moderator assembly from the side of the moderator and reflector plug. The power manipulator and/or the through-wall master-slave manipulators will perform the necessary bolting and unbolting operations. Once the moderator assembly is extracted from the MR plug, it will be transferred to the shear cutting device with the in-cell crane. Once the pipes are cut, the pieces of pipes and the moderator assembly will be placed into baskets, the lids of the baskets will be attached and sealed by welding, the baskets will be decontaminated and transferred to the dedicated storage pits in the maintenance cell. In order to reduce waste, the steel reflector and the beryllium reflector of the moderator and reflector plug will be refurbishable. Unlike the MR plug, the PBW plug will be lowered through a floor valve straight to the turning table equipped with the shear-cutting device. After cutting, the pieces of pipes and the PBW itself will be placed into baskets, which will be transferred to the dedicated storage pits in the maintenance cell after being welded shut and decontaminated.

A large number of operations on highly radioactive components will be performed in the process cell. Established procedures will identify all critical scenarios and define operational procedure for each incident case ahead of time, in order to avoid critical situations such as failure of equipment during operation. These will include robust procedures for the overhead crane and power manipulator. Should an equipment failure occur in the process cell, it will be handled either by through-wall master-slave manipulators or by the power manipulator. If remote handling is unable to perform maintenance of the equipment, the equipment will, after decontamination, be transferred to the maintenance cell.

Process cell equipment

The major equipment operating in the process cell is listed below. For reference, all the equipment will have a radioactive resistance between 1 MGray and 10 MGray. The schematics of the equipment are illustrated in Figure 3.77. The in-cell overhead crane has a lifting capacity of 25 tonnes. It will reach both the process cell and the maintenance cell. The engineering design of the crane will be robust enough to ensure a safe operation in the anticipated hazardous environment. It will be possible to change the grip of the crane remotely to facilitate different lifting operations in the cells.

A *power manipulator* will run on its own bridge in the process cell. It will be the main handling tool for the operations performed in the process cell. It will take part in the decontamination of the process cell, when needed. In case of the need for hands-on maintenance, it will be possible to lift the power manipulator with the overhead crane and to transfer it to the maintenance cell where the power manipulator will rest on a special support. A *shear-cutting device* will be used to cut steel pipes. The dimension of the shear-cutting device is defined, for example, by the size of the pipe diameters, the pipe thicknesses, the movements of the robot and so forth. An electrical motor-driven device is preferable provided that the required strength of the shearing tool can be achieved. A *cold cutting device* will be used for larger cutting operations like separating the shaft from the wheel. The system foreseen is a circular saw or a band saw. The details of the cutting device will be determined by the thickness, the configuration of the internal channels of the

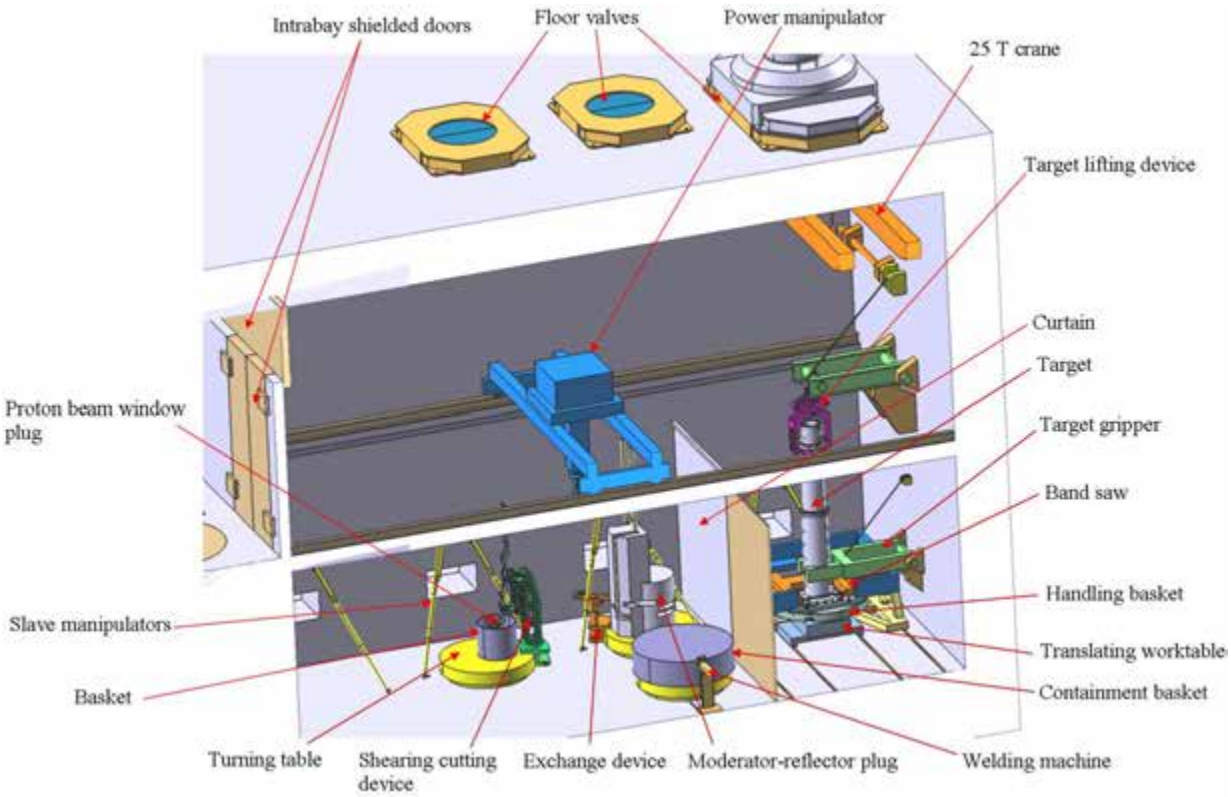

Figure 3.77: Process cell equipment, including a power manipulator, a shear-cutting device to cut steel pipe, a cold-cutting device, several turntables, and other equipment.

shaft and the flexibility of the available technology. The sawing tool will be turn up to 90 degrees so that it will be possible to use it to cut other components, if necessary. The saw is designed so that it will be possible to change the blade by remote handling. Several *turntables* will be used to position and orientate the components as needed. Various jaws and grippers will be fixed on the turning tables, depending on the intended usage.

Other cell equipment includes (but is not limited to) welding machines, lead glass windows with master slave manipulators, HEPA filters, stainless steel liner, floor valves, intra-bay door, lights, translating worktables, target lifting system, target gripper, moderator assembly exchange device, decontamination tools such as brushes, air blower, and vacuum cleaning.

Maintenance cell

The maintenance cell will be connected to the process cell via an intra-bay shielded door. In addition, access for components will be provided via floor valves from the high bay and access for humans via an airlock. The cell will be used for hands-on maintenance on active cells equipment and decontamination operations on tools. The airlock access will be from the technical galleries. The airlock functions as a safety barrier between humans and potentially contaminated areas. In the floor of the maintenance cell there will be access to: 35 pits of 1.2 m diameter used to store standard size baskets, one pit of 3 m diameter to store the baskets to contain the target wheel, one pit of 3 m diameter to temporarily store the entire irradiated target before its transfer to the process cell for cutting operations and one pit of 2 m diameter to store the entire MR plug, (refurbished or irradiated). The pits will be used to store all the waste temporarily before off-site shipment. The pits will be covered with lids that ensure their sealing towards the maintenance cell. The lids also will provide the necessary shielding against irradiation when humans enter the maintenance cell. On the floor of the maintenance cell, the transfer docking port will be located. It will allow the transfer of a basket from a storage pit to a shipment cask docked to the maintenance cell from the transfer area side. Consequently, human access will be possible only if the storage pits lids are closed and if no baskets containing radioactive waste are located on the floor of the maintenance cell. There will be two floor valves of different diameters on its ceiling, connecting the maintenance cell with the high bay. The cell is shown in Figure 3.78.

The maintenance of active cells equipment makes it necessary that the maintenance cell environment is safe for human access, especially in regard to contamination and radiation. Human access requires (for

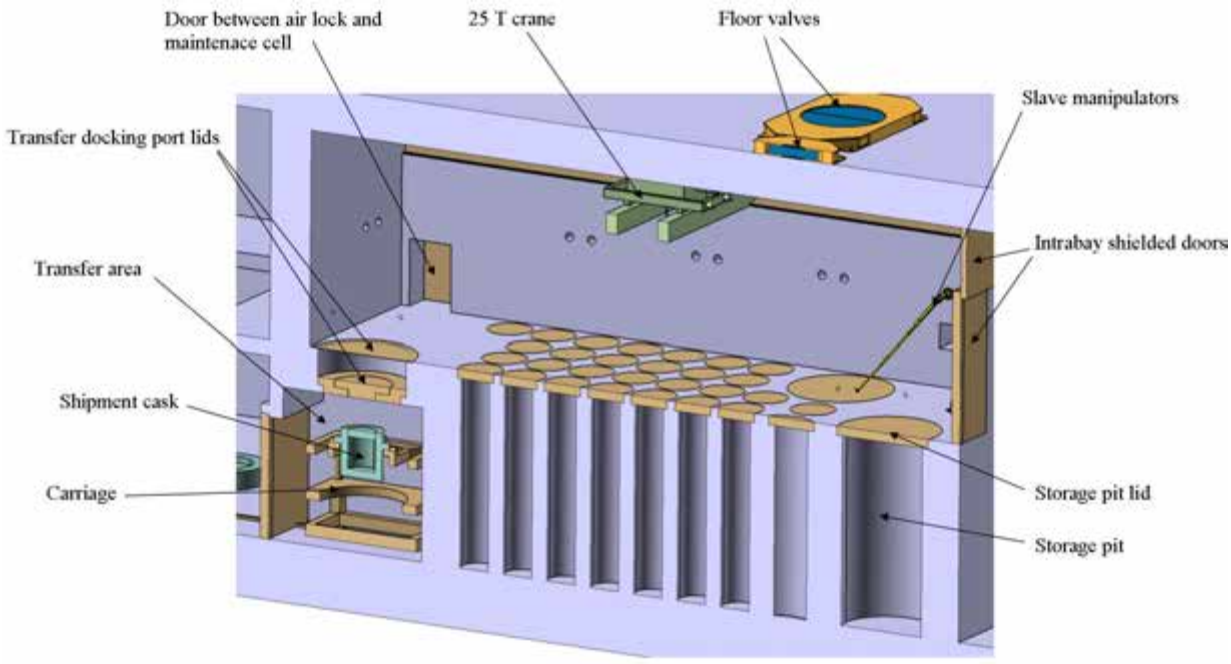

Figure 3.78: Maintenance cell and transfer area equipment

example) that the intra-bay shielding door is closed, that the pressure cascade is within its thresholds, and that no wastebasket is located in the area. The maintenance cell will also be used as the logistical hub for insertion and extraction of wastebaskets in the storage pits and shipment casks docked to the docking port in the maintenance cell floor. It also serves to control the dose rate on the wastebasket surface and eventually to decontaminate it before its introduction into the shipment cask. The contamination level in the maintenance cell will be low because no cutting operations will be performed there. The lids of the storage pits will ensure a sealing between the pit and the maintenance cell. Regular hands-on decontamination of the maintenance cell will ensure an acceptable contamination level. If needed, decontamination by remote handling will be possible by installing slave manipulators in crossings in the maintenance cell walls. Some maintenance operations on maintenance cell equipment such as the intra-bay shielding door will require that the maintenance cell be emptied of radioactive components, in which case the process cell might have to be decontaminated.

The main equipment of the maintenance cell will be an overhead crane, the intra-bay shielding doors, the storage pit lids, the docking port to the transfer area and some general items like lead glass windows, through wall slave-master manipulators, airlock doors, stainless steel liner, lights, decontamination tools, and dose rate measurement equipment. The overhead crane will be able to reach both the maintenance cell and the process cell. The maintenance and process cell cranes provide backup for each other if one crane fails.

Transfer area

The transfer area will be used for docking the shipment cask to the floor of the maintenance cell, in order to transfer the wastebaskets from a storage pit to a shipment cask. The main function of the transfer area will be to provide an area for the safe handling of the wastebaskets when they are introduced into an off-site shipment cask. The shipment cask will be transferred beneath the transfer docking port on a special carriage. The lifting system of the carriage will lift the shipment cask and dock it to the docking port. A tight connection between the cask and the transfer docking port will be secured. The wastebasket will be taken from a storage pit and introduced in the shipment cask via the maintenance cell. Once the waste has been transferred into the shipment cask, the lid will be placed back on top of the cask. Human access to the transfer area will ensure that the cask has been decontaminated to a level within regulations for off-site shipment. The shipment cask will then be transferred to the transport hall for further handling before shipment. The major equipment of the transfer area will be the special carriage used for shipment cask transport from the transfer area to the transport hall. The design of this system depends on the various container sizes to be docked and the shielded door design between the transfer area and the transport hall.

3.5.2 Casks and associated handling devices

General description

Handling casks will be used to transfer irradiated components between the monolith and the active cells. The main components that will be transported by casks are the target, PBW plug, MR plug and the NBGI inserts. There also will be smaller and lighter handling casks for the transfer of some low irradiation level components such as shielding blocks or equipment going through maintenance. These lighter-handling casks will not be described in this report, since the development of these casks will be realised later in the project. The functions to be provided by the main handling casks are 1) lifting and transporting active components from one place to another, 2) limiting the contamination to the surroundings during transport operations, 3) protecting workers and public against radiation and 4) containing waste to provide protection in accordance with the standards developed in the GSO [391]. The high bay crane will transport the casks in the high bay area. The weight of the cask and its built-in component is thus one important criterion for the high bay crane design and rating. For safety reasons, the handling casks will only be lifted a minimal required height above the floor. This is to minimise the impact of a dropping accident and to minimise the radiation exposure to workers through the bottom plate of the casks, as is also discussed in Section 11.4. Furthermore, the hook of the high bay crane will be designed to minimise dropping risks. The dimensions of the various internal handling casks will be adapted to the size of the component they handle and the need for shielding. As the space on the top of the monolith is limited for the positioning of the casks, their design must take these space limitations into account. A summary of the main dimensions and data for the handling casks is given in Table 3.26.

There will also be several general purpose handling casks that will be used for moving slightly contaminated items such as shielding blocks or other equipment from the primary cooling loops. When the shielding is lifted, it will be stored in dedicated areas in the high bay. These handling casks will also provide the functions of shielding, transport and confinement. The design of these casks is less challenging than the design of the four main casks listed in Table 3.26, and their lower weight does not represent a binding constraint for the high bay crane capacity, so details have been left for a later stage. Unlike the four main handling casks, these lower weight casks will not be equipped with built-in internal lifting devices. All lifting operations will be done using overhead cranes. When the handling casks are empty, they will be stored on the high bay floor in a designated location or used for training in the mock up area.

	Unit	Target casks	MR cask	PBW cask	NBGI cask
Max length (including floor valve)	m	7	5	4	3
Max height (including floor valve)	m	8	8	7	7
Max width (including floor valve)	m	4	3	2	1
Max radiation 1 m from cask surface	μSv/h	25	25	25	25
Max weight (including moved component)	t	95	95	95	20

Table 3.26: Main parameters for the internal handling casks used for the target, moderator-reflector (MR), proton beam window (PBW), and neutron beam guide insert (NBGI).

Handling casks engineering concept description

The handling casks will have a mechanical structure composed of cylindrical metal rings that will ensure the mechanical integrity and the integration of the different pieces of internal equipment. On the upper part of the mechanical structure, there will be two handling ears located on each side of the metal cylinder. These will allow the high bay crane equipped with a connection attachment to grab the cask and lift it. The structures also will contain the shielding that is required to fulfil dose limits in the high bay. A lifting unit will be installed on the top of the casks. It will be capable of lifting the plug to be extracted or introduced. This lifting unit must ensure that the item cannot fall during the lifting operation and the transfer of the cask to the active cells. Therefore, the lifting unit will be equipped with a gripper allowing a safe remote extraction and introduction of plugs to and from the monolith and the active cells. The top of the handling casks must ensure enough shielding to permit a worker to safely perform maintenance operations on the lifting unit. A ladder will allow human access to the top of the casks. It will also be possible to remove the top of the casks for exceptional maintenance or decontamination operations.

The bottom of the casks will be equipped with a floor valve consisting of a fixed mechanical frame welded to the down part of the casks. This mechanical structure will fixates two sliding lids guided in the mechanical frame. The drive units moving the two lids will be fixed on the external side of the handling casks, in order to facilitate access during maintenance. In case of failure, it will be possible for a worker to manually move the lids using a turning rod. The bottom part of the casks will be equipped with an alignment structure for correct positioning over the monolith and the active cells. The transfer of a plug into a handling cask will not be possible unless the floor valve is fully open and locked in the open position. During transport, the floor valve will be properly closed. A mechanical device inside the handling casks will be used for the alignment of a plug, in order to reduce the risk of movement of the plug during transport. A camera system installed inside the casks will ensure a sufficient view of the operations. In case of a camera failure, it will be possible for a worker to change the camera from the external side of the casks.

Confinement

Handling cask confinement will be ensured by the cylindrical mechanical steel structure, the top of the cask and the floor valve on the bottom of the cask. The top opening on the top of the cask will allow the chain or wire of the internal lifting unit to grab the component. Due to the clearance between the sliding lids and the frame of the floor valve, the cask will not be airtight. This will not pose a safety hazard for four reasons. First, the plugs are dried in the monolith before movement. Second, the pipe connections can be sealed before lifting. Third, dust is not expected on the exterior of the plugs. And fourth, the movement of

the casks is slow, which keeps the airflow inside the cask stable. To ensure acceptable radiation dosages for the workers in the high bay, metal shielding of the casks is necessary. This metal could be either steel and lead, depending on weight optimisation. The metal shielding surrounding the cask mechanical structure with the floor valve and the top of the casks provides irradiation protection for the workers. The floor valve may be thinner than the shielding around the casks as no worker is expected to be under the casks during transport. The top of the casks will be designed to protect a worker against irradiation during intervention on the top of the cask, even in the presence of waste. The cask confinement requirements will ensure that all operations performed with the cask respect the GSO [391].

Target handling

Once the monolith has been opened and the drive unit of the target has been removed, the shielding blocks around the target can be removed. Before extracting the most irradiated shielding blocks just surrounding the wheel, a floor valve will be installed on the top of the monolith above the target. An alignment structure between the monolith and the floor valve will ensure the correct positioning of the floor valve. The aim of this floor valve is to limit the exchange of air in the monolith and the radiation exposure of personnel when the upper shielding blocks are removed. After the shielding blocks above the wheel have been removed, the cask used for target replacement will be placed on the previously installed floor valve, using the high bay crane. Both the cask floor valve and the floor valve installed on the top of the monolith will be opened and the target will be lifted with the internal lifting unit into the handling cask, as shown in Figure 3.76. Both floor valves will be closed and the cask will be lifted with the high bay crane and transferred to the top of the active cells. There, it will be docked to an appropriate floor valve installed on top of the active cells. Once the target cask has been installed on the active cells floor valve, both floor valves will be opened and the target will be lowered into the active cells.

Proton beam window handling

In order to increase the flexibility of the active cells, floor valves of identical size will be used for both the PBW plug and the MR plug. The handling casks used for these components will be of different sizes, however, and so it will be necessary to install an intermediate steel spacer on the active cells floor valve. This will ensure shielding during transfer operations on top of the active cells. Alignment pins will ensure a correct positioning of both the spacer and the cask on the active cell floor valve. Once the lid on the monolith covering the PBW plug has been opened and the pipes have been disconnected, the shielding blocks above the PBW plug will be removed. A floor valve will be installed on top of the pit and the PBW plug cask will be placed and aligned above the plug on the top of the monolith floor valve. The floor valves, one on the monolith and one on the cask, will be opened, and the PBW plug will be lifted remotely with the cask internal lifting unit into the cask itself. The floor valves will be closed, and the cask will be lifted with the high bay crane and transferred to the top of the active cells where it will be installed on the appropriate floor valve previously equipped with the spacer. Once the PBW cask has been installed on the spacer, the floor valves will be opened. Then, the PBW plug will be lowered into the active cells.

Moderator and reflector plug handling

The handling procedures for the MR plug cask are similar to those for the PBW plug, except that the steel shielding spacer will not be needed for docking the MR plug cask on the floor valve above the active cells.

Neutron beam guide insert handling

Since the NBGI is handled in the experimental halls, its handling procedures have a major interface with experimental hall operations and equipment. The cask will be docked on the side of the monolith, requiring the removal of neighbouring beamlines. The second barrier will be opened and a valve and distance plate will be installed in front of the NBGI. The cask will be connected and the NBGI will be extracted horizontally into it. The cask will be moved to the high bay and tilted, in order to protrude the used NBGI into the active cells. The design of the NBGI handling cask will be compatible with the floor valve design on top of the active cells.

3.6 Fallback and comparative target technologies

In line with decisions taken by the ESS Steering Committee, two additional target concepts that are not the baseline choice have been explored in order to provide a complete and robust technical underpinning for the target design. The water-cooled rotating tungsten target is a back-up option to the baseline concept, developed in order to reduce the technical risk associated with the target station. The water-cooled target concept provides a type of insurance against the possibility that serious unexpected problems may emerge with the baseline option. However, preliminary studies at ESS and other projects show that existing water-cooled spallation target technologies for a proton beam power less than 1 MW cannot simply be rescaled to work with the 5 MW ESS proton beam. Therefore, considerable R&D effort would be needed to realise reliable 5 MW technologies for a water-cooled rotating solid target. The lead-bismuth-eutectic (LBE) target uses liquid metal both as target material and coolant. It was studied as a comparative option for assessing broad environmental implications of different target designs. In the context of that comparison, the baseline option emerged as particularly advantageous.

3.6.1 Water cooled rotating tungsten target

Introduction

Considerable effort has been devoted to the study of a water-cooled rotating tungsten target option, with a focus on identifying solutions to potential problems and critical issues. Some technical designs and materials that might provide solutions to identified problems remained outside the scope of this work. These potential solutions might be worthy of study at a later stage.

The scope of the study presented in this section focuses on examining the basic questions of feasibility for a reference configuration that was identified as a favourable candidate from the point of view of environmental safety. The accidental overheating of the target is a particularly important issue with water cooling, since as temperatures increase beyond 500°C, many metals start to exothermically interact with water vapour in a reaction producing H_2 gas. This becomes a serious safety hazard above 700°C. The after-heat due to radioactive decay at the ESS power level is sufficient for the target to reach such temperatures if active cooling is lost, for example because of a power failure. This mechanism led to the reactor accident in Fukushima, which was made possible by serious safety system flaws. It is a key design goal for ESS to guarantee the highest level of safety for the inhabitants living in the facility's vicinity and for the environment. None of the established water-cooled solid spallation target technologies can be safely used at the ESS power level without substantial additional R&D effort. For this design report, the focus is on demonstrating the feasibility of the chosen target configuration with satisfactory safety margins. For this purpose, the technology does not have to be an optimal concept from all points of view. As the ESS goes into construction, other candidate water-cooled target design concepts will also be investigated in order to develop the best possible design concept for a water-cooled spallation target with 5 MW power.

The target configuration considered for feasibility analysis is described as follows. The spallation volume consists of tungsten rods that are each 10 mm in diameter and 80 mm in length. For protection against corrosion in water, each tungsten rod is canned by a zircaloy tube that is 0.5 mm thick. Tantalum, the conventional cladding material, would substantially enhance the after-heat and would thus aggravate the safety hazard of overheating. The development of canning technology could also open the way for the use of other materials for corrosion protection, such as stainless steel, which react less violently than tantalum or zircaloy with water vapour at elevated temperatures. The canned tungsten rod bundles are vertically placed in a vessel made of stainless steel, and the diameter of the horizontally rotating target wheel is 2.5 m, as in the baseline helium-cooled target option. This cannelloni-shaped water-cooled target has an average density approximately 60% of that of solid tungsten. Heavy water is considered as cooling fluid, in order to avoid a 10% loss in slow neutron yield that light water coolant would imply. The spallation volume is cooled by single-phase cross flow with adequate pressure preload, in order to avoid boiling. The target wheel is sectored as for the helium-cooled option, in order to have enough strength to sustain the pressure preload. The distance between the outside of the vessel and the nearest moderator surface is assumed to be 15 mm.

In this section, cases are identified requiring in-depth experimental, numerical and theoretical studies and tests to reach conclusive answers. The results described in this section contribute to providing a basis for the further assessment of water-cooled target approaches for ESS-class pulsed spallation sources.

Transient water cooling

In order to evaluate the feasibility a tungsten target water-cooling system, some initial thermal analyses have been performed based on a rod cross flow configuration. The cross flow configuration has been chosen, because with required flow speeds for axial flow, the mass flow rate becomes unmanageable. Details of the calculations presented in this section can be found in a more extensive report [392].

The heat load in the rods was evaluated using the MCNPX code, using the reference proton beam and studying the rod with the highest heat deposition. The mean free path of protons at 2.5 GeV is much longer than the diameter of the rod, so a constant heat distribution in the radial direction was studied. The parabolic profile of the heat deposition in the axial direction was reproduced by means of 8 axial sectors with constant heat deposition. The maximum value in the centre of the rods was 4.1 kW cm^{-3} for tungsten, 1.85 kW cm^{-3} for zircaloy and 0.4 kW cm^{-3} for the water [393]. In order to take a conservative approach in the calculations, 5 kW/cm^3 was used for tungsten and 2 kW/cm^3 for zircaloy. The thermal-hydraulic calculations were made for 10 mm diameter tungsten rods canned in 0.5 mm thick zircaloy tubes in a triangular pattern with 1 mm pinch between the tubes, as shown in Figure 3.79. This implies the 61% tungsten and 14% zircaloy volumetric filling ratio. The volume fraction of the tungsten can be increased somewhat by larger rod diameter, thinner canning and smaller tube pinch. The rods are placed vertically between the radii 0.85 m and 1.25 m in the wheel. To fill this concentric area, while removing radial sectors for the cooling water inlet and outlet, requires about 14,000 rods.

For a cross-flow cooling scheme, handbook correlations can provide preliminary approximations of the heat transfer coefficient to be expected [394]. With a bulk water velocity of 1 m s^{-1} between the tubes, the overall heat transfer coefficient is about 10 kW m^{-2} $°C^{-1}$. The heat transfer coefficient is expected to be higher for the cross-flow configuration than for the axial flow. However, it will also be more fluctuating and unevenly distributed around and among the tubes [395]. This has to be investigated further by detailed numerical analysis for the chosen configurations and compared to experiments. The applicability of the handbook correlations for this comparatively low-pinched configuration (compared to usual heat exchangers) should also be assessed. With tangential flow in 33 sectors of the wheel, the total mass flow rate is 290 kg/s, and the overall temperature increase is less than 3°C. By optimisation and more detailed design, for example, by directing higher mass flow to the most heated areas, the mass flow could be decreased and this temperature increased.

A change in the heat transfer coefficient will affect the average temperature of the surface quite strongly, but will have less of an effect on the tungsten temperature increase during the pulse. As a first estimate, the adiabatic temperature increase in the tungsten is about 140°C. The temperature at the outer surface of the canning will determine the limit to boiling. Between the pulses, the rod temperature will not fall quite as low as the water entrance temperature. For initial estimates, it is assumed that the rod temperature has only reached 30°C when the next pulse arrives. Such calculations lead to a peak temperature of 170°C, which is the sum of above mentioned 140°C and 30°C. The water saturation pressure at that temperature is 0.8 MPa, which means that this pressure plus some margin is required to avoid boiling.

The assumption that the heat is deposited instantaneously, which is used in the initial estimate made above is quite conservative. In reality, there is cooling during the pulse, so the surface temperature will not

Figure 3.79: Cut views of the water-cooled target. Left: Rod pattern. Right: Rod support structure.

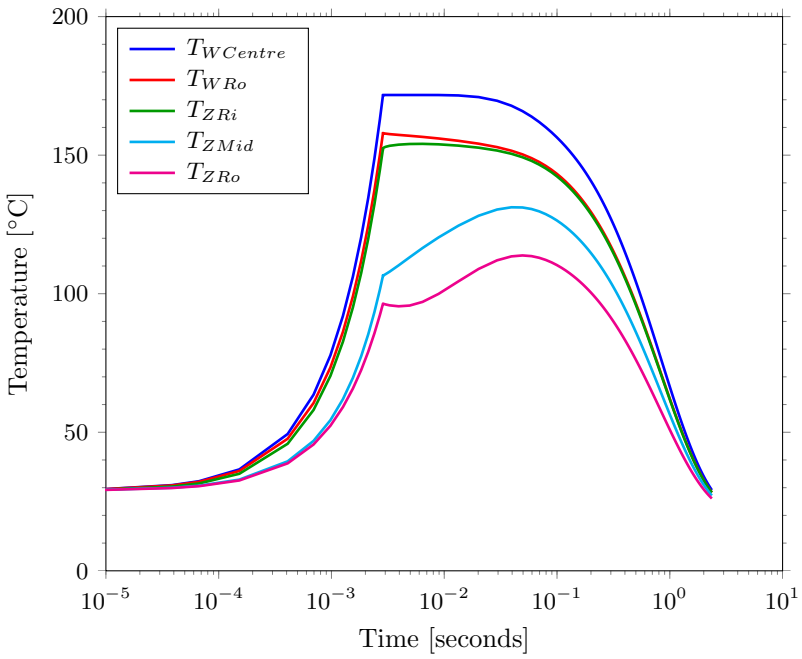

Figure 3.80: Temperatures in the water-cooled target as a function of time for one pulse cycle: $T_{WCentre}$ and T_{WRo} at the tungsten centre and outer edge, and T_{ZRi}, T_{ZMid} and T_{ZRo} at the inner, middle and outer surfaces of the zirconium can.

be quite 180°C during nominal pulses. In addition, the zircaloy also has a lower heat deposition and much lower heat conductivity than the tungsten, which will limit the outer surface temperature further during a pulse. Some rod-axisymmetric thermal simulations have been made on the mid section of the most heated rod, and the calculated results are summarised in Figure 3.80 [392]. The surface temperature estimated there suggests that 0.2 MPa is sufficient to avoid boiling for nominal conditions. However, the simulations are simplified and without known safety margins. A small increase in temperature leads to a large increase in required pressure. Also, the heat transfer at the surface is controlled by the heat transfer coefficient, which will be further investigated. In order to capture the transient heat transfer, the applicability of the modelling tools will also be assessed, because the standard CFD tools for simulations assume stable conditions in both flow and heat transfer.

It is possible to allow some local and temporary boiling at the hottest parts. Such boiling can strongly improve the heat transfer. It appears possible to limit the surface temperature of the lead filled cannelloni to about 200°C at 0.5 MPa [396]. Further investigations will show the feasibility of allowing and using local boiling. However, the configuration of short vertical rods placed with low pinch in a horizontal cross flow is not common and therefore existing experimental verifications are scarce. The conclusion of this preliminary evaluation of the cooling conditions of the water-cooling is that it is possible to remain below the boiling limit, while keeping sufficient pressure. The required pressure is at this stage estimated to be 1 MPa, but abnormal conditions will be further evaluated to determine whether it may be possible to loosen this requirement.

Pressure fluctuations

Pressure fluctuations have also been studied. With microsecond proton pulses, severe thermal shocks will be created in water. For example, an instantaneous temperature rise of 1°C in water at 50°C will cause an instantaneous pressure rise of nearly 1 MPa when all the beam-deposited energy is instantaneously converted into heat. With slower heating over 2.8 ms at ESS, this effect should be reduced substantially, provided that the pressure wave created by the thermal expansion of the rods and the water can freely propagate over 2.8 ms into the cold water across the whole wheel. In this case, values of below 0.1 MPa can be expected. However, if the sectorisation partially or totally prevents this dissipation, higher pressures will arise. Whether or not this occurs depends on the mechanical layout of the wheel.

A further pressure rise in the water will be caused by the quasi-static thermal volume expansion of the rods and, to a lesser extent, of the water [396]. Assuming, for the sake of argument, an average volume increase in the most significant part of the target of 20 cm × 20 cm × 6 cm, an excess volume of about 2 cm^3 will have to be accommodated to avoid a build up of pressure. This again may be absorbed by the total volume of water contained in the wheel, 50 to 100 litres, to arrive at a pressure rise of less than 0.1 MPa. Also, small temporary expansions of the covers of the vessel will mitigate this effect, although undesired vibrations of the vessel may be induced. A more precise assessment of the above dynamic effects, including the dynamic coupling between the cannelloni and the vessel through the water, should be done, based on a more detailed geometry.

Experimental verification

As stated above, the complex water-cooling regime requires experimental verification and benchmarking of the numerical codes. It is of particular importance to investigate the thermal response of the cannelloni during the beam heating over a period of 2.8 ms, and shortly thereafter over a period of about 100 ms, as demonstrated by the studies, presented above. Various approaches to such experiments are at present under investigation at Forschungszentrum-Jülich and ESS-Bilbao. One approach is continuous heating at maximum temperatures. Electrical heating by a DC current of a bundle of cannelloni up to the maximum temperature could be used, with temporary peak temperature of about 200°C. A realistic geometry of the cannelloni and water flow, including adequate pressure pre-load must be provided and a power of about 4.5 kW per cannelloni is required. Such an experiment will provide average heat transfer coefficients at different water flows, pre-loads, heat fluxes and onset of boiling and will thus serve to benchmark the codes applicable for continuous heating regimes. Another approach involves mechanically induced heat pulses. A bundle of cannelloni, pre-heated to about 200°C is driven rapidly into a stream of cold water and the decrease of temperature is measured. The length of time over which the water flow is disturbed will have to be verified, so that the time span of interest, substantially shorter than 100 ms, can be investigated.

An experiment could also be performed with electrically induced heat pulses. In this type of experiment, a bundle of cannelloni or even only its cans, are heated by an electrical pulse over 2.8 ms up to about 200°C, while placed in a realistic geometry and flow of cold water. Since the prime issue is the surface temperature of the cannelloni and its interface with the cooling water, empty pipes with suitable electrical resistivity may be selected to study short term behaviour, when the heat flux from the filling of the cannelloni is not yet relevant. At longer times of around 100 ms, when the heat input from the cannelloni filling starts to matter, this missing heat can be provided by continuing the electrical pulse in an adequate way.

There is also a need for fatigue tests of the cannelloni. In these tests, each cannelloni is submitted to cyclic thermal loads. Temperature rises over 2.8 ms are different in the zircaloy can and the inside tungsten. The interface and, in particular, the thermal contact between the mating materials is of prime importance for the evacuation of heat. About 4 million cycles are accumulated in each cannelloni over 100 days of continuous operation. Cannelloni with adequate pressure at the tungsten-zircaloy interface should be thermally cycled between room temperature and about 200°C. With cycle times for heating up and cooling down of about 10 s (which is not trivial to achieve), 1.7 million cycles will be accumulated over 200 days. Although only thermal cycles with uniform temperature over the cross section of the cannelloni are tested, and the temporary temperature difference between the zircaloy and the tungsten is ignored, the approach should provide insight into the long term thermal behaviour of the cannelloni. Some resilience tests to very high temperatures of around 500°C, which may occur during incidents due to the after heat if no active cooling is available, should also be planned for.

Layout and operation

About 14,000 cannelloni must be manufactured to equip one wheel. The tungsten rods are press fitted into the zircaloy pipes under sufficiently high pressure between the mating parts to ensure good thermal contact. A radial pressure preload between the canning and the rod of 7.2 MPa results from accepting a circumferential stress of 72 MPa in the canning due to the press fitting in the reference configuration. Thus, in the event that pressure buildup occurs due to gas production inside the cannelloni, thermal contact will not be lost unless this pressure is exceeded. To achieve the required preload during manufacture in a reliable and reproducible way, the tungsten-rods and the zircaloy-tubes must be fabricated to micron precision. Assembly procedures, procedures for the closing of the cannelloni and final acceptance criteria

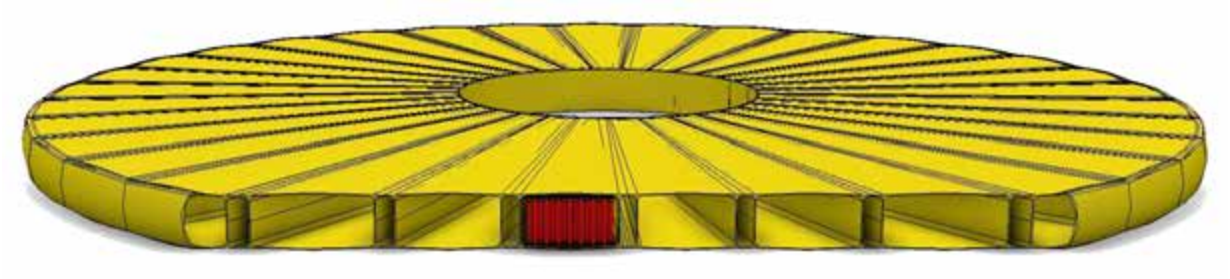

Figure 3.81: Sketch of tungsten rod placement in a sector of the water-cooled target wheel.

must be specified carefully. The global structure of the wheel is made entirely of stainless steel, as shown in Figure 3.81. A separate support holds each cannelloni in place, as shown in Figure 3.79. Perforations in the support provide for good transparency for the passage of water, as discussed above. This holding structure is linked to the global structure of the wheel. Further engineering is required to ensure that the strength of this support is adequate to support at least 45 kg, the weight of each significant part of each target sector, and also to optimise water passage vertically.

Figure 3.81 shows how the wheel is enclosed at the top and bottom by slightly undulated stainless steel sheaths. This shape combines high-pressure resistance with minimum wall thickness. A thickness of 2 mm and wave amplitude of 5 mm resists up to 1 MPa, when a membrane stress of 500 MPa is accepted. This can readily be optimised further by slightly increasing the thickness and/or the wave amplitude. Since the average increase of the water temperature after crossing a target sector is small, no major deformations due to temperature variations around the wheel are expected. With the proposed layout of the wheel, and maintaining a safety distance between the vessel and the adjacent moderator of 15 mm, the distance between the centre of the spallation material and the moderator is 64 mm.

Figure 3.82 shows that the beam entrance window forms an integral part of the wheel, which is thus a monolithic structure, entirely welded together without assembled joints or flanges. The BEW also has a semi-spherical shape. At a thickness of 2 mm and sufficient bulge, pressure resistance to 1 MPa can readily be achieved. The temperature rise in the BEW per pulse is about 30°C to 40°C. Due to the high ratio of cooling surface to mass, a convection coefficient well below 10 kW m^{-2} $°C^{-1}$ is sufficient to ensure adequate cooling. This is much smaller than the convection coefficient required for cooling the cannelloni. As the BEW is among the most critical items in the wheel, it merits detailed studies, including investigations of thermal stresses, dynamic effects and vibrations induced in it via pressure bumps in the cooling water.

Operation

During operation, all standard controls have to be provided and interlocked. These include proper rotation of the wheel, locked to the linac timing; operation of the water cooling system; and the rotating seal and pressure pre-load in the water as well as the measurement of beam position and shape. Safe filling procedures must be devised for the whole circuit and for the wheel which contains more than 2 m^3 of water, in particular. Similarly, scenarios for purging, venting, dry-out and storage of the activated heavy water have to be provided. Shut-off valves will be required to isolate the wheel from the circuit for purposes such as maintenance of the rotating seals or exchange of the wheel. Fast emergency shut-off valves in running circuits must be avoided, since water hammer would aggravate dangerous situations.

During planned shut downs or minor incidental stops, a small water flow should be maintained to evacuate the afterheat safely and to avoid increasing the temperature above the operational level. If the wheel has to be drained, auxiliary gas cooling will be required to avoid temperature rises of several hundred degrees. For intermittent test of the integrity of the wheel, He-leak tests, involving evacuation of the wheel, and pressure tests will be carried out, provided, of course, that the afterheat can be tolerated during such interventions. In principle, it is feasible to instrument the outside of the vessel with temperature sensors and to guide the radiation hard cables to the top of the shaft and transfer the signal through rotating electrical contacts. Such sensors may not be very sensitive to excessive, accidental temperatures inside the wheel, since they are masked by the cooling water.

It is desirable to measure the footprint of the beam on the beam entrance window, as is done for

Figure 3.82: The beam entrance window before the tungsten rods in the water-cooled target wheel.

the proton beam window. In general, pulse-by-pulse measurement of the beam profile is of particular importance to protect the wheel from over-focused beams, which might perforate both the PBW and the BEW. The consequences of such an accident, in particular in terms of down time, are more severe when a large amount of water is lost and the wheel has to be removed, than they would be if only a PBW had to be exchanged. The pulse-by-pulse reproducibility of the footprint and the precision of its measurement will define the safety margin required for a reasonably continuous operation without an excessive rate of interlocks.

SINQ is among the spallation sources most relevant to ESS's water-cooled back-up target design. Its target is cooled with heavy water, using a similar geometry to that foreseen for ESS's water cooling [397]. However, at SINQ the spallation material consists of lead-filled zircaloy tubes. The total energy deposited in the water may be used as a measure for possible corrosion of the target by the water. The SINQ target is routinely changed after it has absorbed an energy of 9,000 MWh, at which point there is no sign of degradation on the actual target. In particular, no adverse corrosion effects have been detected. To put this into perspective for ESS, each of the 33 target sectors on its wheel will have absorbed only 3600 MWh over 5 years (200 days per year of operation). However, the material of the wheel at the exit of the water near the shaft, where all the 33 circuits are merged, is in touch with water that has accumulated higher dose levels. Long-term experience at PSI over some 15 years has shown that no detrimental effects appear on stationary components of the cooling circuit that are not regularly exchanged, such as piping. However, the unprecedented high energy of close to 17 J/g at ESS, combined with the pulse deposited directly in the water will have to be looked into carefully. Temporary very high ionisation and hydrolysis, involving threshold effects, could be present in the water path immediately downstream of the target. The substances and ions might quickly recombine and decay, and thus not be detectable in parts of the water circuit that are further downstream. As yet, no examples of beam-induced energy densities in water comparable to those at ESS have been found. The literature search will continue and advice in radio-chemistry will be sought.

Globally, the technology of heavy water cooling circuits operated in radiation environments is well established, as demonstrated by long term experience at SINQ and other facilities [398]. In ESS's water-cooled target design, the water ducts are made of stainless steel with safety qualified welding and as few flanged connections as possible. They will be designed for a pressure of about 0.7 MPa, taking into account a pressure preload of 0.5 MPa, to prevent cavitation in the pumps, and pressure drop across the whole circuit. Rotating water seals are available from industry, although they would have to be adapted to the specific needs of ESS, including high water flow and radiation resistance. Cleanliness of the water, low electrical conductivity, proper handling and disposal of radioactive isotopes, ^{3}H, ^{17}N, ^{7}Be and radiolysis gas, are important issues that are readily addressed by using delay tanks and resin filters in bypass and recombination stations. Experience from ISIS, LENS and SNS will also be relevant for ESS [399, 400]. Some contamination by deposition of Be-7 along the inside of the pipes has to be expected. If required, local hot spots can readily be shielded. Small quantities of water escaping through incidental leaks, or recuperated continuously from the rotating seals, can be detected by tracking increases in radiation level due to tritium, as is the practice at SINQ. It remains to be determined, however, if the emerging signal can still be detected against the overall tritium background produced during normal operation over prolonged periods, or by previous incidents. This background might be important in the immediate vicinity of the wheel and the top of the rotating shaft.

Fundamental safety issues

Management of the afterheat after prolonged operation is a crucial safety issue for the water-cooled target. The afterheat – or decay heat – is the residual power in the irradiated tungsten due to the decay of radioactive species. If the water-cooled target has a tungsten volume fraction similar to that of the baseline helium-cooled target, a residual power of 47 kW in the water-cooled target's tungsten volume can be assumed [355]. The afterheat decays to about 30 kW after some hours. This heat is dissipated throughout the bulk of the spallation material, uniformly distributed around the wheel over a significant depth of about 20 cm.

The first of a number of afterheat issues is the case in which the flow of water ceases after the beam stops, so that stagnant water remains in the wheel. The pressure preload must be released. Devising a system of cooling via natural convection is difficult in this case, since the migration of heated water through the wheel to the top of the shaft and the return from there of cold water, via a buffer water reservoir or a heat exchanger, would be difficult to make compatible with safety regulations. However, if the stagnant water remains in the target, after some minutes, its temperature will have reached 100°C and it will have evaporated within about half an hour. The phase during which the remaining water boils needs additional study, mainly through experimental tests supported by numerical simulations focusing on the migration of vapour bubbles through the bundle of cannelloni in the radial direction towards the centre of the wheel and into the shaft. The wheel is initially filled with about 1 m^3 of cold water at nearly 0.1 MPa. As it boils, the vapour must be collected close to the top of the shaft, and the tritium carried in the water and vapour at or above 100°C must be contained. After the boiling phase, the wheel will still be filled with water vapour. The temperature will continue to rise and then will stabilise when sufficient removal of heat by radiation sets in. Temperatures well above 400°C are to be expected.

High temperatures can also be reached in the event of a sudden, massive water leak, such as would be caused by a breach of the BEW. In this case, 1 to 2 m^3 of water, pressurised to 1 MPa, would be lost from the wheel. Such a catastrophic scenario could be initiated by continuous beam during an undetected loss of rotation and/or cooling. To prevent such accidents, reliable systems must ensure that the beam is stopped within one or two pulses, or 100 ms, after the wheel stops. Tritium and other isotopes released at elevated temperatures of about 400°C must also be handled safely. In the event of a large breach in the target wheel vessel, the liquid water would be released. In this case, the target vessel would be filled with a mixture of water vapour, helium and possibly also air – a loss-of-coolant accident. The cause for concern is the possible exposure of the tungsten to the high temperature vapour and air due to thermo-mechanical failure of the zircaloy canning tube. A hazardous steam-tungsten interaction is known to begin at a threshold temperature of approximately 600°C. Zircaloy also reacts with oxygen at high temperature, creating hydrogen and zirconium oxides, and is likely to fail due to its crystalline structure. It is therefore important to remove the decay heat and to keep the target temperature below the critical limit of 500°C.

The decay heat in the target wheel volume is balanced by three heat transfer mechanisms: heat conduction though the helium (or air, in case of air ingress) which fills the gap between the target and the shielding; free convection due to the helium (or air) surrounding the target wheel; and thermal radiation from the target vessel towards the shielding block surface. Conservative estimation of the tungsten temperature in the water-cooled target was carried out under the assumption that the decay heat is balanced solely by radiative heat transfer, ignoring the other two heat transfer mechanisms. In order to get a qualitative understanding of the thermal behaviour of the target due to decay heat, it was also assumed that the decay heat is uniformly distributed in the tungsten volume. The temperature of the inner surface of the shielding block was uniformly set to be 100°C, for simplicity. It was also assumed that the surface of the vessel is blackened to have a surface emissivity of 0.7 and that the slightly oxidised surface of the zircaloy cladding has a surface emissivity of 0.4. Given that the radiative heat transfer at the first 50 cm of the outer diameter region of the target wheel dominates, an estimate based on grey body Stefan-Boltzmann law shows that the temperatures at the tungsten surface approach 600°C. This indicates that further engineering efforts are required to keep the tungsten temperature below the critical value of 500°C during a loss-of-coolant accident. However, heat removal by outside gas conduction and convection provides some safety margin. This is an area that will be studied in more detail as the geometrical design is further elaborated.

A number of spallation facilities that rely on water cooling have added a second safety vessel tailored closely to the dimensions of the wheel. However, this would be difficult at ESS, in view of the size of the wheel and the weight of the water or volume of the vapour to be recuperated. A second safety vessel

would suffer from radiation damage and beam induced heating from narrowly focused beams in the same way as would the wheel itself. If this second vessel is not rotating, but remains stationary, an additional PBW must be provided, although the second PBW does not provide additional safety. Therefore, the ESS water-cooled reference design does not call for a second safety vessel. Instead, means must be found to recuperate as much as possible of the water, or in the worst case, the vapour, spilt around the wheel, in a well-tailored sump. Means to dry out the area surrounding of the wheel should also be provided, to recuperate any remaining humidity.

Neutronic performance

The water-cooled cannelloni target is based on the idea of placing spallation material rods canned in zircaloy tubes. Compared to the helium-cooled target option based on a tungsten slab structure, this concept reduces the density of the spallation area. This increases the mean free path of protons, allowing them to interact with oxygen and hydrogen/deuterium. These effects will induce a reduction in neutron yield and a less concentrated source. This neutronic under-performance can be partially compensated for in terms of total system performance, for instance, by optimisation of the premoderator thickness. Analysis shows that a cannelloni target cooled with heavy water can reach 80% of the helium target performance for a single coupled cylindrical para-hydrogen moderator and 1.5 ms of pulse length [401]. On the other hand, this configuration has advantages from a thermal point of view, since it reduces the distance from the spallation material to the cooling media, reducing the thermal gradient inside the target, compared to the helium-cooled option.

Based on these considerations, a new model of the heavy water cannelloni target with the bispectral moderator has been developed for use in its neutronic evaluation, as illustrated in Figure 3.83. This model includes a matrix of 10 mm tungsten rods canned by a 0.5 mm thick layer of zircaloy, cooled by heavy water. Note that the target vessel is made of 7 mm thick aluminium alloy 6061 in this model [402]. The relative position between target and moderator and the thickness of the premoderator have been optimised in order to obtain a preliminary evaluation of the relative performance of this option. The relative position between target and moderator is related to target density. Since the cannelloni target has a much lower average density than the helium-cooled tungsten slab target, the positioning has to be reviewed. Also, the water inside the target produces a significant moderation of the neutron spectrum, so the premoderator can be reduced to 1 cm in thickness.

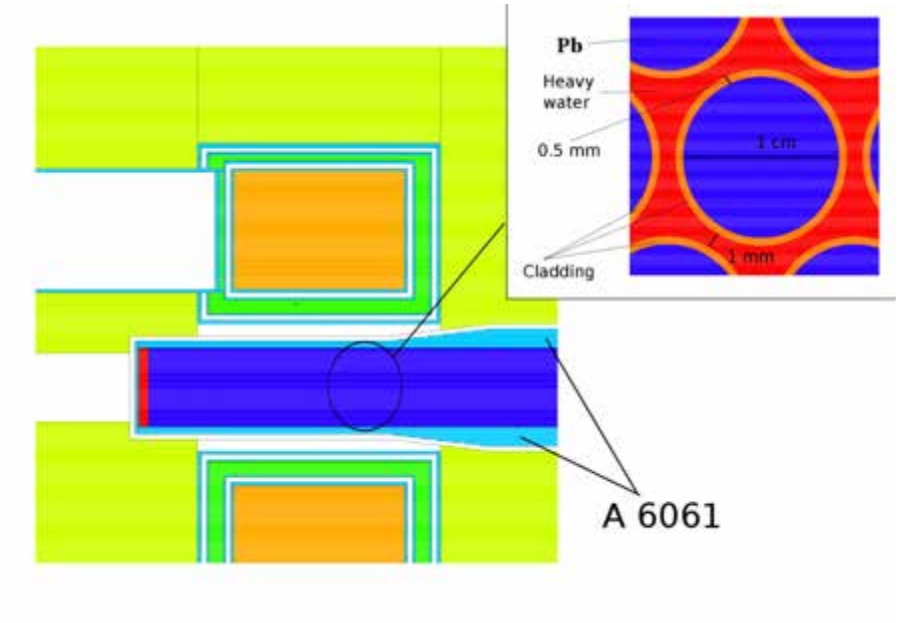

Figure 3.83: Geometrical model for a cannelloni target [393]. The target shown is made of aluminium and lead, but similar principles apply for stainless steel and tungsten.

The new cannelloni configuration reduces the heat load on the moderator by about 10%, mainly due to the lower neutron flux. The improvement for the premoderator is significantly larger, reducing the heat load from about 17 kW to about 11 kW due to the difference in total volume. Thus the backup solution is completely compatible with the cryogenic loops designed for the baseline proposal, and no additional capacity needs to be provided. To summarise, the preliminary neutronic study shows that the cannelloni-type water-cooled tungsten target has manageable disadvantages in neutron performance compared to the helium target option, but that it does not require much modification of the moderator-reflector assembly geometries to achieve the optimum configuration.

Summary

At present, the most powerful spallation sources are SNS, operating at 1 MW average beam power and 60 Hz with microsecond pulse duration, and SINQ, operating at 0.9 MW in DC mode. Extrapolating from these facilities to a water-cooled wheel at ESS is not straightforward. For example, the energy per pulse is about 20 times higher at ESS than at SNS. A water-cooled option has been proposed for ESS, inspired by SINQ, with tungsten rods, contained in zircaloy cans (cannelloni) and cooled by a transverse (cross) flow of heavy water with a velocity of about 1 m/s. Canning in stainless steel may also be an option. As 33 target units are contained in the wheel, so that each unit is hit every 2.4 s, the removal of the average power from each target sector is straightforward. However, understanding the detailed pulsed evolution of the temperature in time and space in and immediately around each cannelloni is much more complex. Different components (tungsten, zircaloy and water) are heated differently by the beam pulse, within a rise time of 2.8 ms.

The thermal interplay among these components over very short time spans measured in milliseconds, the convergence among these different temperatures over 100 ms, and, finally, the decaying average temperature of the whole cannelloni over many seconds is complex and difficult to assess reliably using existing simulation codes. Estimates indicate that temporary peak temperatures well above 100°C on the outer surface of the most loaded cannelloni will be reached. Including phase changes of water with boiling will make the investigation more complex. Thus, at this stage it is assumed that boiling is prevented by pressure pre-loading the water circuit to a value between 0.7 MPa and 1.0 MPa. Possibilities for experimental verification of the thermal regime, most importantly between the time spans of zero to some 100 ms are being investigated. Also, the more global thermal cycling of the cannelloni under fatigue, and in particular the thermal contact between the tungsten rod and the can, must be determined.

The dynamic interplay caused by the pulsed beam between the spallation material and the vessel, coupled to each other by the water, is another phenomenon requiring further investigation. The overall pressure resistance of the vessel up to about 1 MPa does not seem to be a problem and should be amenable to engineering solutions. Such pressure resistance may be required anyway by safety rules for water circuits in which a complex heat source of about 3 MW, contained inside a water volume of about 100 l, is connected at a distance of 6 m to an overhead voluminous water supply of 1 to 2 m^3. The cooling plant and in particular its pumps, heat exchangers, filters and ion exchangers are well established technologies, applied in many facilities around the world. While the lifetime of the wheel is expected to be above 5 years, a number of aspects remain to be studied, such as the effects of radiation damage in the wheel and gas production inside the cannelloni. The production and control of tritium during regular operation and its containment in accidental scenarios also must be investigated in more detail.

Responses to incidents and severe accidents require further investigation and elaboration. For small, incidental stops, for example, loss of water flow, active interlocks are required to stop the beam and to provide means to evacuate the afterheat. For the severe event of a loss-of-cooling accident, water or vapour will be spilt from the wheel into its surrounding area. A second target vessel will not be provided for reasons detailed above, so means to collect the spilt water and to dry out the flooded area should be provided.

3.6.2 Liquid lead bismuth eutectic target

The objective of developing the design of the MEgawatt TArget: Lead bIsmuth Cooled (META:LIC) has been to make available a target solution for comparison with ESS's baseline target design. In this context, the effort to design and validate META:LIC was comparatively limited and priorities have been directed mainly to the target design. However, the decision to develop a liquid lead bismuth eutectic

(LBE) target design is justified by the fact that Europe has developed a remarkable base of experience with LBE technology, and that experience has been very well documented in technical reports, handbooks and scientific papers. In particular, this experience has been gained in the frame of the development of accelerator driven reactor systems that couple a sub-critical reactor core (cooled with liquid lead or LBE) with a liquid LBE high power spallation target and proton accelerator.

The accelerator driven system (ADS) demonstration road map included the design, construction, commissioning, operation, post-operation analysis and decommissioning of the liquid LBE spallation target MEGAPIE (Megawatt Pilot Target Experiment). MEGAPIE has been successfully operated at the Paul Scherrer Institute in Switzerland since 2006, demonstrating the feasibility of liquid LBE high power spallation targets. Moreover, the selection of liquid metal as a prominent comparative solution is also motivated by the relevant operational experience gained in the USA and Japan on the liquid mercury spallation targets at SNS and J-PARC, respectively. This experience is especially important when considering the ancillary systems for liquid metal targets, which are complex.

A more detailed technical report on META:LIC is under preparation as a separate document. In addition to the description of the META:LIC design, below, further elements (e.g. ancillary systems, licensing procedures) considered relevant to operate a liquid metal target have been added. However, due to the limited resources available, the description of these elements is based on the MEGAPIE experience. Their further development would require a more detailed analysis and adaptation to META:LIC's circumstances. The baseline monolith layout conceived specifically for the rotating helium-cooled tungsten target cannot accommodate META:LIC. With relatively minor changes it is possible to adapt existing monolith designs from SNS and J-PARC to ESS. The META:LIC design is conceived as an evolutionary design in which both window and windowless configurations are feasible. This evolutionary design allows the operation of the window configuration both at lower beam power (e.g. the beam power expected during commissioning of the facility) and at full beam power, but with relatively short lifetime. The windowless configuration is potentially capable of power upgrades beyond 5 MW and has a longer lifetime than the window configuration. Both configurations are addressed below.

The META:LIC concept

Figure 3.84 shows the layout of the META:LIC target, which is the same for both the window and the windowless configuration, consisting of three separately replaceable modules. These modules are the target (window/windowless), the pump and the heat exchanger. The heat exchanger and pump modules are submerged in the pool and the target module is attached to the pool. In order to replace individual modules, the whole system is moved on a trolley into the hot cells, where the container can be opened. One of the attractive properties of META:LIC is that the pressure is below ambient pressure within the beam interaction region, which prevents major leakage in case of a leak or break of the window. Figure 3.84 also shows schematically the placement of two moderators that can operate at distinct temperatures for cold and ultra-cold neutrons. Not shown in this figure is a container that safely encloses the whole system, which is described in a later paragraph of this section.

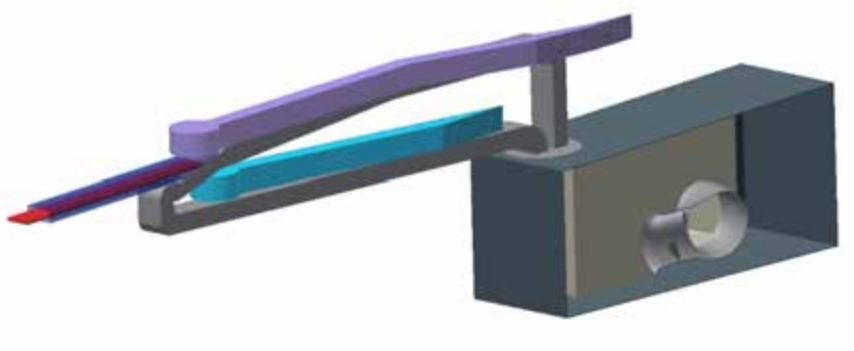

Figure 3.84: The LBE target system consists of the target module, two moderators and a pool with submerged pump and heat exchanger modules. The proton beam arrives from the left along the beampipe and interacts either with structural material (window) or directly with LBE (windowless).

Neutronics and nuclear data assessment

Displacement damage in the side, top and bottom steel walls of META:LIC has been calculated with the parabolic proton beam profile defined for the helium-cooled rotating target. Following 5,000 h at full beam power, the accumulated induced radiation damage amounts to about 15 to 19 dpa in the side and bottom walls. For the window configuration, the window itself is subjected to damage levels up to 50 dpa per 5000 h at the location where the proton beam hits the top steel wall. Under these conditions, helium and hydrogen production are 50,000 appm and 10,000 appm, respectively. These data clearly show that the beam would need to be reconsidered for META:LIC to reduce the peak proton current density. Nuclear heating, neutron and proton flux distributions were calculated using the parabolic proton beam profile. The maximum power density in the LBE amounts to about 2 kW/cm^3. The maximum values of the proton and neutron flux densities are about 3×10^{14} cm^{-2}s^{-1} and 3×10^{15} cm^{-2}s^{-1}, respectively. Figure 3.85 compares the neutron spectral brightness for the baseline helium-cooled target and for META:LIC. The moderator-reflector system and the proton beam parameters optimised for the baseline helium-cooled target have been used for neutronic calculations. The relative positions of the target module and the moderators have been varied to find the position with maximal cold neutron flux, with kinetic energy below 5 meV [403]. Earlier comparisons with a common Gaussian beam profile showed that the neutronic performance was roughly similar between LBE and tungsten [404].

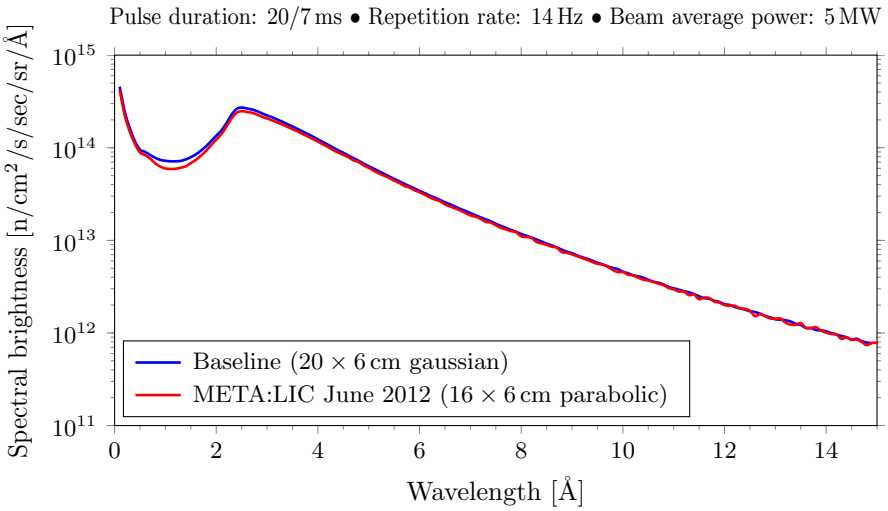

Figure 3.85: Comparison of neutronic performance of the baseline helium-cooled target (RoTHeTa) and the META:LIC target with a cold H_2 moderator.

Window target

The preliminary engineering design of META:LIC has been optimised in both configurations (window and windowless), given the calculated neutronic and heat deposition performance. The window target consists of a proton beam guide with a safety window, an inflow channel leading to a nozzle producing a uniform block velocity profile, a U-bend with an expansion chamber, and an outflow duct. The flow is pumped upwards, then directed into an inclined channel (at a 3 degree angle) and then accelerated by a nozzle into another channel, which is inclined relative to the horizontal plane by a 15 degree angle. This leads to an extremely stable block velocity profile that does not suffer instabilities. The proton beam enters the liquid metal through a solid wall, which is approximately 2 mm thick. The small inclination angle of 15 degrees allows for almost coaxial beam and flow, as in many earlier target designs (e.g. MYRRHA-target, MEGAPIE, EURISOL) in which the coolant is heated quite uniformly, so that a minimal coolant flow rate can be established. On the other hand, due to the inclination, the flow component perpendicular to the beam transports the fluid across the beam in a short time. This is advantageous for pulsed beams, as successive beam pulses interact with fluid that was not subjected to the beam previously.

The target module is installed at a geodesic height above the LBE level in the pool. Therefore when the pumps are not operating, the target module completely drains. A reservoir above the target level could

be provided to remove stored heat in the walls in case of a pump failure. The pressure inside the target module (determined by gravitational pressure and small losses) at the highest elevation is chosen to be slightly above the vapour pressure of LBE. This implies that the pressure at any location within the target is below ambient pressure. The target module is attached to the pool by a plug to allow replacement of the target module structure (excluding LBE inventory). As shown by dedicated investigations, the pulsed nature of the proton beam results in water hammer phenomena in the window target module. Indeed, the energy deposition due to a proton pulse leads to a temperature rise in the material within a short timescale. Due to the inertia of the surrounding LBE, the thermal expansion of the target material in the spallation zone is suppressed. This will result in an initial pressure rise and a shock wave, which potentially leads to high stresses on the container material. The risk of cavitation damage occurs when the pressure wave is reflected, leading to negative pressures.

While for a short pulse target, the time scale of the pulse is too short to allow the target material to expand at all during the pulse and the whole thermal expansion has to be compensated for by a compression of the target material, the time scale for the long pulse target is such that the target material can respond by appreciably expanding during the pulse. In this case, the maximum pressure is no longer proportional to the total energy per pulse, but rather to the sudden change in the heating rate at the beginning and the end of one pulse [405]. Preliminary calculations of pressure development for the META:LIC window configuration have shown that at the container material, peak pressures up to 1 MPa can be reached in normal operating conditions, and the pressure wave will reflect between facing walls. Compared to a short pulse target with sub-microsecond pulses where pressures up to 370 MPa could be expected with these boundary conditions, the pressures calculated here are relatively small. Therefore the risk of cavitation is reduced significantly for long pulse targets such as the ESS target with a 2.86 ms pulse length.

More critical are sudden events like beam trips. Starting with normal operation conditions, the pressures in the window region will significantly decrease due to the inertia of the liquid metal flow and the missing thermal expansion when the beam is suddenly cut-off. Once the flow field conforms to the beam-off conditions, the pressure will increase during the first pulses when the beam starts again. There is insufficient stress relaxation during the first pulses following a beam trip and deformations, so that stresses will be accumulated for several pulses. Countermeasures have been considered, to prevent cavitation issues in the META:LIC target. Two methods have been identified to counteract the water hammer effect and impact of non-steady state conditions such as start-up transients or beam trip. The first is to modify the shape of the pulse at the beginning and end, and the second method is a modification to the design including dedicated expansion volumes.

The maximum pressure in the liquid metal can be reduced if a ramped proton current, and hence a ramped heat deposition, can be provided at the beginning and the end of the pulse. Figure 3.86 shows the influence of the steepness of the ramp on maximum pressure, which can be reduced by a factor of two by having a rise time of about 50 μs. The reduction factor is about 7.5 for a rise time of 200 μs, resulting in

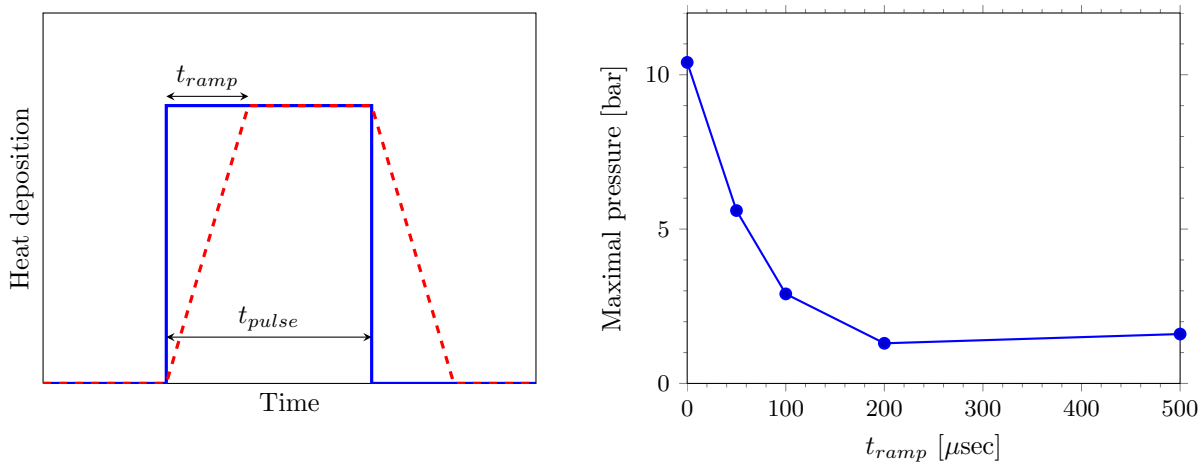

Figure 3.86: Heat deposition and maximum pressure for a ramped proton beam pulse. Left: Heat deposition versus time. Right: Maximum pressure in the target as a function of the ramp time t_{ramp}.

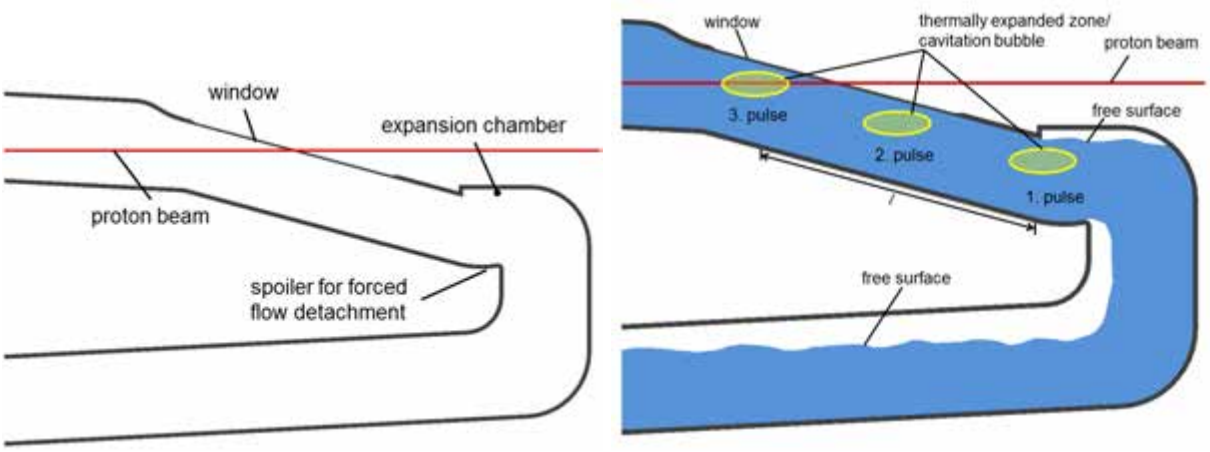

Figure 3.87: META:LIC design with enforced flow detachment. Left: Expansion volume and spoiler. Right: The two free surfaces in the outflow channel and in the expansion volume.

a maximum pressure of just 0.14 MPa. A longer rise time will have no significant effect on the maximum pressure.

The second method to prevent cavitation and high stress on the container material in transient conditions is to adapt the design of the target. In the current design, an expansion volume and a spoiler enforcing flow detachment have been integrated in the U-bend region, as shown in Figure 3.87. This modification leads to two internal free surfaces, one in the outflow channel and the other in the expansion volume. Free surfaces effectively decouple the flow in the beam interaction zone from the flow in the outflow duct. Thus, the establishment of a flow which is capable of accepting the beam can be detected by measurement of the filling level of the inflow channel, where simple and robust technology exists for radiation environments. The introduction of the free surface will also be beneficial for reducing the stress on the target in transient conditions.

Figure 3.87 shows schematically how the integrated free surfaces achieved by the described design modifications interact with transients due to unsteady events (e.g. in the case of a sudden beam trip). Starting with steady-state operation conditions, the fluid pressure in the window region will decrease due to the inertia of the liquid metal flow and the absence of thermal expansion when the beam is suddenly cut off. This sudden change in volume will be compensated for by deformations of the container in the window region and probably cavitation bubbles within the fluid. Once the flow field conforms to the beam-off conditions, the pressure will increase during the first pulses when the beam starts again and the sudden thermal expansion is again compensated for by deformations of the container in the window region. Figure 3.87 depicts the approximate locations of the expansion chamber and the spoiler. Thermal expanded volumes – or cavitation bubbles – are indicated for a time scale corresponding to three successive pulses. The thermal expansion zone is transported downstream with the bulk velocity to the free surface in the expansion volume chamber zone, within 2 or 3 beam pulses. The thermal expansion zone is mitigated when it reaches the free surface. Wall stresses due to the compensation for a missing thermal expansion during a beam trip or during start-up transients after a beam trip, reach saturation after 2 or 3 beam pulses.

Windowless target

The windowless target module mainly differs from the window target module by the fact that the window is removed and a free surface flow is established. Moreover, the water hammer phenomena counter measures (expansion volume and spoiler) are not needed, as high pressure and cavitation zones are neutralised at the free surface. Therefore, the LBE flow is guided back towards the pool by a simple U-bend. The free surface closely follows the shape of the window target module. The geometric dimensions of the windowless target module are nearly identical to those of the window target module. Since it can be assumed that the window is the lifetime limiting structure, removing the window means that the target module lifetime can be extended. The windowless option also provides for proton beam power upgrades [403].

Thermo-hydraulic analysis

The thermo-hydraulics analysis has focused on the calculation of temperature distributions, the feasibility of the expansion volumes within the window target module and the stability of the free surface in the windowless target configuration. The temperature distribution has been calculated with the commercially available program package Star-CCM+ [403]. The computed mean temperature distribution in the fluid and in the target structure are shown in Figure 3.88 for the windowless option. All computed temperatures are within the temperature range that is allowed for the proposed structural material. Thermal stresses are yet to be computed, but are expected to be acceptable for the calculated temperature cycling.

The investigation of the feasibility of the expansion volume proposed for the target with a window, to mitigate cavitation effects, has been conducted with three-dimensional isothermal and transient CFD simulations using the open source CFD tool OpenFOAM Version 2.1 [403]. For both simulations an inflow velocity of 1.5 m/s in the x-direction and vanishing pressure at the outlet has been assumed. Figure 3.89 shows the resulting velocity magnitude distribution of the LBE phase in the interval from $t = 1.5$ s to $t = 3$ s, confirming that the internal free surfaces form at the desired locations. The computed flow velocities of LBE range between 1 and 4 m/s. The material limits related to these velocities are discussed below, but it can already be anticipated that it is crucial that the corrosion limit of the proposed structure material (T91) at the critical locations, that is, at thin walls, should not be exceeded. Less can be said about erosion limits, since these seem to be dependent on the formation of vortices or similar phenomena. Figure 3.89 also shows that non-wetted walls are subject to splashing, so that these structures can be cooled from the inside alone. Splashing can be enhanced by design, if necessary.

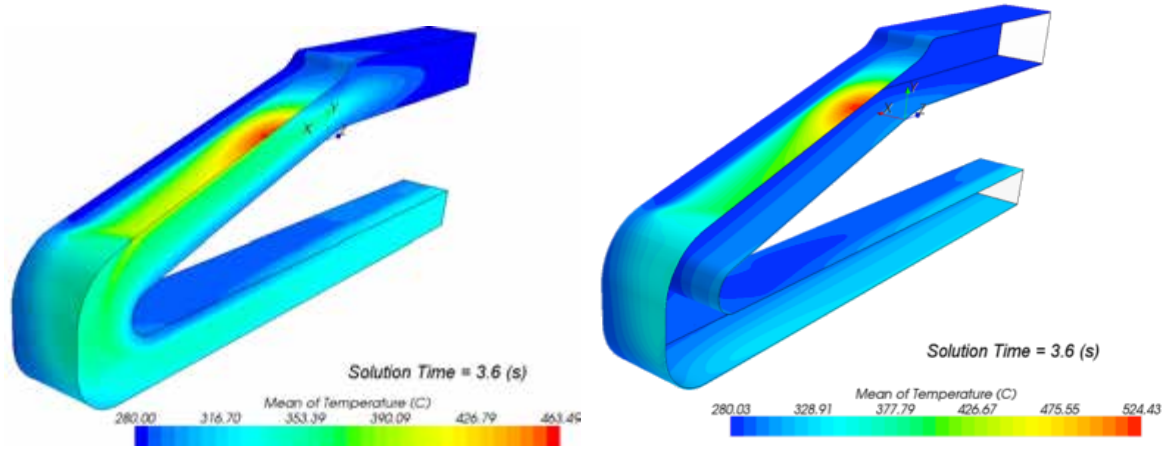

Figure 3.88: Mean temperature distribution in the windowless target option. Left: In the LBE. Right: In the target.

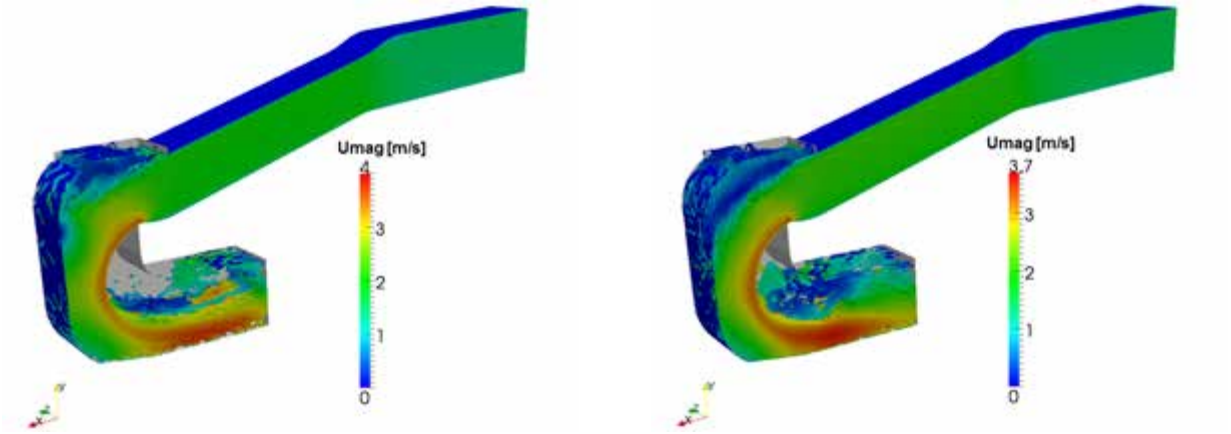

Figure 3.89: Velocity distribution of LBE at two times. Left: At $t = 1.5$ s. Right: At $t = 3$ s.

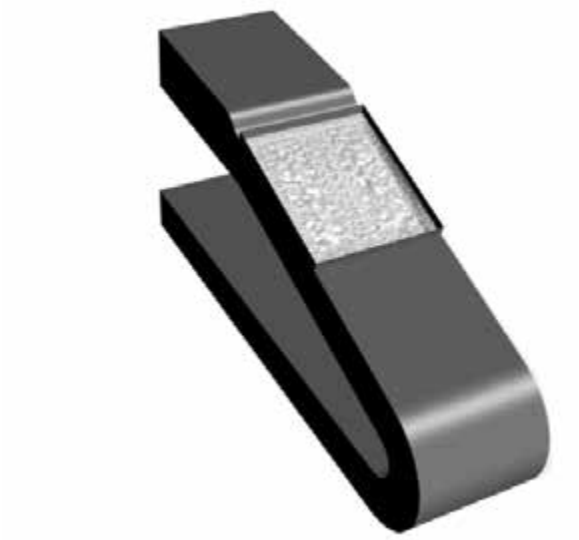

Figure 3.90: Development of the free surface flow in the windowless target, for an iso-surface of volume-of-fluid of 0.5. Some longitudinal standing waves are visible near the sidewalls, originating from the corners at the outlet, but they do not propagate towards the beam centre-line.

The free surface flow condition of the windowless target module has been investigated with an unsteady formulation of the volume-of-fluid. Figure 3.90 shows that these simulations demonstrate the advantageous development of a relatively smooth free surface. Even though some longitudinal standing waves are visible near the sidewalls, originating from the corners at the outlet, they do not propagate towards the beam centre-line [403].

Target module validation

An experimental campaign is foreseen to validate the META:LIC design [403]. The experiment will be focused on thermo-hydrodynamics of the liquid metal flow and will be conducted on a mock-up of the META:LIC target at the LBE loop at the Institute of Physics of the University of Latvia (IPUL). The mock-up is shown in Figure 3.91. The LBE loop at IPUL has a total length of 10 m and contains 1,100 kg of LBE. The loop is equipped with an electromagnetic cylindrical induction permanent magnets pump, which could provide a liquid metal flow rate up to 12.0 l/s at a discharge pressure of 0.4 MPa (compared with a flow rate of up to 30 l/s for the ESS LBE target). Two flow meters of the induction and conduction types, as well as a Venturi tube are installed on the loop.

Figure 3.91: Mock-up of the META:LIC target body.

Structural materials

The structural steels discussed for use in liquid metal targets are the nickel-containing austenitic steel 316L and the nickel-free ferritic/martensitic steel T91. Several corrosion tests and mechanical tests in LBE on both steels have been performed and good summary papers can be found [406,407]. The corrosion resistance of the two classes of steels at higher temperatures depends on the oxygen concentration in the LBE. Indeed, an oxidation mechanism on the steels occurs if the oxygen potential in the LBE is high enough. The oxide that forms on the steel surfaces apparently protects the steels against further corrosive attacks. On the other hand, some observers have suggested that too thick an oxide scale might crack and chip off, opening paths for LBE penetration. Above 500°C, the austenitic steel is susceptible to dissolution attack even at sufficient oxygen potential. In general, austenitic steel does not suffer degraded mechanical properties when exposed to LBE, unlike ferritic/martensitic steels. However, if the steel surface is protected either by an oxide scale or by an artificial iron/aluminium coating, the impact of LBE on the mechanical performance of the steel might be mitigated. One thermo-mechanical load not yet addressed is high-cycle fatigue. Temperature fluctuations like those expected for the LBE-cooled ESS target need to be addressed in specific experiments.

Two different erosion mechanisms are anticipated, causing different types of defects. The first mechanism has been attributed to the flow velocity and the resistance of the oxide layer. In particular, the oxide layer that forms on the steel surface has multiple layers. The outer one is formed by magnetite, while the inner one is a spinel oxide. It has been shown that increasing the flow velocity above 1.4 m/s causes the magnetite layer to disappear due to erosion phenomena. However, the spinel layer resists up to 2 to 3 m/s. Tests at higher LBE velocity have not been performed. The second type of erosion, which is apparently more severe, is due to the formation of vortices in the liquid metal flow. It has been observed that in flow conditions where vortices are generated, the liquid metal attack can be very deep. A thorough understanding of the flow conditions within the LBE loop is therefore mandatory. Note that the block profile of the velocity in the vicinity of the window is very stable and nearly laminar, so that corrosion issues concern other structures like the U-bend.

Irradiation phenomena should also be taken into account for the materials assessment. Indeed, in the proton-neutron irradiation environment, in addition to irradiation hardening, embrittlement due mainly to helium is often observed, which might limit the target lifetime. Investigation of the combined effects of corrosion and irradiation is an ongoing work that is currently being targeted in experiments performed in Bor 60 (LEXURII) and the PIE of MEGAPIE. These experiments will give some initial indications of the possible effects of the combined loads.

Instrumentation

Efforts have been made to assess and evaluate a further qualification route of existing measurement techniques for liquid metal flows, with particular view towards the application to a possible liquid metal target at ESS and its test experiments. The relevant measurement techniques are 1) contact-less flow-metering for the determination of integral flow rates, 2) ultrasound Doppler velocimetry (UDV) for the determination of velocity profiles and 3) contact-less inductive flow tomography (CIFT) for monitoring the three-dimensional velocity distribution in the target.

The contact-less flow meters developed at HZDR are a phase-shift sensor and a rotating single-magnet flow meter. A phase-shift sensor might well be applied for determining the total flow rate at a supposed liquid metal target in environments with low neutron fluxes. In its application, the necessary calibration and a temperature drift have to be taken into account. In contrast to that, the signal of the rotating single-magnet is largely independent of temperature fluctuations of the fluid. However, due to inertia, the time resolution of this sensor is rather limited. The UDV technique is not suited to the harsh environment of an ESS target, but it may well be applied at a lead-bismuth test target in order to identify flow variations due to heat fluxes. Contact-less inductive flow tomography is a promising technique for inferring the flow structure in the ESS target. The CIFT method is based on the fact that a flow under the influence of an externally applied magnetic field induces electrical currents which in turn deform the applied magnetic field [408,409]. The measurable magnetic field deformation outside the volume of the fluid carries information about the current flow state and can be used, by means of solving an inverse problem, for the reconstruction of the flow structure. In order to apply CIFT to ESS conditions, two problems have to be solved in advance: First, given the extreme neutron fluxes in the immediate vicinity of the liquid metal target, the Hall and

Fluxgate sensors used up until now must be replaced by more robust magnetic field sensors. Second, the CIFT inversion technique that has been used mainly on closed flows, or on flow with minor throughput, has to be adapted to flows with a dominant throughput and relatively low sideways or backward directed flow. Given the resulting very small induced fields, the increase in robustness and immunity to external interference is also an important issue. Further R&D activities would be required to investigate the feasibility of the CIFT technique for META:LIC. At present, the focus is on the adaptation of the CIFT method to the IPUL test loop. There is an on-going study to find a coil/sensor configuration that allows, with minimal instrumental effort, reliable identification of flow instabilities and backward directed flow components in the target. It is plausible that relatively simple pick-up coils would be much less sensitive to the expected radiation damage than Hall sensors or Fluxgate sensors. For this reason, a pick-up coil with 192,000 turns was developed and tested at the Mini-LIMMCAST facility which had been previously equipped with Fluxgate sensors. In order to reduce noise sensitivity, a gradiometric version of the pick-up coil was also designed and tested [403, 410].

MEGAPIE experience with different sensors

Temperature sensors proved to be very reliable for MEGAPIE, both inside the target and for the ancillary systems, with both thermocouples and platinum-based resistive sensors [411]. The thermocouple-based leak detector proved to be the most sensitive diagnostics for proper beam centring. Some problems were encountered with heated thermocouples, which were employed in level sensors. The reproducibility and thus the reliability of level determination of the liquid metal in the expansion volume of the MEGAPIE target was compromised, most probably due to LBE and oxides sticking to the sensors during operations. In the cover gas system, purportedly radiation-resistant pressure gauges showed strong radiation-induced drift in two sensors close to the target, resulting finally in the complete failure of one of the gauges.

Reliable pressure measurement is essential inside any new liquid metal target. Pressure gauges should be installed at suitable positions inside the target, to make it possible to gain experience with respect to long term performance in relevant conditions; continuous cross calibration with some external reference measuring the water flow through the target would allow the calibration of these devices. In combination with direct temperature measurements, true flow rates and thermal balances could be established on-line. This would certainly benefit safe operation. This applies to the primary spallation loop as well as to any intermediate cooling loop. One or more electromagnetic flow meters might be included as redundant and diverse devices for determining flow rates. Leak detection inside a liquid metal target should without doubt be based on temperature sensing employing thermocouples. The positive MEGAPIE experience with such devices is amply justifies this conclusion. A decision about whether to include stripe-type leak detectors could only be made after careful investigation into the properties of possible insulator materials. In MEGAPIE, the ZrO_2 turned out to respond very sensitively to changes in the gas composition in the insulation gas volume. In addition, strong and varying temperature and irradiation effects have been observed. Finally, for long-term operation, levels of oxygen in the liquid metal and their effects on materials corrosion should also be controlled and monitored.

Trolley design, interface to monolith and safety concept

The conceptual target station enclosure system pictured in Figure 3.92 provides three physical barriers for LBE while the beam is on. The first barrier represents the META:LIC target module itself. The target module is double-walled, except for the window. The gap between the walls is filled with a cover gas and monitored for contamination. The double-walled proton beam guide and the proton beam entrance window complete the enclosure of the target module. To address the possibility of a leak in the window, the proton beam guide is monitored for contamination and equipped with cold traps for LBE vapour. As the pressure inside the target module is approximately equal to the ambient pressure, there is a negligible differential pressure drop at the proton beam window. An inert inner liner represents the second barrier. It encloses the target module excluding the trolleys and the proton beam entrance window. The pressure inside the inner liner is slightly above the adjacent atmosphere's to prevent the diffusion of oxygen into the atmosphere, which would lead to the formation of explosive gases in the event of a leak in the hydrogen moderator system. The outer liner, which surrounds the hot cells, represents the third barrier for LBE. The pressure inside the outer liner is lower than inside the inner liner. The three physical barriers for the LBE are partially disrupted during maintenance operations when the beam is shut off.

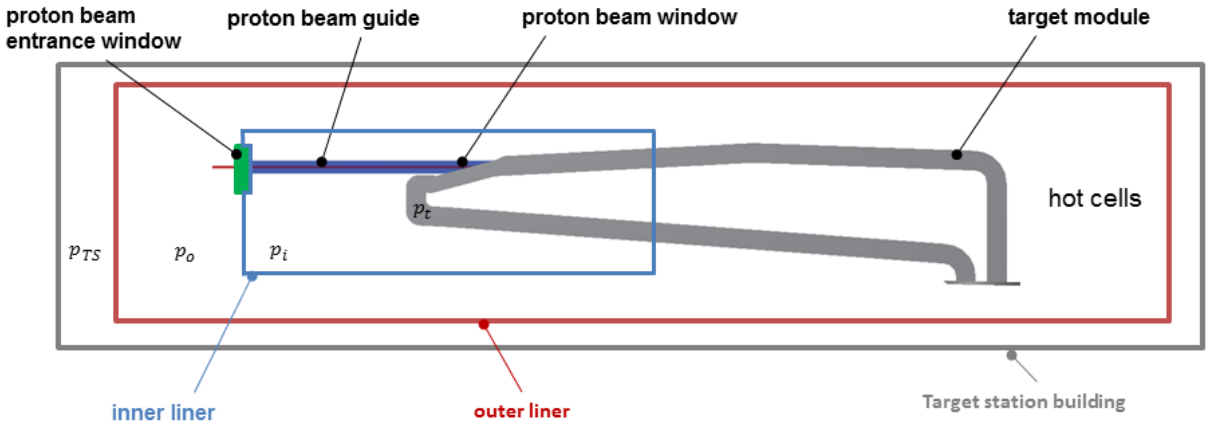

Figure 3.92: META:LIC enclosure concept.

Ancillary systems

Special attention has to be paid to issues of safety and containment in ancillary systems, in addition to safety and containment measures for the target itself. MEGAPIE's experiences are relevant here. At MEGAPIE, the heat removal system and cover-gas system proved to be more expensive than the target and posed significant challenges. MEGAPIE featured an intermediate cooling loop with heat transfer oil as medium, in order to bridge the large temperature difference between the liquid metal on one side and the final heat sink provided by water-cooling under normal pressure on the other side. A big temperature step might also be bridged by other means, such as an intermediate liquid metal loop or a thermosyphon. The MEGAPIE fill (and drain) system worked well, although preheating inside the target would need to be improved compared to MEGAPIE.

In the absence of oil, fire is not a concern in the target, and thus it seems possible to guarantee that a dedicated cold area inside the target stays cold all the time. This would then be the perfect location to install a gas absorber. A cover gas system could be installed, for example to take gas samples or to handle gases that are produced by accident. However, in principle one should consider the option to trap and enclose volatile spallation products inside the target. A cover gas system with an intermediate gas system would have the advantage of being able to handle gases inside the target by trapping and/or gettering them, at least for out-gassing sources, or for tiny leaks. For large leaks, measures similar to those taken at MEGAPIE would be unavoidable.

Licensing issues: radioactivity and accidents

One of the major safety concerns for liquid metal targets is the release of volatile radionuclides, because release of these substances is enhanced by the higher mobility of isotopes within liquid metal compared to a solid target. Furthermore, substantial amounts of highly volatile mercury and highly radiotoxic polonium are produced in LBE. Nevertheless, the success of MEGAPIE at PSI has demonstrated that a 1 MW LBE spallation target can be licensed and safely operated. In particular, PSI had to convincingly demonstrate that the consequences of a very severe accident (as defined by the Swiss Federal Office of Public Health) could be dealt with, and that exposure to the public could be kept below 1 mSv. For ESS, the higher irradiation doses and longer operation times associated with an LBE target would be likely to result in more stringent licensing requirements. However, the ESS facility would be designed in such a way that certain accident scenarios that were relevant for MEGAPIE will not be an issue. For example, it is difficult to imagine scenarios that would result in a complete spill of the liquid metal at ESS. Once accident scenarios for ESS are established, experiences from MEGAPIE can help to identify the most important issues and solve them. There is also a large community developing ADS (MYRRHA) and other LBE-based reactor systems that can supply a wealth of information and will address relevant questions by new research.

Naturally, for reliable safety assessments of a spallation target, the radionuclide inventory has to be known with reasonable accuracy. Calculations have been made for an ESS facility with an LBE-target

geometrically similar to the 2003 design [412, 413]. Similar radionuclide production has been assumed for the current design. For gaseous elements such as hydrogen and the noble gases, instantaneous release from the liquid metal is assumed as a worst case for accidents and for systems for handling the cover gas in routine operation. Oxygen and nitrogen easily form a variety of chemical compounds such as oxides, nitrides, nitrites, and nitrates. Since they only form relatively short-lived radionuclides, and are not produced in large quantities, they are not taken into account into the current design. For elements that have a significant vapour pressure at typical operating temperatures for LBE, recommended functions for conservative estimations of effective vapour pressure and thermodynamic activity coefficients in dilute LBE solutions have been derived for Pb, Bi, Po, Hg, Cd, Tl, and I [414]. Processes for the formation of volatile chemical compounds of various impurities will be investigated within the ongoing R&D program in support of the MYRRHA design. Little experimental data is available on the evaporation kinetics of volatiles from LBE, and it is limited to polonium and mercury [413]. Other physical phenomena that can lead to entrainment of radioactivity into the gas phase are sputtering caused by radioactive decay and aerosol formation [413, 414].

Radionuclide volatilisation in an LBE-based target has been studied. Estimates of the maximum gas phase activities that can occur in the cover gas under equilibrium conditions, that is, for a closed system, have been evaluated omitting the possible formation of volatile compounds among the present impurities. Table 3.27 shows activity and release data for the most important volatile elements at shutdown of the facility after 40 years of operation [414]. Masses of lead and bismuth are given based on the amount of target material present at the start of irradiation. Though a measurable "burn-up" of the material will occur during the four decades of operation, these changes are small compared to the uncertainties introduced by experimental error, simplifications and conservative assumptions, and may safely be ignored. Mercury is the dominating contribution to cover gas activity due to its high volatility and the absence of chemical interactions that could lead to its retention. With respect to the volume, hydrogen isotopes make up the dominating contribution, with helium ranking second at approximately 10% of the gas volume. The contribution of the remaining noble gases and the volatile elements to the gas volume is negligible.

Element	**Liquid phase**		**Gas phase**		**Release fraction**
	Mass [kg]	**Activity** [10^{15}Bq]	**Mass** [ng]	**Activity** [10^{6}Bq]	
Hg	2.99	7.54	1.2×10^{9}	3.2×10^{6}	4.3×10^{-4}
Cd	0.11	0.20	1.9×10^{4}	34.6	1.7×10^{-7}
Cs	0.01	0.28	406.	16.1	5.8×10^{-8}
I	0.01	0.24	2.47	0.07	2.9×10^{-10}
Po	0.03	3.97	0.01	2.4×10^{-3}	6.1×10^{-13}
Tl	1.68	18.30	0.02	2.3×10^{-4}	1.3×10^{-14}
Bi	5.5×10^{3}	23.90	4.41	1.9×10^{-5}	7.8×10^{-16}
Pb	4.5×10^{3}	25.90	0.81	4.5×10^{-6}	1.7×10^{-16}
Rb	0.04	0.62			
Br	0.02	0.57			

Table 3.27: Activity and release data for volatile elements in an LBE-based target after 40 years of operation, sorted by activity in the gas phase. The masses of lead and bismuth listed are the amounts of target material initially present. Mercury is the dominating contribution to cover gas activity due to its high volatility and the absence of chemical interactions that could lead to its retention.

A gas purification system that safely removes both Hg isotopes and Po and other radioactive substances from the cover gas is mandatory. Here, one can build upon the experience gained in the safe operation of such systems with liquid mercury spallation sources at SNS and J-PARC. The off-gas system of SNS consists of a decay tank, two absorbers for binding mercury on a special gold-on-alumina substrate, a copper oxide reactor for converting the hydrogen (tritium) isotopes to water, and two molecular sieves for the absorption of the produced water. Finally, the gas flows over a liquid nitrogen-cooled charcoal absorber to remove the heavier noble gases and residual activity.

In summary, only a small fraction of the volatile nuclear reaction products will escape to the gas phase. Compared to MEGAPIE predictions, the total activity of volatiles in the cover gas phase of an LBE-based

ESS will be orders of magnitude higher, resulting from both the longer and more intense irradiation and the much larger gas volume. Overall, the gas phase activities for the volatile elements predicted here seem to pose no serious safety concerns. Nevertheless, the gas phase has to be purified to reduce its radioactivity to allow for safe maintenance procedures and for routine handling of off-gas.

Radiotoxicity

The radiological hazard of the most dangerous radionuclides was evaluated for MEGAPIE licensing, based on the dose that they generate for the public living near the PSI site in certain accident scenarios. Inhalation, ingestion and direct radiation were considered, to estimate the accumulated dose resulting from each radionuclide. The results of these calculations showed that mercury and polonium isotopes, and iodine isotopes resulting from xenon decay, pose the greatest hazards. Doses caused directly by noble gas release are rather low and mainly caused by direct radiation. Ingestion was found to be the main pathway, indicating that the committed dose can effectively be reduced by administrative methods such as restrictions on the consumption of contaminated agricultural products. During operation, a spallation target facility may be regarded as a closed system having a controlled emission rate of volatile radioactivity. The critical condition is an uncontrolled release due to damage of the target structure, either caused by internal failure or external action.

Two reference accident scenarios were defined for licensing the MEGAPIE target, that differ in their consequences with respect to the containment of radioactivity released from the target [415]. The first is an internal failure in which the target window fails, resulting in a complete spill of the liquid metal, leaving behind a thin layer of LBE sticking to the still hot walls of the target. The second is a failure caused by external events such as an earthquake. Here, in addition to target container damage and a liquid metal spill, ancillary systems such as the off-gas systems are at least temporarily compromised, leading to an unfiltered emission of radioactivity. The inventory used within the MEGAPIE licensing procedure was calculated for an irradiation of 200 days with a proton current of 1.4 mA at 575 MeV [416]. It was assumed that approximately 88 litres of LBE with a mean temperature of 300°C flows out of the target. As a starting point to estimate the release from a pool of LBE, the model of a pool with a 4 m^2 surface area and a depth of 22 mm was introduced [417]. Estimates showed that the activity released from the pool due to mercury and polonium is three orders of magnitude lower than that that released from the thin film of LBE, which remains on the wetted surfaces of the walls of the target. Using the values for evaporated and sputtered activities, the environmental radiological impact and hence the contributed effective dose to the local population was estimated. It was proven to the licensing authorities that even under severe accident scenarios, the population living in the environment of the facility would not be exposed to doses higher than 1 mSv.

The inventory of volatile elements due to LBE is distributed over three source terms: the gas phase of the expansion volume, the spilt LBE below the target, and the LBE surface film adhering to the inner surfaces of the target. Physicochemical and kinetics data about the relevant elements are needed for the assessment of these three source terms. The amount of volatile nuclear reaction products in LBE at the end of irradiation was calculated, for MEGAPIE, to be 64.1 g, of which 43.6 g are radionuclides. To a good approximation, the activities of the single elements are about one order of magnitude lower than that expected for an LBE-based ESS at the end of its irradiation. The noble gases, hydrogen and mercury are the prominent elements in the cover gas phase. Generally, the gas phase inventory of ESS would be higher than at MEGAPIE because of the longer irradiation times and five times higher power, but also because of higher operating temperatures and possibly gas volumes of up to 1000 times larger. Furthermore, a larger amount of liquid metal in ESS may lead to up to a factor of 10 higher dilution and thus lower equilibrium gas phase concentrations. The last three factors, however, greatly depend on details of the design of the system. Among the volatile elements, only the most hazardous mercury and polonium were considered in the assessment of the MEGAPIE reference accident case. The gas phase activity due to these two elements in the cover gas of ESS is predicted to be 1000 times higher than in MEGAPIE.

Summary of the LBE comparative study

The META:LIC target design is an evolutionary design based on existing experience of operating liquid metal targets including SNS, J-PARC and MEGAPIE. Cavitation is a major concern of liquid metal targets subjected to pulsed proton beams. This issue has been addressed for META:LIC and potentially reliable

solutions have been designed. The ESS adoption of a 2.86 ms long pulse substantially reduces container material pressures compared to short pulse targets running with proton beam pulses in the microsecond range. Moreover, the issue of major leakage from the target has also been addressed through design measures such as keeping the target pressure below 1 MPa. A distinctive feature of META:LIC is that analytical flow analysis is possible, enabling the nozzle design to be frozen at an early stage, but retaining the flexibility for adjusting the design when and where needed. Finally, a preliminary overview of needed ancillary systems and instrumentation has been drafted on the basis of the MEGAPIE experience as well as needed data and approaches to prepare the safety and licensing for META:LIC.

Chapter 4

Accelerator

Chapter abstract

Summary: This chapter describes the beam physics and technical design of the accelerator that will provide a safe, reliable, high-power proton beam to the neutron-generating spallation target.

High availability. The top level requirement of 95% availability, set in 2009, strongly influences the baseline design choices. High availability requires that the accelerator must run (after re-tuning) with multiple RF source-cavity stations inoperable. It also requires a segmented cryomodule design, in which each cryomodule may be cooled down or warmed up independently of the others.

The beam physics design description follows the sequence of accelerator sections: the ion source, normal conducting linac, superconducting linac and beam transport sections. This chapter also describes the RF and beam instrumentation systems. ESS actively collaborates with partner laboratories whose accelerators include components similar to those planned for the Lund facility.

The normal conducting linac consists of a radio frequency quadrupole (RFQ) followed by a drift tube linac (DTL). An RFQ similar in design and requirements to that envisioned for ESS is being commissioned at CEA Saclay, and will be tested using ESS parameters.

The superconducting linac is made up of superconducting radio frequency cavities that are immersed in liquid helium at a nominal temperature of 2 K. One set of spoke cavity cryomodules is followed by two sets of elliptical cavity cryomodules, one medium-β and one high-β, where β is the ratio of the proton speed to the speed of light.

Three beam transport sections move the proton beam between the accelerating components and from the accelerator to the target station: a low energy section between the ion source and the RFQ, a medium energy one between the RFQ and the DTL and a high energy section between the end of the linac and the target. These sections contain room temperature focusing and steering magnets.

The radio frequency system converts the AC power from the electrical grid to the radio frequencies required to drive the various accelerator components. Subsystems include the RF sources and conditioners (klystrons and modulators), the RF distribution system and the low level RF controls.

Beam instrumentation will provide detailed information on the condition and location of the proton beam. Such information is critical for the commissioning and for the safe and reliable operation of the accelerator. ESS will contain a dense array of standard beam instrumentation, much of which will be located in the beam transport sections.

Cost savings proposals. This chapter describes the October 2012 FDSL_2012_10_02 baseline accelerator design. Since then a series of proposals have been made that should reduce cost while maintaining the scientific performance with acceptable additional technical risk. These proposals, which principally involve the number of cryomodules and beam energy, are described in Section 4.10. The proposals do not modify the majority of details in this chapter.

4.1 Overview

ESS is an accelerator-driven neutron source. The accelerator is thus a critical component of the ESS facility. The role of the accelerator is straightforward. The accelerator creates protons at the ion source, accelerates them to an appropriate energy and steers them onto the target to create neutrons via the spallation process. A proton kinetic energy of 1–3 GeV is optimal for practical target and moderator designs, and to keep the shielding requirements reasonable. The ESS energy of 2.5 GeV requires an average macro-pulse current of 50 mA to reach a beam power of 5 MW. This current is consistent with the need for high reliability, but leaves some leeway for a potential energy (and thus power) upgrade. The current limit is mainly set by space charge effects at low energy, by the power that can be delivered to the beam in each cavity at medium and high energies, and by beam losses.

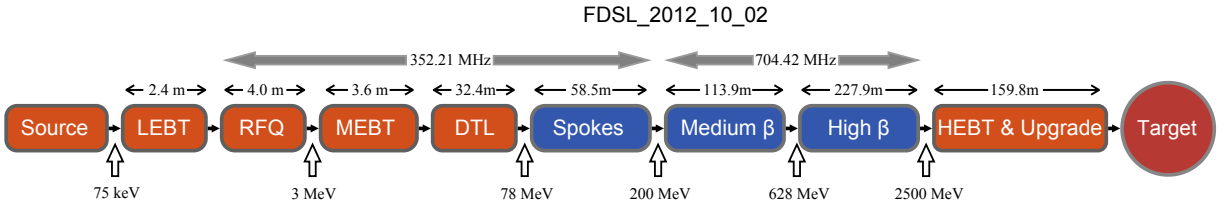

Figure 4.1: Block diagram of the FDSL_2012_10_02 accelerator lattice. The orange items (such as the radio frequency quadrupole and the drift tube linac) are normal conducting, while blue items (the spoke resonators and the medium and high-β elliptical cavities) are superconducting.

The general lay-out of the ESS linac is shown in Figure 4.1. The proton ion source is a compact electron cyclotron resonance source (ECR) similar to the Versatile Ion Source (VIS) in Catania [418], and to the High Intensity Light Ion Source (SILHI) at CEA Saclay [419]. The beam from the ion source is transported through a low energy beam transport (LEBT) section to the radio frequency quadrupole (RFQ) for bunching and acceleration. The RFQ is a four-vane type [420]. A similar High Intensity Proton Injector RFQ (IPHI), which is presently under commissioning at CEA-Saclay, will be tested with realistic ESS performance parameters. The beam is transported from the RFQ and matched to the normal conducting drift tube linac (DTL) through a medium energy beam transport (MEBT) section. Leaving the DTL, the beam enters the superconducting portion of the linac. Acceleration in the superconducting portion of the linac is accomplished via superconducting radio frequency (SRF) cavities constructed from niobium. The cavities are immersed in liquid helium at a nominal temperature of 2 K. An individual tank containing the helium surrounds each cavity. The first superconducting section contains double spoke cavities. Spoke cavities have a large transverse and longitudinal acceptance over this energy range. They are mechanically much stiffer than elliptical cavities, reducing their sensitivity to microphonics and to Lorentz force detuning. The spoke cavity section is followed by two sections of elliptical cavities, medium-β and high-β, where β is the ratio of the proton speed to the speed of light. From the superconducting portion of the linac, the beam is transported via the high energy beam transport (HEBT) section to the target. The target station is not part of the accelerator and is described in Chapter 3. The HEBT section also contains space for potential energy upgrades of the accelerator.

The energy that accelerates the proton beam is provided by the radio frequency (RF) system that converts the AC power from the electrical grid to the appropriate RF frequencies (352.21 MHz and 704.42 MHz) required to drive the various accelerator components. This system includes the RF sources and conditioners (klystrons and modulators), the RF distribution system and the RF controls. Successful operation of an accelerator like that of ESS requires detailed knowledge of the condition and location of the proton beam. The ESS accelerator will be equipped with a dense array of beam instrumentation for this purpose. Designers at ESS and its partners rely heavily on simulation software tools, such as CEA's TraceWin package, which is specifically adapted for evaluating and designing the beam physics of linac machines [421]. Similarly, Oak Ridge National Laboratory's AXCEL software has been used for designing the beam extraction system of the normal conducting linac, and the thermo-mechanical design of the RF system relies on the Fluent suite produced by the ANSYS engineering simulation software company [422]. These software packages incorporate theory, experimental observation and practical experience in their algorithms, allowing ESS designers to profit from relevant accumulated knowledge and experience.

This chapter describes the technical details of the ESS accelerator design. Following a more detailed

overview of the accelerator and its parameters, the chapter reviews the beam physics studies that led to the accelerator design and then describes the various accelerator components. This is followed by a description of the RF and the beam instrumentation systems. Specialised technical systems, such as those for cryogenics and vacuum, required for accelerator operation are described in Chapter 6. The major portion of the chapter describes the baseline design of the accelerator based on specifications that were current in the fall of 2012. Some adjustments to that baseline are being made that will reduce overall costs, while modestly increasing technical risk and maintaining accelerator performance. A preliminary discussion of these adjustments is provided in Section 4.10.

4.1.1 Accelerator parameters

The layout sketched in Figure 4.1 is described in somewhat more detail by the lattice parameters listed in Table 4.1. Top level parameters such as the 5 MW beam power listed in Table 4.2 are rigidly fixed, while lower level parameters are subject to modest evolution. Live parameters, continuously maintained and under configuration change control, are available on-line [423]. The optimum frequency for the accelerating structures is determined by a number of factors. Lower frequencies are favoured due to looser tolerances in manufacturing cavity components. Lower frequencies also have the advantage of reducing RF losses in superconducting cavities, decreasing beam losses through larger apertures, and ameliorating higher order mode (HOM) effects [424] from the high-current beams. Higher frequencies are encouraged by the desire to keep the size of the superconducting cavities small, making them easier to handle and reducing manufacturing costs. The cryogenic envelope and power consumption are also reduced at higher frequencies. Experience shows that a frequency of 600–800 MHz is a good compromise for elliptical structures [425, 426].

The 4% duty factor of the long pulse beam structure is imposed using modulators to drive the klystrons. Special care has to be taken with the design of the RF power source, distribution system and controls, due to severe space limitations; reliability and safety concerns; and high investment and operational costs. While modulators will be shared between several klystrons (as discussed in Section 4.8), the baseline design specifies one klystron per cavity, giving maximum flexibility for beam tuning and robustness against faults. Initial studies show that the linac will – after retuning – be capable of operating with any single individual

Section	**Length** [m]	**Input energy** [MeV]	**Frequency** [MHz]	**Geometric** β	**No. of tanks or modules**	**No. of cells or cavities**	**Temp.** [K]
LEBT	2.4	0.075					
RFQ	4.0	0.075	352.2		4		300
MEBT	3.6	3					
DTL	32.4	3	352.2		4	156	300
Spoke	58.5	78	352.2	0.50	14	28	≈ 2
Medium-β	113.9	200	704.4	0.67	15	60	≈ 2
High-β	227.9	628	704.4	0.92	30	120	≈ 2
HEBT	159.2	2500					

Table 4.1: Radio frequency parameters in the FDSL_2012_10_02 lattice.

Parameter	**Unit**	**Value**
Energy	GeV	2.5
Current	mA	50
Pulse length	ms	2.86
Pulse repetition frequency	Hz	14
Average power	MW	5
Peak power	MW	125

Table 4.2: High level accelerator parameters.

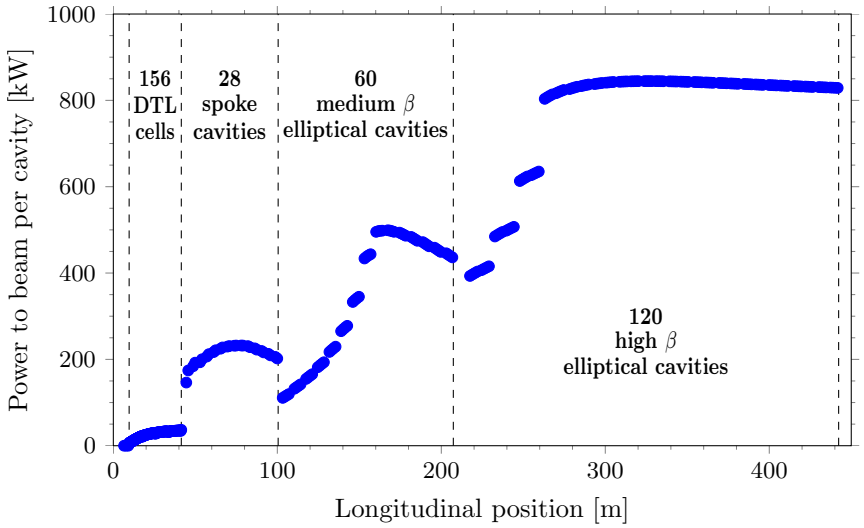

Figure 4.2: Power delivered to a 50 mA beam in each cell of the DTL and in each cavity of the superconducting linac. In the superconducting linac, this is equal to the cavity voltage multiplied by the ratio between the actual and the maximum transit-time factor, by the cosine of the synchronous phase, and by the beam current [427].

superconducting cavity off-line.

In the current design of the superconducting linac, acceleration fields or beam energy gained per cavity are in general limited by the surface electric fields in the cavities, rather than by the power that can be delivered through the power couplers. Figure 4.2 shows the power requirement for the RF sources, based on beam dynamics requirements for a smooth acceleration transition between the different types of structures. The variations within the cavity families are due to varying transit-time factors as the particle velocity changes, and to the requirement that the longitudinal focusing force changes smoothly between the different cavity families. The frequency doubling and consequent change of synchronous phase after the spoke resonator section suggests that the power per cavity should drop by approximately a factor of four, in order to maintain a constant longitudinal focusing force across that boundary. A study of operational experience from SNS is presently underway and it is possible that dedicated machine studies will be conducted at SNS to better understand the extent to which the traditional "rules of thumb" and "good practice" for beam dynamics design apply to high-power superconducting (SC) proton linacs. An optimisation for the best possible use of all RF power available in all klystrons would save cryomodules (and RF sources), which would reduce costs.

4.1.2 Linac configuration

The main components of the linac are shown schematically in Figure 4.1. The engineering design of these is described in other sections of this report. The normal conducting linac design draws on contributions from INFN Catania, CEA Saclay, ESS-Bilbao and INFN Legnaro, while the superconducting cavities and cryomodules are being designed at IPN Orsay and CEA Saclay, and the HEBT at ISA in Århus. This section provides brief descriptions of the different components, focusing on the beam physics aspects.

Ion source

The proton beam is produced in a pulsed microwave-discharge source on a 75 kV platform. It is capable of delivering a proton current of at least 60 mA to give a margin for losses in the LEBT. The time it takes for a pulse to stabilise may reach up to about 100 μs, requiring a LEBT chopper to avoid transient beam losses at higher energies with a risk of radio-activation. The normalised, root mean square (RMS) emittance from the source is expected to be less than 0.20 π mm mrad, as discussed in Section 4.3 on the normal conducting linac. However, the transmission through the linac depends not only on the RMS emittance but also the tails of the particle distribution. These are difficult to measure with the required precision at the

output of the source and also difficult to simulate with ion source codes. Hence, for studies of transmission through the ESS linac, ESS and its partners have assumed that the distribution of particles entering the RFQ follow either the uniform Kapchinskij-Vladimirskij (KV) distribution, or a four-dimensional Gaussian distribution, truncated at 4σ. The former corresponds to a optimistic case scenario for the performance of the ion source, while the latter corresponds to a pessimistic case scenario. As discussed below, the RFQ and the rest of the linac have a very good transmission even in the pessimistic case.

Low energy beam transport (LEBT)

The LEBT has the dual purpose of bringing the beam from the source to the sharp focus required at the RFQ entrance and providing a mechanism for chopping the beam. The chopper produces a beam pulse with sharp flanks and prevents beam from being sent into the linac before the ion source output has stabilised. In the LEBT, the beam energy is low enough that there is only a small power dissipation at the location where the beam is dumped. The energy is also below the Coulomb barrier for nuclear reactions, and radio-activation is thus avoided. The proton beam in the LEBT is partly neutralised by electrons, which are created by ionisation of the residual gas or possibly by injection of free electrons. This is necessary to prevent emittance blow-up caused by the proton-beam space charge. In the current beam optics design, a constant neutralisation of 80% or more is used, independent of beam radius. The focusing in the LEBT is provided by two solenoid magnets. The chopper, consisting of a pair of electrical deflection plates, is located between the two solenoids, and the chopped beam is absorbed on the entrance cone of the RFQ. The chopper will be able to switch off the beam in approximately 100 ns, but it will take longer to switch the beam back on because of the time it takes to re-establish the space-charge neutralisation. This is one reason that a chopper is included in the MEBT, as well.

Radio frequency quadrupole (RFQ)

The beam dynamics of the ESS RFQ are driven by the following five requirements: peak operational beam current of 50 mA; no limit to allowable beam loss below 3 MeV; halo development and beam loss in the high energy linac traceable to the RFQ held to a minimal level; no transverse tails, to avoid their translation into a transverse halo; and phase advances that are matched to adjacent sections. A four vane RFQ composed of four segments of 1 meter each has been designed in order to meet these requirements. The main parameters of the RFQ are presented in Figure 4.3. For a 50 mA beam with a Gaussian distribution

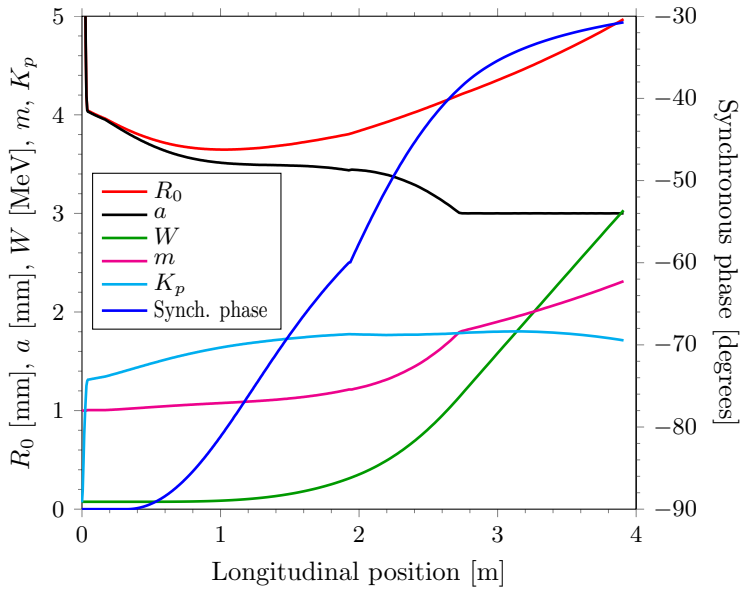

Figure 4.3: Evolution of key parameters along the longitudinal axis of the RFQ. The symbols R_0, a, W, m and K_p represent average aperture, minimum aperture, proton energy, modulation factor and Kilpatrick limit respectively.

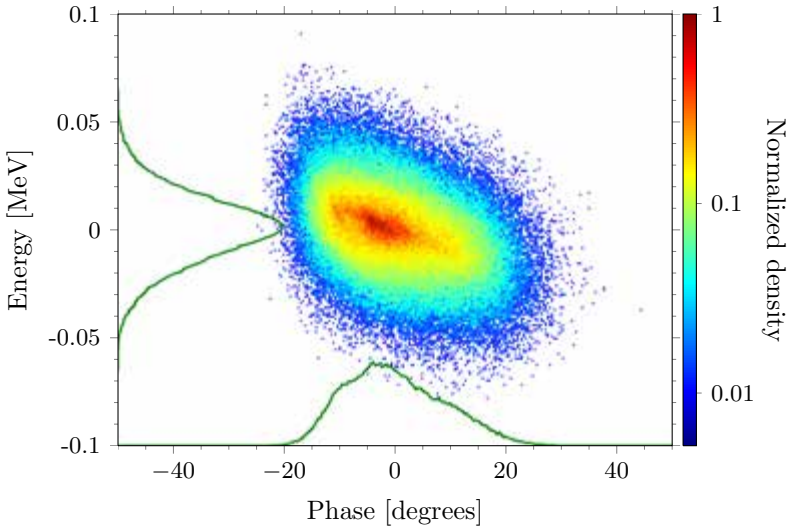

Figure 4.4: The beam distribution in longitudinal phase space at the RFQ output. The horizontal axis is the phase at 352.21 MHz, and the vertical axis is the energy offset from 3 MeV.

truncated at 4σ and 0.20 π mm mrad rms emittance at the entrance of the RFQ, a reasonable transverse emittance growth of 15% is achieved, and the transmission of particles inside the longitudinal acceptance is better than 95%. The RMS longitudinal emittance is 0.34 π mm mrad or 0.13 π deg MeV. Special care has been taken to produce a high quality beam. In particular, no longitudinal tails are formed in the RFQ during the bunching and acceleration process as indicated in Figure 4.4, where one can observe the beam in longitudinal phase space. The current RFQ design is one meter shorter than the 2011 RFQ design, which was composed of five one-meter segments [428]. The rationale for this change is provided in Section 4.3.4.

Medium energy beam transport (MEBT)

The MEBT fulfils four different functions. It has optics to match and steer the beam from the RFQ into the DTL; it has a comprehensive set of beam instrumentation devices; it allows collimation of the transverse particle distribution; and it has a chopper which acts more quickly than the LEBT chopper. The MEBT has three buncher cavities and 10 quadrupole magnets. The number, strengths, and locations of the buncher cavities have been chosen to make bunches short enough so that they see only the essentially linear part of force versus synchrotron phase, but at the same time long enough to avoid a high space charge force that would degrade beam quality. Similar reasoning underlies the design of the magnet lattice, which has been constructed so that the bunches maintain a reasonably large transverse size to avoid a high space charge force, while remaining within the available aperture with enough margin to avoid unnecessary beam loss in the MEBT. In addition, design choices result in a beam that is flat at the position of the chopper target to guarantee chopping efficiency, but round at the locations of the three buncher cavities, since previous experience shows that beam quality degrades when the beam is flat within the cavity. The resulting full beam envelopes (3σ) in the three planes are illustrated in Figure 4.5.

It is very challenging to perfectly fulfil the functions listed above while maintaining the matching between the RFQ and DTL, so some compromises have been made concerning the transverse beam sizes. Nevertheless, the lattice is quite successful at resolving the tensions among multiple competing goals. It provides perfect matching; results in transverse emittance growths of less than 20% and almost no longitudinal emittance growth. Crucially, the halo parameter H increases by less than 0.5 in all three planes, where [429]

$$H = \frac{\sqrt{3\langle x^4\rangle\langle x'^4\rangle + 9\langle x^2x'^2\rangle^2 - 12\langle xx'^3\rangle\langle x^3x'\rangle}}{2\langle x^2\rangle\langle x'^2\rangle - 2\langle xx'\rangle^2} - 2 \tag{4.1}$$

which in turn leads to small beam losses with a peak of less than 1 W in the sixth MEBT quadrupole. Three good locations are identified to collimate the beam and further improve the beam quality. These

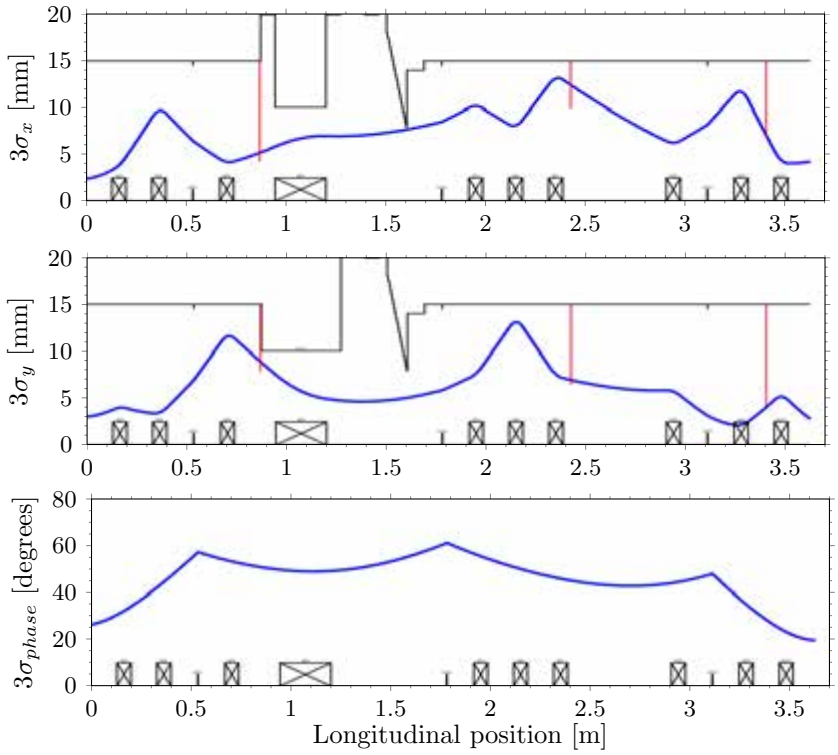

Figure 4.5: Full (3σ) beam distribution envelopes in the MEBT. Locations of collimators and the positions of their jaws are indicated with red lines.

are indicated by red lines in Figure 4.5. Due to mechanical constraints, a collimator must fit between two quadrupoles. The three locations are between the third and fourth quadrupoles, seventh and eighth quadrupoles, and ninth and tenth quadrupoles. Details of the MEBT collimation are presented in Section 4.2.5. A chopper is included in the MEBT to produce a fast-rising edge of the beam pulse. The LEBT chopper is limited in this respect because of the time it takes for the space-charge neutralisation in the LEBT to stabilise. In the MEBT, on the other hand, space charge neutralisation is not an issue, and the rise time of the beam pulse is determined simply by the fall time of the voltage on the chopper plates. Preliminary studies have been made to see where partially deflected particles during the fall (or rise) of the chopper voltage are lost, but conclusions are not yet available at the time of writing.

Drift tube linac (DTL)

The DTL accelerates the protons from 3 to 77.5 MeV in four tanks. A FODO structure with permanent-magnet quadrupoles has been chosen for the transverse focusing. Every second drift tube is empty or equipped with a steering magnet or a beam-position monitor. The beam is almost equipartitioned, and the accelerating field ramps up linearly versus length in the first tank and then stays constant. The synchronous phase ramps up linearly versus cell number in the first tank and is then constant at -24 deg. The tune depression (ratio k/k_0 of phase advance with and without space charge) is kept above 0.4 [430], and the emittance growth is approximately 0.03 π mm mrad in the longitudinal degree of freedom and less transversely, as seen in Figure 4.6.

Superconducting linac

The acceleration of the protons from 77.5 MeV to the final energy of 2.5 GeV is accomplished with three families of superconducting cavities. Double-spoke cavities (with three acceleration gaps) sitting two-by-two in cryomodules take the protons to 200 MeV. Medium-β elliptical cavities with four five-cell cavities per cryomodule accelerate them to 628 MeV, and high-β elliptical cavities also with four five cell cavities per cryomodule bring the beam to 2.5 GeV. The main parameters of the superconducting linac are listed

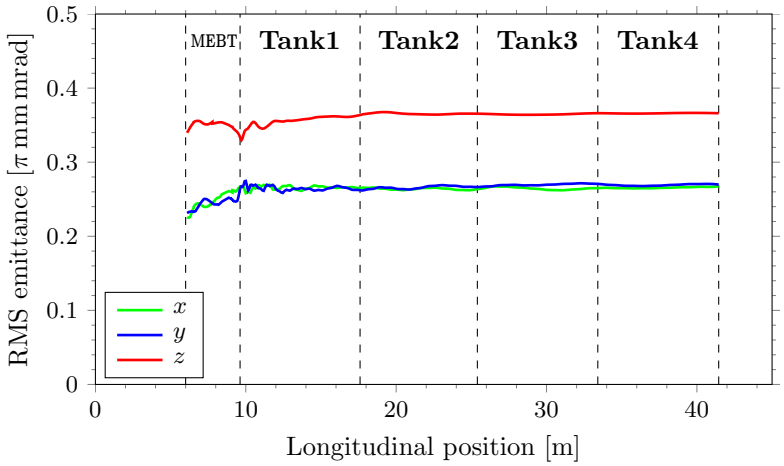

Figure 4.6: Evolution of emittances along the MEBT and DTL. The horizontal origin is at the exit of the proton source, as in the project-wide coordinate system defined in Figure 4.7.

in Table 4.1. Transverse focusing is accomplished with warm quadrupole doublets located between each of the spoke cryomodules, between each of the medium-β cryomodules and between every second high-β cryomodule.

High energy beam transport (HEBT)

The transport line from the end of the last acceleration module to the rotating spallation target consists of three parts [431]. The first ∼100 m on the level of the linac tunnel is reserved for upgrades (apart from a short section after the last cryomodule needed for differential pumping). Here, quadrupole doublets with the same period as in the high-β section keep the beam focused transversely, and between them there are six empty drift spaces that could be replaced by cryomodules in the event of a future energy upgrade. After the upgrade space, the beam is brought achromatically to the surface and the level of the target by two vertical bends, each composed of two dipole magnets in series. After the second bend, when the beam line is horizontal again, a section consisting of quadrupole and octupole magnets expands the beam to the desired 160 mm × 60 mm transverse dimensions on the beam entrance window of the target wheel. There

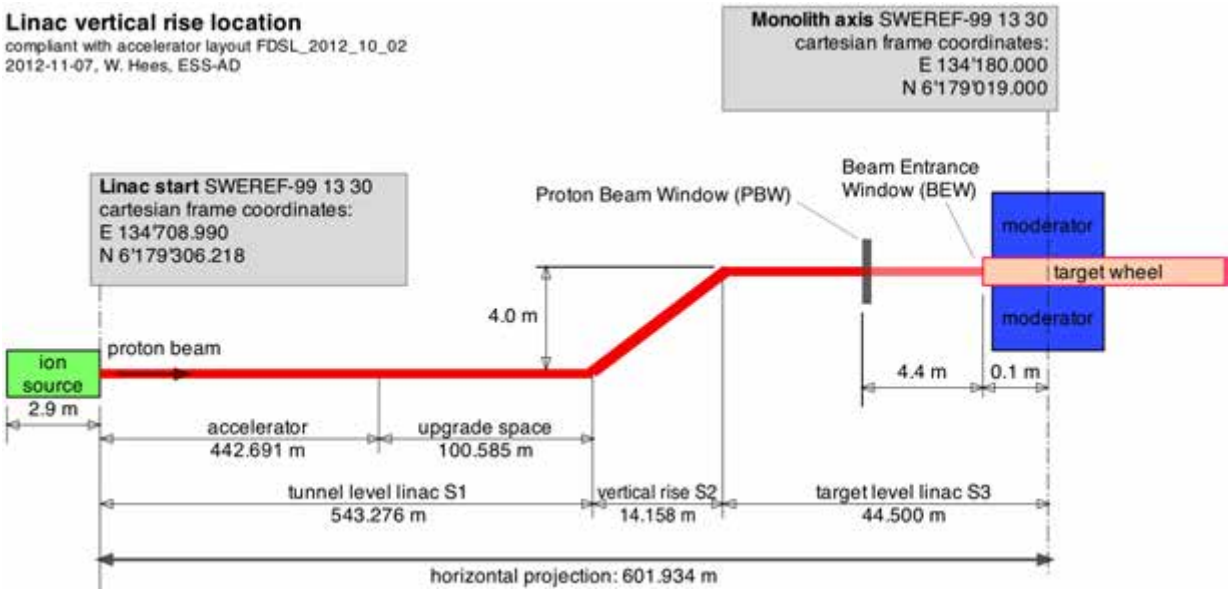

Figure 4.7: End coordinates and overall dimensions of the accelerator, from ion source to target.

is also a beamline on the tunnel level, straight ahead from the accelerator, into a beam tune-up dump that is used for a number of purposes, including for commissioning of the linac before the spallation target is ready for beam; tuning of the linac at start-ups and other occasions; and machine development when the spallation target is not available.

Extraction at intermediate energies

Beam can be extracted at two locations along the accelerator before it reaches full energy. The extraction beamlines have not yet been designed at the time of writing, but there is room in the linac lattice for dipole magnets that deflect the proton beam into these beamlines. Potential uses for extracted beams include beam diagnostics, physics experiments and irradiation targets.

Linac length

A total linac length of 601.934 m from the exit of the ion source to the centre of the target monolith, which is also the centre of the moderators, has been defined as one of the linac high-level parameters. The length of the linear accelerator is 442.691 m, with section lengths listed in Table 4.1. The length of the upgrade space is 101.585 m. The section that lifts the beam 4 m from the tunnel level to the level of the target needs 14.158 m projected on the horizontal plane. The remaining distance up to the monolith centre is 44.500 m. This is illustrated in Figure 4.7.

4.2 Beam physics

The beam physics design of the ESS linac has evolved through numerous iterations and has now reached a high level of maturity. Inputs and constraints influencing the design include: ESS high level parameters as listed in Table 4.2; mechanical properties such as the length of all linac components; constraints such as the maximum cavity gradients and the rating of the power couplers; optimisation criteria such as a desire for a minimum linac length and for small numbers of cavities and cryomodules; requirements such as the need for high beam quality and small losses; and external factors such as the development of production capabilities and collaborations. The primary set of tools for the design work has been the TraceWin suite [432] which includes both design codes (used, for instance, to find the minimum number of cavities and cryomodules needed to accelerate the beam to 2.5 GeV with the given set of requirements), and particle tracking codes that are used to study emittance growth and other multi-particle effects. The resulting configuration is a robust lattice with very small emittance growth, in which design margins and tolerances to faults and parameter variations are balanced with effectiveness in terms of cost and schedule [433]. Although this configuration will produce a linac with excellent properties, further evolution is expected during the next one to two years, as a result of more refined studies and identification of additional requirements. This section mainly deals with the beam physics of the superconducting linac. The beam physics of the other parts of the accelerator are reviewed in Section 4.1.2.

4.2.1 Superconducting linac design and beam dynamics

The layout and optics of the superconducting linac [434] have been designed using GenLinWin from the TraceWin suite of codes. Laws and rules of beam dynamics are used together with external constraints to find the shortest linac that reaches the desired energy of 2.5 GeV. Although length is not the only parameter to optimise, it is closely related to the number of components in the linac, and it thus correlates well with cost and reliability. Other constraints and requirements are met by manually choosing or biasing relevant parameter values. One set of constraints consists of the maximum accelerating fields, obtained from the integral of the longitudinal electrical fields, $E(z)$, in the cavities via the following equation,

$$E_{acc} = \frac{2}{N\beta_{opt/g}\lambda} \int E(z) \cos\left(\frac{2\pi z}{\beta\lambda}\right) dz \tag{4.2}$$

and evaluated at the optimum particle β, i.e. at the value at which the expression reaches its maximum. For the spoke cavities, the number of acceleration gaps, N, is equal to three; $\beta_{opt/g}$ is taken as the optimum β (as listed in Table 4.1) and the wavelength, λ, corresponds to 352.21 MHz frequency. The elliptical cavities have five gaps; $\beta_{opt/g}$ is taken as the geometrical β; and the frequency is 704.42 MHz.

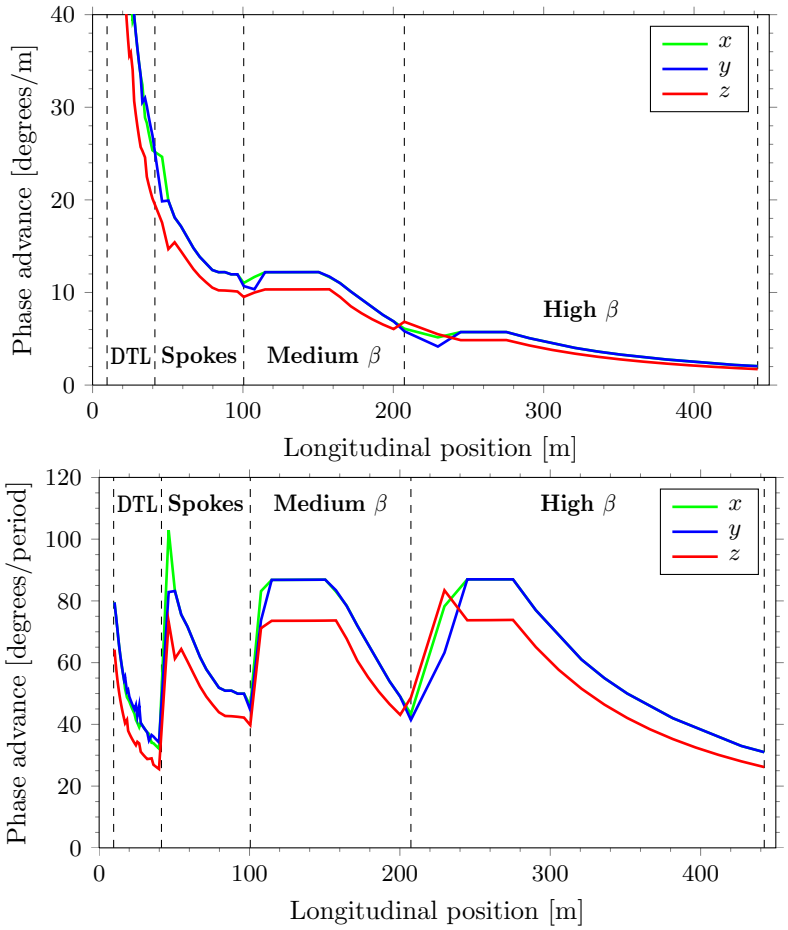

Figure 4.8: The rate of phase advance in the three degrees of freedom, from the DTL to the end of the high-β section. Top: Phase advance per meter. Bottom: Phase advance per lattice cell.

The maximum accelerating fields are 8 MV/m in the spoke cavities, 14.9 MV/m in the medium-β elliptical cavities and 18.4 MV/m in the high-β cavities. The latter two numbers derive from the cavity geometry plus the 40 MV/m peak surface field defined as an ESS high level parameter. Another set of constraints consists of the peak power given to the beam per cavity. This is limited by the power couplers to a maximum of 300 kW for the spoke cavities, 600 kW for the medium-β cavities and 900 kW for the high-β cavities, although these constraints are not binding in the current linac design. Standard design desiderata for high-intensity linacs include having a phase advance per lattice period of less than 90 degrees, smooth phase advance per unit length, and tune depression greater than 0.4. The current linac design meets all these goals.

Figure 4.8 (top) shows phase advances per metre in the three degrees of freedom – horizontal, vertical and longitudinal. They are all smooth functions of the distance along the linac. This avoids the emittance and halo growth that otherwise may result from what T.P. Wangler [435] describes as internal mismatch and consequent charge redistribution at the interface between sections of different focusing strength, even when the beam is RMS-matched at that interface. It also guarantees that matching between the sections is independent of beam current. Phase advances per lattice cell, as shown at the bottom of Figure 4.8, look different because of the different cell lengths. The transverse phase advance is kept below 87 degrees along most of the linac, and the longitudinal phase advance is kept lower than the transverse one by a factor of about 1.2 to keep the beam approximately equipartitioned except at a few locations. If the ratio of phase advances deviates from this factor over more than a few periods and the beam enters the coloured areas of the stability diagram presented in Figure 4.9, simulations reveal emittance transfer between the transverse and longitudinal planes.

The Hofmann stability plot in Figure 4.9 shows the ratio of horizontal phase advance with space charge

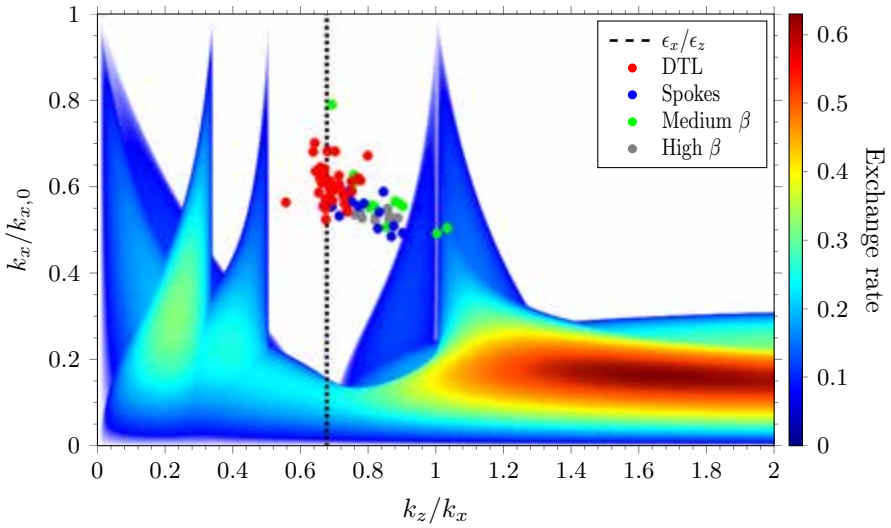

Figure 4.9: Hoffman stability plot showing the rate of emittance exchange between the transverse and longitudinal planes as a function of the ratio between longitudinal and transverse phase advance (horizontal axis) and tune depression, that is, the ratio between the transverse phase advance with space charge and the transverse phase advance without space charge (vertical axis). Emittance exchange is indicated by colour in accordance with the scale on the right hand side of the figure. Coloured dots represent the different lattice cells, and the black vertical dotted line indicates the phase-advance ratio corresponding to equipartitioning.

to horizontal phase advance without space charge is plotted as a function of the ratio of longitudinal to horizontal phase advance. (The relationship between the analogous ratios for the vertical phase advance is essentially the same.) Coloured areas, in which the latter ratio is near a rational number, should be avoided, since coupling between the different planes leads to emittance exchange when the ratio of longitudinal to horizontal phase advance is near a rational number. The dotted vertical line corresponds to equipartitioning such that external focusing relative to internal repulsive space-charge forces is the same in both planes, suppressing the emittance transfer. The coloured dots represent the lattice cells from the DTL through the high-β section. Their positions show that space-charge resonances are almost entirely avoided and that the linac is close to equipartitioned along most of its length. Emittance and halo growth is as serious longitudinally as transversely. A particle that slips out of the RF bucket and stops being accelerated will not experience the correct transverse focusing, and will therefore be lost transversely some distance downstream.

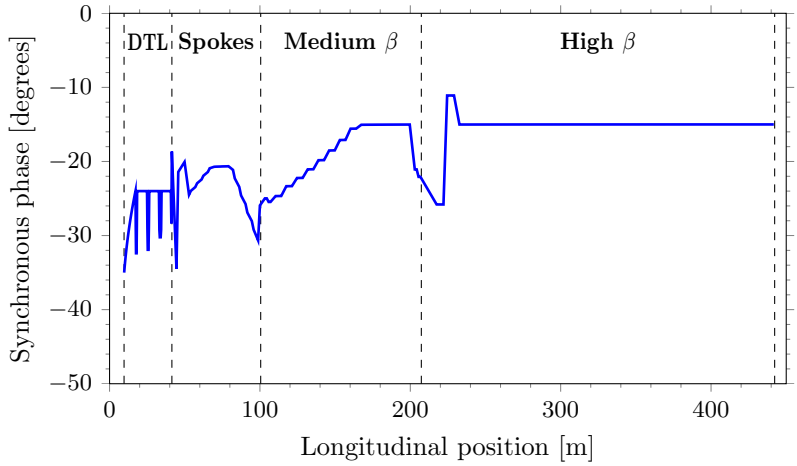

Figure 4.10: Synchronous phase from the DTL to the end of the high-β section.

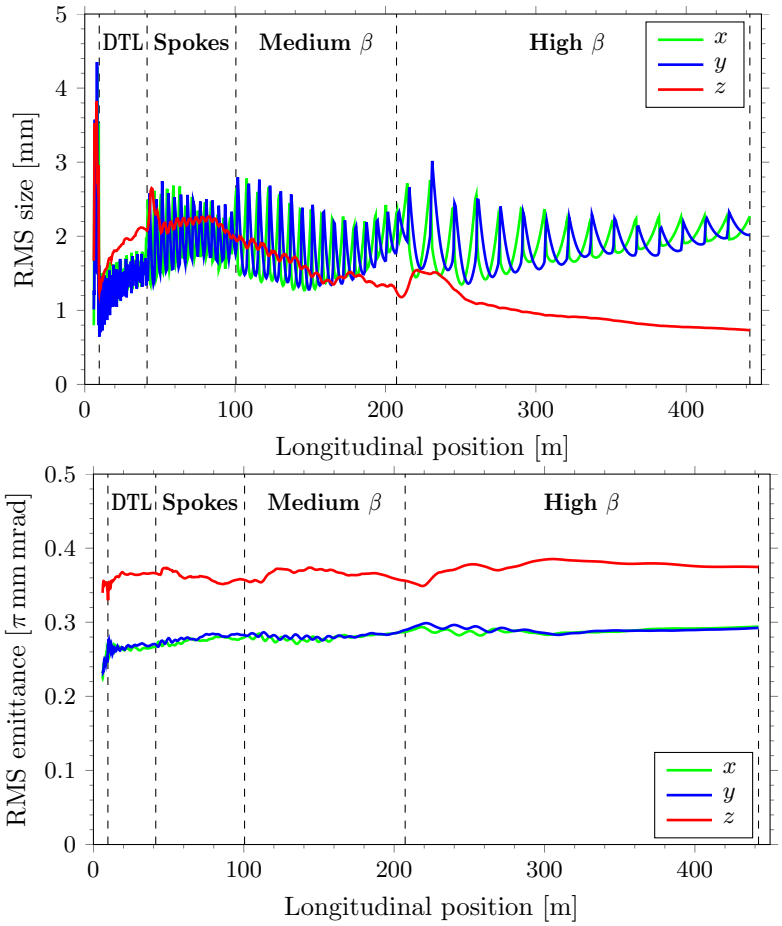

Figure 4.11: Root mean square beam sizes and emittances in the three degrees of freedom, from the MEBT to the end of the high-β section. Top: Beam sizes. Bottom: Emittances.

The synchronous phase, ϕ_s, is plotted in Figure 4.10. It starts out at -35 degrees at the beginning of the DTL to get a sufficient momentum acceptance. Here, the longitudinal emittance is 0.34 π mm mrad, and the RMS $\Delta p/p$ is 0.35%. The synchronous phase increases to -15 degrees towards the end of the medium-β cavities and remains at that value throughout the high-β section, balancing acceleration efficiency with longitudinal acceptance. To ensure a smooth phase advance, variation across the frequency jumps from 352.21 to 704.42 MHz at the end of the spokes, and to capture all particles after the frequency jump, the synchronous phase is also decreased towards the end of the spokes. The longitudinal focusing is thus increased, shortening the bunch as a preparation for the frequency jump. After the jump, the cavity voltages are reduced, contributing to the smooth phase advance. Taken together, these modifications make the frequency jump transparent to the beam.

The resulting linac configuration has beam sizes in the three dimensions as shown at the top of Figure 4.11. These are RMS beam sizes as obtained from a 0.20 π mm mrad Gaussian truncated at 4σ at the entrance of the RFQ. This results from a multi-particle calculation using 100,000 macro-particles and a 3D space-charge model with a $10 \times 10 \times 10$ cell mesh and a space-charge kick applied 25 times per $\beta\lambda$. Emittance growths obtained from the same multi-particle calculations are plotted at the bottom of Figure 4.11, which shows that the emittance exchange and emittance growth are less than 10% through the entire superconducting linac.

4.2.2 Studies of errors and fault tolerances

The plots of beam sizes and emittances shown here were simulated for an ideal linac in which the mechanical alignment of the linac components is perfect, magnetic and electrical fields have mathematically exact

values without temporal drifts or instabilities, and no power-supply ripples exist. In this ideal case, no particle losses in the superconducting sections are seen in simulations, since even the outermost beam particles stay well within the apertures of cavities and quadrupoles. A real linac has many imperfections. The linac configuration must be tolerant to static and dynamic variations in parameter values, and beam losses must stay small within the range of expected variations. Also, the machine should, as far as possible, be able to run even if some components fail. To address these issues, a comprehensive study of alignment and field errors has been initiated, and investigations of the effects of faults and failures have begun [436]. For the superconducting linac, the errors considered include those in quadrupole translations (x, y), quadrupole rotations (x', y', ϕ), quadrupole gradients, quadrupole multipole components, cavity translations (x, y), cavity rotations (x', y'), RF amplitude errors, and RF phase errors.

In a first set of calculations, sensitivities to the different types of errors were compared to find out, for instance, how much quadrupole misalignment has to be introduced in order to obtain the same growth in beam size as produced by a certain amount of cavity misalignment. For each component, such as a quadrupole in the superconducting linac, the error was drawn from a uniform distribution with the given amplitude, producing a linac with randomly misaligned quadrupoles. The amplitude of each type of error was varied in four or five steps. For each type of error and each error amplitude, 1000 linacs were generated, and the maximum growth in beam size among the 1000 linacs was obtained from the tracking of 100,000 macro-particles including space charge through each one. In total, about 40,000 linacs with different random errors were studied. In a second step, all errors were considered simultaneously, although with some simplifying assumptions to make the computing time reasonable. Using information gained from the first set of calculations, the errors were here limited to quadrupole translations ≤ 0.3 mm, quadrupole roll ≤ 1 mrad, gradient errors $\leq 0.75\%$, cavity translations ≤ 3 mm, cavity pitch and yaw ≤ 3 mrad, RF amplitude jitter $\leq 1.5\%$ and RF phase jitter $\leq 1.5\%$.

Quadrupole pitch and yaw were found to be insignificant on the scale of the other errors, and multipole components are still under study. Figure 4.12 shows how the maximum beam radius (outermost particle among the 100,000 over 1000 linacs) grows when the error amplitudes were at these limits, at 2/3 of the limits and at 1/3 of the limits. Not yet included is the effect of errors in the normal conducting linac on those in the cold linac. Also, beam centre corrections have not yet been included, but this is unlikely to have a significant impact, since beam size in the high-β section is dominated by envelope oscillations rather than by beam centre random walk. Furthermore, the error budget has here been divided equally (based on beam size growth) between the different sources of errors, which may not be optimal for reasons of technology and cost.

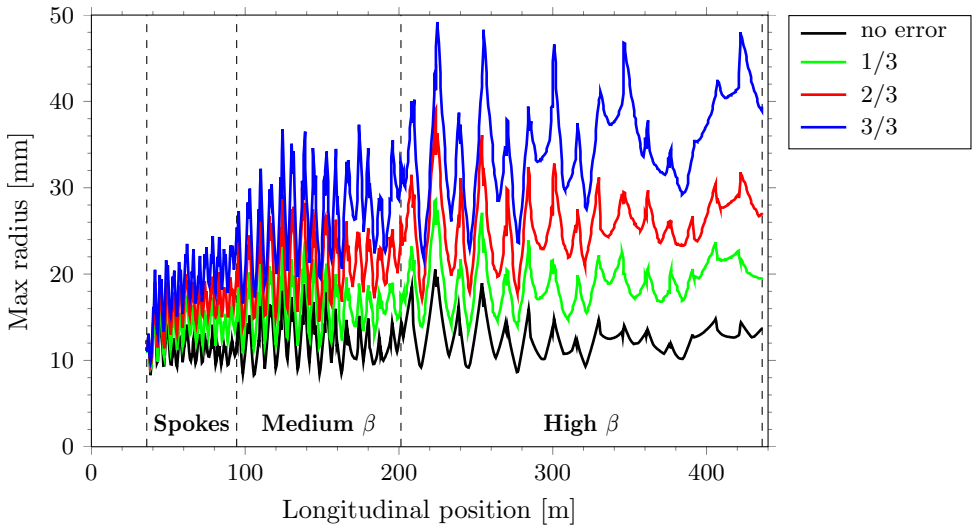

Figure 4.12: Maximum beam radius versus distance with increasing errors. The green curve is with error amplitudes at 1/3 of the values in the text, the red curve is at 2/3, and blue curve is at the full values. The black curve represents a linac with no errors.

4.2.3 End-to-end simulations

Although the different linac structures, such as RFQ, MEBT, DTL, superconducting linac and HEBT, have been designed separately to some extent, and by different collaboration partners, the beam has to pass smoothly from one structure to the next. Some adjustments to the optics have been made during the last year to achieve this. For instance, the focusing towards the end of the RFQ has been adjusted to better match the MEBT, and the DTL was extended by one tank to provide a better transition to the spokes section. To study how the beam physics of one accelerating structure affects that of following structures, end-to-end simulations, starting at the RFQ input and ending at the beam entrance window of the spallation target have been performed. Some results are shown in Figure 4.13, in which the beam density throughout the linac is plotted. The longitudinal acceptance of the linac is illustrated in Figure 4.14. The figure shows the longitudinal phase space at the entrance to the DTL. Particles must be inside the grey area at this location to reach the end of the machine. The grey area thus defines the longitudinal acceptance. The actual beam, starting as a 0.20 π mm mrad Gaussian truncated at 4σ at the entrance of the RFQ, is represented by the coloured distribution at the centre.

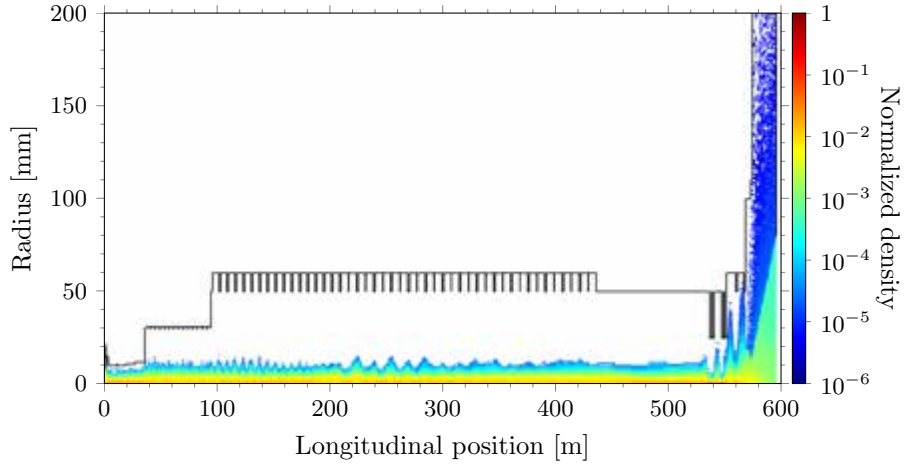

Figure 4.13: Particle density (right scale) as a function of longitudinal distance and radius (left scale) along the linac, from the start of the MEBT to the beam-entrance window on the surface of the target wheel. The large increase in beam size at the end is due to the non-linear optics producing a beam profile of 160 mm $\times$ 60 mm on the target.

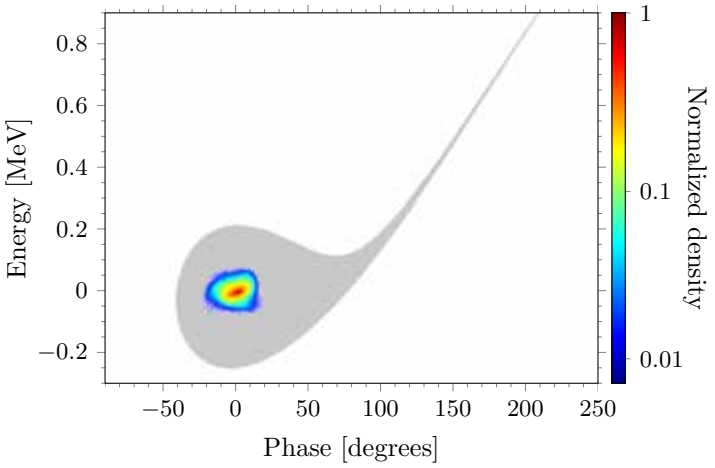

Figure 4.14: Longitudinal acceptance of the linac, referred to the entrance of the DTL. Only particles entering the DTL inside the grey area will reach the end of the linac. The actual beam out of the MEBT is represented by the coloured distribution at the centre.

4.2.4 Energy gain

Figure 4.15 (top) shows the cavity voltage V versus distance, defined as

$$V = \int E(z) \cos\left(\frac{2\pi z}{\beta\lambda}\right) dz \tag{4.3}$$

at optimum β (i.e. at maximum transit-time factor). The gradual increase from one section to the next is required to match the longitudinal focusing between the different linac sections and to get the smooth longitudinal phase advance per metre, as shown in Figure 4.8. Multiplying the voltages by the 50 mA beam current, ratio between actual and maximum transit-time factors and the cosine of the synchronous phase, the power to the beam per cavity is obtained and plotted in Figure 4.2. The increase in beam energy along the length of the linac shown at the bottom of Figure 4.15. The linac is quite tolerant to cavity field errors in that the beam can be accelerated even if cavity voltages are substantially below specifications. If the beam velocity drops too much, the transit time factors become too low, and acceleration ceases. However, this does not happen until the energy gain in the spokes or medium-β sections fall below 70% of nominal values.

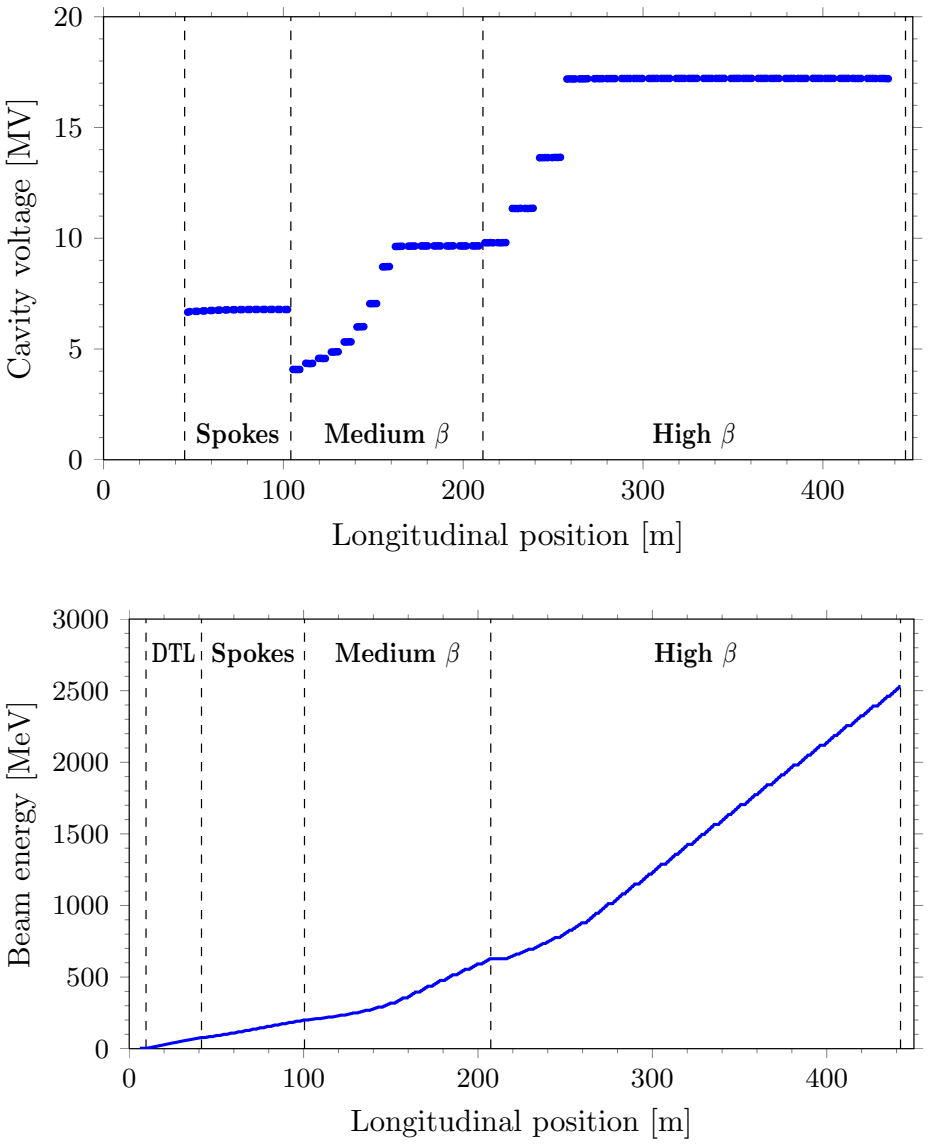

Figure 4.15: Cavity voltage and beam energy versus distance along the linac, from the DTL to the end of the high-β section. Top: Cavity voltage. Bottom: Beam energy.

4.2.5 Beam loss and collimation

The upper limit of acceptable beam losses in high-energy linacs is often set at 1 W/m, and this is also the design goal for beam loss in the ESS linac. Above that limit, activation of accelerator components becomes too large to allow hands-on maintenance with reasonable cool-down times. If lower losses can be achieved, staff working with maintenance in the tunnel will be exposed to less radiation. ESS has therefore taken into account a more ambitious goal, aiming at losses of 0.1 W/m, or even less. The beam dynamics design has not yet reached a level where such small relative losses (1 part, or 0.1 part, in 5×10^6) can be investigated using computational methods. Carrying out such investigations would require computational tools that take account of all relevant physics and include all fields to sufficiently high order while still keeping calculation times reasonably short. In addition, it would also require a good knowledge of all linac parameters including misalignments, field errors, etc., as discussed above, and of starting conditions for the particles that are tracked. It is not yet clear to ESS and its partners whether it will be possible to perform simulations that give the required accuracy and resolution in the halo of the beam, out to five or six standard deviations of the transverse particle distribution.

A pragmatic approach to reducing beam losses, which has been demonstrated to be effective and is used during operation in the SNS linac, is to remove the beam halo with collimators in an initial part of the linac [437]. The SNS linac has collimators in the MEBT, and the installation of MEBT collimators has been considered for the ESS linac as well. Studies have been initiated to identify an optimum collimation scheme in the MEBT [438, 439] and three important facts have been observed:

1. The distribution of halo particles in the phase space is very different from the ellipse formed by particles in the core. Instead, the halo particles tend to have a more irregular distribution. This happens because the halo is produced by resonances driven by the space-charge force.

2. A scheme based on a set of collimators separated by a fixed value of phase advance, such as two collimators separated by 90 degrees or three collimators separated by 60 degrees, is not efficient. This is due to the strong space-charge force, in which the phase advance of individual particles depends strongly on their initial phase space positions at the entrance to the MEBT.

3. A collimation in the later part of the MEBT is more efficient than that in the initial part. Due to the non-linearity of the space-charge force, the motion of some halo particles is chaotic, and two halo particles whose phase space positions are close to each other at the end of the linac could have very different phase space positions at the entrance to the MEBT. This means that a collimator in the initial part of the MEBT has a higher risk of removing particles that are within the core at the end of the MEBT than a collimator located near the end of the MEBT.

In addition, a collimator in the MEBT occupies several centimetres of space and so can be placed only between two quadrupoles. Given these conditions, no guidelines for determining the optimum collimator locations have been found. Instead, we have used a method of first defining halo particles at the end of the MEBT and then observing their distribution in the phase space at potential collimator locations. This has been demonstrated to work reasonably well and the search can be completed in a reasonable time, since the number of potential collimator locations is limited. Figure 4.5 shows locations and jaw positions of three collimators which are optimised for the present RFQ and MEBT. A collimator jaw is placed so that particles carrying about 15 W of beam power are removed for each plane. This corresponds to removing particles beyond 3σ if the distribution is perfectly Gaussian. There is no generic criterion to distinguish particles in the core and halo, and this 3σ has been chosen for two reasons. First, removing particles beyond 3σ from a Gaussian beam with conditions of the ESS MEBT is technologically feasible with a graphite collimator [439]. Secondly, simulations show that the removal of particles beyond 3σ significantly improves the distribution at the end of the linac, while removal of particles beyond 4σ barely improves that distribution.

Figure 4.16 compares the particle distributions in the transverse planes at the end of the MEBT in the cases with and without the presented set of collimators. Reduction of beam halo is visible, particularly for the vertical plane, but the distribution is still far from elliptical, indicating that the collimators must be placed closer than 3σ in order to inject bunches with a perfectly elliptical phase-space distribution into the DTL.

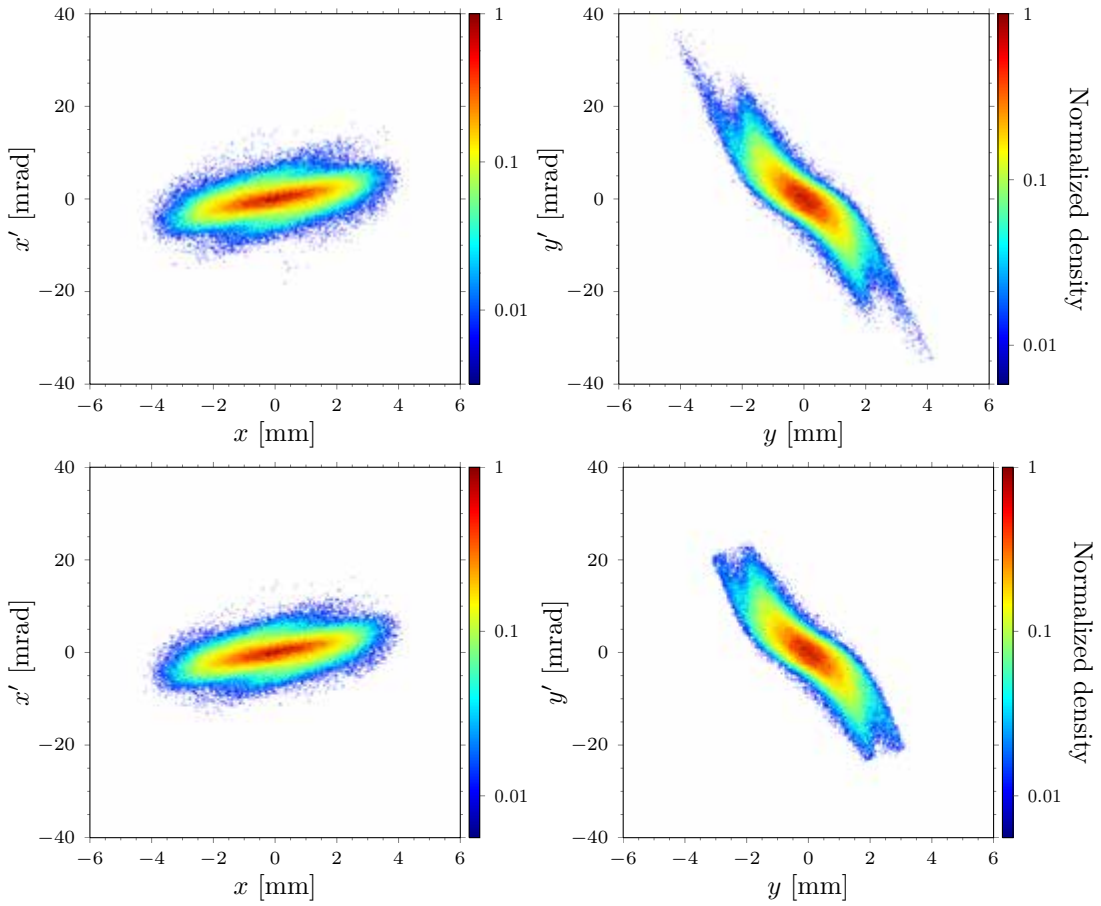

Figure 4.16: Particle distributions in the transverse planes at the end of the MEBT. Top: Without collimation. Bottom: With collimation.

4.2.6 Same-order and higher-order cavity modes

The fundamental passband modes induced by the beam in the superconducting cavities could prove to be dangerous to the longitudinal beam emittance due to their high R/Q compared to the accelerating modes at certain velocities. In some cases, the R/Q of the $4\pi/5$ mode is three times that of the fundamental at the beginning of the medium-β section. To explore the effect of these modes, a pulse train of one million point-like bunches was tracked through the superconducting section of the linac. Each bunch adds to the induced fields, these act on subsequent bunches through a kick-drift-kick model [440], and the resulting bunch energy and time errors are calculated. The size of the error depends on the size of the frequency spread of the modes which was modelled as a Gaussian with a width given by an empirical formula [441]. One thousand linacs with different seeds for the Gaussian spread were used for the simulations.

As an example, Figure 4.17 shows the effect of these modes on the pulse phase space of an early design of the linac layout (top row) and for a more recent design (bottom row), with different velocity partitioning over the three cavity families [442]. Each column shows the phase space at the exit of the linac. The left column shows the case in which no modes are acting. There is cause for concern when the growth due to passband modes, shown in the middle column, is larger than that produced by the acceptable amplitude and phase jitter from the RF sources, shown in the right column. It can be seen that the linac of the top row, which represents an earlier ESS lattice, is susceptible to these modes. The bottom row, corresponding to the FDSL_2012_10_02 linac lattice – the current linac design – shows significantly better performance.

Investigations have also been conducted of the effects of varying the current from the nominal 50 mA to a relatively high value of 150 mA in order to determine if there is a threshold value, and if so, how close the nominal current is to the threshold. The external coupling factor Q_{ext} was also varied from 10^4 to 10^9, although the actual value is expected to be close to that of the accelerating modes at around 10^6.

The results are shown in Figure 4.18. Negligible growth is observed at the nominal current of 50 mA. It is not until 90 mA that the growth starts to exceed that due to RF errors, represented by the dashed line. Losses are seen at this current for external coupling factors Q_{ext} larger than 10^7. Similar investigations have been performed for the higher order modes (HOMs) in both the longitudinal and transverse planes. In most cases, the effect of HOMs on beam quality is negligible, with the exception of the case in which

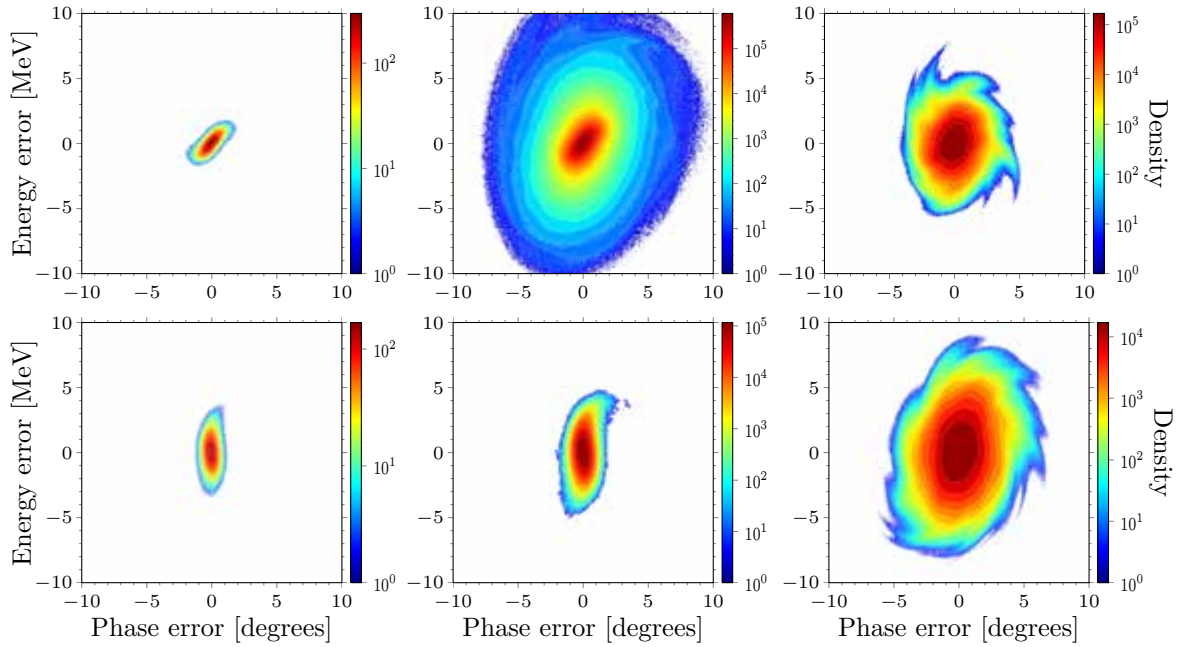

Figure 4.17: Phase space distribution averaged over a macro-pulse of a million point-like bunches, with cavity modes and RF errors, at the linac exit for two lattices. The top row shows an early lattice, while the lower row shows the FDSL_2012_10_02 lattice. The left column depicts the case in which no modes are acting; the middle column depicts the case in which passband modes are acting; and the right column depicts the case in which there are uniformly distributed RF errors.

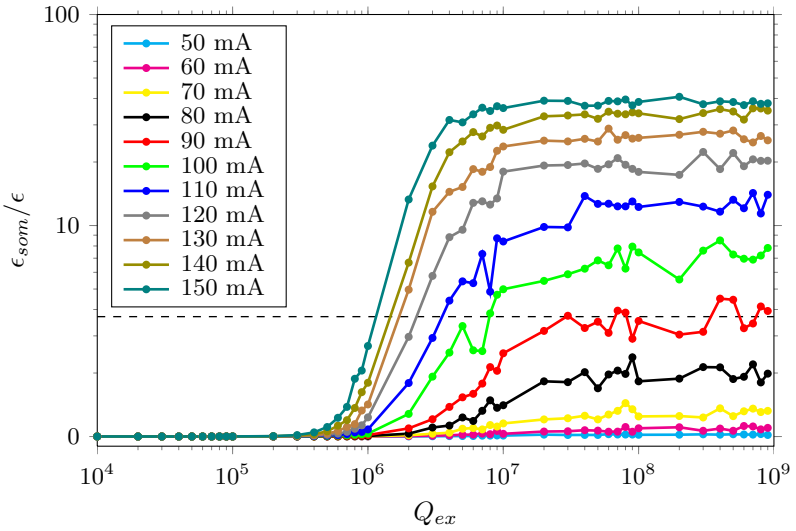

Figure 4.18: The average longitudinal emittance increase for 100 linacs over a set of beam currents, as a function of the external coupling factor Q_{ex} for modes in the fundamental passband. Negligible growth is observed at the nominal current of 50 mA. It is not until 90 mA that the growth starts to exceed that due to RF errors, represented by the dashed line.

the HOM frequency is equal to that of a machine line, i.e. the case in which the HOM frequency is an integer multiple of 352.21 MHz. In this case, the increase in phase space is huge, resulting in lost bunches. It was found that HOMs with high R/Q must be at least 3 MHz from a machine line in order to eliminate problematic effects. HOMs acting in the transverse direction LAO were studied with alignment errors, showing no significant added growth in any cases. Complete details of these calculations may be found in a 2012 paper by Ainsworth [443].

4.2.7 Cost savings proposals

A series of proposals have been made that should reduce cost while maintaining the scientific performance with acceptable additional technical risk. These proposals, which principally involve the number of cryomodules and beam energy, are described in Section 4.10. The proposals do not modify the majority of details in this chapter.

4.3 Normal conducting linac

The normal conducting linac consists of the proton source, LEBT, RFQ, MEBT and DTL. The major challenge with respect to this part of the accelerator is the production of a high quality beam with a well defined temporal pulse, a short emittance and minimal halo. Achieving these three goals will minimise beam losses throughout the high energy part of the linac, while maximising the overall reliability of ESS. The integrated design of this part of the linac is of key importance. It requires the solution of a series of specific problems of accelerator physics, particularly those involving space-charge effects. A particular emphasis has been put on the evaluation of the transient behaviour of the beam due to the chopping process at the entrance to the RFQ. The main features of the source design, including the microwave injection system, beam extraction, and pulse formation inside a neutralised LEBT are described below.

4.3.1 Ion source

ESS will require a proton beam of 50 mA (90 mA in a possible future upgrade), at 75 keV with a maximum emittance of 0.2 π mm mrad, a 14 Hz repetition rate with 2.86 ms pulse length, and 99.9% reliability. In terms of emittance, the TRIPS and VIS sources [418, 444], developed by the LNS group, can largely meet the requirements for ESS in continuous mode. Tests carried out on SILHI [445] confirmed the capability of these sources to meet ESS requirements in pulsed mode as well. In fact, it was observed that for a pulse duration of 3 ms and repetition rates of 10 and 20 Hz, the beam emittance was around 0.15 π mm mrad. The current required for the ESS facility in the baseline configuration can be satisfied by means of a conventional microwave discharge ion source (MDIS) like VIS, based on the direct absorption of electromagnetic waves in a plasma through the electron cyclotron resonance mechanism. Recent studies performed at INFN-LNS have shown that the magnetic field profile exerts a critical influence on plasma properties, especially on density. Two innovative plasma heating methods will be employed. The first is based on non-conventional methods of RF coupling to the plasma that are described below, while the second consists of an optimisation achieved by short plasma confinement. The ESS proton source design merges the best solutions already tested in previous sources with a flexible magnetic system able to produce both standard and new magnetic profiles that will allow increased currents and proton fractions, with reduced emittances and beam halo formation.

A novel magnetic system

The proton source will be similar to the VIS proton source, but the magnetic system will consist of a set of three solenoids, instead of two. The novel magnetic system shown in Figure 4.19 has been designed for very high flexibility, by using three different coils that are energised independently from one another, and that allow polarity changes. One key to obtaining this flexibility is the use of highly purified iron discs between the solenoids to spatially confine the magnetic field produced by each one.[1] Pure iron shielding will also serve to avoid a Penning discharge inside the extraction column and to avoid emittance growth due to

[1]The highly purified iron is composed of a product called ARMCO ®Pure Iron, which is manufactured by AK Steel International.

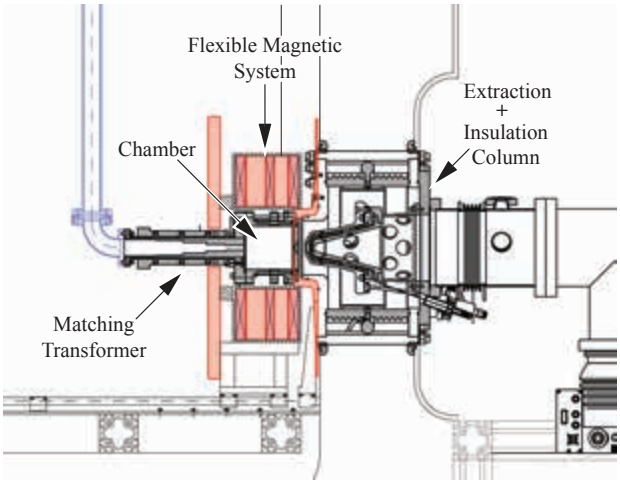

Figure 4.19: The ion source, highlighted in red, with a flexible magnetic system joined to the RF matching transformer and the extraction system to the LEBT.

stray magnetic field. The field will be reduced from 1000 to 100 Gauss over a distance of 1.6 cm regardless of the selected magnetic configurations, as shown in Figure 4.20. The typical shape of the magnetic field for MDIS machines shown by the green line in Figure 4.20 is a quasi-flat profile that is everywhere above the resonance value of 875 Gauss. This ensures electron densities around the cutoff at 2.45 GHz or slightly larger ($n \sim 10^{17}$ m^{-3}), temperatures sufficient for hydrogen ionisation ($T = 15$ to 20 eV) and H_2 molecule lifetimes long enough for complete ionisation and proton generation. Achieving such plasma parameters requires RF power around 1-1.5 kW and background pressures as low as 10^{-5} mbar.

A recent study has investigated the possibility of overcoming the cutoff density by converting the incoming electromagnetic wave into a plasma wave [446]. This study parallels similar investigations in fusion science, in which large plasma densities are needed to fulfil the Lawson criterion [447]. At INFN-LNS, indications that this conversion mechanism occurred have been observed with the VIS source equipped with movable permanent magnets operating at variable frequencies [448]. The process is based on the conversion of an oblique (with respect to the applied magnetic field) electromagnetic wave (called extraordinary mode, or X mode) into an electron oscillation (longitudinal wave) propagating across the magnetic lines, which are called Bernstein waves (BWs). Plasma waves travel in plasmas of various densities and are absorbed at cyclotron harmonics. Since they are sustained by the electron motion, BWs cannot be externally excited, but originate from an X mode interacting with gyro-rotating electrons at the upper hybrid resonance (UHR) [449]. The first experiments show evidence of the formation of a 10 to 20 times

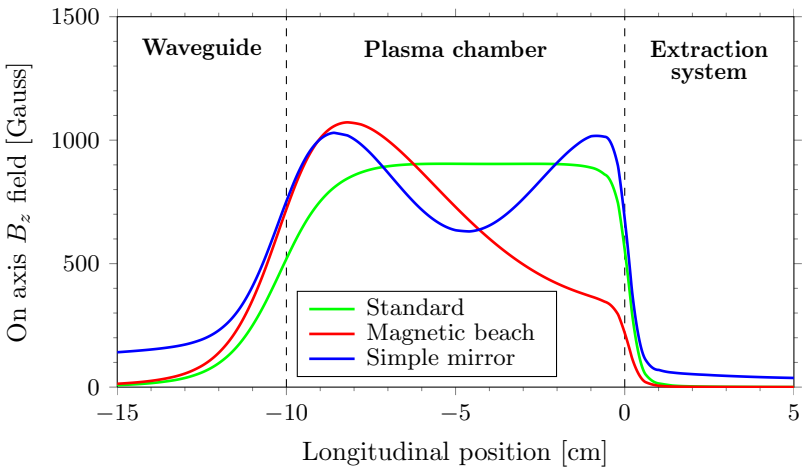

Figure 4.20: Magnetic field profile in the ion source, generated by three independent shielded coils.

over-dense plasma when operating in second harmonic mode. To be converted into a BW, the X mode requires a rapidly dropping magnetic field which makes possible either UHR or second harmonic absorption. This configuration, shown in red in Figure 4.20, is sometimes called a "magnetic beach." It is possible that this second method of RF-plasma energy coupling could significantly enhance output currents, but if it is to be employed at ESS, it will only be after the implications of its use for ion dynamics (the possibility of ion heating as an ancillary mechanism) and beam emittance have been carefully studied.

Another way to optimise the proton generation of an MDIS will be attempted by use of a simple mirror-like trap, such as the one labelled (3) in Figure 4.20. Studies of the balance equations of the different plasma species (H_2, H_2^+, H^+) reveal that their reciprocal abundance is regulated by their relative lifetimes. In a quasi-flat magnetic field, under normal operating pressure, ion lifetime is governed only by collisional diffusion across the magnetic field, which is a rather fast process. The prolongation of H_2^+ molecule lifetime through use of the simple mirror configuration should increase ionisation efficiency, boosting the proton fraction even at moderate RF power, and also improving the reliability of the source.

Microwave coupling

In order to improve the performance of ESS's ion source, a detailed electromagnetic study of the plasma chamber as a cavity has been carried out with an eigenmode solver. This analysis has determined the plasma chamber dimensions required to have a TE111 dominant mode at a frequency around 2.5 GHz. The effect of two different matching transformers on microwave coupling also has been fully studied [450]. Figure 4.21 shows the electric field distribution of the TE111 mode inside a cylindrical resonance cavity with a 101.2 mm length and a 45.3 mm radius. Ion source performance is improved by introducing the matching transformer shown in Figure 4.22, to reduce the reflected power.

Four electrode extraction system

The extraction system consists of four electrodes: a plasma electrode placed on the HV platform at a voltage of 75 kV, plus a set of three electrodes, the first and the last attached to the grounded flange, and between them a repelling electrode placed at a few hundred volts to preserve the space-charge compensation of the LEBT. The extraction has been simulated using the AXCEL simulation code developed at Oak Ridge National Laboratory. Figure 4.23 shows the simulated RMS beam emittance ellipses at $z = 0.14$ m distance from the extraction aperture. The total beam current assumed in the simulation is about 100 mA, with a proton fraction of 90%, and H_2^+ fraction of 10%.

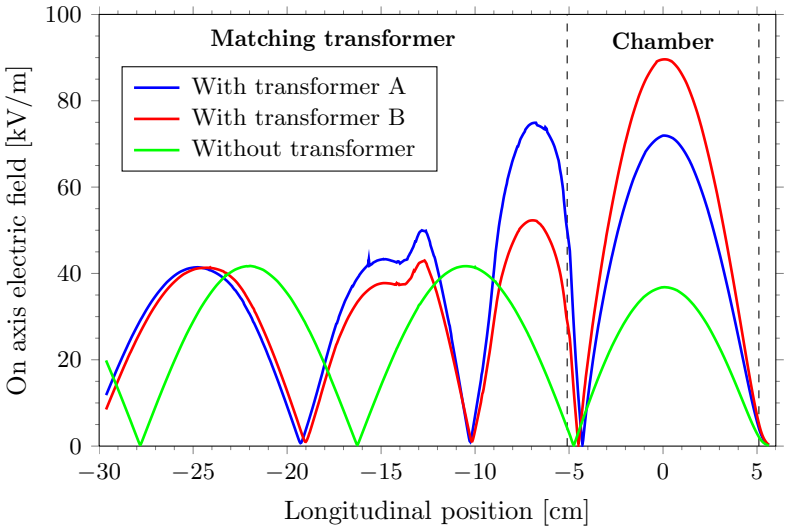

Figure 4.21: Electric field distribution of the TE111 mode inside the ion source plasma chamber – a cylindrical resonance cavity with a 101.2 mm length and a 45.3 mm radius – for three different transformer configurations.

Figure 4.22: Ion source matching transformer, used to reduce the reflected power.

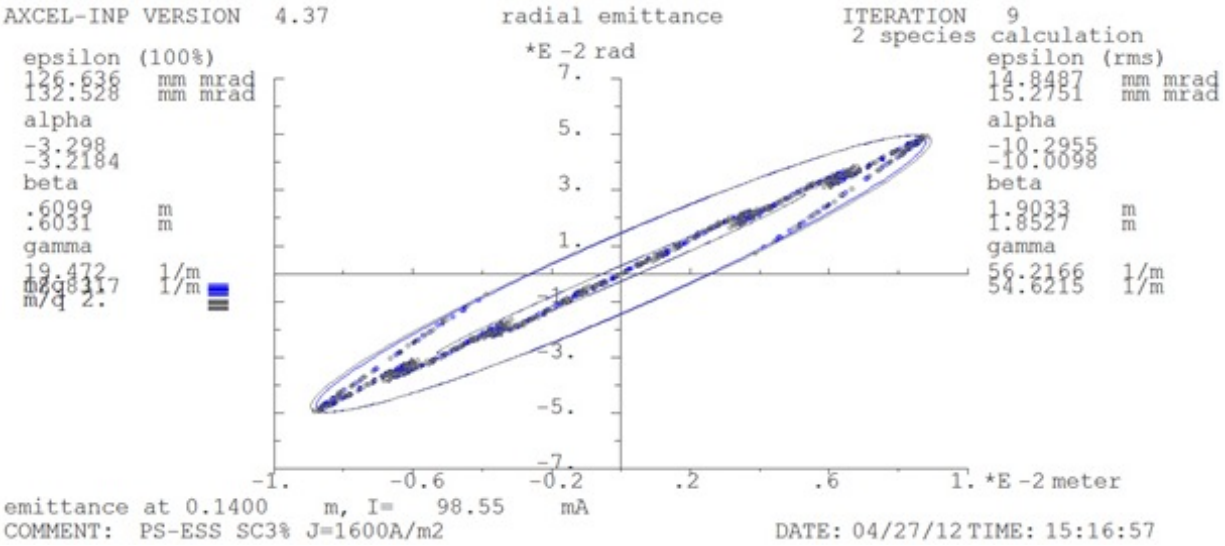

Figure 4.23: Transverse root mean square beam emittance ellipses at $z = 0.14$ m distance from the ion source extraction aperture, simulated by AXCEL.

In summary, requirements for the proton source are quite restrictive. In view of previous experience with sources at INFN-LNS, the needs of the initial phase of the facility will be fulfilled by using a conservative approach, based on a standard MDIS configuration (that is, a VIS-like machine). Possible upgrade requirements are even more stringent in terms of currents (up to 90 mA or more), but possible solutions for source upgrades have already been considered during the design phase, by proposing a novel flexible magnetic system. More standard solutions for performance optimisation (which do not require any *ab initio* design modification) will be implemented, such as the alumina tubes introduced into the plasma chamber. Thus the design effort not only considers current, emittance, efficiency and reliability requirements, but also takes account of continuous MDIS development.

4.3.2 Low energy beam transport

Beam focusing in the LEBT will be performed by a dual solenoid system. The solenoid design is similar to that used in the IFMIF LEBT [448]. The deflecting plates of the chopper are inserted between the solenoids. The total length of the line from the plasma electrode to the RFQ entrance is 2.10 m. Two vacuum pumping systems using turbomolecular pumps (TMP) will be installed in the line, one before the first solenoid and one in between the magnetic elements. The positions of the different optical and monitor components are still under discussion. A preliminary layout is shown in Figure 4.24.

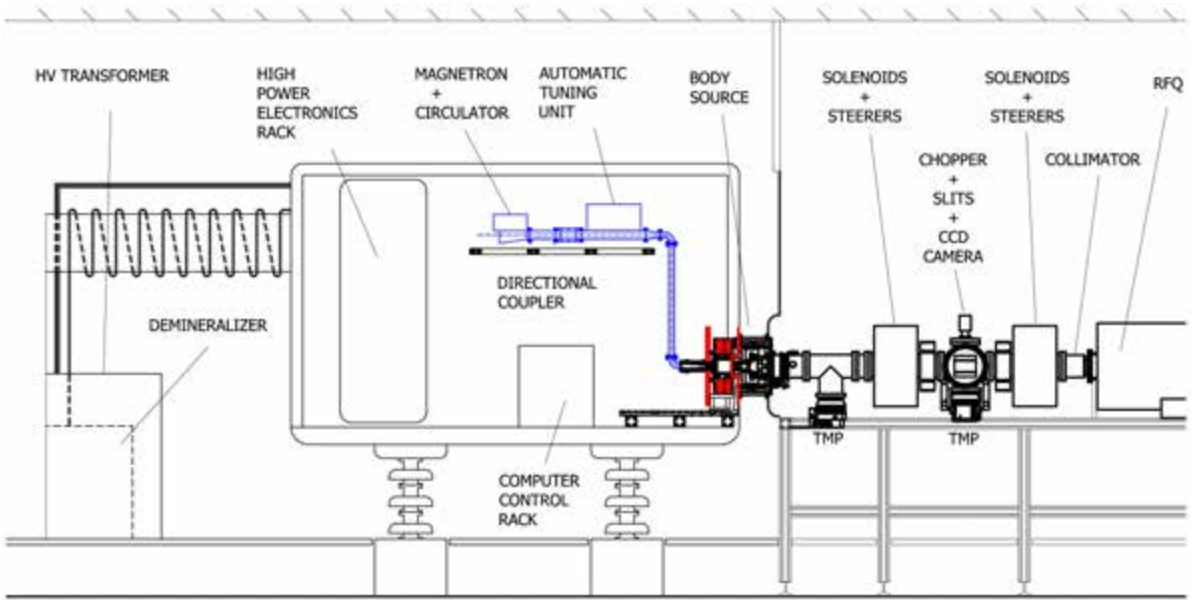

Figure 4.24: Preliminary layout of the ion source and the low energy beam transport. Beam is extracted from the ion source through a LEBT chopper that incorporates beam emittance measurement slits, followed by a collimator just before entrance to the RFQ.

LEBT beam instrumentation

Beam profile measurement will be performed with secondary emission monitor (SEM) grids at two locations in the LEBT, the first between the two solenoids, and the second after the second solenoid. Each grid will be moved by a stepping motor when necessary in order to increase the resolution. The profile measurements will inform the beam steering strategy and will be used to match the beam at the RFQ entrance. In CERN's LINAC4, it has been observed that in SEM grids using tungsten wire, the profile measurement is perturbed by thermionic emission when the beam pulse is longer than 600 μs at a current of 30 mA. The measurable pulse length can be increased by using a carbon wire. ESS plans to carry out emittance measurements to characterise the ion source and beam optics in order to optimise beam injection at the RFQ entrance and to provide beam distribution measurements for end-to-end simulations. The measurements will be performed during the commissioning phase and also during operation for dedicated beam studies. During operation, the system will be installed between the two solenoids, and the slit will be positioned as close as possible to the first solenoid. The SEM grids used for profile measurement will be reused for these measurements. During commissioning, the emittance meter will be positioned [451] at three different locations: after the source, after the first solenoid, and after the second solenoid. The slit will be designed to withstand full beam power. In order to meet this requirement, the slit will be made of graphite, and its geometry will distribute the energy deposition over a large surface area [452].

ESS also plans current measurements. A Faraday cup will be installed after the source; as in the case of the slit, the Faraday cup will be designed to withstand full beam power. This Faraday cup will be integrated into the machine protection system and will be used as a slow mitigation device. In addition, a beam current transformer (BCT) will be installed as close as possible to the RFQ entrance. This BCT also will be integrated into the MPS, and the transformer will be used in conjunction with a second transformer installed at the RFQ exit in order to measure beam transmission. This device is relatively slow, so for commissioning, a fast Faraday cup with a time response on the order of a nanosecond or less will be installed to measure the effect of the LEBT chopper on the current rise time. ESS will use optical beam diagnostics. The emitted light caused by the interaction between the beam and the residual gas can be used for different types of measurements, specifically for the determination of the ion species fractions. With a digital camera installed in the focal plane of a monochromator with a few tens of degree angle with respect to the beam propagation axis, the Doppler shift observation of the H_α hydrogen Balmer series allows isolation of the fluorescence of each ion species in the beam. The ratio of the different types of ions is proportional to the light intensity [453].

4.3.3 LEBT chopping and collimation

In low energy beam transport of high intensity beams, the self-generated repulsion between charged particles can generate a large and irreversible emittance growth. However, the optimum matching of the beam with the RFQ requires high focusing and low emittance. To address this issue, the space-charge neutralisation of the beam charge can be accomplished by ionising the residual gas. The generated electrons are captured by the beam potential, while the generated ions are repelled by the beam and lost on the surface of the vacuum chamber. Such a space-charge compensation (SCC) regime has similarities to a plasma regime but the electric field produced, for example by the pre-chopper, introduces many significant variations especially in the transition regimes. In order to reduce the length of the LEBT chopper, and to keep space free for the installation of diagnostics, the chopper chamber is coupled to the TMP, as shown in Figure 4.25 (left). The design calls for locating the high voltage power source as close as possible to the chopper plate to obtain low impedance connection and to maintain the high switching speed of the electronics (15 ns). A repelling electrode will be inserted in the extraction system and in the RFQ collimator, as shown in Figure 4.25 (right), in order to preserve the SCC from the high electric field located in the extraction system and inside the RFQ.

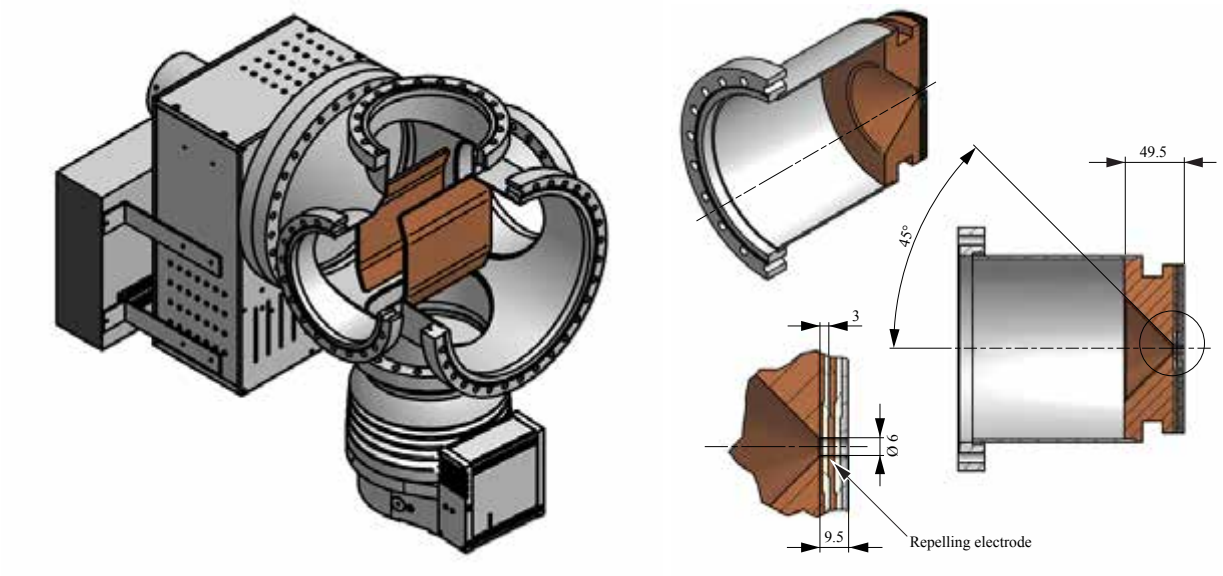

Figure 4.25: Left: LEBT chopper, coupled to a turbomolecular pump, and high and low voltage electronics boxes. Right: RFQ collimator at the end of the LEBT, with integrated repelling electrode.

The extraction system has been simulated with AXCEL and the emittance parameters at the position $z = 0.14$ m [454] have been used as an input for the simulation of the LEBT using the TraceWin code. This software takes into account an SCC map along the LEBT and it is able to perform the optimisation of the optical element parameter so that the RFQ Twiss parameters can be achieved. Figure 4.26 shows the beam trajectory and the emittance shape obtained at the RFQ entrance by using an SCC value of 98%. The shape of the chopper electrodes is indicated at the centre of the LEBT, between the two solenoids. AXCEL and TraceWin also simulate the secondary beam in the simulations, which is made up of H_2^+ in the case of ESS. In sources like VIS and SILHI, the proton fraction can reach 90%. As shown in Figure 4.27, the RFQ collimator was designed to accept the 10 mA secondary beam shape. The RFQ collimator was also designed to dump the high power transported by the chopped beam (90 mA at 75 keV). Due to the position of the chopper, determining the trajectory of the chopped beam is not trivial because the beam is also deflected by the second solenoid. Figure 4.28 shows the radial distribution of the chopped beam and its impact shape over the RFQ collimator.

Time dependent performance

The beam longitudinal front at the end of the LEBT is extremely important for the design of the subsequent accelerator cavities of the linac. The required rise and fall time is 100 ns while the source modulation is

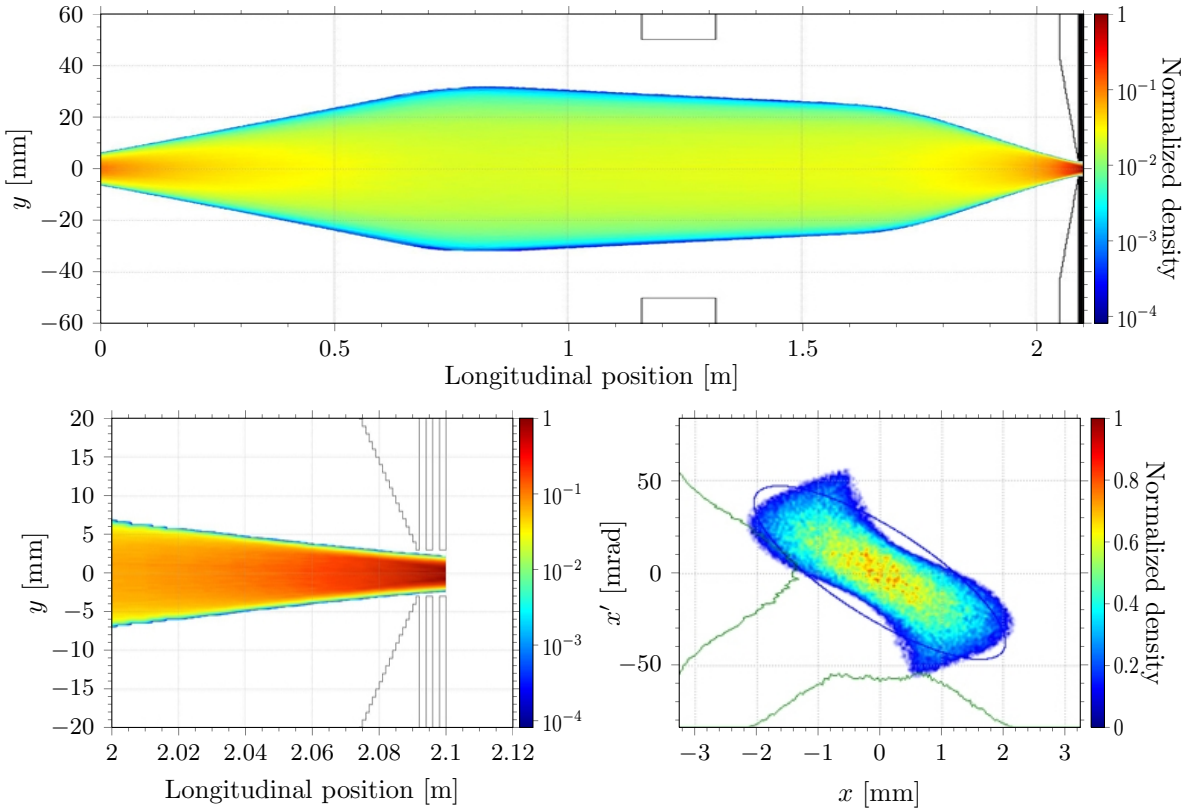

Figure 4.26: Proton beam trajectory in the LEBT and its phase space distribution at the RFQ entrance, with a space charge compensation value of 98%.

able to achieve a 2 μs rise time. The design calls for the chopper to be inserted to cut the slow edge. In addition, fast power electronics with 15 ns transition time were selected. However, the chopper electric field and the difference in the two beam trajectories produce a low SCC value during the transport of the first part of the beam. Relying on previous results about SCC creation time [455] and plasma analysis of the electron gas that neutralises the beam, time dependent simulations show that the pulse beam fall time is below 20 ns, while Figure 4.29 shows that 300 ns is the limit on the fastest possible beam rise time. The longitudinal beam pulse shape obtained from this work is extremely important for the design of the subsequent accelerator cavity and the fast-chopper that must be placed in the MEBT in order to reach 100 ns pulse rise time. More investigations and a series of measurements are planned to confirm and refine these study results at INFN-LNS and CEA-IRFU.

4.3.4 Radio frequency quadrupole

The RFQ presented in Section 4.1 for the FDSL_2012_10_02 baseline lattice is 4.0 m long. However, this section describes a 5 m device that was designed to reduce beam losses below the limit of 1 W/m for protons of 2 MeV or higher. The reduction in length comes mainly from the fact that there is no copper activation that justifies limiting the power loss to 1 W/m in the RFQ [456, 457]. Shortening the RFQ has reduced the potential fabrication and operational risks since fewer tuners and vacuum and RF seals as well as vacuum pumps are required. The construction cost will also be lower as machining and brazing are known to impact significantly the overall cost of the RFQ. Less power dissipated in copper also reduces operational costs. The same methodology and technical choices that are valid for the 5 m results presented below are also valid, and are kept, for the 4 m RFQ design. It should be stressed that the 5 m RFQ was designed for 90 mA. This value corresponds to 75 mA – the upgrade value discussed when the design was proposed – plus a 20% margin. The main parameters of the optimised design proposed for the RFQ are summarised in Table 4.3.

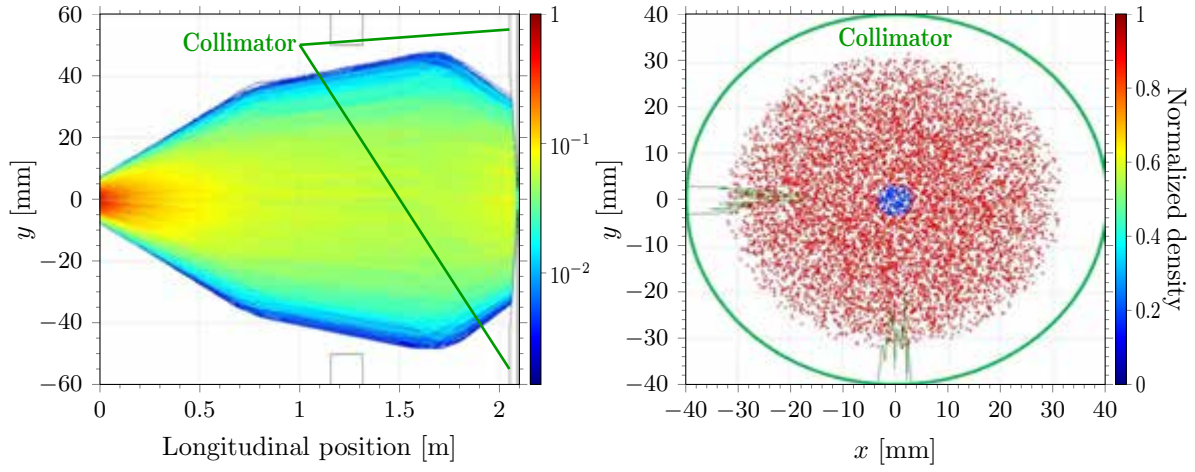

Figure 4.27: Secondary (H_2^+) beam trajectory in the LEBT and its distribution on the collimator.

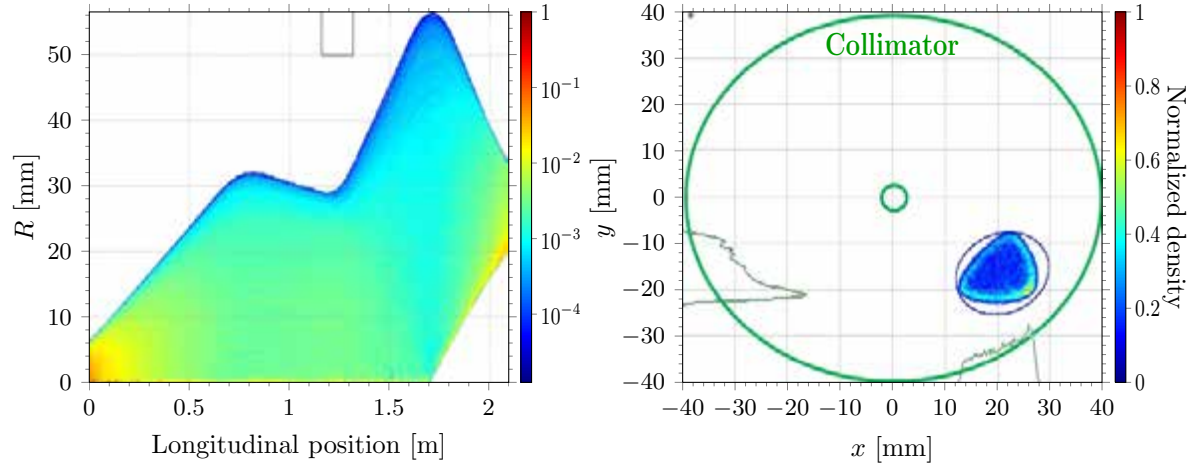

Figure 4.28: Chopped proton beam trajectory in the LEBT its distribution on the RFQ collimator. The chopper deflects the beam out of the centre of the collimator while the solenoids rotate the off-centred beam by 45 degrees.

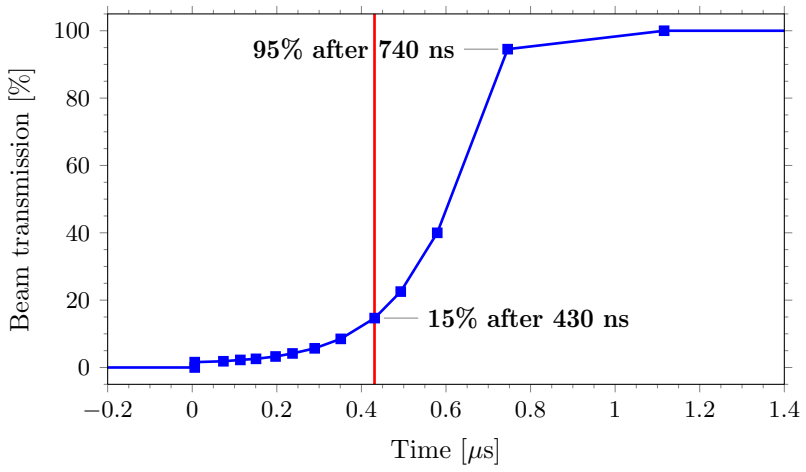

Figure 4.29: Beam pulse rise time out of the LEBT, limited to 300 ns by space charge compensation dynamics. The pulse beam pulse fall time (not shown) is less than 20 ns.

Parameter	Unit	Value
Inter-vane voltage, V	kV	80 to 120
Synchronous phase, ϕ_s	deg	-90 to -31
Minimal aperture, a	mm	3 to 3.9
Modulation factor, mm		1 to 2.06
Vane radius of curvature, ρ	mm	3 (constant)
Vane length, L	m	4.93
Kilpatrick limit, K_p		1.8

Table 4.3: Main parameters of the 5 m RFQ design.

Pole tip

The RFQ pole tip design is a four vane-type structure, divided into five 1 m segments. The design calls for the peak electric fields on the vane surfaces to be limited to a Kilpatrick value of 1.8 A. Transmission of more than 99% is achieved for the nominal current and very low longitudinal emittance beams are delivered to the subsequent RF structures of the linear accelerator. The beam physics design is shaped by multiple considerations: a desire to profit from the experience and expertise of CEA-Saclay; a desire to rely on well-tested and conventional concepts in the RFQ design; a commitment to designing in adequate safety margins; and a commitment to integrating RF and mechanical designs in the early stages of the beam physics design. In addition to these considerations, the design must produce high quality beams and minimise beam losses. In the longitudinal plane, the design should achieve low RMS emittances with a well defined shape in phase space (no tail) in order to lower the risk of hazardous losses at high energy while keeping a high acceleration rate in the linac. Emittance blow-up in the transverse planes is not expected to be an issue. The reference design has also ensured low losses along the RFQ vanes in order to prevent sparking issues.

In addition, design calls for a non-constant voltage. This ensures high values for both the longitudinal and transverse current limits all along the RFQ structure; a constant inter-vane voltage can not preserve the latter limits without dramatically decreasing the aperture. Furthermore, the evolution has been chosen so that the first derivative of the voltage with respect to the longitudinal axis, z, vanishes at both ends of the RFQ. As a consequence, no circulating currents will occur at the RFQ extremities and no additional losses will be experienced at these locations. The rate of growth of the voltage has also been chosen in such a way that the change in the local 2D frequency is acceptable for the RF design. The voltage and the 2D frequency shift, Δf, are shown in Figure 4.30. The latter is given by:

$$\frac{\Delta f(z)}{f_o} = \frac{1}{2}\left(\frac{\lambda}{2\pi}\right)^2 \frac{1}{V(z)}\frac{\partial^2 V(z)}{\partial z^2} \tag{4.4}$$

where f_0 is the fundamental frequency of the empty cavity (without tuners).

The most original feature of the design is the long pure bunching section ($\phi_s = 90$ degrees) composed of 120 non-accelerating cells. This feature, associated with a slow rate of acceleration in the first half of the structure and a large longitudinal acceptance, results in excellent beam transmission, low longitudinal emittances and no transverse emittance growth as indicated in Table 4.4. Figure 4.31 shows that losses are negligible and no particle with a kinetic energy greater than 2 MeV hits the vanes. The longitudinal portrait of the beam at the RFQ output is well defined without any tail, as shown on Figure 4.31.

Parameter	50 mA	90 mA
Total transmission	0.9968	0.9879
Transmission of accelerated particles	0.9939	0.9824
RMS longitudinal emittance (π deg MeV)	0.0985	0.1265
Transverse emittance blow up	1.0602	1.0315

Table 4.4: Emittance growth and beam transmission through the 5 m RFQ at 50 mA and 90 mA.

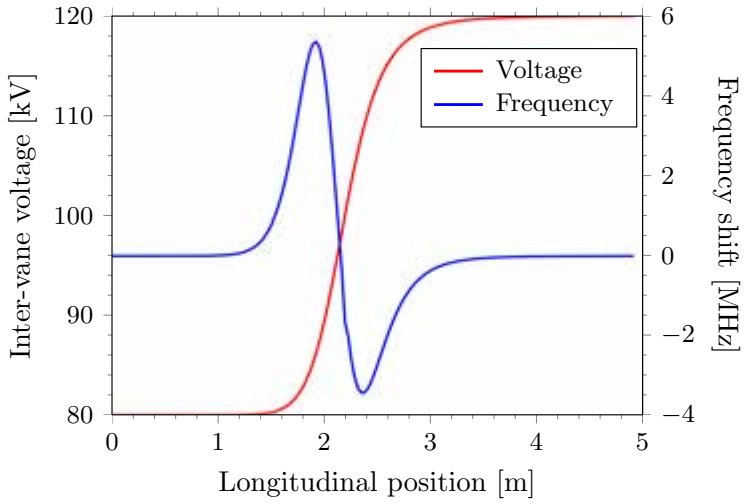

Figure 4.30: RFQ inter-vane voltage and the 2D frequency shift.

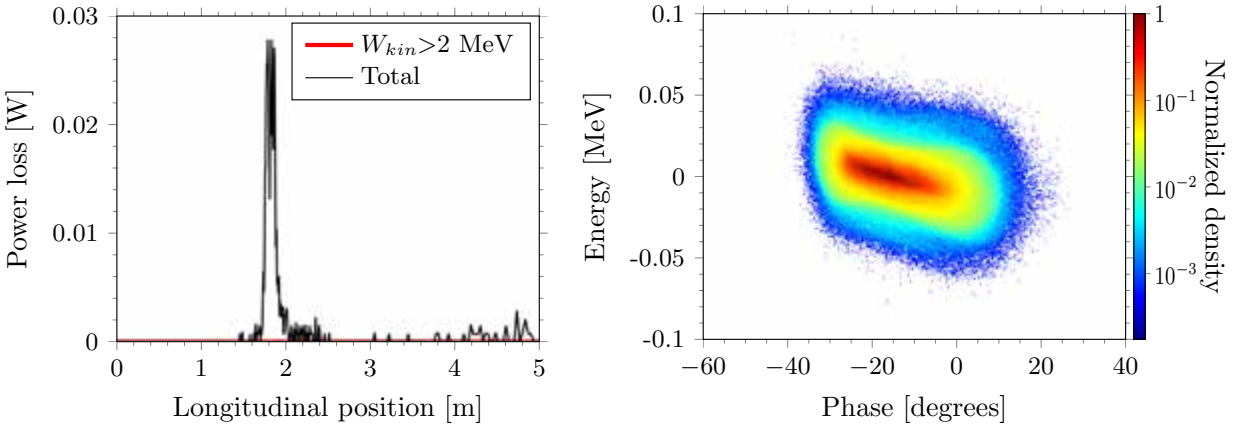

Figure 4.31: Left: Beam power losses along the RFQ. Right: Longitudinal phase space distribution at the RFQ output for an input beam with a current and emittance of 50 mA and 0.2 π mm mrad.

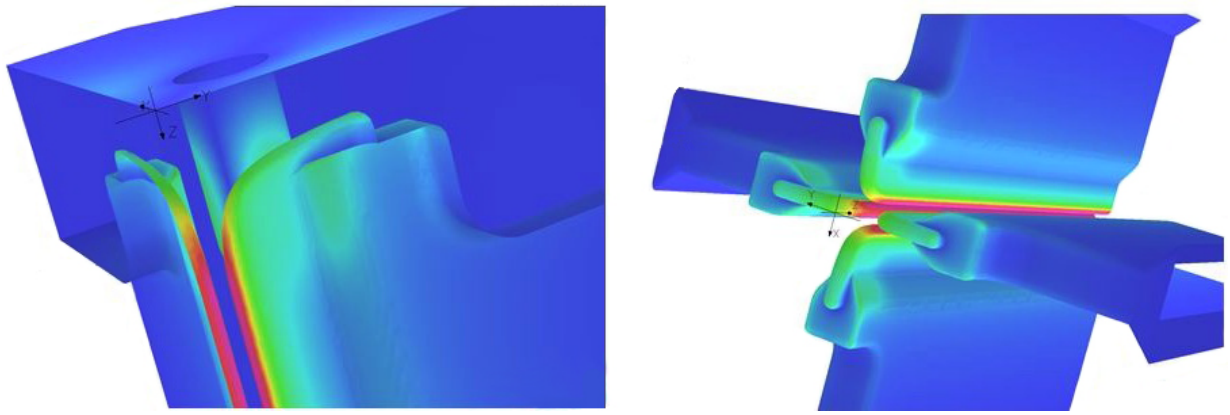

Figure 4.32: 3D views of the RFQ input, showing vane undercuts. The colour-code represents electric field magnitude.

4.3.5 RF design of the 5 m RFQ

Specified parameters for the 2D cross section RF design are frequency, length, mean value of electrode tip-to-axis distance r_0 versus abscissa z along the RFQ (varying between 3.445 mm and 4.737 mm), radius of curvature of electrode tips ($r_0 = 3.0$ mm), and inter-electrode voltage V versus z (from 80 kV at RFQ input to 120 kV at RFQ output). The RFQ cross section is designed to achieve voltage profile $V(z)$ thanks to a modulation of the electrode lateral surfaces geometry. Slug tuners are dedicated to compensating for voltage errors resulting from construction tolerances. The cavity resonance frequency with tuners in electrically null positions is set to 346 MHz, in such a way that most of the tuner position range lies inside the cavity.

Stability analysis shows that the RFQ is naturally stable within a wide range of end-circuit dipolar voltage log-slope parameters, from about -2 up to 0 V/(m/V), so that dipole stabilising rods should not be required with a proper design of RFQ end-circuits. The role of these circuits is two-fold: 1) to tune accelerating-mode boundary conditions to a null quadrupole voltage slope at both ends, in such a way that no current is injected in the end-circuits, and 2) to tune the dipolar voltage log-slope parameter to some value in the stability region. The first condition is achieved with so-called quadrupole rods located close to the vane tips in each quadrant, and the second one with a proper choice of vane undercuts, as shown in Figure 4.32. The dipole stability requirement is found to be satisfied with a 23 mm undercut at the RFQ input and a 25 mm undercut at the output. Quadrupole rod tuning ranges should be 18 to 38 mm at input and 21 to 41 mm at output to cover a comfortable -0.1 to $+0.1$ (V/m)/V tuning interval. With this design, the quadrupole mode closest to the accelerating mode Q_0 is Q_1, with a +1.47 MHz frequency shift (+31.94 MHz quadratic frequency shift). The dipole modes closest to the accelerating mode Q_0 are D_2 and D_3, with -5.25 MHz and +2.56 MHz respective frequency shifts (-60.05 MHz and +42.18 MHz quadratic frequency shifts).

An efficient tuning scheme is defined with $T = 15$ regularly spaced, 80 mm diameter slug tuners, and $S = 2T = 30$ field-sampling points, as shown in Figures 4.33 and 4.34. Tuner axis separation is $\Delta z = 0.334$ m, and the distance between RFQ ends and the closest tuner is about 0.135 m. The RFQ is assumed to be tuned using bead-pull measurement in the magnetically dominant field region. The $S = 2T$ sampling scheme requires the magnetic field perturbation induced by tuners along the bead trajectory to be quite localised. To this purpose, the bead trajectory is set close to the quadrant bottom walls, and field-sampling points will be located at least every $\pm 0.2455 \Delta z = 0.082$ m about each tuner axis. With these distributions, all 15 modes will be available for tuning, which will provide excellent tuning efficiency to null-out undesired spectral components. Theoretically – in the absence of experimental errors – the desired voltage profile can be reconstructed with a relative accuracy of 10^{-4}. Total CW power dissipated by tuners varies from about 700 W at the -17 mm tuner position (gap losses dominate when the tuner is recessed inside the copper wall), to 6,800 W at the +30 mm tuner position (cylinder losses dominate when the tuner is inside the cavity), as shown in Figure 4.35. The average power dissipation is scaled down from the CW power by the operational duty cycle of 4%.

RF power is coupled to the cavity with a half-circular loop, shown in Figure 4.36. Coupled power varies from 469 kW to 23 kW when the loop coupler is rotated by 45 degrees around its own axis. Loop-induced voltage relative perturbation is smaller than 1.8 10^{-3} over the rotation angle range from 0 to 45 degrees. The coupling loop is located at the midpoint between two adjacent tuners, so the magnetic field perturbation induced by the loop along the bead trajectory is limited to a ∼50 mm interval, thus leaving a ∼60 mm space for field-sampling points, between the loop coupler axis and nearby tuner axes, as shown in Figure 4.37. Vacuum ports will be inserted between tuners, reproducing the Linac4 two-diaphragm

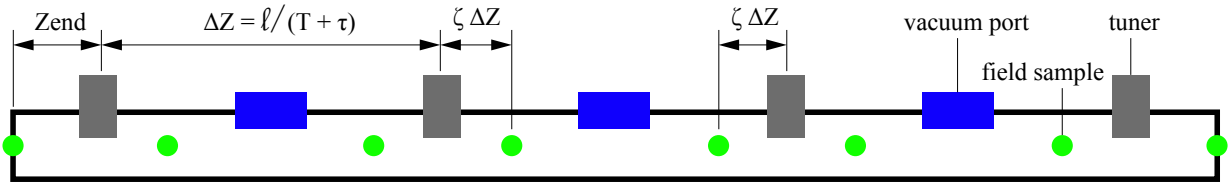

Figure 4.33: Distribution of RFQ tuners and field-sampling locations, in this example with 4 tuners and 8 field-sampling points.

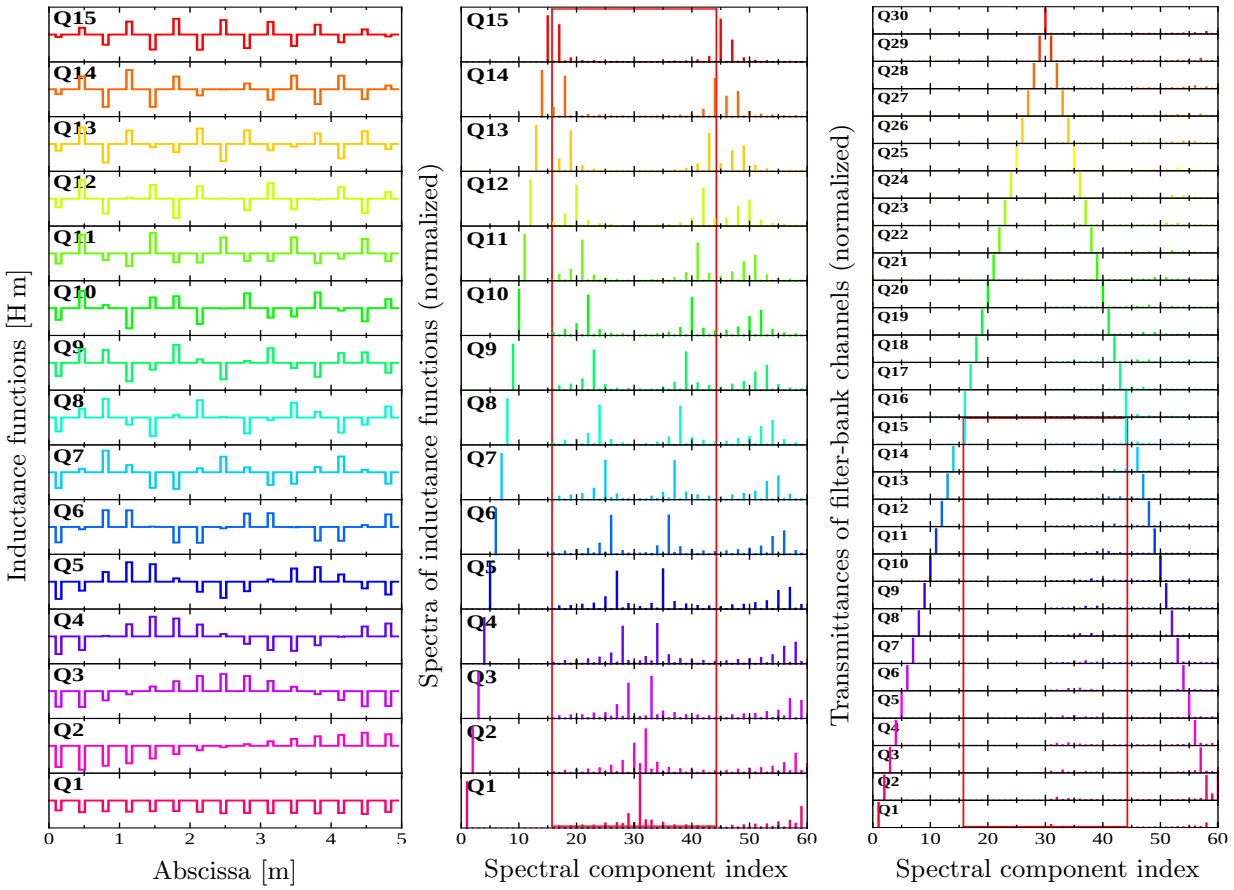

Figure 4.34: Left: RFQ inductance eigenfunctions. Middle: Normalised spectra of inductance eigenfunctions. Right: Transmittance of linear filter-bank for the quadrupole subset. Spurious spectral components of the eigenfunctions are rejected by the filter-bank (red boxes).

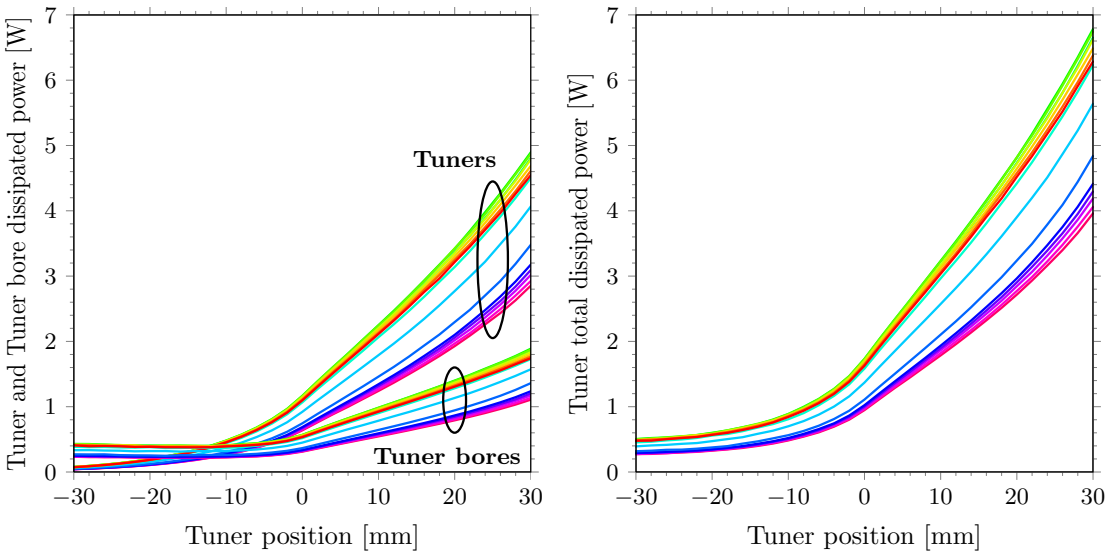

Figure 4.35: Power dissipated by the RFQ tuner assembly. Left: CW power dissipated in tuners and in tuner bores versus tuner position (positive inside RFQ cavity; negative outside cavity) and tuner location (colour-coded). Right: Total CW power dissipated in the tuner assembly versus tuner position and tuner location (same colour code).

design. Positions of the ports with respect to the cavity inner wall will be experimentally adjusted during RF tests following copper parts assembly and prior to the first braze, in order to achieve a perfect match. The compliance of port conductance with RFQ vacuum system requirements still has to be ascertained.

Error analysis is a crucial part of RF design. Tuner position limits are derived from construction errors. Tolerances on the electrode tips' cross section are defined by two quantities, t and δ. The centre of curvature of each electrode tip is located in a square with side $2t$, centred at its theoretical location, while the distance between the realised and theoretical profile of the electrode tip is bounded by δ. Two cases related to different machining options are considered: 1) vane-tips are assumed to be circular, in which case δ is radius tolerance, and 2) vane-tip profiles may be anywhere between $\rho - \delta$ and $\rho + \delta$ limits. These two cases lead to different error volumes in the space of inter-vane capacitance errors. In simulations, the variations of geometrical errors versus abscissa along the RFQ have been assumed to be arbitrary. The value t has been varied between 40 μm and 60 μm, while δ has been varied between 20 μm and 40 μm. The maximum tuner position (including some safety margin) has been shown to be less than or equal to +30 mm for all t and δ values such that $t + \delta \leq 90$ μm in case 1, or δ values such that $t + \delta \leq 80$ μm in case 2, as shown in Table 4.5. The minimum tuner position is greater than or equal to -6.2 mm in all cases.

Voltage and frequency stability of the RFQ under operation are quantified using single-mode perturbation analysis. Figure 4.38 shows what happens when an arbitrary 10^{-4} relative perturbation is applied successively to all 15 modes in each quadrupole and dipole subset of inter-vane capacitance eigenfunctions.

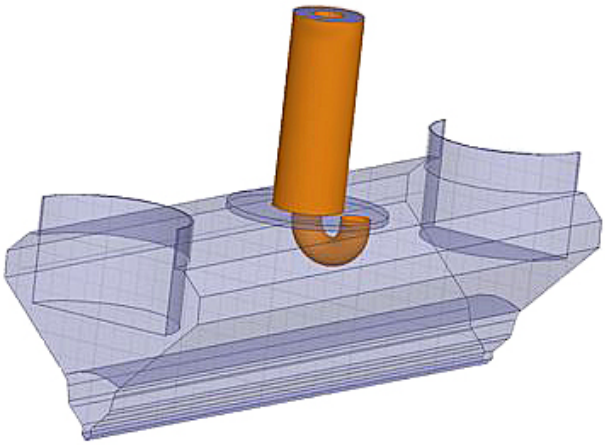

Figure 4.36: The RFQ half-circular power coupler.

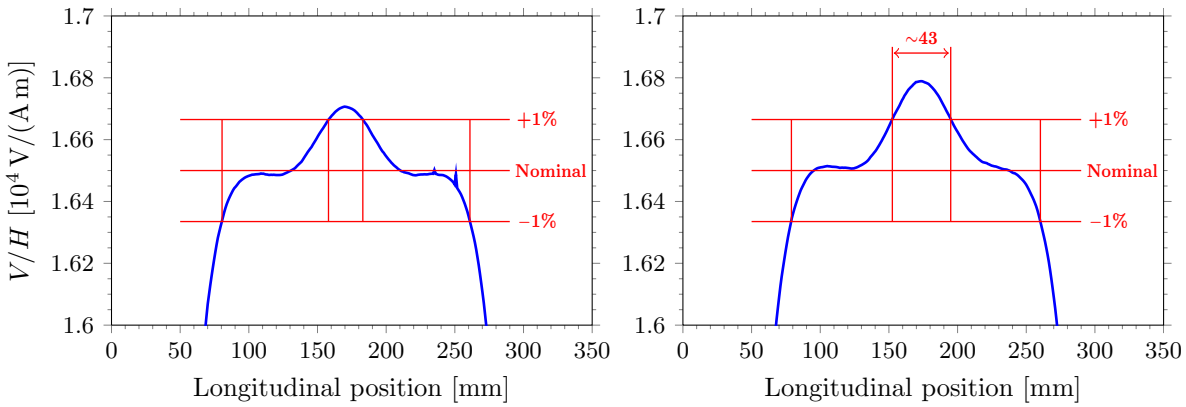

Figure 4.37: Magnetic perturbations from the RFQ power coupler on the tuning bead trajectory, with data from the simulation of a 350 mm long RFQ section with perfect open-circuit boundary conditions. The red boxes show the regions available for field sampling, where the perturbation is smaller than 1%.

	Case 1: circular vane-tip shape			**Case 2: arbitrary vane-tip shape**		
	$t = 40\ \mu$m	$t = 50\ \mu$m	$t = 60\ \mu$m	$t = 40\ \mu$m	$t = 50\ \mu$m	$t = 60\ \mu$m
$\delta = 20\mu$m	$+25.1$	$+27.6$	$+30.1$	$+26.8$	$+29.3$	$+31.9$
	-1.2	-4.0	-7.5	-3.1	-6.3	-10.4
$\delta = 40\mu$m	$+26.9$	$+29.4$	$+32.0$	$+29.5$	$+32.1$	$+34.7$
	-3.2	-6.4	-10.5	-6.5	-10.7	-16.7
$\delta = 60\mu$m	$+28.6$	$+31.2$	$+33.8$	$+32.3$	$+34.8$	–
	-5.4	-9.2	-14.4	-11.0	-17.1	–

Table 4.5: RFQ tuner position limits in mm, versus mechanical errors: location of the pole tip centre of curvature t, and location of the pole tip δ.

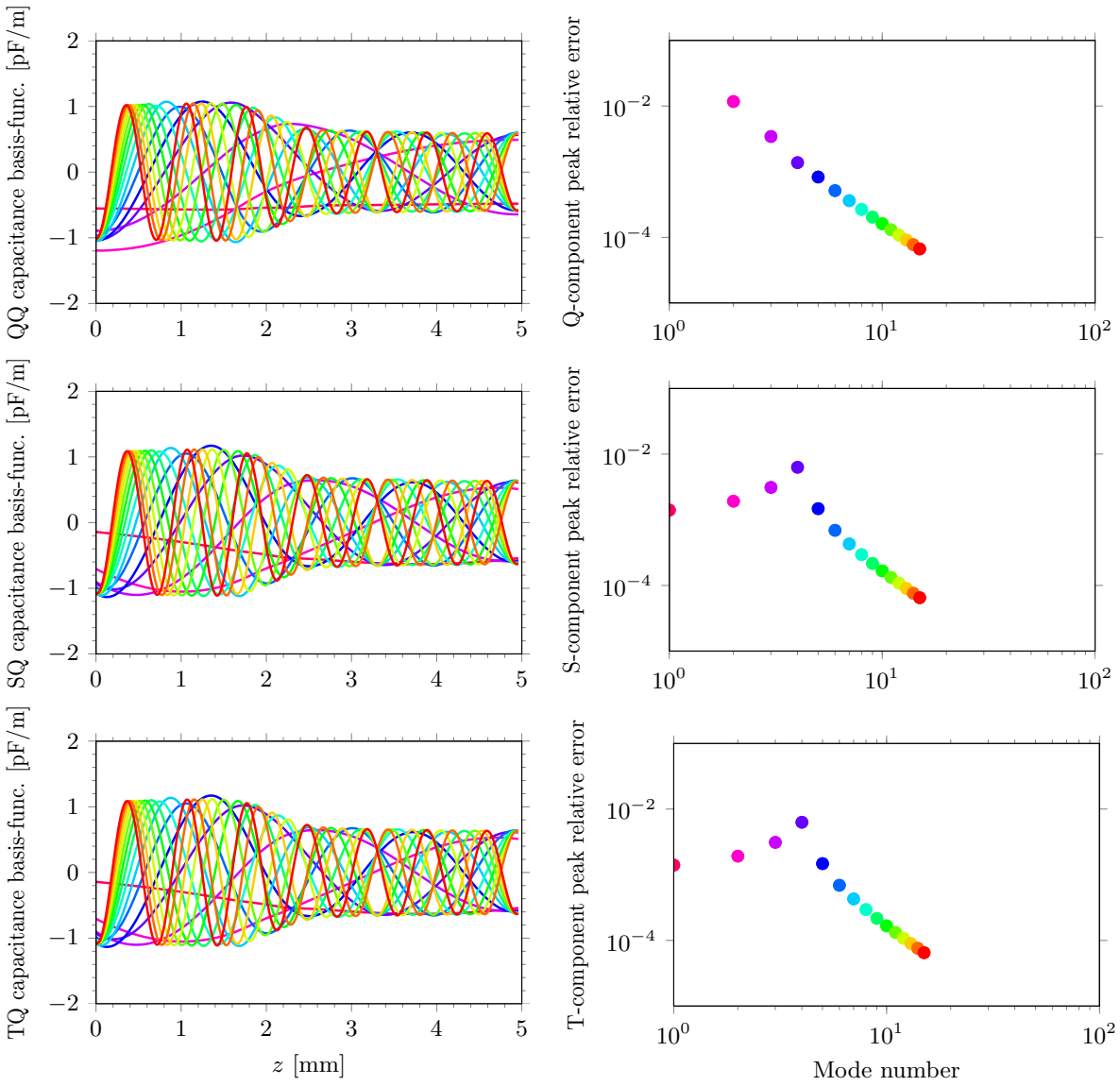

Figure 4.38: Single-mode perturbation analysis. The capacitance peak relative perturbation is 10^{-4} for each mode. From top to bottom: Q, S and T subsets. Left: Normalised capacitance expansion functions. Right: Voltage peak relative perturbations resulting from the capacitance perturbations versus mode index – abscissa 1, 2, etc., correspond to Q_0, Q_1, or D_0, D_1.

The RFQ frequency shift is about 17 kHz (Q_0 capacitance eigenfunction). Voltage error is maximum for Q_1-like perturbation (1.17%) and for D_3-like perturbation (0.63%). Numbers for other amplitudes of relative perturbation are readily obtained by linearity. Voltage errors decrease rapidly with mode index: peak amplitudes of Q_5 and D_5 spectral components are 5.15×10^{-4} and 6.90×10^{-4} respectively. This suggests that the RFQ cooling scheme should be designed in such a way that perturbations occur on fifth-order modes where possible, for instance by alternating cooling water circulation from one 1 m section to the other. RFQ cooling scheme specifications will be derived from thermo-mechanical simulations and sensitivities given by the single-mode analysis.

4.3.6 Medium energy beam transport

Figure 4.39 shows the layout of the MEBT, while Table 4.6 lists its operational parameters. It is 3.6 m long, containing no solenoids, 10 quadrupoles, 3 bunchers, and 4 collimators, but its relatively compact design provides adequate separation for the required diagnostics. The MEBT includes a fast chopper (and beam dump) that complements the slow LEBT pre-chopper, which will be used to sharpen the beam edges produced by the slow-chopper during rising and fall times (∼10 ns), thus eliminating the partially chopped beam that passes through the RFQ [458]. In its fundamentals, the chopping structure is based on CERN's Linac4 design. It consists of an electrostatic travelling wave deflector coupled with a beam dump for dissipating the sectioned beam current, serving the goal of reducing beam losses at higher energies.

The major challenge for the MEBT is to maintain a high quality beam, with a pulse well defined over time, a low emittance and a minimised halo, so as to limit beam losses downstream in the linac while maximising overall reliability. In order to minimise beam loss at the high energy portion of the linac, and the consequent activation of components, a fast chopping scheme has been adopted for the MEBT. Four key features of the MEBT enhance its versatility and effectiveness. First, the MEBT will contain a fast chopper and its corresponding beam dump, which will be able to serve during commissioning as well as in the ramp up phases. Second, the MEBT will be designed so that it can serve as a halo scraping section by means of various adjustable blades. Third, the MEBT will contain instrumentation making it possible to measure the beam phase and profile between the RFQ and the DTL. Finally, MEBT instrumentation will also make it possible to match the RFQ output beam characteristics to the DTL input both transversely and longitudinally. For this purpose a set of ten quadrupoles will be used to match the beam characteristics transversely, in combination with three 352.2 MHz buncher cavities, which will serve to adjust the beam in order to achieve required longitudinal parameters.

In different designs for high-intensity linear accelerators, the MEBT emerges as one of the critical stretches through the accelerator in terms of losses, emittance increase and halo formation. In order to minimise emittance growth along the MEBT section due to the effects of space charge, at a minimum, the MEBT design must supply a solid cross localisation and avoiding sharp changes in localisation strength. To this end, a compact quadrupole with a length of 70 mm is being designed. In addition, some of these quadrupoles, whose field gradients vary between 9 T/m and 30 T/m, are expected to incorporate correcting dipoles in order to minimise any beam misalignments.

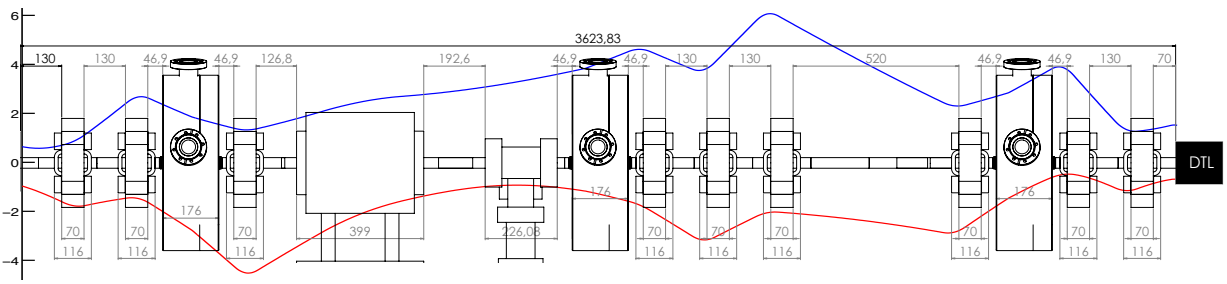

Figure 4.39: Medium energy beam transport layout, containing 10 quadrupoles, 3 bunchers, and 3 collimators. Root mean square beam sizes are also plotted: the horizontal size in blue, and the vertical in red. All sizes are in mm.

Parameter	Unit	Value
Input energy	MeV	3
Input speed, β		0.0798
Total current	mA	50
Particle		protons (H^+)
Number of quadrupoles		10
Minimum quadrupole gradient	T/m	9
Maximum quadrupole gradient	T/m	30
Number of buncher cavities		3
Frequency	MHz	352.21
Peak power per cavity	kW	14
Effective Voltage, E_0TL	kV	150

Table 4.6: Medium energy beam transport operational parameters.

Collimation

Collimation before the linac entrance avoids emittance growth and halo development in high-intensity linacs [459]. MEBT collimators scrape the beam in the transverse plane at 3 locations. For this purpose, four stepping motors are needed per location. The scraper will be used during nominal operation. The collimator system has to be integrated in the interlock system in order to avoid interaction with the beam core. The position of the beam will be provided by a beam position monitor positioned as close as possible to the collimator, whose movement will be held within specified limits. In addition, the temperature and charge deposition will be measured in the scraper. Scrapers will be adapted from the CIEMAT/AVS design shown in Figure 4.40. Designed for IFMIF (5 MeV, 125 mA, CW, D^+), these scrapers are made with water-refrigerated copper alloy due to the proximity of the superconducting structure. A carbon/carbon composite with an additional water cooling system is under consideration. A more detailed explanation of the procedure to find the optimum location is given in an ESS technical report [439]. Figure 4.41 shows a realistic beam distribution at the beginning and end of the MEBT, with and without collimation, while Figure 4.42 show how the 3 halo parameters and 3 beam emittances evolve. Table 4.7 summarises the conclusion that collimation leads to an acceptable beam loss of 1.3%, while significantly reducing the transverse halo parameters.

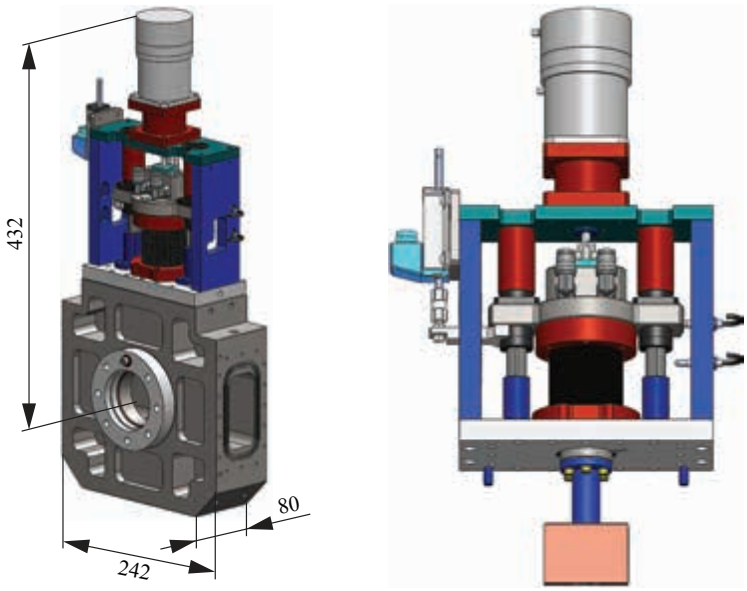

Figure 4.40: MEBT collimator scrapers, based on the AVS and CIEMAT design for IFMIF. Courtesy of I. Podadera and M.A. Carrera.

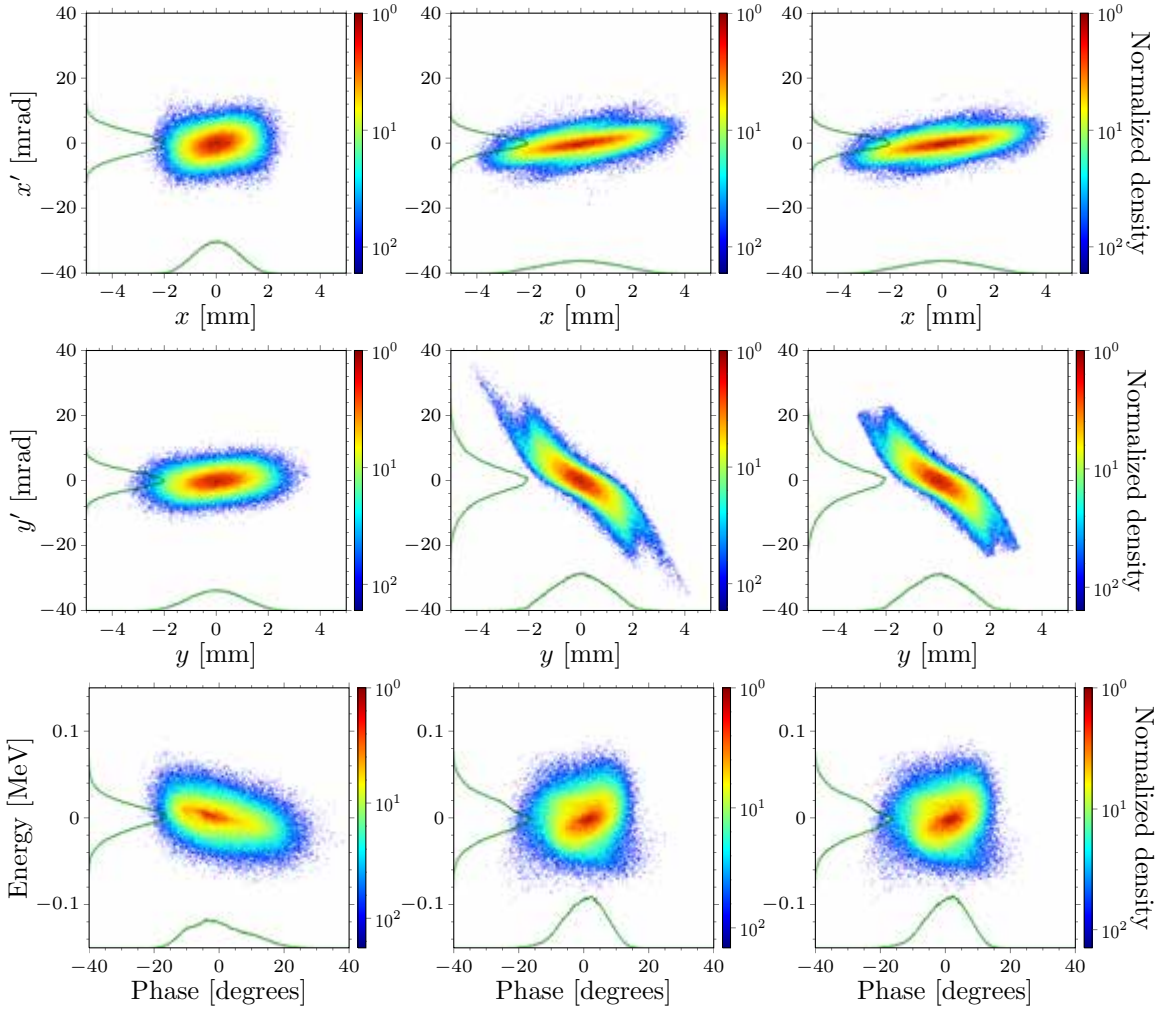

Figure 4.41: Beam phase space distribution through the MEBT. Left: Realistic beam distribution at the RFQ output, and MEBT input. The normalised RMS emittance values are $\epsilon_{xx'}$=0.227 π mm mrad, $\epsilon_{yy'}$=0.230 π mm mrad, and $\epsilon_{zz'}$=0.338 π mm mrad. Middle: Beam distribution at the MEBT output, without any collimation. Right: Beam distribution at the MEBT output, with collimation.

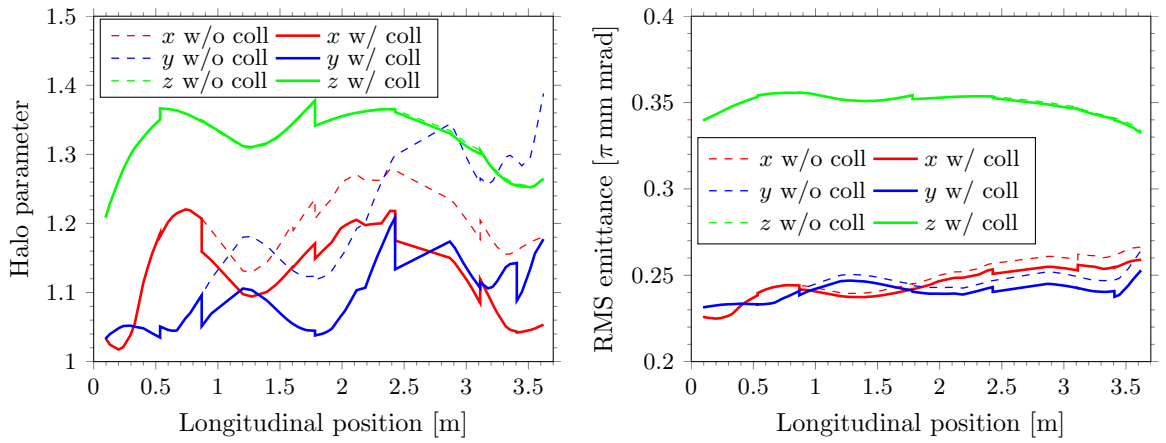

Figure 4.42: Evolution of beam parameters along the MEBT. Left: Halo parameters. Dashed lines are without collimation, while solid lines are with collimation. Right: Emittance evolution without (dashed lines) and with (solid lines) collimation.

Collimation	Beam losses [%]	Emittance growth, $\Delta\epsilon/\epsilon$ Horizontal [%]	Vertical [%]	Long. [%]	Final halo parameter, H Horizontal	Vertical	Long.
OFF	0.05	17.2	14.8	−1.5	1.18	1.39	1.27
ON	1.30	14.1	10.0	−1.8	1.06	1.18	1.27

Table 4.7: Emittance growth through the MEBT and final halo parameter, with and without collimation. Beam losses and emittance growth are acceptable in all conditions, while transverse halo parameters decrease significantly with collimation.

Misalignments, gradient errors and buncher RF errors

Magnet translations, rotations and quadrupole gradient errors have been studied in order to more narrowly specify the requirements for the dipolar components needed for the quadrupoles. Errors are assumed to be uniformly distributed; each value expressed in Table 4.8 represents the maximum-range error, using about 2×10^5 particles as input, as shown in Figure 4.41. In simulations, five error steps have been used: [20%, 40%, ... 100%]. Once the quadrupole and cavity errors have been introduced for each linac scheme; tunable parameters have been adjusted in each linac simulation to maximise transmission while maintaining Courant-Snyder parameters at the end of the line. Steerers embedded in the quads correct beam trajectories for misalignments produced due to manufacture imperfections or alignment errors during the installation phase of the different elements. Figure 4.43 represents the maximum integrated fields required to correct beam trajectories for each steerer. This provides the information needed to specify the magnetic design of the quadrupoles.

Parameter	Unit	Value
Quadrupole displacement (Δx,Δy)	mm	±0.5
Quadrupole longitudinal shift (Δz)	mm	±0
Quadrupole gradient ($\Delta g/g$)	%	±1
Quadrupole rotation (ϕ_x,ϕ_y,ϕ_z)	deg.	±0.1
Cavity displacement (Δx,Δy)	mm	±0.5
Cavity longitudinal shift (Δz)	mm	±0
Cavity rotation (ϕ_x,ϕ_y)	deg.	±0.1
Cavity amplitude error ($\Delta E/E$)	%	±1
Cavity phase error ($\Delta\phi/\phi$)	%	±1
Beam position monitor	mm	±0.1

Table 4.8: Static quadrupole misalignment and buncher RF errors in the MEBT. The errors are uniformly distributed; each value is the absolute maximum range error.

Diagnostics

The 6D beam phase space distribution will be measured in the MEBT at a reduced beam power (100 μs, 50 mA, 1 Hz repetition rate or 10 μs, 50 mA, 14 Hz repetition rate) using a set of six beam position monitors (BPMs). At least two BPMs are essential for time-of- flight measurement, and three for absolute energy measurement. A bunch shape monitor (BSM) is foreseen for bunch length measurements. One beam current transformer (BCT) will be installed at the beginning of the MEBT. The sampling rate of the BCT will be 10 MHz with a resolution of 1% of the nominal beam current. A second BCT will be installed in the DTL tank in order to measure the input current in the DTL. Another BCT will be installed in the normal conducting linac. The current monitors will also measure beam transmission between two monitors and will be integrated into the machine protection system (MPS). Four wire scanners will also be installed. Two of these wire scanners will be equipped with high dynamic range electronics in order to

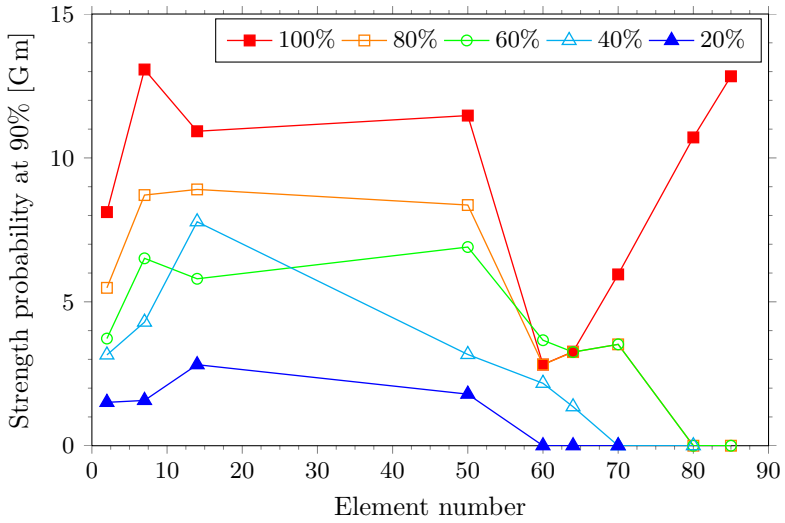

Figure 4.43: Maximum integrated field strength for each MEBT steerer. Results are presented in five steps, going from 20% error up to 100%.

measure the beam transverse halo. Finally, a slit-and-grid emittance measurement system is planned for emittance measurements

Quadrupole design

The design parameters for the MEBT's quadrupoles and their integrated steerers cannot be calculated until the optical layout and mechanical constraints have been completely defined. Regarding the optics, the aperture of the quadrupoles must be fixed according to the beam transverse size and maximum loss restrictions. The quadrupole gradient and length (or integrated gradient/field) are fixed by the optical focusing requirements, and the dipolar steering strength is dictated by the maximum acceptable beam misalignment. Field quality will be defined using optical tracking simulations. Getting these simulations right is especially important for the MEBT's quadrupoles because the steering dipoles will be integrated inside the quadrupoles, resulting in a sextupolar component amounting to about 30% of the dipole steering component (about 5×10^{-3} of the main quadrupole field); the precise value will be determined by future simulations. Otherwise, independent steerers or embedded $\cos\theta$ dipoles will be used. Regarding the mechanical constraints, the maximum distance between quadrupole coil-ends (the maximum physical length) must be set before it is possible to design the coil shape and to select a working current density. The minimum distance from the quadrupole to other devices or quadrupoles is also important because the magnetic field can interfere with them. ESS will conduct a crosstalk study to deal with this issue. Preliminary calculations for the quadrupoles have been based on the following tentative specifications: 34 mm aperture, 20 T/m with 70 mm effective length, 116 mm maximum physical size (length) and 1.5 mrad (∼4 G m) deflection for the steerers.

4.3.7 MEBT buncher cavities

The MEBT includes several buncher cavities that compress the beam longitudinally. The design of the buncher cavities is an iterative process between electromagnetic, thermo-mechanic, RF and beam dynamics perspectives, which also affect the tuner and coupler design. In the electromagnetic design of the buncher cavity, a high shunt impedance per unit length ZT^2 is desirable in order to reduce power consumption and, as a result, simplify the cooling system. Nevertheless, electrical discharges must be avoided by limiting the peak surface electric fields. Using stochastic hill-climbing and a genetic algorithm implementation [460], a configuration has been selected which is judged to deliver the best compromise between these competing goals. Table 4.9 summarises the parameter list of the current electromagnetic design [461]. A study of the tuning system required for the bunching cavity in order to correct the frequency shift due to thermal expansion and manufacturing tolerances was also carried out [462]. The insertion in the cavity of a plunger

Parameter	Unit	ESS	CERN B30	FETS
Frequency	MHz	352.21	357.22	315.86
Q_0		23477	24129	27222
T		0.593	0.56	0.636
V_0T	kV	140	140	160
P	kW	14.02	15.38	11.82
r	MΩ	1.4	1.27	2.35
ZT^2	MΩ/m	11.1	10.11	15.67
$E_{s,max}$	MV/m	27.2	24.25	27.56
Kilpatrick		1.47	1.30	1.49

Table 4.9: MEBT buncher cavity parameters, illustrating the close similarity to CERN B30 and RAL FETS buncher cavities.

tuner in a region of high magnetic field increases the resonant frequency of the TM010 accelerating mode. In this study, one and two hollow cylinders were inserted into the cavity at different positions and different penetration levels. In a latter configuration, a tuning range of almost 2 MHz was obtained, thus doubling the range obtained with only one tuner. In addition, the E_z field along the axis of the cavity was not affected by the presence of the tuners. Finally, the study confirmed that the resonant frequency of the cavity varies very little with the relative positions of the tuners.

Power couplers inject RF power into the bunching cavities, but must also preserve the vacuum in the cavities. This is usually achieved by using an RF ceramic window. The ESS configuration for the coupler contains two additional transitions to the input, output, and window coaxial. Each transition is located at one side of the ceramic window. Thus, by changing the dimensions of the transitions (both length and radius) and the window (radius), the required matching can be obtained. The final dimensions for the input and output flanges will be fixed when the mechanical design of the coupler is addressed. The coupler under study was designed and analysed by a full-wave electromagnetic simulator. The input and output coaxial dimensions for the electromagnetic design were chosen to guarantee a characteristic impedance of $Z_0 = 50\ \Omega$. Those dimensions have been taken as a reference from the coupler of CERN's linac4 chopper line buncher. These dimensions can be changed if required as the design evolves. The ceramic window

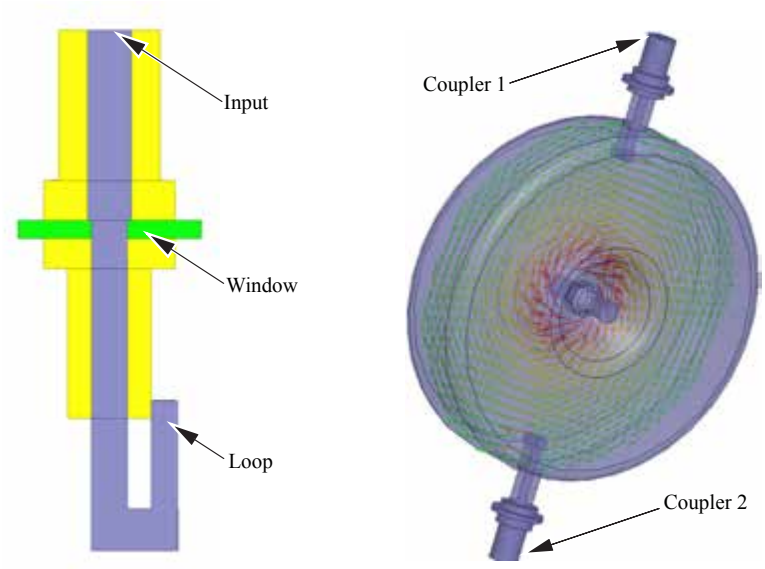

Figure 4.44: Left: Electromagnetic model of the drum-like coupler including the coupling loop designed for the MEBT buncher cavity. Right: Magnetic field intensity H_θ of the TM010 mode resonating in the cavity induced by the power couplers.

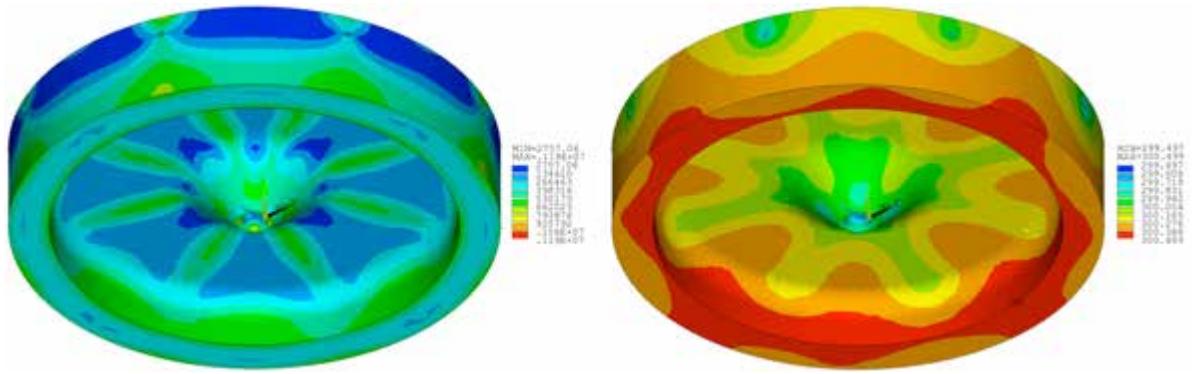

Figure 4.45: Simulations of the MEBT buncher cavities. Left: Temperature. Right: Stress field.

of the ESS MEBT coupler will be a cylinder. The preliminary value for its length is $L_{window} = 6$ mm. Again, this value will be modified if necessary as the design evolves. Once the window transitions of the coupler have been designed, a loop will be added to the model. This loop must inductively couple the power coming from the RF distribution system into the re-bunching cavity, as illustrated in Figure 4.44. This coupling is directly related to the area covered by the loop which ensures the minimum magnetic flux needed [463].

Thermo-mechanical design

The thermo-mechanical design of the buncher cavities relies on ANSYS's Fluent simulation software [422]. Once the actual heat deposition is obtained from EM calculations, that information can be exploited using a user-defined function (UDF) within the FLUENT software environment. The maximum value of the heat flux applied to all zones of the buncher cavity is reached at the "nose" of the copper walls of the buncher cavity, as shown in Figure 4.45. After using the UDF to apply the heat flux to the cavity's

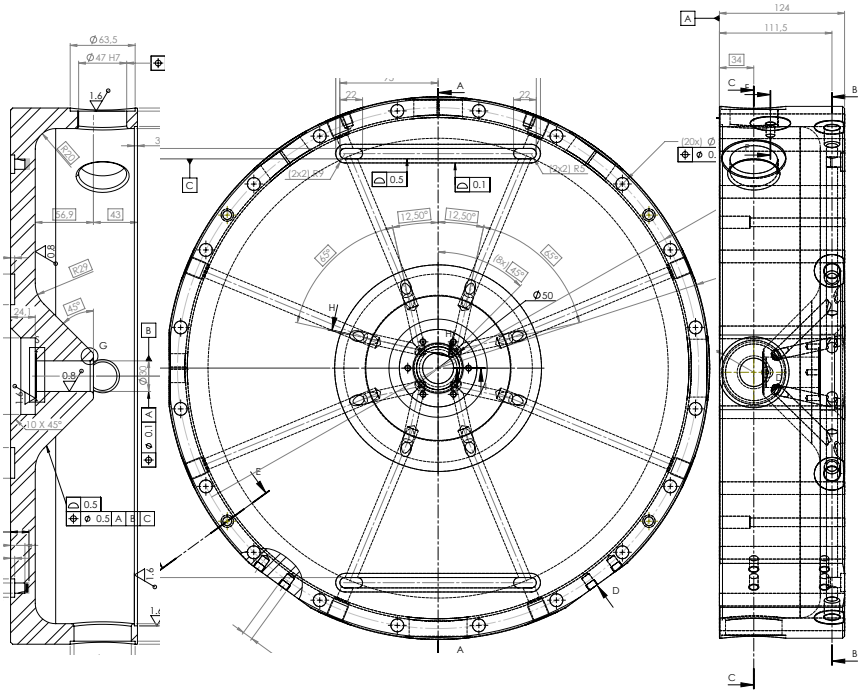

Figure 4.46: Engineering detail of the MEBT buncher cavity, showing its characteristic Maltese cross-shaped cooling channels.

geometry, Fluent is used to solve the computational fluid dynamics problem iteratively. For a 1.4 kW average power on the cavity, the temperature increase reached at the nose is around 2 K, while the rest of the solid has a homogeneous temperature between 300°C and 300.5°C, as indicated in Figure 4.45. Water is circulated inside each channel with a mass flow rate of 0.077 kg/s, reaching 3.6 m/s after the elbow. The average velocity in the rest of the flow is around 2.16 m/s [464]. Once the thermal hydraulic analysis is finished and the temperature field is obtained, a thermo-mechanical analysis can be performed. The most important results obtained from the thermo-mechanical analysis are the stress and strain values, because these parameters set material and geometrical restrictions respectively. The calculated stress field is around 1.2 MPa near the cooling channels drawn in Figure 4.46. This is a very low value, significantly lower than the yield strength of the material (around 270 MPa for oxygen-free tempered copper) and the fatigue strength (115 MPa for treated copper working 3×10^8 cycles). Finally, maximum strain values for x, y and z coordinates are 0.005, located in the nose, where temperature is higher [465].

Manufacturing considerations

The cavity mechanical design addresses two main pieces: the first includes the cavity barrel and one cover, and the second includes the other cover. Each piece will be made in stainless steel. After machining, the commercial flanges will be welded to the body. Once all the components of the cavity are assembled, the interior of the two pieces will be copper-plated at a thickness of 30 μm, creating a layer thick enough for the RF requirements. Both parts will be assembled using HELICOFLEX© metal seals to guarantee the vacuum requirements. This model will be fabricated with all the ports opened and the tuners (one fixed and one movable) in the right positions. The assembled cavity will then be then measured to verify that it meets design specifications and to check the resonant frequency. Afterwards, the cover piece edge will be machined, so that when the full cavity is assembled the gap length will be as small as possible, resulting in the lowest possible resonant frequency. The movable tuner range must be sufficient to deal with the frequency shift due to the thermal expansion of the cavity, which mainly appears on the nose cones of the gap area. Therefore, during operation, the cavity geometry will be very similar to the one obtained by optimising the geometry at 352.21 MHz.

4.3.8 Drift tube linac

The drift tube linac (DTL) will accelerate a proton beam with a 50 mA pulse peak current from 3 to 80 MeV. The DTL is designed to operate at 352.21 MHz, with a duty cycle of 4% (2.86 ms pulse length, 14 Hz repetition period). Permanent magnet quadrupoles (PMQs) are used as focusing elements in a FODO lattice scheme – that is, with half of the drift tubes left empty, leaving space for steerers and beam diagnostics. Figure 4.47 show the overall layout and dimensions of the four DTL tanks. The design is based on the mechanical design and prototyping of the Linac4 DTL [466], and it emphasises respect for practical technological limitations and avoiding beam losses along the DTL structure. The maximum RF power per tank is fixed at 2.15 MW. The surface electric field limit is 1.4 Kilpatrick, to avoid sparking, particularly at the first DTL cells, due to the simultaneous presence of electric and static magnetic fields. The tank length is limited to 8 m (9.3 λ), to avoid stability problems in the RF voltage design. The total number of tanks is four, to reduce the global RF power needed. The DTL beam bore radius widens along

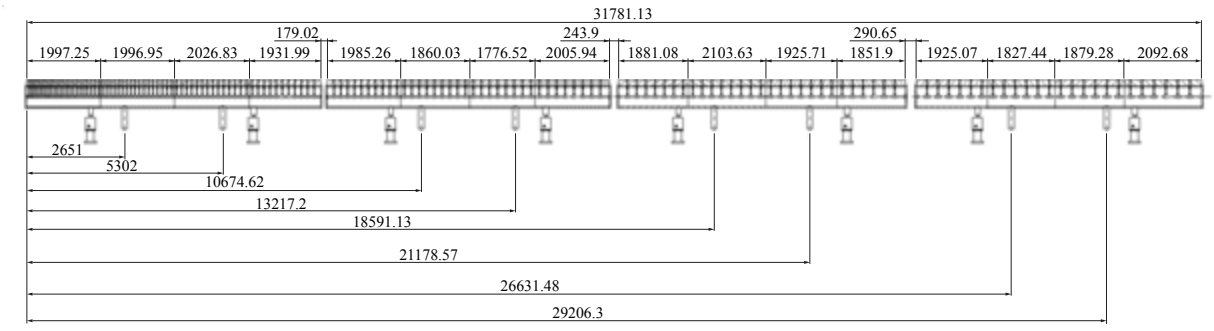

Figure 4.47: Overall layout and dimensions of the four tanks of the drift tube linac.

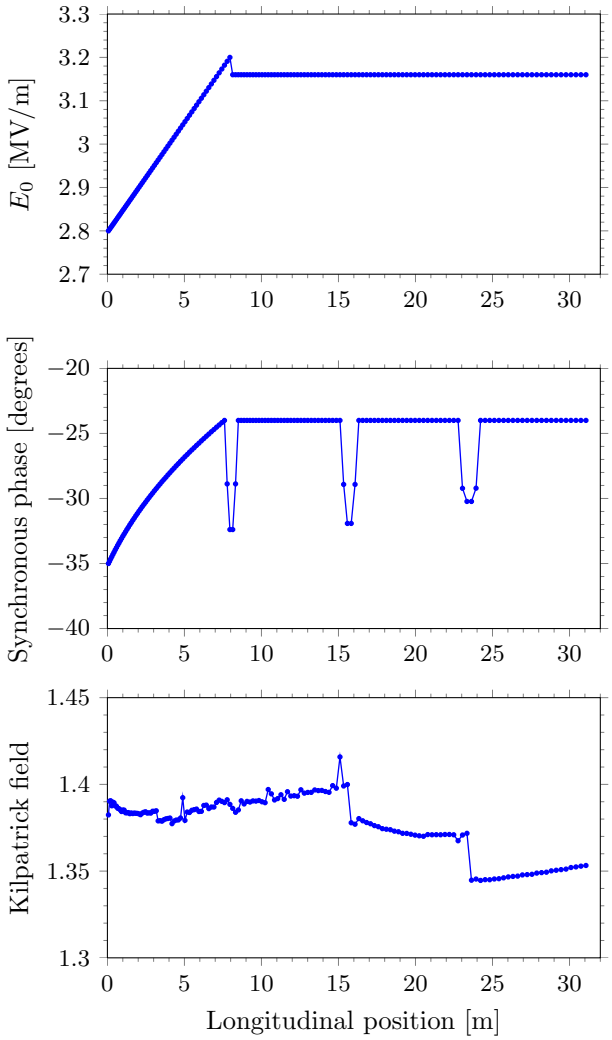

Figure 4.48: Evolution of three key parameters along the DTL: Top: Electric field E_0. Middle: Synchronous phase ϕ_s. Bottom: Surface field.

the length of the DTL to avoid losses. The optimised solution has been found by using GenDTL, from the TraceWin suite of codes. Figure 4.48 shows the evolution of three key parameters along the DTL: Electric field E_0, synchronous phase ϕ_s, and surface field. Half of the drift tubes are empty, available for beam diagnostics and steerers. The permanent magnet quadrupole strengths range from 30 T/m to 70 T/m, permitting an equipartitioned beam evolution, as shown in Figure 4.49, which also show the evolution of the beam distribution along the DTL.

RF design

The presence of DC magnetic field lowers the limit given by Kilpatrick's criterion for electric breakdown [466]. In the first cell of the ESS DTL, the maximum surface electric field is on the drift tube nose at $R = 12$ mm. At that point, the PMQ fringe field ($B' = 70$ T/m) is 0.092 T. This value of B reduces the maximum E_{surf} to 1.4 Kilpatricks, as shown in Figure 4.50. The DTL's RF design is achieved through a multi-step process. Beam dynamics simulations using GenDTL's Superfish routine provide key parameters, including E_0, T, ZT^2, energy gain, synchronous phase, number of cells, and cell and gap lengths, which become inputs into the RF design. The frequency perturbation induced by the stem over each cell is then evaluated. This perturbation can induce a ramped field shape. The stem effect is compensated for by an equivalent variation of the face angle. Once all the cells are resonant at the same frequency, they compose the tank. The accelerating field E_0 is not yet the nominal one: the final adjustment is obtained

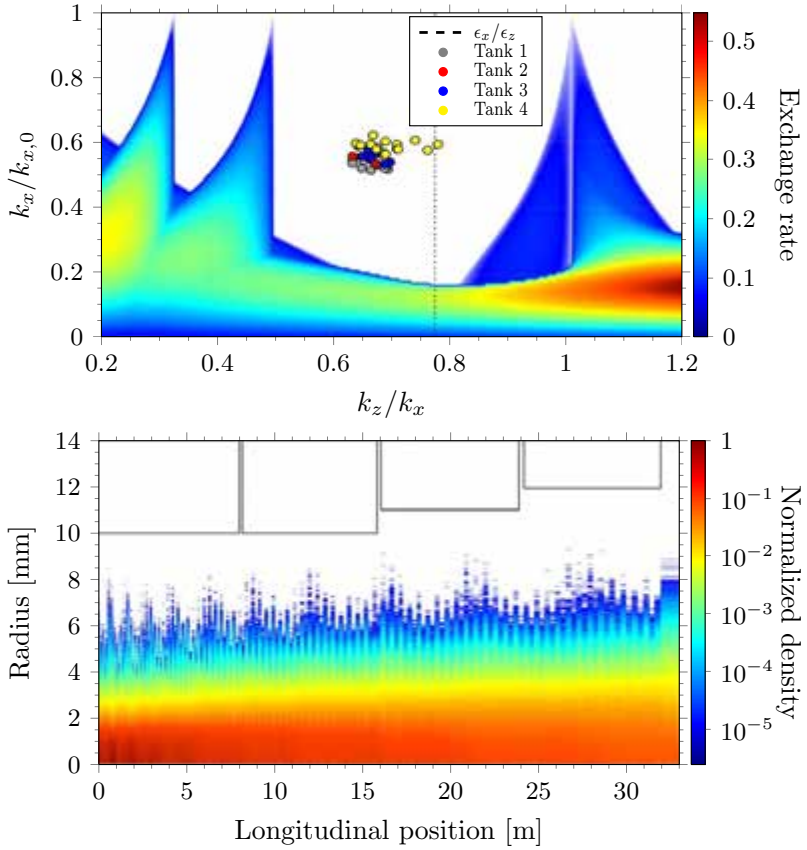

Figure 4.49: Top: Hofmann stability plot for the DTL. Bottom: Evolution of the beam distribution along the DTL.

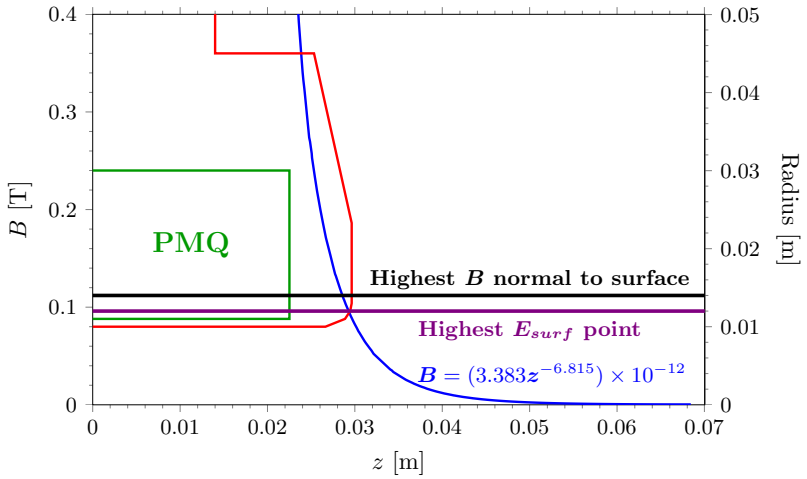

Figure 4.50: Magnetic fringe fields at the point of maximum surface electric field (R = 12 mm) on the drift tube nose in the first cell of DTL tank 1.

by changing face angles once again. Finally, the mechanical feasibility of the drift tube geometries is checked. This design procedure has been validated using 3D simulation software from COMSOL [467], for a representative tank (5.5 m, 26 cells) with an aggressive ramped field. The error obtained with respect to the nominal design is 4%, located in the two end cells, which are used for ramping.

A circuit model of the DTL determines the number of post couplers needed to stabilise each tank [454]. The number of post couplers required per unit length to keep E_0 within specifications ($\pm 1\%$) when a

reasonable perturbation is applied to the end-cells is given by

$$N \geq \frac{|E_{first} - E_{last}|}{E_0} \frac{1}{L_{Tank}} \tag{4.5}$$

Slug tuners in a DTL should compensate for frequency effects due to construction errors. The evaluation of frequency error is achieved by applying realistic tolerances to the important dimensions of the cavity (tank diameter, drift-tube lengths, drift tube diameter, face angles). The tuners have diameters of 90 mm, oriented at 45 degrees with respect to the stem axis and distributed uniformly at 30 cm intervals along the tank. The tuner sensitivity is 3.5 kHz/mm, linear around 50 mm of penetration. One 2.8 MW klystron running at a duty cycle of 4% feeds the required RF power to each tank. The power available at the RF tank input is 2.15 MW (30% margin for waveguide losses and low level RF regulation). The 2.15 MW figure includes power dissipated on copper (including a 25% margin above the values from the Superfish calculations) and beam power. The ESS design calls for two iris power couplers per tank, designed to have overall coupling factors of $\beta_0 = 1 + P_{beam}/P_{cu}$, as shown in Figure 4.47.

Misalignment and RF errors

An error sensitivity study for the various parameters of the DTL has been performed, using 100 DTL models and 1.6×10^5 particles (1 W per particle). A uniform input distribution was assumed, with an overlapped Gaussian halo distribution. The added halo extends to 3σ and the number of particles in the halo were adjusted to have the equivalent of 1 kW of power in the halo. A couple of steerers per axis were used in each tank, to correct the beam centroid in case of PMQ shaking or input beam error with maximum steerer strength (1.6×10^{-3} Tm). Figure 4.51 shows the results of the error sensitivity study of PMQ shake, in 10 steps with the errors listed in Table 4.10. The steerers reduce beam losses by a factor of 10, and reduce the additional emittance growth by 50%.

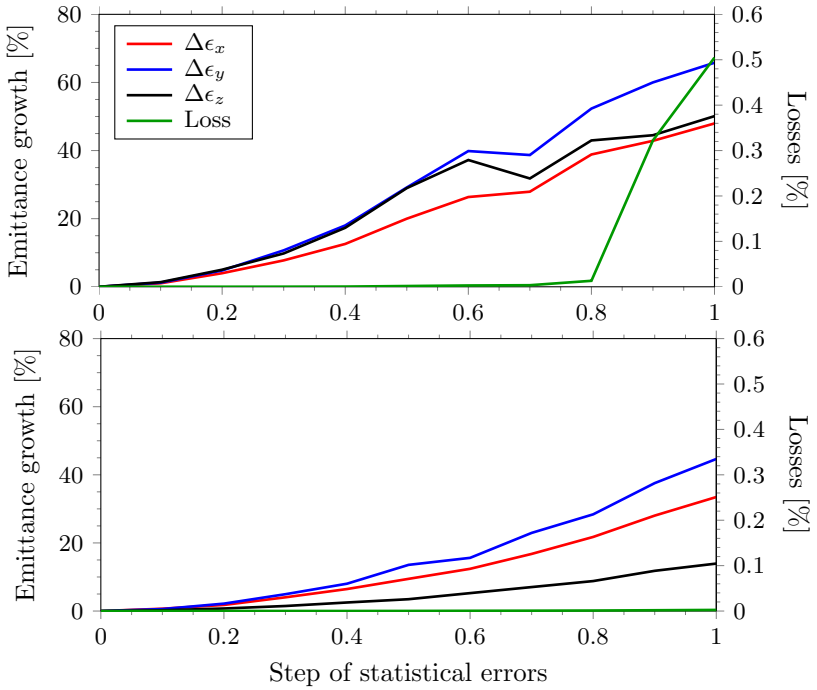

Figure 4.51: Beam losses (green) and emittance growth as a function of quadrupole misalignment error. Top: Without steering correction. Bottom: With steering correction, reducing beam losses by a factor of 10, and reducing emittance growth by 50%.

Parameter	Unit	Value
Maximum accelerating field amplitude (E_0) error	%	±2
Maximum accelerating field phase error	deg.	±2
Maximum transverse quadrupole misalignment error	mm	±0.2
Maximum quadrupole roll error	deg.	±1
Maximum quadrupole strength error	%	±1

Table 4.10: Misalignment and RF errors used for drift tube linac steering correction studies.

4.4 Superconducting RF linac

The superconducting RF linac will be composed of fully segmented cryomodule units installed in the 400 m long cold linac portion of the accelerator. This section describes the technical design of the hardware that makes up the cold section, divided into "spokes", "medium-β" and "high-β" components [468]. The RF and cryogenic environments, which are necessary for the operation of these pieces of hardware, are described elsewhere in this document, as are the beam physics, and the integration and safety aspects of the design and operation of these components.

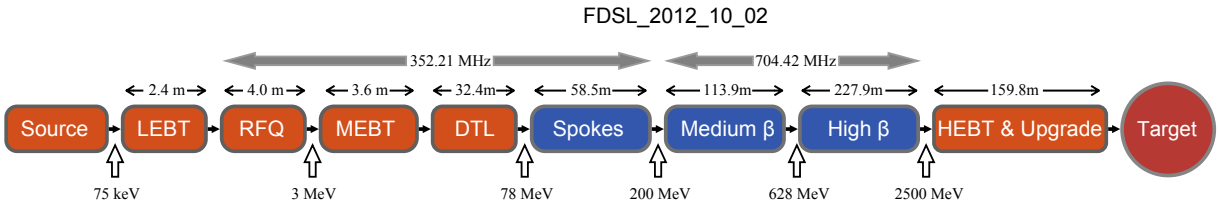

Figure 4.52: Superconducting sectors in the accelerator layout block diagram, coloured blue: spokes, medium-β, and high-β.

Figure 4.52 shows the layout of the ESS linac, with the cold linac components coloured blue. Table 4.11 summarises the composition of the cold linac sectors. In order of increasing energy level, the cryomodules will contain two double-spoke cavity packages, four medium-β cavity packages and four high-β cavity packages. Warm quadrupole doublets and beam instrumentation systems will be installed in between the cryomodules to correct and monitor the beam profile. The main functions of the cryomodules are to provide the positioning and alignment of the SRF cavity package with respect to the beam axis and to reduce thermal losses to the 2 K helium tank. As such, the cryomodules will have the capacity to transfer energy from the RF system to the beam. The main requirements for the cryomodules are listed in Table 4.12. The cryomodule package will be composed of the cryomodule itself and the jumper connection. The jumper connection will link the cryomodule to a valve box on the cryogenic transfer line (CTL), which in turn will be linked to the linac cryoplant. A single vacuum barrier located at the valve box will separate the CTL insulating vacuum from that of the cryomodule. The CTL and cryoplant are described in Chapter 6. The cryomodules will be composed of the SRF cavity packages described below, the supporting system, the alignment system, the thermal and magnetic shields, the internal cryogenic piping and the

Section	Number of modules	Frequency [MHz]	Input energy [MeV]	Cavities per module	Cavities per sector	Module length [m]	Sector length [m]
Spoke	14	352.21	79	2	28	2.9	58.5
Medium-β	15	704.42	201	4	60	5.6	113.8
High-β	30	704.42	623	4	120	6.7	227.9
Total	59				208		400.16

Table 4.11: Main parameters of the spoke, medium-β and high-β sectors.

Parameter	Unit	Value
Alignment	mm	±1
Helium tank operating temperature	K	2
Helium tank operating pressure	kPa	3.1
Thermal shield operating temperature	K	40 to 50
Thermal shield operating pressure	MPa	1.9
Magnetic shield level	mG	14
Power coupler double-wall temperature	K	5 to 150
Power coupler double-wall pressure	MPa	0.14
Insulating vacuum level	mbar	10^{-5}

Table 4.12: Cryomodule requirements.

diagnostic instrumentation. As in the case of the cavity, the cryomodules will come in three different families: the spoke cavity cryomodule, the medium-β elliptical cavity cryomodule and the high-β elliptical cavity cryomodule. Each elliptical cryomodule will contain four superconducting cavity (or resonator) packages, and each package will include the cavity in its helium tank, the fundamental power coupler, the cold tuning system, and the RF pick-up coils. Each spoke cryomodule will contain two spoke resonator packages. The design of the spoke and elliptical cryomodules is driven by the need for thermo-mechanical optimisation and the mechanical stability of the cryo-string assembly.

Tunnel integration

The three families of cryomodules will be sequentially installed inside the ESS tunnel. Figure 4.53 shows the tunnel, including elliptical cavity cryomodules, jumper connections, valve boxes and cryogenic transfer lines. ESS will not use bayonets to connect the cryomodule to the CTL but instead will use a cost effective, low heat-leak solution with a jumper connection and a vacuum barrier. The jumper connections feed the cryomodule's cryo-distribution piping and contain Joule-Thompson control valves, cool-down control valves, 2 K sub-cooler heat exchangers and diagnostic instrumentation. This use of a vacuum-isolated jumper connection for every cryomodule will reduce the total heat load to the linac cryoplant, while maintaining the option to isolate a failing cryomodule. Indeed, the jumper connection will be accessible from the side of the cryomodule, and it will be possible to disconnect it (after a local warm-up) without warming up the CTL.

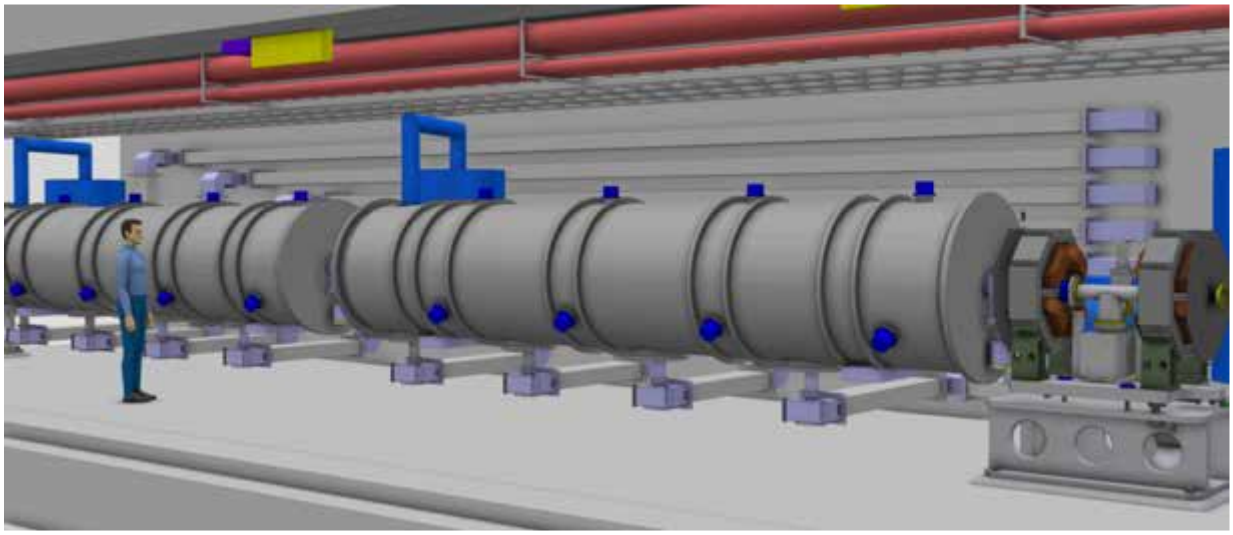

Figure 4.53: Tunnel perspective, showing elliptical cavity cryomodules, jumper connections, valve boxes and cryogenic transfer lines.

The beam elevation is driven by the need to be able to access the biasing system equipped with the power coupler door-knob in the accelerator tunnel. The maintenance of this component will be performed without removing the cryomodule from the beam line. This RF line comprises several components and devices such as RF contacts, insulating foils and diagnostics that are critical for operating the RF power.

4.4.1 Cryogenic operating parameters and flow process

The maximum allowable working pressure for the spoke and elliptical helium tanks is 0.15 MPa: this pressure is consistent with the maximum allowable stress for the design of the spoke resonator, and the helium tank can avoid classification as a pressure vessel if it is operated below 0.15 MPa relative pressure under European Union standards.[2]. Table 4.13 lists the different temperatures and pressures envisioned for use in the cryo-distribution lines of the cryomodules. These are preliminary temperature and pressure ranges for the thermal shield which will be optimised later. The operating pressures and temperatures listed in Table 4.13 were selected to fit the calculation of the pressure and temperature distribution along the CTL. The operating pressures range from 1.9 MPa for the thermal shield piping to 3.1 kPa for the saturated helium tank. In order to prevent contamination of the helium, the sub-atmospheric lines require the use of helium guards around the flanges.

	Temperature [K]	**Pressure** [MPa]
SRF helium tank	2	0.0031
Power coupler double-wall	5 to 150	0.14
Thermal shield	40-50	1.9

Table 4.13: Temperature and pressure levels in the cryogenic transfer lines.

The flow schematic and the process and instrumentation diagrams (P&ID) are similar for the spoke and the elliptical cavity cryomodules. Figure 4.54 shows the flow schematic for a spoke cryomodule, while elliptical cryomodule flow is discussed in Section 4.6. Helium will be used to cool the helium tank containing the SRF cavity packages, the thermal shield and the various heat intercepts. The cryomodules will operate at several temperature levels: 2 K for SRF cavities operation, 40 K to 50 K for the thermal shield cooling and heat intercepts, and 4.5 to 150 K for the power coupler double wall cooling.

Helium tank and cavity

The SRF cavity helium tanks will be cooled down using a specific circuit. The cryogenic transfer lines will feed the cryomodule cryo-distribution line with 4.5 K supercritical helium at 0.3 MPa. During cool down and filling of the SRF cavity, the supercritical helium will be expanded to 0.14 MPa. The SRF cavities will be filled in parallel from the bottom of each helium tank. During normal operation, the dynamic and static heat loads (including beam losses) will be dissipated in the 2 K, 3.1 kPa helium bath, causing vapour to evolve. This very low-pressure (VLP) helium gas will be pumped via the CTL to the linac cryoplant. The 2 K bath will be supplied by the supercritical helium flow, which will be expanded using a Joule-Thomson valve. To improve the 2 K operation, a 2 K subcooler heat exchanger will be installed in each cryomodule, as drawn schematically in Figure 4.55. The 2 K heat exchanger will pre-cool the incoming helium flow (for example, from 4.8 K and 0.3 MPa to 2.2 K) before the Joule-Thomson expansion to 3.1 kPa takes place. The supply helium temperature will vary along the CTL due to the remaining heat load in the CTL and the jumper connections, from 4.5 K at the cryoplant side to 5 K at the first spokes cryomodule. A typical value for the available heat of evaporation after the J-T expansion is 20 J/g, which is used to remove the cavity heat load at 2 K. The returning vapour flow will warm up to around 3.6 K in the subcooler heat exchanger before entering the VLP return line.

The design of the power couplers for the three cavity families is based on work carried out by the High Intensity Pulsed Proton Injectors (HIPPI) project, which is part of a larger European collaboration for accelerator research [469, 470]. In this design, each double-walled power coupler is cooled by a controlled helium flow at about atmospheric pressure. This helium flow is taken from the supercritical helium flow

[2]European Directive 97/23/CE

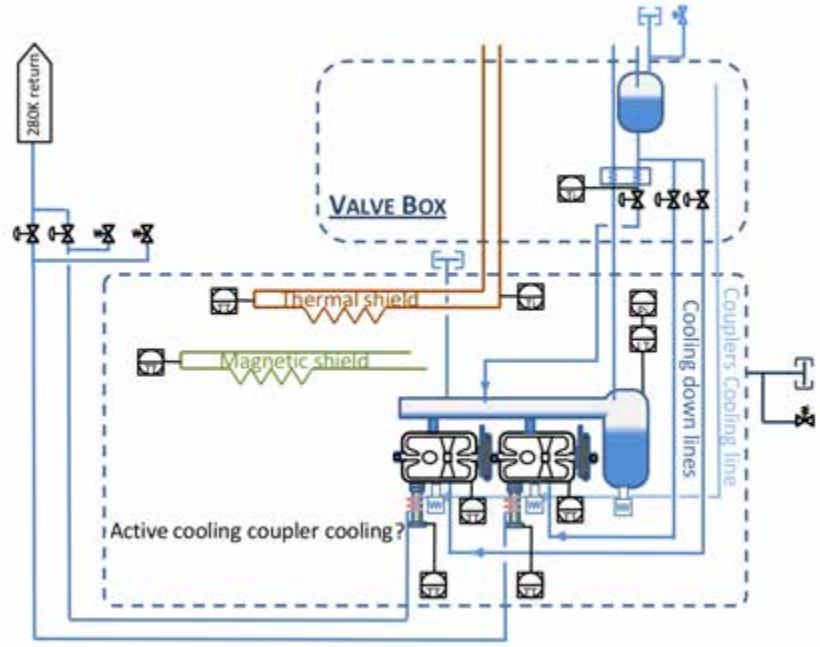

Figure 4.54: Spoke cryomodule cryogenic flow scheme, including cool down lines for the helium tank; cryogenic distribution; magnetic shielding for the SRF spoke resonators; power coupler/cavity ports and cold tuners; filling lines, to distribute helium coming from the cold box to the cryomodule, including a phase separator pipe connected to the helium tanks of the cavities and another small phase separator for LHe level measurement; a double-wall power coupler cooling line, which removes static and dynamic heat loads along the coupler tubes, connected to the SRF spoke resonators; a 40 K to 50 K helium gas line for cooling down and regulating the temperature of the thermal shields; a cooling line for cooling the cold magnetic shields before the SRF spoke cavities; safety devices, including burst disks and relief valves; control and measurement instrumentation (temperature, pressure transducers, LHe level gauge); and heaters for fast re-heating purposes and heat load control.

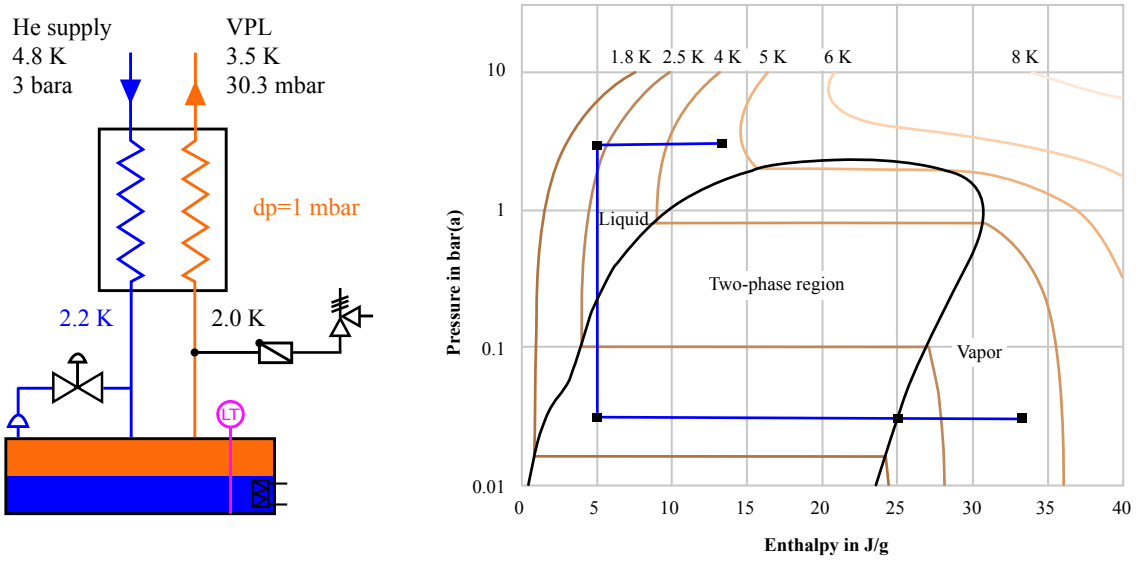

Figure 4.55: Drawing and performance of the 2 K subcooler heat exchanger. Left: Schematic of the cavity circuit showing typical inlet and outlet conditions at the 2 K pre-cooling heat exchanger. Right: State variables in a pressure-enthalpy diagram.

supplied by the CTL. The heat dissipated by the RF power and the power coupler static heat load is extracted by a 40 mg/s flow of helium gas increasing from 5 K to 150 K as it moves along the power coupler double wall. This helium flow is routed away from the power coupler ceramic windows to the exterior of the cryomodule vacuum vessel. The helium flow is collected at atmospheric pressure and sent to the warm helium piping. Each power coupler outlet flow temperature is controlled and an electrical heater permits the ceramic windows to remain above the dew point. The aluminium thermal shield will be actively cooled by gaseous helium flowing at a temperature in the range of 40 K to 50 K and at a pressure of 1.9 MPa. Blankets of multi-layer insulation will be wrapped around the thermal shield and the helium tank [471].

The fully integrated cryomodule will include magnetic shielding to ensure that the residual resistance due to trapped magnetic flux is not greater than 4 nΩ. At 704.42 MHz, this implies that a reduction of the earth field by a factor of 35 is required. A magnetic shield made of high permeability materials will protect the cavity package. The magnetic shield will be passively cooled during the cool-down phase. The cryomodule vacuum vessels will be made of stainless steel in order to generate a homogeneous magnetic field. Each cryomodule will have an independent insulating vacuum (expected level: 10^{-5} mbar), and thus an independent interface to the vacuum systems. Turbomolecular pumps (TMP) will be used to establish the insulating vacuum in order to limit the heat load to the cryogenic system. Pirani and cold cathode vacuum gauges will be attached to the vacuum port. This port may also be used to install a TMP and a roughing pump if needed to maintain vacuum during normal operating conditions.

4.4.2 Cryogenic heat loads

A preliminary heat load calculation makes it possible to estimate the cryogenic cooling capacity using a bottom-up approach that adds static, dynamic and beam loss contributions [472–474]. The static heat load estimate will evolve with the cryomodule design, and is discussed in detail in Sections 4.5 and 4.6. Table 4.14 summarises the calculated static heat load distributions at different temperature levels. The cryogenic duty cycles for the spoke and the elliptical RF cavities are expected to be about 4.65%. Table 4.15 lists the typical dynamic heat losses that are used for calculations related to the three families of cryomodules. The dynamic heat load assumptions include a safety margin (that is, they assume a quality factor, Q_0, lower than nominal). Table 4.15 also records the total heat load to the cryomodules and the global heat load to the superconducting linac, assuming that the heat deposited by beam losses is as large as 1 W/m. Preliminary heat load studies for the valve box and the transfer line have also been completed, as discussed in Chapter 6. The addition of the contribution from control valves and the CTL, makes it possible to estimate the required cryoplant and distribution line capacity. Figure 4.56 shows the contribution of the spoke, high-β and medium-β cryomodules to the total superconducting linac heat load. The dynamic heat load is approximately half of the total heat to be extracted by the cryogenic system.

Sector	**2 K** [W]	**5 K** [W]	**50 K** [W]	**4.5 K equivalent** [W]
Spoke resonator cryomodule	5.0	–	35.0	17.5
Medium-β cryomodule	6.7	1.5	75.0	27.0
High-β cryomodule	7.5	1.5	75.8	29.4

Table 4.14: Static cryomodule heat load estimates at each temperature level.

Cryomodule	**Static load** [W@4.5 K]	**Dynamic load** [W@4.5 K]	**Beam losses** [W@4.5 K]	**Total** [W@4.5 K]
Spoke resonator cryomodule	17.5	18.0	8.7	44.2
Medium-β cryomodule	27.0	67.3	17.1	111.3
High-β cryomodule	29.4	82.0	20.1	131.5
Linac sub-totals	1530	3722	981	6233

Table 4.15: Heat load estimates for spoke, medium-β and high-β cryomodules.

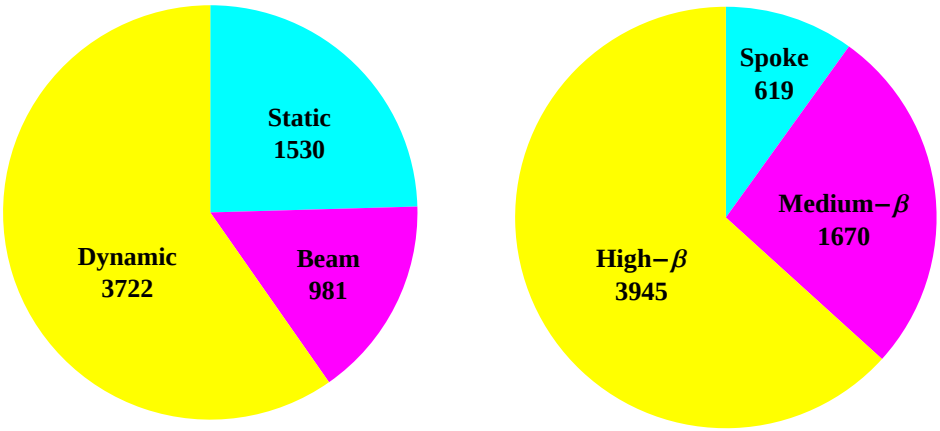

Figure 4.56: Total cryogenic heat loads, in Watts at 4.5 K (equivalent). Left: Total static, dynamic and beam loss heat loads. Right: Total dynamic heat loads in the spoke, high-β and medium-β sectors.

Cryogenic control and operating modes

Cryogenic instrumentation will be used to monitor operating variables and control the valves and interlock systems, relying in many instances on lessons learnt from operating experience at the Large Hadron Collider at CERN [475,476]. The control system and safety equipment will ensure a high degree of reliability during the different operating modes. More than 50 read-back channels will be available for each cryomodule and will be integrated in the EPICS-based controls platform described in Chapter 5. Dedicated PLCs will close some of the control loops for control valves and the appropriate instrumentation. The SRF cavity interlock system will be integrated with the machine protection system described in Section 5.2.2. The positioning and alignment of the cavity packages will be provided by a dedicated support system and laser tracker technique [477].

4.5 Spoke cavities and cryomodules

The superconducting spoke sector of the linac shown in Figure 4.52 will accelerate beam from the normal conducting section to the first family of the elliptical superconducting cavities. The SRF spoke cavity cryomodules will accelerate a proton beam extracted from the DTL at 79 MeV of beam energy up to an energy of 201 MeV at the entrance to the medium-beta cavity section. Acceleration will be performed by a single family of $\beta = 0.5$ bulk niobium double spoke cavities (with three accelerating gaps), operating at a temperature of 2 K, and at a frequency of 352.21 MHz. A total of 28 spoke cavities; grouped in pairs in 14 cryomodules, will take up 58.6 m of length along the linac. The chosen operating accelerating field is 8 MV/m, where the accelerating length is defined to be $(n + 1)\beta\lambda/2$, and n is the number of spoke bars. The required peak RF power to supply one cavity will be about 250 kW for the 50 mA beam intensity, corresponding to 10 kW of average power.

The ESS linac will probably be the first accelerator integrating spoke cavities to be constructed. These structures offer the potential for high performances and other intrinsic advantages. In addition to all the well-known advantages of superconducting cavities (high efficiency, large beam aperture and high reliability) spoke cavities also: have multi-gap capabilities (high real-estate gradients); are compact and naturally stiff (less sensitive to mechanical perturbation such as vibrations); exhibit high cell to cell coupling (no field flatness required); are less sensitive to HOM or trapped modes (due to the high cell to cell coupling); are not susceptible to dipole steering effect (contrary to other low-β cavities such as quarter-wave resonators); make a wide β range accessible; and exhibit a high longitudinal acceptance (accelerating efficiency over a wide β range). Table 4.16 shows that about 15 spoke prototypes of different types have been fabricated and tested worldwide. Other high power proton accelerators currently under design are also considering adoption of spoke technology, including MYRRHA in Belgium, ADS in China, Project-X in the USA and EURISOL in Europe.

Lab	**Type**	**Freq.** [MHz]	**Optimal** β	E_{acc} **max** [MV/m]	V_{max} [MV]	E_{pk}/E_{acc}	B_{pk}/E_{acc} [mT/(MV/m)]
IPN Orsay	Single	352	0.20	4.8	0.8	6.7	14.5
	Single	352	0.36	8.1	2.5	4.7	12.8
ANL	Single	855	0.28	4.4	0.3	5.5	12.7
	Single	345	0.29	8.7	2.2	4.6	12.1
	Single	345	0.40	7.0	2.4	6.3	16.7
	Double	345	0.40	8.6	4.5	4.7	9.1
	Triple	345	0.50	7.6	6.6	3.7	11.5
	Triple	345	0.62	7.9	8.7	3.9	12.0
FZ-Jülich	Triple	760	0.20	8.6	1.4	5.1	13.3
LANL	Single	350	0.21	7.5	1.3	5.1	13.3
	Single	350	0.21	7.2	1.3	5.0	10.1
FNAL	Single	325	0.21	12.0	2.4	3.6	5.8
	Single	325	0.21	16.7	3.4	3.6	5.8
at 2K	Single	325		21			

Table 4.16: Performance at 4 K of spoke resonators worldwide. E_{acc} is accelerating gradient, V_{max} is maximum voltage, E_{pk}/E_{acc} is the ratio of peak electrical field to the accelerating gradient, and B_{pk}/E_{acc} is the ratio of the peak magnetic field to the accelerating gradient.

Electromagnetic design

The spoke cavity electromagnetic design is guided by the choice of frequency, the optimum *beta* and the optimisation of the peak fields. While the most important parameter for the beam is the accelerating field or the voltage seen by the particle, the most important optimisation criterion is the ratio of surface fields to peak fields. The goal is to minimise the peak fields while keeping the accelerating field constant. Another important factor to optimise is the overall length of the cavity: a spoke cavity has a re-entrant shape, and the size of the re-entrant part can be increased to give more volume to store the energy, thus resulting in a decrease of peak field. The drawback of increasing the size of the re-entrant part of the spoke cavity is a lower real-estate gradient due to the larger longitudinal space taken by the cavity for the same voltage. Following beam dynamics simulations, values were established for a set of parameters to enable the double spoke cavities to fulfil ESS requirements. These are summarised in Table 4.17.

CST MicroWave Studio software has been used for the design and optimisation of the cavity, and for its modelling using MWS's 3D CAD tools [478]. The first mode that must be calculated for the design of a spoke cavity is the fundamental mode, TM010, which is used for acceleration. A benchmark study has been performed to determine the number of mesh cells required for the iterative calculations. A convergence

Parameter	**Unit**	**Value**
Pulsed beam mode duty factor	%	4
Frequency	MHz	352.21
Optimal beta, β_{opt}		0.50
Temperature	K	2
B_{peak}	mT	70
E_{peak}	MV/m	35
Accelerating gradient, E_{acc}	MV/m	8.0
L_{acc}	m	0.639
B_{peak}/E_{acc}	mT/(MV/m)	< 8.75
E_{peak}/E_{acc}		< 4.38
Minimum beam tube diameter	mm	50
Maximum power	kW	300

Table 4.17: Spoke resonator cavity main parameters.

of both E_{pk}/E_{acc} and B_{pk}/E_{acc} ratios was observed at approximately 100,000 mesh cells. The main goal of the electromagnetic design is to get these ratios below 4.38 and 8.75 mT/(MV/m), respectively. The optimisation procedure has been divided into three sequential parts. First, the geometry is optimised while ignoring additional ports (such as the RF coupler port) that penetrate into the cavity body. Second, the RF coupler is integrated into the cavity body, with particular attention to external-Q calculations. Finally, calculations are made with all ports present: RF coupler, pick-up probe ports and ports dedicated to the cavity preparation (chemistry and rinsing).

Geometry

The spoke cavity design benefits from 10 years of experience with earlier spoke cavity fabrication at IPNO (l'Institut de Physique Nucléaire d'Orsay/Orsay Institute of Nuclear Physics) by a team that has designed three spoke-type cavities (two single-spoke and one triple-spoke), and has prepared and tested them in vertical and horizontal cryostats at 4 K and 2 K. IPNO's experience in the design of spoke cavities and the feedback IPNO has received from manufacturers has led it to reject both the cylindrical and the racetrack shape for spoke base geometry. The cylindrical shape results in a magnetic field that is too high, while the racetrack shape leads to difficulties in forming the components and, above all, in welding the spoke bases to the cavity body. Consequently, the design optimisation process for ESS started with a conical shape for the spoke base. In order to parametrise the spoke cavity geometry, the impact of 13 parameters on the E_{pk}/E_{acc} and B_{pk}/E_{acc} ratios has been studied using simulation software, as illustrated in Figure 4.57. After analysing approximately 600 cavity models, a parametrisation was selected which gave good results. Two mesh types (hexahedral and tetrahedral) were used to cross check the results. The discrepancies across the different approaches vary from about 4% for the B_{pk}/E_{acc} ratio to about 10% for the E_{pk}/E_{acc} ratio, while the G factor and r/Q values are in perfect agreement. The values of the calculated ratios are 4.54 and 7.27 mT/(MV/m) for E_{pk}/E_{acc} and B_{pk}/E_{acc}. The E_{pk}/E_{acc} ratio is slightly higher than the target value of 4.38, in order to achieve a practicable compromise among cavity length, end-cap shape feasibility and tuning sensitivity.

The spoke cavity design also incorporates a mechanical analysis of the double spoke resonator with its titanium helium tank. A numerical simulation analysis of the behaviour of the cavity and helium tank assembly under pressure has been conducted, permitting the development of a mechanical design of the cavity with its stiffeners and of the helium tank. In addition, an electromagnetic-mechanical analysis was performed in order to estimate the sensitivity of the design to detuning, pressure fluctuations and Lorentz detuning. The spoke 3-gap cavity design has been defined through an RF analysis performed

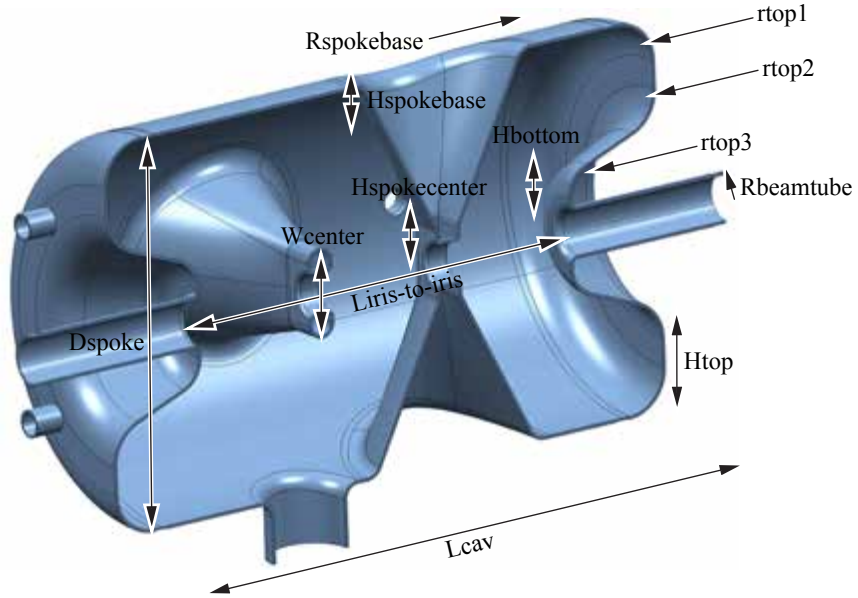

Figure 4.57: Spoke cavity parameters used to optimise the geometry.

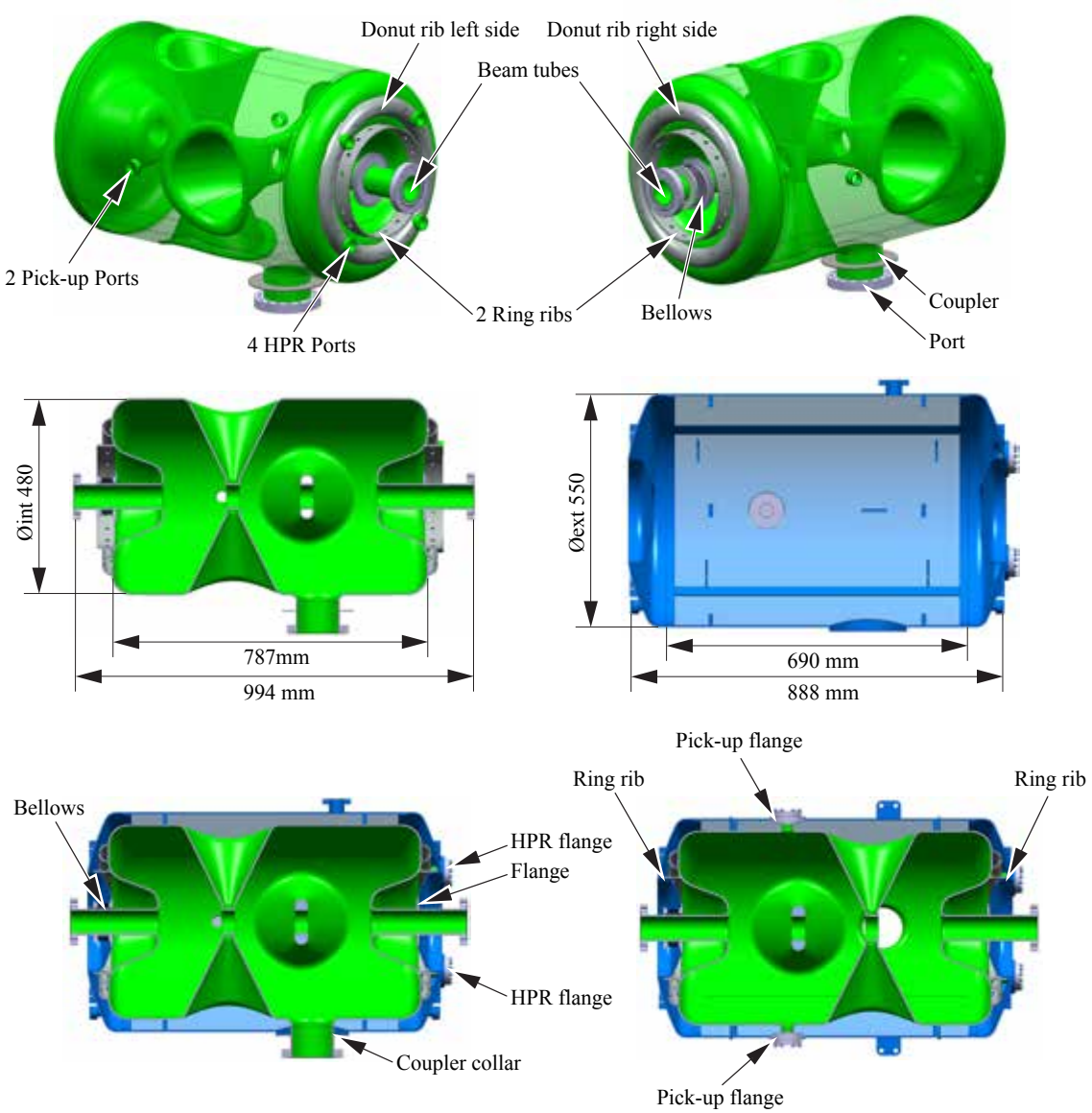

Figure 4.58: Mechanical design of the spoke cavity and helium tank. Top: Double spoke cavity. Bottom: Helium tank assembly.

with MicroWave Studio software. The cavity will be made of niobium and will consist of a cylindrical outer conductor, two spoke bars oriented at 90 degrees with respect to each other and two re-entrant end cups, as shown at the top of Figure 4.58. Additional detail of the spoke cavity package design is provided elsewhere [479].

4.5.1 Mechanical design

Based on mechanical calculations and manufacturing considerations, the thickness of all cavity walls has been fixed to a minimum of 4 mm [480]. The design also calls for several stiffeners in order to reinforce the cavity so that it can withstand external pressure, including two doughnut ribs welded onto the plane area of the end cups, and two ring ribs making a connection between the end cups of the helium tank and the end cups of the cavity. There will be several ports on the cavities, including the fundamental power coupler ports (internal diameter 100 mm), ports for the pick-up antennae (internal diameter 32 mm), and additional ports for cleaning preparation (internal diameter 28 mm) located on one of the end cups for

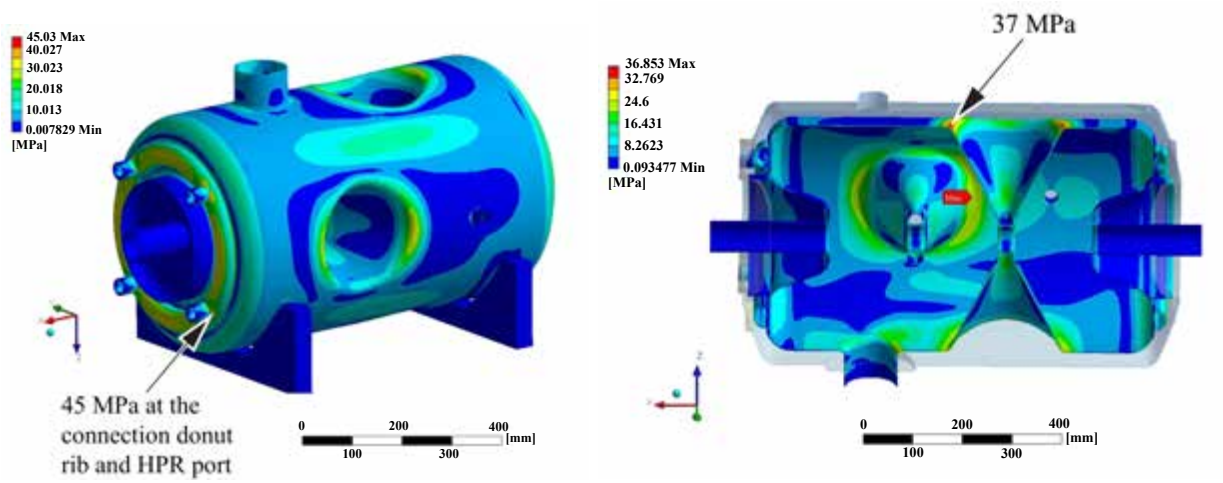

Figure 4.59: Critical areas of von Mises stress, in spoke cavity leak tightness simulations. Left: The critical areas are at the connections between the ports and the reinforcements in configurations with or without helium tank. Right: The critical areas are the top of the spoke bar in the vertical cryostat and in the cryomodule configurations.

the passage of the high pressure rinsing probes. The beam tube aperture is 56 mm. On the high pressure rinsing port side, the beam tube will be connected to the helium tank by a flange. On the other side, a bellows will be connected between the beam tube and the helium tank for the cold tuning system (CTS) discussed in Section 4.5.2). The helium tank will be made of titanium with a wall thickness of 3 mm. As the thermal expansions of niobium and titanium are similar, some welding between the helium tank and cavity is possible and which would contribute to improving the stiffness of the cavity. Reinforcements on each end cup will be used to hang the cold tuning system and the handling tools.

The cavity will undergo different loads during its life-cycle from the manufacturing phase to the operating phase during leak tightness tests, cool down and nominal operation inside the cryostat. The risk of permanent deformation of the cavity is highest at room temperature because of the low yield strength of niobium at 293 K (a pressure value of 50 MPa is commonly chosen). This situation might arise during cool down and leak tightness tests. Several test configurations were analysed using ANSYS finite element analysis software. In the leak test configurations with or without helium tank, the most critical areas are located at the connections between the ports and the reinforcements. Nevertheless, results under pressure showed that the maximum von Mises stresses are less than the yield strength of niobium at room temperature, as shown in the left of Figure 4.59. In the vertical cryostat and in the cryomodule configuration, the critical areas are the top of the spoke bar that limit the allowable pressure load to 0.15 MPa, as shown at the right of Figure 4.59.

Parameter	**Unit**	**Value**
MECHANICAL		
Cavity stiffness, K_{cav}	kN/mm	20
Tuning sensitivity, df/dz	kHz/mm	330
Pressure sensitivity, K_P (free ends)	Hz/mbar	120
Pressure sensitivity, K_P (fixed ends)	Hz/mbar	40
COLD TUNING SYSTEM		
External coupling factor (Q_{ext})		2.4×10^5
Bandwidth	Hz	1,467
Accelerating gradient	MV/m	8

Table 4.18: Spoke cavity frequency sensitivity and cold tuning system parameters. Only the cavity and the end cups of the helium tank are taken into account in calculating the sensitivity due to pressure, K_p.

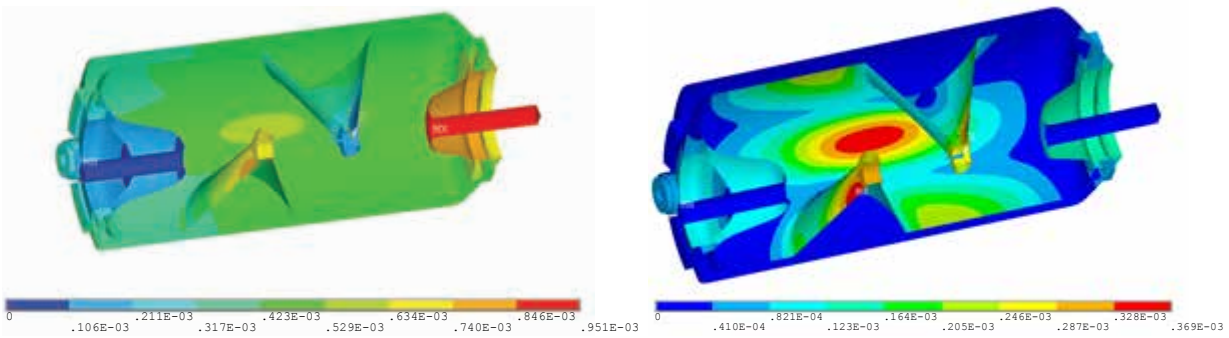

Figure 4.60: Spoke cavity and helium tank deformation under Lorentz pressure. Left: Fixed at one end. Right: Fixed at both ends.

The frequency sensitivity of the cavity during its operation was estimated using ANSYS mechanical-electromagnetic coupling simulations. In these simulations, a quarter of the cavity was meshed and no port was taken into account. An electromagnetic simulation was performed in order to check the frequency and other RF parameters of the cavity. The RF parameters obtained with ANSYS are similar to those from MicroWave Studio. Table 4.18 presents the results of the frequency sensitivity analysis. The results for deformation under Lorentz pressure on the cavity fixed at one and at two ends, are shown in Figure 4.60.

4.5.2 Cold tuning system

For a pulsed machine like ESS, Lorentz force detuning is an important source of resonant frequency detuning, whose effect must be taken into account [481]. Table 4.19 presents the Lorentz factors expected for the spoke cavities, with and without the helium tank attached. The cold tuning system (CTS) is attached to the spoke cavities to adjust *in situ* the resonant frequency of the superconducting cavities in order to counteract frequency shifts due to mechanical perturbations of the cavities. The spoke CTS integrates two different functions: a slow tuning capability over a wide frequency range (typically 1 MHz) and a fast tuning capability over a reduced frequency range (a few kHz). The first function is provided by a mechanical system driven by a stepping motor, and the second function is achieved by means of piezoelectric actuators inserted in the mechanical system of the CTS. The principle of the CTS is to induce a mechanical deformation of the cavity by either pulling or pressing on the cavity extremities in order to change the cavity length, thus resulting in frequency detuning.

The CTS achieves motion resolution fine enough to ensure frequency regulation over a sufficiently wide frequency control range, and integrates piezo actuators to compensate for the Lorentz force. Figure 4.61 shows that the CTS consists of a mechanical system driven by a cold stepping motor operating under vacuum and a reduction gear. The motor drives a ball screw, linked to a double lever arm mechanism, which can act on four rods attached to the cavity. The design is optimised to obtain high rigidity at the lowest possible weight and cost. Table 4.18 lists values for a number of parameters determined by electromagnetic and mechanical studies of the double spoke cavities, which are important data for the

Helium tank	**Ends**	**Lorentz force coefficient, K_L** [Hz/(MV/m)^2]	**Frequency shift at 8 MV/m** [Hz]
No	Free	−6.3	403
No	Fixed	−2.9	186
Yes	Free	−5.3	340
Yes	Fixed	−2.8	180

Table 4.19: Spoke cavity frequency sensitivity: the Lorentz factor, $K_L = df/d(E_{acc}^2)$, with and without the helium tank attached, with free and fixed ends. Note that the cavity bandwidth is 1355 Hz.

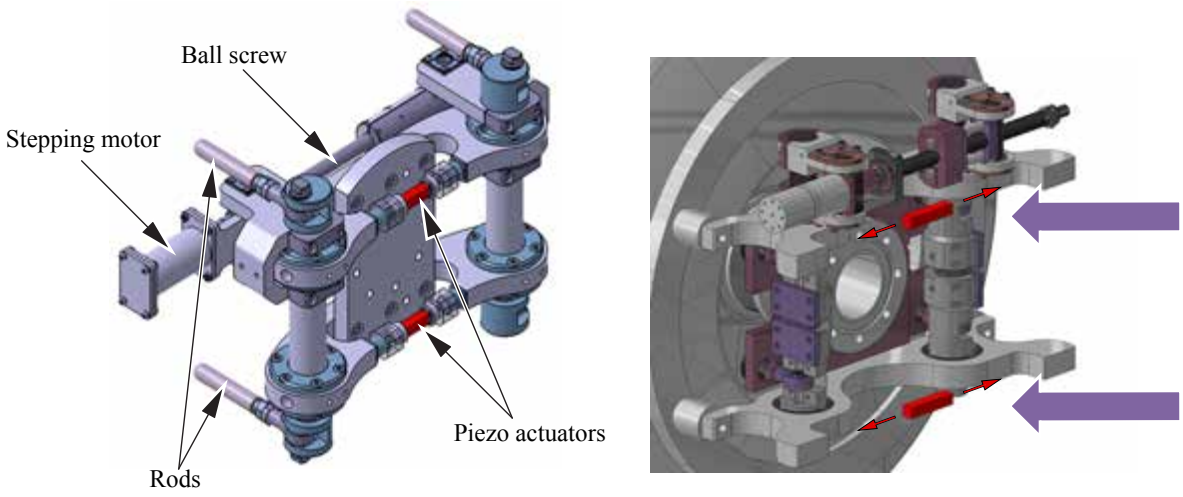

Figure 4.61: The spoke cold tuning system consists of a mechanical system driven by a cold stepping motor operating under vacuum and a reduction gear, with piezo-actuators to compensate for Lorentz forces.

CTS design. The mechanical dual lever arm system that has been chosen as the main option to control the frequency of the cavity *in situ* is inspired by studies and realisations in R&D programs at EURISOL and ADS that have been experimentally validated. For good regulation, the mechanical resolution matches at least one twentieth of the cavity bandwidth. For a cavity frequency of 352.2 MHz and a coupling factor of 2.40×10^5, the bandwidth is 1467 Hz, so the design strives for a resolution of 68 Hz. The CTS must be at least ten times more rigid along the beam axis than the cavity itself. This effectively reduces the effect of the Lorentz forces (and therefore the required size of piezoelectric actuators) and prevents coupling CTS and cavity mechanical resonances modes. The cavity stiffness will be 20 kN/mm, so the CTS requires a stiffness of at least 200 kN/mm.

The tuning sensitivity corresponds to an effective cavity tuning of 330 kHz/mm when the CTS is providing motion. Part of this motion is lost because the CTS stiffness is not an infinite value:

$$\text{Tuning\_sensitivity} \quad = \quad \text{Cavity\_sensitivity} \times \left(1 - \frac{1}{1 + K_{CTS}/K_{cavity}}\right) \tag{4.6}$$

Given the required CTS stiffness, K_{CTS}, of approximately 200 kN/mm, the tuning sensitivity will be about 300 kHz/mm. Using data from simulations under two scenarios (fixed and free cavity ends), the

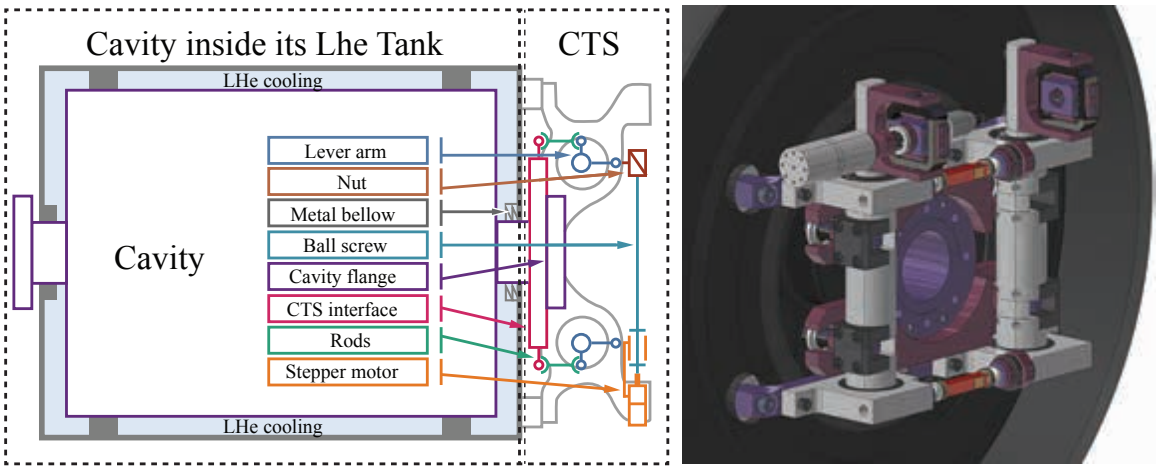

Figure 4.62: Spoke cold tuning system kinematic scheme and 3D model.

Part	Individual compliance [μm/kN]	Number of parts sharing the force	Equivalent compliance [μm/kN]
Rigid lever	2.21	2	1.11
Arms	1	2	0.5
Rods	0.61	4	0.15
Flange frame	5.46	1	5.46
Total compliance			7.22

Table 4.20: Individual and equivalent compliances calculated for several spoke cold tuning system parts. The total stiffness is 138.5 kN/mm.

pressure and Lorentz coefficient also have been calculated. A double arm lever CTS easily offers one to two millimetres of full stroke displacement, which corresponds in the ESS case to a total frequency tuning range of 300 kHz to 600 kHz, a range large enough to compensate for frequency shifts from many sources. A more precise study may be carried out in the future to define the useful range more narrowly. One of the main difficulties in achieving such a wide frequency tuning range is the amount of force that the CTS must generate. For a 2 mm total stroke, the corresponding force is 50 kN, which might add design complexity to some CTS parts and complicate the selection of several mechanical components. For the preliminary design, ESS has chosen an arbitrary maximum stroke of 1.25 mm, requiring the CTS to generate a maximum force of 25 kN.

A kinematic study of the CTS system has been conducted. In the CTS model adopted by ESS, a ball screw system driven by a stepper motor acts on a double lever arm mechanism to provide a much reduced displacement along the beam axis. With this model, it is possible to deal with high forces and fine precision over a long range. Figure 4.62 show the CTS kinetic scheme and the 3D model.

Stiffness and compliance

Several simulations have been performed to define the CTS stiffness along the beam axis, including all of the parts that are subject to mechanical stress from the deformation forces applied to the cavity. Four sub-assemblies are individually subjected to an equal force from the cavity, exclusively along the beam axis, in order to determine their individual compliance. This compliance is divided when several sub-assemblies share the same (or nearly the same) forces. All compliances are then summed when sub-assemblies are fitted in serially from a kinematic point of view. Table 4.20 shows that the results of these simulations are close to the targeted stiffness of 200 kN/mm. Further optimisation will be accomplished by enlarging some mechanical parts, especially on the flange frame, which is exhibits a much higher equivalent compliance than other sub-assemblies. Piezo actuators are often inserted mechanically in series between the cavity and the CTS. In the ESS case, the situation is different due to the force the CTS is required to develop. Consider a 25 kN maximum force to be exerted on the cavity through the piezo-actuators. They would not be able to operate because this value is far above the maximal blocking force found in commercial devices which is around 8 kN for most manufacturers. In order to solve this problem, the ESS design puts the piezo in a rigid lever arm part, as shown in Figure 4.61, which will share the forces applied to the cavity to prevent excessive pressure on the piezo actuators. However, this will reduce the motion provided from the piezo to the cavity. At the present design stage, the piezo-stack size is 36 mm $\times$ 10 mm $\times$ 10 mm.

4.5.3 Fundamental power coupler

The fundamental power coupler for the spoke has the dual role of supplying RF power to the cavity while insulating the cavity vacuum from atmospheric pressure inside the RF line. The core of the spoke power coupler system study is detailed elsewhere [482]. For the ESS double spoke cavity, operated at 8 MV/m, the nominal power for the linac baseline (50 mA, 4% duty cycle) is about 250 kW peak power (10 kW average power). Several upgrade scenarios are being explored for the ESS linac. One upgrade scenario under consideration for the power coupler is a beam current increase to 75 mA. In that configuration, the corresponding RF power requirement is close to 400 kW. A preliminary analysis of possible solutions for the spoke RF coupler has been performed based on recent developments in the EURISOL project. For

this project, a capacitive 352 MHz power coupler has been developed for spoke cavities, which would be mounted on a 56 mm diameter port. A number of window geometries have been studied: cylindrical, disk (with and without chokes) and travelling wave window. For each window type, ANSYS's HFSS software [483] was used to calculate the RF parameters, the surface field on the ceramics, the bandwidth, and the RF losses. An adaptation of this design with a larger coupler diameter has been carried out, to take into account the high peak power requirements and to cope with the increased capability that would be required for a potential upgrade.

Multipacting

Resonant secondary electron emission RF discharge, or multipacting, can disturb the operation of high power microwave generators and particle accelerators. The multipacting phenomenon degrades the frequency response of microwave cavities, thus reflecting the incoming power back to the power amplifier. Multipacting can also cause problems with heating – a result of the RF power dissipated to the device walls as the multipacting electrons strike the walls – which significantly degrades the superconducting properties of the accelerating cavities. It is therefore very important to size each accelerator component to avoid multipacting. The RF power transferred through the coupler to the spoke cavity is 300 kW in CW operation. To accommodate the high peak power requirements and to limit multipacting phenomena between the RF window and the spoke cavity, the coupler diameter must be large. On the other hand, for mechanical and thermal reasons, the coupler diameter cannot be too large. Two studies were performed to determine the optimum diameter for the power coupler. The HFSS software was used to calculate antenna diameters of given 50 Ω and 75 Ω impedances, and different diameters of the power coupler port.

Multipacting in a coaxial waveguide depends mainly on the operation frequency, the power coupler port diameter D, the power coupler impedance Z and the RF power P. The electric field amplitude is lower when the coaxial waveguide impedance is 50 Ω than when it is 75 Ω. The value of the electric field increases as antenna diameter decreases. An analytical formula is used to calculate the maximum RF power. The formula is weighted by a fit corresponding to points of experimental multipacting measurements performed by CERN on the LEP RF power coupler, operating at 352.21 MHz:

$$P_{max} \;=\; (f\,D)^4\,Z \times h\left(\frac{1}{n+1}\right) \tag{4.7}$$

where n is the mode order number and the weight h is a function of $1/(1+n)$. Based on this fit, the SNS RF power coupler design and operating performance have been used as a benchmark to define the ESS optimum power coupler port diameter of 100 mm. A calculation using Equation 4.7 using modes up to eighth order predicts an estimated maximum spoke RF power of about 350 kW.

The final choice for the spoke cavity is a capacitive power coupler mounted on a 100 mm inner diameter port, with an antenna diameter of 43.4 mm, corresponding to a 50 Ω impedance. The maximum peak electric field for 300 kW RF input power in CW is 3 kV/cm inside the air coaxial waveguide. The coupler uses a warm disk ceramic window. Two pipes located on the window outer diameter make it possible to

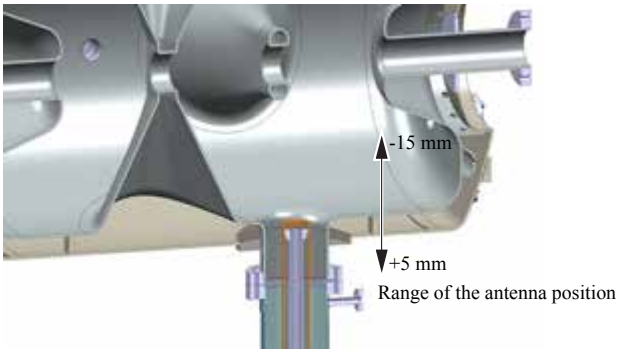

Figure 4.63: The position of the antenna tip can be adjusted relative to the mouth of the spoke coupler port, ranging from 5 mm outside the cavity to 15 mm inside the cavity.

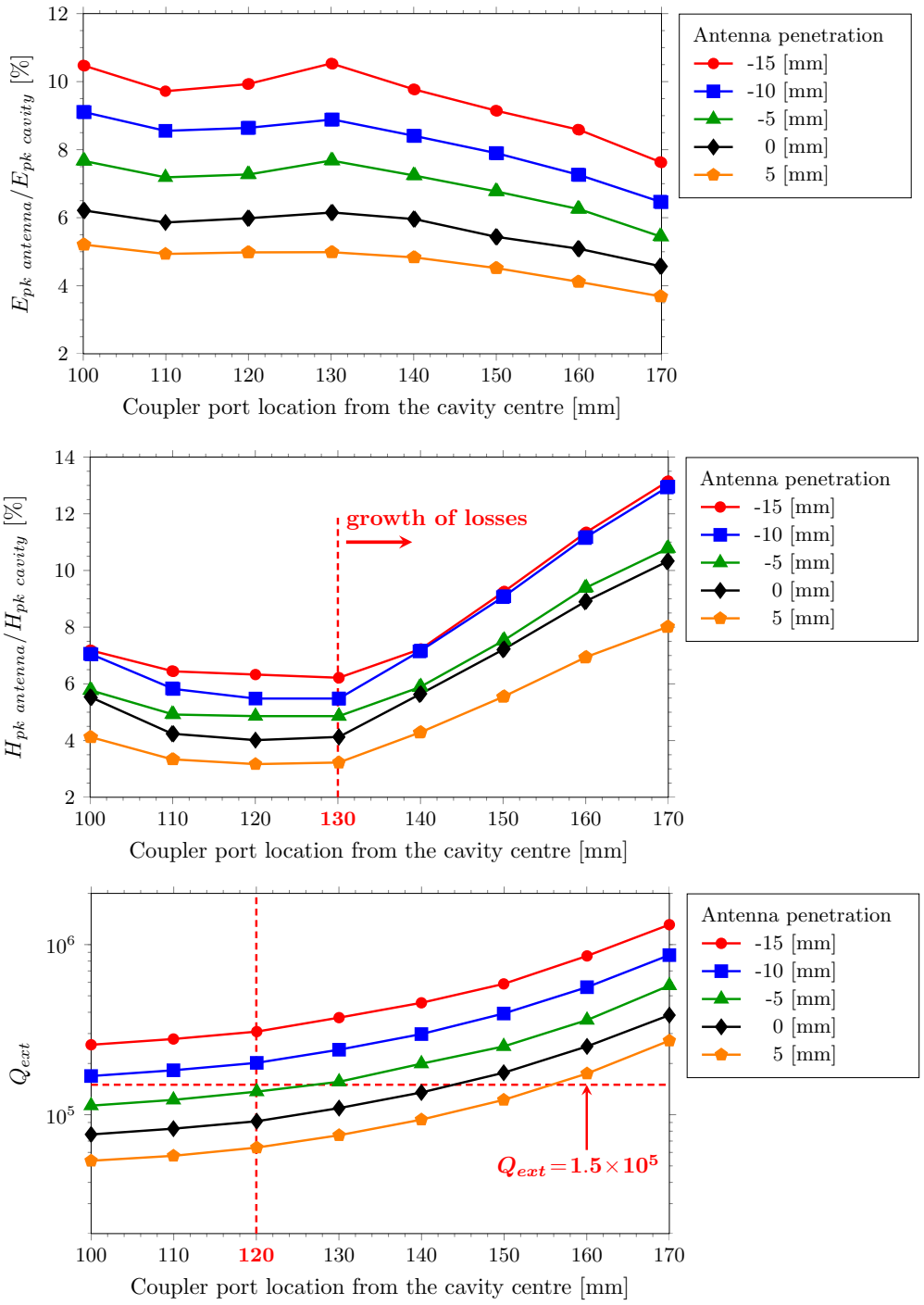

Figure 4.64: Spoke coupler performance versus antenna penetration into the cavity. Top: Peak electric field, E_{pk}. Middle: Peak induction, H_{pk}. Bottom: External coupling factor, Q_{ext}.

air or water-cool the ceramic window. Two of the three diagnostic ports permit the measurement of the vacuum level, and the last port is dedicated to measuring the electronic activity in the area of the ceramic disk when the RF power is travelling through the coupler. Taking these values into account, a range of Q_{ext} values have been calculated that are achieved by varying the antenna tip penetration over a 20 mm range, as shown in Figure 4.63. The peak surface values for the E and B fields on the antenna have been checked for different locations of the coupler port with respect to the cavity centre.

Cavity penetration

The ratio $E_{pk\ antenna}/E_{pk\ cavity}$ varies from 5% to 10% depending on the antenna tip penetration and the location of the coupler port, as shown in the plot at the top of Figure 4.64. For $E_{acc} = 8$ MV/m and $E_{pk}/E_{acc} = 5$, the E_{pk} antenna value is quite low – between 2 MV/m and 4 MV/m. The middle plot shows that the peak surface magnetic field on the antenna is moderate up to 130 mm. Indeed, the coupler port must be integrated to the cavity body below the value of 130 mm. The bottom plot shows that a reference value of 1.5×10^5 can be achieved by setting the coupler port centre to 120 mm from the cavity centre with a 5 mm antenna tip penetration into the cavity. $E_{pk\ antenna}/E_{pk\ cavity}$ is around 7% and $H_{pk\ antenna}/H_{pk\ cavity}$ is less than 5%.

RF window

A coaxial coupler using a single ceramic disk window is well suited for handling the average RF power level of 300 kW in CW operation. The insertion of a ceramic disk inside a coaxial waveguide creates a local mismatch responsible for a partial power reflection. Accordingly, the ESS design modifies and optimises the reflection parameter, S11, for the area around the ceramic disk, so that the maximum RF input power is transferred through the coupler to the spoke cavity. A computed S11 parameter of 61.4 dB is obtained at the nominal frequency. The coupler exhibits a very large bandwidth, approximately 1 GHz, thereby allowing standard fabrication tolerances. The electric field distributions on the window and on the alumina ceramic disk of the RF power coupler are shown in Figure 4.65. The maximum peak electric fields at 300 kW RF input power are 4 kV/cm and 3 kV/cm (in CW operation), respectively, low enough to avoid initiating discharges in the air.

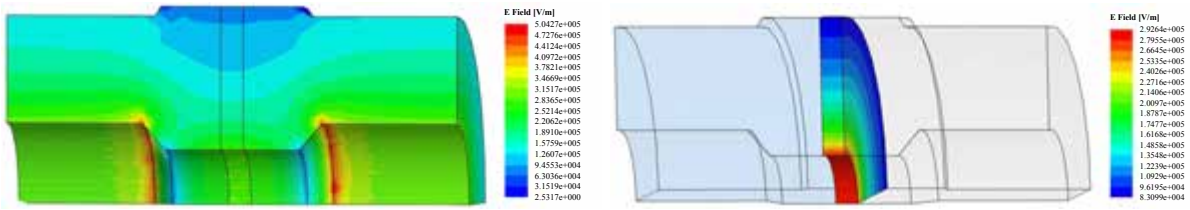

Figure 4.65: Electric field distributions in the spoke power coupler, for an input power of 300 kW. Left: A peak field of 4 kV/cm on the RF window. Right: A peak field of 3 kV/cm on the alumina ceramic disk.

4.5.4 Cryomodules

The RF spoke cavities will be made of niobium enclosed in a titanium (grade 2) liquid helium (LHe) tank. Each SRF spoke cavity will be assembled with its RF power coupler in a clean room meeting ISO 4 standards. Two RF assemblies (SRF spoke cavity + LHe tank + RF coupler), will then then be coupled together via a stainless steel beam line bellow yielding a string of two cavities, as shown in Figure 4.66. To form a complete clean enclosure for future RF operations, two ultra high vacuum (UHV) gate valves will be positioned at each end of this string. The cavity string length from valve to valve is the sum of its components' lengths. Depending on the choice of cold or warm gate valves, cold/warm transitions and dish ends for the cryostat closure may or may not be placed between the RF spoke resonators and the gate valves leading to different lengths of the cavity string. Figure 4.67 shows the length of the spoke cryomodule components, adding up to a total length of 2.900 m. This length dictates the approximate cryomodule length. For the spoke section, the use of cold valves does not increase the section length very much (about 2.1 m).

A spoke cryomodule contains: a cavity string, consisting of 2 SRF spoke cavities inside their helium tanks, 2 RF power couplers, 2 cold tuners, 2 UHV gate valves and optionally including 2 small diameter dished ends for the cryostat closure and two cold-warm transitions; one cold magnetic shield per cavity; a thermal shield; multi-layer insulation blankets covering the cold mass and the thermal shield; several rods for the mechanical anchoring and positioning of the cavity string inside the vacuum vessel; cryogenic piping for the helium distribution inside the cryomodule; vacuum, cryogenic and RF instrumentation for

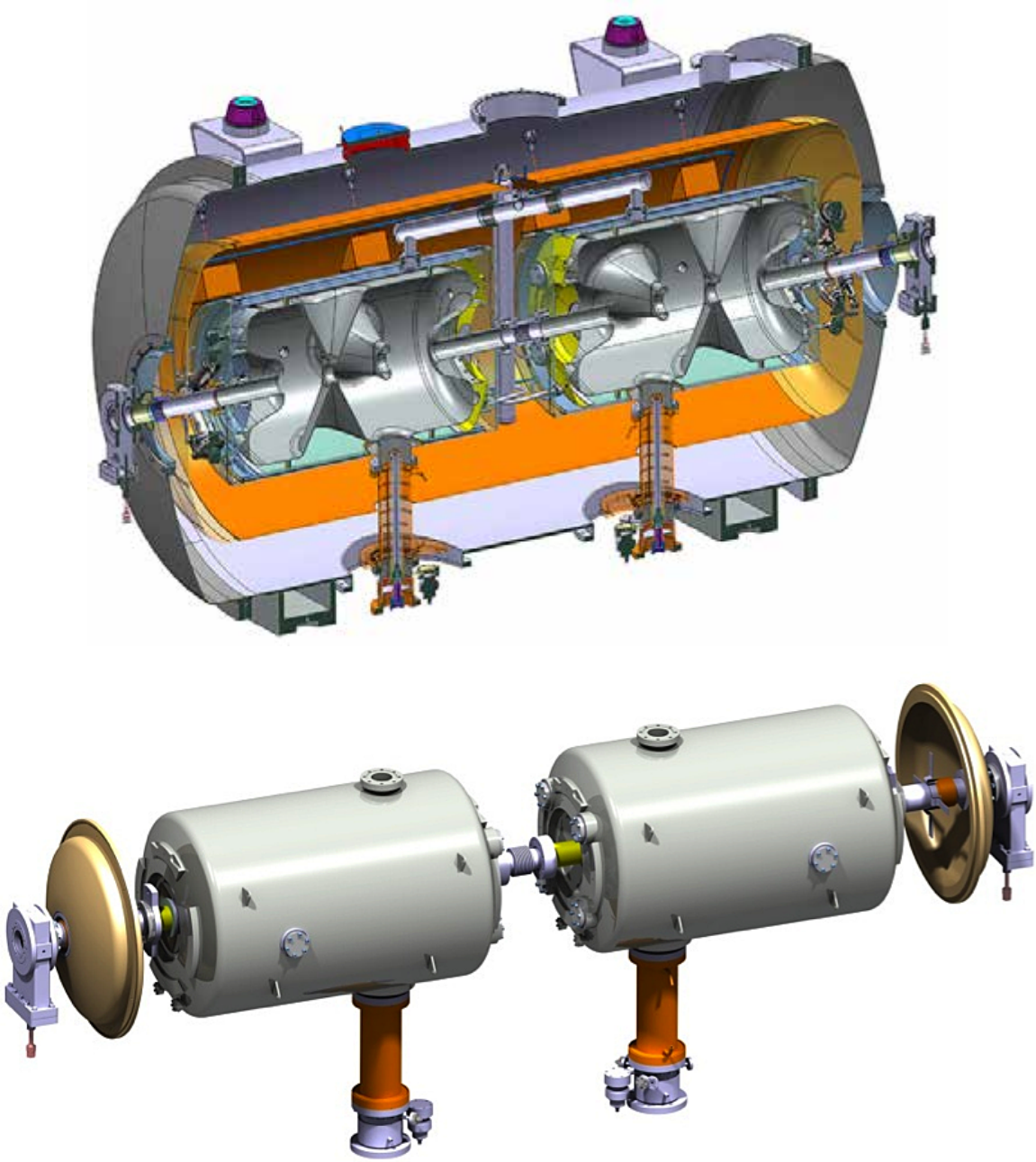

Figure 4.66: A spoke cryomodule string, composed of two spoke cavities. Top: Spoke cryomodule solid model. Bottom: Spoke cavity string assembly.

the cryomodule operations; and a vacuum vessel, equipped with dished ends for the insulation vacuum closure, and alignment devices and several ports for interfacing with the vacuum pumping system, the control and measurement instrumentation, and the safety equipment (relief valves, burst disk, etc.).

Figure 4.68 shows the dimensions of the cryomodule, enclosed by a cylindrical vacuum vessel with dished ends. The cavity string UHV gate valves will be warm valves, located outside the cryomodule. The selection of the warm valve type (rather than warm + cold) necessitates an opening with diameter equal to the valve size on each cryostat dished end. Smaller diameter dished ends, located on each extremity of the string of cavities, were integrated into the design in order to close the vacuum vessel. The dished ends offer the best compromise between space and weight as, being parts of the cavity string, they will be assembled inside the clean room. Dedicated tooling will be designed to handle them.

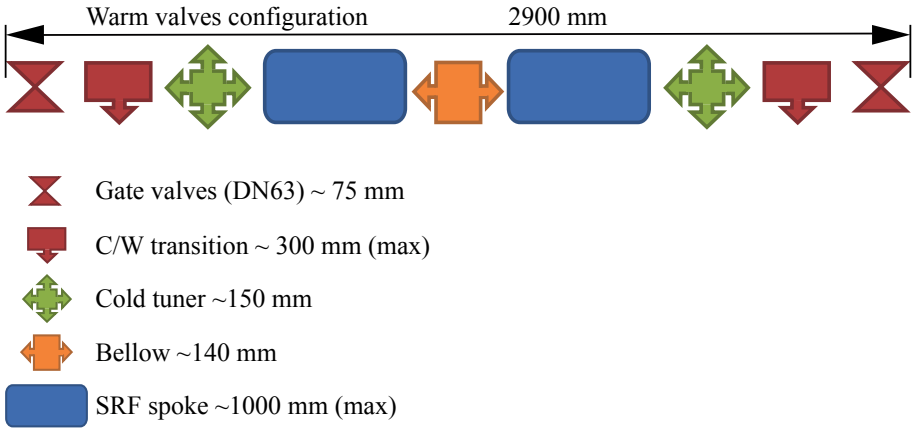

Figure 4.67: Sequence and lengths of the spoke cryomodule components.

Assembly

Different configurations are possible for the coupler orientations and cold tuner positions. Important factors in the choice of configurations include assembly procedure in the clean room and related tooling issues (conceptual design only); distribution of the masses of the string of cavities; support system interfaces; cold magnetic shield interfaces; cryogenic distribution interfaces; vacuum vessel interfaces and dimensions; tunnel interfaces and the tunnel surroundings; RF operations; and maintenance operations. The preferred configuration shown in Figure 4.66 has the RF powers couplers pointing down and centred, and the cold tuners positioned towards the cryomodule ends. During the assembly of the string of cavities in the clean room, RF couplers will be pre-positioned using dedicated tooling designed specifically for this purpose, allowing their pre-alignment, coaxial to within a range of ±1 mm of the nominal position. Vacuum will be established within the cavities before they leave the clean room. Dedicated tooling will also be designed to compensate for the resulting forces on the three bellows. The cryostat diameter of 1300 mm is large enough to accommodate the height of the cavity and power coupler assembly and to permit the insertion

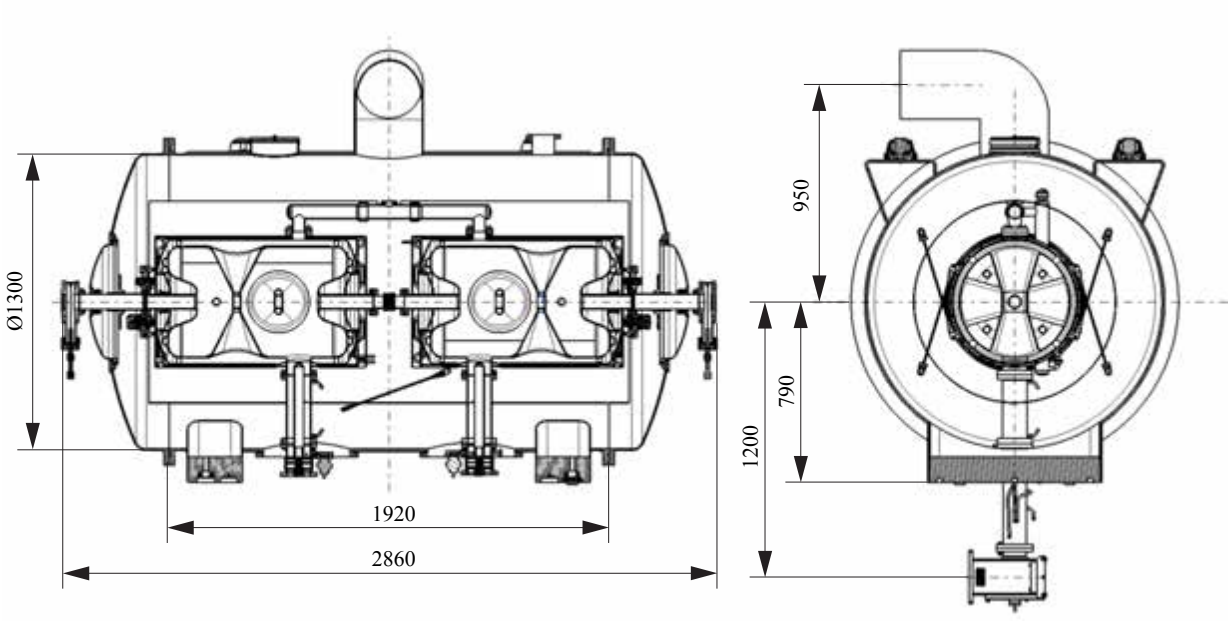

Figure 4.68: Spoke cryomodule cross sectional drawings and dimensions.

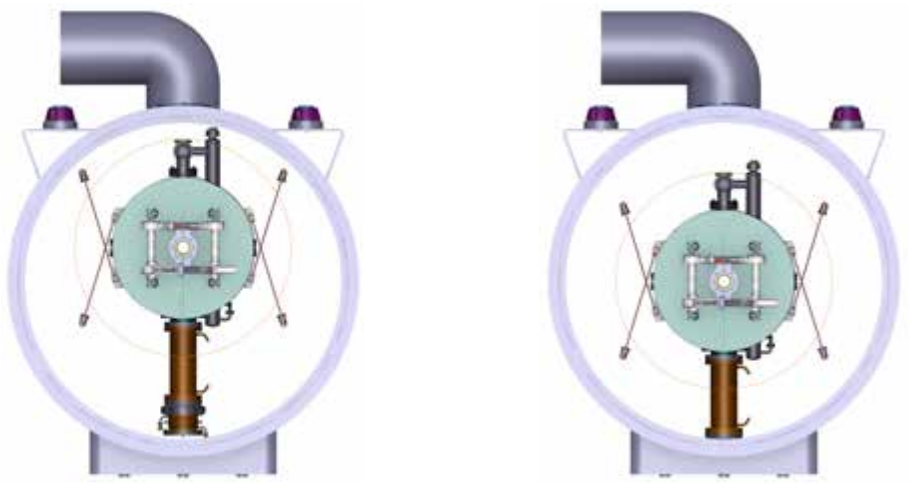

Figure 4.69: Assembling the spoke cavity and power coupler in the cryostat. The diameter of the cryostat accommodates the height of the cavity and power coupler assembly, permitting the insertion of the cavity string into the vacuum vessel. Left: String of cavities during the cryostatting. Right: String of cavities at nominal position.

of the cavity string into the vacuum vessel, as illustrated in Figure 4.69. The vacuum tank wall thickness (currently 12 mm) may be adjusted in the future to fit pressure requirements and requirements for handling, transportation, et cetera.

Three spherical head jacks will support the cryomodule, in order to have an isostatic alignment of the cryomodule. The supporting interface will be used for cryostat levering, support and handling. Taking into account the weight to be sustained and the cavity string length, a supporting system for the cavities based on rods is the preferred solution. This cost effective and already proven solution is compatible with a simple and precise alignment performed from outside the vacuum tank, and makes it possible to correct the alignment at cold temperature. The positioning and alignment of the two cavities with respect to each other will be achieved by means of fixed points placed on the cavities. The mechanical axis of each cavity will be reported on fiducials that will be vertically aligned with the ground supporting devices. These elements will serve as the references for cryomodule alignment inside the tunnel. The main dimensions of the spoke cryomodule are shown in Figure 4.68. Outside the clean room, the cavity string will be built into a cryomodule in three steps. First, the cold magnetic shield (four half shells and a cooling line) is mounted around each spoke cavity's helium tank. Second, the cold tuner is mounted on each spoke cavity. Finally, the thermal shield is placed around the string of cavities and the assembly is inserted into the vacuum vessel using dedicated tooling.

Component	**Static heat load at 50K** [W]	**Static heat load at 2K** [W]
Thermal shield (incl. mag. Shield)	10.0	0.4
Supporting system (rods)	4	0.2
Warm to cold transitions (2 items)	6	0.4
Safety equipment (relief valve and bursting disk)	4.1	0.25
Control valve (3 items)	3	1.5
Two power couplers	–	2.0
Instrumentation	8.0	0.2
Total	35	5

Table 4.21: Static heat loads for the spoke cryomodule. Magnetic shields surround the helium tank of the cavities.

Heat load and cryogenics

Table 4.21 summarises results from estimations of the estimated static heat loads in the spoke cavity cryomodule. The dynamic heat loads are estimated to be 2 W for each of the spoke cavities when the RF and the beam are on, adding to the 1 W/m (or less) of beam losses. The total heat load (equivalent at 4.5 K) for the spoke cavity cryomodule is estimated to be 44.2 W. The spoke cavities are maintained at 2 K in a helium-II bath generated by isenthalpic expansion, through Joule-Thomson valves. The flow process is discussed in Section 4.4.1.

4.6 Elliptical cavities and cryomodules

The superconducting linac contains two types of elliptical cavities, medium-β and high-β, that accelerate the beam from the spoke superconducting linac at 201 MeV up to full energy at 2.5 GeV. The linac layout optimisation has been carried out taking into account the limitation of SRF cavity performance due to electronic field emission. This is reflected in the choice of parameters such as the maximum accelerating gradient E_{acc}, and the peak electric field on the surface E_{pk}. The power couplers run derated, ensuring that it is possible to add a 30% power margin for cavity voltage stabilisation. The medium-β and high-β cryomodules are composed of 60 and 120 elliptical cavities, with β values of 0.67 and 0.92, and operating gradients of 15 MV/m and 18 MV/m, respectively. The duty cycle for the elliptical SRF cavities is expected to be about 4.5%. Elliptical cavity parameters have been chosen taking into consideration not only the state-of-the-art performance of bulk niobium cavities, but also the actual performance of cavities in operating linacs, reflecting the commonly observed on-line performance yield, which differs from the yield observed in single cavity vertical tests.

The maximum surface electric field (E_{pk}) specification is linked to the expected electronic field emission (FE) in elliptical cavities. High pressure water rinsing (HPWR) has proven to be the most efficient processing step to push the FE onset to a sufficiently high gradient so that it is not the main cavity performance limitation. The largest available set of multi-cell, high gradient cavities consists of 9-cell, 1.3 GHz cavities, of the type used in a number of X-ray free electron lasers (XFEL), first developed for use at the TESLA facility in Hamburg, Germany. Using state-of-the-art preparation and cleaning techniques, several laboratories have proven that accelerating gradients at the XFEL specifications (E_{acc} = 23.6 MV/m, corresponding to E_{pk} = 47 MV/m, and B_{pk} = 100 mT) can be obtained on series production. The usable gradient yield statistics from a 50 cavity production run [484] show that a 20 MV/m gradient (corresponding to 40 MV/m peak surface electric field) has been obtained for about 80% to 90% of the cavities. In most cases, field emission-limited cavities can be reprocessed with extra steps of HPWR with an 80% success rate. ESS elliptical cavity peak field specifications are about 20% lower than XFEL values, to ensure a high performance yield despite the larger cavity size and lower βs. Table 4.22 shows the main parameters for the medium-β and high-β cavities. The medium-β cavity package shares most of the mechanical features of the high-β cavity package, including the features of the helium tank, tuner, power coupler, and magnetic shield. The only important difference is the total length, which is shorter for the medium-β package.

Magnetic shielding

One component of the RF surface resistance of the superconducting niobium is due to the magnetic flux trapped during cool down at the moment of the cavity's transition from the normal to the superconducting state. In order to reduce the power dissipated by the cavity, one has to shield the cavity from the external magnetic field. The sensitivity of the niobium surface resistance at 700 MHz to the magnetic field is:

$$\frac{dR_s}{dB_{res}} = 0.3\ [\mathrm{n\Omega/mG}] \tag{4.8}$$

The goal is to limit this component of the surface resistance to a maximum of about 10% of the total surface resistance of $R_{s\ tot}$ = 40 nΩ at 700 MHz and 2 K. The resulting maximum acceptable residual magnetic field on the cavity is therefore $B_{res\ max}$ = 14 mG. Preliminary studies have investigated several options for magnetic shields, including shields at 300 K, shields at cryogenic temperature, and combinations of both types of shield. Calculations were made under the assumption that the magnetic field surrounding the cavity is that of the earth at Lund, (0.5 Gauss, no magnetic component close to the cavity) and that

Parameter	Unit	Value
RF frequency	MHz	704.42
Temperature	K	2
MEDIUM-BETA		
Output energy	MeV	654
Number of cells per cavity		5
Geometric β		0.67
Cavity length	m	1.145
Expected gradient, horizontal	MV/m	15
Expected gradient, vertical test	MV/m	17
Cavity Q_0		6×10^9
Fundamental mode Q_{ext}		6.8×10^5
Fundamental mode R/Q	W	340
Average heat load at nominal gradient	W	5.9
Power coupler power forward power	MW	1.2
Maximum Power transmitted to beam	MW	0.6
HIGH-BETA		
Output energy	MeV	2500
Number of cells per cavity		5
Geometric	β	0.9
Cavity length	m	1.356
Nominal gradient in the linac	MV/m	18
Expected gradient, vertical test	MV/m	20
Geometric β prototype		0.86
Optimum β prototype		0.92
Cavity length prototype	m	1.315
Fundamental mode R/Q prototype	W	477
Fundamental mode Q_{ext} prototype		7.1×10^5
Cavity Q_0 at nominal gradient, prototype		6.0×10^9
Average heat load at nominal gradient, prototype	W	4.5
Power coupler power rating	MW	2
Power coupler forward power	MW	1.2
Maximum power transmitted to beam	MW	0.9
Cell to cell coupling	%	1.8
E_{pk}/E_{acc}		2.2
B_{pk}/E_{acc}	mT/(MV/m)	4.3
Separation between π and $4\pi/5$ modes	MHz	1.2
Iris diameter	mm	120

Table 4.22: Medium-β and high-β elliptical cavity parameters.

this field is parallel to the cavity axis, which represents a worst case scenario. This preliminary study led to the choice of a cold magnetic shield fixed around the helium tank of the cavity, in the vacuum tank. No special equipment is foreseen to enhance the rate of shield cool-down, except the thermal contact with the helium tank. The chosen material ensures good efficiency of the shielding over the critical range of temperature.

Cavity design

One of the main parameters in the design of a multi-cell cavity is the cell-to-cell coupling, κ. Choosing a low κ value enhances cavity efficiency, but at the expense of other desirable features. With increasing κ, it becomes easier to achieve an even field distribution in the cavity, and therefore to control the homogeneity of the peak surface fields among the cells. The frequency separation between the accelerating mode and its neighbour is also increased. Even more important for a high current application, the high κ translates into higher iris diameters, and better higher order mode (HOM) propagation. Designs have been investigated

with κ values ranging from 1.1% to 2.5% for the $\beta = 0.86$ cavity. These investigation lead to conclusion that the loss in cavity efficiency is excessive above $\kappa = 2\%$. One important geometrical parameter for designing a multi-cell elliptical cavity is the wall angle, which is related to mechanical stability, sensitivity to Lorentz force detuning and the ease of cavity preparation (chemical etching, HPWR and drying) which is of key importance for achieving cavity performances. Based on experience with $\beta = 0.50$ and $\beta = 0.65$ cavities, for which wall angles between 5.5 degrees and 8.5 degrees [485, 486] have been explored, ESS has specified a minimum wall angle of 8 degrees. This requirement restricts the range of geometrical cell parameters accessible for cavity optimisation for peak fields, in particular. The main RF cavity parameters are shown in Table 4.22. Taking into account the cryogenic duty cycle (4.7%), the average power dissipated in one cavity on the accelerating mode at 18 MV/m is less than 4.5 W at the $Q_0 = 6 \times 10^9$ specification. The fundamental passband modes impedance are shown in Figure 4.70. Apart from the accelerating mode, only the $4\pi/5$ mode has significant impedance in the energy range of the high-β section, from $\beta = 0.76$ to $\beta = 0.96$. This is unavoidable in this type of cavity.

External coupling and end-groups

The matched external coupling factor $Q_{ext} = 7.1 \times 10^5$ at the specified beam current and nominal gradient. The power coupler connection is a 100 mm, 50 Ω coaxial line. The nominal Q_{ext} value is achieved by combining a 140 mm beam pipe diameter with a conical-shape coupler tip with a penetration of 7 mm into the beam tube, as shown in Figure 4.71. One benefit of using a large beam tube diameter is the reduction of the cut-off frequency for the higher order modes (HOMs). The cavity has identical end cells with straight beam pipes to fully exploit this possibility. Calculations of higher order modes in the cavity

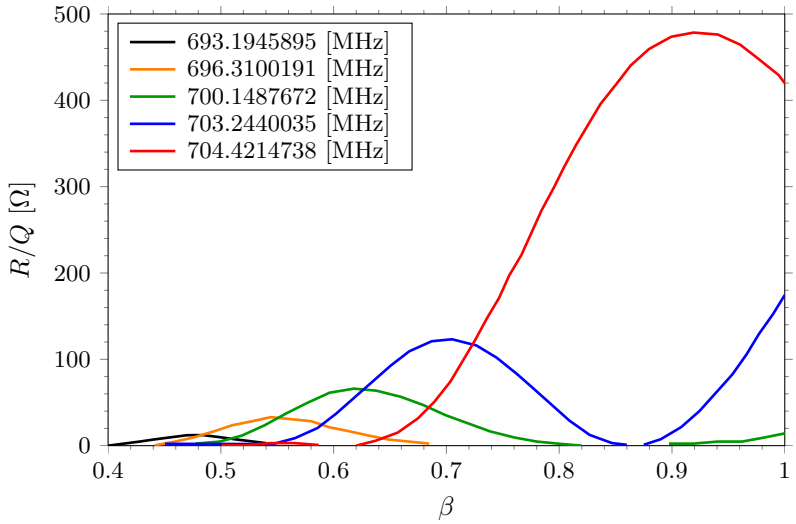

Figure 4.70: Fundamental passband modes in the high-β elliptical cavity, showing R/Q as a function of β. Only the $4\pi/5$ mode has a significant impedance in the range of interest, from $\beta = 0.76$ to $\beta = 0.96$.

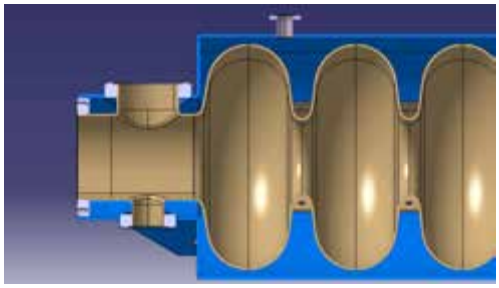

Figure 4.71: Geometry of the high-β elliptical cavity, showing the power coupler port and the titanium helium tank.

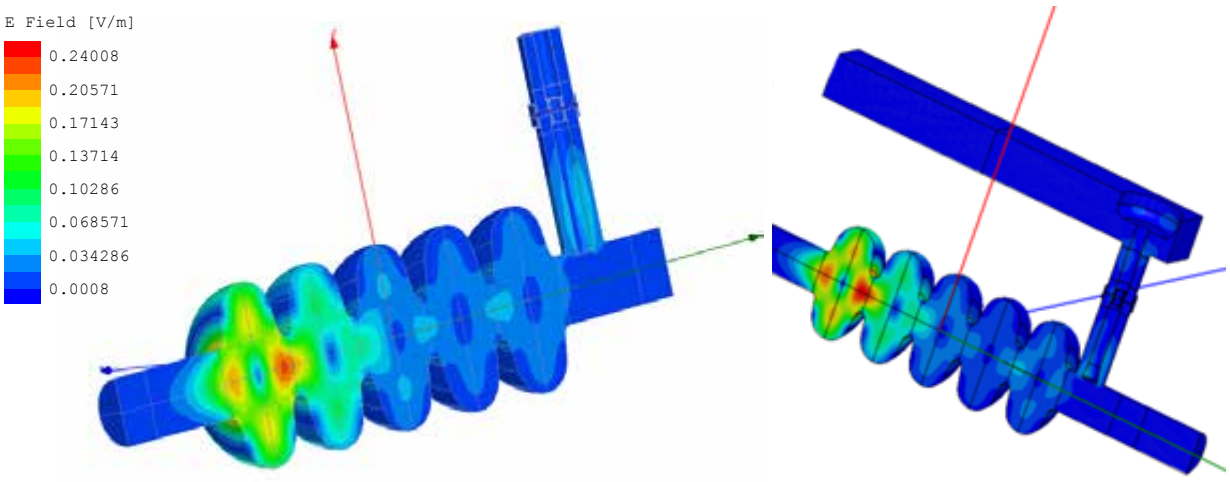

Figure 4.72: Electromagnetic simulations of TM monopole modes in an elliptical cavity. Left: A matched wave guide, with the lowest frequency TM monopole mode at 1420.3 MHz, the closest to the second harmonic of 704.42 MHz (12 MHz away). Right: Unmatched case of a doorknob and a shorted-end wave guide, with the lowest frequency TM monopole mode at 1420.3 MHz.

have been performed with a focus on TM monopole modes, since their excitation is more relevant than the excitation of dipole modes for the beam dynamics in a proton linac [440,487]. The monopole modes of the cavity have been computed using three different RF codes in 2D and 3D with consistent results. Only two HOM monopole bands are below cut-off. At the closest approach, a monopole HOM is 12 MHz above a machine line.

In order to assess the damping provided by the normal conducting parts of the power coupler and bellows located between cavities, these elements have been included in the EM simulations. The RF window of the power coupler, the doorknob waveguide transition and a length of rectangular waveguide terminated by a matched load have been included in the simulation in order to take into account the full coupler transmission characteristics. The simulations in this ideal case indicate that the loaded Q's of the non-propagating monopole HOMs of a single cavity are all in the 10^4 to 7×10^5 range. These low values are

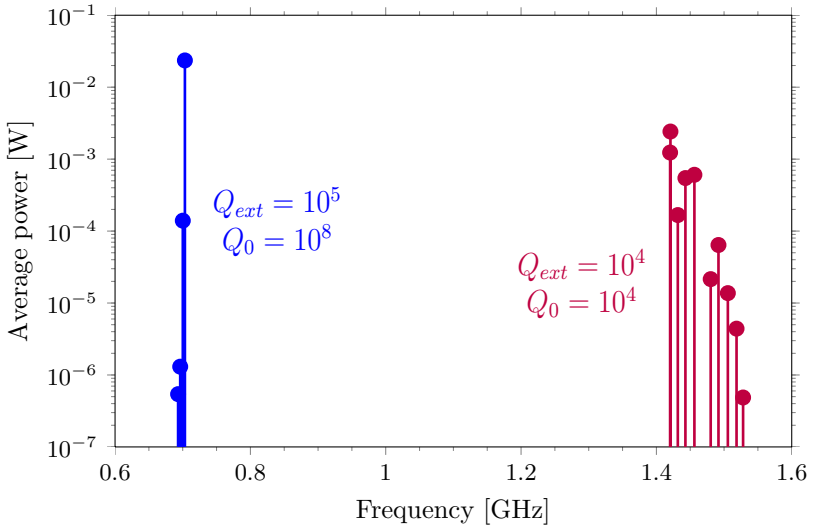

Figure 4.73: Worst-case analysis of average power deposited for elliptical cavity modes below cut-off frequency.

explained by losses on copper surfaces of the power coupler and inter-cavity bellows and by transmission through the RF window.

In reality, the RF network cannot be represented adequately by a matched load over the whole frequency domain considered here. Hence, a worst case scenario has been studied with a rectangular wave-guide terminated by a shorted end, as illustrated in Figure 4.72. The Q_{ext} values obtained in this case are higher than those calculated for the matched case, but they remain in the 10^4 to 10^6 range. The RF power deposited by the beam for the modes below frequency cut-off was also calculated using analytic formulae from Wilson and Biarrotte [488], using nominal beam parameters. The results of this worst-case analysis are shown in Figure 4.73, which plots the average deposited power for the modes under cut-off. The values get even lower when the Q-values are higher than those illustrated in the figure. Thus, it is reasonable to expect values for the average power deposited by the beam lower than 0.02 W, which is comparable to the average power deposited in the fundamental mode, equal to 30 kW. All these simulation results lead to the conclusion that none of the monopole modes below cut-off need extra damping with HOM couplers. However, the two prototype cavities will be equipped with two HOM coupler ports, in order to make possible RF measurements of HOM in real cavities.

4.6.1 Mechanical design

An overview of the elliptical cavity package is shown in Figure 4.74, with emphasis on the cold tuning system. The core of the elliptical cold tuning system study is detailed elsewhere. The helium tank is made of titanium, and the flanges designed for aluminium gaskets are made of niobium-titanium. The tuner is inserted between the cavity flange and the helium tank, similarly to the arrangement in the SPL cavity design with $\beta = 1$ [489]. The tank extends to the beam tube flange on the power coupler side and is stiffened with a series of fins. This layout, shown in Figure 4.71, enhances the ability to set the coupler port as close to the first cavity iris as needed to achieve the correct coupling coefficient for the nominal beam power, and also for potential upgrades. The computed stiffness of the helium tank is 70 kN/mm. Before operation, the cavity must be subjected to safety pressure tests while at room temperature, which elucidate how it may be plastically deformed. The plastic deformation of the cavity during a 5 MPa pressure cycle was evaluated in a test rig. Figure 4.75 shows the distribution of the stress within the cavity cell wall for 0.5 MPa differential pressure. The maximum von Mises stress is 54 MPa, while the maximum deformation is 0.235 mm. The maximal residual deformation is less than 7 μm, which should not be detrimental to the field distribution on the fundamental mode. The parameter $K_P = \Delta f/P$ measures the resonance frequency shift induced by the differential pressure P between the outside and inside of the cavity. The coefficients given in Table 4.23 correspond to elastic deformation, which occurs when the cavity is operated in the cryomodule.

Two prototype cavities will be manufactured and tested in a vertical cryostat. They will be built from high purity bulk niobium sheet with a residual resistivity ratio greater than 250. All flanges are made of niobium-titanium 45/55 alloy directly weldable to niobium. The two prototypes will be equipped with two HOM 50 mm diameter ports making it possible to make RF measurements of HOMs.

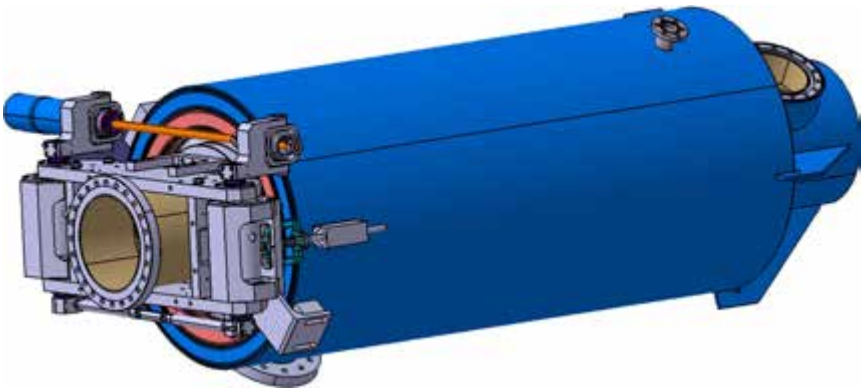

Figure 4.74: High-β elliptical cavity with titanium helium tank and integrated piezo tuner.

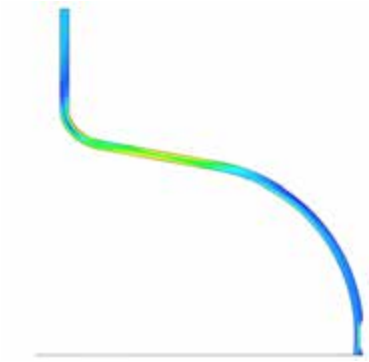

Figure 4.75: Distribution of stress within the elliptical cavity cell wall for 0.5 MPa differential pressure when the ends of the cavity are fixed.

Parameter	Unit	Value
K_L with fixed ends	Hz/(MV/m)^2	-0.36
K_L with free ends	Hz/(MV/m)^2	-8.9
Stiffness	kN/mm	2.59
df/dz	kHz/mm	197
Max von Mises stress per mm elongation	MPa/mm	25
K_P with fixed ends	Hz/mbar	4.85
K_P with free ends	Hz/mbar	-150
Max von Mises stress per bar, fixed ends	MPa/bar	12
Max von Mises stress per bar, free ends	MPa/bar	15

Table 4.23: Mechanical characteristics of the elliptical cavity.

4.6.2 Cold tuning system

Since these cavities are designed to work in pulsed mode, it is important to minimise their sensitivity to Lorentz detuning. To this end, the design calls for stiffening rings to be placed between the cavity cells. The static Lorentz detuning coefficient, $K_L = \Delta f / E_{acc}^2$, measures the resonance frequency shift produced by the mechanical deformation induced by the electromagnetic field in continuous wave excitation. The positions of the stiffening rings and the cavity thickness have been optimised in order to minimise $|K_L|$ when the cavity has fixed extremities. The result is a cavity thickness of 3.6 mm and a stiffening ring radius of 84 mm. With these values, $|K_L| = 0.36$ Hz/(MV/m)^2 for a cavity with fixed ends. An exhaustive list of the corresponding RF and mechanical parameters is given in Table 4.23.

The static Lorentz detuning coefficient depends upon the external stiffness, K_{ext}, experienced by the cavity during operation, which is given by the combined stiffness of the tuner and helium tank. Taking into account the design stiffness of the tank and the measured stiffness of the Saclay V tuner [490], the expected K_{ext} value is about 23 kN/mm. Figure 4.76 shows the variation of the K_L with respect to K_{ext}, according to the formula:

$$K_L = K_{L\infty} + \frac{df}{dz} \frac{\overrightarrow{F_\infty}.\overrightarrow{u_z}/E_{acc}^2}{K_{ext} + K_{cav}} \tag{4.9}$$

The dynamic Lorentz detuning in pulsed operation will be compensated by a fast tuning system, using a Saclay V-type piezo tuner, which has been successfully used for Lorentz detuning compensation in pulsed mode with the 5-cell HIPPI cavity at $\beta = 0.5$ and a frequency of 704 MHz [490]. Similar tuners were also developed and manufactured for the SPL 704 MHz cavities at $\beta = 1$. The piezo elements are 30 mm long stacks with a blocking force of 4 kN, and are able to produce a 3 μm stroke at temperatures below 10 K for a maximum operating voltage of 200 V. In order to ensure a controlled efficiency of the piezo fast tuning system, the preload applied by the frame on the piezo stack is independent of the cavity spring-back force. The Saclay V-type tuner works at cryogenic temperature inside the insulating vacuum tank. It is a

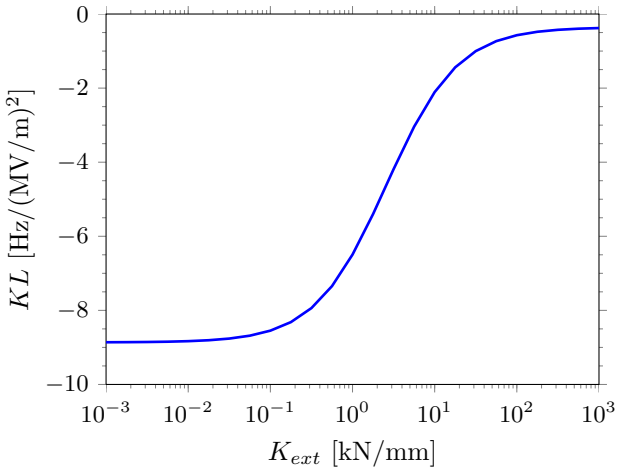

Figure 4.76: Variation of the static Lorentz detuning coefficient of the elliptical cavity, K_L, with respect to the external stiffness, K_{ext}.

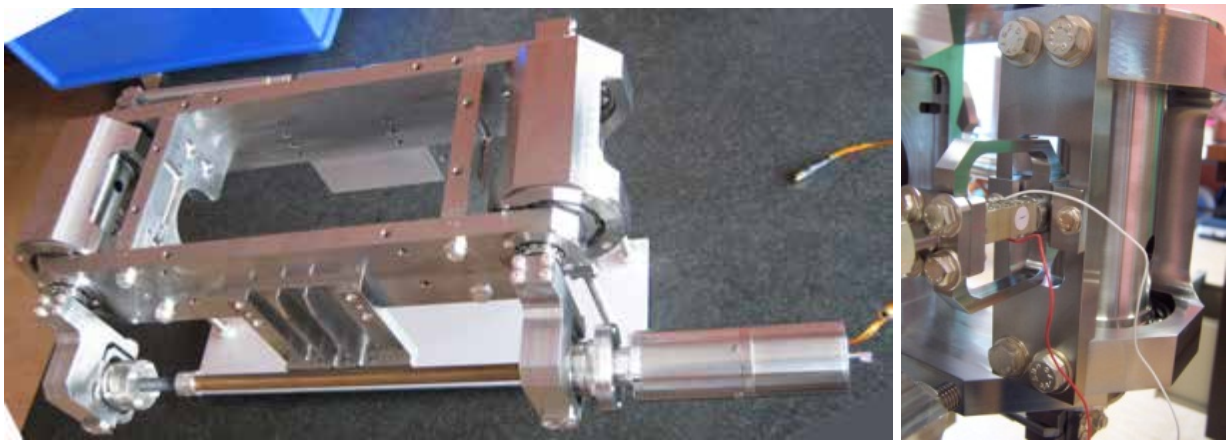

Figure 4.77: Elliptical cavity cold tuning system. Left: Slow tuning mechanism. Right: Piezo stack with the tuner mounted on the cavity.

double lever system driven by a screw with a stepper motor and a planetary gear box. Figure 4.77 shows the proposed slow tuning mechanism. All the surfaces subject to friction are treated with a dry lubricant coating that is efficient at cryogenic temperatures. The tuning range of the slow tuner is ±600 kHz.

4.6.3 Fundamental power coupler

A detailed description of the elliptical cavity power coupler system study is given elsewhere [491]. Thanks to the very low dissipation of power in an SRF cavity, the RF power transferred through the coupler to the cavity is almost entirely converted into beam power. The high-β elliptical cavity linac section run at a maximum gradient of 18 MV/m is the most demanding section for power couplers, with the parameters shown in Table 4.24.

Parameter	**Unit**	**Value**
Nominal peak input power	kW	900
Maximum admissible input power	kW	1200
Maximum duty cycle	%	10

Table 4.24: Elliptical power coupler specifications.

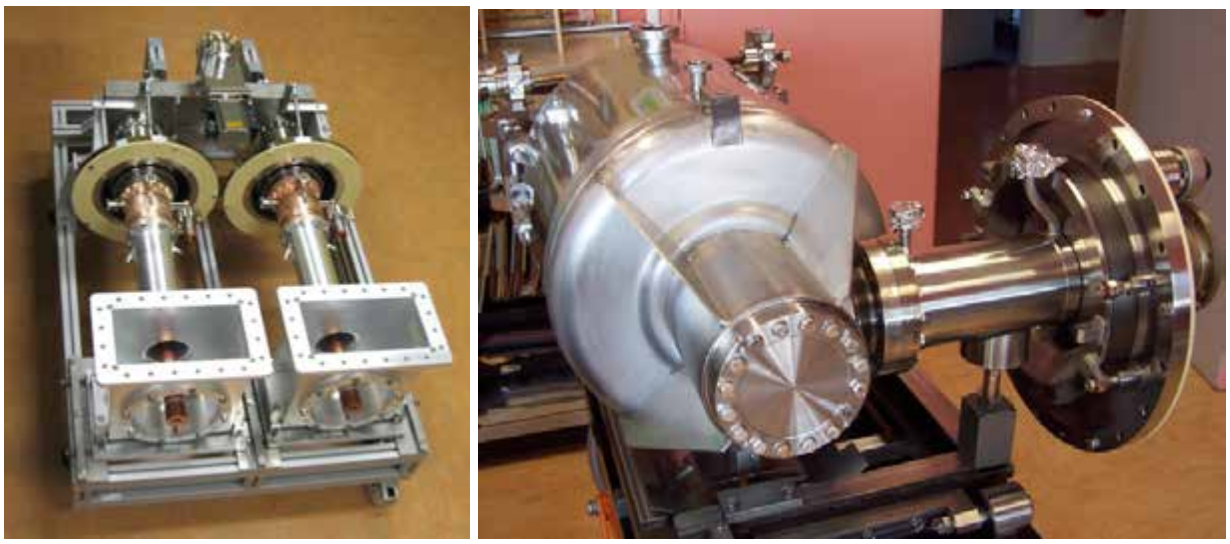

Figure 4.78: Prototype elliptical power coupler tests. Left: CEA-Saclay's 1 MW power coupler. Right: The $\beta = 0.5$ HIPPI cavity equipped with the CEA-Saclay 1 MW power coupler in preparation for the RF power tests in the horizontal cryostat at CryHoLab at Saclay.

Coaxial couplers using a single ceramic disk window are suited for handling both peak power and average power when equipped with active cooling. The 508 MHz KEK-B coupler type stands out as a sound design for handling power levels of hundreds of kilowatts in CW [492]. The KEK design has been adopted for the SNS power coupler specified at a peak power of 550 kW for a frequency of 805 MHz [493]. The 81 couplers of the SNS have proven to operate reliably since the machine's commissioning [494]. A coupler initially specified to handle 1 MW peak power at 704 MHz and a 10% duty cycle has more recently been designed at Saclay following the same RF design principles, and upgrading the cooling of the inner conductor. Prototypes have been tested up to the ESS specifications on a room temperature stand, as shown in Figure 4.78. Tests on an SRF $\beta = 0.5$ have also been carried out up to 1 MW in full reflection mode, which is the most demanding case for peak fields and power dissipation in the coupler [495]. ESS plans to test a pair of these couplers up to 2 MW peak power in order to evaluate the operational margins in terms of peak power. The design of the ESS coupler is directly derived from the HIPPI coupler. The main differences lie in the mechanical interfaces with the cryomodule vessel, the reduced length of the air-side coaxial waveguide, and the cooling channels. The original design was based on water cooling, so the cooling channels of the inner conductor were not optimised for air cooling. However, tests conducted in full reflection mode on a cavity using air cooling have been carried out up to 35 kW average RF power without problems. If air is chosen over water as the cooling fluid, the cooling channels will be modified in the ESS design to achieve a better efficiency with air cooling. The shorter air side coaxial part already reduces RF dissipation and improves the conductance of the channels for air flow.

The coaxial coupler has an outer diameter of 100 mm and an impedance of 50 Ω. The RF window is built around an alumina disk matched with chokes on both the inner and outer conductors. Its transmission characteristics show a very large bandwidth around the nominal frequency. The rectangular waveguide-to-coaxial transition is of the doorknob type, a configuration that is most convenient for the interconnection of the cooling channels of the inner conductor and for the installation of a high voltage capacitor, as shown in Figure 4.79, which also shows the electric field distribution in the transition. The capacitor applies a DC bias on the antenna in case a multipacting barrier coincides with the particular power level of a given cavity. The doorknob RF design helps reduce the peak electric field on the conductors in order to avoid discharges in the air. The maximum peak electric field at 1.2 MW RF input power is 12 kV/cm. The connection between the RF window and the cavity is ensured by a stainless steel double walled tube, which acts as the outer conductor of a coaxial line. Its inner surface is copper plated to minimise RF losses. The double wall encloses the helium gas cooling channels necessary to reduce the static losses to the 2 K temperature of the coupler and to remove the heat produced by the RF dissipation in the copper layer.

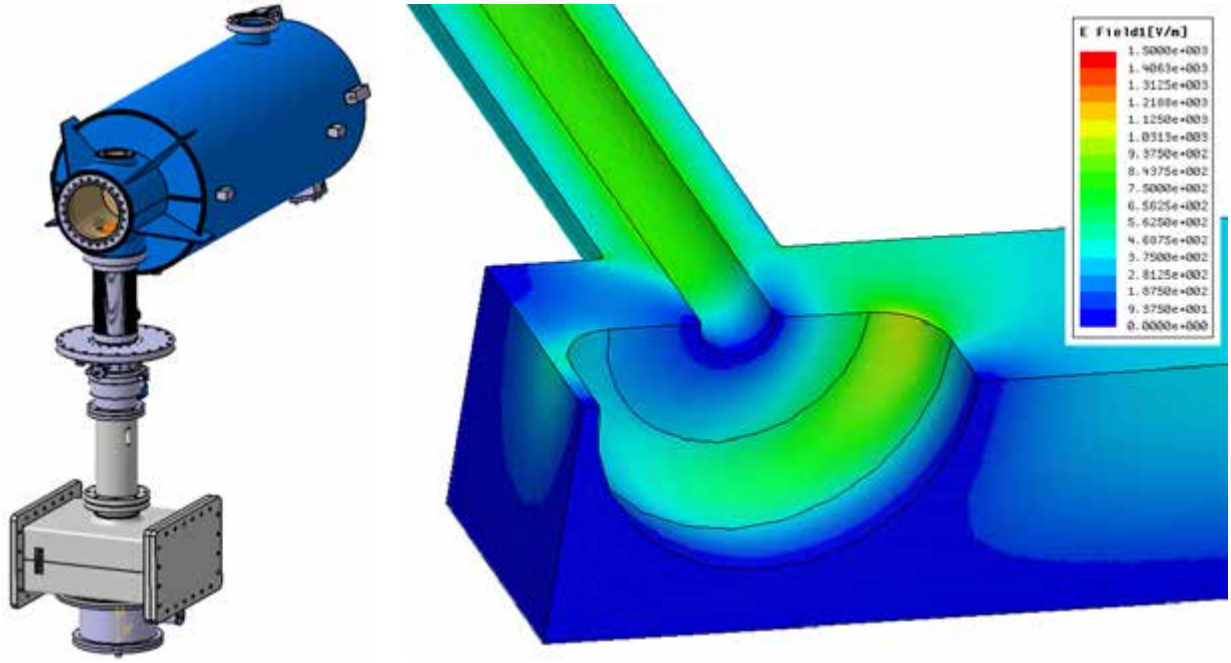

Figure 4.79: Elliptical cavity with power coupler door-knob transition and biasing system. Left: Waveguide-to-coaxial transition. Right: Electric field distribution in the doorknob transition.

4.6.4 Cryomodules

Both the medium-β and the high-β cryomodules house four cavity packages. For the sake of consistency, the cryomodule design shown below is the high-β cavity cryomodule designed for $\beta = 0.86$ cavities. Figure 4.80 shows sketches of the elliptical cryomodule. As in the SNS cryomodule design, the general layout is based on the use of a space frame supporting the cold mass inside the vacuum vessel. The space frame is kept at 300 K inside the insulating vacuum. It is centred within the vacuum vessel axis by three jacks around the diameter of the vacuum vessel and at four levels along the axis of the vessel. During assembly, it is open at the bottom, in order to enable the insertion of the cavity string after clean room assemblage with the power coupler at the bottom. The openings are ultimately closed to increase stiffness. Each cavity is supported by two sets of four cross rods to keep the cavity axis oriented along the beam axis, and by two sets of two axial rods for longitudinal alignment. The thermal shield is held in the frame by insulated supports. The frame allows easy insertion of the cavity string into the vacuum vessel with minimal risk of disturbing the pre-established alignment. Figure 4.81 shows the results from calculations of frame deformations that were performed taking into account the weight of the cavities and of the frame itself, as well as the 3000 N pre-tension applied by each rod. The maximum calculated stress, 65 MPa, is acceptable regardless of the mechanical characteristics of the steel. The cavities are suspended inside the space frame by eight rods located in two cross planes and constrained longitudinally by four more.

The hanging rods shown in Figure 4.82 ensure the positioning and the stability of the cavities at ambient and at low temperatures. They support high mechanical stress values and also limit heat conduction. The transverse and axial rods are about 400 mm and 800 mm long, respectively. The axial rods fix the coupler position during the cool-down, and ensure stability during cold tuning system operation. The cross rods have the biggest mechanical stress values and the highest heat conduction due to their shorter length. Mechanical and thermal calculations have been made only for these components. The rods are made out of titanium TA6V, a material that offers a good compromise between heat conduction and mechanical properties. It provides low heat conductivity over the whole temperature range between 300 K and 2 K (7.56 W $m^{-1}K^{-1}$ to 0.233 W $m^{-1}K^{-1}$). It has a small thermal shrinkage coefficient of 0.0017; a low Young modulus of 110 GPa; and a high yield strength of 1040 MPa. Four types of mechanical stress have been taken into account in the design process: 3000 N pre-tension; weight of the cavities assembly; atmospheric pressure on the coupler; and low temperature shrinkage. Pre-tension provides stability during

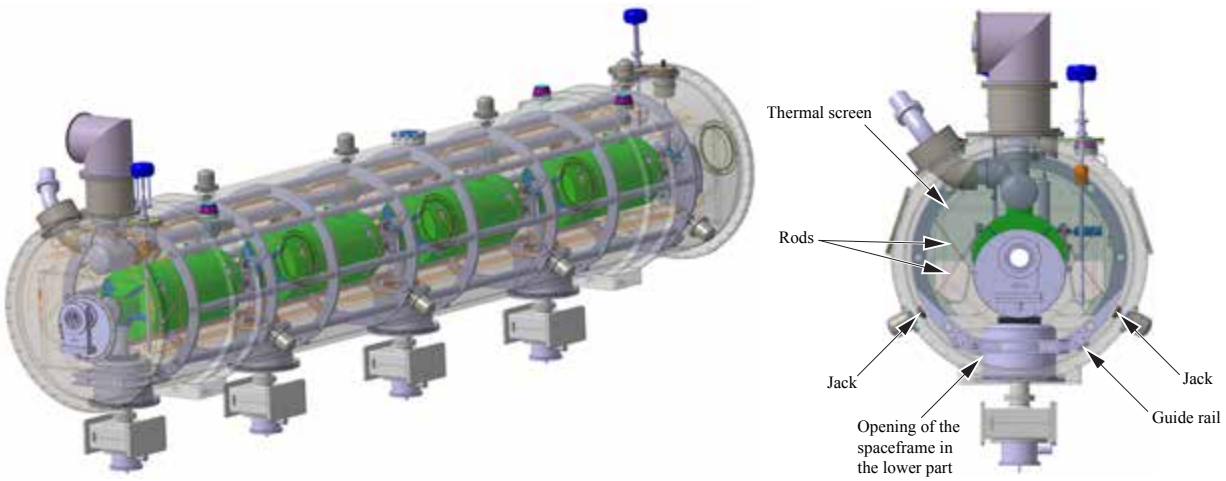

Figure 4.80: Sketches of the high-β elliptical cavity cryomodule. Left: Four cavities in one cryomodule. Right: Cross section of the cryomodule.

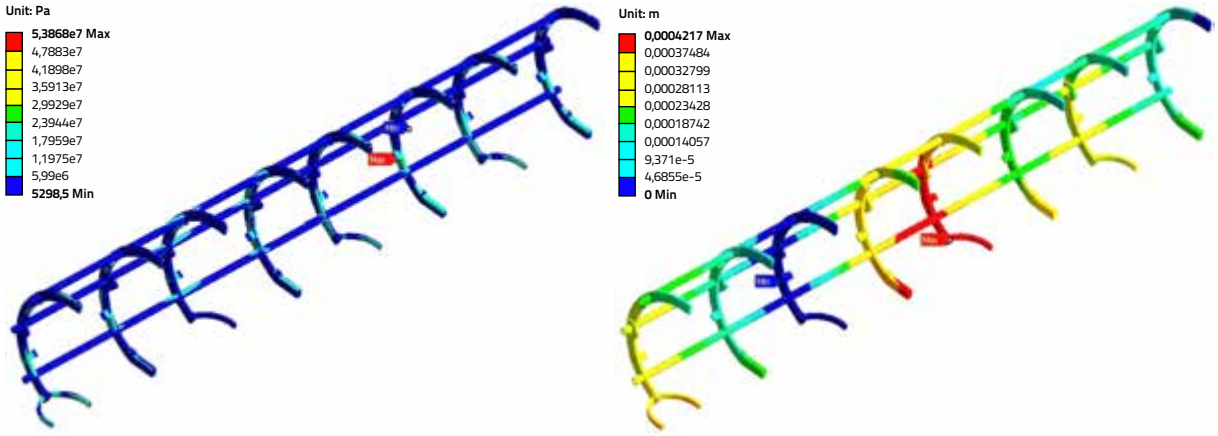

Figure 4.81: Deformations of the elliptical cryomodule spaceframe under gravity loading and pre-tension.

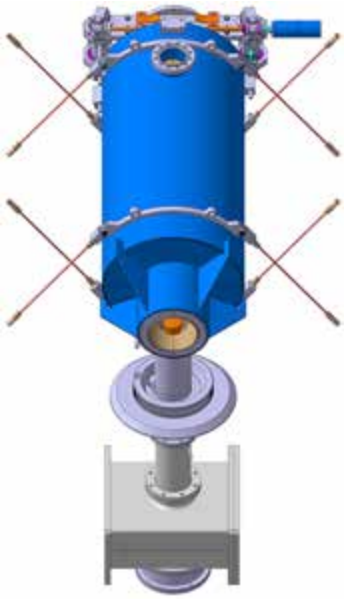

Figure 4.82: Elliptical cryomodule helium tank with transverse and axial hanging rods.

Component	**50 K** [W]	**5 K** [W]	**2K** [W]
Thermal radiation	19		0.7
Supporting system with thermalisation at 50 K	8		0.23
Interface between space frame and thermal shield	20		
Warm to cold transition (2 items)	6		0.4
Safety relief valves	6.8		0.42
Control valves	3		1.5
Coupler conduction from 5 K flange			4
Instrumentation, heaters and actuators	13	1.5	0.2
Total	75.8	1.5	7.5

Table 4.25: Static heat load for one high-β cavity elliptical cryomodule.

post-assembly shipping to the ESS site. The value of 3,000 N is the same as that which has been chosen for SNS. Each cavity (with tank, coupler and magnetic shield) weighs about 2100 N. The atmospheric pressure induces a force of about 6380 N through the coupler. Half of the displacement due to the shrinkage has been allocated to the rods for the stress calculation. Considering the yield strength of each material, the 6 mm diameter of the TA6V rods maintains some safety margin from the mechanical point of view, and eases manufacturing. The increased cryogenic heat load recorded in Table 4.25 is acceptable.

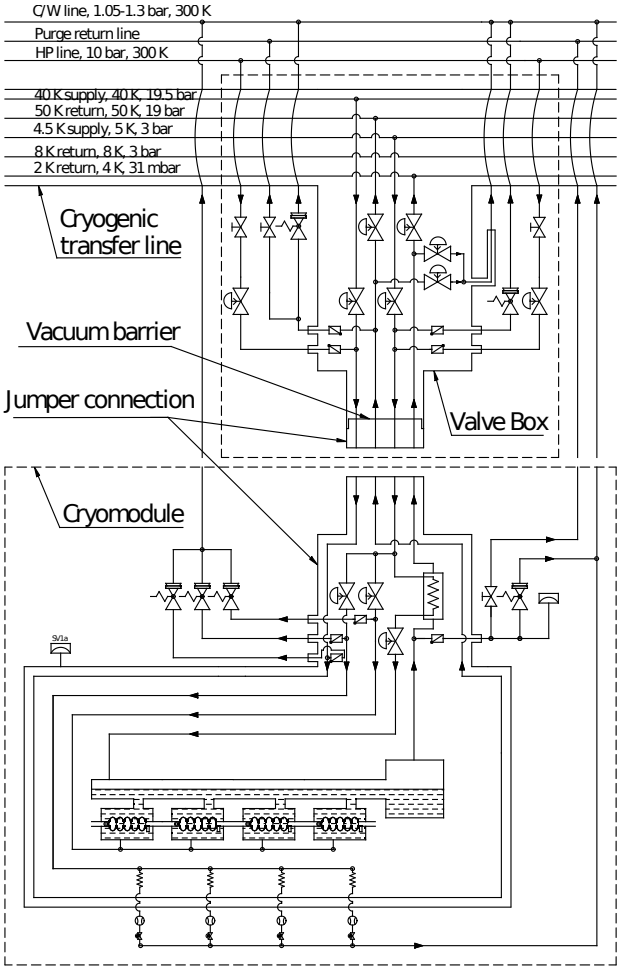

Figure 4.83: Process and instrumentation diagram for the elliptical cavity cryomodule.

Heat load

Static heat loads estimated during the design of the high-β cavity technology demonstrator cryomodule are recorded in Table 4.25. In addition, when the RF and the beam are on, each of the four fundamental power couplers' double-walls is cooled by 40 mg/s of helium flowing at temperatures between 5 K and 150 K. The dynamic heat loads for each of the medium-β and high-β cavities are estimated to be 3.3 W and 4.5 W, respectively. The beam losses (1 W/m) and an additional heat load of 1 W for each coupler also contribute to the dynamic load. Finally, the total heat load (equivalent at 4.5 K) for the medium and the high-β elliptical cavities are estimated at 76 W and 90.6 W per cryomodule, respectively.

Flow scheme

The cryogenic transfer line feeds the cryomodule as described in Chapter 6. Figure 4.83 shows the flow schematic for the elliptical cavity cryomodules. All cryo-distribution cooling lines are routed from the cryomodule to the cryogenic transfer line, except the conditioning lines used for the warm-up and cool-down lines, and the power coupler double-wall return line. The operating pressure ranges from 1.9 MPa for the thermal shield piping to 3.1 kPa for the saturated helium tank. In order to prevent contamination of the helium, the sub-atmospheric operating conditions of the cavity require the use of helium guards around the flanges. A redundant pressure relief system prevents over-pressurisation of the helium tank, holding the pressure below 0.15 MPa.

4.7 High energy beam transport

4.7.1 Layout, optics and beam distributions

The main purpose of the high energy beam transport (HEBT) system is to transport the beam to the main target. Furthermore, the HEBT must be able to transport beams which, especially during the early years, will deviate from the nominal 5 MW beam. A schematic drawing summarising the layout of the HEBT and the functions of the different parts is shown in Figure 4.84. The HEBT includes:

1. A 100 m long, straight underground section S1, to provide space for additional accelerator cryomodules for upgrades in power (energy or current) and/or reliability. In addition, a collimation system is being designed for this section, although its necessity is not yet fully established.

2. An achromatic semi-vertical section, denoted S2, to bring the beam 4 m up from the underground linac tunnel to the target level.

3. A horizontal section S3, that transports the beam to the main target. It includes a beam expander system to match the beam to the nominal target footprint. A fixed collimator, to capture tails of the beam not folded onto the target, will be placed just before the proton beam window (PBW), 4.4 m in front of the target.

4. Two beam dump lines continue in the S1 line of sight, and their associated targets: A tuning and commissioning beamline to match the beam onto the "tune-up dump" and a dispersive beam line capable of measuring the energy spread of the beam.

5. A neutron beam catcher to capture the back-streaming neutrons from the target.

Normal conducting magnets, with their associated power supplies, will be used throughout the HEBT. The last four S3 magnets will be radiation hard, suitable for remote exchange due to the expected high radiation level. Beam transport simulations of the lines have been made using TraceWin/Partran, including 3D space charge. In the energy range from 600 MeV to 2.5 GeV, the RMS energy spread at the exit of the linac is about 1.5×10^{-3}. Transport through the high energy section will further de-bunch the beam, with the highest de-bunching effect occurring at the lowest energy. However, the RMS energy spread at the target, for the 600 MeV beam, is only about 7.8×10^{-3} (0.5 MeV). With such a small energy spread, there is no need to perform bunch rotation.

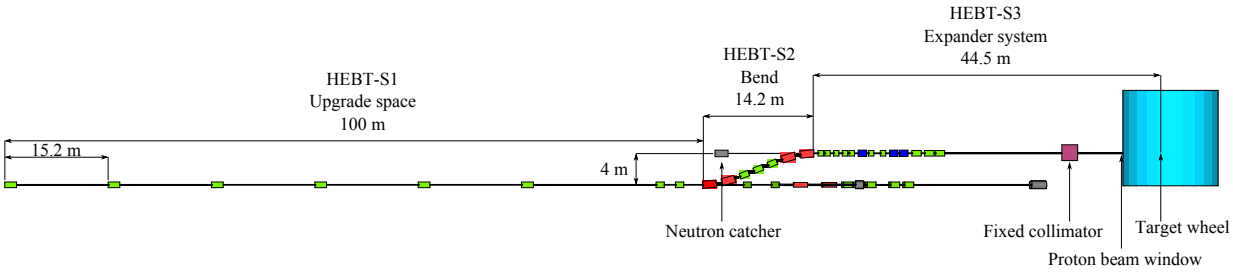

Figure 4.84: High energy beam transport line layout, including quadrupoles (green) and dipoles (red). The target monolith, the fixed collimator and the position of the proton beam window are at the far right. The underground beam dump lines with their targets also can be seen, at the same elevation as the linac.

Collimation and upgrade straight, S1

The 100 m long straight section of the HEBT, S1, will accommodate a system of transverse collimators able to reduce the power in the tails of the beam. As of this writing, the collimator systems are still under development, but it is planned to design the jaws to 3 kW per jaw (right/left/up/down), with good efficiency. The S1 section also provides ESS with the option to undertake a number of upgrades in the future. The most important of these is a possible power upgrade to 7.5 MW, which would be obtained by an RF power increase, a current increase to 75 mA or an energy upgrade to 3.5 GeV [496]. If necessary, the space could also be used for a reliability upgrade by adding additional cryomodules while keeping total beam power constant. The S1 section continues the doublet focusing structure of the linac, which will provide smooth focusing and would therefore facilitate a future upgrade. As shown in the optics layout in Figure 4.85, space is available for an additional twelve high-β elliptical cryomodules. Finally, a beam for a future second target station could be extracted from the S1 section.

Achromatic elevator, S2

Section S2 will transport the beam from underground to the target 4 m up. Two double bends of 2 × 11 degrees and three quadrupoles in between will match the beam at the exit to a vanishing dispersion and

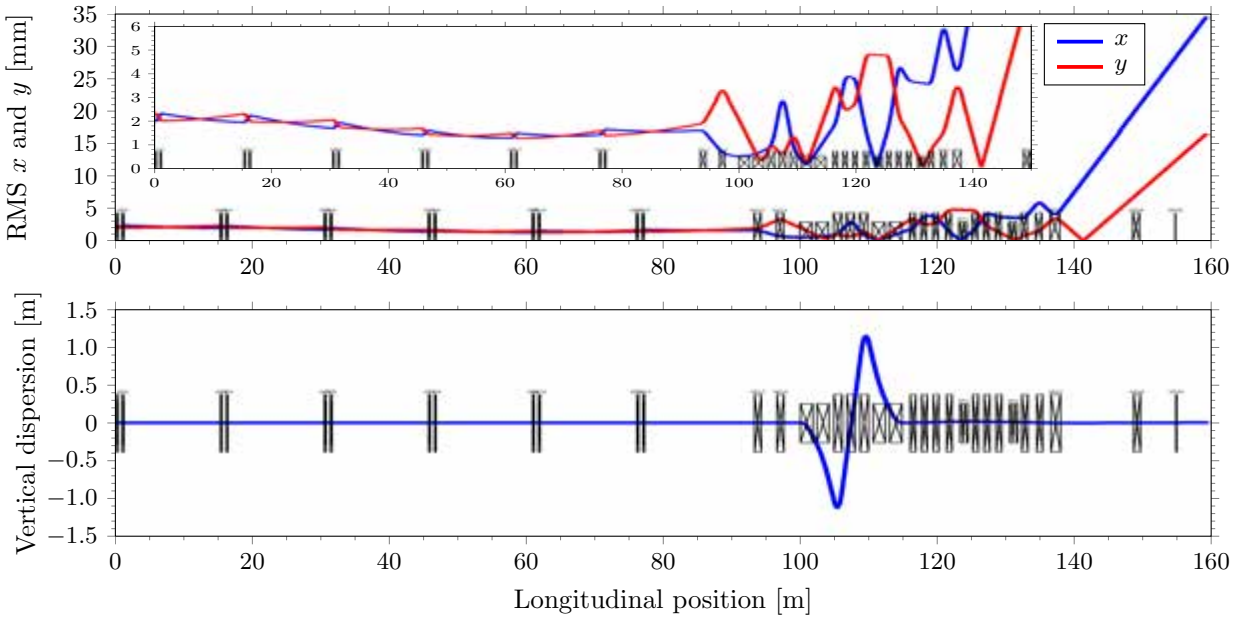

Figure 4.85: Beam size envelopes along the high energy beam transport. Top: The horizontal (blue) and vertical (red) RMS beam envelopes for the nominal beam in the HEBT. The inset shows an expanded view of the beam envelopes in the final approach to the target in section S3. Bottom: Vertical dispersion.

small cross section. Holes in the dipole magnet yokes will allow passage of the beam to the beam dump line and will also let the back-streaming neutrons from the main target pass into the neutron catcher.

Expander and target matching, S3

The straight S3 section will transport the beam onto the main ESS target, using quadrupoles to match it to the required beam footprint measuring ±80 mm horizontally and ±30 mm vertically. To reduce the peak current density on the target, two octupoles will fold the tails of the Gaussian-like beam distribution into a flatter profile. In order to produce a flat distribution in both planes while not introducing coupling between the horizontal and vertical motion, two beam waists have been included in the S3 design, as shown in Figure 4.85. Thus, four quadrupoles will match and form a waist at the first octupole, three quadrupoles will match and produce a waist in the other plane at the second octupole, and three quadrupoles will shape the beam into the required footprint on the target. A proton beam window (PBW) will be placed 4.4 m upstream of the periphery of the rotating target wheel, and will separate the target enclosure from the vacuum system of the accelerator. The PBW will be a cooled aluminium window. Its design is discussed in more detail in Section 3.3.8. The beam assumed in the simulations presently being carried out consists of two overlapping Gaussian distributions, a primary distribution and a secondary one, representing the beam tail/halo. The width of the secondary distribution is five times larger than that of the primary distribution, but it contains only 1% of the particles in the primary distribution. In comparison with simulations of the linac output, this double Gaussian distribution describes *e.g.* $\simeq 10$ times more halo at about 4 RMS, and these simulations are thus quite conservative with respect to tails and corresponding losses.

Figure 4.86 shows the time-averaged particle current density on the target and on the PBW. The rotation of the target effectively enlarges the target area, thus reducing local radiation damage by a factor of $\simeq 50$, as compared to a static target. Note the tails of the beam on the PBW and the flat beam profiles. The target will nominally be exposed to a peak current density of 52 μA/cm^2, while the PBW will be hit by a maximum current density of 84 μA/cm^2, in both cases scaled to the nominal average beam current of 2 mA. For reference, a peak current density of 250 μA/cm^2 would result from a Gaussian beam without any flattening. The fixed collimator will, in the present scenario, intercept 8.3 kW of beam power. There is a correlation between maximum peak current density and the beam power outside the target footprint (hitting the fixed collimator) due to beam-folding by the octupoles. Lower peak current densities can be obtained by sacrificing higher beam powers on the fixed collimator.

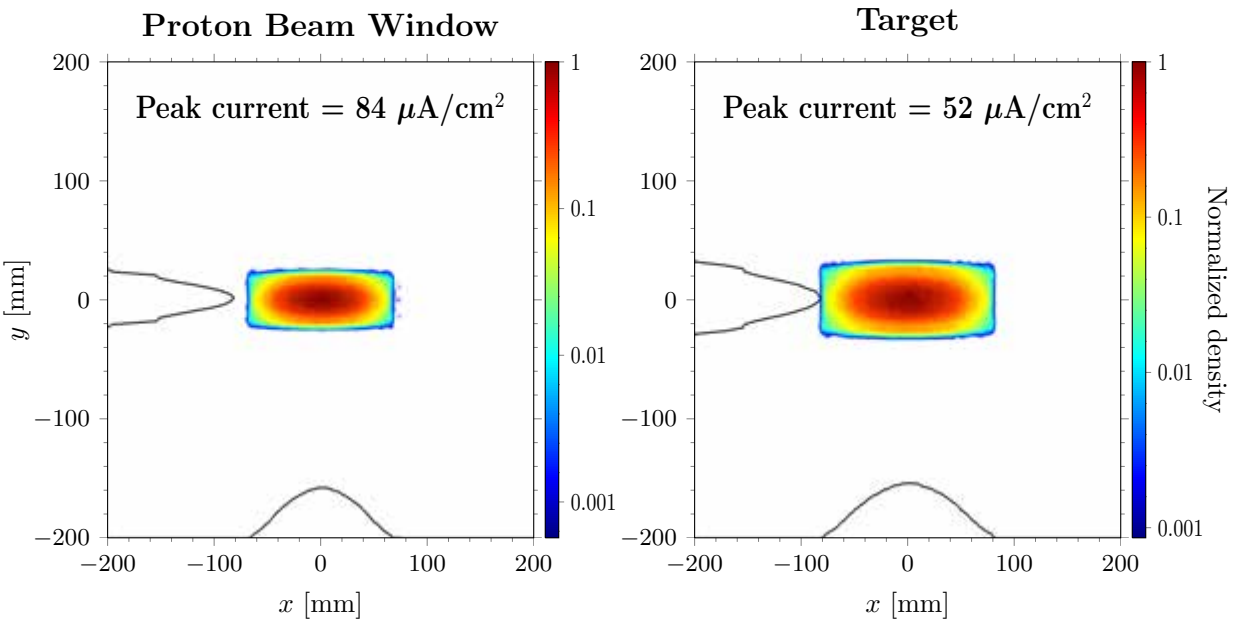

Figure 4.86: Particle density plots. Left: On the proton beam window. Right: On the target. Also shown are projections of the horizontal and vertical beam profiles, on a linear scale.

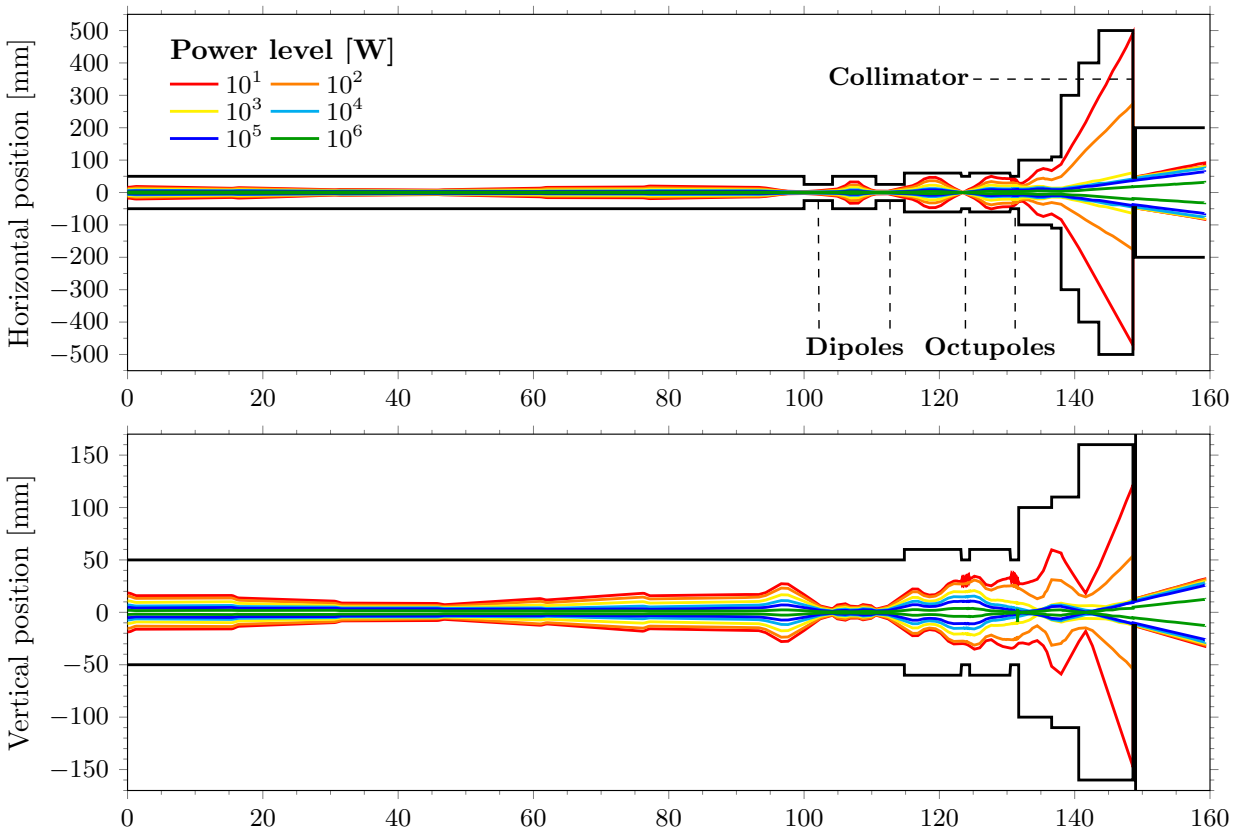

Figure 4.87: Particle density and beam power level contours along the high energy beam transport. The apertures inside the vacuum chambers are outlined. Top: Horizontal. Bottom: Vertical.

Losses and apertures

Tails in the beam may lead to losses unless the apertures are sufficiently large. However, magnet apertures drive costs and therefore have to be optimised carefully. Figure 4.87 shows the transverse power loss contours in both planes, together with the apertures in the magnets and the vacuum chambers that have been designed to balance losses against costs. In this design, there are no beam losses before the fixed collimator. In the figure, each macro-particle corresponds to a 10 W loss. The design calls for a large aperture in front of the fixed collimator. It also calls for smaller apertures in the octupoles as compared to the quadrupoles. Finally, the design of the last quadrupole triplet calls for especially large apertures to accommodate the expansion of the beam on the target. Preliminary simulations indicate that apertures following this design will be sufficient even when more realistic magnetic and alignment errors are introduced. With well-corrected beams, it is possible to avoid almost all of the large relative losses seen with uncorrected beams. First results indicate that the above apertures are sufficient when realistic magnetic and alignment errors are introduced. Clearly, large relative losses are obtained for uncorrected beams, whereas no significant additional losses occur for well-corrected beams.

4.7.2 Collimators and beam dumps

Comprehensive simulations of the beam transport from the linac to the target have been performed, but some contingency margin has to be added in the technical design of the components. In particular, it is vitally important to take account of the power content of the tails of the beam, as too much beam power might damage components and make maintenance difficult. Two collimator systems will be installed in the HEBT, with an appropriate phase advance (of around 90 degrees for halo particles) between them, as preliminarily shown in Figure 4.88. The two systems are necessary to perform an effective collimation. Each system will be designed to capture about 3 kW of beam power with a high collimation efficiency. As a precaution, the first system will be able to capture large-amplitude particles in the beam with a system

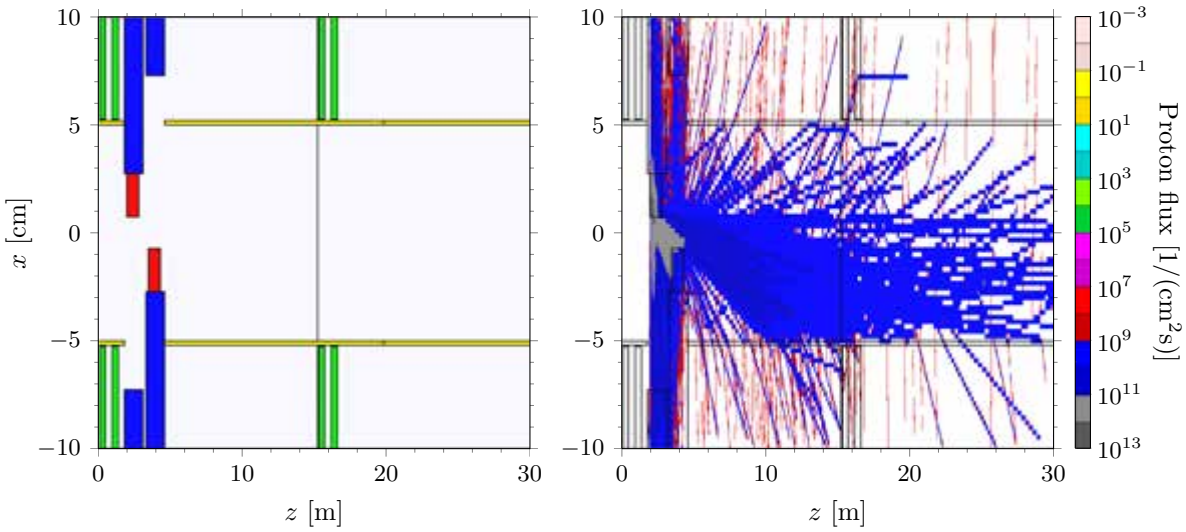

Figure 4.88: Movable collimators. Left: Two periods of the S1 line with beam pipe (yellow) and quadrupole yokes (green). Two beam-intercepting subsystems feature L-shaped, stainless steel jaws (red) to collimate in both planes. The jaws are fixed in a vacuum chamber duct that can be displaced transversely by moving external stainless steel radiation shields (blue). This system will be repeated three periods downstream to scrape halo of opposite phase. Right: Proton flux with $E > 200$ MeV when the jaws are struck by 20,000 halo protons between 3.3 and 10 standard deviations in an exponential distribution. About 6% of the protons hitting the jaws are transmitted, albeit at reduced energy. The populated emittances clearly exceed the HEBT's admittance, necessitating the strategic placement of masks and absorbers.

of transverse movable collimators. The other system will be a fixed collimator. As described above, the octupoles in the S3 section will produce a flat beam distribution at the expense of sending large-amplitude halo particles to even larger amplitudes. Hence a fixed collimator is designed to capture particles outside the beam footprint on the PBW. The collimator will be designed for a power of 25 kW, although lower powers are expected. The movable collimator systems in S1 will occupy parts of the space reserved for future upgrades, and ways to operate without them may have to be found in the long term.

Tune-up dumps and beam lines

During the initial commissioning and start-up of the ESS accelerator, and also during start-up after longer shutdowns, a straight beam line following the S1 line will transport the beam to a commissioning beam dump. This dump is designed for 50 kW, and a quadrupole doublet will expand the beam to 12.5 mm RMS on the dump. During the initial commissioning of the linac, when there will be many phase scans of the cavities, this beam will impinge on the target with varying energies, energy spreads, and transverse widths. A diagnostic line will transport the beam to a second tuning beam dump. This beam line is designed with a large ratio between dispersion and β-function, and hence the energy spread of the beam can be measured directly using profile monitors. Such measurements are otherwise not directly available. The line will also include a quadrupole expansion of the beam to the required 50 kW beam dump. A beam plug (gamma blocker) will be inserted in front of the dumps during maintenance for personnel access to the linac tunnel. The two tuning beam lines will transport the beam to the commissioning beam dumps designed for 50 kW average beam power. They will also be designed for full single pulses, with correspondingly low duty cycles. The dumps will be built to withstand the narrow beams that might occur during the early stages of commissioning. RMS beam widths of 0.5 mm can be handled by the dumps with small repetition rate. Most pulses, after the very early phases of commissioning, will supply nominal RMS beam widths of 12.5 mm.

4.7.3 Magnets and power supplies

One of the main hardware components of the HEBT will be the magnets and their associated power supplies. The main parameters of the magnets and corresponding power supplies appear in Table 4.26. All HEBT magnets will be normal-conducting, designed to provide the necessary fields (at an upgrade energy of 3.5 GeV, including 20% contingency for quadrupoles and octupoles) and to have very high reliability. Efforts have been made to minimise the number of magnet types and power supplies. Only one type of dipole will be used in the S2 and the dump line sections, while four types of quadrupole yoke cross section will be needed. In addition, two high-field beam-folding octupoles are necessary. Finally, a number of correctors, most built into the magnets as corrector coils, have been designed. Magnets have in general been designed for low radiation environments using epoxy-impregnated coils. Most magnets will have a laminated core, to reduce the ramping time constants, except for the six dipoles and the two octupoles which will have solid cores. Magnets will be delivered with mechanical supports, alignment and mounting systems and vacuum chambers.

A large number of warm quadrupole doublets (14 in the spokes section, 36 in the elliptical section) will be needed between cryomodules in the linac, in addition to those in the HEBT. They will be included in a linac warm unit (LWU) magnet assembly as shown on the right of Figure 4.89. In addition to holding the quadrupoles with corrector magnets, each LWU will also include steerers, beam diagnostics and vacuum equipment, and mechanical support. The units will be designed with two different beam pipe apertures (internal diameter 60 mm for the spokes section, and 100 mm for the elliptical section and the HEBT) and a prototype will be built.

Special radiation precautions will be necessary for the magnets located in the final portion of the HEBT near the target. Plans for dealing with this issue are based on experience at other facilities, and at PSI in particular. Even for these magnets, no significant beam losses are expected in excess of 1 W/m. Nevertheless these magnets – that is, the last octupole, the last three large-aperture quadrupoles and the last two steerer magnets – will be exposed during their lifetimes to significant neutron flux from the target and the fixed collimator, ($\simeq$ MGy). Hence they will be built for a long lifetime in a high radiation environment using mineral-insulated cables. Even taking these precautions, the radiation-hard magnets may have to be exchanged at some point. Figure 4.90 shows the design of an environment permitting remote handling and exchange of these radiation-hard magnets in the final stretch of the HEBT. The magnets will be placed in a relatively narrow ditch and covered by shielding blocks from above during operation. All connections, electrical power, electrical monitoring, vacuum, and cooling water will be

Section	**Magnet type**	**Rad. level** [W/m]	**Magnet count**	**PS count**	**Aperture** [mm]	**Magnetic length** [mm]	**Magnet strength** [T]	**Weight** [t]
DIPOLE								
S2	S2D	$\lesssim 1$	6	3	55	1800	1.679	13.9
QUADS								
S1	LWUQP	$\lesssim 1$	12	6	105	247.2	0.533	0.9
S1	S1QP	$\lesssim 1$	2	2	105	530	0.533	2.0
Dump	DQP	$\lesssim 1$	9	9	105	1200	0.686	4.7
S2	S2QP	$\lesssim 1$	3	3	105	1002	0.686	5.6
S3	S3QP	$\lesssim 10$	7	7	126	800	0.79	5.0
S3	S3RHQP1	High	2	2	206	900	0.79	14
S3	S3RHQP2	High	1	1	226	1400	0.79	16
OCTS								
S3	S3O	$\lesssim 10$	1	1	105	1200	0.31	3.2
S3	S3RHO	High	1	1	105	1207	0.66	6.5

Table 4.26: Parameters of the high energy beam transport magnets and corresponding power supplies (PS). All magnets and power supplies are specified for operation at 3.5 GeV including 20% contingency relative to nominal parameters. The magnet strength (in Tesla) represents the pole tip field for the dipole and octupoles, and the integrated strength for quadrupoles. The LWUQP magnet style is also used in the focusing structure of the elliptical cavity linac, where an additional 60 of these magnets will be used.

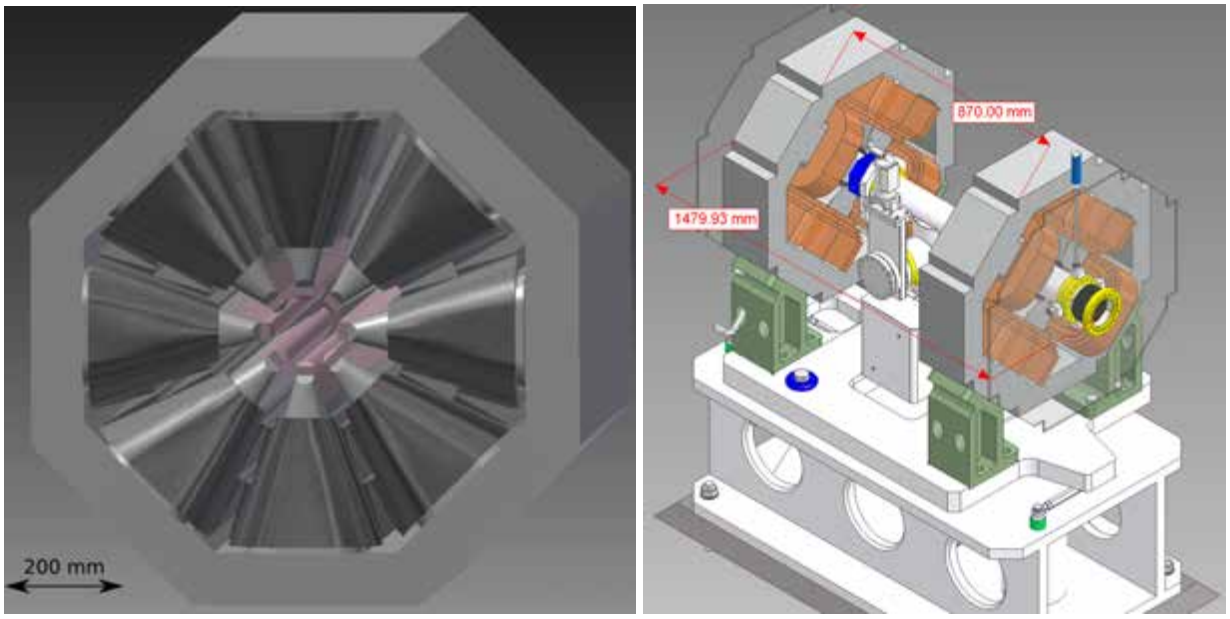

Figure 4.89: Left: A radiation-hard octupole magnet, featuring Permendur poles and conical coils of mineral-insulated cables. Right: The linac warm unit (LWU) magnet assembly that will be used both between cryomodules, and also in the S1 section.

made via holes in the shielding blocks. Long specialised tools will be used to disconnect and connect the magnets. Using an above-mounted crane, a faulty magnet can be lifted to a storage position, possibly in a radiation cask. This procedure can be reversed during the installation of a new magnet. A similar approach may be used for the exchange of other equipment, such as beam diagnostic modules. The amount of concrete shown in the figure is not optimised with respect to shielding but merely illustrates the remote exchange concept.

Magnet power supplies will only require moderate stability, and ramping speeds of several seconds will suffice. High reliability will be required due to the relatively large number of units. The total power consumption of all magnets will be around 350 kW. Where space permits, relatively large copper coils will be used to reduce power consumption and reduce costs.

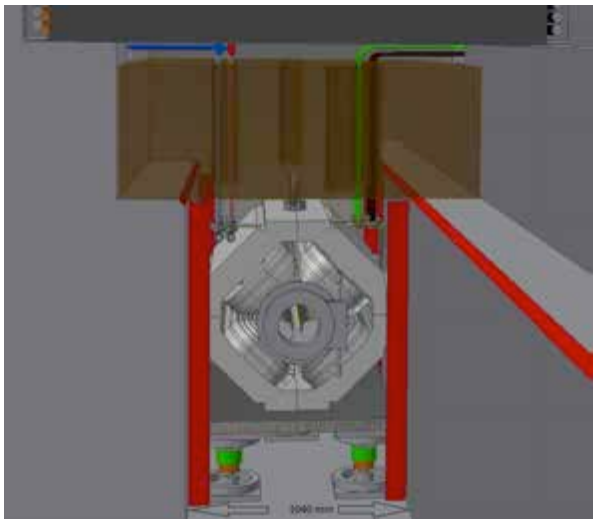

Figure 4.90: Remote connect/disconnect and exchange of the last radiation hard magnet, using long tools and water piping and cabling high above the magnets.

4.8 Radio frequency systems

4.8.1 Overview

The RF system for the linac converts AC line power to RF power at either 352 or 704 MHz for supply to the RF accelerating cavity couplers. The AC conventional power lines on one side and the waveguide power couplers on the accelerating cavities on the other side bound the RF system. To deliver an average beam power of 5 MW with a 4% duty factor (2.86 ms pulse at a rate of 14 Hz), the linac RF systems must supply over 123 MW of peak power. Because of the large power density, 98% of the linac consists of superconducting radio frequency (RF) resonators that are used to transfer power to the beam. Superconducting resonators by nature exhibit 100% beam loading, which poses interesting challenges to the RF system. However, the ESS design is quite different from that of other superconducting linacs. The ESS linac uses protons instead of H^- ions; does not inject into a ring; and is heavily coupled due to high beam current and a large system bandwidth. These three factors might indicate that the tolerances on RF control do not have to be as stringent as would be the case for a low beam current linac injecting into a ring. However, because of the high gradients required in the ESS linac, Lorentz detuning in the superconducting cavities can span over 40 degrees of RF phase. In addition, unlike in short-pulse linacs, the beam pulse length in ESS is much longer than the mechanical response time of the cavity due to Lorentz detuning. ESS's working assumption is that the superconducting cavities are equipped with fast piezo-electric tuners to compensate for the Lorentz detuning.

The normal-conducting section of the linac consists of an RFQ and four drift-tube tanks. It will be powered by five power sources, one for the RFQ and the bunching cavities in the MEBT and one each for the four drift tube tanks. The superconducting section of the linac comes after the normal-conducting section. There are three types of superconducting resonators. The first 28 are spoke resonators operating at 352.21 MHz. The remaining 180 are elliptical cavities operating at 704.42 MHz. As shown in Figure 4.2, the power level for the superconducting section of the linac ranges from 50 kW to 850 kW.

The RF systems provide the RF power required for 50 mA of peak beam current over a pulse length of 2.86 ms at a pulse rate of 14 Hz. The fill and fall time of the cavities will be on the order of 300 μs, so the total RF pulse length will be on the order of 3.5 ms. Thus, the duty factor will be 4.9%. The voltage amplitude will be regulated within a range of less than 0.1% and a phase error of 0.5 degrees. The design will accommodate variation on the order of 5% in cavity-to-cavity coupling strength and Lorentz-detuning factors. The bandwidth of the system will be dictated by the loaded cavity bandwidth. The cavity power coupler is designed to transfer all RF energy to the beam when the beam is passing though the cavity. The optimum coupling value is given by a unique cavity voltage, beam current and R/Q. The baseline design specifies the maximum voltage for each type of cavity. For different cavity voltages, it can be shown that a rather minimal amount of RF energy will be reflected.

With the combination of requirements on cavity gradient, variations in cavity-to-cavity coupling strength and Lorentz-detuning factors, the baseline configuration calls for one cavity per power source. To provide the beam power, it is necessary to take into account loss from the power source to the resonator. A conservative value of 0.2 dB (5%) insertion loss is assumed for this design. For regulation to work properly, a certain amount of power overhead will be required. (The power overhead is defined as the ratio of the maximum output power of the RF source to the operating power.) A sufficient power overhead for regulation is typically 25%. Taking into account insertion loss and power overhead for regulation, the maximum power the RF power source needs to have available is 1.3 times the required beam power. Thus the range in power sources will be from 65 kW to 1100 kW for the superconducting cavities and 1200 kW to 2600 kW for the normal-conducting cavities. The set of high level parameters that have a direct influence on the RF system is shown in Table 4.27. The system-specific requirements are shown in Table 4.28 and the specifications that drive RF system cost are shown in Table 4.29.

The main component of the RF system is the power amplifier. The power amplifier takes pulse power from the modulators and converts the power into RF waves at 352 or 704 MHz. Because of the power levels required, most of the power amplifiers at ESS will be klystrons with a peak power range from 1 to 3 MW. These klystrons will be deployed in the RFQ, DTL, and superconducting elliptical cavity sections. The linac will require about 180 klystrons. The superconducting spoke section of the linac will require less than 300 kW of peak power per resonator at 352 MHz, so klystrons would not be an economical choice. Tetrode amplifiers or induction output tubes are more economical. The tetrode-based amplifier has been tentatively adopted for the spoke section, and will be described in this report.

Parameter	Unit	Value
Maximum beam current	mA	50
Beam current stability	%	1
Beam current control	%	1
Beam current ripple	%	1
Beam current pulse length	ms	2.86
Beam current pulse length stability	ppm	1
Beam current pulse length control	ppm	1
Repetition rate	Hz	14
Cavity gradient amplitude regulation	%	0.5
Cavity gradient phase regulation	degrees	0.5
Permissible AC grid load variation (flicker)	%	1

Table 4.27: High level RF system parameters.

Parameter	Unit	RFQ	Bunch -ers	DTL	Spokes	Med. β	High β
Number of couplers		1	2	4	28	60	120
Average coupler spacing	m	0	1	7	2.1	1.8	1.8
Max power delivered to coupler	kW	1500	15	2200	239	514	872
Min power delivered to coupler	kW	1500	15	2200	165	122	394
Ave power delivered to coupler	kW	1500	15	2200	218	358	786
Max reflected energy per pulse	J	25	0.2	35	60	160	250
Max reflected power	kW	1500	15	2200	239	514	872
Frequency	MHz	352	352	352	352	704	704
Average synchronous phase	deg.	0	90	30	15.2	15.9	14
Loaded Q	10^3	15	15	15	160	640	820
Maximum cavity fill time	μs	50	50	50	400	250	250
Lorentz detuning coefficient	Hz/(MV/m)^2	0	0	0	1	1	1
Lorentz detuning time constant	ms	0	0	0	1	1	1
Slow tuner range	kHz	100	100	100	100	100	100
Slow tuner slew rate	kHz/s	1	1	1	1	1	1
Maximum slow tuner cycles	10^6	1	1	1	0.1	0.1	0.1
Fast tuner range	kHz	0	0	0	10	10	10
Fast tuner bandwidth	Hz	1	1	1	1000	1000	1000
Cav. phase noise (microphonics)	Hz	0	0	0	10	10	10
Cavity drift rate	Hz/s	1	1	1	1	1	1

Table 4.28: Specific RF system requirements.

The RF power amplifiers convert conventional AC line power into a pulsed or DC waveform that can be used to energise the amplifiers. For klystrons, this power converter is called a modulator and for tetrodes, the power converter is called the anode supply. The RF power is delivered from the power amplifier to the accelerating structure via the RF distribution system. The distribution system will be composed of waveguides to minimise loss. The RF distribution system must also protect the RF power amplifier from energy reflections from the accelerating structures during the fill or emptying of the superconducting cavity or during those occasions when the beam current departs from its expected level. For this reason, the design calls for a circulator with a matched load to be placed on the output of the klystrons to act as an isolator. The low-level RF (LLRF) control system is a regulation system to control the RF amplitude and phase. In addition, the LLRF control system will control the fast and slow tuning of the cavities. The system requires both feedback and adaptive feed-forward algorithms. To minimise the required power overhead, adaptive feed-forward will be heavily emphasised. The adaptive feed-forward algorithms will require fairly high speed and sophisticated computing.

Parameter	Unit	RFQ	Bunch -ers	DTL	Spokes	Med. β	High β
RF regulation overhead	%	25	25	25	25	25	25
RF distribution loss budget	%	5	5	5	5	5	5
RF pulse length	ms	2.91	2.91	2.91	3.26	3.11	3.11
Number of couplers per power source		1	1	1	1	1	1
Saturated RF power per power source	kW	1950	20	2900	320	700	1150
Minimum efficiency at operating power	%	43	60	43	70	43	43
Number of power sources per modulator		1	3	1	2	2	2
Max. modulator stored energy per pulse	kJ	10.2	0.2	15	2.5	7.5	13
Modulator Efficiency	%	85	85	85	95	85	85
Total average AC power to modulator	kW	176	2.5	1050	450	2700	11800
Total average cooling rate	kW	155	16.6	956	704	2961	10066
Total average AC power	kW	199	19	1143	1489	3768	13894

Table 4.29: RF system specifications that drive costs.

This section discusses specifics of the engineering requirements for the low-level RF control, the RF power amplifiers, the RF power amplifier power converter, the RF distribution system and the RF gallery layout. Many of the RF systems along the linac are identical or share common features, so only a single sub-set of "test stand" stations is described. This test stand will be used to prototype many of the components described below. Significant differences between the test stand and the operational linac are also described.

4.8.2 Low level RF control

The LLRF system starts at the connection to the probe in the cavity, and ends at the feed-point to the power amplifier. It generates an input signal to the amplifier that drives the cavity to a field with an amplitude and phase that are within 0.5% and 0.5 degrees of a set value that is unique for each cavity.

Uppsala and Lund test stands

Two test stands will need LLRF systems: the FREIA test stand in Uppsala (352.21 MHz), and the Lund test stand (704.42 MHz). The two differ in operational frequency, and in the number of cavities and amplifiers that will be installed. The baseline design of the LLRF system is described below. The design will be similar for both frequencies, differing only for frequency-specific parts, such as local oscillator (LO) generation and mixers. The LLRF system will be built in a chassis, using primarily commercial, off-the-shelf (COTS) parts. The chassis chosen is the μTCA.4 chassis, as this fulfils requirements on flexibility, size and options for redundancy. The μTCA.4 is a standard developed especially for the physics community, and is a highly modular system. It consists of a crate with modules in pairs, with one module facing front and the other back. Sensitive cabling can be routed to the back of the crate where it will be better protected, and the front panels can be used for monitoring and service. The crates support redundant fans and power modules. Each crate will house a number of modules:

1. Crate controller;
2. CPU, running Linux and an implementation of the control box;
3. Timing receiver;
4. Down-mixer (non-COTS);
5. Analog to digital converter (ADC);
6. Field programmable gate array (FPGA);
7. Digital to analog converter (DAC);

8. Up-mixer (non-COTS);
9. Slow tuner interface (possible COTS);
10. Fast tuner interface (possible COTS); and
11. Machine protection system (MPS) interface (non-COTS)

The LLRF system for ESS will be based on a digital control structure, in which the automatic control algorithms will be executed in an FPGA. The input from the cavity will be down-mixed and the RF-signal will be sampled in the ADC. The output from the FPGA will be converted to an analog signal in the DAC, and up-mixed to the RF-frequency with the same LO as used by the down-mixer. This will minimise impacts on phase drifts and frequency errors from the LO, which will be synthesised from the clock signal of the timing system. The absolute value of the amplitude will be measured by the ADC. The timing reference for the phase measurement will be given by the signal from the phase reference line. Four signals will be sampled in parallel: the signal from the cavity; the direct output from the power amplifier; the reflected signal from the cavity; and the phase reference. In addition, the power to the load will be measured with a power meter. The direct output from the amplifier will be used to linearise the amplifier. The reflected signal from the cavity will be used to tune the cavity, and the power to the load will be measured in order to monitor the health of the system.

The automatic control algorithm will be based on a classic PI-control structure with pulse-to-pulse feed-forward compensation. Thus, repetitive phase and amplitude shifts within a pulse will be corrected for by the feed-forward compensation, and the loop gain of the feedback loop can be reduced. This reduces the necessary overhead in the power amplifier while still achieving the specified amplitude and phase performance. In addition, a separate algorithm to linearise the power amplifier in order to increase system performance will be used.

Cavities will be tuned by the LLRF system using the slow, servo-driven tuners, and by monitoring the phase and amplitude of the reflected signal. The set point of the tuning of each cavity will be given by the control system. Piezo electric actuators in the cavities will be used in order to handle Lorentz force detuning. This will be done in a feed-forward network, also implemented in the LLRF system. The superconducting cavities will have two piezo actuators, with the second one used as a spare. The second piezo actuator will also serve, when available, as a vibration pickup to further increase system performance. The system will save time-stamped data from the last pulse for post mortem analysis. A complete LLRF system will be housed in a temperature-controlled rack, together with the driver amplifiers for tuner motors and RF power amplifiers.

Linac

The ESS linac will have one LLRF system per power source. Each system will be housed in a separate temperature-controlled rack, as is the case for the test stand systems. Two main versions of the systems will be made, one for each RF frequency. Each cavity type will have its own parameters for the control algorithms, and each individual cavity will have its unique set-point for phase, amplitude and tuning. The components that will be fitted with LLRF systems include the RFQ, buncher cavities, DTL, spoke cavities, and the medium and high-β elliptical cavities. The cables from the cavities in the tunnel will follow the same path up to the gallery as the cables from the phase reference line. One tap from the line will be used for each cryostat in the superconducting part, and one for each cavity in the normal-conducting part. The cables coming from each cryostat, the cavities and their reference, will be tied together in order to minimise the phase difference introduced over time between them due to temperature variations. Phase differences in the cable to the power amplifier will be handled by the closed loop control system.

4.8.3 Low level distribution

System requirements

The phase reference distribution system (PRDS) will serve as the phase reference for all cavities with low phase noise and low phase drift. The system starts at the output from the master oscillator and ends at the inputs to the LLRF systems. The PRDS requirements for the Lund and Uppsala test stands and for the linac are listed in Table 4.30.

Parameter	Unit	Lund	Uppsala	Linac system
Short term stability	degrees	±0.1	±0.1	±0.1
Long term stability	degrees	±1	±1	±1
Frequency to be delivered	MHz	704.42	352.21	352.21/704.42
Master oscillator power level	dBm	20	20	20
Output power level	dBm	13	13	13
Number of stations to be delivered		8	2	214

Table 4.30: Phase reference distribution system requirements for test stands and linac system.

Design considerations

Coaxial cable and optical fibre are the two most commonly used solutions for PRDS. The fibre solution provides flexibility for active drift compensation using reflectometry and could achieve higher precision, but it is more complex and costs more. It is an attractive and effective approach for a PRDS system when the distance is relatively long and the system serves only a few LLRF systems. The PRDS system serves a large number of LLRF systems, so the coaxial cable solution will probably be simpler and more practical to implement, with temperature control for the main line and a point-to-multipoint scheme for local distribution. Temperature variation along the main line must be kept within ±0.3°C in order to achieve long-term stability of the RF system phase within ±1 degree. ESS's point-to-multipoint local distribution scheme will be an improved version of the point-to-point scheme implemented at SNS. It will considerably reduce the number of tap points along the main line. Figure 4.91 shows a possible point-to-multipoint local distribution scheme for ESS. The disadvantage of this approach is that it is not possible to compensate for the phase drift associated with the use of additional power splitters and cables from cavity probe points to the tap point, and therefore temperature control for splitters and cables is required if ambient temperature varies significantly.

Technical specification

As mentioned above, a coaxial cable-based PRDS is preliminarily proposed for both test stands and the linac, with temperature control for the main line and a point-to-multipoint scheme for local distribution. The test stands require far fewer tap points than the linac – two for the Lund test stand and one for the Uppsala test stand, versus about 60 for the linac system. The length and required input power of the main line are therefore much lower for the test stands, as well. Detailed PRDS technical specifications for test stand and linac systems are listed in Table 4.31.

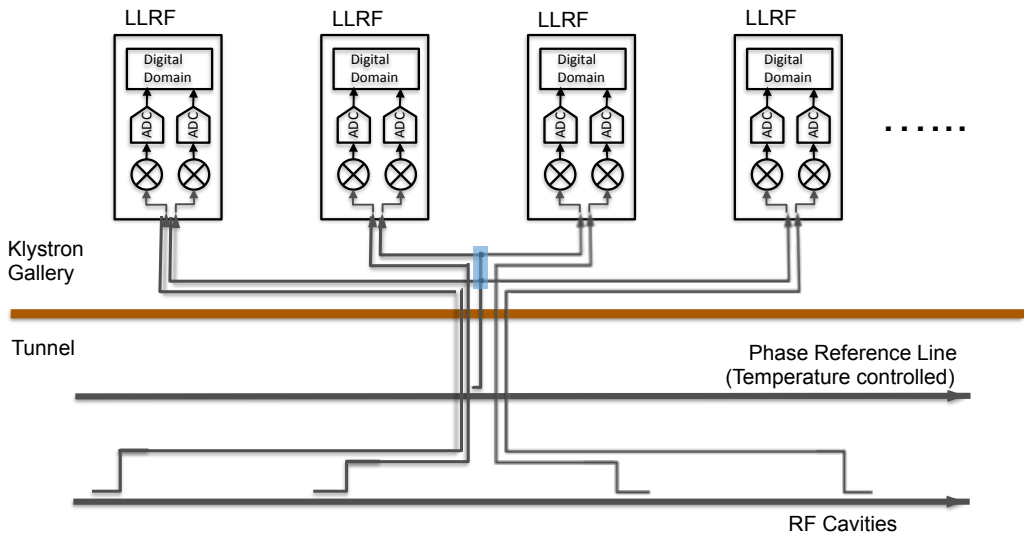

Figure 4.91: Point-to-multipoint scheme for local phase reference distribution system (PRDS).

Parameter	Unit	Lund	Upp-sala	RFQ	MEBT	DTL	Spoke	Med. β	High β
Delivery medium		Coax. cable	Coax. cable	Coax. cable	Coax. cable	Coax. cable	Coax. cable	Coax. cable	Coax. cable
Delivery frequency	MHz	704.42	352.21	352.21	352.21	352.21	704.42	704.42	704.42
Main line temp. var.	°C	±3	±3	±0.3	±0.3	±0.3	±0.3	±0.3	±0.3
Total tap points		2	1	1	1	3	7	15	30
Stations per tap		4	2	1	2	1	4	4	4
Input power	dBm	25	20	50	50	50	50	50	50

Table 4.31: RF phase reference distribution system specifications for test stands and the linac.

4.8.4 Klystrons

Lund test stand

Klystrons are the baseline choice for RF power amplifiers for the Lund test stand. The klystrons will operate at a frequency of 704.42 MHz and the saturation peak power will be 1.2 MW. With the duty cycle targeted for ESS (5%) this means that the average power level at saturation will be about 60 kW. The Lund test stand will power eight klystrons from four modulators. The high voltage power needed for the test stand will be 800 kW, assuming a klystron efficiency of 60%. This is 200 kW per modulator. The pulse form is a flat top at about 100 kV/20 A with a width ranging from a few microseconds up to 3.5 ms (the nominal pulse width is 2.86 ms and the rise/fall times when cavities are fed can be up to 250 μs). The klystrons will be operated at various power levels. For operation with regulation overhead, a power level of 900 kW is assumed (allowing for 25% overhead). Since the efficiency goes down to around 45% at this power level, the high voltage pulsed power still needs to be 200 kW for this case. The anode will operate in a pulsed cathode configuration, avoiding the mod-anode configuration for klystrons because of a number of drawbacks: the mod-anode configuration can become unstable, with electron back-streaming; it would decrease reliability and increase costs about 10% due to the need for special terminals; a crowbar would be required in the HV line, which also would increase costs; and the LLRF system would need to compensate for voltage droop, which may not always be possible. The pulsed cathode configuration, on the other hand, offers the advantages of simplified fault circuits; better stability at lower cost; and excellent voltage regulation.

The klystrons will be placed in an oil tank to protect the electron gun from breakdown, and to cool it. Power will be needed for the electron gun's ion pump, the solenoids that focus the beam and the monitoring system, which includes the waveguide arc sentry that protects the klystrons in case of arcs in the gun area. The total power needed for these purposes is, at the maximum, $20 \times 8 = 160$ kW, or an installed power of 180 kVA (assuming a power factor of $\cos\phi = 0.9$) for the eight klystrons. Cooling will be needed for the klystron body, the solenoids, and the collector which receives most of the power. This will be provided by the gallery cooling system in the form of deionised (DI) water. The gallery will provide DI water at three temperature levels: 20°C, 40°C, and 60°C. The klystrons will be cooled from the mid/low and high temperature loops, with the body and solenoids cooled by the mid temperature loop and the collector cooled by the high temperature loop. All electronics will be cooled from the low temperature loop. The approximate flow-rate needed for the body and solenoid cooling is 115 lpm assuming a $\Delta T = 15$°C. For the collector cooling, the needed flow rate is 770 lpm under the same assumption. The rest of the systems will be attached to the low temperature line, with a flow rate of 40 lpm using 15°C temperature differences. The klystrons will need dry air flow across the output windows in order to avoid arcing. Finally, a pre-driver that amplifies the LLRF signal up to maximum 100 W will be needed. The baseline design calls for a solid state amplifier.

Linac

One klystron will be needed for the RFQ, tuned for 352.21 MHz. For reasons of simplicity, a klystron similar to the DTL klystrons will be used, with peak saturated power of 2,900 kW powered by one modulator, although the requirement for the RFQ klystron is actually somewhat lower (1,700 kW). The RFQ klystron will need the same utilities as the Lund test stand klystrons. Power need will be 145 kW

high voltage pulsed power and 15 kW power for the magnets and other systems. The cooling need for the RFQ klystron will be 15 lpm for the mid temperature loop which will cool the body and magnets, 140 lpm for the high temp loop which will cool the collector, and 5 lpm for the low temperature loop which will cool the other systems. Four 2900 kW klystrons will power the four DTL tanks. These will be powered by four modulators, and they will require the same auxiliary systems as each of the test stand klystrons. The combined pulsed power need for these four klystrons is 1000 kW, and the auxiliary systems will require 80 kW. The corresponding cooling needs are 60 lpm for the mid temperature loop, 20 lpm for the low temperature loop, and 560 lpm for the high temperature loop.

The medium-β section will be powered by the same type of klystrons as the test stand. There will be 60 klystrons, powered by 15 modulators. Average RF power per klystron will be 35 kW, and auxiliary systems will require up to 20 kW, assuming 60% efficiency. The total pulsed power needed is 3500 kW. The auxiliary systems will need 1200 kW. To cool the klystrons, the low temperature system will require a flow rate of 300 lpm, the mid temperature system will require 900 lpm, and the high temperature system will require 3350 lpm. The high-β section will be powered by 120 klystrons of the test stand type. These will be powered by 60 modulators. The average klystron power will be 60 kW. Auxiliary power will be up to 20 kW per klystron, again assuming 60% efficiency. Total pulsed power need will be 12000 kW, and auxiliary power need will be 2400 kW. To cool the high-β section, the low temperature loop will require a flow rate of 600 lpm, the mid temperature loop a flow rate of 1700 lpm, and the high temperature loop a flow rate 11500 lpm.

4.8.5 Modulators

Klystron modulators are high voltage power converters that transfer electrical power to the klystron cathodes from a standard low voltage distribution grid, with the appropriate voltage waveform shape, precision and reliability. Accessory power supplies, such as those for the filament heater, ion pumps or focusing solenoids are not considered part of the klystron modulators. They will be physically separated from the modulators and will be specified and procured separately. All klystron modulators for the linac will be long-pulsed, with pulse lengths on the order of several milliseconds, and of the solid state type. Rather than vacuum tubes, they will use solid state power switches with full on/off controllability, such as insulated gate bipolar transistors (IGBTs) or integrated gate commutated thyristors. This will lead to a considerable gain in terms of reliability, lifetime and maintainability. Due to the fact that all klystron modulators will be able to generate power pulses by themselves, the klystrons will not need a mode anode terminal, which will reduce their cost by up to 10% and increase their reliability considerably.

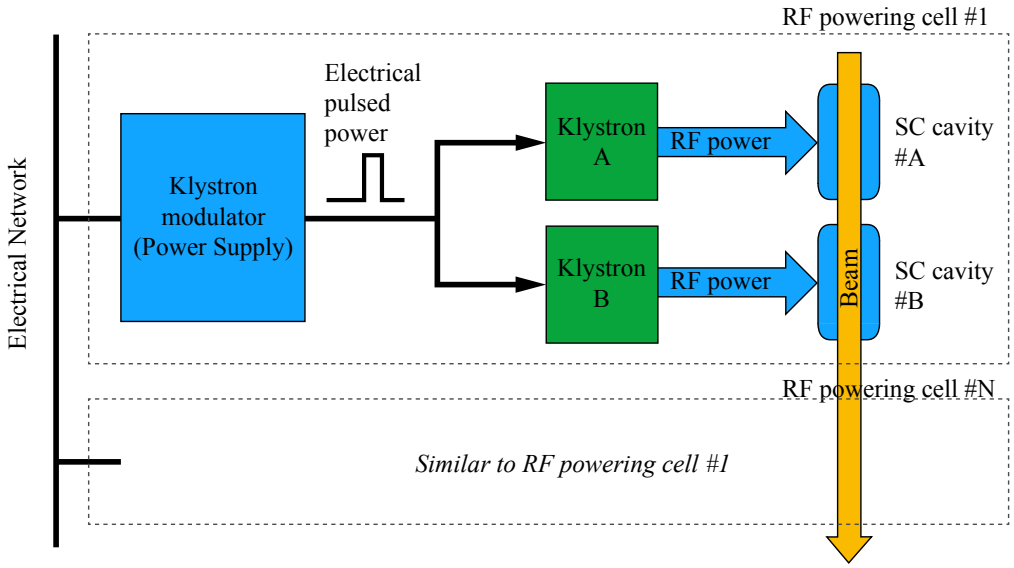

Figure 4.92: General powering scheme for klystrons and superconducting cavities. The example shows the linac high-β section.

Due to the voltage ratings, the use of crowbars in the high voltage cathode lines would require the use of vacuum tubes (thyratrons, ignitrons, etc.) which are to be avoided for reasons of cost, reliability and maintainability. Arc protection will therefore be performed by acting on the modulators "pulser" system, as if the pulse had to be interrupted early. A number of modulator topologies have been suggested in the literature, some of them developed by particle physics laboratories for applications similar to ESS, but unfortunately, not many are offered by well-established manufacturers. The modulator procurement schedule is quite tight, and the most straightforward approach will be to purchase this equipment from existing companies based on their current designs. This implies that ESS will not impose a specific modulator topology on its suppliers. Several topologies, differing considerably from one another, may be used in the accelerator.

Configuration of an RF powering cell

Figure 4.92 shows a simplified schematic of an RF source powering cell for the linac's high-β section. In this section, one modulator will feed two klystrons in parallel. In the medium-β section, one modulator will feed four klystrons in parallel, using the same connection scheme as in the high-β section. In the RFQ and DTL, one modulator will feed one klystron. In all linac sections, each klystron will feed one RF superconducting cavity.

Potential klystron modulator topologies

Figure 4.93 shows four examples of potential modulator topologies. The topology in the top panel is based on a monolithic pulse transformer. The circuit at the primary side of the transformer is at medium voltage and can be installed in a standard air-insulated cabinet. This circuit is formed by a capacitor charger, a main capacitor bank, a solid state switch assembly (usually based on a series association of several switch modules), a transformer demagnetisation circuit (undershoot network) and a passive bouncer system. An active bouncer, based on a fast switch mode power supply, could be an alternative. The pulse transformer increases the voltage to the level required by the cathode (typically above 100 kV) and therefore must be installed in an oil tank. The main drawback associated with this topology is the requirement for a pulse transformer, which is a bulky device that is only available from a single source worldwide. Its advantages are simplicity of construction and operation; higher reliability than alternatives; and easier maintainability since active components, such as semiconductors, are located in air-insulated cabinets, facilitating access for repair, while only the passive components, such as the pulse transformer, auxiliary inductors, and current and voltage sensors, are located within hermetically sealed oil tanks.

The topology in the middle top panel is a variant of the first, in which several primary side circuits are used instead of a single one. This topology is therefore partially modular, which allows for some operational redundancy and facilitates repair by allowing exchange of plug-in modules instead of individual components. Each primary sub-circuit is formed by a capacitor charger, a capacitor bank, a low voltage solid state switch and an undershoot network. These can be designed to operate at low or medium voltage. Each sub-circuit feeds one primary winding of the multi-primary winding (split core) pulse transformer. Due to its parallel switching nature, each solid state switch can be a standard single device. As in the first topology, a single passive bouncer may be used to compensate for the capacitors voltage droop. Besides the drawback associated with the pulse transformer itself, the droop compensation bouncer can be quite bulky and might dissipate a significant amount of power since the bouncer inductor is rated for considerably higher currents (much higher transformation ratio on the pulse transformer). Advantages over the first topology include the utilisation of standard low or medium voltage-rated power switch modules (for example, IGBTs) in single configurations; and modularity of the sub-circuits at the primary side.

The topology in middle bottom panel is transformer-less and almost entirely oil-immersed. A capacitor charger charges a main capacitor bank directly at the voltage level required by the cathode. A solid state switch assembly formed by the series association of several IGBTs is used for pulse forming, with pulse generation (switch closed) and pulse stop (switch open) either at the end of the pulse in normal conditions or abruptly in the case of a klystron arc. A fast switch mode power supply can be used as an active bouncer for capacitor voltage droop compensation in closed loop. This topology requires a high voltage switch assembly rated for the full cathode voltage, which is only available from a single source and is under patent. Furthermore, all components are immersed in an oil tank which both increases the quantity of oil within the system and complicates access to sensitive electronic components for repair.

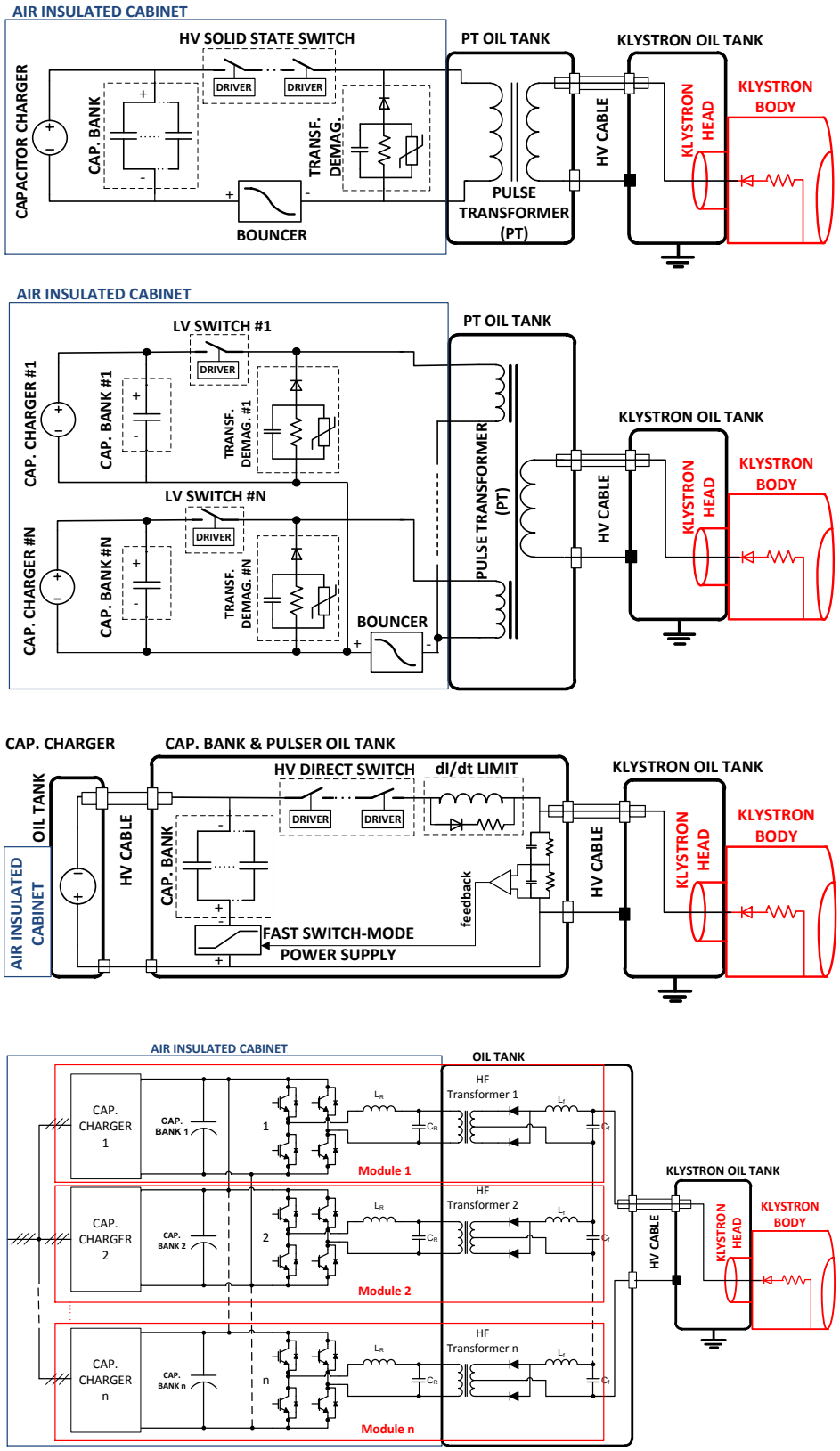

Figure 4.93: Potential modulator topologies: Top: Monolithic pulse transformer with passive bouncer. Middle top: Multi-primary winding pulse transformer with passive bouncer. Middle bottom: Direct switch with active bouncer. Bottom: Multi-level resonant converter.

The topology in the bottom panel is based on the association of several modules in series on the high voltage side and in parallel on the low or medium voltage side. Each module is formed by a capacitor charger, a main capacitor bank, an H-bridge inverter, a parallel resonant filter, a high frequency transformer, a diode rectifier bridge and a passive low-pass filter. All parts of the circuit up to the primary side of the HF transformers are placed in a standard air-insulated cabinet, since these circuits are operating at a low or medium voltage level. The HF transformers and all parts at the secondary side are placed in an oil tank. The primary to secondary side high voltage isolation is performed by the HF transformers. Compensation for capacitor voltage droop can be easily accomplished by acting on the controls of the H-bridges within a closed feedback loop. Due to the "de-queueing" effect (sudden damping of the parallel resonant circuit by load impedance reduction), the output current is self-limited to a safe value, usually two to three times the nominal current before the arc is detected and all H-bridges are switched off. This is the only topology for which all components are standard components that can be procured from at least three different sources. The topology is entirely modular. The potential for oversizing of the H-bridges power switches due to switching losses and reactive power handling with a negative impact on cost and efficiency is the main drawback, although this could be ameliorated by careful design and adoption of soft-switching techniques.

Types of high voltage insulation

Dividing klystron modulators into two parts – the first, at medium voltage, installed in an air-insulated cabinet, and the second, at the output high voltage level, installed in an oil tank – facilitates access for repair and diagnosis. The interface between the two parts could be implemented either by pulse transformers or by high frequency transformers. An entirely oil-insulated solution may be acceptable for ESS, but even in this case, the quantity of oil used should be minimised. Oil-free solutions, or solutions based on dry-type insulation are not acceptable for reasons of long term reliability. While ESS has not yet fully specified the modulator design, it has developed the following design rules:

1. Power parts subject to potentials below 50 kV are to be placed in air-insulated cabinets;
2. Power parts subject to potentials above 60 kV are to be placed in an oil tank; and
3. Power parts subject to potentials between 50 kV and 60 kV may be in oil or air-insulated containers, depending on the specific design.

Oil leakage prevention and oil type

An oil retention bin will be placed underneath oil tanks in order to prevent accidental leakage during operation or storage. If a single tank is used, the capacity of the retention bin must be equal to at least 110% of the oil capacity of the tank. In cases where several tanks are used within the same modulator, the retention bin dimensions will be governed by the same rule, applied to the highest capacity tank. For long term reliability and fire safety, silicon oil is preferred.

Interface specifications

The mains connection for the modulators is AC, three-phase and low voltage – 400 V ± 5%. A single connection port is foreseen to power the entire modulator. At the time of writing it is not clear whether an alternative DC grid will be adopted. A considerable level of flicker could be produced on the grid, because of the long modulator pulse length (about 3.5 ms), unless specific mitigation techniques are undertaken. No international standards exist limiting grid flicker for industrial equipment connected to private networks and absorbing a current higher than 75 A per phase, as will be the case for the modulators. However, ESS has reached an agreement with the local electrical distributor (Lunds Energi) that those international standards applicable to electrical appliances connected to a low voltage distribution grid (400 V) with currents below 75 A per phase will also apply to ESS klystron modulators. The klystron modulators will therefore conform to IEC/TS 61000-3-5 in matters related to flicker on the grid interface [497].[3]

[3]For the purpose of flicker assessment only, it will be assumed that the modulator is supplied from a network with infinite power via a dedicated distribution transformer whose rated power is 10% higher than the nominal average power of the modulator with a short circuit voltage of 5%.

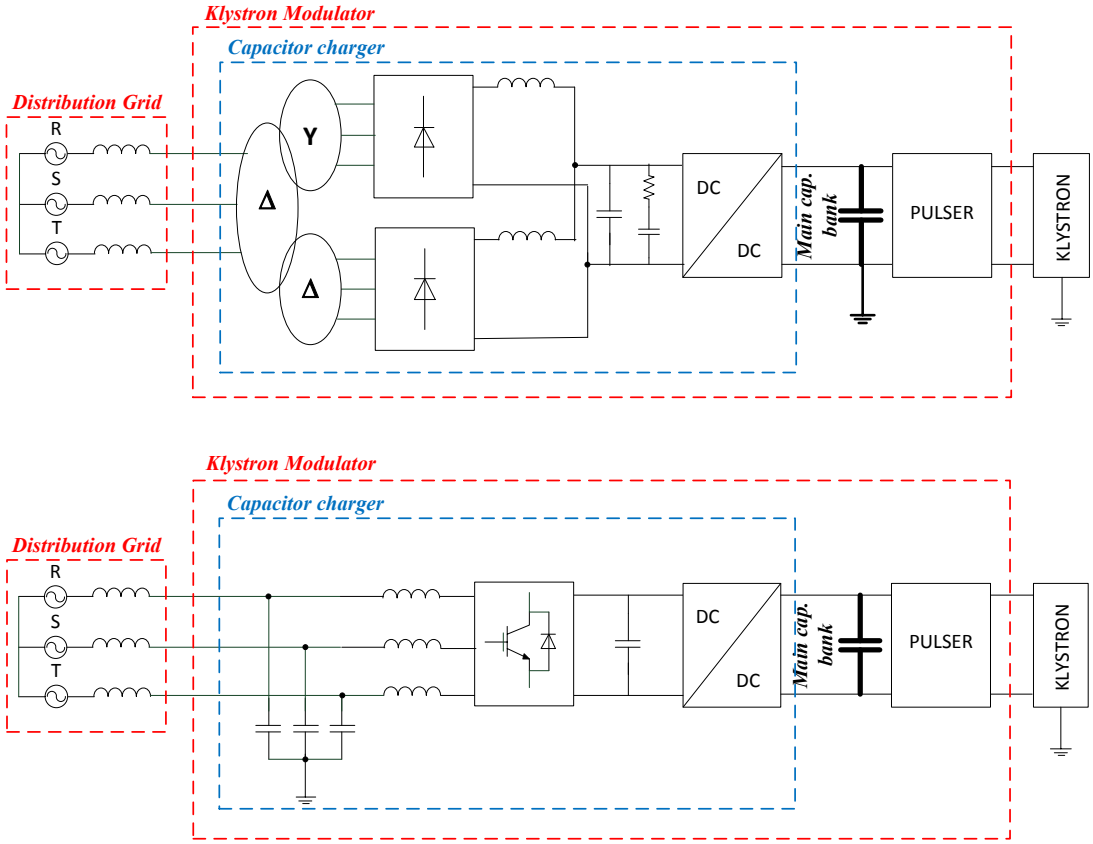

Figure 4.94: Potential capacitor charger topologies that mitigate flicker and emissions of low frequency current harmonics. Top: Twelve pulse rectification front end. Bottom: Sinusoidal current absorption active front end.

The maximum line voltage variation due to pulse operation at 14 Hz, measured at the input of a klystron modulator, is less than 0.2% of the nominal voltage. For matters related to low frequency current harmonic emissions on the grid, the klystron modulators will comply with IEC 61000-2-4 at their power input terminals [498]. The grid power quality will be determined mostly by the input stage of the klystron modulators, which is the capacitor charger. Figure 4.94 shows two alternative topologies for the capacitor chargers addressing the requirements for flicker and low frequency current emission standards. In both cases, a DC/DC converter is used to charge the main capacitor bank at constant power by using a power regulation loop. With the topology shown on the top, all current harmonics up to the 11th order (exclusive) are cancelled, while with the topology shown on the bottom, the current absorbed from the grid is almost purely sinusoidal.

HV link to klystrons

The modulators will be physically disassociated from the klystrons. The electrical connection between the modulator and the klystron (the HV link) is differential, meaning that the output current will return to the modulator via a dedicated cable and not via the common earth. This will avoid spreading leakage currents through unknown grounding loops. The connection between the modulators and the two klystrons will be performed in principle by using high voltage insulated cables and connector assemblies, rated for at least 160 kVDC. A low voltage insulated grounding cable can be used for the low potential side return connection. A feedthrough installed on the modulator's oil tank is appropriate for the internal connection to the return wire. In pulsed power applications, high voltage connectors may fail over time due to rapid and large voltage fluctuations (high dV/dt) between the internal wire and the external connector body at ground potential. Such high dV/dt values originate in the circulation of stray currents to ground via capacitive coupling, progressively degrading isolating materials. ESS will investigate the long term reliability of

high voltage cables and connectors in pulsed mode in partnership with the cable assembly manufacturers. An experimental setup will be developed to test the reliability of such cable assemblies. Should doubts persist about the reliability of the fast, high voltage cable/connector assemblies, an alternative will be developed. In such an alternate system, the high voltage cables would plunge within the oil tank thorough a hermetically sealed tank bushing, conserving the cable isolation gaskets intact at the tank-traversing point. The design would ensure that the high voltage wire contact is made sufficiently below the surface of the oil.

Grounding and electromagnetic compatibility precautions

Internal and external grounding will be adequate to ensure safety and electromagnetic compatibility (EMC) compliance. The enclosure formed by the various assembled cabinets will behave as a Faraday cage in order to limit radiated noise emissions. All cabinets will be individually EMC compliant and they will be bolted together with perforating screws or metallic plates in order to assure a good electrical contact up to very high frequencies. All cabinets and non-active metallic parts will be connected individually to an internal protective earth (PE) bus-bar. The purpose of this connection is to enhance personnel safety, and it may be made using normal grounding wires with appropriate cross sections. A direct link between the modulators PE busbar and the closest building grounding stick is foreseen, with appropriate copper grounding cables of short lengths. A direct link between the modulator oil tank and the klystron oil tanks is also planned using appropriate copper grounding cables of short lengths. Again, the purpose of this connection is to protect personnel rather than to serve EMC purposes.

Local and remote control and interlock links

Three control and interlock links are planned. First, a remote control link will make all modulator control actions and monitoring available in the integrated control system through a link using EPICS based control boxes, as discussed in Chapter 5. Second, there will be a local control system for human machine interface based on a touchscreen display. Third, a hardwired interlock link will connect each modulator to the local RF control system. Table 4.32 lists the logical signals in the hardwired interlock link.

Cooling

Demineralised water cooling will be essential for the modulators. A single inlet/outlet adaptor will be used to interconnect each modulator to the external water cooling circuits. The most dissipative components, such as the power semiconductors, switch assemblies, oil tanks and power inductors, will be water-cooled. The maximum power losses dissipated to the air will not exceed 10% of total modulator losses under nominal operating conditions. The modulators' demineralised water cooling system will meet the requirements listed in Table 4.33.

Electromagnetic compatibility

The klystron modulators will comply with IEC standards with respect to noise emission and immunity, even though these standards were designed for electrical appliances connected to a public low voltage grid. This conservative measure is intended to assure that RF interferences that would disturb the LLRF systems are avoided, especially in proximity to the LLRF systems. The adopted EMC standard references

Signal name	Direction	Purpose
MOD_FAILURE	output	Sum of modulator internal faults.
PULSE_START	input	Reference signal for starting a pulse. The length of this signal will be the length of the HV pulse being generated.
CABLE_CONNECT	output	Check for hardwired interlock cable well plugged in.
MOD_FAST_ABORT	input	Modulator fast power abort.
PULSE_PERMIT	input	Modulator permission to pulse.

Table 4.32: Logical signals in the hardwired modulator interlock link. The direction is with respect to the modulator.

Parameter	Unit	Value
Maximum water conductivity	μS/cm	1.2
Operating pressure	Pa	16
Testing pressure	Pa	24
Maximum inlet/outlet pressure drop	Pa	3
Maximum inlet/outlet temperature rise	°C	15
Maximum inlet temperature	°C	27
Maximum available water flow	m^3/hr	2.5

Table 4.33: Properties of the demineralised water in the modulators.

are: 1) on noise emission: CISPR 11; EN 55011 class B, at the AC mains [499]; and 2) on immunity: IEC-61000-4 (Level 4) on AC mains and all external controls/interlock cables [500].

Safety devices and apparatus

In klystron modulators, as in any other high voltage electrical equipment storing a large quantity of energy, safety is a top priority during design and construction. Specifications must be clear, complete and in compliance with the most advanced safety rules, standards and best implementation practices. Within this context, ESS has adopted the following design and construction rules for the modulators:

1. Capacitor bank(s) will be equipped with an automatic fast discharging system. This system will be formed by an electromechanical HV relay in series with a rugged discharge resistor.
2. Manual short-circuiting power switches will be connected in parallel with each capacitor bank to guarantee full discharge status before any human intervention inside the cabinet takes place. This redundancy feature is mandatory as the automatic discharge system may fail, for instance due to discharge resistance damage or wiring breakdown.
3. A “fast stop” red button will be installed close to the ICS chassis enabling personnel to immediately stop the modulator system. Action on this button will be assigned priority by the PPS and MPS, as it relates to matters of personnel and material safety.
4. Each door to the power cabinets will have an auxiliary switch indicating whether or not the door is open. If this switch moves to the “door open” position, the ICS will activate all capacitor bank automatic fast discharging systems. The switch and fast discharging systems will be designed and engineered for the highest level of reliability.
5. If either the “fast stop” or the door interlock is activated, the ICS will automatically ensure that: all “pulser” switches are deactivated; capacitor charger is inhibited; capacitor automatic fast discharging system is activated; and the main circuit breaker is opened. No software programmable devices will be allowed within the signal processing chains associated with the execution of these safety actions.
6. If required, one or several grounding rods will be installed outside the klystron modulator cabinet. A set of discharging points in the power circuit will guarantee that all capacitors in the circuit and all possible stray capacitances are fully discharged before human intervention.
7. The klystron modulator will be equipped with one voltmeter per capacitor or per capacitor bank.
8. Each oil tank having an oil capacity above 25 l will be equipped with the following interlock and monitoring sensors: one oil pressure switch, one oil over-temperature switch, one oil pressure sensor and one oil temperature sensor.

Klystron arc detection and protection

Klystron modulators are responsible for detecting and extinguishing arcs inside the klystrons. A maximum limit for the energy dissipated within an arc is specified by the klystron manufacturer. It is usually set to 20 J. A factor of two is applied to this limit to provide a safety margin in the design. A constant arc voltage of 50 V will be used to evaluate the arc energy.

Modulator dimensions

The external dimensions of the klystron modulators have been extrapolated from similar projects. It will be possible to view and handle the modulators as a single block although they may be formed by several racks assembled in a common base frame. The maximum external dimensions are 1.5 m × 4 m × 2.2 m (length × width × height).

Reliability, repairability and availability

Equipment must be extremely reliable, require a minimum of maintenance and must facilitate easy replacement of faulty components. The equipment will be operated remotely and continuously, 24 hours per day, for about 250 days per year. Maintenance will be restricted to the annual shutdown period. The estimated service life of the equipment is 140,000 hours over 25 years. All components will be rated according to the "worst-case" design principle. In other words, the "mean time between failures" (MTBF) called for in component specifications will be evaluated under worst-case operating conditions. The MTBF for the klystron modulators must be at least 50,000 hours. The "mean time to repair" (MTTR) for the modulator will be specified with the equipment installed in its final location in the RF gallery where no crane will be available. Requirements call for an MTTR of less than three hours, measured from the instant when the first repair action takes place. Together, these MTBF and MTTR requirements yield an estimated global availability for the approximately 100 modulators of 99.2%.[4]

Testing methodology and facilities

The production of klystron modulators will be divided into three steps: 1) prototypes: one per contractor; 2) pre-series: first unit of the series production for each contractor; and 3) series: remaining units for each contractor.

Klystron modulators will undergo acceptance testing at the manufacturers premises before delivery. ESS will include a testing protocol in the technical specifications that it sends out for tendering that specifies type tests for prototype and pre-series units and routine tests for series units. In both the type and the routine tests, the protocol will call for an initial set of tests at "no power", during which all interlocks, control and command signals, control systems, and water circuits will be individually checked. It will also call for a pressure test of all water circuits in all units. In addition, in the routine tests, all units will be tested at nominal power for about 10 minutes, possibly with a dummy load. The main waveforms and associated parameters will be measured, recorded and analysed for assessment of compliance with technical specifications. In addition, heat run tests lasting at least 12 hours will be performed in the prototype and pre-series tests; a routine arc test will be performed under nominal operating conditions in all units; and EMC measurements of emissions and immunity, low frequency current harmonic distortion and flicker assessment will be performed on the prototypes and pre-series units, according to the procedures outlined in the IEC standards discussed above.

As a complement to this testing campaign, all prototypes will be extensively tested at the Lund RF test stand according to a testing protocol written specifically for prototypes before authorisation is given to the contractors for pre-series and series production. This extensive testing campaign will last for about one year and will be performed both with dummy loads and klystrons. Pre-series units will also be tested at the ESS test stand at nominal power and under realistic machine operating conditions. The load will be a set of two klystrons connected in parallel, of the same type and reference as the ones selected for the accelerator. The pre-series testing campaign will last from a few weeks to a few months, depending on the quality of the systems being delivered. The ESS test stand will allow for the simultaneous testing of 4 modulators at full power with their klystrons or dummy loads. Electrical feeders will supply the required power; water cooling sufficient for 8 klystrons or dummy loads will be provided; appropriate instrumentation will be installed; and a set of devices for handling, transportation and oil manipulation will be provided, as discussed in Chapter 6.

Finally, each series modulator will be commissioned at its final location in the RF gallery with its associated klystrons and RF cavities or with RF dummy loads. The gallery will be designed to allow for the occasional testing of a particular modulator at its final location with a dummy load during normal operation, in case longer term troubleshooting or specific testing is found to be necessary.

[4]This availability estimate added an hour of downtime to the MTTR to account for technicians displacement and preparation for the repair work.

Spare parts and component availability

A certain number of completely functional spare modulator units will be required (in principle, about 5% of the total number of units). This spare capacity will be provided for from the early stages of the tendering process. Options for ordering additional units at an agreed price for a given period of time also will be addressed in the contracts. In addition, a specific set of spare parts, equal to about 5% of the operating inventory of each device type, will be purchased and delivered with the series units. This will include but will not be limited to: capacitor charger units, main capacitor banks, automatic discharge systems and manual grounding switches, pulse-forming units, pulse or isolation transformers if required by the topology, solid state switches or switch assemblies, control cards and chassis, water circuit components, HV pulsed cables and connectors, and high precision measuring devices such as voltage dividers or current transformers. As with the modulator units, options for ordering additional components or subsystems at an agreed price for a given period of time will be addressed in the contracts. Selected components will be acquired from a second source independent from the one used by the contractors, to the maximum extent possible, in order to ensure availability of replacement parts over time. A plan for spare parts storage and inventory management will be put in place during the last two years of the construction phase.

4.8.6 Spoke RF power (352 MHz)

The linac has 28 superconducting spoke cavities at 352 MHz. The power coupled to the beam ranges from 162 kW to 239 kW per coupler for beam current of 50 mA. The RF amplifier powers the spoke cavities via the RF distribution system. Adding 5% loss overhead in the RF distribution system and 25% power overhead for LLRF, the power for the RF amplifier ranges from 225 kW to 350 kW. Spoke amplifier requirements are given in Table 4.34. Each spoke cryomodule contains two spoke cavities, so the Uppsala test stand has two RF chains, each including at least one high-power RF amplifier, DC power supplies, at least one pre-amplifier, RF distribution, a bunker, an LLRF system, and water and air cooling. The centre frequency of the high power amplifier and pre-amplifier is the same as for the superconducting spoke cavities: 352.21 MHz. The beam pulse length is 2.86 ms at a repetition rate of 14 Hz, the fill time of the cavity is no greater than 400 μs, and no forward power is required after the beam pulse. Hence, the RF pulse width will be greater than 3.26 ms and the duty factor of the amplifier and the pre-amplifier will be greater than 4.6%. The loaded Q of the cavity is about 160,000, setting the cavity bandwidth at about 2 kHz. The amplifier bandwidth should be at least 10 times larger than the cavity bandwidth for tuning and regulation delay, so the amplifier 3 dB bandwidth at maximum saturated power will be greater than 200 kHz. The preamplifier bandwidth should be at least twice that of the tetrode amplifier: greater than 400 kHz. The bandwidth of all the components in the RF distribution system will have to be at least twice that of the preamplifier: the design calls for 1 MHz. The distance between the two adjacent spoke cavities is 2.1 m so the average spacing between the amplifiers (and pre-amplifiers) will be no greater than 2.1 m.

High power RF amplifier

The capital and running cost of an accelerator is strongly affected by the RF power amplifiers in a number of ways. The capital cost of the amplifiers (including replacement tubes) is an appreciable part of the total capital cost of the accelerator. Their efficiency determines the electric power required and, therefore, the running cost. The gain of the power amplifier determines the number of stages required in the RF amplifier chain. The size and weight of the amplifiers determines the space required and will therefore, have an influence on the size and cost of the gallery. Hence, power source selection is very important.

Parameter	Unit	Value
Frequency	MHz	352.21
Maximum power at saturation	kW	350
3 dB bandwidth	kHz	200
Pulse width	ms	3.5
Pulse repetition rate	Hz	14

Table 4.34: Spoke amplifier requirements.

Among the different varieties of amplifiers, the tetrode is the cheapest solution by far – it's cost is at most one tenth the cost of the other amplifiers. A tetrode can have a high efficiency depending on the class of operation – in class AB its efficiency may be greater than 65%. The size of the amplifier is determined by the size of the output cavity, which is about one square meter. Its gain is 13 to 15 dB, so that it needs a pre-driver. It can be water-cooled to avoid blower noise. The tetrode can work with standard DC power supplies. It requires power supplies for anode, filament, control grid and screen grid. It also provides a very reliable system. A tetrode doesn't fail suddenly, but shows a graceful degradation, thus facilitating preventive maintenance. For all these reasons, the tetrode will be used as the high power amplifier for the first chain of the Uppsala test stand.

A recent study showed that three tetrode models manufactured by Thales (TH781, TH391 and TH595) could be used. The TH781 model would produce 350 kW at 352 MHz, but at reduced gain and efficiency. Though the TH391 model would offer better gain and efficiency, it is air-cooled, which allows anode dissipation of only 12 kW. The TH595 model is water-cooled and hence has higher anode dissipation of 40 kW, and will lead to a more compact system. The 350 kW power would be generated by combining outputs from two TH595 tetrodes each producing 175 kW, with power combination through a 3 dB hybrid coupler. An anode current above 45 A is not permissible for the TH595, so the tetrode can not be operated in deep class C mode. Calculations suggest that the TH595 tetrodes would operate best in class B, achieving lower harmonic distortion than in class C operation, with more efficiency than in class A operation. A quiescent current of 2 A flowing through the tetrode would lead to dissipation and hence decreased efficiency. To avoid this, control grid power supply will be modulated to make it more negative before and after the RF pulse to get nearly zero quiescent current.

The target anode efficiency of the tetrode amplifier is more than 65%. Tetrode gain decreases during ageing were taken into consideration during calculations of the required pre-driver power. The calculations assumed a gain of 13 dB, leading to a calculated pre-driver output power requirement of 10 kW. The output flange of the tetrode amplifier is 50 Ω, 6-1/8 inch. The input flange of the tetrode amplifier is 50 Ω, 7/8 inch. The spoke cavity will provide a reflected energy of at least 500 J. To protect the tetrode from the reflected energy, a circulator will provide isolation of more than 20 dB. The circulator may be located at the output of each tetrode amplifier, or it can be located after the point at which the output power from the two tetrodes has been combined. After comparing RF distribution systems in terms of size, cost and ease of handling, the RF distribution system shown in Figure 4.95 represents the finalised design. A circulator is present at the output of each tetrode.

The MTBF of the tetrodes will be greater than 3,200 hours, yielding an expected tetrode failure rate of once every 800 hours, or once per month, for a system of four tetrodes. The mean time to repair or replace the tetrode is less than three hours. A two to three hour repair time every 800 hours contributes less than 0.4% of downtime. Care will be taken while designing the output and input cavity so as to make replacement of tetrodes easy.

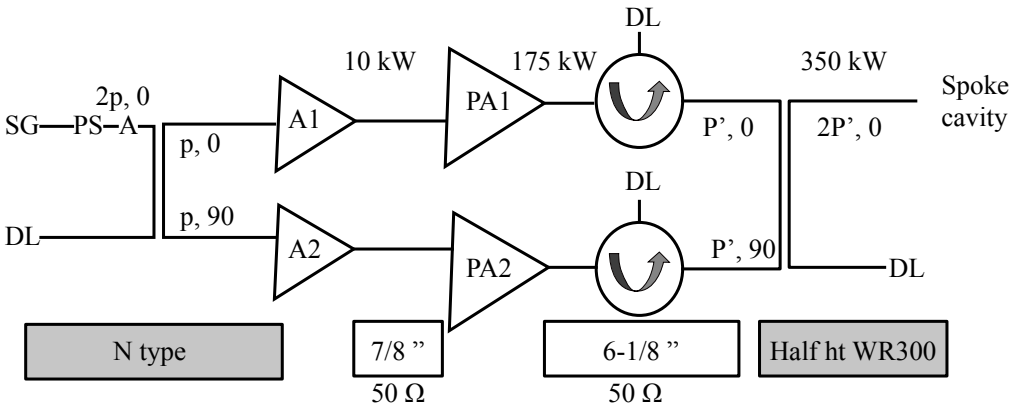

Figure 4.95: Schematic of amplifier and RF distribution layout at the Uppsala test stand. Solid lines indicate RF distribution. PS: phase shifter. A1, A2: attenuators. PA1, PA2: preamplifiers. DL: high power amplifier.

Tetrode power supplies

Figure 4.96 shows a schematic of a tetrode with the DC power supplies. Each tetrode amplifier will need four power supplies: an anode power supply (18 kV, 18 A, average output power = 31 kW), screen-grid power-supply (1.3 kV, 0.7 A), control-grid power-supply (400 V, 0.7 A), and filament power supply (8.8 V, 190 A rms). The anode power supply will be a capacitor charger with capacitor and series switches for the output. The filament, control grid and screen grid power supplies will be commercial of the shelf. All the power supplies will have their own control system for switch-on sequence, control and monitoring. It will have the necessary interlocks to address such issues as cooling failure, over voltage, over current, crowbar et cetera. As there are 4 tetrodes in the Uppsala test stand, it will need four sets of power supplies. Instead of using separate anode power supplies, a single anode power supply with two outputs will be used, thus achieving lower cost and size. Instead of a crowbar, a series switch will be used for protection. When a crowbar is used, if a pulse is missed, the capacitor is discharged, so that the next few pulses are also missed. Series switches avoid this problem, increasing the reliability of the system. The maximum output voltage will be 18 kV. The output pulsed current will be 18 A for each output. The output voltage droop will be less than 1 kV. The average power will be 31 kW. The efficiency will be better than 80%. A series switch that opens when the current exceeds 27 A will be provided. An anode power supply requires a wire burn test to ensure its correct operation during peak voltage and current values. A copper wire of 0.2 mm in diameter and 36 cm long will be used for this test.

Each of the 4 amplifiers will also need a screen grid power supply. The maximum output voltage and current for the screen grid power supply will be 1.3 kV and 0.7 A. Similarly, each of the 4 amplifiers will need one control grid power supply, with maximum output voltage of 400 V and maximum output current of 0.7 A, and one filament power-supply, with maximum output voltage of 8.8 V and maximum output current of 190 A. In order to protect the screen grid and control grid power supplies from high voltage from the tetrode, the tetrode output will be equipped with a high voltage diode in parallel with a high resistance of 2 kΩ, the combination in series with the output.

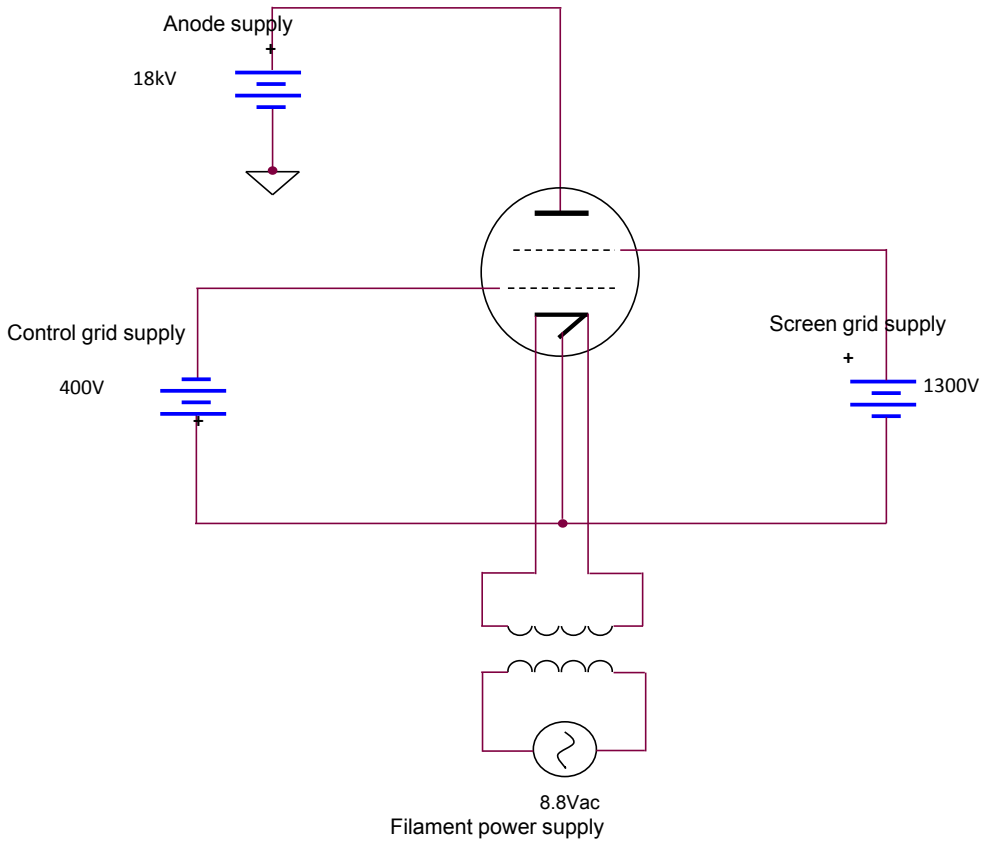

Figure 4.96: Schematic of Uppsala test stand high power tetrode amplifier with DC power supplies.

Pre-amplifier for the high power tetrode

A triode is cheaper than a solid state amplifier, but the low gain of a triode would require the pre-driver to have three stages with two triodes, one solid state amplifier and six power supplies. This rather complex system, combined with the low lifetime of a triode and the rather large number of power supplies, makes the probability of failure relatively high and the system reliability relatively low. In contrast, the solid state amplifier is modular with a built in redundancy, making it more reliable. The test stand will use modular sold state technology for the pre-amplifier. Each module will consist of a laterally diffused metal oxide semiconductor which will have circulators for protection from the reflected power. Modules will be driven in class AB, to avoid non-linearity. A blanking signal will be applied to the amplifier during the absence of the RF pulse, to avoid unnecessary power dissipation and to increase efficiency. The target efficiency of the tetrode amplifier is 50% to 55%. The gain of the preamplifier will be more than 73 dB, so that input power to the pre-amplifier will be from the signal generator. The output flange of the pre-amplifier will be 50 Ω, 7/8 inch, and the input connector will be 50 Ω, 7/8 inch. The solid state amplifier will be modular.

The mean time between failures for the pre-amplifiers will be greater than 6400 hours, so that a pre-amplifier failure can be expected to occur once every 1600 hours, or once every two months, for a system of four pre-amplifiers. Solid state amplifiers also offer built-in redundancy, leading to very stable operation. In the event of a single module failure, redundant modules can be brought online, or the remaining modules can be operated with a higher input power, so as to provide 10 kW power to the tetrode amplifier. The mean time to repair or replace the amplifier is very low, on the order of a few minutes. Using a conservative value of 15 minutes, pre-amplifier repair time will contribute less than 0.05% downtime. Sufficient space must be allocated around the pre-amplifier to facilitate easy replacement of the modules.

RF distribution

A schematic of the RF distribution layout is shown in Figure 4.95. In this design, power on the order of a few mW is divided by a hybrid coupler into two 3 dB down outputs, with a relative phase shift of 90 degrees. Each of these outputs is applied to the pre-amplifier. The pre-amplifier amplifies this output to 10 kW. This 10 kW power is applied at the input of the high power tetrode amplifier, which produces an output power of 175 kW. Each tetrode amplifier is protected by means of a circulator from the reflected power. Outputs of both the tetrodes will have a relative phase shift of 90 between the two. These two outputs are combined with the help of a hybrid coupler to produce 350 kW power. Any phase shift and amplitude errors can be corrected by an attenuator and phase shifter located after the signal generator with the help of LLRF.

As shown in Figure 4.95, there will be four power levels, so there will be more than one type of RF distribution. Power input to the pre-amplifier will be a few mW. N-type SMA connectors and the corresponding 50 Ω cables will be used for this purpose. Power output from the pre-amplifier will be 10 kW. As the maximum power handling capability of 7/8 inch, 50 Ω line at 352 MHz is more than 50 kW, 7/8 inch coaxial line will be used for RF distribution at this power level. Finally, the tetrode amplifier will amplify the 10kW power into 175 kW. At 352 MHz, the maximum power-carrying capability of 50 Ω, 6-1/8 inch line is more than 1 MW. Hence, for peak power of 175 kW, 6-1/8 inch, 50 Ω coaxial line can be used. The spoke cavity may reflect energy of 500 J. To protect the tetrode from the reflected energy, a circulator with isolation of 20 dB will be used. The circulator can be located immediately after the tetrode or after the power from the two outputs has been combined. The size of a circulator using 6-1/8 inch coaxial line is only 0.6 m × 0.6 m × 0.5 m, while the size of a circulator in half height WR2300 waveguide is 2.5 m × 2.5 m × 0.5 m. Hence, a circulator in 6-1/8inch coaxial line will be used immediately after the tetrode amplifier. The outputs of the tetrode amplifier will be connected to the hybrid coupler through the circulator.

The return loss of all the components in the RF distribution system components needs to be better than about 30 dB and the insertion loss of all its components needs to be better than about 0.05 dB. The material of the coaxial line (both 6-1/8 inch and 7/8 inch) needs to have a low loss to satisfy the requirement of 5% of loss overhead in distribution system, so the outer conductor will be composed either of tempered 6061 aluminium alloy – T6 or equivalent – or copper. The magnetic field will be very strong at the inner conductor, which needs to have good conductivity: the material of choice is ETP copper. The inner conductor joint will be made of Be-Cu and Teflon supports may be used. The coaxial line doesn't need pressurisation, so the wall thickness of the outer conductor and inner conductor may be as thin as

1.85 mm and 1 mm respectively. Each RF distribution system (both 7/8 inch and 6-1/8 inch) needs to have dual directional couplers to monitor forward and reflected power. One coupler will be at the input and output of the pre-amplifier and high power tetrode amplifier. The length of the coaxial lines will be kept as short as possible. Each tetrode amplifier chain will have two directional couplers of 6-1/8 inch and 7/8 inch coaxial line. The distribution systems need bends for bending the coaxial line. Each tetrode amplifier chain will have 12 coaxial 6-1/8 inch bends and at least 3 7/8 inch bends.

During cavity fill time (400 μs) and tuning, the circulator has to handle 100% reflection. The power handling capability of 6-1/8 inch, 50 Ω line is more than 1 MW, hence 6-1/8 inch circulator can be used without pressurisation. The insertion loss of the circulator needs to be less than 0.1 dB. The cavity will supply reflected energy of 500 J per pulse. The tetrode is able to withstand a maximum reflected energy of 20 J per pulse, so the circulator will provide isolation of more than 20 dB. As the power level is low, the circulator will not have a temperature compensation loop. The circulator will have an electromagnet whose magnetic field is compensated for changes in the return loss of the circulator. Each tetrode chain will need one circulator. The dummy load will be connected to the third port of the circulator so that under mismatch conditions, power reflected from the cavity is absorbed in the dummy load. The dummy load can be either a water or a ferrite load. A water load would need an RF window separating the coolant from the waveguide. The coolant will be an ethylene-glycol water mixture. There is a chances that the window could develop cracks leading to water leakage inside the RF system. As a result, a ferrite load is preferred over a water load. But due to construction difficulties, ferrite loads are available only in waveguide geometry, so a ferrite load with half height WR2300 will be used along with a 6-1/8 inch coaxial to waveguide adapter. Each tetrode chain will need one ferrite load and one coaxial 6-1/8 inch coaxial to waveguide adapter.

The hybrid coupler will combine the power to 350 kW. One hybrid coupler is needed for each amplifier chain. The hybrid coupler, as well as the rest of RF distribution up to the spoke cavities, needs to be able to handle 350 kW power and 100% reflected power during initial cavity fill time. As the maximum power carrying capability of half height WR2300 is more than 10 MW, it will be used for RF distribution at 350 kW power. The 6-1/8 inch coaxial line can also serve this purpose, but installation and cooling would be difficult, as it contains inner conductor, outer conductor, inner conductor joints and either teflon or ceramic rods to support the inner conductor inside the outer conductor. Hence the length of 6-1/8 inch coaxial line section is kept to a minimum.

The WR2300 half-height RF distribution needs rigid and flexible waveguides, directional coupler, dummy loads, H-bends and E-bends. Each RF distribution system using half-height WR2300 waveguide needs to have dual directional couplers to monitor forward and reflected power. One coupler will be located after the hybrid coupler and the second before the spoke cavity, so for one tetrode chain, the total number of dual directional couplers will be two. Coupling of the dual directional coupler needs to be between 50 to 70 dB, and the directivity of the dual directional coupler needs to be better than 27 dB. The distribution system will need some flexible waveguides to take care of mechanical alignment. Each RF distribution system may need one or two flexible waveguides to take care of mechanical assembly, but for the test stand, the use of flexible waveguides will be avoided as much as possible. The preliminary design calls for one flexible waveguide per tetrode chain.

4.8.7 High power RF distribution (702 MHz)

The 702 MHz high power RF distribution system takes power from the klystrons to the medium-β and high-β elliptical cavity. Each cryomodule contains four cavities. The Lund test stand will have the capacity to test two cryomodules in parallel, with each cavity driven by one klystron, for a total of eight high-β RF distribution systems. Table 4.35 lists the number of components for each medium-β and high-β RF distribution chain. Other relevant parameters are listed in Table 4.36.

Waveguide type, material, and wall thickness

The high power RF distribution system will use WR1150 waveguide, which has an upper cutoff frequency of 1026 MHz – an adequate safety margin over the WR1500 cutoff frequency of 787 MHz. WR1150 waveguide is also thinner and lighter than WR1500, facilitating handling and reducing costs. The output power of the klystrons will be 1250 kW and the cavity filling time will be 250 μs, so the waveguide must be able to handle a peak power of 1250 kW with full reflection during 250 μs or during tuning. The WR1150 waveguide will

Parameter	Unit	Value
Length of waveguide	m	40
Number of E-bends		6
Number of H-bends		6
Number of circulators		1
Number of dummy loads		1
Number of flexible wave guide sections		3
Number of dual directional couplers		2

Table 4.35: Component count for each medium-β and high-β RF distribution chain.

	Units	Lund test stand	RFQ	MEBT	DTL	Spoke	Med. β	High β
RF distbtn. systems		8	1	N/A	4	28	64	120
Frequency	MHz	704	352		352	352	704	704
Peak power	kW	1250	1600		2900	350	800	1250
Waveguide width	in	11.5	23.0		23.0	23.0 half height	11.5	11.5

Table 4.36: High power RF distribution parameters.

not need pressurisation, because its power carrying capability is more than 10 MW. The wall thickness will need to be (only) at least 1/8 of an inch. The WR1150 material needs to have low loss to satisfy the requirement of 5% loss overhead in distribution. Copper waveguides provide a loss of 0.002 dB/m, while aluminium waveguides provide a loss of 0.03 dB/m. Copper is more expensive than aluminium and the density of copper is three times that of aluminium. Thus copper waveguides would be heavier and more expensive than aluminium waveguides. Hence, it has been decided to use Aluminium 6061 – T6, or an equivalent material. The duty factor for the klystron is greater than 4.6%, so the waveguide will handle average power of 60 kW. The waveguide absorbs power of at least 150 W/m, so it needs water cooling.

RF distribution components

The klystron bandwidth will be greater than 100 kHz, and the bandwidth of RF distribution system components must be at least 10 times larger: 1 MHz. Similarly, the return loss of the klystron will be 30 dB, so the return loss for the components of the RF distribution system will have to be better than 30 dB, and the insertion loss needs to be better than 0.05 dB. The RF distribution system will have dual directional couplers for monitoring forward and reflected power. Coupling of the dual directional couplers needs to be between 50 and 70 dB. Directivity of the dual directional couplers needs to be better than 27 dB. One coupler will be located after the high power RF amplifier and the second before the high-β elliptical cavity. Thus, each RF distribution system will have to have two waveguide dual directional couplers, and the Lund test stand will have 16 dual directional couplers. Each RF distribution system will have 6 E-bends and 6 H-bends for bending the waveguides, so that the Lund test stand will have 36 E-bends and 36 H-bends altogether. Each RF distribution system will require as many as three flexible waveguides to take care of mechanical alignment, for a total of up to 24 flexible waveguides in the Lund test stand. During cavity fill time (250 μs) and tuning, the circulator will have to handle 100% reflection.

The power-handling capability of WR1500 waveguide is 1.5 times that of WR1150. To avoid the need for pressurisation, WR1500 wave guide will be used to make the circulator. As the circulator is made up of WR1500 and the RF distribution system is made up of WR1150, all the ports of the circulator will be equipped with adapters for WR 1500 to WR 1150. Insertion loss in the circulator needs to be less than 0.1 dB. The cavity will supply reflected energy of 1100 J per pulse. The klystron will be able to withstand reflected energy of no more than 20 J per pulse, so the circulator will provide isolation of more than 20 dB. Circulators contain anisotropic ferrite materials, so their losses increase with temperature. To have low ferrite losses as well as good isolation, the circulator will have an electromagnet whose magnetic field is compensated for changes in temperature. To achieve high efficiency in the klystrons, the circulator

needs to offer matched impedance, so it will have an electromagnet whose magnetic field is compensated for changes in the return loss of the circulator. Each RF distribution will need one circulator, so the total number of circulators for the Lund test stand will be eight. The dummy load will be connected to the third port of the circulator so that under mismatch conditions, it will absorb power reflected from the cavity. A water load would require an RF window to separate the ethylene-glycol water mixture that is used as coolant from the waveguide, but that window could develop cracks leading to water leakage inside the RF system. For this reason, ESS will use ferrite loads. Each RF distribution will need one circulator.

RF distribution system protection

The RF distribution system will contain various mechanisms to detect arcs, increases in reflected power, or problems with cooling and to send fast signals to the LLRF and to the machine and personnel protection safety systems described in Sections 5.2.2 and 5.2.3, in order to protect equipment and personnel by tripping the system. Arc detectors will be placed in circulators, among other places in the RF distribution system. Reflected power will be monitored by the dual directional coupler. If reflected power is more than 40% during a pulse, the system will be tripped. Flow meters and pressure gauges will be placed throughout the RF distribution system.

4.8.8 RF gallery

Lund test stand

The Lund test stand part of the RF gallery will be housed in the upgrade section which occupies the last 70 to 90 meters of the accelerator building. There will be 1,200 to 2,000 square meters available at this end of the building equipped with the necessary power and cooling utilities. The test facility will use RF for modulator soak tests and klystron RF tests. To successfully carry out these tests, the test facility part of the gallery will require enough cooling capacity and electrical power to power four modulators and eight klystrons and enough HVAC capacity to take up excess heat not dissipated by water cooling systems and to provide stable environmental temperature and humidity for the test facility. It will also need equipment to move and handle both klystrons and modulators, and enough space to house the modulators, the klystrons, and their associated control and monitoring equipment and to record results (the control and monitoring instrument racks). It will also require space to mount the necessary waveguides, circulators, and loads for the operation of modulators and klystrons or beam sticks (for some modulator only tests beam sticks will be necessary), and the equipment required to assemble and mount the waveguides, circulators, loads and other equipment needed for the tests. It will also need space to keep one klystron ready for deployment (warm cathode, solenoid, etc.) and storage space for spares needed for the operation and maintenance of the facility.

The cooling system for the test facility will recycle as much as possible of the excess heat from the equipment for use in the district heating system. This means that ESS will operate without any cooling tower or similar facility. Instead, heat will be dissipated via a heat exchanger into the heating system. Inside the test facility, the preliminary design calls for three general temperature levels: 20°C, 40°C, and 60°C. The coolant will be DI water, with a resistivity of 1 MΩ to 10 MΩ, so the gallery will be equipped with facilities for handling and filtering DI water. As much heat as possible will be dissipated to the high temperature loop since recycling efficiency improves dramatically with higher temperature, so the klystron or amplifier collectors, which dissipate the largest amount of power, will probably routed on the high temperature loop. For logistical reasons, the circulator and load cooling will be routed to this loop as well. The klystron body and magnet cooling will be routed to the mid-temperature loop; and the instrument racks, modulators, etc, will be routed to the low temperature loop. The cooling capacity for the test stand will be able to dissipate 21.6 kW per modulator and 112 kW per klystron, or 950 kW total for the eight klystrons and four modulators. The split between the loops is under discussion. The water cooling system will operate with 10 MΩ water in a loop covering the whole gallery. Nominal pressure will be 8 Pa, max pressure 11 Pa.

The electrical power system in the gallery will provide three phase AC, 690 V for the power equipment and 400 V for other purposes. The installed power needs for the test stand will be 1060 kVA. The cooling and power demands for the test stand are summarised in Table 4.37. The HVAC system will deal with the heat not dissipated by the cooling system, and will provide stable environmental temperature and humidity in the gallery. The gallery will be equipped with several air-handlers. It is expected that the

Linac component	**Count**	**Installed power** [MVA]	**Cooling power** [MW]	**Cooling water flow rate** [l/m]
Klystrons	8	0.12	0.09	860
HV modulators	4	0.96	0.86	83
Sum		1.08	0.95	943

Table 4.37: Cooling and power demands of components to be tested on the Lund test stand.

temperature will be regulated to a value of 22.5 ± 2.5°C. Based on the experience of the SNS gallery adjusted for eight klystrons, the air handling capacity will be 200,000 lpm for the test stand.

Assembly and test

The gallery will require facilities to move heavy equipment, especially the modulators and klystrons, which weigh in at several tons. A faulty klystron may have to be replaced within 4 to 8 hours or a modulator may have to be repaired. It is suggested that a specially constructed forklift be used for the long hauls. At the test stand, a crane will be needed to lift and tilt klystrons in and out of their packaging. A movable crane (not an overhead crane), ready to deploy anywhere along the linac, will also be needed. The test stand must have space so the four modulators and eight klystrons undergoing testing can be set up and tested simultaneously. This means that room is needed for waveguides, circulators, and loads. Space must also be allocated for racks with control and monitoring equipment, including four LLRF racks and four racks of equipment for monitoring signals from the klystrons and the modulators. This equipment will interface with the ICS. The test stand will also require a staging area in which waveguides, cryomodules, klystrons, and other components can be prepared before installation, and an area where spares for modulators, klystrons, loads, circulators, and other RF parts can be stored. Finally, the test stand will require a place where a klystron or other vacuum tube can be kept warm and ready for deployment if a klystron in the tests fails.The preliminary design calls for the staging area, area for spare components, and the space to keep warm klystrons for the test stand to be located in the upgrade space of the gallery.

Stub number	**Linac section**	**Number of parts fed through stub**
1	Source, LEBT, RFQ, MEBT, DTL	5
2	Spoke part	1
3	Spoke part	2
4	Medium-β	1
5	Medium-β	2
6	Medium-β	3
7	Medium-β	4
8	High-β	1
9	High-β	2
10	High-β	3
11	High-β	4
12	High-β	5
13	High-β	6
14	High-β	7
15	Upgrade	1
16	Upgrade	2

Table 4.38: Linac parts fed from the RF gallery by 16 waveguide penetration stubs, according to the BLED FDSL_2012_10_02 layout.

Linac RF gallery

The rest of the RF gallery will mainly house the linac equipment. In the transition area to the tunnel, the design calls for gathering waveguides, penetrations for cables and cooling, etc. into bundles of waveguides, cables and pipes. Linac penetrations will be made by the 16 stubs that are listed together with the parts of the linac they feed in Table 4.38. An overview of the gallery and a typical waveguide penetration stub (from the medium-β section) is shown in Figure 4.97. The picture shows some of the racks (blue), the modulators (grey), the klystrons (blue/black) and the waveguides leading down into the tunnel. Cable trays and water piping are shown, as well as some of the heat exchangers and circulation pumps in a side room of the gallery. In the tunnel, the figure shows four cryomodules, the cryo-transfer line and some jumpers/valves of the cryo-system. Waveguide supports will be provided in the stubs and personnel will assemble the joints down in the shaft. Concrete blocks will then fill the remainder of the space. Polyethylene beads will be used for radiation shielding. Concrete blocks that seal the stub will finalise the radiation shielding. The stub area will be fenced off under normal operation to avoid accidental exposure. Currently, four medium-β and high-β cryomodules are planned per stub, leaving around 30 m between the stubs. Each stub will be modified to accommodate the systems it services.

The normal conducting linac part of the gallery accommodates the RF amplifiers and modulators for the RFQ, the MEBT buncher cavities, and the DTL tanks. These will require power and cooling. The

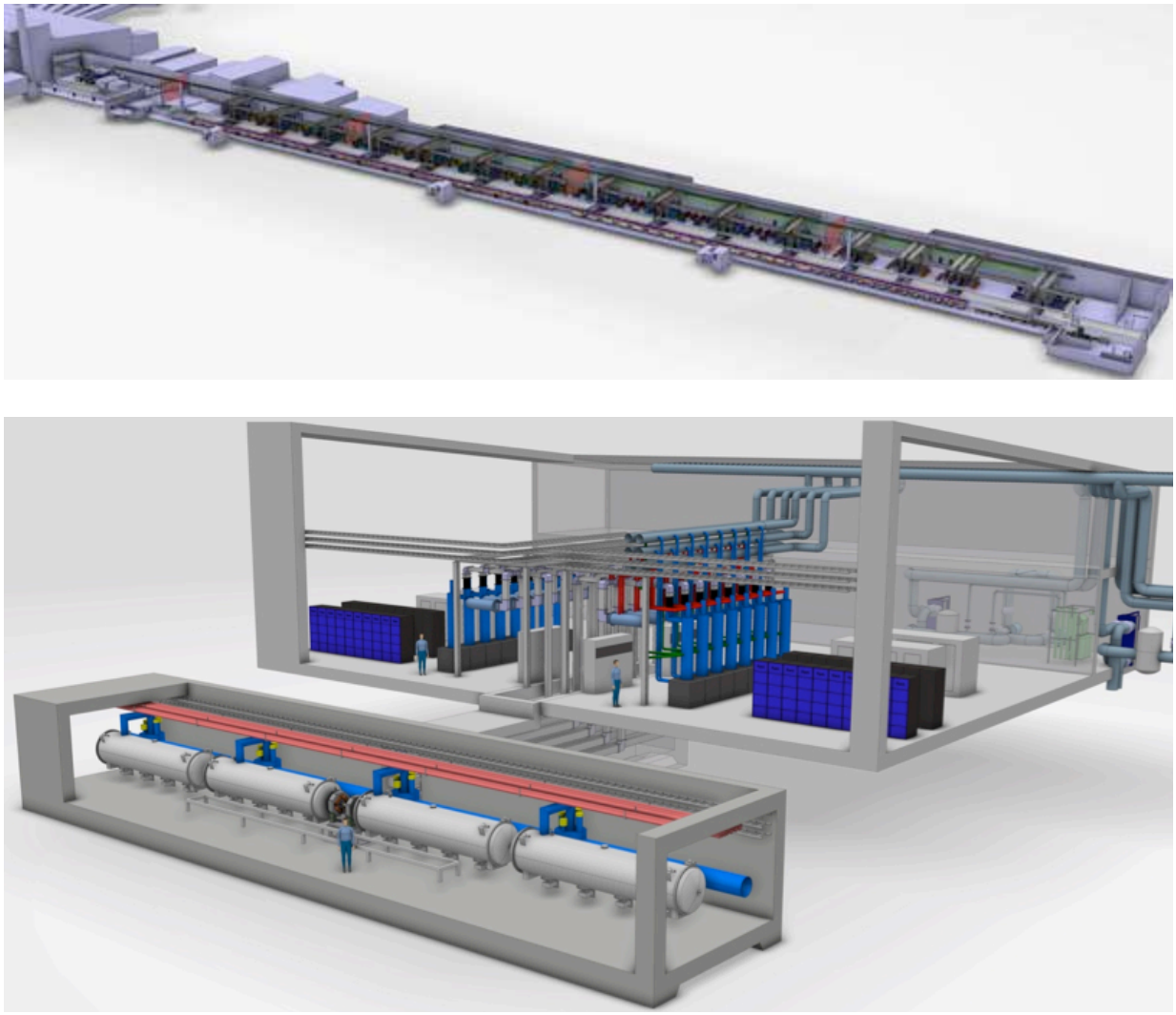

Figure 4.97: Top: An overview of the RF Gallery. Bottom: A typical stub (in the medium-β section) connecting the tunnel with the RF gallery.

Linac section	**Count**	**Installed power** [kVA]	**Cooling power** [kW]	**Cooling water flow rate** [l/m]
Front end				
Source	1	90	81	200
RFQ klystron	1	18	218	210
RFQ klystron modulator	1	240	22	21
Buncher amplifiers	2	3	3	4
DTL tank klystrons	4	72	1044	1000
DTL tank klystron modulators	4	1200	108	105
Sub-total		1623	1476	1540
Spoke section				
HV supplies	14	770	35	35
Predrivers	28	56	50	50
Tetrodes	28	336	1000	956
Sub-total		1162	1085	1041
Medium-β section				
Medium-β klystrons	60	900	4500	4300
HV modulators	15	4500	365	350
Sub-total		5400	4865	4650
High-β section				
High-β klystrons	120	1800	13,470	12,900
HV modulators	60	14,400	1296	1240
Sub-total		16,200	14,770	14,140

Table 4.39: Power and cooling demands for the main linac sections. Cooling flow rates are calculated under the assumption of a temperature rise of 15°C, using deionised water as coolant.

other installations needed in this gallery section include cooling for the source, and tuning (water cooling and temperature regulation) systems for the RFQ and the DTL tanks. The tuning/cooling systems will be part of the RFQ and DTL, so the gallery only needs to provide pump and monitoring power and floor space. It is estimated that the floor space needed is about 30 m for the chilling/tuning systems, and that the power needed for the pumps and monitoring systems is 7 kW per system, totalling 35 kW. The powering and cooling of the source, the buncher amplifiers, the klystrons, and the modulators will need to dissipate power according to the requirements listed in Table 4.39. The HVAC system for the first stub needs a flow of 300,000 lpm, in order to regulate the temperature to 22.5 ± 2.5°C.

Power and cooling needs for the main linac sections are summarised in Table 4.39. The superconducting part of the linac starts in the spoke section, with 28 cavities in 14 cryomodules fed from tetrode tube amplifiers (one amplifier per cavity). The air handling capacity needed for the spoke linac section is expected to be 200,000 lpm. In the medium-β linac section, where the RF frequency changes from 352.21 MHz to 704.42 MHz, 60 medium-β cavities in 15 cryomodules are fed by klystron amplifiers, with four klystrons per modulator. Air handling capacity for this part of the linac is expected to be 1,000,000 lpm. In the high-β section of the linac 120 cavities are each fed by a klystron. Air handling capacity for this part of the linac is expected to be 3,000,000 lpm. The HEBT contains instrumentation, magnets, bending dipole magnets and the upgrade space for the linac. The power needs for this section of the linac are limited, the largest being the total power demanded by the bending dipole magnets. Total magnet power for the whole linac is expected to be 300 kW.

4.9 Beam instrumentation

4.9.1 Design considerations

Successful commissioning and operation of an accelerator relies on the availability of proper beam instrumentation. Residing on the intensity frontier, ESS will place particular demands on the instrumentation systems. A short commissioning phase and a steady ramp-up to ultimate performance will require quality beam measurements to compare with the accelerator model. Reliable operation in support of the neutron science community will require trustworthy systems that protect accelerator hardware from beam-induced damage. ESS beam instrumentation requirements have been developed based on experience at similar facilities, the ESS accelerator and target baseline designs, and initial plans for commissioning. An external committee reviewed beam instrumentation in July 2012, and the current baseline incorporates this committee's input. Use-cases have provided valuable guidance for the definition of system functionality, device quantities and layout, and required performance. Table 4.40 lists the device types that make up the ESS beam instrumentation suite.

Device	Abbreviation
Beam loss monitor	BLM
Beam current monitor	BCM
Beam position monitor	BPM
Emittance slit	Slit
Wire grid	Grid
Faraday cup	FC
Wire scanner	WS
Non-invasive profile monitor	NPM
Imaging system device	Img
Beam halo monitor	Halo
Bunch shape monitor	BSM

Table 4.40: Types of beam instrumentation devices and their abbreviations.

The very first use of instrumentation will occur during commissioning of the ion source and the low energy beam transport (LEBT) line. During this activity, the primary measurements will be the current and emittance measurements. Beam current monitors (BCMs) based on toroids will provide a non-interceptive measurement capability. An emittance system based on slits and secondary emission (SEM) grids has been used to measure similar beams in other facilities, and this design is a reasonable choice for ESS. A Faraday cup (FC) will be cross-calibrated with the BCMs and will also act as a beam stop. A temporary spectrometer line after the first solenoid will provide energy spread measurements. After completion of these measurements, the permanently installed LEBT instrumentation will remain to support all future activities. Figure 4.98 schematically depicts the layout of this permanent instrumentation.

The next major step will be the commissioning of the radio frequency quadrupole (RFQ) and the medium energy beam transport (MEBT) line. As with the LEBT, a temporary spectrometer line will be used to measure the energy spread after the RFQ and then after the MEBT. A slit and grid system will measure the emittance, and BCMs will monitor transmitted current and charge. Fast BCMs will also measure MEBT chopper performance. With the beam bunched by the RFQ, the beam position monitors (BPMs) that depend upon the presence of high frequencies will measure the position and phase to aid

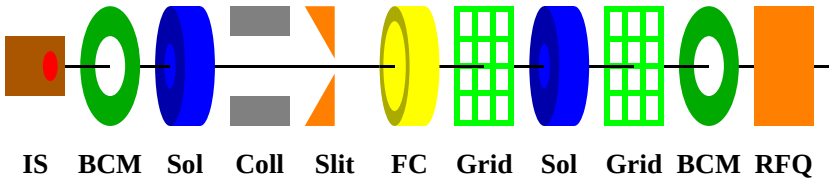

Figure 4.98: Schematic layout of low energy beam transport diagnostics.

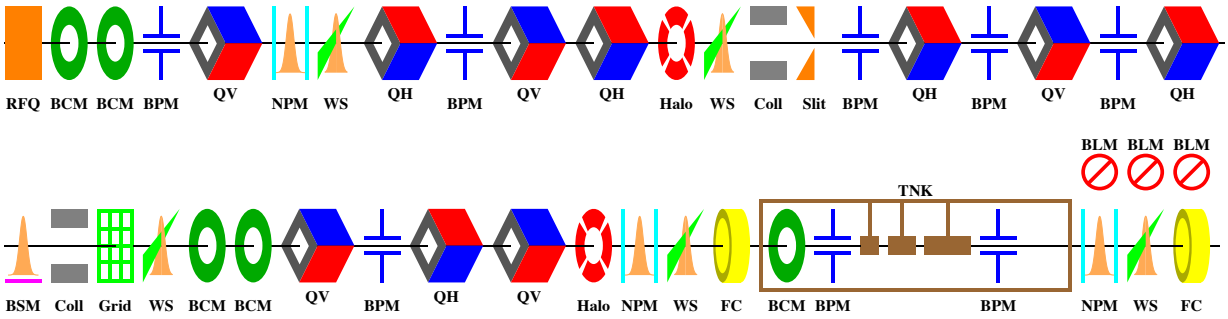

Figure 4.99: Schematic layout of instrumentation for MEBT and the first DTL tank. Buncher cavities are not shown. BCM pairs represent one standard toroid and one fast toroid. The BLM triplet represents one ion chamber, one neutron detector, and one fast loss monitor.

in beam steering, and in setting the phase and amplitude of the RFQ and buncher systems. Longitudinal bunch shape monitors (BSMs) will measure bunch length while wire scanners (WS) will measure the transverse beam size. The layout of the permanently installed instrumentation devices is shown in Figure 4.99, including the first DTL tank. Each drift tube linac (DTL) tank is commissioned in sequence into Faraday cups located after each of the tanks. Space constraints inside the tanks limit the diagnostics to BCMs in some end-walls and BPMs embedded within a few otherwise empty drift tubes. The Faraday cups along with a wire scanner reside within the thin inter-tank chambers. After the DTL is tuned, beam is transported to a Faraday cup at the end of the spoke section. This beam is initially at 80 MeV and is gradually raised to around 200 MeV by tuning the spoke section. Next, this 200 MeV beam is transported to a Faraday cup at the end of the medium-β section and, after tuning, reaches the desired energy of around 600 MeV. Finally, this last insertable Faraday cup is retracted and beam is transported through the high-β section to the linac tuning dump where full energy is eventually achieved. After the linac (and target systems) have been set up, dipoles are energised and the initial beam travels to the target. The ESS facility can then begin the ramp to high power.

During commissioning and tuning procedures, BPMs provide phase information to set up over 200 accelerating structures and also provide the position information required to centre beam in the aperture. Wire scanners support transverse matching, while BSMs support longitudinal matching. BLMs and BCMs measure loss and transmission respectively, and via their interface to the machine protection system (MPS), protect the accelerator components from beam-induced damage. Halo monitors measure the evolution of particles that emerge from the beam core. These particles can cause unwanted activation in the accelerator or unwanted thermal load on collimator and target components. For beam pulses longer than a few percent of the nominal 2.86 ms pulse length, wire scanners can no longer survive in the beam's core, so non-invasive profile monitors (NPM) provide the transverse profile measurements. Since the transverse beam density

Section	BLM	BCM	BPM	Slit	Grid	FC	WS	NPM	Img	Halo	BSM
LEBT	–	2	–	1	2	1	–	–	–	–	–
MEBT	–	4	6	1	1	1	4	2	–	2	1
DTL	12	6	8	–	–	4	4	4	–	1	1
Spokes	42	–	28	–	–	1	5	5	–	3	3
Medium-β	48	2	32	–	–	1	4	4	–	4	4
High-β	60	1	30	–	–	–	4	4	–	4	4
Upgrade	22	2	14	–	–	–	4	4	–	2	2
A2T	20	2	16	–	2	–	3	4	2	4	–
Dump Line	10	2	8	–	1	–	1	1	1	1	–
Total	214	21	142	2	6	8	29	28	3	21	15

Table 4.41: Beam instrumentation device count, organised by accelerator section.

is critically important to the survival of dump and target components, it is measured redundantly by the grids (that can survive the expanded beam), imaging devices (Img) and an NPM that make up the beam-on-target system.

Except for the temporary spectrometer systems for LEBT and MEBT, all of this instrumentation will be permanently installed and available for online measurements. Devices are located according to best practices developed at similar facilities. Where cross-checks are required, diverse measurement techniques are used. Moderate redundancy is employed, such that failure or maintenance of individual devices will not lead to excessive downtime. These considerations have led to the baseline layout of beam instrumentation that is summarised in Table 4.41. The systems that contain all of these devices are discussed in more detail within their respective sections. The instrumentation systems fall into three categories:

1. Insertable devices for commissioning and tuning (emittance slits and grids, Faraday cups), and other interceptive devices used in the core of the beam (wire scanners and bunch shape monitors).

2. Non-interceptive devices used over full dynamic range of beam power (beam loss monitors, beam current monitors, beam position monitors, imaging systems, devices that monitor beam-on-target).

3. Devices most relevant for high power (non-invasive profile and halo monitors in the linac and transport lines)

For category 1 devices, all interceptive devices downstream of the LEBT will limit individual pulses to 5 μC as shown at the top of Figure 4.100. The shaded region represents beam pulse parameters that allow these interceptive devices to survive. One technique to assure survival of all interceptive devices is to assume that the beam current could be as large as the nominal peak current (50 mA), and to then restrict the pulse length to 100 μs or less. The next consideration is a limitation on average current. The tuning dump at the end of the linac will absorb up to 50 kW of beam power, equivalent to 20 μA average current. Similar capability is required of the insertable Faraday cups that provide intermediate beam stops during commissioning and tuning of upstream accelerator sections. To fully characterise the beam that is destined for these FCs and the dump, all category 1 devices are specified to handle 20 μA average and 50 mA peak current. This parameter space is illustrated at the bottom of Figure 4.100. The dots on both of these envelope diagrams represent a useful subset of the beam types that will be present in the ESS accelerator, as summarised in Table 4.42. The diagnostics mode is of particular interest, and will be frequently referenced in the descriptions of individual instrumentation systems.

Some simple guidelines lead to requirements for the various beam instrumentation systems. All devices should survive diagnostics mode beams. When the minimum beam is present, all devices in categories 1 and 2 should produce usable results, although the performance may be derated. For fast tuning beam, all scanning devices (WS and Emit) should be able to take advantage of the 14 Hz repetition rate by moving continuously through the beam and correlating position and measurements in real-time. For fast and slow tuning beams, all category 1 and 2 devices should achieve full performance, even though some may require averaging over multiple pulses, and category 3 devices should produce usable measurements that can be cross-checked with other devices. Insertable devices must not be allowed near the beam core when beam is in long pulse mode. Due to the long beam loading and Lorentz detuning times, this mode is needed primarily to qualify the RF system while beam is transported to the tuning dump. Therefore, BPMs should achieve full performance for these long, infrequent pulses. In high power mode, insertable devices remain retracted from the beam core, and all category 2 and 3 devices should reach full performance.

The supporting electronics for each instrumentation device will contain several interfaces. The primary interfaces are: timing, RF reference, control system network, MPS, power, environmental (electromagnetic, cooling airflow), physical (rack/enclosure), and, of course, the instrumentation device in or on the beam line. Collectively, the first four interfaces determine the data acquisition functionality, and this topic deserves further discussion. The timing system will synchronise all acquisition of beam-based signals, tagging data with the global time stamp discussed in Section 5.2.6. For data associated with a given beam pulse, the time stamp will allow unique identification of that pulse. Waveforms and other precisely sampled data will contain timing information with a precision better than one sample period. A few systems will be synchronised to the RF structure and will require an interface to the RF reference distribution system. These systems include the BPMs and BSMs. In an Experimental Physics and Industrial Controls (EPICS) control system discussed in Chapter 5, the collection of process variables defines the system's interface to the network. Timing events will trigger the update of EPICS process variables containing beam data.

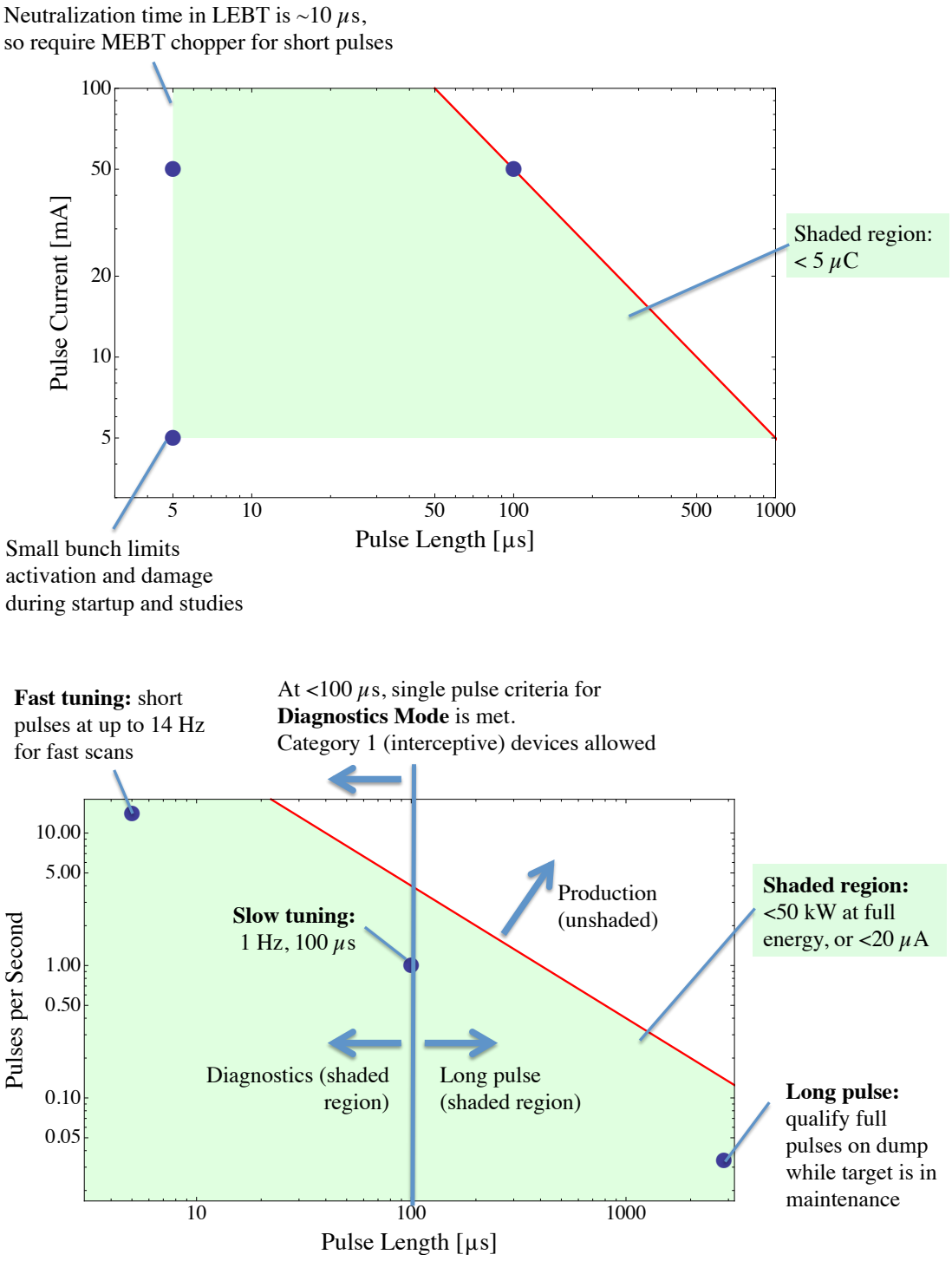

Figure 4.100: Beam pulse parameter envelope for different modes of diagnostic operation. Allowable regions are shaded. Top: For insertable (category 1) instrumentation devices. Bottom: For 50 kW beam to the linac tuning dump.

Each system will present its measurement results in several different sets of process variables, with each set representing a particular time frame and triggered by particular timing events. Measurement results for some typical time frames include: an average over one pulse, an average over a number of pulses, a sample within a pulse, an array of samples over a pulse, and finally, a series of measurements surrounding

Mode	Typical beam	Pulse Length [μs]	Peak current [mA]	Rep. rate [Hz]
Diagnostics	Minimum	5	5	1
	Fast tuning	5	50	14
	Slow tuning	100	50	1
Long pulse	Long pulse	2860	50	.03
High power	Production	2860	50	14

Table 4.42: Typical beam modes and beam parameters used to specify instrumentation performance.

the time of a trigger event (with the option of including pre-trigger data). This last measurement type will provide the post mortem data required by the MPS. It will also support comprehensive data acquisition for machine studies and for diagnosis of subtle issues that do not lead to an MPS trip. In addition to these measurement process variables, all systems will expose additional process variables to allow configuration, status monitoring, and debugging. All insertable devices (category 1) will provide status to MPS such that only diagnostics beam is allowed when they are inserted near the beam core. BLM, BCM, and beam-on-target systems will provide MPS inputs so that beam can be inhibited upon significant beam loss, too much beam (for example, in the case of chopper failure), or undesirable beam properties at the windows, dump, and target. An option to interface the BPMs and halo monitors to MPS will also be provided.

4.9.2 Beam loss monitoring

The beam loss monitoring (BLM) system is arguably the most important diagnostic system of the ESS linac. It has the dual purpose of keeping the machine safe from beam-induced damage and avoiding excessive machine activation by providing critical input to the MPS. Thus, the system must be designed to not have any blind spots. In addition, as the BLM system will be a major tool for beam tune-up, it should also be designed in a way that enables it to pin-point the loss location as precisely as possible. With this in mind, in the cold linac there will be three ionisation chambers (IC) per warm section, located before, between, and after the quadrupoles. The ICs will be placed as close as possible to the beam pipe. Simulations such as that shown in Figure 4.101 confirm that this distribution of detectors will allow losses in either of the quadrupoles to be distinguished from losses upstream [501]. The quadrupoles are the locations where the beam size is largest, and are therefore the most likely loss locations. In the warm linac, there will be one IC per DTL tank (located in the inter-tank region) as well as several neutron detectors (ND) and scintillator-based fast loss monitors.

The required sensitivity is set by the desire to limit machine activation. The chosen criterion is that the BLM system should be able to detect a continuous loss leading to beam pipe activation of 1% of the hands-on maintenance limit (or about 0.01 W/m). The response time, on the other hand, is determined by the ability to detect large fast losses. Simulations show that if the entire beam is lost in a single spot, it can start melting steel or copper in a matter of 2 μs to a few tens of μs in the warm linac (longer in the cold linac) and this figure highly depends on the size and energy of the beam [501]. Thus, the requirements for the BLMs in the low energy part of the accelerator are to detect such full point losses within at most 2 μs. The rest of the BLM system can detect such losses within 10s of μs. SNS or LHC-style ICs may be used, possibly with some modification. When loss signal is too weak to be measured with the BLMs in the low energy part of the warm linac, BCMs will be used to detect high losses and abort the beam if needed. In order to avoid the saturation of the loss monitors for high losses, as must be done to estimate the total dose, a dynamic range of 10^6 is required.

The BLM electronics will provide the pulse average loss, as well as the time distribution of the losses along the pulse. In addition, it will provide a real time input to the MPS if the BLM signal exceeds a pre-determined threshold. At least two different thresholds are foreseen, corresponding to different integration time constants for the signal (e.g. direct signal with natural time constant of the IC, and integrated loss over beam pulse). In addition, the system will monitor the loss integrated over multiple pulses. A major anticipated background in the beam loss measurement will come from x-rays emitted from the accelerating cavities. To correct for this effect, occasional no-beam pulses (at the rate of a fraction of a Hz) will be

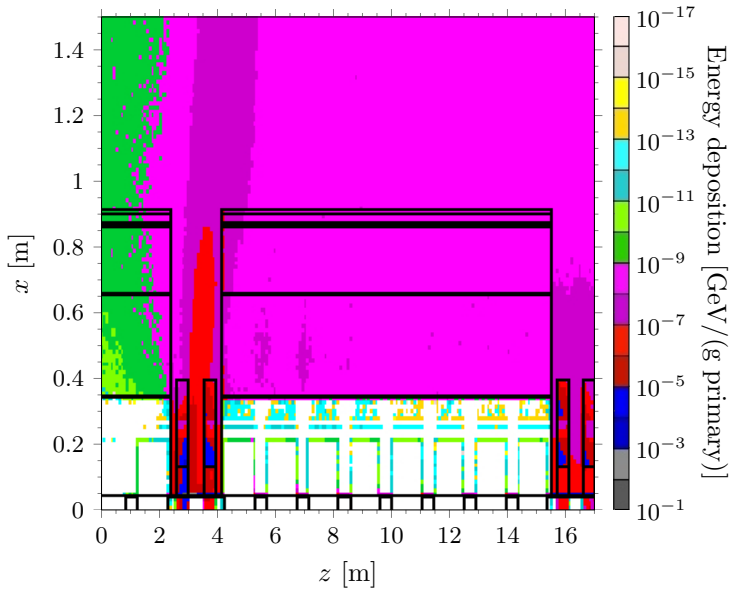

Figure 4.101: Total energy deposition in the (x, z) plane – (horizontal,longitudinal) – over a 17 m range starting about 4 m upstream of a single point of beam loss in the middle of the first quadrupole in a doublet. A cryomodule is located in the 13 m downstream of the loss point. The energy deposition is recorded in units of GeV/g for a single primary proton with an energy of 1 GeV and an impact angle of 1.5 mrad.

required to establish a baseline for subtraction. The BLM system will include a self-test functionality. This is particularly important for its connection to the MPS, which demands fail-safe critical mitigation devices [502]. At low energies, ion chambers are not very effective at detecting beam loss due to the self-shielding from the RFQ and DTL tank. Here differential current measurement will be used as the the primary input to the MPS, while neutron detectors and scintillation detectors will be used as backup devices.

4.9.3 Beam current monitoring

The BCM system will measure the beam current versus time at various locations along the linac. As shown in Table 4.41, the low energy end of the linac contains a denser population of BCMs than the high energy end. This addresses concerns of damaging beam loss that the BLM cannot easily detect. The accelerator-to-target (A2T) and dump sections also contain BCMs. With an accuracy of ±1%, the BCMs will provide the beam current waveform over the macro pulse, the charge per pulse, the average beam current, and the cumulative charge. As the final current measurement devices just upstream of the target, the A2T transformers must provide some additional functionality. The segmented design of the target wheel mandates synchronisation between the beam's time of arrival and the target's azimuthal position, and signals from the A2T BCMs can help to achieve this. Real-time data must also be sent to the beam on target imaging systems and to the neutron instruments. This data will be used to normalise the beam-on-target density measurement, and will be included in the neutron instruments' event stream. The BCM output will be sampled by a fast ADC and stored in local memory, so that the data can be retrieved later and examined upon a user request or machine failure. A slower update rate on the order of a few hertz will be used at the user end for commissioning and machine operation purposes [503].

It is planned to use commercial AC current transformers for most of the BCMs. The upper −3 dB cutoff frequency of the high-bandwidth for these devices is about 1 MHz, corresponding to a measurement rise/fall time of 350 ns. The lower −3 dB cutoff frequency is about 3 Hz, resulting in a droop of up to 4.5% with a 3 ms pulse. One or more fast current transformers may be used to measure the beam current profile with a bandwidth of up to a few gigahertz. These devices are useful to measure the performance of the MEBT choppers or to study an abnormal beam behaviour, where the bandwidth of the AC current transformers is not sufficient. In addition to the absolute current, some of the BCMs will be configured

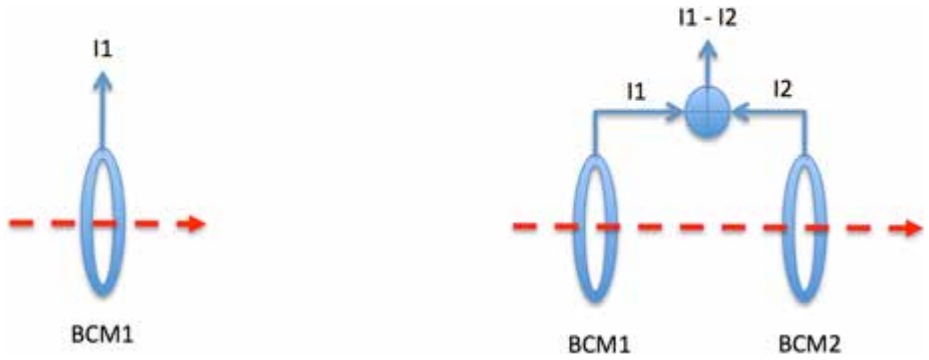

Figure 4.102: Beam current measurements used by the machine protection system. Left: Absolute. Right: Differential.

for a differential current measurement as shown in Figure 4.102. The BCMs will be connected to the machine protection system so that the beam can be shut off if the absolute or the differential current exceeds user-defined thresholds. As with the BLMs, the BCM system will include a self-test functionality. The BCM sensors will include calibration windings so that they can be calibrated on a regular basis using a separate current source.

4.9.4 Beam position and phase

The BPM system is used to measure the beam position, the beam phase and an approximate beam current. The BPM data will be used to correct the beam trajectory during machine commissioning and normal operation. The BPM system will provide the horizontal and the vertical beam position waveform throughout the macro pulse as well as the beam position averaged during the pulse. With beam in the central region of the nominal 100 mm aperture, the system should provide stability of ± 0.1 mm. The beam phase will be measured to an accuracy of ± 1 degree, and will primarily make possible RF cavity phase scans. In addition, differential phase measurements will be used for energy calculations based on time-of-flight between two BPMs. The BPM system will provide the phase waveform throughout the macro pulse and the phase averaged over the pulse. The BPM system will use buttons, except in the DTL drift tubes where special shorted striplines will be used. As far as possible, BPM sensors will be physically attached to each quadrupole, since the normal goal of beam steering is to centre the beam in the quadrupoles. Again, the DTL is the primary exception, since the permanent magnet quadrupoles take most of the available space in a drift tube, forcing the BPM to reside in its own drift tube. In the A2T line, beam should be centred in the octupoles, so BPMs will be located on or near these strong, non-linear magnets.

Adequate performance of the BPM system starts with adequate signal out of the electrodes. Figure 4.103 shows the Fourier spectrum of the button voltage due to a 352 MHz repetitive bunch. For a longitudinally well-focused beam ($\sigma_z \simeq 2$ mm [504]), the amplitudes of some higher harmonics are larger than the fundamental. As the beam gets defocused, though, these harmonics quickly decrease, and with $\sigma_z \gtrsim 50$ mm they become negligible. This suggests using the lower harmonics for the BPM signal processing. On the other hand, processing at accelerating frequency is not desirable due to potential interference with the high power RF sources. This will be overcome by receiving the second harmonic (i.e. 704 MHz) in the first part of the linac (operating at 352 MHz), while processing the fundamental (352 MHz) in the second part of the linac where the RF frequency is 704 MHz. As described in the design considerations, commissioning and tuning may result in a beam that travels through long sections of unpowered linac on its way to the next Faraday cup or dump.

The ability to measure the position of a debunched beam is important, for example during the machine tuning when the aim would be to perform a cavity phase scan while confirming the beam position several hundred meters down stream. Figure 4.104 shows the signal strength before and after debunching throughout the linac with no longitudinal focusing after the spoke section. There should still be enough signal to allow rough beam centring, but resolution will be degraded. The situation is improved by using a Faraday cup at the end of the medium-β section, and using this destination to achieve about 600 MeV before transporting beam to the linac tuning dump.

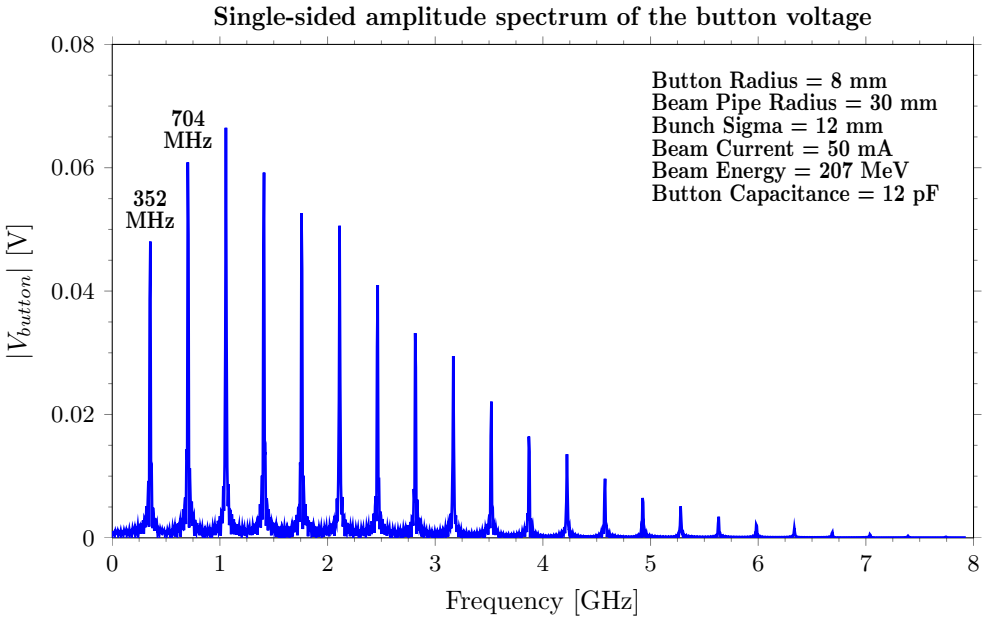

Figure 4.103: Fourier spectrum of the voltage on a button beam position monitor, due to a 352 MHz repetitive bunch.

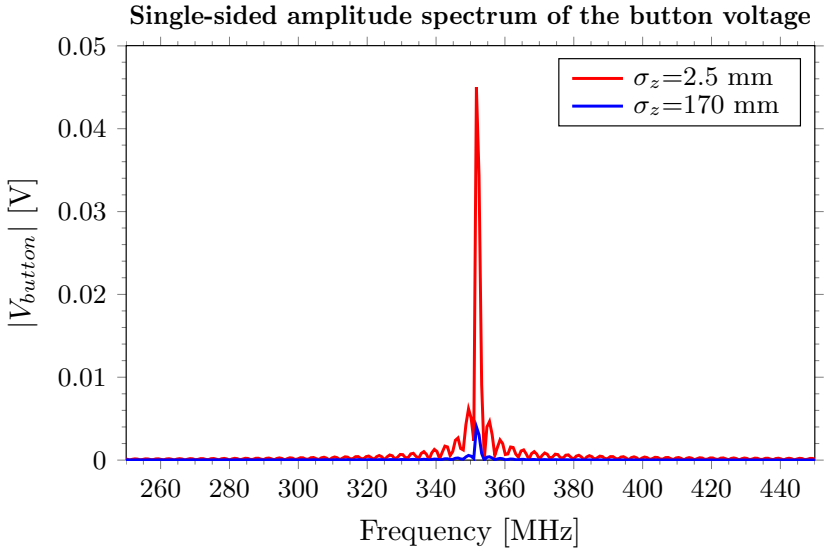

Figure 4.104: Fourier spectrum of the button voltage around 352 MHz before (red) and after (blue) debunching with no longitudinal focusing after the spoke section.

The BPM electronics will have of a fast analog front-end, where the BPM signals will be received by sensitive analog electronics, and level-adjusted and conditioned. Following this, a digital section will digitise the signals and process them in an FPGA. Processing will be narrow band, with a bandwidth of about 1 MHz [505]. Narrow band processing requires some additional correction at the low energy end of the linac, since the sensitivity for a given frequency is not only given by the geometry of the pick-up, but also is a function of the relativistic beta. The BPM electronics should have a large enough dynamic range and a good signal-to-noise ratio so that they give useful results even when the beam amplitude and duration are decreased to the diagnostic mode's minimum beam values of 5 mA and 5 μs respectively. To the extent possible, readout hardware will be shared between the BPM and LLRF systems, since requirements are very similar. As mentioned in the first section, the BPM system will interface to the LLRF reference system as well as the global timing system.

4.9.5 Faraday cups

During commissioning and tuning of the ESS linac, insertable Faraday cups will measure beam current while isolating the downstream accelerator components from beam. The acquisition electronics will measure current ranging from 5 mA to 50 mA with an accuracy better than 1% and a time resolution better than 1 μs. To avoid overheating, the beam must be in the diagnostics mode when any Faraday cups are inserted, except in the LEBT, where a Faraday cup will be installed in between the ion source and the first solenoid, where the beam sizes are relatively large. The LEBT Faraday cup will handle pulses much longer than the diagnostic pulse and might be used in production mode with external cooling. At low energy, the secondary emission yield is large, and this could affect the signal. A bias voltage is foreseen to suppress this secondary emission. For the MEBT Faraday cup, the challenge is to keep the thermal load below the mechanical limits, given the small beam sizes and the large stopping power of 3 MeV protons. This system will feature a wide bandwidth collector, capable of monitoring MEBT chopper performance. Faraday cups will also be installed after each DTL tank. As seen in Figure 4.105, these will be based on the SNS design that includes an energy degrader in front of a graphite collector. The thickness and the material of the energy degrader have been chosen to enable it to stop those particles not accelerated by the DTL cavities. The parameters of the energy degrader are presented in Table 4.43.

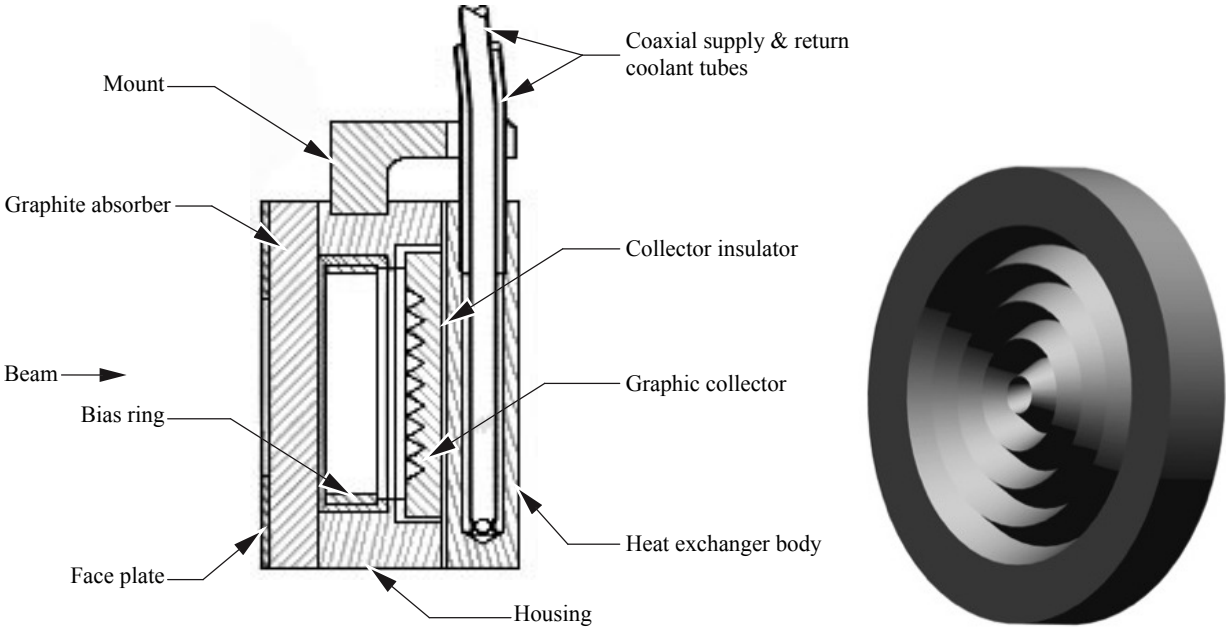

Figure 4.105: The drift tube linac Faraday cup. Left: General view. Right: Detailed view of the graphite energy degrader in front of the collector that enables the Faraday cup to stop those particles not accelerated by the DTL cavities.

The energy degrader absorbs the low energy particles that have fallen out of the accelerating bucket. It also absorbs part of the beam that is at nominal energy, and the scattering will increase the beam size at the collector and reduce the thermal load. The distance between the energy degrader and the collector is about 30 mm. The Monte Carlo code FLUKA [506] has been used to estimate the energy deposition map in the graphite collector and in the energy degrader. In this simplified model, the beam has no divergence and no energy spread, and is round with $\sigma_x = \sigma_y = 3$ mm for each energy case. Table 4.43 records the temperature increase expected for Faraday cups collecting a single, slow tuning pulse 100 μs long with a peak current of 50 mA. The temperature on the collector can be reduced by using the shape presented in Figure 4.105. For the energy degrader, the maximum temperature is reached when the upstream DTL tank is not accelerating the beam. Assuming the same beam parameters at 3 MeV (the input energy of the first DTL tank), the first Faraday cup located at the exit of this tank would reach a maximum temperature of 1760 K. For similar situations, the maximum temperature of the rest of the energy degraders is lower, but additional engineering is required to assure that all cups and their degraders survive the diagnostics mode under all anticipated operating conditions.

Beam energy [MeV]	**Degrader material**	**Degrader thickness** [mm]	**Degrader maximum temperature** [K]	**Collector maximum temperature** [K]	**Transmission** [%]
21.5	Carbon	3	628	1060	98.6
41.1	Carbon	8	456	850	94.7
60.0	Carbon	10	432	697	96.0
77.7	Copper	6	443	492	93.0

Table 4.43: Maximum temperature increase in the degrader and in the collector of Faraday cups collecting a single, slow tuning pulse 100 μs long with a peak current of 50 mA, for four different beam energies.

The Monte Carlo simulations show also that a non-negligible number of particles are created in the energy degrader. The amount of nuclear interaction increases with beam energy and the particles produced can perturb the measurement. The shower created in the energy degrader is dominated by neutral particles (neutrons and γ), but a small number of leptons are also created and can change the charge on the collector. The charge transmitted compared to the quantity of particles in the beam is shown in the last column of Table 4.43. In the worst case, 7% of the beam charge is lost in the energy degrader, so that a correction must be applied to the data in order to meet the accuracy requirements. It has to be noted that the Monte Carlo codes are not able to track particles at very low energy, and this leads to an underestimate of the collector signal.

Two more Faraday cups will be deployed, primarily to act as intermediate beam stops, one at the end of the spoke section at about 200 MeV, and the second between the medium-β and high-β sections at slightly above 600 MeV. Because they function primarily as beam stops and not as measurement devices, the measurement accuracy required of the upstream cups does not apply to these cups. The FC positioned in the spoke section will be located in a standard warm section, between two quadrupoles. The length available for the dump and the longitudinal shielding is 0.46 m. The second FC occupies space provided by a missing cryomodule, a length of around 8 meters. The main concern with these devices is activation, and Monte Carlo simulations have been performed for a 200 MeV and a 623 MeV proton beam. The model of the FC consists of an aluminium cylinder with a length of 0.30 m for the 200 MeV FC. The high energy FC is anticipated to present a more challenging activation issue, so a more complex design is modelled. The FC in this case consists of an aluminium cylinder ($l = 70$ cm, $\varnothing = 12$ cm) surrounded by a tungsten cylinder ($l = 130$ cm, $\varnothing = 30$ cm). The primary proton beam is degraded in the aluminium cylinder, and the tungsten layer acts as shielding.

For the simulation, the irradiation profile is set at 10 days of irradiation with a particle flux of 3.2×10^{13} protons per second, followed by 5 weeks of cooling and 3 more days of irradiation with the same flux. The cooling time after the irradiation is set at 1 day. To simulate the dose rate after the dump is retracted, the irradiation has simply been done with the FC in retracted position. The fixed shielding consists of iron and light concrete ($\rho = 2.34$ g/cm^3), and the size of the shielding has been specified to decrease the dose rate as much as possible while keeping a transverse dimension of less than about 2 m and a longitudinal dimension compatible with the space available. Figure 4.106 shows a map of the dose rate after one day of cooling for the 200 MeV beam stop, and for the downstream stop at 623 MeV. Beam stops at these locations can be designed to support staged commissioning and tuning while still allowing hands-on maintenance of nearby equipment.

4.9.6 Wire scanners

Because they have been deployed successfully at several similar facilities, wire scanners represent a conservative choice for the measurement of transverse beam profiles. They employ a thin wire that scans transversely across the beam. During the scan, the electronics simultaneously acquire the position of the wire and the signal due to the beam-wire interaction. Signal processing and analysis software then reconstructs the beam profile. Unfortunately, the beam-wire interaction causes wire heating and beam loss, limiting the measurement to beams of reduced pulse length and reduced average current. When the wires are in use, beam will be limited to the diagnostics mode as described in Section 4.9.1. As with all insertable

devices, an MPS interface will be required to protect against device damage. The wire scanner will measure the RMS beam sizes with a precision of ±5% and a time resolution of better than 1 μs. Even with beam restricted to diagnostics mode, wire heating presents a challenge for these devices. For the warm linac, thermal analysis of both carbon and tungsten wires led to a choice of 33 μm diameter carbon wire that survives the 3 MeV beam in the MEBT, the most challenging location. The evolution of the maximum wire temperature during measurement of slow tuning beam is presented in Figure 4.107. Equilibrium is reached after 3 pulses and the wire reaches a peak temperature of 2100 K. With fast tuning beam, the wire temperature peaks at 1500 K. At higher energy, the temperature decreases with the stopping power. For example, at the 23 MeV output energy of the first DTL tank, the predicted peak temperature reaches 900 K during measurement of slow tuning beam.

After the DTL, the wire selection criteria must address concerns about particulates emanating from ablated or broken wires. Carbon wires are contraindicated by a test performed at GANIL, where the effect

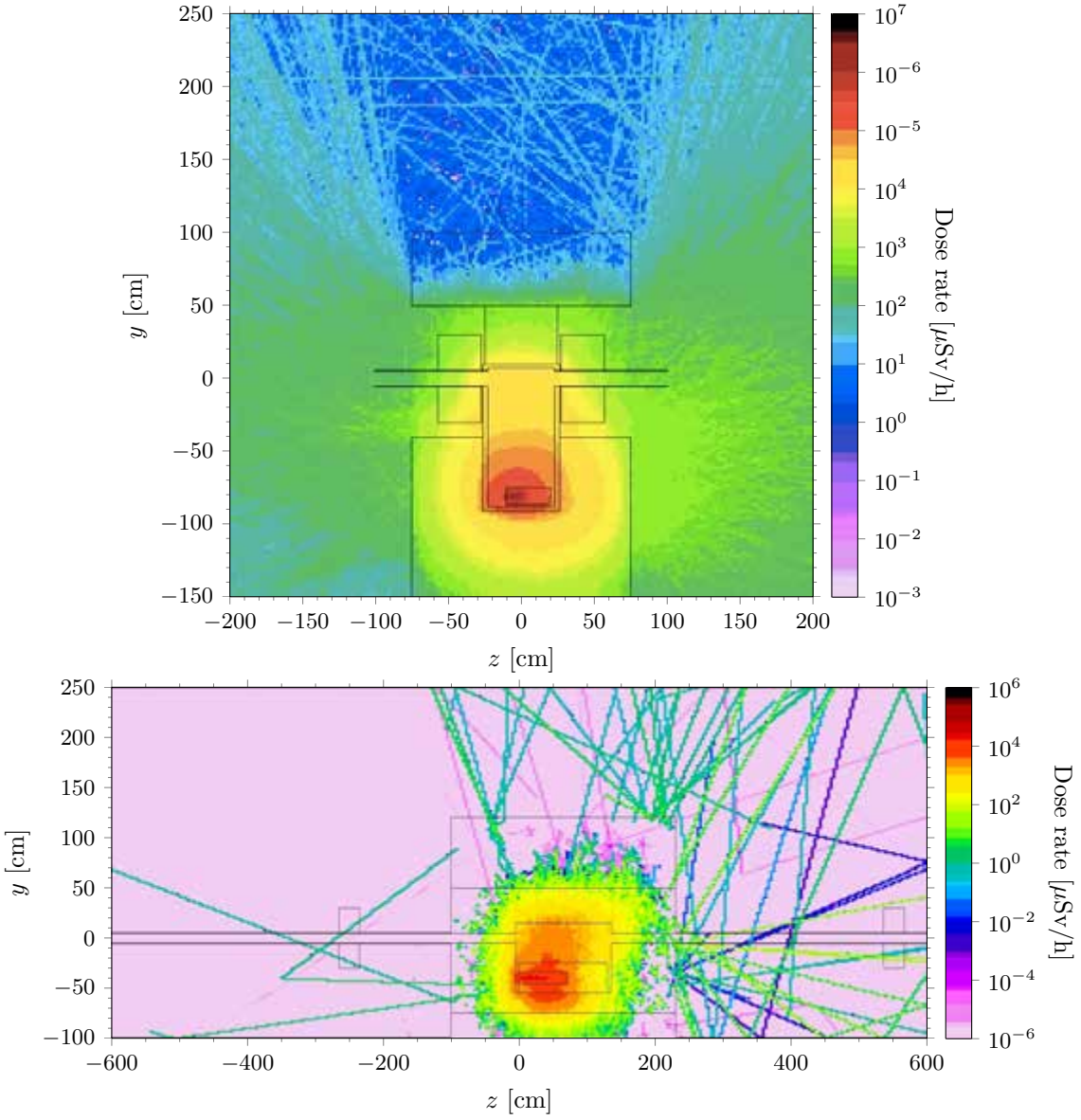

Figure 4.106: Dose rate maps around a beam dump after 10 days of irradiation with a particle flux of 3.2×10^{13} protons per second, followed by 5 weeks of cooling, 3 more days of irradiation with the same flux, and one day of cooling. Top: Around an aluminium dump accepting a 200 MeV beam. Bottom: Around dump composed of aluminium and tungsten accepting a 623 MeV beam.

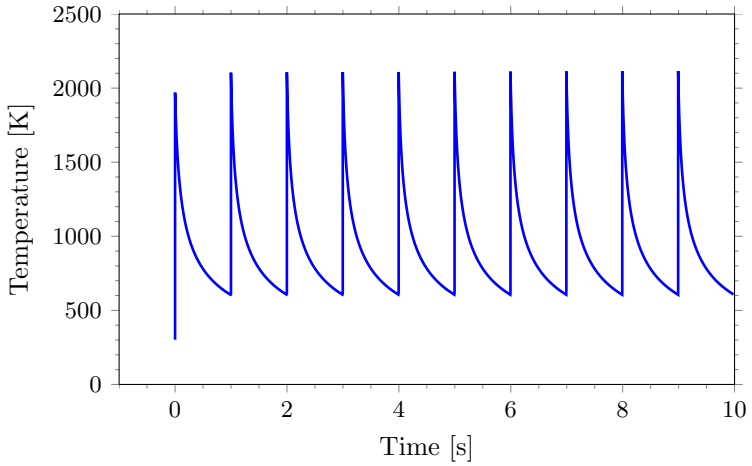

Figure 4.107: Maximum temperature on a 33 μm diameter carbon wire while measuring a 3 MeV slow tuning beam. The beam size is 2 mm RMS in both planes.

of sublimating different wire materials near superconducting cavities was studied. Tungsten seems to be an acceptable material, and will be used for wire scanners in the spoke section and beyond. Additional testing will be performed to qualify this choice. Again, low energy beam induces the largest temperature rise, so an analysis at the 80 MeV output energy of the DTL will highlight any thermal issues. Assuming a beam size of 2 mm RMS in both planes, a 20 μm diameter tungsten wire reaches a maximum temperature of 1600 K during the slow tuning mode and 1200 K during the fast tuning mode. As the energy increases, the energy deposition in the wire decreases. At the minimum ionising energy of $\approx$ 2 GeV, the wire remains below 1000 K while in the core of fast or slow tuning beam.

With materials and sizes selected to enable wire survival, the signal must then be calculated. At 3 MeV, the typical 2 mm RMS beam will induce a secondary emission current of 0.4 mA in a carbon wire that is placed in the beam core. The temperature increase can also be an issue for the measurement, because the thermionic emission increases quickly above 1800 K. During the slow tuning mode, the temperature of the wire is above this threshold at the end of the pulse, leading to an emitted current around 8 μA. This 0.2% effect is only present near the end of the slow tuning pulse. At high energy, the secondary emission

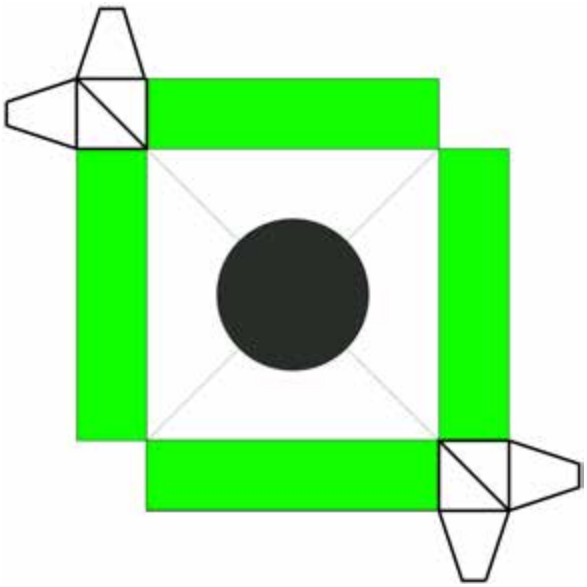

Figure 4.108: Scintillator geometry to measure the shower from a wire scanner. The scintillator is in green, with the light guide outlined in black. The circular beam pipe is in the centre.

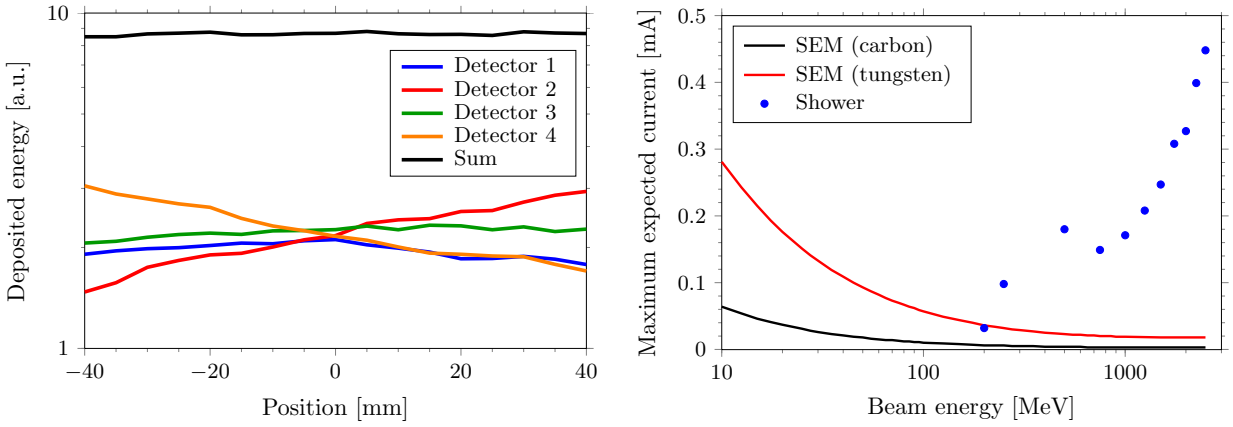

Figure 4.109: Wire scanner performance. Left: Energy deposition on the four scintillators as a function of the wire position, at a beam energy of 1 GeV. Right: Maximum expected current on the wire as a function of the beam energy in SEM mode for carbon wire (black line), tungsten wire (red line) and in shower mode (blue dots).

signal becomes small, and a better way to measure the profile is to measure the shower created by the beam hitting the wire target. In order to determine the best detector geometry, the FLUKA Monte-Carlo code has been used [506]. A physically realisable geometry is shown in Figure 4.108. The detector consists of 4 scintillators positioned around the beam pipe, and the size of each active element is 5 by 5 by 20 cm. Each scintillator will be connected to a photo-multiplier tube (PMT) with a light guide. A distance of 35 cm between the wire and the scintillators will allow the package to fit within the smallest anticipated longitudinal space. The energy deposited in each scintillator as a function of the wire position is shown at the left of Figure 4.109. The plot also shows that the sum of the signals varies by less than 2% with wire position. A summary of signals expected from secondary emission mode and from shower mode is shown at the right of Figure 4.109. The beam sizes are $\sigma_x = \sigma_y = 2$ mm and the current is 50 mA. For the estimated signal provided by the PMT, the scintillator is a lead tungstenate crystal with the geometry shown in Figure 4.108. The light collection efficiency times the photocathode quantum efficiency is assumed to be 10%, the gain of the PMT is 10^4, and a neutral density filter absorbs 90% of the light. Based on this estimate, wire scanners above a few hundred MeV will acquire their signals from the shower detectors. The design of the fork will be similar for all the wire scanners and the wire will be mounted as shown in Figure 4.110. To avoid cross talk between the measurement planes, the wires will not be crossed. One drawback of this design is that the time needed for a vertical and horizontal measurement is increased by a factor of two compared to crossed wire design. A bias voltage will be implemented.

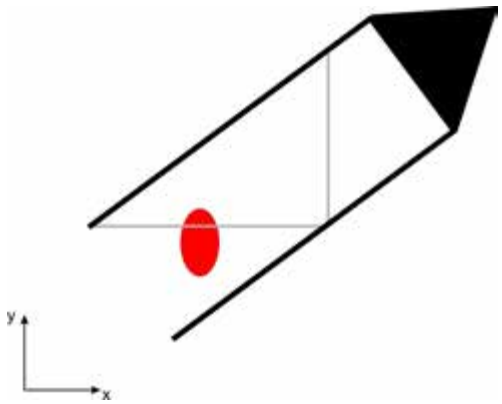

Figure 4.110: Diagram of the wire scanner fork. The beam is represented in red.

4.9.7 Non-invasive profile monitors

Non-invasive methods for measuring beam profiles are being investigated in parallel with the development of the wire scanners. Attractive candidate methods employ three types of devices: ionisation profile monitors (IPM) [507], luminescence profile monitors (LPM) [508] and particle beam scanners (PBS) [509]. These methods could allow measurements of the beam profile during neutron production, since they would not require the use of shorter diagnostics pulses. However, they are often viewed as less exact than wire scanners and may have limited resolution at low beam powers, so invasive devices will be retained for cross calibration even where the non-invasive devices are installed.

Ionisation profile monitor

When ionisation profile monitors are used, as depicted in Figure 4.111, the ionised residual gas particles are collected. The proton beam generates these particles as it passes through the residual gas. An electric field then accelerates the particles towards a detector. In principle, it is possible to detect the generated ions or electrons. The space charge of the beam also produces an electric field that accelerates the particles, disturbing the measurement. For electrons, this effect can be minimised by applying a magnetic field. Of course, this field also bends the proton beam, requiring the addition of one or two corrector magnets. To use the generated ions, the beam space charge effects have to be minimised by applying a very strong external electric field. First simulations show that a field of approximately 600 kV/m will lead to a beam image broadened by about 2.5%. There are two options for the high voltage: two electrodes can have a symmetric voltage applied, or the voltage can be applied to one electrode while the other is grounded. While the first option has the advantage of lower high voltages, facilitating handling, the detector has to be on high voltage, too. The second option has a higher single voltage, but the detector can be at ground potential. One option for a detector at high voltage can be a phosphor screen followed by an optical detector. This option is under evaluation. ESS plans to use the residual gas ionisation profile monitor in the superconducting part of the Linac, located in the warm sections where the residual gas pressure is approximately 10^{-9} mbar.

Luminescence profile monitor

The residual gas luminescence profile monitor, depicted in Figure 4.112, relies on the proton beam's excitation of the residual gas particles, which then emit light while de-exciting. This light can be imaged via an optical system to an area detector. The detector may be an image-intensified camera or a multichannel photomultiplier. One advantage of this method is that no components have to be installed inside the

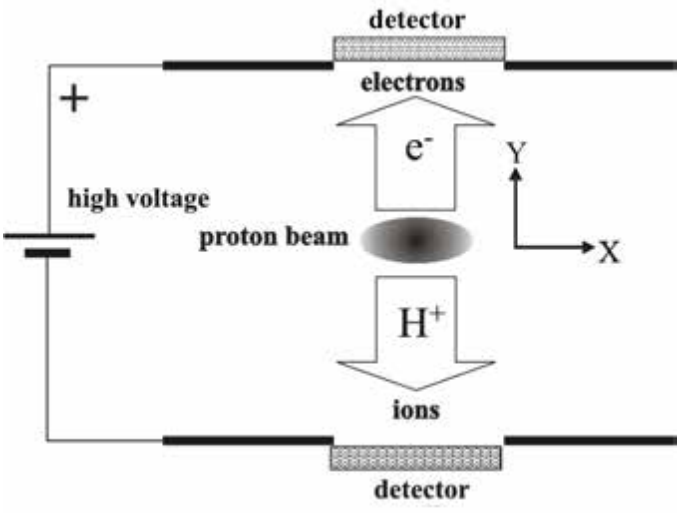

Figure 4.111: Sketch of the basic principle of an ionisation beam profile monitor (IPM). A magnetic field must be imposed to confine the path of the electrons, in order to use them for beam profile measurements.

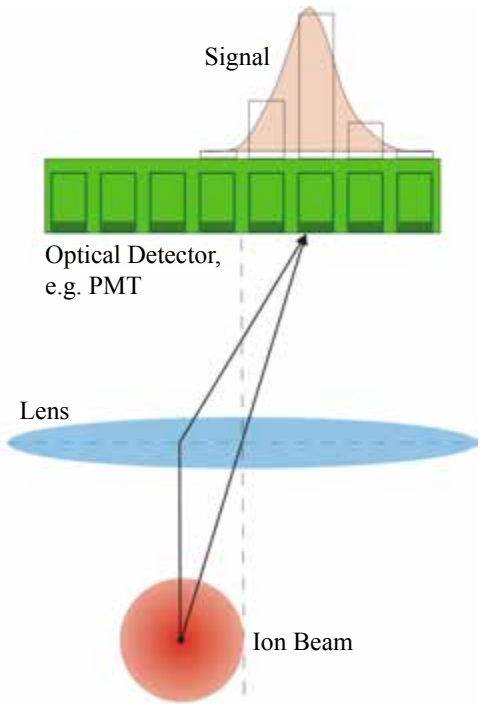

Figure 4.112: Sketch of the basic principle of a luminescence profile monitor (LPM) [510]. The light generated in the residual gas-beam interaction is imaged with a lens system onto a position sensitive detector, like a multichannel-photomultiplier or an intensified camera.

vacuum system. The disadvantages are the rather low cross section and collection efficiency. ESS plans to use this method in the normal-conducting linac, where residual gas pressures above 10^{-8} mbar are expected, and also in the target monolith where the beam passes through helium at atmospheric pressure.

Particle beam scanner

When particle beam scanners are used, a charged particle beam (typically electrons) is sent on a trajectory perpendicular to that of the proton beam, and scanned transversely across the full extent of the beam. The proton beam's electromagnetic fields deflect the diagnostic beam, and this deflection can be used to calculate the proton beam's profile. The disadvantage of this method is its highly experimental nature, which makes it necessary to spend a large effort in development. The advantage is the rather short time of only several μs for one profile scan. Unlike the other methods presented, this technique could measure all types of beam pulses, from the minimum diagnostics mode beam up to high power production beam. Given this advantage, particle beam scanning will be investigated along with the ionisation and luminescence techniques.

4.9.8 Halo monitoring and emittance measurement

In order to keep the losses at a small level, the beam's transverse halo will be measured at several locations along the ESS linac and cleaned with several collimators. In the warm linac, the halo measurement can be performed with wire scanners equipped with high gain and high dynamic range electronics. The charge deposition in the MEBT collimators can be also measured. In the cold linac, this method cannot be employed and two different options are under investigation: 1) use of detector-based Cerenkov light emission, and 2) use of diamond detectors. For both options, the radiation hardness of the materials is an issue and the life time of the detector has not yet been estimated. The drawback of these two methods is that they cannot measure the profile of the beam core, a function provided instead by the noninvasive profile monitors. At a location downstream of the high-β section, a wire scanner equipped with a particle detector telescope will be used in counting mode to measure beam core and halo with the same device.

Emittance measurement

The current beam instrumentation layout includes slit and grid emittance systems at two locations: one in the LEBT for monitoring 75 keV beam from the source, and the other in the MEBT to monitor beam at 3 MeV. Sets of wire scanners described in Section 4.9.6 provide a less direct measure of emittance at several locations throughout the facility. Layout and operation of a slit and grid system is depicted schematically in Figure 4.113. At each slit position, the narrow aperture allows the passage of a beamlet populated by particles that have approximately the same position x and a certain angular distribution. Due to the phase space rotation in the following drift space, the beamlet's angular distribution is transformed into a position distribution and sampled using a profile monitor, in this case a wire grid. Therefore, the profile measurement gives the angle $x'(y')$ for a certain position $x(y)$ and by scanning the slit across the beam, the phase space at the slit can be reconstructed. In order to sample both transverse planes, two slits and two grids are needed. The angular resolution of the system is determined by the profile monitor resolution (e.g. the wire distance) and the drift length. The slit geometry and material affect measurement accuracy. A number of particles will be scattered from the slit aperture edges and the slit aperture width biases the phase space sampling by introducing an angular cut. The larger the aperture, the smaller the cut. The slit also has to absorb most of the beam power. The mechanical design of the slit used at 3 MeV will be similar to the one used for the CERN LINAC4 diagnostic test bench, which is presented in Figure 4.114.

In the LEBT, the emittance system will be positioned in between the solenoids. After the first solenoid, the beam sizes are large and preliminary estimation shows that the slit can stand the full pulse length with full current. The slit will consist of graphite blades with a shape similar to that of the LINAC4 device. An external cooling system is planned. For the MEBT slits, the thermal load will be controlled by restricting the beam to diagnostics mode, and an MPS interface will assure this restriction. The grids will be made with carbon wires in the LEBT, and tungsten wires in the MEBT. At 3 MeV, tungsten wires provide

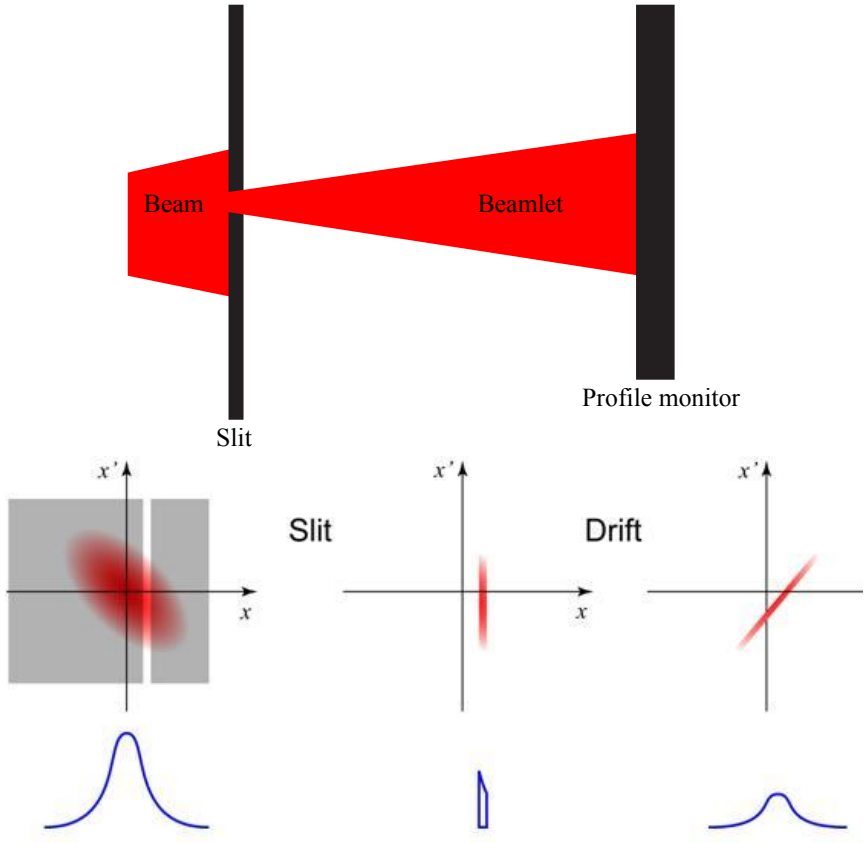

Figure 4.113: Slit and grid system for emittance measurement. Top: Schematic diagram. Bottom: Phase space sampling the beam divergence after beamlet rotation in phase space along the drift from the slit to the profile monitor.

Figure 4.114: Drawing of the LINAC4 slit (courtesy of D. Steyaert and E. Berthome).

better signal, while at 75 keV, the carbon wires will allow the use of the grid for profile measurement of a long pulse. In the MEBT case, a foil will be positioned downstream from the wires, which will have a bias voltage applied. This foil will reduce the cross talk between the wires and maximise the secondary emission signal.

4.9.9 Longitudinal bunch shape

Longitudinal matching needs to be measured and improved wherever the focusing structure of the linac changes. Four bunch length monitors are required at each interface between different linac sections, for this purpose. Bunches in the ESS linac are very short ($10 - 40$ ps full length), and so options to measure the bunch length are limited. Wall current monitors, or any other method based on detecting the fields at the vacuum chamber boundary, have an intrinsic resolution limit that is significantly larger than the bunch length, due to the rather low relativistic beta. This effect is illustrated in Figure 4.115. A bunch shape monitor seems to be the best option. Such a detector is based on measuring secondary electrons from a wire placed in the tail of the beam distribution. Since the process of electron emission does not have a significant delay, very good time resolution can in principle be achieved. Variants of such a

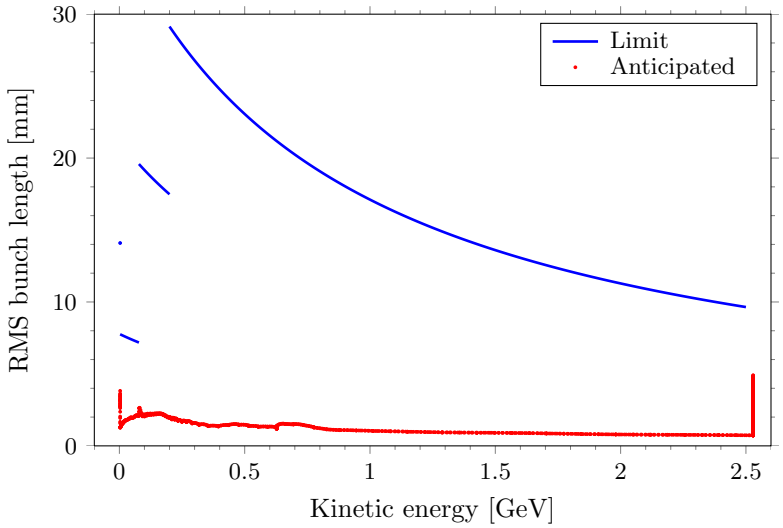

Figure 4.115: The continuous upper line represents the fundamental limit of the measurement of the full length of the bunch – the vacuum chamber wall current pulse length for an infinitely short beam pulse – as a function of energy. The individual points represent the anticipated evolution of the full length of the bunch, according to beam physics calculations.

monitor without a physical wire have been developed at GSI and ANL, and these are interesting options for ESS. These monitors could also in principle be used as wire scanners, but the baseline design separates these functions to allow optimisation of the various devices for their respective applications. The thermal constraints affecting wire selection are similar to those of the wire scanners which are discussed in depth in Section 4.9.6.

4.9.10 Beam-on-target monitoring

To assure that the interface requirements between the linac and the target systems are met, instrumentation will be deployed to measure the beam properties at the proton beam window and the target's beam entrance window. To achieve this, the beam density will be measured with a precision of ±20%, and the beam position with a precision of ±3 mm. The importance of these measurements merits deployment of redundant and diverse measurement techniques. Figure 4.116 shows the layout of beam instrumentation in this region, while Figure 4.117 shows the location of devices within the target monolith. Upstream of the proton beam window, a multi-wire grid will measure horizontal and vertical beam profile. On the downstream surface of the proton beam window, a thin luminescent coating will provide two-dimensional images of the beam density. Thermocouples surrounding the proton beam window will allow beam halo measurement and will be used to protect the window frame. The proton beam density at the target will be imaged by using a luminescent coating on the target's beam entrance window. In between the proton beam window and the target, an instrumentation plug will carry additional diagnostic devices, all residing in the helium at atmospheric pressure that fills the target monolith. These will include:

1. Optics to allow remote viewing of the proton beam window, and the beam entrance window;
2. An NPM consisting of optics to observe beam-induced gas luminescence;
3. A multi-wire grid, in ionisation mode to measure horizontal and vertical beam profile; and
4. Thermocouples to measure beam halo and to protect equipment.

The beam density images and the profile measurements rely on the BCM shown on the left of Figure 4.116 for normalisation. Synchronisation of the the target wheel position with respect to beam arrival time can be performed by using signals from this BCM and, redundantly, by analysing the images of beam and fiducials on the target's beam entrance window. The scope of the beam-on-target systems also includes beam instrumentation devices for the linac tuning dump. At this dump, a luminescent coating will be used to image the beam on the window. Upstream of the dump, a multi-wire grid will provide horizontal and vertical profiles. Experience at SNS provides a basis for the application of luminescent coatings and diamond-machined optics in the helium-filled target monolith [511]. A particular challenge is the development of a coating that will not significantly affect the thermal performance of the thin aluminium proton beam window. Observation of helium gas scintillation at the SNS gives confidence in using this signal for the NPM.

After the final quadrupoles upstream of the target have expanded the proton beam, the reduced beam density allows tungsten wires to survive in the high power beam. The grids will consist of tungsten wires with a diameter of 100 μm. Realistic super-Gaussian beam profiles cause the central wires to reach a maximum temperature of 880 K, far below the melting point of tungsten and the threshold of thermionic emission. This is a conservative estimate for the wires in beam vacuum, and also for wires in the monolith's helium environment, because it only takes credit for radiative cooling. The grids upstream of the proton

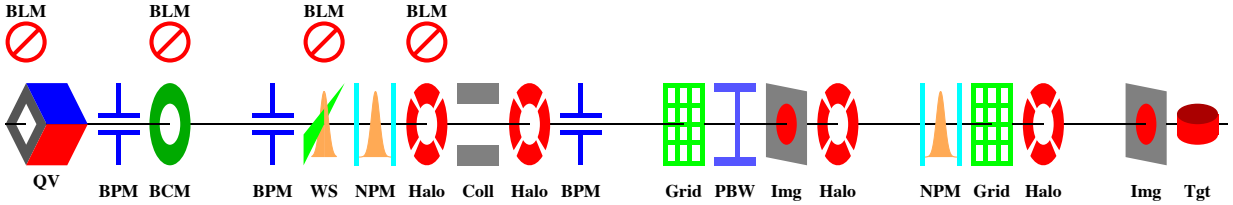

Figure 4.116: Schema of beam instrumentation in the approach to the target.

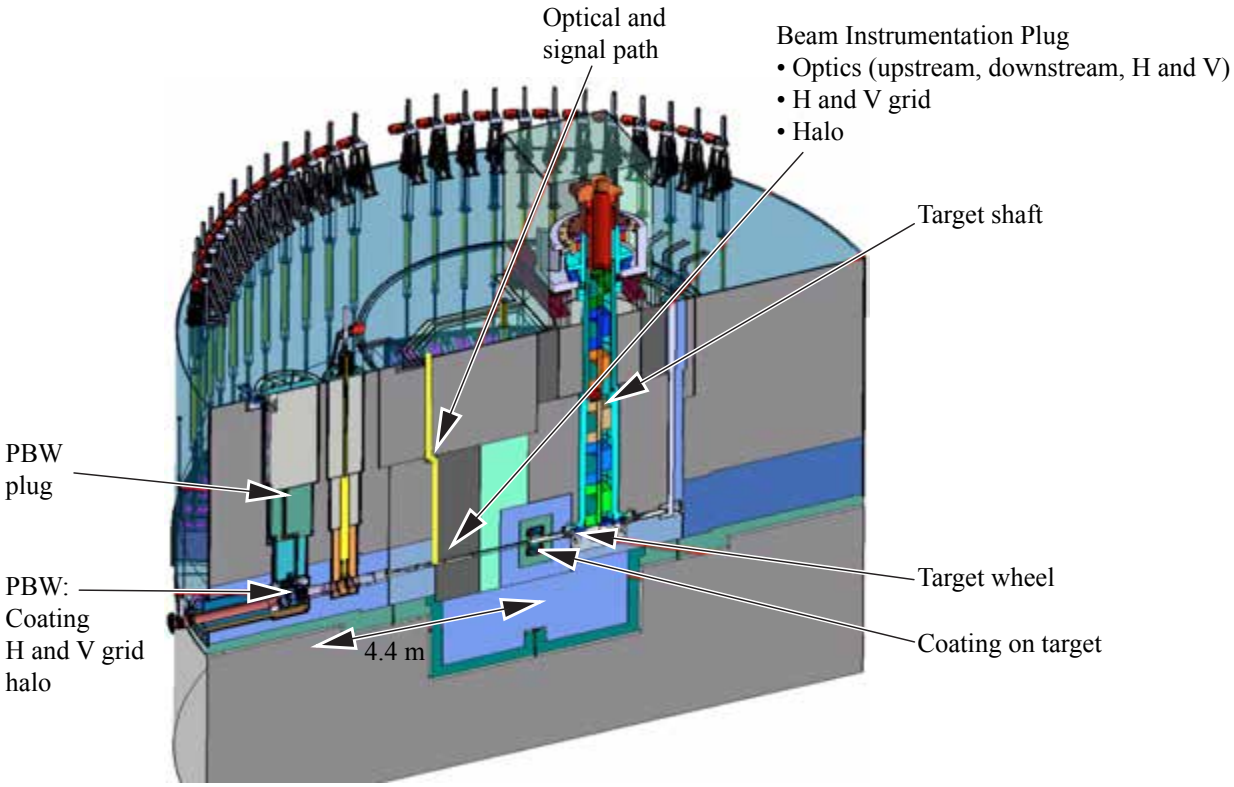

Figure 4.117: Locations of beam-on-target diagnostics within the target monolith.

beam window and the linac tuning dump reside in beam vacuum and will produce a signal resulting from secondary emission and a charged particle shower. According to FLUKA simulation estimations, the central wires will produce a peak signal of 0.35 μA for the horizontal profile and 0.92 μA for the vertical profile. Residing in helium at atmospheric pressure, the grid just upstream of the target will operate in ionisation mode. Assuming a cell depth of 10 mm in the longitudinal direction, the maximum expected signal is around 3.5 mA, with the shower from the upstream PBW producing a background of less than 0.4%. Non-linear response could be an issue, and this effect along with mitigation techniques will be studied during the design phase. These signal levels should allow the grids to achieve the required measurement performance.

4.10 Cost savings proposals

The FDSL_2012_10_02 design described above robustly meets the primary goals of the ESS accelerator. Namely, it provides an average beam power of 5 MW and a peak beam of 125 MW to the target with an availability of 95%. A careful cost estimate of the design has been made. The main cost driver is the RF system, which comprises 37% of the total cost. The 704.42 MHz elliptical cryomodules account for an additional 19%, and the cryogenic plant for another 14% of the total cost. There is always uncertainty in such cost estimates, especially in a project as complex as ESS. Some of the major cost driving components – such as the cryomodules, klystrons, and modulators – will be prototyped in order to reduce this uncertainty. The linac design is being examined to identify possible sources of cost savings based on design optimisations that will help to cope with potential market fluctuations, and to respond to design alterations that may be necessary as a result of prototyping test results. A number of alternatives provide design contingency at the expense of availability and beam quality.

Reducing the number of cryomodules

Reducing the number of cryomodules will have the largest impact on cost because each one that is removed not only deducts the cost of the cryomodule but also removes the need for (and cost of) for the RF power sources that feed the cryomodule. The proton beam power is proportional to the product of the beam current, the duty factor, the number of cavities, and the average energy gain per cavity. Changing the duty factor has the least impact on the accelerator design but makes a significant change to the temporal structure of the neutron beam. This is undesirable from the user point of view, and so changing the duty factor will not be considered. Instead, it is possible to raise the beam current and to increase the average energy gain per cavity, in order to offset the reduction in the number of cryomodules.

Increasing the beam current

Increasing the beam current makes it possible to reduce the number of cryomodules. For example, if the beam current is raised by 10%, then 3 high-β cryomodules out of 30 can be removed along with the associated RF systems. However, the remaining cavities now have to provide more peak power to the beam since the beam current has increased. Increasing the peak power from an RF system increases its cost, but not in proportion to the peak power. It is estimated that for each cryomodule removed, 80% of the cost of a cryomodule and its associated RF system can be credited as savings. Increasing the beam current will increase space charge forces at the low energy end of the linac and will possibly increase the beam emittance. This could cause more beam loss along the linac, and might adversely affect operational performance.

Increasing the cavity gradient

The high-β cavities are designed to operate below a maximum surface field of 40 MV/ m. This conservative value was chosen to maximise both the availability of the linac and also the acceptance yield of the cavity manufacturing process. Raising the maximum allowable surface field to 44 MV/meter permits 3 more high-β cryomodules to be removed. Again, the peak RF power will need to increase from the remaining RF systems so that only 80% of the cost of the cryomodule and RF system can be recovered. Increasing the peak surface field will affect cavity yield and could affect availability.

Uneven variation of the rate of phase advance

Finally, the FDSL_2012_10_02 design requires a phase advance of less than 90 degrees per cell, requires the tune depression factor to stay about 0.4 in all three planes, and requires the phase advance per meter to vary smoothly along the length of the linac. The last requirement reduces the average accelerating voltage in the medium-β linac section. Relaxing this requirement so that the maximum cavity gradient is achieved in every medium-β cavity permits 3 more high-β cryomodules to be removed. Since the RF systems do not have to provide more peak power than initially required in the medium-β section, 100% of the cost of the cryomodule and RF system can be recovered. However, it is estimated that the emittance will increase by 15% in the medium-β section with the relaxed requirement on phase advance. This emittance increase could cause additional beam loss.

In summary, 9 high-β cryomodules out of the existing 30 cryomodules could be removed with a 10% increase in beam current, a 10% increase in peak surface field in the superconducting cavities and the relaxation of the requirement on smooth phase advance though the medium-β section of the linac. These proposals should reduce cost while maintaining the scientific performance with acceptable additional technical risk. All other aspects of the accelerator design nominally remain the same.

Chapter 5

Integrated Control System

Chapter abstract

Summary: The integrated control system (ICS) is responsible for the whole ESS machine and facility: accelerator, target, neutron scattering instruments and conventional facilities. This unified approach keeps the costs of development, maintenance and support relatively low. ESS has selected a standardised, field-proven controls framework, the Experimental Physics and Industrial Control System (EPICS), which was originally developed jointly by Argonne and Los Alamos National Laboratories. Complementing this selection are best practices and experience from similar facilities regarding platform standardisation, control system development and device integration and commissioning. The components of ICS include the control system core, the control boxes, the BLED database management system, and the human machine interface.

The control system core is a set of systems and tools that make it possible for the control system to provide required data, information and services to engineers, operators, physicists and the facility itself. The core components are the timing system that makes possible clock synchronisation across the facility, the machine protection system (MPS) and the personnel protection system (PPS) that prevent damage to the machine and personnel, and a set of control system services.

Control boxes are servers that control a collection of equipment (for example a radio frequency cavity). The integrated control system will include many control boxes that can be assigned to one supplier, such as an internal team, a collaborating institute or a commercial vendor. This approach facilitates a clear division of responsibilities and makes integration much easier. A control box is composed of a standardised hardware platform, components, development tools and services. On the top level, it interfaces with the core control system components (timing, MPS, PPS) and with the human-machine interface. At the bottom, it interfaces with the equipment and parts of the facility through a set of analog and digital signals, real-time control loops and other communication buses.

The ICS central data management system is named BLED (beam line element databases). BLED is a set of databases, tools and services that is used to store, manage and access data. It holds vital control system configuration and physics-related (lattice) information about the accelerator, target and instruments. It facilitates control system configuration by bringing together direct input-output controller (IOC) configuration and real-time data from proton and neutron beam line models. BLED also simplifies development and speeds up the code-test-debug cycle. The set of tools that access BLED will be tailored to the needs of different categories of users, such as ESS staff physicists, engineers, and operators; external partner laboratories; and visiting experimental instrument users.

The human-machine interface is vital to providing a high-quality experience to ICS users. It encompasses a wide array of devices and software tools, from control room screens to engineer terminal windows; from beam physics data tools to post-mortem data analysis tools. It serves users with a wide range of skills from widely varied backgrounds. The Controls Group is developing a set of user profiles to accommodate this diverse range of use-cases and users.

5.1 Overview

5.1.1 Architecture and organisation

From a control system point of view, the ESS machine includes all parts of the facility, including the accelerator, target, neutron-scattering instruments and conventional facilities. The integrated control system (ICS) will connect all parts of the machine into an integrated working entity. ICS will provide control support for all phases of ESS's life-cycle, from commissioning through operation, maintenance and decommissioning. It will provide automatic as well as manual control; monitoring and diagnostics capabilities; and the means to store and retrieve various readings collected by systems and instrumentation. This unified approach will keep the costs of development, maintenance and support relatively low. ESS has selected a standardised, field-proven controls framework, the Experimental Physics and Industrial Control System (EPICS), which was originally developed jointly by Argonne and Los Alamos National Laboratories. Complementing this selection are best practices and experience from similar facilities regarding platform standardisation, control system development and device integration and commissioning.

Figure 5.1: The main components of the control system architecture: The control system core, control box, human machine interface, BLED data management system and the software development environment.

The ICS project is the responsibility of the Controls Group. Since the Controls Group interacts with the majority of the stakeholders involved in the ESS project, it is essential to clearly define the scope of ICS and its interfaces with all parts of the facility before the beginning of the construction phase. The scope of ICS can be presented in terms of organisational blocks, as shown in Figure 5.1:

1. The control system core is the heart of ICS. It includes those computer services that need to run continuously regardless of ICS user activities, such as the archiving of process variable (PV) values; monitoring of alarm states; and slow feedback loops. It also includes the central systems such as timing, the machine protection system (MPS) and the personnel protection system (PPS).

2. Control boxes govern the interaction of ICS with physical equipment. They serve two purposes: At the top, they provide an abstract representation of equipment to higher layers of the control system so that equipment can be monitored and controlled; at the bottom, they implement real-time control loops of the equipment.

3. BLED (beam line element databases) is the name of ICS's central data management system. It is a set of tools and databases used for the central storage, access and management of information regarding the machine and its configuration.

4. The development environment provides vital services that facilitate software consistency and compatibility. It allows for proper development procedures, artifact sharing, code storage, and related functions. It also provides a controlled way to develop upgrades to the ICS software.

5. The human machine interface (HMI) encompasses graphical and non-graphical user interfaces, and also workstations and the layout of the main control room. It provides for site-wide monitoring of ESS's status, and remote access. The HMI encompasses a wide array of devices and software tools, ranging from control room screens to engineer terminal windows, and from beam physics data tools to post-mortem data analysis tools.

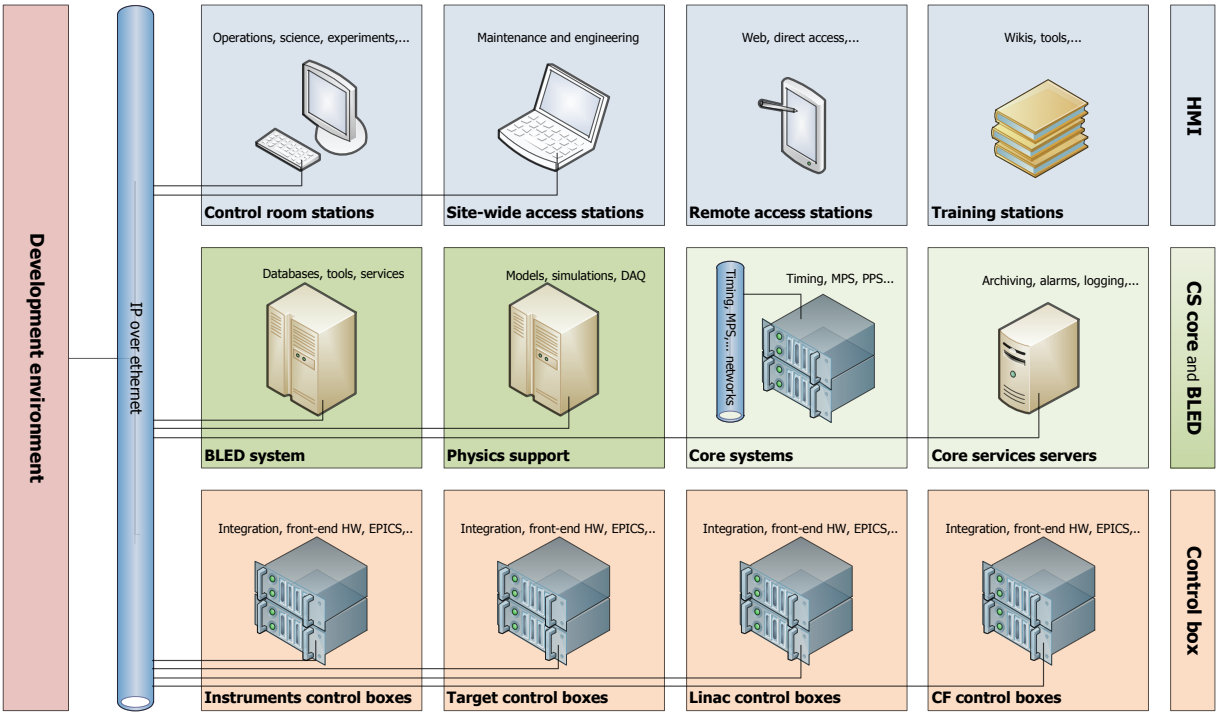

Figure 5.2: The three-tier architecture of the control system. Upper layer: Control system-user interaction. Middle layer: Processing, data management and configuration storage. Bottom layer: Communication with equipment and measurement acquisition.

These organisational blocks can be associated with the three tier [512] architecture of the control system, which is illustrated in Figure 5.2. The ICS subsystems associated with each of the three tiers will run physically on computers meeting requirements specifically set for that tier. The computers of the presentation tier will focus on ergonomics and usability. The computers of the data and services tier will offer high CPU performance and reliability, and will have access to substantial storage capacities. The computers of the resource tier will have a wide assortment of input/output capabilities, reflecting the need for control boxes to communicate with a wide array of equipment. The platform will likely be modular to allow various types of input/output through field buses and custom-developed hardware.

Figure 5.3 presents more detail about the functional layout of the ICS, tying specific functions, subcomponents, and equipment to the logical components of the ICS responsible for, or in communication with, those functions, subcomponents and equipment. The logical components and their functions conform to the three tier architecture of the ICS. The top, or presentation, layer is directly accessible to the user. This is the domain of the human machine interface. The bottom, or resource, layer interacts directly with non-ICS physical equipment. This is the domain of the control boxes. The middle layer includes both services and the data that live within the control system. This tier exposes the overall, aggregated state of the facility to its operators. This is the domain of the ICS core and BLED.

One of the key roles of the ICS architecture is to reduce the complexity of interactions among components. This is a crucial function in large-scale systems, as the number of possible interactions grows

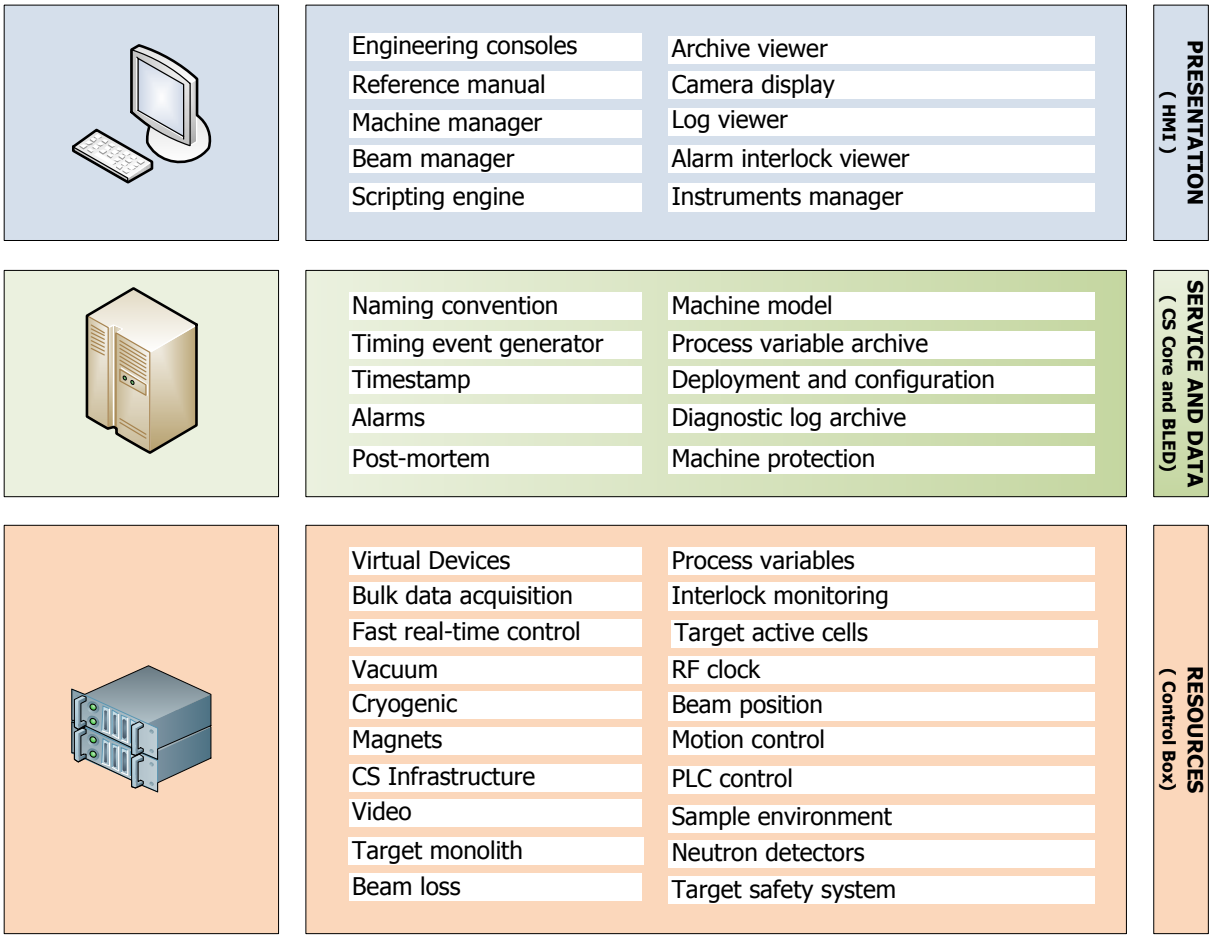

Figure 5.3: Functional layout of the control system, tying specific functions, subcomponents and equipment to the logical components of the ICS responsible for, or in communication with, those functions, subcomponents and equipment. The presentation layer is the domain of the human machine interface. ICS Core and BLED provide services and data. The resource layer is the domain of the control boxes, which interact directly with equipment.

approximately with the square of component instances. To reduce complexity, the architecture imposes the following restrictions on interactions:

1. The components of the presentation tier will interact primarily with components of the service and data tier, whose role is to provide information about the state of the facility to the HMI.

2. In limited circumstances, components of the presentation tier may interact directly with components of the resource tier. These interactions typically will be used for detailed diagnostics or for special-purpose data transfers.

3. A component of the presentation tier can only make use of interfaces exposed by either the resource or the services tier. The presentation tier will make no assumptions regarding implementations and protocols behind these interfaces.

4. The presentation tier will rely on the mediation of the service tier (in particular, on the naming service) to gain initial direct access to the resource tier.

5. Components of the resource tier will be passive. Apart from registering their presence with the service tier, they will not actively establish communication with other components. Service tier components will be responsible for establishing communication with components of the resource tier.

The ICS will be designed as an object-oriented, decentralised, distributed system. Control boxes will interface with and control installed equipment. They will provide network access to the equipment, using physical connections for the hardware and device drivers for the software. ESS machine operation will require precise coordination of its component pieces of equipment. Synchronised equipment handling will be achieved by reaction to timing events broadcast by ICS timing generators. Real-time operating systems or pure hardware implementation will assure precisely timed actions with μs reaction time jitter (timing resolution). In addition to actions triggered by timing events, the equipment control level will service requests from the equipment itself, typically triggered by interrupt signals.

One of the main tasks of a control system is to provide an intuitive representation of the equipment to human users and to transfer commands from human users to the equipment. This will be achieved by constructing a modular HMI interface that will encompass all aspects of human-machine interactions. A separate user interface on top of the integrated control system, which will cater to the specific needs of scientific users, will be provided by the DMSC as part of a software suite, as discussed in Section 2.8.3.

Since the control system of the ESS facility will be very complex, it is important that it be scalable, that is, that there be no a priori upper bound on the size of the control system as a whole. At these scales, it will not be possible to achieve this goal by improving the performance of individual components. Instead, the ICS architecture must make it possible to redeploy components on additional hardware resources to cover additional needs for processing and communication power. To ensure the flexibility to make such redeployments possible, all configuration data and information about the machine will be handled by BLED. Changes to the ICS configuration will be entered into BLED and then propagated through the system where they will take effect, thus minimising the effort needed to introduce changes as well as the possibility of errors. All the code for ICS will be built within a dedicated development environment which will ensure compatibility with set standards and a uniform means of deployment.

Safety and protection systems

In the event of device fault or failure, or detection of non-nominal conditions, ICS will be structured to respond in a way that will prevent damage to equipment and harm or danger to personnel. A number of safety and protection systems will ensure safety during the commissioning, operation and maintenance of the ESS machine. Figure 5.4 provides an overview of the three most important safety and protection systems, ranked in order of the safety and reliability requirements each must meet. These are the target safety system (TSS), the personnel protection system (PPS) and the machine protection system (MPS). TSS covers the target station and adjacent portions of the facility, while both MPS and PPS have machine-wide responsibilities.

The TSS will be responsible for the actions required to operate the target station in compliance with Swedish regulation and ESS's own General Safety Objectives. It will fulfil the highest reliability and safety demands, and will be a safety classified system under Swedish law. The TSS will interact with the MPS

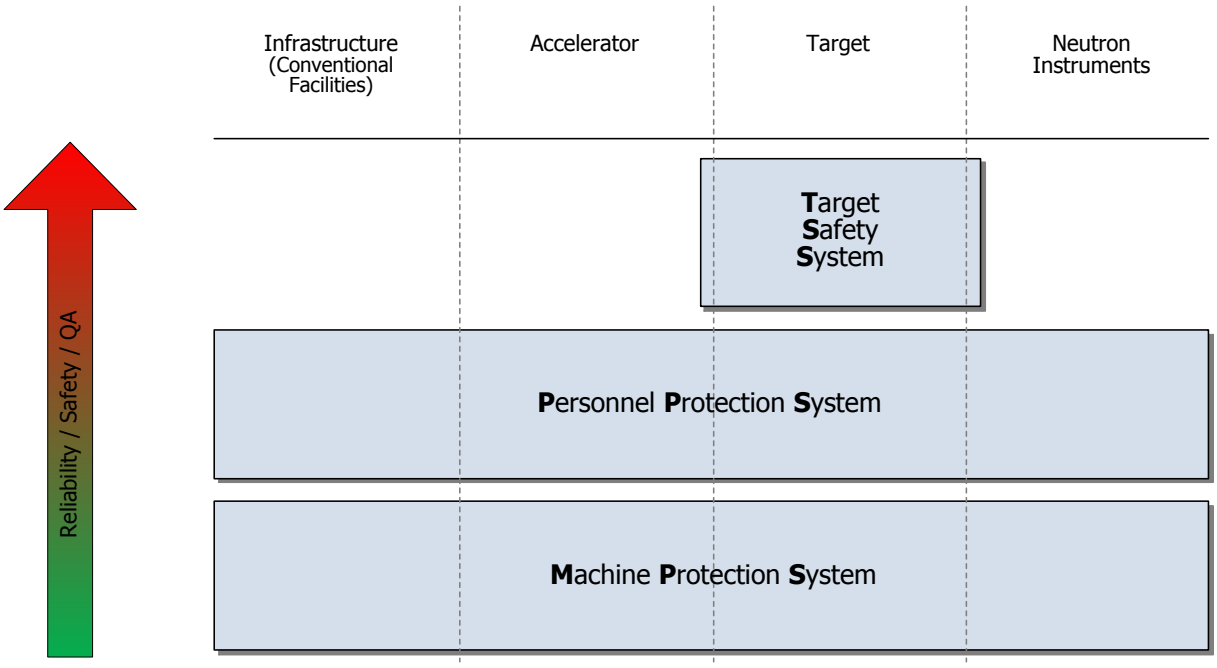

Figure 5.4: Overview of the main safety and protection systems, with the order from bottom to top reflecting increasing demands for reliability and safety: The machine protection system (MPS), personnel protection system (PPS) and target safety system (TSS). The TSS covers only the target station systems, including the A2T (accelerator to target station) section and the intersection between the target and neutron instruments, while the responsibility of MPS and PPS spans the whole machine.

only to request a switch off of the proton beam. The construction and operation of the TSS is described in Section 3.1.5.

The PPS will be responsible for the protection of personnel. Its main focus will be protection against radiological risks, but it may also play a role in protection against other hazards such as electrical shock. The PPS also will be a safety classified system under Swedish law, and will meet the rigorous reliability and safety demands that accompany that classification. The MPS will protect the machine's equipment against damage due to beam losses and malfunctioning components of safety-critical devices by initiating an emergency shutdown of the proton beam. It will not be a safety classified system under Swedish law, but it will be constructed to deliver high levels of reliability and safety.

5.1.2 Infrastructure

Main control room and satellite control areas

The main control room will be the central location from which operations activities will be coordinated. The machine as a whole will be controlled and monitored from the main control room. Neutron instruments will also be monitored from the main control room, but since neutron scientists need proximity to their sample environments and data acquisition hardware, satellite control areas will contain the systems needed for control and monitoring of instruments and sample environment. Data acquisition from the experiments will also be controlled from these areas, as described in more detail in Section 2.8.3.

In the main control room, a large monitor will provide an overview of the state of the machine at a glance. The ESS status application will display a condensed message on this monitor describing the status of the machine with "all OK" / "Error" information. Additional monitors will display more detailed information about the components of the machine, and the main monitor will be able to display component-specific information upon request, as well.

The control room will be built in at least two stages. During installation and commissioning of the machine and the first neutron instruments, a temporary location will serve as the main control room until the building where the permanent control room will be housed has been completed. The main control

room will not contain hardware or analogue signals, but instead will contain only monitors and control stations. This will make it easier to move operations from the temporary to the final control room, as both rooms will be able to exist in parallel while the temporary control room is decommissioned. The main control room will be equipped with a kitchen, sleeping and rest rooms, showers and a control room reception.

Control system data centre

A secure and local data centre will support the main control room, and will house servers for ICS and also for immediate post-processing of data from the experiments. High-speed and secure networks and data storage capabilities will provide the necessary computing infrastructure for ICS and neutron instruments. Data acquired from the experiments will pass through this data centre on their way to permanent storage and analysis at the DMSC facility in Copenhagen, as presented in Figure 2.49. Only authorised personnel will have access to the data centre and related networks.

Networks

ESS will be a high-power, high-profile facility, and so must ensure that security needs are met in its systems for accessing its control system. While complete isolation of ICS from the Internet would provide complete perimeter security, it would also make efficient remote diagnosis and support impossible. Furthermore, it will sometimes be advantageous to be able to control instruments and experiments remotely, as is discussed in Section 2.8. Clearly, a solution is required that couples adequate security with adequate remote access. ESS will achieve this goal by making remote access to ICS possible only through dedicated gateway hosts. In addition, external network access by any resources inside the firewall will be proxied at the firewall to limit the risk of malware or virus infection.

The traffic on ICS internal networks will not be encrypted, since these networks are presumed to be secure and encryption would hinder passive logging and CS diagnostics. Seven independent dedicated networks will provide the infrastructure for ICS operation:

1. A control network that will be used by channel access, the middleware that conveys process variable data [513];
2. A timing network that will be used for time synchronisation and time stamping;
3. An MPS network that will be used for events relevant to machine protection (e.g., detection of a fault in a safety-critical subsystem) and for heartbeat signal;
4. A PPS network that will be used for events relevant to personnel safety, whose design is still under discussion;
5. A programmable logic controller (PLC) network that will be used for reliable implementation of safety/interlock logic, for which reaction times of several 100 ms are acceptable;
6. A video network for video streaming; and
7. A network for collecting beam diagnostic data.

Either standard computer network or optic fibre will be used to provide interconnections among network nodes, depending on requirements with respect to data transfer rates and latency of the systems in question. Where possible, the standard TCP/IP and UDP/IP protocols will be used. The choice of protocol will depend on whether the network needs to be able to establish a fast connection and whether the risk of losing some data is acceptable in order to boost performance. The networks will be constructed with redundant topology, essentially providing two paths involving independent elements (network cards, cables, switches) between every two nodes of the network. Table 5.1 provides an overview of the required data transfer rates and protocols for the various control system networks.

It is expected that two levels of hierarchy will be sufficient for the control system networks, however a third level may be required, depending on the number of nodes. The network infrastructure will be monitored and will be accessible via the same interfaces as other equipment. It will be possible to instantiate, monitor and control devices on a given network node even in case of control system outage through direct local access, remote shell, command line tools, web interface, etc. All network devices will be powered using uninterruptable power supplies.

Network	Transfer rate	Unit	Protocol
Core control	1	Gbps	TCP
Timing	2.5	Gbps	Custom
Machine protection system			Custom
Programmable logic controller	100	Mbps	TCP or UDP
Video	> 1	Gbps	UDP
Beam diagnostics	Maximum available		UDP

Table 5.1: Required transfer rates and protocols for different control system networks.

5.1.3 Hardware framework

The control box is the main building block of the ICS hardware framework. It will provide a platform for running the distributed control framework software (EPICS) and a uniform way to integrate equipment into ICS. Control boxes will act as servers and correspond to input/output controllers (IOCs) in EPICS terminology [514]. In many cases, a physical subsystem will be connected to one or more control boxes which will contain all the control logic for that subsystem (e.g., closing some of the control loops that can be locally closed) and management of the subsystem states. The idea is that a subsystem connected to control boxes can be controlled independently of other subsystems, or it can be simulated, because its external interfaces are well defined. Thus, a control box is also an organisational unit of procurement for ICS. Table 5.2 lists preliminary estimates of the number of control boxes that will be required for the operation of different ESS domains.

Domain	Number of control boxes
Neutron instruments	100
Target	100
Accelerator	350
Conventional facilities	50

Table 5.2: Preliminary estimates of the required number of control boxes per domain.

5.1.4 Software framework

The EPICS control system framework, running on a Linux operating system, will be used for control system services and control box software. EPICS is widely used for system control at many large physics facilities, including proton accelerators at neutron sources (SNS and J-PARC) and electron accelerators, as well as instruments at synchrotrons. SNS and ISIS are considering EPICS for instrument control as well. EPICS is supported by a large community with two annual collaboration meetings and an annual technical meeting. EPICS drivers already exist for many devices, including those used by many neutron instruments. Development of ESS instrument-specific drivers can be carried out in close collaboration with these labs.

A “device” is an abstraction that represents either a single piece of equipment (low-level code for interfacing the hardware) or a virtual device defined in software only (e.g. device models, virtual equipment, etc.). From the ICS point of view, all equipment will be modelled as a device, and a device will be the basic unit of ICS granularity. A device will be the smallest part that can stand alone and it will be loosely coupled to other parts of the ICS. A device is defined as an association of process variables, setpoints, states, configuration that influences the behaviour of the device, and actions, which are logic that is executed upon various triggers, such as state transitions, events, time, or command invocations.

A process variable (PV) usually represents a physical quantity that is typically acquired by sensors, such as thermometers, magnetometers, current meters, or beam monitoring instrumentation. Higher-level entities in the control system also expose process variables, but these do not necessarily have a directly

measurable physical correspondent. The values of these process variables are derived from other process variables. PVs whose values are derived from sensors are read-only. ICS acquires them, but can not influence them directly. On the other hand, actuator-like devices can exert an influence on the machine and can be assigned a target value (e.g., the power supply can be told how much current it is to produce). The desired target value is called a setpoint.

The middleware in EPICS is called channel access (CA). It is responsible for conveying PVs from their sources (e.g., sensors or machine model logic) to their sinks (e.g., the user interface or control loop regulators input). Similarly, CA is responsible for conveying the setpoint values from their sources (e.g., the user interface or control loop regulator's output) to their sinks (e.g., the actuator or logic that drives other actuators).

A device can be associated with one or more process variables whose values define its state. A device can thus be modelled as a finite state machine, in which all possible transitions between states are known in advance. State transitions are performed by the device logic, which is in turn triggered by events, changes of other process variable values, setting of setpoint values, etc. The device's state is determined by the states of the equipment it represents. All the equipment interfaced to the CS will be in exactly one of the following equipment states:

1. Off: Equipment and power supplies are powered down.
2. Operational: Equipment is operating.
3. Non-operational: Equipment is on, but temporarily unavailable for operation. For example, it might be initialising or performing some other lengthy operation in which it is not in a consistent state.
4. Fault: Equipment is not working properly. This state may have several sub-states so that failure can be more precisely defined.

The logic of devices will continue to execute even in case of ICS failures. The devices will detect a failure and act accordingly. Devices will be connected to the control system in parallel compositions rather than serial ones to reduce the probability of failures. Devices will be grouped into systems. The state of a system will be the union of its device states. A device will be able to belong to more than one system. When systems are grouped into further systems and domains, their states will be transferred up the hierarchical chain.

5.1.5 Device integration

During construction, ESS will accept in-kind contributions from project partners, in addition to cash contributions from member states. The Controls Group will provide the organisation and infrastructure to make this kind of collaboration efficient for components within ICS. A well-defined set of procedures, interfaces and hardware that will standardise and integrate the deliveries of different collaborating partners will be provided. This will be achieved by using the control box as both the platform on which the technical architecture of the hardware and software will be based, and as the basic organisational unit of human activities associated with ICS development and implementation. From an organisational standpoint, the control box approach will facilitate collaboration among ESS partners and integration of their work into a coherent whole. A control equipment catalogue will list the hardware supported by ICS based on requirements specified by various stakeholders, as is discussed in Section 5.3.2.

The hardware, software and maintenance associated with each device can be divided into two parts: device integration and device contribution. The Controls Group is responsible for device integration while stakeholder groups are responsible for device contribution.

Device software will be a joint effort of the Controls Group and the stakeholder groups who will use the device. The Controls Group will take responsibility for the parts of the device that involve interaction with the ICS as a whole, such as device instantiation, including registration to BLED, and setting up the connection to remote access middleware via the control box. The Controls Group will also be responsible for those device functionalities that are common to all devices through definition of a common set of properties, as well as for the framework or tool-set to implement equipment control functionality. Stakeholder groups will take responsibility for designing and implementing properties and equipment controls actions, based on the control system framework and tool-set. The Controls Group will provide training to enable stakeholder groups to implement their own high level applications. The training

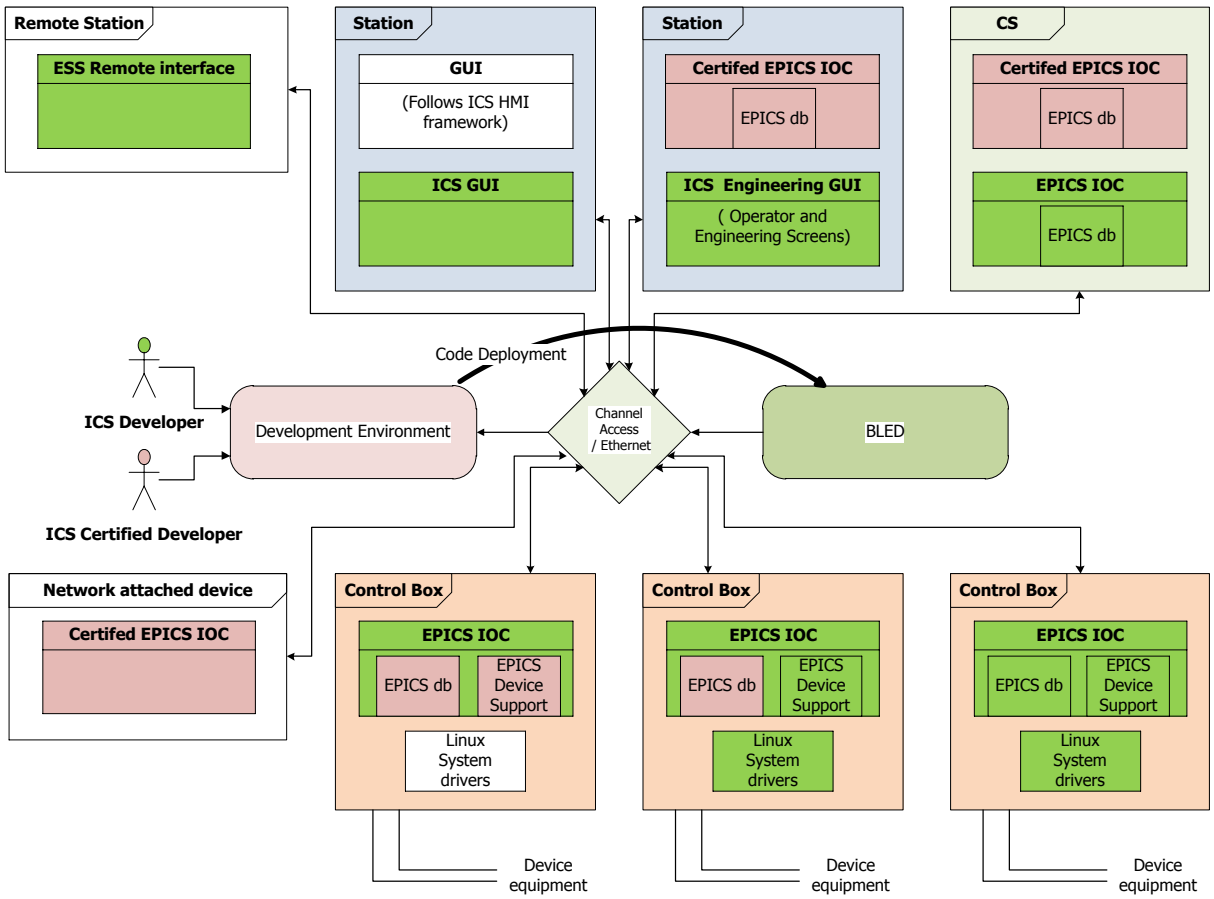

Figure 5.5: ICS integration borders. Green represents ICS development while purple represents development done by ICS-certified developers. White represents software and hardware that are not part of ICS.

will lead to ICS developer certification. In addition, the Controls Group will provide the control system framework, development environment infrastructure, code review, acceptance procedures and support.

The device hardware consists of the equipment itself, and the cables and control box components needed to connect the equipment to ICS. The equipment and cables are a part of the device contribution, and so the Control Group will not be responsible for their maintenance. Any device hardware that is part of the control box, on the other hand, will fall under device integration and will be the responsibility of the Controls Group. Control boxes will be provided and maintained by the Controls Group.

Figure 5.5 shows how both ICS developers (green) and ICS-certified developers (purple) will use the development environment to develop code for device integration. The code will then be deployed to the appropriate control box, station or server using the configuration stored in BLED. The border between device integration and device contribution is shown for eight examples, including three control box examples, a special case of a network-attached device, a server, two station examples and a remote station. Once successfully deployed, the maintenance responsibility for all certified and ICS-developed software will transfer to the Controls Group. The white coloured elements are not under the responsibility of the Controls Group at any time in their life-cycle.

5.1.6 Naming convention

The ESS naming convention [515] is based on a standard developed for the Superconducting Super Collider in the U.S. in the 1980s, and later adopted by other large research facilities, including SNS, FRIB, ITER, and CEBAF. The naming convention was agreed upon and approved at a very early stage of the project in order to establish a standard before names started to evolve. The main purpose was to standardise

meaningful, yet short and mnemonic signal and device names: Given millions of signals to control and thousands of devices to operate, clear communication is essential among operators, physicists and engineers. The format of signal names is:

```
SSSS-BBBB:DDDD-III:TTTIIIXXX
```
(5.1)

where

`SSSS` is the system name, which indicates the part of the facility to which the device provides service. For example, `HB` indicates the high-β sections in the accelerator tunnel and gallery. This links a name to the approximate physical location of the equipment that the device represents.

`BBBB` is the subsystem name, which indicates the context in which a device is used, for example, vacuum (`Vac`) or controls (`Ctrl`).

`DDDD` is the device identifier, for example a beam loss monitor (`BLM`) or a gate valve (`GV`).

`III` is the device qualifier, which is used to distinguish identical devices of the same system-subsystem from one another.

`TTTIIIXXX` is the signal part of the name with type (`TTT`), instance (`III`) and suffix (`XXX`). These are intrinsic to the control system.

Devices are not structured hierarchically through the naming convention. For example, there are four cavities inside a cryomodule. Both cryomodule and cavities are devices, which implies that the internal structure cannot be resolved from the names themselves. Rather, the parent-child relation resides in the BLED configuration database, as is discussed further in Section 5.4.

5.2 Control system core

5.2.1 Safety, the core requirement

The services that run in the core are the heart of the integrated control system. These are the machine protection system (MPS), personnel protection system (PPS), timing system, and general services for logging, alarm monitoring, and archiving of process variable values. These services, together with the safety-classified Target Safety System, form the essential backbone for the safe and efficient control of the machine. The ICS Project is responsible for delivering all these systems with the exception of TSS, which is the responsibility of the Target Division. All of these systems will function together in a highly coordinated way to guarantee the safe and reliable operation of the facility. It is important to emphasise this point. The safety of personnel and of the environment and inhabitants near the ESS site is the highest priority requirement for ICS. ICS will be constructed so that equipment failure cannot endanger anyone working at or visiting the site. Although the production of the brightest source of spallation neutrons for scientific research is the principal purpose of the ESS project, safe operation of the facility takes precedence even over this goal.

The following sections discuss the machine and personnel protections systems. The target safety system is discussed in Chapter 3, but the relationship of this system to ICS is outlined here. The remaining components of the core control system, including the global timing and general system services are discussed in detail following the discussion of the safety systems.

5.2.2 Machine protection system

The main role of the machine protection system is to protect the machine's equipment from damage induced by beam losses and/or malfunctioning equipment. Protection will be achieved by initiating an emergency shutdown upon detection of critical and non-nominal conditions. A wealth of diagnostic instrumentation installed throughout the machine will enable MPS to detect such conditions. This instrumentation will continuously survey the health of equipment and beam, and convey the information it gathers to MPS. Based on the combined reports on the status of all relevant sub-systems and the results of diagnostic measures, MPS will either perform an emergency shutdown of the beam or machine, or will permit beam-based operation. At the same time as MPS seeks to protect equipment from damage, it will also seek

to avoid false emergency shutdowns leading to unnecessary machine downtime; thus the quantity to be optimised by MPS is integrated machine performance. In addition to its protective role, MPS will also enable ESS to trace the origin of an emergency shutdown, helping to identify the responsible subsystem(s) and the nature of the problem. Finally, MPS will play an important role during ESS commissioning and operation by making it possible to load and apply the required operational mode settings to the machine's equipment, and to assure the correctness of the settings once they have been loaded [516].

Design approach of safety-critical systems

The successful design of a complex and mission-critical system, such as MPS, is achieved by applying well-established system safety management methods and techniques [517–519]. These techniques help to prevent, eliminate and control hazards and risks. ESS will use a top-down systems design approach, focusing on the overall facility mission and goals. Within this approach, the terms accident, safety, risk, hazard, and reliability are briefly defined as follows:

Accident is an undesired and unplanned, but not necessarily unexpected, event that results in at least one specified level of loss, for example a fatality, injury, occupational illness, loss of containment, uncontrolled discharge to the environment, or legal claim. An accident has the potential to disrupt nominal safe operations.

Incident is an event that involves no, or only minor, loss but that would have had the potential for loss under different circumstances.

Hazard is a state or set of conditions that, together with other (worst-case) conditions in the environment, will lead to an accident, that is, to a loss event.

Safety is freedom from accidents or losses.

Losses include human injury, equipment damage, environmental pollution, and mission loss, among other things.

Hazard level is a combination of the severity level and likelihood of occurrence of the hazard.

Risk describes a hazard level combined with the likelihood of the hazard leading to an accident plus exposure (or duration) of the hazard.

Reliability is the ability of a system to perform a required function under given conditions for a given time interval.

Availability is the ability of a system to be in a state allowing it to perform the required function at a given instant of time.

The assigned design function for MPS is the execution of an emergency shutdown upon detection of non-nominal or other critical conditions that might lead to damage to the machine's equipment. The time interval during which this function must be assured starts at machine powering and stops when the action, 'shutting down the machine in a controlled and safe way,' has been completed. The concept, design and development of MPS will follow the life-cycle model laid out in the IEC61508 standard to the extent practicable. This model provides an overall context for the development of safety-critical systems under specific standards [519]. Similar life-cycle activities apply to all related MPS systems. Assumptions that are made in the analysis of one MPS system or component will often impose requirements on another system or component, whose compliance with these requirements must be tracked. For example, analysis of the subsystem responsible for shutting down the beam will assume that certain physical conditions will trigger an alarm. This assumption then places a requirement that must be tracked on MPS's alarm-generating subsystem. Similarly, a number of MPS subsystems will be analysed under the assumption that safety-critical fast valves fulfil their safety and reliability requirements.

The IEC61508 standard

The IEC61508 is an international industrial standard for the, "Functional Safety of Electrical/Electronic/ Programmable Electronic Safety-related Systems (E/E/PE, or E/E/PES) [520]." The language of the standard defines functional safety as, "... part of the overall safety relating to the EUC (Equipment Under Control) and the EUC control system that depends on the correct functioning of the E/E/PE safety-related systems and other risk reduction measures." [521] The standard also considers, "... other technology safety-related systems and external risk reduction facilities in order that the safety requirements specification for the E/E/PE safety-related systems can be determined in a systematic, risk-based manner [520]." Central to this standard are the concepts of risk and safety function. IEC61508 proceeds from the following views about risks: Zero risk can never be reached. Safety must be considered from the beginning. Unacceptable risks must be reduced, in keeping with the ALARA (as low as reasonably achievable) principle. The IEC61508 standard covers the complete safety life-cycle, which is separated into 16 phases divided into three main parts: analysis (phases 1-5), realisation (phases 6-13) and operation (phases 14-16).

Safety and reliability can be approached by performing a probabilistic risk assessment, in which component reliability (in terms of component failure rate), and event probability are used in quantitative safety assessment methods. Probabilistic statistical methods allow the determination of the mean time between failure (MTBF), system availability, and probability of mission success or failure. However, a reliability analysis provides a broader overview than the safety analysis, adding consideration of non-critical failures as well as of the acceptability of higher failure rates for non-critical systems. ESS will perform a series of studies to address MPS's reliability. Each study will focus on a specific MPS subsystem, using a variety of modelling approaches. The performance and reliability of MPS will depend on all of its components. The reliability assessments will yield quantitative estimates of the probability of a missed emergency shutdown that is detrimental to machine safety; the probability of a false trigger of an emergency shutdown that interferes with beam availability; and the contributions of MPS components to increasing or reducing the probabilities of each of these two scenarios.

Safety cannot be achieved through component reliability alone. If a system failure would be catastrophic, the failure rate must be made vanishingly low. One way to achieve such extremely low failure probabilities is to apply redundancy, based on the multiplication rule for independent events. However, adding equipment can be impractical or costly. Often, a less expensive way to achieve the same result is to design the system for "inherent fail-safety," that is, to design the system in such a way that its failure modes are not catastrophic. The typical design approach for safety-critical systems is to build the system so that single failures trip mechanisms to initiate a safe shutdown. If the system itself contains a source of hazard, it should be possible to remove this hazard from the system so that its failure modes are no longer catastrophic. Systems, however, can never be made 100% fail safe if they are required to be almost continuously available. Redundancy, fault tolerance, recovery procedures, and self-monitoring are the available design tools to deal with these situations. MPS is such system, and it is dependent on reliable input signals from the related subsystems.

The safety integrity level (SIL), as defined within the IEC61508 standard, is realised through improved system reliability and safety, but also through management, systematic techniques, verification and validation. Software written in accordance with IEC61508 may need to be unit tested, depending on the required SIL level. Table 5.3 shows the IEC61508 standard's acceptable probabilities of failure on demand (PFD) for systems whose services are demanded infrequently, and probabilities of failure per hour (PFH) for continuous operation systems for different safety integrity levels.

Safety integrity level (SIL)	**Probability of failure on demand (PFD)**	**Probability of failure per hour (PFH)**
1	$10^{-1} - 10^{-2}$	$10^{-5} - 10^{-6}$
2	$10^{-2} - 10^{-3}$	$10^{-6} - 10^{-7}$
3	$10^{-3} - 10^{-4}$	$10^{-7} - 10^{-8}$
4	$10^{-4} - 10^{-5}$	$10^{-8} - 10^{-9}$

Table 5.3: Safety integrity levels and permissible probabilities of failure according to the IEC61508 standard.

The MPS design approach using the IEC61508 life-cycle model

"Analysis" is the first part of the IEC61508 life-cycle model. It consists of five phases.

In the first phase of analysis, the concept of the system is defined. Conceptually, the role of MPS is to ensure maximum machine availability. Shutdown might be a failsafe mode, but so might be an auto-diagnose and recovery action, which would avoid machine downtime. In the conceptual phase, failure modes, functions, effects of functions, and their related risk levels for all MPS subsystems must be determined. Compensating measures must be defined and automated. Operators must be alerted, since catastrophic events sometimes happen due to operator misunderstanding. Special focus must be given to the measures required to achieve the machine's mission with respect to beam availability and quality; to identifying the impact on that mission of specific machine functions; and to delegating responsibility for mitigating adverse impacts on that mission. The functional requirements for all the equipment must be established, especially for self-testing functionalities and diagnostics; for cross comparisons of available information and diagnostics; and for implementing self-healing systems or automated early fault detection methods. If an MPS intervention is required, the recovery of the machine must be automated. MPS actions and other controls must be coordinated so that the recovery time is as short as practicable.

In the second phase of analysis, the overall scope of the system is defined. While MPS is a vital part of the ESS project, it will be a supporting system, rather than an intervening one. Its role is to optimise integrated machine performance, that is, to simultaneously enhance safety and machine availability.

The third phase of analysis consists of hazard and risk assessment. The goals of this analysis are both to identify risks and to specify design safety features and procedures to strategically mitigate risks. Hazard and risk analysis techniques include both qualitative and quantitative methods. Qualitative methods answer the question, "What must go wrong to create a system hazard?" while quantitative methods provide estimates of probabilities; rates; and the severity of consequences, accidents and failures. Both approaches will be used to analyse MPS hazards and risks. MPS must protect the machine's equipment against damage, and this requires the identification of risks to the machine, to MPS itself, and to related MPS subsystems. At this point in time, a hazard analysis has been completed for the target station, which focused on radiological risks. The hazard analysis for the accelerator is ongoing, and focuses on identifying events leading to critical beam losses and equipment damage. Within such an analysis, it is also possible to evaluate the required SIL for MPS. This will be based on the number of missions planned per year, the number of years during which missions will be carried out, the SIL of the target system and target safety system, dependencies between the target safety system and MPS, total equipment cost and equipment cost of subsystems and their devices, and damage risk for the project and equipment concerned. A conventional facilities risk and hazard analysis has already been carried out. A neutron instruments analysis will be initiated in spring, 2013.

The fourth phase of analysis involves the determination of overall safety requirements. The results from the hazard and risk analyses will be used to derive high-level requirements for MPS in accordance with the evaluated SIL. For example, one of the top-events identified by the hazard analysis for the target station and the A2T transport line is failure of the first bending magnet, leading to possible contamination in the tunnel area and radiation in the high bay area, and/or to a damaged beampipe. Several safety barriers have been identified to mitigate these risks, such as the installation of radiation monitors connected to MPS which can request MPS to shutdown the beam or close safety vacuum valves. In order to derive top-level requirements from this event, it is necessary to estimate how much time can elapse before the magnet fails and the proton beam melts the beampipe. Several scenarios related to this type of event have to be considered (e.g. different beam sizes, energies, or angles at which the beam hits the beampipe). A preliminary estimate of the time needed for a typical ESS proton beam (with a size of 1–4 mm) to melt the copper or steel of accelerator equipment is on the order of a few μs in the warm linac and 40 μs in the cold linac [501].

The fifth and final phase of analysis involves the allocation of safety requirements. Merging the top-level requirements with the information on ESS operational modes allows the identification of all safety functions for MPS as well as the allocation of these safety functions within the MPS framework (i.e. within MPS-related systems and subsystems). A first draft of ESS operational modes for the machine is provided in an ESS technical report [516]. There will be normal operational modes (such as neutron production at full power) but also machine test modes, allowing for the step-by-step commissioning of the machine. Currently it is expected that the beam permit system (BPS), which will form part of MPS, will be responsible for loading and setting these modes, as well as for verifying the correctness of configuration

settings. Procedures for changing between different operational modes are in the process of being defined.

MPS architecture

An initial proposal for the MPS architecture has been derived from the MPS high-level requirements. Figure 5.6 offers a simplified overview of this design: MPS input devices (MIDs) provide information about beam and machine health by surveying equipment and beam parameters and reporting on beam quality. The machine interlock system (MIS) combines the signals from all MIDs and communicates with MPS output devices (MODs), which have the power to trigger a shutdown of the proton beam. The beam permit system assures that the facility is configured and secured appropriately and that all relevant equipment is operating within the desired set point ranges for the (operational) mode selected by the operators. The post mortem system (PMS) enables ESS to analyse the origins of machine shutdowns.

MPS input devices (MIDs)

The information or measurement collected by an MID will be compared to pre-defined set-point values representing nominal machine operation (so called thresholds), but MIDs will interface the machine interlock system via binary signals, reporting, "OK," or "NOK." The comparison of measurements to setpoints will be carried out on the MID level (for example, within the BLM system). A detected value below the threshold will result in an OK signal to MIS. A measured value above or equal to the threshold will result in an NOK signal to the interlock system, which, in turn, will initiate a mitigation action (i.e. an emergency shutdown of the proton beam, such as an inhibition of the next pulse or a fast abort of the beam). Signals will be transmitted via hard-wired links.

The procedures assuring safe and efficient threshold management for all MIDs must be defined early within the MPS design process as it is crucial not only to detect critical conditions but also to compare the measured values to the correct thresholds. These procedures, as well as the MID threshold settings themselves, are owned by MPS. A special MPS committee will be responsible for threshold management and will define the procedures and interfaces to be used to safely set and modify any MID threshold.

To limit the number of false triggers of an emergency shutdown, the number of MID channels on the level of the interlock system that may provoke an emergency shutdown will be minimised. However, if the required level of reliability cannot be achieved otherwise, redundancy and majority voting strategies will be implemented. A summary of currently-identified MIDs is given in Table 5.4, which also lists separately the MID signals generated by beam instrumentation and by the magnet powering system. The most important diagnostic devices from beam instrumentation, which detect beam losses, will be BLMs and BCMs. BLMs can detect critically high beam losses within a few μs, however they are only sensitive to protons with an energy greater than 50 MeV [522]. BCMs are the beam diagnostics devices which will be used for the detection of beam losses for proton energies less than 50 MeV with a response time of 1 μs to 2 μs. A detailed discussion of beam loss instrumentation can be found in Section 4.9.

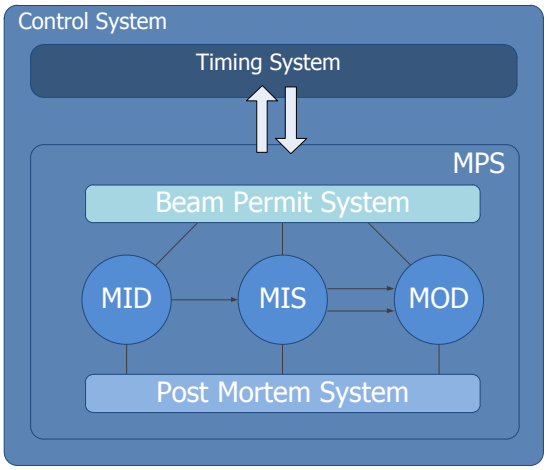

Figure 5.6: Simplified machine protection system architecture.

MPS input device name	Number of devices	Max. number of interlock signals	Fast beam abort	Next pulse inhibit
Timing system	1	1	x	
Beam instrumentation	468	468	x	x
RF modulators	110	110	x	x
Magnet powering system	257	257	x	x
Cryoplant, distribution system	5	5	x	
Vacuum system	10	10	x	
Target station	70	70	x	
Neutron instruments	22	1 aggregated	x	
Control room	1	1	x	
Beam permit system	1	1		
Personnel protection system	1	1 aggregated	x	
Ion source	1	2	x	
LEBT chopper	1	2	x	
Collimation system	12	12	x	
Sub-total	960	941		
Beam instrumentation				
Beam loss monitors	205	205	x	x
Beam current monitors	19	19	x	x
Beam position monitors	142	142	x	x
Wire scanner	28	28	x	
Faraday cup	8	8	x	
Grids	6	6	x	
Slits	2	2	x	
Non-invasive profile monitors	22	22	x	
Imaging devices	3	3	x	
Halo monitor	21	21	x	
Bunch shape monitors	12	12	x	
Sub-total	468	468		
Magnet powering system				
Magnet power supplies	235	235	x	x
MEBT magnet power supplies	20	20	x	x
LEBT magnet power supplies	2	2	x	x
Sub-total	257	257		

Table 5.4: Machine protection system input devices and their signals to the machine interlock system. (Additional input devices may be added.) Mitigation measures include a "next pulse inhibit", enhanced in some cases by a "fast beam abort."

MPS output devices (MODs)

MPS output devices (MODs) are devices which receive a signal from the machine interlock system. There are two different types of signals which can be sent to MODs. The first type of signals are those requesting an action, such as initiating an emergency shutdown of the proton beam or a post mortem event. Examples include switching off the proton beam by switching off the ion source or switching on the LEBT chopper. The post mortem signal will be triggered by the machine interlock system, but propagated to the different devices via the timing system. The second type of signals are informative signals, for example, signals conveying the information that a mitigation action is taking place. MIS status information will be sent to the control room, the target station, the neutron instruments, and also to the beam permit system.

Mitigation devices receiving an emergency shutdown trigger from the MIS will be designed to be fail-safe and reliable. Redundant mitigation devices will be required for switching off the proton beam (e.g. the ion source and the LEBT chopper will be used as redundant devices for certain mitigation techniques).

At the time of writing, two different mitigation techniques have been identified, although they have not yet been validated: the "fast beam abort" (FBA), and the "next pulse inhibit" (NPI). The FBA requires an immediate shutdown of the machine, that is, switching off the ion source and removing the current pulse from the machine. The NPI allows the current pulse to pass to its foreseen destination. An NPI does not shutdown the machine; but it inhibits the extraction of the following n pulses from the source unless the machine has returned to nominal conditions.

The time needed to switch off the ion source is a few tens of a microsecond (30-100 μs), while the LEBT chopper is able to switch off the beam in less than 1 μs. When the MIS receives a mitigation request, it triggers both devices simultaneously, assuring the required redundancy. Other mitigation devices are under evaluation, such as the MEBT chopper. The mitigation devices must provide an additional output signal, informing the machine interlock system that the mitigation action has been successfully completed. If the MIS does not receive this signal, it will trigger a request to switch off the power of the ion source. A mitigation device will also provide its internal overall status to the machine interlock system (OK/NOK), and if the mitigation device detects an internal failure (status signal goes to NOK), MIS will trigger other available mitigation devices to execute an emergency shutdown, as it is not safe to operate the machine with faulty mitigation devices. The communication between MIS and mitigation devices will be implemented via hard-wired links.

Machine interlock system (MIS)

MID signals can be maskable or not depending on the operational mode, which is controlled by the beam permit system. MIS will combine the OK/NOK signals from all MIDs, including masked signals, and will be able to distinguish between masked and unmasked incoming signals. If any MID sends an unmasked NOK signal, the interlock system will communicate with the relevant mitigation devices, which will then complete the necessary mitigation action. MIS will trigger no action when it receives either masked NOK signals or OK signals from the MIDs. The MIS is mainly hardware-based with its own network. The system will be composed of several MIS devices to shorten the connections between MIDs and MODs distributed along the accelerator. Each MIS device will have several inputs to connect several MIDs.

A distributed system requires a fast and reliable network to provide for signal propagation and to exchange important interlock information among the different devices. Optical fibres will be used for this purpose. Depending on the topology, such as daisy chain, star, tree or ring topology, each or some devices will have several outputs in order to connect to the different MODs. The system topology has not yet been defined. The selection will be determined in part on response time, scalability, the number of interlock system devices, signal path redundancy, and the total length of fibres. Table 5.5 describes the advantages and disadvantages of alternative MIS topologies.

The machine interlock system must offer two types of interlock service: local interlock service, in which a single device provides the service, meaning that the MID that detects a fault and the MODs are wired

Criterion	**Star**	**Tree**	**Daisy-chain**
Response time	Minimum	Increased by delay of switch(es)	Depends on the number of hops
Scalability	Limited due to the maximum number of network interfaces in a single device	Scalable with additional level of tree-branches	Limited due to maximum number of hops, due to signal propagation delay
Number of interlock system devices	2 (master and nodes)	3 (master, switches and nodes)	2 (master and nodes)
Signal path redundancy	Requires duplication of all paths and the master	Requires duplication of all paths of the leaves	Requires only one return path from the last node to the master
Total length of fibres	Highest	In between	Lowest

Table 5.5: Advantages and disadvantages of alternative machine interlock system topologies.

Interfaces	Master	Node	Switch
Several output interfaces to connect to MPS output devices	Yes	Optional	No
Several input interfaces to connect to MPS input devices	Optional	Yes	No
Machine interlock system network interface(s)	Yes	Yes	Yes
Interlock logic to correctly react upon a received NOK signal	Yes	Yes	No
Internal memory for post-mortem logs	Yes	Yes	Optional
Interface to timing system to synchronise time and clock	Yes	Yes	Optional
Interface to control system to obtain configuration/logic and to provide post-mortem logs	Yes	Yes	Optional

Table 5.6: Interfaces required for master, switch and node devices in the machine interlock system.

to the same device; and global interlock service, in which at least two geographically separated devices provide the service. For each single incoming emergency request, only one single mitigation action (or two in cases requiring redundancy) will be requested within a pre-defined time interval (probably a few μs); this requirement addresses the need to cope with multiple and/or concurrently occurring emergency shutdown requests, that is, with multiple requests received by the Machine Interlock System within nanoseconds of each other. Depending on the chosen topology, at most three different types of MIS devices will be needed: master, switch and node devices. The needed interfaces for the three device types are summarised in Table 5.6.

The master and node devices must have at least one network interface when no signal path redundancy is required; otherwise, they must have at least two. Additionally, the master and node devices must have an interface to the timing system, which provides synchronisation data to the local time and clock. The master also uses the timing system to dispatch a signal indicating that a mitigation action is taking place to all devices providing data to the post mortem system. If these devices receive the signal from the timing system, they will freeze their circular buffers, needed for post mortem analysis. The master and the node must provide a bidirectional interface to the service and data tier of ICS to receive configuration information and to send information on the device status as well as its logs for the post mortem analysis.

Beam permit system (BPS)

The beam permit system (BPS) is the part of MPS that will assure that the facility is configured and secured appropriately, and that all relevant equipment is operating within the desired set point ranges for the operational mode selected by the operators. There are several alternative implementations possible for such a system, and the final choice is currently under evaluation. One possibility would be a BPS based on PLCs. The PLCs would read the analogue values from the MIDs (such as voltage and/or current of power supplies for the magnets) and compare these values to the pre-defined thresholds for the specific operational mode loaded by the operators. If the validation fails, the beam permit would be revoked and an emergency shutdown request would be sent to the machine interlock system. Another possibility would be a system based mainly on software. This system would validate the correct status of all MIDs, MODs and MIS devices depending on the loaded configuration settings for a certain operational mode. If the validation is finished without any irregularity detected, the BPS would issue a beam permit signal to the machine interlock system, and perhaps to some other systems as well. Only after the beam permit signal had been issued would the machine be allowed to start, and to load the settings required for the operational mode. Every time the machine is stopped, the BPS would revoke the beam permit signal and the device validation would need to be repeated in order to load the next requested operational mode.

Post mortem system (PMS)

The MPS will provide support for a post mortem system to analyse data from many different MPS devices in order to establish the origin of a mitigation request and to assist operation. All devices providing post mortem data will be required to use a standardised data format and standardised data acquisition processes. The post mortem analysis must verify that all MPS devices and MPS subsystems have operated as expected. Within such an analysis, it must be assured that the real origin of the failure leading to a machine shutdown has been tracked down and correctly identified. It has not yet been decided whether

an operator's approval of the post mortem analysis results will be required before restarting machine operation, or whether automated processes will be implemented. In either case, the post mortem analysis will support operators in the main control room as they decide whether the machine is in a safe state to proceed or not. The post mortem service is described in Section 5.2.7.

In order to determine which MPS subsystem(s) first caused the machine to shutdown, all MPS subsystems and devices will be synchronised with the timing system. The required level of precision is currently under evaluation. The machine interlock system will time stamp and monitor incoming signals from all MIDs and MODs and will log signal changes on input interfaces so that it will possible to establish which device(s) reported NOK status first. The interlock system will log output signals as well, in order to have evidence about which mitigation device is triggered first. Every individual MIS device will log its own input and output interfaces. Maskable signals will be logged as well, as they may provide vital information for the post mortem analysis. The results of this type of analysis will also be useful for device performance optimisation. To determine the reason why an MPS device or MPS sub-system reported NOK status, the MPS device must also log its internal status signals and other important parameters.

It is important to separate the safety-critical transfer of post mortem data from normal machine data transfer. The need for a dedicated network is under investigation. The decision will depend on an evaluation of the amount of data liable to be transferred and of how long it is likely to take to finalise post mortem analysis, given that delays in analysis results have the potential to adversely affect machine availability.

Timing system

The timing system provides important input to MPS, enabling all devices involved in machine protection to synchronise their local device time. When applicable, the timing system will provide information about the operational mode to MPS systems, including the machine interlock system, beam permit system, MIDs and MODs. When an emergency shutdown is triggered, the timing system will propagate this information to MIDs and MODs and inform them to preserve their circular log buffers. More information about MPS's interface with the timing system can be found in Section 5.2.6.

MPS response time

The MPS response time is defined as the time needed for the following events to occur: Detection of a failure or a critically high beam loss by one or more MIDs, generation of an NOK signal, propagation of this NOK signal from the MIDs to the machine interlock system, MIS initiation of a mitigation action, and MOD completion of the mitigation action (i.e. emergency shutdown). As mentioned earlier, steel or copper accelerator equipment will begin to melt after a few μs of exposure to the full proton beam for the warm LINAC and after about 40 μs for the cold LINAC. These numbers imply that the MPS response time must be no greater than a few μs in the warm LINAC. Simulations to more precisely define required response times under various circumstances are currently underway.

MPS internal failures

The design function of MPS is to perform an emergency shutdown when non-nominal conditions are detected. Machine safety would be compromised by a non-nominal condition of MPS itself. A failure is an event leaving a component in a state that prevents it from fulfilling its function. Failures in MPS and its constituent components fall into two main categories, depending on their effect on system operation. The first category consists of failures to perform an emergency shutdown, when such a shutdown is desirable. Such failures are referred to as "blind" failures because they imply that incoming shutdown request signals have not been treated and/or transmitted correctly. The second category consists of shutdowns under nominal conditions. In these cases, MPS has acted upon a false failure report resulting from inherent active or passive failsafe measures which trigger an emergency shutdown request upon occurrence. For example, the interruption of an optical fibre within the machine interlock system network will automatically result in an emergency shutdown request. Such actions lead to unnecessary downtime.

Both types of failure affect machine availability, but only the first type compromises machine safety and creates the potential for damage to the machine's equipment. On the MPS component level, such blind failures prevent the correct treatment and transmission of an incoming emergency shutdown request. On the global system level, the concurrence of non-nominal conditions and undetected failures of an MPS

component can result in a missed emergency shutdown. MPS subsystems must allow for the correct detection of non-nominal and critical conditions.

Redundancy is defined as the existence of more technical means than necessary for the required function. Redundancy is one of the design principles that renders a system fault tolerant, that is, that enables a system to continue functioning despite a hardware or software failure.

The MPS will be designed to be failsafe, which means that it will request an emergency shutdown upon detecting an internal failure, thus passing the machine into a safe state. Additional self- monitoring features of the MPS are foreseen as well. Monitoring is an activity intended to observe the actual state of a component and is usually carried out during operation (i.e. in the operating state), in order to detect or anticipate failures. However, such fault failure signals and the related shutdown request compromise machine availability.

Warnings can also be viewed as a type of failure, and their analysis often yields valuable information. Unlike failures leading to false emergency shutdowns, warnings are not critical in and of themselves for MPS functionality, but they provide useful information for maintenance planning and early fault detection, thus making it possible to avoid more serious failures. Faulty components also can be detected by diagnostics and testing. The time needed to repair faulty MPS components may contribute to machine downtime, but it also may make it possible to avoid longer periods of downtime.

Diagnostics services provide mechanisms to detect possible device and network failures, and to avoid false failures leading to unnecessary downtime. These diagnostic mechanisms, together with a failsafe design approach, increase the reliability of the system. Three major types of MIS failures have been identified: 1. Network connection failure (e.g. broken fibre, no power); 2. failure of a device (e.g. no power, broken hardware); and 3. failure of an MID or MOD connection (e.g. broken channel, no power on channel, noise on channel, or broken fibre). For each of these types of failure, a diagnostic measure will be established to allow for early detection and to avoid MIS blindness. When a failure falling into these categories has been detected, a machine shutdown will be requested.

MPS and the timing system are embedded within the integrated control system. Health messages must pass constantly between MPS, the timing system, and other ICS subsystems. If any of the relevant subsystems stops issuing periodic health messages, the other systems will request a shutdown. Some device failures can be detected on the physical layer (e.g. if a neighbouring device detects a loss of signal). Heartbeat or hello packets can help diagnose other failures, like unresponsiveness of the device. Devices will constantly exchange internal health signals. If a particular device stops sending health signals, it will be treated as a failed device and all neighbouring devices will react and send a shutdown request. Any device with output interfaces will be designed so that if it stops driving the output, the output automatically goes to NOK state which then triggers the connected mitigation device(s). The MIS network will be realised with bidirectional fibre connections, where each fibre has an optical transmitter on one side and an optical receiver on the other. Three possible types of MIS network failures have been identified: 1. failure in the transmitter, which would be detected by a receiver as a loss of signal on the physical layer; 2. a broken fibre cable, which would also detected by a receiver as a loss of signal on the physical layer; and 3. failure in a receiver, which would be detected indirectly as a loss of health signal on the data layer. Measures will be implemented in the machine interlock system to monitor the signals indicating these three types of failures. Diagnostic measurement needs are under evaluation.

Applications for MPS status survey

The MPS will include applications offering a permanent survey of MPS functionality and machine status at the machine level, the section or segment level, and at the level of a single MIS device. The machine level view will include information about BPS status, MIS status, the status of machine segments, and the status of the timing system. The segment level view will divide the machine into smaller sections or segments, providing linking elements between the top-level machine view and the detailed device view. The machine segment view will include information about the status of the selected machine segment and the status of all machine interlock system devices in the segment. The MIS device-level view will include information about the status of the device, the status of all inputs (i.e. the status of MIDs), and the status of all outputs (i.e. the status of MODs). Status overview applications for the BPS and the post mortem system will be provided. Specific management tools for the modification of safety-critical configuration settings will be provided for the BPS, the machine interlock system and the post mortem system, as well.

5.2.3 Personnel protection system

The personnel protection system (PPS) will protect personnel against unnecessary exposure to hazards from the machine, including radioactivity and electromagnetic radiation, electrical shock, and other dangerous phenomena, such as faulty ventilation, helium release, or oxygen deficiency hazards. The PPS must support the operational flexibility required for different modes of operation and will, therefore, be sufficiently automated to minimise the need to rely on administrative procedures to protect personnel. The system will be operational 24 hours per day, 7 days per week and 365 days per year. The design process for the PPS includes several analysis and development phases. As a first step, the functional specification of PPS will be defined. Then a segmentation of the ESS machine based on several selection criteria, such as expected radiation levels, will be evaluated. Subsequently, a hazard and risk analysis will be performed in order to define PPS safety functions. Having defined these safety functions, it will be possible to derive technical specifications and complete the PPS design.

Design

The PPS has two main functions: Radiation safety and facility operation management. It therefore consists of two main parts: An access control system and a radiation monitoring and alarm system. The access control system must prevent unauthorised or accidental entry into radiation and/or operational areas. Elements of this system include physical barriers, personal key boxes, door control boxes, emergency stop buttons, cameras for monitoring, beam stoppers, signs, flashing lights, audible warnings, etc., and also a dedicated interlock system, and a set of administrative procedures defining conditions for safe entry into the machine. The radiation alarm system will include radiation sensors to monitor the radiation field directly, and indirect methods such as beam loss monitors.

The aim of the PPS is to protect personnel, rather than the machine. Therefore, this system will be independent and distinct from MPS and other ICS components, so that performance of PPS safety functions will be guaranteed even in the absence of a fully working control system. ESS has set the following PPS design goals:

1. Only registered and authorised personnel will be allowed to enter the ESS machine;
2. All PPS status information will be available to other ICS subsystems, including MPS;
3. A status display will provide all important PPS information independently of the rest of ICS;
4. PPS will be designed so that it is in a secure state in case of any error;
5. The PPS interlock system will provide for redundancy;
6. A radiation monitoring system will be an integral part of PPS;
7. All PPS components will exhibit high degrees of reliability;
8. PPS circuits will be failsafe; and
9. Duplicated circuits or redundant components will be implemented wherever the failure of a single circuit or device could lead to a hazard.

A highly reliable PPS is indispensable for radiation safety management for personnel entering or leaving radiation-controlled areas. To ensure this reliability, the Controls Group will evaluate the possibility of basing the PPS architecture on two tiers of programmable systems performing access control and safety interlocks. In addition, safety functions can be performed by redundant Programmable Logic Controllers (PLCs), which are certified for safety applications. It may be necessary for independent engineers to program the PLCs, providing a certain level of diversity and defence against coding errors. In order to centralise information about the status of PPS equipment, all signal paths will be hardwired from the equipment towards the interlock system.

Functionality

The PPS will manage the entrance to and exit from any given radiation-controlled area according to the classification of the given access mode using two separate PPS subsystems. A dedicated access safety system will guarantee the absence of beam in the zone, and, in some cases, the absence of other types of hazards (such as electrical hazards), as well. In addition, a dedicated access control system will manage access to primary beam zones. The main operating principle for both systems will be, "If there is beam, then there is no access; if there is access, then there is no beam."

Consider, as an example, access to hot areas during accelerator operation. During beam operation, the No Access mode will prohibit all access to the accelerator, target station and neutron instruments. If an access door is opened or a lock is released, PPS will immediately interrupt permission for beam operation. However, it will be possible to enter specific radiation hot areas during beam operation under strict PPS management, in order to support operational efficiency. As a second example, consider access to the target station and radiation monitoring. It will be possible to enter specific areas of the target station and perform repair or maintenance work even when the linac is operational. Radiological exposure during that work will be surveyed by PPS and will be safe for the personnel. A radiation monitoring system will check radiation levels continuously at several static points in the accelerator and in the target station.

5.2.4 Relationship of ICS and the target safety system

The target safety system (TSS) will be implemented and maintained separately from ICS and will comply with safety regulations for nuclear facilities. It is not in the scope of ICS to deal with safety-classified systems. The majority of the systems for the target will not be safety-classified. The current estimate is that it will be possible to control about 80% of target station control signals in the same manner as signals from the rest of the facility. The remaining 20% of signals originating from the target station will be safety-classified (under the jurisdiction of nuclear safety regulations) and will need to be controlled by TSS. TSS will be represented in ICS as another device. ICS will be informed of the status of TSS, and there will be read-back of some TSS signals in the main control system, but ICS will not control those signals. In general, the target station will send information about its status to ICS (that is, to MPS and PPS) so that the proton beam will be switched off in case of non-nominal or critical conditions. However, TSS also will be able to act independently, and, in particular, will be able to switch off the beam on its own when the criticality of an event makes such action appropriate. A series of target-related events requiring protection functions already has been defined, including events such as leaks of helium coolant; signals from the accelerator (beam profile); and external events such as loss of power supply, fire, or earthquake.

5.2.5 Timing and synchronisation

The primary clock source for ESS will be the master oscillator, which is in the domain of the Low-Level RF Group. The master oscillator will generate a 704 MHz primary RF frequency and its subharmonics to provide a very stable phase reference for client devices, such as RFQs, that require the highest level of synchronisation, with jitter at the femtosecond level. (Subharmonic frequencies are frequencies below the fundamental frequency of an oscillator in a ratio of $1/n$, where n is a positive integer [523].) The timing system will complement the master oscillator, offering services to client devices which have less strict jitter requirements, with jitter at the picosecond level. For these devices, distribution of services from the highly stable master oscillator clock would not be cost-effective. These devices might also need more complicated synchronisation procedures than the clock distribution service of the master oscillator alone can provide. Figure 5.7 shows a very broad overview of the timing system. A brief description of its main components is given below.

RF master oscillator and timing system

The timing system will be very closely coupled with the master oscillator, deriving its lower-performance clock from the RF clock. The short-term stability of the RF clock will be regulated by the master oscillator, which will align to the global positioning system (GPS) reference only on a very long time scale. Since the timing system must always be aligned with the RF clock, its notion of absolute time, which it will distribute to client devices, will also derive from the master oscillator, rather than directly from the GPS

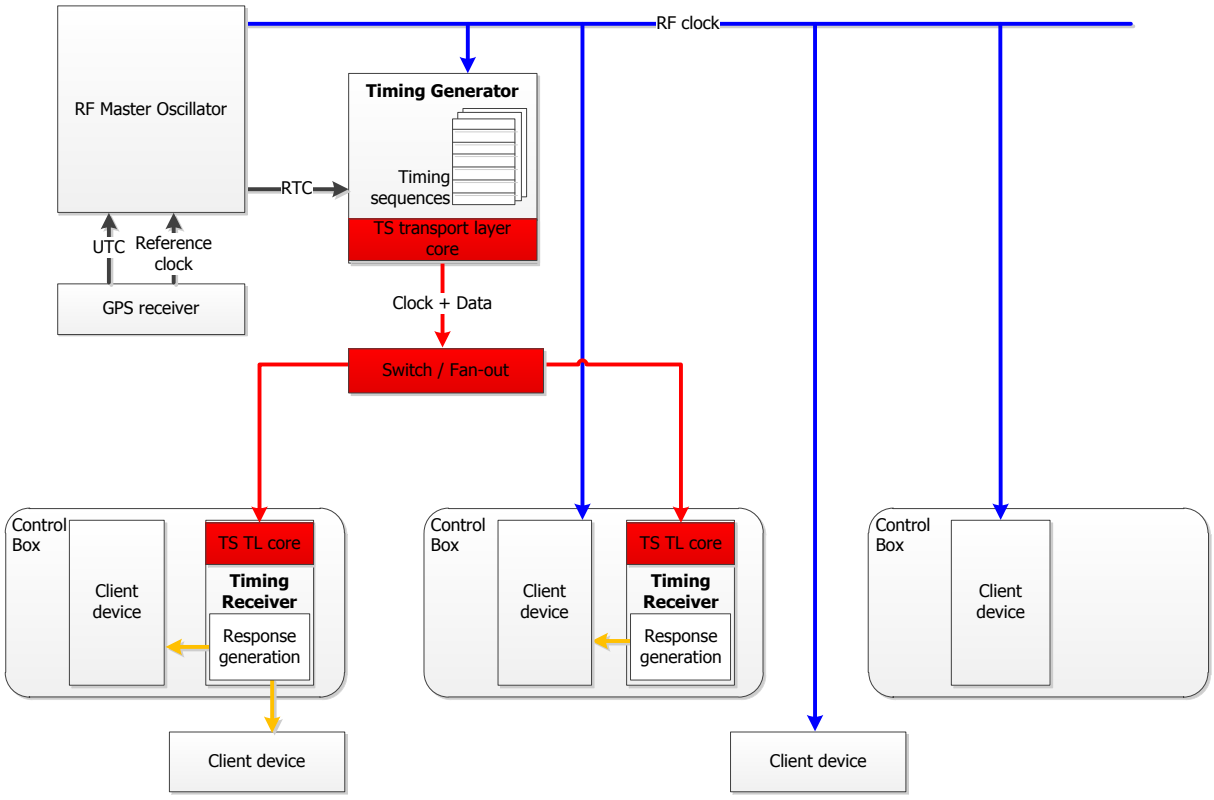

Figure 5.7: Timing system overview. The abbreviations TS and TL refer to the timing system and the transport layer, respectively.

receiver. This means that the timing system may be detuned with respect to the GPS reference on a short-term basis, but will not drift away from it over a longer time scale.

Clock correlations

A single master oscillator will generate the phase reference of the RF parts and the master clock for the timing system. Thus, a common time base and phase will be established between the different systems. A 1 Hz signal will be generated without any approximation, so the choice of the timing frequency will have no influence on the accuracy of the real time clock. Four periods of the bunch frequency of 352.21 MHz will be used as the fundamental clock period, in order to get a reasonable frequency for the field programmable gate array (FPGA) logic of the timing system hardware. An integer number of ticks of this clock will define the full length of the beam macropulse, and the exact beam macropulse repetition rate, which will be slightly different from the nominal value of 14 Hz, as shown in Table 5.7.

Parameter	Unit	Value
Bunch frequency	MHz	352.21
Bunches per event clock period		4
Event clock frequency, f_{event}	MHz	88.0525
Event clock period, T_{event}	ns	11.356861
Event clock ticks per macropulse start		6289464
Beam macropulse repetition rate	Hz	14.000000636
Event clock ticks per macropulse length		251830
Beam macropulse full length	ms	2.859998

Table 5.7: Primary timing system parameters.

Transport layer

The timing system will be responsible for the distribution to client devices of absolute time and the clock that is coupled with the RF master oscillator. To achieve this distribution, a deterministic and high-performance clock and real-time data distribution network is required. This network is the timing system transport layer. Several transport layer solutions of various levels of maturity and performance already exist. For example, there are solutions available from Micro-Research Finland [524] and White Rabbit (IEEE 1588). The transport layer solution must be able to achieve device synchronisation at the 1 ns level or better. The availability and maturity of alternative approaches will also influence ESS's choice. A bi-directional transport layer has been ruled out at the present time.

Timing generator

Figure 5.8 shows the high-level design of the timing generator. The timing generator will serve a number of purposes. It will lock to the 88.0525 MHz master oscillator clock and distribute the clock to timing receivers over the timing system transport layer with low jitter. It will deterministically execute timing event sequences. It will acquire real time clock data from the master oscillator and distribute this data to

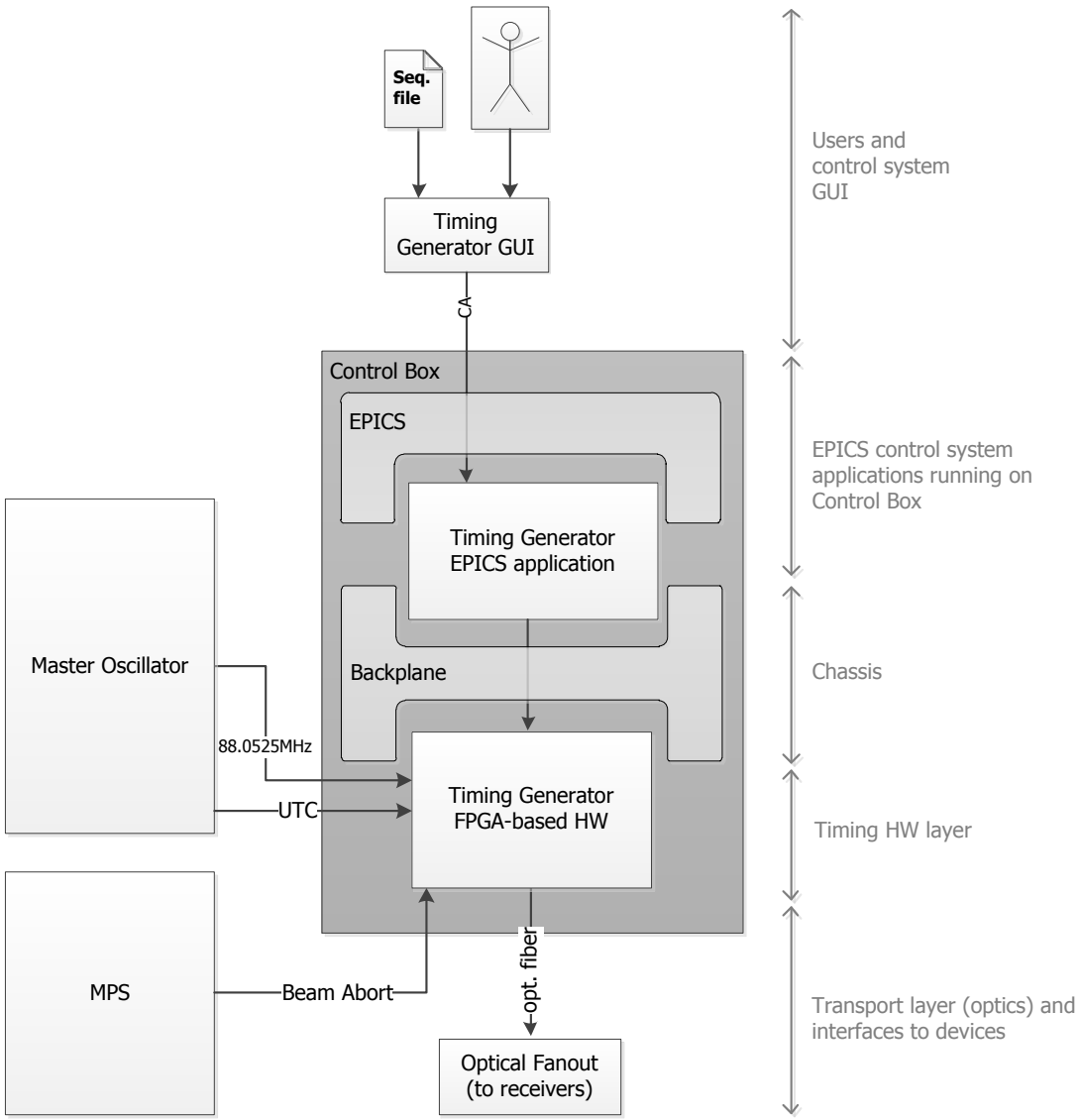

Figure 5.8: Timing generator overview.

timing receivers over the transport layer. And it will condition the execution of event sequences with MPS beam-abort input and distribute beam-abort information to timing receivers, as is shown in Figure 5.9. Procedures for locking to the master oscillator reference clock and distributing this clock at the event clock frequency, f_{event}, to timing receivers with acceptable jitter performance mainly depend on the choice of the timing system transport layer.

Because client devices need to be synchronised with sub-nanosecond precision, the event sequences need to be handled entirely in the timing generator's FPGA-based hardware operating at the f_{event} frequency. The timing generator's EPICS IOC will provide mechanisms for the control system to load a specific timing sequence into the timing system hardware and request and monitor its execution. The start of event sequence execution will always be aligned with the 14 Hz pulse repetition rate in the timing system hardware. Emission times of all events in the event sequence will be defined relative to the start of the pulse. The timing generator must be able to dynamically change event sequences to support beam ramp-

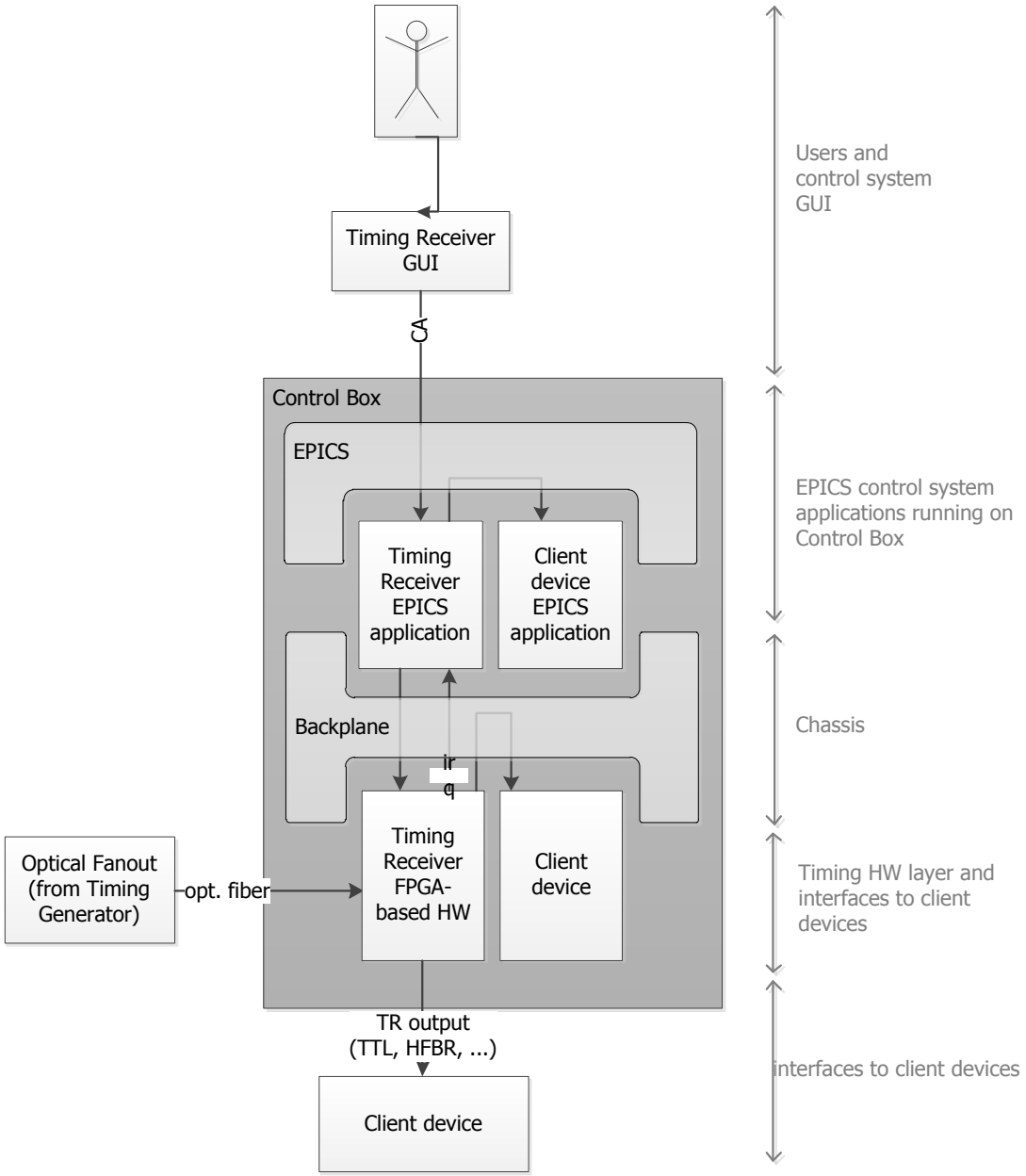

Figure 5.9: Timing receiver overview.

up. The ramp-up rate must be controlled deterministically. The event sequences will be executed at a 14 Hz rate, which will allow enough time for the timing generator software to load the next sequence into the timing generator FPGA while a given sequence is being executed, thus maintaining control over beam ramp-up. To facilitate this mechanism, the timing generator FPGA must be able to internally store two event sequences – one currently being executed and one being programmed by the timing generator software, which will be executed at the start of the next pulse.

Timing receivers

Figure 5.9 shows the high-level design of the timing receivers. The timing receivers also will serve a number of purposes. They will lock to the clock distributed by the timing generator over the timing system transport layer and offer this clock as a service to client devices on an outbound interface. By phase locking to this clock, client devices will be able to synchronise to the timing receiver, to the timing generator and, consequently, to the master oscillator. They will receive data about events from the timing generator over the transport layer. They will generate configurable responses to received events, such as triggers. And they will receive real time clock data from the timing generator for event logging and client device time reference. The timing receiver's EPICS IOC application will provide mechanisms for the control system to configure event responses and other timing receiver services, and to monitor the behaviour of the timing receivers. It also will provide a way for client device applications to interface with the timing receiver on a software level.

There are many factors that influence the phase alignment of clock and responses between two timing receivers, including the granularity of the propagation delay compensation mechanism, temperature changes in the fibre cable, and event clock jitter. Different cable lengths between the timing generator and timing receivers introduce different event propagation delays. A mechanism to compensate for propagation delays will have to be implemented within the timing receiver. This will enable all timing receivers to be completely synchronous in trigger responses, time service and other deterministic services.

For commissioning and testing purposes, timing receivers must be able to function autonomously, without receiving clock and data from the timing generator, and without being connected to the timing system network. Timing system architecture will include a stand-alone mode of operation to satisfy this need. In this mode, the event clock will be generated internally within the timing receiver and the timing receiver will be able to play hypothetical event sequences. For this purpose, the timing receiver will be able to host timing generator logic on both the firmware and software levels.

Control system integration

All timing system components, namely the timing generator and timing receivers, will be hosted by a control box and will be integrated into ICS via EPICS. The EPICS interface will enable control system users to configure timing sequences and responses to events; start and stop execution of event sequences; and monitor the behaviour of timing system components. Since ESS will have a huge number of timing system components across the whole machine and these components will be FPGA-based, the control boxes will support remote firmware update.

Prototyping

An important early step in the development of the timing system was a 2012 prototype that demonstrated its basic concepts. The first timing system prototype was based on a cPCI PlusIO hardware platform with Micro-Research Finland cPCI timing hardware as the transport layer. The choice was consistent with decisions concerning the 2012 control box prototype, discussed in Section 5.3.2, and also took into account the availability of alternative timing system transport layers that fit ESS requirements. On top of the transport layer, some of the timing services were implemented and demonstrated as a proof-of-concept, rather than as a final implementation. Figure 5.10 shows some of the equipment used in the 2012 timing system prototype. Implementation of timing system services will be decoupled from the timing system transport layer technology as much as possible to preserve the option to change the generic COTS (commercial off the shelf) transport layer in the future without losing timing system services that have been customised to meet ESS requirements. In parallel with a highly mature hardware platform such as cPCI, ESS will probably also use a high performance hardware platform. The Controls Group will develop a prototype based on the μTCA.4 platform in 2014.

Figure 5.10: Timing system prototype (2012). Left: A computer monitor showing the GUI for the timing receiver EPICS application, Middle: Control box (2012 version) including a timing receiver, a timing generator and a switch box simulating the MPS system (on the top of the control box). Right: An oscilloscope showing the output of a timing receiver.

5.2.6 Timing system services

The main purpose of the timing system is to precisely synchronise devices across the whole machine. To achieve this, the timing system will offer a variety of services, such as clock distribution, real-time control system data distribution and different triggering mechanisms. Using these services, the timing system must be able to precisely dictate the 2.86 ms long beam pulse with a 14 Hz repetition frequency to a vast number of front-end devices. The various timing system services are discussed in turn below.

14 Hz pulse generation

The 14 Hz beam pulse will be the end result of several devices which are clients to the timing system working in sync. From the timing system perspective, the 14 Hz pulse generation does not necessarily require the actual generation of the physical pulse, but rather involves the generation of a series of predefined events (real-time data packets) and triggers to its client devices. The events and triggers will be synchronised across the whole facility with the required precision.

Event clock

The timing receivers will offer the event clock as a configurable option on outbound interfaces. The timing receiver event clock will be phase aligned to the timing generator and master oscillator.

Event responses

There will be several types of events and triggers at different positions relative to the 14 Hz pulse, for example, at start-of-pulse, end-of-pulse, and pre-trigger (all events yet to be determined), so the timing system architecture will allow for configurable event sequences. The timing system architecture will include a configurable response mechanism to address different client device needs.

Time-stamp service

The timing system will distribute real time clock (RTC) data to client devices to enable precise time-stamping across the whole machine with a time-stamp jitter of better than 1 ns. Because of this jitter requirement, the timing system will implement a deterministic RTC data transmission and synchronisation

between the timing generator and timing receivers, which will be designed so that it does not interfere with event sequence execution and distribution. Since the timing receiver must be phase aligned to the timing generator event clock, the RTC in the timing receiver will never drift away in time from the RTC in the timing generator. Therefore, RTC synchronisation can in principle be done once and for all at timing system start-up. However, resynchronisation will be performed periodically for the sake of robustness. The event period, $T_{event} = 11.356861$ ns, is the smallest possible time-stamp resolution.

Each timing receiver will log received timing events with precise RTC time stamps. This data will be used for diagnostic purposes and for client device time synchronisation when the timing receiver triggers a client device upon receipt of a specific timing event. Alternatively, time-stamp functionality could also be offered to client device hardware directly over a backplane, using real-time data distribution. The time-stamp service will also provide mechanisms for precise time-stamping of data acquired by client devices (e.g. a sensor connected to a DAQ card). So far, two distinct data acquisition use-cases have been identified: 1. A DAQ device outputs one measurement per pulse (usually averaged), which needs to be time-stamped precisely enough to be able to correlate this measurement to a specific pulse, and 2. a DAQ device captures a waveform of data sample within a time frame of the pulse. The waveform will be time-stamped so that waveforms from different DAQ devices can be correlated with each other. In both use cases, the timing event trigger will be used to start data acquisition.

Integration with the machine protection system

Upon detection of faults by the machine protection system, the timing generator must immediately stop the execution of event sequences and, consequently, the generation of beam pulses. Thus, the timing system will be integrated with MPS. The deterministic nature of the event distribution and triggering mechanisms makes the timing system suitable for notifying client devices to lock their data buffers for post-mortem analysis.

Figure 5.11 shows the structure of interactions between MPS and and the timing system. Upon receiving a beam abort signal from an MID (1), the machine interlock system triggers the timing generator (2) to stop execution of the timing sequence (3) and to propagate a "lock buffers" event to all timing receivers (4), which then trigger all devices that implement post mortem data logging to lock the post-mortem data buffers (5). The timing system is also responsible for providing real time clock synchronisation service to all MIDs and MODs, and to all devices that have to provide post mortem logs, so that post mortem data can be merged into a single timeline. The timing system is a safety critical system whose incorrect behaviour would compromise machine safety; thus the timing system is itself an MID, and must provide a binary OK/NOK status signal to the machine interlock system. The timing system will be able to request a switch off the proton beam upon detecting that one or several of its own components have failed.

5.2.7 Control system services

Control system (CS) services refer to software libraries, servers, and standardised interfaces in the control system core in the middle tier of the control system, that provide common functionalities throughout the control system. Some of the required CS services are supplied in the EPICS core, but will require modification to serve ESS needs. For example, EPICS's ready-made data correlation and timing services are insufficient for ESS's needs, and modifications to them will also require modifications to EPICS archivers and logging tools, as described below. The remainder of this section itemises CS services for ESS as identified at the time of writing, and provides a description of the basic common functionality.

Control system permissions

ICS will have a permission system to limit the effects of accidental CS user actions that could otherwise disrupt facility operations. This permission system will establish authority over operational or maintenance access to each particular portion of ICS. Read access of ICS control points will not be constrained by the permission system inside the control network. The permission system will be fine-grained and hierarchical; this approach is well-supported by the underlying EPICS framework and is in use by operating facilities such as SNS and CEBAF. Control system users, and the processes that they run, will be assigned roles and profiles, and access will be controllable down to an EPICS channel-by-channel resolution. It will be possible to modify these roles and profiles over time, so, for example, an operations crew chief may permit

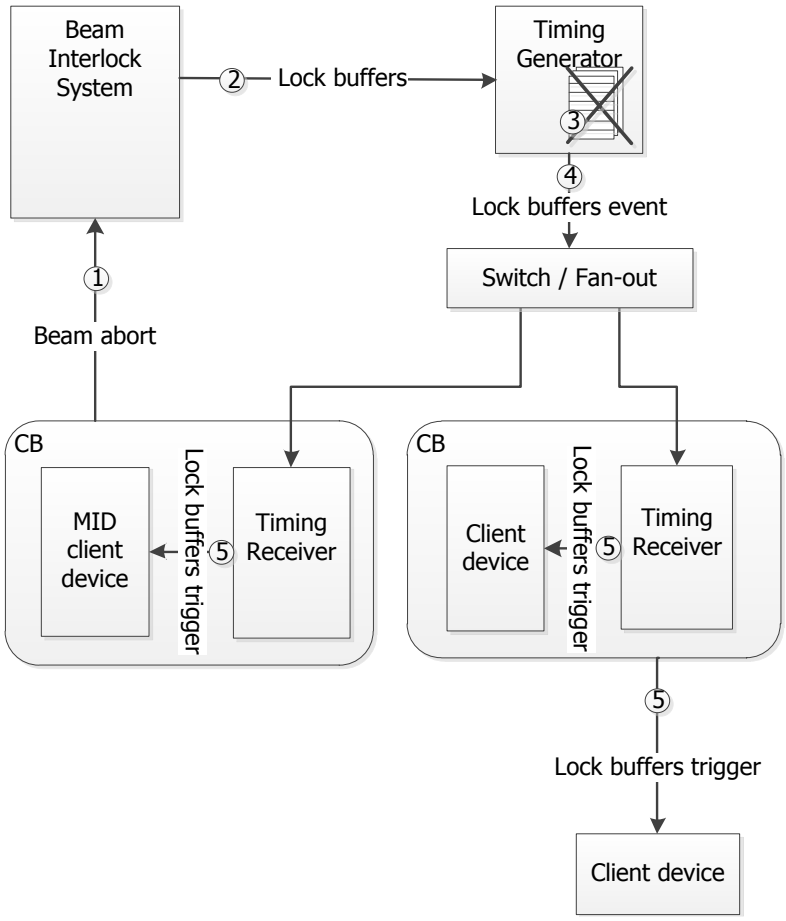

Figure 5.11: Interplay between the timing system and the machine protection system.

access to a specific subsystem to a remote diagnostics user for a specific period of time. Roles and profiles may also change dynamically with machine state. More information on user roles and profiles can be found in Section 5.6.1.

A higher-level permission policy will be in place to guide proper configuration of the ICS permission system and to establish the conditions under which ad hoc permissions may be granted. This policy will be implemented in an ICS permission management application that will be available to the main control room staff crew chief and other authorised personnel. This application will be designed to make it straightforward to control whether a particular user or process has permissions to access controls that affect beam delivery. EPICS also supports channel access gateways [525], which provide a means for many clients to access a process variable while making only one connection to the channel access server that owns the process variable. It also provides additional access security beyond that on the server. It thus protects critical channel access servers while providing access, possibly with restrictions, to needed process variables. These gateways are mostly used to "fan out" readings to multiple clients. If a gateway is deemed necessary for settings, its permission model must be consistent with the ICS permission model described above.

Archiving service and viewer

Archiving is a service dedicated to providing historical information about machine operations. This information is used to evaluate machine performance, diagnose problems and failures, and establish correlations between various settings and measurements for analysis. At ESS, the archiving service will provide a mechanism to store ICS settings, read-backs, and configuration to a permanent location. This service will usually be provided by one or more network archivers. The data archiving structure can be simple, as each record

will consist only of context information, identification of the property, and value of the property. ESS will develop a well-documented and thoroughly reviewed archiving philosophy to guide proper configuration of its archiving service, in recognition of the fact that the design of this application and the availability of archived data will strongly affect the efficiency of machine diagnostics. Archived data will be easily browsable from an archive viewer application that supports many modes of data visualisation, such as time plots (value vs. time), correlation plots (value vs. value), and waterfall plots (trace or other array vs. time or accelerator s-coordinate).

The core EPICS archive service [526] is quite old and is not recommended for use in new installations, so new large installations tend to build their own archive services. ESS will evaluate in detail archivers and archive viewers used at other facilities. For example, LogView at the Relativistic Heavy Ion Collider (RHIC) is a good design example of a logger server and viewer. SNS has developed a relational database archiver, RDB Channel Archiver, that uses data and configuration stored in a relational database. The most appropriate off-the-shelf archiving service and viewer appears to be the BEAUTY archiver that is part of the Control System Studio. ESS will evaluate this archiver to determine whether it suits ESS needs during the development and commissioning phases.

The archiving system and its viewer are intimately connected with the implementation of data correlation, since their primary purpose is to display correlated time plots of historical data with time precisions and accuracies down to the lowest levels of time granularity available in ICS. The archiving system provides two types of service – trending and the archiving service. Trending involves the archiving of process variables over time. Because it is not carried out for control purposes, trending is performed at a slower data rate than the live display of data. Trending data is stored permanently. The archiving service is provided to the user to configure restricted sets of data for special purposes.The archiving service stores historical values of properties in the control system and is connected to specific user demands for data collection. Archiving will be configured on a per-property basis, and may be done on-time (archiving of a value at a certain clock frequency), on-change (archiving of a value as soon as it changes by a configurable amount), or on-event (for example, generating an archive of ring buffer readings on an abort event).

The implementation of the archive viewer will naturally depend on the structure and storage of archive records. This viewer will support the display of historical data and the visual display of control point trends to establish slow correlations over timescales of days to years. This viewer will support efficient, abortable retrieval of data from the archiving service; retrieval of data for a set of properties and process variables; and the presentation of retrieved data as a table or as a chart showing value versus time or other accelerator context information (for example, value in consecutive cycles with the same cycle ID). It will be able to retrieve data within a bounded time interval at a bounded sample rate, or with a limited number of samples, and to filter retrieved data by other accelerator context information, such as by the cycle ID or timing event ID that has triggered a given value. Finally, it will have the ability to export data to common spreadsheet programs and data formats (e.g. CSV) for further manual analysis.

Logging service and viewer

Logging will provide developers and engineers with insight into the current behaviour of ICS components. As such, it will be a valuable diagnostic tool when the control system's functionality doesn't comply with set requirements, allowing developers and engineers to pinpoint and resolve problems. The scope of the logging service will be to record information over limited time intervals. As such it is to be distinguished from the archiving service, which will store historical information from the control system over the entire ESS life-cycle. Additionally, while the archiving system will mainly be concerned with collecting data about the machine and its operation, the logging service will include information on the running of the control system itself, such as software-generated log files. The logging service will collect time-stamped log entries from ICS in a time-frame that is as close to real time as is possible within bandwidth and storage constraints. It will store these entries in a central database to permit efficient queries. This database may be a text file, but other means to store log entries such as a relational database or large-scale databases such as Google BigTable or Spanner will be evaluated for applicability and scalability.

It will be possible to configure the logging system dynamically, without interfering with existing logging activity. This will allow the verbosity of logging to be increased when problems are under investigation, and to be reduced during normal operation so as to limit the amount of network traffic and data storage consumed by logging. Logged data will be easily browsable from a log viewer. It will be possible to filter logged data by the source from which the log entry originates, time-stamp range, verbosity level

and log data contents. It will also be possible to correlate logged data with other data sources, such as data from the archiving service. EPICS provides ready-made services for logging (the "iocLogServer" and "iocLogClient" components). Apart from acquiring EPICS logs, other log files generated by computer nodes (e.g., Linux log files) will also be centrally managed. Use of off-the-shelf services such as "syslog" and "syslog-ng" will be considered. Off-the-shelf viewers for logs also exist (e.g., "LogZilla" and "Apache Chainsaw") and commercial tools for analysing logs are available (e.g., "Splunk"). These tools will be evaluated for suitability to ESS requirements.

Post mortem service

ICS post mortem analysis software will have a modular structure and will use a multi-level analysis framework for the post mortem data. The purpose of this service is to provide an automated analysis, qualification, and categorisation of shutdown events. The modules will present each MPS subsystem that has a connection to the post mortem. They will be easily extensible, to accommodate lessons learnt from operational experience. The input for each module's analysis (i.e. pre-defined analysis procedures and rules governing the interpretation of results) will be provided by the experts responsible for the relevant subsystem. The ability to cross-correlate results from different subsystems will be very useful, and so the post mortem framework will allow users to easily implement and modify correlation functions between different modules while avoiding adverse impacts on overall analysis performance. The framework will provide all necessary infrastructure for the analysis modules and all post mortem logs, and will store results and comments for offline analysis. Such offline analysis will help identify specific categories of shutdown events or scenarios and may facilitate creation of an early fault detection system. The system will be able to execute specific MPS subsystem checks for verification purposes, as well.

Save, restore, and compare

During commissioning and operations, operators will need to create a named and time-stamped "save set" of machine setpoints. This save set will contain sufficient information to make it possible to recreate a given machine operational condition through EPICS settings. BLED will contain a database-driven tool to acquire, restore, and compare these save sets. The compare functionality is often overlooked, but it is an essential function of this system so users can easily see what changes have been made in machine, equipment or diagnostic settings between two save sets. The "Control System Studio" provides save/restore functionality within its "PV Table" view. ESS will evaluate the suitability of Control System Studio's compare functionality for its needs, and will design enhancements if required.

Alarms

Alarms are special types of messages that indicate conditions that require operator awareness, and possibly operator action. Their main purpose is to inform operators of unusual situations, and to enable them to understand the root causes of these situations before failures occur. The delivery of alarms must be guaranteed, which places requirements on network communication (e.g. they cannot be delivered with UDP), but they need not be delivered with real-time priority since their recipients will likely not respond to them in real-time. Alarms may range in criticality level from very low (an innocuous measurement slightly out of nominal range) to very high (possible imminent threat to facility personnel). ESS will establish and support standards for alarm generation by EPICS control system IOC or PV. Data structures for each alarm will include the alarm name generated from the associated PV, device name, system, supersystem, time-stamp, criticality level, and a description of the cause (e.g. the value of the PV that triggered the alarm). ESS will define a limited number of criticality levels which will be documented and reviewed, and which will depend on the potential impact of the underlying cause of the alarm on cost, operational uptime, equipment damage, and personnel safety in ascending order. ESS will survey current practice at several other facilities to guide it in defining criticality levels.

A central alarm server will be responsible for collecting all alarms, storing them in a dedicated database, and dispatching them to running alarm display programs. Operators will be able to efficiently package groups of seemingly correlated alarms together within the scope of a well-designed alarm display program. Alarms will be colour-coded by criticality level, and alarms above a certain criticality level will produce audible signals, as well. There will be two versions of alarm displays: one that is "read-only" and only displays active alarms, and one that is interactive. Alarm displays will also be developed to display a subset

of alarms that are only relevant for certain areas of the machine, such as the injector or instrument stations, for use in those areas. Alarm indications will latch – that is, they will remain on all alarm displays until their state is changed by a user interacting with them on any of the interactive alarm displays. Alarms on the alarm display and in the alarm system will fall into exactly one of a pre-defined number of mutually exclusive states. The precise set of states is still being defined, but is likely to resemble the following list:

1. New: Alarm has arrived but has had no operator interaction.
2. Seen: Operator indicates the alarm has been seen, and has assumed responsibility for follow-up.
3. Assigned: Operator has forwarded the alarm to another group for follow-up.
4. Deferred: Investigation is complete but immediate resolution is not possible (e.g. enclosure access required).
5. Resolved: The cause of the alarm has been resolved.

Changes to alarm states within the alarm display will be stored with the original alarm to evaluate response times and impact on operations, and to help establish maintenance and upgrade priorities. In the view of the EPICS user community, the most promising alarm server and viewer appears to be "BEAST," which is part of the "Control System Studio." ESS will evaluate this toolkit to determine whether it is applicable to ESS's situation and, if so, to determine how it should be adapted to meet the facility's particular needs.

Name services

EPICS was originally designed to avoid the need for a name service; all control point discovery is accomplished dynamically via UDP broadcast and response between channel access clients and servers. ICS will be too large and too complex for this approach to scale well under all anticipated conditions, for example, during simultaneous start of the system or its temporary outage and subsequent restoration. In addition, the control system's network will be segmented in several subnets for maintainability and scalability reasons, a circumstance in which the broadcast-based EPICS Channel Access discovery mechanism will be unable to function unassisted. ESS will resolve this problem by creating a central name service. This service will be similar to the Internet's DNS, but it will look up system control point names in order to locate the IP information of their IOCs.

The name service will follow documented standards for control point naming (PVs and IOCs); will provide the ability to assign user-readable aliases for control points; and will provide a documented interface for translation of a PV or IOC name or alias to a unique control point within the ICS. The record that is returned from a name lookup may also contain other information about the control point, but will not duplicate information that normally resides in the PV configuration itself. The channel access gateway concept may be extended to use data from BLED (as discussed in Section 5.4.3) to provide a mapping of PV name to its whereabouts in the control system. Several implementations of EPICS-friendly name services are presently under development. These include two versions of IRMIS (a relational database of installed IOCs) [527], and other solutions at SNS.

5.3 The control box

The construction of the ESS machine will be geographically and organisationally distributed among many laboratories. It is important that control system integration is implemented in a controlled way that enforces a high level of standardisation. For this reason, ESS has adopted a control box methodology based on the development philosophy established by SNS and further developed at ITER [528]. The control box is simply a server that controls a collection of equipment, for example a neutron instrument or a part of a subsystem. To make the complete control system, these servers need to be interfaced to the middleware so that they can communicate among themselves and with the HMI and ICS core services.

The main advantages of the control box approach are that it allows independent and yet standardised equipment controls development, and encourages and enforces consistency and integration of equipment and subsystems across the machine. The control box approach also facilitates new component testing (for example, of EPICS drivers), allows factory acceptance testing of equipment and subsystems throughout the

control system, and makes it easy to validate technology decisions. Control boxes provide a platform for early risk reduction, helping to prevent unexpected surprises at project integration time, and minimising the waste of time and resources on throw-away hardware and software development.

The control system will be partitioned into separate subsystems that are closed entities and can be assigned to one supplier, such as an internal team, a collaborating institute or a commercial vendor (for example, for the vacuum or cryogenic subsystems). The control box metaphor ensures that these subsystems will be treated as separate entities (for example, they will not share hardware interfaces). Strict guidelines for their development will be provided, enabling a clear assignment of responsibilities and making integration much easier, a particularly vital necessity for distributed control systems. To further ensure that guidelines will be followed, only ICS-certified developers will be entrusted with developing the software that will run on the control boxes.

5.3.1 Distribution and design

The distribution of the control boxes will be optimised taking into account performance, complexity, and cost. In the simplest case, when subsystem equipment is located near the control box, the control box will be directly connected to the equipment with signal cables. Examples might include the ion source and the proton beam chopper, located at the front end of the linac, and the sample environments of the scientific instruments. A single control box will be sufficient for many one-of-a-kind subsystems. In a more complex cases, the equipment may be distributed across a larger area, or may include numerous components. For example, the numerous superconducting cavities, with their associated klystrons and cryomodules, will be spread along most of the linac. In this case, it would be impractical to control a complete subsystem with a single control box. Instead, one control box for each type of equipment will be placed at periodic intervals along the linac.

Control box architecture

The control box forms a link between the physical world of equipment and the abstract functional domain of the control system software. An EPICS IOC associated with specific devices with corresponding drivers and channel access layer will directly correspond to a control box's hardware and connected equipment. The device software will convert input signals to meaningful data and will also make it possible for hardware devices to process software commands. A schematic example of an EPICS-based control box, with software and hardware components and three different equipment interfaces, is shown in Figure 5.12. Control box prototypes from 2011 and 2012 are pictured in Figure 5.13.

The hardware in a generic control box will consist of one or more IOC computers, associated buses, and a crate. The control box may also include one or more I/O modules (analogue-digital converters and digitisers, digital-analogue converters, serial interfaces, etc.) and timing receivers. The exact hardware specifications have not yet been identified at the time of writing. The choice of platform and form factors will be delayed as long as possible, but will be made early enough to allow the development of the timing system, because the timing receivers must be consistent with the control box hardware specifications. More information about the control equipment catalogue that will list the supported I/O modules can be found in Section 5.3.2.

The software in a control box will include an EPICS IOC and either a real-time or a non-real-time operating system, depending on requirements for IOC processing (for example, IOC real-time control loops require an IOC real-time operating system). It will also include a driver in the form of a kernel module that will provide low level access to hardware; EPICS device support, which will implement drivers for communication with the kernel driver; the EPICS database that will maintain the values of all process variables under responsibility of the IOC; the EPICS channel access, which will allow the control box's process variables to be accessed from other computers in the network, and which will be able to retrieve process variable values from other IOCs; and software support for ICS core services and BLED. It will also be possible to deploy the control system logic of a subsystem on one of the control boxes that is a part of the subsystem. The software aspects of the control box will be configurable by the control configurator that is a part of BLED, and which is covered in more detail in Section 5.4.2.

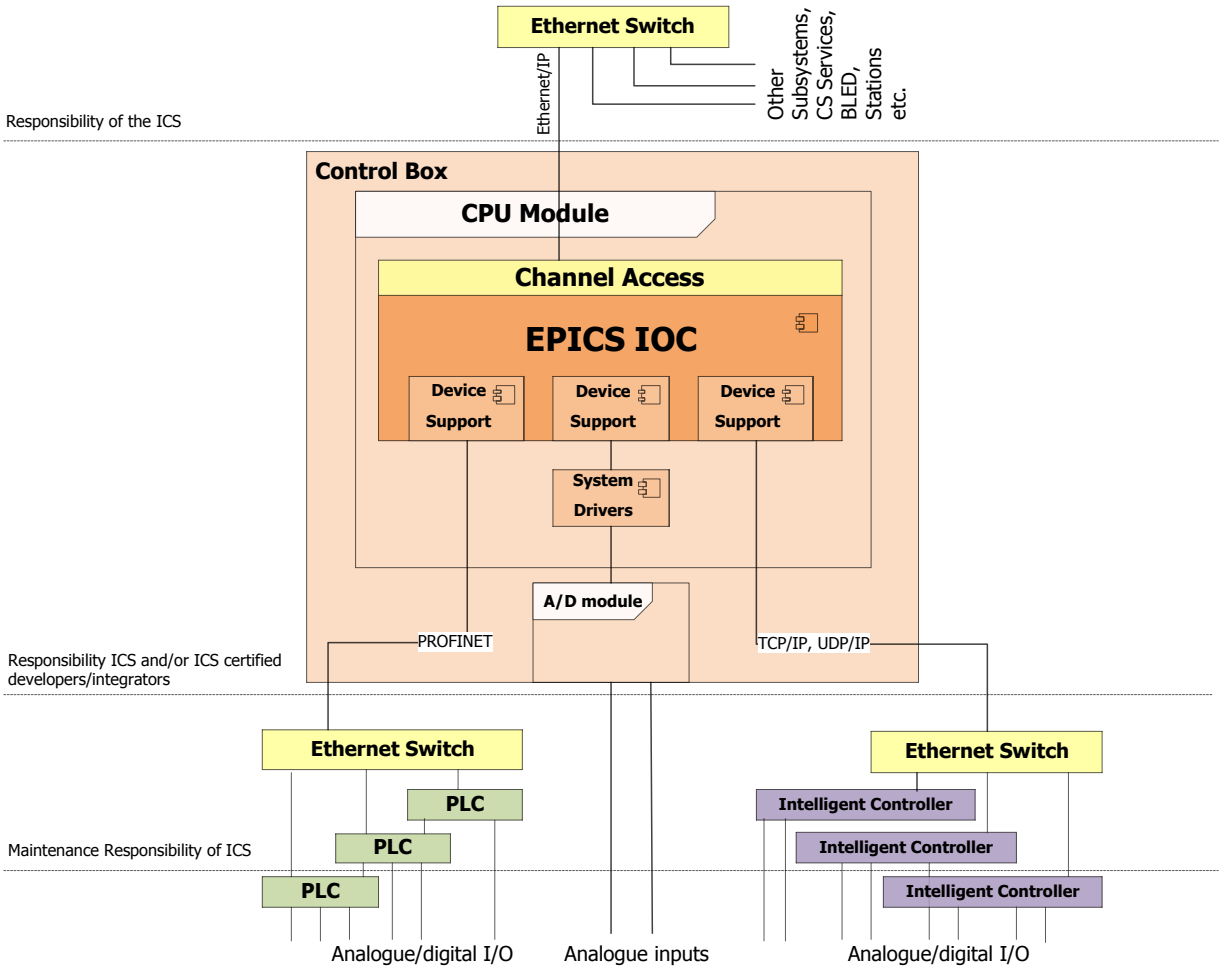

Figure 5.12: A schematic example of control box software and hardware components, showing three different equipment interfaces: The equipment is connected to PLCs, the equipment is connected directly to the analogue-to-digital (A/D) module, and the equipment is connected to some kind of intelligent controller. PLCs and intelligent controllers are not considered to be parts of the control box, while the A/D module is. The levels of ICS responsibilities are represented by dashed lines.

Equipment interface

The control boxes will employ a variety of types of interfaces to equipment. The three most common examples are shown in Figure 5.12. The first example, PLC integration, is discussed in more detail in Section 5.3.4. Another possible interface would make use of an intelligent controller that would close some of the control loops before integration in the ICS takes over. The equipment may also be connected directly to the control box on one of the analogue-to-digital (A/D) modules from the control equipment catalogue described in Section 5.3.2. The type of communication can be either hard real-time or non real-time communication.

A hard real-time equipment interface is needed whenever the control box response to external events must be guaranteed within a certain time frame. This can be satisfied either by using a real-time operating system, or by implementing the functionality in FPGA hardware. When a real-time interface is required, the real-time information will be distributed between subsystems only by means of the timing system. No other real-time communication will propagate between different subsystems. This approach will isolate all aspects of subsystem real-time behaviour. Subsystems can then be developed and fully tested earlier in the process during factory testing, rather than later during site testing, acceptance, and integration.

A non real-time equipment interface takes limited responsibility for making process variables and parameters of hard real-time control loops available to other subsystems and user interfaces. Some equipment

Figure 5.13: Control box prototypes. Top crate: 2011. Bottom crate: 2012.

will have its own real-time control (for example, PLC systems, temperature regulators, motion controllers, or low-level RF fast control feedback loops). When this is the case, the control system will only need to slowly control the parameters of these low-level control loops and monitor their diagnostics (i.e., to monitor PLC registers, the setting of reference temperatures, manipulation of PID control loop parameters, etc.). Other equipment will be required to exhibit real-time behaviour, but can be controlled in a feed-forward manner, as occurs, for example, with the high-level control of the superconducting RF system. In this case, the control system will distribute information about what actions to take (i.e., waveforms defining values of set points as a function of time), while the timing system distributes the time and event triggers.

In order to use the centralised configuration system effectively, each piece of equipment will provide a unique identification which can be read from the controls interface. Equipment identification will not be based on IDs provided by controls components. The use of IP or MAC addresses of equipment controllers for equipment identification would not be sufficient, since these addresses may change when the controls interface component is replaced. The scheme for equipment identification will be provided by the naming convention described earlier in the chapter. In addition to being able to read equipment identifiers by remote access via the control system, it will also be possible to read them using an identifier bar code that will be placed on the casing of the equipment. Equipment will allow complete remote control without manual setting. Autonomous activity of the equipment which could interfere with controls activities will be avoided. In those cases in which it is possible to set a piece of equipment to manual control, it will be possible to read the manual control state with the control system.

5.3.2 Prototyping support and the control equipment catalogue

The selection of the control box hardware platform must take into consideration the availability, reliability, pricing and available support of the needed components. To facilitate early prototyping and proof of concept, early control box prototypes are being built using a variety of platforms. The first prototype was built in 2011, and the second in 2012, based on the cPCI PlusIO hardware platform. Subsequent prototypes will be released annually. After the platform has been set, yearly prototype releases will continue, each adding new support for various I/O modules. Table 5.8 lists the planned support for the control box prototypes for 2012 through 2014. The main purpose of the 2012 release is to provide support for the timing prototype. In 2013, the control box prototype will add support for the MPS prototype and selected PLC and motion controller support. The 2014 control box prototype will support additional specific components to provide control support for prototypes by other stakeholders.

Release year	**Control box platform**	**Support**
2012	cPCI PlusIO	Timing prototype
2013	cPCI PlusIO, microTCA	MPS, PLC, Motion controller
2014	To be determined	Generic AD/DA cards, digitiser, generic camera, power supply controller

Table 5.8: Evolution of support provided in control box prototypes from 2012 to 2014.

Control equipment catalogue

From the earliest design stages of the project, it is important that a certain level of agreement about hardware components and platforms is achieved among different ESS stakeholders. For ICS, ESS will model its approach to tackling the complex equipment discussion and to simplifying the integration of equipment in the control system on the approach that has been successfully employed at ITER. Such an approach will cover the following steps:

1. A study of already available components.
2. The identification of unavailable functionality in the supported hardware.
3. The identification of new hardware able to fill the missing roles.

4. Integration of the component by ICS using the control box and the development environment.

5. Adding the fully supported component to the catalogue, thus making it available to all possible future users.

6. Provision of support and further development for the listed components.

The number of I/O types will be limited to minimise the burden of driver development and maintenance burden. One or several standard bus architecture(s) with standardised I/O modules will be selected.

5.3.3 Neutron instrument and sample environment control

The integrated control system will support neutron beam line instruments, sample environment sets, and detectors. Instrument control systems will be synchronised with the accelerator and data acquisition. Time-stamped settings (meta data) for the instruments and sample environment will be archived so that they can be matched with detected neutrons and accelerator settings, and so that they will ultimately make it possible to replay the experiment.

Close cooperation will continue with instrument designers, developers and associated user communities during the development phase. Moreover, standardisation will be enforced in the laboratories developing individual instruments. Several sample environments will be provided by ESS, but users may also need to be able to plug in their own customised sample environment. ICS will respond to this need, and will be capable of accommodating dynamic changes of the sample environments. Requirements for ICS-compatible sample environments will be provided to users. The control box concept plays an important role in this approach, as illustrated in Figure 5.14. Some of the major issues that need to be addressed by the Neutron

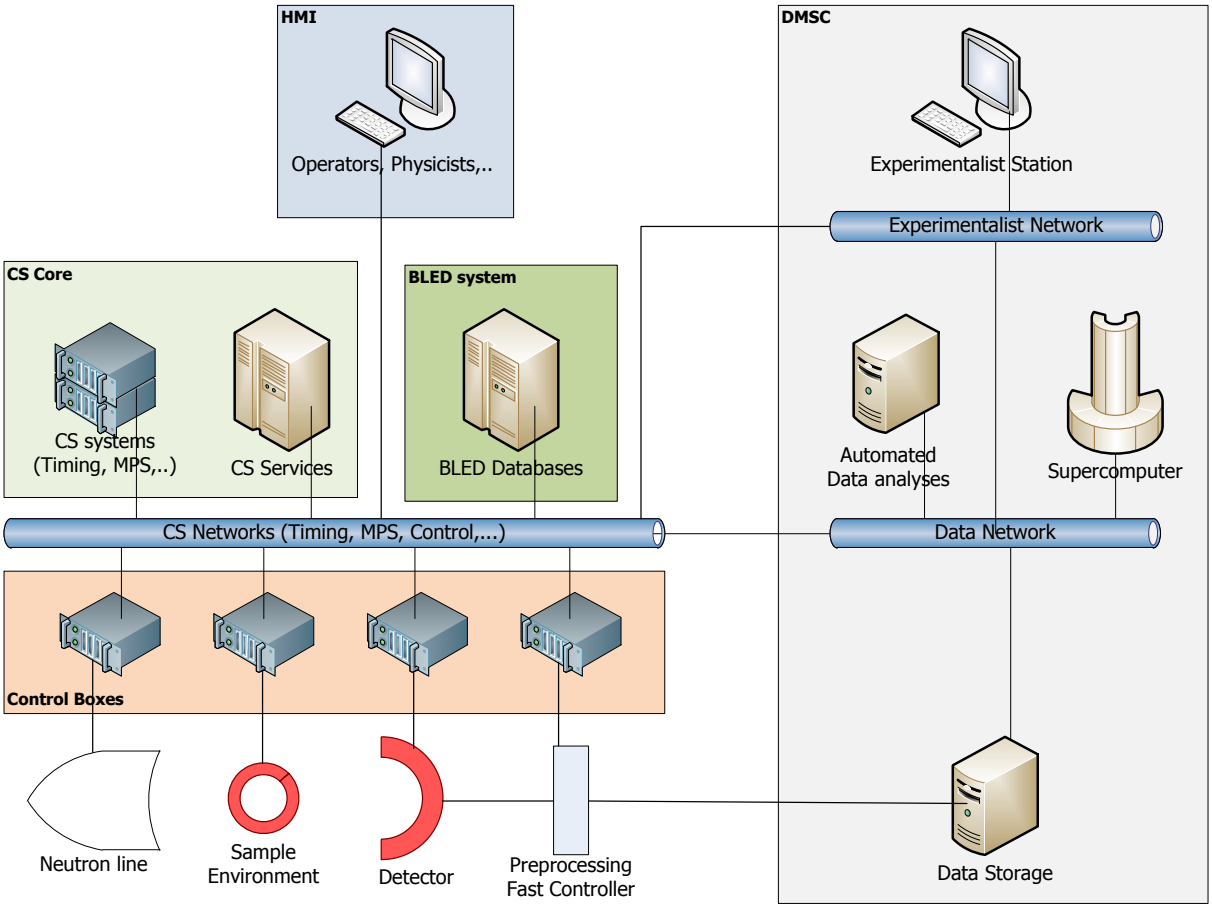

Figure 5.14: Integration of a neutron beamline instrument using control box methodology.

Scattering Systems Project include data acquisition systems, motion control and general automation with an emphasis on standardisation, maintainability, and compatibility between instruments and instrument control systems. These issues are discussed further in Section 2.8.

The instruments will need to receive timing signals from the master oscillator and timing events for the spallation pulses so that detected neutron events can be unambiguously associated with the generating spallation pulse. The timing receivers in the control boxes used to integrate the instruments with ICS will provide this functionality. Acquired experimental data will be transmitted to the data management system and all monitored process variables will be archived using the ICS archiving system. The configuration of the machine at the time of the experiment will be stored in BLED. The systems will use the same timing services for time-stamping, thus making it possible to connect all stored information, whatever its source.

5.3.4 Infrastructure control and programmable logic controllers

Infrastructure such as HVAC and facility monitoring may be controlled by industry-supplied control systems based on programmable logic controllers (PLCs). These PLCs will only be used for controlling slow devices' I/O signals. This approach minimises the risks of faulty code, operating system errors or other malfunctions for the interlocks mechanisms, at the same time as it provides a reasonable degree of independence from the main control system. The advantage of a separate slow control system is that it can run when the main control system is down. Nonetheless, monitoring and control of the industrial control system equipment will also be available through ICS. The connection between the industrial control system and ICS will be implemented with PLC control boxes. The PLCs will be monitored and controlled

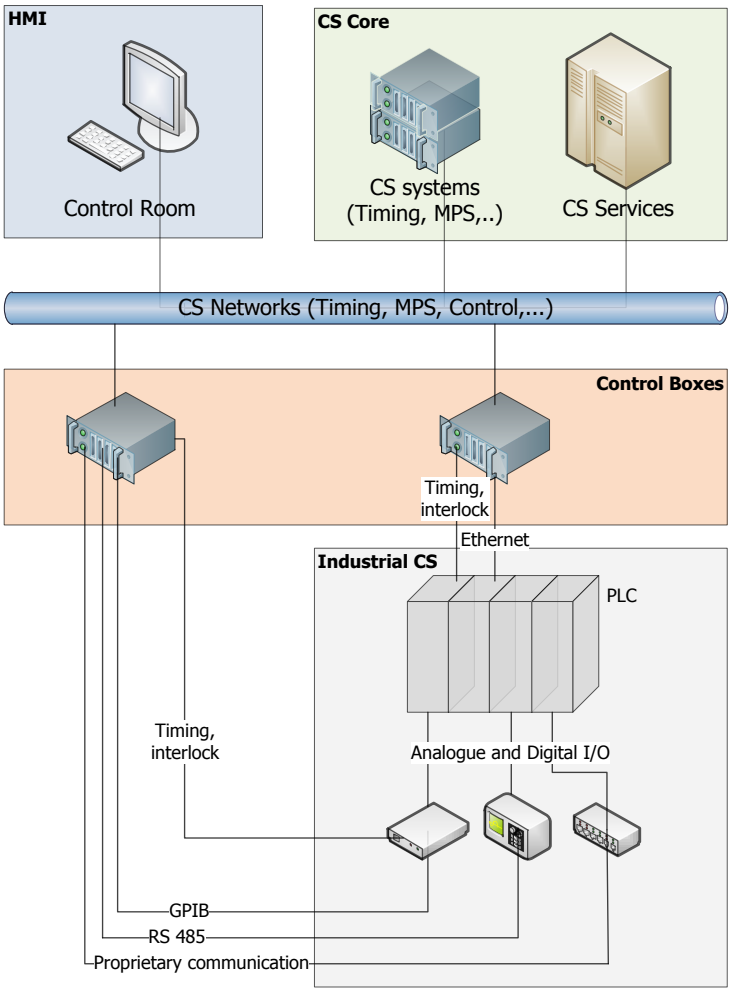

Figure 5.15: Signal exchange between the industrial control system and ICS, via PLC control boxes.

as devices available to to ICS as shown in Figure 5.15. For the most part, PLCs will be used to integrate the cryogenic, facility monitoring, vacuum and HVAC systems into ICS.

5.4 Beam line element databases (BLED)

The machine data needed for development, commissioning, operation and maintenance of ICS will be centrally managed. This system for central management of data has been named BLED. The name BLED was originally derived from Beam Line Element Databases, but the scope of BLED has expanded to include non-beamline elements. With this approach, it will only be necessary to enter data once, which will save time and reduce the chance of errors. BLED will be tightly connected with the software development environment and will present a natural gateway for the introduction of new configurations of the control system. The aim of BLED is thus not just to centrally manage data and ensure their consistency (the benefits of which will be most apparent during integration, commissioning and decommissioning), but also to simplify development and reduce the time and effort required for the code-test-debug cycle. Implementation of BLED will be based on existing solutions, in particular the IRMIS system [527] for maintaining inventory information and the ITER Self Description Database (SDD) toolkit for forward- and reverse-engineering of EPICS databases from/to the BLED's relational database management system model.

5.4.1 Design and architecture

Its databases are the central part of the BLED system. They will be deployed on a server connected to the control network, which will not be accessible to the outside world. External clients will use a web and command line interface provided by the external BLED web application server, which will be able to access BLED databases via a gateway, as shown in Figure 5.16. This setup will make access to BLED possible for developers, remote users and neutron scientists from satellite control areas that would

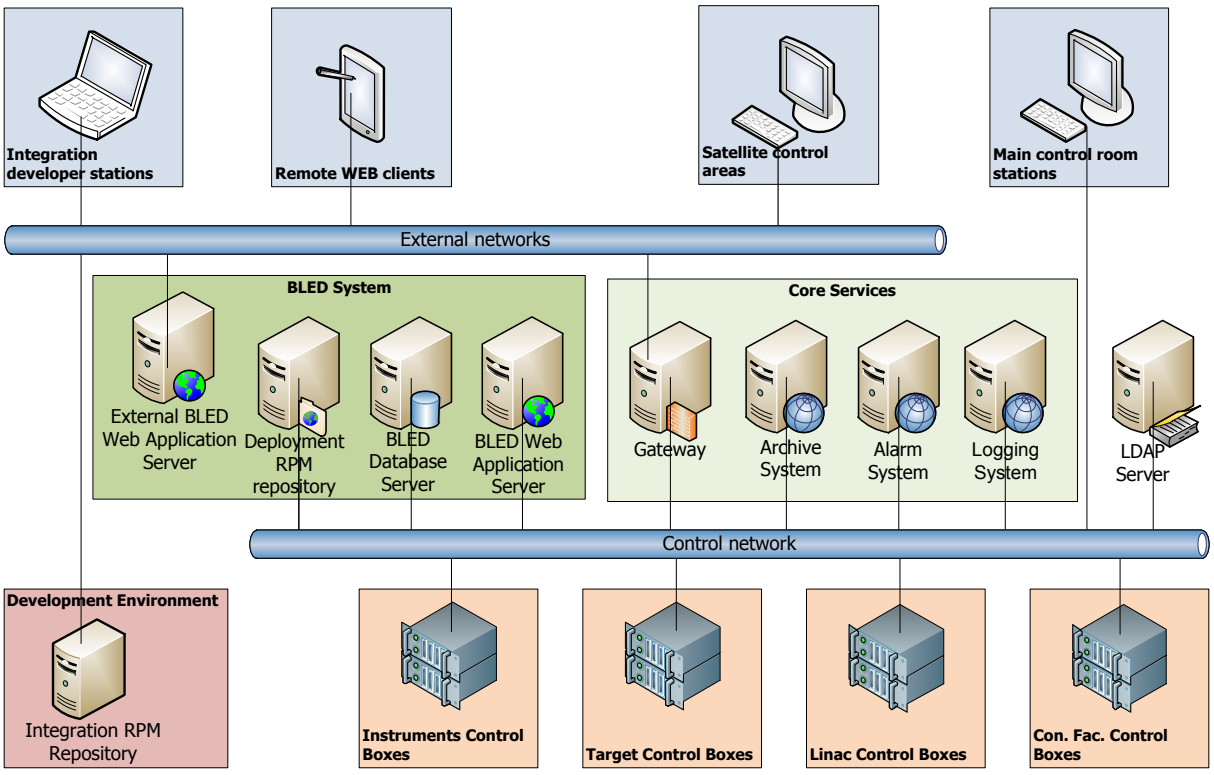

Figure 5.16: Network view of the BLED architecture. An external BLED web application server will provide access to BLED from outside the controls network.

normally be prevented from accessing the control network. The extent of the access has not been defined yet, but will be configurable to some extent. ESS central directory services will be used for user access authentication. Control network clients will also have access to the same functionality using an internal BLED web application server.

Several different tools will be used for interacting with the databases. The tools can be divided into two broad categories: User tools that are purely user oriented (e.g. the naming convention tool), and service tools that will run as services, which require little user interaction (e.g. CS Configurator). User tools must be able to run on a number of different platforms. In addition, some tools should be easily accessible during commissioning. These tools will have the form of web applications, compatible with web browsers endorsed by ESS. The user interface allowing the control system user to perform desired tasks will be accessible by opening a URL specific to each tool. On the other hand, service tools will not need require a web-based user interface, as access will be mainly administrative in nature. They will be command-line based, and will run on the Scientific Linux operating system that has been selected for controls. BLED will use service-oriented architecture [529]. Figure 5.17 displays the logical architecture of BLED. Command line tools, web browsers and possible BLED client applications will access the databases through BLED services.

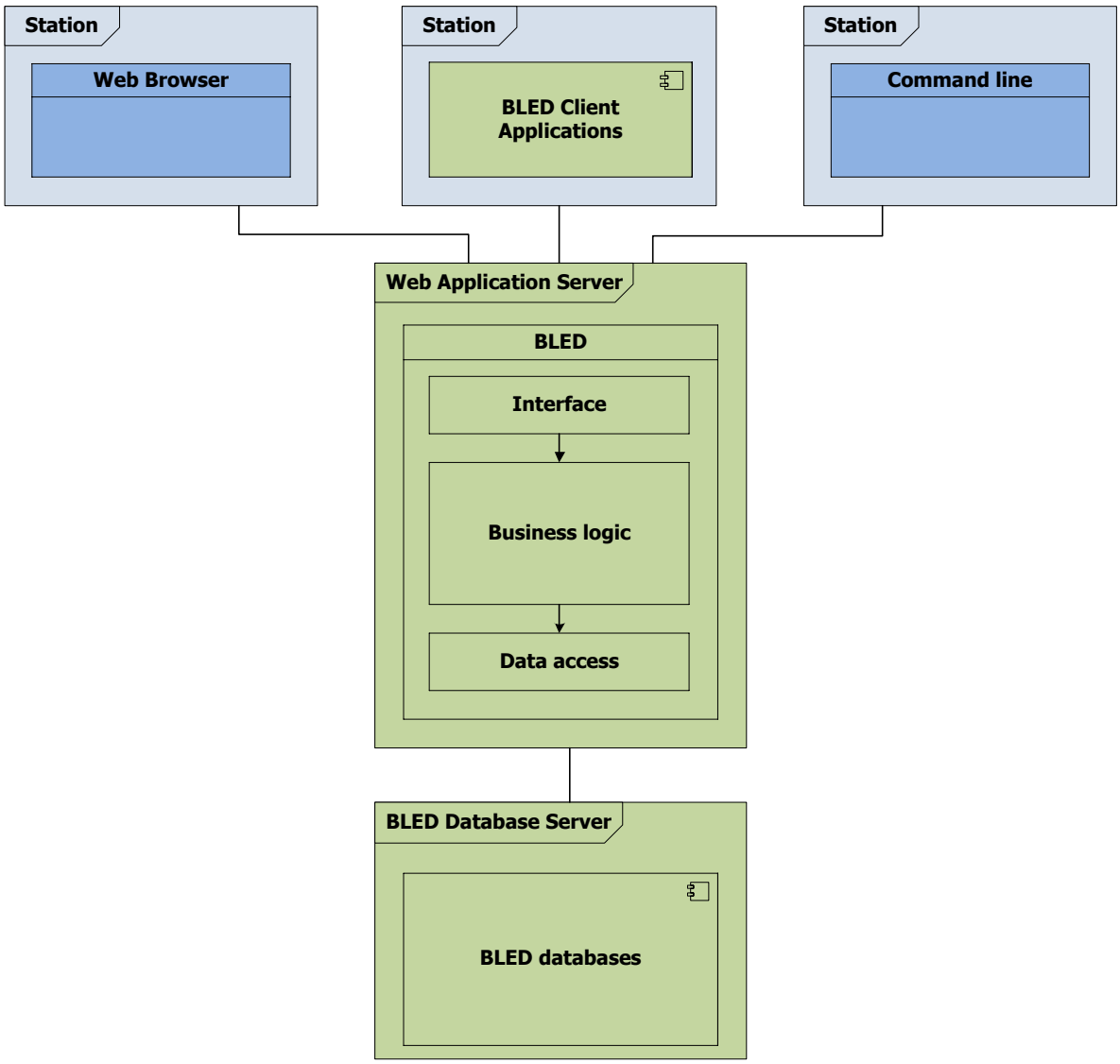

Figure 5.17: BLED's service-oriented architecture.

5.4.2 Functionality

Security

BLED will access the data relevant to each individual user's credentials from the central directory service of the facility. A user will have to identify himself at each attempt to access BLED if there is no running session already in process. Section 5.6 discusses how only control system users will be granted access. Once logged in, a session will be established which will remain active for a predefined period of time or until the control system user logs out. If the session times out, the user will have to log in again. Different users will have different access rights, providing for full, limited, or no functionality for any given tool. Access to databases will be restricted.

Versioning

Versioning is an important feature of BLED. History will be maintained in the versioning system for the configuration of ICS stored in BLED databases. The history will have two important roles. It will make it possible to revert the configuration of the machine to the previous version when the new configuration produces unwanted results. It also will sometimes provide useful context for the interpretation of old data, as results may be easier to explain if the configuration of the system at the time is known.

BLED will provide three special configurations (aliases) at any given moment: Previous, production, and integration testing. The last valid and approved configuration will be named "production." The configuration that was valid before the current one will be named "previous". When the team is testing new or changed parameters, the configuration will be named "integration testing". Once the testing has been completed, the "integration testing" configuration will become "production," and the extant "production" configuration will become "previous." The system will allow the team to set the currently active configuration for each device in the system. This way it will be possible to test different configuration changes at the same time, and there will be no need to simultaneously switch the configuration on all equipment, an operation that would probably not be instantaneous. BLED will use tools that were specifically developed with versioning in mind (e.g. Mercurial) and will not implement the actual history in the database. Instead, BLED itself will provide only the means to track and control different versions stored in the versioning system.

Control system configurator

Control system configurator (CS configurator) is a series of tools and services used to store the data in the BLED databases and also to generate and deploy the configuration to the proper parts of the distributed control system. Control boxes, stations and service servers are computer nodes that are the natural focal points of the control system for middleware deployment. Each computer node will have a unique name, network information and a list of the package management system (RPM) packages that need to be installed for it to perform its system role. The RPM packages will be deployed automatically at the time of installation from the deployment RPM repository and will include the following logical units: Operating system, drivers, applications, EPICS database and device support. Updates to these logical units will take place through the deployment RPM repository. Figure 5.18 shows how code development and control system design and configuration will be deployed to ICS computer nodes.

All the installed units will be configured based on information stored in BLED. A system management server which is a part of the CS configurator service will listen on a dedicated port for deployment of a new runtime configuration and will pull it when it becomes available, or this new configuration may be pushed to a specific computer node by request. Depending on system role, the configuration will belong to one of three categories:

1. IOC configuration: The configuration includes a list of required EPICS modules, sequence of EPICS IOC shell initialisation commands, and EPICS sequencer binaries. This entire configuration is deployed in some local directory for off-line use (/var/opt/codac). After the configuration has been deployed, the IOC is requested to reload the EPICS application with this configuration.

2. CS services configuration: This configuration is generated and imported into services, such as alarm and archiver. All ICS service hosts are then requested via the CS configurator service to restart the

corresponding services. An alternative currently under investigation would be to host the alarm and archive configuration databases in BLED.

3. HMI screens: BLED deploys HMI screens from the deployment RPM repository and notifies all CS users to update their local caches. This notification is accomplished through the CS configurator service and, upon control system user confirmation, the user interface is refreshed. Alternative HMI deployment schemes are currently under investigation, such as storing HMI screens on a network file share or having the control system query BLED for new screens.

During operation, it will be possible to stop the CS configurator service and to completely disconnect BLED from the network. The entire configuration will be stored locally on each computer node. The CS configurator system management server will generate reports of the configuration of any particular part of the system as well as of all computer nodes for which the software or configuration is out of date. Users will be able to use this information to update the nodes requiring a more recent version of the software or configuration to operate properly. Development stations in particular will be similar to a control box in many respects. For example, they will share the same kernel and drivers. Therefore, it makes sense for

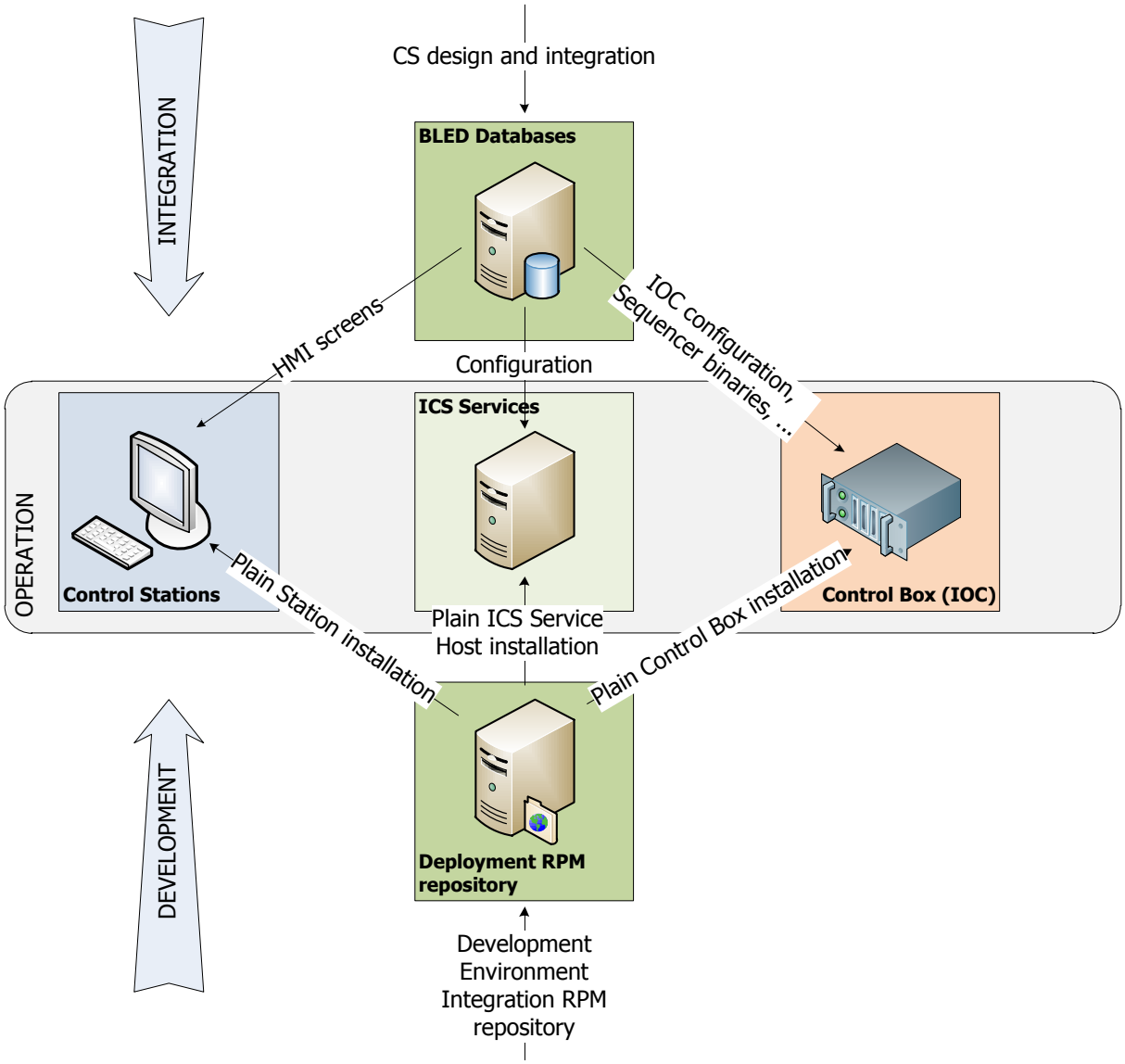

Figure 5.18: Control system configurator for control system computer nodes.

them to be configured from the same RPM repository as the control box. The CS configurator will also provide tools for the integration of new devices. It will generate the basic layout of the EPICS application and databases for the start of development and later incorporate the finished work in the BLED databases. Examples of CS configurator use cases are presented in Section 5.4.4.

Inventory

In a system as large as ESS, it is important to keep track not only of device configurations, but also of their physical locations, since searching for a piece of equipment might make maintenance tasks unnecessarily long and expensive. Because BLED databases will contain information about all physical components of the machine, they provide a natural way to catalogue and locate the physical pieces in the facility. Another use case is to determine all the pieces of equipment that are affected by the failure of any particular piece of equipment. For example, if a power supply is down, information in BLED will make it possible to locate all the equipment connected to that particular power supply. It also will be possible to provide this information to external systems for inventory purposes.

Equipment installation

Tracking of the status and progress of installation is a valuable input to day-to-day planning. It will be possible to store information in BLED about which equipment has already been installed, which equipment has been delivered but not yet installed yet. Even installed equipment may not be completely aligned with the design. For example, the characteristics of a particular device could differ from the ideal design case because the magnetic field is different or because the device is slightly displaced or rotated. In such cases, measurements will be performed on devices and corrections applied to system in a process of calibration. BLED will store the calibration data and so that it can be taken into account when needed, for example, for simulation of the system. BLED will also be able to provide rack-by-rack installation plans which will include information about which equipment belongs in which rack, the appropriate lengths and types of cables, and directions to connect equipment.

Naming tool

To support the naming process, a naming tool will be developed. Use-cases are being studied to collect the requirements for a number of capabilities and services, including filtering and sorting capabilities, as well as automated name generation for systems with a large number of devices. The tool will also enforce the syntax and ensure that ESS Naming Convention [515] rules are fulfilled.

Lattice tool

The accelerator lattice lists most of the devices in the linac and is typically constructed using specialised design tools. Modification of the lattice must be accompanied by a recalculation of the physical parameters of the beam and therefore cannot be done without proper simulation tools. By importing the lattice into BLED, the linac devices will be automatically registered. Another benefit of importing the lattice into BLED is that it can then be exported easily in various file formats supported by different accelerator design tools. Typically, lattice design workflow will take place in the following steps:

1. Create lattice using a design tool (e.g. TraceWin).
2. Import the lattice for a selected part of the accelerator into the BLED database.
3. Examine the lattice (optional).
4. Export the lattice in any of the supported formats.
5. Modify the lattice.
6. Import the new lattice into the database.

Parameter tool

BLED will also hold information about the parameters of the facility. A given parameter may have more than one value. For example, one parameter may be beam energy. In this case, several approved parameter values exist, one for every section of the beamline. Control system users need to be able to view all the parameters currently applied in the machine in order to reference them or to use them in further calculation, design and development. Parameter management workflow will follow the pattern below:

1. A new parameter and value are added to a parameter list.
2. The status of the parameter value is "draft."
3. The technical board assesses the new parameter and either rejects it or accepts it (the status is now "rejected" or "active").
4. An existing parameter value is modified. The old parameter is still active and the change is shown as a draft parameter.
5. The technical board assesses the change and either rejects it or accepts it.
6. If the board accepts the change, the status of the previous version of the value is deprecated and the new value becomes active.
7. The previous value represents one link in the history chain.

5.4.3 Configuration databases

BLED configuration databases are divided into five loosely coupled parts. First is the control configuration part that holds the data that is needed to configure control system software modules. Each module is configured through a set of parameters (field values) that define the module's behaviour, influence the default values of PVs, provide configuration for alarms and archiving, etc. In addition, the IOC in which each module is instantiated is included. Second is the systems part that contains information about all the systems defined during the design of the machine. For the accelerator, the system includes all devices in the lattice and the relevant data are imported with the lattice tool. All the additional supporting devices as well as devices from other domains will also be identified and entered. For devices that have been instantiated, the signals for each device will be specified. Third is the equipment part that includes information about the real hardware that represents the designed system. Fourth is the cabling part that contains information about the cabling that supports the equipment part by providing interconnections between different pieces of equipment. Fifth, and finally, is the location part that stores details about the physical layout of the facility, that is, about the location of buildings and rooms, the types of racks and servers installed in each of them, the location of all the equipment, etc.

Figure 5.19 shows the interfaces and main building blocks of the five parts. The control configuration part represents the configuration model, the systems part represents the system engineering model and the remaining three parts constitute the physical model of the machine. The sections below briefly describe each individual part in slightly more detail; however, only the most important building blocks are presented.

Control configuration

Control configuration will contain information about all the software modules that are part of ICS. The module instances will be connected to the elements stored in the systems part of BLED. Since a device is an extension of the element object, the module instance will also be connected to a device. In this manner, each device will be associated with modules that are needed for the configuration of the device in ICS. The configuration in module instances will be defined using fields, where the field values will represent the actual values of the configuration. The field values in the BLED database will be used to automatically generate the EPICS IOC start-up scripts (the st.cmd files). This top-down approach will give developers the ability to check and track the consistency of the EPICS configuration database files, and to generate an initial set of EPICS files for all devices. The translator will generate basic EPICS database configuration files out of device definitions. The developer will then be able to work on EPICS files using tried and proven EPICS development tools like VisualDCT and text editors of his or her choice. For further streamlining of

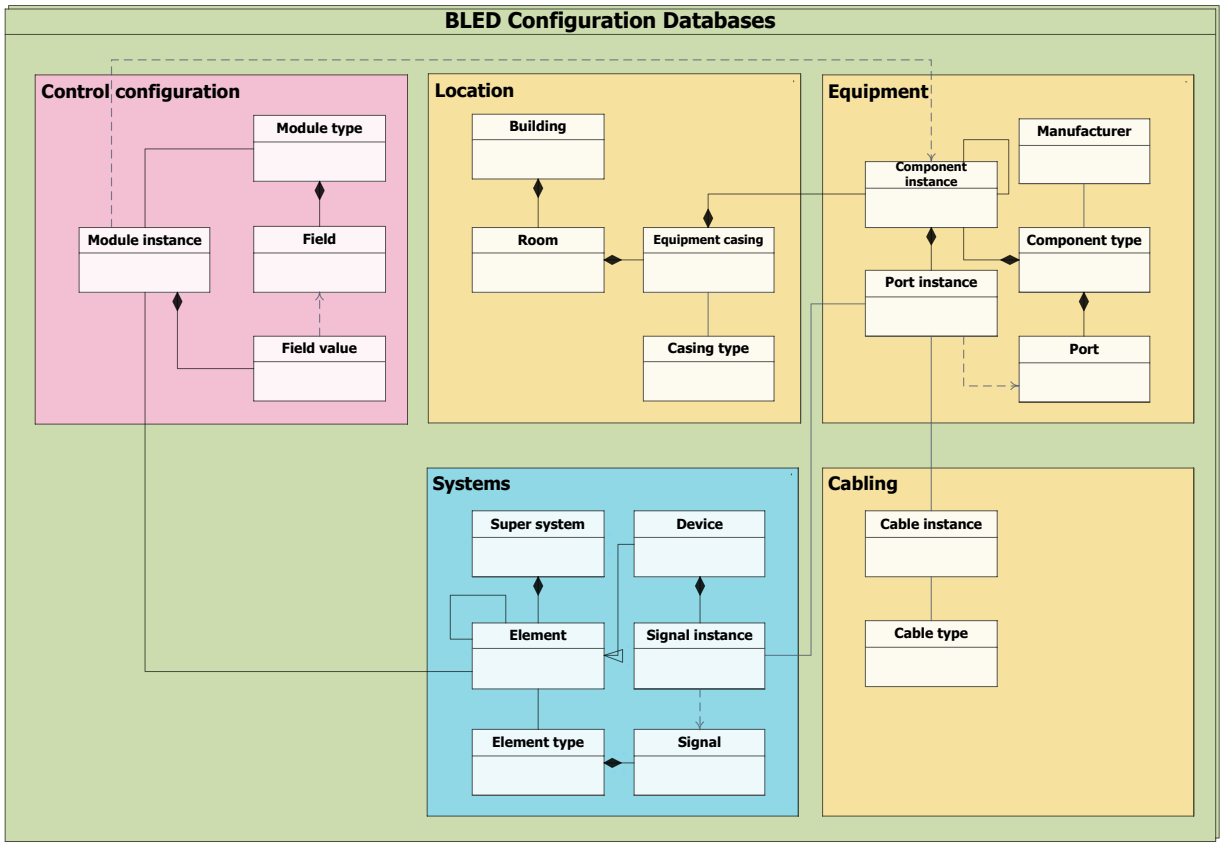

Figure 5.19: An overview of BLED data used for integrated control system configuration.

EPICS development, a special Eclipse RCP editor will be developed. It will provide syntax highlighting, keyword and definition completion tailored specifically for ESS EPICS development. The created/modified EPICS database configuration files will be stored in the version control system and will be pulled back into the BLED database using the SDD-parser tool, which will automatically check consistency and resolve changes that were introduced in the EPICS database.

Systems

The machine will be composed of a number of systems, each of which will itself be composed of a set of interacting elements, and each of which can be implemented to fulfil its specified requirements [530]. A system from one perspective can be viewed as an element from another. Elements define the hierarchical structure of the machine. Each element will be named according to the ESS naming convention, which is described in Section 5.1.6. All elements will be organised in a hierarchical way, which means that each element will have only one parent, although more than one element may have the same parent. A parent may be either another element or a super-system. In addition, each element may also have a predecessor or previous element, which will define the instance which is located directly in front of this entity within the same parent. Elements will also be used to represent virtual systems; such elements are called virtual elements.

A device is an extension of an element object and will not have any children. Instead, the device will have a number of defined signal instances, each of which will be connected to the port instance in the equipment part of BLED. This will make it possible to generate a list of all the components that make up the equipment associated with a particular device. For equipment to be represented in ICS it will have to have at least one signal. A device representation of a node will provide a unique name for the associated computer node, based on the device location in the system hierarchy. Similarly, it will be possible to generate the EPICS PV names combining the device location in the hierarchy with a signal name. Signals will be either physical or virtual.

Equipment

All the equipment that makes up the ESS machine will be listed in the equipment part of BLED. Equipment will consist of different components connected with cables defined in the cabling part of BLED. The connections will be made via ports or, more precisely, via port instances. A device representation of a node will provide the link to the physical components that make up the node. Many components will need an indication of the drivers required to operate them. For boards, this will usually be the OS driver. For other pieces of equipment, this may be the firmware version of the driver that is loaded onto the device. This information will be stored in the component definition. During testing and upgrading, it will be possible to override this in a given component instance, allowing for selective upgrade of a particular component's software. Generating a list of all devices and components associated with those devices that are connected to a particular node will define a list of RPM packages with appropriate drivers and the necessary configuration for their installation on the node.

In the case of computer nodes, the component instances will be associated with the module instances, representing an alternate route for listing all modules needed for the configuration of a particular node. It is not obligatory that each component defined in a component instance have a port instance associated with it. Certain components will not be installed in the control system and thus will not be connected to any other component, for example, replacement components in storage.

Cabling

The cabling part of BLED defines a lists of cables that are associated with port instances in the equipment part. It stores the information about how different components are connected. Each port instance will have only one cable instance associated with it, however a cable instance may be referred to by as many port instances as desired. This approach will support one-to-one, one-to-many (e.g. Y-type), and many-to-many cable connections. The cable type will define the basic properties of the cable, while the cable instance will add information about variables such as the cable length of a particular instance.

Location

The location part of BLED defines the physical or geographical location of equipment. It provides the list of all available rooms and buildings. Within the rooms, all casings (e.g. racks or power-supply units) will be identified. Each equipment casing will contain one or more of the components listed in the equipment part of BLED.

Database tools

ESS's web application server access is intended for regular users who mainly need to inspect or enter data in standardised ways. In this case, BLED will assure the integrity of the process, providing validation of entered data, error checking, and similar services. Less standardised actions, such as database maintenance or repair of broken data, also will need to be done occasionally. While a web tool would be useful for such purposes, it is likely to prove too costly to develop. Instead, regular client applications will be developed, which, at least in the ideal case, only developers and system engineers will have to use. Database management tools also will be used to provide general access and tools to manage the BLED databases.

5.4.4 Use cases

During integration, developers will have to write device support code for each device, which in practice means providing access to all device signals. The following workflow pattern is anticipated:

1. The device element is defined and its signal instances are entered. Then the device is instantiated by assigning module instances to it.

2. A component instance is chosen to which the device is attached. This may be a control box that a developer is using for testing.

3. The control box component instance is associated with equipment casing, and the appropriate equipment is defined by specifying additional components and ports. Cabling information is used to connect components.

4. The device signals are associated with the proper ports.

5. The EPICS IOC signal database template is automatically generated for the selected device. PV default names are generated in accordance with the naming convention, although the developer can choose to override this function.

6. The developer implements the EPICS IOC logic database and writes the device support code.

7. The code is stored in the RPM repository. If the code uses macros referring to PV names instead of naming PVs explicitly, the logic database is checked to ensure that the referred names conform to the naming convention. All the names are added to BLED.

8. The developer may use annotations in the EPICS database file to configure alarm and archiving services.

In addition to providing control system configuration management, BLED data can also serve as the basis for a road map for installation during commissioning. After equipment has been ordered and has arrived on site, data stored in BLED will make it possible to track the status of the devices and to define the installation plan for the installation technician. For example, for a given device, the installation technician will access a mobile application on a tablet PC or mobile phone. For each component and each port, the application will specify the ID of the cable connector to which the device connects. When the installation is complete, the technician will check a check-box, using the mobile application. Once the endpoints of all components have been connected, the technician will be able to launch automated interconnection tests, again from the mobile application, allowing him or her to troubleshoot any cabling problems without leaving the site.

Once the equipment has been installed and connected to a control box, and the relevant device has been defined in BLED, device software deployment will be carried out automatically. First, the equipment and control box will be turned on. The system management server will use the ID of the control box to configure it. Then the OS will be updated or installed, and the drivers for digital cards installed in the control box will be deployed. Finally, the EPICS IOC application will be installed from the repository and started.

Information in BLED databases will also be used when packaging the EPICS IOC application for a particular control box. First, a single st.cmd will be generated by BLED for all the devices associated with the control box. Then a signal database template file will be created for all devices connected to the control box. The most recent device support and logic databases for all devices will be loaded from the repository and included, unless specified differently in the component instance data in the BLED database. The IOC application will be compiled and packaged, and the package will be put in the repository ready for deployment. During debugging and testing it will be possible to make a “hot” change of the configuration of the IOC databases. For example a change in the EPICS logic database would be implemented using the following steps:

1. The proper device is located in the configuration tool.

2. A copy of the EPICS logic database file is opened from the repository or generated from BLED (the tool could have text editing capabilities or even be an integrated version of a visual database configuration tool).

3. The changes are made and set for deployment or re-imported into BLED.

4. The EPICS IOC on the destination control box is stopped and the database file is deployed directly to the control box.

5. The EPICS IOC is restarted.

5.4.5 Online and offline proton beam modelling and simulation

The initial control setpoints for the accelerator will be generated by the offline accelerator design models used by the Accelerator Physics and Engineering Groups. These models are comprehensive, complex, and slow, and will not agree perfectly with observed accelerator performance. The control setpoints are also

far too numerous and low-level for an operator or accelerator physicist to be able to tune efficiently. A real-time, reasonably accurate machine model is therefore necessary to assist operations with accelerator tuning, and to provide modelled optics data to feedback loops and control applications. An online model will be used for this real-time physics modelling of the ESS proton beam. Operators and accelerator physicists will use this model to tune the accelerator. The model itself will be continuously improved to more realistically predict observed accelerator behaviour and measurements. The online model will permit parameter changes to be tested before application to the real accelerator. High level applications will also use the online model to support automatic routine tasks, such as loading the parameters from the running machine and finding optimal magnet and RF settings for a specific goal.

The model will assist operations with accelerator control by providing a "physics view" of groups of accelerator control points. Some outputs will be viewed by physicists and operators to evaluate ESS conditions, and some outputs will be used by control system servers and software to calculate corrections and expected response of control loops. It should be emphasised that the online model is not meant to provide the capability to simulate the entire machine, but only those capabilities that are needed in reasonable real-time by controls or in the main control room.

Accelerator tuning will be performed iteratively over several steps:

1. The offline design model (or later the online model) is used to compute initial values for low-level device setpoints.

2. Initial values for setpoints are corrected by tuning the accelerator based on beam measurements, with assistance from the online model.

3. Differences in tuning are investigated and results are used to improve both online and offline models.

This process is designed to produce ever-closer agreement between the models and accelerator behaviour, which will help reduce tuning time. It is not the responsibility of ICS to provide the algorithms for the low-level device computations. However, ICS will ensure that algorithms are invoked at the proper times, and that their results are delivered to the appropriate applications, services, control points, and/or databases.

Offline simulations will still be necessary to understand detailed beam dynamics and any instabilities that may be generated by errors in linac component production, assembly errors, or other random errors. Offline simulation codes will be flexible enough to include unexpected phenomena arising during the beam commissioning phase. The codes will also provide single and multi-particle capabilities to simulate a reasonably wide range of operations situations. The data required to construct the simulations (e.g., systematic errors associated with component fabrication and alignment errors during installation) will be maintained in a database.

Composition of the online model

A schematic of the relationship between the online model and some other portions of the ICS is shown in Figure 5.20. EPICS provides channel access low-level control points throughout the control system, and all access to ESS hardware will be through EPICS. However, EPICS is very low-level and fine-grained, and does not provide an abstraction layer whereby applications and operators can interact with the accelerator using abstract, physics-level structures such as orbits or other correlated groups of instruments. The online model will adopt the SNS approach, using the XAL development environment [531] as a physics abstraction layer to provide access to these structures in a controls context. The ESS online model will be composed of several elements, including an interface with BLED databases, an interface with XAL, a multi-particle simulator, and a beam envelope simulator. Each of these elements is described in more detail below.

BLED

The online model will have a number of inputs, including the beamline physical layout; calibration information; magnet and RF instantiation information; and installation, aperture, survey data, and magnet and RF settings from the live control system or archiver. It will produce a number of outputs, including expected beam envelopes, betatron functions, and phases at all beamline elements. The lattice tool will save accelerator lattices and configurations in formats suitable for various simulation codes, so the online model will only need to save control system strengths and settings to a BLED database to support realistic offline modelling. There may be several online models active at any time, each representing a different

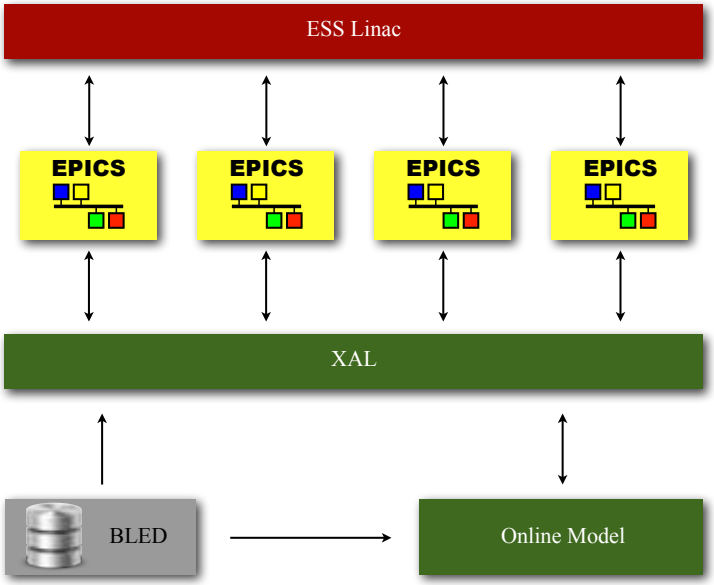

Figure 5.20: Online model dataflow schematic showing interfaces to BLED and XAL. There is no direct interface to EPICS input-output controllers or process variables.

state of the ESS accelerator. One model, the "live" model, will have a special status. This model will represent the best model of the accelerator according to current real-time setpoints, read-backs, and design beamline information, and this is the model that will be used by active controls processes such as orbit correction and feedback systems.

XAL

The implementation of the online model will probably be based on the software HMI framework XAL, which is written in Java and was first developed at SNS [532]. XAL provides a hierarchical physics view of the accelerator and hides most of the underlying control system details. The hierarchy is configured in an XML database, facilitating application sharing across different beamlines, and shielding the programmer from detailed knowledge of signal names. The online model can be consulted for design values, for live machine values, or for user-selected tuning values. It is fundamentally important that the online model, especially the output of the envelope simulator, be fully integrated with XAL. All model properties such as element beta functions and phases, RF cavity gradients and phases, beamline element s-locations and apertures, and tracked particle distributions will be accessible within the ESS XAL framework and to ESS XAL applications.

Multi-particle simulator

The multi-particle simulator will be the section of the ESS online model that calculates transport properties and dynamics of individual protons and groups of protons through the accelerator. It will implement the physics of all linear and non-linear elements of the accelerator using well-documented approximations for maximum performance. It will provide interfaces to select relevant physics through the online model, making it possible to produce results reasonably quickly in a control room context for various studies and enquiries. For example, the live online model will not use beam-gas scattering calculations, although these may be used (at corresponding computational expense) in calculations in another online model dedicated to studying these effects.

The multi-particle simulator will be benchmarked with other offline simulation computations and measurements as much as possible. Indeed, initial beam commissioning activities will often consist of comparing beam measurements to those predicted by the multi-particle simulator portion of the live online model and resolving discrepancies between the two. The multi-particle simulator will be written in a reasonably low-level language (C or its equivalent) to maximise calculation speed, optimisation, and performance.

The multi-particle simulator internals will be well-documented and extensible to include new physics as observed in the live accelerator. Since it is probably impossible to anticipate all modelling needs ahead of time, some aspects of the accelerator are likely to be included in the online model only after their mechanisms are better understood. This was the experience with emittance growth due to beam-gas scattering at SNS, for example.

Beam envelope simulator

The beam envelope simulator will be the section of the online model that calculates transport properties and dynamics of phase space contours through the accelerator, particularly of the ellipses that represent the extent of a certain portion of the proton beam (e.g. 3 σ contours). It will initially implement linear approximations for all physics of dipoles, quadrupoles, RF cavities, space charge, and other elements of the accelerator, although nonlinear calculations may be added to it in the future if they are determined to be important for observed ESS transport behaviour. The beam envelope simulator will be able to reproduce the expected linear behaviour of the beam through all accelerator elements within a few seconds. The beam envelope simulator will also be benchmarked with other offline simulation computations and measurements as much as possible, particularly with regard to observed beam sizes and aspect ratios at beam imaging instrumentation. The beam envelope simulator will be written in Java to integrate as much as possible with XAL, which is also written in Java. ESS will evaluate the capabilities and performance of the existing XAL beam envelope simulator to determine if it addresses ESS needs as-is, if it requires modest additional code contributions to satisfy ESS needs, or if it should be rewritten completely.

Control room interface to the online model

The user will be able to set the properties of the simulator (initial conditions, strength of the magnets, etc.) through the same interface that he or she uses to control the real accelerator wherever feasible, although it is understood that not all properties will have operational analogues; for instance, one cannot set the initial particle phase space distribution in the operational accelerator. This will reduce the burden of training, by making it possible for the user to understand how to use the model once he or she has been trained to use the XAL interface. The online model and live accelerator controls will present visualisations of the results of common computations in the same way, with a clear, persistent visual indication (perhaps a different background colour) to distinguish displays concerning the live accelerator from those pertaining to the online model. The XAL front-end will be capable of displaying comparisons between various online models, including comparisons to the live accelerator. The online model will be capable of using all the physics algorithms implemented in XAL concerning beam dynamics. For example, XAL contains code to optimise the trajectory of the beam (trajectory steering); the online model will be able to access this code to steer the orbit in the simulator and provide a result of the computation. The online model also will be accessible as an independent tool to perform beam dynamics studies.

Model-driven machine operations

The ESS accelerator is designed to have very high availability, with a baseline machine reliability of 95%. Achieving this reliability requires that machine tuning be as time-efficient as possible. Historically, operators and physicists have performed iterations to a new group of machine settings on the accelerator by hand-tuning a small set of machine parameters, even for an initial iteration. However, a philosophy of model-driven accelerator operations probably will be necessary to achieve a machine reliability of 95%. In model-driven machine operations, the first iteration of tuning to a new configuration of the machine is always preceded by iterative optimisation using the model. Operators who need new machine settings to enact some change, such as retuning after an RF cavity trip or changing delivered beam properties, use the new settings that the model recommends based on these optimisations.

There are two overall goals for model-driven machine operations. The first is to reduce the length of time required both to recover from failures and to set up new configurations. The second is to pursue the continuous development and improvement of the accelerator model of the accelerator so that it becomes continually more realistic, while still providing nearly real-time response for tuning applications and failure recovery. If the model is realistic enough and there are enough tuning redundancies, the ESS failure recovery process may ultimately be automated to minimise downtime and support the 95% facility reliability goal.

Development of an accurate model is an ongoing process, since accelerator facilities like ESS are in a constant state of development and modification. The configurator database will support realistic model development because all significant hardware changes will be recorded and available for use by the model. Improvements in machine/model agreement will come from both sides; hardware repairs will move machine performance towards the model, while inclusion of known errors, such as systematic misalignments or measured BPM electronics offsets, will make the model more closely match the machine.

All feedback loops that go through the beam (e.g. orbit feedback) will have loop coefficients. These coefficients will be routinely monitored and compared to those predicted by the model. A routine set of accelerator studies will characterise the accelerator optics for a given set of magnet currents and RF settings. These studies will then be analysed to provide data to improve the model and locate repairable anomalies in hardware performance. Ideally, machine commissioning will provide a great deal of data to understand and improve the model. However, this will only be practicable after instrumentation has been commissioned and determined to be both reliable and precise enough for direct model comparisons. These studies will be performed on a regular and ongoing basis, to track long-term drift and machine reproducibility, and to measure anomalous behaviour before it impacts accelerator uptime.

Existing accelerator modelling codes

There are a wide variety of accelerator modelling codes available, though no single code presently exists that will serve all ESS source, RFQ, superconducting linac, and operational needs during the design, construction, commissioning, and operation phases of the accelerator. As is described in more detail in Chapter 4, ESS beam physics design has been performed using codes from CEA, including Toutatis for the RFQ, GenLinWin for the superconducting linac, and TraceWin for general particle tracking. Though these codes are suitable for machine design, they are monolithic, proprietary, and comparatively complex and slow. They are thus not suitable for direct use in control system online models. Many of the model algorithms in OpenXAL share a family lineage with TraceWin through their common Trace 3D ancestry, making it quite compatible with ESS beam physics design work. ESS personnel will compare existing OpenXAL code capabilities with TraceWin design results, and will engage in the OpenXAL model development collaboration with a view to addressing conflicts and confirming the suitability of OpenXAL for coding the online model.

Since ESS is SRF-dominated, the RF cavity "multi-gap" is the most important electromagnetic structure in design modelling. This element takes account of particle energy gain between gaps, correcting the dynamics according to the transit time factor in the gap, as in the classic work of Lapostolle and Weiss [533]. Space charge is particularly important in ESS due to the 50 mA design beam current. Space charge is implemented in TraceWin as in Trace3D. The impulse is applied in the beam frame, so before each impulse the beam dynamics coordinates are transformed from the laboratory frame to the beam frame. The kick of a 3D ellipsoidal distribution of particles is then applied, and the frame is restored to the laboratory frame. This procedure can be extended to the cases of coupled or tilted beam to modify the transformation matrix used for the change in the reference.

Space charge is modelled in XAL with a generalisation of the Trace3D model, using homogeneous phase space coordinates. XAL was also adapted for the commissioning of the J-PARC accelerator, making available modified code in which the RF gap model is improved for a bunched beam with large phase spread, as is found in the J-PARC transport line [534], and thus implementing a more reliable function for emittance growth. However, XAL has not been tested in a regime resembling ESS's large-current collective effects. Efforts will be made to baseline this model in OpenXAL in conjunction with SNS.

5.5 Software development environment

The development environment is a system composed of services that ensure a simple and consistent software design and development workflow while enforcing a modular approach through the use of **artifacts**. The unified concept of an artifact encompasses all the, documentation, test plans, images, data files and executable files, that are associated with a given element of a software project [535]. In the ESS development environment, all artifacts will have a predefined directory structure and configuration files which specify the procedure to build the artifact and list all required dependencies. The development environment will consist of several services, providing the rather comprehensive set of functions listed in Table 5.9, which

Service	Functionality
Module design	Module skeleton generation
RPM	Artifact packaging and distribution
Mercurial	Versioning control
Eclipse	Artifact development and testing
Maven	Artifact build system
Artifactory	Maven artifact storage and distribution
Jenkins	Continuous integration and software packaging
jUnit	Unit testing
Bugzilla	Bug tracking

Table 5.9: Development environment service functions.

range from module skeleton generation to version control and bug tracking.

In order for the development environment services to run and interact smoothly, a standard approach must be enforced across developers. ESS will use the Jenkins open source continuous integration tool, which is written in Java [536]. Creating repositories according to set standards will enable the Jenkins server [536] to automatically work without any additional configuration. If any discrepancies arise in the repositories they must be fixed. Packaging also requires a great deal of effort since customised package scripts have to be created for each unit. The standard procedures and services will be described on wiki pages which will offer developers a reliable and publicly accessible source of information. To minimise the possibility of developers not following the standards set by ICS, only ICS-certified developers will have access to all the services of the Development Environment.

Software component organisation

Software organisation will be structured into two layers: Artifacts and RPM packages. Both layers will be designed with a modular development approach in mind. While artifacts will be used for source code structuring, RPM packages will be used for installation and binary packaging purposes. Artifacts will have a predefined directory structure that will determine the way source files are organised. This will allow the Maven project development tool [537] to build artifacts without specific build instructions. RPM packages, on the other hand, will have to be individually prepared for packaging. A specification file will have to be generated to define the files included in the package and the proper installation procedure.

Services

Configuration parameters and values will be stored in a BLED database. Each developer will be able to generate artifact base files from the configuration data of the unit. As is usual practice, artifacts will be added into a private artifact repository. This repository will be administered with the Artifactory repository manager [538], which offers fine-grained permission control that is delegated using a platform-independent web user interface. Version control for each artifact will be accomplished using the Mercurial versioning control system [539], which is built with complex modular system development in mind. Developers will be able to locally commit code multiple times before pushing and merging a stable version of their repository with a public one. The integration of development environment services into the control system is depicted in Figure 5.21.

The continuous integration server will build code only from stable branches of public repositories. It will automatically package the build code into RPM packages which will then be stored in an RPM repository. One repository will be created to hold the nightly built packages, while another repository will be created for the sole purpose of making deployment packages available. The developer will decide when a module is stable enough, and has undergone sufficient testing to be updated in the integration repository, but a release manager will decide when an updated integration package has been tested sufficiently for deployment in the control system. Deployment will be executed using BLED, which will move the package into the suitable repository, thus forcing the relevant units to update.

For each artifact, unit tests will be created using the JUnit framework [540]. The framework will then be used for automatic testing of all the built software, facilitating early detection of bugs. The bug tracking

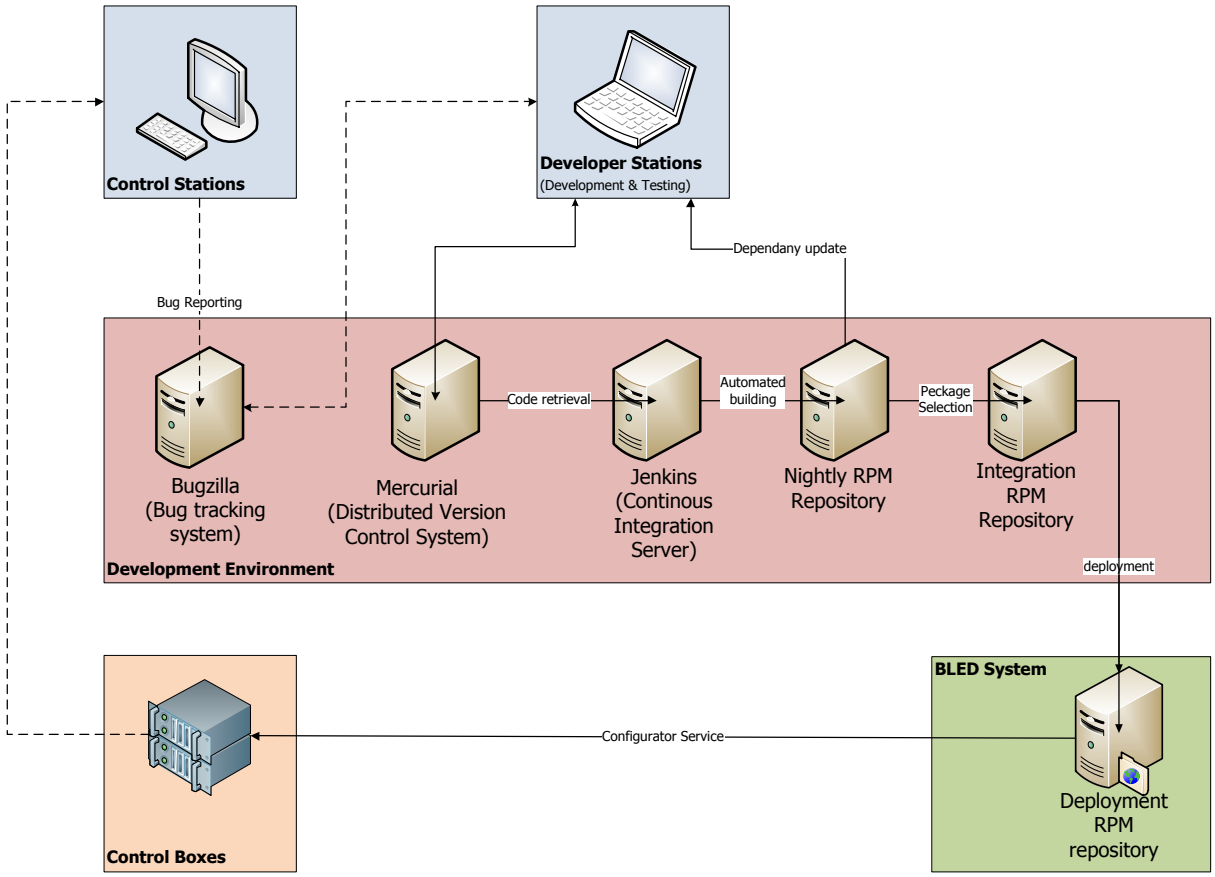

Figure 5.21: Development environment services and their integration into the control system.

system Bugzilla [541] will be used to deal with any bugs that slip by the automatic unit testing regime. With a simple web interface and email notification capabilities, Bugzilla will allow everybody using the control system to report any bugs they find and to receive notifications about bugs identified by other users.

Software development cycle

The software development cycle will join the functionalities of the complete spectrum of development environment services to form a simple yet efficient system. During the design phase, all the system requirements will be gathered, and a project skeleton will be generated, making possible a quick start on the development phase. Development will be an iterative process during which changes will be committed to Mercurial, built with Maven, and then tested. Figure 5.22 provides a schematic overview of this cycle. At the end of each development cycle, after the code has been tested and debugged in order to produce a stable version, the code will be merged in the integration Mercurial branch. This will allow developers to control the distribution of code during deployment and thus reduce the risk of hardware and software malfunctions. Consequently, this will also reduce the work load of testers and of the developers themselves. When a set of newly implemented software needs to be tested, a chosen integration package will be moved into the deployment repository using a BLED tool, which will force the tested unit to upgrade. Tests may be carried out using dedicated test hardware, or may make use of production hardware. All bugs, quirks, and enhancements will be tracked in Bugzilla, providing the people involved with a concise overview of all remaining tasks for each unit.

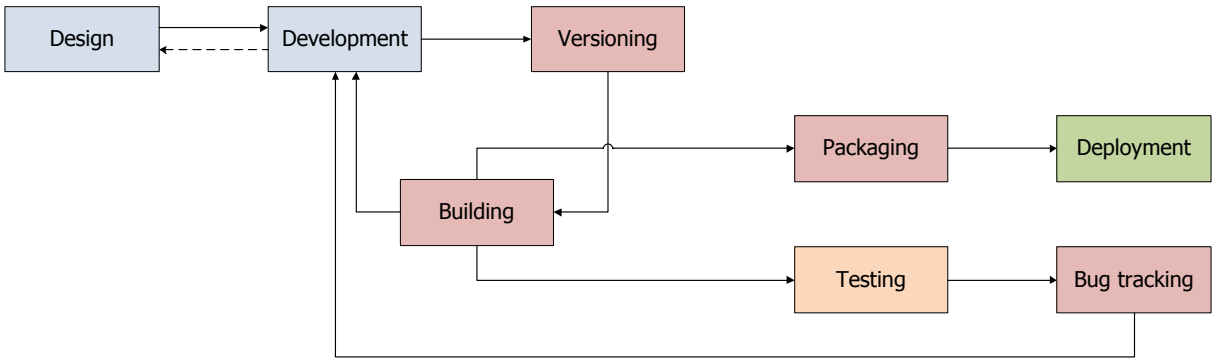

Figure 5.22: The use of development environment services in the software development cycle. The first phase of the cycle is design. During this phase, the control system is broken down into functional units which are defined in detail. When the design is finished, artifact files are generated using BLED and the development phase can begin. During development, code is regularly committed and tested. Bugs are tracked in the tracking system. Once the code is stable, it is packaged and made ready for deployment.

5.6 The human machine interface and the user experience

A control system user is defined to be any person interacting with ICS. User needs will vary depending on their level and area of expertise. Control system users connected with the accelerator and target will be highly-trained ESS staff who are likely to be very familiar with the technical details and development of these systems and associated software. In contrast, the typical neutron instrument user is likely to be a visiting scientist who may be at ESS for as little as one day per year. As a general rule, such scientific visitors will not have participated in the development of the instruments and associated software. They will come from diverse scientific disciplines, ranging from palaeontology to biology, and will also include researchers from the social sciences and the humanities on occasion. ESS's goal is to make it possible for users with little or no neutron scattering experience to operate an instrument, at the same time as it affords more proficient users the opportunity to fully exploit instrument capabilities.

There are significant differences between user interface requirements for the accelerator and target, and requirements for the neutron instruments. The user interface for the accelerator and target will be relatively complete and mature by the time operations begin. On the other hand, the interface for neutron instruments and associated control software will continue to evolve significantly as new instruments are added. Even after all 22 instruments have been installed, the interface will have to respond to ongoing changes and improvements to meet new needs.

ESS is committed to a platform-independent HMI. This requirement constitutes a very flexible and adaptable approach to interfacing users with ICS. The term "station" describes a platform hosting a preset configuration of functionality for each set of user requirements. All configurations will be based on the same basic framework to minimise duplication. This concept enables the human machine interface to ICS to be tailored for a particular type of control system user, ranging from software developer to physicist. The station, with its pre-configured functionality, will provide the software interface between ICS and various applications, as well as a connection point for the interface that scientific visitors will use to control and monitor their experiments. Each station will be responsible for three main tasks: Equipment control, device modelling, and equipment monitoring. The default operating system for stations will be Linux. Since all hard real-time tasks will be handled in dedicated hardware, a non-real-time Linux kernel will be used. Stations and control boxes will use the same Linux distribution.

5.6.1 User roles and profiles

While some characteristics are common to all types of control system users, a detailed classification of users into several roles with different profiles will improve the user experience and minimise the risk of accidents and mistakes. ESS will assume that all control system users are able to read in English, and all user interfaces will be in English. At the moment of writing, there are no plans to adapt any part of HMI for other languages. CS users who prepare automated tasks will be assumed to have a basic understanding

of ICS's scripting language, including of the composition of simple user interfaces. However, they will not be assumed to have mastered advanced topics such as concurrency, networking and asynchronous communication.

Operator

Operators will be responsible for operating the facility so that it carries out scheduled scientific plans. They will also be in charge of monitoring the facility, reacting to deviations from nominal behaviour, and providing periodic operations reports to management. Operators will work in shifts, as the facility will operate around the clock, seven days a week. At the end of the shift, the operator will hand over his or her work to an operator in the following shift, assuring continuity across shifts. The number of operators per shift and in total has not yet determined, and will depend on the exact design of the facility. Multiple operators (about a third of the total) will use ICS concurrently during any given shift. Operators will perform most of their work from the main control room. They will attend one of the control room stations at almost all times during their shift. While an individual operator may be away from a station for periods of several minutes at a time, at any given time, at least one operator will be present at or near a station. Operators will generally work at the facility for a number of years, and they will be trained to master the concepts of operating the facility. However, they will not be expected to master all operations procedures, or to be familiar with all possible conditions of the facility.

Accelerator physicist

Accelerator physicists will have a thorough understanding of the accelerator. They will be particularly active during facility commissioning, during the implementation of new operational modes or major beam tuning activities, and during the commissioning of new instruments. Accelerator physicists will often need to correlate diagnostics data with machine settings in order to improve their understanding of the machine's behaviour. At any given time, several, or perhaps half a dozen, might be expected to be using ICS concurrently. Accelerator physicists will perform their work in the control room or at workstations located on the ESS computer network. Most accelerator physicists will work at the facility for a number of years, although some will be short-term or part-time employees or guests. Accelerator physicists will be familiar with the principles underlying the design and operation of the facility, including the concept of online models. They also will have an in-depth knowledge of an applicable field of physics.

Engineer

Engineers will be in charge of commissioning and maintaining ESS's technical systems. Technical systems include all types of equipment, whether it can be controlled over the ICS or not, and the ICS itself. Engineers will interact most intensely with the facility when subsystems experience failures. While problems usually will be identified first by an operator, it will be the engineer who will have to resolve them. Engineers will also be responsible for ensuring that equipment is accessible over ICS. This includes ensuring physical connectivity to ICS, installing appropriate drivers, configuring ICS to register equipment, and specifying translations from engineering to physical units (calibration). Engineers will view the facility at the level of installed equipment, rather than at the level of higher-level abstractions such as devices or systems. Engineers will need efficient tools to pinpoint pieces of equipment experiencing failures, and to access detailed low-level diagnostics.

The number of engineers has not yet been determined, but several of them might be expected to be using ICS concurrently at any given point in time. Engineers will perform part of their work in the control room or at workstations connected to the ICS network. Engineers will also often need to physically access the equipment. At the point of physical access, they may use mobile terminals to gain access to devices either via ICS, or directly. Most engineers will be employed at the facility for a period of years. However, some engineers will be present on the site only to commission specific pieces of equipment for which they are responsible. Engineers will be highly skilled in their area of expertise (electrical engineering, mechanical engineering, etc.). However, they will not be expected to be familiar with the concepts of operating the ESS facility. They will not be expected to memorise physical location, configuration settings and models of equipment.

Neutron researcher

Neutron researchers will use ICS to request a neutron beam meeting specified parameters at the site of their experiment. As the beam is delivered, ICS will notify the experimentalist, and will provide information about the beam's actual parameters. Some, but not necessarily all, experimental equipment may be under ICS control. Researchers will interact with ICS through the integrated software solution discussed in Section 2.8. The number of experiments and researchers will vary over time. Neutron researchers will work in one of the satellite control areas at a workstation (possibly their own portable computer) connected to the ICS network. Most experimentalists will work at the ESS facility for a relatively short period of time, typically lasting several days to several months. Experimentalists will be highly skilled in their area of expertise. However, their familiarity with the ESS facility will often be limited, and it would be impractical to require them to master low-level details of the facility in order to carry out their experiments. Researchers who wish to automate their experiment will be required to be familiar with a standard scripting language, as well as with the high-level application program interface for interacting with ICS.

5.6.2 High-level application program standards

Users will need a variety of high-level application programs to help them with their tasks. Many of these applications will fall outside the scope of ICS, but a minimum set of requirements will be set by ICS for such applications. ICS documentation will provide a wealth of information regarding the signals and various other parameters available for such applications. Only ICS-certified developers will process high-level applications through the development environment.

The device approach will form the basis for the high-level application standards that ICS will establish. In accordance with this approach's main principles, equipment connected to the control system will be modelled and presented to high-level applications as device-objects with properties. It will be possible to configure stations using predefined device-objects representing the controlled equipment. For all high level applications, the access point to equipment will be the device-object, and configuration of device-objects will be the responsibility of ICS. Device modelling will provide equipment abstraction according to the needs of the higher layers of the control system. It will allow the representation of a piece of equipment by multiple device-objects, and will also permit the representation of several pieces of equipment that form a logical unit by one device-object. In general, flexible combinations between pieces of equipment and device-objects will be possible. Device modelling will be able to use combinations of several pieces of equipment and other device-objects as its building blocks.

High-level applications will enable users to monitor and control equipment in the facility. They will run on one or more stations. The application layer infrastructure will support plug-in architecture, making it easy to add blocks of functionality to the system without having to rebuild the entire application, while at the same time enabling all plug-ins to live within the same process and share data and network connections. Multiple perspectives, that is, distinct arrangements of user interface elements to define task-oriented workspaces, will be available. They are described in more detail below. A consistent look and feel across applications will lower the learning curve for users and will also make it possible for developers to share common components. The behaviour of buttons and other user interface elements associated with specific actions, such as tool bar and menu items, will be standardised across applications. User preferences will be stored centrally, and will persist across time and work stations. A help system will offer contextually-based assistance associated with user interface elements. Applications will give users the ability to access both ICS services and device-objects.

The user interface will be consistent in terms of colour usage (e.g., alarm colour-coding), fonts, graphical symbols and icons, keyboard shortcuts, terminology in textual messages and user interface element layout [542]. The various parts of the user interface will be capable of exchanging information with each other through standard mechanisms such as drag-and-drop. Data exchange with external programs (for example, the exchange of tabular data) will also be possible. Applications will be able to execute lengthy tasks in the background so that they do not block the user interface. Instead, the user interface will provide a progress bar and a "stop" function, while allowing the user to continue using the rest of the application. Every action that a user triggers which takes more than 1 s to execute, will be accompanied by an on-screen indication that the action is "in progress". When problems arise with the user interface, it will not crash. Instead, it will report the condition to the user, and log it in a central logging system.

It will give the user an opportunity to save data and restart the application gracefully. Applications will enable users to view and generate various types of charts, including histogram and correlation (value versus value) charts. Charts will be able to display several data sets simultaneously, with different colours, area fills, and symbols. There will be a zoom feature, and textual readout of value(s) at the mouse location.

Sets of applications will be offered through a variety of perspectives, each tailored to different user needs. Each perspective will be able to host several views, each presenting a specific kind of information (e.g., a property-value table, synoptic display, control panel or chart). Specific perspectives are listed below.

1. The supersystem perspective, focusing on the status of the instruments, target or linac as a whole;
2. The beam perspective, focusing on one of the neutron beams or the proton beam;
3. The engineering perspective, facilitating access to components' low-level engineering interfaces;
4. The supervision perspective, providing an overview of interlocks and other alarm conditions;
5. The design perspective, for use during the design of macros, scripts and custom user interfaces; and
6. The management perspective, for supervision of control system infrastructure, providing information about the status of computers, CPU load, available memory, network utilisation, etc.

Scripting language and a macro mechanism with basic flow control will be part of ICS. High level applications will be implemented in such a way that their functionalities can be used by the macro mechanism. Scripting will be textual. It will be constructed to be simple to learn and extensible. An off-the-shelf interpreted language, such as Python or Perl, will be used for macro scripting.

Chapter 6

Specialised Technical Services

Chapter abstract

Summary: This chapter describes three specialised technical systems: the cryogenic system, vacuum system and test stands. These systems support all three areas of the ESS facility: accelerator, target and experiments. The system designs are conservative and based on experience at other facilities such as CERN, SNS and CEA Saclay. Issues such as the determination of safety factors for the cryogenic system capacity as well as the availability and sustainability of the cryogenic system are also discussed.

The cryogenic system consists of: the linac cryoplant that provides cooling for cryomodules; the test and instruments cryoplant that provides cooling for test stands and liquid helium for instruments; the target cryoplant that provides 16 K helium cooling for the target hydrogen moderators, and the distribution system that connects the linac cryoplant to cryomodules. The linac cryoplant and test/instrument cryoplant share common gas management and storage systems. The target cryoplant system is completely separate due to potential for tritium contamination. The cryogenic systems have been designed to meet sustainability goals through measures such as He conservation and heat recovery.

The vacuum system provides vacuum for the linac beam line, target system and instrument lines. It uses well-established technology and procedures based on experience at similar facilities, including SNS, JLab, J-PARC and LHC, and has low technical risk.

Test stands provide testing and validation of both RF equipment (klystrons and modulators) and cryomodules. Cryogenic connection to cryomodules in the test stands will prototype similar connections in the linac tunnel. The test stand programme accommodates the unavoidable uncertainty in the ESS construction schedule by allowing for RF equipment testing in a temporary location if necessary. Cryomodule testing will be carried out at the ESS site. All cryomodules will be tested at nominal temperatures and RF power levels before tunnel installation. Cryomodule testing will take place at two locations. The Uppsala test stand will test prototype and series production spoke cryomodules. The Lund test stands will test all elliptical cryomodules, and will retain the capability to test spoke cryomodules.

6.1 Cryogenic systems

The cryogenic system is the largest of the specialised technical systems and can be further divided into four subsystems: the linac cryoplant, the target cryoplant, the test stand and instruments cryoplant and the distribution system. The linac cryoplant will provide all the cooling to the 59 cryomodules containing the superconducting RF cavities. The target cryoplant will provide cooling to the 20 K hydrogen in the moderators surrounding the target. The test stand and instruments cryoplant will serve two purposes. It will produce liquid helium (LHe) for distribution in transport Dewars to instruments along the experimental beam lines, and it will provide cryogenic refrigeration to the cryomodule test stands. The main distribution system will provide the cryogenic and warm gas connections between the linac cryoplant and the cryomodules. A smaller distribution system will connect the test stand and instruments cryoplant to the cryomodule test stand. ESS will build this smaller system first and it will serve as a prototype for the main distribution system. The linac cryoplant and test stand and instruments cryoplant will share a common helium recovery, purification and gas handling system. They will also share a common helium gas storage facility. Separate LHe storage Dewars will be provided for these two plants. Due to the possibility of tritium contamination and to allow operational stability of the quite distinct cryogenic processes, the target cryoplant will be completely separate from the other two cryoplants. It will contain its own gas storage system, and will be linked to the target by a separate distribution line. Figure 6.1 is a high-level block diagram showing the ESS cryogenic system and its connections to other ESS components.

The cryoplants and distribution system will be controlled by a programmable logic controller (PLC)-based system which, in turn, will communicate with an EPICS-based Human-Machine Interface. The EPICS system will link the PLCs of the cryoplants and distribution system and allow operator control, data logging, trending and alarms. The detailed accelerator control structure is still under development and lower level connections, in particular between the distribution system and linac cryoplant PLCs, may

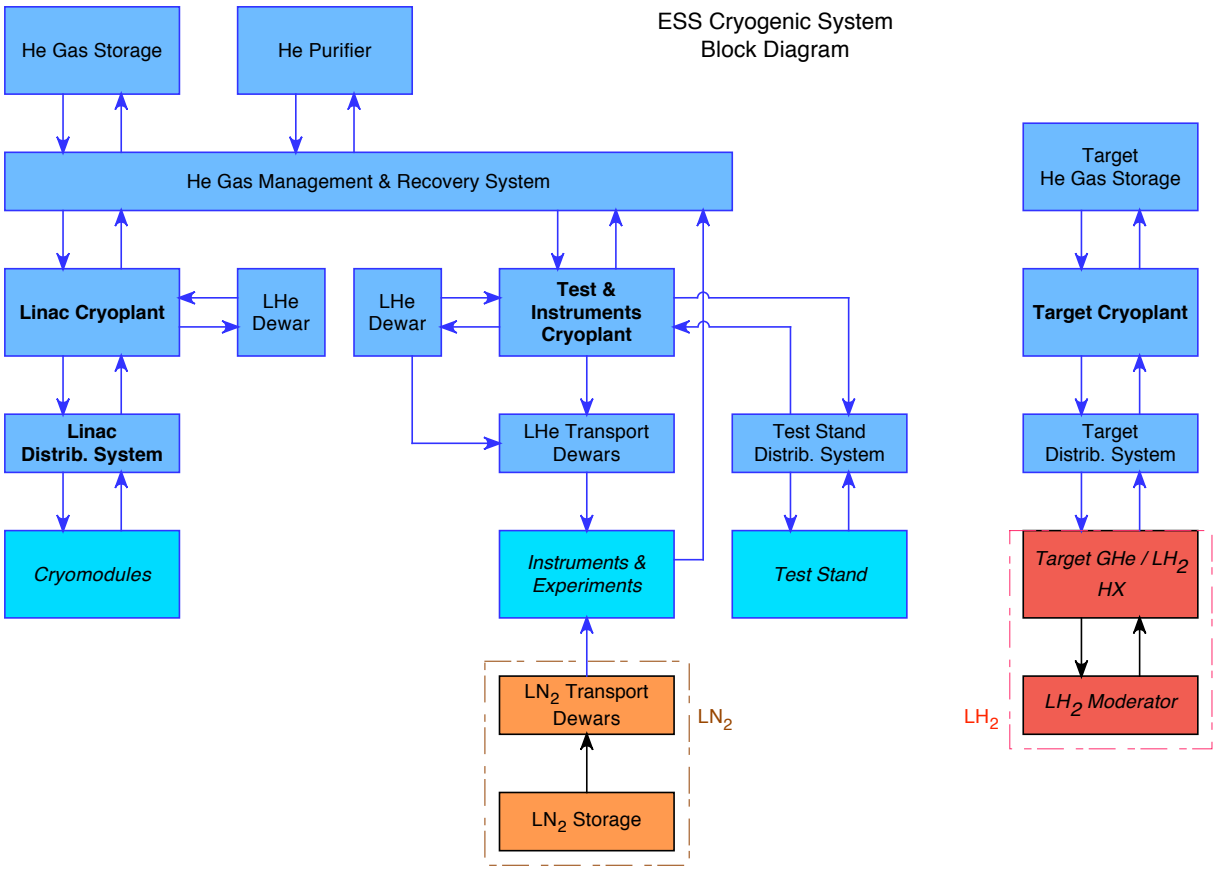

Figure 6.1: Block diagram of the ESS cryogenic system.

be necessary. Outside cryoplant vendors will produce the cryoplant control systems, up to and including the PLC level. ESS will produce detailed technical specifications for these systems, including guidelines for the standardisation of PLC hardware and data structure. ESS-vendor contracts will require vendors to provide all documentation and source code for their control systems. The integrated controls system (ICS) project will specify the details of the interface between the vendor-supplied PLC systems and the ESS controls systems. The ICS will create the EPICS controls as well as the entire control system for the distribution system. Private industry will produce all three cryoplants and the cryogenic distribution system in accordance with ESS performance specifications. The installation and commissioning of these systems will be a shared responsibility between the vendors and ESS.

One of the unique aspects of the ESS project is the attention paid to energy conservation and sustainability. A number of aspects of the cryogenic system reflect this priority. Superconductivity makes ESS possible. Without the use of superconducting RF structures, the energy costs of accelerating the proton beam would be excessive. Superconducting systems require cooling to cryogenic temperatures, which in itself requires energy. ESS attempts to minimise the energy costs of the cryogenic system by: designing the system to minimise the amount of cryogenic cooling required; specifying efficient cryogenic refrigeration plants and recovering as much of the heat removed from the cryogenic system as practical. Techniques to minimise the amount of cooling required include: the use of welded pipe connections rather the more easily demountable but higher heat leak bayonet connections; and the selection of cryogenic plant options (such as a final stage of warm compression for the sub-atmospheric pressure helium lines) that allow easier reduction of cryoplant capacity and minimise the need for active heaters to keep the cryogenic load constant. The linac cryoplant will be specified to operate at about 26% Carnot efficiency, which is in the upper range of possible cryogenic plant efficiency.

The most innovative aspect of the ESS cryogenic system regarding sustainability is the recovery of the heat produced by the warm helium compressors for reuse in the Lund District Heating System. ESS uses a significant amount of helium gas, also a limited resource. The cryogenic systems are designed to be closed cycle, recovering and reusing most of the helium gas. Only in certain abnormal operating conditions will helium be vented to the atmosphere.

Availability refers to the fraction of time that the ESS cryogenics system is able to provide the cooling required. If the cryogenic system is not functioning properly, ESS cannot deliver neutrons to researchers. Thus, a very high availability for the cryogenic system is required. There is significant experience in the operation of large He II cryogenic systems. Properly designed and operated, such systems can achieve availabilities of greater than 98%. There are a number of features in the proposed cryogenic system design that are chosen to help increase availability. Availability is aided by the separation of the more dynamic test stand cryoplant from the linac cryoplant, which will operate at more constant loads. Thus, an unexpected event in the test cryoplant due to an R&D test won't impact the linac operation. Availability of liquid helium for the instruments is increased by the planned LHe storage, which will allow the instruments to operate for a number of days with the target plant shut down. The availability at the individual cryoplant level is helped by the presence of backup helium compressors that can be brought on line quickly in the event of a compressor failure, as well as by the presence of backup control power and backup instrument air supplies. Given the large amount of power required, the primary compressor power wont have a backup, so a site power outage will shut down the cryogenic systems. However, such outages are quite rare in the Lund area.

6.1.1 The linac cryoplant

The linac cryoplant is the largest of the cryoplants and provides cooling at three nominal temperature levels: 40 K to 50 K for the thermal shields of the cryomodules and distribution system; 4.5 K for the power coupler thermal intercepts and 2 K for the SRF cavities. The linac consists of 59 cryomodules operating at 352.21 MHz for the spoke cavities and 704.42 MHz for the elliptical ones. The ESS cryomodules are individual cryogenic units and are cooled in parallel by the cryogenic distribution line. Details of the cryomodule design may be found in Chapter 4. Figure 6.2 is a flow schematic showing typical flows and connections between the distribution line and a cryomodule. Applying lessons gleaned from the experience of other accelerators such as SNS [543], the cryoplant will supply 4.5 K helium at 0.3 MPa to the cryomodules. The actual production of saturated 2 K He II will occur at each individual cryomodule. This approach is thermodynamically more efficient (it minimises the heat leak to the 2 K level) and limits the possibility of two-phase flow in the distribution system.

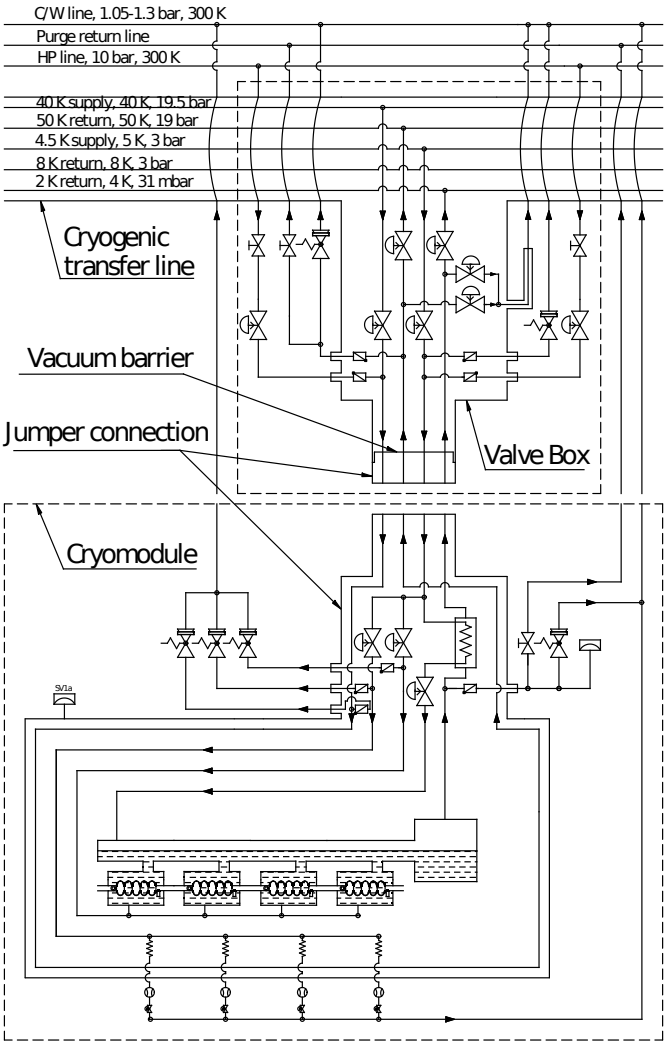

Figure 6.2: Schematic of the helium distribution system of the linac, including fully segmented cryomodules. As an example, a high beta elliptical cryomodule is shown.

To produce the 2 K temperature level in each cryomodule, incoming helium, at temperatures varying from 4.5 K to 5 K along the length of the distribution line and at a pressure of 0.3 MPa, will be pre-cooled by the subcooler to 2.2 K before entering the Joule-Thomson expansion valve. The remaining enthalpy difference by evaporation of helium will be 20 J/g. An overall heat load to the 2 K temperature level of 40 W results in a mass flow of 2 g/s. Choosing the optimum temperature for the cavity operation is essential for the overall efficiency of the cryogenic system. ESS needs to determine if it is true that a reduction in the temperature of the superfluid helium bath to 1.8 K would increase the Q-value of the superconducting cavities by a factor of around 1.5, which would more than compensate for the increased cryogenic effort of providing helium at 1.64 kPa instead of 3.1 kPa saturation conditions. A temperature below 1.9 K, which is the temperature at which superfluid helium reaches its peak heat transfer capability, would avoid thermal run-away at localised hot spots on the cavity surface [544, 545].

The low pressure He gas must be pumped away from the 2 K saturated baths surrounding the cavities and returned to the cryoplant. In plants of this size, there are two options for such a pumping system. One relies solely on cold compressors; the other employs a set of cold compressors followed by a final stage of warm compression. The cryogenic heat load at 2 K in the ESS accelerator will be roughly two-thirds dynamic, resulting from cavity and beam heating, and one-third static heat leak from warmer temperatures. Thus, it is desirable for ESS to use the pumping system that makes it easiest to reduce the 2 K plant capacity when the dynamic load is reduced. The alternative approach of using electric heaters to mimic the dynamic load for a significant length of time is counter to the ESS project goals of energy

efficiency and sustainability. The 2 K capacity may be more easily reduced using a mixture of cold and warm compression for the low pressure He pumping system and this is the approach selected for the linac cryoplant. This approach, which CERN uses in the LHC plants [546], also allows for an easier restart of the 2 K system after a system upset.

Each cavity is equipped with an RF power coupler whose outer conductor is flanged to the 2 K cavity surface. The power couplers need to be cooled by a controlled flow of supercritical helium that warms up from 5 K to around 150 K towards the warm end of the power coupler and returns back as ambient-temperature gas to the linac cryoplant. The appropriate mass flow is regulated at ambient temperature with a flow controller in the return connection at each power coupler. The distribution system will deliver He to the cryomodules for coupler cooling at 0.3 MPa. The current coupler design calls for an operating pressure of 0.14 MPa. That reduction in pressure must be accomplished inside the cryomodules.

Helium gas will be used at supply conditions of 1.95 MPa at 40 K to cool the thermal radiation screens. It will return to the cryoplant at 1.9 MPa and 50 K. This thermal shield will act as a heat sink at 40-50 K for instrumentation wires and support structures as well. Lowering the temperature of the thermal screen from typical values of 50-80 K to the average temperature level of 45 K makes possible a simplified design of the cryomodule without a separate 5 K thermal radiation screen [547]. The ESS Cryogenics Group will further optimise the temperature and pressure specifications for the shield circuit helium as part of the development of the specification of the overall linac cryoplant.

A cool-down line connected at the cryomodule connection box to the 4.5 K helium supply line will achieve the cool down of the whole cryomodule. To guarantee the required temperature gradient along a cryomodule and the required time-temperature history of the cold mass itself, a specified flow rate will be mixed in the valve box, using the cold helium supply on the one hand and the ambient temperature helium gas from the warm-up line on the other hand. For an effective cool-down procedure, this cool-down line will be connected to the bottom of each cavity enclosure. The same line will be able to conduct a warm-up procedure for the whole linac in a fast and uniform way with a helium gas flow of increasing temperature. Because part of the cavity cooling circuit operates at sub-atmospheric pressures, a guard system is required to protect against leakage of outside air into the pure helium gas system from the outside. Therefore all seals of safety relief devices in these circuits, as well as the shaft sealing of cryogenic valves, will be connected to a helium guard system, which will surround these non-welded connections with a pure helium gas atmosphere. The saturation pressure for a 2 K superfluid helium bath is 3.13 kPa. The adjustable J-T valve will create the pressure step and regulate the level in the two-phase pipe. For a given heat load to the 2 K cold mass, the appropriate helium flow rate will be set in this circuit. The return part of this circuit will start with the low-pressure pipe connected to the two-phase pipe in the cryomodule. The overall drop in pressure in the vapour low pressure (VLP) return part of the cavity cooling circuit, including the heat exchanger in the cryomodule, will have to be smaller than 0.25 kPa.

The specific cryoplant cycle design will be produced by the vendor ESS selects to provide the plant. Nonetheless, Figure 6.3 shows a generic schematic of the major components of the linac cryoplant. Determining the capacity of the linac cryoplant requires a detailed analysis of all the possible heat loads. The dynamic and static heat loads have been estimated for the cryomodules described in Chapter 4, and for the distribution system. These estimates are based on current understanding of the designs and on the expected performance of cavities and couplers. The dynamic loads (RF and beam loss) have a built in safety factor as they assume conservative performance of the cavities and the maximum acceptable beam load. During 2013, these estimates will be refined as the designs are developed. By September of 2013, formal technical notes on the cryomodule heat load and the distribution heat load will be prepared by the responsible groups. These will serve as an input into the final sizing of the Linac cryoplant. Both the heat load analysis and the proposed plant sizing will be peer reviewed by external experts in September 2013. This approach will provide plant sizing information in sufficient time for the specification of the Linac cryoplant in 2014. A current estimate, sufficient for costing and planning, is 1724 W at 2 K, 1223 W at 5 to 8 K and 7872 W at 40 K. There is also expected to be an 7.2 g/s liquefaction load at 4.5 K for coupler cooling. These numbers do not include any safety factor except for those associated with the cavity dynamic loads and with beam heating. The determination of the appropriate safety factors is discussed in Section 6.1.5. A cryoplant of this size is similar to those used at the JLab 12 Gev Upgrade [548] and at the LHC [546]. Such a cryoplant, while certainly a custom order, is well within the current state of the art.

The inventory of liquid helium for the cold part of the linac, including the distribution system, will be 12,000 l. Gaseous helium storage at ambient temperature will keep the helium inventory at the discharge

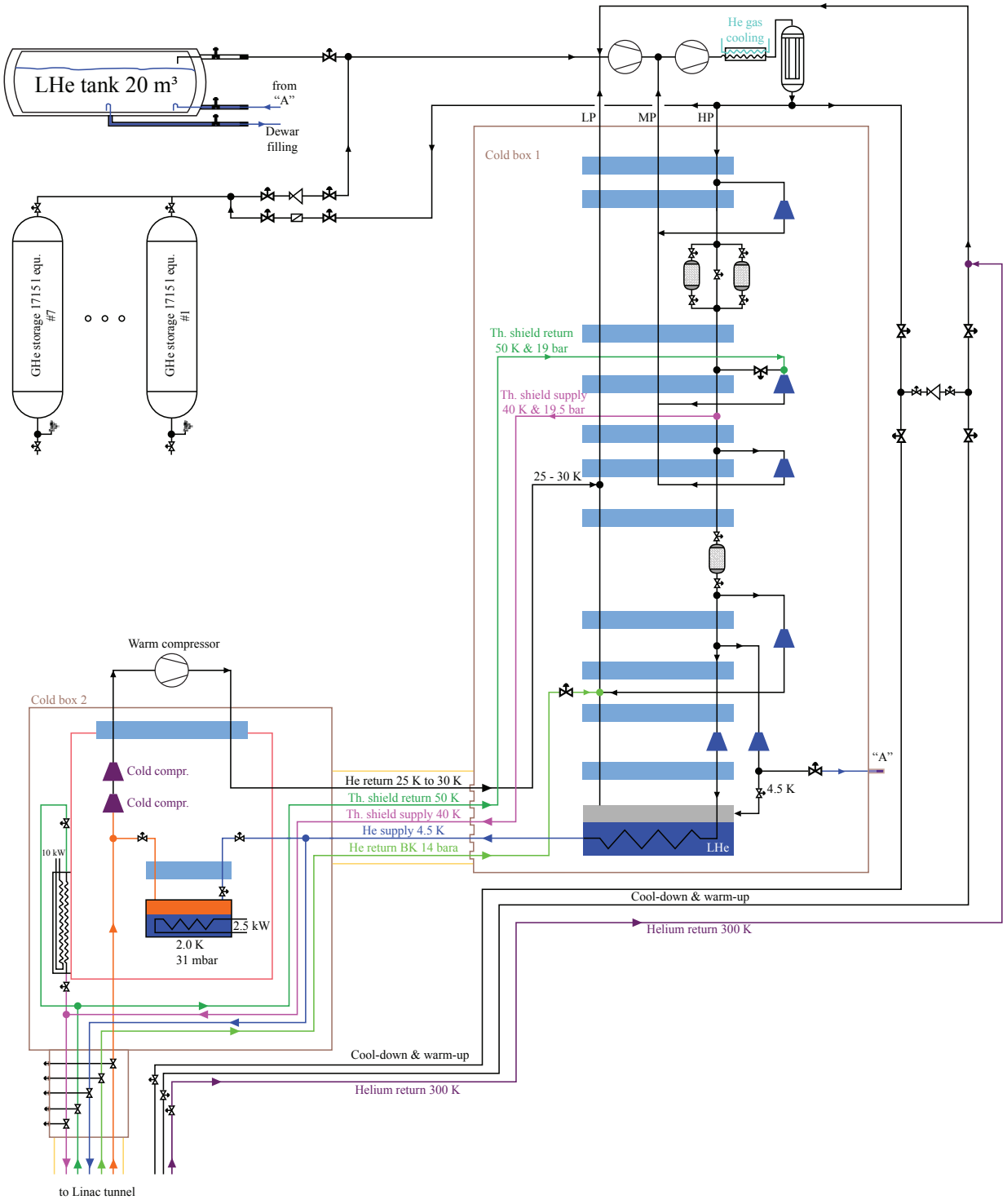

Figure 6.3: Generic schematic of the linac cryoplant.

pressure of the cryoplant compressors, which is 2 MPa. Seven cylindrical gas tanks with a diameter of 3.7 m and a length of 10 m will be sufficient to store the necessary amount of helium gas, since one of these tanks can store an equivalent amount of 1,750 l liquid helium. The exact size and number of tanks will be determined by ESS in consultation with potential vendors. Additionally, a liquid helium storage tank of 20 m^3 will be installed to store helium for a second fill and to compensate for helium losses during operation. The Linac Cryoplant will share gas storage and management with the Test Stand and

Instruments Cryoplant.

6.1.2 Test stand and instruments cryoplant

This cryoplant will serve two functions. During ESS operations, the test stand and instruments cryoplant will provide liquid helium to the various instruments along the neutron beam lines. The number, type and position of the instruments requiring LHe will change over the lifetime of ESS. This feature, along with the relatively small LHe requirements for a single experiment, has led the ESS Cryogenics Group to select delivery of LHe via portable Dewars rather than through a dedicated distribution system. There will be a dedicated room temperature return header along all the neutron beam lines to collect the He gas from the instruments. This gas will be returned from the instruments to the cryogenics building, where it will be purified and returned to gas storage. This system will reduce helium losses during normal operations to the absolute minimum.

Estimates have shown that the nominal instrument requirements for LHe is 17 l/h with an expected peak rate of 35 l/h. In order to allow for uncertainties in instrument LHe needs, and to compensate for possible degraded operation of the plant, the test stand and instruments cryoplant will be sized to liquefy at least 50 l/h. This cryoplant will also include a 5000 litre LHe storage tank that will create a buffer volume to compensate for unexpected plant shut downs and to supply unexpected peak needs. The instruments are also expected to require up to 200 l/h of liquid nitrogen (LN_2). This will be provided by on-site storage filled by an external vendor on a regular basis. In order to limit the number of refills, a total of 50 m^3 of LN_2 storage, divided among several Dewars, will be provided. Once used by the instruments, the nitrogen gas will be safely vented into the outside air.

The second function of this cryoplant is to provide cryogenic cooling for the cryomodule test stands. Each of the 59 cryomodules will be tested under full RF and cryogenic operating conditions prior to installation in the ESS tunnel. Based on the current ESS schedule and cryomodule production rates, the Cryogenics Group has determined that three test stands will be required: one dedicated to the spoke cryomodule testing and two dedicated to the medium-β and high-β cryomodules. In order for the results of the testing to be unambiguous, the cryoplant should provide refrigeration at the same temperature levels as will be used in the operating linac. Thus, the cryoplant must provide cooling at 40 K, 4.5 K and 2 K. As in the case of the linac cryogenic system, the cryoplant will provide helium at 4.5 K and 0.3 MPa to the cryomodules and the conversion to 2 K saturated He II will take place inside the cryomodule. The connections to the cryomodules on the test stands will have the same design as those in the linac tunnel. This will allow early validation and experience with the linac distribution line design. One issue that is yet to be resolved is the method by which the sub-atmospheric-pressure helium is pumped off the He II bath in the cryomodules under test. This may be accomplished by a set of cold compressors or by a set of room temperature vacuum pumps. The final choice will be made during the design and specification phase scheduled for completion by mid 2013. Regardless of the choice made, all helium pumped off the 2 K baths will be recovered, purified and reused.

The refrigeration capacity of this plant at the various temperature levels is based on the worst-case assumption that ESS will have to operate all three test stands simultaneously under full RF power. The resulting plant has a 4.5 K equivalent capacity of 500 W to 600 W. A plant with this refrigeration capacity can easily be designed to operate as a liquefier producing the 50 l/h required. Even after ESS begins operating, there will still be a need for some cryomodule testing to support both the repair of cryomodules and the development of upgraded cryomodules. The test stand and instruments cryoplant will be designed to meet both this need and the instrument liquid helium needs. The test stand and instruments cryoplant will be located in the cryogenics buildings, along with the linac and target cryoplants and adjacent to the cryomodule test stand area. The instrumentation and test cryoplant will be the first of the ESS cryoplants to be procured, installed and commissioned. As such, it will provide valuable experience and training for the ESS cryogenics team.

6.1.3 Target cryoplant

A key feature of the ESS target will be the hydrogen moderators, which will use hydrogen at 20 K and 1.5 MPa to reduce the energy of the neutrons before they reach the instrument lines. The neutrons will deposit significant amounts of energy into the hydrogen that will have to be removed to maintain the hydrogen at its nominal operating temperature of 20 K. The target cryoplant will provide the cooling for

the hydrogen moderators. The heat deposited into the hydrogen will be removed via a heat exchanger that will transfer the heat from the hydrogen circuit to a gaseous He circuit operating at 16 K which is connected to the target cryoplant. Both the helium and hydrogen circuits will be closed loops and will be separated from each other. Only heat will transfer between them. This approach is similar to that used for the LH2 moderators at SNS [549] and J-PARC [550] as well as in larger hydrogen target experiments [551]. The design and procurement of the hydrogen moderators and associated hydrogen circulation loops, including the helium/hydrogen heat exchanger, is provided as part of the target system described in Chapter 3. Current analysis shows that the required capacity of the target cryoplant is 25 kW at 16 K, without including a safety factor [552]. Due to the helium circuits proximity to the target, there is the possibility of tritium contamination in the target cryoplant. ESS will manage this risk in two ways. First, the target cryoplant will be completely separate from the other cryogenic systems, with its own He gas management and storage systems. In addition, the target cryogenic plant will be designed to prevent the automatic venting of helium at warm-up.

6.1.4 Distribution system

Figure 6.4 shows how the linac cryogenic distribution system starts at the connection boxes of the linac superconducting RF cryomodules and moves out through the cryogenic transfer line (CTL) to the linac refrigeration plant, hosted in a common cryoplant facility at the high-energy end of the linac. Key design features of the distribution system are:

- All cryogenic supply and return lines will be placed in one common, vacuum-jacketed cryogenic transfer line, the diameter of which will mainly be determined by the VLP helium return pipe.
- An intermediate temperature thermal shield, operating at the same temperature as the cryomodule shields (40 K/50 K), will be included in the CTL, valve box and jumper sections.
- Each cryomodule will be connected to the cryogenic transfer line via jumper connections with a U-shape design. Cryogenic valves situated in a vacuum-insulated valve box will allow the separation of single cryomodules from the cryogenic transfer line.
- The jumper sections will be welded connections within a common vacuum jacket rather than separate bayonet connections.
- The system will allow individual warm up and cool down of a cryomodule, while keeping the rest of the system at cryogenic temperatures.
- A vacuum barrier in the jumper connection will separate the vacuum of the transfer line and the individual cryogenic insulation vacuum of the cryomodules.
- High-pressure helium gas will cool the thermal radiation shields. This temperature level additionally serves as a first level of heat interception.
- Supercritical helium will be supplied in a second circuit feeding the superfluid helium cooling of the superconducting cavities. The supercritical helium flow will be pre-cooled in a 2 K subcooler at each cryomodule. A cool-down line, bypassing the precooling heat exchanger, will connect to the supercritical supply line as well.

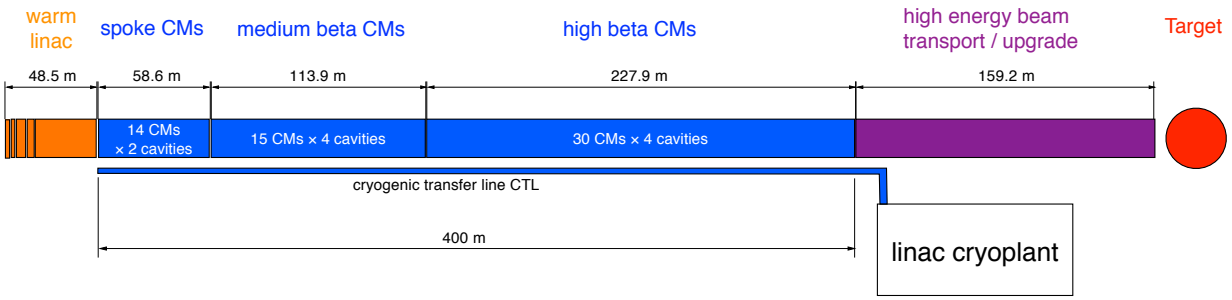

Figure 6.4: Schematic of the linac cryogenic distribution system.

- The pressure drop in the precooling heat exchanger in each cryomodule should be smaller than 0.1 kPa at the low-pressure vapour side, while sub-cooling the incoming helium flow to a temperature below 2.2 K.
- The acceptable pressure drop in the VLP line mainly determines the pipe dimension of the cryogenic transfer line. The maximum allowable pressure drop in the vapour helium return system at the 3.1 kPa pressure level is 0.25 kPa over the whole length of the 450 m VLP line.
- A part of the supplied supercritical helium will be used for cooling the RF power couplers. The flow will warm up to 150 K cooling the power coupler and will return to the cryoplant at ambient temperature.

The design of the CTL assumes that all cryogenic elements in the linac will be cooled using one cryogenic plant, which will be located at the high power end of the linac. The schematic of the CTL in Figure 6.2 shows the interconnection of the CTL with a typical cryomodule. The allowable pressure drop for the heat exchanger on the vapour return side is 0.1 kPa. This sets the limit for the pressure drop of the VLP return pipe and the jumper connection to less than 0.15 kPa. The major influencing parameter of the cryogenic transfer line is the necessary diameter of the VLP return pipe. On one hand, there is a cross section restriction on this big-diameter pipe that determines the vacuum enclosure pipe that finally needs to fit in the tunnel layout. On the other hand, there is a limited margin of permissible pressure drop for the 450 m long cryogenic transfer line on the order of $\Delta p < 0.15$ kPa. Figure 6.5 shows the accumulated heat load versus length of the gas return pipe starting from the spoke cryomodules towards the cryoplant.

The heat load to the 2 K cavity circuit is 1.9 kW directly in the cryomodules. Additionally, there is a heat load to the supply helium in the CTL and to the jumper connection and interconnection boxes. The CTL heat load is reduced as much as possible by introducing an 8 K return line, which lifts the majority of the heat load to the 5 to 8 K temperature level. Therefore the accumulated heat load at the cryoplant side of the CTL adds up to 2.1 kW, as shown in Figure 6.5. A pressure drop calculation of the sub-atmospheric pressure vapour flow determines the overall pressure drop to be 0.1 kPa for an inner pipe diameter of 260 mm, for example. At each cryomodule connection, the flow coming from the cryomodule

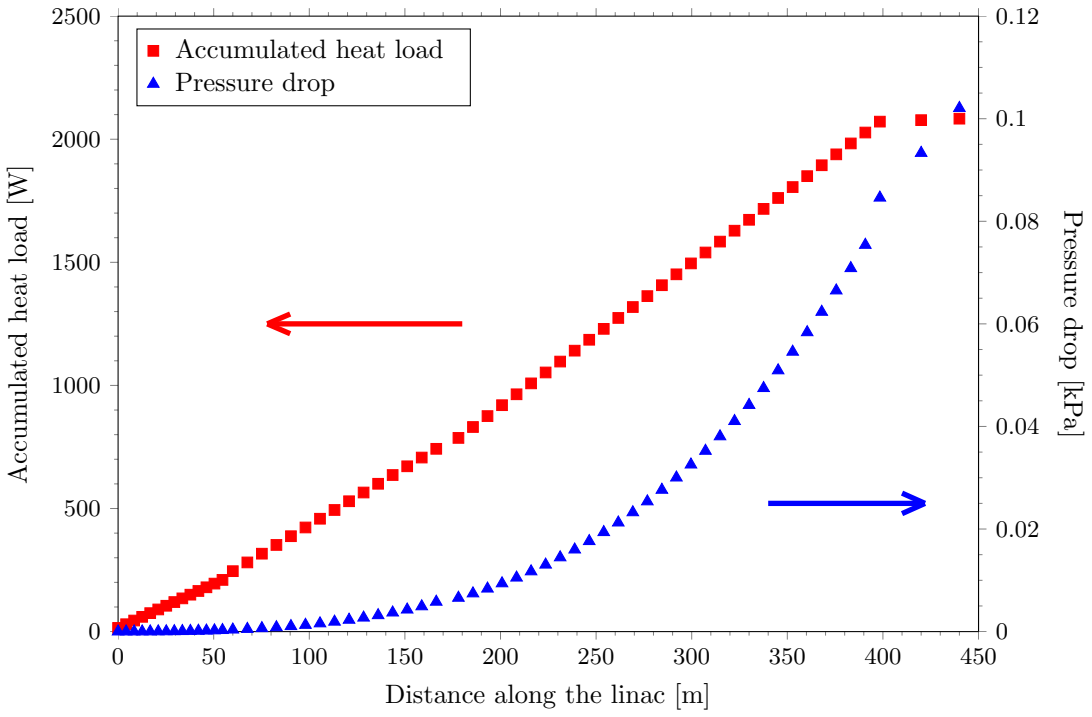

Figure 6.5: Cumulative heat load and resulting pressure drop in the VLP return line starting at the spoke cryomodules of the Linac and moving towards the cryoplant. Also see Figure 6.4. The inner pipe diameter for this example is 260 mm. No safety factor for heat loads is applied in this calculation.

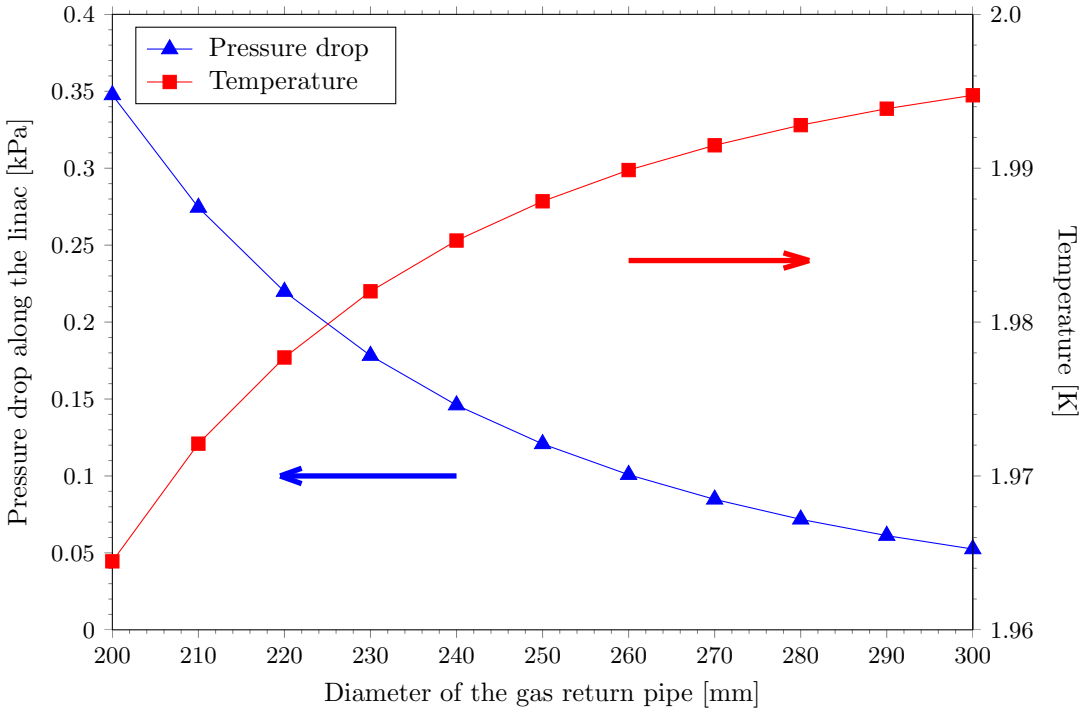

Figure 6.6: Pressure drop and temperature change along the full length of the VLP return line pipe, starting from the spoke cryomodule, as a function of the inner diameter of the pipe. The starting temperature at the first spoke cryomodule is set at 2.0 K. The right-side vertical axis measures temperature at the other end of the Linac on the cryoplant side. The allowable pressure drop in the gaseous helium return pipe is 0.1 kPa and should not exceed 0.15 kPa. No safety factor for heat loads was applied in this calculation.

mixes with the flow of the VLP return pipe. A straight drift section after each T-intersection adds a heat load of 0.2 W/m to the VLP pipe that increases the flow temperature up to 4.3 K within the cryogenic transfer line.

Figure 6.6 shows the pressure drop and temperature change along the full length of the gas return pipe as a function of the pipe diameter. The pressure drop decreases with increasing pipe diameter, reaching the specified limit of 0.1 kPa at a diameter of 260 mm. This pressure difference along the gas return pipe causes a change of saturated vapour pressure in the two-phase pipe for different cryomodules along the Linac. Figure 6.6 also shows the maximum temperature difference caused by the change in saturated vapour pressure along the cryogenic transfer line plotted against the gas return pipe diameter (blue diamonds). For a given temperature of the helium bath in the first spokes, the resulting temperature difference at the last cryomodule is about 10 mK for a pipe diameter of 260 mm. The design of the distribution system is ongoing. The Cryogenics Group is still studying a number of issues, such as the number, type and location of safety valves; the number of warm helium lines; the design of the cool-down line and the final line sizes. ESS will finalise these design decisions in 2013.

6.1.5 Safety factors for cryoplant capacities

In large scientific facilities such as ESS, the precise determination of the cryoplant cooling capacities is complicated. This results from a number of factors. At this stage of the project, prior to significant prototype testing, the static and dynamic heat loads of the cryogenic components have been calculated, but are not yet verified. Even after all prototypes are complete, subsequent degradation of cryogenic component performance may lead to higher heat loads. Additionally, over time the performance of the cryoplant may be reduced due to equipment failures. Another complication is that the amount of uncertainty will vary between temperature levels and in the case of ESS, from cryoplant to cryoplant. For example the 40 K to 50 K shield heat load, which is mostly independent of cavity performance, can be determined with less uncertainty than the 2 K heat load. Similarly, the 16 K heat load for the target cryoplant has

Cryoplant	Temperature [K]	F_o	F_{ud}	F_{us}
Linac	2	1.15	1.0	1.5
	4.2	1.15	1.0	1.5
	16	–	–	–
	40/50	1.15	–	1.3
Test and instruments	2	1.15	1.0	1.5
	4.2	1.15	1.0	1.5
	16	–	–	–
	40/50	1.15	–	1.3
Target	2	–	–	–
	4.2	–	–	–
	16	1.15	1.3	1.5
	40/50	–	–	–

Table 6.1: Cryoplant safety factors for each cryoplant and each temperature level.

been determined by well-understood neutronics calculations, and is thus predicted with a high degree of confidence. One approach for dealing with this uncertainty is to multiply the expected cryogenic loads by a safety factor to determine the final capacity of the cryoplants. There are hazards in this approach. One has to be careful not to apply safety factors on top of safety factors, resulting in an overly conservative and costly system. Alternatively, being overly optimistic and applying too small a safety factor can result in a cryoplant that is too small to meet actual operating requirements. These hazards are best avoided by being very explicit and clear about the definition and size of the safety factors used.

The ESS cryogenics team will use the following formula to determine each cryoplants cooling capacity at a given temperature [553]:

$$C = F_o \left(F_{ud} Q_d + Q_b + F_{us} Q_s\right) \tag{6.1}$$

where:

- C is the total cooling capacity of cryoplant at a given temperature
- F_o is the operational safety factor
- F_{ud} is the uncertainty factor on the dynamic heat loads (i.e. those associated with RF cavities and couplers)
- F_{us} is the uncertainty factor on static heat loads
- Q_d is the predicted dynamic heat load
- Q_b is the predicted beam heat load
- Q_s is the predicted static heat load

The operational safety factor F_o takes into account the desirability of having some operating space in which to control the plant. It also allows some margin for seasonal temperature variations, and degraded plant performance due to minor maintenance issues. F_{us} and F_{ud} take into account the uncertainty in predicting the exact static and dynamic heat loads. Table 6.1 lists the ESS safety factors for each cryoplant and each temperature level. The clarity of this approach allows for straightforward reviews. The value of $F_o = 1.15$ is an estimate based on industry experience. The lowest safety factor (1.3) is associated with 40 K to 50 K static loads and the dynamic loads associated with the target, as these loads have been calculated with the highest degree of confidence. The safety factors associated with both the cavity dynamic heat load and the beam heating are set to 1.0. This results from the baseline estimates of these values already containing safety margin. The operational safety factor is still applied to these values as well. The safety factors may be adjusted as the project continues and additional design and performance data becomes available. The plant capacities and safety factors must be firmly determined before the plant specification is released for

bidding by industry. At the earliest, this will occur in the first quarter of 2014 for the test stands and instruments cryoplant.

Experience shows that maintaining a high purity of the helium gas is key to cryoplant availability [554]. ESS will use well-established operating procedures along with helium purification systems and monitoring of the helium gas purity to address this issue.

6.2 Vacuum systems

6.2.1 Accelerator vacuum systems

Front end systems

The front-end systems comprise the Ion Source (IS), Low Energy Beam Transport (LEBT), Radio Frequency Quadrupole (RFQ) and Medium Energy Beam Transport (MEBT). With the exception of the MEBT, these systems will be designed to handle the high hydrogen gas loads needed for ion source operation. While the vacuum systems will be suitably sized to manage these loads, the pump exhaust will also be handled in an appropriate manner to eliminate the potential for the formation of explosive mixtures. Safety considerations will be addressed in the design and the design will comply with applicable codes and standards for the handling of hydrogen.

Since beam energy levels in the front end systems are relatively low, no specific actions will need to be taken to reduce vacuum levels below those dictated by beam transport requirements in order to allow hands-on maintenance. The radiation levels anticipated will not impact the selection of vacuum equipment. The use of elastomers, such as EDP or Viton, for sealing is well-accepted, but ESS will use metal seals and CF-style flanges where possible. The use of TMPs (turbomolecular pumps) is appropriate for the continuous pumping of the high hydrogen gas flows that will need to be pumped from the IS and LEBT sections. Dry scroll pumps will also be used for initial evacuation and will back these TMPs. The use of closed cycle cryo-pumps is also an option, however, hydrogen inventory and the impact of routine regeneration will need to be considered if ESS decides to use this type of pump.

The greatest risk when pumping hydrogen is the formation of an explosive mixture at hydrogen concentrations in the air as low as 4.5%. Even with the low flow rates anticipated, it is prudent to dilute the hydrogen concentration below the explosive limit by gas ballasting the scroll pumps with nitrogen to produce an exhaust stream below the critical concentration. This will eliminate the potential for explosive mixtures forming with the oxygen in the air in the vicinity of the pump's electric motor, switches or other electrical equipment. ESS will use this strategy no matter which type of primary pump it decides to use. Due to the potential for hydrogen explosions, ESS will not use hot filament gauges. Emergency power is not essential for these systems if TMPs are used, since the run down time will allow an orderly shut down of the systems and extensive precondition of the systems will not be required to bring them back on line. If cryo-pumps are used, consideration will need to be given to the provision of emergency power to prevent the unscheduled warm up of the pumps. Vacuum gauging and manual vent valves to bring the systems up to atmospheric pressure will be fitted.

Pumping will be distributed along the length of the RFQ and will be designed to provide sufficient pumping speed to maintain RFQ pressure at an operational level and to minimise gas flow into the MEBT. The use of TMPs for the RFQ has several advantages: commonality with the pumping systems used for the ion source and LEBT; reducing the need for spares; providing continuous operation by avoiding the need for periodic regeneration, which will extend machine availability unless redundant pumps are used; and improving operational safety since hydrogen inventory will not be accumulated in the pumps. The optional use of cryo-pumps has the same disadvantages as delineated in the previous section, and the exhausted gas stream would be handled in a similar way. Pneumatically operated gate valves will be provided at both the entrance and exit of the RFQ to allow preconditioning of the LEBT and isolate the MEBT during RFQ maintenance and conditioning. The valves will be sized to have sufficient aperture to ensure that the gate seal is outside the tails of the beam profile. The valve between the RFQ and MEBT will be a normally closed (NC) valve (power to open) which will isolate the RFQ from the MEBT in the event of power failure or loss of vacuum. Each TMP (or cryo-pump) will be equipped with inlet gate valves to allow individual pumps to be isolated from the system. The comments regarding emergency power in the previous section also apply in this case. The RFQ will be fitted with vacuum gauging and a manual vent

valve to bring the RFQ up to atmospheric pressure. Again, the use of elastomers, either EDP or Viton, for sealing is considered acceptable but ESS will use metal seals and CF style flanges where possible.

Since the gas loads associated with the MEBT will be primarily due to outgassing, the use of ion pumps will be a suitable choice for this application. Noble ion pumps are preferred to suppress any tendency for argon instability. RF screens will be required at the inlet to each ion pump to prevent the regurgitation of gas from the ion pumps into the systems as a result of the RF power. A fixed mechanical pumping system using a TMP backed by a scroll pump is preferred for the initial evacuation of the MEBT prior to bring the ion pumps online. An NC gate valve (one that closes automatically upon loss of power or vacuum) will be installed between the MEBT and warm linac to isolate the system in the event of power failure or loss of vacuum. Emergency power will be considered to maintain MEBT vacuum during a power outage, eliminating the need to bring the mechanical pumping system online in order to restart the ion pumps. The MEBT will be fitted with vacuum gauging and a manual vent valve to bring the system up to atmospheric pressure.

Drift tube linac

As is the case with the MEBT, the gas loads associated with the drift tube linac DTL tanks will be primarily due to outgassing and the use of ion pumps will be a suitable choice for this application. Noble ion pumps will be used to suppress any tendency for argon instability. RF screens will be required at the inlet to each ion pump to prevent the regurgitation of gas from the ion pumps into the systems as a result of the RF power. The ion pumps will be connected directly to the DTL tanks. Initial evacuation of each DTL tank will be accomplished using a mobile pump cart prior to bringing the ion pumps online. This connection will be made via a gate valve fitted to the DTL tank. This valve will be interlocked with the pump cart via an electrical connector, which will connect the gate valve to the pump cart. Tank and pump cart pressures will be used as valve interlock commands. It is anticipated that it will be possible to use elastomers or the sealing of drift tubes, post couplers, slug tuners, etc. Silver coated "C" seals or a similar approach will be used in these sealing areas to maintain RF coupling between components. NC gate valves will be installed between individual DTL tanks and the low energy differential pumping section to isolate individual tanks in the event of power failure or loss of vacuum. RF heating of the valve seals may be an issue with the higher energy tanks and will need to be investigated before valve selection is finalised, especially if a minimum aperture beam line is used. This could require the use of valves which provide RF resistance in the opened position by providing electrical contact between the flanges.

Emergency power will be required to maintain the DTL tanks under vacuum during a power outage, which will eliminate the need to reconnect a mobile pump cart prior to bringing the ion pumps back online due to a loss of tank vacuum ($> 10^{-4}$ mbar). Each tank will be fitted with vacuum gauging and a manual vent valve to bring the tank up to atmospheric pressure. To provide the maximum possible pumping speed in a limited space, it is anticipated that a getter pump will be used to provide the pumping between the RF window and iris. The getter pump will be provided with an isolation gate valve to allow the getter to be reactivated when heated. A TMP backed by a scroll pump would be used to pump out the gas released during this reactivation. Emergency power will be optional for the RF window pumping system, since the pumps of the DTL tank will be available during a power outage to pump the RF window cavity through the iris. Each RF window will be fitted with vacuum gauging. The RF window will be vented through the iris into the DTL tank. Once more, the use of elastomers for sealing is considered acceptable, but ESS will use metal seals and CF style flanges where possible. The windows will use a brazed assembly. In addition to providing for the location of the between-tank isolation valves, tank interconnections will also be used to accommodate beam instrumentation as needed. The diameter of the tank interconnecting beam line will be minimised within the limits required to accommodate the tails of the beam to limit heating. While elastomers would be acceptable, ESS will use metal seals and CF style flanges where possible.

Low energy differential pumping section

The low energy differential pumping section (LEDP) provides a pressure reduction between the last DTL tank and the first spoke cavity in order to limit the flow of gas from the warm section of the machine into the cold section. The LEDP will have distributed ion pumps and a beam tube that will provide the minimum conductance possible in order to generate the maximum pressure gradient within the physical constraints dictated by physics and the installation. This section will also include beam instrumentation

and a fast closing valve to protect the first spoke cavity from an inrush of gas that may result from a loss-of-vacuum event occurring in the warm section of the machine. Emergency power will maintain the LEDP under vacuum during a power outage in order to protect the cold section of the machine. The LEDP will be fitted with vacuum gauging, fast valve sensor and a manual vent valve with micron filter to bring this section up to atmospheric pressure. With the limited beam aperture, metal seals and CF style flanges will be used where possible. Valve sealing will be limited to the use of elastomers (EDP or Viton). Following fabrication of the LEDP beam pipe, it and other components will be extensively cleaned prior to assembly in a class 10/100 clean room to minimise the potential for contamination of the cold section of the machine during and following installation.

Cold linac

The accelerating cavities of the spoke, medium-β and high-β cryomodules will be cooled with helium at cryogenic temperatures and as a result will be self-pumping. Each unit will be fitted with vacuum gauging and a manual vent valve with micron filter to allow each section to be brought up to atmospheric pressure. The cavities will be conditioned prior to installation in the tunnel and connection to the warm sections. This connection will be made under clean room conditions using portable clean rooms to minimise the potential for particulate contamination of the cavities. Following connection and evacuation of the warm sections, the interconnecting valves to adjacent cryomodules will be opened. As each warm section is installed, the vacuum jackets of cryomodules adjacent to it will be evacuated using a portable pump cart. Once the vacuum jackets are under vacuum, the cryomodule will be ready for cool down. The pump cart can be removed once the cryomodule has been cooled down, since this will provide self-pumping of the vacuum jacket due to the cold surfaces. Beam line connections will be made using metal seals and CF style flanges where possible.

The linac warm units will provide the beam line connection between individual spoke cavity modules and cryomodules. These sections will have a centrally located ion pump, beam instrumentation, vacuum gauging and manual vent valve with micron filter to allow them to be brought up to atmospheric pressure. The warm sections will be isolated from the cryomodules during installation by isolation gate valves located on the end of each adjacent cryomodule. While elastomers would be acceptable for sealing, ESS will use metal seals and CF style flanges where possible. Emergency power will be provided to maintain the warm sections under vacuum during a power outage to minimise the flow of gas into the cold sections of the machine. Following fabrication of the warm beam pipe, this and other components will be extensively cleaned prior to assembly in a class 10/100 clean room to minimise the potential for contamination of the cold sections of the machine during installation.

High energy differential pumping section

The high energy differential pumping section (HEDP) will provide a controlled pressure increase between the last high-β cryomodule and the HEBT in order to limit the flow of gas from the warm section of the machine into the cold section. The HEDP will have distributed ion pumps and a beam tube providing the minimum conductance possible in order to generate the maximum pressure gradient within the physical constraints dictated by physics and the installation. This section will also include beam instrumentation and a fast closing valve to protect the final cryomodule from an inrush of gas from the HEBT into the cold sections of the machine in the event of a loss of vacuum in the HEBT. Emergency power will be provided to maintain the HEDP under vacuum during a power outage in order to protect the cold section of the machine. The HEDP will be fitted with vacuum gauging, fast valve sensor and a manual vent valve with micron filter to bring this section up to atmospheric pressure. With the limited beam aperture, metal seals and CF style flanges will be used where possible. Valve sealing will be limited to the use of elastomers (EDP or Viton). Following fabrication of the HEDP beam pipe, this and other components will be extensively cleaned prior to assembly in a class 10/100 clean room to minimise the potential for contamination of the cold section of the machine during and following installation.

High energy beam transport

The high energy beam transport (HEBT) beamline runs from the HEDP to the target and tuning beam dump windows, with the allowable pressure rising to about 10^{-6} mbar as the beam line approaches the

target and tuning beam dump windows. The pressure in the proximity of the HEDP must be lower than this to minimise the flow of gas into the last cryomodule.

The size of the beamline will expand rapidly as it moves from the vicinity of the collimator to the target and tuning beam dump windows. Since this area will be activated, special precautions will be required for maintenance, in particular, the use of shielding and long-handled tools or remote handling techniques. These requirements and the larger beamline pose challenges in the selection of the appropriate metal seal design for the beam line flanges and in provisions to allow remote leak testing. For hands-on maintenance upstream of the collimator, a gamma blocker will be rotated into the beamline to block the back-streaming of radiation from the target, tuning beam dump or collimator. Radiation hard components will be used when available and these components will need to exhibit a high level of reliability. Local shielding and a strategy using redundancy of components needs to be considered in the vacuum design for these radiation areas.

Ion pumps will be used for the pumping of the HEBT. They are the most suitable option because they have no on-board electronics and controllers can be located remotely. Vacuum instrumentation will be of concern in the radiation areas and will require careful consideration and selection of equipment during the design process. Valves will be metal sealed where possible. Corrosion as a result of nitrous oxide forming from the irradiation of the air will also be a consideration, especially if bellows are used. It is currently planned to install a fast valve upstream of the collimator to protect the upstream beam line in the event of a break in the target. A similar fast valve will implemented upstream of the tuning beam dump window to protect the linac in case of its rupture. Emergency power will be provided so that access is not required to re-evacuate the beamline using mobile pump carts to restart ion pumps in case of a power outage. The interface with the target will be at the "safety isolation valve", which is a part of the second confinement safety barrier of the target station, on the upstream side of the valve. The Target Division will be responsible for the proton beamline downstream of this valve up to and including the target window. This will be a radiation area and a design will be developed that will provide for the disconnection and reconnection of the proton beamline from the safety isolation valve using long-handled tools or remote handling techniques. Remote leak testing after the connection has been reestablished will also be required. The design adopted will be integrated into the maintenance strategy for the safety isolation valve and window. Corrosion as a result of nitrous oxide will also be a consideration if bellows are used.

The proton beam line will terminate at the window in front of, but not connected to, the tuning beam dump. The window design has yet to be completed although it is currently anticipated that it will be water-cooled. This will be a radiation area and the design will be compatible with replacement by the use of long-handled tools or remote handling techniques. One option for the vacuum connection would be the use of a clamshell-style clamp, with metal seal, that could be opened and closed using long-handled tools. After release from the clamp, the flanges could be opened using a double bellows arrangement that would be installed in the final section of the beam line. The bellows assembly would be evacuated to open the flange connection to the window, allowing its replacement, and pressurised to close the connection. The capability to leak test the connection after mating will also be required. With the level of radiation that can be anticipated, consideration must be given in the design to the potential for corrosion of the bellows as a result of the production of nitrous oxide. The type of connections adopted for the water connections to the window is outside the scope of responsibility of the vacuum group.

Target systems

The vacuum group will assist in designing the vacuum interface and proton beam window, the target safety valve located in the proton beam line and the interconnecting beam line between these two components. Since the area will be activated, the design developed will be compatible with replacement by the use of long-handled tools and/or remote handling techniques. Since these components form part of the beam line, helium leak testing will be required. Although the HEBT will operate at a relatively high pressure, on the order of 10^{-6} mbar, a reasonable level of leak tightness will need to be achieved following the change out of components to minimise the gas load to which the HEBT ion pumps will be exposed so as to limit maintenance requiring the change out of pumps due to saturation. The vacuum group will also provide assistance in the design of embedded vacuum system within the He target cooling circuit and the He monolith circuit.

6.2.2 Instruments and neutron beam lines

The vacuum group will provide support during the development of instruments and neutron beam lines; providing guidelines for the design of vacuum chambers and components, and selection of vacuum components and equipment; conducting material testing, such as outgassing studies on materials to be installed in a vacuum environment; providing advice and review during the design of instrument chambers and components from a vacuum prospective, for example, concerning weld design and material selection; inspecting fabricated components and chambers for vacuum compatibility; witnessing vacuum testing at vendor premises and providing for the testing and start up of the various vacuum systems following installation. The vacuum group also will provide support on vacuum-related issues during the design and installation of the initial suite of instruments. Ongoing discussions will be held with the scientists responsible for the design of these instruments and with those responsible for other vacuum tasks that may be required. Vacuum resources will be adjusted as required to accommodate the needs of instrument design and installation. Approximately 2900 m of neutron guide will be installed to support the full suite of instruments. It is anticipated that vacuum pumps will be required at about 20 m intervals along the neutron guides and that they will need to provide an operating pressure in the 10^{-3} to 10^{-4} mbar range. The vacuum group will assist in the vacuum design of the neutron guides and interfacing components, such as choppers, and will design, procure, fabricate and install the vacuum pumping equipment needed to support this activity. It is anticipated that the neutron guides will be pumped with mobile pumping units allowing the ready exchange of units for servicing. It is estimated that 30 to 40 mobile pumping units will be required for the neutron guides needed to support the initial suite of instruments.

Vacuum facilities will be provided to support both construction and pre-operation activities. These facilities will include: outgassing test chambers for the investigations of materials and components; general purpose bake-out and drying ovens for the preparation of equipment prior to installation; support equipment including pump carts, leak detectors etc.; class 10/100 cleaning area and washing area for the preparation of warm sections and other critical components prior to installation; pump carts, leak detectors and other equipment specifically needed for “clean” cryomodule vacuum assembly such as making and breaking beamline connections in the cold linac; portable clean rooms to support the making of “clean” beamline connections; and provision of limited spares-holding to support vacuum operations through pre-operational activities. Pump carts, leak detectors, cold traps and other equipment needed to support vacuum operations on activated and/or contaminated circuits will also be provided.

6.3 Test stands

Test stands for the cryomodules and RF systems will be employed in both Uppsala and in Lund.

6.3.1 Uppsala test stand

The FREIA laboratory at Uppsala University serves as a Facility for Research Instrumentation and Accelerator Development [555]. The construction of the 1000 m^2 FREIA laboratory hall will be completed in July 2013. The hall will have separate areas for three RF test bunkers, for RF power generation equipment, for a helium liquefier and cryogenic storage facility, for a vertical cryostat, for equipment mounting, for a control room, for a small workshop, for equipment storage and for offices (located at a mezzanine) and contain general laboratory infrastructure like power and fluid distribution systems. A sketch of the inside of the hall is shown in Figure 6.7. A helium cryogenic facility and a general purpose test cryostat will be delivered in December 2013 and commissioned by May 2014. The bunkers will be built up during 2013 using steel loaded concrete blocks.

The first project for which the FREIA Laboratory will be used is the development and prototyping of the RF system for the ESS superconducting spoke cavities, to be followed by the high power testing of the first prototype ESS spoke cryomodule. In a first phase, the functionality of the tetrode-based RF power system will be demonstrated in tests in which one power system is used to power a single spoke cavity. In a second phase, the prototype spoke cryomodule containing two superconducting spoke cavities will be tested at high power, requiring the simultaneous operation of two complete RF systems. Testing of the 14 production spoke cryomodules will also be carried out in the Uppsala test facility. The first RF power source with control and distribution equipment is scheduled to arrive before December 2013. The RF source will first be commissioned and tested using a water cooled load. The first prototype spoke cavity

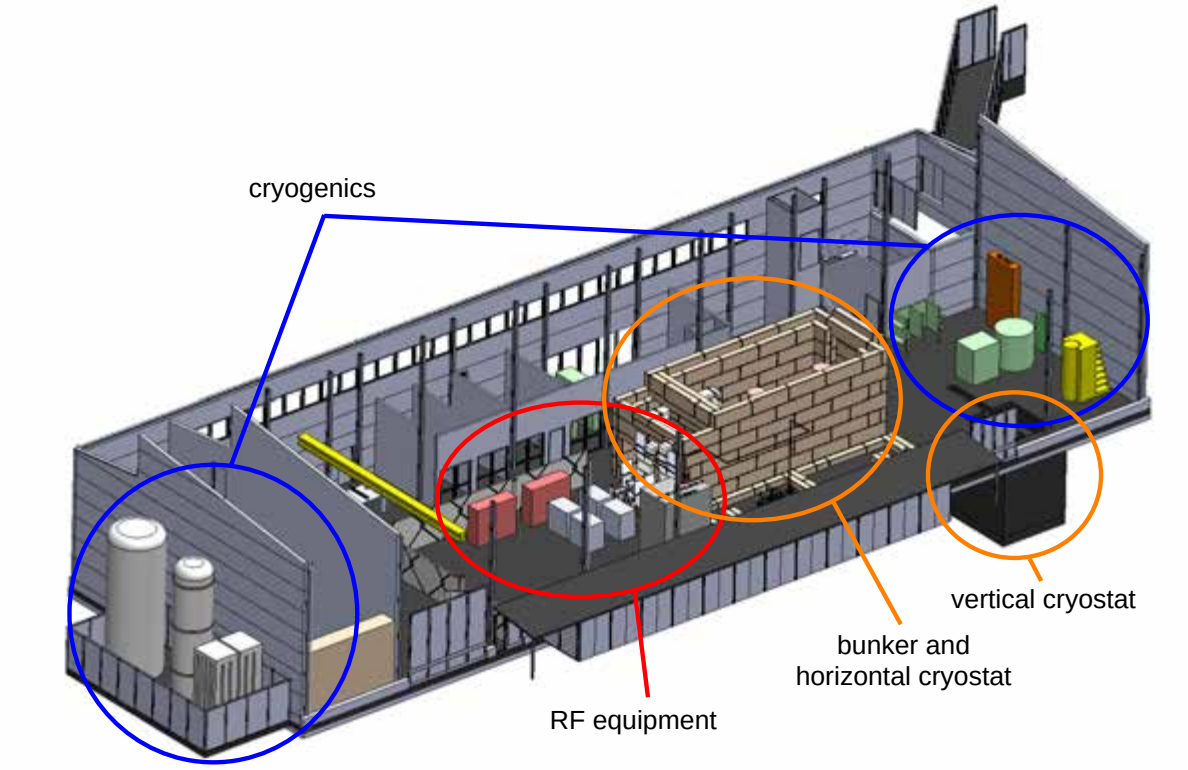

Figure 6.7: Interior layout of the Uppsala FREIA test stand hall.

is expected to arrive in May 2014. It will be installed in the horizontal test cryostat and tested with an RF source during the second half or 2014. The prototype spoke cryomodule is scheduled to arrive in mid 2015. It will be tested at high power during the second half of 2015 and the first half of 2016. Thereafter, FREIA can be used for acceptance testing of the series spoke cryomodules as they are delivered from the production line.

Three major components are required for the ESS test program in Uppsala; RF equipment, cryogenics and the test stand infrastructure.

RF equipment

Reliable development of an energy efficient and resource effective RF system requires testing of the individual components and the complete RF system in a realistic environment. Thus an RF test facility is required with which the different concepts, topologies and elements of the RF system can be investigated in an in-depth test program. The RF test facility requires a complete RF system consisting of an LLRF system, high power RF amplifier, RF distribution system and spoke cavity, as shown in Figure 6.8. The LLRF system will generate the low power RF signal and adjust the individual amplitude and phase to the spoke cavities. The LLRF will also measure the field in the cavities and tune the cavity frequency to adjust for so-called Lorentz force detuning caused when the high power RF pulse starts filling the cavity volume. The spoke cavities will require an RF power of 350 kW at 352.21 MHz with 3.5 ms pulse length and 14 Hz repetition rate. Tetrode type vacuum tubes will be used as the high power RF amplifiers in combination with solid state pre-amplifiers. The layout of the proposed RF sources is described in detail in Section 4.8.6. For commissioning and initial testing, the high power amplifiers will be connected to a water cooled RF load. Thereafter, they will be connected to the superconducting spoke cavities. Prototype testing of the spoke cryomodules requires the addition of a second RF power amplifier and distribution chain. This will make it possible to power both cavities in a cryomodule simultaneously. The second chain

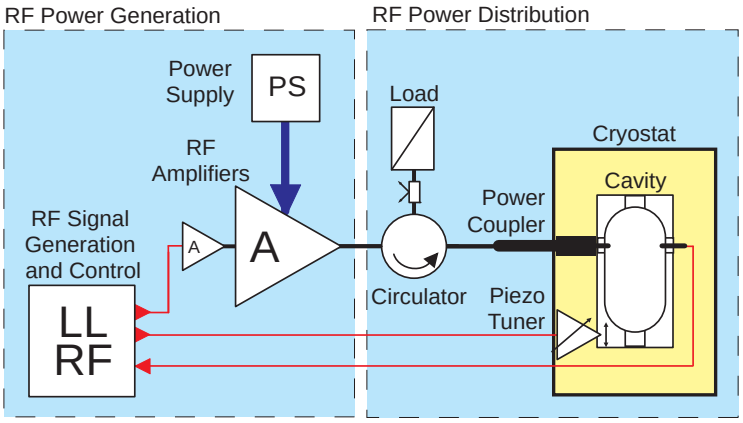

Figure 6.8: Possible configuration of RF equipment to power a superconducting spoke cavity in FREIA.

will be modelled on the first chain, with improvements based on lessons gained from experience.

Cryogenics

Figure 6.9 shows the layout of the FREIA cryogenic facility, including a helium liquefier, liquid and gas helium storage, liquid helium distribution valve box, impure helium gas recovery system and a liquid nitrogen distribution system. The capacity of the cryogenic facility is designed to provide 30 W cooling power at 2 K to a superconducting cavity or other device in the cryostat. The helium liquefier will provide a 2-phase mixture of gas and liquid helium at 4.4 K, 0.13 MPa at the output of its cold box into a liquid helium storage Dewar. From this Dewar the liquid helium will be distributed to external users and cryostats connected to the distribution valve box. The temperature of the liquid helium can be decreased additionally in the 2 K cold box of the cryostat to cool superconducting cavities. A sub-atmospheric pumping system will be used to decrease the helium pressure as required to keep the liquid bath temperature at 2 K. The helium liquefier plant will consist of a 4 K cold box, a helium cycle compressor (1.3 MPa output pressure) as well as high and medium pressure helium gas storage. An oil removal system to clean the helium gas leaving the compressor, a high pressure gas distribution panel and automatic control system will also be included but are not shown in Figure 6.9. In addition, a liquid nitrogen storage tank and distribution system will be used for pre-cooling of the liquefier cold box in order to increase its liquefaction capacity. Liquid nitrogen will also be used for the thermal shield cooling of the test cryostat.

The combination of storage Dewar and distribution valve box provides the possibility to deliver liquid helium both to the test cryostat and to other users. This ensures upgrade possibilities to add other test cryostats as well as the filling of liquid helium transport Dewars for external experiments. The large volume storage Dewar can serve as a buffer supply of liquid helium when the required liquid helium flow exceeds the flow directly from the liquefier. This makes it possible to run experiments in the test cryostat with feed boxes required cooling power exceeding the liquefier power, as well as enhancing the filling speed for transport Dewars. The 2 K liquid helium flow will be created inside the test cryostat. To provide 30 W cooling power requires a 1.5 g/s 2 K liquid helium flow. Including losses and accounting for gas helium in the 2-phase flow, we estimate that this requires a 2 times larger 2-phase flow from the 2 K cold box and a 1.5 times larger 2-phase flow from the 4 K liquefier cold box. The required liquefaction capacity is therefore 4.6 g/s at 4.4 K which is equivalent to 140 l/h. The actual liquefier capacity will be in the order of 120 l/h. The 2000 l volume of the liquid helium storage Dewar serves as buffer to provide the additional required flow during full dynamic thermal load operation in the test cryostat (i.e. with full RF power on two spoke cavities). The storage Dewar will be refilled during intermediate breaks when there is only static thermal load in the test cryostat.

Test stand infrastructure

The test stand infrastructure consists of a versatile horizontal cryostat and a concrete bunker for radiation protection purposes. Initially the test stand will contain a single 2 K type cryostat with a horizontal vacuum tank. The cryostat will have a direct connection to the cryogenic facility and a vacuum pumping system.

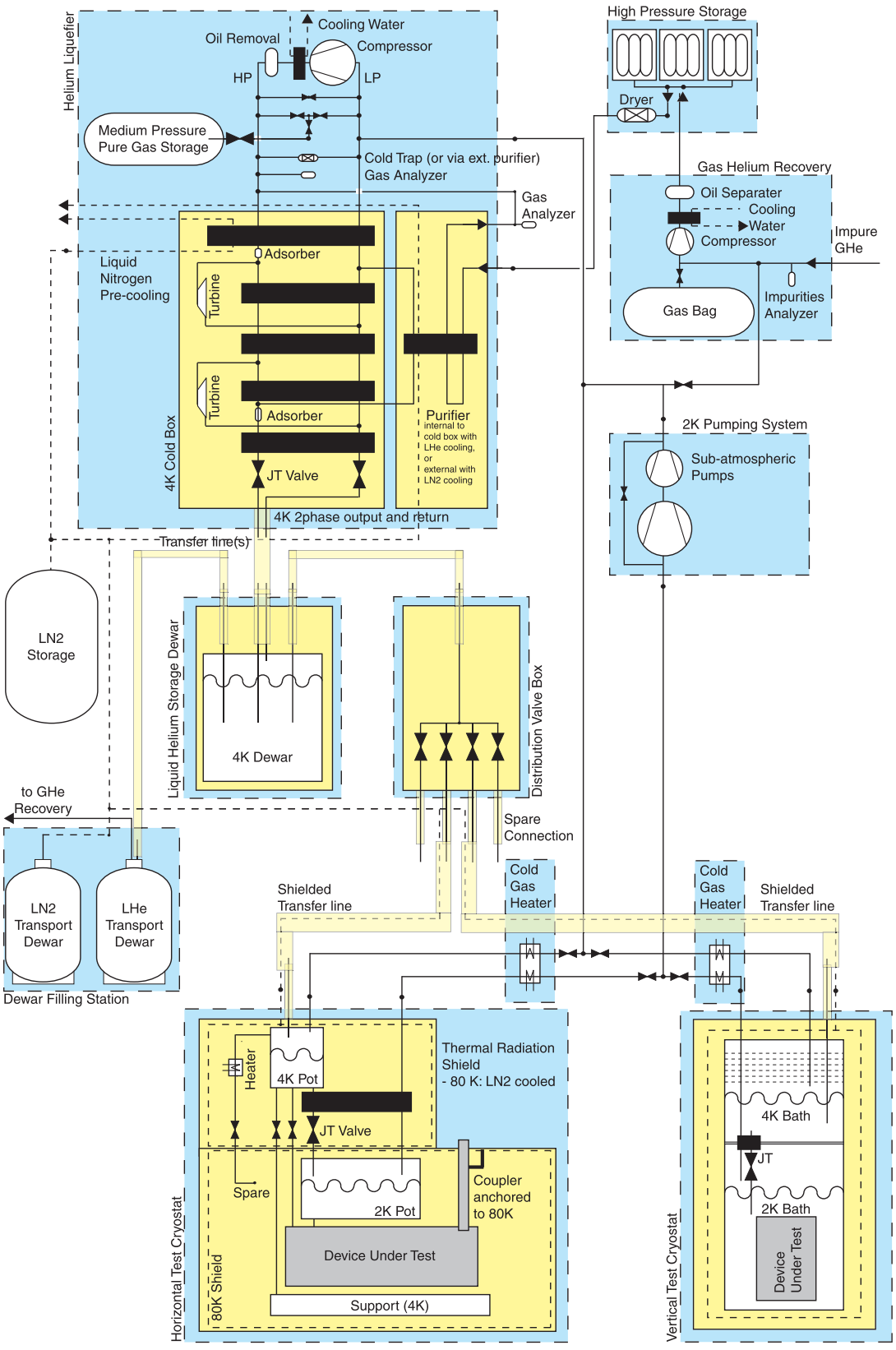

Figure 6.9: Layout of the FREIA test stand cryogenic facility including horizontal and vertical test cryostats.

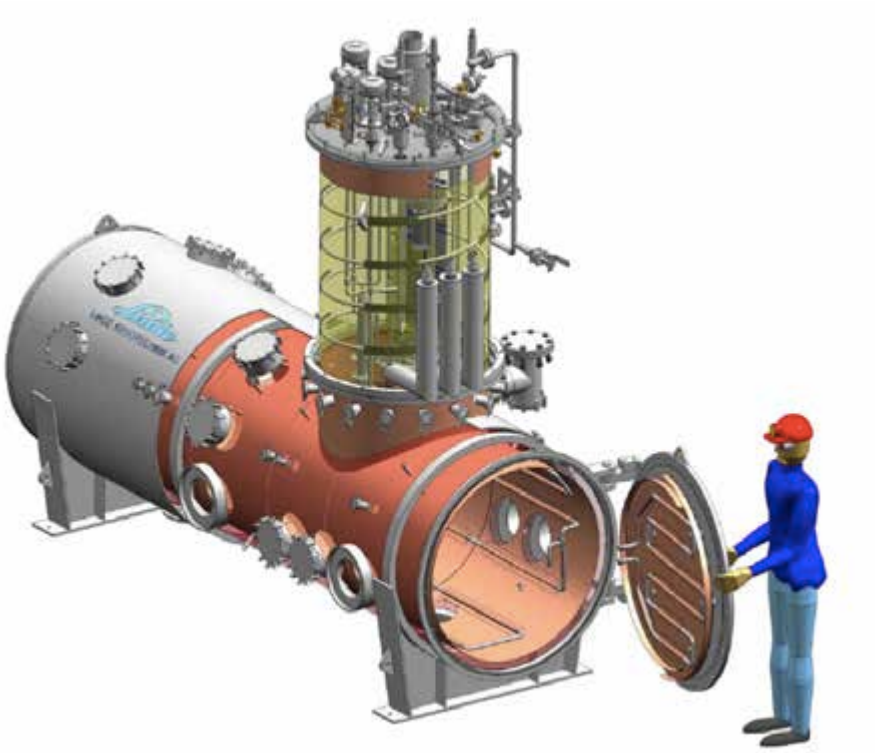

Figure 6.10: Layout of the HoBiCaT cryostat [556]. The vertical feed box includes a liquid helium reservoir and 2 K cold box.

The facility will be designed such that other cryostats, with either horizontal or vertical vacuum tanks, can be added later on. The design of the initial test cryostat will be adopted from the CHECHIA cryostat at DESY, CryHoLab at CEA Saclay and the BESSY HoBiCaT facility [556–559], with small improvements. These cryostats have been designed for horizontal testing of superconducting cavities at temperatures between 1.8 and 4.2 K with help of an integrated cryogenic feed box. The thermal radiation shield is typically cooled with liquid nitrogen. The HoBiCaT cryostat is shown in Figure 6.10. This cryostat has an internal volume that is sufficiently large for the installation of two superconducting cavities. It has doors at both ends to allow easy access to the interior volume of 1.1 m diameter by 3.5 m length. The cavities slide into the cryostat on a rolling table. Power couplers can penetrate the vacuum vessel through feedthroughs on the side. Diagnostic ports are provided for additional instrumentation. The FREIA cryostat will be installed inside a bunker with 80 cm thick walls of iron ore concrete (4.0 kg/dm^3), a common Swedish alternative to barite concrete. The bunker will have an internal volume 4 m wide by 9.6 m long and 4.8 m high. This will enable simultaneous installation of both the horizontal test cryostat and the prototype spoke cryomodule.

During the ESS construction phase the FREIA facility is available for test of the complete spoke cryomodules. Testing of the prototype spoke cryomodule has already prepared the facility for the acceptance testing: RF systems have been extensively tested, staff is familiar with installation and testing of a spoke cryomodule. The bunker is designed such that a cryomodule can be installed simultaneous with the horizontal cryostat leaving the possibility open to continue tests on RF systems or a cavity. Cryomodules can enter the FREIA hall through the access door and work space between bunker and cryogenic plant. The bunker wall on that side can be opened to install the cryomodule.

6.3.2 Lund test stand phase I: RF equipment tests

The Lund test stand will serve two distinct purposes: during phase I, the main RF equipment prototypes – the modulators and the klystrons – will be acceptance-tested. In phase II, the series production cryomodules will be acceptance-tested. The test bench for phase I will consist mainly of a hall equipped with

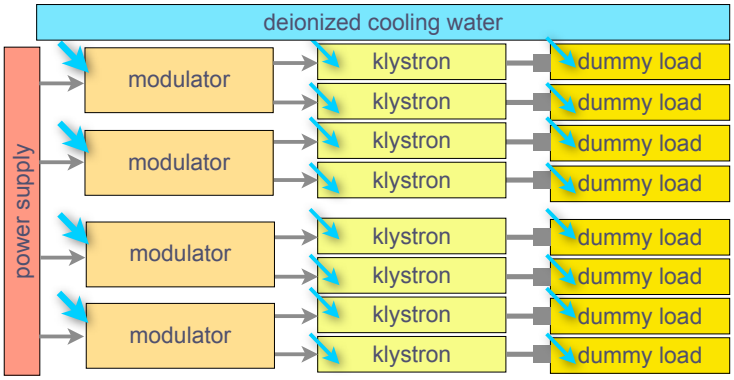

Figure 6.11: Block diagram of the RF soak test structure in phase I of the Lund test stand.

requisite electrical power, electrical grounding, cooling water and HVAC. This will allow extended soak tests of the high power RF equipment prototypes from different manufacturers, providing a solid base for their acceptance. The test bench for phase II will consist mainly of bunkers, the test stand cryoplant and the accepted modulator and klystron prototypes as RF power sources. This will allow site acceptance tests (SAT) of all of ESS cryomodules, with full cryogenic load at the final operating temperature and with full RF load on all cavities in parallel. The acceptance – or reception – tests of the RF equipment prototypes are described in Section 4.8.5. The tests themselves will be run by RF-testing personnel. There are no plans for a 24-7 operator presence, as the tests should run automatically for most of the time. Test-stand personnel will supervise the automated operation of the utilities and perform occasional maintenance interventions.

The RF equipment test stand will be placed in an industrial hall (factory or large lab space) that will provide standard 3-phase electrical power for both modulator and klystron soak tests. It will be equipped with electrical grounding that allows high power/high voltage equipment to be operated safely and free of power disturbances. It will also be equipped with primary cooling water and a secondary deionised water loop to evacuate most of the heat generated by the tests. Finally, it will have sufficient ventilation to keep the temperature in the hall at 24 ± 3 C, in order to create a stable environment for reproducible tests. The test stand will be equipped with all auxiliary services necessary for the tests, such as access control, fire safety, lighting, offices, control room, rest rooms, workshops and logistics areas (storage and handling spaces). Special care will be taken to avoid pollution by oil spills from the RF equipment. This can include oil barriers and oil separators in the drain sumps on top of the precautions mentioned in the discussion about oil leakage in Section 4.8.5. During the soak tests the RF equipment should ideally be set up in its final configuration (i.e. similarly to how the series production will be installed in the klystron gallery). See also the discussion about reception tests at the end of Section 4.8.5. A schematic of the test setup is shown in Figure 6.11. The actual physical setup of the test equipment has not yet been decided and depends on the available surface. The requirements for utilities are listed in [560], with a summary of the most important points in Table 6.2.

The baseline location for the test stand is the upgrade space of the klystron gallery on the ESS site, because it is explicitly designed for housing the RF equipment in question. The availability of both civil engineering structures and utilities at the projected start date can not, however, be guaranteed. Therefore, using an existing industrial facility in Lund as a fallback solution during an initial period is being studied. The small number of pieces of equipment to be tested makes the logistics of phase I relatively simple,

Parameter	**Unit**	**Value**
Total installed power	kVA	1300
Deionised cooling water resistivity	MΩ	> 10
Dissipated cooling power	kW	1200
HVAC temperature	°C	24 ± 3

Table 6.2: RF equipment test stand building and utilities requirements.

compared to phase II. Nonetheless, ESS will carry out detailed planning to ensure that delivery and installation of the testing equipment, auxiliary equipment and RF equipment goes as smoothly as possible. The RF equipment to be tested will arrive from a number of different manufacturers. The modulators will be supplied by at least three different companies and the klystrons by three or four different companies. The test stand will provide of enough storage space to accommodate the successive or simultaneous installation of all equipment, taking into account the challenges of coordinating delivery schedules across multiple manufacturers.

ESS will select manufacturers of klystrons and modulators based on the results of equipment testing. Thus, it is of key importance to ensure the comparability of test results across manufacturers. The modulator soak tests are foreseen to take place over 12 months. All modulators will be tested in parallel under identical conditions, to allow a fair comparison of the different models. The klystron soak tests are foreseen to take place over six months. Klystrons also will be tested in parallel under identical conditions. The modulators will first be tested without any of the other RF equipment attached, i.e. without the klystrons. After an initial period of testing lasting roughly six months, the modulators fitness will be evaluated individually. If enough of the modulators are deemed fit to serve as power sources for the klystron tests, these tests will begin. During this second period of testing, the klystron tests will overlap with the remaining modulator tests, saving time in the overall testing schedule. For the klystron tests, all RF equipment must be installed, including waveguides, circulators, dummy loads and LLRF systems, as described in Section 4.8.2. If the individual modulator tests determine that there is an inadequate number of modulators that are fit to serve as power sources for the Klystron tests, the start of the klystron tests will be postponed until testing has identified an adequate number of reliable modulators.

If the phase I tests are conducted off the ESS site, this part of the test stand will be decommissioned after termination of the RF equipment tests. The building will be prepared for return to the owners. The tested RF equipment will be transferred to the klystron gallery upgrade space on the ESS site, where it will be used to provide power for the cryomodule testing program in phase II. If the phase I tests have been conducted in the klystron gallery upgrade space on the ESS site, this part of the test stand will be transformed and expanded to serve as the test stand for phase II.

6.3.3 Lund test stand phase II: elliptical cryomodule acceptance tests

In phase II, the series production elliptical cavity cryomodules will be acceptance-tested, while testing of the spoke cavity cryomodules series production remains an option. Detailed descriptions of the cryomodules can be found in Section 4.4. The main purpose of the cryomodule site acceptance tests is to verify the proper functioning of the series production cryomodules. Both cryogenic and RF operability will be evaluated. Another goal is to measure key parameters of the cryomodules subsystems, such as heat loads of the cryogenic components and resonant efficiencies of the RF components. Another important part of the testing process is the *in situ* conditioning of the main RF power coupler. In phase II, the test stand will need substantial operational support from the test stand personnel. This support will include operation of the cryoplant, supervision of the automated operation of utilities and occasional maintenance interventions. The tests themselves will be run by RF testing personnel, cryomodule testing personnel and mechanical and instrumentation installation crews. There will be a permanent test stand operator presence during all testing hours. Cryomodule site acceptance tests require full RF power to the cavities, which produces x-ray emissions from the cryomodules. Therefore, the cryomodule tests have to be conducted in concrete bunkers, which shield the surroundings from this radiation. The tests also require a constant flow of cold helium in order to maintain the cryomodules at their operating temperature, which makes the proximity of the test stand to a correctly dimensioned helium cryoplant indispensable.

The cryomodule test stand will have three bunkers, two for the elliptical cavity cryomodules (both medium beta and high beta) and one for the spoke cavity cryomodules. Each bunker will be fully equipped with wave guides, cryogenic transfer line, valve boxes and jumper connections, as well as assorted ancillary equipment. The RF power supplies, i.e. the moderators and klystrons, will be located outside the bunkers, and the waveguides will be fed from the power supplies into the bunkers through suitable chicanes. The bunkers have to be big enough to allow easy and rapid installation and disconnection of the cryomodules in order to minimise turn-around times. ESS will equip the test stand with all auxiliary services necessary for the tests, such as access control, fire safety, lighting, offices, control room, rest rooms, workshops and logistics areas (storage and handling spaces).

During ESS construction, this test stand is not intended for cryomodule prototype R&D and testing,

Bunker	Modules [m]	Warm [m]	Inner [m]	Wall [m]	Chicanes [m]	Outer [m]
Elliptical	7	2	11	1 + 1	2	15
Elliptical	7	1	8	1 + 1	2	11
Spoke	4	1	5	1 + 1	2	9

Table 6.3: Lund test stand bunker lengths.

Bunker	Inner [m]	Wall thickness [m]	Chicanes [m]	Outer [m]
All	5.5	1 + 1	1.5	9

Table 6.4: Lund test stand bunker widths.

nor for cavity testing. There will be limited space in the test stand area for staging of the cryomodules, but not for long term storage. At a later stage of the ESS project, more test facilities and associated spaces will become necessary, e.g. a clean room suite for cryomodule assembly and repair as well as a vertical cavity test stand. Ideally, the test bunkers will have the same cross section as the accelerator tunnel, so as to create a realistic test bench not only for testing the main functions of the cryomodules, but also for testing many other parts of the accelerator installation process. While space and cost considerations may not permit this, at least one of the bunkers must be comparable in size to the linac tunnel, and the other two must be adequately sized to allow rapid installation and disconnection of testing equipment. The length of the bunkers should allow easy manoeuvring around the installed cryomodules. At least one of the bunkers should be long enough so that both warm inter-module sections could be installed with the cryomodule, if combined tests or space verifications should be desired. The total length will include space for personnel access (chicanes), and the total width will include space for the wave guide chicanes.

Tables 6.3 and 6.4 show the bunker lengths and widths, based on the lengths of the different types of cryomodules, the desired additional space to install warm sections, space for passage around the modules, an assumed wall thickness of 1 meter and space needed for access chicanes. The actual physical setup of the bunkers and the test equipment has not been finalised as this Technical Design Report goes to press. It will depend on the available surface and the positioning of the utility headers. A preliminary layout is shown in Figure 6.12, and a block diagram of the test setup is shown in Figure 6.13.

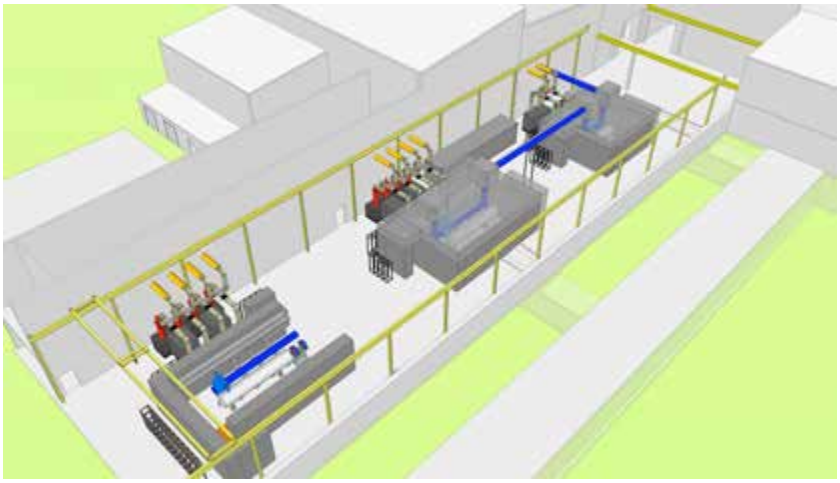

Figure 6.12: Preliminary layout of the cryomodule site acceptance test stand in phase II.

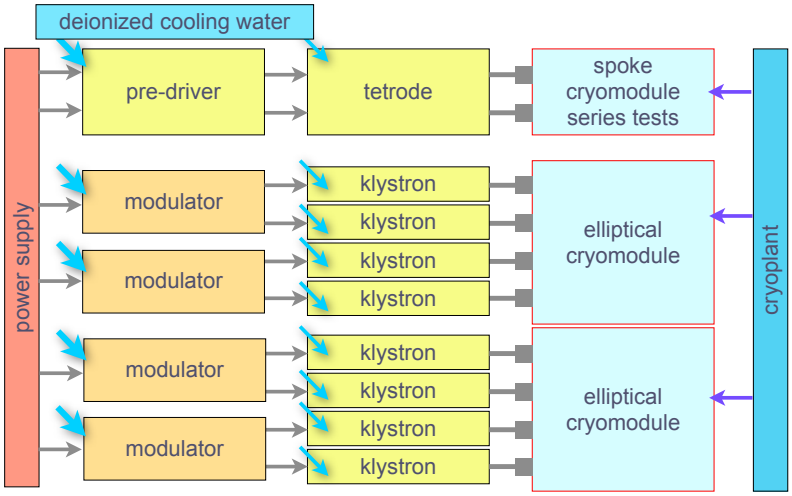

Figure 6.13: Block diagram of the cryomodule site acceptance test stand in phase II.

Cryogenics

The cryoplant providing cryogenic cooling for the cryomodule test stand will be located in the cryogenics buildings alongside the klystron gallery upgrade space. The cryoplant will supply refrigeration at conditions which are very similar to the conditions in the accelerator, as discussed in Section 6.1. The worst-case scenario is the simultaneous testing of three cryomodules with full RF power. The cryoplant and distribution system will be dimensioned to adequately supply cooling for this scenario. Tables 6.5 and 6.6 show the heat load contributions and the installed heat load capacities for the three test bunkers and the distribution system [472]. The expected installed (4.5 K equivalent) capacity of the test and instrumentation cryoplant is seen to be 437 W. However, to provide adequate capacity to produce 50 l/hr of liquid helium and to operate one test stand at the same time, the plant will be sized to be between 500 W and 600 W

	2 K							**5 K**		**50 K**
	Static			**Dynamic**				**Stat.**	**Dyn.**	**Stat.**
	Other [W]	Valves [W]	Tot. [W]	Couplers [W]	Beam [W]	Cavity [W]	Tot. [W]	[W]	[g/s]	[W]
Spoke CM	3.5	1.5	5.0	2.0	2.9	4.0	8.9	0	0	35
Medium-β CM	5.2	1.5	6.7	4.0	5.6	13.2	22.8	1.5	0.16	75
High-β CM	6.0	1.5	7.5	4.0	6.7	18.0	28.7	1.5	0.16	76

Table 6.5: Cryomodule heat load estimates.

	2 K static [W]	**2 K dynamic** [W]	**5 K** [W]	**4.5 K liquid** [g/s]	**40 K** [W]
Cryomodule prediction	19.2	45.2	3	0.32	186
Distribution line prediction			77		252
Total prediction	19.2	45.2	80	0.32	438
Installed power	33.1	52.0	137	32 [W]	654
Installed 4.5 K equivalent	99.4	155.9	103	32 [W]	47
Total installed 4.5 K equivalent			437		

Table 6.6: Summary of heat loads and installed capacity for the test and instruments cryoplant.

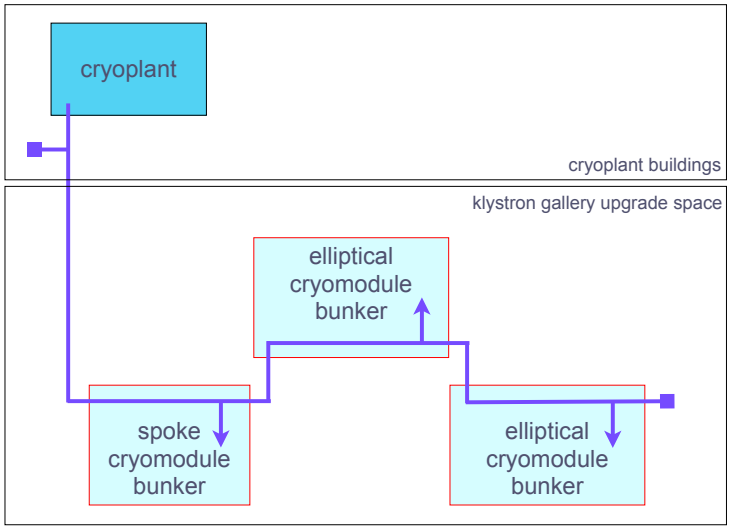

Figure 6.14: Schematic of the Lund test stand cryoplant, distribution line and test bunkers.

(4.5 K equivalent). All heat loads and capacities mentioned rely on preliminary heat load estimates for the cryomodules and have to be revised once more accurate values are known.

A schematic view of the cryoplant, the transfer line, the valve boxes and the cryomodule bunkers is shown in Figure 6.14. The distribution system, i.e. the transfer line and the valve boxes, will be as close to the final design of the linac system as possible, as discussed in Section 6.1.4. They need to differ in one aspect, however: simultaneous and independent operation of the three bunkers calls for a separate low pressure vapour return line for each of the cryomodules. This is needed to allow 2 K operation of some of the cryomodules while others are cooling down. Three independent vapour return lines will comfortably fit into the space of the full-sized vapour return line as needed for the tunnel. Therefore, the overall design and sizing of the test stand transfer line will be very close to the linac transfer line. The same is true for the valve boxes and jumper connections linking the transfer line to the cryomodules. The requirements for space and utilities are listed in Table 6.7. The cryomodule tests have to be performed as close to the final installation site (i.e. the accelerator tunnel) as possible in order to avoid damage to the modules during transport. An ideal location is the upgrade space in the klystron gallery. It has the required size, comes already prepared for the RF power equipment and is located very close to the cryogenics buildings. Figure 6.15 shows the location of the klystron gallery upgrade space and the cryogenics buildings. The klystron gallery upgrade space, the cryogenics buildings and the necessary utilities will be available in good time according to the main construction schedule.

Phase II planning, logistics, schedules and sequencing

The test stand is designed to be able to process three cryomodules in parallel: one spoke cryomodule and two elliptical cryomodules. Medium and high beta cavities have different lengths, which makes the routing of the RF wave guides from the klystrons to the power couplers different for these two types of cryomodule. The bunkers will have to have enough flexibility to adapt to either of the wave guide layouts, but re-routing is time consuming and should not be attempted more than once during the main test run. According to the construction project planning, the cryomodules will be arriving from the manufacturers

Parameter	Unit	Value
Total installed power	kVA	1800
Dissipated cooling power	kW	1700
HVAC temperature	24 ± 3	°C

Table 6.7: Lund test stand phase II building and utility requirements.

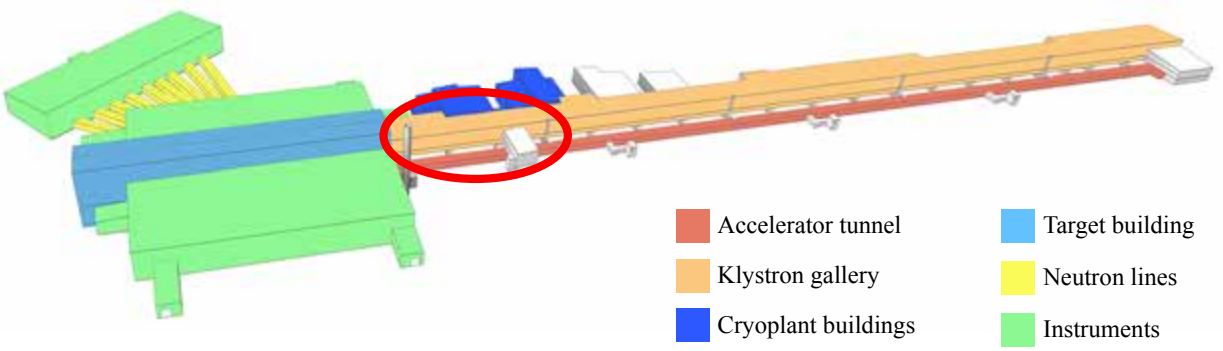

Figure 6.15: Location of the cryomodule test stand (red circle) among the ESS surface buildings.

over a long period. The 14 spoke cryomodules will arrive over a period of 14 months, the 15 medium beta cryomodules over a period of 14 months and the high beta cryomodules over a period of 28 months.

Some of the main pieces of equipment will be manufactured by suppliers and have a non-negligible lead and manufacturing time. This concerns mainly the cryogenic equipment such as the test and instruments cryoplant, the transfer line, valve boxes and jumper connections. Installation and commissioning of all equipment in the test stand area can start when Conventional Facilities hands over the klystron gallery upgrade space and relevant cryogenics buildings. It needs to be finished by the time the first cryomodules arrive. Main pieces of equipment are the RF power sources (modulators, klystrons), wave guides, bunkers, cryogenic transfer line, valve boxes and jumper connections. The test stand, including bunkers and RF power equipment will remain in place until a potential upgrade of the linac calls for their removal. This upgrade is not yet planned, but can be expected to happen many years after completion of the ESS facility. Therefore no plans are being made for the decommissioning or relocation of the test stand at this stage. There are 59 cryomodules of three different types to be tested in total: 14 spoke cryomodules, 15 medium beta cryomodules and 30 high beta cryomodules. Cryomodules are expected to arrive from the manufacturer with an average cadence of one cryomodule every month per type of cryomodule. This means that each bunker needs to process one cryomodule per month. Experience from other testing facilities, such as the XFEL Accelerator Module Test Facility [561], has shown that testing of a cryomodule takes at least two weeks, including installation and disconnection. An extra burden to the ESS test stand is the necessity to condition the RF main power couplers when installed in the cryomodules, adding around one week per cryomodule to the length of the test. Turnaround time for one cryomodule in the test stand is estimated at between three and four weeks, once the test stand is up and running at full speed.

After a cryomodule is tested on the test stand, it will be prepared for tunnel installation. This preparation can be done in the logistics part of the test stand area, where a space of around 200 m^2 is reserved for this purpose. However, there are no significant storage spaces included in the test stand, only buffering spaces for logistical purposes. If there is any delay in cryomodule installation, additional storage will have to be provided elsewhere.

Risk assessment and crucial interdependencies

The test stand will provide a service to other projects within the ESS programme and its planning, installation and operation are very closely linked to a number of other projects. These include cryomodules, RF equipment, cryoplant and conventional facilities, to name but the most important. Other minor interdependencies might become more significant over time, and project planning and execution must always remain flexible enough to respond to the changing circumstances. The cryomodule testing program will be one of the first major technical activities on site. As such it provides opportunities for prototyping other systems such as the Integrated Control System (ICS), vacuum systems, machine protection systems etc. It also will afford the opportunity for training cryogenic and RF operations staff. The complexity of the cryomodule test stand facility and its importance in meeting the project schedule means that significant planning and careful oversight will be required.

The biggest uncertainty is the production schedule of the cryomodules. Any delay will have implications for the test stand operation, which will either need to be delayed and/or sped up to recover lost time.

Availability of tested and accepted RF equipment is absolutely necessary. If not enough of the modulator or klystron prototypes qualify in phase I for operation of phase II, the two elliptical cryomodule bunkers can not be run in parallel and testing of cryomodules will be delayed. In the unlikely case that not even half of the RF equipment qualifies, no elliptical cryomodule can be tested as planned. A detailed risk assessment is necessary and will be performed during the course of the project preparation.

The test stand and instruments cryoplant will be the first cryoplant to be procured, installed and operated by the ESS Cryogenics Group. Availability is therefore not obvious. Tight integration between the test stand team and the cryoplant team will be implemented to mitigate this risk. The test stand will be one of the - if not the - first major activity in the buildings on the ESS site. Availability of buildings and utilities at the promised date can not be taken for granted and progress needs to be closely monitored. The integrated control systems (ICS) project will provide the control system for the test stand. Its personnel will use part of this effort to run a vertical integration test of all of their subsystems. This might create delays in the installation and commissioning of the test stand. A machine protection system (MPS) is not necessary for the test stand, but the test stand could be used as a test bench for parts of the MPS, if this does not disrupt the tests.

Chapter 7

Conventional Facilities

Chapter abstract

Summary: The term "conventional facilities" refers to the spaces required to house the ESS research equipment, machines and instruments and to accommodate the human beings who will either make use of the facility directly, or who will support its operation and maintenance, be they ESS staff, guest researchers or visitors. The overall goal of the Conventional Facilities (CF) project is to deliver the physical space for a sustainable research facility in a sustainable way. CF is also responsible for the mechanical and electrical services necessary for the proper functioning of the facility. This chapter describes the main components of the completed ESS facility, and provides preliminary sketches of several key parts.

The methodology used to accomplish the CF mission is described. As the ESS programme proceeds, different aspects will come into focus at different points in time. The chapter provides an overview of the most important issues for CF in the different programme phases, including the organisational setup, handling of internal and external requirements, the design process and the management of consultants work and the procurement and management of contractors.

Location and conditions at the site have been studied by CF in terms of geography, current infrastructure, archaeology and scientific and industrial environment, and ground conditions have been analysed. The chapter reviews site characteristics, summarises the findings of a study of ground conditions, and describes potential foundation solutions, including the advantages and disadvantages of the different approaches.

Logistics within the site pose a challenge, since the facility stretches over a considerable area. It is the responsibility of CF to create an efficient and functional logistics network. The chapter presents the main logistics issues, and an overview of CF's approach to dealing with them.

Earthworks needed to create roads, parking spaces and landscaping, including the detention ponds required to treat storm water, are described. The specific requirements of the storm water system that will protect external recipients from pollution from the facility receive particular attention.

Buildings must reflect the ESS core values of excellence, openness and sustainability. The buildings that will be constructed on the ESS site are described, including both their function and significant aspects of their design. The main parameters influencing the design of buildings on site are loads, deformation requirements, radiation protection, required volumes and logistics.

Main services include electrical systems, the building management system, water cooling systems, water supply systems, waste water systems and the ventilation system, among others. The chapter describes the various service systems and discusses the most important aspects of their design and of interfaces among them, and with other parts of the facility.

7.1 Methodology

The Conventional Facilities project (CF) is one of the projects in the programme for constructing ESS. The overall goal of the CF project is to deliver the physical space for a sustainable research facility in a sustainable way. This includes meeting energy-related objectives and requirements, creating a good working environment for employees during operations, including accessibility features, creating an outdoor environment that promotes biodiversity and sustainable transportation and using environmentally sound material. Delivering the project in a sustainable way means creating a safe working environment during construction, always adopting a life-cycle perspective on the ESS facility, fulfilling requirements imposed as part of the Swedish environmental and construction permitting process and delivering the project within schedule and within budget.

CF must ensure the correct input for the design and construction works. Therefore, comprehensive coordination with other projects such as the Accelerator, Target, Neutron Scattering System and Energy project, is needed. Internal requirements and interfaces between divisions are established and defined within the scope of the coordination work. To ensure timely deliverables, to meet quality requirements, and to stay within budget, a major part of the CF organisation will participate during several phases of

Figure 7.1: Preliminary site layout.

the project. Many of the employees who will be involved in construction and commissioning are already at work during the design phase. This approach will ensure knowledge transfer to the coming phases. For similar reasons, when the programme enters the operation and maintenance phase, CF will probably be staffed mainly by employees transferred from the construction organisation. Figure 7.1 shows a preliminary sketch of the layout of the main components of the ESS facility on the site.

7.1.1 Design

The purpose of the design is to deliver the blueprints and other documentation necessary for construction of conventional facilities in an efficient manner, on schedule and within budget. The design will be developed in collaboration with other ESS projects to ensure fulfilment of ESS's overall and specific requirements. The design encompasses architecture, civil and structural engineering, system installations and earthworks. It is by necessity managed progressively and evaluated in phases, starting with a feasibility study, and followed by a preliminary design and then a detailed design, using building information models (BIM) and design manuals. Responsibility for design management rests with design coordinators with different areas of expertise and specialisation, and is characterised by close cooperation with construction management.

The general mission of CF is to *provide space for the ESS facility.* This overarching mission breaks down into three major categories: fulfilling society's requirements; providing space for people; and providing

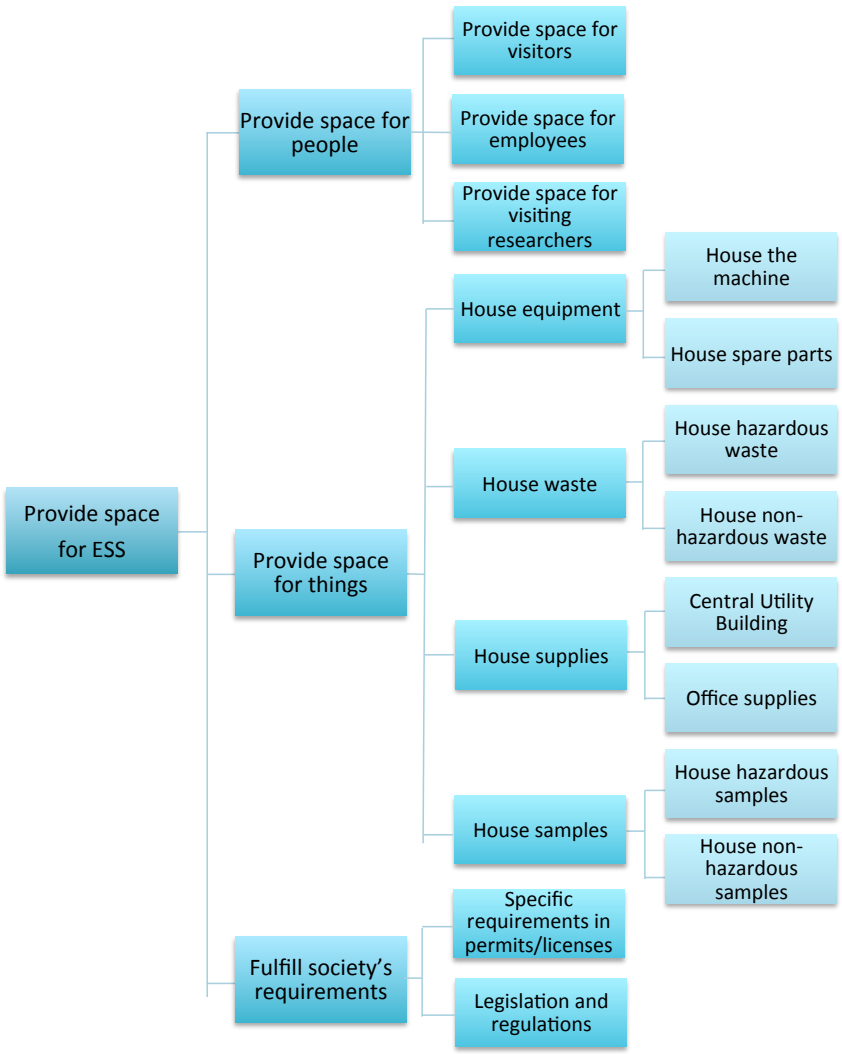

Figure 7.2: Preliminary functional analysis for conventional facilities.

space for things. These categories can be further broken down into requirements and functions, as shown in Figure 7.2. The "things" that need to be housed can be divided into four major areas: accelerator, target, instruments and "other". Most internally generated requirements concern the first three groups. To ensure that it meets externally generated societal requirements during the construction period and throughout the facility's lifetime, ESS must obtain the necessary regulatory permits and licenses, as discussed in more detail in Chapters 10 and 11.

Environmental permit

In the application for an environmental permit, which is the responsibility of the Health, Safety and Environment (HSE) Division, ESS has made a great many environmental commitments, most of which are detailed in the ESS environmental impact assessment (EIA) [562] and the ESS technical description (TD) [563]. These commitments constitute the minimum level of environmental performance that will be expected from the facility; the Swedish authority may impose additional requirements when it grants the environmental permit. The environmental commitments affect the whole organisation, but those relevant to CF are either commitments that specifically address the construction works (thus, CF has sole responsibility for the commitment), or they are commitments that address other parts of the facility (e.g., parts of the machine), which are therefore primarily the responsibility of other parts of the organisation, but which have implications for the design of the buildings and/or site.

The commitments relevant for CF have been identified, and internal responsibility for meeting CF commitments has been delegated. The commitments will be fulfilled by integrating requisite features into drawings, specifications, procedures for the work on-site and other contractual documents. As the ESS programme proceeds, the fulfilment of environmental commitments will be verified through established procedures.

National construction permit

In addition, ESS has submitted an application for a license to commence construction to the Swedish Radiation Safety Authority under the terms of the Swedish Radiation Protection Act. Again, the licensing process is the responsibility of the HSE Division. More detailed information about this application is available in Chapter 11.

Regional building permit

The local authorities in Lund municipality are in the process of developing detailed land use plans for the ESS site and the Brunnshög district. ESS is one of the linchpins of Lund's comprehensive plan for the Brunnshög district [564]. When the detailed land use plan has been established for the site, ESS will submit the requisite applications for building permits to the Department of Housing and Urban Development in Lund (*Stadsbyggnadskontoret*) in accordance with the detailed land use plan.

Sustainability and environmental performance

The host countries vision of a sustainable research facility is encapsulated in the first three of the "four Rs" of the ESS energy concept [565]: Responsible (an energy efficient facility); Renewable (using 100% renewable energy sources); and Recyclable (recycling excess heat produced during operations). Sustainability is one of the organisation'ss core values, along with openness and excellence. ESS's environmental policy states that ESS will contribute to society and be a world-leading model of environmental sustainability for research facilities by: practising sustainable activities every day at ESS, at all levels, and in all aspects of the organisation; always viewing the ESS facility from a life-cycle perspective; striving for excellence through a process of continual improvement and innovative initiatives to prevent adverse environmental impacts; openly demonstrating leadership in environmental commitment with owners, users, collaborators, and suppliers; establishing and maintaining an appropriate environmental management system; and complying with national laws and regulations, as well as with stakeholder requirements.

Several aspects of environmental performance have to be taken into consideration and balanced against each other, in the scope of CF work. These include: biodiversity on site; transportation within the site, as well as to and from the site; energy efficiency of systems and buildings; the sustainability performance of materials being used as construction materials; the indoor environment; and social sustainability. ESS

is considering the adoption of a building environmental classification system as a tool to facilitate a balanced and coherent approach to the different aspects of environmental performance. Several different classification systems are under consideration, including international approaches such as LEED [566] and BREEAM [567], as well as Swedish national systems such as *Miljöbyggnad* (Environmental Building) [568]. The decision about which system to use, and to what extent, has not yet been made.

In order to protect and preserve the ESS facility and operation, a number of risk mitigation measures will be necessary. The main objective of these measures is to protect the facility from sabotage or other threats. For security reasons, detailed information is not presented here. These concerns are analysed in a separate, confidential report. For purposes of Swedish law, the Swedish Radiation Safety Authority regards ESS as a non-nuclear facility. This is discussed in detail in Chapters 10 and 11. Nevertheless, ESS will use some of the Swedish regulations regarding security at nuclear facilities as a reference and guide for its own security strategy. Detailed information about ESS's fire safety strategy is available in a separate internal report [569].

Energy strategy

Efficient energy use, adaptable indoor climate, and robust systems are goals for CF. It is essential that all buildings and systems supporting the actual research programs can perform according to the overall energy strategy, which seeks to capture every possible efficiency in energy use, and to ensure decreases in carbon dioxide emissions [570]. ESS will choose energy systems and indoor climate solutions that simplify the implementation of efficient electric energy use, requiring systems that are reliable, responsible, recyclable and renewable. Examples of practices that serve these energy goals include: using demand-controlled ventilation flows and lighting wherever possible; using heat recovery in air-handling units where applicable; designing low-temperature heating systems; orienting buildings to make the best use of natural daylight; and using energy-saving control technologies for lighting, such as movement sensors and daylight detection.

Design manual

The ESS Design Manual is an obligatory tool for ESS personnel and consultants during the development of the feasibility study, the preliminary design and the detailed design, as there will be several consulting offices working in numerous disciplines and towards various objectives. The Design Manual will help to secure design conformity. Its proper use will enable the organisation to recognise design solutions and ensure that quality standards are met in different objects. Another purpose of the manual is to guarantee efficient construction by using a limited number of preferred solutions. For the immediate future, the manual will be divided into two parts covering structural and system installation issues. The Table of Contents of the structural part is:

1. Introduction and design philosophy;
2. Standards, codes, norms and complementary design rules;
3. General design requirements;
4. ESS material and design determination;
5. Load conditions;
6. Load combinations;
7. List of accredited cross-sectional members, bolts and welding seams;
8. General detail design requirements;
9. Health and safety requirements;
10. Geotechnical information and data reports;
11. Fire safety strategy report;
12. Steel cross sections and
13. Design report template.

Figure 7.3: The main areas addressed by the building programme.

Building programme

During 2011, CF compiled a building programme to form the basis of the building project at ESS [571]. The main areas addressed by the building programme are summarised in Figure 7.3. The programme focused on dividing the functions into easily identifiable parts, describing workflow and flow of materials in different parts of the facility and showing examples of typical cross sections. In addition, the programme summarised a preliminary estimate of space requirements and of the allocation of space to different functions. Although the most recent version of the building programme document is dated 9 January, 2012, the programme has been updated continuously by development of the digital model and further discussions about space allocation. The updates mainly concern accelerator tunnel dimensions and design of stub concept for

waveguides going from the klystron gallery to the tunnel; klystron gallery change of layout, dimensions and functions; target building increased in length and widened to accommodate functions; and instrument buildings revised as the preliminary layout of first instruments has evolved. The building programme forms part of the brief for the architectural competition. The result of the competition will influence the overall exterior design considerably.

7.1.2 Architectural design competition

ESS will be one of the most advanced science infrastructures ever built. The scientific and symbolic value of the facility for the university town of Lund, Sweden and for the global science community calls for a work of architectural and functional excellence. Many of the buildings are technical utility buildings of an industrial nature, which poses specific limits and further challenges the architectural design. The size and location of the facility demand creative and innovative ideas for landscaping and transportation infrastructure. Given the decades-long time scale for the ESS project, sustainability must be a watchword for designers. This means that ESS should not only comply with the environmental, safety and planning standards in place today, but should also lead the science community toward a future of sustainable building and design, in keeping with progressive planning principles that foster sustainable and enriching lifestyles.

The summer of 2012 saw the launch of the architectural design competition for ESS, which was undertaken under European Union rules and regulations[1]. Under EU directives, submissions remained anonymous until the jurys final decision and there was no presentation of submitted proposals by the participating teams during the contest period. An ESS memorandum laid out the criteria for evaluating entries. In addition to the overall quality of the architectural design, there were five criteria: flexibility; economic feasibility; functional feasibility; safety; and sustainability and environmental impact.

The prequalification process selected contestants for the architectural design competition, with a total of 24 initial entries. Four entries did not meet the formal criteria and were eliminated. A shortlist of nine teams was prepared during the prequalification meetings with the jury, ranking the submitted references according to the requested criteria. After a short presentation by each of the nine companies, the jury discussed strengths, weaknesses, opportunities and risks. The five top-ranked teams who were invited to participate in the next stage of the design contest.

All teams received notice on 13 June, 2012. Two days later, the five participating teams were invited to join a start-up meeting at ESS. CF, ESS directors, ESS users and Lund municipality officials gave a general introduction. The participants met with members of the jury and were given the opportunity to ask questions and visit the site. After this introduction the competition was officially launched. During the competition, a questions and answers forum was set up on the Internet, enabling registered teams to submit questions to the competition secretary. About 100 topics and subtopics were addressed, with questions answered and additional files, maps and CAD files supplied to the contestants during the summer. Full documentation of all items and activities on the forum was made available to the jury. On 28 September, 2012 all proposals were received at ESS. A number of meetings were held with the jury during October. Experts within the fields of architecture, landscaping, economy and user aspects were invited to give their assessment of the proposals and supply the jury with insights and discussion helpful to the decision process.

On 19 February, 2013 the Steering Committee endorsed the final decision of the board, and selected Henning Larsen Architects A/S in collaboration with COBE ApS, SLA A/S, and NNE Pharmaplan A/S to become the ESS architects. Their proposal excels in many aspects, providing the facility with a clear concept for the overall design of the site as well as suggesting suitable building types and designs for the various functions. The centrepiece target building is characterised and is instantly recognisable by its overhanging, oval roof. The roof provides an ordering principle for the various buildings around the target area. In front of the target building a dense campus area is planned around several open urban spaces between the buildings, as shown in Figure 7.4. Reception, offices, labs and visitor facilities are planned for this area. The area between ESS and Science Village will be landscaped into an entrance park.

[1]The design competition was governed by Directive 2004/18/EC of the European Parliament and of the Council. For the contest itself, Title III, Rules governing design contests, applied.

Figure 7.4: The central campus, in an artists impression by the architects Henning Larsen Architects A/S in collaboration with COBE ApS, SLA A/S, and NNE Pharmaplan A/S. The target station is in the background, characterised and instantly recognisable by its overhanging, oval roof.

7.1.3 Feasibility study, preliminary design and detailed design

Feasibility study

The purpose of the feasibility study is to develop concepts and to sort out viable main options taking into consideration prevailing scheduling issues. The study will also be used as an instrument to determine the budget with a margin of error under 12%, and to ensure the option of recapture without project delays if necessary. Five items will be used as discussion points during the study: demands and objectives, requirements and constraints, location on the site, conceptual solutions, and proposal.

"Demands and objectives" touch on subjects such as descriptions of activities, ESS visions and concepts, preliminary investigations and goals for maintenance and operation. "Requirements and constraints" deal with the choice of consultants, key requirements and milestones, machine plan and principal flow charts, issues pertaining to governmental entities, reference objects and study visits, analysis of eventual excessive requirements and schedules as well as the budget for the feasibility study and preliminary design. "Location on the site" includes analysis of traffic logistics, site conditions and general plans, geotechnical investigation and site layout plans. "Conceptual solutions" deal with conditions analysis, layouts and functional compliance, study of concept solutions and decisions about preferred solutions. "Proposal" encompasses a summary of objectives, requirements and constraints, site disposition, layouts and flow charts, architectural sketches, basic system installation description, quality, volumes and estimated operational and building cost and project end date.

The completed feasibility study will include the following topics: logistics; layouts; site plan; architectural and structural sketches, facades, plans and sections in scales of 1:400 and 1:200; architectural description in short; structural description in short; system installations description in short with so-

lutions in principle plus cost evaluation; process description in short plus cost evaluation; geotechnical information report; geotechnical data report; design manuals covering structural and system installation issues; specific issues pertaining to governmental entities; reference objects; and cost evaluation with a deviance less than twelve per cent.

Preliminary design

In the preliminary design phase, the feasibility study and alternative part solutions will be assessed with analysis of schedules for different construction methods and levels of prefabrication. The budget will be evaluated with a margin of error below five per cent. The preliminary design will be used to facilitate fulfilment of the project goals and to evaluate what actions are necessary to ensure success. In the detailed design, the feasibility study will be used as an instrument to guarantee that proper quality is achieved and that schedules and budget are met. Six items will be used as discussion points during the preliminary design phase: ESS decision and declaration of goals; programme clarification; the site; development of concepts; main proposal and alternatives; and summary of the feasibility study and the preliminary design.

"ESS decision and declaration of goals" includes programme consent of the feasibility study and decision on preferred concept with alternatives. "Programme clarification" establishes basic demands and constraints, detailed requirements and refinement, equipment programme, social patterns, influence of equipment on buildings and installations, programme presentation, preliminary agreements with governmental entities and detailed analysis of excessive requirements. "Study of the site" details plans, localisation of services, emission limitations and sets degrees of freedom for traffic. "Development of concepts" treats flexibility of alternative construction methods, development of architecture and structural solutions, development of system installation solutions, specialists studies, system installation volume requirements, canalisation coordination and effects on schedules, budget and operation costs. "Main proposal and alternatives" touches on alternative part solutions, evaluation of alternatives, preliminary decisions on alternatives, remaining alternatives, descriptive list of content, evaluation of construction methods, detailing of structures, the schedule, costing and decision on alternatives. In the "summary of the feasibility study", documents will be coordinated, valued and decided on, necessary decision-making executed and reference documents collected, budget calculated and presentations planned.

Deliverables of the preliminary design are: previous feasibility study; architectural drawings and descriptions with plans scaled 1:100 and 1:200, sections, facade elevations and a room book; structural drawings and descriptions including foundation plans scaled 1:100 and 1:200, structural sketches, plans and crucial sections scaled 1:100 and 1:200, retaining walls drawings, pile plans and estimation of reinforcement as well as structural steel; system installation schemes, drawings, descriptions and statement of construction methodology for system installations; building related process schemes, drawings, descriptions with statement of construction methodology and a final decision on interfaces; and cost evaluation with a margin of error below five per cent.

Detailed design

The detailed design encompasses and implements the preliminary design decisions. All drawings and documents necessary for construction will be reviewed and collected in appropriate sub-projects. There might be a need for very early engagement of contractors; this would require careful planning and execution of tender packages. It should be noted that the detailed design phase will continue for a number of years after the first proton beam, even if at a much-reduced pace, following instrument engineering and late developments.

7.1.4 Construction, commissioning, operation, and decommissioning

Construction

The most basic function of CF is to provide space for the ESS facility. Contractors will carry out the actual construction works. CF will be responsible for organising and coordinating the works on-site during the construction phase, and also for the work carried out on-site by other divisions. CF will be responsible for setting objectives for the construction works, collaborating with the HSE Division in obtaining the necessary permits, defining the requirements that will be imposed on contractors, creating incentives for contractors to take all relevant aspects of their work into consideration (e.g. health and safety, environment

and quality aspects) and reviewing the work carried out by the contractors. The management systems of the contractors will be used to as great an extent as possible – provided that they fulfil the requirements set by ESS – in order to make the work more efficient.

Several requirements have to be met before construction can begin on-site. All necessary permits have to have been granted. It may be necessary to apply for the building permit in several stages in order to avoid delay should one or more parts of the building permit be controversial. ESS must check each permit carefully to ensure that it takes account of all requirements. CF needs to procure one or several contractors. The most suitable set-up, in terms of cost- and time-saving, will be a partnering contract with incentives. The contractors need time to prepare the work in terms of planning, procurement of subcontractors, etc. If possible, the contractors will participate during the detailed design phase and, in some case, even during the preliminary design phase. During construction, CF will be stationed on-site. Keeping the works within schedule is a great challenge. Therefore, detailed planning in which construction work, deliveries and logistics are coordinated is crucial. Keeping within budget will be critical for the success of the project. Processes and procedures will be developed to ensure an easy and efficient way to keep track of costs.

Commissioning

Detailed information about conventional facilities commissioning work is given in Chapter 9, but in brief the responsibility of CF includes design management, construction, and testing and commissioning. The goals of "design management" are to define the extent of commissioning works, and to ensure, by incorporating correct facilities, that commissioning can be carried out. The goals of "construction" are to ensure that works are carried out in full conformance with relevant requirements and quality management systems; to ensure that building information management guidelines are followed; and to require the contractor to develop a detailed commissioning method statement. The goals of "testing and commissioning" are to establish a CF commissioning team; to carry out functional tests to ensure verification of all requirements on a system working in a stand-alone mode; and to coordinate tests to ensuring verification of all requirements on a complete plant or building when all relevant systems are in operation and are fully interconnected.

Operation and maintenance

The cornerstones of CF operation and maintenance responsibility are to maintain the "four Rs" of the ESS energy concept: responsible, renewable, recyclable and reliable. CF responsibilities under operation and maintenance include building maintenance and support, fire and safety, electrical systems, and water systems.

"Building maintenance and support" includes energy management. ESS will recycle energy from cooling the machine into the district heating system operated by Lunds Energi. Systems in radioactive areas, such as ventilation, heating and cooling water circuits and waste water, need proper design and monitoring in order to ensure safety at all times. Given the complexity of the facility and the presence of (low) levels of radiation, there will be a need for an internal, ESS staff-based, "fire and safety" emergency squad. The role of this squad will be to assist the local fire brigade in technical assessment of emergency situations, such as how to handle a fire and when and where to enter. Laws, norms, standards and working procedures generally govern the operation and maintenance of "electrical systems". This applies especially to high and low voltage systems that must be handled by certified staff. "Water systems" treatment plants will supply deionised water to cooling systems and laboratories. Water cooling systems will be used as primary cooling media, but will also be used as a secondary system connected to a cryogenic cooling plant.

Conventional building systems will be controlled and monitored by the integrated control system (ICS) in a safe and logical way in order to prevent mistakes and incorrect actions. The ICS is described in Chapter 5. In order to minimise risks associated with remote handling, vital functions will be physically interlocked or hardwired. The facility will operate 24 hours a day, seven days a week, requiring at least six shift teams. Each shift will include one building management system (BMS) control engineer; one electrical, low and medium voltage (LV and MV), engineer; one fire alarm engineer; one security system and communication engineer; and one HVAC engineer. Additional staff, required on a 40 hour a week basis, are: one technical operations manager; two building finishes engineers; and one administrator. There will be a total of 34 in-house employees.

The CF operation and maintenance functions also include operating an asset management system to

support a planned maintenance system. This system will generate work orders, both for preventive and breakdown maintenance. Maintenance records will be created and kept. The asset management system will also manage spare parts and service agreements with contractors. Critical spare parts need to be stored on site. There will be full redundancy for systems or devices that have the potential to fully or partially shut down ESS operations when they malfunction. A risk analysis will be carried out to identify critical spare parts that are involved in such a shutdown bottleneck. Spare parts with a long lead-time for delivery will also be treated as critical and will be stored on-site.

Decommissioning

The decommissioning planning includes design management (ensuring that system and structural design will allow for decommissioning); construction (documenting all materials used); and operation and maintenance (properly training personnel, conducting relevant quality assurance procedures, maintaining records and managing waste). Further information about ESS decommissioning planning is given in Chapter 10.

7.1.5 Building information modelling

Developing an information management system adequate to meet the comprehensive project goals poses unique challenges for CF. The complexity of the facility in combination with the complexity of the design, construction and operations processes, which involve a large number of internationally and temporally distributed stakeholders, require the implementation of a common data environment including the definition of intelligent and coordinated 3D-models with meta-data for all disciplines. For these reasons, building information modelling (BIM) guidelines were developed during autumn 2011 comprising specifications for digital information modelling and delivery for all design disciplines within CF [572].

BIM at ESS encompasses a combination of different databases and model files, such as 3D models, 2D models, cost estimates, and schedules. The integrated process in which BIM is used is called "virtual design and construction." The principles for BIM refer to common denominators for information models and are based on international (ISO) and Swedish standards, reflecting state-of-the-art information modelling techniques. Careful account has been taken of the diversity of design disciplines and of the long periods of time over which model-based data will have to be managed.

The BIM process has three components. First, the *process definition* states what information is to be delivered for different purposes and how this process is organised. These definitions are mainly derived from Swedish national guidelines such as *Bygghandlingar* 90 Parts 7 and 8 [573]. Second, the *data model* defines what information models are used and how they are structured. Application-specific definitions are applied in combination with common exchange formats. Third, the *naming conventions* explain the different criteria governing how things are defined. These criteria are mainly derived from Swedish Standards, such as the BSAB96 classification system and SB CAD Standard, in combination with the ESS naming conventions [515, 574, 575].

The BIM guidelines formalise the integrated information management required for the 3D-design of CF, digital documents and 2D drawings, design review and 3D coordination, quantity take-off, cost estimation and control, scheduling, as-built documentation and CE marking and facility management. The BIM guidelines are defined in harmony with the overall product life-cycle management (PLM) and 3D modelling principles as applied at ESS. It was recognised that the conditions for PLM and 3D modelling differ fundamentally for CF in terms of technical infrastructure, methodology and processes as compared to those at the ESS Design Office. For example, the Design Office applies a common CAD tool (Catia v6) for all disciplines. The CAD tool is directly integrated with the PLM-solution Enovia, called CHESS within ESS. Such a principle and choice of CAD tool would not be suitable or feasible in CF design, construction or operations processes. The BIM guidelines and related processes bridge this gap, and ensure integration of the information modelling processes at CF into the overall information modelling processes at ESS. A specific area within the CHESS system has been developed during spring 2012 according to the BIM guidelines. The area is called BLESS – Building Lifecycle at ESS. BLESS allows external and temporary actors involved in the design, construction and operations processes of CF to integrate with the overall information management at ESS.

BIM and data coordinators and models managers, working closely with project and design managers at CF and the Design Office, coordinate the BIM guidelines and the processes necessary to implement them. Each design discipline, contractor and supplier involved at CF is required to assign a BIM leader

to ensure proper application of BIM. With the ESS programme moving into the preliminary design phase, the number of actors in the design process will increase substantially as will the amount of model-based information.

7.2 Location and conditions at the site

ESS will locate its facility on a 74.2 hectare site identified on the Swedish national mapping system as Östra Odarslöv 13:5, situated northeast of the town of Lund in the region of Skåne in southern Sweden. Figure 7.5 shows maps of the region with the site shaded in blue, on the outskirts of the Brunnshög district. The district is undergoing extensive growth and development, within regional land use plans that call for a mixed-use neighbourhood with about 3,000 dwellings and businesses providing employment for 20,000 to 25,000 individuals by 2025 [564]. In addition, Lund and the surrounding region are home to a thriving knowledge-based industrial sector, including such major international companies as Ericsson, Tetra Pak and Alfa Laval. ESS is just northeast of the site designated for the MAX IV synchrotron. ESS and MAX IV construction plans call for an area between the two facilities, the "Science Village, which will include shared infrastructure and services for both facilities.

The site is located on a ridge of gently sloping hills. The ground level in the area varies between 74 m and 82 m above sea level, with the highest part in the south-western corner of the site. Agriculture was originally the predominant land use on the site, but construction has displaced the farm of Korsbäck, which used to occupy a parcel of fertile land in the central portion of the site. There is a residential building on Odarslövsvägen (Route 946) that may be retained as guest quarters during a transitional period. The marl pit (marlstone quarry) in the middle of the site will be removed. A minor road currently under the jurisdiction of a community association that extends north from Odarslövsvägen towards Odarslövs church passing through a tunnel under the E22 will be replaced with a walking and cycling route. The company Kopparstaden AB owns a 65 m high wind power station that is located within the site on its eastern boundary. The wind power station will continue to operate in its present form. Figure 7.6 shows a photograph of the site taken from above in 2011, and gives a close-up view of the Korsbäck farm.

7.2.1 Archaeology and environs

Any archaeological remains that may exist within the ESS property are protected under the Heritage Conservation Act (SFS 1988:950). An archaeological investigation that is required prior to construction is currently underway. The County Administrative Board must grant permission for any displacement of fixed ancient remains. The application process to the County Administrative Board for the necessary permits so that construction can proceed has also begun, with appropriate measures to conserve significant artefacts and to record information about their placement within the site. The archaeological investigation is being carried out in several steps: archaeological survey step 1 [576]; archaeological survey step 2 [577]; trial excavation; and final excavation. Step 2 was carried out in spring 2012 with the aim of clarifying the dating and conservation conditions of the ancient remains identified in step 1. The "trial excavation" took place in autumn 2012 with the aim of deepening knowledge about the ancient remains and of clarifying the archaeological delimitation, content, dating and scientific potential. Figure 7.7 shows two pots that were excavated from a grave on the ESS property that dates back more than a millennium and a half. The "final excavation" is planned for summer 2013, to be completed before on-site work can begin.

Connections to the site

ESS's location allows for fast and efficient travel to and from the facility for researchers and other visitors from Europe and other parts of the world. From the site, travellers can reach Copenhagen's International Airport by car or train in less than an hour. For vehicular access, the site is conveniently located between two public roads, the E22 highway and Odarslövsvägen (Route 946). The E22 highway currently carries about 30,000 vehicles per day past the site, while Odarslövsvägen carries about 1,000 vehicles per day. Neither road is significantly congested at the present time. Traffic in the area will increase as the district of Brunnshög expands to the south of the ESS site, and development of the MAX IV and ESS research facilities will also contribute to this increase. Partly to mitigate this increase in traffic, regional authorities will construct a tramway from Lund Central Station to the area. In addition, local buses and bicycle routes will be available.

Figure 7.5: Maps of the ESS location. Top: Copenhagen/Malmö area. Bottom: Northeastern part of Lunds outskirts. The ESS site is shown as a blue shaded area.

Figure 7.6: The ESS site in 2011. Left: Viewed from above, the site is located in the foreground of the photograph, with Lund in the middle and Malmö in the background. Right: Korsbäcks farm located in the centre of the future ESS facility.

Figure 7.7: Pots found on the ESS property in a grave more than 1500 years old.

A well-developed technical infrastructure is already available in the vicinity of the ESS site, including electricity, water, district heating, and fibre optic network. While the site does not yet have water and sewer connections, VA-Syd (the water and sewer-company) has indicated that it has ample capacity available.

7.2.2 Ground conditions

Earlier geotechnical investigations

Geotechnical investigations have been carried out in several stages as part of the project, beginning as early as 2002. This investigation will be completed in early 2013, with the delivery of the Ground Investigation Report (GIR) and the Geotechnical Design Report (GDR). In 2008 the following investigations were performed: soil and rock sounding (Jb3), Swedish ram sounding (HfA), core drilling (Kb), helical auger sample (Skr) and installations of open system for groundwater observation. A seismic survey, or multi-channel analysis of surface waves (MASW), was carried out in one investigation to enable ESS to calculate the undrained initial shear modulus of the rock and soil. In 2010, an additional investigation was carried out which included more soil/rock soundings (Jb3), helical auger samplings (Skr) as well as further installation of open system for groundwater observations. The aim was to increase the reliability of findings by tightening the investigation grid. Also in 2011, an EIA for the construction of ESS was conducted with

the following investigations: helical auger sampler (Skr), soil/rock sounding (Jb3), core drilling (Kb), and installation of open system for groundwater observation.

Ground and geotechnical investigations in 2012

The 2012 investigations started with a geophysical survey consisting of resistivity (electromagnetic mapping) and magnetometry surveys. The resistivity survey was completed in several sections with the goal of evaluating the overall conditions of soil and rock and to locate areas containing sediments and sand. Figure 7.8 shows a typical section with soil and the underlying sedimentary rock (red colour). The aim of the magnetometry survey was to find the dolerite dikes in the sedimentary rock. The resistivity survey

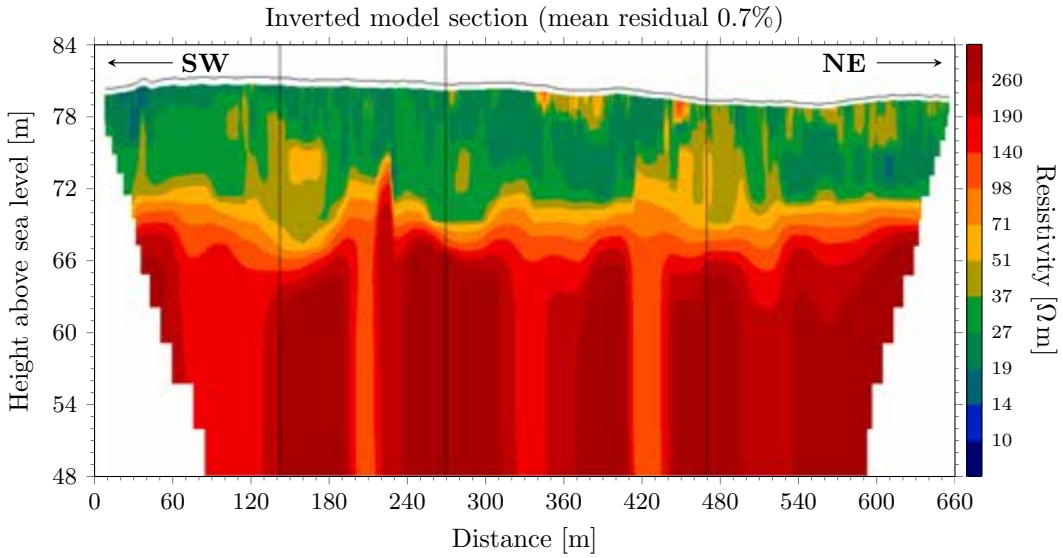

Figure 7.8: Ground resistivity versus depth along a 660 m section.

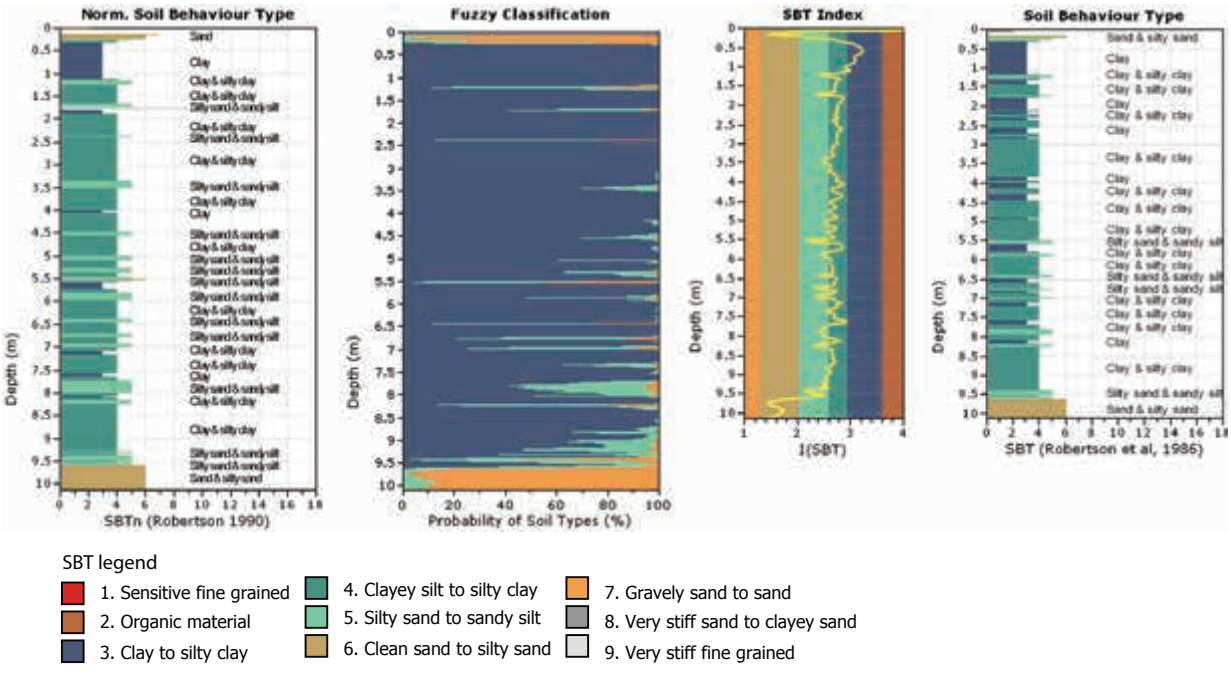

Figure 7.9: Cone penetration test results in clay till ending in the transition zone.

was followed by a large number of cone penetration test (CPT), helical auger samples (SKR) and field vane tests (Vb) in the soil. For undisturbed samples from soil and rock, core drilling (Kb) was carried out, together with soil/rock sounding (Jb-total/Jb-3) for determining the level of the sedimentary rock. Finally, different hydro-geological investigations was conducted with installation of pumping wells and groundwater tubes with filter tips (Rf), flow logging and test pumping. Figure 7.9 shows a typical result and evaluation from CPT-sounding in soil ending in the transition zone.

Soil and rock classifications were primarily carried out at the field, with ocular classification of cores and auger sampling. After that, the disturbed samples from auger drilling were analysed to determine classification, bulk density, natural water ratio, liquid limit and grain size distribution for selected samples of clay till. The soil samples have also been classified according to Swedish "AMA Anläggning 10, concerning risk of frost and material type [578]. The undisturbed core samples of soil and rock were subjected to classification tests and advanced laboratory testing. Rock classification included bulk density, moisture content, slake durability, uniaxial compression test, Brazilian (tensile) test and point load test measurements. Soil classification tests included sieve analysis, grain density, plasticity index, grain size distribution and moisture content. Advanced tests on clay till included an odometer test performed at a constant rate of strain (CRS), and a consolidated anisotropic undrained tri-axial test (CAU) with acoustic measurements and cyclic loading.

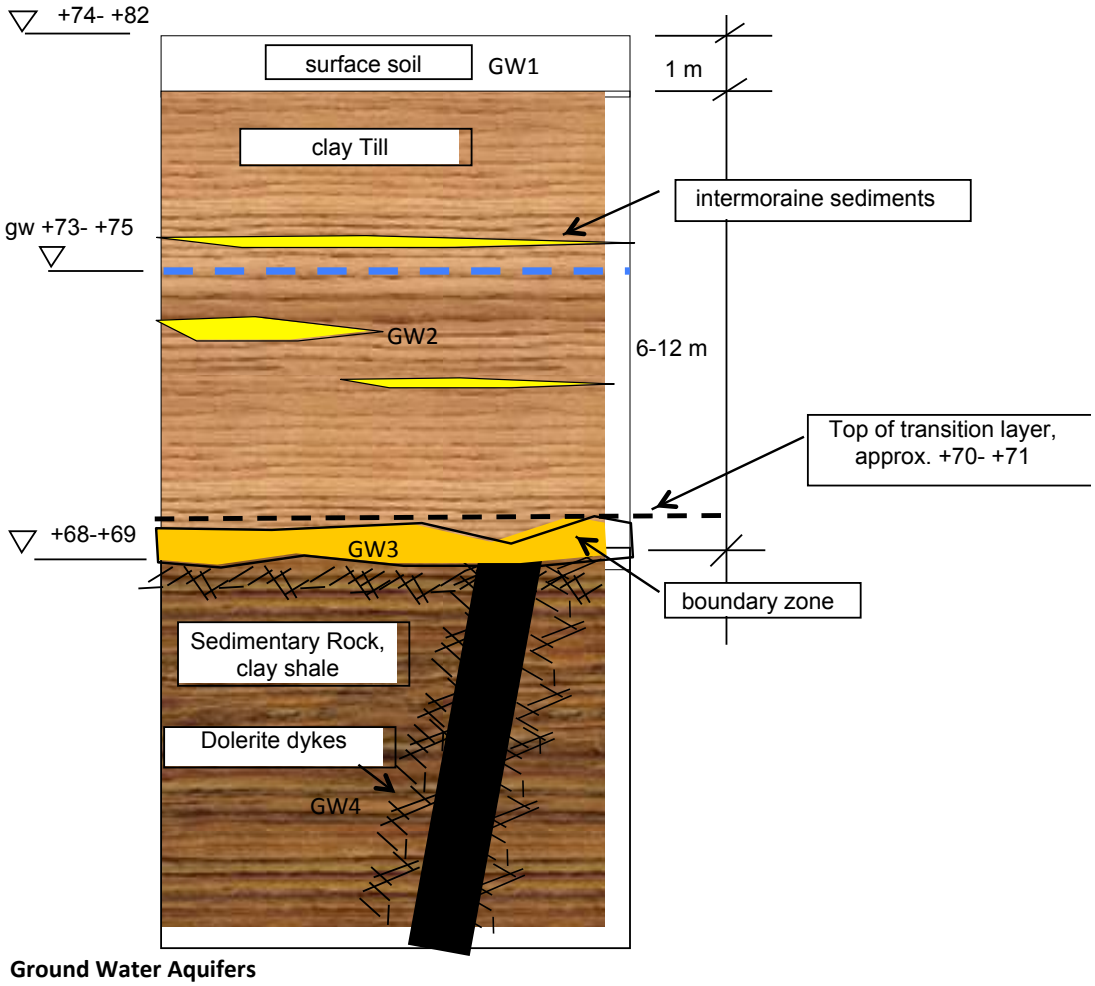

Figure 7.10: Conceptual model of the soil and rock at the ESS site.

Groundwater

Preliminary evaluations resulted in the conceptual soil and rock model presented in Figure 7.10. The soil layers are dominated by clay till, resting on top of sedimentary rock 8 m to 12 m below ground level, which corresponds to 68 m to 69 m above sea level. The topsoil consists of sandy and clayey soils with a substantial amount of organic material. Locally, intermoraine sediments of sand are found between the clay till layers. Based on the investigations available, there is a zone between the soil and rock that is difficult to classify as either soil or rock. The investigation results indicate that the boundary zone is permeable and hydraulically in contact with water-bearing joints in the rock. The underlying rock consists of clay shale and has intrusions of dolerite dikes. Five dolerite dikes have been detected in the area.

Groundwater is present in three different aquifers corresponding to the conceptual soil and rock model in Figure 7.10: in the upper part of the soil (GW1); in the intermoraine sediments (GW2); and in the upper part of the rock and boundary zone (GW3) together with fissures and joints in the dolerite dikes

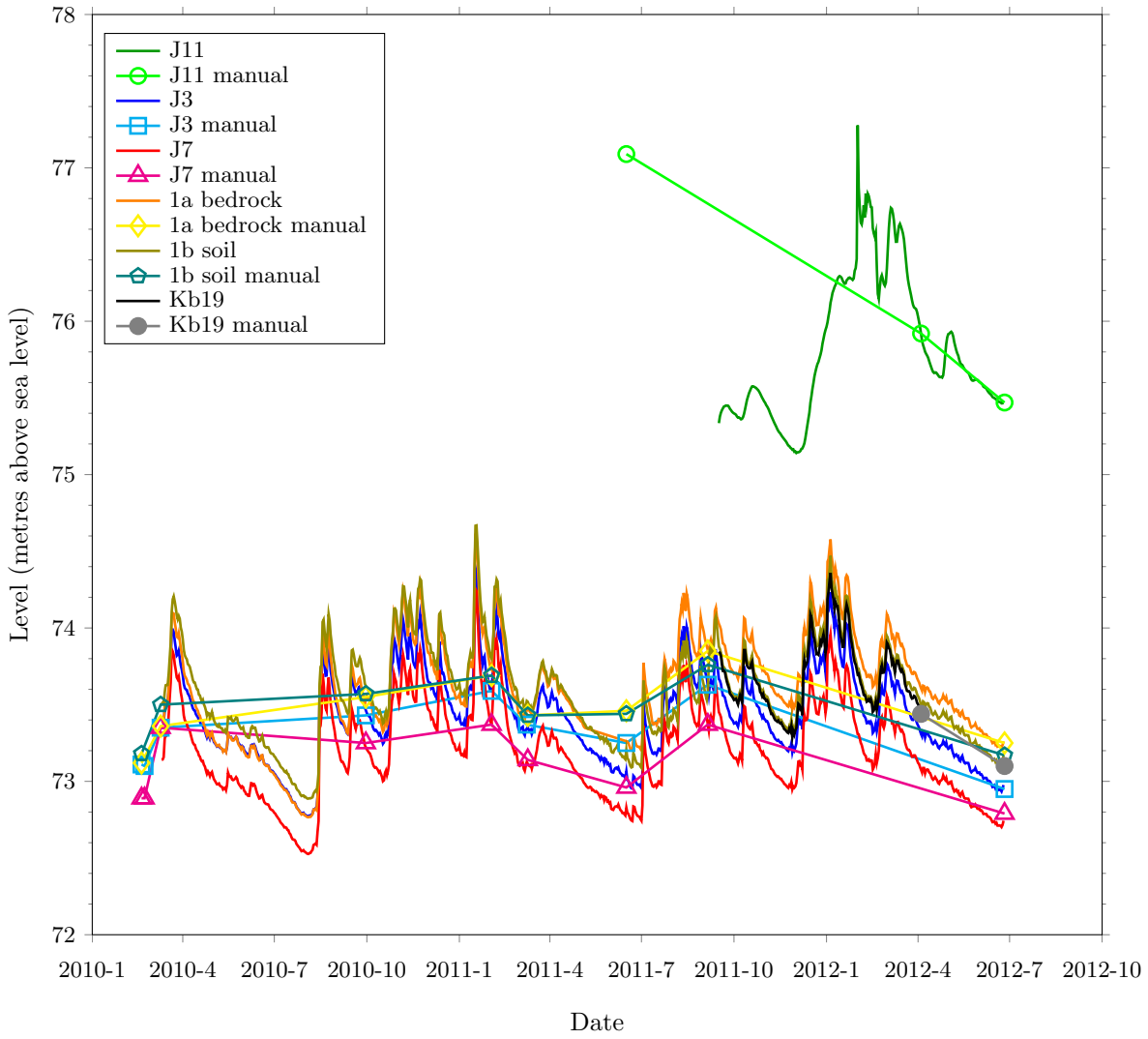

Figure 7.11: Groundwater levels in pipes installed in soil and rock from 2010 to 2012. Lines with points show manual measurements, while continuous lines show automatic measurements with permanent monitoring data loggers. The legend indicates soil measurements with an index J or a qualifier *soil*, while rock measurements are marked with an index Kb or a qualifier *bedrock*. There are no significant differences between the hydraulic head in the soil aquifer and in the boundary zone aquifer, including the upper fractured rock. The green line $J11$ is from measurements near the marl pit, showing locally higher groundwater levels in the upper layers.

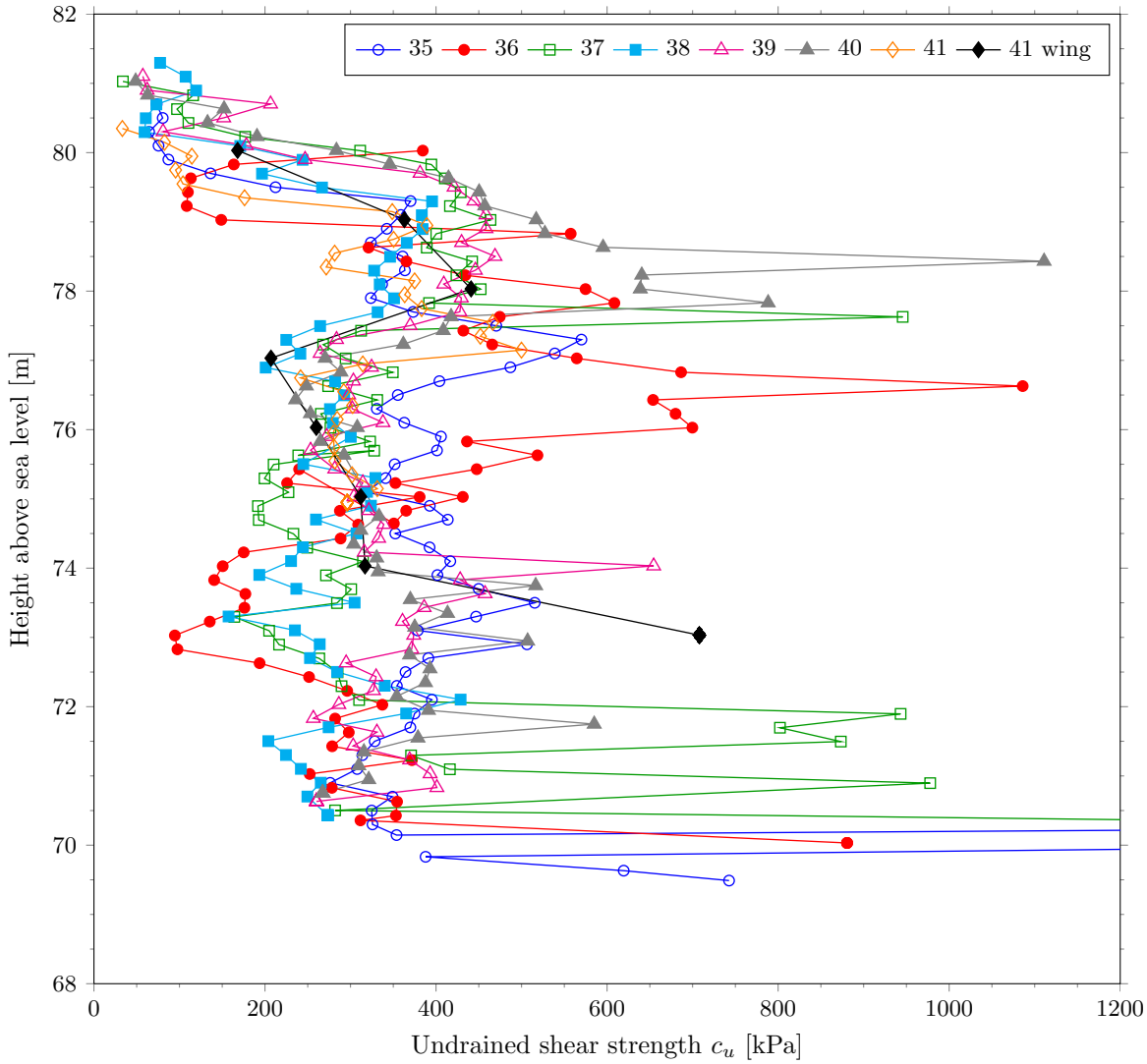

Figure 7.12: Measurements of undrained soil shear strength c_u, showing an example where its value in the clay till is derived from several vane tests in borehole 40 and from cone penetration tests in boreholes 35 to 41. The derived values are then used to establish an average value that is used for design.

(GW4). The clay till units and the undisturbed rock are considered to be practically impermeable or to have very low permeability. Generally, the ground water levels vary between 70 m to 75 m above sea level, corresponding to levels 3 m to 5 m below ground level. In the southwest part of the area and around Korsbäcks farm, ground water levels are mainly at 73 m to 74.5 m above sea level. Figure 7.11 shows groundwater levels over a two year period. Groundwater flows in two directions in the area; towards the north-northeast and towards the south-southwest. Around the marl pit there is a local, radial flow in the upper layers, as illustrated by the green curve in Figure 7.11.

7.2.3 Preliminary values from the ground and geotechnical investigations

Tables 7.1, 7.2 and 7.3 present average and range values from a preliminary evaluation of soil and rock parameters. These values may change slightly upon delivery of the GIR and the GDR. The values for undrained shear strength C_u that are shown in Table 7.2 and Figure 7.12 are derived from cone penetration (CPT) tests correlated with *in situ* methods such as vane tests. Drained cohesion, friction angle and modulus values based on undrained shear strength are derived empirically and will be correlated with the advanced laboratory testing.

Soil layers	**Water content** [%]	**Liquid limit** [%]	**Density** γ [kN/m^3]	**Density** γ' [kN/m^3]
Upper clay till	11 - 24	17 - 36	20 (19 - 23)	10 (9 - 13)
Lower clay till	14 - 20	17 - 36	22 (21 - 23)	12 (11 - 13)
Boundary zone	–	–	18	11

Table 7.1: Soil water content, liquid limit, and densities. "Upper clay till" is above 78 m above sea level, "lower clay till" is below 78 m, and the "boundary zone" is between 70 m and 71 m.

Parameter	**Unit**	**Average**	**Range**
Upper clay till			
Deformation modulus, E_{50}	MPa	30	20 - 40
Pre-consolidation pressure, σ'_c	kPa	500	400 - 600
Undrained shear strength, C_u	kPa	100	80 - 150
Undrained shear strength, c'	kPa	0	0 - 10
Undrained shear strength, ϕ'_k	deg	32	31 - 33
Lower clay till			
Deformation modulus, E_{50}	MPa	50	40 - 70
Pre-consolidation pressure, σ'_c	kPa	1000	800 - 1200
Undrained shear strength, C_u	kPa	250	200 - 450
Undrained shear strength, c'	kPa	50	20 - 90
Undrained shear strength, ϕ'_k	deg	32	31 - 33
Boundary zone			
Deformation modulus, E_{50}	MPa	50	30 - 70
Pre-consolidation pressure, σ'_c	kPa	1000	800 - 1200
Shear strength, ϕ'_k	deg	38	37 - 39

Table 7.2: Soil strength and deformation characteristics.

Parameter	**Unit**	**Average**	**Range**
Density, γ	kN/m^3	27	26 - 30
Compressive strength, σ'_c	MPa	40	25 - 105
Tensile strength, σ'_t	MPa	4	3 - 16
Deformation modulus, E_{50}	MPa	10000	7000 - 22000

Table 7.3: Rock strength and deformation characteristics in the clay shale between 66 m and 40 m above sea level.

Modulus values	M_{virg0} [MPa]	k_{virg}	$M_{virg100}$ [MPa]	$M_{virg500}$ [MPa]	M_{rel0} [MPa]	k_{rel}	M_{rel100} [MPa]	M_{rel500} [MPa]
Sample ID								
Kb22.6.786-789	20	38	24	39	66	174	83	153
Kb23.4.521-524	16	34	19	33	112	115	123	169
Kb24.5.658-661	13	40	17	33	72	137	86	140
Kb25.6.776-779	20	26	23	33	59	71	66	94
Kb26.7.862-865	10	26	13	23	45	70	52	80

Table 7.4: Compression modulus values obtained through constant rate of strain (CRS) tests. The modulus values M_{virg} and M_{rel} at a certain normal stress σ are assumed to follow Equations 7.1 and 7.2.

Constant rate of strain tests with unloading and reloading have been carried out on five different samples. The compression modulus has been evaluated both for the virgin and also for the reloading branch, with the results listed in Table 7.4. The modulus values M_{virg} and M_{rel} at a certain normal stress σ are assumed to follow Equations 7.1 and 7.2.

$$M_{virg}(\sigma) = M_{virg0} + k_{virg}\,\sigma \quad (7.1)$$

$$M_{rel}(\sigma) = M_{rel0} + k_{rel}\,\sigma \quad (7.2)$$

Comparing these results with the modulus values obtained from CPT tests, the values from the reloading branch at stress level between 100 kPa and 200 kPa are in best agreement. Typical values of the bulk modulus from the cyclic triaxial tests are in the range of 150 MPa to 650 MPa. The values obtained from the acoustic measurements were even higher – around 8 GPa.

7.2.4 Utility supplies to the site

The ESS facility places considerable demands on the power grid. The power output is estimated at approximately 40 MW and the energy consumption at around 250 GWh. For this reason, ESS will be connected to the 130 kV network. A 130 kV overhead line passes outside the site, which is part of EON's regional grid. The overhead line has a high capacity and is well suited for connecting a facility of the size and character of ESS. Three overhead lines should be connected to a new receiving station within the ESS site, as shown in Figure 7.13. The receiving station will supply the facility with electricity. During operations, the ESS facility will produce large amounts of waste heat. Figure 7.13 shows how the facility will be connected to the district heating grid for the distribution of waste heat. The total amount of waste heat is estimated to be almost 200 GWh annually. Communication systems with high capacity and availability are required for the ESS facility. Several fibre-based communication links will be constructed to connect the facility to the national and international systems, also as shown in Figure 7.13. The figure also shows how the ESS facility will connect to the Lund municipal water supply grid at a connection point in the southern corner of the site. Waste water from ESS will be connected to the municipal waste water system at the same point.

7.3 Logistics, earthworks and buildings

As the facility will stretch over a considerable area, it is important to establish a coherent design for the site, facilitating communication between all parts and providing a scheme of transportation which can serve logistics, social interaction, gradual addition of further buildings and instrument halls as well as providing an underlying grid for the landscaping. A list of logistical issues includes the handling of activated equipment, sample handling, transport of heavy equipment, and loading bays and access roads. Activated equipment, machine parts and materials enclosed in casks will be loaded and shipped from the southwest end of the target building. This area must be connected to the hot cells and the high bay over the target. Preferably, a hall should be arranged to accommodate a heavy flatbed truck so that the high bay overhead crane can load it. Weights of many tons are expected and safety regulations for this type of transport are rigorous.

Sample handling requires a sample reception area that is central to the general lab building, but which is separated from public access and connected to the instrument halls. The functions of receiving, tagging, shipping and storing samples for experiments will be carried out here. Sample transportation is not heavy, but is frequent. The prepared sample will often be bulky and may require connections to cooling, electrical and other supplies. Transport from the sample environment lab to the instrument is a main concern; it must be swift and preferably indoors. The sample environment is discussed in more detail in Chapter 2.

The accelerator and supporting utility buildings rely on transports of heavy equipment and replacement machinery for the klystrons, cryogenic facility and the accelerator. An assembly hall at the start of the accelerator and additional space in the upgrade area of the klystron gallery will be used for transport and logistics. Sufficient loading bays and road transports are required. Generally all workshop areas need loading bays and access roads for deliveries. The requirements are indicated in the building programme.

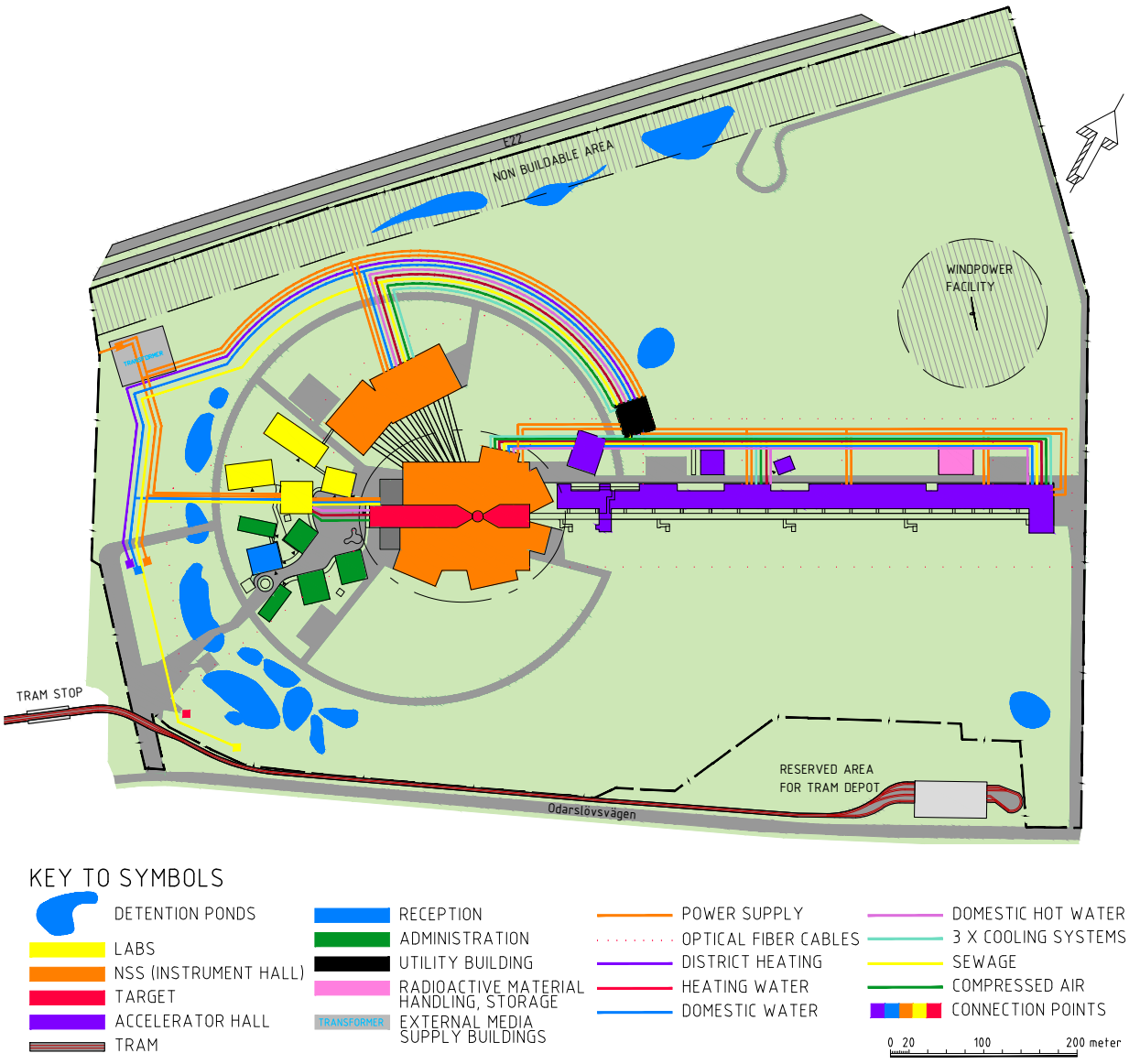

Figure 7.13: Utility supplies to the site – power, communication, heat, water and sewage.

Goods reception

The plant will have numerous local loading bays for varying sizes of cargo transport by lorry. The bays will be designed to fit the expected amounts and sizes of goods to and from the installations and will be equipped with the necessary lift tables, climate shelters and motorised gates and walkway doors. A shared, single location for goods reception for all ESS needs is foreseen. For security reasons and for convenience in handling external transports arriving at ESS, the single location is the most practical solution. The goods reception will be located in such a way that access to the site and reception of goods can be handled from one point in the security system. Special attention will be given to the sample reception area and to the ability to handle heavy transports, transports of encased radioactive inventory, gases and samples.

Waste management systems

Waste will be generated in all parts of the ESS facility, with the majority generated in offices, the canteen and cafeterias, instrument halls, accelerator buildings and target. The waste management system is dimensioned according to the estimated number of 500 to 700 persons who are expected daily at the ESS site [579]. The waste is divided into two main categories – hazardous and non-hazardous material.

Hazardous material includes radioactive, biological and electrical waste. Non-hazardous material includes household, office and packaging waste. Chapter 10 provides additional detail about the handling of radioactive waste. All waste, except chemical hazardous waste from the laboratories, will be stored in a separate building, awaiting disposal [563]. Hence, efficient waste management requires good logistics within the site. An overview of waste streams has already been made [579], and will be further detailed regarding amounts and types of waste for the design purposes of the waste management building. Chemical hazardous waste will be stored adjacent to the premises where it has been generated, awaiting disposal [563].

Elevators

The facility will be equipped with elevator systems so that accessibility requirements under Swedish law are met. The final design of elevator systems will be preceded by a logistics analysis to get the right sizing based on usage rate and the calculated amount of people and goods. The buildings will be planned so that staircase use is encouraged for environmental and health reasons.

7.3.1 Heavy lifting

Overhead crane systems will be installed so that transport requirements in each building are met. The design of each overhead crane will be based on analysis of the capacity and operating range. Table 7.5 contains a preliminary estimate of the list of cranes needed.

Special lifting requirement in instrument hall next to monolith

Close to the monolith in the target area, the overhead cranes of the instrument building will not reach the shielding blocks and other items that need to be lifted. Underneath the high bay floor a complicated lifting requirement needs to be solved, the guide insert including its cask represent a weight of 20 t. The target crane proposal shown in Figure 7.14 is currently under discussion. Additionally, an outrigger (javelin bar) with a lifting capacity of 7.5 t reaching 10 m is proposed on the instrument hall bridge cranes.

Mobile units

There will be a number of locations where the use of overhead cranes will be impractical or ruled out by overhead installations or other reasons. In the klystron gallery, a vehicle-based (robotic) system for lifting and transporting components at maintenance and/or replacement is suggested. Pads running on pressurised air may also be considered useful for moving machinery in this area. The accelerator tunnel requires a special vehicle-based system to facilitate the transport and lifting of accelerator elements, cooling systems and other items along the length of the tunnel.

Location	Description	Number	Capacity [t]
High bay	High capacity	1	95
Active cells		several	–
Target instrument hall	Overhead	4	30
Target instrument hall	Javelin bar	1	7.5
Close to monolith	Guide insert & cask	1	20
Labs		several	0.25 - 0.50
Far instrument hall		1	10
Neutron guides	Shielding blocks		
Cryogenic facility, vacuum & workshops	Smaller	several	10
Front end building		1	10
Waste storage building		1	30

Table 7.5: A preliminary list of cranes. The active cell and waste storage building cranes cranes will have a special design. The front end crane could be replaced by an elevator.

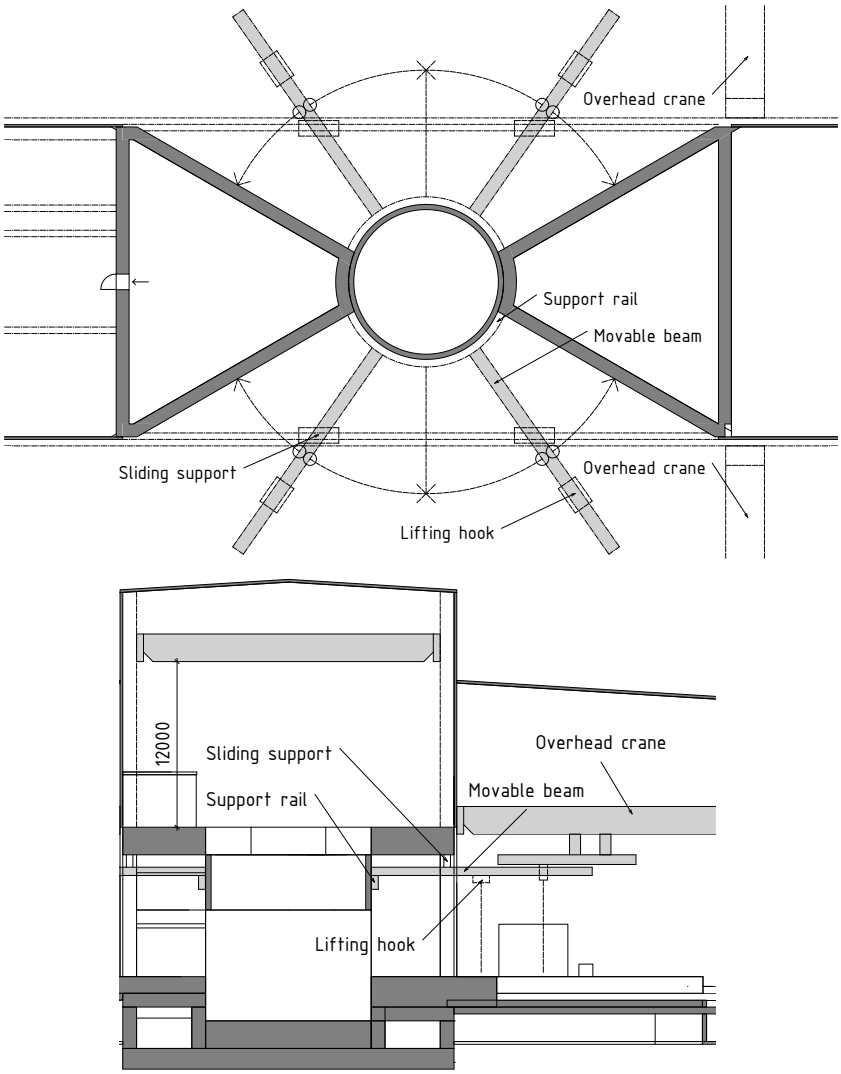

Figure 7.14: Preliminary layout for the target monolith crane. Top: Plan view. Bottom: End view.

7.3.2 Earthworks

Landscaping and urban planning of the ESS site requires the same level of careful attention as the design of the buildings. As the facility stretches out over almost 1 km^2 of land and the chosen site is on a ridge rising above the surrounding landscape, ESS will direct particular attention towards layout on the site, flexible development, transportation within the site and views towards the site from neighbouring locations. Safety barriers will be integrated into the landscape design, to avoid giving a fenced-in impression. The Scandinavian climate can be challenging in winter, with snow and wind combining to render roads inaccessible and causing failures in technical infrastructure. Landscaping design will be used to moderate the adverse effects of climate.

Terracing for the accelerator, target and instruments will be carried out to accomplish a common ground level, balancing the masses within the designated area, which minimises the need for transport of soil. Landscaping integrating buildings with roads, drainage, ditches and storm water detention ponds follow as functions of specified building heights. Use of storm water ponds and open ditches will provide a pleasant outdoor environment on-site. Planting trees and bushes as well as other landscaping elements will contribute to obtaining a soft and green environment around the facility and to connecting it with the surrounding farmland. Landscaping, including choice of plants and design of bodies of water, will promote biodiversity [562]. This will be achieved in different ways, for example, by using native plants, using plants

that attract insects, or by designing ponds with gentle slopes, giving insects and other small animals access to the water.

Roads

A system of roads, bicycle and pedestrian paths is planned around the buildings to facilitate transport and access for various types of traffic across the site. This system will be designed to encourage walking and bicycling. These are divided into several categories, ranging from heavy transport roads, designed to carry loads in excess of 100 tons, to light truck transports and walking paths. All road structures will be dimensioned with respect to each category of vehicle and nature of transport and will be provided with an asphalt surface. One-way streets for heavy traffic will be built with a width of 4.5 m, and if a two-way street is needed the width will be 7.5 m. Roads for light truck transports will be built with a width of 6.0 m and for only passenger cars 5.0 m. Bicycle and pedestrian paths will have a width of 3.5 m. Sustainability has to be taken into consideration when planning the road structures on-site. Pedestrians and bicyclists will be given priority over car traffic. Furthermore, wherever possible, the walking paths will be planned to facilitate public transport to and from the site.

Parking space

Lund has compiled a separate parking standard for Brunnshög where the ESS site is located [580]. This standard must be followed in terms of both car and bicycle parking. However, the building permit stage will take into consideration that the ESS facility is unique, with a large proportion of guest researchers who visit the facility temporarily. Their choice of accommodation and transport during their time at the facility will influence the logistics on-site. The need for parking space will also be affected by the expansion of other modes of transportation, e.g. bicycle paths, tram and bus services, to the ESS facility. According to the parking standard for Brunnshög, 0.4 to 0.5 bicycle spaces should be built per employee. This implies about 350 bicycle spaces for ESS. However, this value may be affected by the fact that ESS is a special workplace and by the future expansion of other modes of transportation. Bicycle parking facilities should be located near the entrance and be equipped with good lighting, weather protection and reasonable security to prevent thefts. Approximately 175 parking spaces for employees and visitors to ESS will be built. In addition, parking areas will be provided for a large number of transport vehicles operating within the site.

Some of the parking areas may be planted with armoured grass coating to minimise the storm water impact. A system for treating polluted storm water will be developed for the parking spaces in which storm water will be led to the southernmost drainage company Odarslöv-Puggängarna. The treatment system will be designed in order to clean the water in such a way that the storm water running to the stream Sularpsbäcken will not be detrimental to the environmental status of the stream or its surroundings [563].

Storm water

Surface and drainage water within the area runs in three different directions and three existing drainage companies connected to the area handle the water.

1. “V Odarslöv – Hoby av å r 1943”, akt 769
2. “Odarslöv – Puggängarna av å r 1945”, akt 833
3. “Odarslöv – Igelösa av å r 1945”, akt 832

The catchment areas for each company are shown in Figure 7.15. Of the total site area of approximately 74 hectares, 32 hectares drain to company 1, around 27 hectares to company 2, and about 15 hectares to company 3.

When an area formerly used for cultivation is developed, the amount of impermeable surfaces increases and the possibility for the water to infiltrate the soil decreases. The result is that the amount of storm water generated within the area will increase. To avoid an overload on the drainage companies, with flooding problems as a result, the storm water flow from the development site needs to be collected in detention ponds with regulated outlets. In these ponds, it will be certified that the drainage from the actual connected surfaces does not exceed the dimensioned magnitudes of the drainage companies. By

Figure 7.15: Map of the three water drainage catchment areas.

using these criteria for dimensioning of the storm water system, the amount of water leaving the area will not change compared to existing conditions.

The main principle for handling of storm water within the area is to use a combination of pipes and open systems. The storm water will mainly be collected through pipes leading to the ponds for the necessary detention. But open storm water systems can also be integrated in the area, where they can be used not only as a technical solution for storm water runoff but also as an aesthetic element in the area which increases biological diversity and enhances ecological values. The detention ponds are located in the lower areas of the site in order to use the natural runoff of the area and to avoid problems of backwater in the systems. The locations have also been chosen with consideration to the position of the existing drainage companies. The detention pond located in the northwest occupies 6,500 m^2, the pond located in the south occupies 7,200 m^2 and the pond in the east occupies 3,150 m^2.

For the dimensioning of open storm water systems on the property, a rainfall with a statistical return time of 100 years has been used in order to ensure that heavier rain situations could be taken care of within the site and as an extra precaution to avoid overload on the drainage companies. They will be designed to promote sedimentation, and the flow to the drainage companies will be unchanged compared to the

situation prior to construction of the facility. There will be a closing device on the detention ponds in order to facilitate sample taking, treatment and removal of polluted storm water [563]. During construction of the facility, the southernmost drainage company, number 2, will not receive any storm water from the site, due to environmental considerations. For detailed information see the Storm Water ID-report [581].

7.3.3 Buildings

The buildings at the ESS facility should reflect the core values of excellence, openness and sustainability. Section 7.1.1 describes the environmental classification system that is being considered for the design and construction of ESS, which will facilitate and guide the consideration and balancing of different dimensions of sustainability. With respect to buildings, the following dimensions of sustainability are of special importance: accessibility, work environment, choice of materials and substances, energy, and quality.

Accessibility

Everybody should be able to visit the facility; therefore it is important that physical accessibility on-site is good. The buildings, the design of the rooms, the furnishings and the equipment must all facilitate accessibility for the disabled. ESS must meet legal requirements affecting both buildings and properties [582,583]. Additional requirements will be detailed in the building permit, which is the purview of Lund municipality. In practice, accessibility is multi-dimensional; for example, differences in levels must not impede access for individuals using wheelchairs, signage should be distinct enough so that people with limited vision are able to find their way independently and hearing aid loops should be installed in auditoriums [584].

Work environment

In order to create a sustainable research facility, the work environment must be good. The design will take the work environment during operation into consideration, as well as the work environment during construction. The buildings will be designed so that inappropriate physical strains are avoided when working in the buildings, and the possibilities to operate and maintain the facility in a safe manner will be taken into consideration [585]. Furthermore, a healthy indoor environment is important for the work environment. Important aspects of the indoor environment include temperature, ventilation, air-borne pollutants, daylight and noise. ESS will develop quantitative requirements for the indoor environment, which will be integrated into the design process. In addition, intangible qualitative dimensions will be taken into consideration, such as design features that foster information exchange, creativity and innovation.

Choice of materials and substances

The choice of construction materials and materials for furnishings and fittings is a factor influencing the sustainability of a building in several ways. For example, some materials and substances may generate pollution in the building during operations, such as volatile compounds that are emitted to the air, affecting the indoor environment. On the other hand, some materials have an environmental impact during the building life-cycle – they may affect the energy efficiency of the building, they may be harmful to workers during decommissioning, etc. The choice of materials may affect the need for maintenance, repair and exchange. The life-cycle of a given material may have an environmental impact. For example, toxic substances or hazardous waste may be generated during the production of the material.

Energy

Over the life-cycle of a building, the energy used during operations constitutes approximately 80% of the total energy use. Hence, the energy efficiency of the buildings and the recovery of surplus heat from the facility affect its sustainability performance to a great extent. The energy concept is described in more detail in ESS Energy Design Report [570], from an ESS point of view. Furthermore, the energy concept could be visualised through different features in the building, showcasing the responsibility, renewability and recyclability.

Quality

In order to make buildings sustainable, quality must be considered. The quality of the ESS buildings must be of an appropriate level so that the schedule can be maintained within budget, without compromising the functionality of the facility. By defining a certain level of quality, requirements can be integrated into the design and construction works. Furthermore, by estimating the life-cycle cost (LCC) of different alternatives, the most cost efficient solution over the building's lifetime can be found.

7.3.4 Accelerator buildings

The accelerator buildings are comprised of three main parts: accelerator tunnel, front end building, and klystron gallery. The cut-and-cover accelerator tunnel has culverts for waveguides to the klystron gallery and emergency exits. The tunnel includes personnel protection system doors and gates to seal off access to the accelerator during operation. The front end building includes underground housing for the ion source, LEBT, RFQ, MEBT, DTL and staging area. The klystron gallery houses radio frequency power sources, klystrons and modulators, and the cryogenic facility, which contains cold-box and compressor buildings for the accelerator, the target and the instruments. In addition to these structures, the tunnel will have culverts connecting it to the cryogenic building and a drop hatch space for access from the upgrade area in the klystron gallery. The structural design includes a non-piled, *in situ* cast, reinforced concrete tunnel.

Figure 7.16 (left) shows the tunnel section of 5.4 m × 3.3 m, and also shows the interconnection with the accelerator tunnel via reinforced concrete underground stubs that are 3.3 m wide, and 12.6 m long. The klystron gallery will provide a clear width of about 18 m and a clear height of about 9 m. Figure 7.16 (right) shows the labyrinth structure of the tunnel emergency exit that is necessary for shielding purposes. The tunnel will rest on over-consolidated clay till with very high shear strength and deformation modulus, thus long-term deformations and live load-induced deformations will be small and acceptable. The design of the tunnel has to consider that the interconnected target building will rest on piles, but there should be no difficulties finding a proper structural solution for the interface. The tunnel foundation level will be +74.4 m above sea level, with base slab upper edge at +74.8 m. These levels have been chosen to ensure safe shielding distance to the transition layer between +70 m and +71 m, and to optimise the logical relationship between topography, mass balancing, the klystron gallery, the target building and the experimental halls.

As the tunnel will run on a groundwater ridge and the average groundwater level is approximately at the foundation level, exterior drainage is not necessary. The tunnel will be covered by an embankment and located at a safe distance from the klystron gallery for shielding reasons. Excavated clay and clay till will be used for backfill and for the embankment under controlled conditions, ensuring proper shielding capability. The design of the tunnel, stubs and emergency exits will be robust, with five emergency exits, including one to the front end building, and eighteen stubs to the klystron gallery. Tunnel expansion joints will be radiation-proof and placed in between stubs at a spacing of 70 m to 80 m.

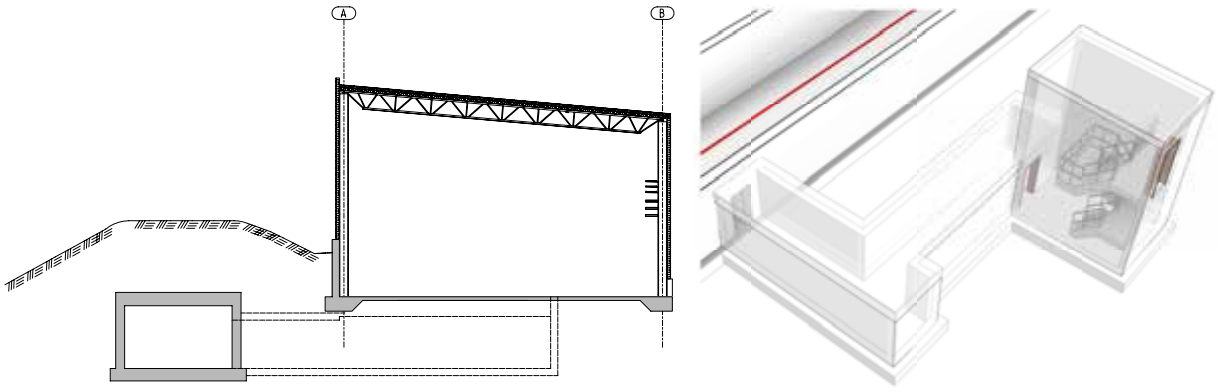

Figure 7.16: Accelerator tunnel and klystron gallery. Left: Standard section of the tunnel and the klystron gallery, showing an underground interconnecting stub. Right: Emergency exit labyrinth, from the accelerator tunnel.

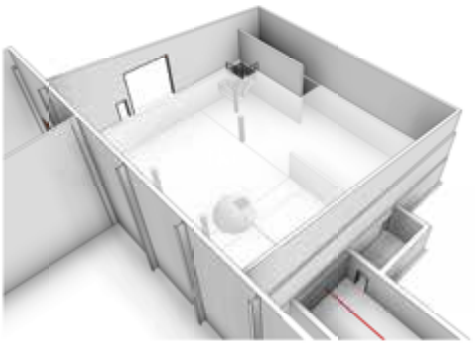

Figure 7.17: Perspective view of the front end building.

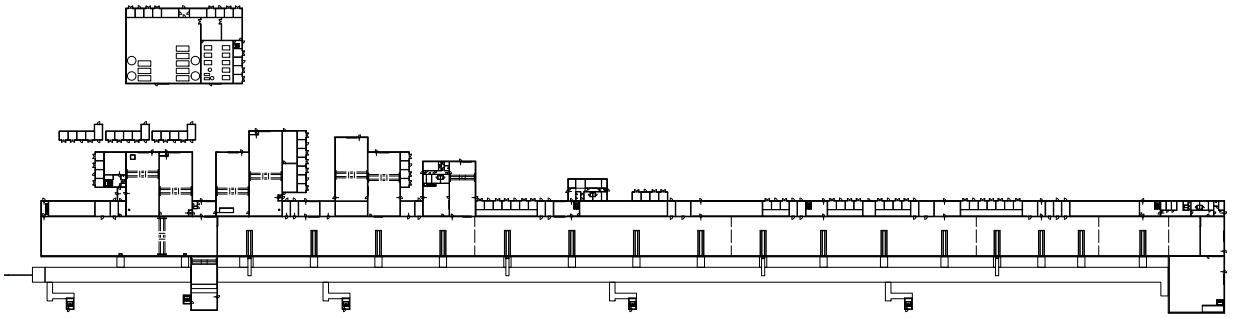

Figure 7.18: Plan view of the klystron gallery plan. The proton beam runs from the front end building on the northeast (at the right), to the target station – not shown – on the southwest (at the left). The 16 underground stubs that connect the tunnel and the klystron gallery are shown.

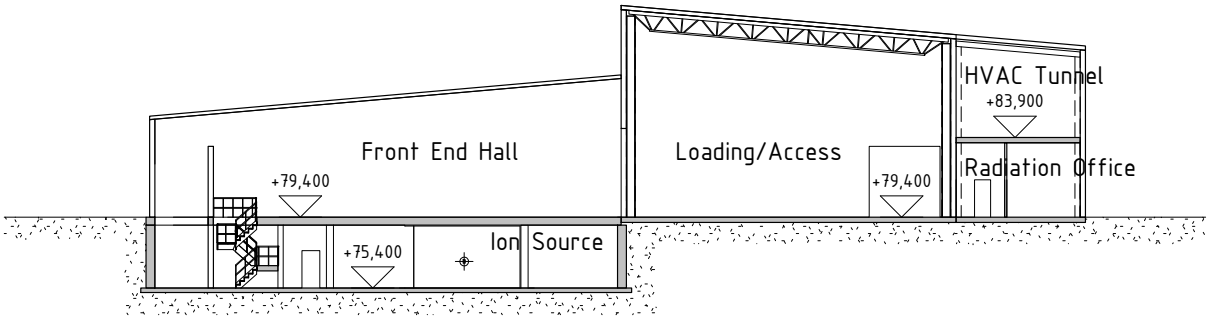

Figure 7.19: Klystron gallery cross section at the front end building (northeast end of tunnel).

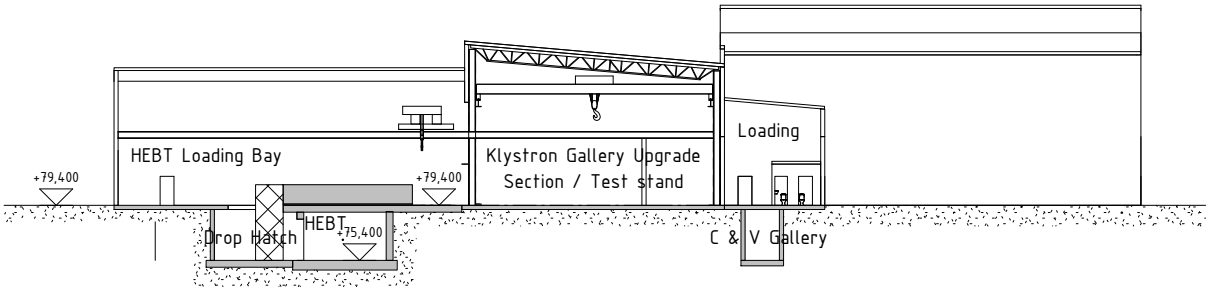

Figure 7.20: Klystron gallery assembly hall and cold box building (southwest end of tunnel).

The front end building that is shown in perspective view in Figure 7.17 has the same structural requirements as the tunnel and the klystron gallery. It is an *in situ* cast, reinforced concrete extension of the tunnel 20 m × 25 m, with a steel superstructure 25 m × 25 m connecting to the klystron gallery.

Klystron gallery

The klystron gallery shown in plan view in Figure 7.18 houses radio frequency power sources, klystrons and modulators, in a building at surface level that runs parallel to the accelerator tunnel. The klystron gallery is spatially separated from the adjacent buildings for fire protection. Figure 7.19 shows a cross section view of the klystron gallery at the front end building. Parallel to the klystron gallery along its northern facade, workshop buildings will provide areas for maintenance, shops, laboratories and storage. Additional adjacent facilities along the northern facade will include HVAC, and the cryo-building comprising compressor and cold-box buildings. Figure 7.20 shows the spatial relationship of the klystron gallery and the cold box building.

The structural design of the klystron gallery will comprise a floor slab of reinforced concrete and a steel frame structure with a corrugated steel roof. The main frame will consist of H-shaped steel columns arrayed along the northern and southern facade with a spacing of 6 m. Columns will support steel trusses spanning the gallery in some 18 m. The main stability of the superstructure will be achieved via flexural rigidity at the column foot, vertical and horizontal bracings within the wall and the roof structure. Additionally, corrugated steel roof and wall cladding will amplify rigidity to the system. The point of intersection to the structural design of the accelerator tunnel will be the upper outlines of the stubs within the klystron gallery and the adjacent floor slab, as shown in Figure 7.21.

The klystron gallery is supported via an elastically bedded, reinforced concrete floor slab (200 mm thick) resting on a layer of pressure-resistant insulation. The shielding embankment of the accelerator tunnel is partly supported by a reinforced concrete socket rigidly interconnected with the floor slab. This cantilever socket also allocates vertical load impact from the exterior wall and facade. In between the stubs and right beneath the floor slab, an arched strip foundation provides sufficient load-bearing capacity for vertical load impact and flexural bending moment, imposed by earth pressure and column support forces.

The average groundwater level is well below the level of the foundation. Nevertheless, the reinforced concrete floor slab is designed in water non-permeable concrete. The utilisation class for water non-permeable concrete is determined to be “A” and the permitted crack width $w \leq 0.30$ mm. The exposition class for the concrete is determined as “XC4” for the bottom and “XC1” for the top. Due to traffic of rubber

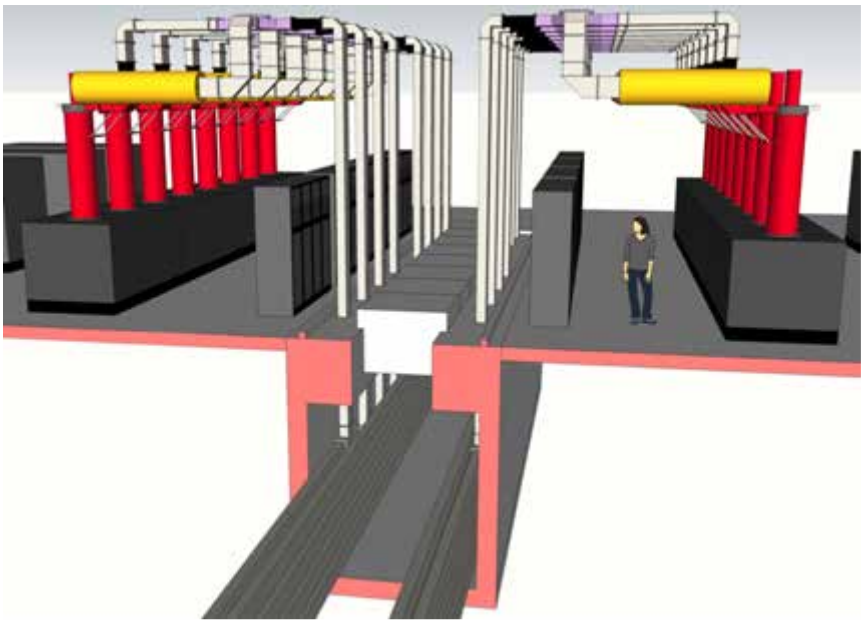

Figure 7.21: Structural intersection of the accelerator tunnel and the klystron gallery, at the upper outlines of the stubs within the klystron gallery and the adjacent floor slab.

wheel forklifts, the top of the floor slab receives the additional requirement class "XM3". Serviceability Limit State combinations with regard to crack-width control are based upon the assumption of expansion joints and slip support (double foil layers between insulation and floor slab). The shear force distribution along the expansion joints is verified applying slip shear force anchors. Arched strip foundations and floor slab are to be cast *in situ* simultaneously, reducing the constraint forces.

7.3.5 Target building

At the target station, the proton beam hits the target and the neutrons are produced by the clash. The target in itself is a highly complicated piece of machinery enclosed in a number of servicing systems and safety barriers. The complexity of this building and its close interaction with the target systems by necessity puts most of its design into the hands of the machine designers. However, the exterior, roof, cladding materials and proportioning, as well as the symbolic value of its function make its architecture worthwhile to study further. The main components of the target building include the accelerator-to-target tunnel; a target monolith; servicing cells for cooling and other systems; handling cells for activated materials; a high bay area above the monolith to service inserts by overhead crane; space allocated for services and safety barrier systems; and an area for shorter instruments. Figures 7.22 and 7.23 show perspective and section views of some of the target building and adjacent structures.

A number of structural issues are highlighted in the target building. Heavy loads on overhead cranes place emphasis on the right choice of load-bearing structure. The weight of the shielding elements close to the monolith puts high demands on the slab. Safety demands for rigidity and earthquake scenarios add further requirements to the target building. In addition to meeting all the demands placed on the structure, the building must have excellent logistics and provide workspaces for man and machine that are comfortable and functional. The structural design of the target building comprises a piled base slab of reinforced concrete, four stabilising reinforced concrete walls, a reinforced concrete hot cell structure, a precast concrete slab and column structure from the base slab to the high bay slab and a steel superstructure from the high bay to the roof, including two major trusses spanning beam port sectors.

Even though geotechnical conditions are very good, *in situ* cast reinforced concrete piles is a necessary solution to meet extreme deflection limits and loads. With a non-piled solution with foundation in the very capable clay till, the building would continue to move under monolith erection, and move in a complicated pattern under major shielding operations. These movements would be difficult to calculate as geotechnical characteristics always vary and shielding operations may be randomly executed, and have been determined to be unacceptably large and unpredictable. The *in situ* cast reinforced base slab will be given a differentiated thickness to meet variable loads and demands on basement free height. The logical relationship between topography, mass balancing, accelerator tunnel and klystron gallery levels, gives an excavation level as low as +72 m and quite close to the transition layer between +70 m and +71 m. To ensure excavation stability, the transition layer water pressure will have to be lowered and controlled during construction.

The four stabilising walls are absolutely necessary to keep beam port sectors free from intruding structural elements and maintain the greatest possible flexibility. They are by necessity symmetrical, stretching out from the monolith to external walls, supporting slabs and high bay trusses and guaranteeing sufficient resistance to an earthquake or aeroplane crash. The hot cell core for processing, storage and maintenance, together with remote handling bays, determines the width of the target building. The core structure will be in reinforced heavy concrete, while remote-handling bays may be precast concrete slab and column structures. Pile and column spacing will follow a structural grid formulated by hot cell and external walls and a longitudinal spacing of 6 m, apart from at the monolith, where piles will be concentrated. Precast slabs need to be pre-stressed and complemented with reinforced *in situ* concrete.

The high bay steel structure with columns, bracing, roof trusses and two main trusses supporting the high bay slab over beam port sectors, also will support an overhead crane with a capacity of 95 t. A ring-formed reinforced concrete wall supported by the high bay slab will enclose the sealed cell on top of the monolith. This will ensure that high bay loads from flask and shielding handling are not transferred to the monolith. In the accelerator to target zone, high loads from equipment and shielding will occur on several slabs. Together with logistical demands this may require a specific pile and column spacing as well as structural slab solution.

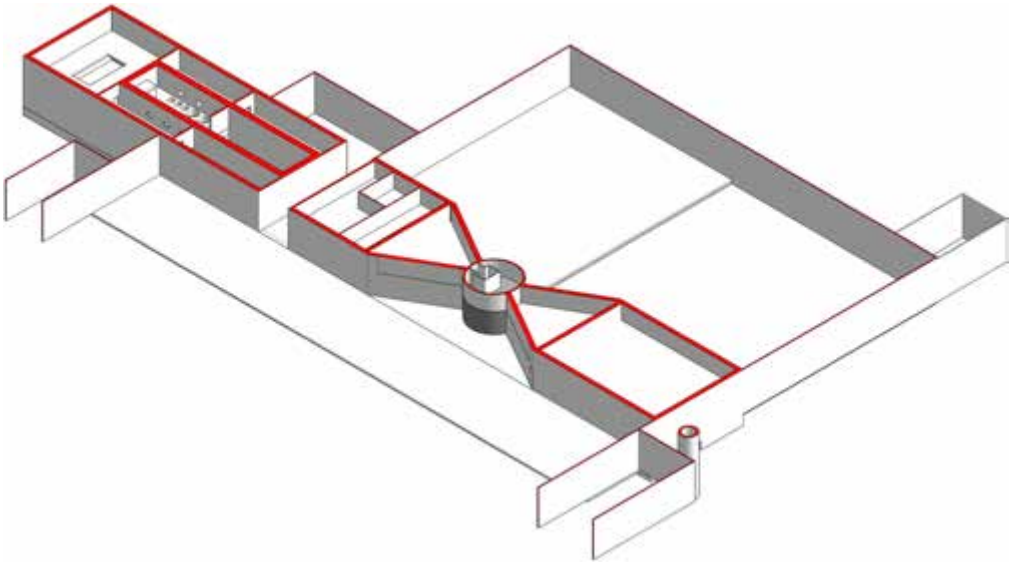

Figure 7.22: Perspective view of the target building and parts of experimental halls at ground level.

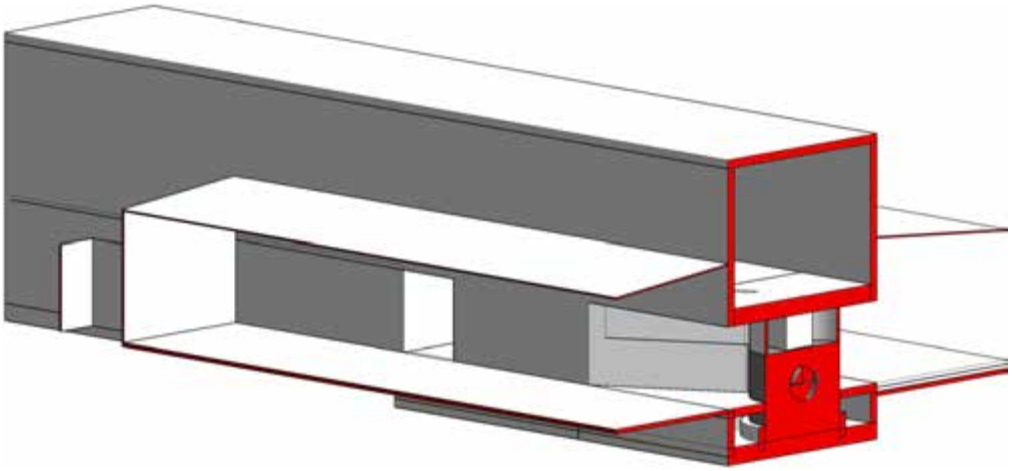

Figure 7.23: Section through the target building, monolith, and parts of experimental halls.

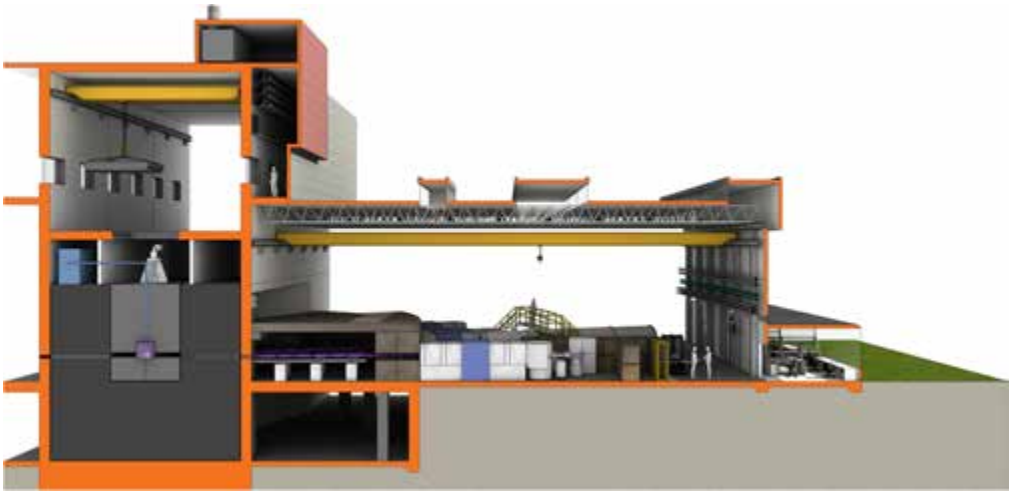

Figure 7.24: Target building and experimental halls [571].

7.3.6 Experimental halls

The experimental halls contain the instrument stations where the neutrons from the source are applied to the samples and detected by the instruments. Instruments in themselves range in space allocation from a couple of square metres up to large installation of hundreds of square metres. The neutron guides leading up to the instruments are planned at lengths ranging from about 10 m up to 156 m. The 156 m extensions of the neutron guides are likely to require a separate enclosure, leading to the experiment hall. Instruments will be built and altered during the entire lifetime of ESS and therefore require flexible and expandable building concepts. Experimental halls also contain: instrument support systems and lifting devices; user laboratories close to the instrument stations; control hutches and offices at the instruments inside the hall; mechanical, electrical and optical workshops and support laboratories; and offices and meeting rooms in adjacent areas.

Figure 7.24 shows a conceptual picture of the target building and experimental halls that are close by. The structural design of these halls is comprised of piled base slabs of reinforced concrete supporting steel superstructures and reinforced concrete culverts. For the same reasons as for the target building, piles are necessary to meet extreme deflection limits and loads. With a non-piled solution with foundation in the very capable clay till, the buildings would continue to move under Monolith erection as they are interconnected to the Target building, and move in a pattern that cannot be determined under various shielding operations. Chapter 2 gives more detailed information about shielding. Deformations dependent on shielding operations would be decaying but still large and unpredictable and therefore have been determined to be unacceptable.

The *in situ* cast reinforced base slabs may be given a differentiated thickness to meet variable loads and pile spacing. Variable pile spacing is necessary to allow culverts to run between pile rows. Steel piles spacing at 2 m by 2 m or more would allow the base slab structural solution to be optimal without beams. Culverts will be used for efficient system installation distribution to instruments, and therefore there will be no need for slab recesses for system installation distribution. Steel superstructures with columns, bracing and roof trusses will support overhead cranes covering experimental hall areas. There will be no structural structures obstructing areas in beam port sectors. Satellite experimental hall(s) will not have to support extreme shielding loads but still suffer to extreme deflection limits, and will therefore be given the same principal structural solution with piled base slab supporting steel superstructure.

7.3.7 Central laboratory, DMSC, office and auxiliary buildings

Different solutions to meet the need for laboratory buildings are under consideration. A centralised laboratory building containing many user laboratories was assumed for the design contest, and in the building programme [571]. These laboratories provide users of instruments the possibility to prepare research and follow up on experiments. They include: a chemical laboratory; a biological laboratory; an actinides laboratory; an NMR laboratory; and a sample reception facility. Some of the laboratories use large and heavy equipment and are in many ways as much workshops as laboratories, and therefore may need to be placed on the ground floor. In addition to the central laboratories, a variety of instrument-specific labs are placed directly at the instrument locations, providing special support to the instruments. These installations may also include mechanical workshops and utilities for handling special services or heavy equipment.

The Data Management and Software Centre is to be built in Copenhagen. Chapter 2 describes the activities at the DMSC, ranging from instruments control and data acquisition to data visualisation and analysis. The DMSC is located at the Northern Campus of University of Copenhagen (KU), in close collaboration with KU, the Technical University of Denmark and all other Danish universities. The DMSC may be located in a purpose-built building, or as a part of another building.

ESS will require a central office building with offices for administration, scientists, directors and other personnel as well as a separate user office. Preferably, the office will be connected to public spaces for visitors, meeting rooms, exhibition space and auditoriums. The central office building should contain at least the following components: offices, with a mixture of open plan and single office rooms; meeting rooms; an auditorium; exhibition space; and a lounge, science room and library. Some of the auxiliary buildings and functions will be located in the Lund Science Village. There are on-going discussions regarding guesthouse, recreation, conference facilities and canteen.

Entrance

The entrance area will be directed towards the town centre and the Science Village development between Max IV lab and ESS. Visitors and workers will get a welcoming feeling from the moment of arrival at the facility. As a user, efficient handling of everyday routines will be taken care of by the reception area staff. As a visitor, a clear and visually communicative environment will aid navigation around the site. The reception staff needs to handle a great many tasks including receiving users and visitors, managing access control systems, sample reception and goods handling, security checks and clearances, dosimeter handling for staff and visitors, tours of the facility for visitors and general guidance and services related to all ESS departments. The entrance foyer should have a lounge area, restrooms and meeting facilities outside the security-controlled area suitable for visitors. An auditorium of reasonable size would also preferably be placed in this area. How visitors from the general public and schools might study the operations at ESS is a subject worth looking into; the possibility to offer for example, a viewing platform in the experiment halls next to the target building should be considered.

Guesthouse and recreation facilities

ESS will receive thousands of users, students and other guests every year. Suitable accommodation close to the research facilities must be provided. Many users stay at the facility during experiments and need to be close to their laboratory for shorter or longer periods. The guesthouse could provide the following functions: simple hotel-like accommodation; recreational facilities for guests and staff; and a canteen. Recreational facilities for the users and staff, connected to the guesthouse, might include a gym, pool, jacuzzi, sauna, lounge and social areas that can be reserved for dinners, meetings or get-togethers is planned.

Ventilation stack

A ventilation stack is needed to reduce the concentration of radioactive emissions in the air, in case of radioactive emissions to the air in the accelerator tunnel and/or in the target building. The stack needs to be at least 40 m above the surrounding ground level.

Central utility building

Some support systems are optimised, technically as well as economically, by locating their main equipment centrally, in a single central utility building (CUB). The CUB will contain the following systems and equipment: a water cooling system, with heat pumps, cooling machines, heat exchangers, pumps and valves; a compressed air system, with compressors, dryers, filters, buffer tanks; a process water system, with deionised makeup water and water treatment equipment; heating system, with heat exchangers, pumps and valves; electrical supply (for CUB equipment), with MV-switchgear, transformers, and LV-switchgear; and local control equipment for the systems and equipment. The CUB will be divided into rooms containing different systems, with redundancy and back-up power supplies, split into fire compartments to ensure high safety, good maintenance level and high reliability.

External utility supply buildings

An overview of external utility supply is shown in Figure 7.13. Some utility connection points will be located on the ESS site. In order to make a harmonious impression, equipment in the hand-over points will be arranged in a way that balances the landscape and building design in general. An example of this is the connection point for electrical power, which will have HV (130 kV) switchgear, transformers, MV (20 kV) switchgear and probably emergency generator sets. The space needed and the height of the HV equipment and transformers makes it difficult to create a building with a low profile. Gas-insulated switchgear, as in Figure 7.25, is somewhat smaller than air-insulated switchgear.

Control centre

The control room represents a central and crucial function at the facility. Here all processes are monitored and controlled around the clock, 7 days a week. The central space occupies a number of control workstations. Typically these will include six to nine computer display panels per seat, keyboards, communication and safety panels. Controls will likely be divided into target, accelerator, conventional facilities,

Figure 7.25: Typical gas-insulated 130 kV switchgear.

and instrument data acquisition. A central meeting space is required adjacent to the seats. A central display showing an overview of the operational status will be visible across the room. Several categories of personnel will man the control room; accelerator and target scientists as well as operators working on shift. The control room is discussed from the perspective of control functionality in Section 5.6. All personnel must be given the room needed to work together and to facilitate work around the clock. Several meeting spaces are needed for debriefing at shifts and for special operations planning. Individual offices are needed for permanent staff close to the control room. A kitchen and lunchroom as well as a lobby for relaxation are suggested. Changing rooms with showers and rest cabins are needed. A separate viewing room for visitors is suggested, reached independently of the control room area entrance.

Conference facilities

As work in teams is ever increasing, the need for meeting rooms and conference facilities is growing. ESS will provide excellent services with a varied and flexible approach to the contemporary way of work. Open and closed spaces will be mixed to create an environment that encourages interaction and meetings. Meeting rooms will be fully equipped for communication. Varied furnishings and wallboards might be considered.

Canteen

A canteen serving users and staff is seen as a crucial function for social interaction and scientific success at ESS. The canteen should be capable either of serving meals produced on-site or of receiving catering on a daily basis for a large number of people. Lighter meals as well as breakfast, coffee, tea, fruit and sweets should be available around the clock.

Storage

Generally, the need for temporary storage of equipment, materials, consumables and other goods is stressed within most operational procedures at ESS. The planning of buildings will take this into account and provide both dedicated storage spaces and allow for local storage of various items in experiment halls, laboratories, workshops, cryogenics building and klystron areas. In building terms, general storage aside, special areas and even buildings will be required for safety and security reasons including storage of gas, flammables, hazardous substances and material sensitive to magnetism, shock, high or low temperatures, etc.

Waste building

All waste except chemical hazardous waste will be stored in a separate building, awaiting disposal. There are several legislative requirements concerning premises where waste is stored which must be fulfilled. These include requirements that the building be equipped with leakage protection, that hazardous waste

be stored separately from non-hazardous waste and that different hazardous waste fractions be stored separately from each other. The waste management system is further described in Section 10.4, and any specific requirements on the waste building will be identified in the more detailed analysis of the waste streams that will be performed.

7.4 Electric power services

Table 7.6 shows a summary of load levels anticipated for the different main consumers of electrical power. The optimal strategy for distribution of grid power from secondary substations is under study. The final choice will depend on technical, economic and environmental considerations. A conventional cable solution has some limitations and disadvantages compared to an alternative bus-bar supply solution. The final solution is likely to differ between the more industrial parts of the ESS facility and the parts accessible to the public. Life-cycle cost analyses will determine the choice. On-going investigations and coordination between all parts of the facility, including all machine and research equipment, will provide the information basis for more detailed design considerations in the upcoming preliminary design.

Electric power will be supplied to ESS at a high voltage level (130 kV). It will be transformed to a medium voltage level (20 kV) for distribution within the facility. In immediate proximity to the loads, substations with redundant structure, containing 20 kV switchgear and transformers, will transform the medium voltage power to low voltage power (e.g. 690 V or 400 V). In addition, a number of systems will use extra low voltage (ELV) power (less than 50 V), including systems related to fire safety, security, surveillance, communication and building management. The different load centres place different requirements on the quality of the electrical supply, depending on the consumers. However, some base requirements are common for the whole electric power system and grid: it must not jeopardise the safety of staff and visitors; its design must facilitate operation and maintenance; the adverse consequences of faults must be minimised; disturbances should be mitigated at their source, in general; dimensions must be based on a life-cycle cost analysis; and sustainability must be an integral part of design and operational decision making. These requirements will be met by following applicable Swedish legislation, Swedish and international standards and good engineering practice.

Primary distribution substations

ESS will be connected to the 130 kV sub-transmission grid in the area. Today, there is a three-direction interface where two regional grid branches supply the Eastern Receiving Station for the city of Lund. To connect the research facility, the three-direction interface will be replaced by a new substation, erected close to the site. The capacity of either of the two feeding 130 kV lines is enough to allow uninterrupted operation when one line is disconnected for maintenance or for other reasons. The switchyard can be designed to facilitate instant redundancy in case of a fault in one of the power transformers or bus bars.

Load type	**Main power** [MW]	**Aux. power** [MW]	**Back-up** [MW]	**Comment**
Accelerator	23.5	4.2	–	Assume 15% of total power is LLRF & controls
RF-test hall	1.1	TBD	–	Power is independent of Accelerator supply
Target station	6.0	0.3	TBD	Control & containment systems need UPS
Experiment halls	4.8	TBD	TBD	Option of 10 MW available at all 4 halls
Cryoplant: accelerator	4.3	0.2	0.8	Helium recovery and control system backup
Cryoplant: target	2.2	0.2	0.2	Control system (only) backup
Computing & controls	TBD	TBD	TBD	30 min of UPS power for safe shutdown
Heat recovery	8.2	0.7	–	Cooling is not needed if accelerator stops
Facilities	3.0	–	0.3	Emergency lighting & security for 12 hours

Table 7.6: Estimate of requirements for installed electrical power. The values cannot be simply summed to directly calculate the electrical power consumption. Cryoplant back-up power is for both a common helium recovery and storage system, and for controls. Target station values are preliminary estimates.

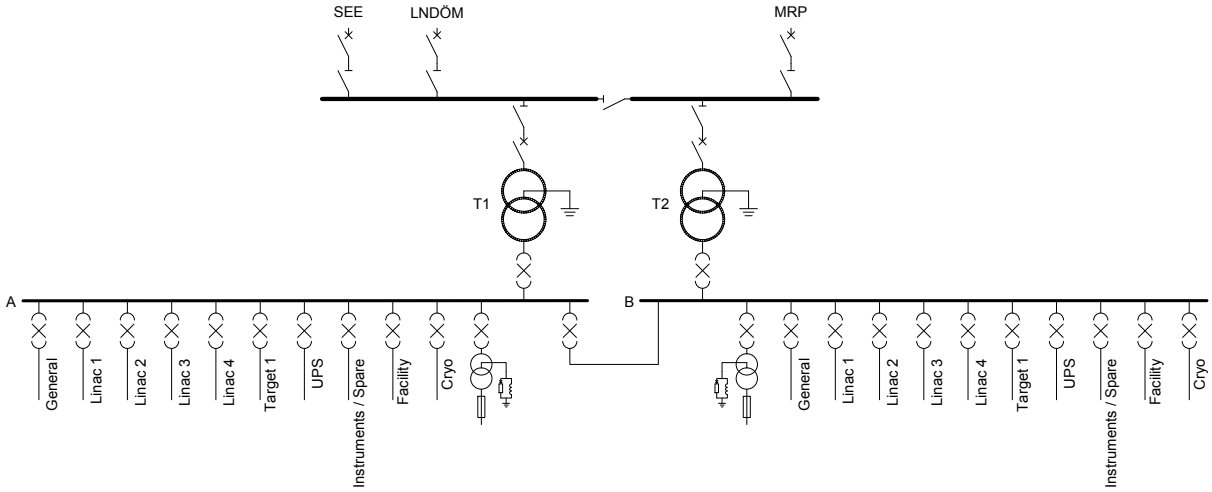

Figure 7.26: Primary distribution substation single-line diagram.

Essentially, there are three different types of 130 kV switchgear. The most expensive, in terms of investment cost, is gas-insulated switchgear, with all components such as switching devices and bus bars contained in sealed gas caskets. Air-insulated switchgear, installed indoors, consists of equipment that is equivalent to that used for outdoor installations. Buildings housing air-insulated switchgear must be larger than those required for gas-insulated switchgear. The least expensive investment costs are incurred with outdoor air-insulated installations. This is the most common approach to power distribution grid switchgear, since it does not have any infrastructure to veil, such as the switching devices and the bus bar. Thus, there is more flexibility for functions such as reconstruction and maintenance of the switchgear, although the installation makes a larger visible impact on the landscape.

The ESS switchyard area uses indoor 130 kV switchgear, either air-insulated or gas-insulated, together with power transformers and medium voltage switchgear. The substation will either be fitted into one large building, or divided into at most three separate smaller buildings. The 130 kV voltage will be transformed by two power transformers to a medium voltage level suitable for distribution to secondary distribution substations closer to the load centres. The power transformers will be an important component of a robust and safe power supply for ESS. Each power transformer will be able to bear the whole load of ESS plus other nearby loads, such as Science Village. This is necessary for maintenance and to reduce the risk of downtime due to transformer failure. The power transformers require proper ventilation. They will be oil-insulated and placed on concrete foundations that can contain the entire volume of oil from the transformer tank. The power transformers will reflect the need for low losses because of the high duty cycle. Due to the irregularity of certain loads, low transformer impedance is important, for example to minimise unwanted voltage deviations throughout the site.

Electrical power grids in Sweden operate as monopolies, based on a concession system and regulated by the Energy Market Inspectorate. EON Elnät is the owner and operator of the regional 130 kV sub-transmission grid while Kraftringen Nät has the concession for lower voltage grids in the area. Two possible grid connection solutions have been identified. The first is a grid connection at 130 kV. ESS would own and operate transformers in the primary distribution substation, with the grid connection interface between ESS and EON Elnät. In the second solution the grid connection is at the medium voltage level. Kraftringen Nät would own and operate transformers in the primary distribution substation, with the grid connection interface between ESS and Kraftringen Nät.

7.4.1 Medium voltage systems

Site power will be distributed at a medium voltage (MV) level of 20 kV. Although this is slightly more expensive than with 10 kV distribution equipment, it has the advantages of higher short circuit power, which improves power quality, and lower currents, which result in lower energy losses and lower magnetic fields. The availabilities of spare parts for 10 kV and 20 kV are roughly equivalent. The ESS MV

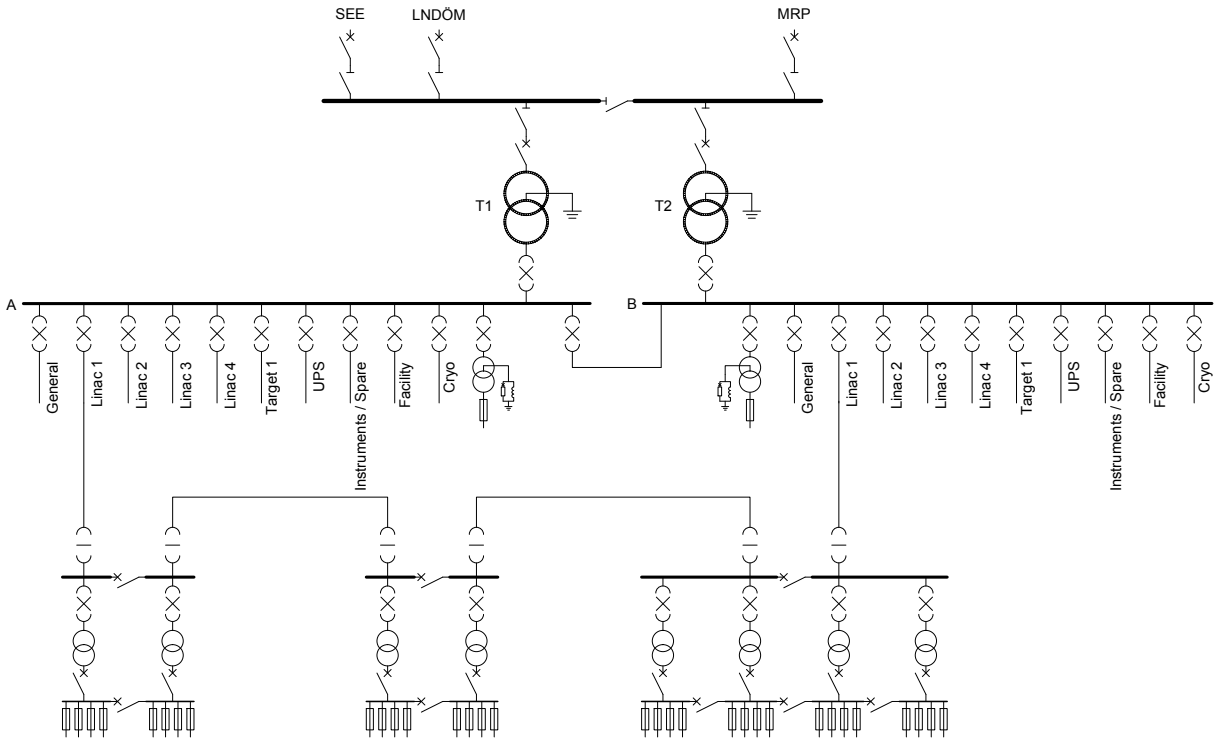

Figure 7.27: Loop power distribution to medium voltage substations.

power grid will be built and will perform as a regular distribution power grid. This will make it possible to use standard and conventional MV switchgear devices and equipment, which will result in a more manageable grid structure that allows for easy operation and monitoring. Safety, reliability, serviceability and sustainability will be prioritised in the selection of switchgear design and type. The area reserved for the primary distribution substation is approximately 100 m by 200 m. A single-line diagram that illustrates the proposed layout of the primary substation is shown in Figure 7.26.

Medium voltage system earthing and earth fault protection

Medium voltage systems in Sweden, with a few exceptions, operate as isolated or arc suppression coil-compensated networks. Conventional Facilities has chosen to embrace this standard for reasons of experience and maintenance. It is necessary to create a neutral point in the MV power grid, due to the vector group of the primary substation power transformers. This will be achieved with grounding transformers at each section of the MV bus bar – for example, a transformer with zigzag winding – which would also be used for internal substation power supply. An arc suppression coil will be installed at each neutral point, connected in parallel with a neutral earthing resistor. This will create an isolated resonance-earthed distribution grid, which will reduce the earth fault currents to safe levels. Fault clearance during earth faults can be achieved without risk of interference to adjacent feeders, by choosing a proper earthing resistance.

Medium voltage cables

The power will be distributed to substations around the facility by MV cables that are designed to handle planned load currents, but which also include flexibility to handle higher load levels. The MV grid will be constructed with feeders interlinked in loops for redundant and flexible supply. Despite the loop structure, the MV grid will not be operated in a meshed manner. Figure 7.27 provides a single-line diagram illustrating loop distribution to substations. The cable design is a balance between investment cost and power losses, taking account of both economic and environmental considerations – the investment cost is higher for a larger cable, but the energy losses are lower.

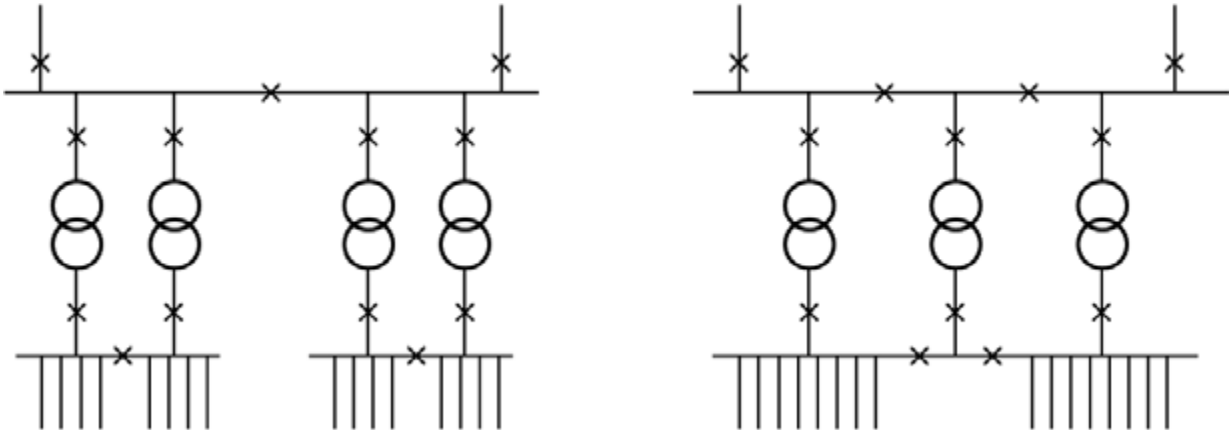

Figure 7.28: Two examples of the provision of spare medium voltage transformers. Left: Four 2000 kVA transformers are grouped into two pairs, each bearing a 60% load. The entire load of one pair can be supplied by a single transformer, briefly loaded at 120%. Right: Three 2500 kVA transformers. Two operate under an 85% load, while a spare transformer has no load.

Secondary distribution substations

Several secondary distribution substations, inside or close to the ESS site, will use a standardised substation that includes transformers, MV switchgear and low voltage switchgear. Additional equipment such as UPS and filters will be provided where appropriate. The standard substation concept has several advantages: it is easy and safe operation, it has fewer spare parts, it has flexibility to adjust to late changes, and it also has flexibility to adapt to future upgrades. It is possible that the low voltage switchgear will be located inside the main buildings rather than in the secondary substation buildings, in order to ensure faster and easier operation. Each substation will be connected to at least two medium voltage feeders, for flexibility and redundancy, as indicated in Figure 7.28.

Spare transformer capacity is needed, for redundancy and to facilitate maintenance. Figure 7.28 shows two examples of this approach. On the left of the figure are four 2000 kVA transformers, grouped into two pairs. All 4 transformers bear a 60% load. In case of transformer failure, the entire load of one pair can be supplied by a single transformer, briefly loaded at 120%. Alternatively, on the right of the figure are three 2500 kVA transformers. Two operate under an 85% load, while one (spare) transformer has no load. If an active transformer fails, its entire load is supplied by the spare. The transformers will transform the medium voltage to a suitable lower distribution voltage of 400 V for conventional loads, somewhat higher for process loads. Both dry-type and oil-insulated transformers are under consideration.

Safe and easy operation and maintenance join reliability, sustainability and economy as important influences on the choice of transformers and switchgear type and layout. The ring main unit MV switchgear in the standard substation design normally includes four switching devices, generally circuit breakers, in cubical cabinets. The switchgear will be designed with some free space to leave open the option of adding more switches in the future. In general, the design will take into account the possibility of future extensions of the switchgear. The design will also provide easy access for operational actions and maintenance, prioritising protection of human beings and equipment. The switchgear will include the appropriate number of switches for a given purpose and will be designed with withdraw-able or removable parts, so that contact with unprotected live parts is prevented. Switchgear will be arc-certified and in compliance with valid standards, minimising the risk of harmful pressure, heat or gas in case of events such as short circuits.

Power quality

Proper power quality is essential for the proper functioning of machines and other electrical equipment. The level of power quality can be described in terms of compatibility between emitted electrical disturbances and immunity to electrical disturbances. Common power quality problems include harmonics, transients and flicker. The operating principle is to take care of disturbances at the source. That is the only way to

guarantee high power quality to all consumers. In addition, all equipment will be adequately designed to ride through voltage dips arising from the external grid. There is no way to mitigate all such disturbances at the source, since they may originate from such causes as lightning strikes at overhead lines and similar unavoidable accidents.

The grid owner ensures a certain level of power quality in the grid. This means that ESS can expect a certain level of power quality at the grid connection point, but it also implies that there are requirements imposed on the facility in the grid connection point. Since there will be both disturbing equipment and sensitive equipment within ESS, proper power quality must be ensured not only at the interface between ESS and the grid owner but also within the ESS internal power system. This can be achieved by requirements on the loads immunity and allowed maximum emittance. Installation of equipment designed to mitigate the disturbance may also be necessary. In general, such equipment will be installed close to the source of disturbance in order to ensure proper power quality to other loads. Harmonics cause losses and capacity reduction in transformers and cables. Mitigation of harmonics close to the source reduces losses and increases the available capacity in the power system.

Power monitoring and control

The entire ESS distribution power grid system will be monitored by a supervisory control and data acquisition (SCADA) system. The system provides the capability of performing actions on specific objects and equipment. Essential information, such as voltage, active and reactive power, and an event list will be included in the monitoring system. The power grid SCADA will communicate this information, as well as the status of connected objects, to the integrated control system (ICS). Server redundancy is essential. If the main server should go down, or if it should be undergoing upgrades, the backup server must take over seamlessly. By the same token, when the main server comes back online, it must takeover seamlessly from the backup server. Both the SCADA system and CF's programmable logic controllers (PLCs) will be updated via a timing system service provided by ICS, to ensure a correct time stamp for alarms and sensor data.

Back-up power

Some consumers will be very sensitive to outages in the power supply. System wide outage has historically happened once every 20 years in the adjacent sub-transmission system. It is not practical to install uninterruptable power to the entire facility. Instead, efforts have been made to identify the most sensitive loads in terms of human safety and economic values, such as delicate or expensive equipment. The cryoplant may be equipped with an emergency backup generator to get the plant in a fail-safe mode in case of a longer interruption. The instrument stations may have parts of their loads supplied on a battery-secured grid in order to permit the safe shut down of equipment. Other examples of loads that will be supplied with backup power are emergency lighting, control room equipment and emergency ventilation.

In many cases, the primary purpose of providing backup power is to ensure that safe and controlled shutdown of specific functions is possible and that computer systems remain online. This can often be achieved by ordinary uninterruptable power systems (UPS). Both local and central UPS solutions will be considered. It is possible that some loads will be connected to local UPS units while other loads will be connected to a central UPS unit. The central UPS build implies that all the UPS services for emergency backup are linked together through one or more centralised systems. However, the centralised UPS can be divided into smaller subsystems that provide better redundancy conditions compared to individual independent uninterruptable power supplies. The centralised battery pack should be constructed with interlinked smaller battery units to improve the redundancy further.

Backup power will be delivered by an ordinary MV loop distributing prioritised power to the entire site. The backup power supply will be located at the primary distribution substation. During normal operation, the backup power loop will be energised from the ordinary MV-level supply. If the supply fails, the MV bus bar circuit breakers will open and the backup system will take over the supply for the prioritised loop automatically. For safety reasons, the backup system will be designed so that operator intervention is required to restore normal operation. Dedicated low-voltage racks supplying prioritised power will be co-located with the ordinary switchgear to achieve simplicity in deployment and operation of the backup power system. Equipment requiring backup power will be connected to these racks.

The technology of the backup power supply will be considered carefully, as the different approaches

each have advantages and drawbacks. Diesel generators are relatively cheap and use familiar commercial-off-the-shelf (COTS) technology, but they require continuous maintenance and fuel storage. The diesel fuel is flammable, which poses an environmental hazard and requires special storage and handling. Battery supplies may be available in the power range required, but they are relatively expensive. However, battery systems require less maintenance, the backup is "immediate and they will not leak fuel. Hydrogen fuel cells offer an emerging battery technology. They may become COTS for MV at the required power level during the construction phase, or during the ESS lifetime.

Electrical interfaces

In general the interface between the power supply system and the other internal systems is at the outgoing low voltage breakers of the secondary substations, or at outgoing low voltage breakers in separate low voltage distribution rooms.

The accelerator will be the single largest consumer of ESS power and it is physically the largest system. The power consumption of the accelerator varies along the path between the ion source and the target. To accommodate the power variation along the beam path, standardised substations will be distributed along the stubs in a way that keeps the low-voltage cable lengths within reasonable limits. The number of substations necessary depends on the supply voltage required by the modulators. For design purposes, a main power voltage of 690 V has been proposed. This voltage represents a worst-case scenario in the sense that it requires the largest number of substations. Substations for klystron gallery, tunnel and ion source will be located at the klystron gallery. The interface between the electric power supply system and the modulators will be at the outgoing low voltage breakers of the substation.

Target power consumption is very small, compared to the accelerator. Nonetheless, the expected demand requires a few dedicated substations. The interface between the electric power supply system and the loads within the target is at the outgoing low voltage breakers at the substations.

Within the experimental halls, there will be laboratories and more permanent infrastructure supporting the experimental work. It is important that the electrical system for the instruments is flexible and has sufficient design margin to adapt to changes in the configuration and location of the neutron instruments. Basically, the neutron instrument suite will always be a "work-in-progress". New instruments will be developed and obsolete instruments retired over the entire lifetime of ESS. The interface between the power supply system and the instruments will be at the instruments.

The cryogenic compressors will be supplied by substations located close to the end of the klystron gallery and the beginning of the target building. A voltage level of 3.3 kV is preferred over a lower voltage of 400 V. The intention is to use the same voltage level for cooling pumps and heat pumps. The interface will be at the outgoing breakers in the substations.

The conventional facility system electrical interfaces are currently under review. Some interfaces will occur with air compressor systems, data systems and conventional building systems. For example, there will be a need for conventional 400 V power along the accelerator tunnel, to supply lighting, ventilation and tools during maintenance, among other purposes. This need will be supplied by dedicated substations.

7.4.2 Low and extra low voltage systems

Rooms for low voltage (LV) systems operating below 1 kV focus on accessibility, interchange ability, flexibility and management aspects. There are two categories of LV rooms: for machine supply and for common power. LV distribution rooms for machine supply rely on several secondary distribution substations will be deployed around the facility. Each substation will contain transformers and MV switchgear that connect to LV switchgear in separate rooms located close to the load. Space for additional equipment is reserved in these rooms. The final design and placement of substations and LV rooms will be based upon power demand investigations and analysis. Electrical distribution rooms for common power use floor oriented LV rooms in each building that contain distribution boards connecting to local LV wiring.

Ducts

Ducts will be sized to cover the requirements for cable installation related to conventional facility installations, with spare capacity for flexibility and future changes. In addition, Conventional Facilities will collaborate with other divisions to ensure that ducting systems allocate adequate space for other cable

systems, such as control systems. The cable support could be arranged using floor ducts, trays and ladders, wall channels or piping. Type, material and structure will depend on system design criteria and requirements. Cable support will be separated into at least three parts (power cables, communication cables and cables for fire and safety systems). In addition, separate support will be provided for control and machine cables.

A separate dedicated piping system of blown fibre pipes will provide the backbone for communication between the facility distribution room, building distribution rooms and floor or area distribution rooms. This common piping system provides capacity for all communication fibre optics needed. In the more industrial-like premises of the accelerator tunnel, gallery, target building and experiment buildings, the main ducting system will include a grid of cable ladders/trays mostly starting from secondary distribution points. In more public parts of the facility such as offices, labs, reception rooms and guest facilities, the ducts could be concealed above ceilings or recessed to give a discreet impression. The installation must not obstruct access to other systems. The use of installation floors is recommended, to accommodate flexibility for control room and computer rooms.

Lighting

Artificial indoor lighting will be selected to provide for energy efficiency and a comfortable lighting environment for ESS personnel and visitors. The lighting system will be adapted to the best available technology, which means lighting systems applied with latest technology for lamps and control technology to ensure long maintenance intervals and minimised energy use. LCC analyses will determine the best solution for each application. LED technology is currently in an intensive development phase and is likely to become prominent for indoor lighting use in the next few years. Outdoor lighting design must meet norms and standards and provide for a safe transportation environment within the site. Entrance lighting will be in focus in order to create good conditions to guide visitors, staff and goods flow. Special attention will be directed to illumination of the site and surroundings for safety purposes.

Guidance and emergency lighting will comply with European regulations, and exit signs will meet the guidelines in the ESS fire safety strategy document [569]. Power supplies will be backed up to secure lighting in the event of evacuation during power failure. Lighting control through a generic technical communication network covering light fitting groups provides opportunities for energy-savings. Lighting control such as presence detection, daylight adaptation and also monitoring of safety light fitting status will be implemented.

Extra low voltage

Extra low voltage systems with voltages less than 50 V will be incorporated into the buildings with a focus on accessibility, interchange ability, flexibility and management aspects. ELV system premises include a central facility distribution room that contains central distribution equipment from which the building plot backbone emanates, and an access point for external telecommunication grid, with separate confinements for BMS, Security and IT equipment. A central ELV room in each building, and floor or area distribution rooms, contain equipment from which building backbone emanates. BMS, security and IT equipment are separately confined. ELV distributions rooms with servers, spare servers and other equipment will also serve the main control room and the back-up control room.

Building management system, and fire detection and alarm

A building management system supervisory control and data acquisition (BMS/SCADA) system will be used to control, regulate and monitor the status of all conventional facility-related building systems. The system architecture will be open protocol and expandable, allowing full flexibility for the future. Source code will be fully available and owned by ESS. Users will operate the system through a graphical interface. The BMS system will communicate information as well as the status of connected objects to the integrated control system. The possibility of integration with preventive maintenance systems or asset management systems will be evaluated. Server redundancy and seamless transfers from main to backup servers is essential for both the power grid SCADA and the BMS/SCADA systems. Sections 5.2.5 and 5.2.6 discuss how both SCADAs receive timing system services from the ICS.

Addressable fire alarms based on smoke detectors, alarm push buttons, et cetera, will provide early warning in case of fire or smoke accumulation. Fire alarms will be connected to the municipal fire brigade

and have automatic transmission of fire alarms. Details of the ability to transfer information to the supervisory security system and ICS are provided in the Fire Safety Strategy Report [569]. The evacuation alarm system is a part of the automatic fire alarm system. Alarming equipment, consisting of audible sounders in combination with visual signals, is activated automatically when smoke is detected, or manually with push buttons [569]. All functions related to fire safety are controlled directly from the fire alarm system, enabling these functions to be monitored on the same level. Control examples include: evacuation alarms, audible and visual alarms, fire door controls, release of access controlled doors, lifts, ventilation, and smoke management. These alarms and functions will be fully integrated with the Personnel Protection System described in Section 5.2.3.

Communication systems

A generic communication cable system will comply with the latest applicable standards for categorised communication networks. The facility and building backbone will be three separated optical fibre networks terminating in building, floor, and area distribution rooms. The network will support BMS, security and IT systems. The communication network will connect local outlets via LAN. Communication points for WLAN (wireless data communication) and for mobile communication will cover the needs of the facility. An intercom system will be installed for vocal communications from doors, gates and similar locations to the reception and control rooms. Images from intercom locations where a CCTV camera is located will automatically be presented in the responding monitor when the intercom call is received. After completion of the call, the presentation will return to the previous image selection.

A mobile communication system will be installed with complete indoor and outdoor coverage, enabling users to send and receive text messages both manually and automatically from security systems. The control room will be equipped with a radio communication system suitable to communicate with the fire brigade, police, and other emergency responders. The system will conform to the Swedish national "RAKEL" system. The radio system will also cover outdoor areas on the ESS site.

Other extra low voltage systems

Restrooms accessible for the disabled, rest cabins and some other areas will be equipped with an emergency alarm system. Alarms will be indicated both optically and acoustically outside each room and also in the security system terminal in the control room. There will also be cable TV service access points, for distributing national and international TV-channels.

7.4.3 Electrical environment and grounding

Electrical installations will be designed to provide a good and safe electrical environment. All parts of the facility will be equipped with grounding and protection systems that integrate various protective and functional aspects. The foundation of the grounding system will be an extensive grounding grid using concrete reinforcement in the base slab, basement and other underground concrete constructions. The system will be shared by all systems and will connect the various buildings to define a common ground potential for the total site.

A common grounding system for both high, medium and low voltage systems according to norms is planned. All substations will use the same common ground potential in order to counteract differences within the electrical systems, despite the large number of substations and the relatively large geographical distribution area within ESS. The grounding will be designed to meet the specific needs of different equipment. For example, where pulses with high-rise times, i.e. with high frequency content, are expected, a solution providing low inductance and high surface area such as flat straps could be considered. An equipotential system ensures personal protection against electric shock. The system defines certain non-electrical conductive parts and connects them to common ground potential to avoid differences in voltage level. The common ground potential could also serve as a part of a functional grounding wire grid to ensure clean earth. Ground potential could be made accessible by ground bars in strategic places.

Every building in the ESS facility will be equipped with both external and internal lightning protection to protect buildings, equipment and people. The lightning protection system will follow EN 62305 [586–589] performance standards, and will include different levels of over-voltage protection devices in strategic locations. The system will be connected to common ground potential in the various buildings. Protection

against interference will be developed taking into consideration general regulations, EMC directives, CE norm, filter technology etc. Means to handle electric and magnetic fields will be ensured by choice of methods and materials during the detailed design phase. Distance to sensitive parts of the operation and various shielding actions will also be considered. For some areas it is essential to minimise or protect against static electricity, such as in areas with sensitive electronic equipment or in areas that pose explosion risks.

7.5 Water systems

ESS needs water in different qualities for different purposes, often within the same building. Lund municipality's external tap water grid will supply the water needed, except possibly for some purchases of deionised water for the process water system. Municipal water in Sweden meets national standards for victuals, so there is no need for a water purification plant for drinking water. The municipal system will provide cold and hot water to all installations in cleaning rooms, rest rooms, staff rooms, etc. in all buildings. On-site systems will provide several different levels of water purification, required for certain special purposes, such as for the neutron science laboratories and for the cooling and heating systems for the accelerator, target and instruments. Some of these purification systems will be supplied by the municipal water system. ESS will provide on-site water storage for fire extinguishing sprinklers and hydrants.

An internal domestic cold-water pipe network will provide the ESS facility and each heating substation with domestic cold water. Internal tap water consumption will be measured with flow meters for each building. Back-flow protection will be installed to the required extent. Hot domestic water will be produced in heat exchangers in heat substations located in each building, using waste heat from the process during beam operation and district heating when the beam is off and no waste heat is produced. Cold and hot water will be distributed to all consumers by an insulated pipe network. Insulated pipes will also carry circulating hot water. The outgoing hot-water temperature will be between 55°C and 60°C. Some electrical hot water boilers may be used locally for low-consumption and distantly located consumers.

7.5.1 Cooling water system

The facility requires more than 40 MW of electrical power to operate, most of which is converted to waste heat, and must be removed. The ESS cooling system accomplishes two goals. The primary goal is to remove waste heat and provide adequate cooling and temperature control for all systems to assure safe and efficient facility operation. The second goal is to recycle as much of the waste heat as practicable and provide it to external customers. To accomplish these goals, the cooling system is designed with a series of heat exchangers, pumps, heat pumps, piping, and possibly other chiller systems that use water as the primary heat exchange medium to transport heat generated from facility systems to external customers. In order to achieve an energy efficient heat recovery, it is of considerable value to cool equipment at as high temperatures as possible. The ambition is to build an energy-efficient, sustainable and robust cooling water system. The water cooling system for the ESS facility will be built for the scope outlined in Figure 7.29.

One way to achieve the secondary goal of re-using the waste heat is to use it for other applications within ESS. For example, return water flow at appropriate temperatures will be used for heating office buildings. Another way is to make this energy available for external use, for example by directing the high temperature water cooling return flow through heat exchangers to an off-site district heating system. All options are currently being kept open pending decisions at a later stage in the project, as final optimisation requires more detailed information from the different machines and conventional facilities.

A backup system will be installed to insure personnel safety and to protect valuable ESS systems and machines in the event of unexpected conditions such as the unavailability of the district heating systems. Backup solutions may include a dry air cooler and tap water. The capacity of the system will be determined later on based on requirements to maintain cooling for critical systems.

The net cooling demand is estimated to be 29 MW. Table 7.7 shows how these demands can be met by providing cooling water at three different temperature levels. The final determination of the number of cooling levels will be made based on machine requirements and an economic evaluation of heat recovery. The detailed design of the cooling water system will be completed using standard machines, equipment and components such as pumps, heat exchangers, heat pumps, piping components, tanks and vessels. Construction materials are to be standard austenitic stainless steels. In some special applications other

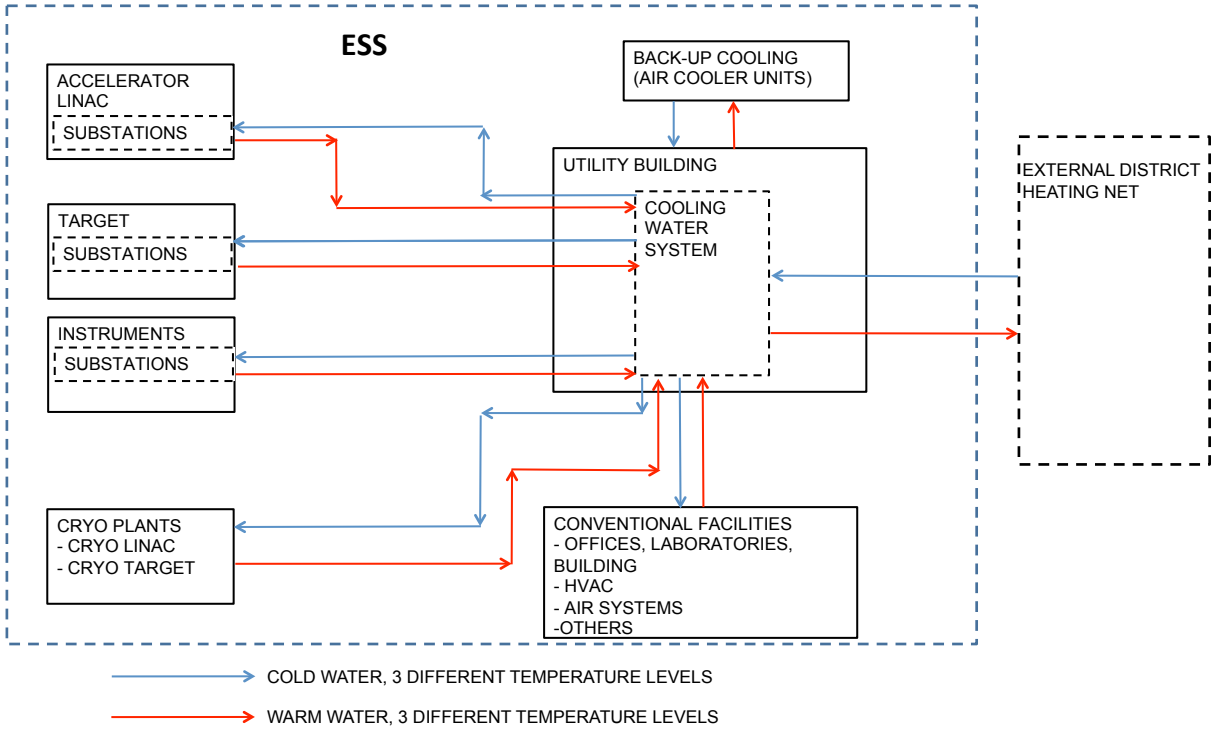

Figure 7.29: Schematic arrangement of the water cooling system.

Temperature level	**Supply temp.** [°C]	**Return temp.** [°C]
Low	5 – 15	30 – 35
Medium	30 – 35	40 – 50
High	40 – 50	75 – 80

Table 7.7: Water cooling system temperature levels.

materials like high-grade steels or thermo-plastics may be used. Governing codes are appropriate EU Directives required for CE marking systems and components. The cooling water system primarily uses deionised and demineralised water and possibly (for some outdoor applications) ethylene glycol/water mixtures.

7.5.2 Deionised process water

Deionised water will be used in all cooling and heating water circulation systems for the accelerator, target, and instruments. Purified process water will be produced in a central plant and will be distributed via a pipe network to all sub-stations. The deionised process water system will consist of two units, each of which is able to service 60% of the need. One unit together with a storage tank will provide the plant with enough water during service time. Filters will continuously purify the circulating water in each cooling loop so that the levels of organic particles and ions are within the required limits. Purifiers will be located in the different substations. There is great variation in the amount of water to be purified, depending on operating modes. The level of the deionisation and purification for the feed system will meet the specific demand for each system and loop as required.

There are different ways to produce the process water – for example by reverse osmosis and ion exchange – requiring further investigation to choose the best option. The different levels of purity appropriate for each system are being determined. The quality, purity and resistivity will be controlled and monitored continuously. The high demand for process water during fill-up and start-up poses a special issue. There

are three possible routes to address this issue: buy deionised water, install a temporary facility or build a large-capacity permanent facility. After commissioning, the need for water during normal operation is comparatively low, mainly to compensate for leakages and service in the systems. Thus, different solutions may be used during the topping-up process and during normal operation.

7.5.3 Cooling water requirements

Heat is removed from each point that requires cooling with ordinary water-to-water heat exchangers, with requirements from target, cryoplants, accelerator, ion source, instruments and facilities that vary in different operating modes. The full implications of the different operational modes are still being evaluated, but a preliminary list is shown in Table 7.8. Certain systems will run at reduced capacities in the different operational modes, or may be shut down and not require any cooling. This will result in varying demands on the cooling water system. Another factor influencing the cooling system is the seasonal variation in ambient temperatures. This changes the demand for heating and cooling in conventional buildings (offices, laboratories etc.). These seasonal variations will affect the demands on the cooling system and how much power it can deliver to other customers. Future work is planned to perform computer-based mass and energy balance simulations to optimise the cooling system design, and to ensure it will accommodate all operating mode variations. However, the "beam on target" mode has the highest cooling demand, as presented in Table 7.9. The cooling points listed represent about 80% to 85% of the total cooling demand.

Accelerator

The linear accelerator comprises both the accelerator tunnel itself and the klystron gallery. The total cooling requirement for the system is divided among components in the tunnel and gallery. Most of the cooling demand is for klystron gallery equipment. Although a majority of the klystron gallery cooling demands will be met using water, the low level RF (LLRF) equipment requires approximately 500 kW of air cooling. The HEBT magnets require approximately 250 kW of cooling. The RFQ and DTL tanks in the accelerator tunnel require not only cooling, but also more stringent temperature control requirements than the rest of the accelerator systems. A separate cooling and temperature control loop may be provided for this equipment. Cooling for the RFQ and DTL is estimated to be less than 200 kW.

Target

The target substation cools four sub-systems: the main target material cooling loop, which is connected to two inner gas cooling systems that use helium and nitrogen; a cooling loop for thermal moderators, inner and outer reflectors, the monolith shielding, beam dump, and water purification systems; a cooling loop for monolith flush, helium purification, and proton beam window systems that are primarily gas cooled; and a cooling loop to provide constant temperature regulation in ventilated zones for connection cells, utility rooms, and active cells. Target moderators will be kept at cryogenic condition with a hydrogen system. This small cooling demand is supplied from a cryogenic helium plant.

Cryoplants

Chapter 6 discusses how three separate cryoplants will provide helium at cryogenic conditions. The largest of the three plants provides helium at 2 K for accelerator cooling. A second system provides helium at 16 K to the target moderators. The main cryoplant cooling demands are the condensers in the helium compressors and cooling of the oil in the compressors. The third cryoplant – the test stand and instruments

Mode	**Duration** [h/y]
Full operation	5000
Down-time	1900
Intermediate (e.g. start-up, shutting down)	1700

Table 7.8: Operating hours per year in different operating modes.

System	Cooling loop	Supply temp. [°C]	Return temp. [°C]	Total power [MW]
Accelerator	Low	17	34	4.3
	Medium	32	39	2.0
	High	47	78	8.4
	Sub-total			**14.7**
Target	Low	10	26	4.3
	Medium	30	67	3.2
	Sub-total			**7.5**
Cryoplant	Low	9	35	0.5
	Medium	32	60	3.2
	High	60	87	3.2
	Sub-total			**6.9**
Instruments	Low	12	27	**1.6**
Buildings	Low	12	27	4.0
	Medium	32	42	0.2
	High	47	77	−6.0
	Sub-total			**−1.8**
	Total estimated cooling demand			**28.9**

Table 7.9: Estimated water cooling power demands in the extreme case of the "beam on target" operating mode. The high temperature cooling loop of the "Buildings" system has a negative cooling demand because it provides heat.

cryoplant – serves two functions. During operations, it provides liquid helium to the various instruments on the neutron beam lines. Its second function will be to provide cryogenic cooling for the cryomodule test stand. Cooling requirements for this third system are an order of magnitude smaller than for the other two plants. There will be a large difference between supply and return water-cooling temperatures for both the condenser cooling and in the oil cooling circuits. Consequently, cooling will be done in several stages to maximise heat recovery.

Instruments

The specific instruments to be included in the initial 2019 suite are currently in review. Cooling will be provided for the initial seven instruments, with provision to expand the cooling system to accommodate new instruments as they come on line. Cooling will be required for both individual instruments and instrument support equipment. The initial estimated cooling requirement for instruments and instrument support is approximately 1.6 MW, and is likely to be highly distributed.

Conventional facilities

Other cooling demands currently being investigated include compressed air systems, conventional building heating and cooling, and heating for potable water supplies. Two air compressor systems are currently planned, one with dry filtered air for valve actuators and control, and one for general shop air. Conventional facility building heating and cooling requirements will also be provided by the cooling system, with current estimates of approximately 5 MW of cooling and 6 MW of heating, pending additional definition. Heat for conventional buildings will be provided, as much as possible, by waste heat from the technical infrastructure.

7.5.4 Cooling water interfaces

Generally, cooling water will be supplied from the primary cooling water distribution system to cooling substations located near the accelerator, target, cryoplant and instrument systems. The cooling substations will include heat exchangers that transfer heat from these systems to the primary water-cooling system.

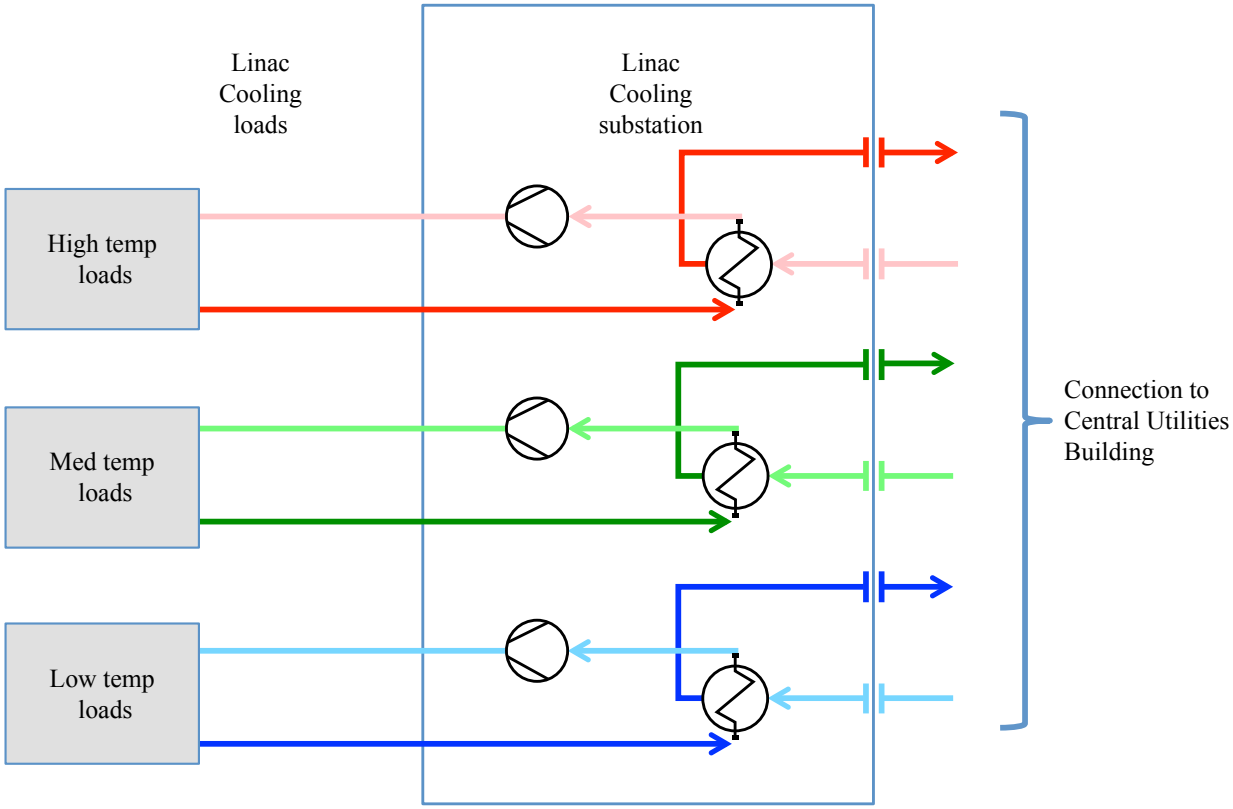

Figure 7.30: Accelerator water cooling system interfaces. Cooling substations located in rooms immediately adjacent to the klystron gallery building will require an area of approximately 450 m^2.

Distribution pumps, expansion tanks and water treatment equipment will also be located at these cooling substations.

Accelerator

Cooling water will be supplied from the cooling substation to the different cooling points in the klystron gallery. Cooling water for the equipment in the accelerator tunnel will also be supplied from one of the cooling substations. Figure 7.30 shows a schematic of the accelerator cooling system. The linac is located in the accelerator tunnel, and the klystron gallery equipment is in a building that runs parallel to that tunnel. The klystron gallery connects to the tunnel through a number of transverse galleries that are called stubs. Accelerator cooling substations require an area of approximately 450 m^2. These substations will be located in rooms immediately adjacent to the klystron gallery.

Target

The target individual subsystem cooling loads are managed by a cooling system internal to the target system. The interface between this target cooling system and the facility cooling system is a target cooling substation. Cooling water will be supplied from the cooling water distribution system to this target cooling substation located in or near the target building. The cooling substation will include heat exchangers that transfer heat from the target cooling loop to the water cooling system. Figure 7.31 shows a schematic of the target cooling system. The target cooling substation is located outside of and adjacent to the target station building so that it is outside the boundary of any radioactive zone. The target cooling substation occupies an area of approximately 50 m^2.

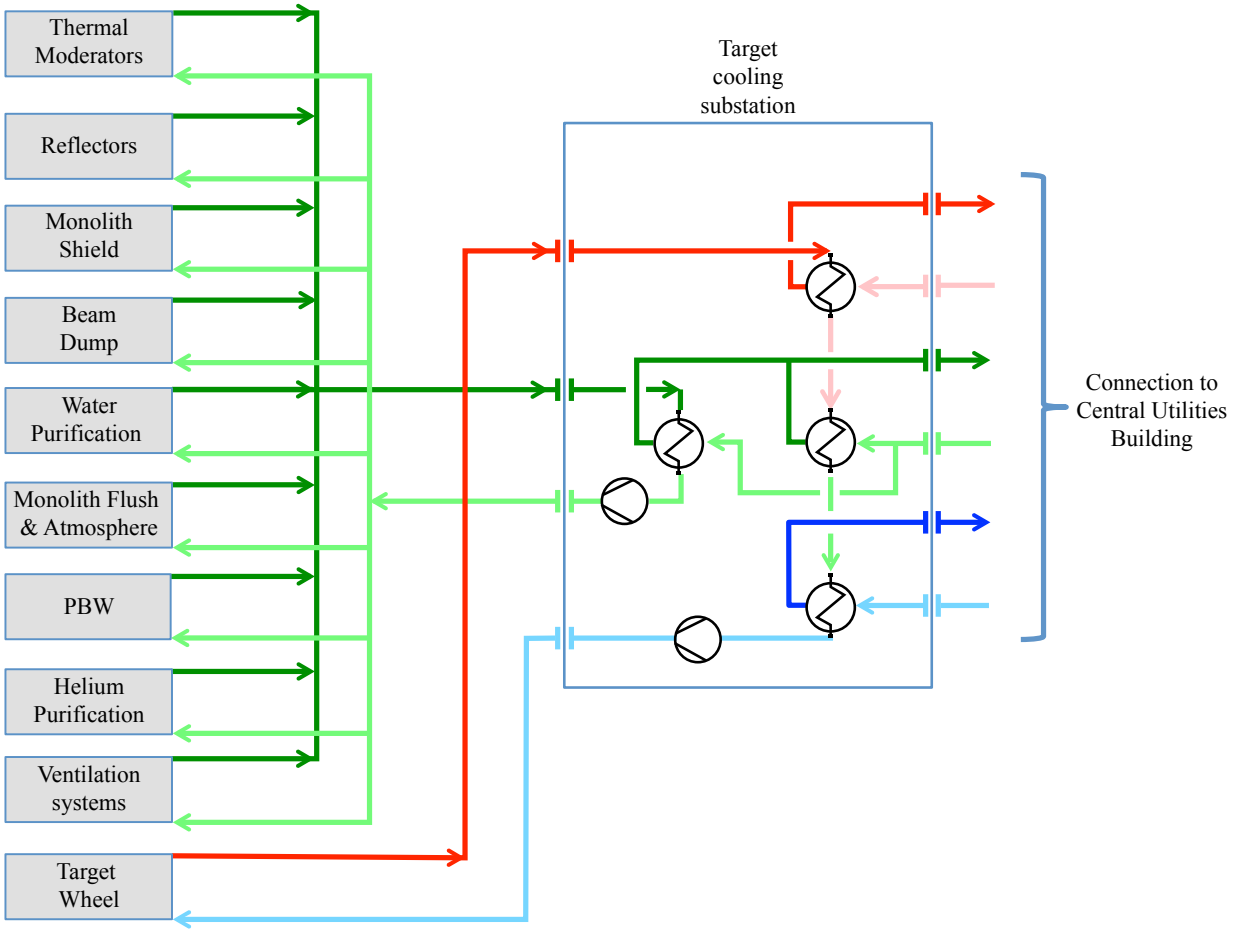

Figure 7.31: Target building water cooling system interfaces. The single cooling substation is outside the radioactive zone boundary, with an area of approximately 50 m^2.

Instruments

The specific interfaces between the cooling system and instruments have yet to be defined pending further definition of the instrument suite. Currently, the instrument cooling demands will all be met with the low temperature range cooling loop. It is anticipated that the cooling demands for the instruments will be highly distributed, with the possible result of not recovering much waste heat from this system.

Cryoplant

Cooling water will be supplied from the overall cooling water distribution system to a cooling substation located near the cryoplants. Figure 7.32 shows the general configuration of the interface between the cooling substation and the cryoplants. A single, integrated cooling substation will support both the accelerator and target cryoplants. The substation for the smaller instrument cryoplant will be a separate system, as this cryoplant will be operational before the two larger cryoplants.

Conventional facilities

The interface between the cooling system and other conventional facilities is currently in review. Interfaces will be required for air compressor systems, and conventional building heating and cooling. Cooling for air compressors and conventional building cooling will be provided from the low temperature range cooling loop. Heating for buildings will be provided from waste heat in the medium and high temperature cooling loop return streams. In some cases, this heat may not be sufficient for buildings. In that case, additional heat may be provided from interface with the Lund district heating system.

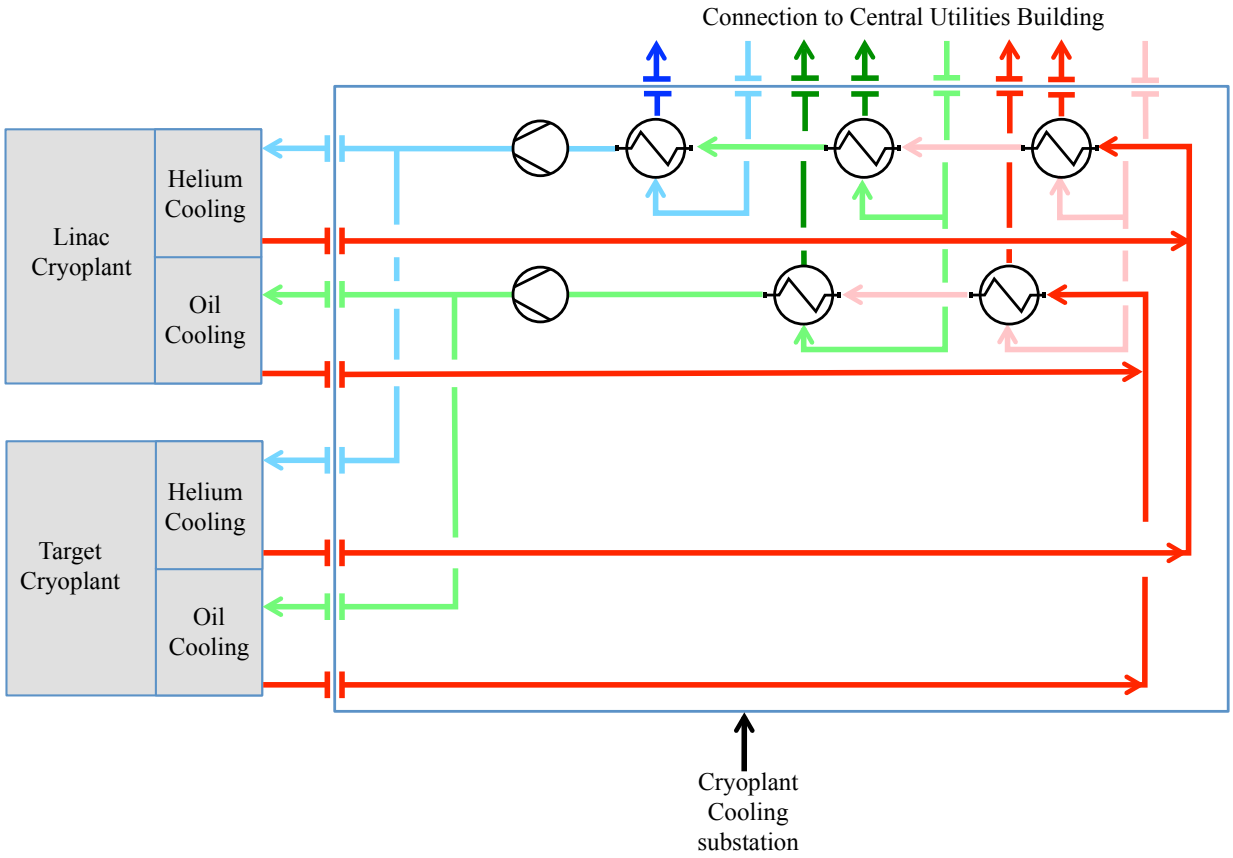

Figure 7.32: Cryoplant water cooling system interfaces. A single, integrated cooling substation will support both the accelerator and target cryoplants.

Instrumentation and controls

Instrumentation and controls for the accelerator cooling system are largely undefined at this point. Instruments will be required to monitor coolant flow rate, temperature, pressure, and cooling water quality. Acoustic noise, pump and compressor vibration, and leak rate monitoring may be required. In addition, instruments will be required to monitor and control circulation pump power and heat pump compressor power. Cooling water quality and treatment systems are also required for the cooling system. The cooling system will use an integral, continuous, on-line monitoring system that is fully integrated with the ICS to manage cooling water quality. Alarms and shut downs will be provided as part of the general infrastructure of control by ICS.

District heating

The central utility building contains all the heat pumps necessary to produce the required cooling capacity for the three cooling loops. A large amount of heat is produced on the condenser when a heat pump cools, the sum of the cooling energy and the electrical energy supplied to the heat pump compressor. To recover this energy for use in the Lund district heating system, the hot-side temperature of the heat pump must be lifted to a useful level of about 80°C to 90°C. If this temperature lift is not of interest for economic reasons, the energy will be released to the ambient air in some type of cooling equipment, in which case the energy is wasted.

Table 7.10 shows the calculated number of heat pumps and heat exchangers, based on the assumption that all energy will be recovered and transferred to the district heating system. The heat exchangers in the high-temperature cooling loop will be cooled directly from the return pipe side of the district heating system. In the part of Lunds district heating system where ESS will be located, the return temperature varies between 45°C to 50°C over the year. The supply temperature from the heat exchangers to the

Parameter	Unit	Cooling system		
		Low	Medium	High
Cooling capacity	MW	10	7	14
Heating capacity	MW	15	12	14
Number of heat pumps		3	2	–
Heat pump capacity	MW	5	6	–
Number of heat exchangers		–	–	2
Heat exchanger capacity	MW	–	–	7

Table 7.10: Number of heat pumps or heat exchangers in each cooling system.

supply pipe side of the district heating system will be in the range of 75°C to 80°C. Further investigation is required to determine if this temperature level is enough to feed into the district heating system.

Other external interfaces

If companies in business such as greenhouses, fish farms, or biogas production want to start activities in the vicinity of ESS, it is technically possible for them to use the low-temperature energy from the cooling systems instead of building their own heat plant. Users with lower temperature requirements could interface with the return pipe side on the cooling system low or medium cooling loops. This means that they can have supply temperatures to their heating systems of about 35°C to 45°C.

7.5.5 Waste water and storm water

The main waste water system will be connected to the Lund municipal waste water system. Waste water within the site will be diverted by gravity flow pipes and if needed by pumping stations and pressure pipes to the connection point. The radioactive waste water system will collect potentially irradiated waste water from any process in the facility. The floor drains and piping layout will be designed for gravity flow, from which the contaminated waste water will be pumped up to waste storage tanks. If no radioactivity is measured in the waste water in the tank, it will be released to the main waste water system. Chapter 10 has more detailed information about potentially radioactive waste water. Section 7.3.2 describes the storm water system that is designed for local disposal. It consists of drains, gravity flow pipes that allow water to infiltrate the soil, pump stations and at least one storm water detention pond in order to release storm water outside ESS to drainage companies.

7.6 Main services

7.6.1 Compressed air and gas systems

Three different types of compressed air are provided. Two systems provide pressurised air for common pneumatic tools and cleaning during maintenance and installations, and instrument air for instruments and machine systems. Pressurised air and instrument air is produced in the central utility building, and is distributed by a ring system to various systems and consumer locations, where a substation ensures that sufficient capacity is available using a buffer tank with local controls. Figure 7.33 shows how the third system produces extra dry instrument air with an extremely low dew point as required for some specific instrument, machine and system purposes, by using normal instrument air as “raw material” at the local consumer site.

The substation for extra dry instrument air consists of a buffer tank and an adsorption dryer for removing moisture down to −70°C. Standard air compressors provide most pressurised air, but oil-free compressors are used for instrument air and extra dry instrument air. Table 7.11 shows the air quality that is expected for each of the three systems, determined by the standards laid out in ISO 8573 [590].

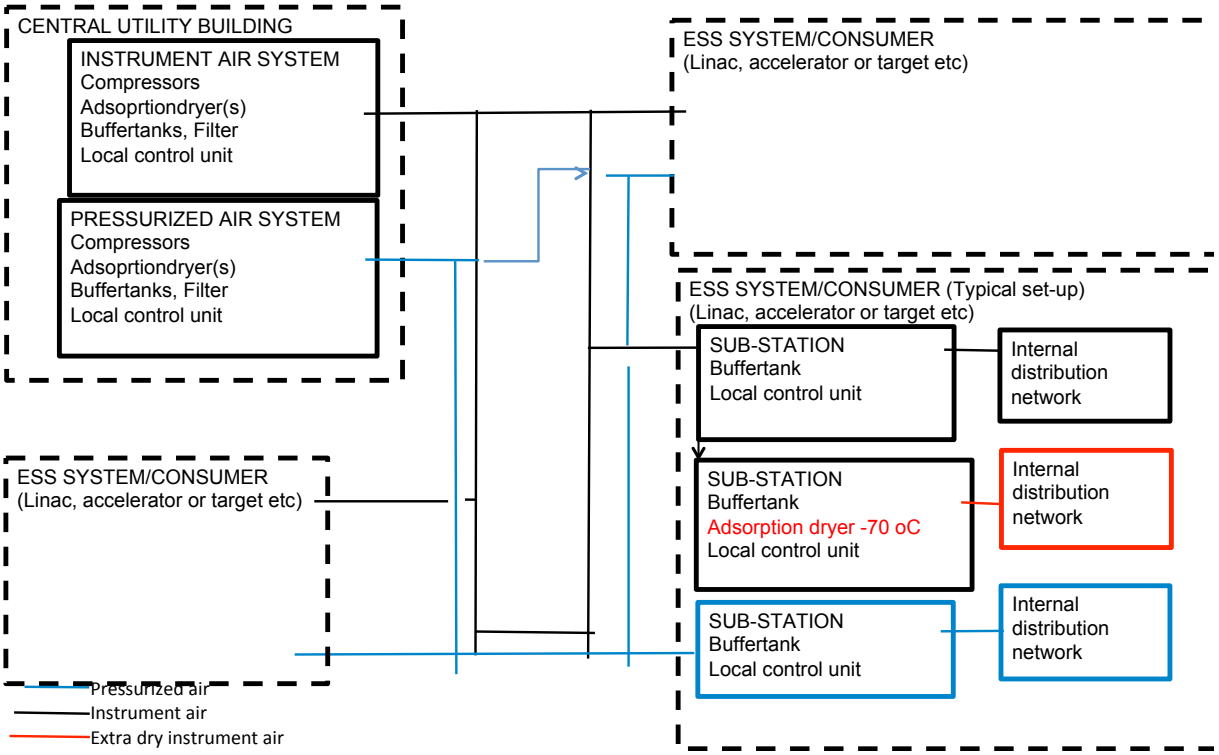

Figure 7.33: Compressed air systems: pressurised air, instrument air, and extra dry instrument air.

Compressed air type	Dust content class	Oil content class	Moisture content class
Pressurised air	2	2	3 or 4
Instrument air	1	0	2
Extra dry instrument air	1	0	1

Table 7.11: Compressed air system qualities, using the standards laid out in ISO 8573 [590].

Helium, nitrogen, hydrogen and other gas systems

Gas distribution systems will provide storage, transfer, flow control and distribution services for the buildings. Helium, nitrogen and hydrogen will be distributed from outdoor tanks for liquefied gases together with evaporators and distribution pipes into the buildings. Other gases will be delivered either from mobile single gas bottles, bundles of gas bottles or bottles located in discharge central rooms, and distributed out to consumers by installed pipe networks.

7.6.2 Heating and ventilation

The primary heating system is based on internal waste heat from the cooling process when the plant is in operation and complemented with district heating from the Lund municipal heating network during beam shutdowns. The heating system will be designed as an internal district heating circulation system with a primary underground pipe network from the central utility building to heating substations with heat exchangers for secondary heating systems and hot water generation located in each building. The heating substations consist of shunts and pumps for different types of secondary heating circulation systems, for example, radiator loops or air-heating loops. For the accelerator, an additional heat exchanger is required, since this system is exposed to radiation during beam operation.

The large industrial-style premises will be heated through ventilation and local fanned-air heaters.

Smaller areas such as staff rooms will be heated by radiator systems. Electrical radiators will heat some areas, such as electrical rooms and distantly located rooms with a low power demand. Other types of premises, such as offices, labs and public areas, will be heated by low-temperature floor heating systems. The goal is to design all heating water systems with as low a temperature as possible considering the balance between pressure losses through heating coils and low-temperature waste heat from the process in order to use as much of the waste energy as possible.

All normal ventilation systems are designed to ventilate, dispose and recycle heat from processes in each building. Supply air will be added, mixed and, if necessary, displaced. Exhaust air will be evacuated in the usual manner and recycled in the air-handling unit. A number of protective ventilation systems will be provided for laboratories and workshops. All fume cupboards and flexible and fixed local extraction devices will be connected to the local extraction systems, and the area pressure will be balanced by additional air-conditioned supply air.

Accelerator and klystron gallery ventilation

During operation, the accelerator tunnel is air-conditioned by a number of air-conditioning units. Each unit consists of a filter-cooling coil, heating coil and fan-section, designed to fulfil appropriate temperature and humidity demands. The air pressure is atmospheric, as the tunnel is not ventilated during operation. The tunnel will be ventilated with fresh air only during service and maintenance stops, when the proton beam is off. The ventilation system will start after a delay. Supply air will be taken down to the front end of the tunnel by a supply air-handling unit containing outdoor air damper, filter, heating and cooling coils and a frequency controlled supply air fan via ducts and a supply air grill. The exhaust system contains an exhaust grill at the end of the tunnel, airtight ducts and damper, HEPA-filter and a frequency controlled exhaust fan connected to an extract duct network and the central ventilation stack. The ventilation system runs with high airflow for a period when it starts, in order to obtain a low level of activation in the tunnel. Thereafter, it runs with a lower airflow adapted to hygienic demands for maintenance personnel and in order to maintain appropriate climate and humidity demands. The accelerator tunnel is at a slightly negative pressure during ventilation, with respect to both ambient pressure and also to pressure in the klystron and front end buildings.

The klystron gallery air-handling units will provide the areas with filtered temperature regulated air. The units will be equipped with filter sections, mixing chamber, rotating heat recovery wheel, heating and cooling coils and frequency controlled supply and exhaust fans. The units will be controlled for energy efficient air-conditioning to fulfil the climate demands in the klystron building. Supply air will be distributed via a duct network and displaced supply air devices on floor level along the long sidewalls.

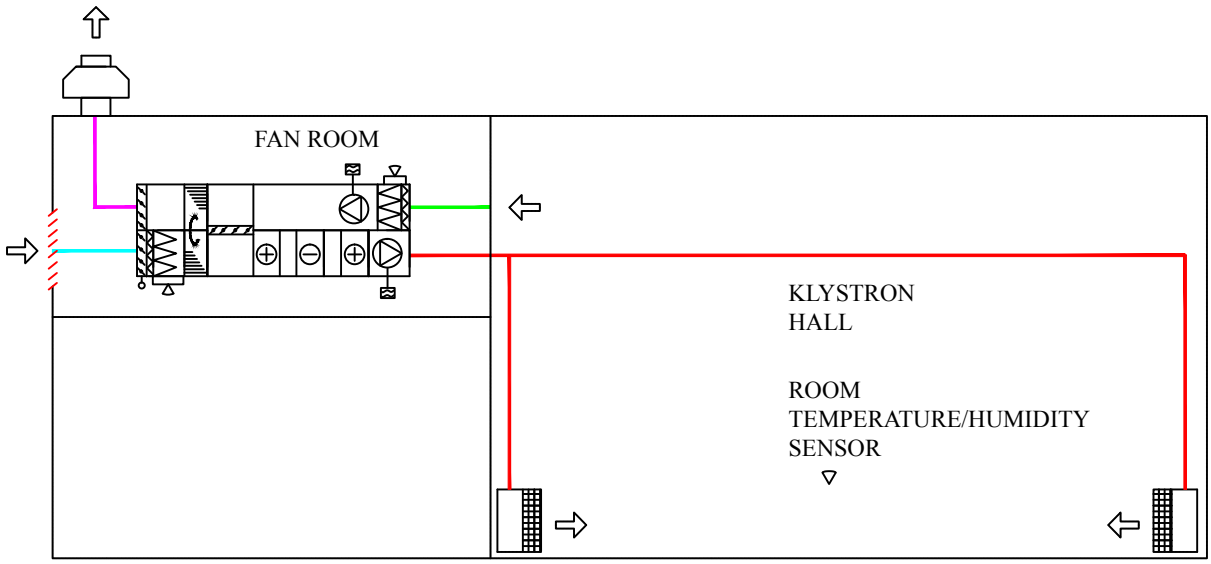

Figure 7.34: Air-handling in the klystron gallery building.

The system will maintain a slight overpressure compared to the accelerator tunnel. Figure 7.34 shows the klystron gallery air handling system.

Target ventilation

Target HVAC ventilation systems will be designed to complement the physical barriers and to provide an integrated containment system to minimise the emission of radioactive particles through the ventilation stack. There will be several types of classified air exhaust systems, which will serve process, storage and maintenance rooms within the active area, as well as connection areas and the utility rooms with pump, decay, and purification rooms. These systems will get compensating filtered and temperature regulated air from air-handling units and supply air devices located in the high bay, from which the air will be transferred through airtight ducts and dampers into the active areas. Ordinary air-handling units will ventilate other areas inside the target building. Active areas will have a slightly lower air pressure than either the ambient pressure or the pressure of areas with no radiation, during operation. A slightly negative pressure relative to ambient pressure will result in the continuous exhaust of air from these regions.

Experimental hall ventilation

Experimental hall air-handling units will provide the areas with filtered temperature-regulated air. These units will be equipped with filter sections, mixing chamber, rotating heat recovery wheel, heating and cooling coils and frequency controlled supply and exhaust fans. They will be controlled for energy efficient air conditioning to fulfil the climate demands in the instrument halls. The supply air will be distributed to the area via a duct network and high level mixing supply air devices.

7.6.3 Fire extinguishing systems

There will be various fire extinguishing systems around the facility. Different concepts have been analysed, including systems needed in rooms not accessible to the fire brigade and systems needed to limit the consequences of a fire. Rooms with a high level of radiation will probably have gaseous fire suppression systems installed. Areas where a fire can develop rapidly and where the consequences cannot be accepted, such as the klystron gallery, will also be equipped with fire suppression systems. Such systems could be equipment integrated gaseous systems, but an overhead system such as a water sprinkler, has also been analysed. In the case of a fire, the extinguishing water might contain hazards, such as radioactivity, hazardous chemicals or infectious samples. A separate tank system to collect potentially contaminated extinguishing water is under consideration for premises posing such a risk, in order to ensure that the operation of the municipal waste water treatment system will not disrupted. Similarly, gates or valves in the detention ponds can be closed for water sampling, treatment or disposal, in order to ensure that fire extinguishing water that is drained into the storm water system will not damage the environment.

7.6.4 Security systems

Figure 7.35 shows a block diagram of a typical security system structure. All security systems will have full functionality at central unit level, in case of main power or back-up power supply failure for at least 12 hours, unless otherwise indicated. Some critical parts of the security systems such as servers, switches and similar equipment will be connected through a UPS that will keep the power supply steady for at least 30 minutes, to permit a controlled shutdown sequence. Security systems will be independent, and will not be connected to external IT communication. An error in one system will not affect the functionality of other systems. All security systems will function autonomously without depending on servers or other peripherals, and will be equipped with time synchronisation over a common external time base. Some parts of the security system interact with the integrated control system. For example, common interlocks function as part of logical functions for ICS and associated safety systems, MPS, PPS and TSS, as discussed in Sections 3.1.5, 5.2.2, 5.2.3, and 5.2.4. The generic cable system that is part of the general security system will be a separate system provided with sabotage control and monitoring. The security cable system, designed for TCP-IP communications, could be a part of the general building cable system. If so, it will be clearly marked and securely separated, with labels, so that confusion is avoided. No connection through a virtual local area network or mixing of domains other than security LANs will be allowed.

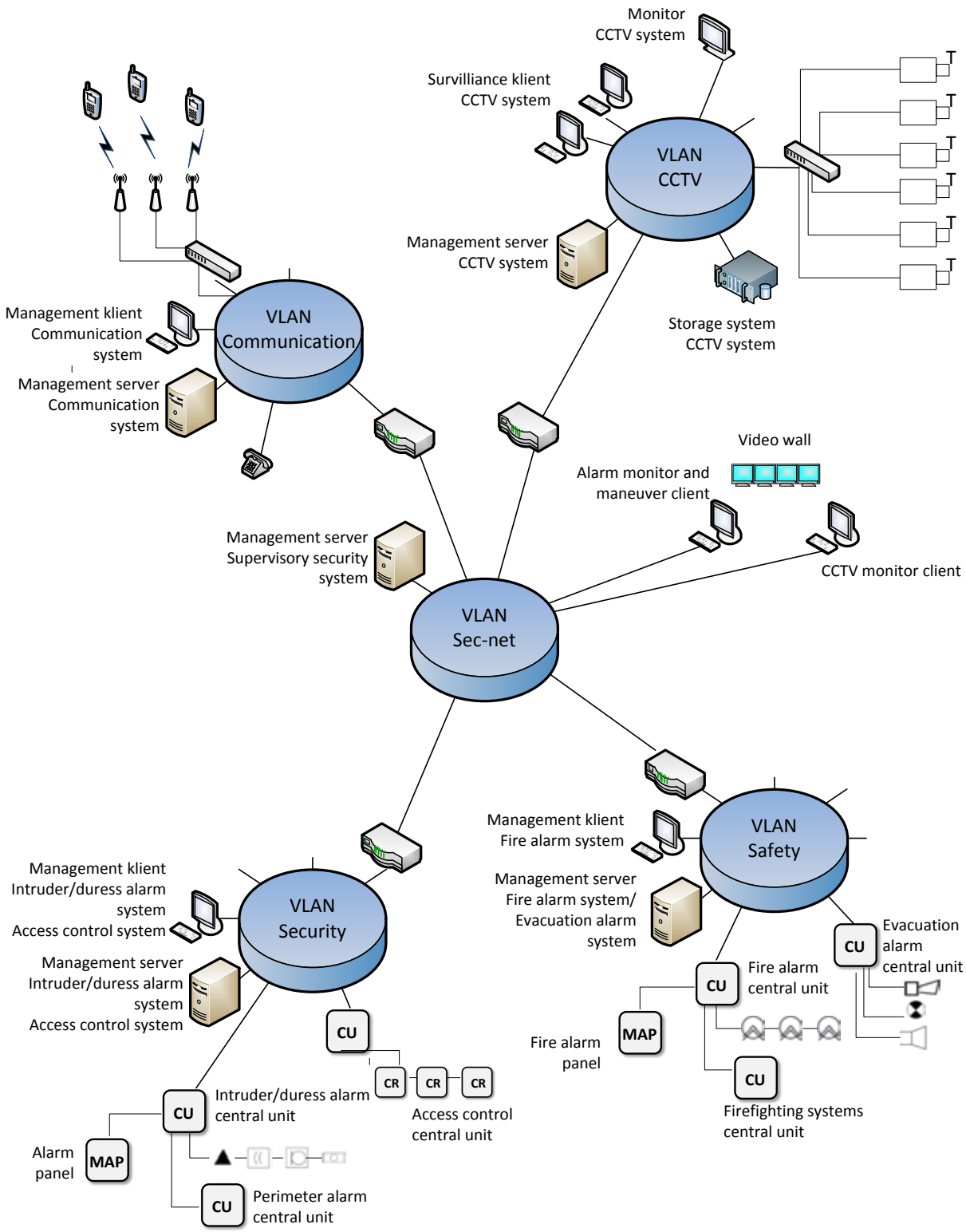

Figure 7.35: Block diagram of a typical security system structure.

Intrusion alarm

The intrusion alarm system will be designed and executed in accordance with the corresponding SSF 130:6 [591] or equivalent European code. All openings and glass in the perimeter and the building facades will be protected with alarm devices that generate an alarm upon unauthorised entrance or when glass is broken. Additional protection, such as volume protection, will be provided for certain areas within the premises, such as reception and control rooms. Manoeuvrability of such alarm zones will preferably be implemented through the access control system. Assault alarms will be part of the intrusion alarm system. An outer perimeter protection system will be an intrusion alarm sub-system, with the main purpose of monitor the site externally. Any movement in the designated areas will generate an alarm that interacts with CCTV-cameras.

Access and door controls

The access control system will use proximity cards and will be adapted to the MIkron FARE Collection System (MIFARE) standard, providing functions such as anti-passback, both on global and local mode as well in hard and soft mode. Some doors, such as entrance doors and doors leading to restricted areas, will be possible to control remotely through the access control system from the supervisory security system. On-site external security devices will also be controlled remotely. It will be possible to transfer information to the supervisory security system and the control system. Some passages need an interlock function and monitoring, such as doors to restricted areas due to radiation and control room fire doors. All door control and monitoring will be a part of the intruder alarm and access control system. Interlock functions will be hardwired and will not depend on logical conditions in servers.

Surveillance systems

All parts of the CCTV system will comply with Open Network Video Interface Forum standards. The CCTV system is primarily intended for: visual verification of events triggered by alarms, identification of people from intercoms, and similar functions; manual and automatic camera “patrols” of guarded areas; and recording of all images as a basis for investigations. There is no general need for permission to install a CCTV system, according to Swedish laws governing public surveillance, although some cameras may be disallowed, such as at the entrance gate. The system will be equipped with intelligent video analysis, of a type that has to be determined. Each individual camera in the system will be equipped with built-in, real-time video motion detection. The system will be integrated with other systems and will act automatically within the programmed settings. The ability to manage and locate cameras on drawings will be provided. For example, automatic display of the image will occur with the choice of camera in graphical interfaces. Other features may include dynamic zoom through lateral positioning, or similar functions. It will be possible to transfer any information to the supervisory security system and the control system.

Supervisory security system

The main objectives of the supervisory security system are to monitor all underlying systems and to present alarms and events. To some extent the system will also include control functionality. At a minimum, the supervisory security system will connect to: intrusion alarms, assault alarms, external perimeter protection, access control, door control, fire alarm, and elevator alarms. Other systems closely related to safety, such as the personnel protection system discussed in Section 5.2.3, will also be connected. The system will interact with underlying systems, both at the server levels and at the central unit levels, depending on the type of system, with presentation in the control room. Control panels connected directly to the underlying security system will also be available in the main control room, in case of failure in the supervisory security system. Figure 7.36 shows normal and emergency modes of operation.

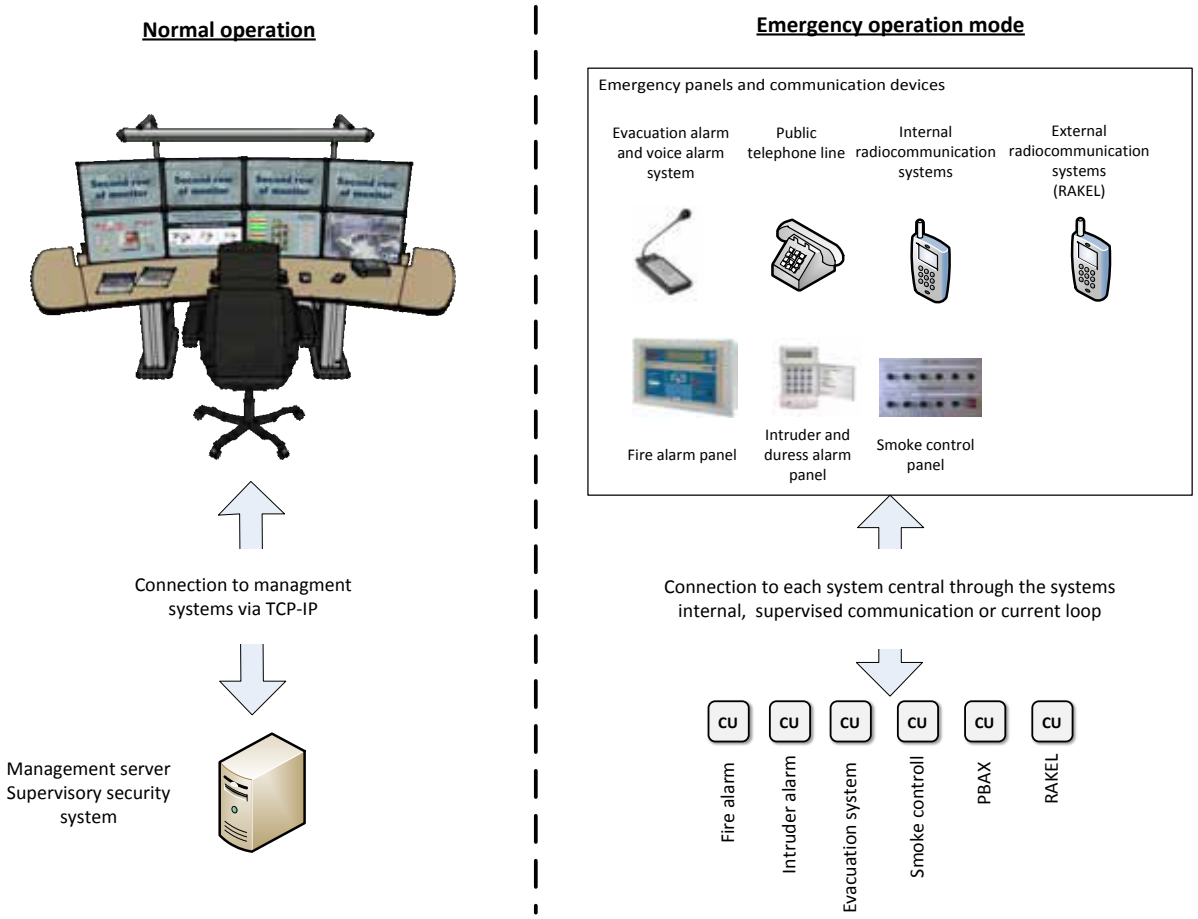

Figure 7.36: Normal and emergency operation modes for the supervisory security system.

Chapter 8

Integration

Chapter abstract

Summary: The ESS integration strategy facilitates the success of the programme by progressively combining system elements in accordance with design requirements. It sets out procedures to ensure that interim assembly configurations are tested repeatedly, in order to assure the necessary flow of information and data across interfaces, to reduce interference risk and to minimise errors.

Quality management and quality assurance. ESS is implementing a quality management system based on the principles of ISO-9001. Systems engineering will ensure the efficient management of non-conformities and change requests. A uniform way of operating in civil engineering work and facility construction is defined through a building information modelling system.

Norms and standards. The internal manual, *Standards, Norms and Guidelines Recommended for the Design and Construction of ESS,* constitutes a platform of standards recognised to be valid and applicable. The Standards Working Group is responsible for keeping the platform current with evolving norms and standards adopted by relevant national and international agencies and professional groups.

Components standardisation. ESS will maintain a centralised, freely accessible database of standardised components that will guide personnel in Lund and at partner laboratories during the selection of devices for their applications. Benefits from components standardisation include economies of scale, reduced burden on procurement offices, ease of maintenance and supply and more efficient management of inventory.

Design integration focuses on the interconnections between system components. The plant breakdown structure allows easy interface identification and provides a framework for the coherent organisation of document and CAD assembly structures. Configuration management is achieved through configuration identification, interface and document management and change control. The plant layout is the three-dimensional model virtualisation of the facility. It is robustly linked to the proton and neutron beam lattices by BLED, the centralised system of databases and tools and services that is used to store, manage and access data.

Survey and alignment helps to accomplish the required positioning accuracy of the ESS components. A surface monument network will be connected to the accelerator axis, the target ports and the neutron lines in order to establish a relation between the global position coordinates and the components.

Life-cycle management. Product life-cycle management (PLM) encompasses the tools and procedures developed to ensure component traceability from design through installation, operation and decommissioning. Life-cycle management at ESS is currently based upon Dassault Systemes Enovia V6.

Installation. The first major challenge for integration activities is to successfully bring the facility through the installation process. The goal is to achieve system assembly and interconnection, while accomplishing all quality-related tasks such as acceptance testing and component alignment.

8.1 Introduction

Thousands of ESS scientists and engineers will participate in the facility's design, construction and operation. ESS employees will collaborate with and support researchers from a wide variety of disciplines using the experimental instruments. Research laboratories in 17 countries, as well as private vendors from across the globe, will be involved in the manufacture of sophisticated technical components for the facility. Coordination of these multiple actors and complex functions is essential to the successful realisation of the ESS programme. This chapter explains how ESS will approach the integration process to guarantee that all systems and subsystems, coming from disparate sources, precisely match and work together.

The purpose of ESS's integration strategy [592] is to facilitate the success of the ESS programme by progressively combining system elements in accordance with design requirements. The strategy calls for a structured iterative process, that alternates with verification and validation processes [593] as appropriate. ESS's integration strategy requires the identification and description of all boundaries, whether physical or logical, between system elements and the satisfaction of all functional, performance and design requirements and constraints. It sets out procedures to ensure that interim assembly configurations are tested repeatedly to assure the necessary flow of information and data across interfaces to reduce interference risk and minimise errors.

8.2 Quality, norms and standards

Quality management and quality assurance

ESS is implementing a quality management system [594] based on the principles of ISO-9001 [595]. The system is designed to build quality into ESS operation through established and documented policies, processes and best practices. Key parts of the quality management system include management responsibility, resource management, continuous improvement, supporting processes and the programme processes. As a part of the quality management system, ESS applies systems engineering [596] as an interdisciplinary approach and means to support the successful realisation of systems. ESS engineers employ a systems engineering approach to define user needs and required functionality in the development cycle, to ensure that necessary requirements documentation is carried out, and to achieve design synthesis and system validation in the context of the complete facility.

The systems engineering approach will encompass all technical tasks in the design, construction, commissioning and operation of ESS and all of its subsystems. Activities will be monitored to ensure that trace links between the requirements and verification and validation activities are maintained. Systems engineering will also ensure the efficient management of non-conformities and change requests. In order to ensure a uniform way of operating in civil engineering work and facility construction, a building information modelling system [572], adapted to ESS's modelling strategy and requirements, is defined. The system contains requirements for the management of information, aimed at creating a structured and uniform working method. In this approach, programme uncertainties are continuously identified, analysed and managed during the life-cycle. Uncertainties include both opportunity and risk. Opportunities are captured for the benefit of the programme, while risks are identified and mitigated through the risk management process [597].

Norms and standards

The structure to be used is derived from a perspective based on the legal requirements related to radiation protection, as indicated in Figure 8.1.

The ESS change control board (CCB) has approved the establishment of a continuous working process called *Standards, Norms and Guidelines recommended for the design and construction of ESS* [598], called the SNG document. This document is referenced by the Safety Analyses Report (SAR), which ESS is required to produce by the Swedish Radiation Safety Authority, and constitutes a platform of standards recognised to be valid and applicable to ESS. Responsibility for implementing the process rests with the Norms and Standards Working Group (NSWG), which is responsible for keeping current with evolving norms and standards adopted by relevant national and international agencies and professional groups. Figure 8.1 lists some of these agencies and groups. The NSWG will update the SNG document continuously as more knowledge is gained and as further details of the ESS design develop, with the intent to provide

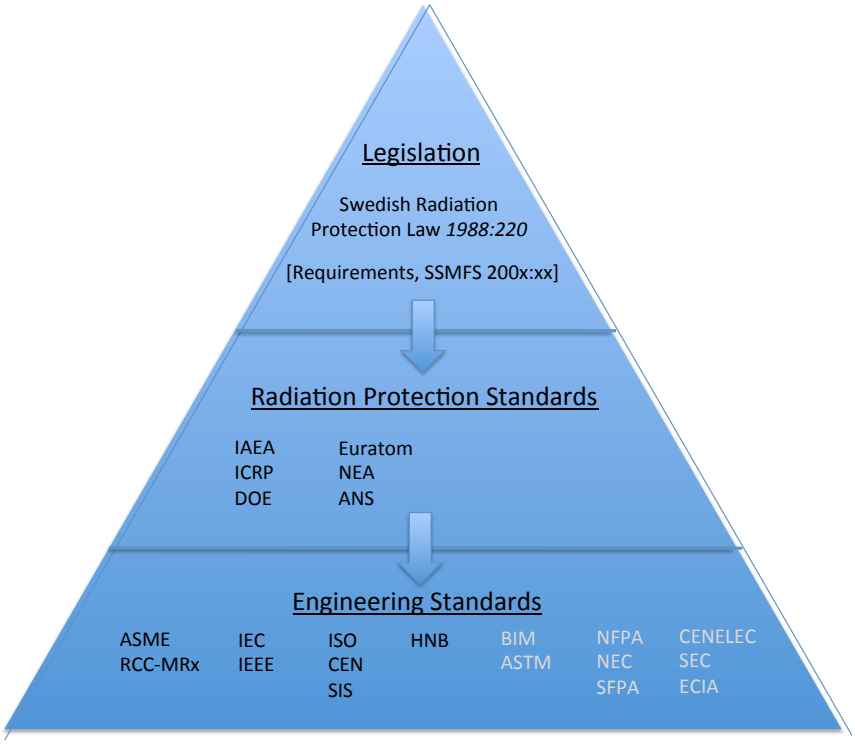

Figure 8.1: A hierarchy of standards: legislation, radiation protection, and engineering standards.

a comprehensive and easily accessible reference on standards for all ESS divisions, research collaborators, and outside vendors. Specific tasks associated with this work include:

- Keeping the report [598] up to date about current ESS standards and norms.
- Searching for new standards that could be useful to ESS and push implementation of common standard throughout ESS.
- Searching for new revisions of already applied standards and push implementation of common standards throughout ESS.
- Arranging for subscriptions to standards and ensure availability thereof within ESS.
- Distributing information within ESS about adopted changes and updates.
- Managing ESS subscriptions to relevant journals, working paper series, professional association and governmental and international agency reports.

Component standardisation

Although ESS will be a unique, custom-built machine, the project offers several opportunities for component standardisation, ranging from simple items such as flange connections through complex components such as pumping systems, electrical connectors, safety systems and conventional infrastructure. The benefits from components standardisation are several. Among others, it allows economies of scale, reduces the burden on procurement offices, promotes ease of maintenance and supply, and provides for more efficient management of inventory. ESS will maintain a centralised, freely accessible database of standardised components which will guide ESS personnel and partner laboratories during the selection of devices for their applications. This database will contain detailed product specifications, such as component materials, manufacturers, part numbers and possible alternative components as well. ESS guidelines will favour commercial products and careful analyses will be called for before undertaking costly and lengthy components redesigns. ESS will focus on robust and cost-effective life-cycle management, which will be necessary to

handle inevitable component obsolescence, since the ESS project will span a period of over 40 years from construction through operation and decommissioning.

8.3 Design integration

Design integration [592] emphasises the development of a holistic approach by promoting multidisciplinary, extensive collaboration among key stakeholders and design professionals from conception to completion. From the design integration perspective, any system is itself made up of other interdependent systems. The approach focuses on the interconnections among system components, whether those are across the departments and disciplines of a human organisation, or across the equipment and functions of a physical facility.

Plant breakdown structure

The plant breakdown structure (PBS) provides a visual road map for integration and helps delineate activities subsequently addressed in the work breakdown structure (WBS) [599]. The PBS allows easy interface identification, efficient control of the design progress and tracking of changes to the plant configuration, which are monitored during its life-cycle. Also, the PBS provides a framework according to which the document and CAD assembly structures are coherently organised. The scope of the plant breakdown structure (PBS) is to describe the functional breakdown of the plant in systems, sub-systems, loops, equipment and parts. It ensures that each element of the plant is uniquely identified as soon as it is created during the evolution of the design and manufacturing process in accordance with the ESS naming convention described in Section 5.1.6 that is implemented by the ICS Project, and that all relevant

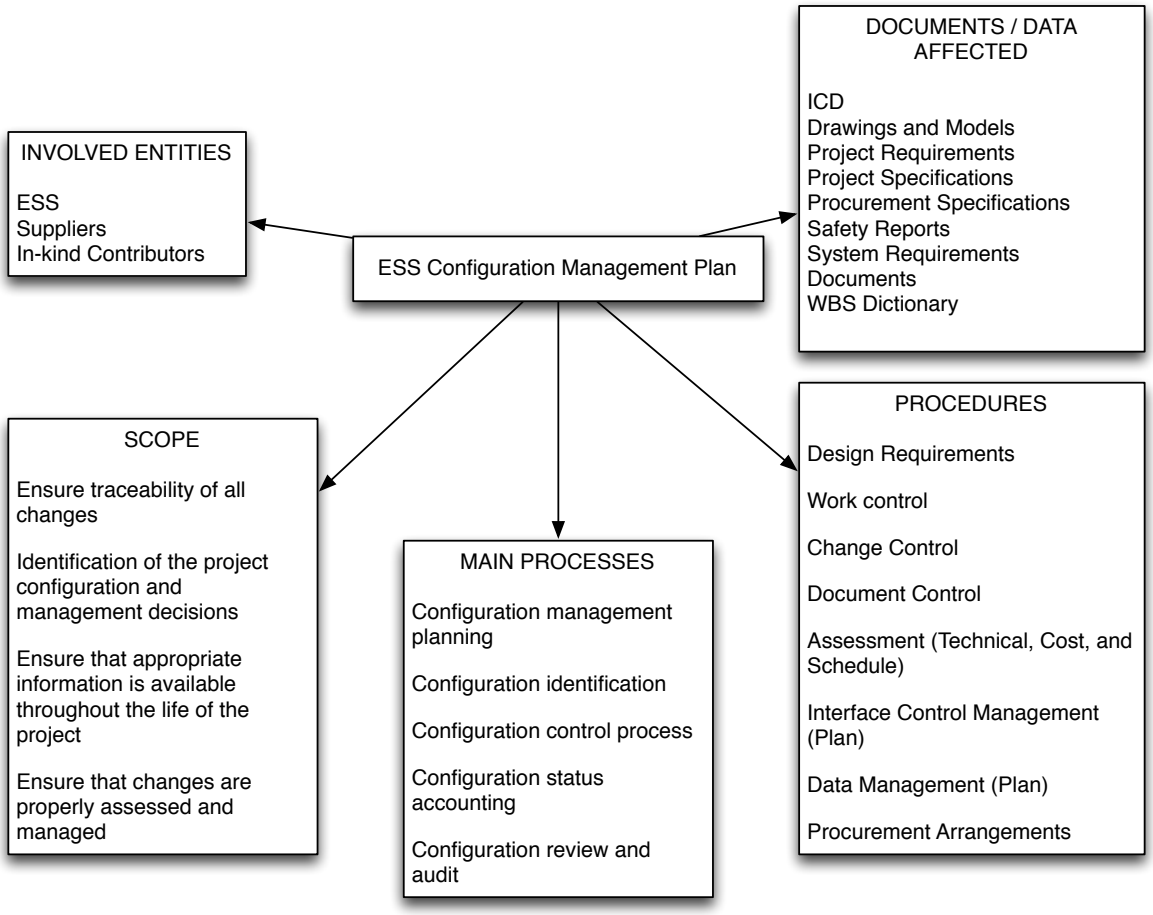

Figure 8.2: Configuration management plan.

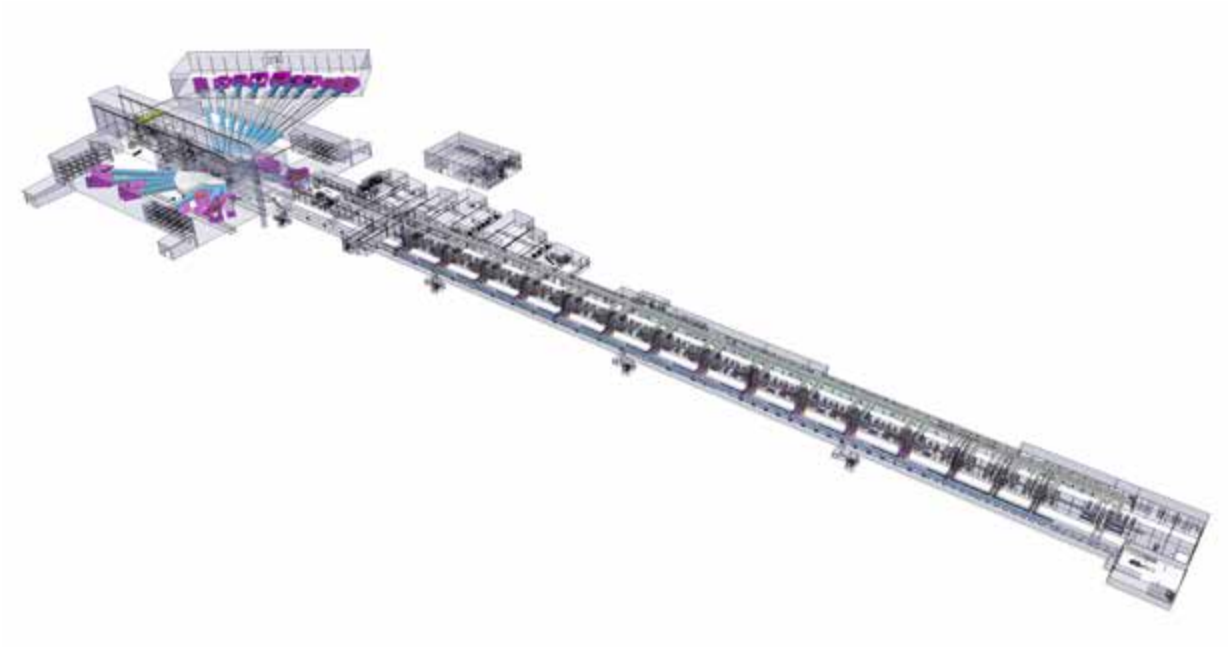

Figure 8.3: Isometric view of the ESS plant layout.

information, such as requirements, analyses, and 3D models, is linked to the corresponding element. The PBS is organised as a product tree [600]. The elements in a subset of the PBS serve to fulfil the function of their top common node. The elementary parts of the plant are the leaves of the tree structure. The PBS is deliverable-oriented, the main deliverables being the accelerator, the RF source, the target station, each neutron line inclusive of the relevant instruments, the cryoplants, the test stands, the offices, the control system, and the power station. The graphical representation of the PBS tree makes the verification of the ESS configuration status intuitive and efficient.

Configuration management

The activity of configuration management (CM) ensures that accurate information, consistent with the physical and operational characteristics of the project, is available at any point of time. The ability to rapidly identify and retrieve this information is vital to achieve cost-effective construction, to maintain the configuration of the plant, and to support future upgrades. Configuration management concerns requirements, design changes, interfaces and risk management. The key elements for fulfilling the configuration management objectives are configuration identification, interface management, change control and document management. Figure 8.2 identifies the main elements of the CM plan. The *The ESS Configuration Management Plan* [601] contains operational details.

ESS plant layout

The ESS plant layout (EPL) is a three-dimensional model representing the virtualisation of the whole facility. As such, the EPL depicts the physical arrangement of equipment, buildings and any related infrastructure within the ESS site (water pipelines, electrical lines, conduits, survey monuments and so forth). Figure 8.3 shows an isometric view of the EPL assembly.

Robust data flow

One of the BLED databases contains the information provided by the Beam Physics Group that is necessary to define the machine and neutron line lattices and layouts. It is of the utmost importance to guarantee a robust data flow from BLED to all stakeholders involved in the engineering and virtual modelling of ESS systems and subsystems. The virtual model is divided into three major deliverables, corresponding to the three major ESS sub-projects: the accelerator 3D model (AD), the target station 3D model (TS) and

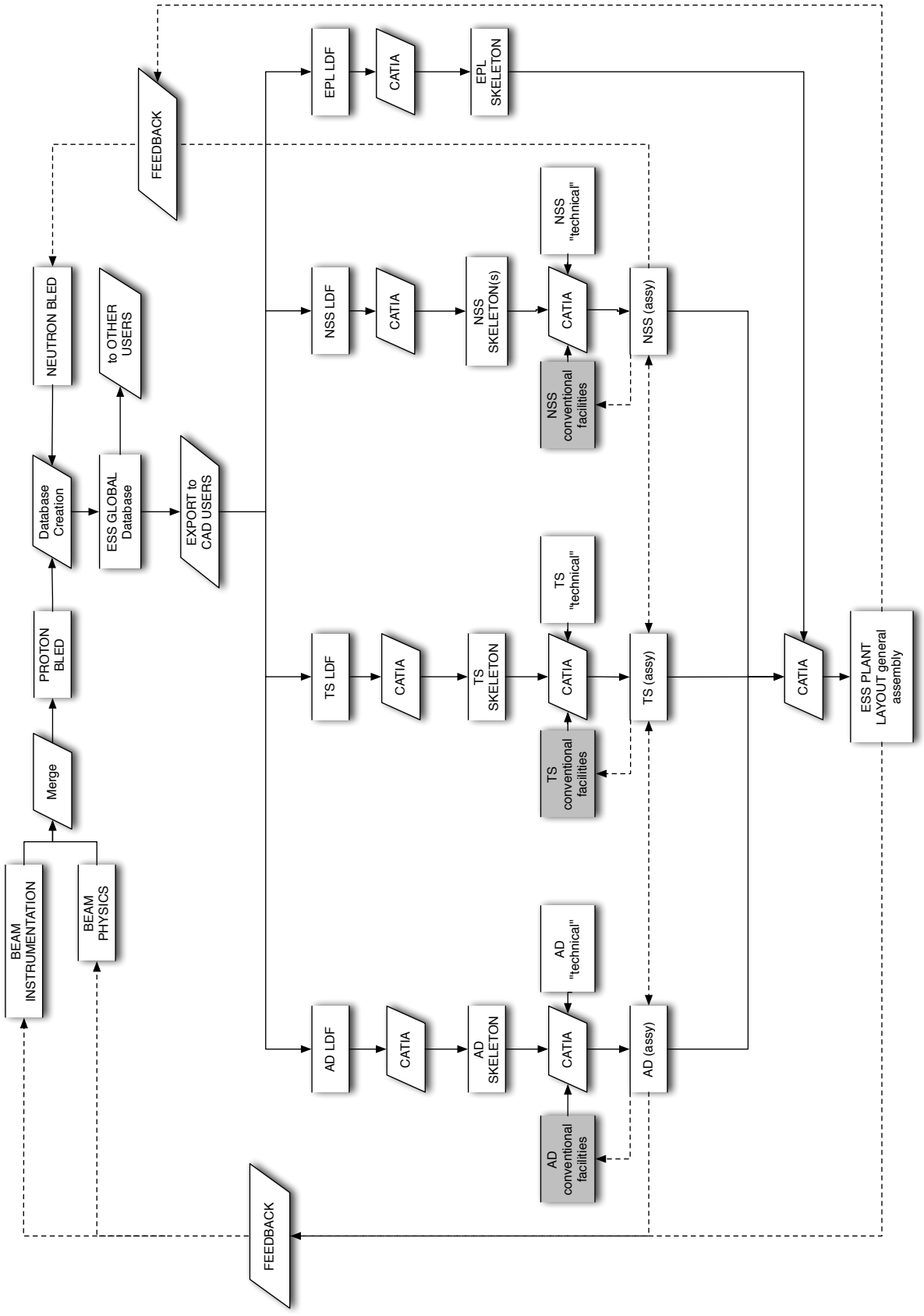

Figure 8.4: Data flow between BLED and the ESS plant layout.

the neutron science 3D model (NSS). The relevant conventional facilities building models are organised as subsystems of these major areas. Data communication is achieved by first extracting from BLED the location data files (LDF), a data set containing the spatial coordinates of the relevant devices. LDFs then allow the creation of so-called "skeletons", e.g. three-dimensional lines embedded in the CATIA drawing containing start and end points (slots) locating the position of the various 3D entities. Figure 8.4 describes the data flow from BLED to EPL and highlights the merging of conventional facilities models into the CATIA environment [602].

8.4 Coordinate systems, survey and alignment, and installation

This section outlines the survey and alignment requirements and the tools and techniques that will be used to accomplish the required positioning accuracy of the ESS components. The specifications for any given device are dictated by the relevant beam optics calculations. The alignment team will assist during the design of components in order to guarantee a proper fiducialisation. Once the construction phase is complete, the group will maintain the precision of the alignment during repairs, replacements, upgrades, and operations for the life of the project.

The site-wide coordinate system and the machine coordinate system

The ESS site-wide coordinate system (SCS) is defined and established as the main coordinate system for the facility [603]. The SCS origin is located underground and south west of the ESS site in order to guarantee that all objects have positive coordinates. The Cartesian SWEREF-99 13 30 coordinate system is used to orient the SCS axes and to determine the E and N origin coordinates. The SCS Z axis points vertically up. Its origin coincides with RH 2000 national altitude reference system zero, located at zero altitude according to the Normaal Amsterdams Peil (NAP). This is approximately 80 m below the ESS surface site. The target monolith is located 500 m to the north and 500 m to the east from the SCS origin. The linac forms a 28.5 degree angle with the SCS east axis, rotated counter clockwise. The absolute locations of the site-wide coordinate system origin, the linac start and the monolith axis are given in Table 8.1, while Figure 8.5 shows the locations of key points in the site-wide coordinate system.

Surface and tunnel networks

Standard Global Positioning System technology will allow surveyors to establish the monuments surface network within the degree of accuracy called for by this type of installations. Monuments above and below ground will be referenced by optical measurements with the purpose of establishing a relationship among SCS, the global position coordinates and the machine coordinate system (MCS). In this way, the surface monument network will be connected to the accelerator axis, the target ports and the neutron lines.

Both wall and floor monuments will be installed. In the accelerator tunnel ceiling, a survey clear zone will be reserved as well, guaranteeing an unobstructed view of the whole accelerator tunnel line which will be useful for theodolite global surveys. The monument network will be installed after the concrete walls and floor have cured to ensure monument position stability. The beamline will not follow the gravitational equipotential (that is, it will not follow the curvature of the earth). The advantage of freeing the beamline from the need to follow the curvature of the earth is that it permits a straight (flat) beam path, although the tunnel floor will follow the surface of the earth. Over the approximately 600 m longest dimension of the linac hall, this results in a disagreement with the equipotential curve of about 28.2 mm. This is comparable to the civil construction error of the floor, so no special constraints are necessary in its installation. The differences between the beamline and the level floor will be resolved in the support stands. The floor monuments in the linac hall will be spaced in a 5 m or less rectangular grid; with an analogous arrangement for the wall monuments. A large enough number of monuments will be visible at any laser tracker station in order to minimise laser tracker location error. Figure 8.6 shows typical wall and floor monuments, mounted with spherical retro-reflectors.

Coordinate measuring devices and component fiducialisation

The most efficient instrumentation for the network observations will be the combination of a laser tracker with a digital level. Laser trackers will contribute mainly to horizontal positional accuracy and digital

Point	**East coordinate** [m] SWEREF-99 13 30	**North coordinate** [m] SWEREF-99 13 30
Site-wide coordinate system origin	133680.000	6178519.000
Linac start (accelerator origin)	134708.990	6179306.218
Monolith axis (target origin)	134180.000	6179019.000

Table 8.1: Absolute locations of key points in the SWEREF-99 13 30 coordinate system. The site-wide coordinate system origin is located at zero altitude according to the Normaal Amsterdams Peil.

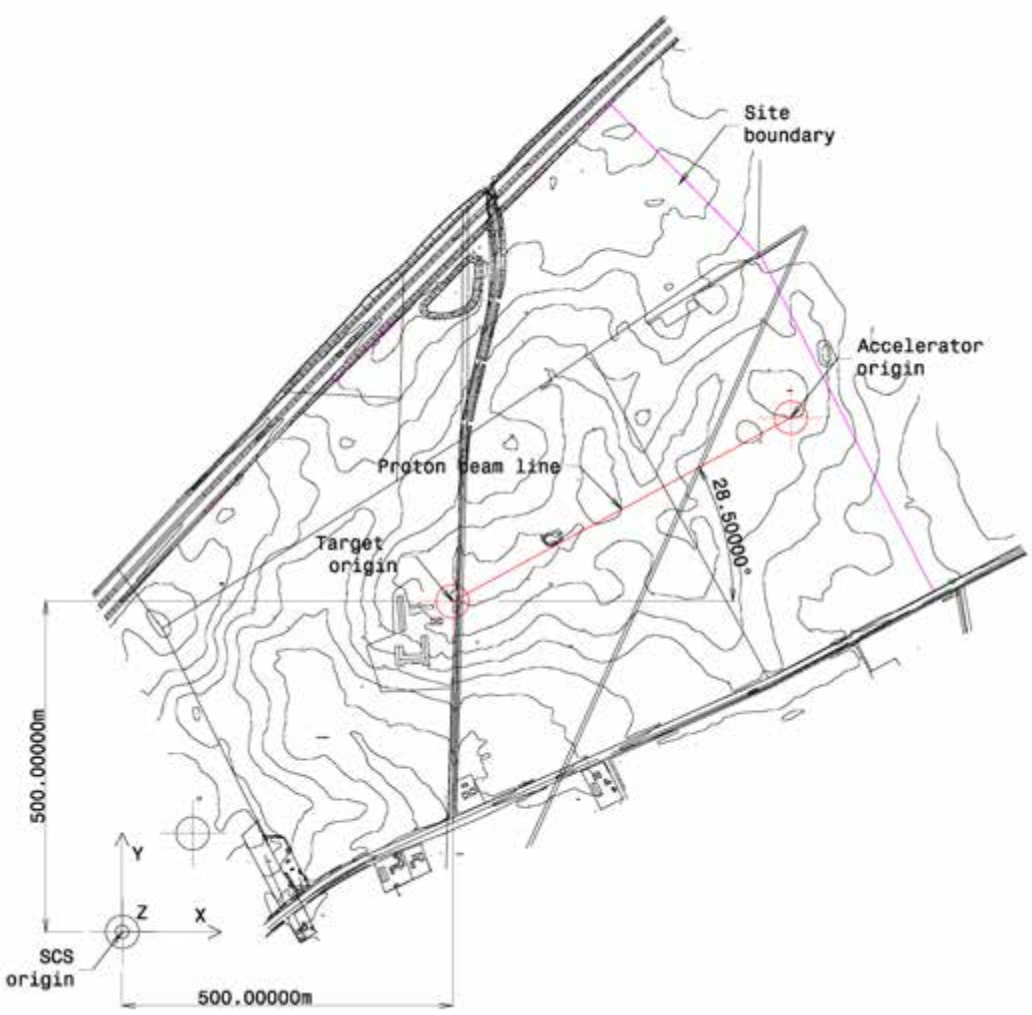

Figure 8.5: The site-wide coordinate system origin, the linac start (accelerator origin), and the monolith axis (target origin) on the ESS site. The absolute locations of these two points are listed in Table 8.1.

levels to vertical positional and rotational accuracy. The ESS project will use laser trackers with standard 38.1 mm diameter spherical mounted retro-reflectors and digital levels in combination with INVAR rods. Only two types of alignment instruments are necessary for the ESS installation, laser trackers and coordinate measuring machine (CMM) arms. Laser trackers include testing and calibration utilities with their delivery. A typical measurement session begins with these utilities. CMM arms require periodic recalibration at the manufacturer's service facility.

For each component on the beamline, there will be two sets of fiducials in order to reference the internal parts of the component, which are normally not accessible, to the component's external casing, and the external casing to the area in which the component is installed. The primary set of fiducials, or references,

Figure 8.6: Survey monuments and receptacles. Left: Wall mounted survey monuments. Middle: Floor mounted monuments. Right: Receptacles for laser tracker spherical retro-reflectors.

will be located within the device. An example of an internal reference is the exposed pole tips of a room temperature magnet or the entrance and exit flanges of a superconducting cavity. The secondary set of fiducials will be located externally, and will consist of pin receptacles used for housing the laser tracker retro-reflector, such as those shown on the right of Figure 8.6. They will be placed on the device away from the beamline, where they can be easily accessed and viewed in order to check for component position drift over time.

8.5 Life-cycle management

ESS and its collaboration partners need to be able to create, update and reuse information related to building and maintaining the ESS assets in a controlled and traceable manner throughout the design, manufacturing, commissioning, operation, maintenance and decommissioning phases. A framework project was initiated in spring 2011 whose goal is to align short and long term operations, to harmonise work practices, and to create a strategy for a common platform for integration and exchange of data following a system engineering philosophy [596].

The platform strategy requirements are based on the following principles:

- Strive to achieve a single unified software platform.
- Simplify the number of integration points between software products where possible.
- Adopt modern tools that can outlast the construction phase.
- Follow ESS adopted standards.
- Integrate the work process between civil and mechanical engineering.
- Avoid redundancy in data and information.

8.6 Installation

The scope of work of installation consists of several tasks designed to guarantee that systems are successfully assembled and interconnected. The production of installation layouts and the development of installation procedures directly support this goal. In order to assure that all operations comply with defined quality standards, the installation team collaborates on the definition of requests for information, coordinates the collection of written information about supplier capabilities, and is involved in site and factory acceptance tests. The installation team takes part in the design validation of components that may have an impact on the installation and alignment performance of the associated systems, and is actively involved in inventory activities. Figure 8.7 describes the ESS process flow for factory and site acceptance tests [604].

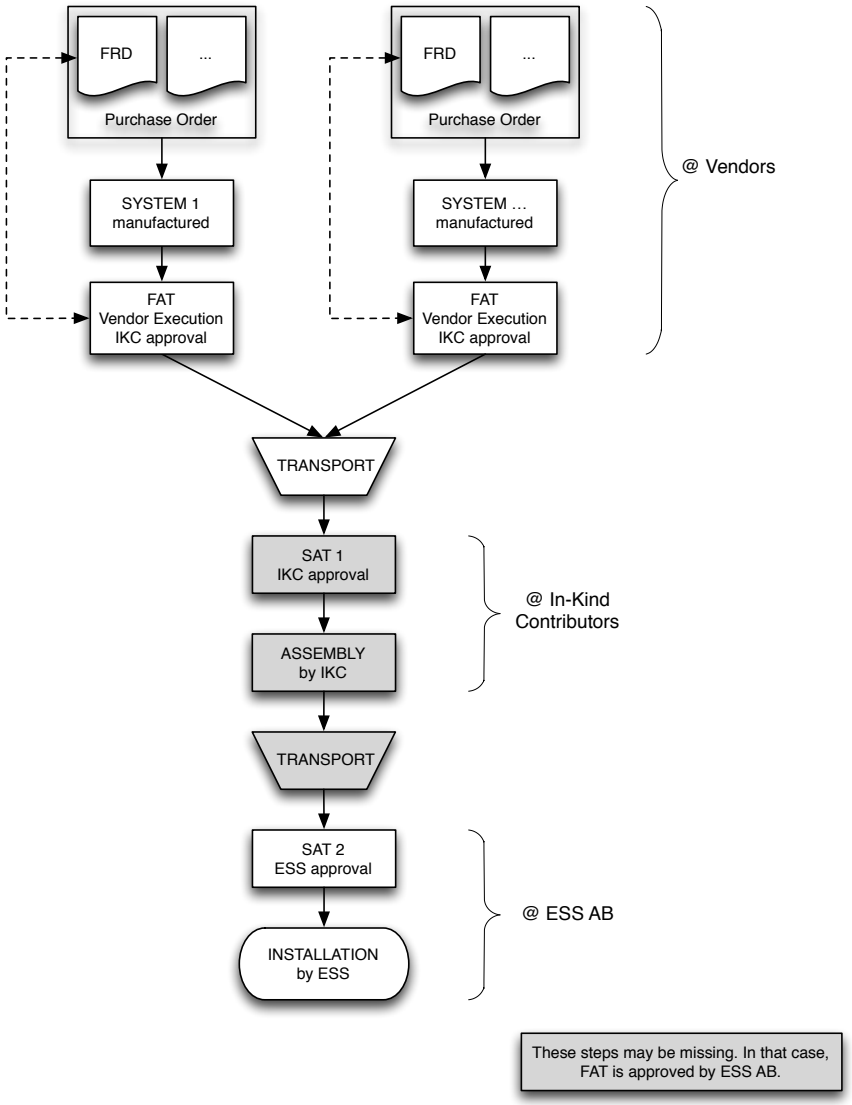

Figure 8.7: The process flow for factory acceptance testing and site acceptance testing.

Chapter 9

Commissioning

Chapter abstract

Summary: For a complex facility such as ESS, the transition from construction to operation has to be planned well ahead and early in the construction phase so that it can be made in an organised and effective manner. Experience from other research facilities shows that managing the interface between systems during start-up requires planning and structured procedures in order to keep to schedule and manage risks for personnel and equipment. This chapter describes the technical aspects of this transition for all major parts of the facility: the conventional facilities including technical infrastructure, the accelerator, the target, the instruments and the integrated control systems. The chapter presents a schedule for the transition stretching from when the first building is completed and taken into operation in 2016 to when the last of the 22 instruments is completed in 2025 and 5 MW of power is reached.

Strategy and methodology. Building on experience from other research facilities, ESS has developed a commissioning strategy and methodology. A main element of this strategy is an initial proton beam commissioning with a staged approach and early start. This will be followed by an aggressive early increase in beam power, in order to identify any machine limitations as soon as possible, before a large number of users are expecting reliable beam. Naturally, the commissioning and power ramp-up will comply with the limits set by the licenses and permits ESS has been granted by the relevant legal authorities. Systems will be commissioned first without beam, and later with beam.

The conventional facilities commissioning includes bringing all the conventional parts and systems of the facility into an operational state such that they perform all intended functions and meet design and operational criteria. Buildings and systems will be completed and commissioned in a timely fashion in order to allow efficient and early installation and commissioning of machine and instruments systems.

The accelerator will be commissioned in stages: The front-end and ion source will be commissioned first, followed by the drift tube linac; the superconducting linac with spoke resonators, all medium and high beta elliptical cavities; and finally the high energy beam transport (HEBT) and the transfer to the target. For commissioning of the first stages, a movable beam dump and a provisional control system will be used to allow parallel installation of the later stages.

The target station will be the last major machine component to be commissioned. It includes the neutron production systems (target, moderators and pre-moderators, proton beam window), the ancillary systems and the safety systems (shielding, confinement barriers). Activation levels will be kept low during the initial stages of commissioning in order to allow hands-on work.

The neutron instruments will be commissioned individually as the construction of each instrument is completed. The instruments will first be commissioned without beam followed by a commissioning with beam and later a period of scientific commissioning where the instrument is brought into scientific operation suitable for external users.

9.1 Introduction

Experience from other research facilities show that the transition from construction to operations for a complex facility such as ESS requires a significant a planning effort already at an early stage in order to efficiently reach operational requirements, keep to schedule and manage risks for personnel and equipment. The purpose of this chapter is to describe the technical aspects of how ESS will make the transition from the construction phase into the operations phase on a high level, that is how the main technical systems of ESS will be commissioned together. The management, organisation and approval procedures for this transition are described in the Transition to Operations document [605].

The scope of this chapter includes all parts of the facility: the conventional facilities including technical infrastructure, the accelerator, the target and the instruments. In terms of programme schedule, it stretches from when the first building is completed and taken into operation in 2016 to when the last of the 22 instruments is completed in 2025 and 5 MW of power is reached. Notably, it includes the commissioning of the machine, the production of the first neutrons, the power ramp-up and the commissioning of the instruments. More precisely, the commissioning of any system at ESS starts with the completion of the installation and ends with routine operation at full specification. This chapter describes the key activities and technical aspects related to the commissioning of the main systems of the facility. The activities and schedules presented in this chapter follow the project specifications for the construction and operation of the accelerator, the target, instruments and conventional facilities [42, 606–609]. It is important to note that it is not a project specification in itself.

This chapter describes the strategy and methodology to be applied, the commissioning of the conventional facilities, the accelerator, the target station and the instruments and clarifies a few key definitions. It builds on lessons learnt from other facilities, in particular from the commissioning of the SNS and the MEGAPIE target experiment. A few key lessons are listed in Section 9.8. In the chapter, the commissioning of the control systems, the data management systems and machine- and personnel protection systems are described together with aforementioned main parts of the facility but it also has a section of its own. The requirements and limits set by licensing and regulatory requirements are described throughout the document.

Definitions

1. **Beam commissioning:** initial transport of beam through a beam line, following equipment installation during the construction phase.
2. **Cold commissioning:** Start up of systems without producing a proton beam. Approximately no ionising radiation or radioactive materials is generated.
3. **Hot commissioning:** Start up of systems including producing a proton beam. Ionising radiation and radioactive materials can be generated.
4. **Power ramp-up:** Increase in the operational power on target in the period 2019 to 2025 to 5 MW.
5. **Machine reliability:** Machine reliability: the fraction of the time scheduled for neutron production that high power beam is delivered on target [42].
6. **Machine availability:** the fraction of the time (over a year) that the machine is available for neutron production with a high power beam being delivered to the target [42].

9.2 Strategy and methodology

The overall strategy for the initial commissioning of beam through the accelerator, and for the subsequent increase in machine performance to its design levels is described here. Initial beam commissioning culminates with the delivery of beam on the target and production of first neutrons in 2019. A primary aspect of the initial beam commissioning is a staged approach with an early start. The period following the initial beam commissioning through 2025 involves increasing the beam power, operational hours, machine reliability and the deployment of the scientific instruments to meet ESS goals. In this power ramp-up period, an aggressive early increase in beam power is planned, to identify any machine limitations as soon as possible, before a large number of users are expecting reliable beam.

The commissioning and power ramp up must be conducted within the limits set by the licenses and permits given. The Environmental Court will set conditions for the construction and operation of the facility for all matters not concerning radiation. The Radiation Safety Authority will set conditions for all matters concerning radiation and radioactive materials. According to the plan agreed with the authority, a license will be granted for ESS construction, another for test operation (commissioning) and later full operations at full power. Accordingly, permits and licenses will set conditions for commissioning both with and without beam. Reporting to relevant authorities during commissioning will continue, just as did reporting to the same authorities during construction. An open dialogue, monitoring and inspections are foreseen and it is expected that the licensing authorities will follow the commissioning of the facility closely.

Further, every care will be taken not to damage the machine or expose personnel to undue risks. This may in fact impose more restrictive limits than the licenses. The machine protection system (MPS) and the personnel protection system (PPS) must therefore be commissioned early and reach a level of functionality that can properly protect machine and personnel during commissioning. The ESS accelerator will be the worlds most powerful proton accelerator and many of its systems represent state of the art technologies. As ESS is a green-field site, none of the systems will have a history of institutional support at the central site. Having all these systems work together in concert will be challenging, and beam commissioning is the first time all the supporting systems truly need to work in an integrated fashion. Discovering the inevitable issues that will surface during beam commissioning as soon as possible will give system developers an early opportunity to modify their systems. In fact, the commissioning of sections of the accelerator will be a valuable integration exercise. As such, a staged approach to beam commissioning is planned in order to facilitate early system adjustments.

The staged commissioning provides several opportunities to run systems together, as opposed to installing all the ESS accelerator systems before attempting to run beam. Four commissioning stages are envisioned for the period 2016 through 2019. Lessons learnt in the early commissioning will facilitate commissioning in later periods, when more is at stake, and will also facilitate the initial power ramp-up. As an example of this approach, the SNS beam-commissioning period is shown schematically in Figure 9.1, indicating seven commissioning stages over about 3.5 years [610]. The initial commissioning stages involved accelerator beam-lines of only a few meters. The latter commissioning periods covered much more involved tasks, such as the entire superconducting linac and the entire ring and transport line systems. However less time was needed for these latter tasks, in large part due to the lessons learnt from earlier commissioning experiences. Providing early commissioning stages will be beneficial in the long run, but will require special arrangements initially. The early beam commissioning will require early building occupancy and utility support and the use of a temporary control room setup, and it will coincide with other construction activities on site. Beam commissioning during the construction period need not preclude construction and installation activities in downstream parts of the accelerator, in the target and instrument areas. Installing a temporary shield wall beyond the commissioning beam stop can permit installation activities to proceed downstream in the same tunnel. This was the case for the early commissioning activities at SNS shown in Figure 9.1.

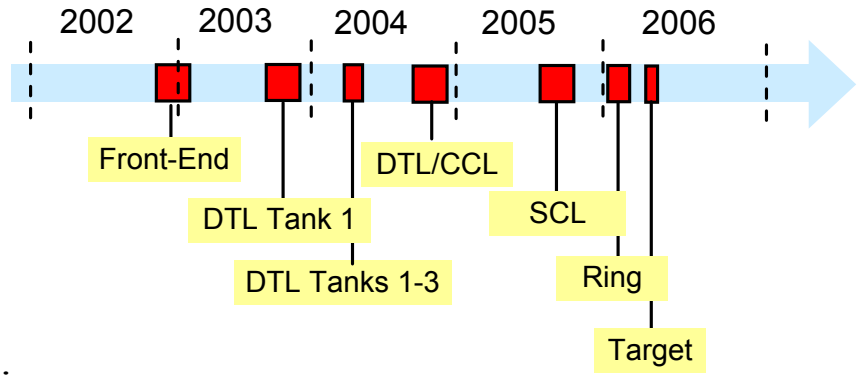

Figure 9.1: Beam commissioning during the SNS construction period, with the commissioning durations indicated in red. Courtesy of SNS.

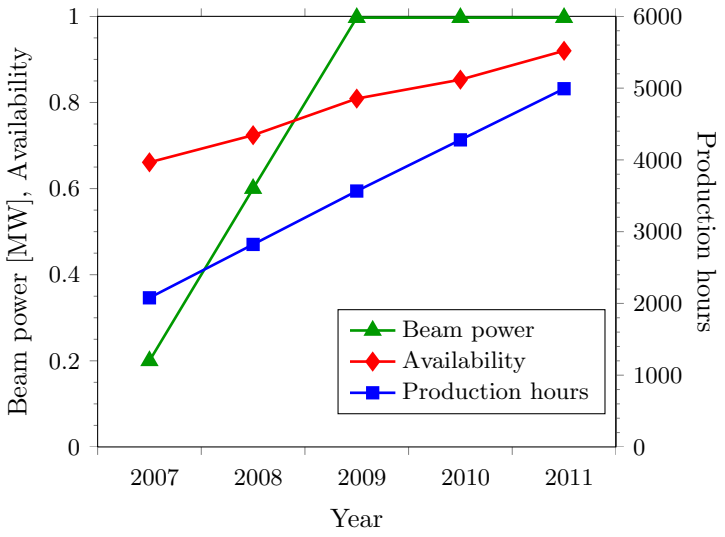

Figure 9.2: Operational metrics for the first 5 years of SNS operations following the initial proton beam on target. The beam power is the maximum beam power delivered during each fiscal year. Courtesy of SNS.

Following the initial delivery of a proton beam to the neutron target in 2019, including the commissioning of the initial set of instruments, a transition to a fully operational facility is planned. In this power ramp-up period, the operational power on target, the operational hours per year, the machine reliability and the number of operational instruments will approach the final facility performance levels, capable of delivering the scientific productivity expected from ESS. Throughout this period there will be a transitional emphasis from accelerator and target development towards an emphasis on supporting the neutron science.

As ESS represents unprecedented accelerator power levels and aims for world-class accelerator reliability, some years will be required to reach full capabilities. Low machine reliability in the initial years during power ramp-up is expected for a new world-class, first-of-a-kind facility. As 2025 approaches, with a large suite of instruments deployed, the disruptions caused by extended machine downtimes will have more severe consequences, and there will be a larger resistance to any change in the accelerator operation that may risk reliability. As such, an aggressive early push on the proton beam power ramp-up is planned, which will help identify any machine weaknesses and allow for appropriate modifications before a large neutron user community is in place at ESS.

This strategy is similar to that employed at SNS. The SNS original transition to operations plan called for a rapid increase in beam power to 1.4 MW over three years, accompanied by slower increases in beam reliability, neutron production hours and reliability [611]. Some actual SNS operational metrics over the first five years following initial delivery of proton beam on target are shown in Figure 9.2. There was an aggressive initial increase in the beam power over the first three years of operation. With the aggressive push for extended high power accelerator operation during the SNS power ramp-up, equipment shortcomings were identified early and efforts initiated for remediation. The identification of equipment issues requiring upgrades in the initial years at SNS is reflected in the low initial level of machine reliability. However, remedial actions taken during 2007-2009 led to reliability increases later on [612]. After 2009, the supported neutron user base had significantly increased, and there was a growing resistance to risking further beam power increases, which could adversely impact reliability [613].

After a neutron scattering instrument construction project is complete, it will enter a hot commissioning phase, using the spallation neutrons to characterise the performance of the instrument. As part of the instruments commissioning readiness review, the instrument team will have prepared a comprehensive commissioning plan. At full power and 95% reliability, instrument commissioning will take at least six months and could take up to two years. For instruments entering the commissioning phase in the initial years of ESSs operations, these plans will take into account the fact that beam operations will be at low power and low reliability. The scientific partners associated with the instrument will be working with the

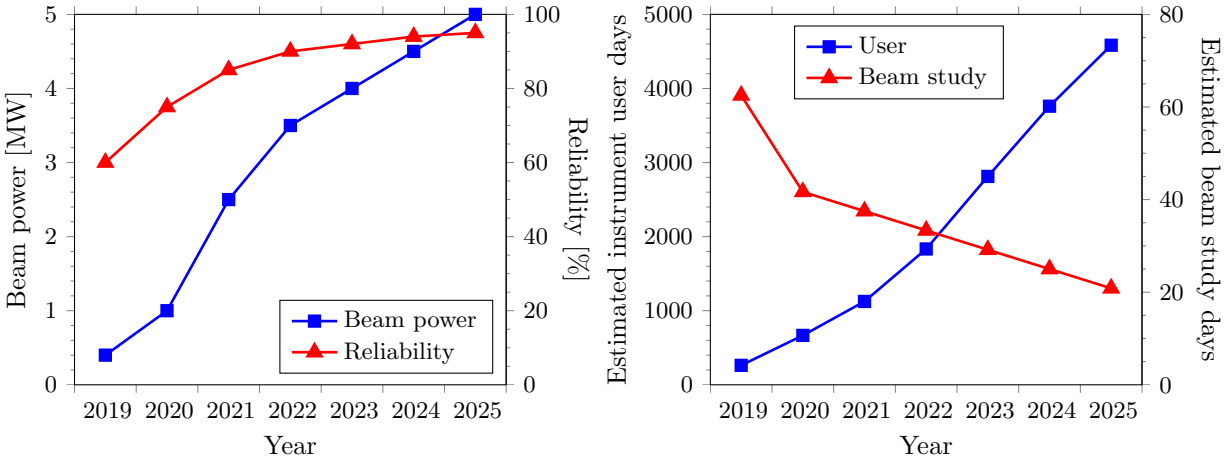

Figure 9.3: High-level goals during the transition period to full operations. Left: The accelerator parameters, indicating a rapid initial increase in power and reliability. Right: Estimates of delivered number of instrument user days and number of days of beam study, approaching the design expectation at the end of 2025.

instrument staff on the commissioning and subsequent early operations of the instruments. These partners will be fully cognisant of the operational status and risks associated with experiments at a facility still building up its experience and capabilities.

Taking into consideration the issues described above, a schedule for delivery of the high level ESS performance goals by the end of 2025 is shown in Figure 9.3. The accelerator parameters shown in Figure 9.3 (left) indicate an aggressive push early on, reaching 90% of full power within 3 years. Machine reliability is expected to be quite low initially, as equipment issues are addressed. Approaching 95% reliability at the end of the transition period will be one of the primary challenges. Figure 9.3 (right) indicates the build-up of operational support for neutron science. Figure 9.4 presents the high level schedule for the main activities and milestones for the transition to operations phase. In reality the beam availability will be low and reliability poor in the initial stage of the commissioning with beam and during the power ramp up. However, a preliminary operations schedule has been produced for planning purposes [614] for the first year in the operations phase. This schedule is shown in Figure 9.5.

9.3 Conventional facilities

For conventional facilities, commissioning means bringing all the conventional parts and systems of the facility, which are completed mechanically and electrically, into an operational state such that they perform all intended functions and meet design criteria. Commissioning tests will verify that the works have been carried out in conformance with technical specifications and relevant standards. When this is complete, witnessed and documented, the plant is ready to be handed over for further installation and commissioning of the related machine parts, that is, of the accelerator, target and instruments or parts thereof.

Commissioning requirements and methodology

The successful implementation of any installation plan is dependent on a properly conducted commissioning procedure prior to handover. Conventional Facilities will already have ensured during the design stage that the requirements and extent for the commissioning work have been clearly defined. Factory acceptance tests and other special demands, if any, will have been specified. BLED databases will have been populated and BIM guidelines will have been followed. The specification and design drawings will address and incorporate appropriate facilities for commissioning. Subsequently, the system installation subcontractor during the construction phase will be required to develop and submit a detailed commissioning method statement for each system, specifying which tests are to be performed and how they will be carried out and documented.

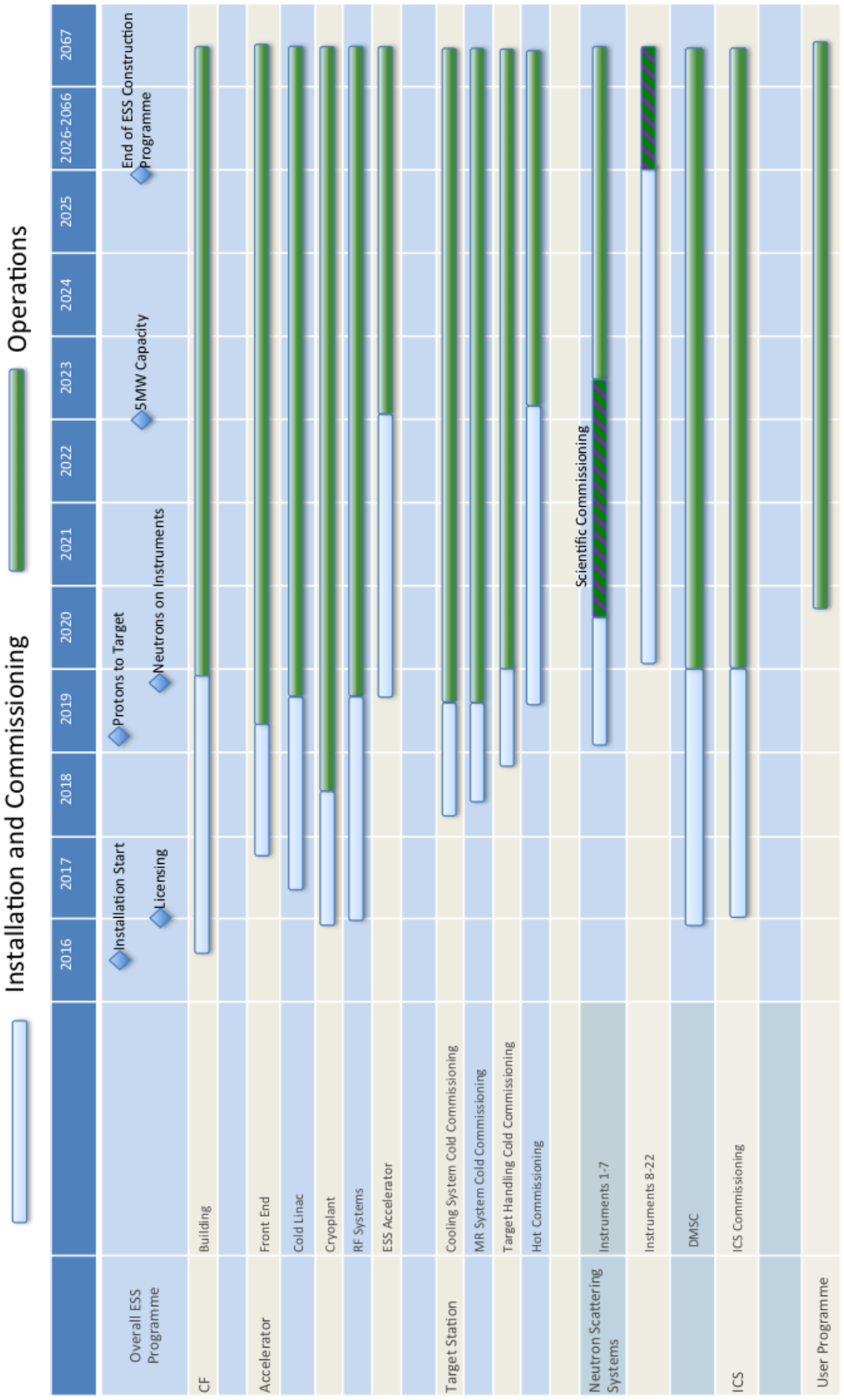

Figure 9.4: High level timelines for system commissioning during the transition to operations. Both installation and commissioning activities, and operations activities fall within the operations phase of the programme.

2019

	Jan					Feb							Mar						
Week	1	2	3	4	5	6	7	8	9	10	11	12	13						
Mon	31	7	14	21	28	4	11	18	25	4	11	18	25						
Tue	1	8	15	22	29	5	12	19	26	5	12	19	26						
Wed	2	9	16	23	30	6	13	20	27	6	13	20	27						
Thu	3	10	17	24	31	7	14	21	28	7	14	21	28						
Fri	4	11	18	25	1	8	15	22	1	8	15	22	29						
Sat	5	12	19	26	2	9	16	23	2	9	16	23	30						
Sun	6	13	20	27	3	10	17	24	3	10	17	24	31						

	Apr				May				June										
Week	14	15	16	17	18	19	20	21	22	23	24	25	26						
Mon	1	8	15	22	29	6	13	20	27	3	10	17	24						
Tue	2	9	16	23	30	7	14	21	28	4	11	18	25						
Wed	3	10	17	24	1	8	15	22	29	5	12	19	26						
Thu	4	11	18	25	2	9	16	23	30	6	13	20	27						
Fri	5	12	19	26	3	10	17	24	31	7	14	21	28						
Sat	6	13	20	27	4	11	18	25	1	8	15	22	29						
Sun	7	14	21	28	5	12	19	26	2	9	16	23	30						

	Jul					Aug							Sept						
Week	27	28	29	30	31	32	33	34	35	36	37	38	39						
Mon	1	8	15	22	29	5	12	19	26	2	9	16	23						
Tue	2	9	16	23	30	6	13	20	27	3	10	17	24						
Wed	3	10	17	24	31	7	14	21	28	4	11	18	25						
Thu	4	11	18	25	1	8	15	22	29	5	12	19	26						
Fri	5	12	19	26	2	9	16	23	30	6	13	20	27						
Sat	6	13	20	27	3	10	17	24	31	7	14	21	28						
Sun	7	14	21	28	4	11	18	25	1	8	15	22	29						

	Oct					Nov							Dec						
Week	40	41	42	43	44	45	46	47	48	49	50	51	52						
Mon	30	7	14	21	28	4	11	18	25	2	9	16	23						
Tue	1	8	15	22	29	5	12	19	26	3	10	17	24						
Wed	2	9	16	23	30	6	13	20	27	4	11	18	25						
Thu	3	10	17	24	31	7	14	21	28	5	12	19	26						
Fri	4	11	18	25	1	8	15	22	29	6	13	20	27						
Sat	5	12	19	26	2	9	16	23	30	7	14	21	28						
Sun	6	13	20	27	3	10	17	24	1	8	15	22	29						

: Shutdown 205 days (4920 hours)
: Restart 64 days (1536 hours)
: MIT 69 days (1656 hours)
: TNP 27 days (648 hours)

2020

	Jan					Feb							Mar						
Week	1	2	3	4	5	6	7	8	9	10	11	12	13						
Mon	30	6	13	20	27	3	10	17	24	2	9	16	23						
Tue	31	7	14	21	28	4	11	18	25	3	10	17	24						
Wed	1	8	15	22	29	5	12	19	26	4	11	18	25						
Thu	2	9	16	23	30	6	13	20	27	5	12	19	26						
Fri	3	10	17	24	31	7	14	21	28	6	13	20	27						
Sat	4	11	18	25	1	8	15	22	29	7	14	21	28						
Sun	5	12	19	26	2	9	16	23	1	8	15	22	29						

	Apr				May				June										
Week	14	15	16	17	18	19	20	21	22	23	24	25	26						
Mon	30	6	13	20	27	4	11	18	25	1	8	15	22						
Tue	31	7	14	21	28	5	12	19	26	2	9	16	23						
Wed	1	8	15	22	29	6	13	20	27	3	10	17	24						
Thu	2	9	16	23	30	7	14	21	28	4	11	18	25						
Fri	3	10	17	24	1	8	15	22	29	5	12	19	26						
Sat	4	11	18	25	2	9	16	23	30	6	13	20	27						
Sun	5	12	19	26	3	10	17	24	31	7	14	21	28						

	Jul					Aug							Sept						
Week	27	28	29	30	31	32	33	34	35	36	37	38	39						
Mon	29	6	13	20	27	3	10	17	24	31	7	14	21						
Tue	30	7	14	21	28	4	11	18	25	1	8	15	22						
Wed	1	8	15	22	29	5	12	19	26	2	9	16	23						
Thu	2	9	16	23	30	6	13	20	27	3	10	17	24						
Fri	3	10	17	24	31	7	14	21	28	4	11	18	25						
Sat	4	11	18	25	1	8	15	22	29	5	12	19	26						
Sun	5	12	19	26	2	9	16	23	30	6	13	20	27						

	Oct					Nov							Dec						
Week	40	41	42	43	44	45	46	47	48	49	50	51	52	53					
Mon	28	5	12	19	26	2	9	16	23	30	7	14	21	28					
Tue	29	6	13	20	27	3	10	17	24	1	8	15	22	29					
Wed	30	7	14	21	28	4	11	18	25	2	9	16	23	30					
Thu	1	8	15	22	29	5	12	19	26	3	10	17	24	31					
Fri	2	9	16	23	30	6	13	20	27	4	11	18	25	1					
Sat	3	10	17	24	31	7	14	21	28	5	12	19	26	2					
Sun	4	11	18	25	1	8	15	22	29	6	13	20	27	3					

: Shutdown 204 days (4896 hours)
: Restart 24.3 days (584 hours)
: MIT 45.7 days (1096 hours)
: TNP 92 days (2208 hours)

Figure 9.5: Provisional beam schedule for the year when first neutrons are produced (2019), and for the first year in the operations phase (2020). The schedule indicates when machine is shutdown (magenta), when its is started (orange), when operated for machine studies (yellow) and when it is producing neutrons (green). During power ramp-up and early commissioning stages the availability will be low and reliability poor. During the long shut down in the winter-spring the high-β cryomodules will be installed and most likely also instrument beam ports will be opened/installed.

Commissioning team

The conventional facility commissioning team will include a BMS subcontractor engineer, a subcontractor representative engineer, an ESS specialist consultant engineer and an ESS installation coordinator. Additional personnel, including system specialists, will join the team as and when required.

Staged commissioning

In order to line up with time schedules for commissioning of the various machine parts, conventional facility commissioning will be flexible and will be performed step-by-step. Conventional facility installation will be logistically complicated, including temporary installations due to late completion of permanent infrastructure. Details will be developed as machine requirements are consolidated. A tentative conventional facility commissioning time schedule is shown in Table 9.1. Generally the commissioning works will be divided into adjustments and tests on completion. Tests on completion are divided into two stages. First, functional tests verify that all requirements on a system are met when working in a stand-alone mode. Second, coordinated tests verify that all requirements on a complete plant or building are met when all relevant systems are in operation and are fully interconnected. Responsibility for carrying out adjustments

Period	Facility
Summer 2015 to autumn 2016	Accelerator building
Spring 2017 to winter 2017/18	Target station building
Summer 2017 to winter 2018/19	Instrument buildings
Summer 2019	Offices
Summer 2019	Laboratories
Autumn 2019	Canteen and guest house

Table 9.1: Tentative conventional facility commissioning schedule.

and conducting tests rests with the subcontractor. It is the task of the subcontractor to prove that the system installation is in accordance with the specification and all relevant norms and regulations. All tests must be be documented in test records and these records will be a part of the handing-over documentation submitted by the subcontractor.

Installation tests and other prerequisites for the commissioning works already will have been executed during system installation works and will be governed by the respective quality system of the subcontractor or, if works have been executed directly by ESS, by ESSs own Quality Manual. Any such quality system will at minimum comply with AMA (*Allmän Material och Arbetsbeskrivning*) [578]. These prerequisites include (but are not limited to) installation inspections including hidden works; flushing and leakage control of all pipe works; cleaning and leakage control of all ventilation ducts; insulation resistance test and colour coding of all electrical installations and cable works; labelling of all installations; and ensuring that the building envelope or relevant part thereof is completed. Assemblies, apparatus and components – whether separated or composite – must meet requirements on design, specifications and CE marking in accordance with the European Machine Directive SS-EN ISO 12100:2010 and Swedish law (SFS 2011:791) as well as the Work Environment Authority regulations (AFS 2008:3 and AFS 2009:5).

Documentation that must be available includes as-built drawings, an extensive photographic and video database, and operation and maintenance manuals. Operating procedures will be developed and validated as part of commissioning with associated training for ESS staff that will be responsible for operating the systems. Consideration will also be given to developing a 3D data base for all structures and components based on as-built conditions. When the above conditions have been fulfilled for a building and the service systems in it, the building can be declared “ready-for-occupancy”. Note that SNS negotiated an intermediate completion stage called “ready for [machine] installation”, which allowed storage and early installation work to begin before a building was “ready-for-occupancy”.

9.4 Accelerator

The installation of accelerator and target components will begin as soon as occupational readiness has been achieved and buildings and the installation of infrastructure such as electricity, water, ventilation and communications has been completed. The different subsystems will be installed and taken into operation in stages, each with readiness reviews, ensuring that all dependencies of one subsystem on another are fulfilled and verified. Completion of the readiness review, and follow-up on any review recommendations will take place before beam commissioning begins. Detailed commissioning plans will be written for all systems during the construction phase, at the same time that all necessary procedures, software tools and instruments are developed. Commissioning plans will describe the goals for the commissioning stage and the activities needed to achieve these goals.

Staged commissioning

The commissioning plan is based on the concept of a stepwise completion of the infrastructure and conventional facilities. In order to use the available time in an efficient manner, the linac tunnel, the klystron building and the infrastructure are made available for commissioning in four stages, including supporting infrastructure such as electrical power, cooling water, piping for cryogenic fluids, et cetera. Each stage allows the complete installation of a section of the accelerator and its associated support equipment. Section commissioning will take place while work on the buildings for the next stage continues to take place.

The four stages, which also correspond to portions of the accelerator where beam-stops are planned for tuning purposes during operation, are:

1. The front-end: ion source, LEBT, RFQ, and MEBT.
2. The drift tube linac
3. The superconducting linac with spoke resonators, all medium and high-β elliptical cavities.
4. The high energy beam transport and final approach to the target.

The initial stages cover relatively small sections of beam-line, but offer an early opportunity for integrated operation of systems needed for production of beam. Lessons learnt in this early period will facilitate commissioning of the more involved later commissioning stages. This is a primary motivation for striving for early stages of beam commissioning. Stages 1 and 2 require that electrical power, cooling water and other services are installed. Cryogenics are not used until stages 3 and 4. Cryogenic plant commissioning for the accelerator is thus part of stage 3.

The accelerator is planned to be taken into operation already after the commissioning of the medium-β section, with a temporary drift section installed for the high-β section. The energy above 600 MeV will be sufficient to drive the spallation reaction with a power of about 1 MW to 1.5 MW and produce neutron beams. The cryomodules and associated RF equipment for the high-β section can then be installed during the first three years of power ramp up. The installations would be carried out mainly during the long annual shutdowns. The staged installation of the high-β cryomodules affects the power ramp-up only marginally and it reduces schedule risk substantially.

Beam dumps and shielding

The beam destinations for the stages described above will have insertable beam stops for use during beam study periods that can also be used for commissioning. The ionising radiation created by the beam on these beam-dumps will be appropriately shielded with a temporary wall so that installation and construction work may continue downstream. The insertable beam stops will receive beam up to the nominal energy (at that position in the accelerator) and at the nominal current, but the beam pulses will be much shorter than nominal, down to 10 to 20 μ s, and the pulse repetition rate will be much lower, so that radiation can be kept at acceptable levels. It will still be possible to verify full operation of a majority of subsystems during each of the three commissioning stages, however, because the instantaneous beam power will reach its nominal value. Full power beam commissioning will be performed when the spallation target is in operation, since the accelerator itself will not be equipped with a beam dump that can handle the full average power of 5 MW

Testing before installation

Hardware components will arrive from factories and laboratories around the world for installation. All major components will be tested before they are sent to Lund. This includes ion source, RFQ, DTL tanks, cryomodules, RF sources and many other items. Linac structures will be tested at dedicated facilities at several collaborating accelerator laboratories. The normal conducting accelerator up through the RFQ will be tested for an extended amount of time, on the order of 6 months, at full power and with beam before it is delivered to Lund.

There is a comprehensive plan for testing the linac RF and cryomodule components. Manufacturers will test the RF klystrons as part of the acceptance criteria, and the high power modulators will be tested in place as they are installed in the klystron gallery in Lund. Testing is also planned for the superconducting cavities and cryomodules. Cavities will be tested in vertical tests to assure that they meet the design criteria, including an appropriate margin to account for the typically higher vertical test results compared to operation in a final horizontal assembly. Cavities that do not meet specifications will be further processed as needed before assembly into strings used for cryomodule fabrication. The baseline plan calls for cryomodules to be tested at high power at test stands in Uppsala (352 MHz structures) and on-site in Lund (704 MHz elliptical structures). If the cryomodules do not meet specifications, they will be shipped back to the manufacturer for repair.

If the equipment delivery and installation schedule does not permit high power testing and repair of cryomodules that do not meet full specification, another strategy is to install the cryomodules in the tunnel as they arrive, forgoing the high power RF test, as was done at SNS. In this approach, some installed cryomodules may need to be removed and upgraded later. The superconducting linac design is quite flexible and can accommodate reduced superconducting cavity performance.

Under-performing installed cryomodules still provide some acceleration and additional neutron production. Also, because of the early cryomodule installation, the supporting RF systems will be subjected to operational experience sooner. Cryomodule removal, upgrade and re-insertion in the linac would occur during the power ramp-up period of 2019 – 2025. Spare cryomodules for each of the families are planned, to facilitate this process, and missing cryomodules (taken out for repair) can also be tolerated for most of the linac. Also, *in situ* plasma-processing cavity remediation techniques are under development at SNS for the purpose of reducing the field-emission limitations, which is by far the most common type of superconducting cavity operational limitation.

Commissioning with beam

Commissioning here means the initial operation of the linac sections with beam, after final installation activities in Lund. System experts will develop plans and test each of the supporting technical systems individually, prior to beam commissioning. It is foreseen that a readiness review with the Radiation Safety Authority will occur prior to each stage of commissioning to ensure that adequate personnel and machine protective controls are in place. The reviews will also cover individual system preparations and tests. In each commissioning stage, an important part of the commissioning plan includes testing the machine protection interlock systems with tightly controlled beam spills, to verify their integrity.

Stage 1: Front-end

The first commissioning stage encompasses the ion source, low energy beam transport, radio frequency quadrupole, and medium energy beam transport. This section is about 10 m long altogether. Although some of this equipment will have been run with beam at collaborator sites, this will be the first beam acceleration at Lund. A key goal of this commissioning stage is integrated operation of all systems that the ESS will use for the acceleration and control of beam. This portion of the accelerator does not require tunnel enclosure, as the radiation levels will be minimal. In addition to verifying the integrated operation of the ESS sub-systems (timing, machine protection, controls systems, magnets, RF, vacuum, cooling etc.), beam quality will be quantified with a variety of measurements. The beam instrumentation group will test beam position monitors, beam current monitors, emittance and profile-measurement systems. While much of the RF equipment will have been tested before commissioning, the RF group will verify that the low-level RF system works properly with beam. This commissioning stage will also be the first opportunity for high level software tools to be exercised, for instance trajectory correction, RF phase scans and transverse matching.

Stage 2: Drift tube linac

The drift tube linac (DTL) will be installed in the linac tunnel, with supporting RF equipment in the klystron gallery. It comprises about 30 m of beam-line. The beam destination is a planned beam stop in a differential pumping section between the warm linac and the cold linac. This stage will involve the first significant beam acceleration. The primary beam tuning in this stage will be setting the RF amplitude and phase of the DTL klystrons. This will also provide an opportunity for testing system changes implemented as a result of lessons learnt from the first stage of commissioning, and possibly further refined.

Stage 3: Superconducting linac

The superconducting linac includes the spoke, medium-β and high-β cavity family types, and drift sections provided for future energy upgrade. It covers an energy range of about 80 MeV to 2500 MeV and corresponds to about 400 m. Beam will be directed to a straight-ahead tuning dump at the end of the linac, which includes a small portion of the HEBT system. Using a beam-line without bends greatly simplifies the beam tuning over such a wide energy range. The cryogenic system will be needed for this stage of commissioning and this stage also represents the first large-scale use of high power RF with beam. Before

beam commissioning commences, the RF group will qualify each superconducting cavity, to determine its safe operational limits (without beam) in the actual ESS machine environment. This step will identify upgrade needs for the superconducting RF equipment.

The primary beam tuning activity will be to set up each RF source with respect to the beam. Transverse matching at the lattice transitions between cavity types will be done, and the beam quality at the final energy will be measured with profile measurements. Running the superconducting RF with beam will also provide an opportunity to test the feedback and feed-forward systems of the low-level RF systems to compensate for the beam loading effects. Also, this will be the first opportunity to run beam at high enough energy to get meaningful response from beam loss monitors, which are a critical protection element.

Stage 4: High energy beam transport and target approach

The final beam commissioning will take place through the high-energy beam transport (HEBT) system to the target. Prior to commissioning, the target systems will need to be tested, and the systems reviewed and approved for low power beam readiness. This includes the target and all supporting systems such as the cryogenic moderators, shutters, neutron choppers, beam dump and initial beam instruments. Remote handling methods for critical systems will have to be demonstrated. In addition to delivering the beam to the target, this transport line has the important function of qualifying the beam properties as suitable for high power delivery to the target. These systems will be commissioned at low power, and procedures will include provisions for ensuring proper beam position, peak beam density, and allowable beam-halo levels at the target (halo here refers to the radial extent of beam at the periphery of the target). Beam diagnostics to be employed in this stage include profile measurements, beam position monitors, beam harp device, halo measurement systems, and imaging systems for the beam at the vacuum window and at the target.

Beam power ramp-up

A beam power ramp-up period will follow the initial delivery of beam on target, after a review of operational-readiness-for-high-power is performed by the the Radiation Safety Authority.

The average proton beam power on target is the product of the beam energy, the beam current, the beam macro-pulse length and the pulse repetition rate. Increases in average beam power will be modulated primarily by incrementally increasing the repetition rate and the macro-pulse length. Initially, the pulse repetition rate will be increased, reaching 14 Hz after about one year of operation. This will allow the neutron instruments to be commissioned at their final 14 Hz data acquisition rate as soon as possible. Also, some accelerator performance issues, such as Lorentz detuning, will be become more severe as the pulse length increases, and increasing the pulse length may require more development time than increasing the repetition rate. Pulse length issues will be investigated during beam study periods early on, at low repetition rates. If the final beam energy is below the 2.5 GeV design level due to cryomodule performance, the poor-performing structures will be swapped with spares, and re-worked in the planned superconducting RF facility discussed above, during the period of 2019 – 2025.

Another important issue during the initial power ramp-up period is gaining an understanding of the activation of the in-tunnel beam-line components from beam loss, and its impact on maintenance. Translating the beam loss monitor measurements during operation into residual activation of in-tunnel equipment after beam shut-down is largely an empirical exercise. The previously described machine protection qualification during the initial beam-commissioning period serves the purpose of assuring prompt protection against machine damage. However it is possible to cause significant residual activation of tunnel components with beam loss levels that do not cause equipment failure. To protect against buildup of higher than expected residual activation, limits on slower, time-averaged beam loss measurements will be set based on activation measurements taken in the tunnel. This effort will also involve optimisation of the placement of loss monitors to ensure that beam loss monitors adequately cover all beam-line areas. The operational run periods between residual activation measurement surveys will start at a frequency of every few days, and be extended to once a month after four years (2023). The beam power increase from one run to the next will be limited to less than a factor of two initially, and reduced to increases in the range from 10% to 20% as the final 5 MW power level is approached.

As 2025 approaches, a primary operational constraint will be the 95% reliability goal. In particular, downtimes covering fractions of a day or more are particularly disruptive for users. Many users will only

System	Subsystem	Test
Target	Shaft and drive	Run at up to 25 Hz.
	Target segments	Leak test at pressure.
	Target Safety System	Demonstrate trip signals generated for all defined cases.
Primary helium loop	Pump, heat exchanger, filter	Pressure and flow tests without target.
	Full loop with target	Full operational test without heat.
Target secondary loop	Nitrogen loop	Pressure leak tests, full flow testing without heat.
Moderator	Helium refrigerator	Full heat load test with resistive heater.
	Hydrogen loops	Loop testing without moderators.
	Hydrogen loops	Loop testing with moderators.
	Hydrogen loops	Off normal and venting tests.
Water loops	Reflector, PBW, shielding loops	Pressure decay leak testing.
	Reflector, PBW, shielding loops	Fill and drain testing.
	Reflector, PBW, shielding loops	Full flow testing.
	Inert cover gas system	Demonstrate design gas flow rates, I&C.
Gas	Monolith Helium system	Monolith helium fill and gas analysis.
	Helium distribution	Operational check of all warm helium systems.
	Nitrogen distribution	Operational check.
	Vacuum	Operational check and leak rate measurements.
	Activated off-gas	Leak check, flow tests to stack or holding tank.
Monolith	Primary shutters	Test cycle times, safety system performance.
	Neutron beam windows	Test leak tightness of all windows installed on beam lines.
	Beam dump cooling	Test flow rates and leak tightness of dump.
Remote handling	Hot cell operations	Test all operations that require full remote handling for beam operations $>$ 100 kW.
	High bay operations	Practise component replacement.
	Waste handling	Test target disposal method.
Instrumentation & control	All subsystems	Demonstrate proper operation and integration with overall ESS system.

Table 9.2: Stage 1 target station commissioning tests, without beam.

be at ESS for two to three days, and will have invested considerable time into planning experiments. If reliability is threatened by operation at higher power, the beam power will be limited to provide reliable operation. A key effort for the accelerator system owners during the period 2019-2025 will be to identify and remediate equipment issues that cause downtime. Also, exploiting the full flexibility inherent in a superconducting linac design to maximise machine reliability will be useful for achieving 95% reliability. For instance, it will be possible to continue running beam with an RF cavity or klystron offline, or even a high voltage convertor modulator (powering two RF sources) offline, over much of the linac. Model-based rapid adjustment of a superconducting RF linac setup to adapt to a failed cavity has been shown to work [615]. Developing fault recovery tools to quickly adapt the accelerator setup to work around failed components will be a major high level controls effort in the period 2019-2025.

9.5 Target station

The time frame for accelerator commissioning will be rather long. The target station will be the last major machine component to be commissioned. Target commissioning will demonstrate both the appropriate

performance and also the safe functioning of the target systems during operation (with beam on target), and also during maintenance. Operating procedures will be validated and documented and ESS operating staff trained. The commissioning will include the neutron production systems (target, moderators and premoderators, proton beam window, etc.), the ancillary systems and the safety systems (shielding, confinement barriers, etc.).

Stage 1: Commissioning without beam

The first stage of target commissioning will be performed without any beam on the target, allowing for the correction and adjustment of parameters as necessary. A preliminary set of pre-beam commissioning tests is given in Table 9.2.

This stage will proceed in parallel with accelerator commissioning, up until beam commissioning on the tune-up beam dump system. Systems will initially be tested separately, followed by integrated system testing with multiple systems including the overall instrumentation and control systems using documented operating procedures. Physical and functional interfaces with the accelerator, instruments and conventional facilities, which can be tested without beam, will be verified to be acceptable. Handling procedures and tooling for components such as the target, which will be activated beyond hands-on levels even at low initial beam power levels, will be fully demonstrated. Some safety functions will be tested in this stage (usage of portable sealed sources, etc.), without creating any active inventory. Proper operation of all safety systems required for beam operation will be tested and verified. Responsible engineering work package managers will define the required testing for their systems.

Stage 2: Commissioning with low power beam

The second stage of target commissioning starts when the proton beam is first delivered to the target. A preliminary set of low power commissioning tests is given in Table 9.3. The pace of the low power ramp up may be limited by activation and contamination levels, in those cases in which "hands-on" levels are desired for unexpected maintenance on systems such as primary loops and off-gas systems. Procedures for the second stage of commissioning are still being defined.

Irradiation will start with very low power on target (of the order of 1% of the nominal 5 MW). Some low power measurements will be performed before progressively increasing the power, with intermediate stabilised plateaus. In this phase, first neutrons will be measured at the beam lines. Extensive radiation surveys will be done to identify any shielding weaknesses. Some special tests can be done at this low power, involving the safety interlock systems; for instance safety systems related to the beam profile shape can be tested by reducing the beam spot size (something that can be done only at low power). The functioning of systems like the heat removal system, or the cooling loops, can be tested and compared with predictions from calculations, and with previous measurements done during the tests. While slowly increasing the beam power, efforts will concentrate on the precise measurements of fluxes, on additional tests of the cooling loops and heat removal systems, on radiation mappings, and on investigating the performance and safety of the target station, to match the expected operating and licensing requirements.

Target beam commissioning includes tests and qualifications of the accelerator to target interface. Beam profile measurements will be performed for both accelerator and target. The correct functioning of the beam profile monitors is essential, as the peak current density will be controlled at all times during irradiation. First neutrons will be detected by the instruments and moderator neutronic performance will be measured and compared to acceptance criteria. Target station monitoring will be tested by validating and understand control signals from the target, such as pressure sensors and target temperature measurements. When possible, physical parameters will be measured directly by independent redundant systems through the target control system, in order to cross check and validate the normal output signals.

Radiation protection monitoring will be performed at certain key points of the facility, including dose measurements at the beam exits and radiation gas monitors. Spallation products (volatiles and possibly non-volatiles) will be measured in the gas systems using conventional spectroscopy methods. One surprise in SNS was that the xenon and krypton would adsorb on dust and also on the gold filter used to remove mercury from the helium cover gas, which gave unexpectedly high dose rates in unexpected locations. For ESS there might also be surprises from activated dust transport. There should also be an effort to evaluate tritium production and transport. Another area of interest would be the production of free hydrogen and oxygen in the water loops by radiolysis.

System	Subsystem	Test
Target	Shaft and drive	Run at 25 Hz.
	Target Safety System	Demonstrate front end trip for a loss of rotation.
	Beam diagnostics	Establish beam density profile and location on target segments.
Primary helium loop	Pump, heat exchanger	Compare measured temperatures with predictions.
	Filter system	Measure activation in filter room due to trapped dust.
Target secondary loop	Nitrogen loop	Compare measured temperatures with predictions.
Moderator	Full loop	Compare measured temperatures and pressure fluctuations with predictions.
	Neutronic performance	Measure brightness and time structure from both moderators.
	Transfer lines	Measure vacuum levels with beam, and measure activation.
Water loops	Reflector, PBW, shielding loops	Compare measured temperatures with predictions.
	Inert cover gas system	Measure gas production by radiolysis.
Gas	All subsystems	Confirm normal operation with beam.
	Activated off-gas	Measure dose rates and stack releases. Measurements of spallation products and comparison with predictions.
Monolith	Shielding	Survey all areas after each significant increase in beam power.
	Beam dump	Compare measured temperatures with predictions.

Table 9.3: Stage 2 target station beam commissioning tests, with low power beam.

Safety barriers for the internal confinement of radioactive contamination will be tested, along with zoning confinement for helium and hydrogen hazards. These functions are assured by the HVAC and confinement devices (penetrations). Handling systems will be tested before active beam commissioning. If possible, remote handling systems will be used during initial installation for the target, proton beam window and moderator/reflector plugs. Hot cell operations that will be done remotely will be tested before beam operations. The correct functionality of key waste handling operations will be demonstrated. The interdependences of different target control sub-systems will be tested, including transient responses – for example, moderator loop control system response to pressure transients. Protective actions will be tested during integration with the overall accelerator control system, including alarm response procedures. Target protection system and safety-related beam shutdown operations will be tested before first beam on target, and also at low power.

Very low power target commissioning may be performed without some ancillary systems, but all ancillary systems must be fully operational well before full power operation.

Stage 3: Beam power ramp-up

As discussed in the accelerator section, following the initial target beam delivery, there will be a progressive ramp-up of the beam power (energy and repetition rate). The target systems will have to withstand operation at full power. This includes, for instance, the cryogenic loops, which will have to operate at maximum heat deposition in the moderators, close to 10 kW per module. In general, most of the tests listed in Table 9.3 will be repeated at full power to arrive at routine operation of the target. A key aspect concerns safety, related to activation levels, shielding, and functioning of containment barriers. Radiation levels and the residual neutron field outside the shielding will be monitored at full power.

9.6 Instruments

For the neutron scattering instruments, the transition from the construction into operations has two phases – cold and hot, as indicated in Figure 9.6.

Stage 1: Cold commissioning without neutrons

The end of the construction of an individual instrument is marked by a successful completion of the "cold commissioning" phase, after which all instrument components function as anticipated for operations, but without receiving neutrons from the target. High level instrument systems and tests are indicated in Table 9.4. The end of cold commissioning for an instrument will be marked by a "readiness-for-operations" document, approved by an appointed operations manager. The individual beam shutter cannot be opened prior to this approval. The main focus of this phase is to ensure that all components and sub-systems of an instrument system work according to specifications; that communication channels and exchange of signals between accelerator and target are established and working; that safety-relevant systems such as safety interlock systems work according to design and that their functionality complies with local rules and regulations.

Stage 2: Hot commissioning with neutrons

Once an instrument is ready for "hot commissioning", the focus is on testing it under real operational conditions with an emphasis on finding and rectifying bugs and issues, and on keeping pace with the proton beam power ramp up. Radiation surveys will be carried out at very low power on target. During this period, extensive radiation surveys will be done to identify any shielding weaknesses as the accelerator power is increased to its final operating power of 5 MW. The exact details for the hot commissioning of a neutron scattering instrument will be detailed in the *Instrument Commissioning Schedule*.

In order to move the instrument from the commissioning phase into the operational user mode, further administrative requirements include the availability of two database-driven systems, one of which accepts proposals including user, sample, instrument, sample environment and scheduling information, and the other of which tracks samples on their way through the facility, from arrival to check-and-release following radiation protection procedures. Neutron scattering personnel will begin the transition from construction into operations in 2019, in accordance with the construction schedule. Pre-operations – the beginning of operations and use of laboratories such as sample environment, neutron optics or detectors – will already

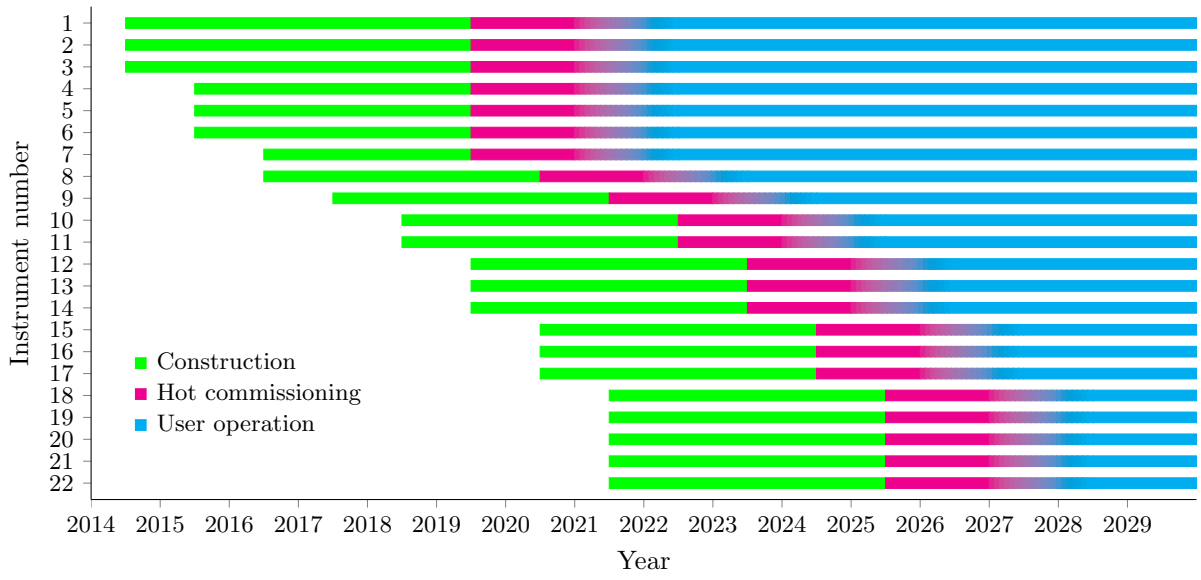

Figure 9.6: Instrument construction schedule. The construction period for each instrument (green) ends with "cold" commissioning, followed by a period of "hot" commissioning (red) before the instrument moves into normal user operation (blue).

Sub-system	Test
Choppers	Receive signals from accelerator timing system. Feedback to instrument motion control, data acquisition and instrument control system.
Guides	Measure vacuum levels.
Motion stages	Feedback to instrument motion control, data acquisition and instrument control system.
Safety interlock system	Feedback to instrument motion control, data acquisition and instrument control system. Communicate with machine protection system.
Detectors & neutron monitors	Feedback to instrument motion control, data acquisition and instrument control system.
Data reduction	Access raw data from data acquisition system and conversion from instrument coordinates to physical coordinates.
Data analysis	Access and analyse reduced data sets.
Data storage	Archive and store data in accordance with data management policies.

Table 9.4: Basic instrument systems tests during the cold (construction) and hot (operations) commissioning phases prior to user operation (operations), for instruments 1 to 22. Cold commissioning: Simulated signals to test detector systems or using portable neutron source, if appropriate licensing is provided, with instrument shutter closed. Instrument must be fully functional. Hot commissioning: Using spallation neutrons coming from the target with instrument shutter open. Instrument must be fully functional.

have commenced in 2018, depending on when such laboratories are handed over as "ready-for-occupancy" by Conventional Facilities.

9.7 Integrated control systems

A functioning control system is a pre-requisite for the commissioning and acceptance of all devices (accelerator, target, conventional facilities and instruments) for the operations phase. Core components of the control system will be tested and accepted before installation of the accelerator, target and instruments begins. High-level applications that will provide the integration of all devices via a uniform look-and-feel to test and accept devices before and during beam commissioning will be developed in parallel with the installation and commissioning of devices during the construction phase.

The core control system components are global timing, system services, machine protection and personnel protection. The global timing system provides clock synchronisation for all devices. System services include management of alarms, the logging and archiving of data from process variables, management of control system configuration settings and the post-mortem service for detailed analysis of events which have caused the machine to shutdown or to stop proton beam production.

The machine protection system (MPS) is a non-safety class system whose purpose is to protect the machines equipment from damage due to malfunctioning components (of equipment) and due to non-nominal and/or critical beam losses. If the MPS detects critical or non-nominal machine conditions, the proton beam will be switched off and further beam injection will be inhibited until the origin of the failure has been eliminated and further beam operation is considered to be safe. The personnel protection system (PPS) is a safety-class system whose purpose is to protect personnel against unnecessary radiological exposure from the ESS machine, electrical shock hazard and other dangerous phenomena (such as loss of oxygen in the tunnel, helium release, etc.). If personnel enter into areas where exposure to radiation is possible, no beam operation will be allowed and will be interrupted immediately.

All these systems must be tested and operational for the installation and commissioning of the machine equipment with (and without) beam and will be fully exploited and integrated before the ESS operation phase starts. An external review of the final control system is foreseen before formal operations can begin, encompassing all aspects of the control system so that the necessary levels of security, safety, integration, and reliability can be assured. If other control systems for some sub-systems are identified at this time, which are not (yet) part of the ICS, these systems will be tagged for integration.

Operational modes and support from MPS and PPS

The different configuration settings for all beam and machine modes will be located in a common database, which is embedded in the ICS. The matrix shown in Figure 9.5 provides an overview of the currently foreseen operational modes, i.e., of the various machine and beam mode combinations.

MPS and PPS must protect the machines equipment and ESS personnel, but at the same time, these systems must support operational flexibility which is required during the installation, commissioning and operation phases of the ESS machine. In this context, the ESS machine consists of the accelerator, target station, ICS, energy platform, and conventional facility suite layout. It is important to define sequences of actions to be taken in order to bring the machine, for example, from a state of maintenance to a state in which it produces neutrons at full power; i.e., to operate the machine means to bring the machine into different *states*. Several *operational machine state*s have been identified, including maintenance, machine development, restart, and full power neutron production among others. The states consist of several operational modes, where each operational mode represents a combined set of one beam and one machine mode.

A machine mode refers to a specific machine configuration and provides an overview of whether the machine is powered or not, whether the machine (or parts of it) can be accessed by personnel or not, etc. Additionally the machine mode defines the source and the intended destination of the proton and neutron beams within the machine layout. Before starting any beam-based operation, all transport systems must be ready and validated for the setting. The beam permit system, which is part of the MPS ,will perform this validation. Different intended destinations for the proton beam are, for example, interceptive stops such as Faraday cups, the tuning dump line or the target station.

The machines equipment will be installed and commissioned stepwise and the machine modes will be set up according to these different steps, allowing for high operational flexibility. Especially during installation and commissioning, it must be possible to install equipment, for example, in the cold LINAC while performing beam-based tests in the warm LINAC. In order to do so, the machine modes will also be individually applicable for each segment of the machine and not for the full machine only. For example

BEAM-MODE.qualifier	**MACHINE-MODE.qualifier**												
	SHUTDOWN.segment	COOLDOWN.segment	ACCESS.segment	WARMUP.segment	CALIBRATION.segment	RECOVERY	ABORT	NAHZ.segment	STANDBY.segment	SETUP.segment	PREPARE-TARGET.segment	PRODUCTION.power	STUDIES
NO-BEAM	x	x	x	x	x	x	x	x	x				x
PROBE-BEAM.segment										x			x
SETUP-BEAM.segment										x			x
PREPARE-PHYSICS-BEAM											x		x
STABLE-BEAM.power												x	x
BEAM-TRIP												x	x
BEAM-ABORT						x			x	x	x	x	x

Table 9.5: Matrix of beam-modes and machine-modes. The *segment* mode qualifier refers to a part of the machine. For example STANDBY.LINAC is true if the LINAC is ready for beam injection after it has been fully tested. The *power* mode qualifier has values such as LOW-POWER and HIGH-POWER. A cell marked with a cross "x" indicates that a beam-mode and a machine-mode have the potential to both be simultaneously true. For example, the SETUP-BEAM beam-mode cannot be true if the ACCESS machine-mode is true.

ACCESS is a machine mode, which can be ON for the LEBT (i.e. access is allowed in the LEBT segment) but OFF for the DTL (i.e. access is not allowed in the DTL segment): ACCESS.LEBT=ON and ACCESS.DTL=OFF. If access rights are violated, the access permit will be removed and possible beam operation will be interrupted by the PPS. The machine mode SETUP validates the intended destinations of the proton beam: SETUP.DTL.FC.4 indicates that the proton beam will be stopped in the fourth Faraday cup in the DTL.

A beam mode is defined through specific beam parameters, such as peak current, pulse structure, beam power, pulse repetition rate, etc. Several different types of beam modes are needed in order to commission and operate the machine with beam in a safe way: beam parameters for the "probe beam mode are chosen such that the beam is considered to be safe. A safe proton beam can reach any destination within the accelerator and target station layout and has no potential to damage the equipment. The probe beam settings can be different for the LINAC (ending in the tuning dump line) and the A2T line (ending in the target station). Usually, the probe beam modes will be used in a first step of beam-based operation.

In a second step, the setup beam modes will be used to tune the accelerator and take measurements for diagnostic purposes as well as for the preparation of the target station for full power neutron production. After the accelerator and the target station have been prepared for full power production, the so-called stable beam modes will be used to indicate a stable neutron production at medium or full power to the different users. There are two more beam modes foreseen: beam trip and beam abort, where "beam trip reflects a short interruption of the proton beam due to a minor problem of the machine and "beam abort indicates a serious problem resulting in a longer interruption of beam and neutron production. The beam permit system permanently crosschecks the beam parameter settings (for example, verifying that the voltage on specific magnets is as expected for a given condition and mode) and if non-nominal conditions are detected, beam operation will be interrupted by the MPS.

Controls commissioning strategy for device integration

The major structures in the facility – Accelerator, Target and Instruments – will be brought online in stages during installation and commissioning. At every point in this process the control system for each of these devices will have to be tested individually. The integration of these devices into the main control system will occur as each of these devices is commissioned. The Controls Group will have an Integration Support Group working in tandem with machine and neutron instrument personnel, to provide the necessary support. The schedule for final control system integration will follow along with the end of commissioning of the major structures. Following this step-by-step process, the ICS will be built for the entire facility. Major sub-systems such as Cryogenics and Vacuum (and others) will be developed by outside contractors and delivered to ESS. The ICS project team will accomplish the integration of their control systems into the main Control System in time for the use of these systems for commissioning of the Machine and Instruments.

Conventional facility controls

Electrical Power, Heating, Ventilation, Air Conditioning, and Water Systems as well as Safety and other sub-systems provided by Conventional Facilities will be integrated early in the development of the Control System, as they are also pre-requisites for the installation of the Machine and Instrument devices. The schedule for the integration of these control systems will be determined by the delivery time of each sub-system.

Main control room and data centre

The main control room will be the place where operations activities will be centred, and every part of the machine will be controlled and monitored from this central location without exception. Neutron Instruments will also be monitored from the main control room, but since neutron scientists will need to be near their sample environments and data acquisition hardware, satellite control areas will exist. These satellite areas will contain the systems needed for control and monitoring of instruments and sample environment, which in most cases will only be monitors and user stations. In addition, data acquisition for the experiments may also be controlled from these areas as the electronics for the experiments will be located as close as possible to the sample environments in most cases.

A secure and local data centre supports the control systems main control room where servers for both the control system and immediate post-processing of data from the experiments will be housed. High-speed and secure networks and data storage capabilities will provide the necessary computing infrastructure for both machine and instrument operation. Data acquisition from the experiments will pass through this data centre on its way to permanent storage and analysis at the DMSC facility in Copenhagen. Only authorised personnel will have access to the main control room and related networks.

The control room will be built in at least two stages. During installation and commissioning of the machine and the first instruments, a temporary control room will be built. The temporary control room will serve the role of the main control room until the building where the main control room will be housed is completed. Since the main control room will not contain any hardware, only monitors and control stations, it will be possible to move operations from the temporary to the final control room relatively easily as both rooms will exist in parallel for a time until the temporary control room can be decommissioned. The final control room will be equipped with a kitchen, sleeping and rest rooms, showers and a reception.

9.8 Operational lessons learnt from other facilities

SNS target system reliability

In general target systems achieved high reliability with only a few exceptions. A number of factors that are believed to have helped are:

1. Simplicity was emphasised in design.

2. All support systems and shielding were designed for full 2 MW operation.

3. Operating technician staff were in place for installation and commissioning and were very well trained and had well developed normal-operating and alarm response procedures.

4. A full-scale prototypical primary mercury loop was constructed and operated leading to many improvements in the loop and target design. For example, extreme flow-induced cavitation was found with the first target design, resulting in a redesign.

5. A prototypical cryogenic moderator loop was tested during preliminary design, which resulted in changing the type of circulator and also validated the control system design with cold accumulator to reduce pressure fluctuations.

6. Redundant pumps were used for all water loops with automatic switch over.

7. Extensive remote-handling testing was done both during early design and for over six months on-site prior to first beam on target

SNS target system operations

1. Primary pump continuous testing was only done for a few days and did not identify a problem found during the first long-term pump operation over a period of months. During operation, the vertical shaft grease seal and also the helium barrier seal failed, requiring beam shut down and repairs.

2. Inadequate vendor monitoring of design changes in the moderator led to a problem with one short supply tube and a moderator that could not operate at power. This was later repaired in place.

3. Deflections within the inner reflector plug during handling were not adequately evaluated and the initial on-site lift may have contributed to transfer line leaks requiring removal and repair.

4. Not enough design work was done to develop leak check methods for the target mercury loop after a target change. When one target did not pass the leak check after installation, there was an intense effort to develop methods in a full remote-handling environment, which was difficult.

5. The 7.5 kW moderator refrigerator had numerous problems and caused a loss of reliability during the first few years. Installation of an instrument in the warm leg to the cold box detected hydrocarbons coming from the compressor system and led to a final fix of the system. Such instrumentation should be part of the initial design and refrigerator procurement should be closely monitored. Early on-site testing is needed.

6. The accumulators in the moderator loops may be damaged or may leak, and should therefore be designed to be accessible. Both SNS and J-PARC have had to replace an accumulator.

MEGAPIE target

Experience with the MEGAPIE target provides information concerning the design, construction, operation and dismantling of a liquid metal target operating at the 1 MW level [616].

1. In general, simplification of the target design is desirable, for instance the use of only one electromagnetic pump, instead of two as were used in MEGAPIE.

2. For the heat removal system, it is desirable to avoid oil as a medium for an intermediate cooling loop, and the corresponding fire safety equipment. Possible alternative solutions could be direct water-cooling of LBE or an intermediate liquid metal loop.

3. Information stemming from the analysis of the operation of the gas systems includes: light gases are the greatest contributors to pressure build-up in the target cover gas system. In the experiment, one of the pressure transducers failed during operation, demonstrating the importance of having more measuring devices for a reliable measuring system. Moreover, leaks of radioactive xenon isotopes produced in the LBE were detected in the insulation gas system, corresponding to roughly 1% of the amount of the total inventory in the cover gas system. The issue of leaks between target components should be taken into account in the target design.

Chapter 10

Emission Control

Chapter abstract

Summary: This chapter gives an overview of the progress ESS has made in developing a waste management strategy for irradiated materials. It addresses regulatory requirements, radiological characterisation, waste treatment and conditioning, waste disposal, decommissioning, and environmental impact. ESS is committed to the safe management of radioactive waste and emissions during the entire life-cycle of the facility. ESS has already made substantial progress in estimating levels of radioactive waste and emissions, and in developing protocols for managing waste. The main finding is that waste can be successfully handled, transported and disposed of in accordance with Swedish law. ESS will be a good neighbour, and will not damage the health of the community or the environment.

Requirements. The chapter provides an overview of Swedish radiation safety regulations relevant for the licensing, operation and decommissioning of the facility. The Swedish waste management system and Sweden's waste management policies are also reviewed.

Radiological characterisation. Within the Swedish radwaste system, the generator of radioactive waste must provide information about the radionuclide inventory before the removal of the waste into final repositories is permitted. Nuclide inventories were estimated for the most important components of the target station using Monte Carlo techniques. The same method was used to estimate residual activity within the linac tunnel and in the shielding wall and surrounding soil. The inventory database that was created is currently being evaluated by SKB, the Swedish company in charge of final disposal of the radwaste. Source terms for environmental analysis also were derived using this direct methodology. Two additional methods were used to verify and validate the nuclide inventory results.

Waste management. ESS has developed a waste management logistical plan that divides waste streams into categories according to a risk-based assessment, and proposes a treatment protocol optimised for each specific material's characteristics. Waste shipping and disposal plans have been evaluated and found to be feasible.

Operational waste and emissions. Preliminary estimates of the radioactive waste and emissions generated in fluid systems indicate that the purification systems will function well and that safe management of radionuclides is readily achievable.

Environmental impact analyses. The annual dose to a reference person from exposure due to operational release of radionuclides was estimated, and the radiological consequences of potential accidental releases were evaluated. The results show that ESS is well within Swedish regulatory requirements.

Decommissioning. Immediate dismantlement is the preferred decommissioning strategy, with the goal of returning the site to green field status.

10.1 Radiation safety requirements

The overall ESS safety approach is laid out in the general safety objectives (GSO) [391], which are described in more detail in Chapter 11. Radiation protection is a main priority throughout the project lifetime, through all stages of conceptual and detailed design, fabrication of components and construction, commissioning, operation, planned and unplanned maintenance, and eventual dismantling and decommissioning. The GSO concentrates upon setting limits for radiation doses. In many cases, ESS limits are stricter than those required by Swedish law. Although ESS is a non-nuclear facility, the Swedish Radiation Safety Authority (SSM) is empowered to regulate the operation of accelerators and sealed radiation sources, to provide for the protection of workers and the public during activities involving ionisation radiation, and to regulate the transport of radioactive substances. The regulations that apply are discussed at some length in Section 11.2. According to SSM regulations, limits on the release of radioactive substances depend on the doses received by a critical group or a reference group designed to be representative of people living in the vicinity of the facility. Section 11.3 discusses this in some detail, including the *classification of events*. The limits on radiological doses to the public and facility employees and visitors are summarised in Table 11.3.

ESS has set 0.05 mSv as the upper annual dose limit for the general public in normal operation.

The release of liquid waste to the municipal sewage water treatment is also regulated by SSM. Radioactive waste water must be controlled before its release, which implies that storage and treatment facilities must be in place. For nuclear facilities (unlike ESS), SSM requires that the dose estimation methodology be described and approved by SSM. The calculations must be based upon measured dispersion data and knowledge of the circumstances in the most affected area during the time period concerned. Although not legally bound to do so, ESS has declared that it will abide by the intention of this regulation [617].

According to Swedish regulation, it is the responsibility of the holder of a licence to own or operate a facility dealing with nuclear materials to prepare for the management and disposal of radioactive waste products from the facility and to decommission and dismantle the facility. Therefore, ESS is responsible for the safe management and disposal of radioactive waste deriving from its operation, and for decommissioning and dismantling the facility after it has been taken out of service. It is ESS's responsibility to plan, build and operate the facilities and systems that are needed for this purpose, and to conduct related research and development. Radioactive waste from ESS will be handled and disposed of within the Swedish system for management of radioactive waste and spent nuclear fuel. Established disposal facilities will be used that meet the legal requirements for each specific category of waste. Similarly, transport of activated materials will comply with Swedish ADR (Accord Dangereux Routier) regulation and established practice, based on IAEA transport recommendations (TS-R-1). Selected transport containers will meet the legal requirements for each category of material being moved.

10.2 Radiological characterisation of the waste

Preliminary ESS estimates of the radiation levels and associated shielding requirements were assessed for different parts of the facility.

Linear accelerator

ESS has developed an approach [618], including both methodology and tools, to assess activation levels and associated shielding of the ESS accelerator. The input parameters and tools used in this approach reflect current assessment capability, and the approach is based upon conservative assumptions that provide an appropriate margin of safety, given the still developing level of knowledge and understanding of the accelerator system. Monte Carlo simulations complemented with analytical predictions were used to estimate the thickness of the lateral shielding of the accelerator tunnel. A tunnel configuration placed underground is proposed as a reference for further detailed evaluations. An ordinary concrete shielding wall one meter thick was assumed in the analysis, for the purpose of minimising the activation of the soil surrounding the concrete. In this respect, two situations were analysed: i) normal linac operation and ii) accidental full beam loss. For the second case, the expected integrated equivalent dose from full beam loss outside the predicted shields has to comply with exposure limits given a cut-off time of 50 ms. The amount of earth shielding required in addition to the one meter thick wall of concrete was derived to meet the exposure criteria for controlled, supervised and public areas. It was concluded from the investigation

that a shielding thickness of about six meters of earth will be required for the option designating the site as a supervised area, and eight meters of earth for a public area designation.

Additionally, a preliminary estimate of the required shielding in the HEBT zone was performed. Calculations have shown that two meters of iron block followed by a 40 cm thick layer of ordinary concrete will be required to shield the bending magnet in the linac-to-target connection zone. This estimation accounts only for 1 W/m beam loss along the magnet and aims to reduce the prompt radiation to a level of 1 μSv/h. Evaluations considering backscattering of the neutrons from the target area are necessary to correctly size the magnet shielding in order to insure safe working conditions in the area. The proposed thickness of the shielding guarantees an integrated dose in case of accident below the acceptable limit with sufficient margin to cut off the beam. Analysis of options to reduce the shield thicknesses in compliance with the ALARA principle will be conducted in the future.

The residual field inside the tunnel was further evaluated using a simple geometry to model unshielded beam loss consequences upon the machine structure, concrete wall and air inside. Residual dose levels obtained in these preliminary calculations are high. One hour after shut-down in the high energy zone of the accelerator, dose rates of a few hundreds of micro-Sieverts per hour were found. Consistent with these results, the high energy end of the linac might be classified as a radiation-controlled area with restricted access. Activation of the concrete wall and adjacent soil shielding was also estimated to permit a preliminary quantitative evaluation of the radioactive waste likely to arise during the lifetime of the facility (40 years of operation). About 1.50×10^4 tonnes of concrete shielding from the accelerator tunnel (in a volume of 6.37×10^3 m^3) will need to be cleared during ESS decommissioning. The recent implementation of the clearance concept [619] within Swedish legislation leads to the characterisation of this concrete through an identification of its clearance index. It was concluded that only the first 20 cm of concrete surrounding the tunnel (3500 tonnes) have the potential to require special handling for disposal, while the remaining concrete will be suitable for free release. Section 10.3 discusses further the concept of clearance under Swedish law.

Release of radioactive materials into the environment was also assessed, guiding the evaluation and definition of potential sources for environmental contamination analysis, a major topic addressed by the ESS design. Based on these estimations, further complex studies were carried out to model the migration of contaminants through the environment and to assess its impact. Activity concentrations of radionuclides of major concern in terms of contaminant migration into the groundwater were derived for the first one meter of soil surrounding the concrete tunnel wall. The ESS accelerator design will include protective measures to isolate the soil from groundwater in order to prevent the exchange of contaminated water. A preliminary evaluation of the activity released in the atmosphere from the linac tunnel accounting only for the air exchange rate inside the entire tunnel volume was also carried out. It was found from this conservative analysis that a more realistic model will be required to aid in the design of the ventilation system inside the accelerator tunnel. Various scenarios of the release of radioactivity into the air from the accelerator tunnel were analysed and compared.

Target, moderator and reflector assembly

A basic calculation model of the target, moderator and reflector assembly (TMRA), optimised in terms of neutron yield from the moderator face, was the starting point of calculations investigating various parameters involved in the activation analysis, as reported in an ESS technical report [620]. The geometry model used for radiation transport analysis is shown in Figure 10.1. The most important parameters for the calculation model are described in the 2011 target station design update [339], while the material compositions used are described in another technical report [355]. The total specific activity and decay heat in the tungsten target as a function of decay time are given in Table 10.1. More detailed results of the spatial distributions of the activity and decay heat versus decay time in the target wheel will be derived in the future. Estimates of the α-emitters in the tungsten target after five years of operation show that ^{148}Gd is by far the main contribution. The tritium activity produced in the target after 5000 hours of operation is calculated to be at the level of 1.5×10^{15} Bq for the tungsten. A similarly large amount of tritium – 1.2×10^{15} Bq – is produced in the beryllium reflector, as recorded in Table 10.2.

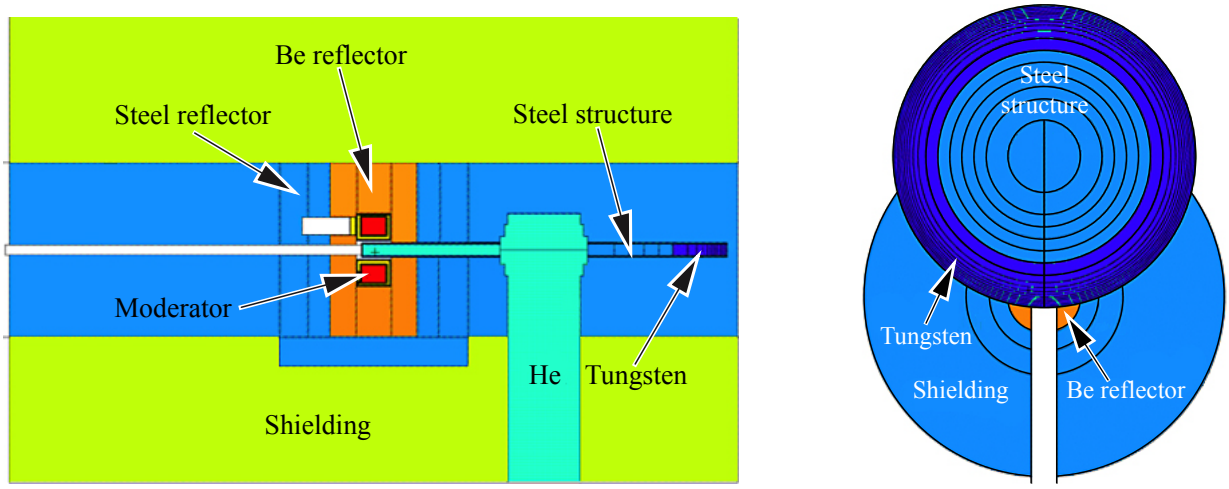

Figure 10.1: Geometric model of the target, moderator and reflector assembly (TMRA) used in decay calculations. Left: Side view of the TMRA. Right: Plan view.

Decay time [y]	**Total activity** **Wheel** [10^{15}Bq]	**Layers & shroud** [10^{15}Bq]	**Decay heat** **Wheel** [kW]	**Layers & shroud** [kW]
0	467	8.239	41.5	1.54
0.02	111	3.718	3.16	0.291
1	12.0	1.278	0.355	0.094
3	4.4	0.678	0.120	0.053
5	3.0	0.426	0.059	0.038
7	2.3	0.289	0.032	0.028
9	1.9	0.205	0.018	0.022

Table 10.1: Total activity and decay heat as a function of decay time for the tungsten target wheel and the stainless steel layers and shroud.

Target station component	**Material**	**Tritium activation** [10^{12}Bq]
Target wheel	Tungsten	613.1
Shroud #1	Stainless steel	14.6
Shroud #2	Stainless steel	14.2
Target coolant	Helium	0
Target coolant alternative	Heavy water	2.3
Moderator coolant	Water	0.6
Moderator cladding	Aluminium	0.9
Pre-moderator		2.0
Moderator		0.02
Reflector	Beryllium	1180.0
Reflector shield	Stainless steel	19.4
Total	Helium coolant	1455.6
Total alternative	Heavy water coolant	1457.9

Table 10.2: Tritium activation produced in target station components during 5000 hours of operation.

Instruments and beamlines

For the first beamline shielding calculations, a generic source term will be obtained, which will capture the specifics of the high energy component of the direction of the beamlines with regard to the incident proton beam. Subsequent calculations will be performed to investigate the shielding required at a generic beamline. For rough estimates of the shielding around neutron beam tubes, the approach outlined by Gallmeier [621] may be used.

10.2.1 Source term for waste disposal classification

Within the Swedish waste system, the complete nuclide inventory (T > 5 years) must be reported by the producer before disposal of radwaste is allowed to proceed. In compliance with this requirement, ESS has submitted a description of the nuclide inventories in the principle components of its waste to SKB, the Swedish Nuclear Fuel and Waste Management Company. This information, and other nuclide vectors that are part of an inventory database created by ESS which is under analysis within SKB, will be used for design and safety assessment and for various licensing and regulatory purposes. The preliminary estimates for activation of the quadrupoles are shown in Figure 10.2. The right hand panel shows the decay over time of total specific activity (in black) and the contributions of individual radioisotopes (in colour), following irradiation over 40 years, corresponding to the lifespan of the ESS facility. The left hand panel shows the percentage of total activity attributable to individual isotopes over time.

Figure 10.3 shows estimated total activity as a function of decay time for the proton beam window's aluminium window pane and frame, and for its steel flanges after 5000 hours of operation, corresponding to the component's expected lifetime. Additional information about the most important contributors to the total activity of the PBW module are provided in a separate technical report [622]. The total activity of the tungsten target wheel and the ^{3}H contribution to that activity are shown in Figure 10.4 as a function of the decay time after 5 years of irradiation, which is the expected lifetime of the target. Table 10.3 provides additional detail about the most important contributors to the total activity. The total activity of the beryllium reflector and the tritium contribution is also shown in Figure 10.4 as a function of the decay time after 5000 hours (one year) of operational irradiation. Table 10.4 provides additional detail about the most important contributors to total activity in the beryllium reflector material.

10.2.2 Source terms for environmental analysis

Another ESS technical report [623] describes the preliminary assessment of the potential source term for radioactive waste discharges that will occur during the routine operation of the ESS facility. These dis-

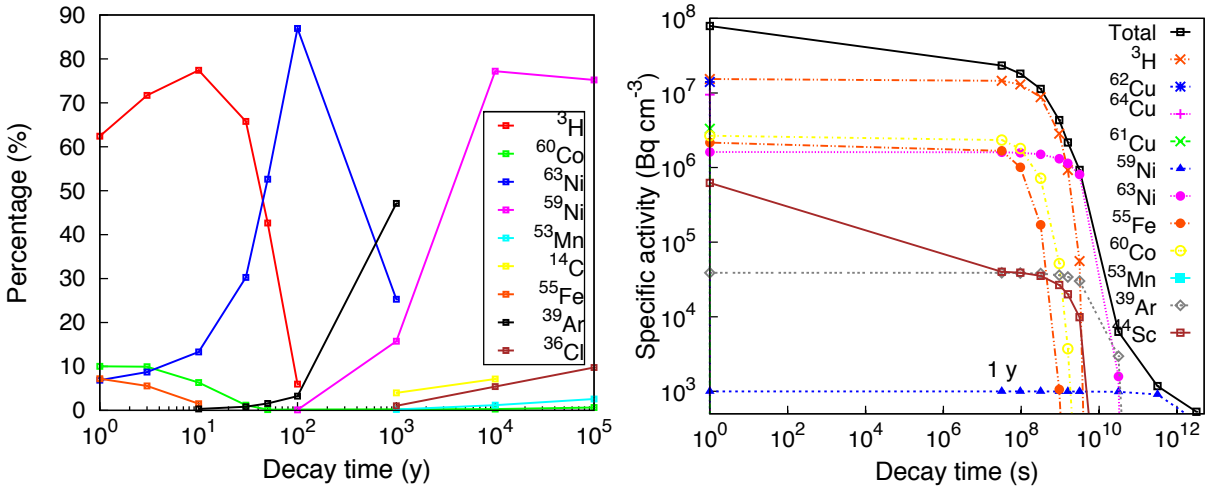

Figure 10.2: Quadrupole activation decay curves after 40 years of irradiation with a 2.5 GeV proton beam, and 1 W/m beam losses. Left: Percentage of activity due to particular radioisotopes as a function of time. Right: Specific activity due to particular radioisotopes as a function of time.

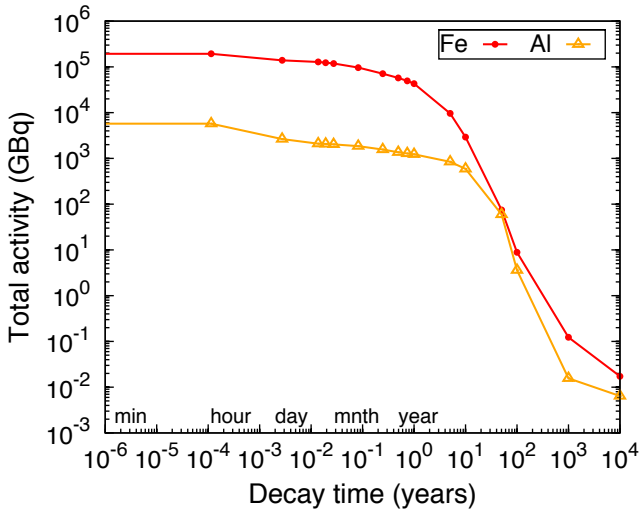

Figure 10.3: Total activity in the aluminium and steel (iron) components of the proton beam window as a function of decay time after 5000 hours of operation.

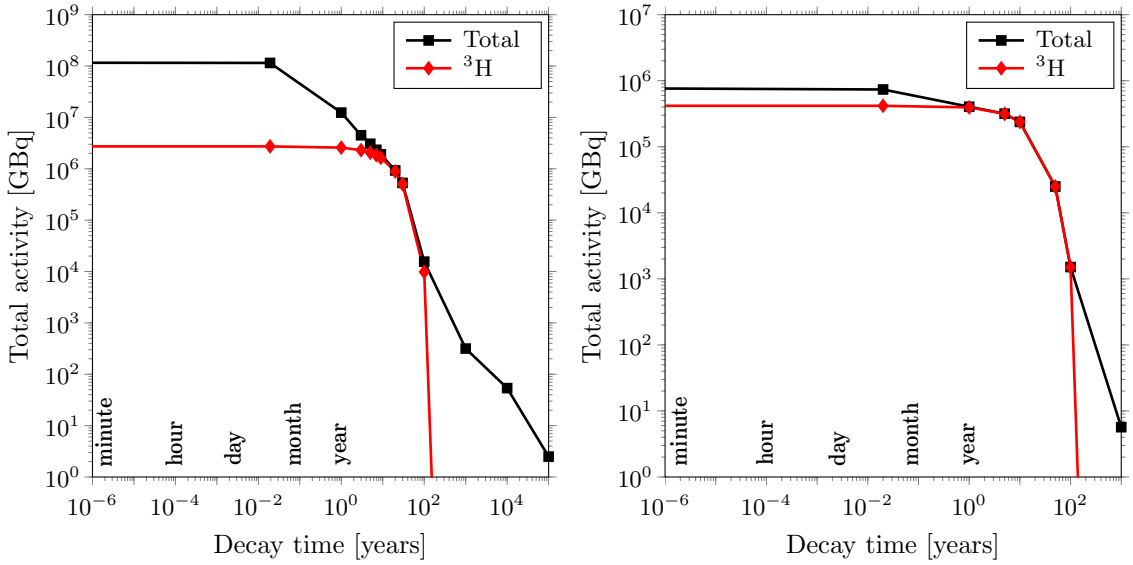

Figure 10.4: Total activation and tritium contribution decay curves after irradiation. Left: Target wheel after 5 years of irradiation. Right: Beryllium reflector after 5000 hours (one year) of operational irradiation.

charges are in the form of gaseous discharges to the atmosphere from the stack and aqueous discharges to public sewers or via contamination of the groundwater underneath the linac and its further migration into the environment. The initial identification of the main sources of discharges has been completed. Subsequently, the nuclide vector breakdown was identified analysing both sources of hazards: activation and contamination. ESS estimates of the production activity [355,618,624], together with available experimental data from previous experience were used for identification of the radionuclide vector that potentially might be discharged via the airborne and the waterborne routes. Radioactive inventories associated with the linac tunnel and surroundings as well of the majority of the target station components have already been calculated under conservative assumptions about operating conditions. The results of this earlier work represent the starting point for the environmental source term evaluation.

A complete understanding of the release and diffusion of radioisotope products depends upon many parameters and will require experimental work reproducing ESS conditions. Furthermore, the effects of the ventilation systems and filters, some of whose details are still being worked out, will have tremendous

Nuclide	**Decay time** [years]					
	6	40	10^2	10^3	10^4	10^5
^{3}H	83.4	96.4	72	0	0	0
^{14}C	0	0	0	0.3	0.6	0
^{36}Cl	0	0	0	0	0	0.7
^{39}Ar	0	0	0.1	0.7	0	0
^{59}Ni	0	0	0	0	0.2	1.3
^{79}Se	0	0	0	0.1	0.8	2.2
^{81}Kr	0	0	0	0.1	0.9	12.3
^{91}Nb	0	0.1	1.6	31.6	0	0
^{93*}Nb	0	0	0.3	12.6	14.9	0.3
^{94}Nb	0	0	0	0.2	0.8	0.7
^{97}Tc	0	0	0	0	0.2	4
^{99}Tc	0	0	0	0	0.2	2.7
^{137}La	0	0	0	1.4	8.7	57.6
^{148}Gd	0.2	0.9	11.6	0.1	0	0
^{150}Gd	0	0	0	0	0.3	5.6
^{154}Dy	0	0	0	0	0.2	4.3
^{157}Tb	0.1	0.6	9.3	7.2	0	0
^{154}Dy	0	0	0	0	0.2	4.3
^{163}Ho	0	0	0.7	29.7	53.4	0

Table 10.3: Fractional contributions (in %) of the most important nuclides to the total activity of the target wheel requiring disposal, as a function of decay time after 5 years of irradiation. Other nuclide contributors are not subject to disposal.

Nuclide	**Decay time** [years]							
	0.02	1	5	10	50	10^2	10^3	10^4
^{3}H	57	97.7	99.3	99.7	100	99.7	0	0
^{5}He	0	0	0	0	0	0	0	0
^{6}H	0	0	0	0	0	0	0	0
^{8}Li	0	0	0	0	0	0	0	0
^{9}Li	0	0	0	0	0	0	0	0
^{7}B	40	0.7	0	0	0	0	0	0
^{8}B	0	0	0	0	0	0	0	0
^{10}B	0	0	0	0	0	0.3	98	99.3
^{14}C	0	0	0	0	0	0	2	0.7
^{54}Mn	0.1	0.1	0	0	0	0	0	0
^{55}Fe	1.1	1.5	0.7	0.3	0	0	0	0
^{59}Fe	1.5	0	0	0	0	0	0	0

Table 10.4: Fractional contributions (in %) of the most important nuclides to the total activity of the beryllium reflector as a function of decay time, after 5000 hours (one year) of operational irradiation.

consequences for the source term's quantitative evaluation. In this stage of the design project, only qualitative assessment of the above processes can be done based mainly on the existing operational experience of similar facilities with appropriate scaling for ESS conditions. With the development of the design, more specific information will be available, permitting further refinement.

It is convenient to define radionuclide categories and report the results of emission monitoring as a breakdown of released activities corresponding to the given categories. Each category has either a critical or a representative radionuclide, for which the dose conversion coefficient is the greatest or the most representative one, respectively. Such impact presentation is simple and conservative. To illustrate the relative importance of the different radionuclide categories, the effective doses to the reference person have to be calculated for ESS release data using the estimated dose conversion coefficients. The selection of

radionuclide categories and representative radionuclides for this analysis is: i) ^{3}H, ii) ^{7}Be, iii) Short-lived gases (^{11}C), iv) Other beta/gamma (^{60}Co), v) Radioactive iodine (^{126}I) and vi) α-emitters (^{148}Gd).

Accuracy and validation

Computer codes and nuclear data are used to estimate radioactivity level, but their reliability must be validated. In the work carried out so far, ESS has relied on two methodologies. The first uses an updated spallation model, INCL4.6-Abla07, and the second relies on an evaluation of nuclear cross section data for p+W reactions at energies up to 3 GeV. INCL4.6 [625] and Abla07 [626] are two codes describing the two steps of spallation reactions (intra-nuclear cascade and de-excitation phase). Their combination has been widely recognised as resulting in one of the most reliable spallation models available [627]. Two types of empirical validation are needed when using these codes to study a spallation target. The first type of validation involves the use of elementary nuclide production cross sections and the second relies on nuclide production yields in a thick target. The two approaches are complementary, since the former gives a precise idea of the reliability of the model for a given observable (e.g. ^{148}Gd production from proton-tungsten interaction from tens of MeV up to a few GeV), while the latter takes into account contributions to isotope production from all types of particles with their energy spectra. In other words the first one helps to understand what has been learnt from the second one. A useful summary of the work that has been done on elementary production is provided in a paper by Leprince. [628].

Careful comparisons show that, for the most part, calculation results fit the experimental data on nuclide production versus incident proton energy within a factor of two, and sometimes approach "perfect" agreement, over the whole energy range, i.e. from a few tens of MeV up to 2.6 GeV [629, 630]. In some cases, discrepancies larger than a factor two have been identified, but almost always for low energy protons and often when the cross section production is low (around 0.01 mb). Similar empirical validation would be valuable not only for protons, but for all potential projectiles (i.e. secondary particles), but data are very scarce. This benchmark could be used to estimate uncertainties, a point which is addressed below. Validation on thick targets, implying that transport issues, slow down, and secondary particles have been taken into account is in progress. Two sets of data on residue production yields can be used within the ESS target study: data from a tungsten target irradiated with 800 MeV protons [631], and lead and bismuth samples inserted in a mercury target irradiated with 2.83 GeV protons [632]. The agreement of calculation results with the first set of empirical data is very good, with ratios that are often smaller than two, even if some cases require careful study and the help of validation on thin target materials discussed above [633]. Validation work to benchmark the model with a projectile energy close to the ESS value of 2.5 GeV, using the second data set, is planned in the near future.

Evaluation of nuclear cross section data for p+W reactions at energies up to 3 GeV

The evaluation of cross sections for proton-induced reactions for tungsten has been carried out to improve the reliability of the data used for activation calculations for the target. The work included the selection and analysis of available experimental data for tungsten using the tools from the BEKED code package of KIT [634], calculations using advanced nuclear models, and the statistical combination of measured data with results of calculations based on available and obtained covariance information about measurements and model calculations. The activation data file contains cross sections for 10,182 proton-induced reactions at primary energies from 0 to 3 GeV for the tungsten isotopes ^{180}W, ^{182}W, ^{183}W, ^{184}W, and ^{186}W. The range of residual nuclei is from $Z = 1$ to 75. A technical report is being written, although additional work is necessary in order to construct similar data bases for other projectiles (neutron, deuterium, tritium, Helium-3 and α) to take secondary particles into account. Nonetheless, the currently available database can be used to build a radionuclide inventory for ESS in the many cases where nuclide production is due mainly to protons.

Target calculations

The INCL4.6-Abla07 model, implemented in MCNPX, has been used to estimate nuclide inventory and radioactivity level in the detailed target geometry that is pictured in Figure 10.1. Irradiation history and decay were taken into account in these estimations by use of the CINDER'90 code. Some of the results of estimated activity of spallation products in the tungsten target at shut down and after nine years of decay are presented in Figure 10.5. Total activity after five years is due only to tritium and to a few nuclei whose

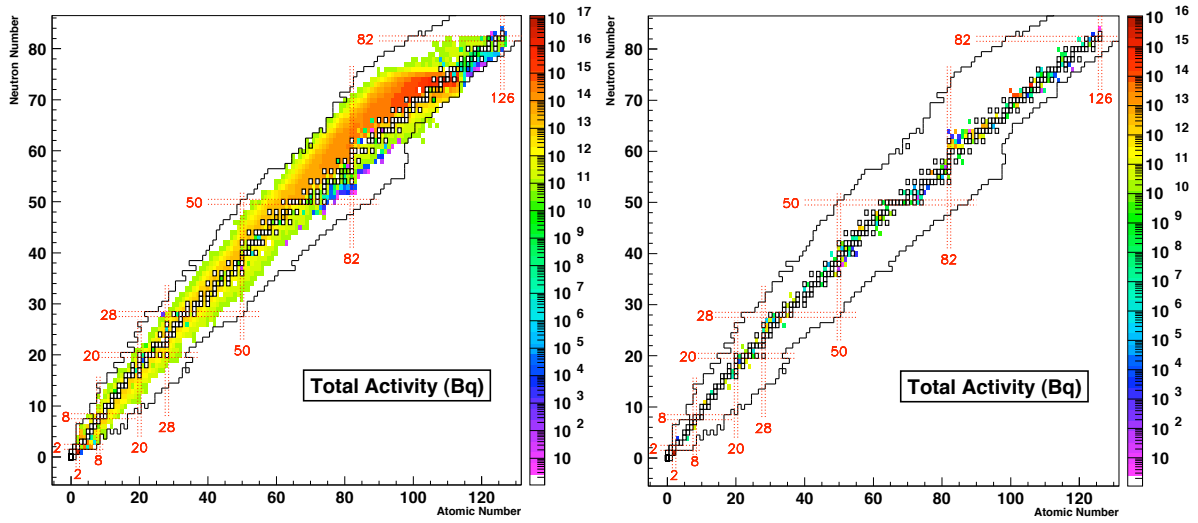

Figure 10.5: Nuclide map of total activity in the tungsten target, estimated by using the INCL4.6-Abla07 model. The colour scale is in Becquerels. Left: At final shut down. Right: After 9 years of decay.

atomic weights are close to that of tungsten. Uncertainties on residue production yields and activation can be determined nucleus by nucleus, by convoluting the proton energy spectrum that produces each isotope with the ratio between calculation and experimental data obtained from the benchmark with a thin target (elementary mechanism). This gives an estimate of the degree of uncertainty. In the absence of experimental data, either a neighbour of the isotope can be used or an imprecise but reliable estimate can be generated.

The INCL4.6-Abla07 reaction model gives good results for elementary nuclide production cross section and residual production yields on tungsten in the ESS energy range. That is, calculations obtained using the model fit experimental data within a factor of two, most of the time. Target calculations have been carried out using this model. Using experimental validation results, it is possible to assess uncertainties even where direct data is not available. A validated activation data file has been prepared for proton-induced reactions on tungsten up to 3 GeV using available experimental data and results of advanced model calculations. The data permit the calculation of the activity and nuclide inventories produced during irradiation in the tungsten target with high accuracy using any activation code. Such evaluations should be extended to other materials of interest with the objective of developing a full data library for proton and neutron-induced activation cross sections up to 3 GeV.

10.3 Waste management

Well thought-out plans for waste management are crucial for any installation producing radioactive waste. For a large and complex facility such as ESS, this planning must progress in tandem with the design of the facility. ESS has issued a preliminary waste management plan [635], which forms the basis for much of the material in this section of the technical design report. Estimation of the volumes of different types of waste was one of the main issues addressed in that plan, since possession of this information is prerequisite to planning for everything from the capacity of treatment and storage facilities to transport and disposal needs. Separate estimates were carried out for operational waste and for the waste that will be generated during decommissioning. The waste management plan identified and categorised waste streams according to the types of treatment that they will require, the end state to which that treatment will bring them, and the arrangements and facilities that will be used for their final disposal. It reported how the different elements of ESS waste will fit within the Swedish waste classification system, which is described in detail in an SKB handbook [636]. The waste management plan also laid out the design principles and good practices that ESS will use to minimise activation and the volume of radioactive waste generated, with a focus on how waste management concerns will be addressed in standard operating and maintenance procedures. It identified all feasible options for waste treatment and conditioning and waste disposal,

	Unit	High activity	Intermediate activity	Low activity
Specific power	[kW/m^3]	≥ 2		
Surface dose rate	[mSv/h]		> 2	< 2
Needs cooling?		Yes	No	No
Needs shielding?		Yes	Yes	No

Table 10.5: Radioactivity waste categorisation – activation levels.

defined the planning process and strategy that ESS will use to optimise its waste management plans, and provided the rationale for the waste management choices that have been made.

10.3.1 Waste classification

All radioactive waste will be handled and disposed of within the Swedish system for management of radioactive waste. ESS will therefore classify its wastes in accordance with Swedish practice into the following categories, each of which specifies the mode of final disposal:

1. Free release material: Material which can be freely released under Swedish law, also known as exempt waste.
2. Very low level waste: Waste which can be disposed of in landfill-type repositories on-site.
3. SFR-waste: Short-lived low- and intermediate level waste which can be disposed of in the Swedish final repository for such waste, known as SFR, operated by SKB in Forsmark, Sweden.
4. SFL-waste: Long-lived low-and intermediate level waste which in future can be disposed of in the Swedish facility for long-lived waste, known as SFL, that will be built by SKB.
5. SFK-waste. Heat-generating waste, a category which includes spent nuclear fuel.

This system is similar to the IAEA Classification of Radioactive Waste [637], but has been adapted to the existing or planned waste disposal facilities in Sweden. In the Swedish system, all waste that is transported to final disposal must be accompanied by a description that includes its waste categorisation. These descriptions form a basis for the regulatory authority to grant permission for the disposal of the waste package in the disposal facility, and they provide a record for posterity of the contents of the disposal facility. The basic criteria used to determine whether radioactive waste activation is *high, intermediate* or *low* are summarised in Table 10.5. In addition, waste is classified as *short-lived* if the dominant content of radionuclides have a half-life of less than 31 years, and as *long-lived* if it has a significant content of radionuclides with a half-life of more than 31 years.

Clearance

Recently, the clearance concept has been implemented in the Swedish regulatory system for radioactive waste [619]. Materials or objects conforming with specified criteria for clearance are released from further control by the regulatory body. The clearance index (CI) for a material containing a mixture of radionuclides is calculated by means of Equation 10.1, where A_i is the specific activity due to the component nuclide i, L_i is the clearance level for the nuclide i, and activities and clearance levels are measured in units of Bq/g.

$$CI = \sum_{i}^{N_{nuclides}} \frac{A_i}{L_i} \tag{10.1}$$

For ESS purposes, the clearance index was used to categorise components of the waste stream for each decay period as follows:

1. Any material for which the CI was less than or equal to one was classified as exempt waste, suitable for free release.

2. Materials for which the CI for the material as a whole was greater than one, but the CI for its constituent nuclides with half lives greater than 30 years was less than one were classified as short-lived, low and intermediate level wastes.
3. Materials for which the CI for nuclides with half lives greater than 30 years was greater than one were classified as long-lived low and intermediate level waste.
4. Materials with specific decay heat greater than 2 kW/m^3 and activation levels above 104 TBq/m^3 would be classified as heat-generating waste. ESS will produce no waste in this category.

This methodology was used to assemble an ESS clearance levels library. A post-processing code was created to read this database and to calculate the CI for each material at each decay time. In addition, waste categorisation was facilitated by sorting the clearance indexes according to the half lives (greater or less than 30 years) of the constituent nuclides in the material. This approach has been used to determine the waste classifications of the highly activated components of the target station [622]. Waste classification for other components of the facility is on-going.

10.3.2 Rate of waste generation

The amounts of waste of each type that will be generated have been estimated for the baseline design of the facility, and for the operation and maintenance protocols that are still undergoing optimisation. Thus the estimates reported here are subject to evolution and update in the future. Waste classification is based on Monte Carlo calculations for highly activated components and on experience at similar facilities. Further details about the evaluation of wastes generated during operation and decommissioning are given in a technical report [635].

During its 40-year operational life, ESS is expected to generate a total of 14,669 tonnes of waste, of which 10,230 tonnes will be sent for off-site disposal, while the remaining 4,439 tonnes will be suitable for free release. The bulk of this operational waste will be solid waste (estimated at 9,825 tonnes), made up mainly of metal, including a large fraction of ferrous metals. Over three quarters of the solid waste (77%) derives from the replacement of the instruments every 10 years. Less than 6% of the solid waste (554 tonnes) is classified as long-lived waste. The overwhelming majority of the operational waste stream will be suitable for disposal in the final repository for short-lived low and intermediate level waste in Forsmark. Some metallic waste (39 tonnes) will be suitable for free release and on-site disposal after decontamination of pipes and equipment used in the target station. Disposal solutions for 13 tonnes of beryllium waste are under analysis, with the potential for disposal in the SFL facility that SKB plans to build as a final repository for long-lived waste. In addition to the metal wastes, operational waste is estimated to include 8 kg of sealed sources used for calibration of the instruments, 192 tonnes of oil (including 179 tonnes of silicon oil from the klystrons), 200 tonnes of ion exchangers, approximately 39 m^3 of combustible waste, and 4,400 tonnes of plastic waste from the replacement of the detector shielding every 10 years. The plastic waste will be suitable for free release on-site, perhaps after a short period of storage to allow for radioactive decay.

Decommissioning will generate an estimated total of 50,572 tonnes of waste, of which 71% (35,956 tonnes) will be suitable for free release on site. The great majority (31,156 tonnes) will be very low level waste concrete from dismantled shielding, plus 800 tonnes of very low level waste from dismantling the target, all suitable for free release on site, perhaps after some period of storage. Another 3,500 tonnes of concrete waste will originate from the internal side of the accelerator tunnel wall. Additional concrete waste from the accelerator itself and the parts of the monolith shielding closest to the target (962 tonnes) will be long-lived waste. Decommissioning will also generate an estimated 10,154 tonnes of metal waste, mainly ferrous metals from the target monolith and the components of the linac, all of which are likely to be short-lived wastes suitable for the SFR facility. Finally, 4,000 tonnes of soil from the area surrounding the concrete wall of the linac will be suitable for free release on site after storage for decay where necessary.

10.3.3 Management of radioactivity on-site

Several aspects of the management of radioactivity on site are analysed in the ESS waste management plan, including assignment of responsibilities, waste collection and segregation systems, the waste characterisation system, traceability of waste, waste storage options, treatment and conditioning and packaging, and a flow chart of waste streams and timing. The most important items are briefly described below.

Waste characterisation system

ESS will rely on three complementary methods for waste characterisation: Monte Carlo calculations, the matrix method, and on-site radiation detection and measurement. An important limitation of direct Monte Carlo calculations is the fact that all input parameters (material composition and radiological history) must be known before launching the simulations. Experimental validation of the calculations is desirable because of the uncertainties associated with nuclear models and simplifications in the geometry of modelled components. The matrix method is based on the calculation of nuclide production yields for selected target materials and particle spectra, which are representative of materials at ESS. The calculations require tabulated cross sections for all particles, energies and reactions of interest. To determine clearance indexes, this method can be used to define constraints on the activity of gamma emitters in such a way that when these constraints are met, the activity of hard-to-measure nuclides is automatically below the clearance levels. The activity of gamma emitters can then be evaluated by means of dose rate measurements. ESS has started to evaluate the nuclide production cross sections for proton-induced reactions of hazardous nuclides [638] and intends to continue this work with the creation of a database of evaluated neutron yields as a basis for developing a book-keeping record based on the matrix method.

Radiation detection and measurement at ESS will be based on a gamma measurement station to quantify the activity distribution of gamma emitters. The station will include a counting chamber with scintillation detectors and one or more germanium detectors. In addition to its use in distinguishing between materials that can be handled in a normal workshop and those requiring a special workshop for handling radioactive materials, this station will be used for determining clearance indexes, and deciding which materials are suitable for free release. For massive waste (whose weight is greater than 1 tonne), the phenomenon of self-absorption is particularly important. Exclusive reliance on gamma-spectroscopy measurement of the whole object would introduce large errors in the characterisation because of the unknown distribution of activity. In these cases, sample measurements will be coupled with Monte Carlo calculations. Additionally, the station will be used for the detection and measurement of surface contamination.

Traceability

An important element of waste management is ensuring the traceability of waste during the multi-step process that begins with the dismantling of a component and ends with its final disposal. ESS's book-keeping system for waste-handling and disposal will require documentation of the quantity of each component of waste, its radioactivity and composition, which in turn implies that theoretical and experimental methods for the determination of the radionuclide inventory will be developed, as discussed above. The ESS database will be harmonised with the Studsvik waste management system, referred to by its Swedish acronym as SVALA, which deals with waste treatment and conditioning and with on and off-site transportation issues, and also with the new SKB database dealing with final disposal information which is currently under development.

Waste storage options

At the time of writing, waste storage options in ESS's active cells are being analysed in term of space requirements over time. (Technical details about the active cells may be found in Section 3.5.) Through the analysis of specific decay heat and activity levels [622] it has been determined that the target wheel will be suitable for classification as intermediate level waste following five years of decay time in storage. All other components will meet the requirements for the intermediate level waste classification upon shut-down, and will require only about one year of storage. Additional details about active cell storage capacity requirements and data relevant for waste stream planning are provided in the preliminary waste management plan. ESS is also considering the possibility of developing an interim storage facility that would house some waste during the facility's entire lifetime. This facility would comply with the demands of Swedish law and IAEA guidelines [639]. The preliminary waste management plan contains more information about the requirements that such a facility must meet and the outlines of the proposed approach.

Treatment, conditioning and packaging

The preliminary waste management plan also outlines potential methods for treating and conditioning a number of components of the ESS waste stream, including spent ion exchange resins and tritiated water.

It also discusses packaging options and requirements for storage and transport. These packaged wastes will be shipped for disposal at the SFR final repository. The assessment in the waste management plan is based upon reference handling sequences, but potential variants are also being evaluated. Final details will be agreed upon in consultation with SKB subject to approval by SSM.

10.3.4 Transportation of radioactive waste off-site

Transport of radwaste from ESS to Studsvik and SKB facilities will comply with ADR regulation and existing practice in Sweden. Important transportation issues are summarised below, and further details are available in a technical report focusing on these issues [640].

Low level waste in IP-2 containers

The concept for the transport of low radiation level waste to Studsvik assumes a fleet of ISO IP-2 containers operating between the facilities with an estimated turnaround period of 10 to 15 weeks. The containers will be filled with variable numbers of boxes of various sizes loaded with scrap and waste. For waste with surface dose rates above the acceptable level, the packed boxes will have a lining about 30 mm thick. After the waste has been removed, the boxes, inserts and containers will be cleaned and transported back to ESS following protocols for radioactive transport (ADR Class 7).

Intermediate level waste in special packaging

Waste with higher radiation levels will require more specialised transport containers (type B) in order to assure low enough surface dose rates and meet other ADR requirements. For special wastes such as the target, moderator-reflector plug and the proton beam window plug, preliminary assessments of surface dose rates greater than or equal to 2 mSv/h and A2 values (that is, activity values obtained in accordance with IAEA methodologies for so-called “normal” radioactive materials) indicate that type B containers may be needed for shipping. For example, the estimated A2 value for the transport of the tungsten target after 5 years of operation followed by 5 years of cooling is about 8 TBq. Comparing this value with the total activity of the target (under the same conditions) of about 3000 TBq shows clearly that target should be transported via a type B container [641].

Shielding calculations for the design of containers

Calculations for the optimisation of shipping container shielding for the highly activated components of the target station are summarised below. Details are available in a separate technical report [642].

Two types of geometry models were used for Monte Carlos simulations of the container loaded with the ESS target. In the first model, it was assumed that the target was not dismantled before it was placed in its shipping container, while in the second model, it was assumed that the target was dismantled and packed in a cylindrical container with a radius of 30 cm and a height of 65 cm. Gamma spectra calculated as a function of decay time were used as the source term for shielding calculations, as illustrated in Figure 10.6, which focuses on the external layer of the target wheel. Table 10.6 shows activity of the high gamma energy nuclides within the tungsten target. The optimisation criteria respected ESS’s dose limits of 2 mSv/h at contact and 0.1 mSv/h at 1 meter from the outer surface of the container. The calculations showed very similar results for the model with the intact target wheel loaded in a shipping cask and the model with the dismantled target inserted in a cylindrical drum, as can be seen in the two maps of photon dose rates in Figure 10.7. However, the mass of the cask holding the dismantled target is substantially lower.

This analysis demonstrates that dismantling the target prior to shipment has several advantages. The cost of the shipping container would be substantially lower, and it could be designed for use with other activated components as well. Furthermore, the licensing process would be facilitated by avoiding a customised container to accommodate the odd shape of the wheel. Radioactive transport on Swedish roads generally requires a permit, but probably not for every single occasion. On the other hand, there are costs and risks associated with dismantling the wheel within the active cells. A final decision will weigh these costs and risks against the advantages of the smaller cylindrical container.

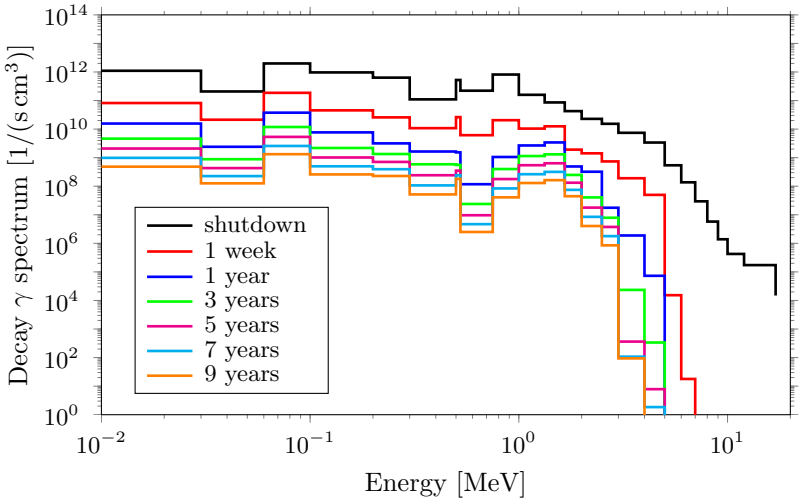

Figure 10.6: Gamma-radiation spectra in the external layer of the tungsten target wheel, after various decay times.

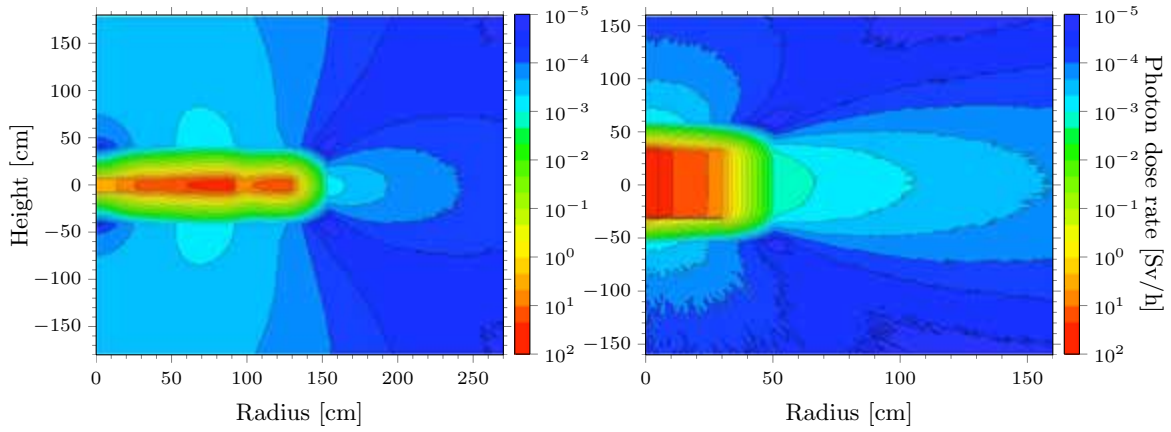

Figure 10.7: Photon dose rate maps [Sv/h] for the iron cask loaded with an activated target wheel, 5 years after final shut-down. Left: Intact target wheel (side = 20 cm, end = 27 cm). Right: Dismantled wheel (side = 20 cm, end = 26 cm).

Nuclide	**Activity at shut-down** [10^{12}Bq]	**Activity after 5 years** [10^{12}Bq]
^{22}Na	0.5	0.1
^{54}Mn	4.0	0.1
^{60}Co	6.6	3.4
^{154}Eu	6.6	3.4
^{172}Lu	847.0	115.0
^{173}Lu	1150.0	92.1
^{182}Ta	994.0	0.02

Table 10.6: Gamma-ray activity within the target at shut-down and after 5 years of cooling.

10.3.5 Waste treatment and conditioning options

The Swedish system for the disposal of short-lived low and intermediate level waste in the SFR facility specifies several acceptable options for the pre-disposal treatment and conditioning of the waste. These are:

1. Cement solidification, in which ion-exchange resins or sludge are mixed with concrete in drums or moulds.
2. Cement stabilisation, in which scrap metal and refuse are placed in molds and cement is poured over the waste.
3. Cement stabilisation (alternate methodology), in which the waste is placed in 100 litre drums, which are then put inside 200 litre drums. Concrete is then poured in-between the drums.
4. Bitumen stabilisation, in which ion-exchange resins are dried and mixed with bitumen, and then poured into molds or drums.
5. De-watering, in which wet ion-exchange resin is pumped into a concrete tank and water is removed by suction.

The preliminary waste management plan summarises treatment and conditioning methods for the waste together with information about the waste containers that will be used. In those cases in which it is proposed to store radioactive waste or to defer decommissioning for an extended period of time, ESS will give due consideration to the principle stated by the IAEA that, "decisions on radioactive waste management made at one step may foreclose alternatives for, or otherwise affect, a subsequent step" [643]. Swedish law requires that ESS specify the "best available technique" for the management of each type of waste. ESS has developed a best available technique statement [644] to optimise waste management for tritium production and release. Similar statements will be developed to define optimum waste management techniques for other components of the waste stream. However, it is premature to make such commitments for those waste packages destined for ultimate disposal in an SFL facility since the waste assessment criteria for that facility have not yet been completely specified. Determining the best available technique for handling the beryllium waste from the reflectors deserves particular caution.

10.3.6 Requirements for final repository capacity

The Swedish regulatory authorities require the producer of radwaste to provide a complete nuclide inventory ($T > 5$ years) before disposal is permitted. ESS has already submitted a database containing the nuclide inventories of the most important components of its waste stream to SKB, and has used this database to develop a rough estimate of the final repository capacity that will be required for waste disposal. This estimate is based on a conversion factor specifying one cubic meter of capacity for every tonne of raw waste destined for either the SFR or SFL final repository. The results are listed in Table 10.7. The capacities of the SFR and SFL repositories are 200,000 m^3 and 10,000 m^3, respectively. Thus, ESS waste will require only 12% of the total SFR capacity and only 15% of the total SFL capacity. The assumption that beryllium waste will go to the SFL repository is reasonable, given that beryllium waste from the Studsvik reactor will go there. ESS continues to work collaboratively with SKB to identify indicator

Source of waste	**Short-lived waste (SFR)** [m^3]	**Long-lived waste (SFL)** [m^3]	**Long-lived waste (SFL) or other** [m^3]
Target station and accelerator-to-target		554	13
Operational waste	9,663		
Decommissioning	13,654	962	
Total	23,317	1,516	13

Table 10.7: Capacity requirements for the final waste repositories.

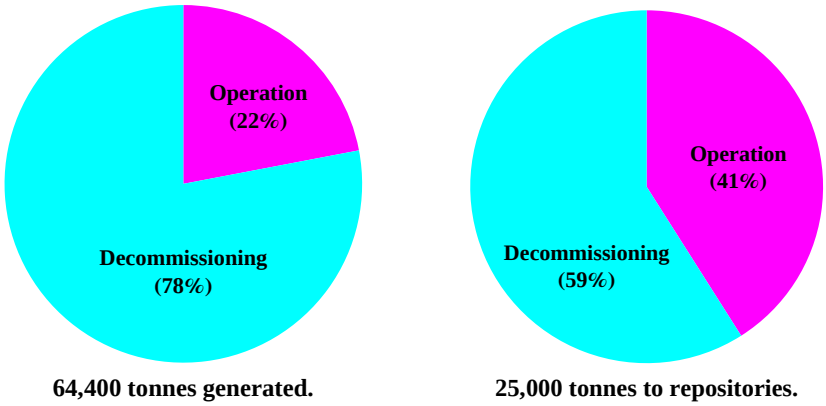

Figure 10.8: Operational and decommissioning components of waste. Left: All waste generated. Right: Waste destined for a radioactive waste repository.

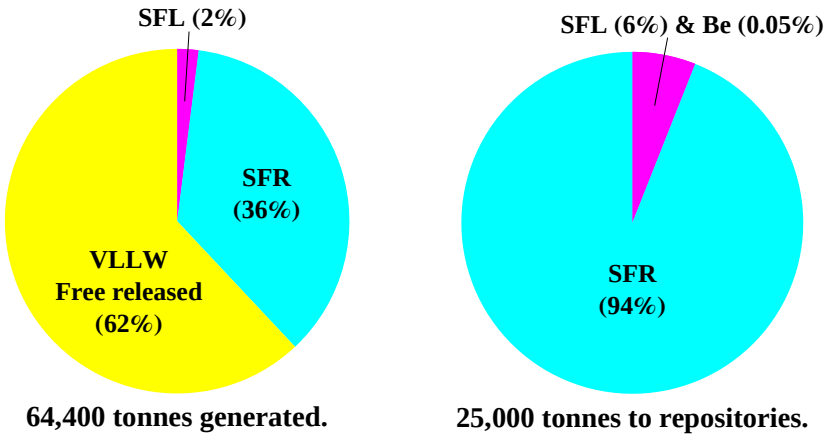

Figure 10.9: Final disposition of waste. Left: All waste generated. Right: Waste destined for a radioactive waste repository.

nuclides in order to include ESS waste in the design and safety assessment of the SFL, and to facilitate complementary licensing for the SFR, should this prove necessary.

The charts in Figure 10.8 show the proportions of ESS waste that will be generated during operations and decommissioning. More than three quarters of the total waste (78%) will derive from the decommissioning of the facility, as will well over half (59%) of the waste requiring disposal in a final repository. The left panel of Figure 10.9 shows the division of ESS radwaste among three modes of ultimate disposal (free release, SFR and SFL), while the right panel deals only with waste that will require disposal in a final repository. Well over half (62%) of the total waste will be suitable for free release, and the overwhelming majority (94%) of the waste requiring disposal will be suitable for the SFR repository.

10.4 Operational waste and emissions

This section provides preliminary estimates of the radioactive waste generated in the fluid systems of the ESS facility. First, it analyses the processes responsible for contamination of the fluid coolants described in Chapter 3 and presents estimates of the production rates of the contaminated by-products of the purification systems. Information about the waste stream arising from the purification and ventilation systems is necessary to develop a waste management plan and to develop working procedures during maintenance activities. Next, the estimated source term for atmospheric releases during routine operation is presented. Two distinct release operations are analysed: on-line emissions and emissions resulting from processing. The derived source term (that is, the breakdown of radionuclides and activity) scales well with

that defined for routine operation of the ISIS facility. The outcome is the input data for the environmental impact analysis of normal ESS operation. Finally, a parametric study analysing the performance of the helium cooling circuit purification system is briefly described. The final amount of tritiated water and its specific activity were derived as a trade-off between the amount of hydrogen added to the coolant and the purification flow rate. The analysed systems perform well – safe management of radionuclides is readily achievable.

10.4.1 Radioactive waste in fluid cooling systems – preliminary estimates

Contamination of the fluid coolants

Two types of fluid coolants are used in ESS systems: helium, which is used in the target assembly; proton beam window; and internal shielding, and water, which is used in the linac machine including collimators; premoderator and moderators; reflectors; and outside shielding. Radionuclide production inside fluid cooling systems has two sources: activation during operation; and contamination as a result of corrosion, erosion, and/or diffusion of radionuclides from activated surroundings. Activation of fluid coolant is easily calculated by means of computer codes, as discussed in Section 10.2 [355, 620], but it is difficult to quantify the contamination of the coolants resulting from the various processes. Despite this, preliminary estimates are required for development of the design of the coolant systems, in particular identification of the purification systems; derivation of the associated waste to be handled during operation; and establishment of working procedures for use during maintenance. The distribution of the radionuclides within the coolants has been predicted based on data from the literature and on the previous experiences of other facilities, scaled to reflect operating conditions.

The rate of loss of activity due to corrosion is proportional to the fractional rate of loss of mass from a given component. Corrosion is not uniform, but overall loss of thickness on the order of 5 μm/y is a reasonable assumption considering the values used in the SNS design (2.5 μm/y with stainless steel) [647]. A conservative estimate for ESS was derived by assuming an average distance to the nearest cooling channel of 20 cm, corresponding to a fractional rate of loss of activity from monolith steel of 10^{-10} to 10^{-8} per year. The diffusion and chemical removal process in the tungsten target is described in a 2002 report, which concludes that that tritium, all halogens, and noble gases must be assumed to have significant diffusion rates [646]. The calculated half-lives for different elements within the target are given in Table 10.8.

Group	**Element**	**Diffusion**		**Emission**	
		Half-life	**Unit**	**Half-life**	**Unit**
	H	2	h	rapid	
Halogens		2	h	rapid	
Noble gases		100	d	20	h
Dust formation		**(1000)**	y	–	
IVa	C	5×10^{9}	y	3×10^{11}	y
Transuranic metals	Fe	7×10^{10}	y	–	
Alkali metals	K	3×10^{11}	y	4×10^{13}	y
Lanthanides	Y	5×10^{11}	y	–	
Chalcogens	S	5×10^{14}	y	4×10^{21}	y
Pnictogens	P	3×10^{22}	y	1×10^{42}	y
Refractory metals	Hf	9×10^{26}	y	–	
Alkaline metals	Ba	6×10^{29}	y	–	

Table 10.8: The diffusion half-life of representative elements within the tungsten target and the emission half-life of volatile elements in the dust. The elements included have the highest diffusion rates for their respective group. Hydrogen diffusion is not well understood [645] – the value given here represents the highest possible diffusion rate given the available data. Data for halogen diffusion in tungsten are absent from the literature and no evidence suggests halogen retention. Therefore halogen diffusion is conservatively given a value equal to that of hydrogen. Noble gas diffusion is similarly uncertain. The diffusion rate given here is an estimate based upon arguments presented by Jensen [646].

Also appearing in Table 10.8 is an entry for dust formation half-life. Clearly, dust formation is the dominant release process for all elements except hydrogen, halogens, and noble gases. For other activated structural materials (stainless steel and aluminium), the diffusion rates of all elements are negligible due to low operating temperatures. In these materials, the dominant release process is corrosion. The target diffusion numbers were generated assuming 550°C uniform temperature within the blocks and active chemical removal at the target surface. The emission numbers were generated assuming diffusion from a 10 μm dust particle at 200°C, and only elements with active chemical removal in a reducing helium atmosphere are listed in this column. The tungsten target is prone to ablation and dust formation. An ablation rate of 10 μm/y of all surfaces is a reasonable upper limit for target deterioration [648,649]. This amounts to 0.07% of the target mass becoming dust per year, or roughly 3 kg/y to 4 kg/y. The operating assumption is that 1% to 5% of this dust potentially may coat the interior surfaces of the target-cooling loop, while the remainder will be removed via cyclonic filtration. One concern is the propensity of the dust to emit volatile radionuclides. The emission half-times for the elements are given in Table 10.8. Given the values, the nuclides that have been identified as mobile due to diffusion from the target are also rapidly liberated from the dust. Other elements remain in the dust for very long periods of time.

Radioactive waste purification systems

The main isotopes present in the coolants arising from activation as well as from potential contamination are described in a 2011 technical report [623], while purification items used within the coolant systems are described in another report [650]. Ion exchangers employed in all water cooling loops, accepting 1% to 5% of the flow, remove all corrosion products and all radionuclides other than tritium at a rate equivalent to the corrosion rate. Scaling values from nuclear industry standards, a volume of 0.8 m^3/y is anticipated. A rough estimate of the activity present in the ion exchangers, for 10^{16} Bq/y activation in the monolith steel with a corrosion rate of 10^{-8}/y, gives roughly 10 GBq of total activity in the ion exchangers. Cyclonic filters in the helium cooling streams are expected to be almost 100% effective at removing ablation dust due to the large grain size of the target [648]. Table 10.9 shows the radionuclide inventory of the collected dust, per gram, for the five highest-activity nuclides after one year of operation. Because of the relatively large grain size of the dust (typically greater than 1 micron), cyclonic filtration with efficiencies greater than 99.9% will limit potential releases from this process to under 10 MBq, assuming that no more than 0.01% of the dust becomes airborne during processing.

High efficiency particulate air (HEPA) and activated charcoal filters that are used in the linac tunnel ventilation system, in the active cell ventilation, and in other ventilation outlets are assumed to be greater than 99.9% efficient in removing airborne solid particles [651]. The performance of the tritium scavenging system, which is based on copper oxide, cold traps and molecular sieves, is analysed in detail in a technical report [645], and is summarised in Section 10.4.3. The scavenging system removes tritium from the helium cooling loops by converting it to hydrogen tritium oxide, and also effectively removes other volatile radionuclides from the helium stream. The waste streams arising from the purification and ventilation systems are summarised in Table 10.10. Quantitative prediction of the amounts and associated activation of the derived waste depicted in this table is the subject of further analysis.

Nuclide	**Activity per unit mass** [10^6Bq/g]
^{185}W	500
^{181}W	400
^{179}Ta	30
^{173}Lu	20
^{172}Hf	7

Table 10.9: Radionuclide activity per gram of collected target dust for the top five nuclides, sorted by activity. Three to four kg of dust is expected to be collected each year.

Source systems	Waste type	Main nuclide(s)	Activity accum. rate [Bq/y]	Matter accum. rate	Unit
Cyclonic filter	Dust	Spallation mixture	$< 10^{13}$	4	[kg/y]
Water cooling	Ion exchangers	Corrosion products ^{7}Be, ^{56,57,58,60}Co, ^{55}Fe, ^{52}Mn, ^{67}Cu	$< 10^{13}$	~ 1	[m^3/y]
Ventilation	HEPA filters	^{7}Be, spallation dust etc.	$< 10^{11}$	~ 4	[m^3/y]
Helium circuit	Molecular sieves	Xe-127, I-125 etc	$< 10^{14}$	< 100	[kg/y]
	CuO (no regeneration)	^{3}H	tbd	2000	[kg/y]
	Hydrogen tritium oxide	^{3}H	5×10^{14}	500	[l/y]

Table 10.10: Activity and matter accumulation rates from operational waste streams in the purification and ventilation systems.

10.4.2 Source term for atmospheric releases

The source term for atmospheric releases can be separated into two distinct release pathways: operational emissions from tunnel ventilation, and process emissions from handling tritiated water and dismantling targets. Based upon dose estimates, only nuclides that are emitted at a rate of 25 MBq/y are listed. The justification for setting the cutoff at this level of activity is that the most radiotoxic nuclide in the facility is ^{148}Gd, and a release of 25 MBq/y of ^{148}Gd would give a dose of 10 μSv to the nearest neighbour. All other isotopes have significantly lower dose factors for all pathways and the highest dose due to 25 MBq/y release is from ^{125}I, at 0.2 μSv, as discussed in Section 10.5.

Emissions from linac tunnel ventilation

Linac tunnel ventilation is the only possible source of immediate, continuous activity release. The design of the ventilation system, and its performance in mitigating radioactive releases, has not yet been optimised. For estimation purposes, it is assumed that air from the tunnel will be continuously vented to release moisture and heat. Assuming this to be the case, the released isotopes and their quantities are reported in Table 10.11, applying the additional assumptions of either a one-day air turnover period, or a two-day turnover period when the beam is on. The HEPA filter in the ventilation stream efficiently captures 99.9% of the ^{7}Be. Clearly, emissions can be controlled significantly by throttling the ventilation back. If radiation protection issues were the only concern, tunnel air could circulate in a sealed system, only ventilating after the beam has been off for at least an hour, since the tunnel is inaccessible due to prompt radiation when the beam is on. Under this option, the source term for airborne release is greatly reduced due to the decay of the short-lived β-emitters.

Nuclide	Chemical form	Source term (one-day turnover period) [Bq/y]	Source term (two-day turnover period) [Bq/y]
^{3}H	Water vapour	8.8×10^{6}	8.8×10^{6}
^{7}Be	BeO_2 aerosol	1.0×10^{7}	1.0×10^{7}
^{11}C	CO & CO_2 gas	2.6×10^{12}	1.3×10^{12}
^{13}N	NO_2 gas	2.7×10^{12}	1.3×10^{12}
^{15}O	Oxygen gas	1.5×10^{12}	7.5×10^{11}
^{41}Ar	Argon gas	4.1×10^{10}	2.0×10^{10}

Table 10.11: Source term for atmospheric release from tunnel ventilation during online operations. Air from the tunnel will be continuously vented to release moisture and heat when needed, with a one-day or a two-day turnover period.

Nuclide	Chemical form	Activity [Bq]	Release fraction	Source term [Bq/y]
^{3}H	Water vapour	5×10^{14}	0.01	5×10^{12}
^{125}I	HI, HIO_3	10^{8}	0.01	10^{6}

Table 10.12: Source term for atmospheric release coming from on-site cementation of tritiated contaminated water. The release for ^{125}I is included for reference, despite a very low release rate.

Emissions from processing tritiated water

Table 10.12 records the contribution to atmospheric releases that comes from processing tritiated water, which comes from activated cooling water systems. The release of tritium assumes on-site cementation of tritiated water with more than 99% efficiency [652]. Tritiated water processing must be assumed to release ^{125}I (1% evaporation loss) and all long-lived noble gases. The quantification of these releases is described in a 2012 technical report [646]. Noble gases, however, can be selectively distilled and captured, making their release negligible. Tritiated water processing is assumed to take place once yearly after at least 1200 days of decay-time. At processing time there will be roughly 3×10^9 Bq of ^{85}Kr and ^{42}Ar distilled from the molecular sieves. These may be included in the source term for release if no effort is made to retain them. However, the doses due to these releases are small. Neither of these noble gases emit significant gamma radiation, and therefore they do not contribute to the external plume dose. ^{42}Ar has radioactive progeny, ^{42}K, but a release rate of 3×10^9 Bq/y of ^{42}Ar when considering the plume passage rate of 3 m/s to a distance of 330 m, corresponds to a yearly release of 5 MBq of ^{42}K. This is small compared to the 25 MBq/y limit discussed above. Note that ^{42}K in secular equilibrium with the stored ^{42}Ar will not be released during cementation.

Emissions from target dismantlement

Finally, hot cell operations that cut the target shaft will necessarily generate small releases of activated steel as aerosols, along with small amounts of aggregated and activated tungsten dust, as recorded in Table 10.13. The amounts of airborne particulates are estimated using the following conservative assumptions: 0.1% of the stainless steel in the shaft is cut, and 0.1% of the cut material has a size distribution allowing transport as suspended particles. These particles will pass through 99.9%-efficient HEPA filtration, therefore a release factor of 10^{-9} on the shroud is possible, though unlikely. The total radioactive inventory of the shaft after one year of decay time is 1.3×10^{15} Bq. Therefore, releases from this source are on the order of 1 MBq every five years. This low-level of release is negligible. Similarly, 1% of all tungsten dust that has been formed due to ablation (accounting for 0.07% of the total target per year) is assumed to be present in the dismantled region and taken into the ventilation system. This is also filtered with at least 99.9% efficiency, so a release fraction of 4×10^{-8} is assumed for the spallation products. Target processing takes place once every five years after one year of decay-time. If the decision is taken to dismantle the target, the tritium release may be as much as one part in a thousand of the total inventory, under a worst-case-scenario. Such a release is unlikely because the target bricks themselves should remain intact during the procedure.

Nuclide	Chemical form	Activity [Bq]	Release fraction	Source term [Bq/5y]
^{3}H	Gas	0.5×10^{15}	10^{-3}	5×10^{11}
^{148}Gd	Dust or aerosol	8×10^{11}	4×10^{-8}	3×10^{4}
^{179}Ta	Dust or aerosol	8×10^{15}	4×10^{-8}	3×10^{7}
^{181}W	Dust or aerosol	10×10^{15}	4×10^{-8}	5×10^{7}

Table 10.13: Source term for atmospheric release from target dismantlement, in units of Becquerels every 5 years. The release for ^{148}Gd is included for reference, despite a very low release rate.

10.4.3 Tritium control

Tables 10.11 and 10.12 show that tritium is a major contributor to release and to the radionuclide inventory. The main finding of the 2012 report [645] devoted to the theoretical analysis of the performance of the helium purification system is that tritium control can be achieved by copper oxide conversion to hydrogen tritium oxide, and subsequent capture on cold traps and molecular sieves. However, ordinary cold traps exhibit low efficiency, and are preferably combined with absorbers or getters [653]. Without this system, the tritium level in the cooling gas would approach 500 TBq per year, a level that would pose a hazard in cases of helium leaks. The total 500 TBq of tritium must not be released into the environment. This was demonstrated in a 2012 analysis of the intake of tritiated water [654,655], which showed that environmental release would result in a dose to a reference person living just outside the site fence that would exceed the ESS limit of 50 μSv/y.

The proposed system operates with an assumed 100 ppm (by pressure) hydrogen addition to the helium. This H_2 scavenges tritium from surfaces by exchange reactions forming HT [645]. A 3 g/s purification-loop flow transports the HT (in addition to the added H_2) to heated copper oxide where it is converted to water. This water is then frozen out of circulation in a -20°C cold trap. Additional helium drying is achieved by passage through cold molecular sieves. One major advantage of the system is that the cold molecular sieves also capture other radioactive impurities, namely noble gases and halogens. Operating as stated, the system will generate roughly 100 kg of tritiated water per year with an activity approaching 600 TBq, (6 GBq/ml). The steady state tritium activity in the helium will be under 200 Gbq. This process consumes copper oxide at a rate of 2 tons per year, and uses less than 100 kg of molecular sieves, both of which may be regenerated on-site if necessary. These conditions result in a balance between operational safety and the volume of radioactive waste generated. Depending on the eventual needs of the facility, operating conditions may be altered.

It should be underlined again that the release rate of tritium from the target is not known, and that the worst case was assumed for the investigation. This conservative hypothesis will stay in place until relevant experimental data becomes available, as discussed in Section 10.2.

Conclusions

All of the fluid systems, except the linac and hot cell ventilation, are closed systems, and no online operational emissions will occur from them. Diffusion and ablation of the tungsten target do not represent sources for online operational releases, and the mobile activity introduced by these processes can be managed easily. The amount of additional waste that is generated by such management is reasonably scaled to the facility. It is clear that safe radionuclide management is easily achievable, and that the feasibility of ESS as a whole is not compromised by the production of radioactivity on site.

10.5 Environmental impact analyses

10.5.1 Dose calculations and methodologies

Estimates of the magnitude of operational routine releases of radionuclides from the ESS facility are needed to ensure that the public is not exposed to radiation in excess of dose limits ESS has set for itself. In the work carried out so far, the focus has been on the atmospheric dispersion pathway. Preliminary evaluation of dispersion via the ground pathway is reported here as well. The estimates for surface water flow are currently underway. The dose calculation methodologies for the various internal and external dose contributions are very similar for the two last dispersion pathways. In particular, they all use the same "reference person," a statistical construct designed to be representative of individuals living near the facility. The radiological consequences of possible accidental releases have also been estimated.

An ESS technical report [656] provides an overview of the methodologies and models developed to estimate dose factors due to atmospheric dispersion through the relevant exposure routes. In the work that has been completed so far, the aim of the analysis has been to establish and demonstrate the validity of calculation methodologies. All available site-specific data were used in the analysis. Several values for the ventilation stack height were analysed, from 25 m to 65 m. Particular attention was devoted to tritiated water vapour, including a modelling approach that is built on the assumption that all water entering the body of an exposed person will have the same tritium concentration. Calculations suggest

that the reference person may have an intake in the range of 0.5×10^{-8} Bq to 2.0×10^{-8} Bq of tritium per Bq released, corresponding to an annual dose range from 0.9×10^{-19} Sv/Bq to 3.6×10^{-19} Sv/Bq [655]. Calculations of the doses to persons living at different distances and in different directions from the facility can then be made, and it is possible to evaluate the influence of the atmospheric release height on dose to inhabitants in the area around ESS.

Inhalation, ingestion and external dose estimates

In another technical report [657], the calculation endpoints were ingestion and inhalation doses from exposure to each Bq released to the atmosphere of various radionuclides during routine operation, using the source term estimates given in Table 10.11 for different pathways. The total dose from intake of tritiated water was estimated on the basis of the methodology described above. The general principles and methodologies of the ECOSYS model, which is the food chain dose model in the European ARGOS [658] and RODOS [659] emergency management decision support systems, can be applied for any contaminant radionuclide with the provision of adequate radionuclide-specific data. This model was used for the ingestion dose estimates in the project.

The ESS facility will produce a large number of "exotic" radionuclides, whose behaviour in the environment has never been investigated. However, from knowledge about physicochemical equivalents, it is possible to parametrise the ECOSYS model. ECOSYS required a number of location-specific parameters (e.g, human diets, animal feeding regimes) as well as an improvement of some of the generic parameters, where parametrisation was old and no longer in touch with state-of-the-art knowledge [657]. For both of these purposes, the work benefited from recent Nordic project work [660]. External doses from a range of potentially important contaminants from routine airborne releases were also calculated in accordance with methodologies for estimation of doses from releases during routine operation [661], with contributions from three pathways: from the contaminated plume during its passage; from the external dose from deposition of airborne contaminants on surfaces; and from the external dose from deposition of airborne contaminants on humans. External dose calculations were made for those additional radionuclides that were identified as being of major concern, with the results shown in Table 10.14.

Annual dose rates from routine airborne releases

Based on quantitative estimates of the most important contaminants that may be released during routine operation, as discussed in Section 10.4, it is possible to estimate doses to population groups within 2 km from the facility. Release heights of 25 m to 65 m above ground were used for these estimates. Figure 10.10 illustrates total annual doses from routine releases of radionuclides to the air as a function of distance from ESS. The doses are estimated for representative persons living within 2 km of the facility who are assumed to consume locally produced foodstuffs, taking into account all radioisotopes defined as source terms in

Nuclide	**Release rate** [Bq/y]	**Ingestion** [nSv/y]	**Inhalation** [pSv/y]	**Extern. (plume)** [μSv/y]	**Extern. (depos.)** [pSv/y]	**Extern. (skin)** [pSv/y]	**Tritium** [μSv/y]	**Total** [μSv/y]
^{3}H	5.5×10^{12}						0.032	0.032
^{7}Be	1.0×10^{7}	0.025	0.23		5.1	0.17		0.00003
^{11}C	2.6×10^{12}			0.14				0.14
^{13}N	2.7×10^{12}			0.13				0.13
^{15}O	1.5×10^{12}			0.027				0.027
^{41}Ar	4.1×10^{10}			0.003				0.003
^{125}I	1.0×10^{6}	0.23	2.1		0.15	0.007		0.00023
Total	1.2×10^{13}	0.26	2.3	0.30	5.2	0.18	0.032	0.33

Table 10.14: Annual dose rate contributions from routine releases to air at 45 m during normal operation. Doses are received by individuals living 660 m away and include the pathways of ingestion, inhalation, external exposure from the contaminated plume, deposited contaminants in the environment, and deposited contaminants on human skin. The incorporation of tritium (mostly via ingestion and inhalation) is treated separately.

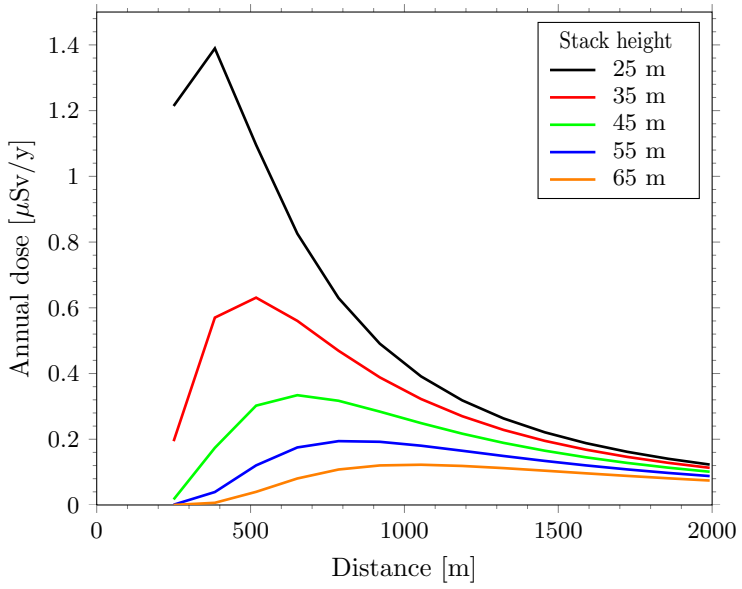

Figure 10.10: Total annual dose rate from routine releases of radionuclides to the air as a function of distance from stacks of different heights.

Section 10.4 that are released to the air. They include contributions from internal and external exposures, as described above.

Table 10.14 gives an estimate of the annual doses received through different pathways for the most important radionuclides. The inhalation and ingestion doses are conservatively shown for the age class of one-year-olds, as this age group generally receives the highest doses. The nuclides ^{11}C and ^{13}N, released as gases, each contribute about 40% of the total annual dose. The largest annual dose from a single pathway, summed across all nuclides, is 0.3 μSv/y, due to external γ-exposure from radionuclides in the plume. This value is less than the 10 μSv/y limit proposed by ESS for a single pathway. Further, calculations show that by reducing the ventilation rate of the linac tunnel from once a day to once every two days, the release rate of radionuclides can be reduced by about a factor two. For either of the linac tunnel ventilation rates, the total annual dose contribution across all pathways and nuclides is well below the annual dose rate limit of 50 μSv/y.

In addition, there is a contribution to airborne release from dismantling the target once every five years. This contribution is almost negligible, since the largest estimated released amount of any contaminant is less than 50 MBq (for ^{181}W), and the highest total dose conversion factor of all radionuclides examined as potentially important is 4×10^{-13} Sv/Bq (for ^{148}Gd). Table 10.15 shows the total doses from airborne releases occurring once every five years of each of the most important radionuclides in terms of total dose conversion factors and released amounts in connection with the target dismantling process. The release of ^{148}Gd in this process is estimated to be several orders of magnitude less than that of ^{181}W, and the total dose conversion factor for ^{181}W is also a couple of orders of magnitude less than that for ^{148}Gd. The total dose is the sum of the external dose from deposition on surfaces, the external dose from the passing plume, the external dose from contamination on skin, the internal dose from ingestion (for 1 year olds) and the internal dose from inhalation (also for 1 year olds). The doses from the target dismantling operation are also very small compared with the annual dose rate limit of 50 μSv/y.

10.5.2 Groundwater migration

Preliminary calculations have been made of the migration of activated groundwater towards the ESS site fence, at a distance of 250 m. The calculations assume a linac beam loss of 1 W/m, and standard shielding of 0.6 m to 0.8 m of concrete. The model applied is based on a typical soil and groundwater activation code combined with the groundwater migration model TRACE/PARTRACE, originally developed and tested for pesticide transport with groundwater, but extended to radioactive nuclide transport [662]. Figure 10.11 indicates that even fast-migrating nuclides, such as tritium and ^{36}Cl, require several hundred to several

Nuclide	Total dose conversion factor [10^{-15}Sv/Bq]	Release [GBq]	Total dose [μSv]
^{148}Gd	406	0.00003	0.010
^{172}Hf	1.26	0.005	0.007
^{172}Lu	0.206	0.005	0.001
^{173}Lu	0.669	0.008	0.005
^{175}Hf	0.310	0.002	0.0005
^{179}Ta	0.181	0.030	0.005
^{181}W	0.448	0.050	0.020
^{182}Ta	1.43	0.003	0.004
^{185}W	0.324	0.020	0.007
Total			0.060

Table 10.15: Dose parameters for selected potentially important radionuclides during target dismantlement releases. Total dose conversion factors, releases and total doses are calculated for the nearest inhabitant living about 330 m south of the facility.

thousand years to reach the site boundary. Thus, no radioactive nuclides will move off-site during the lifetime of the facility (operation plus decommissioning), and there is no risk to the public from groundwater activation. Even for long-lived ^{36}Cl (with a half-life of 300,000 years), the activity concentration at the site fence will be less than 0.4% of the original source concentration at the accelerator, an amount far below the established limits. This low level is due to dilution effects. No ^{36}Cl will appear at the fence before several thousand years of migration.

These estimates are based on the assumption of very low hydraulic conductivity (10^{-6} m/d), as measured on a limited number of soil specimens. An extended campaign of hydro-geological measurements on soil samples from the site is under way, and migration calculations will be repeated if deviating soil parameters are found. Additionally, the nuclide concentrations produced within the site boundary by activation near the accelerator are not completely negligible, according to the first activation and migration calculations. This has to be taken into account in decommissioning work, particularly with respect to tritium in the vicinity of the accelerator.

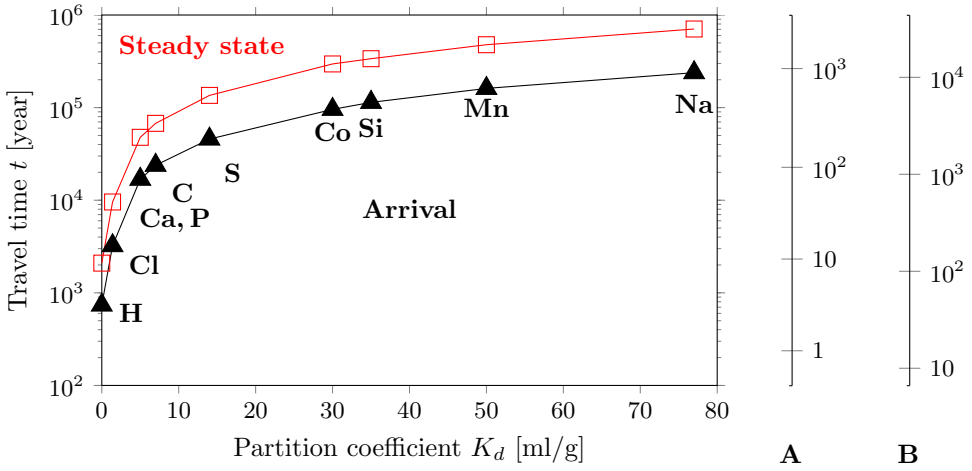

Figure 10.11: Groundwater migration travel times for selected radionuclides, as a function of the nuclide partition coefficient K_d between soil and water. The black line shows the travel time until the site boundary is reached, while the red line shows the travel time until steady state conditions occur. A hydraulic conductivity of 10^{-6} m/d is assumed.

Sample types	Sample size	Unit	Samples per year
Ground water (wells), drinking water	50	litre	2
Stream and lake water	50	litre	2
Sediment	100	g	1
Aerosols and gases (air sampler with charcoal cartridge)	106	m^3	12
Precipitation	50	litre	12
Grass	1	m^2	4
Milk	10	litre	2
Cereals	1	kg	1
Lichen/moss	200	g	1

Table 10.16: Sample types and rates for monitoring releases of radionuclides to the environment.

Monitoring releases of radionuclides to the environment

The ESS General Safety Objectives [391] state that ESS will be operated in such a way that it protects the public and the environment from harm. For this purpose, ESS needs to demonstrate that operational releases of radioactive substances to the environment do not exceed permitted levels and that the annual radiation exposure of a person representing the more highly exposed members of the public do not exceed dose limits. These individuals are assumed to live either at Östra Torn, 330 m south of the site, or at Vastra Odarslov, 660 m to the west. All planned operational releases of radioactive substances will be monitored in order to document that that they are below authorised limits. In the case of releases to the atmosphere, stack monitors will quantify releases of tritium, radioactive gases and particulates. A person located at the perimeter of the site will potentially be exposed to gamma radiation from airborne radioactivity releases and from radioactivity deposited on the ground. External gamma dose monitoring can be carried out, for example with passive devices such as thermoluminescent dose meters. A monitoring programme outside the facility will collect environmental samples for analysis of key radionuclides, such as tritium. This programme will document possible radioactive contamination of the local environment, and the radiation exposure of the representative person from ingestion of food contaminated by radioactive emissions. Table 10.16 shows typical sample types, sites and sampling frequencies for a monitoring programme. Prior to ESS commissioning, a baseline study will be carried out to provide information on radionuclides present in the environment. Some radionuclides produced from ESS operation also occur naturally (for example tritium and ^{7}Be). It is necessary to know the background levels of these radionuclides in order to evaluate the impact of ESS operation.

10.5.3 Accidents

Estimates of the radiological consequences of hypothetical accidental releases have also been carried out. Definitions of the categories of design basis accidents (DBA) are given in Chapter 11. Indications about the source term for DBAs were derived from an ESS technical report [663], which also recommended that ESS perform a sensitivity study varying the specific release factors for volatiles and aerosols. A separate analysis ranking the contaminants that might be released during a defined hypothetical accident by their importance with respect to dose was carried out first [664]. The findings of this study were used as the basis for dose calculations for a design basis accident [665]. The second study investigated two scenarios: the first with a volatile release fraction of 0.001% and the second with a volatile release fraction of 0.5%. In both scenarios, it was assumed that noble gases and tritium would be released to the atmosphere from a 45 m stack, whereas the amounts of volatiles and aerosols will vary depending on the exact scenario.

Table 10.17 gives an overview of the estimated dose to a reference person located 660 m from the site for the most important radionuclides for average design basis accident conditions. Table 10.18 shows estimated doses for worst-case design basis accident conditions. The total dose estimated from the 0.001% volatile release fraction DBA scenario is almost 0.2 mSv, well below the design basis accident limit of 50 mSv. The doses, dominated by tritium intake mainly via ingestion, are higher under the 0.5% volatile release fraction scenario, with a total estimated dose around 6 mSv. In this case the doses are dominated by radioiodine intake, again, mainly via ingestion. Doses were conservatively calculated for a release during the plant

Nuclide	Ingestion [μSv]	Inhalation [nSv]	External (plume) [nSv]	External (deposition) [nSv]	External (skin) [nSv]	Tritium [mSv]	Total [μSv]
^{3}H						0.18	180.
^{120}I		0.62	5.2	0.86	0.064		0.007
^{123}I	0.004	0.40	0.24	0.48	0.060		0.005
^{125}I	8.4	28.	0.017	3.9	0.018		8.4
^{126}I	0.11	0.47	0.006	0.22	0.023		0.11
^{121}Xe			0.015				
Total	8.5	30.	5.5	5.4	0.17	0.18	190.

Table 10.17: Estimated doses following a design basis accident that releases a combined volatile fraction of 0.001% into the atmosphere. Doses shown are received through different pathways for a range of particularly important radionuclides. Ingestion and inhalation doses are given here for 1 year olds, in order to be conservative. The total estimated dose is almost 0.2 mSv, well below the design basis accident limit of 50 mSv, dominated by tritium intake, mainly via ingestion.

Nuclide	Ingestion [mSv]	Inhalation [μSv]	External (plume) [μSv]	External (deposition) [μSv]	External (skin) [μSv]	Tritium [mSv]	Total [μSv]
^{3}H						0.18	180.
^{120}I		0.30	2.5	0.42	0.031		3.3
^{123}I	0.002	0.23	0.14	0.27	0.034		2.7
^{125}I	5.4	18.	0.11	2.5	0.012		5400.
^{126}I	0.18	0.82	0.11	0.37	0.041		0.18
^{121}Xe			0.14				0.14
Total	5.6	20.	0.14	3.6	0.12	0.18	5900.

Table 10.18: Estimated doses following a design basis accident that releases a combined volatile fraction of 0.05% into the atmosphere. Doses shown are received through different pathways for a range of particularly important radionuclides. Ingestion and inhalation doses are given here for 1 year olds, in order to be conservative. The total estimated dose is around 6 mSv, dominated by radioiodine intake, mainly via ingestion.

growth season. If the accident occurred outside the plant growth season, the dose would be about a factor of 50 lower. All doses in this chapter are effective doses, so thyroid organ doses would be some 25 times higher. According to ECOSYS calculations, the ingestion doses would be reduced by about a factor of 50 if consumption of local food products is avoided over the first few critical months. Doses to individuals living 1 km from the site would be almost a factor of 10 lower than those to individuals living just outside the site fence. These doses are well within the limits listed in Table 11.3.

10.6 Decommissioning

Swedish regulations require that an initial decommissioning plan be prepared during the design of the ESS facility, with periodic updates during ESS's operating life, and a final plan due immediately prior to decommissioning. Some operational details do not have to be defined in the initial decommissioning plan, since personnel, contractors and technologies are likely to change substantially over the operating life of the facility. The initial version of the decommissioning plan will be submitted to the Swedish Radiation Safety Authority (SSM) as part of the licensing process for the facility. Equipment, materials and buildings within the controlled area of the ESS premises will be decommissioned following the scheduled operational period of 40 years. Two issues fundamental to the initial decommissioning plan have already been examined: the general decommissioning strategy, and the desired endpoint (greenfield or brownfield status). Options have been ranked, and the decommissioning procedures and documentation for other facilities that are similar

in size and overall purpose to ESS have been studied. Technical and financial aspects have been identified and advantageous solutions selected. An preliminary version of the initial decommissioning plan has been compiled, and will be submitted to SSM after some elaboration of details and possibly after some minor revisions.

The initial decommissioning plan must address: licensing conditions; staffing and training; organisation and administrative control; cost estimation; waste management; emergency management; radiation and physical protection; on and off-site monitoring and quality assurance. It must also address the following critical tasks: characterisation of the facility, including surveys of radiological and other hazards; record keeping; removal of highly radioactive material; decontamination of surfaces and equipment; dismantling techniques: remote control versus manual skills; and final radiation survey and completion of decommissioning procedure.

Decommissioning strategies

On one hand, the decommissioning task is unique because ESS is a unique facility, so there are a number of open questions. On the other hand, national legislation in Sweden covers the general issue of decommissioning [666, 667] and international guidance is also available from the International Atomic Energy Commission [668–670]. According to both Swedish law and the IAEA, the fundamental task for decommissioning planning is to define two (or more) strategies or options, one more probable and the other less probable, that a facility could adopt for its overall approach to decommissioning. These two approaches are referred to as the "reference" and "fallback" options. Three reasonable approaches for ESS decommissioning are: 1. Immediate decommissioning, including prompt (or at least continuous) removal of all radioactive materials to a pre-designated disposal site; 2. Delayed or deferred decommissioning, including a safe enclosure period for the natural decay of radionuclides; and 3. Phased decommissioning, with periods of consecutive deferral and active dismantling.

A good example of the analysis of decommissioning strategies is given in a report about the decommissioning of the Eurochemic reprocessing plant in Belgium [671]. After reviewing international guidance [668, 672] and the experience of comparable facilities, ESS has chosen immediate dismantlement (ID) as the "reference" strategy. A five-year decommissioning period, presumed to be from 2065 to 2070, is more than adequate. There are four key advantages to the strategy of immediate dismantlement. First, the radiation level of the ESS structure in shutdown conditions (after the removal of the last target) will not exceed the level of the operating facility, so it will not pose a significant threat to the environment. Second, the compactness of the operational unit assures that only a small amount of removable or dispersive contamination will be present on surfaces. Third, as the ESS structure is rather unique, it is of primary importance that the accumulated experiences of the operating staff should be used as much as possible. Planning and training staff to carry out dismantling activities for areas with elevated radiation levels will be more feasible if the facility uses the ID strategy. And fourth, cost estimation is more straightforward and less inaccurate for the ID strategy than for the other options. Optionally, a model of phased decommissioning can also be elaborated as the "fallback" option for the initial version of the decommissioning plan.

Greenfield site restoration and reuse

The second fundamental issue is to specify the desirable endpoint of decommissioning operations in terms of site restoration. This, in turn, determines the post-decommissioning level of regulatory oversight for the site, and the uses to which the site may be put. The two endpoint options are to return the site to green field status, or to leave the site in brown field status. If the site is returned to green field status, it can be reused without any further restriction. Buildings will be either demolished or reused, with an unconditional release (clearance) from regulatory control. Under brown field status the site can only be used for special purposes (e.g. a new radiological facility, a non-radioactive waste dump etc.), with a conditional release (clearance) from regulatory control. The initial decommissioning plan will state that the ESS goal is to return the site to green field status, permitting unrestricted reuse of the site.

Previous experience – ITER and the Budapest Neutron Centre

Unlike nuclear research reactors, the decommissioning of large spallation sources is far from commonplace. ESS has found it useful to study the decommissioning planning and experiences of two facilities with com-

parable levels of radiological threats. The decommissioning plan of the ITER experimental fusion facility proposes a phased decommissioning strategy, with an outline in the facility's 2001 design report [673]. It will start with a five-year decommissioning period for the main assemblies, followed by a de-activation (safe enclosure) period of five to 50 years. After the de-activation period, the facility will be handed over to a new organisation inside the ITER host country. The main factor underlying the decision to pursue the phased decommissioning approach is the high activity level of ITER's reactor vessel. In contrast, ESS has no components with comparably high activity levels.

Budapest Neutron Centre has a 10 MWth research reactor using low-enriched uranium fuel. It was completely refurbished during a seven-year break from operations, with the complete removal and exchange of the reactor vessel and some internal components. These operations were quite similar to decommissioning, so the experience was used in writing the decommissioning plan that was first elaborated in 1997-1998, and then submitted in 2010 as a part of the periodic safety assessment. The Centre chose immediate dismantlement as its reference strategy, taking place around 2030-2040, with a planned duration of 10 to 15 years from shutdown. The plan shows that the early removal of the most active part of a facility eases operations with the less active components. If the key operational challenge of providing temporary storage for the highly active components is solved, there is no need for a more expensive safe enclosure option.

Alternative decommissioning methodologies

As part of the process of preparing the initial decommissioning plan, ESS has evaluated alternative decommissioning methodologies, and has scrutinised the previous experiences of related projects, including MEGAPIE at PSI in Switzerland; the DR-1, DR-2 and DR-3 facilities in Risø Denmark; Rossendorf in Germany, and the reactor vessel removal KFKI in Hungary. These experiences will be described in detail in ESS's initial decommissioning plan.

Waste management during decommissioning

Collectible radioactive decommissioning waste is different from operational waste. The amount of decommissioning waste generated within a given time period is generally larger, and it displays a wider variety of physical characteristics. The dismantling process will require that a certain part of the facility is assigned as temporary storage area; ideally, two separate areas will be designated for radioactive and clearable waste. The ESS premises are large enough to host these buffer areas safely. Radioactive material and waste present at the time of the final shutdown will contribute to the "radionuclide vector". Categorised according to their origin, the types of waste that will be present on-site include left-over operational wastes that were not released as effluents during the operational period (most of these wastes will be kept in designated waste storage locations); structural materials that were in use in the final operational campaign, such as the last target and activated assemblies; building material such as steel, concrete, and other metals; and contaminated laboratory equipment. All of these waste types fall within the regulatory framework discussed earlier, including the requirement to categorise the components of the waste stream in terms of method of final disposal, and the methodology for calculating the clearance index for specific components of the waste.

Financial and organisational issues including decommissioning costs

Swedish regulatory authorities recommend that cost estimates in the initial decommissioning plan be based on analysis of the following conceptual groups of decommissioning activities: pre-decommissioning actions; facility shutdown activities; procurement of general equipment and material; dismantling activities, waste processing, storage and disposal; site security, surveillance and maintenance; site restoration, clean-up and landscaping; project management, engineering and site support; and research and development. Instead of providing a rough estimate of decommissioning costs as a "given percentage of construction costs," the "unit cost method" developed by Jeong et al. [674] may be used for ESS. This approach is generally applicable to the ESS facility (apart from spent fuel management issues) although it was primarily intended for research reactors. ESS cost estimates will also benefit from the valuable assessments of alternative approaches compiled by an expert group supported by the OECD Nuclear Energy Agency [675].

Engineering design for efficient dismantling and disposal

International best practice, as detailed in several IAEA reports [676, 677], and the conclusions of an ESS-specific engineering report [678], lead to a number of engineering design recommendations. Every structural material which can be activated by the primary protons and the generated neutrons should be analysed prior to installation in order to reveal impurities (e.g. rare earth metals) which may contribute to radioactive inventory. While this is not completely possible for the field concrete shielding of the high energy linac section, some upper limits will be set. As a general principle the more active parts will be removed first so the remaining dose burden will be mitigated, although this is only one factor in the optimisation procedure. Moreover, parts with dispersible radioactivity should be easily accessible in order to avoid contamination of originally clean areas. This includes items such as worn-out insulation. Some parts with enhanced radioactivity will be removed by remote controlled operations (robotics). For manual removal of highly radioactive elements, shielding will be built by means of cranes or high capacity transport vehicles. Space will be reserved for their installation. Monitoring equipment will be built in areas of significant external dose rate and/or surface contamination. Materials of equipment and structures which will probably require decontamination will already be under study and observation during the construction phase in order to select the optimum method and means of decontamination. Finally, an overall system of record keeping for materials and operations in the controlled area of the facility will be used.

Key participants in decommissioning

In addition to the Swedish Radiation Safety Authority (SSM), key participants in decommissioning activities in Sweden at the present time include Studsvik Nuclear AB, a nuclear technology and radiological research company, and SKB, the Swedish Nuclear Fuel and Waste Management Company. Studsvik was originally majority government-owned, but it was turned over to private investors by the Swedish government in the 1970s, retaining its headquarters in Nyköpping, Sweden [679, 680]. SKB was created as a cooperative effort of the Swedish nuclear power companies after Sweden enacted legislation in the 1970s requiring them to manage and dispose of any nuclear waste they generated, and to operate licensed repositories for radioactive waste [681].

Chapter 11

Safety and Security

Chapter abstract

Summary: ESS will be designed to a high level of safety in order to meet the expectations of the users, the personnel and the regulatory requirements. This applies to aspects of safety such as radiation, fire, cryogenics, chemicals, heavy loads and other hazardous items or situations. The security of the facility will be designed to meet the basic in-house security rules and regulatory requirements, as well as the need from the users and personnel to work in an open and friendly atmosphere.

Licensing of ESS is focused on the regulatory radiation safety requirements from the Swedish Radiation Safety Authority (SSM). Thus, the chapter mainly deals with the radiation safety principles for ESS design. The fundamental safety functions, the safety barriers and the safety systems are generally described.

Passive safety is the fundamental safety principle. The accelerator proton beam hits the target material and neutrons are produced in the spallation process. When the proton beam stops, the production of neutrons stops. Residual heat is removed from the tungsten target by passive conduction, convection and radiative cooling, even without any active systems.

Three confinement barriers contain the substantial nuclide inventory in the target, caused by proton bombardment. All possible other nuclide inventories at ESS will have at least two safety barriers.

11.1 Safety principles

ESS will be a complex facility with the potential to pose a variety of hazards to human beings and the environment. ESS prioritises prevention of harm to employees, the public, and the environment from both radiation and conventional safety threats. In 2011, ESS formally adopted the following project-wide set of *general safety objectives* (GSO) [391]:

- "To protect individuals, society and the environment from harm arising from the construction, operation and decommissioning of the ESS facility.
- To ensure that in normal operation, exposure of personnel to hazards within the facility is controlled, kept within prescribed limits, and minimised.
- To prevent accidents with high confidence.
- To ensure that any abnormal operational event has minimal consequences for ESS personnel and for the public.
- To minimise the hazardous waste arising from the operation and decommissioning of ESS, both in its quantity and level of hazard potential."

These overarching goals will guide ESS through all phases of its multi-decade life-cycle, through all stages of conceptual and detailed design, fabrication of components and construction, commissioning, operation, planned and unplanned maintenance, and eventual dismantling and decommissioning. The GSO govern the design and implementation of the specific safety systems and programmes.

In accordance with well-established international best practice, a few basic principles constitute the framework for the ESS safety programme: exposure to hazards will be *as low as reasonably achievable* (ALARA); multiple and redundant levels of safety barriers and protective systems will provide *defence-in-depth*; ESS design will incorporate both *passive* and *active* safety measures; and an ongoing process of *review and assessment* of safety systems will shape the entire engineering design process. These principles will enforce the *safety culture* within the ESS organisation. Maintaining that safety culture will be a top priority for ESS management.

As low as reasonably achievable

ESS will keep exposures to hazardous materials as low as reasonably achievable. The ALARA principle means that ESS will make every reasonable effort to minimise exposure to radiation, even when exposure falls far below dose limits prescribed by Swedish law (as will usually be the case). ESS will operate on the principle of achieving the lowest level of exposure that is consistent with the purpose for which the licensed activity is undertaken, taking into account the state of technology, the financial cost of achieving further reductions in exposure, and the impact of further reductions on the project's scientific objectives. Application of the ALARA principle implies that predicted doses (during the design phase) and actual doses (during operational phases) should generally decrease as the project proceeds and new data become available, permitting more precise and more realistic estimations of dose levels. ESS will maintain documentary records of the predicted and measured personnel and environmental exposures, in accordance with Swedish law and International Committee for Radiation Protection guidelines and as a necessary step for implementation of ALARA best practice.

Review and assessment

Throughout the engineering design process, ESS personnel will conduct safety reviews and assessments to ensure that the design satisfies the top-level safety objectives and is in compliance with SSMFS 2008:27 [682]. These assessments will include analyses of: normal operation; maintenance; incidents and accident scenarios; waste handling and waste storage; commissioning and test operation; and decommissioning. The results of these analyses will be available to assist the preparation of documentation for regulatory applications.

Safety culture

No set of protocols, rules or laws by itself can guarantee the safe operation of a complex facility. Organisations have cultures, and those cultures affect the safety of their operations. INSAG [683] described a "safety culture" as:

> "... that assembly of characteristics and attitudes in organisations and individuals which establishes that, as an overriding priority, ... safety issues receive the attention warranted by their significance."

Indicating the importance of this issue, a subsequent INSAG report [684], offers recommendations to tackle the practical and managerial challenges to building and maintaining such a safety culture. The management of ESS embraces the INSAG recommendations, and is committed to fostering a safety culture that nourishes an open and constructive attitude towards safety concerns and an organisation-wide commitment to a continuous process of safety improvement.

Quality assurance management

High quality of design, materials, structures, components and systems, operation and maintenance is vital for the overall safety of ESS. Quality assurance programs will ensure the development of a safe design (including design of process and safety systems, design of safety barriers, design of modifications and safety analysis). Appropriate conservative assumptions and safety margins will be used for design and construction.

11.1.1 Confinement barriers and defence-in-depth

Safety engineers at nuclear facilities such as power plants have refined and developed the concept of "defence-in-depth" through years of practical experience. The approach allows facilities to compensate for potential human and technical failures by building several levels of redundant protection into the facility design, including sequential safety barriers to prevent the release of radioactive material to the environment. A failure at one level of a system is compensated by the barriers in place at the next level. While nuclear facilities pioneered the defence-in-depth approach, it can be and has been fruitfully applied to other types of facilities. ESS will use a set of physical confinement barriers that operate independently of one another to prevent and mitigate potential releases of radioactive isotopes. Demonstration of the adequacy of this set of barriers is an important part of the safety analysis. ESS will apply the defence-in-depth concept in order to minimise deviations from normal operation, to prevent accidents, and to mitigate the consequences of abnormal events.

In accordance with the principles laid down by the International Atomic Energy Agency working group INSAG (International Nuclear Safety Advisory Group), ESS will implement the defence-in-depth approach via four safety levels with procedures and systems: to minimise deviations from normal operation; to monitor and document deviations from normal operation and to intervene *before* such deviations progress to accidents; to control accidents if they do happen; and to mitigate the adverse effects of accidents. Table 11.1 provides more detail about this multi-level approach to safety. ESS has chosen to apply the defence-in-depth strategy, which implies that there will be confinement barriers in different parts of the facility. The confinement barriers are shown in Table 11.2.

Passive safety systems

Passive safety systems rely on facility features whose very nature acts to prevent accidents or to limit the adverse consequences of accidents. Passive safety systems rely predominantly on natural laws and material properties, and provide protection independently of human intervention. The ESS design constitute of two such fundamental characteristics of passive safety systems. The first crucially important feature of ESS's design from the safety perspective involves the linear accelerator. The linac will depend on the continuous input of power from the electrical grid to produce beam. This is a powerful safety feature, because if the external power supply is interrupted for any reason, the accelerator will automatically shut itself down. Unlike nuclear reactors, there is no danger of ESS "going critical" once it has been accidentally or deliberately cut off from the power grid. The second important feature of the ESS design from the

Level	Objective	Tool
1	Prevention of abnormal operation and failures.	Conservative design and high quality in construction and operation. Qualification of materials in the target environment. Continuous survey and documentation during manufacturing and testing. Simple operation to reduce probability of human error. Redundancy, diversity and separation principles in active safety systems. Qualification of personal in all life-cycle phases. Quality assurance system covering the safety related activities by ESS and the subcontractors and partners.
2	Detection of deviations from normal operation and provision of means to prevent development of sequences leading to accident conditions.	Independent or redundant control, limiting and protection systems as well as other surveillance features including environmental radiation monitoring.
3	Control of accidents.	Engineered safety features and protection systems to prevent accident progression. Radioactive materials confined within a containment system.
4	Control of severe accident conditions and prevention of accident progression.	Procedures for mitigation of accidents in order to ensure that radioactive releases are kept as low as reasonably achievable.

Table 11.1: Levels of defence-in-depth to compensate for potential human and technical failures..

System	Number of barriers	Confinement barriers
Target	3	Target wheel envelope Monolith confinement Target building
Target systems	2	Monolith confinement Target building
Hot cell	2	Hot cell confinement Target building
Proton accelerator	2	Accelerator beampipe Accelerator tunnel
Neutron scattering instruments	3	Neutron guide shielding Neutron guide tunnel and bunker Instrument component confinement
Waste disposal building	2	Cask/package Building

Table 11.2: Confinement barriers for radiological protection.

safety perspective involves the cooling function of the ESS target station. The most likely reason for a loss of cooling system function is an electric power interruption. Although this guarantees an instantaneous shut-down of the accelerator, heat production in the target will continue for some time. ESS's adoption of a rotating, helium-gas-cooled tungsten target of 2.5 m diameter, which offers a large enough surface area for passive radiative cooling to avoid dangerous temperatures with a significant safety margin, passively eliminates this risk, even in the absence of an active cooling system.

Active safety systems

ESS's active safety systems will include mechanical, electrical and instrumentation and control components. They will ensure that the facility operates safely, and that safety is maintained in the event of an incident. For example, active safety systems will provide for cooling of the target material during normal beam operation. Other active safety systems will make sure that the beam is shut down and that components such as the target material are cooled in the event of an incident. Note that cooling of the target material will be done actively by gas cooling although from a defence-in-depth perspective, this function is not formally required since the cooling can be done passively. Active safety systems also encompass ESS protocols governing installations and training programs to ensure that all employees act in accordance with prevailing instructions and in compliance with Swedish regulation SSMFS 2008:27 [682]. ESS protocols will lay out a fixed schedule for maintenance, testing and adjustment of many mechanical and electrical safety devices, and for radiation monitoring of the experimental instruments.

11.2 The licensing application and regulatory processes

While ESS is a non-nuclear facility, it will produce activated materials. In developing its safety programmes, ESS has profited from decades of collaboration and exchange among regulators and facility operators within the nuclear community about how to handle such materials. The International Atomic Energy Agency (IAEA) is an important actor in this exchange, publishing reports and guidelines that analyse crucial safety issues, summarise the lessons learnt from industry experience, and establish best practices. This accumulated collective knowledge base informs ESS's own safety objectives and programme.

The licensing process of ESS is given by three different legal acts in Sweden, as shown in Figure 11.1; the Radiation Protection Act, the Environmental Code and the Planning and Building Act. In March 2012, ESS sent in the formal application to the Swedish Radiation Safety Authority (SSM) asking for a permit to construct. The Preliminary Safety Analysis Report (PSAR) [685] constitutes the basis of the application. The PSAR describe the overall technical concept, potential risks and the mitigation of those risks and the waste management of the radioactive material. In March 2012, ESS also sent in an application to the Swedish Environmental Court asking for permissibility to construct and operate ESS outside Lund. An Environmental Impact Assessment (EIA) forms the basis for the application. Continuous work has been done for the facility planning layout process towards the Lund municipality in accordance with the Planning and Building Act. In these matters, ESS has a strong connection and cooperation with both Max-lab and the Lund municipality regarding the planning of the whole area northeast of Lund.

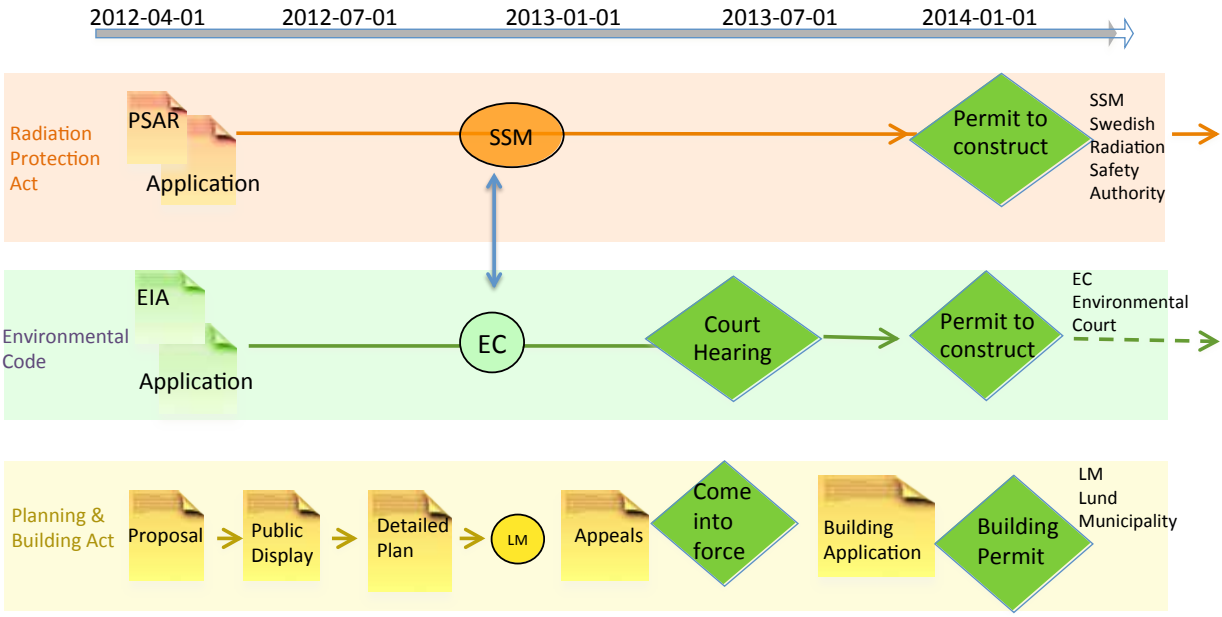

Figure 11.1: Licensing process for construction permits.

Radiation regulations

The Swedish Radiation Protection Act (SFS 1988:220) governs activities and facilities emitting radiation in Sweden. The main purpose of the act is to protect humans and the environment from the harmful effects of radiation. Under power conferred by the act, the Swedish government has issued Radiation Protection Government Regulation (SFS 1988:293). In its turn, under power conferred by this regulation, the SSM has issued a large number of authority regulations supplementing the Radiation Protection Act and Government Regulation. For nuclear facilities, the Nuclear Activities Act (SFS 1984:3) applies. However, ESS does not qualify as a nuclear facility under the definition laid out by the Nuclear Activities Act. Under both the Radiation Protection Act and the Nuclear Activities Act, SSM is appointed as the regulatory authority.

A number of SSM regulations apply to ESS. These include SSMFS 2008:27, which regulates the operation of accelerators and sealed radiation sources; SSMFS 2008:51, which provides for the protection of workers and the public during activities involving ionisation radiation; SSMFS 2008:52, as amended by SSMFS 2010:1, which provides for the protection of outside workers who work with ionising radiation; and SSMFS 2010:2, which regulates the handling of radioactive waste and releases from activities with open radiation sources. In addition, the Swedish Civil Contingencies Agency (MSB) Regulation MSBFS 2011:1, on road and terrain transports of dangerous goods (ADR-S), will apply to the transport of radioactive substances to and from ESS. In the SSM regulations that apply to ESS, there are no specific regulations regarding accidental conditions, although both SSMFS 2008:27 and SSMFS 2008:28 require regulated facilities to develop an action plan for handling unexpected events from a radiation protection point of view.

SSM may, when granting a permit under the Radiation Protection Act, or at any point during the term in which the permit is valid, set permit conditions for ESS. While ESS is not a nuclear facility, it has taken into account those aspects of nuclear facility regulation that seem relevant to ESS activities in developing its own internal protocols and guidelines, which in many circumstances are more stringent than the national regulations [617]. ESS has declared that it will abide by the intention of this regulation. ESS has set 0.05 mSv as the upper annual dose limit for the general public, but aims at not exceeding 0.01 mSv per year for any of three exposure pathways: direct radiation, inhalation and ingestion.

11.3 Radiological safety

The radiological safety focuses upon limiting the doses for the ESS personnel as well as the environment. The limitation and estimation of radioactivity doses are based on regulations from SSM for facilities with major radioactive inventories. In particular, SSMFS 2008:17 requires that "events" be classified according to the probability of occurrence, and specifies that reference doses be established for each event class, which should not be exceeded. ESS has also taken into account experience from similar facilities around the world. The limiting doses are established for normal operation and for different hazardous events, which might occur during the lifetime of the spallation neutron source.

Classification of events

All possible incidents and accidents that might happen at the ESS facility, including normal operation, are categorised into four classes depending on the predicted annual frequency of such events. The classification of the events is presented in Table 11.3, using frequency values adopted from licensing practice in Western Europe [686]. The definitions of event classes are given below and the list of initiating events with their classification is provided in the document setting out ESS's *General Safety Objectives* [391].

- **H1: Normal operation.** Normal operating regime includes different maintenance phases of the facility, including events and disturbances during the normal operation occurring more or less frequently but where a relevant safety system is available. The restart of the facility can be done after repairs that fall within the range of normal maintenance.
- **H2: Incidents.** Events which are unusual, but which are expected to happen at some point during the lifetime of the ESS facility are classified as incidents. The expected frequency of these events varies from 10^{-2} times up to less than once per year. The facility should be able to restart after several weeks of repair following an incident.

Event	Description	Frequency [1/y]	Unit	Rad. workers	Non-exposed workers	Public (effective dose)
H1	Normal operation	≥ 1	[mSv/y]	10	0.05	0.05
H2	Incidents	10^{-2} – 1	[mSv]	20	0.5	0.5
H3	Unexpected events	10^{-4} – 10^{-2}	[mSv]	50	5	5
H4	Design basis accident	10^{-6} – 10^{-4}	[mSv]	100	50	50
–	Beyond design basis accident	$\leq 10^{-6}$				

Table 11.3: Classification of radiation hazard events and summary of the General Safety Objective limits on radiological doses.

- **H3: Unexpected events.** Events that are not expected to occur during the lifetime of the ESS facility are classified as unexpected events. The predicted frequency of these events varies from 10^{-4} to 10^{-2} times per year. The facility should be able to restart after several months of repairs following an unexpected event.
- **H4: Design basis accidents (DBA).** Events which are very unlikely to occur within the lifetime of the facility are classified as DBA events. The predicted frequency of these events ranges from 10^{-6} to 10^{-4} times per year. The facility will be designed and constructed to withstand DBA events, within specific limits.
- **Beyond design basis accidents (BDBA).** Events which are not expected to happen within the lifetime of the facility are classified as BDBA events. The frequency of these events is less than 10^{-6} times per year. The facility probably would not be able to restart after a BDBA.

The commissioning process will include conservative and realistic assessments of the facility's capacity to cope with normal operation, incidents, unexpected events and DBA events. BDBA events have such a low probability that they will not be included in the commissioning safety assessments. Nevertheless, BDBA events will be analysed during the ESS design phase in order to evaluate alternative emergency response scenarios by the relevant authorities. As part of this analysis, ESS will estimate the potential radiological impact of BDBA events. Preliminary evaluations indicate that the radiological impact of BDBA events would not be dramatically larger than that of the DBA events that the facility will be designed to withstand.

General radiation safety requirements

Under Swedish law, the regulations regarding risk and exposure limits for ionising radiation are different for employees and the general public. The summary of the GSO for radiation hazards towards workers with risk for exposure to ionising radiation, non-exposed workers at ESS as well as general public together with the collective dose for ESS staff is presented in Table 11.3. The upper dose limits for H1-H4 events are also provided.

Staff

ESS employees are divided into two classes: those who might be exposed to ionising radiation during their duties and non-exposed employees. The latter group will not have access to areas where there is a risk for radiation exposure. In accordance with Swedish regulation SSMFS 2008:51, the maximum annual effective dose for workers shall not exceed 50 mSv, while the cumulative dose over five years is limited to 100 mSv. Swedish law requires that employee doses be individually monitored, and that doses be monitored online in real time during an employee's presence in radiation risk areas. The Swedish regulations [687] prescribe an annual effective dose limit of 1 mSv for employees who are not exposed to radiation.

In accordance with the ALARA principle, ESS guidelines call for more restrictive dose limits than does Swedish law [391]. For ESS employees whose duties might subject them to radiation exposure, dosage should not exceed 10 mSv per year. The ESS goal for non-exposed employees is 0.05 mSv per year. In addition to the individual dose limits for ESS workers, ESS has adopted a maximum collective annual

effective dose, which includes exposures for subcontractors, consultants, and other non-employees present at the facility. ESS has set this collective limit at 1 personSv per year. ESS will also comply with Swedish exposure limits for pregnant women, in accordance with SSMFS 2008:5 [687], which requires that once the employer becomes aware of the pregnancy, the maximum effective dose to a foetus may not exceed 1 mSv during the remainder of the pregnancy.

In case of incident conditions, the Swedish regulations for employees working with ionising radiation is taken as a reference. In accordance with SSMFS 2008:51 [687] the maximum annual effective dose must not exceed 50 mSv, while the total obtained dose during five years has to be lower than 100 mSv for employees. ESS guidelines again set a more restrictive limit of 20 mSv per year. Since there are no governmental requirements related to dose limits for non-exposed workers, ESS guidelines call for the same dose limit as for general public, namely 1 mSv per year [687]. ESS will also comply with the Swedish regulatory requirement that rescue efforts that could lead to an effective dose higher than 100 mSv, may only be performed by volunteers in possession of valid scientific information about the radiation danger.

The public and the environment

Under SSMFS 2008:51 [687], the effective annual dose limit for individuals from the general public who do not work with ionisation sources shall not be higher than 1 mSv. In specified exceptional circumstances, SSM allows for a higher effective dose for a single year provided that the average over five consecutive years does not exceed 1 mSv per year. Again, ESS guidelines call for more restrictive dose limits than does Swedish law, with 0.05 mSv as the upper annual dose limit for the general public. The doses to a representative individual must be estimated with appropriate documentation of methodology. In July, 2012, ESS submitted a dose assessment report to SSM describing likely exposure of the representative person including living conditions, food pathways and a statistical analysis of meteorological dispersion conditions. The analysis demonstrated adequate protection of the environment and biosphere [688]. The results from the activation calculation performed [618] show that ESS radiation emissions will not harm any species or the ecosystem as a whole.

The maximum effective dose for general public must not depend on incident or accident conditions. ESS will estimate release doses for H2 events, and will describe in detail the steps to be taken to mitigate the consequences of releases during such events. In general, SSMFS 2008:51 [687] stipulates that the annual effective dose from H2 events shall not exceed 1 mSv per person who does not work with ionisation sources. In exceptional circumstances, SSM allows for a higher effective dose for a single year provided that the average over five consecutive years does not exceed 1 mSv per year. The calculation results of the released doses under accident conditions will help to determine which measures ESS should apply to mitigate accident consequences and protect employees and the general public. In accordance with [391], ESS guidelines call for the following maximum effective doses to the public: 0.5 mSv/event for H2 events, 5 mSv/event for H3 and 50 mSv/event for H4 events.

11.3.1 Safety functions

The IAEA [689] has identified three fundamental safety functions that,

> "...shall be performed in operational states, in and following a design basis accident and, to the extent practicable, on the occurrence of those selected accident conditions that are beyond the design basis accidents:
>
> - control of the reactivity;
> - removal of heat from the core; and
> - confinement of radioactive materials and control of operational discharges, as well as limitation of accidental releases"

Because ESS is not a nuclear facility, these safety functions must be adapted to fit its circumstances. A spallation source neither creates the reactivity threat posed by a fission reactor nor has the same level of decay heat arising from a fission process. The fundamental safety functions in a spallation source are: stopping the spallation process (by stopping the proton beam); removal of afterheat from the target; and confinement of radioactive materials and control of operational discharges, as well as limitation of

accidental releases. There is no need for active cooling of the helium-cooled tungsten material of the target after shut down of the proton beam [690]. However, active cooling of the target is required during proton beam on the target. While the design of the complete ESS safety programme is an ongoing effort, progressing in an integrated way with the design of the entire facility, the outlines of its basic principles and functions have been established.

Stopping the proton beam

The proton beam will be stopped in the case of any of the following events:

- Loss of target wheel rotation (to avoid compromising the first target confinement barrier)
- Loss of active cooling of the target material on the target wheel (to avoid compromising the first target confinement barrier)
- Loss of cooling of the moderator hydrogen (to avoid an uncontrolled pressure rise that could harm the first and second target confinement barriers)
- Loss of cooling of the pre-moderator water (to avoid an uncontrolled pressure rise that could harm the first and second target confinement barriers)
- Loss of cooling of the reflector (to avoid compromising the first and second target confinement barriers as well as the first confinement barrier of the reflector)
- Loss of cooling of the proton beam window (to avoid compromising the first PBW confinement barrier)
- Loss of vacuum in the accelerator tub (to avoid compromising the accelerator confinement barrier as well as protection of the machine)

The beam will also be stopped (for personnel protection) in the case of: personnel entrance into the target rooms above the monolith; personnel entrance into the accelerator tunnel; or personnel presence in the neutron instruments if there is no appropriate shutter in the line of sight if the personnel, or if an installed shutter fails to close. Abnormal beam steering can also lead to the loss of vacuum in the accelerator, which also turns the beam off. Several levels of safeguards will protect against personnel exposure within the neutron instruments. The high-radiation environment of the instrument will be searched and closed off before the shutter is opened. However, if a person is accidentally locked inside one of the neutron instruments despite these precautions, he or she will be able to trip the proton beam. In addition, an emergency switch will shut down the beam in case equipment malfunction leads to an unsolicited shutter opening. The uncontrolled release of high beam power can lead to serious damage and/or long repair times of the accelerator, the target station and neutron instruments. It is therefore crucial to maximise the operational efficiency of the facility by avoiding accidents. But also any interruptions of operations due to repair and/or maintenance work should be limited to a shortest time possible.

Figure 5.4 shows the relation between the main safety and protection systems at the ESS facility: the target safety system (TSS), the personnel protection system (PPS) and the machine protection system (MPS). The TSS addresses the actions required to operate the target station in accordance with the Swedish nuclear regulatory guidelines, and must fulfil the highest reliability demands. It covers the target station systems, the A2T (Accelerator to Target Station) section, and the intersection between target and neutron instruments. The TSS interacts with the accelerator, mainly to request a machine shutdown (switch off of the proton beam). The PPS and MPS will be designed for the protection of personnel and machine equipment throughout the conventional facilities, the accelerator, the target station and the neutron instruments. The reliability demands for the PPS are higher than those for the MPS. Details on the MPS and PPS are described in Chapter 5. Both MPS and PPS are under the responsibility of ICS.

Cooling systems, removal of afterheat and confinement of the radioactive inventory

Cooling systems for the following components must be operational for a safe performance of the facility: the target material in the target wheel and its confinement; the hydrogen moderator; the water pre-moderator; the reflector; the proton beam window; and the monolith shielding. Controlled ventilation of the following

components is required for the mitigation and/or reduction of releases of radioactive substances to the environment: the target monolith; the target station connection cells; the target station building; the target station active cell; the accelerator tunnel; and the waste treatment building. Confinement of the radioactive inventory will to be controlled via the leak tightness of the first barrier (the target wheel shroud), and the second barrier (the monolith lining). Controlled pressure relief will be operational for the following cooling systems: the target wheel; the moderator (safety valve outside the monolith); the pre-moderator (safety valve outside the monolith); and the proton beam window. Controlled pressure relief will also be provided for the monolith in case of a moderator fire, explosion, or similar event.

11.3.2 Safety systems

Redundancy and diversity in active safety systems provide multiple levels of protection for personnel, the general public, and the environment. The following safety systems have been identified:

- Target safety system
- Personnel protection system,
- Target wheel cooling system,
- Target moderator cooling system,
- Target pre-moderator cooling system,
- Target reflector cooling system
- Target proton beam window cooling system
- Target wheel confinement system
- Target monolith confinement ventilation system
- Target building confinement ventilation system
- Active cells ventilation system
- Accelerator tunnel ventilation system
- Target monolith pressure relief system
- Target moderator pressure relief system
- Target pre-moderator pressure relief system
- Target proton beam window pressure relief system
- Target component handling system

Safety classification of facility systems

There are standards that deal with safety classification of systems and components for nuclear power plants. Safety classification is based on event classes with adopted maximum environmental impact that govern reliability requirements for different systems. A similar approach can be applied for ESS but it is not relevant to talk about breakdowns in the same way as in a nuclear fission reactor. However, one can determine which systems and components that are most important to prevent the release to the environment of radioactive nuclides during an accident and those essential for fulfilment of a safe operation of ESS. For ESS one safety class is suggested with the criteria given below. The following systems, structures and components are defined as radiation safety classified:

- System that has a confinement barrier function.
- Control system that provides information on safety related process parameters and the ability to control safety features.

- System for mitigating release of radioactivity to the environment.
- Monitoring system for monitoring of radioactive emissions during normal operation and accidents.
- Systems for protection of confinement barriers.
- Systems for the supply of power and media to the system defined as safety related.
- Structures that prevent the spread of contamination within the facility.
- Structures that carry static loads and protects safety related systems.
- Fire mitigation systems for protection of safety related systems.

Some external systems that are not in this list – such as cranes – could compromise these classified safety systems. The risk could come from pressurised components, accumulated heat, potential chemical reactivity, or mass, (e.g. in case of an earthquake). Such components must be secured if they are in the vicinity of classified components, or they can simply be eliminated.

11.4 Conventional safety

The radiation safety question is important both for the public as well as for the ESS employees. The conventional safety is mainly an occupational safety issue for the ESS employees and the visiting scientists. For ESS construction the main focus will be on: fire safety; hydrogen; cryogenic safety; pressure vessels; electrical safety; chemical handling; and heights and heavy loads.

Fire safety

Prevention of fire is essential especially in high-energy physics facilities as ESS. A typical fire can arise from electrical cabinets, cables and high-voltage equipment. Other sources must also be considered in the analysis. The need for local fire fighting capabilities at ESS has to be analysed in more detail. At present no on-site local fire brigade is foreseen. A fire in the accelerator, target, instrument buildings and waste building may give rise to release of radioactive gases.

Hydrogen

Hydrogen will be used as ion source of the accelerator and as a moderator in the target monolith. The handling and use of hydrogen in the accelerator will be done according to existing regulations. The main hazard of handling and operating with hydrogen is the risk of explosion. Hence, the system will be designed to be intrinsically safe. Hydrogen has a low ignition point and therefore it is vital to remove or limit all possible ignition sources, e.g. electrical connections. The assessments of radionuclide inventory in the accelerator do not indicate that this will be of any major radiological risk. Within the target monolith there will be two circuits of hydrogen at 20 K and 1.5 MPa, which will be cooled by cryogenic helium. Empty rooms within the monolith will be filled with helium, which will reduce the risk of hydrogen explosion within the target. Further analyses of the potential risk have to be evaluated.

Cryogenics

The use of cryogenics liquids and evacuated vessels constitute a potential explosion hazard and risk of suffocation. Oxygen deficiency hazards must be considered in every space where cryogenics are present. A complete risk analysis will qualify the zone of operation. Experience and construction guidelines and regulations from existing accelerator laboratories will be used. Adequate ventilation and expansion volumes will be considered. Cryogenic safety will also be important for the safety at the instruments where liquefied nitrogen and helium will be used for experiments.

Pressure vessels

Apart from the cryogenic safety, ordinary pressure vessels regulations apply as any normal industrial activity. Pressure vessels or pressurised systems containing water will or may occur in the heat recycling systems and the cooling systems.

Electrical safety

Electrical safety is of vital importance, especially in the klystron gallery where several high-voltage components will be installed. Swedish regulations specifically give the distance between high-voltage equipment if to perform maintenance during operation.

Chemical handling

At the laboratories and at the instruments, safe handling of chemicals will be important. All chemicals that are handled within ESS are under restriction of REACH [691], the European legislation for handling of chemicals. The chemicals, which are planned to be used at ESS must be registered in a database, updated by ESS and containing safety fact sheets for handling of the individual chemicals.

Height and heavy loads

An important part for the occupational safety will be preventive measures regarding heights and handling of heavy loads. Specific regulations apply for the construction of cranes and lifting devices but also the planning of how the heavy load will be internally transported (lifting zones) will be done from a safety point of view. Work places and/or work task involving high heights will be analysed, estimated from a point of risks and followed by mitigating actions or procedures.

11.5 Security

The security of ESS will be designed to meet the basic in-house security rules and fulfilment of regulatory requirements as well as the need from the users and personnel to work in an open and friendly atmosphere. Apart from the obvious in-house security rules in preventing stealth and protection of equipment, the security requirements will be treated and integrated together with the safety requirements. Especially the zoning of the facility will be integrated taking into account radiation safety, fire safety and security. Systems for entry and zoning permissions will be designed and maybe fully integrated with the personal protection system described in Section 5.2.3.

Chapter 12

Conclusions

After more than 20 years of work we find ourselves at the point where the construction of ESS will begin. This comes about thanks to the dedication of countless hundreds, and perhaps thousands, of people who have contributed to bringing the project to where it is today. The publication in 2013 of the *Technical Design Report* demonstrates the fruits of that work – the scientific drive, the technological inventiveness, the administrative determination. We could not have reached this point without the support of our funding bodies and, ultimately, of the taxpayers who support the funding bodies. We are well aware of the responsibility we carry. We will deliver.

The TDR comes one year after the *Conceptual Design Report* (CDR) was published. It is not simply one year advanced from the CDR, but rather contains the work, the studies and the designs contributed by perhaps four times as many people as contributed to the CDR. There has been a multiplicative process in play. Equally well, whilst the CDR was more or less a stand-alone document, the TDR is but one of the whole sheaf of documents of more than one thousand pages that together represent the current state of knowledge. They in turn stand on the foundation studies and technical reports that have been produced over the last few years in Lund, in the laboratories of our partner countries and indeed around the world.

This body of knowledge has reached a certain state of maturity. It is, thanks to the nature of a scientific facility, incomplete. It will always be incomplete. However it represents what is both necessary and sufficient to allow a clear decision from funding bodies around Europe to officially start the construction phase of ESS.

As Ivan Turgenev said:

> *If we wait for the moment when everything, absolutely everything is ready, we shall never begin.*

It is time to begin!

Glossary

A2T	Accelerator to Target
ACS	Advanced Cyclone System
ADC	Analog to Digital Convertor
ADR	Accord Dangereux Routier
ADS	Accelerator Driven Reactor System
ADU	Accelerator Design Update project
ALARA	As Low As Reasonably Achievable
AMA	Allmän Material och Arbetsbeskrivning
ANL	Argonne National Laboratory, Argonne, USA
ANS	American Nuclear Society
ANSI	American National Standards Institute
ANT	Advanced Neutron Technologies
appm	Atomic Parts Per Million
ASIC	Application Specific Integrated Circuit
ASME	American Society of Mechanical Engineers
BAG	Swiss Federal Office of Public Health
Bas-P	Byggarbetsmiljösamordnare Planering
Bas-U	Byggarbetsmiljösamordnare Utförande
BDBA	Beyond Design Basis Accident
BEW	Beam Entrance Window
BC	Bandwidth Control
BCM	Beam Current Monitor
BCT	Beam Current Transformer
BDBA	Beyond Design Basis Accidents
BH90	Swedish recommendations for design and construction documentation
BHM	Beam Halo Monitor
BIM	Building information model/modelling
BLED	Beam Line Element Databases
BLM	Beam Loss Monitor
BLESS	Building Lifecycle at ESS
BMS	Building Management System
BNL	Brookhaven National Laboratory, Upton, USA
Brazil test	Laboratory test for tensile strength in rock according to ISRM 2007
BPM	Beam Position Monitor
BPS	Beam Permit System
BSAB96	Swedish classification system for building and Civil Engineering Works
BSM	Bunch Shape Monitor
BW	Bernstein Waves

CA	Channel Access
CAD	Computer Aided Design
CAMEA	Continuous Angle Multiple Energy Analyser
CAU	Consolidated Anisotropic Un-drained tri-axial test
CCB	Change Control Board
CCTV	Closed Circuit Television (Surveillance)
CDR	Conceptual Design Report
CE	The CE marking or formerly EC mark
CEA	Commissariat à l'Énergie Atomique
CEA-IFRU	CEA - Institut de Recherche sur les lois Fondamentales de l'Univers, Saclay, France
CEBAF	Continuous Electron Beam Accelerator Facility (See JLab)
CEED	Complex Environment Engineering Diffractometer
CERN	European Organisation for Nuclear Research
CF	Conventional Facilities division
CFD	Computational Fluid Dynamics
CGS	Cover Gas System
CHESS	Collaboration Home of ESS
CIEMAT	Centro de Investigaciones Energéticas Medioambientales y Tecnologicas
CIFT	Contactless Inductive Flow Tomography
CKM	Cabibbo-Kobayashi-Maskawa
CM	Configuration Management
CONCERT	ESS-CEA study on a multipurpose HPPA accelerator
COTS	Commercial Off The Shelf (equipment)
CPT	Cone Penetration Test according to ISO/DIS 22476-1
CPU	Computational Processing Unit
CRL	Compact Refractive Lenses
CRS	Constant Rate of Strain test, according to BS 1377
CS	Control System
CTL	Cryogenic Transfer Line
CTS	Cold Tuning System
CUB	Central Utility Building
CVD	Chemical Vapour Deposition
CW	Continuous Wave
DAC	Digital to Analog Converter
DB	DataBase
DBA	Design Basis Accident
DBTT	Ductile to Brittle Transition Temperature
DCF	Dose Conversion Factor
DESY	Deutsches Elektronen-Synkrotron, Hamburg, Germany
DFT	Density Functional Theory
DH	District Heating system
DI	Deionised (water)
DMSC	Data Management and Software Centre, Copenhagen, Denmark
DOE	U.S. Department of Energy
dpa	Displacements Per Atom
Drainage company	A community association having a jointly-owned facility to drain mainly arable land
DTL	Drift Tube Linac
DTU	Technical University of Denmark
DU	Design Update

E-BOM	Engineering Bill of Materials
ECR	Electron Cyclotron Resonance
ECR	Engineering Change Request
EERC	E.ON ENERGY RESEARCH CENTRE
EIA	Environmental Impact Assessment
ELV	Extra Low Voltage (< 50 V AC)
EM	Electromagnetic
EMC	Electromagnetic Compatibility
ENSA	European Neutron Scattering Association
EPICS	Experimental Physics and Industrial Controls
EPL	ESS Plant Layout
ERDA	Electron Recoil Detection Analysis
ESFRI	European Strategy Forum for Research Infrastructures
ESRF	European Synchrotron Radiation Facility, Grenoble, France
EUC	Equipment Under Control
EURISOL	EURopean ISOL
eV	Electron Volt
FAT	Factory Acceptance Test
FBA	Fast Beam Abort
FC	Faraday Cup
FEA	Finite Element Analysis
FEL	Free Electron Laser
FEM	Finite Element Method
FES	Front End Systems
FMECA	Failure Modes, Effects, and Criticality Analysis
FPD	Full Power Day
FPGA	Field Programmable Gate Array
FPY	Full Power Year
FREIA	Facility for Research instrumentation and Accelerator Development, Uppsala University
FRIB	Facility for Rare Isotope Beams, East Lansing, USA
FSAR	Final Safety Analysis Report
FWHM	Full Width at Half Maximum
FZJ	Forschungs Zentrum Jülich, Jülich, Germany
GANIL	Grand Accélérateur National d'Ions Lourds
GDR	Geo-technical Design Report
GEANT	Monte Carlo computer code for high energy particles transport simulation
GEDEON	GEstion DEchets par des Option Nouvelles
GEM	GEneral Materials diffractometer
GEMs	Gas Electron Multipliers
GISANS	Grazing Incidence Small Angle Neutron Scattering
GIR	Ground Investigation Report
GRID	Wire Grid
GSI	Gesellschaft für SchwerIonenforschung, Darmstadt, Germany
GSO	General Safety Objectives
HEBT	High Energy Beam Transport
HEDP	High Energy Differential Pumping
HEPA	High Efficiency Particulate Air
HfA	Dynamic probing according to SS-EN ISO 22476-2
HMI	Human Machine Interface
HOM	Higher Order Mode
HRS	Heat Removal System

HSE	Health, Safety and Environment
HTO	Hydrogen Tritium Oxide
HV	High Voltage (> 1 kV AC)
HVAC	Heating, Ventilation, and Air Conditioning
HZB	Helmholtz-Zentrum Berlin, Berlin, Germany
HZG	Helmholz-Zentrum Geesthacht
HZDR	Helmholtz-Zentrum Dresden-Rossendolf, Dresden, Germany
IAEA	International Atomic Energy Agency
IAS	Integration, Acceptance and Support activities
IC	Ionisation Chamber
ICC	Integrated Control Centre
ICND	International Collaboration for the development of Neutron Detectors
ICS	Integrated Control System
ID	Immediate Dismantlement
IE	Initiating Event
IEC	International Electrotechnical Commission
IFMIF	International Fusion Materials Irradiation Facility
IGES	Initial Graphics Exchange Specification
IGBT	Insulated Gate Bipolar Transistor
IGCT	Integrated gate Commutated Thyristors
ILL	Institut Laue-Langevin
INFN	Istituto Nazionale di Fisica Nucleaire
INFN - LNS	INFN -Laboratori Nazionale del Sud, Catania, Italy
INS	Inelastic Neutron Scattering
INSAG	International Nuclear Safety Advisory Group
I/O	Input-Output
IOC	Input-Output Controller
IPF	Instrumented Protective Function
IPHI	Injecteur de Proton de Haute Intensité
IPM	Ionisation Profile Monitor
IPNO	l'Institut de Physique Nucléaire d'Orsay, Orsay, France
IPUL	Institute of Physics, University of Latvia, Latvia
ISD	Imaging System Device
ISIS	ISIS Pulsed Spallation Neutron Source, Didcot, United Kingdom
ISO	International Organisation for Standardisation
ITER	International Thermonuclear Experimental Reactor, Cadarache, France
Jb3, Jb-total	Swedish soil- and rock sampling according to SGF Report 2:99 and 1:2006
J-PARC	Japan Proton Accelerator Research Complex, Tokai, Japan
J-SNS	Japanese Spallation Neutron Source
JAERI	Japan Atomic Energy Research Institute, Tokai, Japan
JLab	Thomas Jefferson National Accelerator Facility
Kb	Core drilling of soil and rock for core samples, according to SS-EN ISO 22475-1
KEK	High Energy Accelerator Research Organisation, Tsukuba, Japan
KEKB	KEK B factory project
KIT	Karlsruher Institut für Technologie, Karlsruhe, Germany
KU	Copenhagen University, Copenhagen, Denmark
LAN	Local Area Network
LANL	Los Alamos National Laboratory, Los Alamos, USA
LANSCE	Los Alamos Neutron Science Center, Los Alamos, USA
LBE	Lead-Bismuth Eutectic
LBNL	Lawrence Berkeley National Laboratory, Berkeley, USA
LCC	Life Cycle Costing

LDF	Location Data Files
LDV	Laser Doppler Vibrometer
LEBT	Low-Energy Beam Transport
LEDP	Low Energy Differential Pumping
LEKAB	Lunds Energikoncernen AB
LHC	Large Hadron Collider
LH_2	Liquid Hydrogen
LHe	Liquid Helium
Linac	Linear Accelerator
LINXS	Lund Institute for Neutron and X-Ray Science
LLLW	Low-Level Liquid Waste
LLRF	Low Level RF
LO	Local Oscillator
LOCA	Loss-of-Coolant Accident
LOFA	Loss-of-Flow Accident
LOHS	Loss-of-Heat Sink
LPM	Luminescence Profile Monitor
LTCF	Lost Time due to Component Failure
LV	Low Voltage (< 1 kV AC)
LWU	Linac Warm Units
MASW	Multichannel Analysis of Surface Waves
MAWP	Maximum Allowable Working Pressure
MAX IV	The MAX IV Laboratory comprising MAX-lab and the MAX IV project, Lund, Sweden
MCNPX	Monte Carlo N-Particle eXtended
MCS	Machine Coordinate System
MDIS	Microwave Discharge Ion Source
MEA	Membrane-Electrode Assembly
MEBT	Medium Energy Beam Transport
MEGAPIE	Megawatt Pilot Experiment, PSI
MEP	Mechanical Electrical Plumbing
META:LIC	MEgawatt TArget: Lead bIsmuth Cooled
MID	MPS Input Device
MIS	Machine Interlock System
MOD	MPS Output Device
MOF	Metal-Organic Framework
MOSFET	Metal Oxide Semiconductor Field Effect Transistor
MPS	Machine Protection System
MR	Moderator-Reflector
MSGCS	Micro-Strip Gas Counters
MTBF	Mean Time Between Failures
MTTR	Mean Time to Repair
MYRRHA	A multipurpose neutron source for R&D applications based on ADS
MV	Medium Voltage (50 kV – 1 kV AC)
NBGI	Neutron Beam Guide Inserts
NC	Normally Closed
NMI3	Integrated Infrastructure Initiative for Neutron Scattering and Muon Spectroscopy
NMR	Nuclear Magnetic Resonance
NPI	Next Pulse Inhibit
NPM	Non-invasive Profile Monitor
NSE	Neutron Spin Echo
NSWG	Norms and Standards Working Group
nToF	Neutron Time of Flight
NuPECC	Nuclear Physics European Collaboration Committee

ODH	Oxygen Deficiency Hazards
OLED	Organic Light Emitting Diodes
ORNL	Oak Ridge National Laboratory, Oak Ridge, USA
P&ID	Process and Instrumentation Diagram
PBS	Particle Beam Scanner
PBS	Product Breakdown Structure
PBW	Proton Beam Window
PCS	Pressure Control System
PCV	Pressure Control Valve
PE	Protective Earth
PED	Pressure Equipment Directive
PFD	Probability of Failure on Demand
PFH	Probability of Failure per Hour
PGS	Power generation and storage systems
PID	Piping and Instrument Diagram
PLC	Programmable Logic Controller
PLM	Product Lifecycle Management
PMQ	Permanent Magnet Quadrupole
PMR	Pre-moderator/Moderator/Reflector
PMS	Post Mortem System
PMT	Photo-Multiplier Tube
PPS	Personnel Protection System
PRA	Probabilistic Risk Assessment
PRDS	Phase Reference Distribution System
PSAR	Preliminary Safety Analysis Report
PSB	Partnership for Structural Biology
PSD	Particle Size Distribution
PS-ESS	Proton Source ESS
PSI	Paul Scherrer Institut, Villigen, Switzerland
PV	Process Variable
QA	Quality Assurance
QENS	Quasi-Elastic Neutron Spectroscopy
RAKEL	RAdioKommunikation för Effektiv Ledning
RF	Radio Frequency
RFA	Release Factors for Aerosols
RFQ	Radio Frequency Quadrupole
RFV	Release Factor for Volatiles
RGEC	Radioactive Gases and Effluents Confinement
ROM	Rough Order of Magnitude
ROTHETA	Rotating Helium gas cooled Tungsten (ESS target)
RPM	RPM Package Manager, recursively referring to a package management system
RRM	Repetition-Rate Multiplication
RTC	Real Time Clock
RTD	Resistance Temperature Detector
RWTH Aachen	Aachen University, Aachen, Germany
SANS	Small Angle Neutron Scattering
SAR	Safety Analysis Report
SAT	Site Acceptance Test
SB	Safety barrier
SB11	Swedish recommendations for CAD: Svensk Byggtjänst - Rekommendationer 11
SC	Superconducting

SCADA	Supervisory Control And Data Acquisition
SCC	Space Charge Compensation
SCL	Superconducting Linac
SCRF	Superconducting Radio Frequency
SCS	Site-wide Coordinate System
SEM	Scanning Electron Microscope
SEM	Secondary Emission Monitor
SEOP	Spin Exchange Optical Pumping
SFK-waste	Heat-generating radioactive waste
SFL	Framtida slutförvar för långlivat låg-och medelaktivt avfall, a site for long-lived radioactive waste
SFL-waste	Long-lived low-and intermediate level waste
SFR	Slutförvaret för kortlivat radioaktivt avfall, a final repository for short-lived radioactive waste
SFR-waste	Short-lived low- and intermediate level waste
SI	System Internationale
SIL	Safety Integrity Level
SILHI	High Intensity Light Ion Source
SINQ	Continous Spallation Neutron Source
SKB	Svensk Kärnbränslehantering AB
Skr	Auger sampling according to SS-EN ISO 22475-1
Slake durability	Test on clay stone according to ISRM 2006 part 2
SLLW	Solid Low-Level Waste
SMA	Serviceability, Maintainability and Accessibility
SNG	Standards, Norms and Guidelines
SNS	Spallation Neutron Source, Oak Ridge, USA
SPIRAL2	Système de Production d'Ions Radioactifs en Ligne 2
SRF	See SCRF
SS	Swedish Standard
SSC	Superconducting SuperCollider
SSM	Strålsäkerhetsmyndigheten; The Swedish Radiation Safety Authority
STEP	Standard for the Exchange of Product model data
STF	SäkerhetsTekniska Föreskrifter
SysML	System Modelling Language
TE	Total Elongation
T&E	Test and Evaluation
TDR	Technical Design Report
TLA	Three Letter Acronym
TMP	TurboMolecular Pump
TMR	Target/Moderator/Reflector
TOF	Time of Flight
TRIP	Transformation Induced Plasticity
TS	Target Station
TS	Timing System
TSS	Target Safety System
TTF	Tesla Testbed Facility
TÜV	Technischer Überwachungsverein
UCS	Laboratory test for compressive strength in rock
UDV	Ultrasound Doppler-Velocimetry
UHV	Ultra High Vacuum
UPR	Upper Hybrid Resonance
UPS	Uninterruptable Power System
UTS	Ultimate Tensile Stress

V&V	Verification and Validation
Vb	Field vane test according to ISO/DIS 22476-9
VIS	Versatile Ion Source
VLP	Very Low Pressure (helium)
WBS	Work Breakdown Structure
WFM	Wavelength-Frame Multiplication
WLAN	Wireless Local Area Network
WS	Wire Scanner
WSF	Wavelength-Shifting Fibres
XFEL	X-Ray Free Electron Laser
YS	Yield Stress

Bibliography

[1] E. H. Lehmann and D. Mannes. 'Wood investigations by means of radiation transmission techniques.' *Journal of Cultural Heritage*, 13(3, Supplement):S35–S43, 2012. ISSN 1296-2074. doi:10.1016/j.culher.2012.03.017. Wood Science for Conservation.

[2] C. Castelnovo, R. Moessner, and S. L. Sondhi. 'Magnetic monopoles in spin ice.' *Nature*, 451:42–45, 2008.

[3] S. Mühlbauer et al. 'Skyrmion lattice in a chiral magnet.' *Science*, 323(5916), 2009.

[4] D. Butler. 'Europe is warned of a 'neutron drought'...' *Nature*, 379:284, 1996.

[5] D. Butler. '...and warns of need for more neutron sources.' *Nature*, 396:8, 1998.

[6] D. Richter and T. Springer. 'A twenty years forward look at neutron scattering facilities in the OECD countries and Russia.' Technical report, European Science Foundation, Organisation for Economic Co-operation and Development Megascience Forum, 1998.

[7] European Neutron Scattering Association (ENSA). *Survey of the Neutron Scattering Community and Facilities in Europe*, 1998.

[8] European Science Foundation (ESF) and European Neutron Scattering Association(ENSA). *Survey of the Neutron Scattering Community in Europe*, 2005.

[9] F. H. Bohn et al. 'European source of science.' In *The ESS Project*, volume 1. European Spallation Source, May 2002.

[10] D. Richter. 'New science and technology for the 21st century.' In *The ESS Project*, volume 2. European Spallation Source, May 2002.

[11] F. H. Bohn et al. 'Technical report.' In *The ESS Project*, volume 3. European Spallation Source, May 2002.

[12] G. S. Bauer et al. 'Technical report status 2003.' In *The ESS Project*, volume 3 Update. European Spallation Source, Dec 2003.

[13] 'Instruments and user support.' In K. Clausen et al., editors, *The ESS Project*, volume 4. European Spallation Source, May 2002.

[14] European Strategy Forum on Research Infrastructures. *Strategy Report on Research Infrastructures - Roadmap 2010*. Luxembourg, Publications Office of the European Union, 2011. ISBN: 978-92-79-16828-4.

[15] 'ESS Science Symposia.' http://www.europeanspallationsource.se/ess-science-symposia, last accessed March 24 2013.

[16] Editors E. Janod, F. Leclercq-Hugeux, H. Mutka, J. Teixeira. 'Neutrons, sciences and perspectives.' *The European Physics Journal Special Topics*, 213, 2012.

[17] Komitee Forschung mit Neutronen. 'Perspectives of neutron research in Germany.' http://sni-portal.uni-kiel.de/kfn/kfn/SP11/Perspektiven_der_Neutronenforschung_in_Deutschland_2011-engl.pdf, last accessed March 25 2013.

[18] H. Abele. 'The neutron. Its properties and basic interactions.' *Progress in Particle and Nuclear Physics*, 60(1):1–81, 2008.

[19] S. Profumo, M. J. Ramsey-Musolf, and S. Tulin. 'Supersymmetric contributions to weak decay correlation coefficients.' *Physical Review D*, 75, 2007.

[20] K. H. Lee, P. E. Schwenn, A. R. G. Smith, et al. 'Morphology of all-solution-processed "bilayer" organic solar cells.' *Advanced Materials*, 23(6):766–770, 2011. ISSN 1521-4095. doi:10.1002/adma.201003545.

[21] S. Schorr. 'The crystal structure of kesterite type compounds: A neutron and X-ray diffraction study.' *Solar Energy Materials and Solar Cells*, 95(6):1482–1488, 2011. ISSN 0927-0248. doi:10.1016/j.solmat.2011.01.002. Special Issue: Thin film and nanostructured solar cells.

[22] A. J. Parnell, A. D. F. Dunbar, A. J. Pearson, et al. 'Depletion of PCBM at the cathode interface in P3HT/PCBM thin films as quantified via neutron reflectivity measurements.' *Advanced Materials*, 22(22):2444–2447, 2010. ISSN 1521-4095. doi:10.1002/adma.200903971.

[23] S.-I. Nishimura, G. Kobayashi, K. Ohoyama, et al. 'Experimental visualization of lithium diffusion in Li_xFePO_4.' *Nature Materials*, 7(9):707–711, 2008. ISSN 14761122.

[24] A. Magraso, J. M. Polfus, C. Frontera, et al. 'Complete structural model for lanthanum tungstate: A chemically stable high temperature proton conductor by means of intrinsic defects.' *Journal of Materials Chemistry*, 22:1762–1764, 2012. doi:10.1039/C2JM14981H.

[25] G. Gebel, S. Lyonnard, H. Mendil-Jakani, et al. 'The kinetics of water sorption in Nafion membranes: A small-angle neutron scattering study.' *Journal of Physics: Condensed Matter*, 23(23):234107, 2011.

[26] V. Keppens, D. Mandrus, B. C. Sales, et al. 'Localized vibrational modes in metallic solids.' *Nature*, 395(6705):876–878, 1998.

[27] Y. Yan, I. Telepeni, S. Yang, et al. 'Metal-organic polyhedral frameworks: High H2 adsorption capacities and neutron powder diffraction studies.' *Journal of the American Chemical Society*, 132(12):4092–4094, 2010. doi:10.1021/ja1001407. PMID: 20199070.

[28] C. M. Brown, Y. Liu, T. Yildirim, et al. 'Hydrogen adsorption in HKUST-1: A combined inelastic neutron scattering and first-principles study.' *Nanotechnology*, 20(20):204025, 2009.

[29] C. R. Clarkson, M. Freeman, L. He, et al. 'Characterization of tight gas reservoir pore structure using USANS/SANS and gas adsorption analysis.' *Fuel*, 95(0):371–385, 2012.

[30] Y. B. Melnichenko, L. He, R. Sakurovs, et al. 'Accessibility of pores in coal to methane and carbon dioxide.' *Fuel*, 91(1):200–208, 2012.

[31] S. Yang, J. Sun, A. J. Ramirez-Cuesta, et al. 'Selectivity and direct visualization of carbon dioxide and sulfur dioxide in a decorated porous host.' *Nature Chemistry*, 4(11):887–894, 2012.

[32] A. E. Whitten et al. 'Cardiac myosin-binding protein C decorates F-actin: Implications for cardiac function.' In *Proceedings of the National Academy of Sciences*, volume 105, pages 18360–18365. 2008.

[33] M. P. Christie, A. E. Whitten, G. J. King, et al. 'Low-resolution solution structures of Munc18:Syntaxin protein complexes indicate an open binding mode driven by the Syntaxin N-peptide.' *Proceedings of the National Academy of Sciences*, 109(25):9816–9821, Jun 2012. ISSN 1091-6490 (Electronic); 0027-8424 (Linking). doi:10.1073/pnas.1116975109.

[34] A. M. Hofmann, F. Wurm, E. Hühn, et al. 'Hyperbranched polyglycerol-based lipids via oxyanionic polymerization: Toward multifunctional stealth liposomes.' *Biomacromolecules*, 11(3):568–574, 2010. doi:10.1021/bm901123j. PMID: 20121134.

[35] S. V. Ghugare, E. Chiessi, B. Cerroni, et al. 'Biodegradable dextran based microgels: A study on network associated water diffusion and enzymatic degradation.' *Soft Matter*, 8(8):2494–2502, 2012.

[36] C. Sanson, O. Diou, J. Thévenot, et al. 'Doxorubicin loaded magnetic polymersomes: Theranostic nanocarriers for MR imaging and magneto-chemotherapy.' *ACS Nano*, 5(2):1122–1140, 2011. doi: 10.1021/nn102762f.

[37] K. Wood et al. 'Coupling of protein and hydration-water dynamics in biological membranes.' In *Proceedings of the National Academy of Sciences*, volume 104, pages 18049–18054. 2007.

[38] J. Pieper et al. 'Transient protein softening during the working cycle of a molecular machine.' *Physical Review Letters*, 100:228103, 2008.

[39] S. E. Oswald et al. 'Quantitative imaging of infiltration, root growth, and root water uptake via neutron radiography.' *Vadose Zone Journal*, 7(3):1035–1047, 2008.

[40] D. R. Lee et al. 'Polarized neutron scattering from ordered magnetic domains on a mesoscopic permalloy antidot array.' *Applied Physics Letters*, 82, 2003.

[41] B. Van de Wiele, A. Manzin, A. Vansteenkiste, et al. 'A micromagnetic study of the reversal mechanism in permalloy antidot arrays.' *Journal of Applied Physics*, 111(5):053915, 2012.

[42] D. Argyriou. 'ESS preliminary operations project specification.' Internal Document ESS-0001132, European Spallation Source, 28 Nov 2012.

[43] B. Lonetti, M. Camargo, J. Stellbrink, et al. 'Ultrasoft colloid-polymer mixtures: Structure and phase diagram.' *Physical Review Letters*, 106(22):228301, 2011.

[44] J. Gummel, M. Sztucki, T. Narayanan, et al. 'Concentration dependent pathways in spontaneous self-assembly of unilamellar vesicles.' *Soft Matter*, 7(12):5731–5738, 2011.

[45] K. Bressel, M. Muthig, S. Prévost, et al. 'Mesodynamics: Watching vesicle formation in situ by small-angle neutron scattering.' *Colloid & Polymer Science*, 288(8):827–840, 2010.

[46] A. P. R. Eberle and L. Porcar. 'Flow-SANS and Rheo-SANS applied to soft matter.' *Current Opinion in Colloid and Interface Science*, 17(1):33–43, 2012.

[47] T. C. B. McLeish, N. Clarke, E. de Luca, et al. 'Neutron flow-mapping: Multiscale modelling opens a new experimental window.' *Soft Matter*, 5(22):4426–4432, 2009.

[48] R. S. Graham, J. Bent, N. Clarke, et al. 'The long-chain dynamics in a model homopolymer blend under strong flow: Small-angle neutron scattering and theory.' *Soft Matter*, 5(12):2383–2389, 2009.

[49] J. Penfold and I. Tucker. 'Flow-induced effects in mixed surfactant mesophases.' *The Journal of Physical Chemistry B*, 111(32):9496–9503, 2007.

[50] D. J. Waters, K. Engberg, R. Parke-Houben, et al. 'Structure and mechanism of strength enhancement in interpenetrating polymer network hydrogels.' *Macromolecules*, 44(14):5776–5787, 2011.

[51] H.-G. Peng, M. Tyagi, K. A. Page, et al. 'Inelastic neutron scattering on polymer electrolytes for lithium-ion batteries.' In *Polymers for Energy Storage and Delivery: Polyelectrolytes for Batteries and Fuel Cells*, volume 1096 of *ACS Symposium Series*, chapter 5, pages 67–90. American Chemical Society, 2012.

[52] F. Barroso-Bujans, F. Fernandez-Alonso, J. A. Pomposo, et al. 'Macromolecular structure and vibrational dynamics of confined poly(ethylene oxide): From subnanometer 2d-intercalation into graphite oxide to surface adsorption onto graphene sheets.' *ACS Macro Letters*, 1(5):550–554, 2012.

[53] M. Laurati, P. Sotta, D. R. Long, et al. 'Dynamics of water absorbed in polyamides.' *Macromolecules*, 45(3):1676–1687, 2012.

[54] A. R. G. Smith, K. H. Lee, A. Nelson, et al. 'Diffusion - The hidden menace in organic optoelectronic devices.' *Advanced Materials*, 24(6), Dec 2011.

[55] H. Cavaye, P. E. Shaw, A. R. G. Smith, et al. 'Solid state dendrimer sensors: Effect of dendrimer dimensionality on detection and sequestration of 2,4-dinitrotoluene.' *The Journal of Physical Chemistry C*, 115(37):18366–18371, 2011. doi:10.1021/jp205586s.

[56] A. Angus-Smyth, R. A. Campbell, and C. D. Bain. 'Dynamic adsorption of weakly interacting polymer/surfactant mixtures at the air/water interface.' *Langmuir*, 28(34):12479–12492, 2012. doi:10.1021/la301297s.

[57] W. Wang, G. Kaune, J. Perlich, et al. 'Swelling and switching kinetics of gold coated end-capped poly(N-isopropylacrylamide) thin films.' *Macromolecules*, 43(5):2444–2452, 2010.

[58] A. Zarbakhsh, J. R. P. Webster, and J. Eames. 'Structural studies of surfactants at the oil-water interface by neutron reflectometery.' *Langmuir*, 25(7):3953–3956, 2009.

[59] M. Chen, C. Dong, J. Penfold, et al. 'Adsorption of sophorolipid biosurfactants on their own and mixed with sodium dodecyl benzene sulfonate, at the air/water interface.' *Langmuir*, 27(14):8854–8866, 2011. doi:10.1021/la201660n.

[60] X. Zhang, B. C. Berry, K. G. Yager, et al. 'Surface morphology diagram for cylinder-forming block copolymer thin films.' *ACS Nano*, 2(11):2331–2341, 2008.

[61] M. S. Hellsing, V. Kapaklis, A. R. Rennie, et al. 'Crystalline order of polymer nanoparticles over large areas at solid/liquid interfaces.' *Applied Physics Letters*, 100(22):221601–4, 2012.

[62] T. Chatterjee, C. A. Mitchell, V. G. Hadjiev, et al. 'Hierarchical Polymer-Nanotube Composites.' *Advanced Materials*, 19(22):3850–3853, Oct 2007.

[63] D. W. Schaefer and R. S. Justice. 'How nano are nanocomposites?' *Macromolecules*, 40(24):8501–8517, Oct 2007.

[64] N. J. Wagner and E. D. Wetzel. 'Advanced body armor utilizing shear thickening fluids.', Jun 2007. US Patent 7,226,878.

[65] Y. S. Lee and N. J. Wagner. 'Rheological properties and small-angle neutron scattering of a shear thickening, nanoparticle dispersion at high shear rates.' *Industrial and Engineering Chemistry Research*, 45(21):7015–7024, 2006. doi:10.1021/ie0512690.

[66] P. Akcora, S. K. Kumar, V. García Sakai, et al. 'Segmental dynamics in PMMA-grafted nanoparticle composites.' *Macromolecules*, 43(19):8275–8281, 2010. doi:10.1021/ma101240j.

[67] P. Vandoolaeghe, A. R. Rennie, R. A. Campbell, et al. 'Adsorption of cubic liquid crystalline nanoparticles on model membranes.' *Soft Matter*, 4:2267–2277, 2008. doi:10.1039/B801630E.

[68] Y. Gerelli, L. Porcar, and G. Fragneto. 'Lipid rearrangement in DSPC/DMPC bilayers: A neutron reflectometry study.' *Langmuir*, 28(45):15922–15928, 2012. doi:10.1021/la303662e.

[69] A. Lopez-Rubio and E. P. Gilbert. 'Neutron scattering: A natural tool for food science and technology research.' *Trends in Food Science & Technology*, 20(11-12):576–586, 2009. ISSN 0924-2244. doi:10.1016/j.tifs.2009.07.008.

[70] S. Z. Fisher, M. Aggarwal, A. Y. Kovalevsky, et al. 'Neutron diffraction of acetazolamide-bound human carbonic anhydrase II reveals atomic details of drug binding.' *Journal of the American Chemical Society*, 134(36):14726–14729, 2012. doi:10.1021/ja3068098.

[71] J. P. Abrahams et al. 'Structure at 2.8 Å resolution of F_1-ATPase from bovine heart mitochondria.' *Nature*, 370(6491):621–628, 1994.

[72] B. P. Pedersen et al. 'Crystal structure of the plasma membrane proton pump.' *Nature*, 450(7172):1111–1114, 2007.

[73] J. Kellosalo et al. 'The structure and catalytic cycle of a sodium-pumping pyrophosphatase.' *Science*, 337(6093):473–476, Jul 2012.

[74] E. Balog et al. 'Direct determination of vibrational density of states change on ligand binding to a protein.' *Physical Review Letters*, 93:28103, 2004.

[75] Z. Bu et al. 'Coupled protein domain motion in Taq polymerase revealed by neutron spin-echo spectroscopy.' In *Proceedings of the National Academy of Sciences*, volume 102, pages 17646–17651. 2005.

[76] O. G. Mouritsen. *Life - As a Matter of Fat: The Emerging Science of Lipidomics*. Springer, Berlin Heidelberg, 2005.

[77] K. Simons, E. Ikonen, et al. 'Functional rafts in cell membranes.' *Nature*, 387(6633):569, 1997.

[78] A. Chenal et al. 'Deciphering membrane insertion of the diphtheria toxin T domain by specular neutron reflectometry and solid-state NMR spectroscopy.' *Journal of Molecular Biology*, 391(5):872–883, 2009.

[79] A. P. Le Brun, S. A. Holt, et al. 'Monitoring the assembly of antibody-binding membrane protein arrays using polarised neutron reflection.' *European Biophysics Journal with Biophysics Letters*, 37(5):639–645, 2008.

[80] C. Johnson et al. 'Structural studies of the neural-cell-adhesion molecule by X-ray and neutron reflectivity.' *Biochemistry*, 44(2):546–554, Dec 2005.

[81] L. A. Clifton et al. 'Low resolution structure and dynamics of a colicin-receptor complex determined by neutron scattering.' *Journal of Biological Chemistry*, 287(1):337–346, Jan 2012.

[82] S. Garg et al. 'Noninvasive neutron scattering measurements reveal slower cholesterol transport in model lipid membranes.' *Biophysical Journal*, 101(2):370–377, 2011.

[83] C. K. Wang, H. P. Wacklin, and D. J. Craik. 'Cyclotides insert into lipid bilayers to form membrane pores and destabilize the membrane through hydrophobic and phosphoethanolamine-specific interactions.' *Journal of Biological Chemistry*, 288, in press 2013. doi:10.1074/jbc.M112.421198.

[84] K. C. Thompson, A. R. Rennie, M. D. King, et al. 'Reaction of a phospholipid monolayer with gas-phase ozone at the air/water interface: Measurement of surface excess and surface pressure in real time.' *Langmuir*, 26(22):17295–17303, 2010.

[85] D. Lingwood and K. Simons. 'Lipid rafts as a membrane-organizing principle.' *Science*, 327(5961):46–50, 2010.

[86] I. Vattulainen and O. G. Mouritsen. 'Diffusion in membranes.' In P. Heitjans and J. Kärger, editors, *Diffusion in Condensed Matter: Methods, Materials, Models*, pages 471–509. Springer-Verlag, Berlin, 2nd edition, 2005.

[87] C. L. Armstrong, M. A. Barrett, A. Hiess, et al. 'Effect of cholesterol on the lateral nanoscale dynamics of fluid membranes.' *European Biophysics Journal*, pages 1–13, 2012.

[88] C. L. Armstrong et al. 'Co-existence of gel and fluid lipid domains in single-component phospholipid membranes.' *Soft Matter*, 8(17):4687–4694, 2012.

[89] C. L. Armstrong et al. 'Diffusion in single supported lipid bilayers studied by quasi-elastic neutron scattering.' *Soft Matter*, 6(23):5864–5867, 2010.

[90] M. Rheinstädter. 'Dynamics of soft matter.' chapter Lipid Membrane Dynamics, pages 263–286. Springer, 2012.

[91] A. Stradner, G. Foffi, N. Dorsaz, et al. 'New insight into cataract formation: Enhanced stability through mutual attraction.' *Physical Review Letters*, 99(19):198103, 2007.

[92] F. Roosen-Runge, M. Hennig, T. Seydel, et al. 'Protein diffusion in crowded electrolyte solutions.' *Biochimica et Biophysica Acta (BBA)-Proteins & Proteomics*, 1804(1):68–75, 2010.

[93] M. Heinen, F. Zanini, F. Roosen-Runge, et al. 'Viscosity and diffusion: Crowding and salt effects in protein solutions.' *Soft Matter*, 8(5):1404–1419, 2012.

[94] V. L. Ginzburg. 'Nobel Lecture: On superconductivity and superfluidity (what I have and have not managed to do) as well as on the "physical minimum" at the beginning of the XXI century.' *Review of Modern Physics*, 76:981–998, Dec 2004. doi:10.1103/RevModPhys.76.981.

[95] J. M. Tranquada et al. 'Neutron-scattering study of the dynamical spin susceptibility in $YBa_2Cu_3O_{6.6}$.' *Physical Review B*, 46:5561–5575, 1992.

[96] L. W. Harriger, O. J. Lipscombe, C. Zhang, et al. 'Temperature dependence of the resonance and low-energy spin excitations in superconducting $FeTe_{0.6}Se_{0.4}$.' *Physical Review B*, 85:054511, Feb 2012. doi:10.1103/PhysRevB.85.054511.

[97] N. Tsyrulin, R. Viennois, E. Giannini, et al. 'Magnetic hourglass dispersion and its relation to high-temperature superconductivity in iron-tuned $Fe_{1+y}Te_{0.7}Se_{0.3}$.' *New Journal of Physics*, 14(7):073025, 2012.

[98] P. Bourges and Y. Sidis. 'Novel magnetic order in the pseudogap state of high-T_C copper oxides superconductors.' *Comptes Rendus Physique*, 12(5-6):461–479, 2011. ISSN 1631-0705. doi: 10.1016/j.crhy.2011.04.006. Superconductivity of strongly correlated systems — Supraconductivité des systèmes fortement corrélés.

[99] T. Fennell et al. 'Magnetic Coulomb phase in the spin ice $Ho_2Ti_2O_7$.' *Science*, 326(5951):415–417, 2009.

[100] D. J. P. Morris, D. A. Tennant, S. A. Grigera, et al. 'Dirac strings and magnetic monopoles in the spin ice $Dy_2Ti_2O_7$.' *Science*, 326(5951):411–414, 2009. doi:10.1126/science.1178868.

[101] L. J. Chang, S. Onoda, Y. Su, et al. 'Higgs transition from a magnetic Coulomb liquid to a ferromagnet in $Yb_2Ti_2O_7$.' *Nature Communications*, 3:992, 2012.

[102] H. v. Löhneysen et al. 'Fermi-liquid instabilities at magnetic quantum phase transitions.' *Review of Modern Physics*, 79:1015, 2007.

[103] M. Enderle et al. 'Two-spinon and four-spinon continuum in a frustrated ferromagnetic spin-1/2 chain.' *Physical Review Letters*, 104:237207, 2010.

[104] C. H. Back, D. Weller, J. Heidmann, et al. 'Magnetization reversal in ultrashort magnetic field pulses.' *Physical Review Letters*, 81:3251–3254, Oct 1998. doi:10.1103/PhysRevLett.81.3251.

[105] S. J. Gamble, M. H. Burkhardt, A. Kashuba, et al. 'Electric field induced magnetic anisotropy in a ferromagnet.' *Physical Review Letters*, 102:217201, May 2009. doi:10.1103/PhysRevLett.102.217201.

[106] S. O. Mariager, F. Pressacco, G. Ingold, et al. 'Structural and magnetic dynamics of a laser induced phase transition in FeRh.' *Physical Review Letters*, 108:087201, Feb 2012. doi:10.1103/PhysRevLett.108.087201.

[107] H. Zabel and K. Theis-Bröhl. 'Polarized neutron reflectivity and scattering studies of magnetic heterostructures.' *Journal of Physics: Condensed Matter*, 2003.

[108] A. Ohtomo and H. Y. Hwang. 'A high-mobility electron gas at the $LaAlO_3/SrTiO_3$ heterointerface.' *Nature*, 427(6973):423–426, 2004.

[109] C. A. F. Vaz. 'Electric field control of magnetism in multiferroic heterostructures.' *Journal of Physics: Condensed Matter*, 24:333201, 2012.

[110] M. L. Baker, T. Guidi, S. Carretta, et al. 'Spin dynamics of molecular nanomagnets unravelled at atomic scale by four-dimensional inelastic neutron scattering.' *Nature Physics*, 8:906–911, Sep 2012.

[111] P. C. Canfield et al. 'Still alluring and hard to predict at 100.' *Nature Materials*, 10(4):259, 2011.

[112] Y. W. Long, N. Hayashi, T. Saito, et al. 'Temperature-induced A-B intersite charge transfer in an A-site-ordered LaCu(3)Fe(4)O(12) perovskite.' *Nature*, 458(7234):60–63, 2009.

[113] D. Kan, T. Terashima, R. Kanda, et al. 'Blue-light emission at room temperature from Ar^+-irradiated $SrTiO_3$.' *Nature Materials*, 4(11):816–819, 2005.

[114] M. Azuma, W. Chen, H. Seki, et al. 'Colossal negative thermal expansion in BiNiO3 induced by intermetallic charge transfer.' *Nature Communications*, 2:347, 2011.

[115] M. Burrard-Lucas, D. G. Free, S. J. Sedlmaier, et al. 'Enhancement of superconducting transition temperature of FeSe by intercalation of a molecular spacer layer.' *arXiv preprint arXiv:1203.5046*, 2012.

[116] E. H. Kisi and C. J. Howard. *Applications of Neutron Powder Diffraction*. Oxford Series on Neutron Scattering in Condensed Matter. Oxford University Press, 2008.

[117] V. M. Nield and D. A. Keen. *Diffuse Neutron Scattering from Crystalline Materials*. Oxford Series on Neutron Scattering in Condensed Matter. Oxford University Press, 2001.

[118] C. C. Wilson. *Single Crystal Neutron Diffraction from Molecular Materials*. Series on Neutron Techniques and Applications. World Scientific, 2000.

[119] T. E. Engin, A. V. Powell, R. Haynes, et al. 'A high temperature cell for simultaneous electrical resistance and neutron diffraction measurements.' *Review of Scientific Instruments*, 79(9), Sep 2008. ISSN 0034-6748. doi:{10.1063/1.2979011}.

[120] K. M. Ok, D. O'Hare, R. I. Smith, et al. 'New large volume hydrothermal reaction cell for studying chemical processes under supercritical hydrothermal conditions using time-resolved in situ neutron diffraction.' *Review of Scientific Instruments*, 80(12), Dec 2010. ISSN 0034-6748. doi:{10.1063/1.3514990}.

[121] H. Wu, W. Zhou, and T. Yildirim. 'High-capacity methane storage in metal-organic frameworks M_2(dhtp): The important role of open metal sites.' *Journal of the American Chemical Society*, 131(13):4995–5000, Apr 2009. ISSN 0002-7863. doi:{10.1021/ja900258t}.

[122] P. J. McGlinn, F. C. de Beer, L. P. Aldridge, et al. 'Appraisal of a cementitious material for waste disposal: Neutron imaging studies of pore structure and sorptivity.' *Cement and Concrete Research*, 40(8):1320–1326, Aug 2010. ISSN 0008-8846. doi:{10.1016/j.cemconres.2010.03.011}.

[123] R. I. Walton, F. Millange, R. I. Smith, et al. 'Real time observation of the hydrothermal crystallization of barium titanate using in situ neutron powder diffraction.' *Journal of the American Chemical Society*, 123(50):12547–12555, Dec 2001. ISSN 0002-7863. doi:{10.1021/ja011805p}.

[124] S. Takami, K.-I. Sugioka, T. Tsukada, et al. 'Neutron radiography on tubular flow reactor for hydrothermal synthesis: In situ monitoring of mixing behavior of supercritical water and room-temperature water.' *The Journal of Supercritical Fluids*, 63:46–51, Mar 2012. ISSN 0896-8446. doi:{10.1016/j.supflu.2011.11.010}.

[125] R. Haynes, S. T. Norberg, S. G. Eriksson, et al. 'New high temperature gas flow cell developed at ISIS.' *Journal of Physics Conference Series*, 251(012090), 2010. ISSN 1742-6588. doi:{10.1088/1742-6596/251/1/012090}. Proceedings of the International Conference on Neutron Scattering, ICNS2009.

[126] D. P. Riley, E. H. Kisi, and T. C. Hansen. 'Self-propagating high-temperature synthesis of Ti_3SiC_2: II. kinetics of ultra-high-speed reactions from in situ neutron diffraction.' *Journal of the American Ceramic Society*, 91(10):3207–3210, Oct 2008. ISSN 0002-7820. doi:{10.1111/j.1551-2916.2008.02637.x}.

[127] W. F. Kuhs and T. C. Hansen. 'Time-resolved neutron diffraction studies with emphasis on water ices and gas hydrates.' In H. R. Wenk, editor, *Neutron Scattering in Earth Sciences*, volume 63 of *Reviews in Mineralogy & Geochemistry*, pages 171–204. Mineralogical Society of America, 2006. ISBN 978-0-939950-75-1. doi:{10.2138/rmg.2006.63.8}.

[128] V. P. Ting, M. Schmidtmann, P. F. Henry, et al. 'The kinetics of bulk hydration of the disaccharides alpha-lactose and trehalose by in situ neutron powder diffraction.' *MedChemComm (Journal of the European Federation for Medicinal Chemistry)*, 1(5):345–348, Dec 2010. ISSN 2040-2503. doi: {10.1039/c0md00093k}.

[129] P. Albers, E. Auer, K. Ruth, et al. 'Inelastic neutron scattering investigation of the nature of surface sites occupied by hydrogen on highly dispersed platinum on commercial carbon black supports.' *Journal of Catalysis*, 196(1):174–179, 2000.

[130] D. Lennon, I. Silverwood, N. Hamilton, et al. 'Application of inelastic neutron scattering to studies of CO2 reforming of methane over alumina-supported nickel and gold-doped nickel catalysts.' *Physical Chemistry Chemical Physics*, 2012.

[131] A. G. Stepanov, A. A. Shubin, M. V. Luzgin, et al. 'Molecular dynamics of n-octane inside zeolite ZSM-5 as studied by deuterium solid-state NMR and quasi-elastic neutron scattering.' *The Journal of Physical Chemistry B*, 102(52):10860–10870, 1998.

[132] I. P. Silverwood, N. G. Hamilton, C. J. Laycock, et al. 'Quantification of surface species present on a nickel/alumina methane reforming catalyst.' *Physical Chemistry Chemical Physics*, 12(13):3102–3107, 2010. ISSN 1463-9076. doi:{10.1039/b919977b}.

[133] C. R. Gardner, C. T. Walsh, and Ö. Almarsson. 'Drugs as materials: Valuing physical form in drug discovery.' *Nature Reviews Drug Discovery*, 3(11):926–934, 2004.

[134] J. Bauer, S. Spanton, R. Henry, et al. 'Ritonavir: An extraordinary example of conformational polymorphism.' *Pharmaceutical Research*, 18(6):859–866, 2001.

[135] C. K. Leech, S. A. Barnett, K. Shankland, et al. 'Accurate molecular structures and hydrogen bonding in two polymorphs of ortho-acetamidobenzamide by single-crystal neutron diffraction.' *Acta Crystallographica Section B: Structural Science*, 62(5):926–930, 2006.

[136] M. R. Johnson, M. Prager, H. Grimm, et al. 'Methyl group dynamics in paracetamol and acetanilide: Probing the static properties of intermolecular hydrogen bonds formed by peptide groups.' *Chemical Physics*, 244(1):49–66, 1999.

[137] H. N. Bordallo, B. A. Zakharov, E. V. Boldyreva, et al. 'Application of incoherent inelastic neutron scattering in pharmaceutical analysis: Relaxation dynamics in phenacetin.' *Molecular Pharmaceutics*, 9(9):2434–2441, 2012. doi:10.1021/mp2006032.

[138] M. D. King, A. R. Rennie, K. C. Thompson, et al. 'Oxidation of oleic acid at the air-water interface and its potential effects on cloud critical supersaturations.' *Physical Chemistry Chemical Physics*, 11(35):7699–7707, 2009. ISSN 1463-9076. doi:{10.1039/b906517b}.

[139] M. D. King, A. R. Rennie, C. Pfrang, et al. 'Interaction of nitrogen dioxide (NO2) with a monolayer of oleic acid at the air-water interface - A simple proxy for atmospheric aerosol.' *Atmospheric Environment*, 44(14):1822–1825, May 2010. ISSN 1352-2310. doi:{10.1016/j.atmosenv.2010.01.031}.

[140] H. M. Kwaambwa, M. Hellsing, and A. R. Rennie. 'Adsorption of a water treatment protein from Moringa oleifera seeds to a silicon oxide surface studied by neutron reflection.' *Langmuir*, 26(6):3902–3910, Mar 2010. ISSN 0743-7463. doi:{10.1021/la9031046}.

[141] P. Westerhoff and B. Nowack. 'Searching for global descriptors of engineered nanomaterial fate and transport in the environment.' *Accounts of Chemical Research*, 2012.

[142] F. Ridi, E. Fratini, and P. Baglioni. 'Cement: A two thousand year old nano-colloid.' *Journal of Colloid and Interface Science*, 357(2):255–264, 2011.

[143] H. N. Bordallo, L. P. Aldridge, and A. Desmedt. 'Water dynamics in hardened ordinary portland cement paste or concrete: From quasielastic neutron scattering.' *The Journal of Physical Chemistry B*, 110(36):17966–17976, 2006.

[144] H. N. Bordallo, L. P. Aldridge, P. Fouquet, et al. 'Hindered water motions in hardened cement pastes investigated over broad time and length scales.' *ACS Applied Materials & Interfaces*, 1(10):2154–2162, 2009. doi:10.1021/am900332n. PMID: 20355849.

[145] N. Malikova, S. Longeville, J. M. Zanotti, et al. 'Signature of low-dimensional diffusion in complex systems.' *Physical Review Letters*, 101(26):265901, 2008.

[146] D. Pearson, A. Allen, C. G. Windsor, et al. 'An investigation on the nature of porosity in hardened cement pastes using small angle neutron scattering.' *Journal of Materials Science*, 18(2):430–438, 1983.

[147] K. D. Knudsen, J. O. Fossum, G. Helgesen, et al. 'Pore characteristics and water absorption in a synthetic smectite clay.' *Journal of Applied Crystallography*, 36(3):587–591, 2003.

[148] I. Vouldis et al. *Novel Materials for Energy Applications: A Decade of EU-Funded Research*. European Communities, 2009. ISBN 978-92-79-11379-6.

[149] M. Karlsson. 'Perspectives of neutron scattering on proton conducting oxides.' *Dalton Transactions*, 42(2):317–29, Jan 2013.

[150] I. Ahmed, C. S. Knee, M. Karlsson, et al. 'Location of deuteron sites in the proton conducting perovskite $BaZr_{0.50}In_{0.50}O_{3-y}$.' *Journal of Alloys and Compounds*, 450(1-2):103–110, Feb 2008. ISSN 0925-8388. doi:10.1016/j.jallcom.2006.11.154.

[151] J.-C. Perrin, S. Lyonnard, and F. Volino. 'Quasielastic neutron scattering study of water dynamics in hydrated nafion membranes.' *The Journal of Physical Chemistry C*, 111(8):3393–3404, 2007. doi:10.1021/jp065039q.

[152] M. Karlsson, D. Engberg, et al. 'Using neutron spin-echo to investigate proton dynamics in proton-conducting perovskites.' *Chemistry of Materials*, 22(3):740–742, 2010. doi:10.1021/cm901624v.

[153] M. Strobl, I. Manke, N. Kardjilov, et al. 'Advances in neutron radiography and tomography.' *Journal of Physics D: Applied Physics*, 42(24):243001, 2009.

[154] V. K. Peterson, Y. Liu, C. M. Brown, et al. 'Neutron powder diffraction study of D_2 sorption in Cu_3(1,3,5-benzenetricarboxylate)$_2$.' *Journal of the American Chemical Society*, 128(49):15578–15579, 2006. doi:10.1021/ja0660857.

[155] T. Yildirim and M. R. Hartman. 'Direct observation of hydrogen adsorption sites and nanocage formation in metal-organic frameworks.' *Physical Review Letters*, 95:215504, Nov 2005. doi:10.1103/PhysRevLett.95.215504.

[156] X. Lin, I. Telepeni, A. J. Blake, et al. 'High capacity hydrogen adsorption in Cu(II) tetracarboxylate framework materials: The role of pore size, ligand functionalization, and exposed metal sites.' *Journal of the American Chemical Society*, 131(6):2159–2171, 2009.

[157] J. M. Simmons, T. Yildirim, A. Hamaed, et al. 'Direct observation of activated hydrogen binding to a supported organometallic compound at room temperature.' *Chemistry-A European Journal*, 18(14):4170–4173, 2012.

[158] P. A. Georgiev, D. K. Ross, A. D. Monte, et al. 'In situ inelastic neutron scattering studies of the rotational and translational dynamics of molecular hydrogen adsorbed in single-wall carbon nanotubes (SWNTs).' *Carbon*, 43(5):895–906, 2005. ISSN 0008-6223. doi:10.1016/j.carbon.2004.11.006.

[159] A. J. Ramirez-Cuesta and P. C. H. Mitchell. 'Hydrogen adsorption in a copper ZSM5 zeolite: An inelastic neutron scattering study.' *Catalysis Today*, 120(3-4):368–373, 2007. ISSN 0920-5861. doi:10.1016/j.cattod.2006.09.024. Proceedings of the Korea Conference on Innovative Science and Technology (KCIST-2005): Frontiers in Hydrogen Storage Materials and Technology.

[160] F. Salles, D. I. Kolokolov, H. Jobic, et al. 'Adsorption and diffusion of H_2 in the MOF type systems MIL-47(V) and MIL-53(Cr): A combination of microcalorimetry and QENS experiments with molecular simulations.' *The Journal of Physical Chemistry C*, 113(18):7802–7812, 2009. doi: 10.1021/jp811190g.

[161] F. M. Mulder, B. Assfour, J. Huot, et al. 'Hydrogen in the metal-organic framework Cr MIL-53.' *The Journal of Physical Chemistry C*, 114(23):10648–10655, 2010. doi:10.1021/jp102463p.

[162] L. Ulivi, M. Celli, A. Giannasi, et al. 'Inelastic neutron scattering from hydrogen clathrate hydrates.' *Journal of Physics: Condensed Matter*, 20(10):104242, 2008.

[163] P. A. Georgiev, A. Giannasi, D. K. Ross, et al. 'Experimental Q-dependence of the rotational J=0-to-1 transition of molecular hydrogen adsorbed in single-wall carbon nanotube bundles.' *Chemical Physics*, 328(1):318–323, 2006.

[164] M. M. Murshed and W. F. Kuhs. 'Kinetic studies of methane–ethane mixed gas hydrates by neutron diffraction and Raman spectroscopy.' *The Journal of Physical Chemistry B*, 113(15):5172–5180, 2009. doi:10.1021/jp810248s. PMID: 19354304.

[165] D. K. Staykova, W. F. Kuhs, A. N. Salamatin, et al. 'Formation of porous gas hydrates from ice powders: Diffraction experiments and multistage model.' *The Journal of Physical Chemistry B*, 107(37):10299–10311, 2003. doi:10.1021/jp027787v.

[166] N. Sharma, V. K. Peterson, M. M. Elcombe, et al. 'Structural changes in a commercial lithium-ion battery during electrochemical cycling: An in situ neutron diffraction study.' *Journal of Power Sources*, 195(24):8258–8266, 2010. ISSN 0378-7753. doi:10.1016/j.jpowsour.2010.06.114.

[167] N. Kardjilov, A. Hilger, I. Manke, et al. 'Industrial applications at the new cold neutron radiography and tomography facility of the HMI.' *Nuclear Instruments and Methods A*, 542(1-3):16–21, 2005. ISSN 0168-9002. doi:10.1016/j.nima.2005.01.005. Proceedings of the Fifth International Topical Meeting on Neutron Radiography — ITMNR-5.

[168] A. Senyshyn, M. Mhlbauer, K. Nikolowski, et al. '"In-operando" neutron scattering studies on Li-ion batteries.' *Journal of Power Sources*, 203(0):126–129, 2012. ISSN 0378-7753. doi:10.1016/j.jpowsour.2011.12.007.

[169] W. Schweika, R. P. Hermann, M. Prager, et al. 'Dumbbell rattling in thermoelectric zinc antimony.' *Physical Review Letters*, 99:125501, Sep 2007. doi:10.1103/PhysRevLett.99.125501.

[170] M. Christensen, A. B. Abrahamsen, N. B. Christensen, et al. 'Avoided crossing of rattler modes in thermoelectric materials.' *Nature Materials*, 7(10):811–815, 2008. ISSN 14761122.

[171] H.-R. Wenk. 'Application of neutron scattering in earth sciences.' *JOM (member journal of the Minerals, Metals and Materials Society)*, 64:127–137, 2012. ISSN 1047-4838. doi:10.1007/s11837-011-0223-y.

[172] G. Grellet-Tinner, C. M. Sim, D. H. Kim, et al. 'Description of the first lithostrotian titanosaur embryo in ovo with neutron characterization and implications for lithostrotian Aptian migration and dispersion.' *Gondwana Research*, 20(2-3):621–629, 2011. ISSN 1342-937X. doi:10.1016/j.gr.2011.02.007.

[173] A. D. Fortes, I. G. Wood, D. Grigoriev, et al. 'No evidence for large-scale proton ordering in Antarctic ice from powder neutron diffraction.' *The Journal of Chemical Physics*, 120:11376, 2004.

[174] S. Siano, W. Kockelmann, U. Bafile, et al. 'Quantitative multiphase analysis of archaeological bronzes by neutron diffraction.' *Applied Physics A: Materials Science & Processing*, 74:1139–1142, 2002.

[175] F. Grazzi, L. Bartoli, F. Civita, et al. 'Neutron diffraction characterization of Japanese artworks of Tokugawa age.' *Analytical and Bioanalytical Chemistry*, 395(7):1961–1968, 2009.

[176] F. Grazzi, L. Bartoli, F. Civita, et al. 'From Koto age to modern times: Quantitative characterization of Japanese swords with time of flight neutron diffraction.' *Journal of Analytical Atomic Spectrometry*, 26(5):1030–1039, 2011.

[177] F. Grazzi, P. Pallecchi, P. Petitti, et al. 'Non-invasive quantitative phase analysis and microstructural properties of an iron fragment retrieved in the copper-age Selvicciola Necropolis in southern Tuscia.' *Journal of Analytical Atomic Spectrometry*, 27(2):293–298, 2012.

[178] F. Salvemini, F. Grazzi, S. Peetermans, et al. 'Quantitative characterization of Japanese ancient swords through energy-resolved neutron imaging.' *Journal of Analytical Atomic Spectrometry*, 27:1494–1501, 2012. doi:10.1039/C2JA30035D.

[179] S. Paul. 'The neutron and the universe–History of a relationship.' *arXiv preprint arXiv:1205.2451*, 2012.

[180] J. Rathsman, P. Christiansen, and M. Lindroos, editors. *Proceedings from the Workshop on Neutron, Nuclear, Neutrino, Muon and Medical Physics at ESS (3N2MP)*. Lund, 2009.

[181] 'ESS Science and Scientists: Fundamental Physics Parallel Session.' Berlin, Apr 2012.

[182] V. Cirigliano, Y. Li, S. Profumo, et al. 'MSSM baryogenesis and electric dipole moments: An update on the phenomenology.' *Journal of High Energy Physics*, pages 1–23, 2010.

[183] C. A. Baker, D. D. Doyle, P. Geltenbort, et al. 'Improved experimental limit on the electric dipole moment of the neutron.' *Physical Review Letters*, 97(13):131801, 2006.

[184] V. V. Fedorov, I. A. Kuznetsov, et al. 'Neutron spin optics in noncentrosymmetric crystals as a new way for nEDM search.' *Nuclear Instruments and Methods B*, 252:131–135, 2006.

[185] P. A. Vetter et al. 'Search for oscillation of the electron-capture decay probability of ^{1}42Pm.' *Physics Letters B*, 670(3):196–199, 2008.

[186] M. Baldo-Ceolin et al. 'A new experimental limit on neutron-antineutron oscillations.' *Zeitschrift für Physik C Particles and Fields*, 63:409–416, Feb 1994.

[187] H. V. Klapdor-Kleingrothaus, E. Ma, and U. Sarkar. 'Baryon and lepton number violation with scalar bilinears.' *Modern Physics Letters A*, 17(33):2221–2228, 2002.

[188] H. Rauch and S. A. Werner. *Neutron Interferometry.* Clarendon Press, Oxford, 2000.

[189] H. Bartosik, J. Klepp, C. Schmitzer, et al. 'Experimental test of quantum contextuality in neutron interferometry.' *Physical Review Letters*, 103(040403), Jul 2009.

[190] H. Abele et al. 'Qubounce: The dynamics of ultra-cold neutrons falling in the gravity potential of the Earth.' *Nuclear Physics A*, 827:593c–595c, Aug 2009.

[191] J. S. Bell. 'On the Einstein Podolsky Rosen paradox.' *Physics*, 1(3):195, 1964.

[192] S. Kochen and E. Specker. 'The problem of hidden variables in quantum mechanics.' *Journal of Mathematics and Mechanics*, 17(1):59–87, 1967.

[193] W. Schott, T. Faestermann, P. Fierlinger, et al. 'An experiment to measure the bound-beta decay of the free neutron.' *Hyperfine Interactions*, 193(1–3):269–274, 2009. doi:10.1007/s10751-009-0011-z.

[194] L. L. Nemenov. 'Neutron decay into a hydrogen atom and an anti-neutrino.' *Soviet Journal of Nuclear Physics*, 31:115–119, 1980.

[195] L. L. Nemenov and A. A. Ovchinnikova. 'Effects of scalar and tensor interactions on the atomic decay of the neutron, n. $--$ >. H+n-bar.' *Soviet Journal of Nuclear Physics (Eng. Trans.)*, 31:659–660, 1980.

[196] W. Schott et al. 'An experiment for the measurement of the bound-beta decay of the free neutron.' *European Physical Journal A*, 30:603–611, 2006.

[197] J. Byrne. 'Two-body decay of the neutron: A possible test for the existence of right-handed weak currents.' *EPL (Europhysics Letters)*, 56(5):633, Dec 2001.

[198] H. Abele et al. 'Is the unitarity of the quark-mixing CKM matrix violated in neutron beta-decay?' *Physical Review Letters*, 88(211801), May 2002.

[199] K. H. Klenø, K. Lieutenant, K. H. Andersen, et al. 'Systematic performance study of common neutron guide geometries.' *Nuclear Instruments and Methods A*, 696:75–84, 2012.

[200] T. Kamiyama. Private communication, 2012.

[201] K. L. Krycka, R. A. Booth, C. R. Hogg, et al. 'Core-shell magnetic morphology of structurally uniform magnetite nanoparticles.' *Physical Review Letters*, 104:207203, May 2010. doi:10.1103/PhysRevLett.104.207203.

[202] P. Mueller-Bushbaum, E. Metwalli, J.-F. Moulin, et al. 'Time of flight grazing incidence small angle neutron scattering.' *European Physics Journal Special Topics*, 167:107–112, 2009. doi:10.1140/epjst/e2009-00944-5.

[203] J. Stahn, U. Filges, and T. Panzner. 'Focusing specular neutron reflectometry for small samples.' *The European Physical Journal - Applied Physics*, 58(01), 2012.

[204] M. Ohl, M. Monkenbusch, N. Arend, et al. 'The spin-echo spectrometer at the Spallation Neutron Source (SNS).' *Nuclear Instruments and Methods A*, 696:85–99, 2012. doi:http://dx.doi.org.ludwig.lub.lu.se/10.1016/j.nima.2012.08.059.

[205] P. Fouquet, G. Ehlers, B. Farago, et al. 'The wide-angle neutron spin echo spectrometer project WASP.' *Journal of Neutron Research*, 15:39–47, 2007. doi:10.1080/10238160601048791.

[206] M. Karlsson, P. Fouquet, I. Ahmed, et al. 'Dopant concentration and short-range structure dependence of diffusional proton dynamics in hydrated $BaIn_xZr_{1-x}O_{3-x/2}$ (x = 0.10 and 0.50).' *Journal of Physical Chemistry C*, 114:3292–3296, 2010. doi:10.1021/jp910224s.

[207] F. Tasset. 'Zero field neutron polarimetry.' *Physica B*, 157:627–630, 1989.

[208] K. Zeitelhack. 'Report on the International Collaboration of Neutron Detectors.' He-3 Replacements Workshop, IEEE Nuclear Science Symposia, 2011.

[209] A. Cho. 'Helium-3 shortage could put freeze on low-temperature research.' *Science*, 326(5954):778–779, 2009. doi:10.1126/science.326_778.

[210] D. Kramer. 'For some, helium-3 supply picture is brightening.' *Physics Today*, 64:20, 2011.

[211] D. A. Shea and D. Morgan. 'The helium-3 shortage: Supply, demand, and options for Congress.' Congressional Research Service, Library of Congress, http://digital.library.unt.edu/ark:/67531/metadc31373/, Sep 2010.

[212] T. M. Persons and G. Aloise. 'Neutron detectors: Alternatives to using helium-3.' United States Government Accountability Office GAO-11-753, Sep 2011.

[213] International Collaboration for the Development of Neutron Detectors. www.icnd.org, last accessed Jan 2013.

[214] *2nd International 10B BF3 Detectors Workshop*, 2012.

[215] O. Knotek, E. Lugscheider, and C. W. Siry. 'Tribological properties of B—C thin films deposited by magnetron-sputter-ion plating method.' *Surface and Coatings Technology*, 91(3):167–173, 1997.

[216] S. Ulrich, T. Theel, J. Schwan, et al. 'Magnetron-sputtered superhard materials.' *Surface and Coatings Technology*, 97(1):45–59, 1997.

[217] M. J. Zhou, S. F. Wong, C. W. Ong, et al. 'Microstructure and mechanical properties of B_4C films deposited by ion beam sputtering.' *Thin Solid Films*, 516(2):336–339, 2007.

[218] M. L. Wu, J. D. Kiely, T. Klemmer, et al. 'Process–property relationship of boron carbide thin films by magnetron sputtering.' *Thin Solid Films*, 449(1):120–124, 2004.

[219] S. Ulrich, H. Ehrhardt, J. Schwan, et al. 'Subplantation effect in magnetron sputtered superhard boron carbide thin films.' *Diamond and Related Materials*, 7(6):835–838, 1998.

[220] O. Tavsanoglu, O. A. Yucel, and M. Jeandin. 'A functionally graded design study for boron carbide and boron carbonitride thin films deposited by plasma-enhanced dc magnetron sputtering.' In *TMS Annual Meeting 1*, pages 279–285. 2008.

[221] C. Hoglund, J. Birch, K. Andersen, et al. 'B_4C thin films for neutron detection.' *Journal of Applied Physics*, 111(10):104908–104908, 2012.

[222] European Spallation Source AB. 'A method for producing a neutron detector component comprising a boron carbide layer for use in a neutron detecting device.' international patent application number PCT/SE2011/050891 http://patentscope.wipo.int/search/en/detail.jsf?docId=WO2013002697&recNum=287&docAn=SE2011050891&queryString=evaporators&maxRec=194643, 30 Jun 2011.

[223] H. Pedersen, C. Höglund, J. Birch, et al. 'Low temperature CVD of thin, amorphous boron-carbon films for neutron detectors.' *Chemical Vapor Deposition*, 2012.

[224] B. Alling, C. Höglund, R. Hall-Wilton, et al. 'Mixing thermodynamics of $TM_{1-x}Gd_xN$ (TM= Ti, Zr, Hf) from first principles.' *Applied Physics Letters*, 98:241911, 2011.

[225] K. Andersen, T. Bigault, J. Birch, et al. 'Multi-grid boron-10 detector for large area applications in neutron scattering science.' *arXiv preprint arXiv:1209.0566*, 2012.

[226] I. L. Langevin. 'Ionizing radiation detector.' French patent application FR no. 10/51502, 2 Mar 2010.

[227] J. Ollivier, H. Mutka, and L. Didier. 'The new cold neutron time-of-flight spectrometer IN5.' *Neutron News*, 21(2):22–25, 2010.

[228] N. J. Rhodes, A. G. Wardle, A. J. Boram, et al. 'Pixelated neutron scintillation detectors using fibre optic coded arrays.' *Nuclear Instruments and Methods A*, 392(1-3):315–318, 1997. ISSN 0168-9002. doi:10.1016/S0168-9002(97)00261-1. Position-Sensitive Detectors Conference 1996.

[229] M. L. Crow, J. P. Hodges, and R. G. Cooper. 'Shifting scintillator prototype large pixel wavelength-shifting fiber detector for the POWGEN3 powder diffractometer.' *Nuclear Instruments and Methods A*, 529(1-3):287–292, 2004. ISSN 0168-9002. doi:10.1016/j.nima.2004.04.167. Proceedings of the Joint Meeting of the International Conference on Neutron Optics (NOP2004) and the Third International Workshop on Position-Sensitive Neutron Detectors (PSND2004).

[230] Partec Ltd. (supplier). http://www.parttec.com/index.html, last accessed Jan 2013.

[231] T. Nakamura, E. M. Schooneveld, N. J. Rhodes, et al. 'A half-millimetre spatial resolution fibre-coded linear position-sensitive scintillator detector with wavelength-shifting fibre read-out for neutron detection.' *Nuclear Instruments and Methods A*, 606(3):675–680, 2009. ISSN 0168-9002. doi:10.1016/j.nima.2009.05.013.

[232] T. Nakamura, T. Kawasaki, T. Hosoya, et al. 'A large-area two-dimensional scintillator detector with a wavelength-shifting fibre readout for a time-of-flight single-crystal neutron diffractometer.' *Nuclear Instruments and Methods A*, 686(0):64–70, 2012. ISSN 0168-9002. doi:10.1016/j.nima.2012.05.038.

[233] H. O. Anger. 'Scintillation camera.' *Review of Scientific Instruments*, 29(1):27–33, 1958. doi:10.1063/1.1715998.

[234] M. Heiderich, R. Reinartz, R. Kurz, et al. 'A two-dimensional scintillation detector for small angle neutron scattering.' *Nuclear Instruments and Methods A*, 305(2):423–432, 1991. ISSN 0168-9002. doi:10.1016/0168-9002(91)90562-5.

[235] G. Kemmerling, R. Engels, N. Bussmann, et al. 'A new two-dimensional scintillation detector system for small-angle neutron scattering experiments.' *IEEE Transactions on Nuclear Science*, 48(4):1114–1117, 2001.

[236] R. Engels, R. Reinartz, and J. Schelten. 'A new 64-channel area detector for neutrons and gamma ray.' *IEEE Transactions on Nuclear Science*, 46(4):869–872, 1999.

[237] I. Stefanescu, Y. Abdullahi, J. Birch, et al. 'Development of a novel macrostructured cathode for large-area neutron detectors based on ^{10}B-containing solid converter.' *Nuclear Instruments and Methods A*, (submitted).

[238] M. Russina, F. Mezei, and F. Trouw. 'New capabilities in spectroscopy on pulsed sources: Adjustable pulse repetition rate, resolution and line shape.' In *Proceedings of the 15th Meeting of the International Collaboration on Advanced Neutron Sources, ICANS-XV*, page 349. Japan Atomic Energy Research Institute, Mar 2001.

[239] V. Antonelli et al. 'The design of a CFRP chopper disc for a time-of-flight spectrometer.' In *18th International Conference on Composite Materials*, 21.-26.8.2011. 2011.

[240] H. Stelzer. 'Quaterly report of work package K1.' Internal Report, European Spallation Source, May–Jul 2011.

[241] M. Monkenbusch. 'Multi-chopper design considerations.' Internal paper, Forschungszentrum Jülich, May 15 2011.

[242] H. Abele et al. 'Characterization of a ballistic supermirror neutron guide.' *Nuclear Instruments and Methods A*, 562:407–417, Jun 2006.

[243] C. Schanzer et al. 'Advanced geometries for ballistic guides.' *Nuclear Instruments and Methods A*, 529(1–3):63–68, Aug 2004.

[244] S. Mühlbauer et al. 'Performance of an elliptically tapered neutron guide.' *Physica B*, 385-386:1247–1249, Nov 2006.

[245] T. Hils et al. 'Focusing parabolic guide for very small samples.' *Physica B*, 350:166–168, 2004.

[246] H. Wolter. 'Spiegelsysteme streifenden einfalls als abbildende optiken fuer röntgenstrahlen.' *Annalen der Physik*, 6(10):94–114, 1952.

[247] H. Wolter. 'Verallgemeinerte schwarzschildshe spiegelsysteme streifender reflexion als optiken fuer röntgenstrahlen.' *Annalen der Physik*, 6(10):286–295, 1952.

[248] M. R. Eskildsen et al. 'Compound refractive optics for the imaging and focusing of low-energy neutrons.' *Nature*, 391:563–566, 1998.

[249] T. Oku et al. 'Development of a Fresnel lens for cold neutrons based on neutron refractive optics.' *Nuclear Instruments and Methods A*, 462(3):435–441, 2001.

[250] Paul Scherrer Institut and RISØ-DTU. 'Swiss-Danish neutron instrumentation work packages for the European Spallation Source (ESS), 2011-2014.' Internal Report, 15 Jul 2011.

[251] 'Vorhabenbeschreibung: Mitwirkung der zentren der helmholtz-gemeinschaft und der Technischen Universität München an der Design-Update-Phase der ESS.' *Jülich*, 2011. http://www.essworkshop.org/Meetings/20110111_Copenhagen/Vorhabenbeschreibung_Verbundvorhaben_%20ESS.pdf.

[252] M. . Könnecke. 'Swiss work packages for the European Spallation Source 2011-2014.' Internal Report WP5 2012.

[253] T. Gahl. 'The PSI 2nd gen motion control technology at SINQ focusing on applications in extreme environments.' In *Presentatation at Design and Engineering of Neutron Instruments (DENIM) Conference at Rutherford Laboratory*. http://www.isis.stfc.ac.uk/news-and-events/events/2012/denim-photos/technical-presentation---motion-control---gahl-t-psi13337.pdf, Sep 2012.

[254] C. Pradervand and T. Gahl. 'Motor and encoder standards for SwissFEL-applications.' PSI Elektronik Netzwerk https://controls.web.psi.ch/TWiki-4.1.2/pub/Main/StandardMotorsAndEncoders/SwissFEL_motor_and_encoder_standards_rev1-1.pdf, 2012.

[255] F. Darmann. 'Electrical engineering guidelines to be applied to neutron beam instruments and subassemblies - information for vendors - NBIP-ES-410-1032C Attachment B.', 2010.

[256] D. Beltran. *ALBA hardware guidelines.* ALBA – Computing Division, CCD-GDCTHW-ES-0001 rev 1.2, 2007.

[257] J. Destraves, T. Gahl, M. Kenzelmann, et al. '2nd gen SINQ instruments electronics.' ICANS XIX poster presentation, Grindelwald, Switzerland, Mar 2010.

[258] European Synchrotron Radiation Facility (ESRF). 'IcePAP - motion control at the ESRF.' http://www.esrf.eu/Instrumentation/DetectorsAndElectronics/icepap, last accessed Jan 2013.

[259] 'Experimental Physics and Industrial Control System.' http://www.aps.anl.gov/epics/index.php, last accessed Jan 2013.

[260] ABB. 'FRIDA - Dual arm concept robot from ABB.' http://www.abb.com/cawp/abbzh254/8657f5e05ede6ac5c1257861002c8ed2.aspx, last accessed Jan 2013.

[261] Physikalische Instrumente (PI). 'Hexapod platform and control system from Physik Instrumente (PI).' http://www.physikinstrumente.com/en/products/hexapod_tripod/hexapod_tripod_controller.php, last accessed Jan 2013.

[262] P. K. Willendrup, E. Knudsen, K. Lefmann, et al. 'McStas - A neutron ray-trace simulation package.' http://www.mcstas.org, last accessed Jan 2013.

[263] 'Mantid.' http://www.mantidproject.org, last accessed Jan 2013.

[264] P. D. Adams, P. V. Afonine, G. Bunkóczi, et al. '*PHENIX*: a comprehensive Python-based system for macromolecular structure solution.' *Acta Crystallographica Section D*, 66(2):213–221, Feb 2010. doi:10.1107/S0907444909052925. See also PHENIX homepage www.phenix-online.org.

[265] 'Single sign-on - Wikipedia, the free encyclopedia.' http://en.wikipedia.org/wiki/Single_sign-on, last accessed Jan 2013.

[266] 'PANDATA.' http://www.pan-data.eu, last accessed Jan 2013.

[267] 'The Cluster of Resarch Infrastructures for Synergies in Physics (CRISP).' http://www.crisp-fp7.eu, last accessed Jan 2013.

[268] 'eduroam.' http://www.eduroam.org, last accessed Jan 2013.

[269] M. Fromme, A. Houben, K. Lieutenant, et al. 'Virtual Instrumentation Tool for Neutron Scattering at Pulsed and Continuous Sources.' http://www.helmholtz-berlin.de/forschung/grossgeraete/neutronenstreuung/projekte/vitess/index_en.html, last accessed Jan 2013.

[270] C. L. Jacobsen and S. Skelboe. 'Data format at ESS for data acquisition and storage.' Technical Report, University of Copenhagen, 2013.

[271] S. Campbell. 'ADARA - Initial test of live streaming reduction.' http://www.youtube.com/watch?v=iGAIWoPMbL4&feature=plcp, Aug 2012. YouTube.

[272] S. Campbell. 'ADARA - Testing multiple listeners and reduction paths.' https://www.youtube.com/watch?feature=player_detailpage&v=vP4KiiwBh08, Aug 2012. YouTube.

[273] 'ROOT - A Data Analysis Framework.' http://root.cern.ch/drupal/, last accessed Jan 2013.

[274] 'NeXus scientific data format.' http://www.nexusformat.org/, last accessed Jan 2013.

[275] 'ICAT.' http://www.icatproject.org, last accessed Jan 2013.

[276] T. Otomo. Private communication, Sep 2012.

[277] P. Peterson, M. Doucet, S. Campbell, et al. 'Live analysis and high performance computing at SNS.' NOBUGS (New Opportunities for Better User Group Software) 2012 presentation, September 24-26 2012.

[278] L. Mohanambe and S. Vasudevan. 'Anionic clays containing anti-inflammatory drug molecules: Comparison of molecular dynamics simulation and measurements.' *The Journal of Physical Chemistry B*, 109(32):15651–15658, 2005. doi:10.1021/jp050480m. PMID: 16852983.

[279] P. M. Bentley and R. Cywinski. 'Evidence for a spin emulsion.' *Physical Review Letters*, 101:227202, Nov 2008. doi:10.1103/PhysRevLett.101.227202.

[280] S. L. Holm and K. Lefmann. Private communication, 2012. Niels Bohr Institute, University of Copenhagen.

[281] J. C. Smith. Private communication, 2012.

[282] R. J.-M. Pellenq, A. Kushima, R. Shahsavari, et al. 'A realistic molecular model of cement hydrates.' *Proceedings of the National Academy of Sciences*, 106(38):16102–16107, 2009. doi:10.1073/pnas.0902180106.

[283] J. J. Thomas, H. M. Jennings, and A. J. Allen. 'Relationships between composition and density of tobermorite, jennite, and nanoscale $CaOSiO_2H_2O$.' *The Journal of Physical Chemistry C*, 114(17):7594–7601, 2010. doi:10.1021/jp910733x.

[284] Y. Miao, Z. Yi, C. Cantrell, et al. 'Coupled flexibility change in cytochrome P450cam substrate binding determined by neutron scattering, NMR, and molecular dynamics simulation.' *Biophysical Journal*, 103:2167–2176, 2012.

[285] U. Ryde, L. Olsen, and K. Nilsson. 'Quantum chemical geometry optimizations in proteins using crystallographic raw data.' *Journal of Computational Chemistry*, 23(11):1058–1070, 2002. ISSN 1096-987X. doi:10.1002/jcc.10093.

[286] 'Stochfit-Stochastic Methods for Modeling X-ray and Neutron Reflectometry.' http://stochfit.sourceforge.net/, last accessed Jan 2013.

[287] S. M. Danauskas, D. Li, M. Meron, et al. 'Stochastic fitting of specular X-ray reflectivity data using *StochFit*.' *Journal of Applied Crystallography*, 41(6):1187–1193, Dec 2008. doi:10.1107/S0021889808032445.

[288] M. Björck and G. Andersson. '*GenX*: An extensible X-ray reflectivity refinement program utilizing differential evolution.' *Journal of Applied Crystallography*, 40(6):1174–1178, Dec 2007. doi:10.1107/S0021889807045086.

[289] 'GenX.' http://genx.sourceforge.net/index.html, last accessed Jan 2013.

[290] T. Perring. 'Advanced visualisation and quantification of neutron data.' NOBUGS (New Opportunities for Better User Group Software) 2012 presentation, September 2012.

[291] 'Horace.' http://horace.isis.rl.ac.uk/, last accessed Jan 2013.

[292] 'TobyFit.' http://tobyfit.isis.rl.ac.uk/, last accessed Jan 2013.

[293] 'McPhase.' http://www.mcphase.de/, last accessed Jan 2013.

[294] 'SansView.' http://danse.chem.utk.edu/sansview.html, last accessed Jan 2013.

[295] 'Atomic Simulation Environment.' https://wiki.fysik.dtu.dk/ase/, last accessed Jan 2013.

[296] G. Kresse and J. Furthmüller. 'Efficiency of ab-initio total energy calculations for metals and semiconductors using a plane-wave basis set.' *Computational Materials Science*, 6:15, 1996. See also http://www.vasp.at.

[297] G. Kresse and J. Furthmüller. 'Efficient iterative schemes for ab initio total-energy calculations using a plane-wave basis set.' *Physical Review B*, 54:11169, 1996. See also http://www.vasp.at.

[298] S. J. Plimpton. 'Fast parallel algorithms for short-range molecular dynamics.' *Journal of Computational Physics*, 117, 1995. See also http://lammps.sandia.gov/index.html.

[299] F. Plewinski. 'Description of the target station barriers and zones.' Technical Report EDMS 1253318, European Spallation Source, 2012.

[300] R. Hanslik, M. Butzek, J. Bajus, et al. 'Design of the ESS target station shielding.' Technical Report ESS 03-150-T, Forschungszentrums Jülich, 2003.

[301] European Spallation Source. *Quality management plan*, 2012. ESS-0000126.

[302] K. Jonsdottir. *Risk analysis TS full construction.* European Spallation Source, 2012. ESS-0001053.

[303] Dassault Systems. 'Dymola, multi-engineering modeling and simulation.' http://www.3ds.com/products/catia/portfolio/dymola, last accessed 14 Feb 2013.

[304] Modelica®. 'Modelica 3.2 media library user's guide.' https://modelica.org/, last accessed 14 Feb 2013.

[305] B. E. Ghidersa, M. Ionescu-Bujor, and G. Janeschitz. 'Helium Loop Karlsruhe (HELOKA): A valuable tool for testing and qualifying ITER components and their He cooling circuits.' *Fusion Engineering and Design*, 81(8–14):1471–1476, Feb 2006.

[306] B. E. Ghidersa, V. Marchese, M. Ionescu-Bujor, et al. 'HELOKA facility: Thermo-hydrodynamic model and control.' *Fusion Engineering and Design*, 83(10–12):1792–1796, Dec 2008.

[307] Karlsruhe Institute of Technology. 'Complex experiments, experimental design (KEK).' http://www.inr.kit.edu/english/64.php, last accessed 14 Feb 2013.

[308] E. Noah. 'Recommended structural material compositions for neutronic and activation studies.' Technical Report EDMS 1170528, European Spallation Source, 2011.

[309] S. A. Maloy. *AFCI Materials Handbook: Materials Data for Particle Accelerator Applications.* NM: Los Alamos National Laboratory, Los Alamos, 2006. LA-CP-06-0904, Revision 5.

[310] M. G. Horsten and M. I. de Vries. 'Tensile properties of type 316L(N) stainless steel irradiated to 10 displacements per atom.' *Journal of Nuclear Materials*, 212–215:514–518, Sep 1994.

[311] Y. Dai. 'Suitability of steels as ESS mercury target container materials.' In *Proceedings of the 13th Meeting of the International Collaboration on Advanced Neutron Sources, ICANS-XIII.* 1995. ESS-PM-4.

[312] K. Saito et al. 'Tensile properties of austenitic stainless steels irradiated at SINQ target 3.' *Journal of Nuclear Materials*, 343:253–261, 2005.

[313] S. Maloy et al. 'Shear punch testing of candidate reactor materials after irradiation in fast reactors and spallation environments.' *Journal of Nuclear Materials*, 417(1):1005–1008, 2011.

[314] J. R. Weeks et al. 'Effects of high thermal and high fast fluencies on the mechanical properties of type 6061 aluminum on the HFBR.' In *Effects of Radiation on Materials: 14th International Symposium*, volume 2, pages 441–452. American Society for Testing and Materials, Jan 1990.

[315] P. Ferguson. 'Private communication.', 2012.

[316] Y. Dai and D. Hamaguchi. 'Mechanical properties and microstructure of $AlMg_3$ irradiated in SINQ target-3.' *Journal of Nuclear Materials*, 343(1–3):184–190, Aug 2005.

[317] S. Maloy et al. 'The effect of 800 MeV proton irradiation on the mechanical properties of tungsten at room temperature and at 475 °C.' *Journal of Nuclear Materials*, 345:219, 2005.

[318] S. A. Maloy, R. S. Lillard, W. F. Sommer, et al. 'Water corrosion measurements on tungsten irradiated with high energy protons and spallation neutrons.' *Journal of Nuclear Materials*, 431:140, 2012.

[319] A. T. Nelson, J. A. O'Toole, R. A. Valicenti, et al. 'Fabrication of a tantalum-clad tungsten target for LANSCE.' *Journal of Nuclear Materials*, 431(1–3):172–184, Dec 2012.

[320] M. Matolich. 'Swelling in neutron irradiated tungsten and tungsten - 25 percent rhenium.' *Scripta Metallurgica*, 8(7):837–842, Jul 1974.

[321] E. Noah and S. Iyengar. 'Fatigue and oxidation resistance of tungsten and its alloys.' Technical Report EDMS 1218205, European Spallation Source and Lund University, 2012.

[322] L. Commin, M. Rieth, B. Dafferner, et al. 'Oxidation study of pure tungsten.' Technical Report EDMS 1165708, Karlsruhe Institute of Technology, 2012.

[323] 'ITER materials assessment report (MAR).' ITER Doc. G 74 MA 10 01-07-11 W0.3 (internal project document distributed to the ITER participants).

[324] N. Watanabe. 'Neutronics of pulsed spallation neutron sources.' *Reports on Progress in Physics*, 66(3):339, Mar 2003.

[325] T. Kai et al. 'Coupled hydrogen moderator optimization with ortho/para hydrogen ratio.' *Nuclear Instruments and Methods A*, 523(3):398–414, May 2004.

[326] T. Kai et al. 'Neutronic performance of rectangular and cylindrical coupled hydrogen moderators in wide-angle beam extraction of low-energy neutrons.' *Nuclear Instruments and Methods A*, 550(1–2):329–342, Sep 2005.

[327] F. Mezei and M. Russina. 'Neutron-optical component array for the specific spectral shaping of neutron beams or pulses.' European Patent EP1468427 B1, 2002.

[328] D. B. Pelowitz, editor. *MCNPX User's Manual, Version 2.7.0*. LA-CP-11-0438. Los Alamos National Laboratory report, Apr 2011.

[329] K. Niita, N. Matsuda, Y. Iwamoto, et al. *PHITS: Particle and Heavy Ion Transport Code System*. JAEA, Japan Atomic Energy Agency, 2010. Version 2.23, JAEA-Data/Code 2010-022.

[330] K. A. V. Riper. *Moritz User's Guide*. White Rock Science, 2000-2012 (2012).

[331] 'Monte carlo modeling interface program.' http://www.fds.org.cn/en/software/mcam_1.asp.

[332] H. Tsige-Tamirat and U. Fischer. 'CAD interface for Monte Carlo particle transport codes.' In *The Monte Carlo Method: Versatility Unbounded in a Dynamic Computing World*. American Nuclear Society, LaGrange Park, IL, April 2005.

[333] Y. Wu et al. 'CAD-based interface programs for fusion neutron transport simulation.' *Fusion Engineering and Design*, 84(7–11):1987–1992, Jun 2009.

[334] D. Filges and F. Goldenbaum. *Handbook of Spallation Research: Theory, Experiments and Applications*. Wiley-VCH, 2010.

[335] K. Batkov, F. Mezei, A. Takibayev, et al. 'Optimisation of the coupling between the ESS accelerator and target: Sensitivity to the proton beam profile.' In *20th Meeting of the The International Collaboration on Advanced Neutron Sources, ICANS XX*. Bariloche, Río Negro, Argentina, Mar 2012.

[336] Y. Nara, N. Otuka, A. Ohnishi, et al. 'Relativistic nuclear collisions at 10 AGeV energies from p+Be to Au+Au with the hadronic cascade model.' *Physical Review C*, 61(2):024901, 1999.

[337] H. W. Bertini. 'Intranuclear-cascade calculation of the secondary nucleon spectra from nucleon-nucleus interactions in the energy range 340 to 2900 MeV and comparisons with experiment.' *Physical Review*, 188(4):1711–1730, 1969.

[338] M. B. Chadwick et al. 'ENDF/B-VII.0: Next generation evaluated nuclear data library for nuclear science and technology.' *Nuclear Data Sheets*, 107(12):2931–3060, 2006.

[339] Target Division. 'Target station design update baseline.' Technical Report EDMS 1166507, European Spallation Source, 2011.

[340] Institut Laue-Langevin. 'ILL Yellow Book 2008.' http://www.ill.eu/?id=1379, 2008.

[341] F. Mezei. 'ESS target-moderator performance estimates.' Technical Report ESS-0002734, European Spallation Source, 10 May 2010.

[342] A. Konobeyev, U. Fischer, and L. Zanini. 'Advanced evaluations of displacement and gas production cross sections for chromium, iron, and nickel up to 3 GeV incident particle energy.' In *Proceedings of the 10th International Topical Meeting on Nuclear Applications and Utilization of Accelerators, AccApp11*. Knoxville, TN, US, Apr 2011.

[343] K. Lefmann and K. Nielsen. 'McStas, a general software package for neutron ray-tracing simulations.' *Neutron News*, 10(3):20–23, 1999.

[344] P. Willendrup, E. Farhi, and K. Lefmann. 'McStas 1.7: A new version of the flexible Monte Carlo neutron scattering package.' *Physica B*, 350(1–3):E735–E737, Jul 2004.

[345] E. Klinkby et al. 'Interfacing MCNPX and McStas for simulation of neutron transport.' *Nuclear Instruments and Methods A*, 700:106–110, 2013.

[346] D. Baxtor, A. Crabtree, P. Ferguson, et al. 'Spallation Neutron Source moderator overview.' In *IAEA Advanced Moderator Workshop*. Tsukuba, Japan, Nov 2011.

[347] F. X. Gallmeier, M. Wohlmuther, U. Filges, et al. 'Implementation of neutron mirror modeling capability into MCNPX and its demonstration in first applications.' *Nuclear Technology*, 168(3):768–772, Dec 2009.

[348] U. Filges et al. 'Optimization criteria for the bi-spectral moderator and their application for deriving figure of merit for the MCNP-based optimization of the European Spallation Source target-moderator-reflector system.', 2012. Paul Scherrer Institute (PSI) Internal Report.

[349] T. McManamy, M. Rennich, F. Gallmeier, et al. '3 MW solid rotating target design.' *Journal of Nuclear Materials*, 398(1–3):35–42, Mar 2010.

[350] R. Hanslik. 'Sicherheitstechnische analyse und auslegungsaspekte von abschirmungen gegen teilchenstrahlung am beispiel von spallationsanlagen im megawatt bereich.' Technische Berichte des Forschungszentrums Jülich 4225, ISSN 0944-2952, D468, Forschungszentrums Jülich, 2006.

[351] Siempelkamp. 'ESS target shielding – selection of materials, workpackage 3.1.' Technical Report, Siempelkamp Nukleartechnik GmbH, Krefeld, Germany, Dec 2003.

[352] ANSYS®. 'Academic research, release 14.0.'

[353] Y. Chen, F. Arbeiter, and G. Schlindwein. 'A comparative study of turbulance models for conjugate heat transfer to gas flow in a heated mini-channel.' *Numerical Heat Transfer*, 61(1):38–60, 2012.

[354] A. Takibayev. 'Technical note on heat deposition in tungsten target.' Technical Report EDMS 1164465, European Spallation Source, 2012.

[355] D. Ene. 'Evaluation of ESS safety concerns assuming two basic concepts of the target station.' Technical Report EDMS 1183351, European Spallation Source, 2011.

[356] C. Kharoua. 'Design calculation report. Estimation of the impact of the after heat - LOCA.' Technical Report EDMS 1164510, European Spallation Source, 2012.

[357] PLANSEE GmbH. *Catalog: Tungsten Material Properties and Applications*. http://www.plansee.com/en/Materials-Tungsten-403.htm.

[358] AFCEN (Association Française pour les régles de Conception, de construction et de surveillance en exploitation des matériels des Chaudières Electro Nucléaires). 'RCC-MR:2007 – design and construction rules for mechanical components of nuclear installations applicable to high temperature structures and to the ITER vacuum vessel.' http://www.afcen.org/, 2007.

[359] T. Lebarbé, D. Hyvert, S. Marie, et al. 'Presentation of RCC-MRx code 2010 for sodium reactors (SFR), research reactor (RR) and fusion (ITER): General overview and CEN-workshop.' *ASME Conference Proceedings*, Volume 1: Codes and Standards(PVP2011-57614):393–399, 2011.

[360] T. Shea. 'Diagnostic AIR.' ESS internal talk, 2012.

[361] P. Sabbagh. 'Cycle assumptions for fatigue analysis.' Technical Report, European Spallation Source, 2012.

[362] P. Sabbagh. 'Technical note on fatigue analysis.' Technical Report EDMS 1225592, European Spallation Source, 2012.

[363] J. Wolters, F. Albisu, G. S. Bauer, et al. 'Thermo-mechanical assessment of the disk target concept for the spallation neutron source in the Basque.' In *Proceedings of the 8th International Topical Meeting on Nuclear Applications and Utilization of Accelerators, AccApp07*. 2007.

[364] M. Berrada and J. Wolters. 'Leakage rate in labyrinth-seal systems.' Fzj-zat, Forschungszentrums Jülich, Oct 2012.

[365] M. Berrada and J. Wolters. 'Catalog: RDDM-rotatory direct drive motors.' *INA-Drives & Mechatronics*, pages 50–54, 2012.

[366] H. Haas. *Lebensdauerversuche an Kugellagern bei 120° C in Helium-Atmosphaere*. Forschungszentrums Jülich, 1986. ISSN 0366-0885.

[367] M. Berrada and J. Wolters. 'Catalog: Axial and radial roller bearings.' *INA- Rolling and plain bearings*, pages 50–54, 2012.

[368] P. Sabbagh and C. Kharoua. 'Flow blockage and its consequences on the temperature rise.' Technical Report EDMS 1225425, European Spallation Source, 2012.

[369] Y. Kasugai, K. Otsu, and T. Kai. 'Monitoring system of mercury target failure using radioactivity measurement.' *19th Meeting on Collaboration of Advanced Neutron Sources, ICANS XIX*, (398):35–42, 2010.

[370] K. Ferrell. 'Materials selection for the HFIR cold neutron source.' Technical Report ORNL/TM-99-208, Oak Ridge National Laboratory, 1999.

[371] Y. Beßler, M. Butzek, C. Tiemann, et al. 'MR design and simulation report.' Technical Report EDMS 1254214 (In preparation), Forschungszentrums Jülich, 2012.

[372] Y. Beßler, C. Tiemann, M. Butzek, et al. 'Schweißbarkeit und festigkeitsverhalten hochfester aluminiumlegierungen für den einsatz in spallations-neutronen-quellen.' Technical Report EDMS 1254224, Forschungszentrums Jülich, 2012.

[373] H. Ullmaier, A. Moslang, G. S. Bauer, et al. 'Spallation neutron for radiation damage research on nuclear materials.' In *Proceedings of the 16th Meeting of the International Collaboration on Advanced Neutron Sources*. Dusseldorf-Neuss, Germany, May 2003.

[374] M. Göhran. '2nd interface meeting between beam dump development within WU10.3 and appointed persons within the A2T group.' Technical Report EDMS 1226623, European Spallation Source, 2012.

[375] G. Schlindwein, F. Arbeiter, and J. Freund. 'Start-up phase of the HELOKA-LP low pressure helium test facility for IFMIF irradiation modules.' In *Tenth International Symposium on Fusion Nuclear Technology, ISFNT-10*. 2010.

[376] Dresser Roots®, Dresser Inc. *Catalog: Blowers, Compressors and Controls*, 2011.

[377] Siemens Turbomachinary Equipment GmbH. *Reference List of Siemens Turbomachinary Equipment GmbH (Extract)*, Nov 2011.

[378] H. Teixeira. 'Preliminary design of a hurricane system for tungsten particulate capture, from helium coolant gas stream, on the spallation reaction.' Technical Report EDMS 1192485, Advanced Cyclone Systems, SA, 2012.

[379] R. Salcedo, J. Paiva, and C. Sousa. 'Hurricane/Mechanical ReCyclone® performance at pilot-scale.' Technical Report EDMS 1192485, Advanced Cyclone Systems, SA, 2012.

[380] F. Koch and H. Bolt. 'Self passivating W-based alloys as plasma facing material for nuclear fusion.' *Physica Scripta*, page 100, Mar 2007.

[381] B. Guidersa and J. X. Zhou. 'System analysis of the helium loop for ESS target.' Unpublished, KIT, Karlsruhe Institute of Technology.

[382] F. Plewinski, P. Nilsson, and P. Sabbagh. 'Intermediate cooling circuit for target He cooling - ingress into the helium cooling target circuit – TSDU Baseline V2 (N_2).' Technical Report EDMS 1226049, European Spallation Source, 2012.

[383] P. Nilsson et al. 'Helium purification - first design estimates.' Technical Report, European Spallation Source, 2013. In preparation.

[384] M. S. Yang, R. P. Wang, Z. Y. Liu, et al. 'The helium purification system of the HTR-10.' *Nuclear Engineering and Design*, 218:163–167, 2002.

[385] A. Ciampichetti, A. Aiello, G. Coccolutoa, et al. 'The coolant purification system of the European test blanket modules: Preliminary design.' *Fusion Engineering and Design*, 85(10–12):2033–2039, Dec 2010.

[386] K. Liger, X. Lefebvre, A. Ciampichetti, et al. 'HCLL and HCPB coolant purification system: Design of the copper oxide bed.' *Fusion Engineering and Design*, 86(9–11):1859–1862, Oct 2011.

[387] M. Göhran. 'Wall thickness calculation for hot cells.' Technical Report EDMS 1223237, European Spallation Source, 2012.

[388] Nuclear Industry Guidance. *An Aid to the Design of Ventilation of Radioactive Areas, Issue 1*, Jan 2009.

[389] *Norme Francaise ISO 11933-4: Composants pour enceintes de confinement, Partie 4: Systèmes de ventilation et d'épuration tels que filtres, pièges, vannes de régulation et de sécurité, organes de contrôle et de protection*, Sep 2001.

[390] *Norme Internationale, ISO 10648-2, Enceintes de confinement, Partie 2: Classification selon leur étanchéité et méthodes de controles associées*, Dec 1994.

[391] T. Hansson and P. Jacobsson. 'General safety objectives for ESS.' Technical Report EDMS 1148774, European Spallation Source, 2011.

[392] P. Nilsson et al. 'Estimates for water cooled tungsten rods.', 2012. In preparation.

[393] F. Sordo, M. Magan, J.-P. de Vicente, et al. 'Neutronic and thermohydraulic simulations.', 2012. In preparation.

[394] A. Zhukauskas. 'Heat transfer for tubes in crossflow.' In *Advances in Heat Transfer*, volume 8, page 93. Academic Press, 1972.

[395] K. Thomsen, M. Butzek, F. Gallmeier, et al. 'Options for water cooling of a SINQ-type canneloni at high power.' In *Proceedings of the 10th International Topical Meeting on Nuclear Applications and Utilization of Accelerators, AccApp11*. Knoxville, TN, US, Apr 2011.

[396] J. Wolters et al. 'CFD simulations and thermohydraulic analysis.', 2012. In preparation.

[397] K. Thomsen, F. Heinrich, M. Butzek, et al. 'Some technical issues for a cannelloni spallation-target at high power.' *Nuclear Instruments and Methods A*, 682:42–48, Aug 2012.

[398] W. Wagner, P. Vontobel, and Y. Dai. 'Materials issues for the SINQ high-power spallation target.' *International Journal of Materials Research*, (102):1101–1105, 2011.

[399] P. Sokol. 'Design and operating experience with a beryllium target for neutron generation.' In *Proceedings of the 20th Meeting on Collaboration of Advanced Neutron Sources, ICANS XX*. 2012.

[400] R. S. Lillard, D. L. Pile, and D. P. Butt. 'The corrosion of materials in water irradiated by 800 MeV protons.' *Journal of Nuclear Materials*, 278(2–3):277–289, Apr 2000.

[401] M. Magán, S. Terrón, F. Sordo, et al. 'Union of compact accelerator-driven neutron sources (UCANS) I & II, calculations for ESS-Bilbao low energy target.' *Physics Procedia*, 26:124–131, 2012.

[402] M. Magán, S. Terrón, K. Thomsen, et al. 'Neutron performance analysis for ESS target proposal.' *Nuclear Instruments and Methods A*, 680:61–68, Jul 2012.

[403] C. Fazio et al. 'ESS 2012 LBE technical report.' Technical report, Karlsruhe Institute of Technology, 2012.

[404] E. Noah et al. 'TSCS final report on lead options for the ESS target.' Technical Report EDMS 1108740, European Spallation Source, 2010.

[405] J. Wolters. 'FP7 - neutron source ESS - investigation of upgradeability of ESS.' Technical Report GA No. 202247, European Community.

[406] C. Fazio et al. *Handbook on Lead-bismuth Eutectic Alloy and Lead Properties, Materials Compatibility, Thermal-hydraulics and Technologies*. ISBN 978-92-64-99002-9. OECD/NEA (Organisation for Economic Cooperation and Development/Nuclear Energy Association), 2007.

[407] C. Fazio et al. 'Proceedings of the international DEMETRA workshop on development and assessment of structural materials and heavy liquid metal technologies for transmutation systems.' *Journal of Nuclear Materials*, 415(3):227–459, Aug 2011.

[408] F. Stefani and G. Gerbeth. 'A contactless method for velocity reconstruction in electrically conducting fluids.' *Measurement Science and Technology*, 11:758–765, 2000.

[409] F. Stefani, G. Gerbeth, and T. Gundrum. 'Contactless inductive flow tomography.' *Physical Review E*, 70(056306), 2004.

[410] T. Wondrak, V. Galindo, G. Gerbeth, et al. 'Contactless inductive flow tomography for a model of continuous steel casting.' *Measurement Science and Technology*, 21(045402), 2010.

[411] L. Zanini et al. 'Experience from the post-test analysis of MEGAPIE.' *Journal of Nuclear Materials*, 415:367–377, 2011.

[412] 'ESS update report.' http://neutron.neutron-eu.net/n_documentation/n_reports/n_ess_reports_and_more/106, Dec 2003.

[413] J. Neuhausen. 'Environmental compliance report concerning the radioactive inventory.' EC-FP7 Project ESS-PP Deliverable D 8.2, Paul Scherrer Institute (PSI), 2010.

[414] J. Neuhausen. 'Environmental compliance report concerning the target material.' EC-FP7 Project ESS-PP Deliverable D 8.1, Paul Scherrer Institute (PSI), 2010.

[415] F. Groeschel, J. Neuhausen, A. Fuchs, et al. 'Intermediate safety report, treatment of the reference accident case.' MPR-3-GF34-001/0, Paul Scherrer Institute (PSI), 2006.

[416] E. Pitcher. 'Summary report on neutronics work in support of MEGAPIE.' Technical report, Los Alamos National Laboratory (LANL), 2002.

[417] C. Perret. 'Sicherheitsbericht zum MEGAPIE-experiment an einem target mit flussigem bleibismuth-eutektikum in der neutronenquelle SINQ des PSI-west.' Technical report, Paul Scherrer Institute (PSI), 2002.

[418] S. Gammino et al. 'Tests of the Versatile Ion Source (VIS) for high power proton beam production.' In *19th International Workshop on ECR Ion Sources, ECRIS 2010, Proceedings*, MOPOT012. Grenoble, 2010.

[419] R. Gobin et al. 'High intensity ECR ion source (H^+, D^+, H^-) developments at CEA/Saclay.' *Review of Scientific Instruments*, 73(2):922–924, Feb 2002.

[420] L. M. Young. 'Operations of the LEDA resonantly coupled RFQ.' In *Particle Accelerator Conference, PAC 2001*, volume 1, pages 309 – 313. 2001.

[421] CEA France. 'TraceWin linac beam physics simulation package.' http://irfu.cea.fr/Sacm/logiciels/index3.php, last accessed 21 Jan 2013.

[422] ANSYS. 'Product description for Fluent simulation software.' http://www.ansys.com/Products/Simulation+Technology/Fluid+Dynamics/Fluid+Dynamics+Products/ANSYS+Fluent, last accessed 21 Jan 2013.

[423] European Spallation Source. 'ESS parameter tables.' https://bled.esss.dk/ParametersEditor/?pl=High%20Level%20Parameters, last accessed 23 Jan 2013.

[424] H. Padamsee et al. *RF Superconductivity for Accelerators*. ISBN 978-3-527-40842-9. Wiley-VCH, 2008.

[425] F. Gerigk et al. 'Choice of frequency, gradient and temperature for a superconducting proton linac.' Technical Report CERN-AB-2008-064, Cern, A&B Department, Sep 2008.

[426] M. Harrison, S. Peggs, et al. 'ESS Frequency Advisory Board report.' Internal Report ESS-doc-250-v1, European Spallation Source, Jul 2010.

[427] M. Eshraqi et al. 'Design and beam dynamics study of hybrid ESS linac.' In *IPAC2011 Proceedings*, WEPS062. 2011.

[428] A. Ponton. 'Investigations of diffferent pole tips geometries for the ESS RFQ, part 1.' ESS AD Technical Notes ESS/AD/0009, European Spallation Source, March 2011.

[429] C. K. Allen and T. P. Wangler. 'Beam halo definitions based upon moments of the particle distribution.' *Physical Review ST Accel. Beams*, 5(124202), Dec 2002.

[430] J. Lagniel. 'Halos and chaos in space-charge dominated beams.' In *EPAC96 Proceedings*, page 163. 1996.

[431] A. I. S. Holm et al. 'The high energy beam transport system for the European Spallation Source.' In *IPAC 2011 Proceedings*, THPS050. 2011.

[432] R. Duperrier et al. 'CEA Saclay codes review for high intensities linacs computations.' In *International Conference on Computational Science, ICCS 2002, Proceedings*, pages 411–418. 2002.

[433] H. Danared. 'Design of the ESS accelerator.' In *IPAC 2012 Proceedings*, THPPP071, page 3904. 2012.

[434] M. Eshraqi et al. 'End to end beam dynamics of the ESS linac.' In *IPAC 2012 Proceedings*, THPPP085, pages 3933–3935. 2012.

[435] T. P. Wangler. *RF Linear Acclerators*. Wiley-VCH, 2nd edition, 2008.

[436] M. Eshraqi, H. Danared, and R. Miyamoto. 'Beam dynamics of the ESS superconducting linac.' In *Proceedings of the 52nd ICFA Advanced Beam Dynamics Workshop on High-Intensity and High-Brightness Hadron Beams*, TUO3B02. 2012.

[437] D. Jeon et al. 'Formation and mitigation of halo particles in the Spallation Neutron Source linac.' *Physical Review ST Accel. Beams*, 5(094201), Sep 2002.

[438] R. Miyamoto et al. 'Numerical study of a collimation system to mitigate beam losses in the ESS linac.' In *IPAC2012 Proceedings*, MOPPC027, page 541. 2012.

[439] R. Miyamoto, I. Bustinduy, B. Cheymol, et al. 'Beam loss and collimation in the ESS linac.' In *Proceedings of the 52nd ICFA Advanced Beam Dynamics Workshop on High-Intensity and High-Brightness Hadron Beams*, WEO3A02. Beijing, China, 2012.

[440] M. Schuh et al. 'Influence of higher order modes on the beam stability in the high power superconducting proton linac.' *Physical Review ST Accel. Beams*, 14(051001), May 2011.

[441] S. Molloy. 'An empircal study of HOM frequencies.' Technical Report ESS-doc-92-v2, European Spallation Source, 2011.

[442] R. Ainsworth. *Thesis in preparation.* Ph.D. thesis, Royal Holloway, University of London, to be published in 2013.

[443] R. Ainsworth and S. Molloy. 'The influence of parasitic modes on beam dynamics for the European Spallation Source linac.' *Nuclear Instruments and Methods A*, 2012. ISSN 0168-9002. doi:10.1016/j.nima.2012.11.034.

[444] L. Celona et al. 'Status of the Trasco Intense Proton Source and emittance measurements.' *Review of Scientific Instruments*, 75(5):1423–1426, 2004.

[445] R. Miracoli et al. 'Note: Emittance measurements of intense pulsed proton beam for different pulse length and repetition rate.' *Review of Scientific Instruments*, 83(056109), 2012.

[446] D. Mascali et al. 'Electrostatic wave heating and possible formation of self-generated high electric fields in a magnetized plasma.' *Nuclear Instruments and Methods A*, 653-1:11–16, Oct 2011.

[447] H. P. Laqua. 'Electron Bernstein wave heating and diagnostic.' *Plasma Physics and Controlled Fusion*, 49(R1), 2007.

[448] G. Castro et al. 'Comparison between off-resonance and electron Bernstein waves heating regime in a microwave discharge ion source.' *Review of Scientific Instruments*, 83(02B501), 2012.

[449] F. F. Chen. *Introduction to the Plasma Physics and Controlled Fusion.* London Press, 2nd edition, 1986.

[450] L. Neri. 'RF system design report.' Internal Report ADU_1.6.2.1.6, European Spallation Source, 2012.

[451] B. Cheymol et al. 'First results from beam measurements at the 3 MeV test stand for CERN Linac4.' In *DIPAC 2011 Proceedings*, MOPD52, page 167. 2011.

[452] B. Cheymol et al. 'Design of the emittance meter for the 3 and 12 MeV Linac4 H^- Beam.' In *IPAC 2010 Proceedings*, MOPE052, page 1089. 2010.

[453] F. Senée et al. 'Diagnostics for high power ion beams with coherent fiber for IFMIF-EVEDA injector.' In *DIPAC 2009 Proceedings*, TUPB14, page 197. 2009.

[454] F. Grespan. 'Equivalent circuit for postcoupler stabilization in a drift tube linac.' *Physical Review ST Accel. Beams*, 15(010101), Jan 2012.

[455] A. Ismail et al. 'Space charge compensation in low energy proton beams.' In *LINAC 2004 Proceedings*, TUP15, page 324. Sep 2004.

[456] L. Tchelidze and J. Stoval. 'Estimations of residual dose rates and beam loss limits in the ESS linac.' ESS AD Technical Note ESS/AD/0039, European Spallation Source, Apr 2012.

[457] L. Tchelidze and J. Stoval. 'Estimations of residual dose rate and beam loss limits in the ESS linac.' ESS AD Technical Note ESS/AD/0026, European Spallation Source, Feb 2012.

[458] Linac4 Beam Coordination Committee - Meeting 17. Pre-chopper and 3 MeV chopper beam dynamics. CERN, 29 Jul 2010. http://indico.cern.ch/conferenceDisplay.py?confId=101517.

[459] F. Gerigk et al. 'High current linac design with examples of resonances and halo.' In *LINAC 2002 Proceedings*, page 569. Gyeongju, Korea, 2002.

[460] J. L. Munoz and I. Rodriguez. 'Multiphysics design of ESS-Bilbao linac accelerating cavities.' In *Proceedings of the COMSOL Conference 2011*. Stuttgart, 2011.

[461] O. Gonzalez et al. 'Preliminary electromagnetic design of the re-bunching RF cavities for the ESS MEBT.' ESS AD Technical Note ESS/AD/0036, European Spallation Source, Mar 2012.

[462] O. Gonzalez et al. 'Electromagnetic design of the tuning system for the re-bunching cavities of the ESS MEBT.' ESS AD Technical Note ESS/AD/0035, European Spallation Source, Mar 2012.

[463] O. Gonzalez. 'Electromagnetic design of a power coupler for the ESS MEBT.' Internal Report ADU_1.6.4.1.9, Accelerating Structures Group, ESS Bilbao, 2012.

[464] A. Ghiglino et al. 'Rebunching cavity: Preliminary design report.' ESS AD Technical Note ESS/AD/0037, European Spallation Source, Mar 2012.

[465] A. Ghiglino et al. 'Rebunching cavity: Results of first iteration with real heat generation.' ESS AD Technical Note ESS/AD/0038, European Spallation Source, Mar 2012.

[466] S. Ramberger et al. 'Drift tube linac design and prototyping for the CERN LINAC4.' In *LINAC 2008 Proceedings*, MOP049, page 184. 2008.

[467] 'COMSOL multiphysics modeling and simulation software.' http://www.comsol.com/, last accessed 22 Jan 2013.

[468] M. Lindroos et al. 'Parameter choices for the ESS linac design.' In *Proceedings of LINAC 2012*. Tel Aviv, Israel, To be published.

[469] 'CARE: Coordinated Accelerator Research in Europe for Particle Physics. Description of European collaborative research programme.' http://ec.europa.eu/research/infrastructures/pdf/care.pdf, last accessed 22 Jan 2013.

[470] 'High Intensity Pulsed Proton Injectors (HIPPI).' http://mgt-hippi.web.cern.ch/mgt-hippi/, last accessed 22 Jan 2013.

[471] C. Darve, G. Ferlin, M. Gautier, et al. 'Thermal performance measurements for a 10 meter LHC dipole prototype (cryostat thermal model 2).' LHC-Project-Note-112, CERN, 1998.

[472] X. Wang, W. Hees, and T. Köttig. 'Preliminary heat load estimates of some cryogenic components for ESS.' ESS AD Technical Note ESS/AD/0041, European Spallation Source, Jun 2012.

[473] C. Darve. 'Cryogenics for the new European Spallation Source.' In *Proceedings of the International Cryogenic Engineering Conference, ICEC23*. 2012.

[474] X. Wang, J. Weisend II, T. Koettig, et al. 'ESS linac cryogenic plant.' In *Proceedings of the International Conference on Cryogenics and Refrigeration (ICCR)*. 2013.

[475] P. Gomes, E. Blanco, et al. 'The control system for the cryogenics in the LHC tunnel.' LHC-Project-Report-1169, CERN, 2008.

[476] C. Darve, C. Balle, J. Casas-Cubillos, et al. 'Instrumentation status of the low-β magnet systems at the Large Hadron Collider (LHC).' In *Proceedings of the International Cryogenic Engineering Conference, ICEC22*. 2010.

[477] M. Jones, H. M. Durand, D. Missiaen, et al. 'Status report on the survey and alignment of the accelerators at CERN.' In *Proceedings of the 9th International Workshop on Accelerator Alignment*. Sep 2006.

[478] 'Computer Simulation Technology (CST) Microwave Studio (MWS) Simulation Software.' http://www.cst.com/Content/Products/MWS/Overview.aspx, last accessed 5 Jan 2013.

[479] G. Olry et al. 'Spoke cavity RF design.' Internal Report TR-ADU_1.4.2.2.8, Institut de Physique Nucleaire d'Orsay, 2012.

[480] P. Duchesne et al. 'Spoke cavity mechanical design.' Internal Report TR_ADU_1.4.2.2.20, Institut de Physique Nucleaire d'Orsay, 2012.

[481] N. Gandolfo et al. 'Spoke cold tuning system conceptual design.' Internal Report TR_ADU_1.4.3.3, Institut de Physique Nucleaire d'Orsay, 2012.

[482] E. Rampnoux et al. 'Spoke power coupler conceptual design.' Internal Report TR_ADU_1.4.4.4, Institut de Physique Nucleaire d'Orsay, 2012.

[483] S. Bousson et al. 'Spoke cavity developments for the EURISOL driver.' In *Proceedings of the 2006 Linear Accelerator Conference, LINAC 06*. Knoxville, USA, Aug 2006.

[484] D. Reschke et al. 'Analysis of RF results of recent nine-cell cavities at DESY.' In *SRF 2009 Proceedings*, TUPPO051, page 342. 2009.

[485] J. L. Biarrotte et al. '704 MHz superconducting cavities for a high-intensity proton accelerator.' In *1999 Workshop on RF Superconductivity, SRF99, Proceedings*, WEP005, page 384. 1999.

[486] G. Devanz et al. 'Stiffened medium beta 704 MHz elliptical cavity for a pulsed proton linac.' In *13th International Workshop on RF Superconductivity , SRF 2007, Proceedings*, TUP81. Beijing, China, 2007.

[487] S. Kim. 'Higher order mode analysis of the SNS superconducting linac.' In *Particle Accelerator Conference, PAC 2001, Proceedings*, MPPH149, page 1128. 2001.

[488] P. B. Wilson. 'High energy electron linacs: Applications to storage ring RF systems and linear colliders.' SLAC-PUB-2884 (rev.), Stanford Linear Accelerator Center, Stanford University, Stanford, California, 1991.

[489] J. Plouin et al. 'Optimized RF design of 704 MHz beta=1 cavity for pulsed proton drivers.' In *Proceedings of the 15th International Conference on RF Superconductivity, SRF 2011*, MOPO034. 2011.

[490] G. Devanz et al. 'High power pulsed tests of a beta=0.5 5-cell 704 MHz superconducting cavity.' In *15th International Conference on RF Superconductivity, SRF 2011, Proceedings*, TUPO002, page 1459. 2011.

[491] J.-P. Charrier, S. Chel, M. Desmons, et al. '704 MHz high power coupler and cavity development for high power pulsed proton linacs.' In *Proceedings of the XXIV Linear Accelerator Conference, LINAC08*, THP006. 2008.

[492] S. Mitsunobu et al. 'High power input coupler for KEKB SC cavity.' In *The 1999 Workshop on RF Superconductivity, SRF99, Proceedings*, WEP032, page 505. 1999.

[493] I. Campisi et al. 'The fundamental power coupler for the Spallation Neutron Source (SNS) superconducting cavities.' In *Particle Accelerator Conference, PAC 2001, Proceedings*, MPPH153, page 1140. 2001.

[494] M. Stirbet. 'Retrospective on fundamental power couplers for the Spallation Neutron Source at Oak Ridge.' In *XXV Linear Accelerator Conference, LINAC10, Proceedings*, THP051, page 866. 2010.

[495] G. Devanz et al. 'Cryogenic tests of a 704 MHz 1 MW power coupler.' In *IPAC 2010 Proceedings*, WEPEC001, page 2884. 2010.

[496] M. Lindroos et al. 'Upgrade strategies for high power proton linacs.' In *IPAC 2011 Proceedings*, WEPS064, page 2646. http://accelconf.web.cern.ch/accelconf/IPAC2011/papers/weps064.pdf, San Sebastian, Spain, 2011.

[497] *Electromagnetic compatibility (EMC) - Part 3-5: Limits - Limitation of voltage fluctuations and flicker in low-voltage power supply systems for equipment with rated current greater than 75 A*. International Electrotechnical Commission, http://webstore.iec.ch/webstore/webstore.nsf/Artnum_PK/43153, 2009.

[498] *Electromagnetic compatibility (EMC) - Part 2-4: Environment - Compatibility levels in industrial plants for low-frequency conducted disturbances*. International Electrotechnical Commission, http://webstore.iec.ch/webstore/webstore.nsf/ArtNum_PK/28826?OpenDocument, 2002.

[499] *Industrial, scientific and medical equipment - Radio-frequency disturbance characteristics - Limits and methods of measurement*. International Electrotechnical Commission, http://webstore.iec.ch/webstore/webstore.nsf/Artnum_PK/43918, 2009.

[500] *Electromagnetic compatibility (EMC) – Part 4-4: Testing and measurement techniques – Electrical fast transient/burst immunity test*. International Electrotechnical Commission, http://webstore.iec.ch/webstore/webstore.nsf/Artnum_PK/977673, 2012.

[501] L. Tchelidze. 'In how long the ESS beam pulse would start melting steel/copper accelerating components?' ESS AD Technical Note ESS/AD/0031, European Spallation Source, Feb 2012.

[502] A. Nordt. 'Machine protection system requirement document.' Internal Report, European Spallation Source, 2012.

[503] H. Hassanzadegan. 'Beam current monitors requirement document.' Internal Report, European Spallation Source, June 2012.

[504] S. Peggs, editor. *ESS Conceptual Design Report*. ESS-2012-001. European Spallation Source AB, Lund, Sweden, available at https://dl.dropboxusercontent.com/u/24187786/ess/CDR_final_120206.pdf, 6 Feb 2012.

[505] H. Hassanzadegan. 'Beam position and phase monitors requirement document.' Internal Report, European Spallation Source, June 2012.

[506] 'FLUKA particle physics Monte Carlo simulation package.' http://www.fluka.org/fluka.php, last accessed 23 Jan 2013.

[507] T. Giacomini et al. 'Ionization profile monitors - IPM @ GSI.' In *Proceedings of DIPAC 2011*, TUPD51, page 419. Hamburg, Germany, 2011.

[508] C. Böhme, J. Dietrich, V. Kamerdzhiev, et al. 'Beam profile monitoring at COSY via light emitted by residual gas.' In *Proceedings of DIPAC 2009*, TUPB10, pages 185–187. Basel, Switzerland, 2009.

[509] W. Blokland, S. Aleksandrov, S. M. Cousineau, et al. 'Electron scanner for SNS ring profile measurements.' In *Proceedings of DIPAC 2009*, TUOA03, page 155. Basel, Switzerland, May 2009.

[510] N. I. Balalykin, C. Boehme, O. I. Brovko, et al. 'Development of beam position and profile monitor based on light radiation of atoms excited by the beam particles.' In *Proceedings of RuPAC XIX*, WEHP42. Dubna, Russia, 2004.

[511] T. J. McManamy, T. Shea, W. Blokland, et al. 'Spallation Neutron Source target imaging system operation.' In *Proceedings of Tenth International Topical Meeting on Nuclear Applications of Accelerators (AccApp11)*. http://www.new.ans.org/store/c_5, Apr 2011.

[512] P. D. Sheriff. *Fundamentals of N-tier Architecture*. Barnes & Noble, 2006.

[513] J. O. Hill et al. *EPICS R3.14 Channel Access Reference Manual*. 2010.

[514] M. R. Kraimer et al. *EPICS: Input / Output Controller Application Developer's Guide*. 2004.

[515] G. Trahern. 'ESS Naming Convention.' ESS/AD/0005, European Spallation Source, 2010.

[516] A. Nordt, F. Plewinski, and T. Shea. 'Operational machine states and modes.' ESS AD Technical Note ESS/AD/0044, European Spallation Source, Sep 2012.

[517] H. E. Roland and B. Moriarty. *System Safety Engineering and Management*. John Wiley and Sons, 1990.

[518] N. G. Leveson. 'A new accident model for engineering safer systems.' *Safety Science*, 42:237–270, 2004. doi:doi:10.1016/S0925-7535(03)00047-X.

[519] D. Smith and K. Simpson. *Safety Critical Systems Handbook: A Straightforward Guide to Functional Safety, IEC 61508 (2010 Edition) And Related Standards, Including Process IEC 61511, and Machinery IEC 62061 and ISO 13849*. Butterworth-Heinemann (Elsevier), Oxford, England and Burlington, MA, third edition, 2011.

[520] 'Functional safety of electrical/electronic/programmable electronic safety-related system - part 1: General requirements.' Industrial Safety Standard IEC 61508-1, first edition, International Electrotechnical Comission (IEC), 1998.

[521] 'Functional safety of electrical/electronic/programmable electronic safety-related system - part 4: Definitions and abbreviations.' Industrial Safety Standard IEC 61508-4, second edition, International Electrotechnical Comission (IEC), 2010.

[522] M. Stockner. *Beam loss calibration studies for high energy proton accelerators*. Ph.D. thesis, Vienna Technical University - Institute for Theoretical Physics, 2008.

[523] 'Definition from Wikipedia: Subharmonic.' http://en.wikipedia.org/wiki/Subharmonic, last accessed 21 Feb 2013.

[524] J. Pietarinenn. 'MRF Timing System.' Timing workshop CERN, http://www.mrf.fi/pdf/presentations/MRF.CERN.Feb2008.pdf, Feb 2008.

[525] 'EPICS Process Variable Gateway.' http://www.aps.anl.gov/epics/extensions/gateway/index.php, last accessed 21 Feb 2013.

[526] 'EPICS Channel Archiver and Archive Viewer.' http://ics-web.sns.ornl.gov/kasemir/archiver/, last accessed 21 Feb 2013.

[527] 'IRMIS: Integrated Relational Model of Installed Systems.' http://irmis.sourceforge.net/, last accessed 21 Feb 2013.

[528] A. Wallander. 'Plant system I&C architecture.' Version 2.3, ITER, 7 Feb 2011.

[529] T. Erl. *Service-Oriented Architecture: Concepts, Technology, and Design*. Prentice Hall, 2005.

[530] 'ISO/IEC 15288:2008, Systems and software engineering - System life cycle processes.', 2008.

[531] J. Galambos et al. 'XAL – The SNS application programming infrastructure.' In *Proceedings of EPAC 2004*. Lucerne, Switzerland, 2004.

[532] I. Verstovsek, K. Zagar, and T. Satogata. 'European Spallation Source control system study.' Technical Report CSL-DOC-10-53451, CosyLab, 2010.

[533] P. Lapostolle and M. Weiss. 'Formulae and procedures useful for the design of linear accelerators.' Technical Report CERN-PS-2000-001, European Organisation for Nuclear Research, (CERN - PS Division), http://cdsweb.cern.ch/record/428133/files/, last accessed 10 Apr 2013, 2010.

[534] C. K. Allen, M. Ikegami, et al. 'XAL online model enhancements for J-PARC commissioning and operation.' In *Proceedings of the 2007 Particle Accelerator Conference*, MOPAN029. Albuquerque, NM USA, available at http://accelconf.web.cern.ch/accelconf/p07/PAPERS/MOPAN029.PDF, last accessed 10 Apr 2013, 2007.

[535] 'Definition of the term "artifact" in PC Magazine's online encyclopedia.' http://www.pcmag.com/encyclopedia_term/0,1237,t=artifact&i=37999,00.asp, last accessed 18 Feb 2013.

[536] 'Jenkins CI home page.' http://jenkins-ci.org/, last accessed 19 Feb 2013.

[537] 'Apache maven project homepage.' http://maven.apache.org/general.html, last accessed 19 Feb 2013.

[538] 'Artifactory open source repository manager homepage.' http://www.jfrog.com/home/v_artifactory_opensource_technology, last accessed 19 Feb 2012.

[539] 'Mercurial SCM homepage.' http://mercurial.selenic.com/, last accessed 19 Feb 2013.

[540] 'JUnit software testing framework homepage.' http://junit.sourceforge.net/, last accessed 19 Feb 2013.

[541] 'Bugzilla home page.' http://www.bugzilla.org/, last accessed 21 Feb 2013.

[542] D. Gurd et al. 'Human-Machine Interface (HMI) Standard [for SNS].' https://ics-web.sns.ornl.gov/hmi/hmiStandard.pdf, Mar 2003.

[543] C. Rode. 'The SNS superconducting linac system.' In *Proceedings of the 2001 Particle Accelerator Conference, PAC2001*, pages 619 – 623. IEEE, 2001.

[544] T. Peterson. 'Notes about the limits of heat transport from a TESLA helium vessel with a nearly closed saturated bath of helium II.' Report 1994-18, TESLA, Hamburg, 1993.

[545] S. Van Sciver. *Helium Cryogenics*. Plenum Press, New York and London, 2012.

[546] P. Lebrun. 'Large cryogenic helium refrigeration system for the LHC.' In *Proceedings of the 3rd International Conference on Cryogenics & Refrigeration, ICCR2003*, pages 11–13. 2003.

[547] N. Ohuchi et al. 'Study of thermal radiation shields for the ILC cryomodule.' *Advances in Cryogenic Engineering*, 57A:292–936, 2012.

[548] D. Arenius et al. 'Overview and status of the 12 GeV cryogenic system upgrade at JLab.' *Advances in Cryogenic Engineering*, 55:1087–1091, 2010.

[549] M. White. 'Spallation Neutron Source (SNS).' In *Advances in Cryogenic Engineering: Proceedings of the Cryogenic Engineering Conference - CEC*, volume 613 of *AIP Conference Proceedings*, pages 15–24. 2002.

[550] T. Aso. 'Design result of the cryogenic hydrogen circulation system for 1 MW pulse spallation neutron source (JNSN) in JPARC.' In *Advances in Cryogenic Engineering: Transactions of the Cryogenic Engineering Conference - CEC*, volume 823 of *AIP Conference Proceedings*, pages 763–770. 2005.

[551] J. Weisend II et al. 'The cryogenic system for the SLAC E158 experiment.' *Advances in Cryogenic Engineering*, 47A:171–179, 2002.

[552] S. Gallimore. 'Private communication.', 2012.

[553] T. Peterson. 'Recent cryogenics activity and plans at Fermilab. Presentation at 2010 cryogenic operations workshop.' List of workshop presentations available at: http://www.triumf.info/hosted/cryo-ops/program.html, 2010.

[554] 'Cryogenics operations workshop.' Vancouver, BC, hosted by TRIUMF. Presentations available at http://www.triumf.info/hosted/cryo-ops/committee.html, 2010.

[555] R. Ruber, V. Ziemann, and T. Ekelöf. 'RF development for ESS.' Internal Memo RR/2009/02, Uppsala University, 2009.

[556] J. Knobloch et al. 'HoBiCaT – A test facility for superconducting RF systems.' In *Proceedings of the 11th Workshop on RF Superconductivity*, MOP48, page 173. DESY, 2003.

[557] P. Clay, J. Desvard, R. Duthil, et al. 'Cryogenic and electrical test cryostat for instrumented superconducting RF cavities (CHECHIA).' In P. Kittel, editor, *Advances in Cryogenic Engineering*, volume 41 of *A Cryogenic Engineering Conference Publication*, pages 905–910. Springer US, 1996.

[558] H. Saugnac et al. 'Cryogenic installation status of the "CRYHOLAB" test facility.' In *Proceedings of the 10th Workshop on RF Superconductivity*, PZ007, page 632. Tsukuba, Japan, 2001.

[559] H. Saugnac et al. 'CryHoLab, a horizontal cavity test facility: New results and development.' In *Proceedings of the 11th Workshop on RF Superconductivity*, MOP46, page 168. DESY, 2003.

[560] A. Sunesson. 'Utility requirements for test stand.' Internal Document RFS-TST-UTIL-REQ, version 1.2, European Spallation Source, Aug 2012.

[561] L. Lilje. 'XFEL: Plans for 101 cryomodules.' In *Proceedings of the 13th International Workshop on RF Superconductivity*, MO102. Beijing, China, 2007.

[562] A. Bokenstrand. 'Miljökonsekvensbeskrivning (environmental impact assessment).' ESS-0000007, submitted to Swedish regulatory authorities, European Spallation Source, 7 Mar 2012.

[563] C. Sverdrup and A. Bokenstrand. 'Teknisk beskrivning (technical description).' Submitted to Swedish regulatory authorities ESS-0000006, European Spallation Source, 7 Mar 2012.

[564] Lund Building Office (Stadsbyggnadskontoret). 'Fördjupning av översiktsplanen Brunnshög.' Lund municipal detailed land use plan and comprehensive plan for Brunnshög, 2 Mar 2012.

[565] 'Energy for sustainable science. ESS energy solution.' European Spallation Source brochure, Sep 2011.

[566] LEED. 'U.S. green building council enironmental classification system.' For more information see: http://new.usgbc.org/leed, last aqccessed 22 Feb 2013.

[567] BREEAM. 'BRE trust environmental assessment method and rating system.' For more information see: http://www.breeam.org, last accessed 22 Feb 2013.

[568] Sweden Green Building Council. 'Miljöbyggnad, environmental classification system.' For more information see: http://www.sgbc.se, 2012.

[569] B. Yndemark. 'Feasibility study – Fire safety strategy report.' ESS-0002381, European Spallation Source, 30 Oct 2012.

[570] T. Parker. 'ESS energy design report.' Technical Report ESS-0001761, European Spallation Source, 22 Jan 2013.

[571] B. Kildetoft. 'ESS building program, version 9.' Internal Document, European Spallation Source, Jan 2012.

[572] H. Norberg. 'BIM guidelines for conventional facilities and civil engineering work.' Internal Document ESS-0000340, European Spallation Source, 2011.

[573] 'Bygghandlingar 90: Del 7 redovisning av anläggning, del 8, digitala leveranser för bygg och förvaltning, utgåva 2.' See: http://www.bygghandlingar90.se/.

[574] Svensk Byggtjänst. 'BSAB 96. System och tillämpningar. Utgåva 3 (classification system).' For more information, see: http://bsab.byggtjanst.se/BSAB/Om, 2005.

[575] *CAD-lager. SB11.* Sv Byggtjänst AB, Utgåva 3, 2011. Rekommendationer för tillämpning av SS-ISO 13567.

[576] A. Lagergren. 'Östra Odarslöv 13:5 (skifte 1 och 2).' UV Rapport 2012:42, Arkeologisk utredning steg 1 2011, Dnr 421-3129-2011, Swedish National Heritage board, Riksantikvarieämbetet, 2011.

[577] A. Lagergren. 'Östra Odarslöv 13:5, ESS.' UV Rapport 2012:120, Arkeologisk utredning steg 2 2012, Dnr 421-4393-2011, Swedish National Heritage board, Riksantikvarieämbetet, 2012.

[578] Svensk Byggtjänst. *AMA Anläggning 10, Swedish edition*. Edita Västra Aros AB, Västerås, 2011.

[579] P. Jacobsson. 'ID-report – Handling of non-rad waste and chemical substances.' ESS-0000010, European Spallation Source, 2011.

[580] 'Detaljplan för Östra Odarslöv 13.5 m fl i lund.' Lunds kommun utställningshandling, planbeskrivning, 2012.

[581] L.-O. Hartzén, P. Svensson, and C. Ranelycke. 'Storm water; ID-report – Supporting document for the licensing process.' ESS-0000013 Revision 2, European Spallation Source, 24 Nov 2011.

[582] 'BVF: Förordning (1994:1215) om tekniska egenskapskrav på byggnadsverk m.m.' Svensk författningssamling SFS 1994:1215, 1994.

[583] 'PBL: Plan- och bygglag (2010:900).' Svensk författningssamling SFS 2010:900, 2010.

[584] 'Swedish Agency for Disability Policy Coordination [Myndigheten för Handikappolitisk Samordning].' See: http://www.handisam.se, last accessed 22 Feb 2013.

[585] 'Swedish Work Environment Authority [Arbetsmiljöverket].' See: http://www.av.se, last accessed 22 Feb 2013.

[586] *Protection against lightning - Part 1: General principles*. SS-EN 62305-1, 2nd edition, 2011.

[587] *Protection against lightning - Part 2: Risk management*. SS-EN 62305-2, 2nd edition, 2012.

[588] *Protection against lightning - Part 3: Physical damage to structures and life hazard*. SS-EN 62305-3, 2nd edition, 2011.

[589] *Protection against lightning - Part 4: Electrical and electronic systems within structures*. SS-EN 62305-4, 2nd edition, 2011.

[590] 'ISO 8573-1:2001 Compressed air quality standards.', 2001.

[591] *SSF 130 Utgåva 8, Regler för projektering och installation av inbrotts- och överfallslarmanläggning*. Svenska Stöldskyddsföreningen, 2012. ISBN: 9789189234574.

[592] NASA. *NASA Systems Engineering Handbook*. NASA/SP-2007-6105 Rev1. NASA, 2007.

[593] C. Haskins. *Systems Engineering Handbook*. INCOSE, 3rd edition, 2006.

[594] L. Berdén. 'Quality management policy.' Internal Document ESS-0000126 Rev1, European Spallation Source, 2012.

[595] Kvalitetsledning, SIS/TK 304. *Quality Management Systems - Requirements (ISO 9001:2008)*, 2008.

[596] R. Duperrier. 'System engineering policy.' Internal Document ESS-0000967, European Spallation Source, 2011.

[597] M. Klein Velderman. 'ESS risk management policy.' Internal Document ESS-0000111 Rev 1, European Spallation Source, 2012.

[598] T. Hansson. 'Standards, norms and guidelines recommended for the design and construction of ESS.' Internal Document ESS-0000034, Rev1, European Spallation Source, 2012.

[599] K. Forsberg et al. *Visualizing Project Management*. John Wiley & Sons Inc., 3rd edition, 2005.

[600] G. Lanfranco. 'The ESS plant breakdown structure.' Internal Document ESS-0000940, Rev1, European Spallation Source, 2012.

[601] G. Lanfranco. 'The ESS configuration management plan.' Internal Document ESS-0000254, Rev1, European Spallation Source, 2012.

[602] G. Lanfranco. 'The process flow from beam line element design to 3D virtual models at ESS.' Internal Document ESS-0000941, Rev1, European Spallation Source, 2012.

[603] G. Lanfranco. 'The site-wide coordinate system (SCS) at ESS.' Internal Document ESS-0000091, Rev1, European Spallation Source, 2012.

[604] G. Lanfranco. 'Factory and site acceptance tests.' Internal Document ESS-0000465, Rev1, European Spallation Source, 2012.

[605] P. Carlsson. 'Transition to operations plan.' Internal Document ESS-0001937, European Spallation Source, 29 Nov 2012.

[606] S. Gysin. 'ESS accelerator systems construction project specification (ACCSYS).' Internal Document ESS-0001156, European Spallation Source, 28 Nov 2012.

[607] O. Kirstein. 'Neutron scattering systems project specification.' Internal Document ESS-0000817, European Spallation Source, 28 Nov 2012.

[608] G. Trahern and M. Rescic. 'ESS specification for integrated control system, construction phase.' Internal Document ESS-0001121, European Spallation Source, 22 Nov 2012.

[609] M. Eneroth, M. Åberg, and L. Persson. 'Project specification for conventional facilities construction phase (2013 -2019).' Internal Document ESS-0002388, European Spallation Source, 21 Nov 2012.

[610] S. Henderson. 'Recent commissioning results from the Spallation Neutron Source.' In *Proceedings of the 39th ICFA Advanced Beam Dynamics Workshop on High-Intensity and High-Brightness Hadron Beams, HB2006*, MOAP02. Tsukuba, Japan, 2006.

[611] T. Mason and N. Holtkamp. 'The Spallation Neutron Source: Operational aspects and reliability in the transition from commissioning to fully committed user operation.' Technical Report No 102000000-TR0004, Spallation Neutron Source.

[612] R. Cutler et al. 'Oak Ridge National Laboratory Spallation Neutron Source electrical systems availability and improvements.' In *Proceedings of the 2011 Particle Accelerator Conference*, TUP274. NY, USA, 2011.

[613] J. Galambos. 'Spallation Neutron Source operational experience at 1 MW.' In *Proceedings of the 46th ICFA Advanced Beam Dynamics Workshop on High-Intensity and High-Brightness Hadron Beams, HB2010*, TUO2C01. Morshach, Switzerland, 2010.

[614] 'Report on operations.' Internal Report (draft), The Cross Functional Working Group (CFWG) European Spallation Source, Dec 2012.

[615] J. Galambos et al. 'A fault recovery system for the SNS superconducting cavity linac.' In *Proceedings of LINAC 2006*, MOP057, pages 174–176. Knoxville, Tennessee USA, 2006.

[616] L. Zanini et al. 'Experience from the post-test analysis of MEGAPIE.' *Journal of Nuclear Materials*, 415(3):367, Aug 2011.

[617] C. Carlile. 'Application for permission under the Swedish Radiation Protection Act.' ESS letter to regulatory authorities ESS-0000043, European Spallation Source, 2012.

[618] D. Ene. 'Radiation protection studies for the ESS superconducting linear accelerator.' Technical Report EDMS 1093060, European Spallation Source, 2010.

[619] Swedish Radiation Safety Authority. *The Swedish Radiation Safety Authority's regulations and general advice concerning clearance of materials, rooms, buildings and land in practices involving ionising radiation*, 2011. SSMFS 2011:2.

[620] D. Ene. 'Activation studies on ESS target concepts: Sensitivity analysis.' Technical Report EDMS 1093916, European Spallation Source, 2010.

[621] F. Gallmeier. 'CNCS beam line shielding calculations.' CNCS-05-70-DA0001-R00, SNS, USA, 2004.

[622] D. Ene. 'Assessment of the radioactive inventory in terms of the waste characterization for final disposal.' Technical Report EDMS 1259515, European Spallation Source, 2012.

[623] D. Ene. 'Proposal for the source term definitions: Normal operation nuclides break down lists.' Technical Report EDMS 1183350, European Spallation Source, 2011.

[624] D. Ene. 'Activation studies of the shielding structures for the EURISOL 4 MW target station in terms of the waste characterization for final disposal.' In *Proceedings: First International Workshop on Accelerator Radiation Induced Activation*. PSI, Switzerland, 2008.

[625] A. Boudard et al. 'New potentialities of the Liège intranuclear cascade (INCL) model for reactions induced by nucleons and light charged particles.' *Physical Review C*. Submitted 2012.

[626] A. Kelic et al. 'ABLA07 - towards a complete description of the decay channels of a nuclear system from spontaneous fission to multifragmentation.' In *Contribution to the Joint ICTP-IAEA Advanced Workshop on Model Codes for Spallation Reactions*, NDS-530, page 181. IAEA INDC, 2008.

[627] 'Nuclear data services.' Technical report, International Atomic Energy Agency IAEA, http://www-nds.iaea.org/spallations, last accessed 18 Feb 2013.

[628] A. Leprince et al. 'Excitation functions on thin ^{nat}W target from the new INCL4.6-Abla07.' Internal Report CEA-Irfu 12-61, CEA, 2012.

[629] Y. Titarenko, V. Batyaev, A. Titarenko, et al. 'Measurement and simulation of the cross sections for nuclide production in ^{56}Fe and ^{nat}Cr targets irradiated with 0.04- to 2.6-GeV protons.' *Physics of Atomic Nuclei*, 74(4):523–536, Apr 2011. doi:10.1134/S1063778811040168.

[630] R. Michel et al. 'Cross sections for the production of radionuclides by proton-induced reactions on W, Ta, Pb and Bi from thresholds up to 2.6 GeV.' *Journal of Nuclear Science and Technology*, 2(Suppl.):242, 2002.

[631] J. L. Ulmann et al. 'APT radionuclide production experiment.' Technical Report LA-UR-95-3327, Los Alamos National Laboratory, 1995.

[632] Y. Kasugai et al. 'Measurement of radioactivity induced by GeV-protons and spallation neutrons using AGS accelerator.' Research Report 2003-034, Japan Atomic Energy Research Institute, 2004.

[633] A. Leprince et al. 'Reliability and use of INCL4.6-Abla07 spallation model in the frame of European Spallation Source target design.' In *Proceedings of the 12th International Conference on Radiation Shielding, ICRS-12/17th Topical Meeting of the Radiation Protection and Shielding Division of the American Nuclear Society, RPSD-2012*. 2012.

[634] A. Konobeyev et al. 'Computational approach for evaluation of nuclear data including covariance information.' *Journal of the Korean Physical Society*, 59(2):923–926, Aug 2011.

[635] D. Ene. 'ESS radwaste streams evaluation. Basis for waste management planning.' Technical Report ESS-0001922, European Spallation Source, 2012.

[636] L. Almqvist. 'Avfallshandbok – låg- och medelaktivt avfall, version 2.0.' DokumentID 1195328, Svensk kärnbränslehantering AB (SKB), 2009.

[637] 'Classification of radioactive waste – general safety guide.' IAEA Safety Standards Series No. GSG-1, International Atomic Energy Agency, Vienna, 2009.

[638] A. Y. Konobeyev et al. *Evaluated activation cross section data for proton induced nuclear reactions on W up to 3 GeV incidence energy*. Number 7628 in KIT Scientific Reports. KIT Scientific Publihing, 2012.

[639] 'Predisposal management of radioactive waste, including decommissioning.' IAEA Safety Standards Series No. WSR-2, International Atomic Energy Agency, Vienna, 2000.

[640] D. Ene. 'Transport of radioactive waste from ESS.' Technical Report, European Spallation Source, 2012.

[641] 'Regulations for the safe transportation of the radioactive material.' IAEA Safety Standards Series No. SSR-6, International Atomic Energy Agency, 2012.

[642] D. Ene. 'Shielding calculations for ESS high activated target system.' Technical Report EDMS 1242978, European Spallation Source, 2012.

[643] 'Development of specifications for radioactive waste packages.' IAEA TECDOC 1515, International Atomic Energy Agency, Vienna, Oct 2006.

[644] D. Ene. 'Proposal for approach to be used for determining 3H release reduction.' Technical Report ESS-0001921, European Spallation Source, 2011.

[645] M. Jensen et al. 'Controlling the tritium contents in cooling helium.' Technical Report EDMS 1230258, European Spallation Source, 2012.

[646] M. Jensen. 'Management of operational emissions and waste.' EDMS 1225860, Hevesylab, Risø, 2002.

[647] L. Jacobs. Private communication, 2012.

[648] C. Kharoua. 'Filtering system for the potential tungsten dust.' Technical Report EDMS 1192485, European Spallation Source, 2012.

[649] R. Moorman. 'Dust borne activities in gas-cooled spallation sources experience from gas cooled reactors and from fusion devices.' Technical Report EDMS 1185536, European Spallation Source, 2011.

[650] P. Nilsson. 'Purification guesstimates.' Technical Note 1251578 ver. 0.1, European Spallation Source, 2012.

[651] United States Department of Energy, http://www.hss.doe.gov/nuclearsafety/techstds/docs/handbook/index_hdbk1169.html. *DOE nuclear air cleaning handbook*, last accessed Apr 20, 2013.

[652] 'Management of waste containing tritium and carbon-14.' IAEA Technical Reports Series TRS-421, International Atomic Energy Agency, Vienna, Jul 2004.

[653] K. Liger. 'Private communication.' CEA Cadarache, 2012.

[654] K. Andersson and S. Nielsen. 'Intake of tritiated water vapour released from ESS facility airborne releases.' Technical Report EDMS 1241368, DTU Nutech, Technical University of Denmark, 2012.

[655] D. Ene. 'Intake of tritiated water vapour and radioactive carbon released from ESS facility: Airborne releases, synthesis of work.' Technical Report ESS1241368, European Spallation Source, 2012.

[656] K. Andersson et al. 'Methodology to be used for detailed calculation of dose factors (discharge limits) during operation of the ESS facility.' Technical Report EDMS 1225821, European Spallation Source, 2012.

[657] K. Andersson et al. 'Inhalation and ingestion doses from the most important potential contaminants from routine airborne releases at ESS.' Technical report EDMS 1225821, European Spallation Source and DTU Nutech, Technical University of Denmark, 2012.

[658] 'Argos System.' http://www.argos-system.org, last accessed 19 Feb 2013.

[659] J. Ehrhardt. 'The RODOS system: Decision support for off-site emergency management in Europe.' *Radiation Protection Dosimetry*, 73(1–4), 1997.

[660] S. P. Nielsen and K. G. A. (editors). 'PardNor – PARameters for ingestion dose models for NORdic areas – Status report for the NKS-B activity 2010.' Technical Report, Risoe National Laboratory for Sustainable Energy, Technical University of Denmark, Roskilde, Denmark, Jan 2011. ISBN 978-87-7893-304-1.

[661] K. G. Andersson and S. P. Nielsen. 'External doses from the most important potential contaminants from routine airborne releases at ESS.' EDMS 1259513, European Spallation Source and DTU Nutech, Technical University of Denmark, 2012.

[662] 'Forschungszentrum Jülich.' http://www.fz-juelich.de, last accessed 25 Nov 2012.

[663] T. Hansson. 'Specification for revised dose assessment.' Technical Report ESS-00000056/1, European Spallation Source, 2012.

[664] K. G. Andersson and S. P. Nielsen. 'Radionuclides to be considered in dose estimates following accidental airborne releases.' Technical Report EDMS 120905, European Spallation Source, 2012.

[665] K. Andersson and S. Nielsen. 'Note on evaluation of doses received from airborne releases due to a hypothetical severe design basis accident (DBA) at the ESS installation.' Technical Report ESS-1246094, European Spallation Source, 2012.

[666] C. H. Sen. 'Preliminary decommissioning plan for ESS.' Technical Report N-11/179, Studsvik Nuclear AB, 2011.

[667] Swedish Ministry of the Environment. 'Sweden's fourth national report under the Joint Convention on the safety of spent fuel management and the safety of radioactive waste management.' Ds 2011:35, Ministry Publications Series, Stockholm, 2011.

[668] 'Decommissioning of small medical, industrial and research facilities.' IAEA Technical Reports Series TRS-414, International Atomic Energy Agency, 2003.

[669] 'Decommissioning of medical, industrial and research facilities.' IAEA Safety Standard Series WS-G-2.2, International Atomic Energy Agency, 1999.

[670] 'Decommissioning of nuclear facilities other than reactors.' IAEA Technical Reports Series TRS-386, International Atomic Energy Agency, 1999.

[671] L. Teunckens et al. 'Decommissioning of the Eurochemic reprocessing plant, strategies, experiences and developments.' In *Decommissioning in Belgium: Proceedings of the Belgian Nuclear Society Annual Conference*. 1999.

[672] 'Financial aspects of decommissioning.' IAEA TECDOC 1476, International Atomic Energy Agency, 2005.

[673] *Summary of the ITER Final Design Report*. International Atomic Energy Agency, Vienna, Jul 2001.

[674] K. S. Jeong et al. 'Structures and elements for the decommissioning cost estimations of nuclear research reactors.' *Annals of Nuclear Energy*, 34:326 –332, 2007.

[675] 'Selecting strategies for the decommissioning of nuclear facilities, a status report.' Technical Report (originally published in *Radioactive Waste Management*) No. 6038, Nuclear Energy Agency (NEA) and Organisation for Economic Co-operation and Development (OECD), 2006.

[676] 'Design lessons drawn from the decommissioning of nuclear facilities.' TECDOC 1657, International Atomic Energy Agency, 2011.

[677] 'Managing low radioactivity material from the decommissioning of nuclear facilities.' IAEA Technical Reports Series TRS-462, International Atomic Energy Agency, 2008.

[678] M. Rogante. 'Contributions to the decommissioning issue of the ESS project.' RE-ESSHU-01-2009, Rogante Engineering, Cinitanova Marche, 2009.

[679] 'Studsvik AB.' http://www.studsvik.com, last accessed 19 Feb 2013.

[680] 'Wikipedia: Studsvik.' http://en.wikipedia.org/wiki/Studsvik, last accessed 16 Nov 2012.

[681] 'SKB.' http://www.skb.se, last accessed 19 Feb 2013.

[682] 'Regulation on operation of accelerators and sealed radiation sources.' Swedish Radiation Safety Authority SSMFS 2008:27, 2008.

[683] 'Safety culture.' Technical Report INSAG-4, International Nuclear Safety Advisory Group of the International Atomic Energy Agency, 1991.

[684] 'Key practical issues in strengthening safety culture.' Technical Report INSAG-15, International Nuclear Safety Advisory Group of the International Atomic Energy Agency, 2002.

[685] S. Nordlinder et al. 'Preliminary safety analysis report for ESS.' Technical Report ESS-0000002/1, European Spallation Source, 2012.

[686] R. Moormann. 'Safety & licensing of the European Spallation Source (ESS).' Report Jul 4136, Forschungszentrum Jülich, 2004.

[687] 'Regulation on basic regulations for protection of workers and public at activities with ionisation radiation.' Swedish Radiation Safety Authority SSMFS 2008:51, 2008.

[688] S. Nordlinder. 'Dose assessment for severe accidents at ESS.' Technical Report ESS-0000488/1, European Spallation Source, 2012.

[689] 'Safety of nuclear power plants: Design, requirements.' IAEA Safety Standard Series NS-R-1, International Atomic Energy Agency, 2000.

[690] C. Kharoua. 'Design calculation report, estimation of the impact of the after heat – LOCA.' Technical Report EDMS 1164510, European Spallation Source, 2011.

[691] 'Registration, evaluation, authorisation and restriction of chemical substances (REACH).' European Community Regulation No. 1907/2006, http://ec.europa.eu/environment/chemicals/reach/reach_intro.htm, last accessed 22 Feb 2013.